Sun. Sep 14, 2025

Sun. Sep 14, 2025 5:30 PM - 6:30 PM JST | Sun. Sep 14, 2025 8:30 AM - 9:30 AM UTC Hall A(MP)

[WR] Welcome Reception

Sun. Sep 14, 2025 3:00 PM - 5:30 PM JST | Sun. Sep 14, 2025 6:00 AM - 8:30 AM UTC Resit. Desk

[Regist] Registration

©APSORC25

Mon. Sep 15, 2025

Award Lecture | Award

Mon. Sep 15, 2025 9:15 AM - 10:10 AM JST | Mon. Sep 15, 2025 12:15 AM - 1:10 AM UTC Hall S(Int'l)

[AW1] Award Session 1: Kimura Award 2025

9:25 AM - 10:10 AM JST | 12:25 AM - 1:10 AM UTC

[AW01]

FROM LAWRENCIUM TO SEABORGIUM AND HASSIUM - AND BACK

*Matthias Schädel[1] (1. GSI Helmholtzzentrum für Schwerionenforschung GmbH (Germany))

Award Lecture | Award

Mon. Sep 15, 2025 10:25 AM - 11:20 AM JST | Mon. Sep 15, 2025 1:25 AM - 2:20 AM UTC Hall S(Int'l)

[AW2] Award Session 2: Hevesy Medal Award 2021

10:35 AM - 11:20 AM JST | 1:35 AM - 2:20 AM UTC

[AW02]

Developments in gamma-ray spectrometry, activation analysis, digital autoradiography and design of low-activation structural Materials: mathematical modelling and experimental solutions

*Vladimir P Kolotov[1] (1. Vernadsky Institute of Geochemistry and Analytical Chemistry of Russian Academy of Sciences (Russia))

Plenary Talk | Plenary Talk

Mon. Sep 15, 2025 11:25 AM - 12:10 PM JST | Mon. Sep 15, 2025 2:25 AM - 3:10 AM UTC Hall S(Int'l)

[PL1] Plenary Talk 1 by Yoshio Takahashi

11:25 AM - 12:10 PM JST | 2:25 AM - 3:10 AM UTC

[PL01]

Environmental behaviors of radionuclides studied by advanced X-ray absorption spectroscopy

*Yoshio Takahashi[1] (1. The University of Tokyo (Japan))

Invited & Contributed Talk | [R1]Nuclear Chemistry

Mon. Sep 15, 2025 1:30 PM - 3:00 PM JST | Mon. Sep 15, 2025 4:30 AM - 6:00 AM UTC Hall A(MP)

[R1] Nuclear Chemistry

1:30 PM - 2:00 PM JST | 4:30 AM - 5:00 AM UTC

[R1-01(Invited)]

Recent progress in the study of thorium-229 isomer

*Koji Yoshimura[1] (1. Okayama University (Japan))

2:00 PM - 2:20 PM JST | 5:00 AM - 5:20 AM UTC

[R1-02]

Development of extraction and trapping apparatus for ^{229m}Th ions and half-life measurement of singly charged ^{229m}Th

*Yudai Shigekawa[1,2], Atsushi Yamaguchi[1], Katsuyuki Tokoi[3], Nozomi Sato[1], Hidetoshi Kikunaga[4], Kenji Shirasaki[4], Yoshitaka Kasamatsu[3], Michiharu Wada[5], Hiromitsu Haba[1] (1. RIKEN (Japan), 2. University of Tsukuba (Japan), 3. Osaka University (Japan), 4. Tohoku University (Japan), 5. KEK (Japan))

2:20 PM - 2:40 PM JST | 5:20 AM - 5:40 AM UTC

[R1-03*]

Barrier distribution and excitation function measurements of ^{51}V+^{159}Tb for estimating optimal reaction energy for new element synthesis

*Yuki Yamanouchi[1,2], Pierre Brionnet[2], Satoshi Sakaguchi[1,2], Tomasz Cap[3], Margaux Forge[4], Takumi Fukatsu[1], Hiromitsu Haba[2], Daiya Kaji[2], Sota Kimura[5], Kouji Morimoto[2], Yuya Michimoto[1,2], Toshitaka Niwase[1,2], Hideyuki Sakai[2], Masaomi Tanaka[6,2] (1. Department of Physics, Kyushu University (Japan), 2. RIKEN Nishina Center (Japan), 3. National Centre for Nuclear Research (Poland), 4. Université de Strasbourg (France), 5. KEK Wako Nuclear Science Center (Japan), 6. Faculty of Arts and Science, Kyushu University (Japan))

2:40 PM - 3:00 PM JST | 5:40 AM - 6:00 AM UTC

[R1-04*]

Direct mass measurement of ^{252}Cf fission fragments with MRTOF-MS

*Gen Otsuka[1], Toshitaka Niwase[1], Sota Kimura[2], Hiromitsu Haba[3], Hironobu Ishiyama[3], Marco Rosenbusch[3], Satoshi Sakaguchi[1], Peter Schury[2], Michiharu Wada[2,4] (1. Department of physics, Kyushu University (Japan), 2. Wako Nuclear Science Center, (WNSC), Institute of Particle and Nuclear Studies (IPNS), High Energy Accelerator Research Organization (KEK) (Japan), 3. RIKEN Nishina Center for Accelerator-Based Science (Japan), 4. Institute of Modern Physics, Huizhou branch, Chinese Academy of Science (China))

©APSORC25

Invited & Contributed Talk | [R7]Environmental Radiochemistry

Mon. Sep 15, 2025 1:30 PM - 3:00 PM JST | Mon. Sep 15, 2025 4:30 AM - 6:00 AM UTC Hall S(Int'l)

[R7] Environmental Radiochemistry

1:30 PM - 2:00 PM JST | 4:30 AM - 5:00 AM UTC

[R7-01(Invited)]

A RAPID ANALYSIS OF RADIOSTRONTIUM IN ENVIRONMENTAL WATER USING STRONTIUM SORBENTS

*Yoshimune Ogata[1], Haruka Minowa[2], Sadao Kojima[1], Yuka Kato[3], Keisuke Sueki[4], Shinji Sugihara[5], Tetsuya Arinobu[1] (1. Aichi Medical University (Japan), 2. The Jikei University School of Medicine (Japan), 3. Aloka Co. Ltd. (Japan), 4. Tokyo Metropolitan University (Japan), 5. Oita University (Japan))

2:00 PM - 2:20 PM JST | 5:00 AM - 5:20 AM UTC

[R7-02]

EFFECTS OF CALCIUM APPLICATION ON CAESIUM UPTAKE AND TRANSLOCATION IN PLANTS

*Masashi Kihana[1], Mutsumi Yamagami[1], Yoshihito Ohtsuka[1], Yuichi Takaku[1,2], Yusuke Unno[1], Akira Takeda[1] (1. Department of Radioecology, Institute for Environmental Sciences (Japan), 2. Faculty of Pure and Applied Sciences, Tsukuba University (Japan))

2:20 PM - 2:40 PM JST | 5:20 AM - 5:40 AM UTC

[R7-03*]

ASSESSING POST-REMEDIATION MOBILITY RISKS OF URANIUM(IV) THROUGH COLLOIDAL TRANSPORT AND ISOTOPIC SIGNATURES

*Xinyi Shi[1], Xiaoyan Wei[1], Duoqiang Pan[1], Wangsuo Wu[1] (1. Lanzhou University (China))

2:40 PM - 3:00 PM JST | 5:40 AM - 6:00 AM UTC

[R7-04*]

Soil properties: The case study of the Coffee Field, AIRID Training Center, Chiang Mai University, Thailand.

*Khemruthai Kheamsiri[1], Naofumi Akata[2], Chutima Kranrod[2], Hirofumi Tazoe[2], Tarika Thumwijit[3], Ilsa Rosianna[1], Haruka Kuwata[1], Krit Khetanun[4], Narit Yimyam[4], Yusuke Unno[5], Akira Takeda[5] (1. Graduate School of Health Sciences, Hirosaki University (Japan), 2. Institute of Radiation Emergency Medicine, Hirosaki University (Japan), 3. Faculty of Associated Medical Sciences, Chiang Mai University (Thailand), 4. Faculty of Agriculture, Chiang Mai University (Thailand), 5. Department of Radioecology, Institute for Environmental Sciences (Japan))

©APSORC25

Invited & Contributed Talk | [R7]Environmental Radiochemistry

Mon. Sep 15, 2025 3:15 PM - 4:25 PM JST | Mon. Sep 15, 2025 6:15 AM - 7:25 AM UTC Hall S(Int'l)

[R7] Environmental Radiochemistry

3:15 PM - 3:45 PM JST | 6:15 AM - 6:45 AM UTC

[R7-05(Invited)]

Environmental Analysis by Accelerator Mass Spectrometry

*Hiroyuki Matsuzaki[1] (1. MALT, The University of Tokyo (Japan))

3:45 PM - 4:05 PM JST | 6:45 AM - 7:05 AM UTC

[R7-06]

Retrospective overview of the results of radionuclide measurements in the liquid radioactive discharges of the Krško Nuclear Power Plant and the Sava River water

*Željko Grahek[1] (1. Ruđer Bošković Institute (Croatia))

4:05 PM - 4:25 PM JST | 7:05 AM - 7:25 AM UTC

[R7-07*]

Study on colloid and radionuclide co-migration model in saturated porous system based on the interaction forces between colloids.

*Qi Tan[1], Xiaoyan Wei[1], Zhen Xu[1], Duoqiang Pan[1], Wangsuo Wu[1] (1. Lanzhou University (China))

©APSORC25

Contributed Talk | [R6]Radiation and Radioisotopes in Life Science

Mon. Sep 15, 2025 1:30 PM - 3:10 PM JST | Mon. Sep 15, 2025 4:30 AM - 6:10 AM UTC Hall B(Small)

[R6] Radiation and Radioisotopes in Life Science

1:30 PM - 1:50 PM JST | 4:30 AM - 4:50 AM UTC

[R6-01]

MODELING BIOKINETICS OF INSOLUBLE CESIUM-ABSORBED PARTICLES FOLLOWING INTRATRACHEAL ADMINISTRATION IN MICE

*Kentaro Manabe[1], Yutaka Yamada[2], Takamitsu Morioka[2], Kazuhiko Ninomiya[3], Satoru Endo[3], Masatoshi Suzuki[4,5] (1. JAEA (Japan), 2. QST (Japan), 3. Hiroshima University (Japan), 4. Tohoku University (Japan), 5. F-REI (Japan))

1:50 PM - 2:10 PM JST | 4:50 AM - 5:10 AM UTC

[R6-02*]

In Vivo Imaging of ^{95m}Tc-DTPA as a Radiotracer Alternative to Clinical ^{99m}Tc-DTPA Using Electron-Tracking Compton Camera (ETCC)

*Kaiji Tanaka[1], Ryota Iwasaki[1], Ryuta Kiuchi[1], Koya Yoshida[1], Hiroyasu Matsushita[1], Hiroyuki Kimura[2], Masato Asai[3], Yoji Kitamura[4], Takashi Kozaka[4], Hidekazu Kawashima[5], Tsuyoshi Fukuzawa[1], Shigeto Kabuki[1], Kyoshi Nishijima[6], Etsuo Kunieda[7], Junko Kushida[1] (1. Tokai University (Japan), 2. Kyoto University (Japan), 3. Japan Atomic Energy Agency (Japan), 4. Kanazawa University (Japan), 5. Kyoto Pharmaceutical University (Japan), 6. Kanagawa University (Japan), 7. Tokyo General Hospital (Japan))

2:10 PM - 2:30 PM JST | 5:10 AM - 5:30 AM UTC

[R6-03]

Potential involvement of rhizodeposition from white lupin in cesium dynamics in the rhizosphere soil

*Hiroshi Uchibayashi[1], Satoshi Asaeda[1,2], Akiko Maruo[1], Hayato Maruyama[1], Toshihiro Watanabe[1], Yong-Gen Yin[3], Nobuo Suzui[3], Yuta Miyoshi[3], Yusaku Noda[3], Kazuyuki Enomoto[3], Naoki Kawachi[3], Yusuke Unno[4], Takuro Shinano[1] (1. Hokkaido University (Japan), 2. Hiroshima Prefectural Technology Research Institute (Japan), 3. National Institutes for Quantum Science and Technology (QST) (Japan), 4. Institute for Environmental Sciences (Japan))

2:30 PM - 2:50 PM JST | 5:30 AM - 5:50 AM UTC

[R6-04*]

Flexible Scintillator for non-invasive visualization of nutrient transport in plants

*XIAORUI ZHOU[1], Ai Kaiho Soma[1], Yuko Kurita[1], Natsuko Kobayshi[1], Keitaro Tanoi[1,2] (1. Graduate School of Agricultural and Life Science, The University of Tokyo (Japan), 2. Fukushima Institute for Research, Education and Innovation (Japan))

2:50 PM - 3:10 PM JST | 5:50 AM - 6:10 AM UTC

[R6-05]

Sodium-induced dot-like accumulation of ^{137}Cs in rice root grown under low K^+ condition

*Jun FURUKAWA[1], Satomi KANNO[2] (1. Univ. of Tsukuba, CRiES (Japan), 2. Nagoya Univ., IAR (Japan))

Contributed Talk | [R1]Nuclear Chemistry

Mon. Sep 15, 2025 3:15 PM - 4:35 PM JST | Mon. Sep 15, 2025 6:15 AM - 7:35 AM UTC Hall A(MP)

[R1] Nuclear Chemistry

3:15 PM - 3:35 PM JST | 6:15 AM - 6:35 AM UTC

[R1-05]

Separation of Sm and Nd from spent fuel powder by pyrochemical process

*Mu Lin[1], Fangli Fan[1], Zhi Lin Qin[1] (1. Institute of Modern Physics, Chinese Academy of Sciences (China))

3:35 PM - 3:55 PM JST | 6:35 AM - 6:55 AM UTC

[R1-06]

High temperature retention of radioactive iodine by silver-loaded zeolite under varying atmospheric conditions

*Haohan Zhang[1], Xuandong Kou[1,2], Robert Eichler[1,2] (1. Paul Scherrer Institut (Switzerland), 2. University of Bern (Switzerland))

3:55 PM - 4:15 PM JST | 6:55 AM - 7:15 AM UTC

[R1-07*]

COPRECIPITATION OF ^{211}At WITH SAMARIUM HYDROXIDE TOWARD IDENTIFICATION OF CHEMICAL SPECIES OF At

*Ryoutarou Masuda[1,2], So Hashiba[1,2], Hiroki Aoto[1], Masashi Kaneko[1], Hiroyuki Kazama[1], Hiromitsu Haba[2], Yousuke Kanayama[2], Yudai Shigekawa[2,3], Akihiro Nambu, Yoshitaka Kasamatsu[1,2] (1. Osaka University (Japan), 2. RIKEN (Japan), 3. Tsukuba University (Japan))

4:15 PM - 4:35 PM JST | 7:15 AM - 7:35 AM UTC

[R1-08*]

Synthesis of UO_2 nanoparticles by microplasma in molten salt

*Junhan Luo[1], Yuexiang Lu[1] (1. Tsinghua University (China))

©APSORC25

Contributed Talk | [R6]Radiation and Radioisotopes in Life Science

Mon. Sep 15, 2025 3:25 PM - 4:45 PM JST | Mon. Sep 15, 2025 6:25 AM - 7:45 AM UTC Hall B(Small)

[R6] Radiation and Radioisotopes in Life Science

3:25 PM - 3:45 PM JST | 6:25 AM - 6:45 AM UTC

[R6-06]

Beta-ray imaging in vivo is a good tool for elucidating nutrient element (phosphate) absorption mechanisms in plant roots

*Satomi Kanno[1], Pascale David[2], Laurent Nussaume[2] (1. Nagoya University IAR (Japan), 2. CEA (France))

3:45 PM - 4:05 PM JST | 6:45 AM - 7:05 AM UTC

[R6-07]

Diverse mechanisms of salt tolerance in the genus *Vigna*

*Yusaku Noda[1], Nobuo Suzui[1], Yong-Gen Yin[1], Yuta Miyoshi[1], Kazuyuki Enomoto[1], Naoki Kawachi[1], Keitaro Tanoi[2], Jun Furukawa[3], Ken Naito[4] (1. QST, Takasaki (Japan), 2. UTokyo (Japan), 3. Tsukuba Univ (Japan), 4. NARO (Japan))

4:05 PM - 4:25 PM JST | 7:05 AM - 7:25 AM UTC

[R6-08]

Plant RI Imaging at Tohoku University: Advancing Plant Science Through Radioisotope Visualization

*Hiroshi Watabe[1], Yohei Kikuchi[1], Shozo Furumoto[1] (1. Tohoku University (Japan))

4:25 PM - 4:45 PM JST | 7:25 AM - 7:45 AM UTC

[R6-09]

Spatiotemporal analysis of Ca transport dynamics in tomato using Ca-45 tracer and compact multiprobe system

*Yusuke Shikanai[1], Takuma Hirashima[1], Yong-Gen Yin[2], Nobuo Suzui[2], Mitsutaka Yamaguchi[2], Yuto Nagao[2], Akihiro Saito[1], Naoki Kawachi[2], Kyoko Higuchi[1] (1. Tokyo University of Agriculture (Japan), 2. Takasaki Institute for Advanced Quantum Science, National Institutes for Quantum Science and Technology (Japan))

©APSORC25

Contributed Talk | [R7]Environmental Radiochemistry

Mon. Sep 15, 2025 4:45 PM - 6:05 PM JST | Mon. Sep 15, 2025 7:45 AM - 9:05 AM UTC Hall S(Int'l)

[R7] Environmental Radiochemistry

4:45 PM - 5:05 PM JST | 7:45 AM - 8:05 AM UTC

[R7-08]

Comparative Uptake Behavior of Iodide and Iodate by Corals in Seawater

*ZHIYUAN SHI[1], Yuichi Takaku[2], Shinya Yamasaki[2], Yudai Shigekawa[2], Kimikazu Sasa[3], Keisuke Sueki[2], Aya Sakaguchi[2] (1. University of Tsukuba, Environmental Studies (Japan), 2. University of Tsukuba, Institute of Pure and Applied Sciences (Japan), 3. University of Tsukuba (UTTAC), Tandem Accelerator Complex (Japan))

5:05 PM - 5:25 PM JST | 8:05 AM - 8:25 AM UTC

[R7-09]

Development of analytical method for low-level radiostrontium in seawater using strontium sorbent

*Haruka Minowa[1], Yoshimune Ogata[2], Sadao Kojima[2], Yuka Kato[3], Keisuke Sueki[4], Shinji Sugihara[5], Tetsuya Arinobu[2] (1. The Jikei University Shcool of Medicine (Japan), 2. Aichi Medical University School of Medicine (Japan), 3. Aloka Co., Ltd. (Japan), 4. Tokyo Metropolitan University (Japan), 5. Oita University (Japan))

5:25 PM - 5:45 PM JST | 8:25 AM - 8:45 AM UTC

[R7-10]

Effect Analysis of I-129 to the Environment Generated due to the Decay of Te-129m Discharged by the Fukushima Nuclear Accident

*Haruo M Sato[1], Ryo Ikeda[1] (1. Okayama University (Japan))

5:45 PM - 6:05 PM JST | 8:45 AM - 9:05 AM UTC

[R7-11*]

ATMOSPHERIC ^{210}Pb ACTIVITY CONCENTRATIONS IN NORTH KAZAKHSTAN URANIUM MINING AREA

*Assel Aidosovna Bagramova[1], Aya Sakaguchi[2,3], Kohei Sakata[2], Junko Takahashi[3], Aidana Zhumalina[1], Satoru Endo[4], Tsuyoshi Kajimoto[4], Masaharu Hoshi[5], Kassym Zhumadilov[1] (1. Eurasian National University, Department of Nuclear Physics, New Materials and Technologies (Kazakhstan), 2. University of Tsukuba, Institute of Pure and Applied Sciences (Japan), 3. University of Tsukuba, Center for Research in Radiation, Isotopes and Earth System Sciences (Japan), 4. Hiroshima University, Graduate School of Advanced Science and Engineering (Japan), 5. Hiroshima University, The Center for Peace (Japan))

©APSORC25

Contributed Talk | [R1]Nuclear Chemistry

Mon. Sep 15, 2025 4:50 PM - 6:10 PM JST | Mon. Sep 15, 2025 7:50 AM - 9:10 AM UTC Hall A(MP)

[R1] Nuclear Chemistry

4:50 PM - 5:10 PM JST | 7:50 AM - 8:10 AM UTC

[R1-09*]

Internal Conversion Electron Spectroscopy Using a Silicon Drift Detector (SDD) for Elucidation of Excited-State Structure in Superheavy Nuclei

*Naoto Miyashita[1], Masato Asai[2], Naoyuki Kitagawa[1], Tomoki Fujii[1], Toshitaka Niwase[1], Satoshi Sakaguchi[1] (1. Kyushu University (Japan), 2. Japan Atomic Energy Agency (Japan))

5:10 PM - 5:30 PM JST | 8:10 AM - 8:30 AM UTC

[R1-10*]

Evaluation of radiation tolerance of solar cell detectors using tandem accelerator at Kyushu University

*Hiroto Watanabe[1], Toshitaka Niwase[1], Yuki Yamanouchi[1,2], Tomoki Fujii[1], Naoto Miyashita[1], Naoyuki Kitagawa[1], Yuya Michimoto[1], Ryosuke Shikada[1], Gen Otsuka[1], Satoshi Sakaguchi[1], Takashi Teranishi[1], Hiroyuki Makii[3], Masato Asai[3], Yutaka Watanabe[4] (1. Department of Physics, Kyushu University (Japan), 2. RIKEN Nishina Center for Accelerator-Based Science (Japan), 3. Advanced Science Research Center, Japan Atomic Energy Agency (Japan), 4. Wako Nuclear Science Center, Institute of Particle and Nuclear Studies, High Energy Accelerator Research Organization (KEK) (Japan))

5:30 PM - 5:50 PM JST | 8:30 AM - 8:50 AM UTC

[R1-11*]

Progress for the development of a new detector system for studying the β-delayed fission

*Tomoki Fujii[1], Toshitaka Niwase[1], Yuki Yamanouchi[1], Naoyuki Kitagawa[1], Naoto Miyashita[1], Yusuke Tanaka[1], Satoshi Sakaguchi[1], Yoshikazu Hirayama[2], Yutaka Watanabe[2], Hiroari Miyatake[2] (1. Kyushu University (Japan), 2. Wako Nuclear Science Center, KEK (Japan))

5:50 PM - 6:10 PM JST | 8:50 AM - 9:10 AM UTC

[R1-12*]

Development and performance evaluation of Multi-Sampling Ionization Chamber using intense slow heavy ion beams with mass numbers around 10

*Ryosuke Shikada[1], Masaomi Tanaka[2], Naoyuki Kitagawa[1], Tomoki Fujii[1], Gen Otsuka[1], Hiroto Watanabe[1], Toshitaka Niwase[1], Satoshi Sakaguchi[1] (1. Department of Science, Kyushu University (Japan), 2. Faculty of Arts and Science, Kyushu University (Japan))

©APSORC25

Contributed Talk | [P1]Radiation Safety and Management

Mon. Sep 15, 2025 5:00 PM - 6:00 PM JST | Mon. Sep 15, 2025 8:00 AM - 9:00 AM UTC Hall B(Small)

[P1] Radiation Safety and Management

5:00 PM - 5:20 PM JST | 8:00 AM - 8:20 AM UTC

[P1-01*]

MEASUREMENT OF ^{36}Cl PRODUCTION RATE IN POWER CABLE SHEATHS IRRADIATED AT CERN CHARM FACILITY

*Tatsuhiro Kimura[1], Go Yoshida[2], Hiroshi Matsumura[2], Masumi Matsumura[1], Toshiya Sanami[2], Robert Froeschl[3], Davide Bozzato[3], Arnaud Devienne[3], Masaki Ishida[2], Eisuke Watanabe[2], Kiyokazu Tsugane[2], Eunji Lee[2], Ryoken Shiobara[4], Masahiro Mitsuhashi[4], Hiroshi Yashima[5], Yuuki Hirano[4], Yusuke Nakayashiki[4], Koji Oishi[4], Saori Kurita[6], Miki Nakada[6], Takuya Saze[6], Bui Ngoc Thien[7], Tsutomu Takahashi[1], Tetsuro Yoshida[1], Kimikazu Sasa[1] (1. Tsukuba University (Japan), 2. KEK (Japan), 3. CERN (Switzerland), 4. JER (Japan), 5. Kyoto University (Japan), 6. NIFS (Japan), 7. SOKENDAI (Japan))

5:20 PM - 5:40 PM JST | 8:20 AM - 8:40 AM UTC

[P1-02]

Development of a surface contamination monitor for alpha particles using an outer-layer scintillating fiber

*Sho Toyama[1], Misako Miwa[1], Wataru Kada[1,2], Shigeo Matsuyama[1,2] (1. Department of Quantum Science and Energy Engineering, Graduate School of Engineering, Tohoku University (Japan), 2. Center for Fundamental Research on Nuclear Decommissioning, Tohoku University (Japan))

5:40 PM - 6:00 PM JST | 8:40 AM - 9:00 AM UTC

[P1-03]

THE SHIELDING ABILITY AND RADIOACTIVATION OF NOVEL CERAMICS

*Hiroaki Terato[1], Midori Isobe[1], Hiroyuki Mori[2], Yuriko Mannami[2], Naoyuki Osada[3], Yoshinori Sakurai[3] (1. Okayama University (Japan), 2. Mitsuishi Taika Renga Co. Ltd. (Japan), 3. Kyoto University (Japan))

©APSORC25

Poster Presentation | [R7]Environmental Radiochemistry

Mon. Sep 15, 2025 6:30 PM - 8:00 PM JST | Mon. Sep 15, 2025 9:30 AM - 11:00 AM UTC Poster

[Poster] R7

[P-R7-01]

Study on Activity of Cesium-137 in the Coastal and Offshore Waters of Taiwan

*chun hao Chen[1], Jian Wei You[1], Liang Yu Tao[1], Wan Ling Chen[1] (1. Radiation Monitoring Center (Taiwan))

[P-R7-02]

Study on the Activity of Cesium-137 in Surface Soils of Taiwan

*Jian-Wei You[1], Hui-I Lo[1], Wan-Ling Chen[1] (1. Radiation Monitoring Center, Nuclear Safety Commission. (Taiwan))

[P-R7-03]

Research on the environmental behavior of radionuclides released from Rokkasho reprocessing plant at IES

*Shinji Ueda[1], Hidenao Hasegawa[1], Hideki Kakiuchi[1], Yoshihito Ohtsuka[1], Koichi Abe[1] (1. Institute for Environmental Sciences (Japan))

[P-R7-04]

Measurements of hydrogen deposition velocities of forest soil by using D_2 gas

*Masaru Nagai[1], Hideki Kakiuchi[1], Tsuyoshi Masuda[1] (1. Institute for Environmental Sciences (Japan))

[P-R7-05]

Spatial transports of ^{7}Be and ^{22}Na from the Arctic to the Sea of Japan side of Honshu, Japan.

*Keisuke Yoshida[1], Masayuki Umeda[1], Masahiro Yamashita[1], Masanao Nakano[1], Mutsuo Inoue[2] (1. Japan Atomic Energy Agency (Japan), 2. Kanazawa University (Japan))

[P-R7-06]

Trends of ^{129}I/^{127}I ratios and I-129 concentrationsfor environmental samples of Japan

*Sota Nagaoka[1], Noeru Kato[1], Xiaoshui Wang[1], Wataru Nitta[1] (1. Japan Chemical Analysis Center (Japan))

[P-R7-07]

Radon Concentration Measurement in Water Samples using Plastic scintillator pellets: Evaluation of Efficiency and Detection Limit

*Masahiro Hirota[1], Koichi Sakakibara[2], Kazuki Sawahata[3], Yuka Kato[3] (1. Research Center for Advanced Science and Technology, Shinshu University (Japan), 2. Faculty of Science, Shinshu University (Japan), 3. ALOKA Co., Ltd. (Japan))

[P-R7-08]

Experimental method for estimation of ^{210}Pb gamma-ray attenuation in sediment sample using ^{241}Am point source

*Haifeng Shen[1], Satoru Miyata[1], Katsuyuki Suzuki[1], Wataru Nitta[1], Yuji Ohta[1], Hidesuke Itadzu[2] (1. Japan Chemical Analysis Center (Japan), 2. SEIKO EG&G CO.,LTD (Japan))

[P-R7-09]

Biological Tritium Analysis in Taiwan

HuanChing Huang[1], HueiWen Tsai[1], PingJi Huang[1], *WanJyun Wei[1] (1. National Atomic Research Institute (Taiwan))

©APSORC25

[P-R7-10*]

DISTRIBUTION OF ^{137}Cs, ^{90}Sr AND ACTIVITY RATIO OF ^{90}Sr/^{137}Cs IN SOIL AROUND FDNPP

*Riku Kawase[1], Kazuhiko Ninomiya[2], Takashi Yoshimura[1] (1. The University of Osaka (Japan), 2. Hiroshima University (Japan))

[P-R7-11]

Spatiotemporal variations of ^{134}Cs and ^{228}Ra concentrations of surface waters in the off-Doto area (2018-2025)

*Ryoma Arakaki[1], Kaisei Mashita[1], Mutsuo Inoue[1], Yukiko Taniuchi[2], Takuya Nakanowatari[2], Seiya Nagao[1] (1. Kanazawa University (Japan), 2. Japan Fisheries Research and Education Agency (Japan))

[P-R7-12]

EFFECT OF ENVIRONMENTAL CONDITIONS ON STRONTIUM ADSORPTION OF FLUVO-AQUIC SOIL COLLOIDS

*Lingling Ma[1], Yang Shao[1] (1. Institute of High Energy Physics, Chinese Academy of Sciences, (China))

[P-R7-13]

Spatiotemporal variation of FDNPP-derived ^{137}Cs in/around the Bering Sea

*Daichi Koshiishi[1] (1. Kanazawa university (Japan))

[P-R7-14]

RADIOCARBON DATING OF VERDIGRIS ON THE BRONZE FITTINGS ATTACHED TO THE RAFTERS OF THE MAIN HALL, IZUMO TAISHA SHRINE

*Hirotaka Oda[1], Tetsuya Yamada[2], Tsukamoto Toshio[2] (1. ISEE, Nagoya Univ. (Japan), 2. Gangoji Institute Res. Cultural Property (Japan))

[P-R7-15]

A preliminary study- minute-level analysis of environmental gamma dose rate and precipitation

Wei-Min Li[1], *Chi-Wen Hsieh[1], Chuan-Pin Lee[2,3], Yu-Jie Li[4], Chun-Yi Fang[4], Wei-Hsiang Tseng[1], Yu-Cheng Tsai [1] (1. Department of Electrical Engineering, National Chung Cheng University (Taiwan), 2. Center for Energy and Environmental Research, National Tsing Hua University, Hsinchu City 300044, Taiwan (Taiwan), 3. Radioactive Waste Disposal Technology Research and Development Center, National Tsing Hua University, Hsinchu City 300044, Taiwan (Taiwan), 4. Radiation Monitoring Center, Nuclear Safety Commission, Kaohsiung City 833172, Taiwan (Taiwan))

[P-R7-16*]

Measurement of Radioactive Cesium Transfer Factors from Fukushima-Contaminated Soil to Plants

*Yuzuha Mimura[1], Kazuki Daikoku[1], Ayuto Kato[2], Mai Kondo[2], Sawa Ishikawa[1], Mizuki Sumihama[3], Takashi Saito[4], Haruki Minowa[5], Hiroaki Tanigawa[1], Miki Tanigawa[1], Michio Okada[1] (1. Osaka University (Japan), 2. Gifu University (Japan), 3. Osaka University / Gifu University (Japan), 4. Shokei Gakuin University (Japan), 5. Jikei University. Sch. Med. (Japan))

[P-R7-17]

A comparison between wet-only and total deposition of ^{137}Cs observed in Namie Town, Fukushima Prefecture, Japan

*Hidenao Hasegawa[1], Yoshihito Ohtsuka[1], Naofumi Akata[2], Shinji Ueda[1], Shinji Tokonami[2] (1. Institute for Environmental Sciences (Japan), 2. Hirosaki University (Japan))

[P-R7-18]

Synergistic Coordination-Reduction Interface for Electrochemical Reduction Extraction of Low-Impurity Uranium from Seawater

*Huanhuan Liu[1], Wenkun Zhu[1] (1. Southwest university of science and technology (China))

[P-R7-19]

Self-Absorption Correction Method Validation for Pb-210 quantification using Gamma Spectrometry

*Dante Nakazawa[1], Shigekazu Hirao[2], Kunihiro Sakai[1], Atsuo Suzuki[1] (1. Mirion Technologies (Canberra) KK (Japan), 2. Institute of Environmental Radioactivity at Fukushima University (Japan))

[P-R7-20]

Temporal changes of ^{3}H and ^{129}I in seawater collected at mooring buoy near the marine discharge outlet of the Rokkasho Reprocessing Plant

*Hisaki Kofuji[1], Shinichi Gasa[1], Natsuko Akihama[1] (1. Japan Marine Science Foundation (Japan))

[P-R7-21*]

Depth-Dependent Measurement of Radioactive Cesium Activity Concentration in a 30 cm Soil Core from Fukushima

*Kazuki Daikoku[2], Mizuki Sumihama[2,3], Haruka Minowa[4], Yuzuha Mimura[2], Takeshi Saito[1], Sawa Ishikawa[2], Mai Kondo[3], Ayuto Kato[3], Michio Okada[2] (1. Shokei Gakuin University (Japan), 2. The University of Osaka (Japan), 3. Gifu University (Japan), 4. Jikei Univ. Sch. Med. (Japan))

[P-R7-22]

Efficient Photoassisted Uranium Recovery from Fluorine-Containing Wastewater by Ag/WO_{3-x} with Surface Defect and Heterostructure

*Jia Lei[1], Duo Zhang[2], Shuao Wang[2] (1. Southwest University of Science and Technology (China), 2. Soochow University (China))

[P-R7-23*]

Density of Radioactive Cesium-Rich Microparticles in Contaminated Soils

*Koyo Takeuchi[1], Shinya Yamasaki[1], Satoshi Utsunomiya[2], Yuichi Takaku[1], Keisuke Sueki[1], Yudai Shigekawa[1], Aya Sakaguchi[1] (1. University of Tsukuba (Japan), 2. Kyusyu University (Japan))

[P-R7-24*]

Evaluation of the ability of *Saccharomyces cerevisiae* to reduce U(VI) by anaerobic respiration

*IORI YAMAMOTO[1], Shinya Yamasaki[1], Yuichi Takaku[1], Yudai Shigekawa[1], Aya Sakaguchi[1], Keisuke Sueki[1] (1. University Of Tsukuba (Japan))

[P-R7-25]

Measured and theoretical gamma air dose rates in archived soil samples collected in Japan

*Keiko Tagami[1], Shigeo Uchida[1] (1. National Institutes for Quantum Science and Technology (Japan))

[P-R7-26]

TRITIUM CONCENTRATION IN NATURAL WATER SAMPLES COLLECTED AT TOMIOKA TOWN LOCATED NEARBY FDNPP

*Naofumi Akata[1], Haruka Kuwata[1], Khemruthai Kheamsiri[1], Rosianna Ilsa[1], Yuisa Kitayama[1], Honoka Fukuda[1], Ryohei Yamada[1], William James Stephenson[1,2], Yasuyuki Taira[3], Hideki Saito[4], Noriyuki Takizawa[4] (1. Hirosaki University (Japan), 2. Colorado State University (United States of America), 3. Nagasaki International University (Japan), 4. Tomioka Town Hall (Japan))

[P-R7-27*]

DGT application to study dynamic speciation of uranium in moderately basic environments

*Adrien Constandache[1], Takumi Saito[2] (1. Department of Nuclear Engineering and Management, School of Engineering, the University of Tokyo, 7-3-1 Hongo, Bunkyo-ku, Tokyo 113-8656 (Japan), 2. Nuclear Professional School, School of Engineering, the University of Tokyo, 2-22 Shirakata-Shirane, Tokai-mura, Ibaraki 219-1188 (Japan))

[P-R7-28]

Vertical distribution of ^{129}I, ^{137}Cs, ^{3}H and ^{36}Cl in unsaturated zone observed at Koriyama, Japan

*Tomoko Ohta[1], Keith Fifield[2], László Palcus[3], Stephen G. Tims[2], Stefan Pavetich[2], Hiroyuki Matsuzaki[4], Daisuke Tsumune[5,6], Hiroshi Hayami[6], Yasunori Mahara[7] (1. Nagaoka University of Technology (Japan), 2. The Australian National University (Australia), 3. HUN-REN Institute for Nuclear Research (Hungary), 4. The University of Tokyo (Japan), 5. Tsukuba University (Japan), 6. Waseda University (Japan), 7. Kyoto University (Japan))

[P-R7-29]

Radioactivity of Sulfurous Sinter Deposit from Beitou Hot Spring.

*Takashi Saito[1], Yuto Takahashi[1], Taiga Kaseda[2], Hibiki Shirata[2], Toru Takahashi[2], Shunsuke Hashizume[2], Yuya Koike[3], Mototaka Nakamura[4] (1. Shokei Gakuin University (Japan), 2. Graduate School of Science and Technology, Meiji University (Japan), 3. Meiji University (Japan), 4. Study of European Radon-spa Therapy (Japan))

[P-R7-30*]

Efficient Tritium Enrichment via Direct Seawater Electrolysis: Achieving High Separation Factor and Recovery in a Low-Volume System

*CHIH-YI LAI[1], Mariel Gonzales Tecson[1], Liang-Yu Tao[2], Chun-Hu Chen[1] (1. National Sun Yat-sen University (NSYSU) (Taiwan), 2. Radiation Monitoring Center, Nuclear Safety Commission (Taiwan))

[P-R7-31*]

TRACING RADIONUCLIDES IN THE MARINE ENVIRONMENT USING THE NEW ”MILEA” ACCELERATOR MASS SPECTROMETRY FACILITY, REZ, CZECH REPUBLIC

*Petros Leivadaros[1], Ole Christian Lind[2], Hilde Elise Heldal[3], Christos Tsabaris[4] (1. Czech Technical University in Prague (Czech Republic), 2. Norwegian University of Life Sciences (Norway), 3. Institute of Marine Research (Norway), 4. Hellenic Centre for Marine Research (Greece))

[P-R7-32]

NATURAL RADIOACTIVITY AND RADON INTENSITY IN DIFFERENT TYPES OF ROCK SPECIES AND SOIL IN KOREA

*Kilyong Lee[1], Sungwon Kim[2], Minyong Park[1], Sang-Ok Lee[3], Seung Hwan Lee[2], Jung-Ki Shin[1], Seongjae Jeong[1], Jaeseung Heo[1], Seonghun Choi[1], Sangyong Kim[1] (1. Neosiskorea Co., Ltd (Korea), 2. Korea Institute of Geoscience and Mineral Resources (Korea), 3. Korea National University of Heritage (Korea))

Poster Presentation | [P1]Radiation Safety and Management

Mon. Sep 15, 2025 6:30 PM - 8:00 PM JST | Mon. Sep 15, 2025 9:30 AM - 11:00 AM UTC Poster

[Poster] P1

[P-P1-01]

Minor accidents occurred at the Isotope Science Center, the University of Tokyo from FY2020 to FY2025

*Shogo Higaki[1], Naoki Kosaka[1], Atsuko N. Ozeki[1], Masaomi Takahashi[2], Tomokazu Suzuki[2] (1. The University of Tokyo (Japan), 2. The University of Osaka (Japan))

[P-P1-02]

Radiation Safety Issues in the Dose Assessment Building for Advanced Radiation Emergency Medicine at QST Specializing in Radiochemistry and Bioassays

*Kohei Iwaya Iwaya[1], Hatsuho Seno[1], Guosheng Yang[1], Eunjoo Kim[1], Yoshinari Shiino[1], Takeshi Maeda[1], Norihiro Miyaushiro[1], Ktsumi Uzawa[1], Atsushi Kitagawa[1], Munehiko Kowatari[1], Osamu Kurihara[1] (1. National Institutes for Quantum Science and Technology (Japan))

[P-P1-03]

ACTIVATION ASSESSMENT MANUAL FOR ACCELERATOR DECOMMISSIONING: DEVELOPMENT, REVISION, AND CONTRIBUTION TO INTERNATIONAL STANDARDIZATION

*Hiroshi Matsumura[1], Kazuyoshi Masumoto[1], Go Yoshida[1], Akihiro Toyoda[1], Hajime Nakamura[1], Taichi Miura[1], Eisuke Watanabe[1] (1. High Energy Accelerator Research Organization (KEK) (Japan))

[P-P1-04]

DEVELOPMENT OF A METHOD FOR ^{36}Cl ACTIVITY ANALYSIS IN ACTIVATED POWER CABLE SHEATH AT A LARGE-SCALE PROTON ACCELERATOR FACILITY USING ACCELERATOR MASS SPECTROMETRY (AMS)

*Go Yoshida[1], Hiroshi Matsumura[1], Masumi Matsumura[2], Tatsuhiro Kimura[2], Masaki Ishida[1], Eisuke Watanabe[1], Kiyokazu Tsugane[1], Ryoken Shiobara[3], Masahiro Mitsuhashi[3], Masaaki Yamada[3], Koji Oishi[3], Koichi Nishikawa[1], Akihiro Toyoda[1], Hajime Nakamura[1], Taichi Miura[1], Kimikazu Sasa[2], Thien Ngoc Bui[4], Hiroshi Yashima[5] (1. KEK (Japan), 2. University of TSUKUBA (Japan), 3. Japan Environment Research Co., Ltd. (Japan), 4. SOKENDAI (Japan), 5. Kyoto University (Japan))

[P-P1-05]

PRETREATMENT METHOD FOR MEASURING TRITIUM RADIOACTIVITY IN POWER CORD SHEATHS AT A LARGE-SCALE PROTON ACCELERATOR FACILITY

*Ryoken Shiobara[1], Masahiro Mitsuhashi[1], Masaaki Yamada[1], Go Yoshida[2], Akihiro Toyoda[2], Masaki Ishida[2], Kiyokazu Tsugane[2], Hiroshi Matsumura[2], Eisuke Watanabe[2], Hajime Nakamura[2], Taichi Miura[2], Koji Oishi[1] (1. Japan Environment Research (Japan), 2. High Energy Accelerator Research Organization (Japan))

[P-P1-06]

ANALYSIS OF AIRBORNE DUST COLLECTED IN THE J-PARC NEUTRINO EXPERIMENTAL FACILITY

*Eisuke Watanabe[1,2], Eunji Lee[1,2], Kazutoshi Takahashi[1,2], Kiwamu Saito[1,2], Yoshinobu Sakakibara[1,2], Hiroshi Matsumura[1], Go Yoshida[1], Kiyokazu Tsugane[1], Seiji Nagaguro[1,2], Kotaro Bessho[1,2], Hirohito Yamazaki[1,2] (1. KEK (Japan), 2. J-PARC Center (Japan))

[P-P1-07]

OPTIMIZATION OF PINHOLE COLLIMATORS FOR ACTIVATION IMAGING WITH GEGI5 AND ITS PERFORMANCE VALIDATION AT KEK PHOTON FACTORY

©APSORC25

*Kiyokazu Tsugane[1], Go Yoshida[1], Hiroshi Matsumura[1], Akihiro Toyoda[1], Hajime Nakamura[1], Kazuyoshi Masumoto[1], Taichi Miura[1], Eisuke Watanabe[1], Satoshi Shinohara[1], Hiroshi Miyauchi[1] (1. High Energy Accelerator Research Organization (Japan))

[P-P1-08]

MONITORING RADIONUCLIDES IN THE HELIUM GAS CIRCULATING THROUGH THE TARGET CHAMBER AT THE J-PARC HADRON EXPERIMENTAL FACILITY

*Kotaro Bessho[1,2], Hiroaki Watanabe[1,3], Ruri Kurasaki[1,3], Masayuki Hagiwara[1,2,4], Eisuke Watanabe[1,2], Eunji Lee[1,2], Kazutoshi Takahashi[1,2], Yoshimi Kasugai[1], Hirohito Yamazaki[1,2] (1. J-PARC Center (Japan), 2. Radiation Science Center, KEK (Japan), 3. Institute of Particle and Nuclear Physics, KEK (Japan), 4. QST, NanoTerasu Center (Japan))

[P-P1-09*]

NON-DESTRUCTIVE AND ON-SITE ASSESSMENT FOR ACTIVATED CONCRETE IN 500 MeV PROTON BEAMLINE USING GAMMA DETECTORS

*Thien Ngoc Bui[1], Go Yoshida[2], Kotaro Bessho[2], Kiyokazu Tsugane[2], Akihiro Toyoda[2], Ryuki Asakubo[3], Hirokazu Kawamura[3], Fumiyoshi Nobuhara[3], Hiroshi Matsumura[2], Eisuke Watanabe[2], Hajime Nakamura[2], Taichi Miura[2] (1. Accelerator Science Program, SOKENDAI: 1-1 Oho, Tsukuba, Ibaraki, Japan, 305-0801, (Japan), 2. Radiation Science Center, High Energy Accelerator Research Organization (KEK): 1-1 Oho, Tsukuba, Ibaraki, Japan, 305-0801 (Japan), 3. Tokyo Nuclear Service Co. Ltd.: 19-2 Midorigahara 4chome, Tsukuba, Ibaraki, Japan (Japan))

[P-P1-10]

INFORMATION SHARING SYSTEM FOR THE PERSONAL MANAGEMENT OF ITINERANT RADIATION WORKERS

*Kazunori SATO[1], Akihiro Hio[1], Koji Kodama[1], Shunnosuke Takahashi[1], Hiroshi Watabe[1] (1. Tohoku University (Japan))

Poster Presentation | [P3]Environmental Integrated Knowledge of Radionuclides Dynamics Studied from the Fukushima Accident

Mon. Sep 15, 2025 6:30 PM - 8:00 PM JST | Mon. Sep 15, 2025 9:30 AM - 11:00 AM UTC Poster

[Poster] P3

[P-P3-01*]

Factors controlling dissolved ^{137}Cs activities in Matsukawa-ura lagoon, a semi-closed estuary, after the Fukushima accident

*Takuya Niida[1,2], Hyoe Takata[3], Sho Watanabe[4], Shinya Namura[2], Toshihiro Wada[3] (1. Graduate School of Symbiotic Systems Science and Technology, Fukushima University (Japan), 2. Laboratory for Instrumentation and Analysis, Environmental Engineering Division, KANSO TECHNOS CO., LTD (Japan), 3. Institute of Environmental Radioactivity, Fukushima University (Japan), 4. Fukushima Prefectural Research Institute of Fisheries Resources (Japan))

[P-P3-02*]

OPTIMIZATION OF ^{90}Sr ANALYSIS METHOD FOR THE RESIDUE OF SUSPENDED PARTICULATE MATTER (SPM) SAMPLES AFTER SEPARATION OF ^{129}I

*Shota Morishita[1], Akihito Matsushima[1], Kazuhiko Ninomiya[1] (1. Hiroshima University (Japan))

[P-P3-03]

Cellular effects induced by radiocesium-bearing microparticles (CsMPs)

*Masatoshi Suzuki[1,2], Satoru Endo[3], Kazuhiko Ninomiya[3], Koichi Chida[1], Manabu Fukumoto[1] (1. Tohoku University (Japan), 2. Fukushima Institute for Research, Education and Innovation (Japan), 3. Hiroshima University (Japan))

[P-P3-04]

Fukushima Daiichi NPP-derived radiocesium concentrations in the off-southern Hokkaido, Japan in 2018-2019

*Yuhei Shirotani[1], Shota Kambayashi[1], Naoko Murakami Sugihara[1], Mutsuo Inoue[2] (1. MARINE ECOLOGY RESEARCH INSTITUTE (Japan), 2. Kanazawa University (Japan))

[P-P3-05*]

Comparative Analysis of Canopy Characteristics and Their Influence on ^{137} Cs Migration in Different Fukushima Forest Plots

*Hao Wang[1] (1. University Of Tsukuba (Japan))

[P-P3-06]

Uptake and Elimination of Radiocesium-137 in the Wild Silkmoth *Antheraea yamamai*

*Yusuke YOSHIDA[1], Masaomi TAKAHASHI[1], Akihiro Tohsaki[1], Toshimasa MITAMURA[2], Zenta KAJIURA[3], Risako OHARA[1], Takayuki HONDA[4], Toru TAKAHASHI[4], Satoshi INOSE[4] (1. The University of Osaka (Japan), 2. Fukushima university (Japan), 3. Shinshu University (Japan), 4. Meiji University (Japan))

[P-P3-07]

How the hillslope groundwater discharge controls the dissolved radiocesium concentration of surface water in a forest headwater catchment

*Hiroaki Kato[1], Hiroki Nakada[1], Yuma Niwano[1], Yuichi Onda[1] (1. Center for Research in Radiation, Isotopes, and Earth System Sciences (Japan))

Poster Presentation | [P4]Radionuclide Migration Dynamics: Radioactive Waste Disposal and Environmental Impact Assessment

Mon. Sep 15, 2025 6:30 PM - 8:00 PM JST | Mon. Sep 15, 2025 9:30 AM - 11:00 AM UTC Poster

[Poster] P4

[P-P4-01*]

One-dimensional nanostructure arrays with Schottky Junction enhanced charge separation for the photoelectrocatalytic selective removal of Uranium from wastewater

*Shuyang Li[1] (1. southwest university of science and technology (China))

[P-P4-02]

Unveiling the critical role of the surface hydroxyl groups for electric assisted uranium extraction from the fluorine contained

*Tao Chen[1] (1. Southwest University of Science and Technology (China))

[P-P4-03]

Oxygen vacancy-mediated enhancement of catalytic removal of UO22+ by MOF@COF S-scheme

*Yuqian Zhong[1,2], xinpeng wang[1], liyong yuan[2], weiqun shi[2] (1. Guangxi University (China), 2. The Institute of High Energy Physics of the Chinese Academy of Sciences (China))

[P-P4-04]

The Migration Behavior and Microscopic Mechanisms of Typical Actinides Under the Influence of Environmental Colloids

*Zhen Xu[1], Duoqiang Pan[1], Wangsuo Pan Wu[1] (1. Lanzhou University (China))

[P-P4-05*]

Adsorption and Transport of Te(IV) in Soils Relevant to A Lead-cooled Fast Reactor Environment

*Zhihao Liu[1], Zibo Gao[1], Yujia Lin[1], Huiling Wang[1], Lili Li[2], Muyi Ni[1], Peng Lin[2] (1. Sino-French Institute Nuclear Engineering & Technology (Sun Yat-sen university) (China), 2. China Nuclear Power Technology Research Institute Co., Ltd., Shenzhen, Guangdong (China))

[P-P4-06]

Estimation of nuclide migration behavior considering suspended soil particles in a brackish lake

*Takuma Sawaguchi[1], Toshihisa Sasaki[2], Taro Shimada[1], Seiji Takeda[1] (1. Japan Atomic Energy Agency (Japan), 2. Visible Information Center, Inc. (Japan))

[P-P4-07*]

Mechanism of Eu(III) adsorption and mineral alteration response of Tamusu clay rocks

*Mingwei Wang[1] (1. Sino-French Institute of Nuclear Engineering and Technology, Sun Yat-sen University (China))

[P-P4-08]

Study on the determination of evaluation parameters for assessing radionuclide migration due to surface runoff

*Taro Shimada[1], Naruyuki Ueshima[2], Masakazu Namekawa[2], Shizuka Takai[1], Seiji Takeda[1] (1. Japan Atomic Energy Agency (Japan), 2. NAIS Inc. (Japan))

[P-P4-09]

©APSORC25

Migration of ^{90}Sr and ^{60}Co in the groundwater-soil system surrounding the long-distance effluent pipeline of a proposed NPP: Diffusion experiments and solute transport simulation

*Yu Jia Zhou[1,3], Yuan Chen[2], Li Li Li[3], Pin Chuan Li[5], Yu Han Wu[1,4,6], Liang Ming Kang[1] (1. Sun Yat-sen University (China), 2. State Key Laboratory of Nuclear Power Safety Technology and Equipment, China Nuclear Power Engineering Co., Ltd (China), 3. China Nuclear Power Technology Research Institute Co., Ltd. (China), 4. Guangdong Engineering Technology Research Center of Nuclear Safety & Emergency Response Tech (China), 5. School of Nuclear Science and Engineering, East China University of Technology (China), 6. Key Laboratory of Strategic Mineral Resources of the Upper Yellow River, Ministry of Natural Resources (China))

Poster Presentation | [P5]Environmental Radiochemistry Applicable for Nuclear Non-Proliferation, Disarmament, and Nuclear Security

Mon. Sep 15, 2025 6:30 PM - 8:00 PM JST | Mon. Sep 15, 2025 9:30 AM - 11:00 AM UTC Poster

[Poster] P5

[P-P5-01]

Analysis of $^{140}Ba/^{140}La$ detections at the CTBT Okinawa radionuclide monitoring station in May 2010

*Akiko Furuno[1], Yuichi Kijima[1], Toshiyuki Kurihara[1], Yutaka Tomita[1] (1. Japan Atomic Energy Agency (Japan))

[P-P5-02]

ANALYSIS OF CARBON AND FINE CHARCOAL PARTICLES IN SOIL WITH SOIL PROFILE SURVEY

*Maiko Ikegami[1], Jun Inoue[2], Satoshi Fukutani[1], Koichi Takamiya[1], Hiroshi Yashima[1], Tadashi Mukai[1], Tomonori Adachi[1], Yasuhito Igarashi[1] (1. Institute for Integrated Radiation and Nuclear Science, Kyoto University (Japan), 2. Osaka Metropolitan University (Japan))

[P-P5-03]

Classification of molten particles collected in Hiroshima City based on FIB-TOF-SIMS analysis

*kei nagone[1], yousuke ishii[1], tetsuo sakamoto[1], satoru endo[2], yasuhito igarashi[3] (1. kogakuin univ. (Japan), 2. Hiroshima Univ. (Japan), 3. Kyoto Univ. (Japan))

[P-P5-04]

Vertical profiles of radionuclides and other indices in soil at the site of the remains ofNagasaki Medical College

*Satoshi FUKUTANI[1], Maiko Ikegami[1], Hiroshi Yashima[1], Satoru Endo[2], Naoko Fukuda[3], Sumi Yokoyama[3], Tadashi Mukai[1], Tomonori Adachi[1], Jun Inoue[4], Koichi Takamiya[1], Yasuhito Igarashi[1] (1. Institute for Integrated Radiation and Nuclear Science, Kyoto University (Japan), 2. Graduate School of Advanced Science and Engineering, Hiroshima University (Japan), 3. Atomic Bomb Disease Institute, Nagasaki University (Japan), 4. Department of Geosciences, Graduate School of Science, Osaka Metropolitan University (Japan))

Opening Ceremony

Mon. Sep 15, 2025 8:45 AM - 9:15 AM JST | Sun. Sep 14, 2025 11:45 PM - 12:15 AM UTC Hall S(Int'l)

[OP] Opening Ceremony

©APSORC25

Tue. Sep 16, 2025

Plenary Talk | Plenary Talk

Tue. Sep 16, 2025 8:45 AM - 9:30 AM JST | Mon. Sep 15, 2025 11:45 PM - 12:30 AM UTC Hall S(Int'l)

[PL2] Pleanary Talk 2 by Chirstoph E. Duellmann

8:45 AM - 9:30 AM JST | 11:45 PM - 12:30 AM UTC

[PL02]

Synthesis and chemical studies of superheavy elements

*Christoph E Duellmann[1,2,3] (1. Johannes Gutenberg University Mainz (Germany), 2. GSI Helmholtzzentrum fuer Schwerionenforschung GmbH, Darmstadt (Germany), 3. Helmholtz Institute Mainz (Germany))

Invited & Contributed Talk | [S1]Evolution of the Periodic Table of the Elements

Tue. Sep 16, 2025 9:35 AM - 10:45 AM JST | Tue. Sep 16, 2025 12:35 AM - 1:45 AM UTC Hall S(Int'l)

[S1] Evolution of the Periodic Table of the Elements

9:35 AM - 10:05 AM JST | 12:35 AM - 1:05 AM UTC

[S1-01(Invited)]

Status and Prospect of the SHE Chemistry at IMP

*Zhi Qin[1], Yang Wang[1] (1. Institute of Modern Physics, CAS (China))

10:05 AM - 10:25 AM JST | 1:05 AM - 1:25 AM UTC

[S1-02]

First results of Cn and Fl chemistry experiments at the Superheavy Element Factory

*Nikolay Aksenov[1] (1. Flerov Laboratory of Nuclear Reactions, Joint Institute for Nuclear Research (Russia))

10:25 AM - 10:45 AM JST | 1:25 AM - 1:45 AM UTC

[S1-03]

Fast Chemistry Experiments Beyond Flerovium

*Patrick Steinegger[1,2], Georg Tiebel[1,2], Annie Bukowski[3], Titeana Cook[3], Rugard Dressler[1], Robert Eichler[1,4], Charles M. Folden III[3], Jenna Garcia[3], Isaac Haynes[3], Dominik Herrmann[1], Yuta Ito[5], Amelia Kirkland[3], Jordan Mildon[3], Tetsuya K. Sato[6], Evgeny Tereshatov[3], Alexander Vögele[1], Vera Zakusilova[3] (1. Paul Scherrer Institut (Switzerland), 2. ETH Zürich (Switzerland), 3. Texas A&M University (United States of America), 4. University of Bern (Switzerland), 5. Wako Nuclear Science Center (Japan), 6. Japan Atomic Energy Agency (Japan))

©APSORC25

Invited & Contributed Talk | [P2]ICP-MS Based Radioanalytical Chemistry and Related Applications

Tue. Sep 16, 2025 9:45 AM - 10:55 AM JST | Tue. Sep 16, 2025 12:45 AM - 1:55 AM UTC Hall A(MP)

[P2] ICP-MS Based Radioanalytical Chemistry and Related Applications

9:45 AM - 10:15 AM JST | 12:45 AM - 1:15 AM UTC

[P2-01(Invited)]

In situ Sm-Nd geochronology of xenotime by LA-MC-ICP-MS

*Yueheng YANG[1], Bohang Xie[2], Lei Xu[1], Zhichao Liu[3], Shitou Wu[1], Chao Huang[1], Lie-Wen Xie[1] (1. Institute of Geology and Geophysics, Chinese Academy of Sciences (China), 2. College of Earth and Planetary Science, University of Chinese Academy of Sciences (China), 3. School of Earth Sciences and Engineering, Sun Yat-sen University (China))

10:15 AM - 10:35 AM JST | 1:15 AM - 1:35 AM UTC

[P2-02]

Advances of ICP-MS analysis of actinides at atto-gram levels and its radioecological applications

*Jian Zheng[1], Keiko Tagami[1], Xiang Gu[1], Guosheng Yang[1], Shigeo Uchida[1] (1. National Institutes for Quantum Science and Technology (QST) (Japan))

10:35 AM - 10:55 AM JST | 1:35 AM - 1:55 AM UTC

[P2-03]

Determination of ultra-trace ^{237}Np and Pu isotopes in drinking and surface waters by SF-ICP-MS

*Xiang Gu[1,2], Jian Zheng[1], Guosheng Yang[1], Keiko Tagami[1], Tatsuo Aono[3], Fengchang Wu[2] (1. National Institutes for Quantum Science and Technology (Japan), 2. Institute of Eco-environmental and Soil Sciences, Guangdong Academy of Sciences (China), 3. Fukushima Institute for Research, Education and Innovation (Japan))

Invited & Contributed Talk | [P2]ICP-MS Based Radioanalytical Chemistry and Related Applications

Tue. Sep 16, 2025 11:10 AM - 12:00 PM JST | Tue. Sep 16, 2025 2:10 AM - 3:00 AM UTC Hall A(MP)

[P2] ICP-MS Based Radioanalytical Chemistry and Related Applications

11:10 AM - 11:40 AM JST | 2:10 AM - 2:40 AM UTC

[P2-04(Invited)]

Application and limitations of MC-ICPMS measured ^{236}U/^{238}U as an ocean tracer

Huei-Ting Lin[1], *Chuan-Chou Shen[2,3], Hong-Wei Chiang[4], Jian-Ming Chen[1], Yu-Chen Chou[1] (1. Institute of Oceanography, National Taiwan University (Taiwan), 2. Department of Geosciences, National Taiwan University (Taiwan), 3. Research Center for Future Earth, National Taiwan University (Taiwan), 4. Research Center for Environmental Changes, Academia Sinica (Taiwan))

11:40 AM - 12:00 PM JST | 2:40 AM - 3:00 AM UTC

[P2-05]

Determination of uranium isotope ratios of single uranium particle by multiple collector inductively coupled plasma mass spectrometry

*Jumpei Tomita[1], Ryohei Tomita[1], Takumi Yomogida[1], Daisuke Suzuki[1], Kenichiro Yasuda[1] (1. Japan Atomic Energy Agency (Japan))

©APSORC25

Invited & Contributed Talk | [R9]Interdisciplinary and Multidisciplinary Topics

Tue. Sep 16, 2025 1:30 PM - 3:00 PM JST | Tue. Sep 16, 2025 4:30 AM - 6:00 AM UTC Hall S(Int'l)

[R9] Interdisciplinary and Multidisciplinary Topics

1:30 PM - 2:00 PM JST | 4:30 AM - 5:00 AM UTC

[R9-01(Invited)]

Introduction of research activities related to radiochemistry at F-REI

*Tatsuo Aono[1] (1. Fukushima Institute for Research, Education and Innovation (Japan))

2:00 PM - 2:20 PM JST | 5:00 AM - 5:20 AM UTC

[R9-02]

TATTOOS – a future large-scale radionuclide production infrastructure in SWITZERLAND: a status report

*Robert Eichler[1,2], Nicholas van der Meulen[1], Daniela Kiselev[1], Christian Baumgarten[1], Aleksandar Ivanov[1], Sven Jollet[1], Remi Martinie[1,3], Sophie Harzmann[1], Daniel Laube[1], Maryam Mostamand[1], Nils Preiss[1], Thomas Rauber[1], Davide Reggiani[1], Jochem Snuverink[1], Patrick Steinegger[4,1], Stuart Warren[1], Hui Zhang[1] (1. Paul Scherrer Institute (Switzerland), 2. University of Bern (Switzerland), 3. EPF Lausanne (Switzerland), 4. ETH Zurich (Switzerland))

2:20 PM - 2:40 PM JST | 5:20 AM - 5:40 AM UTC

[R9-03]

UV-Vis-NIR spectroscopy combined with Hyperspectral Imaging for Actinide Concentration Determination during Ion Exchange Processes

*Bradley Childs[1], Tsuyoshi A. Kohlgruber[1], Silvina A. Di Pietro[1], Maryline G. Ferrier[1], Scott A. Simpson[1], Emma R. Tardiff[1], Hiroshi H. Saito[1], Saurabh Narain[1], Kiel S. Holliday[1], Lawrence E. Banks[1] (1. Lawrence Livermore National Laboratory (United States of America))

2:40 PM - 3:00 PM JST | 5:40 AM - 6:00 AM UTC

[R9-04*]

Development and Preliminary Experimental Study of an In-Situ Raman-Based High-Temperature and High-Pressure Water Corrosion Testing Platform

*Hu Wen Zhen[1], Li Lili[2], Ouyang Kun [2], Du Yingzhe[2], Yang huan[3], Ling Peng[2], Ni Muyi[1] (1. Sun Yat-sen University (China), 2. CGN Research Institute Co., Ltd (China), 3. Shenzhen Technology University (China))

©APSORC25

Invited & Contributed Talk | [P5]Environmental Radiochemistry Applicable for Nuclear Non-Proliferation, Disarmament, and Nuclear Security

Tue. Sep 16, 2025 1:30 PM - 3:00 PM JST | Tue. Sep 16, 2025 4:30 AM - 6:00 AM UTC Hall B(Small)

[P5] Environmental Radiochemistry Applicable for Nuclear Non-Proliferation, Disarmament, and Nuclear Security

1:30 PM - 2:00 PM JST | 4:30 AM - 5:00 AM UTC

[P5-01(Invited)]

Characterizing environmental samples for long-lived radionuclides with emphasis on 1940-1950 nuclear events in Japan and Australia

*Mathew P. Johansen[1], D.P. Child[1], M. Peterson[1], E. Young[1], M.A.C. Hotckis[1] (1. Australian Nuclear Science and Technology Organisation (Australia))

2:00 PM - 2:20 PM JST | 5:00 AM - 5:20 AM UTC

[P5-02]

Soil Survey Methodology for Identifying the "Black Rain" Deposition

*Yasuhito Igarashi[1], Satoru Endo[2], Koichi Takamiya[1], Jun Inoue[3], Hiroshi Yashima[1], Maiko Ikegami[1], Yayoi Inomata[4], Satoshi Fukutani[1], Tadashi Mukai[1], Tomonori Adachi[1], Naoko Fukuda[5], Sumi Yokoyama[5], WG Meteorology and Soil (1. Institute for Integrated Radiation and Nuclear Science, Kyoto University (Japan), 2. Graduate School of Advanced Science and Engineering, Hiroshima University (Japan), 3. Osaka Metropolitan University (Japan), 4. Institute of Nature and Environmental Technology, Kanazawa University (Japan), 5. Atomic Bomb Disease Institute, Nagasaki University (Japan))

2:20 PM - 2:40 PM JST | 5:20 AM - 5:40 AM UTC

[P5-03]

THE “BLACK RAIN” GENERATED BY THE HIROSHIMA ATOMIC BOMBWAS ACID RAIN

*Tadashi Mukai[1,2], Tomonori Adachi[3,1], Jun Inoue[2], Hiroshi Yashima[1], Satoshi Fukutani[1], Koichi Takamiya[1], Maiko Ikegami[1], Yasuhito Igarashi[1] (1. Institute for Integrated Radiation and Nuclear Science, Kyoto University (Japan), 2. Graduate School of Science, Osaka Metropolitan University (Japan), 3. ATOX CO.,LTD. (Japan))

2:40 PM - 3:00 PM JST | 5:40 AM - 6:00 AM UTC

[P5-04]

Synchrotron-Based Analysis of Spherical Iron Oxide Particles Found in Hiroshima Bay

*Yukihiko Satou[1], Satoru Endo[2], Ryoga Akaji[2], Takahisa Shobu[1], Aki Tominaga[1], Takehiro Sumita[3] (1. Japan Atomic Energy Agency (Japan), 2. Hiroshima University (Japan), 3. Kyushu University (Japan))

©APSORC25

Invited & Contributed Talk | [R3]Actinide Chemistry and Nuclear Energy Chemistry

Tue. Sep 16, 2025 3:05 PM - 4:35 PM JST | Tue. Sep 16, 2025 6:05 AM - 7:35 AM UTC Hall A(MP)

[R3] Actinide Chemistry and Nuclear Energy Chemistry

3:05 PM - 3:35 PM JST | 6:05 AM - 6:35 AM UTC

[R3-01(Invited)]

INNOVATIVE APPROACHES TO ACTINIDE HALIDE SPECIATION FOR NUCLEAR FUEL CYCLE ADVANCES

*Ken Ronald Czerwinski[1], Jason Victor[1], Renee Olney[1] (1. University of Nevada, Las Vegas (United States of America))

3:35 PM - 3:55 PM JST | 6:35 AM - 6:55 AM UTC

[R3-02]

SYNTHESIS AND ADSORPTIVITY OF NOVEL BIFUNCTIONAL MONOAMIDE-DIAMIDE RESIN FOR SELECTIVE SEPARATION OF ACTINYL IONS

*Masanobu Nogami[1], Keigo Uchida[1], Shion Matsumoto[1], Chikage Abe[2], Tomoo Yamamura[3] (1. Kindai Univ. (Japan), 2. Tohoku Univ. (Japan), 3. Kyoto Univ. (Japan))

3:55 PM - 4:15 PM JST | 6:55 AM - 7:15 AM UTC

[R3-03]

EFFICIENT SEPARATION of Cs(I) FROM SIMULATED HIGH-LEVEL LIQUID WASTE WITH NEW CALIX[4]-CROWN-6 ETHERS

*Zhijun Guo[1], Tengfei Cui[1], Zhen Xu[1], Haolong Wang[1], Qiang Jin[1], Zongyuan Chen[1] (1. Lanzhou University (China))

4:15 PM - 4:35 PM JST | 7:15 AM - 7:35 AM UTC

[R3-04]

Thiol unit-functionalized ultrastable two-dimensional polymer for adsorption of palladium ions in a nitric acid medium

*Hao WU[1], Naoki Osawa[2], Yan Wu[1], YueZhou Wei[1], WeiQun Shi[1], Seong-Yun Kim[3] (1. Shanghai Jiao Tong University (China), 2. Nagaoka University of Technology (Japan), 3. Tohoku University (Japan))

©APSORC25

Invited & Contributed Talk | [R5]Activation Analysis

Tue. Sep 16, 2025 3:15 PM - 4:25 PM JST | Tue. Sep 16, 2025 6:15 AM - 7:25 AM UTC Hall S(Int'l)

[R5] Activation Analysis

3:15 PM - 3:45 PM JST | 6:15 AM - 6:45 AM UTC

[R5-01(Invited)]

The Role of Prompt γ-ray Analysis in Geology

*Takashi Sano[1], Takahito Osawa[2], Masaya Miyoshi[3], Masataka Kawaguchi[4], Mitsunori Ishimoto[4] (1. National Museum of Nature and Science (Japan), 2. Japan Atomic Energy Agency (Japan), 3. Fukuoka University (Japan), 4. The University of Tokyo (Japan))

3:45 PM - 4:05 PM JST | 6:45 AM - 7:05 AM UTC

[R5-02]

Complete analysis with high-resolution Prompt Gamma Activation

*Zsolt Revay[1] (1. Technical University Munich, Heinz Maier-Leibnitz Center (MLZ) (Germany))

4:05 PM - 4:25 PM JST | 7:05 AM - 7:25 AM UTC

[R5-03]

Machine Learning Methods Applied to Prompt Gamma Activation Analysis

*David Knezevic[1], Daniel Boschmann[2], Christian Stieghorst[1], Dimitrije Maletic[3], Zsolt Révay[1] (1. Heinz Maier Leibnitz Zentrum (MLZ), Technische Universität München (Germany), 2. Institute of Automation Technology Helmut Schmidt University, Hamburg (Germany), 3. Institute of Physics Belgrade (Serbia))

©APSORC25

Invited & Contributed Talk | [P5]Environmental Radiochemistry Applicable for Nuclear Non-Proliferation, Disarmament, and Nuclear Security

Tue. Sep 16, 2025 3:15 PM - 4:25 PM JST | Tue. Sep 16, 2025 6:15 AM - 7:25 AM UTC Hall B(Small)

[P5] Environmental Radiochemistry Applicable for Nuclear Non-Proliferation, Disarmament, and Nuclear Security

3:15 PM - 3:45 PM JST | 6:15 AM - 6:45 AM UTC

[P5-05(Invited)]

Quality Assurance for a global network

*Nikolaus Hermanspahn[1] (1. CTBTO (Austria))

3:45 PM - 4:05 PM JST | 6:45 AM - 7:05 AM UTC

[P5-06]

EFFICIENCY EVALUATION OF AN AUTOMATED SOLID-PHASE EXTRACTION SYSTEM FOR MONITORING RADIOSTRONTIUM (^{90}Sr) IN SOIL SAMPLES

*Phachirarat Sola[1,3], Hirofumi Tazoe[2], Naofumi Akata[2], Chutima Kranrod[2], Rawiwan Kritsananuwat[3] (1. Thailand Institute of Nuclear Technology (Public Organization) (Thailand), 2. Institute of Radiation Emergency Medicine, Hirosaki University (Japan), 3. Nuclear Engineering, Chulalongkorn University (Thailand))

4:05 PM - 4:25 PM JST | 7:05 AM - 7:25 AM UTC

[P5-07]

ANALYSIS OF FISSILE MATERIAL USING FISSION TRACK METHOD IN NUCLEAR FALLOUT SAMPLES COLLECTED ON DAIGO FUKURYU MARU

*Koichi TAKAMIYA[1], Maiko IKEGAMI[1], Naoyuki OSADA[1], Yasuhito IGARASHI[1] (1. Institute for Integrated Radiation and Nuclear Science, Kyoto University (Japan))

©APSORC25

Invited & Contributed Talk | [R2]Radioanalytical Chemistry and Nuclear Forensics

Tue. Sep 16, 2025 4:40 PM - 6:10 PM JST | Tue. Sep 16, 2025 7:40 AM - 9:10 AM UTC Hall B(Small)

[R2] Radioanalytical Chemistry and Nuclear Forensics

4:40 PM - 5:10 PM JST | 7:40 AM - 8:10 AM UTC

[R2-01(Invited)]

Speciation study on the origin and history of trace amount of uranium in environmental samples

*Takumi Yomogida[1] (1. Japan Atomic Energy Agency (Japan))

5:10 PM - 5:30 PM JST | 8:10 AM - 8:30 AM UTC

[R2-02]

ANALYSIS OF IMPURITIES OF URANIUM ORE CONCENTRATES USING HAND-HELD RAMAN SPECTROSCOPY

*HIROKI NISHIWAKI[1], Yoshiki Kimura[1], Tomoki Yamaguchi[1] (1. Japan Atomic Energy Agency (Japan))

5:30 PM - 5:50 PM JST | 8:30 AM - 8:50 AM UTC

[R2-03]

High-Precision Boron Isotope Ratio and Quantification Analysis at the Picogram Level Using Isotope Dilution Total Evaporation Negative Thermal Ionization Mass-spectrometry

*Zahra Zandvkili[1], Katsuhiko Suzuki[1,2], Junko Kikuchi[2], Yoshitaka Takagai[1] (1. Fukushima university (Japan), 2. Submarine Resources Research Center, Japan Agency for Marine-Earth Science and Technology (JAMSTEC) (Japan))

5:50 PM - 6:10 PM JST | 8:50 AM - 9:10 AM UTC

[R2-04]

EVOLUTION OF RADIOCHEMISTRY FROM THE PERSPECTIVE OF A LABORATORY CHARACTERISING NUCLEAR WASTE

*Christèle COLIN[1], Céline GAUTIER[1], Marina FAURE[1] (1. cea (France))

Invited & Contributed Talk | [R5]Activation Analysis

Tue. Sep 16, 2025 4:40 PM - 6:10 PM JST | Tue. Sep 16, 2025 7:40 AM - 9:10 AM UTC Hall S(Int'l)

[R5] Activation Analysis

4:40 PM - 5:10 PM JST | 7:40 AM - 8:10 AM UTC

[R5-04(Invited)]

New Research Reactor Project at the Monju site

*Masaji Arai[1] (1. Japan Atomic Energy Agency (Japan))

5:10 PM - 5:30 PM JST | 8:10 AM - 8:30 AM UTC

[R5-05]

ARCHAEOMETRY STUDIES AT MLZ – USING CHEMICAL ANALYSIS WITH NEUTRONS, MULTIVARIATE STATISTICS AND ARTIFICIAL INTELLIGENCE

*Christian Stieghorst[1], Daniel Boschmann[2], Mauro Guerra[3], Daniel Pinheiro[3], Werner G. Häusler[4], Nikola Jovancevic[5], Antonio J.M. Silva[6], Benilde F.O. Costa[7] (1. Heinz Maier-Leibnitz Zentrum (MLZ) - Technical University of Munich (Germany), 2. Institute of Automation Technology Helmut Schmidt University (Germany), 3. LIBPhys-UNL, LA- REAL, Department of Physics, NOVA School of Science and Technology (Portugal), 4. Technical University of Munich, Physics Department (Germany), 5. Department of Physics, Faculty of Science, University of Novi Sad (Serbia), 6. University of Madeira, School of Technologies and Management, CITUR (Portugal), 7. University of Coimbra, CFisUC, Physics Department (Portugal))

5:30 PM - 5:50 PM JST | 8:30 AM - 8:50 AM UTC

[R5-06]

INAA for investigating the causes of colour differentiation of the popular *Haji*-ware in the Japanese Medieval capital

*Makoto TOMII[1], Koichi TAKAMIYA[2], Makoto INAGAKI[2], Yutaka CHIBA[2], Atsushi ITO[2], Masaaki KIDACHI[3], Hideo YOSHII[2] (1. Taisho University (Japan), 2. Kyoto Univeristy (Japan), 3. Ritsumeikan University (Japan))

5:50 PM - 6:10 PM JST | 8:50 AM - 9:10 AM UTC

[R5-07]

SURVEY ON RADIOACTIVE CESIUM MIGRATION BETWEEN ENVIRONMENTAL AND BODY OF WILD BOAR (*Sus scrofa*) LIVING IN FUKUSHIMA PREFECTURE, JAPAN

*MICHIKO FUKUSHIMA[1], Yamato TSUJI[1], Yuto Iinuma[2], Hitoshi KOMATSU[3], Yuuya SUGAWARA[4], Shota MOCHIZUKI[4], Takashi SAKATA[1], Kimie MURAKAMI[3], Kouta KANDA[3] (1. Ishinomaki Senshu University (Japan), 2. Kyoto University (Japan), 3. Fukushima Prefecture Centre for Environmental Creation (Japan), 4. Fukushima University (Japan))

©APSORC25

Invited & Contributed Talk | [R3]Actinide Chemistry and Nuclear Energy Chemistry

Tue. Sep 16, 2025 4:45 PM - 6:15 PM JST | Tue. Sep 16, 2025 7:45 AM - 9:15 AM UTC Hall A(MP)

[R3] Actinide Chemistry and Nuclear Energy Chemistry

4:45 PM - 5:15 PM JST | 7:45 AM - 8:15 AM UTC

[R3-05(Invited)]

Separation of Actinide Elements Based on Molecular Design

*Weiqun Shi[1] (1. Shanghai Jiao Tong University (China))

5:15 PM - 5:35 PM JST | 8:15 AM - 8:35 AM UTC

[R3-06]

Metal phosphonate frameworks (MPFs) for f-block metal separation

*Kai Lv[1], Liangping Xiong[1], Songzhu Qi[1] (1. Institute of Nuclear Physics and Chemistry (INPC), China Academy of Engineering Physics (CAEP) (China))

5:35 PM - 5:55 PM JST | 8:35 AM - 8:55 AM UTC

[R3-07]

Amino Acid Decorated Phenanthroline Diimide as Sustainable Hydrophilic Am(III) Masking Agent with High Acid Resistance

*Bin Li[1] (1. Tsinghua University (China))

5:55 PM - 6:15 PM JST | 8:55 AM - 9:15 AM UTC

[R3-08*]

Adsorption behavior and chemical states of vanadium on iron(II)-bearing clay minerals

*Shiori Morii[1,2], Takumi Yomogida[1,2], Masami Nakada[1], Yoshio Takahashi[2] (1. Japan Atomic Energy Agency (Japan), 2. The University of Tokyo (Japan))

©APSORC25

Contributed Talk | [R8]Education and Outreach

Tue. Sep 16, 2025 9:45 AM - 10:55 AM JST | Tue. Sep 16, 2025 12:45 AM - 1:55 AM UTC Hall B(Small)

[R8] Education and Outreach

9:45 AM - 10:15 AM JST | 12:45 AM - 1:15 AM UTC

[R8-01]

HUMAN RESOURCE DEVELOPMENT FOR RADIATION SCIENCE AT F-REI

*Hiroshi Watabe[1], Atsushi Toyoshima[2], Hiroki Kanda[2], Shin'ichi Goto[3] (1. Tohoku University (Japan), 2. Osaka University (Japan), 3. Niigata University (Japan))

10:15 AM - 10:35 AM JST | 1:15 AM - 1:35 AM UTC

[R8-02]

LINKING RADIOELEMENT SPECIATION, WORKFORCE DEVELOPMENT, AND GLOBAL COLLABORATION IN RADIOCHEMISTRY FOR EMERGING NUCLEAR TECHNOLOGIES

*Ken Ronald Czerwinski[1] (1. University of Nevada, Las Vegas (United States of America))

10:35 AM - 10:55 AM JST | 1:35 AM - 1:55 AM UTC

[R8-03]

What Can Be Learned from Years of Testing of Education And Training Course for Radiation Workers

*Satoru Nakashima[1], Kuninobu Inada[1], Akihito Matsushima[1], Ryoji Koba[1], Hiroaki Teramoto[1] (1. Hiroshima University (Japan))

Contributed Talk | [S1]Evolution of the Periodic Table of the Elements

Tue. Sep 16, 2025 11:00 AM - 12:00 PM JST | Tue. Sep 16, 2025 2:00 AM - 3:00 AM UTC Hall S(Int'l)

[S1] Evolution of the Periodic Table of the Elements

11:00 AM - 11:20 AM JST | 2:00 AM - 2:20 AM UTC

[S1-04]

Isothermal Gas Chromatographic Behavior of Volatile Oxychlorides of Short-lived Molybdenum and Tungsten as a Model of Element 106, Seaborgium

*Tetsuya K. Sato[1,2], Hina Natori[2,1], Ryo Otani[1], Ryota Aoki[2], Kazuaki Tsukada[3], Yuta Ito[4], Masato Asai[1], Minoru Sakama[5], Shinichi Goto[6], Katsuhisa Nishio[1], Hiroyuki Makii[1], Riccardo Orlandi[1], Yuichiro Nagame[1] (1. Japan Atomic Energy Agency (Japan), 2. Ibaraki University (Japan), 3. Tohoku University (Japan), 4. KEK (Japan), 5. Tokushima University (Japan), 6. Niigata University (Japan))

11:20 AM - 11:40 AM JST | 2:20 AM - 2:40 AM UTC

[S1-05]

Towards Next-Generation Techniques for Superheavy Element Detection in Liquids

*Pavel Bartl[1], Lucie Sifnerova[1], Daniela Dvorakova[1], Vaclav Zach[2], Charles M. Folden III[3], Mojmir Nemec[1], Jon Petter Omtvedt[4], Jan John[1] (1. CTU in Prague (Czech Republic), 2. NPI CAS (Czech Republic), 3. TAMU (United States of America), 4. UiO (Norway))

11:40 AM - 12:00 PM JST | 2:40 AM - 3:00 AM UTC

[S1-06*]

SOLVENT EXTRACTION OF Zr AND Hf WITH (O, O-) AND (S, S-) DONOR PHOSPHATE TOWARD CHEMICAL STUDY OF Rf

*Yudai Itakura[1,2], Masashi Kaneko[1], Hiroyuki Kazama[1], Kojiro Nagata[1], Ruilin Wang[1,2], Miyu Konno[1], Enni Khult[1,2], Kyosuke Shibamoto[1,2], Kenta Mori[1], Ryota Kikuchi[1], Kazushi Kawamoto[1], Hiromitsu Haba[2], Yousuke Kanayama[2], Yudai Shigekawa[2], Akihiro Nambu[2], Yoshitaka Kasamatsu[1,2] (1. Department of Chemistry, Graduate School of Science, The University of Osaka (Japan), 2. Nishina Center for Accelerator-based Science, RIKEN (Japan))

Contributed Talk | [S3]Outreach for Education on Radiation and Radioactivity after Fukushima Nuclear Accident

Tue. Sep 16, 2025 11:10 AM - 11:50 AM JST | Tue. Sep 16, 2025 2:10 AM - 2:50 AM UTC Hall B(Small)

[S3] Outreach for Education on Radiation and Radioactivity after Fukushita Nuclear Accident

11:10 AM - 11:30 AM JST | 2:10 AM - 2:30 AM UTC

[S3-01]

FUTURE PERSPECTIVES OF NUCLEAR AND RADIOCHEMISTRY EDUCATION IN THE NEW ERA OF THE SILK ROAD ACCORDING TO CHINESE NUCLEAR ENERGY DEVELOPMENT

*Wangsuo Wu[1] (1. Lanzhou University (China))

11:30 AM - 11:50 AM JST | 2:30 AM - 2:50 AM UTC

[S3-02]

DISSEMINATION OF FOOD REFERENCE MATERIALS FOR MEASUREMENT OF RADIOACTIVITY AFTER FDNPP AND THEIR APPLICATIONS IN PROFESSIONAL TRAINING AND EDUCATION

*Yoshitaka Minai[1], Tsutomu Miura[2], Chushiro Yonezawa[3], Yukiko Okada[4], Fumihiro Arakawa[5], Yoshinobu Uematsu[6], Akira Okada[7], Isao Kojima[8], Takao Osawa[8], Kazutoshi Kakita[8], Shoji Hirai[4] (1. Musashi University and Nedzu Chemical Laboratory (Japan), 2. National Institute of Advanced Industrial Science and Technology (Japan), 3. Japan Institute of International Affairs (Japan), 4. Tokyo City University (Japan), 5. NH Foods Ltd. Research and Development Center (Japan), 6. Japan Accreditation Board (Japan), 7. Toshiba Co. Ltd. (Japan), 8. Japan Society for Analytical Chemistry (Japan))

©APSORC25

Contributed Talk | [P2]ICP-MS Based Radioanalytical Chemistry and Related Applications

Tue. Sep 16, 2025 1:30 PM - 2:50 PM JST | Tue. Sep 16, 2025 4:30 AM - 5:50 AM UTC Hall A(MP)

[P2] ICP-MS Based Radioanalytical Chemistry and Related Applications

1:30 PM - 1:50 PM JST | 4:30 AM - 4:50 AM UTC

[P2-06]

Radiochemical Analysis of Technetium-99 in Seawater: Resin-Based Preconcentration and Separation with Tracer Validation

*Feng-Yun Jimmy Huang[1], Aya Sakaguchi[2], Ching-Wen Cheng[1], Yuichi Onda[2] (1. Department of Medical Imaging and Radiological Sciences, Central Taiwan University of Science and Technology (Taiwan), 2. Center for Research in Radiation, Isotopes, and Earth System Sciences, University of Tsukuba (Japan))

1:50 PM - 2:10 PM JST | 4:50 AM - 5:10 AM UTC

[P2-07]

Homogeneity and stability testing of carrier-free ^{135}Cs standard solution

*Shiho ASAI[1], Taiyo Tajima[2], Aya Sakaguchi[2], Yasushi Sato[1], Katsuhiro Shirono[1] (1. National Institute of Advanced Industrial Science and Technology (AIST) (Japan), 2. University of Tsukuba (Japan))

2:10 PM - 2:30 PM JST | 5:10 AM - 5:30 AM UTC

[P2-08*]

Investigation of curium isotope measurements by mass spectrometry

*Yuya Kasuga[1], Kazuaki Tsukada[2], Masato Asai[4], Yuichi Takaku[3], Shinya Yamasaki[3], Yudai Shigekawa[3], Keisuke Sueki[3], Aya Sakaguchi[3] (1. Graduate School of Science and Technology Degree Programs in Pure and Applied Sciences Master's Program in chemistry University of Tsukuba (Japan), 2. Research Center for Accelerator and Radioisotope Science (RARiS), Tohoku university (Japan), 3. Institute of Pure and Applied Sciences, University of Tsukuba (Japan), 4. Advanced Science Research Center Japan Atomic Energy Agency (Japan))

2:30 PM - 2:50 PM JST | 5:30 AM - 5:50 AM UTC

[P2-09*]

Synthesis of Neptunium Isotopes via the ^{238}U+p Reaction for the Production of the Np Spike

*Nami Matsuzawa[1], Hayato Ogawa[2], Akihiko Yokoyama[3], Hiromitsu Haba[4], Yudai Shigekawa[4,5], Akihiro Nambu[4], Yousuke Kanayama[4], Hiromichi Shimizu[4], Yuichi Takaku[5], Shinya Yamasaki[5], Keisuke Sueki[5], Aya Sakaguchi[5] (1. Graduate School of Science and Technology, Degree Programs in Pure and Applied Sciences, Master's Program in Chemistry, University of Tsukuba (Japan), 2. Graduate School of Science and Technology, Degree Programs in Life and Earth Sciences, Master's Program in Environmental Sciences, University of Tsukuba (Japan), 3. Institute of Science and Engineering, Kanazawa University (Japan), 4. Nishina Center for Accelerator-Based Science, RIKEN, Wako (Japan), 5. Institute of Pure and Applied Sciences, University of Tsukuba (Japan))

©APSORC25

Poster Presentation | [R1]Nuclear Chemistry

Tue. Sep 16, 2025 6:30 PM - 8:00 PM JST | Tue. Sep 16, 2025 9:30 AM - 11:00 AM UTC Poster

[Poster] R1

[P-R1-01*]

Experimental and theoretical study on the coloration of the red uranyl nitrate thiourea complex

*So Hashiba[1], Hiroyuki Kazama[1], Masashi Kaneko[1], Ryoutarou Masuda[1], Kosuke Misawa[1], Yoshitaka Kasamatsu[1] (1. Graduate School of Science, The University of Osaka (Japan))

[P-R1-02]

Design and Synthesis of Tertiary Amine–Bridged Bis(picolinate) Ligands for Chemical State Control of U-235m

*Hiroyuki Kazama[1], So Hashiba[1], Kazushi Kawamoto[1], Kosuke Misawa[1], Ryotaro Masuda[1], Terumi Yokoyama[1], Ryota Kikuchi[1], Masashi Kaneko[1], Yoshitaka Kasamatsu[1] (1. The University of Osaka (Japan))

[P-R1-03*]

Synthesis and structual analysis of $\{(n\text{-}C_mH_{2m+1})_4N\}_2[Th(NO_3)_6]$

*Kosuke Misawa[1], Hiroyuki Kazama[1], Masashi Kaneko[1], Ryoutarou Masuda[1], So Hashiba[1], Koji Yoshimura[2], Yoshitaka Kasamatsu[1] (1. The University of Osaka (Japan), 2. Okayama University (Japan))

[P-R1-04]

Preparation of Simulated MOX Ceramic Nuclear Fuel Microspheres by Microwave-assisted Internal Gelation Process

*WEI TIAN[1], Fangli Fan, Zhi Qin (1. Institute of Modern physics (China))

[P-R1-05]

Radiation-Tolerant Graphene Oxide-Carbon Quantum Dots Composite Membrane for Actinium-225 Solution deacidification

*Jing Bai[1], Baitong Zhang[1], Zhigang Ning[1], Qinggang Huang[1] (1. INSTITUTE OF MODERN PHYSICS, CHINESE ACADEMY OF SCIENCES (China))

[P-R1-06*]

Verification of Excitation Functions in Fast Neutron Induced Reactions Using Activation Method

*Shoma Tsuruta[1], Shinichi Goto[1], Yasuhide Cho[1], Hidetoshi Kikunaga[2] (1. Niigata University (Japan), 2. Tohoku University (Japan))

[P-R1-07]

THICK TARGET YIELD NORMALISED PER ACCELERATED PARTICLE

*Hidetoshi Kikunaga[1], Shin'ichi Goto[2] (1. Research Center for Accelerator and Radioisotope Science, Tohoku University (Japan), 2. Graduate School of Science and Technology, Niigata University (Japan))

[P-R1-08]

Production of carrier-free ^{182}Ta tracer via photonuclear reaction

*Takuya Yokokita[1], Yuki Honda[1], Hidetoshi Kikunaga[1] (1. Tohoku University (Japan))

[P-R1-09*]

Study of Lu-DOTA using Lu-177 produced by photonuclear reaction

©APSORC25

*Miona Tofuku[1], Kazuhiko Akiyama[1], Hidetoshi Kikunaga[2], Shiro Kubuki[1] (1. Tokyo Metropolitan University (Japan), 2. Research Center for Accelerator and Radioisotope Science (Japan))

[P-R1-10]

Production of non-carrier added ^{7}Be by the ^{nat}Li(d,x)^{7}Be reaction

*Akihiro Nambu[1], Hiromichi Shimizu[1], Yousuke Kanayama[1], Yudai Shigekawa[1], Sayantani Mitra[1], Hiromitsu Haba[1] (1. RIKEN Nishina Center for Accelerator-Based Science (Japan))

[P-R1-11*]

Improving the Purity of ^{225}Ac from Thorium Spallation at TRIUMF for Targeted Alpha Therapy Applications

*Elena Timakova[1,2], Eleanor Dunling[1], Justin Bailey[1], Paul Schaffer[1,3,4], Cornelia Hoehr[1,5] (1. Life Sciences, TRIUMF (Canada), 2. Physics, University of British Columbia (Canada), 3. Radiology, University of British Columbia (Canada), 4. Chemistry, Simon Fraser University (Canada), 5. Physics, University of Victoria (Canada))

[P-R1-12]

Optimizing temperature conditions for efficient Zn/Cu thermal separation in ^{64,67}Cu production

*Naoki Takashima[1], Masako Kawabata[1], Akio Ohta[1], Shoji Motoishi[1], Hideya Saeki[1], Yasuki Nagai[1], Yasuhiro Koguchi[1], Kazuyuki Hashimoto[2], Shunsuke Fujino[2], Masatoshi Itoh[3], Hidetoshi Kikunaga[3], Kazuaki Tsukada[3] (1. Chiyoda Technol Corporation (Japan), 2. Japan Atomic Energy Agency (Japan), 3. Tohoku University (Japan))

[P-R1-13*]

Production and separation of ^{149}Tb by the ^{133}Cs + ^{20}Ne reaction

*Yasuhito Kawakami[1], Shin-ichi Goto[1], Masato Asai[2], Tetsuya Kaneko Sato[2], Kazuaki Tsukada[4], Yuta Ito[3], Ichiro Nishinaka[5] (1. Niigata University (Japan), 2. JAEA (Japan), 3. KEK (Japan), 4. RARiS (Japan), 5. QST (Japan))

[P-R1-14]

OPTIMIZING BEAM TRANSPORT AND TARGET THICKNESS FOR 1-30 KEV MUON STOPPING POWER STUDIES

*Ayato Miura[1], Kazuhiko Ninomiya[2], Makoto Inagaki[3], Sohtaro Kanda[4], Yutaka Ikedo[4], Yu Oishi[4], Koichiro Shimomura[4], Yuga Nakazawa[5], Takashi Yoshimura[1] (1. The University of Osaka (Japan), 2. Hiroshima University (Japan), 3. Kyoto University (Japan), 4. Institute of Materials Structure Science, KEK (Japan), 5. Accelerator Laboratory, KEK (Japan))

[P-R1-15*]

ADSORPTION EXPERIMENTS OF MONOVALENT CATIONS ONTO FERROCYANIDE CRYSTALS: TOWARD ELUCIDATING THE CHEMICAL PROPERTIES OF FRANCIUM

*Hiroki Nakada[1], Yoshitaka Kasamatsu[2], Koichi Takamiya[1] (1. Kyoto University (Japan), 2. Osaka University (Japan))

[P-R1-16]

Development of a Functionalized Surface for Alpha-particle Detectors for Use in Liquid Phase

*Ryo Otani[1], Tetsuya K. Sato[1,2], Erina Takeuchi[1], Yuta Miyachi[1,2], Hina Natori[1,2], Maki Honda[1], Yuichiro Nagame[1] (1. Japan Atomic Energy Agency (Japan), 2. Ibaraki University (Japan))

[P-R1-17]

Detector calibration for Si detector by using a light emitting diode

*Toshitaka Niwase[1], Tomoki Fujii[1] (1. Kyushu University (Japan))

[P-R1-18*]

Determination of γ-ray intensity of ^{196m2}Au and 263.8-keV transition

*Yasuhide Cho[1], Shin-ichi Goto[1], Masato Asai[2], Tetsuya Sato[2], Yuta Ito[3], Kazuaki Tsukada[4], Hidetoshi Kikunaga[4]
(1. Graduate School of Science Technology, Niigata University (Japan), 2. JAEA (Japan), 3. WNCS, KEK (Japan), 4. RARiS, Tohoku University (Japan))

Poster Presentation | [R5]Activation Analysis

Tue. Sep 16, 2025 6:30 PM - 8:00 PM JST | Tue. Sep 16, 2025 9:30 AM - 11:00 AM UTC Poster

[Poster] R5

[P-R5-01]

Precision of simulation for radioactivities produced at a vicinity of nuclear core of KUR

*Norikazu Kinoshita[1], Takuma Noto[1], Kazuaki Kosako[1], Hitoshi Nakashima[1], Yuki Sasaki[1], Kazuyuki Torii[1], Makoto Inagaki[2] (1. Shimizu Corporation (Japan), 2. Kyoto University (Japan))

[P-R5-02]

Evaluation of Total Fluorine Content in the Materials for Laboratory use and Consumer Products Using Instrumental Neutron Activation Analysis

*Yoshiaki Furusho[1], Manabu Takayanagi[1], Tsutomu Miura[2] (1. GL SCIENCES INC. (Japan), 2. AIST (Japan))

[P-R5-03]

Improving the Reliability of Instrumental Neutron Activation Analysis by using the Internal Standard Method

*Tsutomu Miura[1], Hideaki Matsue[2], Koich Takamiya[3], Mitsunori Ishimoto[4] (1. National Institute of Advanced Industrial Science and Technology (Japan), 2. Japan Atomic Energy Agency (Japan), 3. Institute for Integrated Radiation and Nuclear Science, Kyoto University (Japan), 4. Nuclear Professional School, School of Engineering, University of Tokyo (Japan))

[P-R5-04]

Application of INAA to trace metal analysis of polymetallic sulfide ores collected from seafloor massive sulfide deposits

*Jun-ichiro Ishibashi[1], Shin Toyoda[2], Kotaro Yonezu[3], Tatsuo Nozaki[4], Yutaro Takaya[5], Hisao Yoshinaga[6], Koichi Takamiya[6] (1. Kobe Ocean-Bottom Exploration Center, Kobe University (Japan), 2. Institute of Paleontology and Geochronology, Okayama University of Science (Japan), 3. Department of Earth Resources Engineering, Kyushu University (Japan), 4. School of Creative Science and Engineering, Waseda University (Japan), 5. Department of Systems Innovation, The University of Tokyo, Tokyo (Japan), 6. Institute for Integrated Radiation and Nuclear Science, Kyoto University (Japan))

[P-R5-05]

ACTIVATION ANALYSIS OF $PM_{2.5}$ SAMPLES COLLECTED IN HACHIOJI, TOKYO

*Yasuji Oura[1], Shuto Kazama[1], Junya Kaneko[1] (1. Tokyo Metropolitan University (Japan))

[P-R5-06]

PLAN FOR NEUTRON IRRADIATION FACILITIES AND NEUTRON ACTIVATION ANALYSIS INSTRUMENTS IN THE NEW RESEARCH REACTOR AT THE MONJU SITE

*Makoto Inagaki[1], Koichi Takamiya[1], Tsutomu Miura[2], Koshin Washiyama[3], Kazuhiko Akiyama[4], Takahito Osawa[5], Yoshitaka Kasamatsu[6], Naoki Shirai[7], Kunihiko Tsuchiya[8], Go Yoshida[9], Nobuhiro Sato[1] (1. Institute for Integrated Radiation and Nuclear Science, Kyoto University (Japan), 2. Research Institute for Material and Chemical Measurement, National Institute of Advanced Industrial Science and Technology (Japan), 3. Advanced Clinical Research Center, Fukushima Medical University (Japan), 4. Graduate School of Science, Tokyo Metropolitan University (Japan), 5. Nuclear Science Research Institute, Japan Atomic Energy Agency (Japan), 6. Graduate School of Science, The University of Osaka (Japan), 7. Faculty of Science, Kanagawa University (Japan), 8. Oarai Nuclear Engineering Institute, Japan Atomic Energy Agency (Japan), 9. Radiation Science Center, High Energy Accelerator Research Organization (KEK) (Japan))

[P-R5-07*]

NON-DESTRUCTIVE DEPTH PROFILE QUANTIFICATION OF CARBON CONTENTS IN JAPANESE SWORD BY MUON LIFETIME ANALYSIS METHOD

*Kousei Yakushi[1], Kenya Kubo[2], Makoto Inagaki[3], Go Yoshida[4], Soshi Takeshita[5], Patrick Strasser[5], Naritoshi Kawamura[5], Yasuhiro Miyake[5], Koichiro Shimomura[5], Tsutomu Saito[6], Kazuhiko Ninomiya[1] (1. Hiroshima University (Japan), 2. International Christian University (Japan), 3. Kyoto University (Japan), 4. KEK Radiation Science Cebter (Japan), 5. KEK IMSS (Japan), 6. National Museum of Japanese History (Japan))

[P-R5-08]

DEVELOPMENT OF A NEW NON-DESTRUCTIVE ELEMENTAL ANALYSIS METHOD FOR TRACE COMPONENTS USING MUON-INDUCED GAMMA RAYS

*Makoto Inagaki[1], Kazuhiko Ninomiya[2], Go Yoshida[3], Kosei Yakushi[2], Eisuke Watanabe[3], Hiroki Nakada[1], Izumi Umegaki[4], Michael Kenya Kubo[5] (1. Institute for Integrated Radiation and Nuclear Science, Kyoto University (Japan), 2. Graduate School of Advanced Science and Engineering, Hiroshima University (Japan), 3. Radiation Science Center, High Energy Accelerator Research Organization (KEK) (Japan), 4. Institute of Materials Structure Science, High Energy Accelerator Research Organization (KEK) (Japan), 5. College of Liberal Arts, International Christian University (Japan))

[P-R5-09*]

ELEMENTAL DEPTH DISTRIBUTION ANALYSIS OF JAPANESE GOLD PRODUCTS FROM LATE 16TH CENTURY USING MUONIC X-RAYS

*Atsuya Yukawa[1], Tsutomu Saito[2], Motonobu Tampo[3], Idumi Umegaki[3], Soshi Takeshita[3], Yasuhiro Miyake[3], Koichiro Shimomura[3], Kazuhiko Ninomiya[1] (1. Hiroshima university (Japan), 2. National Museum of Japanese History (Japan), 3. IMSS KEK (Japan))

©APSORC25

Poster Presentation | [R8]Education and Outreach

Tue. Sep 16, 2025 6:30 PM - 8:00 PM JST | Tue. Sep 16, 2025 9:30 AM - 11:00 AM UTC Poster

[Poster] R8

[P-R8-01]

THIRTY YEARS OF THE RADIATION EDUCATION FORUM

*Yoshimune Ogata[1], Seiichi Shibata[2], Ryuichi Tanaka[2], Yukio Yoshizawa[2], Tadashi Asakura[2], Sayoko Ohmori[2], Kazuko Ohno[2], Kazuo Sakai[2], Keisuke Sueki[2], Masatune Hatakeyama[2], Soichi Hayashi[2], Tomohiro Watanabe[2] (1. Aichi Medical University (Japan), 2. Radiation Education Forum (Japan))

[P-R8-02]

TERMINOLOGY ON RADIOCHEMISTRY AND NUCLEAR CHEMISTRY IN JAPANESE: HISTORICAL ASPECTS AND PRESENT STATUS

*Yoshitaka Minai[1] (1. Musashi University and Nedzu Chemical Laboratory (Japan))

[P-R8-03]

Activities of the Education Division of the Japan Society of Nuclear and Radiochemical Sciences

*Atsushi Shinohara[1], Mitsuru Ebihara[2], Michiko Fukushima[3], Yasushi Kino[4], Takafumi Kitazawa[5], Yuya Koike[6], Hisaaki Kudo[7], Motoyuki Matsuo[8], Yoshitaka Minai[9], Haruka Minowa[10], Satoru Nakashima[11], Yoshimune Ogata[12], Yasuji Oura[2], Takayuki Sasaki[13], Tsutomu Sekine[4], Keisuke Sueki[14], Tatsuya Suzuki[15], Akihiko Yokoyama[16], Go Yoshida[17] (1. Osaka Aoyama University (Japan), 2. Tokyo Metropolitan University (Japan), 3. Ishinomaki Senshu University (Japan), 4. Tohoku University (Japan), 5. Toho University (Japan), 6. Meiji University (Japan), 7. Nigata University (Japan), 8. The University of Tokyo (Japan), 9. Musashi University (Japan), 10. The Jikei University School of Medicine (Japan), 11. Hiroshima National College of Maritime Technology (Japan), 12. Aichi Medical University (Japan), 13. Kyoto University (Japan), 14. University of Tsukuba (Japan), 15. Nagaoka University of Technology (Japan), 16. Kanazawa University (Japan), 17. High Energy Accelerator Research Organization (Japan))

[P-R8-04]

AN EXAMPLE OF RADIATION EDUCATION IN JAPANESE ELEMENTARY SCHOOLS - MY EXPERIENCES BEFORE AND AFTER THE FDNPP -

*Yukiko Okada[1], Naoto Hagura[2], Takehiro Toda[3] (1. Tokyo City University Atomic Energy Research Laboratory (Japan), 2. Tokyo City University Faculty of Science and Engineering Department of Nuclear Safety Engineering (Japan), 3. RADO Co., Ltd (Japan))

©APSORC25

Poster Presentation | [S1]Evolution of the Periodic Table of the Elements

Tue. Sep 16, 2025 6:30 PM - 8:00 PM JST | Tue. Sep 16, 2025 9:30 AM - 11:00 AM UTC Poster

[Poster] S1

[P-S1-01*]

QUANTUM CHEMICAL CALCULATIONS ON COMPLEXES OF No AND ALKALINE EARTH METALS EXTRACTED BY Sr RESIN FROM HDEDTP SOLUTION

*Ruilin Wang[1,2], Eisuke Watanabe[2,3], Takuya Yokokita[2,4], Yudai Itakura[1,2], Miyu Konno[1], Enni Khult[1,2], Kyosuke Shibamoto[1,2], So Hashiba[1,2], Hiromitsu Haba[2], Yudai Shigekawa[2], Akihiro Nambu[2], Yousuke Kanayama[2], Hiromichi Shimizu[2], Masashi Kaneko[1], Hiroyuki Kazama[1], Kojiro Nagata[1], Yoshitaka Kasamatsu[1] (1. Graduate School of Science, OSAKA University (Japan), 2. Nishina Center, RIKEN (Japan), 3. Radiation Science Center, KEK (Japan), 4. RARiS, Tohoku University (Japan))

[P-S1-02]

DEVELOPMENT OF THE LEGEND SYSTEM TOWARDS THE CHEMICAL STUDY OF Nh

*YANG WANG[1], Zimeng Jia[1], Shiwei Cao[1], Yunfei Cui[1], Zhi Qin[1] (1. Institute of Modern Physics,CAS (China))

[P-S1-03*]

Extraction of the group 2 elements and Pb(II) with TODGA-resin towards the chemical experiment with element 102, No

*Enni Khult[1,2], Ruilin Wang[1,2], Masashi Kaneko[1], Hiroyuki Kazama[1], Kyosuke Shibamoto[1,2], Miyu Konno[1,2], Yudai Itakura[1,2], Kenta Mori[1], Ryota Kikuchi[1], Kazushi Kawamoto[1], Ryotaro Masuda[1,2], Hiroki Aoto[1], So Hashiba[1,2], Hiromitsu Haba[2], Akihiro Nambu[2], Koichi Takamiya[3], Makoto Inagaki[3], Eisuke Watanabe[2,4], Takuya Yokokita[2,5], Yousuke Kanayama[2], Hiromichi Shimizu[2], Yudai Shigekawa[2,6], Yoshitaka Kasamatsu[1,2] (1. The University of Osaka (Japan), 2. RIKEN (Japan), 3. KURNS (Japan), 4. KEK (Japan), 5. Tohoku University (Japan), 6. University of Tsukuba (Japan))

©APSORC25

Poster Presentation | [S2]Radiopharmaceutical Sciences

Tue. Sep 16, 2025 6:30 PM - 8:00 PM JST | Tue. Sep 16, 2025 9:30 AM - 11:00 AM UTC Poster

[Poster] S2

[P-S2-01]

ON-LINE MONITORING OF ^{177}Lu SEPARATION BY EXTRACTION CHROMATOGRAPHY

*Kenji Shirasaki[1], Kohshin Washiyama[2], Tomoo Yamamura[3] (1. Institute for Radiation Science, The University of Osaka (Japan), 2. Advanced Clinical Research Center, Fukushima Global Medical Science Center, Fukushima Medical University (Japan), 3. Institute for Integrated Radiation and Nuclear Science, Kyoto University (Japan))

[P-S2-02]

RECOVERY OF ASTATINE-211 WITH PURE WATER AFTER DRY DISTILLATION SEPARATION

*Kazuhiro Ooe[1], Masashi Murakami[2], Yukiyoshi Kon[2], Atsushi Toyoshima[2], Yoshifumi Shirakami[2] (1. Radioisotope Research Center, Institute for Radiation Sciences, The University of Osaka (Japan), 2. Institute for Radiation Sciences, The University of Osaka (Japan))

[P-S2-03]

Thin-layer chromatography for astatine solutions containing reducing agents

*Ichiro Nishinaka[1], Kazuyuki Hashimoto[2], Akihiko Yokoyama[3] (1. Takasaki Institute for Advanced Quantum Science, National Institutes for Quantum Science and Technology (QST) (Japan), 2. Nuclear Science Research Institute, Japan Atomic Energy Institute (JAEA) (Japan), 3. College and Institute of Science and Engineering, Kanazawa University (Japan))

[P-S2-04*]

Flow-Electrolytic Labeling of ^{211}At for Radiopharmaceutical Synthesis in Targeted Alpha Therapy

*Akina Mitsukai[1], Yoshihumi Shirakami[2], Masashi Murakami[2], Kazuki Kajiyama[2], Sadaaki Kimura[3], Atsushi Toyoshima[2] (1. Graduate school of Science, the University of Osaka (Japan), 2. Institute for Radiation Sciences (Japan), 3. Alpha Fusion Inc. (Japan))

[P-S2-05]

CHROMATOGRAPHIC ANALYSIS OF ASTATINE IN METHANOL SOLUTIONS TOWARD STANDARDIZATION OF THE QUALITY OF ASTATINE SUPPLY SOLUTION

*Shigeki Watanabe[1], Masashi Murakami[2], Ichiro Sasaki[1], Kazuhiro Ooe[2], Yukiyoshi Kon[2], Tomoyuki Ohya[3], Jun Ichinose[3], Katsuyuki Minegishi[3], Kotaro Nagatsu[3], Atsushi Toyoshima[2], Noriko S Ishioka[1] (1. Takasaki Institute for Advanced Quantum Science, National Institutes for Quantum Science and Technology (Japan), 2. Institute for Radiation Sciences, The University of Osaka (Japan), 3. Institute for Quantum Medical Science, National Institute for Quantum Science and Technology (Japan))

[P-S2-06]

CHROMATOGRAPHIC ANALYSIS OF ASTATINE IN AQUEOUS SOLUTIONS FOR STANDARDIZATION OF THE QUALITY OF ASTATINE SUPPLY SOLUTION

*Masashi Murakami[1], Shigeki Watanabe[2], Ichiro Sasaki[2], Kazuhiro Ooe[1], Yukiyoshi Kon[1], Tomoyuki Ohya[2], Jun Ichinose[2], Katsuyuki Minegishi[2], Kotaro Nagatsu[2], Noriko S. Ishioka[2], Atsushi Toyoshima[1] (1. The University of Osaka (Japan), 2. National Institute for Quantum Science and Technology (Japan))

[P-S2-07*]

SYNTHESIS AND CHARACTERIZATION OF STRONGLY PHOTOLUMINESENCE NITRIDOTECHNETIUM(V) AND RHENIUM(V) COMPLEXES

©APSORC25

*Sodai Miyamoto[1], Takashi Yoshimura[2] (1. Department of Chemistry, Graduate School of Science, The University of Osaka (Japan), 2. Radioisotope Research Center, Institute for Radiation Science, The University of Osaka (Japan))

[P-S2-08*]

SYNTHESIS OF CRYPTAND-BASED CHELATING LIGANDS FOR STABLE Pb(II) COMPLEXES IN NUCLEAR MEDICINE APPLICATIONS

*Eishun Kawagishi[1], Kojiro Nagata[2], Masashi Kaneko[1], Hiroyuki Kazama[1], Hiroki Aoto[1], Haruka Maeda[1], Terumi Yokoyama[1], Yoshitaka Kasamatsu[1] (1. Graduate School of Science, The University of Osaka (Japan), 2. Core Facility Center, The University of Osaka (Japan))

[P-S2-09]

Synthesis of Lanthanum, Barium, and Actinuim Complexes with The 15-Membered Cyclic Ligand Having Phosphonate Arms

Kenshin Yamashita[1], Kenta Hamasaki[1], Kenji Shirasaki[1], Takuya Yokokita[2], Hidetoshi Kikunaga[2], Kazuaki Tsukada[2], Tatsuo Yajima[3], *Takashi Yoshimura[1] (1. The University of Osaka (Japan), 2. Tohoku University (Japan), 3. Kansai University (Japan))

[P-S2-10*]

SYNTHESIS OF MACROCYCLIC 1,2-HYDROXYPYRIDINONE-BASE LIGAND FOR ^{227}Th AND ^{89}Zr RADIOPHARMACEUTICALS

*Terumi Yokoyama[1], Hiroyuki Kazama[1], Masashi Kaneko[1], Kojiro Nagata[2], Hiroki Aoto[1], Haruka Maeda[1], Eishun Kawagishi[1], Yoshitaka Kasamatsu[1] (1. Graduate School of Science, The University of Osaka (Japan), 2. Core Facility Center, The University of Osaka (Japan))

[P-S2-11*]

SYNTHESIS AND PROPERTIES OF BARIUM, LANTHANUM, AND ACTINIUM COMPLEXES WITH THE 18-MEMBERED CYCLIC LIGAND WITH PYRIDINE PHOSPHONATE ARMS FOR RADIOPHARMACEUTICALS

*Kaseki Matsuda[1], Kazuaki Baba[1], Kojiro Nagata[1], Kenji Shirasaki[1], Takuya Yokokita[2], Hidetoshi Kikunaga[2], Kazukaki Tsukada[2], Tatsuo Yajima[3], Takashi Yoshimura[1] (1. The University of Osaka (Japan), 2. Tohoku University (Japan), 3. Kansai University (Japan))

[P-S2-12]

Development of an Imaging Probe Targeting Adrenal Aldosterone Synthase (CYP11B2)

*Hiroyuki Kimura[1], Yusuke Yagi[2], Riko Fuseda[3], Takaaki Murakami[4], Marina Omokawa[5], Masakatsu Sone[6], Hiroyuki Yasui[3], Nobuya Inagaki[4], Hideo Saji[7] (1. Agency for Health, Safety and Environment, Kyoto University (Japan), 2. Department of Radiological Technology, Faculty of Medicinal Science, Kyoto University of Medical Science (Japan), 3. Laboratory of Analytical and Bioinorganic Chemistry, Division of Analytical and Physical Sciences, Kyoto Pharmaceutical University (Japan), 4. Department of Diabetes, Endocrinology and Nutrition, Graduate School of Medicine, Kyoto University Hospital (Japan), 5. Faculty of Medicine, Dentistry and Pharmaceutical Sciences, Okayama University (Japan), 6. Department of Metabolism and Endocrinology, St. Marianna University School of Medicine (Japan), 7. Department of Patho-Functional Bioanalysis, Graduate School of Pharmaceutical Sciences, Kyoto University (Japan))

[P-S2-13]

Improved in vivo stability of astatobenzoyl compounds by conjugating with D-oligopeptides

*Hiroyuki Suzuki[1], Mutsuho Murata[1], Kento Kannaka[1], Souma Kitagawa[1], Souta Tatusta[1], Kazuhiro Takahashi[2], Tomoya Uehara[1] (1. Chiba University (Japan), 2. Fukushima Medical University (Japan))

[P-S2-14*]

Analysis of cell death induced by short-lived alpha-emitting radionuclides

*Soichiro Magara[1], Koki Mayusumi[1], Erina Hilmayanti[1], Kazuhiro Ooe[2,3], Atsushi Toyoshima[2,3], Koichi Fukase[1,2,3], Kazuya Kabayama[1,2,3] (1. Department of Chemistry, Graduate School of Science, The University of Osaka (Japan), 2. Forefront Research Center, Graduate School of Science, The University of Osaka (Japan), 3. Institute for Radiation Sciences, The University of Osaka (Japan))

[P-S2-15*]

Structural Stability of Radio-activated Gold Compounds via Neutron Irradiation

*KAZUKI KAJIYAMA[1], Akina Mitsukai[1], Masashi Murakami[2], Yoshifumi Shirakami[2], Koichi Takamiya[3], Jun Kataoka[4], Atsushi Toyoshima[2] (1. Graduate School of Science, The University of osaka (Japan), 2. Institute for Radiation Sciences, The University of Osaka (Japan), 3. Institute for Integrated Radiation and Nuclear Science, Kyoto University (Japan), 4. Research Institute for Science and Engineering, Waseda University (Japan))

[P-S2-16*]

Development of Dual-Modality Microspheres Containing Gold Nanoparticles for Radioembolization: X-ray CT and SPECT-Visible

*Koino Nakamura[1], Naoyuki Ukon[2], Kohshin Washiyama[2], Daichi Kuroiwa[3], Hirofumi Sekino[3], Hiroshi Ito[3], Yoshitaka Takagai[1] (1. Fukushima University (Japan), 2. Fukushima Medical University Advanced Clinical Research Center (Japan), 3. Fukushima Medical University School of Medicine (Japan))

[P-S2-17]

Synthesis and evaluation of mPEG-modified [^{211}At]AuNP(s): Towards the development of cancer treatment through intratumoral administration

*Yuichiro Kadonaga[1], Hiroki Kato[1], Hiroaki Shimamoto[1], Xuhao Huang[1], Erina Hilmayanti[1], Kazuhiro Ooe[1], Atsushi Shimoyama[1], Kazuya Kabayama[1], Xiaojie Yin[1], Hiromitsu Haba[1], Masashi Murakami[1], Atsushi Toyoshima[1], Koichi Fukase[1] (1. The University of Osaka (Japan))

[P-S2-18*]

Dose-Dependent Cytotoxic Profiling of Astatine-211 for Targeted Alpha Therapy

*Jumpei Ueno[1], Koki Mayusumi[1], Masayuki Takamatsu[1,2], Atsushi Shimoyama[1,2,3], Kazuya Kabayama[1,2,3], Koichi Fukase[1,2,3] (1. Department of Chemistry, Graduate School of Science, The University of Osaka (Japan), 2. Institute for Radiation Science, The University of Osaka (Japan), 3. Forefront Research Center, Graduate School of Science, The University of Osaka (Japan))

[P-S2-19]

Dosimetry in targeted alpha particle therapy with astatine-211 in single cells using Al_2O_3:C, Mg-based fluorescent nuclear track detector

*Jun Hu[1], Tamon Kusumoto[1], Satoshi Kodaira[1] (1. Institute for Radiological Sciences, National Institutes for Quantum Science and Technology (QST), Japan (Japan))

[P-S2-20*]

Development of Astatine-Labeled Functional Proteins for Cancer Therapy

*Koki Mayusumi[1], Kazuya Kabayama[1,2,3], Kazuko Kaneda-Nakashima[1,2,3], Junichi Takagi[4], Hiroaki Suga[5], Kazuhiro Ooe[2,3], Atsushi Toyoshima[2,3], Koichi Fukase[1,2,3] (1. Dept. of Chem., Grad. Sch. of Sci., The University of Osaka (Japan), 2. FRC, Grad. Sch. of Sci., The University of Osaka (Japan), 3. Inst. for Radiation Sciences, The University of Osaka (Japan), 4. Inst. for Protein Research, The University of Osaka (Japan), 5. Grad. Sch. of Sci., The University of Tokyo (Japan))

[P-S2-21]

Random and Site-Specific Conjugation of TCO to Anti-PD-L1 Monoclonal Antibodies for In Vitro Click Labeling: A Step Toward Pretargeted ImmunoPET Imaging Agents

*Feng-Yun Jimmy Huang[1], Ruey-Jing Huang[2], Ching-Wen Cheng[1], Kuo-Ting Chen[3] (1. Department of Medical Imaging and Radiological Sciences, Central Taiwan University of Science and Technology (Taiwan), 2.

Department of Diagnostic Radiology, Hualien Armed Forces General Hospital (Taiwan), 3. Department of Chemistry, National Dong Hwa University (Taiwan))

[P-S2-22]

SYNTHESIS AND EVALUATION OF ASTATINE-211-LABELED FAP-INHIBITOR RADIOPHARMACEUTICALS

*Masayuki Takamatsu[1,2], Atsushi Shimoyama[1,2], Ayaka Aso[1], Taketo Toda[1], Jumpei Ueno[1], Koki Mayusumi[1], Kazuya Kabayama[2], Yuichiro Kadonaga[2], Yoshifumi Shirakami[2], Tadashi Watabe[2,3], Taku Yoshiya[4], Kazuhiro Ooe[2], Atsushi Toyoshima[2], Hiromitsu Haba[5], Jens Cardinale[6], Frederik Lars Giesel[6], Kazuko Kaneda Nakashima[2], Koichi Fukase[1,2] (1. Grad. Sch. Sci., The Univ. of Osaka (Japan), 2. IRS, Osaka Univ., The Univ. of Osaka (Japan), 3. Grad. Sch. Med., The Univ. of Osaka (Japan), 4. Peptide Institute, Inc. (Japan), 5. RIKEN (Japan), 6. University Hospital Düsseldorf (Germany))

[P-S2-23*]

Development of Novel Radioimmunotherapeutic AgentsTargeting Epithelial Cell Adhesion Molecule

*Sato Oshige[1], Takumi Iwasawa[2], Marina Omokawa[3], Yoji Kitamura[4], Takashi Kozaka[4], Yusuke Yagi[5], Takiko Daikoku[6], Kazunori Kato[2], Hiroyuki Kimura[7] (1. Kanazawa University (Japan), 2. Toyo University (Japan), 3. Okayama University (Japan), 4. Division of Animal Disease Model, Kanazawa University (Japan), 5. Kyoto University of Medical Science (Japan), 6. Division of Animal Disease Model, Research Center for Experimental Modeling of Human Disease, Kanazawa University (Japan), 7. Kyoto University (Japan))

[P-S2-24]

Activities of Alpha-tergeted Therapy using astatine-211 at Osaka University in Japan

*Kazuya Kabayama[1], Atsushi Toyoshima[1], Koichi Fukase[1] (1. Institute for Radiation Sciences, University of Osaka (Japan))

[P-S2-25]

Efforts by the Japanese Astatine Community toward clinical application of alpha emitter ^{211}At

*Kohshin Washiyama[1], Takashi Nakano[2], Mikako Ogawa[3], Hiroki Kanda[2], Kazuya Taki[4] (1. Fukushima Medical University (Japan), 2. The University of Osaka (Japan), 3. Hokkaido University (Japan), 4. Sumitomo Heavy Industries, Ltd. (Japan))

Poster Presentation | [S3]Outreach for Education on Radiation and Radioactivity after Fukushima Nuclear Accident

Tue. Sep 16, 2025 6:30 PM - 8:00 PM JST | Tue. Sep 16, 2025 9:30 AM - 11:00 AM UTC Poster

[Poster] S3

[P-S3-01]

Unique educational materials for social outreach related to low-level radionuclides

*Mutsuo Inoue[1], Shinya Ochiai[1] (1. LLRL K-INET Kanazawa Univ. (Japan))

©APSORC25

Wed. Sep 17, 2025

Plenary Talk | Plenary Talk

Wed. Sep 17, 2025 8:45 AM - 9:30 AM JST | Tue. Sep 16, 2025 11:45 PM - 12:30 AM UTC Hall S(Int'l)

[PL3] Plenary Talk 3 by François Guérard

8:45 AM - 9:30 AM JST | 11:45 PM - 12:30 AM UTC

[PL03]

^{211}At-radiolabeling chemistry for targeted alpha therapy: recent progress and remaining challenges

*François Guérard[1] (1. Nantes Université (France))

Invited & Contributed Talk | [S2]Radiopharmaceutical Sciences

Wed. Sep 17, 2025 9:35 AM - 10:45 AM JST | Wed. Sep 17, 2025 12:35 AM - 1:45 AM UTC Hall S(Int'l)

[S2] Radiopharmaceutical Sciences

9:35 AM - 10:05 AM JST | 12:35 AM - 1:05 AM UTC

[S2-01(Invited)]

Isotope Mass Separation at CERN-MEDICIS :clinical research with High Molar Activity radiotherapeutics

*Thierry Stora[1] (1. CERN (Switzerland))

10:05 AM - 10:25 AM JST | 1:05 AM - 1:25 AM UTC

[S2-02]

Production of ^{155}Tb via α-particle induced reaction on ^{153}Eu

*Yudai Shigekawa[1,2], Ryotaro Masuda[3], Sayantani Mitra[1], Akihoro Nambu[1], Yoshitaka Kasamatsu[3], Hiromitsu Haba[1] (1. RIKEN (Japan), 2. University of Tsukuba (Japan), 3. Osaka University (Japan))

10:25 AM - 10:45 AM JST | 1:25 AM - 1:45 AM UTC

[S2-03*]

Developing robust targetry and radiochemistry of antimony-119 for pre-clinical applications in radioligand therapy

*Aivija Grundmane[1,2], Caterina F Ramogida[1,2], Valery Radchenko[2,3] (1. Simon Fraser University (Canada), 2. TRIUMF (Canada), 3. University of British Columbia (Canada))

Invited & Contributed Talk | [P4]Radionuclide Migration Dynamics: Radioactive Waste Disposal and Environmental Impact Assessment

Wed. Sep 17, 2025 9:45 AM - 10:55 AM JST | Wed. Sep 17, 2025 12:45 AM - 1:55 AM UTC Hall B(Small)

[P4] Radionuclide Migration Dynamics: Radioactive Waste Disposal and Environmental Impact Assesment

9:45 AM - 10:15 AM JST | 12:45 AM - 1:15 AM UTC

[P4-01(Invited)]

In Situ Measurement of Tritium behavior in Lead-Bismuth Reactor

*Muyi Ni[1,3], Yingwu Jiang[1], Junkang Yang[1], Peng Lin[2,3], Shiying Li[2], Xiajie Liu[2,3] (1. Sun Yat-sen University (China), 2. China Nuclear Power Technology Research Institute Co. (China), 3. CNPRI-SYSU Joint Research Center for Coolant Chemistry of Nuclear Reactor (China))

10:15 AM - 10:35 AM JST | 1:15 AM - 1:35 AM UTC

[P4-02]

Migration and Deposition of Radioactive Liquid Effluents in the Soil-Groundwater System Surrounding Terrestrial Discharge Pipelines

*Yuan CHEN[1], Han-yu WU[2], Le-wen SUN[2], Qiao-ya LIN[2], Jie YANG[1], Ming-liang KANG[2] (1. State Key Laboratory of Nuclear Power Safety Technology and Equipment, China Nuclear Power Engineering Co., Ltd. (China), 2. Sino-French Institute of Nuclear Engineering and Technology, Sun Yat-sen University (China))

10:35 AM - 10:55 AM JST | 1:35 AM - 1:55 AM UTC

[P4-03]

A Study on Application AI-Enhanced Multivariate Association Analysis for Environmental Radiation Monitoring Prediction Model in Taiwan

*Wei-Hsiang Tseng[1], Chuan-Pin Lee[2,3], Yu-Jie Li[4], Chin-Yi Fang[4], Yu-Cheng Tsai[1], Wei-Min Li [1], Zih-Shiuan Chiou[1], Yu-Hung Wang[3], Shih-Chin Tsai[5,3], Tzu-Chen Liao[3], Chi-Wen Hsieh[1] (1. Department of Electrical Engineering, National Chung Cheng University (Taiwan), 2. Center for Energy and Environmental Research, National Tsing Hua University (Taiwan), 3. Radioactive Waste Disposal Technology Research and Development Center, National Tsing Hua University (Taiwan), 4. Radiation Monitoring Center, Nuclear Safety Commission (Taiwan), 5. Nuclear Science and Technology Development Center, National Tsing Hua University (Taiwan))

©APSORC25

Invited & Contributed Talk | [S2]Radiopharmaceutical Sciences

Wed. Sep 17, 2025 3:00 PM - 4:30 PM JST | Wed. Sep 17, 2025 6:00 AM - 7:30 AM UTC Hall S(Int'l)

[S2] Radiopharmaceutical Sciences

3:00 PM - 3:30 PM JST | 6:00 AM - 6:30 AM UTC

[S2-07(Invited)]

Development of At-211 YF2, a PSMA-targeted agent: from bench to bedside, and academia to industry

*Yutian Feng Feng[1] (1. Duke University Medical Center (United States of America))

3:30 PM - 3:50 PM JST | 6:30 AM - 6:50 AM UTC

[S2-08]

Production of ^{211}At/^{18}F-labeled PSMA compounds for radiotheranostics under Investigational GMP

*Sadahiro Naka[1,2], Yoshifumi Shirakami[3], Kazuhiro Ooe[3], Kenta Kurimoto[1,2], Toshihiro Sakai[1], Masashi Murakami[3], Yukiyoshi Kon[3], Hiromitsu Haba[4], Atsushi Toyoshima[3], Tadashi Watabe[1,3], Noriyuki Tomiyama[1,3] (1. Department of Radiology, Graduate School of Medicine, The University of Osaka (Japan), 2. Department of Pharmacy, The University of Osaka Hospital (Japan), 3. Institute for Radiation Sciences, The University of Osaka (Japan), 4. Nishina Center for Accelerator-Based Science, RIKEN (Japan))

3:50 PM - 4:10 PM JST | 6:50 AM - 7:10 AM UTC

[S2-09*]

Astatine dry distillation: evaluating co-distillation of radionuclidic impurities and target starting material.

*Ellinor Hansson[1,2], Charlotte Ytterbrink[1], Tom Bäck[1], Erik Leidermark[1,4], Holger Jensen[3], Björn Eriksson[2], Sture Lindegren[1], Emma Aneheim[1,4] (1. Gothenburg University (Sweden), 2. Atley Solutions (Sweden), 3. Copenhagen University Hospital (Denmark), 4. Sahlgrenska University Hospital (Sweden))

4:10 PM - 4:30 PM JST | 7:10 AM - 7:30 AM UTC

[S2-10*]

Neutron activation of gold nanoparticles for imaging of pharmacokinetics

*Nanase Koshikawa[1], Yuka Kikuchi[1], Jun Kataoka[1], Kazuo Skipjack Tanaka[1], Katsuyuki Tokoi[2], Akina Mitsukai[2], Hiroki Aoto[2], Masashi Murakami[2], Yuichiro Kadonaga[2], Atsushi Toyoshima[2], Hiroki Kato[2], Kazuhiro Ooe[2], Koichi Takamiya[3] (1. Waseda Univ. (Japan), 2. Osaka Univ. (Japan), 3. Kyoto Univ. (Japan))

©APSORC25

Invited & Contributed Talk | [R3]Actinide Chemistry and Nuclear Energy Chemistry

Wed. Sep 17, 2025 3:00 PM - 4:30 PM JST | Wed. Sep 17, 2025 6:00 AM - 7:30 AM UTC Hall A(MP)

[R3] Actinide Chemistry and Nuclear Energy Chemistry

3:00 PM - 3:30 PM JST | 6:00 AM - 6:30 AM UTC

[R3-15(Invited)]

URANYL COORDINATION WITH BIOLOGICAL LIGANDS ANALYZED BY HERFD-XANES SPECTROSCOPY

*Akihiro Uehara[1], Daiju Matsumura[2], Daisuke Akiyama[3], Akira Kirishima[3], Shino Homma-Takeda[1], Teruaki Konishi[1], Kenji Ishii[4] (1. Institute for Radiological Science, National Institutes for Quantum Science and Technology (QST) (Japan), 2. Materials Sciences Research Center, Japan Atomic Energy Agency (Japan), 3. Institute of Multidisciplinary Research for Advanced Materials, Tohoku University (Japan), 4. Synchrotron Radiation Research Center, National Institutes for Quantum Science and Technology (QST) (Japan))

3:30 PM - 3:50 PM JST | 6:30 AM - 6:50 AM UTC

[R3-16*]

Structure Elucidation of Uranyl Complexes using DOSY

*Christian Urbank[1,2], Koichiro Takao[2], Lisa Vondung[1] (1. University of Hamburg (Germany), 2. Tokyo Institute of Science (Japan))

3:50 PM - 4:10 PM JST | 6:50 AM - 7:10 AM UTC

[R3-17*]

Development of synthetic method for partially oxidized phthalocyanine complexes extensible to minor actinides

*Takumi Saito[1], Miki Harigai[1], Hisao Yoshinaga[1], Takashi Shimada[1], Tomoo Yamamura[1] (1. Kyoto University (Japan))

4:10 PM - 4:30 PM JST | 7:10 AM - 7:30 AM UTC

[R3-18*]

Coordination-Driven In-situ Reduction and Extraction of Neptunium

*Huaixin Hao[1], Shuyun Zhang[2], Jin Chen[1], Jing Su[2], Zhipeng Wang[1], Chao Xu[1] (1. Tsinghua University (China), 2. Sichuan University (China))

©APSORC25

Invited & Contributed Talk | [P4]Radionuclide Migration Dynamics: Radioactive Waste Disposal and Environmental Impact Assessment

Wed. Sep 17, 2025 3:00 PM - 4:30 PM JST | Wed. Sep 17, 2025 6:00 AM - 7:30 AM UTC Hall B(Small)

[P4] Radionuclide Migration Dynamics: Radioactive Waste Disposal and Environmental Impact Assesment

3:00 PM - 3:30 PM JST | 6:00 AM - 6:30 AM UTC

[P4-06(Invited)]

Enhanced Uranium Mobility via Colloidal Transport: Implications for Remediation Strategies in Contaminated Sites

*Duoqiang Pan[1], Xiaoyan Wei[1], Xinyi Shi[1], Wangsuo Wu[1] (1. Lanzhou University (China))

3:30 PM - 3:50 PM JST | 6:30 AM - 6:50 AM UTC

[P4-07]

Stability and transport of Ce(IV)-Borate intrinsic colloid

*Zongyuan CHEN[1,2], Ganlin Zu[2], Kang Chen[2], Qiang Jin[1,2], Zhijun Guo[1], Wangsuo Wu[1,2] (1. MOE Frontiers Science Center for Rare Isotopes, Lanzhou University (China), 2. school of nuclear science and technology, Lanzhou University (China))

3:50 PM - 4:10 PM JST | 6:50 AM - 7:10 AM UTC

[P4-08*]

Study on the Adsorption and Migration Behavior of Radioactive ^{210}Po in Lead–Bismuth Reactors

*Yuqing Wang[1], Chenyu Liu[1], Hanyu Wu[1], Shengqing Wang[1], Muyi Ni[1] (1. Sun Yat-sen University (China))

4:10 PM - 4:30 PM JST | 7:10 AM - 7:30 AM UTC

[P4-09]

The adsorption of U(VI) on chlorite: Batch, modeling and XPS study

*Qiang Jin[1], Zongyuan Chen[1], Zhijun Guo[1], Wangsuo Wu[1] (1. Lanzhou University (China))

©APSORC25

Invited & Contributed Talk | [R3]Actinide Chemistry and Nuclear Energy Chemistry

Wed. Sep 17, 2025 4:45 PM - 6:15 PM JST | Wed. Sep 17, 2025 7:45 AM - 9:15 AM UTC Hall A(MP)

[R3] Actinide Chemistry and Nuclear Energy Chemistry

4:45 PM - 5:15 PM JST | 7:45 AM - 8:15 AM UTC

[R3-19(Invited)]

Study on Consolidation Behavior and Radionuclides Immobilization Mechanism of Radioactive Wastes by Cold Sintering Process

*Xiangbiao Yin[1], Yuezhou Wei[1] (1. University of South China (China))

5:15 PM - 5:35 PM JST | 8:15 AM - 8:35 AM UTC

[R3-20]

RECENT PROGRESS IN SOLIDIFICATION AND CONDITIONING OF HIGH-/INTERMEDIATE-LEVEL AND LONG-LIVED RADIONUCLIDE-BEARING LIQUID WASTE IN CHINA: A PATRIAL REVIEW

*Yumeng Hou[1], meng Wei[1] (1. CNNC Long' an Co., Ltd. (China))

5:35 PM - 5:55 PM JST | 8:35 AM - 8:55 AM UTC

[R3-21]

DEVELOPMENT OF A LOW-TEMPERATURE DECONTAMINATION MEDIUM

*Katerina Cubova Cubova[1], Jan Houzar[1], Mojmir Nemec[1] (1. Czech Technical University in Prague, Dpt of Nuclear Chemistry (Czech Republic))

5:55 PM - 6:15 PM JST | 8:55 AM - 9:15 AM UTC

[R3-22*]

Study on removal of the nuclear fuel materials from waste liquid using flocculation and precipitation method

*Lucie Šifnerová[1], Fuminori Honda[2], Yu Tachibana[2], Takeru Matsuishi[2], Toshiaki Hiyama[2] (1. Czech Technical University (Czech Republic), 2. Kyushu University (Japan))

©APSORC25

Contributed Talk | [R3]Actinide Chemistry and Nuclear Energy Chemistry

Wed. Sep 17, 2025 9:45 AM - 10:45 AM JST | Wed. Sep 17, 2025 12:45 AM - 1:45 AM UTC Hall A(MP)

[R3] Actinide Chemistry and Nuclear Energy Chemistry

9:45 AM - 10:05 AM JST | 12:45 AM - 1:05 AM UTC

[R3-09]

Measurement of Sr-90/Cs-137 ratios of smear samples collected in reactor buildings of the Fukushima Daiichi Nuclear Power Station using beta-ray spectrometry

*Asako Shimada[1], Yoshihisa Iida[1], Yu Maruyama[1] (1. Japan Atomic Energy Agency (Japan))

10:05 AM - 10:25 AM JST | 1:05 AM - 1:25 AM UTC

[R3-10]

Studies of Cerium Oxide Nanoparticles Aggregation and Dissolution Mechanisms from Nuclear Fuel Debris

*Cong Chao[1], Yiwei Zhang[2], Miguel Pineda[1], Eric S Fraga[1], Naokazu Idota[2], Takehiko Tsukahara[2], Panagiota Angeli[1] (1. Department of Chemical Engineering, University College London (UK), 2. Laboratory for Zero-Carbon Energy, Institute of Integrated Research, Institute of Science Tokyo (Japan))

10:25 AM - 10:45 AM JST | 1:25 AM - 1:45 AM UTC

[R3-11*]

Uranium Dissolution Behavior from Fuel Debris Pellets and Micro-Nanoparticles

*Tongyu XU[1], Naokazu IDOTA[1], Yuma DOTSUTA[2], Yukihiko SATOU[2], Toru KITAGAKI[2], Takehiko TSUKAHARA[1] (1. Institute of Science Tokyo (Japan), 2. Japan Atomic Energy Agency (Japan))

©APSORC25

Contributed Talk | [S2]Radiopharmaceutical Sciences

Wed. Sep 17, 2025 11:00 AM - 12:00 PM JST | Wed. Sep 17, 2025 2:00 AM - 3:00 AM UTC Hall S(Int'l)

[S2] Radiopharmaceutical Sciences

11:00 AM - 11:20 AM JST | 2:00 AM - 2:20 AM UTC

[S2-04*]

THE REACTIONS OF RARE EARTH ELEMENTS AND ACTINIUM WITH THE TWELVE-MEMBERED AZA-MACROCYCLIC LIGAND HAVING PHOSPHONIC PYRIDINE ARMS

*Kenta Hamasaki[1], Kazuaki Baba[1], Kojiro Nagata[2], Kenji Shirasaki[3], Takuya Yokokita[4], Hidetoshi Kikunaga[4], Kazuaki Tsukada[4], Tatsuo Yajima[5], Takashi Yoshimura[3] (1. Department of Chemistry, Graduate School of Science, The University of Osaka (Japan), 2. Core Facility Center, The University of Osaka (Japan), 3. Radioisotope Research Center, Institute for Radiation Sciences, The University of Osaka (Japan), 4. Research Center for Accelerator and Radioisotope Science, Tohoku University (Japan), 5. Department of Chemistry and Materials Engineering, Faculty of Chemistry, Materials and Bioengineering, Kansai University (Japan))

11:20 AM - 11:40 AM JST | 2:20 AM - 2:40 AM UTC

[S2-05*]

CORRELATION BETWEEN COORDINATION STRUCTURES AND ELECTRONIC PROPERTIES OF CYCLEN-BASED COMPLEXES WITH HEAVY P-BLOCK ELEMENTS

*Hiroki Aoto[1], Hiroyuki Kazama[1], Masashi Kaneko[1], Kojiro Nagata[2], Haruka Maeda[1], Eishun Kawagishi[1], Terumi Yokoyama[1], Yoshitaka Kasamatsu[1] (1. Graduate School of Science, The University of Osaka (Japan), 2. Core Facility Center, The University of Osaka (Japan))

11:40 AM - 12:00 PM JST | 2:40 AM - 3:00 AM UTC

[S2-06*]

Basic Performance Evaluation of an Electron-tracking Compton Camera Using Multiple Radionuclide Point Sources and Multi-Source Imaging with 18F-FDG

*Ryota Iwasaki[1], Kaiji Tanaka[1], Ryuta Kiuchi[1], Shigeto Kabuki[1], Hiroyasu Matsushita[1], Koya Yoshida[1], Hiroyuki Kimura[2], Yoji Kitamura[3], Takashi Kozaka[3], Masato Asai[4], Hidekazu Kawashima[5], Kyoshi Nishijima[6], Tsuyoshi Fukuzawa[1], Yoshio Kunieda[7], Junko Kushida[1] (1. Tokai University (Japan), 2. Kyoto University (Japan), 3. Kanazawa University (Japan), 4. Japan Atomic Energy Agency (Japan), 5. Kyoto Pharmaceutical University (Japan), 6. Kanagawa University (Japan), 7. Tokyo General Hospital (Japan))

Contributed Talk | [P4]Radionuclide Migration Dynamics: Radioactive Waste Disposal and Environmental Impact Assessment

Wed. Sep 17, 2025 11:10 AM - 11:50 AM JST | Wed. Sep 17, 2025 2:10 AM - 2:50 AM UTC Hall B(Small)

[P4] Radionuclide Migration Dynamics: Radioactive Waste Disposal and Environmental Impact Assesment

11:10 AM - 11:30 AM JST | 2:10 AM - 2:30 AM UTC

[P4-04*]

Simulation of Tritium Multi-Medium Transport and Food Chain Transfer in Marine Environments with Human Dose Assessment

*Junyang Zeng[1], Lili Li[2], Yingzhe Du[2], Ziliang Hou[2], Youting Wu[3], Shiying Li[2], Hanyu Wu[1], Zhihao Liu[1], Peng Lin[2], Muyi Ni[1], Xiajie Liu[2] (1. Sun Yat-sen University (China), 2. China Nuclear Power Technology Research Institute (China), 3. Ocean University of China (China))

11:30 AM - 11:50 AM JST | 2:30 AM - 2:50 AM UTC

[P4-05*]

Shelf sea sediments as a dynamic sink for strontium, cesium, and cobalt: Redox-sensitive trapping mechanisms mediated by iron-clay synergy

*Lewen Sun[1], Qiaoya Lin[1], Xiaobo Zhang[2], Maoran Wang[1], Yu Zhang[1], Zezu Chen[1], Mingliang Kang[1] (1. Sun Yat-sen University (China), 2. Southern Marine Science and Engineering Guangdong Laboratory (Zhuhai) (China))

Contributed Talk | [P4]Radionuclide Migration Dynamics: Radioactive Waste Disposal and Environmental Impact Assessment

Wed. Sep 17, 2025 4:45 PM - 5:25 PM JST | Wed. Sep 17, 2025 7:45 AM - 8:25 AM UTC Hall B(Small)

[P4] Radionuclide Migration Dynamics: Radioactive Waste Disposal and Environmental Impact Assesment

4:45 PM - 5:05 PM JST | 7:45 AM - 8:05 AM UTC

[P4-10*]

Radionuclide behavior in bedrock for safe disposal of nuclear waste

*Noora Pakkanen[1], Marja Siitari-Kauppi[1] (1. University of Helsinki (Finland))

5:05 PM - 5:25 PM JST | 8:05 AM - 8:25 AM UTC

[P4-11*]

ANTIMONY MIGRATION IN COASTAL ENVIRONMENT: SYNERGISTIC ADSORPTION MECHANISM OF ORGANIC MATTER AND MINERAL PARTICLES UNDER UV-C IRRADIATION

*Qiaoya lin[1], lewen sun[1], xiaobo zhang[2], mingliang kang[1] (1. Sun Yat-sen University (China), 2. Southern Marine Science and Engineering Guangdong Laboratory (China))

©APSORC25

Contributed Talk | [S2]Radiopharmaceutical Sciences

Wed. Sep 17, 2025 4:45 PM - 6:05 PM JST | Wed. Sep 17, 2025 7:45 AM - 9:05 AM UTC Hall S(Int'l)

[S2] Radiopharmaceutical Sciences

4:45 PM - 5:05 PM JST | 7:45 AM - 8:05 AM UTC

[S2-11]

Preparation of Tc Medical Solution Dissolved with Minute Amount of Pure Water or Saline Solution

*Masato Asai[1], Hiroyuki Kimura[2], Shigeto Kabuki[3], Tetsuya Sato[1], Kazuaki Tsukada[1,4], Yuta Ito[1,5] (1. Japan Atomic Energy Agency (Japan), 2. Kyoto University (Japan), 3. Tokai University (Japan), 4. Tohoku University (Japan), 5. KEK (Japan))

5:05 PM - 5:25 PM JST | 8:05 AM - 8:25 AM UTC

[S2-12]

Separation of trace medical isotopes from natural thorium decay chain

*Lifeng Chen[1], Yuezhou Wei[1], Xuexiang He[1], Wannian Feng[1] (1. University of South China (China))

5:25 PM - 5:45 PM JST | 8:25 AM - 8:45 AM UTC

[S2-13]

PREPARATION OF SCANDIUM-47 LABELLED PSMA-617 FOR RADIOTHERANOSTIC APPLICATION

*Yoshifumi Shirakami[1], Masashi Murakami[1], Akina Mitsukai[1], Kazuki Kajiyama[1], Kazuko Kaneda Nakashima[1], Yuichiro Kadonaga[1], Atsuko Saito[1], Sadahiro Naka[1], Tadashi Watabe[1], Kenji Shirasaki[1], Takuya Yokokita[2], Hidetoshi Kikunaga[2], Atsushi Toyoshima[1] (1. The University of Osaka (Japan), 2. Tohoku University (Japan))

5:45 PM - 6:05 PM JST | 8:45 AM - 9:05 AM UTC

[S2-14]

Development of automatic synthesis system of [^{18}F]FBPA synthesis from[^{18}F]HF ([$^{18}F^-$]) and basic evaluation.

*Yasukazu Kanai[1], Yoshihide Hattori[2], Sadahiro Naka[3], Toshihiro Sakai[4], Koji Ono[1], Mitsunori Kirihata[2] (1. Osaka Medical and Pharmaceutical University (Japan), 2. Osaka Metroplitan University (Japan), 3. The University of Osaka (Japan), 4. Hanwa Intelligent Medical Center (Japan))

Poster Presentation | [R2]Radioanalytical Chemistry and Nuclear Forensics

Wed. Sep 17, 2025 6:30 PM - 8:00 PM JST | Wed. Sep 17, 2025 9:30 AM - 11:00 AM UTC Poster

[Poster] R2

[P-R2-01]

Non-Spectrometric Identification of Alpha Emitters Using TPX-3CAM

*Mariko Segawa[1], Ichiro Nishinaka[2], Makoto Maeda[1], Patwary M.D Kawchar[1,3], Yosuke Toh[1] (1. Japan Atomic Energy Agency (Japan), 2. National Institutes for Quantum Science and Technology (Japan), 3. Comilla University (Bangladesh))

[P-R2-02]

COMPARISON OF AGE DATING USING THERMAL IONIZATION MASS SPECTROMETER WITH ALPHA SPECTROMETER

*Erlina Noerpitasari[1], Yoshiki Kimura[2], Umino Yuji[2], Tomoki Yamaguchi[2] (1. National Research and Innovation Agency of Indonesia (Indonesia), 2. Japan Atomic Energy Agency (Japan))

[P-R2-03]

Efficiency Calibration Method of Ge Semiconductor Detectors for Determination of Low-Energy γ-Ray Emitting Nuclides and Validation of the Method

*Takumi Ono[1], Hidesuke Itadzu[1], Masayuki Mizui[1] (1. SEIKO EG&G (Japan))

[P-R2-04*]

ENERGY CONVERSION OF γ-RAY USING SOLID MATERIALS

*Hikaru Yamabe[1], Jun Kumagai[1], Yoshiyuki Hirano[1], Muneaki Yamamoto[1], Tetsuo Tanabe[1], Tomoko Yoshida[1] (1. Nagoya University (Japan))

[P-R2-05]

DEVELOPMENT OF LOW-VOLUME ELECTROLYTIC ENRICHMENT BY SPE MEMBRANE FOR TRITIUM IN WATER SAMPLES

*Yoshihito Ohtsuka[1] (1. Institute for Environmental Scieneces (Japan))

[P-R2-06]

TLC plates containing fluorescent indicators are useful for analysis of alpha-particles and beta^{+}-rays

*Kento Kannaka[1], Hiroyuki Suzuki[1], Kazuhiro Takahashi[2], Tomoya Uehara[1] (1. Chiba University (Japan), 2. Fukushima Medical University (Japan))

[P-R2-07*]

Concentration of Radioactive Iodine Using Forward Osmosis Membrane

*ZHAOYANG SI[1], Tamao Tanji[1], Yoshitaka Takagai[1], Takahiro Osaki[2], Yuji Katayama[2] (1. Fukushima University (Japan), 2. Asahi Kasei (Japan))

©APSORC25

Poster Presentation | [R3]Actinide Chemistry and Nuclear Energy Chemistry

Wed. Sep 17, 2025 6:30 PM - 8:00 PM JST | Wed. Sep 17, 2025 9:30 AM - 11:00 AM UTC Poster

[Poster] R3

[P-R3-01]

Elution of Sr and Cs from geopolymers under radiation environments

*Norikazu Kinoshita[1], Yuki Sasaki[1], Kazuyuki Torii[1], Makoto Inagaki[2] (1. Shimizu Corporation (Japan), 2. Kyoto University (Japan))

[P-R3-02]

MEASUREMENT OF SPECTROSCOPIC PROPERTIES OF U(VI) HYDROXO COMPLEXES USING TIME-RESOLVED LASER LUMINESCENCE SPECTROSCOPY

*Euo Chang Jung[1], Hee-Kyung Kim[1], Wansik Cha[1], Hye-Ryun Cho[1], Sang-Ho Lee[1] (1. Korea Atomic Energy Research Institute (Korea))

[P-R3-03]

Study on cost optimization of geological disposal of high level solid waste containing Am and Cm under high-level liquid waste partitioning strategy

*Xiantao Meng[1], Meng Wei[1], Meilan Jia[2] (1. CNNC Long'an Co. Ltd. (China), 2. China Institute for Radioation Protection (China))

[P-R3-04*]

Redox Stabilization of Am(V) in a Biphasic Extraction System Boosts Americium/Lanthanides Separation Efficiency

*Huaixin Hao[1], Xue Dong[1], Jing Chen[1], Zhipeng Wang[1], Chao Xu[1] (1. Tsinghua University (China))

[P-R3-05]

Generation and Accumulation Behavior of I-131 in Spent Fuel Reprocessing Plant

*Duo Ma[1], Shuai Liu[1], Long Cao[1], Zongqing Bao[1], Lingling Kong[1] (1. CNNC Longan Co., Ltd. (China))

[P-R3-06*]

GAS-PHASE REACTION OF Th, U, Np, Pu, Am, AND Cm IONS WITH O_2 IN A REACTION CELL IN ICP-MS/MS

*Kazushi Kawamoto[1], Hiroyuki Kazama[1], Masashi Kaneko[1], Ruilin Wang[1], Yudai Itakura[1], Enni Khult[1], So Hashiba[1], Kyosuke Shibamoto[1], Kenta Mori[1], Ryota Kikuchi[1], Tatsuya Suzuki[2], Kenji Konashi[3], Chikage Abe[3], Yoshitaka Kasamatsu[1] (1. Graduate school of science, the university of Osaka (Japan), 2. Department of Nuclear Technology, Nagaoka University of Technology (Japan), 3. International Research Center for Nuclear Materials Science, Institute for Materials Research, Tohoku University (Japan))

[P-R3-07]

Solvent extraction of trivalent actinides and lanthanides with high concentrations of tri-*n*-butyl phosphate and nitrate ion from high-level radioactive liquid waste using multistage centrifugal contactor

*Masaumi Nakahara[1], Yuichi Sano[1] (1. Japan Atomic Energy Agency (Japan))

[P-R3-08*]

SYNTHESIS AND REDOX PROPERTIES OF DINUCLEAR U(IV) COMPLEXES WITH SCHIFF BASE MULTIDENTATE LIGANDS

*Nao Yoshida[1], Keisuke Morimoto[1], Kenji Shirasaki[1], Atsushi Shinohara[1], Takashi Yoshimura[1] (1. The University of Osaka (Japan))

©APSORC25

[P-R3-09]

Novel Continuous Decomposition Technology for Radioactive Organic Liquid Waste Based on a Modified Emulsion Flow Device

Takanori Hoshino[1], *Yoichi Arai[1], Sou Watanabe[1], Masahiro Nakamura[1], Hideya Suzuki[2], Yasutoshi Ban[1] (1. Japan Atomic Energy Agency (Japan), 2. Emulsion Flow Technologies Ltd. (Japan))

[P-R3-10*]

Effect of substituents on the solvent extraction of lanthanides using diglycolamide ligands

*Kenta Mori[1], Hiroyuki Kazama[1], Masashi Kaneko[1], Ruilin Wang[1], Yudai Itakura[1], Miyu Konno[1], Enni Khult[1], Kyosuke Shibamoto[1], Ryota Kikuchi[1], Kazushi Kawamoto[1], Yoshitaka Kasamatsu[1] (1. The University of Osaka (Japan))

[P-R3-11]

DFT Study of Substituent Effect on MA/Ln Separation Using BTPhen-type Ligands

*Yuto Fukasawa[1], Satoru Nakashima[1] (1. Hiroshima University (Japan))

[P-R3-12]

Dissolution Behavior of UTi_2O_6 Solid Phase in Aqueous Media

Takuma Koyama[1], Daisuke Akiyama[2], Akira Kirishima[2], Taishi Kobayashi[1], *Takayuki Sasaki[1] (1. Kyoto University (Japan), 2. Tohoku University (Japan))

[P-R3-13*]

Enhanced Uranium Adsorption via Sulfonation of Polyether Ether Ketone

*xin Yu Song[1], Peng Liu[1] (1. Harbin Engineering University (China))

[P-R3-14]

Estimation of tritium amount in activated charcoal by the soaking and burning method

*Miki Nakada[1], Chie Iwata[1], Masahiro Tanaka[1] (1. NIFS (Japan))

[P-R3-15*]

Exploration of uranium adsorption properties of polyimide dixime-based uranium adsorption membrane materials

*Yanxin Jiang[1], Peng Liu[1] (1. Harbin Engineering University (China))

[P-R3-16]

All-in-One: Photo-Responsive Lanthanide-Organic Framework for Simultaneous Sensing, Adsorption, and Photocatalytic Reduction of Uranium

*zhiwei huang[1,2], KongQiu Hu[2], Lei Mei[2], WangSuo Wu[1], WeiQun Shi[2,3] (1. Lanzhou University (China), 2. Institute of High Energy Physics, Chinese Academy of Sciences (China), 3. Shanghai Jiao Tong University (China))

[P-R3-17*]

Chemical characterization of Platinum group alloys in fused borosilicate glasses

*Mizuki Kato[1], Haruaki Matsuura[1], Isamu Sato[1], Yuki Oiwa[1], Sayaka Chiba[1], Haruka Tada[2], Hiroki Izumi[2] (1. TOKYO CITY UNIVERSITY (Japan), 2. IHI Corporation (Japan))

[P-R3-18]

Influence of Actinide Radiotoxicity on Nuclear Waste Disposal Frameworks in Spent Nuclear Fuel Reprocessing Systems

*Shuai Liu[1], Meng Wei[1], Jianquan Liu[1] (1. CNNC Long'an Co. Ltd. (China))

[P-R3-19*]

Adsorption and separation performance of platinum group metals using a novel MPE-TDGA/SiO_2-P adsorbent

*Mai Tanaka[1,2], Naoki Osawa[3], Hao Wu[4], Seong-Yun Kim[1] (1. Tohoku university (Japan), 2. JNFL (Japan), 3. Nagaoka university (Japan), 4. Shanghai Jiao Tong University (China))

[P-R3-20]

Analytical Strategy for Evaluating High-Specific-Activity ^{177}Lu in Theranostic Radiopharmaceutical Production

*Miki Harigai[1], Kazumi Nakano[2], Kenji Shirasaki[3], Hiroyuki Kimura[4], Tomoo Yamamura[1] (1. Institute for Integrated Radiation and Nuclear Science, Kyoto University (Japan), 2. Agilent Technologies, Inc. (Japan), 3. Institute for Radiation Science, The University of Osaka (Japan), 4. Institute for Environmental Safety and Health, Kyoto University (Japan))

[P-R3-21*]

Separation behavior of MA(III) from simulated high-level liquid waste using TEHDGA and HONTA impregnated XAD7-HP adsorbents

*Masahiko Kubota[1,2], Seong-Yun Kim[1], Tsuyoshi Arai[3], Sou Watanabe[4], Tatsuya Ito[5], Ryuji Nagaishi[5] (1. Tohoku University (Japan), 2. Japan Nuclear Fuel Chemical Analysis Co., Ltd (Japan), 3. Shibaura Institute of Technology (Japan), 4. Nuclear Fuel Cycle Engineering Laboratories, Japan Atomic Energy Agency (Japan), 5. Collaborative Laboratories for Advanced Decommissioning Science (CLADS), Japan Atomic Energy Agency (Japan))

[P-R3-22]

Synthesis of simulated radioactive waste containing ^{241}Am for evaluation of hydrogen generation

*Riko Ikarugi[1] (1. Japan Atomic Energy Agency (Japan))

[P-R3-23]

Adsorption behavior of fission product elements on synthesized tungsten oxide type inorganic adsorbent supported in silica beads

*HanYu Wang[1], Xianwei Wang[1], Wenzun Luo[1], Naoki Osawa[1], Tatsuya Suzuki[1] (1. Nagaoka University of Technology (Japan))

[P-R3-24]

Chemical stability of sulfur-containing functionalized silica-based adsorbents under nitric acid conditions for platinum group metals adsorption

*Naoki Osawa[1], Mai Tanaka[2], Hao Wu[3], Tatsuya Suzuki[1], Seong-Yun Kim[2] (1. Nagaoka University of Technology (Japan), 2. Tohoku University (Japan), 3. Shanghai Jiao Tong University (China))

[P-R3-25]

Establishment of a multi-element ICP-MS/MS quantitative method for quality assurance of high-specific-activity Lu-177 preparations

Miki Harigai[1], Kazumi Nakano[2], Kenji Shirasaki[3], Hiroyuki Kimura[4], *Tomoo Yamamura[1] (1. Institute for Integrated Radiation and Nuclear Science, Kyoto University (Japan), 2. Agilent Technologies, Inc. (Japan), 3. Institute for Radiation Science, The University of Osaka (Japan), 4. Agency for Health, Safety and Environment, Kyoto University (Japan))

[P-R3-26*]

Adsorption and separation performance of minor actinides and lanthanides using MPEDGA/SiO_2-P adsorbent

*Riho Okajima[1,2], Masahiko Kubota[1], Seong-Yun Kim[1] (1. Department of Quantum Science and Energy Engineering, Graduate School of Engineering, Tohoku University (Japan), 2. Japan Nuclear Fuel Limited (Japan))

[P-R3-27]

Spent Nuclear Fuel Reprocessing and Regeneration in Accelerator Driven Advanced Nuclear Energy System

*Fangli Fan[1] (1. Institute of Modern Physics, Chinese Academy of Sciences (China))

[P-R3-28*]

ADSORPTIVITY OF TRIPHOSPHINE TRIOXIDE-IMPREGNATED ANION EXCHANGE RESINS FOR RECOVERY OF URANIUM FROM SEAWATER

*Shion Matsumoto[1], Yukito Tounai[1], Masanobu Nogami[1], Chikage Abe[2] (1. KINDAI University (Japan), 2. TOHOKU University (Japan))

[P-R3-29]

Solidification and Stabilization Treatment of Liquid Nuclear Fuel Waste Containing Oil

Takeru Matsuishi[1], Toshiaki Hiyama[1], *Fuminori Honda[1] (1. RIC, Kyushu University (Japan))

[P-R3-30*]

A Study on the Preliminary Evaluation of the Nuclide Monitoring for Modelling at High-Level Radioactive Waste Disposal Site

*WooBeom Ha[1], DoWon Hyun[1], SangHeon Lee[1], JongSoon Song[1] (1. chosun university (Korea))

©APSORC25

Poster Presentation | [R4]Nuclear Probe in Chemistry

Wed. Sep 17, 2025 6:30 PM - 8:00 PM JST | Wed. Sep 17, 2025 9:30 AM - 11:00 AM UTC Poster

[Poster] R4

[P-R4-01*]

MEASUREMENT AND FIRST-PRINCIPLES CALCULATION OF LOCAL FIELDS AT THE NUCLEI OF In/Cd DOPANTS IN ANATASE TiO_2

*Hiiro Amaike[1], Hokuto Shinmei[1], Wataru Sato[1], Tomonori Ida[1] (1. Kanazawa University (Japan))

[P-R4-02*]

Synthesis and ^{61}Ni Mössbauer measurements of Hofmann-Type Supramolecular Complex Using 3-Fluoropyridine

*Yayoi Shinohara[1], Kosuke Kitase[1], Shinji Kitao[4], Takumi Kubota[5], Yasuhiro Kobayashi[4], Makoto Seto[4], Daisuke Akahoshi[2,3], Takahumi Kitazawa[1,3] (1. Department of Chemistry, Faculty of Science, Toho University (Japan), 2. Department of Physics, Faculty of Science, Toho Univercity (Japan), 3. Research Centre for Materials with Integrated Properties, Toho University (Japan), 4. Institute for Integrated Radiation and Nuclear Science, Kyoto University (Japan), 5. Agency for Health, Safety and E nvironment, Kyoto University (Japan))

[P-R4-03*]

MAGNETIC PROPERTIES OF Zn FERRITE $Zn_xFe_{3-x}O_4$

*Hibiki Hirahara[1], Taisuke Ito[1], Wataru Sato[1,2] (1. Graduate School of Natural Science and Technology, Kanazawa University (Japan), 2. Institute of Science and Engineering, Kanazawa University (Japan))

[P-R4-04*]

^{61}Ni Mössbauer Spectroscopic and Chemical Characterization for Supramolecular Fe(4-cyanopyridine)$_2$[Ni(CN)$_4$] Host Framework Materials

*Tamaki Chiba[1], Kosuke Kitase[1], Shinji Kitao[4], Yasuhiro Kobayashi[4], Takumi Kubota[5], Makoto Seto[4], Daisuke Akahoshi[1,3], Takahumi Kitazawa[3,2] (1. Department of Chemistry, Faculty of Science, Toho University (Japan), 2. Department of Physics, Faculty of Science, Toho University (Japan), 3. Research Centre for Materials with Integrated Properties, Toho University (Japan), 4. Institute for Integrated Radiation and Nuclear Science, Kyoto University (Japan), 5. Agency for Health, Safety and Environment, Kyoto University (Japan))

[P-R4-05*]

EFFECT OF INDIUM CONCENTRATION ON THE PHOTOCATALYTIC PERFORMANCE AND LOCAL STRUCTURE OF $SrTiO_3$

*Ibuki Ejiri[1] (1. Graduated school of Natural Science and Technology, Kanazawa University (Japan))

[P-R4-06*]

INITIAL STATE OF CAPTURED MUON IN COPPER ATOM AND CHEMICAL ENVIRONMENTAL DEPENDENCE ON MUON CAPTURE

*Miu Nomura[1], Satoaki Den[1], Naoko Nishino[1], Kazuhiko Ninomiya[1], I-Huan Chiu[2], Shunsuke Asari[3], Akira Sato[3], Takashi Yoshimura[3], Alex Amato[4], Sayato Biswas[4], Lars Frieder Gerchow[4], Carlos Vigo[4], Chennan Wang[4], Charles Hillis Mielke III[4], Debarchan Das[4], Fabian Hotz[4], Gianluca Janka[5], Hubertus Luetkens[4], Katharina von Schoeler[4], Narongrit Ritjoho[6], Thomas Prokscha[4], Toni Shiroka[4], Zaher Salman[4], Zurab Guguchia[4] (1. Hiroshima University (Japan), 2. Japan Atomic Energy Agency (Japan), 3. Osaka University (Japan), 4. Paul Scherrer Institute (Switzerland), 5. ETH Zürich (Switzerland), 6. Suranaree University of Technology (Thailand))

©APSORC25

Poster Presentation | [R6]Radiation and Radioisotopes in Life Science

Wed. Sep 17, 2025 6:30 PM - 8:00 PM JST | Wed. Sep 17, 2025 9:30 AM - 11:00 AM UTC Poster

[Poster] R6

[P-R6-01]

HETEROGENEOUS DISTRIBUTION OF HTO IN ORGANISMS

*Tsuyoshi Masuda[1], Takahito Moriwaki[1] (1. Institute for Environmental Sciences (Japan))

[P-R6-02]

Glutathione, applied to roots site-specifically, inhibits the movement of cadmium in roots of oilseed rape plants (*Brassica napus*)

*Shin-ichi Nakamura[1], Taku Yuzawa[1], Tianyi Zhou[1], Ryotaro Iida[1], Nobuo Suzui[2], Yonggen Yin[2], Yuta Miyoshi[2], Yusaku Noda[2], Kazuyuki Enomoto[2], Ryohei Yamagaya[2], Takahiro Sato[2], Yasuyuki Ishii[2], Naoki Kawachi[2], Akihisa Shinozawa[1], Kanna Sato-Izawa[1] (1. Tokyo University of Agriculture (Japan), 2. National Institutes for Quantum Science and Technology (Japan))

[P-R6-03]

Characteristics of Tritium, Hydrogen, and Oxygen Isotope Compositions in Surface Water Across Thailand

*Chonlada Pitakchaianan[1], Kanyanan Kosinarkaranun[1], Pantiwa Kumsut[1], Tatsuhide Hamasaki[1], Ryuta Hazama[1], Anawat Rittirong, Koichi Sakakibara, Yoshiyuki Hirano, Koki Kashiwaya, Yoshimune Ogata, Yuka Kato, Wanwisa Sudprasert, Kiadtisak Saenboonruang, Kanokwan Khamanek, Soontree Khuntong, Donruedee Toyen, Archara Phattanasub, Monthon Yongprawat, Chakrit Saengkorakot, Piyawan Krisanangkura, Chittranuch Chantarot (1. Osaka Sangyo University (Japan))

[P-R6-04]

Characteristics of ^{7}Be and ^{210}Pb in the Atmosphere of Bangkok, Thailand

*Kanyanan Kosinarkaranun[1], Chonlada Pitakchaianan[1], Pantiwa Kumsut[1], Ryuta Hazama[1], Tatsuhide Hamasaki[1], Anawat Rittirong[2], Hisakazu Muramatsu[3], Pannipa Noithong[4], Wanwisa Sudprasert[5] (1. Osaka Sangyo University (Japan), 2. Osaka University (Japan), 3. Shinshu University (Japan), 4. Roi Et Provincial Office of Learning Encouragement, DOLE (Thailand), 5. Kasetsart University (Thailand))

[P-R6-05*]

Analysis of leaf position-dependent phosphorus allocation in a deciduous woody plant *Populus alba* L.

*Aoi Hirata[1], Yuko Kurita[1], Ryohei Sugita[2], Natsuko Kobayashi[1], Keitaro Tanoi[1,3] (1. Graduate School of Agricultural and Life Science, The University of Tokyo (Japan), 2. Radioisotope Research Center, Nagoya University (Japan), 3. Fukushima Institute for Research, Education and Innovation (Japan))

[P-R6-06]

Photosynthate Allocation in Soybean: Influence of Sink-Source spatial Relationships

Ai Kaiho-Soma[1], Yuko Kurita[1], Natsuko I. Kobayashi[1], Tomoko M. Nakanishi[1,2], *Keitaro Tanoi[1,2] (1. Graduate School of Agricultural and Life Sciences, The University of Tokyo (Japan), 2. Fukushima Institute for Research, Education and Innovation (Japan))

[P-R6-07]

BIOIMAGING AND XPDT TREATMENT USING HIGHLY LUMINESCENT NANOCOMPOSITE SCINTILLATORS

*Václav Čuba[1], Xenie Lytvynenko[1], Lenka Prouzová[1], Jan Bárta[1] (1. Czech Technical University in Prague (Czech Republic))

[P-R6-08]

Experimental systems for the internal and external exposure of silkworms to radioactive cesium for evaluating biological effects.

Sota Tanaka[1], Sho Amano[2], *Tadatoshi Kinouchi[3] (1. Faculty of Bioresource Sciences, Akita Prefectural University (Japan), 2. Oita University Faculty of Medicine (Japan), 3. Institute for Integrated Radiation and Nuclear Science, Kyoto University (Japan))

©APSORC25

Poster Presentation | [R9]Interdisciplinary and Multidisciplinary Topics

Wed. Sep 17, 2025 6:30 PM - 8:00 PM JST | Wed. Sep 17, 2025 9:30 AM - 11:00 AM UTC Poster

[Poster] R9

[P-R9-01]

ROBUST AND OPTIMIZED POLYGONAL MESH MODELING OF 3D-CAD/CG INTRICATE SHAPES USING THE INDUSTRIAL-STANDARD PRE/POST-PROCESSING TOOLS ON PHITS

*Minoru Sakama[1], Hiroto Nakano[1], Makoto Kobayashi[2], Takuya Saze[2], Ken'ichi Fujimoto[3] (1. Tokushima University (Japan), 2. National Institute for Fusion Science (Japan), 3. Kagawa University (Japan))

[P-R9-02]

In Vivo Tracking of ^{131}I-Cobravenom to Enhance Cobra Antivenom Production

*Nantanat Chailanggar[1], Wiranee Sriwiang[1], Piriya Kaeopookum[1], Surasak Akesowan[2], Orawan Khow[2], Narongsak Chaiyabutr[2] (1. Thailand Institute of Nuclear Technology (Thailand), 2. Queen Saovabha Memorial Institute (Thailand))

[P-R9-03]

THE IMPACT OF γ-IRRADIATION ON THE STABILITY OF VARIOUS CLAYS

*ALICIA Negron-Mendoza[1], Benjamín Leal-Acevedo [1], Isabel Gamboa De Buen[1], Javier Gutiérrez- Romero [1], Sergio Ramos-Bernal [1], Claudia Camargo-Raya[1], Elizabeth Chacón-Baca [2], Alejandro Heredia[1], Alfredo Rojas-Vivas[1], María José Rodríguez-Albarrán [1] (1. Instituto de Ciencias Nucleares, Universidad Nacional Autonoma de México (Mexico), 2. Facultad de Ciencias de la Tierra. Universidad Autónoma de Nuevo León (Mexico))

[P-R9-04*]

SMOOTHING OF ENERGY SPECTRUM DATA USING AN ε-FILTER FOR CONVOLUTIONAL NEURAL NETWORKS TO ESTIMATE DEPTH DISTRIBUTION OF RADIOISOTOPES IN SOIL

*Souya Horikawa[1], Kanata Nokubo[1], Ken'ichi Fujimoto[1], Minoru Sakama[2], Kazumasa Inoue[3], Masahiro Fukushi[4] (1. Kagawa University (Japan), 2. Tokushima University (Japan), 3. Tokyo Metropolitan University (Japan), 4. Tsukuba International University (Japan))

[P-R9-05]

Application of multi-point ^{14}C dating of fossil calcareous assemblages for reconstructing relative sea level fluctuation

*Yuzuko Tsukahara[1], Tetsuya Komatsu[1], Natsuko Fujita[1], Nariaki Nishiyama[1], Hideaki Maemoku[2] (1. Tono Geoscience Center (JAEA) (Japan), 2. Hosei University (Japan))

[P-R9-06]

Monitoring of TFWT concentrations in fish using Electrolytic Enrichment method for ALPS treated water discharged into the ocean

*Takaya Yabuta[1], Yurika Sasanami[1], Satoshi Tan[1], Takayuki Otsuki[1], Wataru Niita[1], Keiko Morimoto[2] (1. Japan Chemical Analysis Center (Japan), 2. Kyushu Environmental Evaluation Association (Japan))

[P-R9-07]

MODULATION TRANSFER SPECTROSCOPY OF CESIUM ATOMS TOWARD FULLY OPTICAL QUANTITATIVE ISOTOPE DETECTION

*Leo Matsuoka[1] (1. Hiroshima Institute of Technology (Japan))

[P-R9-08]

ADSORPTION OF BA AND SR USING ZEOLITE SYNTHESIZED FROM INDUSTRIAL WASTES

*Takaaki Wajima[1] (1. Chiba Univeristy (Japan))

©APSORC25

[P-R9-09]

PLATFORMS FOR SUPPLYING SHORT-LIVED RADIOISOTOPES FOR BASIC AND APPLIED SCIENCES IN JAPAN

*Hiroki Kanda[1], Takashi Nakano[1], Mitsuhiro Fukuda[1], Hiromitsu Haba[2], Noriko S. Ishioka[3], Hidetoshi Kikunaga[4], Kotaro Nagatsu[5], Atsushi Toyoshima[6,7], Hiroshi Watabe[8] (1. RCNP, Osaka University (Japan), 2. RIKEN Nishina Center (Japan), 3. QST Takasaki (Japan), 4. RARiS Mikamine, Tohoku University (Japan), 5. QST QMS (Japan), 6. IRS, Osaka University (Japan), 7. Osaka University (Japan), 8. RARiS Aobayama, Tohoku University (Japan))

Poster Presentation | [P2]ICP-MS Based Radioanalytical Chemistry and Related Applications

Wed. Sep 17, 2025 6:30 PM - 8:00 PM JST | Wed. Sep 17, 2025 9:30 AM - 11:00 AM UTC Poster

[Poster] P2

[P-P2-01]

Optimisation of conditions for the quantitative analysis of I-129 in smear samples collected inside the Fukushima Daiichi Nuclear Power Station by alkaline fusion and ICP-MS/MS

*Maki Honda[1], Asako Shimada[1], Yoshihisa Iida[1] (1. JAEA (Japan))

[P-P2-02]

Control of Zirconium-90 for Strontium-90 determination using thermal ionization mass spectrometry (TIMS)

*Norbert Kavasi[1], Tatsuo Aono[1] (1. Fukushima Institute for Research, Education and Innovation (F-REI) (Japan))

[P-P2-03]

Sensitivity improvement for radionuclide analysis using ICP-MS/MS with desolvating nebulizer

*YASUYUKI SHIKAMORI[1], CHIKAGE ABE[1], KAZUYA IDEMITSU[1], YASUYOSHI NAGAI[2] (1. Tohoku University (Japan), 2. Central Research Institute of Electric Power Industry (Japan))

©APSORC25

Contributed Talk | [R3]Actinide Chemistry and Nuclear Energy Chemistry

Wed. Sep 17, 2025 11:00 AM - 12:00 PM JST | Wed. Sep 17, 2025 2:00 AM - 3:00 AM UTC Hall A(MP)

[R3] Actinide Chemistry and Nuclear Energy Chemistry

11:00 AM - 11:20 AM JST | 2:00 AM - 2:20 AM UTC

[R3-12]

Studies on Adsorption and Desorption Characteristics of Lanthanides using a Polydimethylsiloxane Sponge Incorporated with Soft-donor Ligands

*YIWEI ZHANG[1], Atsuro Furuichi[1], Ki Chul Park[1], Naokazu Idota[1], Takehiko Tsukahara[1] (1. Institute of Science Tokyo (Japan))

11:20 AM - 11:40 AM JST | 2:20 AM - 2:40 AM UTC

[R3-13*]

Mutual separation of lanthanides by extraction chromatography in hydrochloric acid solution

*WENZUN LUO[1], Putra Rahma Andri[1], Chikage Abe[2], Suzuki Tatsuya[1] (1. Nagaoka University of Technolygy (Japan), 2. Tohoku University (Japan))

11:40 AM - 12:00 PM JST | 2:40 AM - 3:00 AM UTC

[R3-14*]

Selective Recovery of Lanthanide Ions Using Spiropyran-Based Photoswitchable Adsorbents

*Kai Peng[1], Naokazu Idota[1], Takehiko Tsukahara[1] (1. Institute of Science Tokyo (Japan))

Thu. Sep 18, 2025

Plenary Talk | Plenary Talk

Thu. Sep 18, 2025 8:45 AM - 9:30 AM JST | Wed. Sep 17, 2025 11:45 PM - 12:30 AM UTC Hall S(Int'l)

[PL4] Plenary Talk 4 by Kazuhiko Ninomiya

8:45 AM - 9:30 AM JST | 11:45 PM - 12:30 AM UTC

[PL04]

ELEMENTAL ANALYSIS METHOD USING MUONS: APPLICATIONS FOR ASTEROID AND ARCHEOLOGICAL SAMPLES

*Kazuhiko Ninomiya[1,2] (1. Natural Science Center for Basic Research and Development, Hiroshima University (Japan), 2. Graduate School of Advanced Science and Engineering, Hiroshima University (Japan))

Invited & Contributed Talk | [R4]Nuclear Probe in Chemistry

Thu. Sep 18, 2025 9:35 AM - 10:45 AM JST | Thu. Sep 18, 2025 12:35 AM - 1:45 AM UTC Hall S(Int'l)

[R4] Nuclear Probe in Chemistry

9:35 AM - 10:05 AM JST | 12:35 AM - 1:05 AM UTC

[R4-01(Invited)]

Application of muon spin imaging spectroscopy to material science

*Mototsugu Mihara[1], S. Ishitani[1], K. M. Kojima[2], A. Sato[1], K. Yasuda[1], G. Takayama[1], T. Sugisaki[1], Y. Kimura[1], M. Fukuda[1], M. Fukutome[3], R. Taguchi[1], S. Shimizu[1], K. Horie[1], R. Imai[1], S. Ide[1], K. Shimizu[4], M. Kamon[4], M. Fukushima[4], Y. Mizoi[5], A. Koda[6], S. Kanda[6], W. Sato[7], D. Nishimura[8], M. Tanaka[9] (1. Department of Physics, The University of Osaka (Japan), 2. TRIUMF (Canada), 3. Niigata University (Japan), 4. KYOKUGEN, The University of Osaka (Japan), 5. Osaka Electro-Communication University (Japan), 6. KEK (Japan), 7. Kanazawa University (Japan), 8. Tokyo City University (Japan), 9. Kyushu University (Japan))

10:05 AM - 10:25 AM JST | 1:05 AM - 1:25 AM UTC

[R4-02]

^{61}Ni Mössbauer Spectroscopy on Hofmann-type coordination polymer

*Kosuke Kitase[1], Takafumi Kitazawa[1], Yasuhiro Kobayashi[2], Makoto Seto[2], Shinji Kitao[2], Takumi Kubota[3] (1. Toho University (Japan), 2. Institute for Integrated Radiation and Nuclear Science, Kyoto University (Japan), 3. Agency for Health, Safety and Environment, Kyoto University (Japan))

10:25 AM - 10:45 AM JST | 1:25 AM - 1:45 AM UTC

[R4-03]

LOCAL STRUCTURE OF CADMIUM IMPURITIES IN STRONTIUM TITANATE STUDIED BY THE TIME DEFFERENCIAL PERTURBED ANGULAR CORRELATION METHOD

*Sayaka Komatsuda[1], Wataru Sato[1], Akihiro Taniguchi[2], Yoshitaka Ohkubo[2] (1. Kanazawa University (Japan), 2. Kyoto University (Japan))

©APSORC25

Invited & Contributed Talk | [P3]Environmental Integrated Knowledge of Radionuclides Dynamics Studied from the Fukushima Accident

Thu. Sep 18, 2025 9:40 AM - 10:50 AM JST | Thu. Sep 18, 2025 12:40 AM - 1:50 AM UTC Hall B(Small)

[P3] Environmental Integrated knowledge of Radionuclides Dinamics Studied from the Fukushima Accident

9:40 AM - 10:10 AM JST | 12:40 AM - 1:10 AM UTC

[P3-01(Invited)]

How the forested areas have worked to radiocesium migration in a river system after the Fukushima nuclear accident

*Seiji Hayashi[1], Hideki Tsuji[1] (1. National Institute for Enviromental Studies (Japan))

10:10 AM - 10:30 AM JST | 1:10 AM - 1:30 AM UTC

[P3-02]

TREND OF CS-137 IN LEAVES, BRANCHES, AND TREE RINGS OF FIR (*Abies firma*) IN ISHINOMAKI AREA OF MIYAGI PREFECTURE, JAPAN

*MICHIKO FUKUSHIMA[1], takeshige MATSUTANI[1], Tomoyuki NEMOTO[1], Kiyotane YODA[1], Amares CHATT[2] (1. Ishinomaki Senshu University (Japan), 2. Dalhousie University (Canada))

10:30 AM - 10:50 AM JST | 1:30 AM - 1:50 AM UTC

[P3-03]

Increase in dissolved Cs-137 concentration in bottom water layer at summer stratification from a mountainous lake, Lake Akagi-Konuma in Gunma Prefecture, Japan

*Seiya Nagao[1], Shinji Otori[1], Kanako Shiozawa[2], Takashi Akutsu[2], Kyuma Suzuki[2], Shinya Ochiai[1] (1. Kanazawa University (Japan), 2. Gunma Prefectural Fisheries Experiment Station (Japan))

©APSORC25

Contributed Talk | [R2]Radioanalytical Chemistry and Nuclear Forensics

Thu. Sep 18, 2025 9:45 AM - 10:45 AM JST | Thu. Sep 18, 2025 12:45 AM - 1:45 AM UTC Hall A(MP)

[R2] Radioanalytical Chemistry and Nuclear forensics

9:45 AM - 10:05 AM JST | 12:45 AM - 1:05 AM UTC

[R2-05]

FROM SPECIATION TO SIGNATURE DISCOVERY: INTEGRATED APPROACHES IN THE CONSORTIUM FOR NUCLEAR FORENSICS

*Ken Ronald Czerwinski[1] (1. University of Nevada, Las Vegas (United States of America))

10:05 AM - 10:25 AM JST | 1:05 AM - 1:25 AM UTC

[R2-06]

VERIFICATION OF THE SEGMENTATION APPROACH IN PARTICLE SHAPE MEASUREMENT FOR ELECTRON MICROSCOPE IMAGE ANALYSIS - APPLICATION IN NUCLEAR FORENSICS

*Yoshiki Kimura[1], Tetsuya Matsumoto[2], Yuichi Kijima[1], Yutaka Tomita[1] (1. Japan Atomic Energy Agency (Japan), 2. Power Computer (Japan))

10:25 AM - 10:45 AM JST | 1:25 AM - 1:45 AM UTC

[R2-07]

Study of Rapid Analysis Methods for Pu Isotopes in Atmospheric Particulate Matter Samples

*Yang Shao[1], Lingling Ma[1], Ziao Li[1], Futao Xin[1] (1. Institute of High Energy Physics, Chinese Academy of Sciences (China))

Contributed Talk | [R2]Radioanalytical Chemistry and Nuclear Forensics

Thu. Sep 18, 2025 11:00 AM - 11:40 AM JST | Thu. Sep 18, 2025 2:00 AM - 2:40 AM UTC Hall A(MP)

[R2] Radioanalytical Chemistry and Nuclear forensics

11:00 AM - 11:20 AM JST | 2:00 AM - 2:20 AM UTC

[R2-08*]

Development of Graphene–Macrocycle Hybrid Nanomaterials and Its Application to Cesium Separation

*Jiawei Xu[1], Naokazu Idota[2], Takehiko Tsukahara[1,2] (1. Department of Materials Science and Engineering, Institute of Science Tokyo (Japan), 2. Laboratory for Zero-Carbon Energy, Institute of Integrated Research, Institute of Science Tokyo (Japan))

11:20 AM - 11:40 AM JST | 2:20 AM - 2:40 AM UTC

[R2-09]

Decontamination of contaminated Raspberry Pi module as a surrogate for sensitive electronics by Cyber Clean® Putty

*Zakir Kazi[1], Jaleh Semmler[2], Tim Munsie[1] (1. Defence Research & Development Canada (DRDC) (Canada), 2. Canadian Nuclear Laboratories (CNL) (Canada))

©APSORC25

Contributed Talk | [R4]Nuclear Probe in Chemistry

Thu. Sep 18, 2025 11:00 AM - 12:00 PM JST | Thu. Sep 18, 2025 2:00 AM - 3:00 AM UTC Hall S(Int'l)

[R4] Nuclear Probe in Chemistry

11:00 AM - 11:20 AM JST | 2:00 AM - 2:20 AM UTC

[R4-04]

Chemical state of Fe and electrical conduction properties of dense sintered $Sr_{1-x}Ln_xFeO_{3-\delta}$ and $SrFe_{1-x}Ln_xO_{3-\delta}$ (*Ln*: Y, lanthanoid) with cubic perovskite structure

Keina Nagai[1], Chihiro Kato[1], Taizo Yoshino[1], Ryutaro Maehara[1], Kosuke Shido[1], Takayuki Sugimoto[1], *Takuya Hashimoto[1], Fumito Fujishiro[2], Motoyuki Matsuo[3] (1. Nihon University (Japan), 2. Kochi University (Japan), 3. The University of Tokyo (Japan))

11:20 AM - 11:40 AM JST | 2:20 AM - 2:40 AM UTC

[R4-05]

Mechanism of Half-Iron Morin Transition in the Nb-Doped Hematite

*Satoru Nakashima[1], Habibur Rahman[1], Shiro Kubuki[2] (1. Hiroshima University (Japan), 2. Tokyo Metropolitan University (Japan))

11:40 AM - 12:00 PM JST | 2:40 AM - 3:00 AM UTC

[R4-06]

Preparation and ^{61}Ni Mössbauer Spectroscopy for Supramolecular Bridging Cyanide Complexes containing $[Ni(II)(CN)_4]^{2-}$ unit

*Takafumi Kitazawa[1,2], Kosuke Kitase[1], Shinji Kitao[3], Yasuhiro Kobayashi[3], Takumi Kubota[4], Makoto Seto[3] (1. Department of Chemistry, Faculty of Science, Toho Universityoho University (Japan), 2. Research Centre for Materials with Integrated Properties, Toho University (Japan), 3. Institute for Integrated Radiation and Nuclear Science, Kyoto University (Japan), 4. Agency for Health, Safety and Environment, Kyoto University (Japan))

©APSORC25

Contributed Talk | [P3]Environmental Integrated Knowledge of Radionuclides Dynamics Studied from the Fukushima Accident

Thu. Sep 18, 2025 11:00 AM - 12:00 PM JST | Thu. Sep 18, 2025 2:00 AM - 3:00 AM UTC Hall B(Small)

[P3] Environmental Integrated knowledge of Radionuclides Dinamics Studied from the Fukushima Accident

11:00 AM - 11:20 AM JST | 2:00 AM - 2:20 AM UTC

[P3-04]

Activity ratio of Sr-90 and Cs-137 in different environmental samples collected from the Fukushima exclusion zone

*Norbert Kavasi[1], Tatsuo Aono[1] (1. Fukushima Institute for Research, Education and Innovation (F-REI) (Japan))

11:20 AM - 11:40 AM JST | 2:20 AM - 2:40 AM UTC

[P3-05*]

Fundamental study on the rapid analytical method for radioactive Cs-containing particles by PHITS

*Tsubasa Matsumura[1], Shinya Yamasaki[2], Keisuke Sueki[2], Yudai Shigekawa[2], Aya Sakaguchi[2] (1. Graduate School of Science and Technology, Degree Programs in Pure and Applied Sciences, Master's Program in Chemistry,University of Tsukuba (Japan), 2. Institute of Pure and Applied Sciences,University of Tsukuba (Japan))

11:40 AM - 12:00 PM JST | 2:40 AM - 3:00 AM UTC

[P3-06]

Development of an analytical method for ^{90}Sr in using ICP-DRC-MS/MS with O_2+NH_3 reaction gas

*Kazuma Koarai[1], Makoto Matsueda[1], Kayo Yanagisawa[1], Yusuke Watanabe[1] (1. Japan Atomic Energy Agency (Japan))

©APSORC25

Fri. Sep 19, 2025

Contributed Talk | [R1]Nuclear Chemistry

Fri. Sep 19, 2025 9:00 AM - 10:00 AM JST | Fri. Sep 19, 2025 12:00 AM - 1:00 AM UTC Hall S(Int'l)

[R1] Nuclear Chemistry

9:00 AM - 9:20 AM JST | 12:00 AM - 12:20 AM UTC

[R1-13]

Development of Radiochemical Techniques for the Measurement of (n,2n) Cross Sections at the National Ignition Facility

*John Despotopulos[1], Kelly Kmak[1], Daniel Pitman-Weymouth[2], James Benstead[2], Tom Braun[1], Tony Huynh[1], Justin Jeet[1], William Kerlin[1], Samantha Labb[1], Elvin Monzon[1], Rhyan Reynolds[1], Nicholas Ruof[1], Brian Sammis[1], Dawn Shaughnessy[1], Keenan Thomas[1], Todd Wooddy[1], Charles Yeamans[1] (1. Lawrence Livermore National Laboratory (United States of America), 2. Atomic Weapons Establishment (UK))

9:20 AM - 9:40 AM JST | 12:20 AM - 12:40 AM UTC

[R1-14]

Measurement of the ^{73}As(n,g) cross section at thermal neutron energies

*Kelly Nora Kmak[1], John Despotopulos[1], Connor Holiski[1], William Kerlin[1], Nicholas Scielzo (1. Lawrence Livermore National Laboratory (United States of America))

9:40 AM - 10:00 AM JST | 12:40 AM - 1:00 AM UTC

[R1-15]

Experimental study on noble gas transport in liquid lead using the Gas-jet facility at PSI

*Haohan Zhang[1], Robert Eichler[1,2] (1. Paul Scherrer Institut (Switzerland), 2. University of Bern (Switzerland))

©APSORC25

Contributed Talk | [R3]Actinide Chemistry and Nuclear Energy Chemistry

Fri. Sep 19, 2025 9:00 AM - 10:00 AM JST | Fri. Sep 19, 2025 12:00 AM - 1:00 AM UTC Hall A(MP)

[R3] Actinide Chemistry and Nuclear Energy Chemistry

9:00 AM - 9:20 AM JST | 12:00 AM - 12:20 AM UTC

[R3-23]

Burnup determination of irradiated U-Mo dispersion fuel by chemical methods

*Hyejin Cho[1], Nam uk Kim[1], Yang-Soon Park[1], Minjae Ha[1], Junhyuck Kim[1], Hye-Ryun Cho[1], Jai Il Park[1] (1. Korea Atomic Energy Research Institute (Korea))

9:20 AM - 9:40 AM JST | 12:20 AM - 12:40 AM UTC

[R3-24]

Small-Scale Experiments, Big-Scale Impact: Insights into Anion Exchange Chemistry in Pu Recovery

*Maryline G Kerlin (Ferrier)[1], Bradley C Childs[1], Scott A Simpson[1], Silvina A Di Pietro[1], Tsuyoshi A Kohlgruber[1], Emma R Tardiff[1], Hiroshi H Saito[1], Saurabh Narain[1], Kiel S Holliday[1], Lawrence Eddy Banks[1] (1. Lawrence Livermore National Laboratory (United States of America))

9:40 AM - 10:00 AM JST | 12:40 AM - 1:00 AM UTC

[R3-25]

Experimental Study on Pyrolytic Incineration Mechanism of trialkylphosphine oxide(TRPO)

*Duo Ma[1], Wei Xu[2], Meng Wei[1], Longhao Cao[1] (1. CNNC Longan Co., Ltd. (China), 2. China Institute for Radiation Protection (China))

©APSORC25

Contributed Talk | [P3]Environmental Integrated Knowledge of Radionuclides Dynamics Studied from the Fukushima Accident

Fri. Sep 19, 2025 9:00 AM - 10:00 AM JST | Fri. Sep 19, 2025 12:00 AM - 1:00 AM UTC Hall B(Small)

[P3] Environmental Integrated knowledge of Radionuclides Dinamics Studied from the Fukushima Accident

9:00 AM - 9:20 AM JST | 12:00 AM - 12:20 AM UTC

[P3-07]

Aging Effect on the Decontamination Efficiency of ^{137}Cs from Clay Minerals Using Cationic Surfactant

Akihito Matsushima[1], Herry Wijayanto[2], *Satoru Nakashima[1] (1. Hiroshima University (Japan), 2. National Research and Innovation Agency of Indonesia (Indonesia))

9:20 AM - 9:40 AM JST | 12:20 AM - 12:40 AM UTC

[P3-08]

Impact of plutonium originating from Fukushima Daiichi Nuclear Power Plant accident in the environment: an overview of a decade studies

*Jian Zheng[1], Junwen Wu[2], Keiko Tagami[1], Guosheng Yang[1], Tatsuo Aono[3] (1. National Institutes for Quantum Science and Technology (QST) (Japan), 2. Shantou University (China), 3. Fukushima Institute for Research, Education and Innovation (Japan))

9:40 AM - 10:00 AM JST | 12:40 AM - 1:00 AM UTC

[P3-09]

Effect of Gamma Dose and pH on Methyl Iodide Formation in 2 mM NaI and 5 mM MEK Aqueous Solutions

*Jei-Won Yeon[1], Minsik Kim[2] (1. Korea Atomic Energy Research Institute (Korea), 2. Korea Institute of Toxicology (Korea))

Contributed Talk | [R3]Actinide Chemistry and Nuclear Energy Chemistry

Fri. Sep 19, 2025 10:10 AM - 10:50 AM JST | Fri. Sep 19, 2025 1:10 AM - 1:50 AM UTC Hall A(MP)

[R3] Actinide Chemistry and Nuclear Energy Chemistry

10:10 AM - 10:30 AM JST | 1:10 AM - 1:30 AM UTC

[R3-26]

Complexation and Redox Behavior in Np(V)-HA-Fe(II) System

*Yuxiao Guo[1], Chao Xu[1] (1. Tsinghua University (China))

10:30 AM - 10:50 AM JST | 1:30 AM - 1:50 AM UTC

[R3-27]

HARNESSING BIOPOLYMERS FOR SUSTAINABLE REMOVAL OF RADIOACTIVE ELEMENTS

*Mohammed Fouda Hamza[1], Yuezhou Wei, Xiangbiao Yin, Amr Fouda, Eric Guibal (1. Prof. School of Nuclear Science and Technology, Univ. of South China, Hengyang 421001, China (China))

©APSORC25

Contributed Talk | [S2]Radiopharmaceutical Sciences

Fri. Sep 19, 2025 10:10 AM - 11:10 AM JST | Fri. Sep 19, 2025 1:10 AM - 2:10 AM UTC Hall S(Int'l)

[S2] Radiopharmaceutical Sciences

10:10 AM - 10:30 AM JST | 1:10 AM - 1:30 AM UTC

[S2-15]

^{225}Ac/^{213}Bi MEDICAL GENERATOR FOR RAPID PRODUCTION OF RADIOLABELED PEPTIDES

*Aleksandr N. Vasiliev[1], Stanislav V. Ermolaev[2], Elena V. Lapshina[2], Darya R. Khaliullina[2], Boris L. Zhuikov[2] (1. Shenzhen MSU-BIT University (China), 2. Institute for Nuclear Research of the Russian Academy of Sciences (Russia))

10:30 AM - 10:50 AM JST | 1:30 AM - 1:50 AM UTC

[S2-16]

Investigating radiopharmaceuticals for targeted alpha therapy with Direct Alpha Spectroscopy on living cell cultures

*Peter Kunz[1,2], Mahsa Farasat[1], Behrad Saeedi[1], Luke Wharton[1], Sidney Shapiro[3], Chris Vinnick[2], Corina Andreoiu[2], Hua Yang[1,2], Madison Daignault[2], Meghan Kostashuk[4], Nicholas Pranjatno[2], Myla Weiman[1] (1. TRIUMF (Canada), 2. Simon Fraser University (Canada), 3. University of British Columbia (Canada), 4. McMaster University (Canada))

10:50 AM - 11:10 AM JST | 1:50 AM - 2:10 AM UTC

[S2-17]

Production of ^{225}Ac via the ^{226}Ra(p,2n)^{225}Ac reaction at RIKEN

*Akihiro Nambu[1], Yousuke Kanayama[1], Hiromichi Shimizu[1], Masataka Imamura[1,2], Shota Kimura[1,2], Daiki Mori[1,2], Yuichiro Wakitani[2], Takahiro Mikamoto[2], Yudai Shigekawa[1], Sayantani Mitra[1], Hiromitsu Haba[2] (1. Nishina Center for Accelerator-Based Science, RIKEN (Japan), 2. Japan Radioisotope Association (Japan))

©APSORC25

Contributed Talk | [P2]ICP-MS Based Radioanalytical Chemistry and Related Applications

Fri. Sep 19, 2025 10:10 AM - 11:10 AM JST | Fri. Sep 19, 2025 1:10 AM - 2:10 AM UTC Hall B(Small)

[P2] ICP-MS Based Radioanalytical Chemistry and Related Applications

10:10 AM - 10:30 AM JST | 1:10 AM - 1:30 AM UTC

[P2-10]

Rapid Determination of Uranium isotopes and Ra-226 in Water Samples Using ICP-QQQ-MS

*Ivana Coha[1,2], Norbert Kavasi[3], Marko Štrok[2], Leja Rovan[2], Dorice Seif[4], Marta Jagodic Hudobivnik[2], Željko Grahek[1] (1. Ruđer Bošković Institute (Croatia), 2. Jožef Stefan Institute (Slovenia), 3. Fukushima Institute for Research, Education and Innovation (Japan), 4. University of Dar es Salaam (Tanzania))

10:30 AM - 10:50 AM JST | 1:30 AM - 1:50 AM UTC

[P2-11]

The application of ICP-MS/MS for the analysis of actinides and Sr-90 in bioassay samples for rapid dose assessment in radiation emergency medicine

*Guosheng Yang[1], Eunjoo Kim[1], Jian Zheng[1], Hirofumi Tazoe[2], Munehiko Kowatari[1], Osamu Kurihara[1] (1. National Institutes for Quantum Science and Technology, Japan (Japan), 2. Institute of Radiation Emergency Medicine, Hirosaki University (Japan))

10:50 AM - 11:10 AM JST | 1:50 AM - 2:10 AM UTC

[P2-12]

Determination of trace level I-129 by ozone reaction ICP-QMS/QMS

*Yanbei Zhu[1], Daiki Asakawa[1] (1. National Institute of Advanced Industrial Science and Technology (Japan))

Closing Ceremony

Fri. Sep 19, 2025 11:20 AM - 11:45 AM JST | Fri. Sep 19, 2025 2:20 AM - 2:45 AM UTC Hall S(Int'l)

[CL] Closing Ceremony

Sun. Sep 14, 2025 5:30 PM - 6:30 PM JST | Sun. Sep 14, 2025 8:30 AM - 9:30 AM UTC Hall A(MP)

[WR] Welcome Reception

Sun. Sep 14, 2025 3:00 PM - 5:30 PM JST | Sun. Sep 14, 2025 6:00 AM - 8:30 AM UTC Resit. Desk

[Regist] Registration

©APSORC25

Award Lecture | Award

Mon. Sep 15, 2025 9:15 AM - 10:10 AM JST | Mon. Sep 15, 2025 12:15 AM - 1:10 AM UTC Hall S(Int'l)

[AW1] Award Session 1: Kimura Award 2025

9:15 AM - 9:25 AM JST | 12:15 AM - 12:25 AM UTC

Introduction

9:25 AM - 10:10 AM JST | 12:25 AM - 1:10 AM UTC

[AW01]

FROM LAWRENCIUM TO SEABORGIUM AND HASSIUM - AND BACK

*Matthias Schädel[1] (1. GSI Helmholtzzentrum für Schwerionenforschung GmbH (Germany))

7th Asia-Pacific Symposium on Radiochemistry *September 14 ~ 19, 2025 • Kunibiki Messe • Shimane, Japan*

FROM LAWRENCIUM TO SEABORGIUM AND HASSIUM – AND BACK

Matthias Schädel

GSI Helmholtzzentrum für Schwerionenforschung GmbH: Planckstraße 1, Darmstadt, Germany, 64291, m.schaedel@gsi.de

About a century ago, during their stay with Niels Bohr in Copenhagen, the physicist Yoshio Nishina and the chemist Kenjiro Kimura joint and started a fruitful interdisciplinary collaboration. Back in Japan, their experiments unveiled symmetric nuclear fission [1] and they discovered the β^--emitting isotope ^{237}U [2]. Because of a long half-life, ^{237}Np was not observed. Before focusing on heavier elements in my contribution, I will briefly show results from our discovery of ^{243}Np and ^{244}Np [3], obtained with an early version of the Automated Rapid Chemistry Apparatus (ARCA) [4] at the GSI.

Half a century ago, results from first chemical studies on elements 103 and 104, lawrencium, Lr, and rutherfordium, Rf, respectively, justified placing Lr at the end of the actinide series in the Periodic Table of the Elements (PTE) and Rf, as a group-4 element, at the beginning of a new series of transition elements; today termed superheavy elements (SHE) [5]. However, questions remained about their detailed chemical properties and electronic configuration. From the mid-1980s on, automated chemical techniques matured to a level that detailed chemical studies of Lr, Rf, and the group-5 element dubnium, Db, came into reach [6-8]. In these experiments, which I will touch in an exemplary way, the first goal was a comparison of chemical properties with lighter homologs in the PTE. Concurrently, theoretical calculations on atomic and molecular properties [9] made a deeper understanding of experimental results possible and provided means to unravel the influence of increasingly strong relativistic effects on chemical properties.

After series of experiments, some showing unexpected properties, however, often explained by theory [9], it was at the beginning of the 1990s that the time was ripe to move beyond Db and prepare for and perform studies on element 106, seaborgium, Sg, at the GSI [10]. Sg experiments provided a special challenge because of shorter half-lives and lower cross sections, i.e., lower production rates. I will outline these aspects, present experiments, discuss their results with an emphasis on the aqueous phase chemistry [11,12], and, if time permits, briefly mention gas-phase chemistry [13].

With its ability to *in-situ* form volatile tetroxides, the group-8 element hassium, Hs, provides unique opportunities for chemical [14] and nuclear studies. Prime examples are deeper insights into the nuclear structure of ^{269}Hs and the discovery of the doubly magic nuclide ^{270}Hs [15]. More recently, the *in-situ* formation and first investigation of $Sg(CO)_6$, the first organic compound of a SHE studied in the gas-phase, was successful [16]. This provides great perspectives for further investigations of new classes of SHE compounds in the gas-phase.

A completely different approach and technique, as compared with "classical" heavy and superheavy chemistry experiments, was successfully applied in the determination of the first ionization potential of Lr [17]; the first atomic property directly measured for Lr was in excellent agreement with results from up-to-date theoretical calculations.

Of importance for todays and future SHE chemistry experiments were lessons learned especially from the Sg experiments and consequences drawn from these lessons. One is the crucial importance of applying physical pre-separators, like the gas-filled recoil separator TASCA [18]. Built at the GSI in 2005, it opened up new frontiers and yielded seminal insights in nuclear and chemical properties of SHE [19,20]. In addition, successful SHE experiments require automated, fast and continuously operating chemical separations with highly efficient detection systems of sufficiently good resolution for α-spectroscopy. While all of this is successfully applied in gas-phase chemistry up to Mc [21], it remains a major challenge for liquid phase chemistry. Looking into the future, a fascinating aqueous phase experiment could be the measurement of the redox potential of Sg(VI) to Sg(IV). While such a Sg experiment remains fictional now, one possibly essential component, a flow electrolytic chromatography apparatus, was developed and applied to measure the redox potential of Md^{3+} to Md^{2+} [22]. In combination with a separation technique like SISAK [23], in principle, chemical separations of SHE can be continuously carried out in the liquid phase. Presumably, miniaturization and interfacing the individual components will provide a major challenge, as well as a detection system for α-spectroscopy coupled to a continuously running liquid-phase chemistry experiment.

Not part of this contribution, a brief overview over the present status of superheavy element research worldwide and a summary of more recent results from chemical and nuclear studies at the GSI, Darmstadt, will be presented elsewhere in a Plenary Lecture at this conference [19]. Further reviews, including earlier techniques and results, can be found in Ref. [24] and, with the focus on liquid phase chemistry, in [25,26].

Copyright on 7th Asia-Pacific Symposium on Radiochemistry 2025 - AW01 -

ACKNOWLEDGMENTS

The author is most grateful and feels deeply honored as the recipient of the Kimura Award 2025 of the Japan Society of Nuclear and Radiochemical Sciences. Special thanks and my deepest appreciation goes to all the colleagues, including their institutions, who, in often very large and long-term international collaborations, enabled the experiments and results I am presenting. Among many others, I like to emphasize the crucial role of my colleagues at the GSI, Darmstadt, and the pleasure and honor of working with, and, from 2010 to 2015, being a member of the Research Group for Superheavy Elements at the Advanced Science Research Center of the Japan Atomic Energy Agency, Tokai-mura, Japan.

References

[1] Y. NISHINA, T. YASAKI, H. EZOE, K. KIMURA and M. IKAWA, "Fission Products of Uranium produced by Fast Neutrons", Nature, 146, 24 (1940).
[2] Y. NISHINA, T. YASAKI, H. EZOE, K. KIMURA and M. IKAWA, "Induced ß-Activity of Uranium by Fast Neutrons", *Phys. Rev.*, **57**, 1182 (1940).
[3] K.J. MOODY et al., „New Nuclides: Neptunium-243 and Neptunium-244", *Z. Phys. A – Atomic Nuclei",* **328**, 417 (1987).
[4] M. SCHÄDEL, W. BRÜCHLE, B. HAEFNER, „Fast radiochemical separations with an automated rapid chemistry apparatus", *Nucl. Instrum. Methods Phys. Res.*, **A264**, 308 (1988).
[5] MATTHIAS SCHÄDEL, "The Chemistry of Superheavy Elements", *Angew. Chem. Int. Ed.*, **45**, 368 (2006).
[6] M. SCHÄDEL, "Chemistry of the Transactinide Elements", *Radiochim. Acta*, **70/71**, 207 (1995).
[7] M. SCHÄDEL, "Chemistry of superheavy elements", *Radiochim. Acta*, **100**, 579 (2012).
[8] MATTHIAS SCHÄDEL and YUICHIRO NAGAME, "From SRAFAP to ARCA and AIDA – developments and implementation of automated aqueous-phase rapid chemistry apparatuses for heavy actinides and transactinides", *Radiochim. Acta*, **107**, 561 (2019).
[9] VALERIA PERSHINA, In: *The Chemistry of Superheavy Elements*, pp. 135-239, MATTHIAS SCHÄDEL, DAWN SHAUGHNESSY, Eds., Springer, Heidelberg, Germany (2014).
[10] M. SCHÄDEL et al, "Chemical properties of element 106 (seaborgium)", *Nature*, **388**, 55 (1997).
[11] M. SCHÄDEL et al., "First aqueous chemistry with seborgium (element 106)", *Radiochim. Acta*, **77**, 149 (1997).
[12] M. SCHÄDEL et al., "Aqueous chemistry of seaborgium (element 106)", *Radiochim. Acta*, **83**, 163 (1998).
[13] A. TÜRLER et al., "First measurement of a thermochemical property of a seaborgium compound", *Angew. Chem. Int. Ed.*, **38**, 2212 (1999).
[14] Ch.E. DÜLLMANN et al., "Chemical investigation of hassium (element 108)", *Nature*, **418**, 859 (2002).
[15] A. TÜRLER et al., "On the decay properties of ^{269}Hs and indications for the new nuclide ^{270}Hs", *Eur. Phys. J. A* **17**, 505 (2003).
[16] J. EVEN et al., "Synthesis and detection of a seaborgium carbonyl complex", *Science*, **345**, 1491 (2014).
[17] T.K. SATO et al., "Measurement of the first ionization potential of lawrencium, element 103", *Nature*, **520**, 209 (2015), and T.K. SATO et al, "First Ionization Potentials of Fm, Md, No, and Lr: Verification of Filling-Up of 5f Electrons and Confirmation of the Actinide Series", *J. Am. Chem. Soc.*, **140**, 14609 (2018).
[18] A. SEMCHENKOV et al., "The TransActinide separator and chemistry apparatus (TASCA) at GSI – optimization of ion-optical structures and magnet designs", *Nucl. Instrum. Methods B* **266**, 4153 (2008).
[19] CHRISTOPH E. DÜLLMANN, "Synthesis and chemical studies of superheavy elements", *Plenary Lecture Contribution to this APSORC 2025 conference*, to be published.
[20] CHRISTOPH E. DÜLLMANN et al., "Five decades of GSI superheavy element discoveries and chemical investigation", *Radiochim. Acta* **110**, 417 (2022).
[21] A. YAKUSHEV et al., "Manifestation of relativistic effects in the chemical properties of nihonium and moscovium revealed by gas chromatography studies", *Front. Chem.* **12**, 1474820 (2024).
[22] A. TOYOSHIMA et al., "Measurement of the Md^{3+}/Md^{2+} Reduction Potential Studied with Flow Electrolytic Chromatography", *Inorg. Chem.*, **52**, 12311 (2013).
[23] JON PETTER OMTVEDT et al., "SISAK Liquid-Liquid Extraction Experiments with Preseparated ^{257}Rf", *J. Nucl. Radiochem. Sci.*, **3**, 121 (2002).
[24] ANDREAS TÜRLER and VALERIA PERSHINA, "Advances in the Production and Chemistry of the Heaviest Elements", *Chem. Rev.*, **13**, 1237 (2013).
[25] JENS VOLKER KRATZ and YUICHIRO NAGAME, In: *The Chemistry of Superheavy Elements*, pp. 309-374, MATTHIAS SCHÄDEL, DAWN SHAUGHNESSY, Eds., Springer, Heidelberg, Germany (2014).
[26] YUICHIRO NAGAME, JENS VOLKER KRATZ and MATTHIAS SCHÄDEL, "Chemical studies of elements with $Z \geq 104$ in liquid phase", *Nucl. Phys. A*, **944**, 614 (2015).

Copyright on 7th Asia-Pacific Symposium on Radiochemistry 2025 - AW01 -

Award Lecture | Award

Mon. Sep 15, 2025 10:25 AM - 11:20 AM JST | Mon. Sep 15, 2025 1:25 AM - 2:20 AM UTC Hall S(Int'l)

[AW2] Award Session 2: Hevesy Medal Award 2021

10:25 AM - 10:35 AM JST | 1:25 AM - 1:35 AM UTC

Introduction

10:35 AM - 11:20 AM JST | 1:35 AM - 2:20 AM UTC

[AW02]

Developments in gamma-ray spectrometry, activation analysis, digital autoradiography and design of low-activation structural Materials: mathematical modelling and experimental solutions

*Vladimir P Kolotov[1] (1. Vernadsky Institute of Geochemistry and Analytical Chemistry of Russian Academy of Sciences (Russia))

©APSORC25

7th Asia-Pacific Symposium on Radiochemistry *September 14 ~ 19, 2025 • Kunibiki Messe • Shimane, Japan*

DEVELOPMENTS IN GAMMA-RAY SPECTROMETRY, ACTIVATION ANALYSIS, DIGITAL AUTORADIOGRAPHY AND DESIGN OF LOW-ACTIVATION STRUCTURAL MATERIALS: MATHEMATICAL MODELLING AND EXPERIMENTAL

Vladimir P. Kolotov

Vernadsky Institute of Geochemistry, and Analytical Chemistry of Russian Academy of Sciences, Moscow, Russia

The presentation in occasion of George Hevesy Medal award focuses on the most important results in different areas obtained for some period.

Among the topics are computer's processing of gamma-ray spectrometric information for different purposes, testing tools for evaluating the quality of gamma-ray spectrometry software, estimation of true coincidences effect for voluminous sources, remote gamma-ray spectrometric monitoring of radioactivity of extended objects, application of relational databases for on line storing, managing and consolidating analytical information.

Other subjects are development of methodology of quantitative gamma-activation analysis in non-uniform field of activating radiation as well as some examples of its application for analysis of polymetallic ores and detonation nanodiamonds, which are promising carriers for (radio) pharmaceutical substances.

Computer based method for processing and interpreting a series of autoradiographic images has been developed to increase the informative value of the autoradiography method for screening analysis of large-area thin sections (rock and ore samples).

Several examples demonstrate the effectiveness of combining the abilities of nuclear and non-nuclear elemental analysis techniques for the development of chemical analysis and radiochemical applications.

Conception for design of new class of structural materials with accelerated decrease of the induced radioactivity (low-activation structural materials) is discussed. The central part of the conception is mathematical modelling and computer program for evaluation of high-order nuclear transmutations under neutron irradiation with arbitrary energy distribution. The important influence of impurity elements and isotopic composition for activation and decay kinetics of the induced radioactivity for various materials must be taken in the consideration. The tasks of analytical support for development of low-activation structural materials are formulated. The effect of nuclear transmutations caused by neutron irradiation on the phase stability of some structural materials is studied.

Copyright on 7th Asia-Pacific Symposium on Radiochemistry 2025 - AW02 -

Plenary Talk | Plenary Talk

Mon. Sep 15, 2025 11:25 AM - 12:10 PM JST | Mon. Sep 15, 2025 2:25 AM - 3:10 AM UTC Hall S(Int'l)

[PL1] Plenary Talk 1 by Yoshio Takahashi

11:25 AM - 12:10 PM JST | 2:25 AM - 3:10 AM UTC

[PL01]

Environmental behaviors of radionuclides studied by advanced X-ray absorption spectroscopy

*Yoshio Takahashi[1] (1. The University of Tokyo (Japan))

©APSORC25

7th Asia-Pacific Symposium on Radiochemistry *September 14 ~ 19, 2025 • Kunibiki Messe • Shimane, Japan*

Environmental behaviors of radionuclides studied by advanced X-ray absorption spectroscopy

Yoshio Takahashi[1,2]

[1]*Department of Earth and Planetary Science, Graduate School of Science, The University of Tokyo, 7-3-1 Hongo, Bunkyo, Tokyo 113-0033, Japan*
[2]*Isotope Science Center, The University of Tokyo, 2-11-16 Yayoi, Bunkyo, Tokyo 113-0032, Japan*

In geochemistry and environmental chemistry, understanding the elementary processes of the behavior of elements by analyzing their chemical species (i.e. molecular geochemistry) contributes to a better understanding of the evolution of the universe, the earth, and life, and to the prediction of future environment, resources, and climate. This is basically similar to the studies of environmental radiochemistry. However, we need to consider several additional point in the environmental radiochemistry, which deals with chemistry related to radionuclides [1]: first, by gaining knowledge beyond the framework of the conventional periodic table, the behavior of all elements can be treated more systematically. The second is that the natural abundance of these elements is generally low, which needs more sensitive analysis in particular for speciation work to develop molecular geochemistry of radionuclides. Actually, tools developed in radiochemistry have often provided breakthroughs in molecular geochemistry and contributed to the understanding of the systematics of elemental behavior, especially as societal demands have made the development of such sensitive methods significant in this field. An example of such method is laser-induced fluorescence (LIF) spectroscopy, which has high-sensitivity and various information on the speciation of some elements [2], which was developed quickly in the field of environmental geochemistry in 1990s and subsequently used in trace element geochemistry afterwards. In a sense, this field is at the front of trace element geochemistry, and similar situation may be valid to the application of X-ray absorption fine structure (XAFS) spectroscopy. Thus, I would like to present systematic understanding of environmental behavior of various elements including radionuclides based on advanced XAFS spectroscopy mainly based on our achievement in this field.

Generally, XAFS at hard X-ray region including X-ray absorption near-edge structure (XANES) and extended X-ray absorption fine structure (EXAFS) are frequently employed, which provide information of (i) valence and symmpetry of the target element and (ii) local structures in the vicinity of the targe element such as interatomic distances to neighboring atoms and coordination number. To get the spectra, fluorescens mode using Si or Ge detector to detect X-ray fluorescence intensity from a target element is commonly used to get the XAFS spectra of trace elements. To conduct more sensitive analysis, high energy resolution fluorescence detection (HERFD) using both in energy-dispersive or wavelength-dispersive detector is very powerful to decrease the signal of the target element to background signal (XRF of other elements and scattered X-ray). In addition, to discuss the migration of radionuclides, interaction with light elements (e.g., organic matter) is also important, which can be also considered using XAFS in the soft X-ray region.

In this presentation, as examples of their applications to environmental radiochemistry two topics, (i) studies on the migration of radionuclides emitted by the Fukushima Dai-ichi Nuclear Power Plant (FDNPP) accident in 2011 [3,4] and (ii) the development of advanced XAFS, which consists XANES and EXAFS. The former topic must be summarized from various scientific and engineering perspectives, and the various geochemical processes and migration behavior of radionuclides learned from these studies are important for predicting the behavior of radionuclides in the terrestrial environment [5]. In particular, I would like to discuss migration of radiocesium at earth surface in particular on the affinity of cations to phyllosilicates. In addition, radiocesium-bearing silica microparticles (CsMP) emitted from the accident will be also referred to, as the X-ray spectroscopy plays an important role for the characterization of CsMPs.

The latter topic is important for a comprehensive understanding of the environmental behavior of all elements, which is also related to the first topic, because the highly sensitive analytical tool for the speciation of trace elements is necessary in all fields of environmental geochemistry. The high sensitivity method can be achieved by high energy resolution detection of fluorescent X-rays using either a crystal analyzer or a high energy resolution detector such as a transition edge sensor (TES)[6]. In particular, high energy resolution fluorescence detection XANES (HERFD-XANES) provides more speciation information than conventional XANES [7], which needs to be applied in a wide range of geochemistry in the future. Among the major radionuclides, radiocesium and U were the focus in this part. Radiocesium, which is abundant and volatile in the reactor, is the main radionuclide emitted from the FDNPP accident, and adsorption on phyllosilicates is the main reaction controlling radiocesium behavior [8]. On the other hand, the behavior of U is particularly important for the safety assessment of the geological disposal of radioactive waste, since the treatment of direct disposal will be adopted in many countries in the future.

Copyright on 7th Asia-Pacific Symposium on Radiochemistry 2025

References

[1] Y. Takahashi, A. Yamaguchi, T. Yomogida, Environmental geochemistry of radionuclides (Environmental radiochemistry), Treatise on Geochemistry (Third Edition) 6 (2025) 105–150.

[2] Y. Takahashi, T. Kimura, Y. Minai, Direct observation of Cm(III)-fulvate species on fulvic acid-montmorillonite hybrid by laser-induced fluorescence spectroscopy, Geochim. Cosmochim. Acta 66 (2002) 1–12.

[3] N. Yoshida, Y. Takahashi, Land-surface contamination by radionuclides from the fukushima Daiichi nuclear power plant accident, Elements 8 (2012) 201–206.

[4] Y. Igarashi, T. Kogure, Y. Kurihara, H. Miura, T. Okumura, Y. Satou, Y. Takahashi, N. Yamaguchi, A review of Cs-bearing microparticles in the environment emitted by the Fukushima Dai-ichi Nuclear Power Plant accident, J. Environ. Radioact. 205–206 (2019) 101–118.

[5] Y. Takahashi, Q. Fan, H. Suga, K. Tanaka, A. Sakaguchi, Y. Takeichi, K. Ono, K. Mase, K. Kato, V.V. Kanivets, Comparison of solid-water partitions of radiocesium in river waters in Fukushima and Chernobyl areas, Sci. Rep. 7 (2017) 12407.

[6] W. Li, S. Yamada, T. Hashimoto, T. Okumura, R. Hayakawa, K. Nitta, O. Sekizawa, H. Suga, T. Uruga, Y. Ichinohe, T. Sato, Y. Toyama, H. Noda, T. Isobe, S. Takatori, T. Hiraki, H. Tatsuno, N. Kominato, M. Ito, Y. Sakai, H. Omamiuda, A. Yamaguchi, T. Yomogida, H. Miura, M. Nagasawa, S. Okada, Y. Takahashi, High-sensitive XANES analysis at Ce L2-edge for Ce in bauxites using transition-edge sensors: Implications for Ti-rich geological samples, Anal. Chim. Acta 1240 (2023) 340755.

[7] T. Yomogida, D. Akiyama, K. Ouchi, Y. Kumagai, K. Higashi, Y. Kitatsuji, A. Kirishima, N. Kawamura, Y. Takahashi, Application of high-energy-resolution X-ray absorption spectroscopy at the U L3-edge to assess the U(V) electronic structure in FeUO4, Inorg. Chem. 61 (2022) 20206–20210.

[8] A. Yamaguchi, Y. Kurihara, K. Nagata, K. Tanaka, S. Higaki, T. Kobayashi, H. Tanida, Y. Ohara, K. Yokoyama, T. Yaita, T. Yoshimura, M. Okumura, Y. Takahashi, Molecular geochemistry of radium: A key to understanding cation adsorption reaction on clay minerals, J. Colloid Interface Sci. 661 (2024) 317–332. org/10.1016/j.jcis.2024.01.120.

Copyright on 7th Asia-Pacific Symposium on Radiochemistry 2025

Invited & Contributed Talk | [R1]Nuclear Chemistry

Mon. Sep 15, 2025 1:30 PM - 3:00 PM JST | Mon. Sep 15, 2025 4:30 AM - 6:00 AM UTC Hall A(MP)

[R1] Nuclear Chemistry

1:30 PM - 2:00 PM JST | 4:30 AM - 5:00 AM UTC

[R1-01(Invited)]

Recent progress in the study of thorium-229 isomer

*Koji Yoshimura[1] (1. Okayama University (Japan))

2:00 PM - 2:20 PM JST | 5:00 AM - 5:20 AM UTC

[R1-02]

Development of extraction and trapping apparatus for ^{229m}Th ions and half-life measurement of singly charged ^{229m}Th

*Yudai Shigekawa[1,2], Atsushi Yamaguchi[1], Katsuyuki Tokoi[3], Nozomi Sato[1], Hidetoshi Kikunaga[4], Kenji Shirasaki[4], Yoshitaka Kasamatsu[3], Michiharu Wada[5], Hiromitsu Haba[1] (1. RIKEN (Japan), 2. University of Tsukuba (Japan), 3. Osaka University (Japan), 4. Tohoku University (Japan), 5. KEK (Japan))

2:20 PM - 2:40 PM JST | 5:20 AM - 5:40 AM UTC

[R1-03*]

Barrier distribution and excitation function measurements of ^{51}V+^{159}Tb for estimating optimal reaction energy for new element synthesis

*Yuki Yamanouchi[1,2], Pierre Brionnet[2], Satoshi Sakaguchi[1,2], Tomasz Cap[3], Margaux Forge[4], Takumi Fukatsu[1], Hiromitsu Haba[2], Daiya Kaji[2], Sota Kimura[5], Kouji Morimoto[2], Yuya Michimoto[1,2], Toshitaka Niwase[1,2], Hideyuki Sakai[2], Masaomi Tanaka[6,2] (1. Department of Physics, Kyushu University (Japan), 2. RIKEN Nishina Center (Japan), 3. National Centre for Nuclear Research (Poland), 4. Université de Strasbourg (France), 5. KEK Wako Nuclear Science Center (Japan), 6. Faculty of Arts and Science, Kyushu University (Japan))

2:40 PM - 3:00 PM JST | 5:40 AM - 6:00 AM UTC

[R1-04*]

Direct mass measurement of ^{252}Cf fission fragments with MRTOF-MS

*Gen Otsuka[1], Toshitaka Niwase[1], Sota Kimura[2], Hiromitsu Haba[3], Hironobu Ishiyama[3], Marco Rosenbusch[3], Satoshi Sakaguchi[1], Peter Schury[2], Michiharu Wada[2,4] (1. Department of physics, Kyushu University (Japan), 2. Wako Nuclear Science Center, (WNSC), Institute of Particle and Nuclear Studies (IPNS), High Energy Accelerator Research Organization (KEK) (Japan), 3. RIKEN Nishina Center for Accelerator-Based Science (Japan), 4. Institute of Modern Physics, Huizhou branch, Chinese Academy of Science (China))

©APSORC25

Recent progress in the study of thorium-229 isomer

Koji YOSHIMURA[1] on behalf of Thorium Team
[1]*Research Institute for Interdisciplinary Science, Okayama University, 3-1-1 Tsushimanaka, Kita-ku, Okaya 700-8530 JAPAN*

Thorium-229, a unique isotope of thorium, possesses an exceptionally low-lying nuclear excited state at approximately 8 eV—known as the isomeric state ^{229m}Th. This state has attracted significant attention as it is the only known nuclear transition accessible via direct laser excitation. Since nuclei are highly insensitive to external perturbations, they offer the potential to realize extraordinarily stable quantum systems. Laser manipulation of nuclear states could pave the way for the development of a "nuclear clock" with precision surpassing that of conventional atomic clocks. Such a breakthrough would not only mark a fundamental advancement in physics but also hold immense promise for technological and industrial innovation.

Interest in the unique properties of ^{229}Th dates back to the 1970s, but detailed characterization of its nuclear isomer remained elusive for decades. A major breakthrough came in 2016, when a German research group successfully observed internal conversion electrons from the isomeric state for the first time [1], spurring rapid progress in the field. Subsequent achievements using techniques such as microcalorimetry [2, 3], magnetic bottle spectrometry [4], and X-ray pumping [5] have followed. In 2023, direct observation of vacuum ultraviolet transitions from optical crystals implanted with radioactive ion beams (RI beams) marked another significant milestone [6]. As the precision of energy and lifetime measurements improved, a major breakthrough was achieved in 2024 with the first successful laser excitation of ^{229}Th embedded in a solid-state crystal [7]. Multiple host crystals have since been used for laser excitation experiments, and high-resolution laser spectroscopy is now underway. Meanwhile, rapid progress is being made in trapping and laser-cooling ^{229}Th ions for future excitation studies [8].

In addition to these developments, a phenomenon known as "quenching"—a significant shortening of the isomeric lifetime induced by laser or X-ray irradiation in solid media—has been observed [9]. Understanding this process is crucial, as it may offer a practical method to reset the long-lived isomeric state in solid-state systems. Going forward, high-resolution laser spectroscopy and X-ray absorption fine structure (XAFS) measurements[10] are expected to provide deeper insights into the electronic and coordination environments of thorium in various solid hosts, accelerating the development of optimal materials for nuclear clock applications.

In light of these advances, the global race to develop a functioning nuclear clock has entered a new phase. This presentation will provide an overview of recent progress in nuclear clock research, discuss potential applications in fundamental physics, and explore the broader scientific and technological implications of this emerging field.

References

[1] L.Wense, *et al.* , "Direct detection of the ^{229}Th nuclear clock transition", Nature 533, 47 (2016).

[2] A. Yamaguchi, *et al.* , "Energy of the ^{229}Th Nuclear Clock Isomer Determined by Absolute γ-ray Energy Difference", Phys. Rev. Lett. 123, 222501 (2019).

[3] T. Sikorsky, *et al.* , "Measurement of the ^{229}Th Isomer Energy with a Magnetic Microcalorimeter", Phys. Rev. Lett. 125, 142503 (2020).

[4] B. Seiferle, *et al.* , "Energy of the ^{229}Th nu-clear clock transition", Nature 573, 243 (2019).

[5] T. Masuda, *et al.* , " Nature X-rayX-ray pumping of the ^{229}Th nuclear clock isomer", Nature 573, 238–242 (2019).

[6] S. Kraemer, *et al.* , "Observation of the radiative decay of the ^{229}Th nuclear clock isomer", Nature 617, 706–710 (2023).

[7] J. Tiedau,*et al.* , "Laser Excitation of the Th-229 Nucleus", Phys. Rev. Lett. 132, 182501 (2024); R. Ellwell, *et al.* , "Laser Excitation o fthe ^{229}Th Nucelar Isomeric Transition in a Solid-State Host",Phys. Rev. Lett. 133, 013201 (2024); C. Zhang, *et al.* , "^{229}ThF4 thin films for solid-state nuclear clocks", Nature 636, 603 (2024); C. Zhang, *et al.* , "Frequency ratio of the ^{229m}Th nuclearisomeric transition and the ^{87}Sr atomic clock"

[8] A. Yamaguchi, *et al.* ., "Laser spectroscopy of triply charged ^{229}Th isomer for a nuclear clock", Nature 629, 62–66 (2024).

[9] T. Hiraki, *et al.* , "Controlling ^{229}Th isomeric state population in a VUV transparent crystal", Nat. Commun. 15, 5536 (2024).

[10] S. Takatori, *et al.* , "Characterization of the thorium-229 defect structure in CaF_2 crystals", New Journal of Phys. 27, 043024 (2025).

Copyright on 7th Asia-Pacific Symposium on Radiochemistry 2025 - R1-01 -

7th Asia-Pacific Symposium on Radiochemistry *September 14 ~ 19, 2025 • Kunibiki Messe • Shimane, Japan*

Development of extraction and trapping apparatus for ^{229m}Th ions and half-life measurement of singly charged ^{229m}Th

Yudai Shigekawa[1,2], Atsushi Yamaguchi[3], Katsuyuki Tokoi[4], Nozomi Sato[1], Hidetoshi Kikunaga[5], Kenji Shirasaki[6], Yoshitaka Kasamatsu[4], Michiharu Wada[7], and Hiromitsu Haba[1]

[1]*Nishina Center for Accelerator-Based Science, RIKEN: 2-1 Hirosawa, Wako, Saitama, 351-0198, Japan, yshigekawa@ied.tsukuba.ac.jp*
[2]*Institute of Pure and Applied Sciences, University of Tsukuba: 1-1-1 Tennodai, Ibaraki, 305-8577, Japan*
[3]*Quantum Metrology Laboratory, RIKEN: 2-1 Hirosawa, Wako, Saitama, 351-0198, Japan*
[4]*Graduate School of Science, Osaka University: 1-1 Machikaneyama, Toyonaka, Osaka, 560-0043, Japan*
[5]*Research Center for Accelerator and Radioisotope Science, Tohoku University: 1-2-1 Mikamine, Taihaku-ku, Sendai, Miyagi, 982-0826, Japan*
[6]*Institute for Materials Research, Tohoku University: 2-1-1 Katahira, Aoba-ku, Sendai, Miyagi, 980-8577, Japan*
[7]*KEK Wako Nuclear Science Center: 2-1 Hirosawa, Wako, Saitama, 351-0198, Japan*

The ^{229}Th nucleus has an extremely low-energy isomeric state, ^{229m}Th. The decay mode of ^{229m}Th varies depending on its electronic state. Although the internal-conversion (IC) process and γ-ray emission of ^{229m}Th were recently observed, the electronic bridge (EB) process has never been observed. The singly charged ^{229m}Th (^{229m}Th$^+$) is a promising candidate that decays by the EB process. In this study, we extracted ^{229m}Th^{2+} ions to an ion trap and produced ^{229m}Th$^+$ ions by a charge exchange reaction between ^{229m}Th^{2+} and nitric oxide gas. We were able to observe the IC electrons emitted after the extraction of the ^{229m}Th$^+$ ions to a microchannel plate detector. The IC-electron detection allowed us to count the number of ^{229m}Th$^+$ ions in an ion trap, enabling the determination of the nuclear decay half-life of ^{229m}Th$^+$ for the first time. The obtained half-life was significantly different from those of the IC decay and the γ-ray emission, indicating the presence of the EB decay.

1 Introduction

The first excited state of the ^{229}Th nucleus, ^{229m}Th, has an excitation energy of only 8.36 eV [1] above the ground state (^{229g}Th). This excitation energy is very close to the binding energy of valence electrons, leading to the variation of the decay modes of the isomer depending on the electronic states. The internal conversion (IC) process [2] and γ-ray emission [3] of ^{229m}Th have been recently observed. However, the electronic bridge (EB) decay of ^{229m}Th, which is a higher-order γ-ray emission involving the transfer of the nuclear excitation energy to the transition of an atomic electron, has yet to be observed. One of the candidates for the electronic states in which ^{229m}Th decays dominantly by the EB decay is the singly charged ^{229m}Th (^{229m}Th$^+$) [4]. In previous studies [2,3], the Munich group extracted ion beams of ^{229m,g}Th^{3+}, ^{229m,g}Th^{2+}, and ^{229m,g}Th$^+$ recoiling from a ^{233}U source using an RF-funnel gas cell. When ^{229m,g}Th$^{3+,2+}$ ions were extracted to the surface of a microchannel plate (MCP) detector, ^{229m}Th ions were neutralized on the MCP surface and the IC electrons emitted from the ^{229m}Th atoms were observed. However, no IC electrons were observed upon the extraction of ^{229m,g}Th$^+$, which indicated that ^{229m}Th$^+$ rapidly deexcited during the ion extraction from the gas cell. Hence, the lifetime of ^{229m}Th$^+$ was deduced to be less than the ion extraction time (~10 ms), which was shorter than the theoretically predicted values [4]. In the experiments, the atomic electrons of ^{229m}Th$^+$ may have been excited during the stopping process of the high-energy ^{229m}Th ions in the gas cell, which potentially opened the IC process with a half-life of ~7 μs. Therefore, in this study, we developed a method to produce ^{229m}Th$^+$ by low-energy collisions, namely, a charge-exchange reaction between ^{229m}Th^{2+} and nitric oxide (NO) gas in an ion trap. We also developed a method to count the number of ^{229m}Th$^+$ ions in an ion trap, which allowed us to measure the nuclear decay half-life of ^{229m}Th$^+$.

2 Apparatus

We developed an apparatus for extracting and trapping ^{229m,g}Th ions (Fig. 1). First, ^{229m,g}Th ions (^{229m}Th 2%, ^{229g}Th 98%) that recoiled from a ^{233}U source were decelerated by He gas and pushed to an RF carpet. The ions were then extracted from the central hole of the carpet and transported to a quadrupole ion trap through a quadrupole ion guide (QPIG). The ion trap was filled with 0.4 Pa of argon (Ar) and a small quantity of NO (<10^{-5} Pa). Ar was used for cooling ions and NO was used for producing ^{229m,g}Th$^+$ by the charge exchange reaction. The ions extracted from the ion trap were subjected to mass separation by a quadrupole mass separator (QMS) and transported to an MCP detector.

This apparatus allowed us to extract mass-separated ^{229m,g}Th^{2+} ions at a rate of ~2.0×10^4 ions/s (including ~400 ions/s of ^{229m}Th^{2+}). We also confirmed the production of ^{229m,g}Th$^+$ ions by loading and trapping ^{229m,g}Th^{2+} ions for some time.

Copyright on 7th Asia-Pacific Symposium on Radiochemistry 2025 - R1-02 -

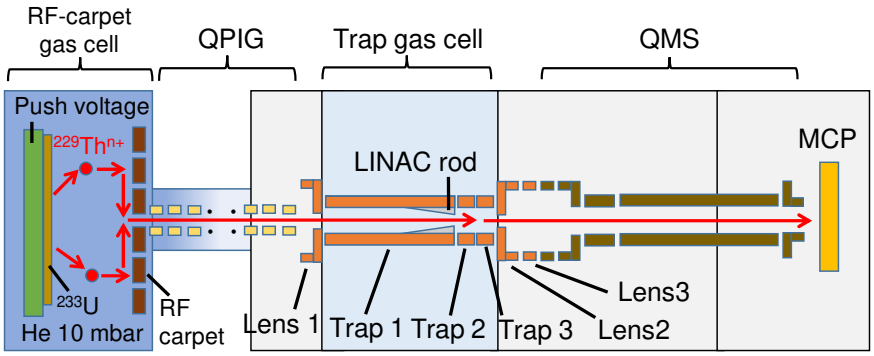


Fig. 1. Apparatus for extracting and trapping ^{229m,g}Th ions.

3 IC-electron measurement

The number of ^{229m}Th ions in the ion trap can be counted by counting the IC electrons emitted after the extraction of the ions on the MCP detector. We first confirmed whether the IC electrons were detected when ^{229m,g}Th$^+$ ions were extracted on the MCP detector. We extracted ion bunches of ^{229m,g}Th$^+$ with a bunch width of ~3 μs. Electron signals were detected after the arrival of the ion bunches at the MCP detector, and the decay curve of the electron counts showed a half-life of ~7 μs. Because the IC half-life of ^{229m}Th neutralized on a MCP detector is known to be ~7 μs, we successfully observed the IC electrons emitted after the extraction of ^{229m}Th$^+$ on the MCP detector.

4 Half-life measurement of ^{229m}Th$^+$

We measured the number of ^{229m}Th$^+$ in the ion trap as a function of the trapping time by counting the IC electrons of ^{229m}Th using the MCP detector. The number of ^{229m}Th$^+$ as a function of the trapping time showed a growth and decay curve. The growth of the number of ^{229m}Th$^+$ is related to the reaction rate between Th^{2+} and NO, while the decay is related to the sum of the nuclear decay constant of ^{229m}Th$^+$ (λ) and the reaction rate (Γ_1) between Th^+ and NO. The reaction rate Γ_1 was independently obtained by measuring the ion counts of ^{229g}Th$^+$ as a function of the trapping time. By subtracting Γ_1 from $\lambda + \Gamma_1$, the nuclear decay half-life of ^{229m}Th$^+$ was determined for the first time. We confirmed that the nuclear decay half-lives of ^{229m}Th$^+$ obtained at different pressures of NO were consistent within error. The determined half-life was ~10^5 times longer than that of the IC decay and ~10^3 times shorter than that of the γ-ray emission, indicating the presence of a new decay mode, namely, EB decay.

5 Conclusions

We developed an apparatus for extracting and trapping ^{229m,g}Th ions. ^{229m,g}Th^{2+} ions were extracted from a ^{233}U source and ^{229m}Th$^+$ ions were produced by a charge exchange reaction between ^{229m}Th^{2+} and NO gas. We extracted ^{229m}Th$^+$ ions on the MCP detector and successfully observed the IC electrons of ^{229m}Th. By counting the ^{229m}Th$^+$ and ^{229g}Th$^+$ ions as a function of the trapping time, we determined the nuclear decay half-life of ^{229m}Th$^+$ for the first time.

ACKNOWLEDGMENTS

^{233}U used in this study was provided by the ^{233}U cooperation project between the Japan Atomic Energy Agency and the Inter-University Cooperative Research Program of the Institute for Materials Research, Tohoku University (proposal numbers 17K0204, 17F0011, and 18F0014). This work was supported by JSPS KAKENHI Grant Numbers JP17H01081, JP19K23445, JP20K14500, JP21H04473, JP23K25904, and JP23H00094.

References

[1] J. Tiedau *et al.*, "Laser Excitation of the Th-229 Nucleus," *Phys. Rev. Lett.*, **133**, 013201 (2024).
[2] L. von der Wense *et al.*, "Direct detection of the ^{229}Th nuclear clock transition," *Nature*, **533**, 47 (2016).
[3] B. Seiferle *et al.*, "Lifetime Measurement of the ^{229}Th nuclear isomer," *Phys. Rev. Lett.*, **118**, 042501 (2017).
[4] F. F. Karpeshin and M. B. Trzhaskovskaya, "Impact of the ionization of the atomic shell on the lifetime of the ^{229m}Th isomer," *Nucl. Phys. A*, **969**, 173 (2018).

Copyright on 7th Asia-Pacific Symposium on Radiochemistry 2025 - R1-02 -

7th Asia-Pacific Symposium on Radiochemistry *September 14 ~ 19, 2025 • Kunibiki Messe • Shimane, Japan*

Barrier distribution and excitation function measurements of $^{51}V+^{159}Tb$ for estimating optimal reaction energy for new element synthesis

Y. Yamanouchi[1,2], P. Brionnet[2], S. Sakaguchi[1,2], T. Cap[3], M. Forge[4], T. Fukatsu[1], H. Haba[2], D. Kaji[2], S. Kimura[5], K. Morimoto[2], Y. Michimoto[1,2], T. Niwase[1,2], H. Sakai[2], M. Tanaka[2,6]

[1]*Department of Physics, Kyushu University: 744, Motooka, Nishi-ku, Fukuoka 819-0395*
[2]*RIKEN Nishina Center: 2-1 Hirosawa, Wako, Saitama 351-0106, Japan*
[3] *National Centre for Nuclear Research: asteura 7, 02-093 Warsaw, Poland*
[4]*Université de Strasbourg: CNRS, IPHC UMR 7178, F-67000 Strasbourg, France*
[5]*KEK Wako Nuclear Science Center: Wako, Sataima 351-0106, Japan*
[6]*Faculty of Arts and Science, Kyushu University: 744, Motooka, Nishi-ku, Fukuoka 819-0395, Japan*

The major difficulty in the synthesis of superheavy elements is the extremely small and energy-sensitive cross sections. To estimate the optimal beam energy, we have been developing a method based on the quasielastic scattering. This method has been verified only with relatively light projectiles from ^{22}Ne to ^{48}Ca. Recently, we tested the validity of this method using the $^{51}V+^{159}Tb$ system at SRILAC/GARIS-III. The ^{51}V beam has been chosen because it is used for the search of element 119 at RIKEN. The experimentally derived optimum energy (E_{opt}) matches the side-collision barrier (B_{side}), confirming the reliability of the method for ^{51}V beam on deformed nuclei around $A \approx 160$.

1 INTRODUCTION

Elements up to oganesson have been discovered, completing the seventh period of the periodic table. The discovery of superheavy elements is critically important for deepening our understanding of the stability of nuclei and the limits of their existence. Search for new elements of the eighth period is being conducted at several facilities. At RIKEN, element 119 is being searched using a $^{51}V+^{248}Cm$ hot fusion reaction. The production cross section of the superheavy nuclei is extremely small, and it takes several years of experiments to synthesize a new element. Even a few percent change in the reaction energy can reduce the cross section by more than one order of magnitude. For example, Fig. 1 is the excitation function for the reaction of $^{248}Cm(^{48}Ca, 4n)^{292}Lv$ [1,2] and shows a deviation of only about 4% in beam energy can drastically reduce the cross section. Therefore, the reaction energy is a crucial experimental parameter in the search of new elements. However, its theoretical predictions range widely, making it difficult to determine the reaction energy based solely on the predictions.

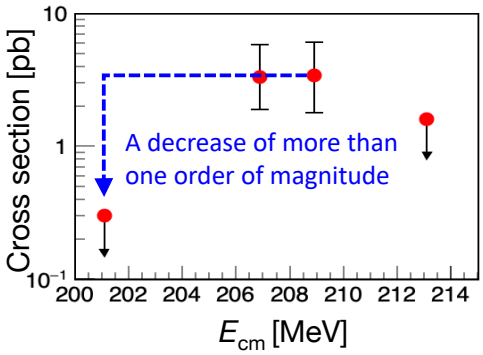


Fig. 1. The evaporation residue excitation function for the reaction of $^{248}Cm(^{48}Ca, 4n)^{292}Lv$ [1,2]. Red points with arrows indicate an upper limit.

2 OBJECIVES, METHODS and RESULTS

Under these circumstances, we have been developing a method to estimate the optimal reaction energy based on the experimentally obtained quasielastic (QE) barrier distribution [3,4]. Although this method has been systematically studied for various projectile nuclei ranging from ^{22}Ne to ^{48}Ca with ^{248}Cm target, it has not yet been validated using a reaction system involving ^{51}V and deformed nucleus. Therefore, a systematic investigation using ^{51}V beam is necessary.

The aim of the present study [5] is to advance our understanding of the mechanism of heavy-ion fusion reactions involving deformed nuclei, and to improve both the precision and accuracy of the estimated optimal reaction energies. We measured the fusion reaction and quasielastic scattering of the $^{51}V+^{159}Tb$ system at Super-conducting RIKEN Linear

Copyright on 7th Asia-Pacific Symposium on Radiochemistry 2025- R1-03* -

Accelerator (SRILAC) using gas-filled recoil ion separator (GARIS-III) [6]. The former and the latter data are used to determine the optimal reaction energy E_{opt} and the quasielastic barrier height respectively, which are compared to investigate the mechanism of the heavy-ion fusion reaction involving a deformed target nucleus.

Previous studies have indicated that, for reactions involving prolately deformed nuclei, the fusion barrier associated with the so-called *side collision*—where the projectile first contacts the equatorial region of the target (denoted B_{side})—provides a reliable proxy for the energy that maximizes the evaporation-residue yield. In the present work, we have undertaken examination of this conjecture by directly comparing the experimentally determined optimal beam energy E_{opt} with B_{side} for the ^{51}V+^{159}Tb system. Figure 2 shows the *xn* channels evaporation residue excitation function with B_{side} and E_{opt}. The result indicates that the beam energy can be set equal to B_{side}, taking into account the experimental efficiency. Our results confirm the reliability of the QE barrier distribution method for estimating optimal reaction energies involving a ^{51}V beam and deformed target nuclei with mass numbers around 160. In this presentation, we will report on the measurement methods, analysis, and results.

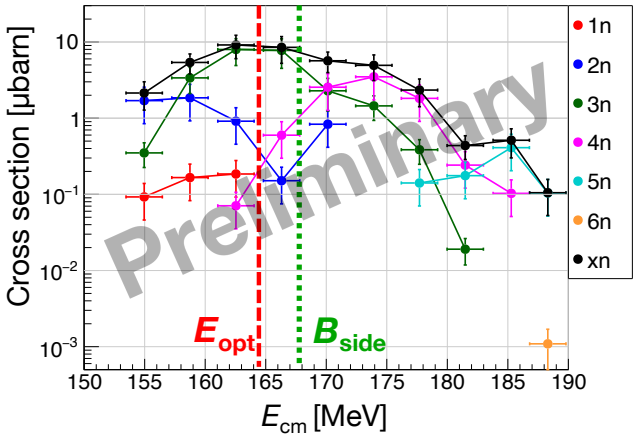


Fig. 2. *xn* channels excitation function for the ^{51}V+^{159}Tb fusion reaction. The vertical dashed line(red) represents the value of E_{opt} and the vertical dotted line(green) represents the value of B_{side}.

3 DISCUSSION

In our paper [5], we reported significant enhancements of the cross sections for charged-particle emission channels compared to neutron emission channels, notably observing an $\alpha 3n$ cross section approximately an order of magnitude higher than that of the $3n$ channel. These findings, in comparison with reactions with lighter projectiles such as ^{48}Ca and ^{50}Ti on the same ^{159}Tb target, suggest projectile-dependent fusion dynamics. These results will also be briefly introduced in our presentation.

References

[1] S. Hofmann *et al.*, Eur. Phys. J. A **48**, 62 (2012).
[2] Yu. Ts. Oganessian, *et al.*, Phys. Rev. C **70**, 064609 (2004).
[3] T. Tanaka *et al.*, Phys. Rev. Lett. **124**, 052502 (2020).
[4] M. Tanaka, S. Sakaguchi *et al.*, J. Phys. Soc. Jpn. **91**, 084201 (2022).
[5] P. Brionnet *et al.*, Phys. Rev. C **110**, 064601 (2024).
[6] H. Sakai *et al.*, Eur. Phys. J. A **58**, 238 (2022).

Copyright on 7th Asia-Pacific Symposium on Radiochemistry 2025- R1-03* -

7th Asia-Pacific Symposium on Radiochemistry *September 14 ~ 19, 2025 • Kunibiki Messe • Shimane, Japan*

Direct mass measurement of ^{252}Cf fission fragments with MRTOF-MS

G. Otsuka[1], T. Niwase[1], S. Kimura[2], H. Haba[3], H. Ishiyama[3], M. Rosenbusch[3], S. Sakaguchi[1], P. Schury[2], M. Wada[2, 4]

[1] *Department of Physics, Kyushu University, Fukuoka, 819-0395, Japan*
[2]*Wako Nuclear Science Center (WNSC), Institute of Particle and Nuclear Studies (IPNS), High Energy Accelerator Research Organization (KEK), Wako 351-0198, Japan*
[3]*RIKEN Nishina Center for Accelerator-Based Science, Wako 351-0198, Japan*
[4]*Institute of Modern Physics, Huizhou branch, Chinese Academy of Science, Huizhou 516000, China*

1 Introduction

The mass of a nucleus is a physical quantity unique to each nuclide. Experimental measurement and determination of the mass of nucleus play an important role in understanding nuclear structure and reactions in nuclear chemistry and nuclear physics. In particular, in the field of astrophysics, the *r*-process, which produces neutron-rich nuclei through successive and rapid neutron capture followed by β^--decays, is considered responsible for the production of approximately half of the heavy nuclides in the nature beyond iron. High precision mass measurements of neutron-rich isotopes are required for further understanding of *r*-process [1]. However, due to the difficulty of the experimental accessibility in this region, direct mass measurements have progressed slowly. While the masses of nuclides near the stable nuclides have been measured with high precision, many of those are determined indirectly such as measurement of *Q* values of decay. In this study, we directly measure the masses of neutron-rich isotopes produced in the spontaneous fission of ^{252}Cf and compare the results with the literature value of 2020 Atomic Mass Evaluation (AME20) [2, 3].

2 Experiment and Analysis

We have performed this mass measurement at RIKEN with a multi-reflection time-of-flight mass spectrograph (MRTOF-MS) [4]. The experimental setup consisted of a cryogenic He gas cell, ion transport system, a radio-frequency quadrupole (RFQ) trap, and the MRTOF-MS [5]. A ^{252}Cf source is installed in front of the gas cell. The fission fragments from ^{252}Cf source are stopped and thermalized in the He gas cell. The thermalized ions are extracted to the RFQ by an rf-carpet [6] and transported to flat trap [7], where the ions are accumulated. Subsequently, accumulated ions are injected into the MRTOF-MS. After the ions make a certain number of reflections, the TOFs of the ions of interest are measured.

Figure 1 shows the observed isotopes in our study, stable nuclides [8] around them and magic number line. 26 isotopes of 7 elements have been observed.

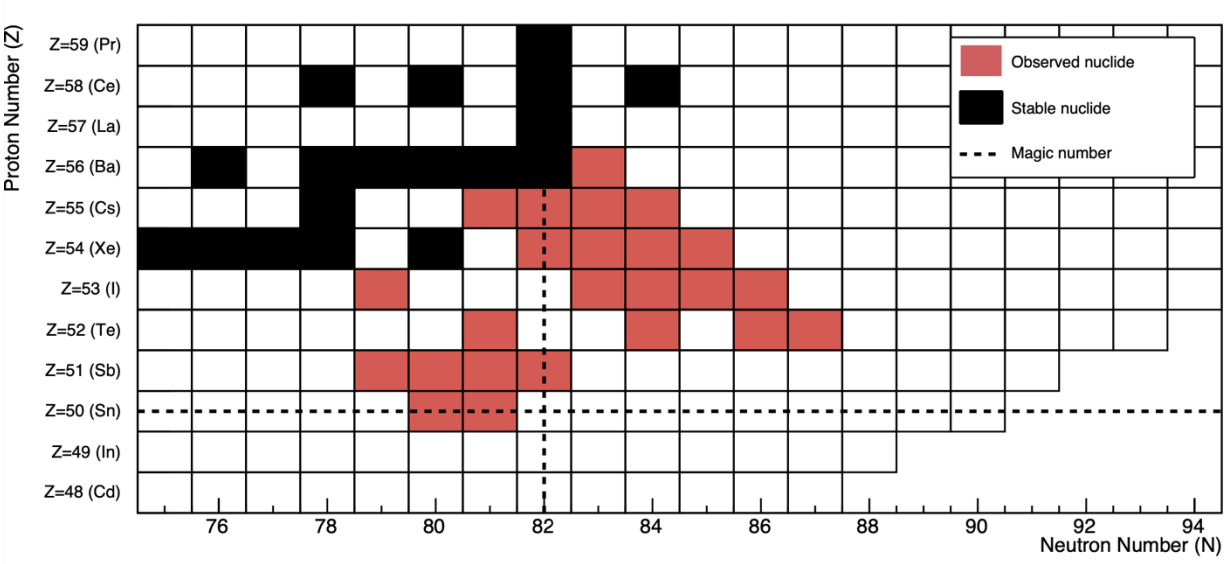


Fig. 1. Location of the observed nuclides on the nuclear chart. The red squares represent the observed nuclides. The black squares represent the stable nuclides. The two dotted lines represent magic number, $Z = 50$ and $N = 82$.

Copyright on 7th Asia-Pacific Symposium on Radiochemistry 2025- R1-04* -

The single-reference method [9] was used to determine the masses of the observed ions by measuring the time-of-flight ratio to a reference ion. In this method, m_X, the mass of analyte ion X, is given by Eq.(1):

$$m_{\mathrm{X}} = \left(\frac{t_{\mathrm{X}}-t_0}{t_{\mathrm{ref}}-t_0}\right)^2 m_{\mathrm{ref}}, \quad (1)$$

where t_X and t_{ref} are the time-of-flight of analyte ion and the reference ion, respectively. m_{ref} represents the mass of the reference ion, t_0 is the delay between the time-to-digital converter start signal and ion's actual ejection from the ion trap.

The atomic mass of nuclide, M_X, is given by Eq.(2):

$$M_{\mathrm{X}} = q_{\mathrm{X}}\left[\left(\frac{t_{\mathrm{X}}-t_0}{t_{\mathrm{ref}}-t_0}\right)^2 m_{\mathrm{ref}} + m_{\mathrm{e}}\right], \quad (2)$$

where q_X is charge state of the analyte ion, and m_e is the electron mass.

The analysis is ongoing, details and results will be presented and discussed at the symposium.

References

[1] H. Schatz, *International Journal of Mass Spectrometry* **349,** 181 (2013)
[2] W. Huang, M. Wang, F. Kondev, G. Audi and S. Naimi, *Chinese Physics C* **45**, 030002 (2021).
[3] M. Wang, W. Huang, F. Kondev, G. Audi and S. Naimi, *Chinese Physics C* **45**, 030003 (2021).
[4] P. Schury, M. Wada, Y. Ito, F. Arai, S. Naimi, T. Sonoda, H. Wollnik, V.A. Shchepunov, C. Smorra and C. Yuan, *Nuclear Instruments and Methods in Physics Research Section B: Beam Interactions with Materials and Atoms* **335**, 39 (2014).
[5] S. Kimura, M. Wada, H. Haba, H. Ishiyama, S. Ishizawa, Y. Ito, T. Niwase, M. Rosenbusch, P. Schury and A. Takamine, *Phys. Rev. C* **110**, 045810 (2024).
[6] M. Wada, Y. Ishida, T. Nakamura, Y. Yamazaki, T. Kambara, H. Ohyama, Y. Kanai, T. M. Kojima, Y. Nakai, N. Ohshima, A. Yoshida, T. Kubo, Y. Matsuo, Y. Fukuyama, K. Okada, T. Sonoda, S. Ohtani, K. Noda, H. Kawakami and I. Katayama, *Nuclear Instruments and Methods in Physics Research Section B: Beam Interactions with Materials and Atoms* **204**, 570 (2003).
[7] Y. Ito, P. Schury, M. Wada, S. Naimi, C. Smorra, T. Sonoda, H. Mita, A. Takamine, K. Okada, A. Ozawa and H. Wollnik, *Nuclear Instruments and Methods in Physics Research Section B: Beam Interactions with Materials and Atoms* **317**, 544 (2013).
[8] F. Kondev, M. Wang, W. Huang, S. Naimi and G. Audi, *Chinese Physics C* **45**, 030001 (2021).
[9] Y. Ito, P. Schury, M. Wada, S. Naimi, T. Sonoda, H. Mita, F. Arai, A. Takamine, K. Okada, A. Ozawa and H. Wollnik, *Phys. Rev. C* **88**, 011306 (2013).

Copyright on 7th Asia-Pacific Symposium on Radiochemistry 2025- R1-04* -

Invited & Contributed Talk | [R7]Environmental Radiochemistry

Mon. Sep 15, 2025 1:30 PM - 3:00 PM JST | Mon. Sep 15, 2025 4:30 AM - 6:00 AM UTC Hall S(Int'l)

[R7] Environmental Radiochemistry

1:30 PM - 2:00 PM JST | 4:30 AM - 5:00 AM UTC

[R7-01(Invited)]

A RAPID ANALYSIS OF RADIOSTRONTIUM IN ENVIRONMENTAL WATER USING STRONTIUM SORBENTS

*Yoshimune Ogata[1], Haruka Minowa[2], Sadao Kojima[1], Yuka Kato[3], Keisuke Sueki[4], Shinji Sugihara[5], Tetsuya Arinobu[1] (1. Aichi Medical University (Japan), 2. The Jikei University School of Medicine (Japan), 3. Aloka Co. Ltd. (Japan), 4. Tokyo Metropolitan University (Japan), 5. Oita University (Japan))

2:00 PM - 2:20 PM JST | 5:00 AM - 5:20 AM UTC

[R7-02]

EFFECTS OF CALCIUM APPLICATION ON CAESIUM UPTAKE AND TRANSLOCATION IN PLANTS

*Masashi Kihana[1], Mutsumi Yamagami[1], Yoshihito Ohtsuka[1], Yuichi Takaku[1,2], Yusuke Unno[1], Akira Takeda[1] (1. Department of Radioecology, Institute for Environmental Sciences (Japan), 2. Faculty of Pure and Applied Sciences, Tsukuba University (Japan))

2:20 PM - 2:40 PM JST | 5:20 AM - 5:40 AM UTC

[R7-03*]

ASSESSING POST-REMEDIATION MOBILITY RISKS OF URANIUM(IV) THROUGH COLLOIDAL TRANSPORT AND ISOTOPIC SIGNATURES

*Xinyi Shi[1], Xiaoyan Wei[1], Duoqiang Pan[1], Wangsuo Wu[1] (1. Lanzhou University (China))

2:40 PM - 3:00 PM JST | 5:40 AM - 6:00 AM UTC

[R7-04*]

Soil properties: The case study of the Coffee Field, AIRID Training Center, Chiang Mai University, Thailand.

*Khemruthai Kheamsiri[1], Naofumi Akata[2], Chutima Kranrod[2], Hirofumi Tazoe[2], Tarika Thumwijit[3], Ilsa Rosianna[1], Haruka Kuwata[1], Krit Khetanun[4], Narit Yimyam[4], Yusuke Unno[5], Akira Takeda[5] (1. Graduate School of Health Sciences, Hirosaki University (Japan), 2. Institute of Radiation Emergency Medicine, Hirosaki University (Japan), 3. Faculty of Associated Medical Sciences, Chiang Mai University (Thailand), 4. Faculty of Agriculture, Chiang Mai University (Thailand), 5. Department of Radioecology, Institute for Environmental Sciences (Japan))

©APSORC25

7th Asia-Pacific Symposium on Radiochemistry *September 14 ~ 19, 2025 • Kunibiki Messe • Shimane, Japan*

A RAPID ANALYSIS OF RADIOSTRONTIUM IN ENVIRONMENTAL WATER USING STRONTIUM SORBENTS

Yoshimune Ogata[1], Haruka Minowa[2], Sadao Kojima[3], Yuka Kato[4] Keisuke Sueki[5], Shinji Sugihara[6], Tetsuya Arinobu[7]

[1]*Aichi Medical University: 1-1 Yazakokarimata, Nagakute, Aichi, Japan, 480-1195, yoshimune.ogata@aichi-med-u.ac.jp*
[2]*The Jikei University School of Medicine: 3-25-8, Nishisinbashi, Minato, Tokyo, Japan, 105-8461, minowa@jikei.ac.jp*
[3]*Aichi Medical University: 1-1 Yazakokarimata, Nagakute, Aichi, Japan, 480-1195, kojima@aichi-med-u.ac.jp*
[4]*Aloka Co. Ltd., 1-20-8 Nakacho, Musashino-shi, Tokyo, Japan, 180-0006, Japan, yuka.kato@aloka.co.jp*
[5]*Tokyo Metropolitan University: 1-1, Minamiosawa, Hachioji, Tokyo, Japan, 192-0364, ksueki727@gmail.com*
[6]*Oita University: 1-1 Idaigaoka, Hasama-machi, Yufu, Oita, Japan, 879-5593, sugihara-shinji@oita-u.ac.jp*
[7]*Aichi Medical University: 1-1 Yazakokarimata, Nagakute, Aichi, Japan, 480-1195, b1050561@gmail.com*

The conventional methods to analyse radiostrontium in environmental water are time-consuming complicated procedures using a lot of deleterious substances. A rapid, simple and safe analysis of radiostrontium is desired. We attempted to develop a new method using a barium silicate-based strontium sorbent. The procedure took several hours to obtain analytical results, and no deleterious substances was used. The minimum detectable concentration of ^{90}Sr was 0.6 Bq L^{-1} in seawater, which is one-fiftieth of the legal wastewater concentration limit, 30 Bq L^{-1}.

1 INTRODUCTION

Since ^{89}Sr and ^{90}Sr tend to accumulate in bones and to increase a risk of bone cancer and leukaemia, therefore there is a high social interest in the results of measurements of environmental water. Because ^{89}Sr and ^{90}Sr are pure beta emitters they must be chemically separated from other elements before radioactivity measurement. The conventional analytical methods require the use of large amounts of deleterious substances, skilled techniques, and two to three weeks to obtain the results [1]. A rapid, simple and safe analysis of radiostrontium is desired.

We have been researching a rapid measurement method for radiostrontium using a sorbent whose main component is barium silicate (Pureceram MAq®, hereafter P-MAq, Nippon Chemical Industrial Co., Ltd.). The solvent is a white powder, the particle size 2-300 μm, that is insoluble in water and selectively sorbs Sr. After adding P-MAq to a sample water and stirring for 4 hours, it can sorb about 90% of Sr in the water. In this report, the Sr sorption properties of P-MAq are reported and some recommended analytical methods are shown.

2. MATERIALS AND METHODS

2.1 Required Amount of the Sr Sorbent

The Sr sorbent, each amount was 50, 100, 120, 130 and 150 mg, was added to 100-mL simulated seawater spiked with ^{85}Sr. The water was stirred for 240 min. Along the stirring, 2 mL of the water was collected at intervals from 15 to 240 minutes, and filtered with a syringe filter (pore size 0.45 μm). The activity of the filtrate water, i.e.; the liquid phase, was measured with a gamma counter (WIZARD^2, PerkinElmer Co. Ltd.).

2.2 Behavior of Major Elements in Seawater and Cs

To investigate the behavior of the major elements in seawater, Na^+, K^+, Mg^{2+}, and Ca^{2+}, 100 mg of P-MAq was added to 100-mL artificial seawater. Along the stirring, 2 mL of the water was collected at intervals from 5 to 120 minutes, and filtered with the syringe filter. The concentrations of the elements were measured with an ICP-AES (Thermo Jarrel Ash, IRIS/AP).

To investigate the behavior of radiocaesium, artificial seawater including 1 kBq of ^{134}Cs was prepared and 100 mg of P-MAq was added. Along the stirring, 2 mL of the water was collected at intervals from 10 to 240 minutes and filtered with the syringe filter. After stirring for 3 hours, the sample was left for 23 hours, and finally the solid phase (P-MAq) and liquid phase were separated by centrifugation. The radioactivity of the filtrate, and separated P-MAq was measured using an HPGe semiconductor detector (GEM-35190S, ORTEC).

2.3 The Minimum Detectable Concentration

The Minimum Detectable Concentration (MDC) in Bq L^{-1} was calculated by the following equations;

$$n_{DL} = \frac{2}{t} + \sqrt{\frac{4}{t^2} + 8\frac{n_b}{t}} \quad (1), \qquad A_{DL} = \frac{n_{DL}}{60 \cdot \varepsilon \cdot Y} \quad (2), \text{ and} \qquad MDC = A_{DL}\frac{1000}{V} \quad (3)$$

here, t is the measurement time (min), n_b is the background (cpm), n_{DL} is the minimum detectable count rate (cpm), ε is the counting efficiency, Y is the chemical yield of Sr, A_{DL} is the minimum detectable activity (Bq) and V is the sample volume (mL).

3. RESULTS AND DISCUSSION

Copyright on 7th Asia-Pacific Symposium on Radiochemistry 2025 - R7-01 -

3.1 Required Amount of the Sr Sorbent

Figure 1 shows the change over time in the ^{85}Sr residual rate in the filtrate. The sorption rate to P-MAq was about 90% after 4 hours for 130 mg or more. Therefore, 130 mg of P-MAq was required to absorb Sr in 100 mL of seawater.

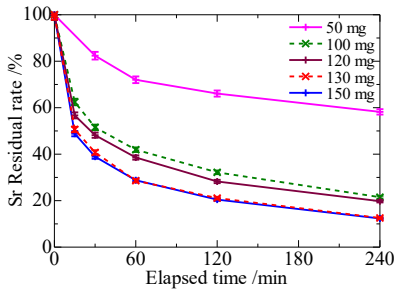


Fig. 1 The ^{85}Sr residual rate in the filtrate.

3.2 Behavior of major elements in seawater and Cs

Figure 2 shows the change over time in the four elements in the solution. The concentrations of those elements were almost constant over the range of stirring times from 5 to 120 minutes, and more than 98% remained in the solution. The adsorption rate to P-MAq is considered to be less than 2%. It was confirmed that the main elements in seawater, such as Na, K, Mg, and Ca, were not adsorbed on P-MAq.

As for Cs, the residual rate of ^{134}Cs in the solution after 2 hours of stirring was over 95%. The activity of ^{134}Cs in the sorbent was measured for 1,000 seconds with the HPGe detector. It was below the detection limit, and the Cs adsorption rate was below 0.001%. It was verified that Cs was not sorbed at all to P-MAq. If a solution included some radiocaesium, P-MAq can be applied to separate radiostrontium.

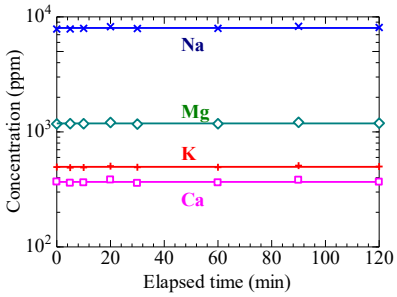


Fig. 2 The concentration of the four elements in the solution.

3.3 The Analysis Method

A recommended procedure of the Sr analyses method using P-MAq [2] is as follows;

(1) Filter the environmental water through a membrane filter to remove suspended solids, and add 200 μL of 4M HCl to 50 mL of sample
(2) Add 65 mg of P-MAq and stir for 4 hours
(3) Suction filtering with a 22 mmϕ membrane filter (pore size 0.45 μm)
(4) Put the filter on a planchet and dry
(5) Measure the sample with a low background gas flow counter

The other methods are using liquid scintillation counter; these methods will be shown at the conference.

3.4 The Minimum Detectable Concentration

By the method above, the measurement time was 60 min, the background of the gas flow counter was 0.12 cpm, the counting efficiency for ^{90}Sr was 10%, the chemical yield was 90%, and the sample volume was 50 mL. The MDC was calculated to be 0.6 Bq L^{-1}, which was one-fiftieth of the legal wastewater concentration limit, 30 Bq L^{-1}.

4. CONCLUSIONS

A new analysis method of radiostrontium in environmental water was suggested. Sixty-five milligram of a strontium solvent, Pureceram®MAq, was added to 50 mL of sample water, and stirring for 4 hours. The sorbent was collected on a membrane filter by suction filtration. After drying, the sample was measured for 60 minutes with a low background gas flow counter. The MDC was calculated to be 0.6 Bq L^{-1}, which was one-fiftieth of the legal wastewater concentration limit, 30 Bq L^{-1}. The procedure took under 6 hours to obtain the results, and no deleterious substances was required. This demonstrated that the method can be applied to the rapid and safe analysis of radiostrontium.

ACKNOWLEDGMENTS

We would like to thank the late Dr. Michio Aoyama for his valuable cooperation and advices. We thank Nippon Chemical Industrial Co. Ltd. for providing Pureceram MAq for research use. This research was partially supported by the following grants; (1) Radiation Safety Research Promotion Fund (JPJ007057) 2021, "Development of a safe, rapid, and inexpensive analytical method for strontium in water, (2) Environmental Radioactivity Research Network Center (Grant No. F-21-19, F-22-06, P-23-12, P-24-09), and (3) JST FY2024 Grant-in-Aid for Scientific Research Substrate C, Grant No. 24K08310.

References

[1] Ministry of Education, Culture, Sports, Science and Technology, *Radioactivity Measurement Series 2, Radioactive Strontium Analysis Method Revised in 2003*, (2003) (in Japanese)
[2] H. Minowa, et. al., "Characterization of barium silicate-based adsorbent for Sr in seawater and terrestrial water", *Proc. 21st Workshop of Environ. Radioactivity*, Tsukuba, Mar. 12-13, 2020, p.176, KEK (2020) (in Japanese)

7th Asia-Pacific Symposium on Radiochemistry *September 14 ~ 19, 2025 • Kunibiki Messe • Shimane, Japan*

EFFECTS OF CALCIUM APPLICATION ON CAESIUM UPTAKE AND TRANSLOCATION IN PLANTS

Masashi Kihana[1], Mutsumi Yamagami[1], Yoshihito Ohtsuka[1], Yuichi Takaku[1, 2], Yusuke Unno[1], Akira Takeda[1]

[1] *Department of Radioecology, Institute for Environmental Sciences:, Obuchi 1-7, Rokkasho, Aomori, Japan, 039-3212*
Email Address: m.kihana@ies.or.jp, yamagami@ies.or.jp, ohtsuka@ies.or.jp, unno@ies.or.jp, takeda@ies.or.jp
[2] *Present address: Faculty of Pure and Applied Sciences, Tsukuba University: Tennodai 1-1-1, Tsukuba, Ibaraki, Japan, 305-8577, Email Address: takaku.yuichi.fp@u.tsukuba.ac.jp*

When an accident occurs at a nuclear facility, radioactive contamination of the surrounding areas becomes a major concern, and it is extremely important to reduce internal radiation exposure due to radiation protection. Based on previous nuclear accidents, countermeasures targeting radiocaesium (e.g., ^{134}Cs, ^{137}Cs) which is one of the most abundantly released radionuclides are particularly necessary. One such strategy for reducing internal radiation exposure is to suppress the translocation of Cs from soil or plant shoots to edible parts. We focused on the application of calcium (Ca) as a potential approach to mitigate Cs accumulation in crops. In this study, we conducted experiments on Arabidopsis thaliana and Oryza sativa L. involving root application, foliar spraying, and immersion of rice panicles as Ca application. The results indicated that Cs uptake and translocation were suppressed in all cases by Ca application.

1. INTRODUCTION

As observed in the Fukushima Daiichi Nuclear Power Plant accident, various radionuclides are released into the environment after nuclear accident, among which radiocaesium is notable for its relatively large amount release.

Radiocaesium in the plume released into the atmosphere are deposited onto land surfaces over time and its concentration in soil and plant shoots is then increased. Crops grown in the area may uptake radiocaesium from both soil and leaf surfaces, eventually translocating it into edible parts. This can result in increased internal radiation dose for humans who consume the crops. Therefore, the reduction of radiocaesium in edible parts of plants is an important issue to radiation protection.

It is known that caesium (Cs) is uptake into plant tissue through transporters involved in potassium (K) uptake, and thus a method has been developed to suppress Cs influx by K fertilization [1]. However, Cs uptake through other transporters has also been reported [2,3]. Under high K concentrations (0.2 mM or higher), Cs uptake occurs mainly through voltage-independent cation channels (VICCs), some of which are inhibited by millimolar levels of calcium (Ca) [4]. Based on this, we focused on Ca application as a method for suppressing Cs uptake and translocation. In this study, we used *Arabidopsis thaliana* (*Arabidopsis*) as a major plant of dicotyledons, and *Oryza sativa L.* (rice) as a major plant of monocotyledons and crop species. This presentation reports the effects of Ca application in various parts of these plants on Cs uptake and translocation.

2. MATERIALS AND METHODS

2.1 Suppression of Caesium-133 Uptake and Translocation by Calcium Addition to Culture Medium in *Arabidopsis* and Rice

Arabidopsis was grown for three weeks on MS-agar medium with a 0.01 µM of stable Cs (^{133}Cs), and 0.5, 1.0, 2.0 and 3.0 mM of Ca. The ^{133}Cs concentration in shoots were measured for each Ca concentration.

Rice seedlings were grown in soil for three weeks, then hydroponically for six weeks. Thereafter, they were cultivated for two weeks in double-strength Kasugai-solution containing a 0.01 µM of ^{133}Cs, and 0.2, 0.5, 1.0, 3.0, 6.0 and 10 mM of Ca. The concentration of ^{133}Cs in the leave were determined by using an ICP-Q-MS (Agilent 7700).

2.2 Suppression of Caesium-133 Uptake and Translocation by Foliar Application of Calcium During the Vegetative Stage in Rice

Rice plants were grown outdoors in soil and treated twice weekly during the vegetative stage with foliar application of a 1.25 µM of ^{133}Cs, and several concentrations (0, 2.0, 5.0, 10, 20 and 30 mM) of Ca solution. After harvest, the ^{133}Cs concentration in the brown rice was measured by using the ICP-Q-MS.

2.3 Suppression of Caesium-133 Translocation to Panicles by Immersion in Calcium Solution During the Ripening Stage in Rice

Copyright on 7th Asia-Pacific Symposium on Radiochemistry 2025 - R7-02 -

Rice grew hydroponically outdoors. One week before heading, the ^{133}Cs concentration in the hydroponic solution was adjusted to 0.01 µM. During flowering and ripening stages, which was between two and three months after planting, rice panicles were immersed twice weekly in solutions with Ca concentration of 0, 2.5, 5.0, 10, and 20 mM. After harvest, the ^{133}Cs concentration in brown rice was analyzed by using the ICP-Q-MS.

3. RESULTS AND DISCUSSIONS

3.1 Suppression of Caesium-133 Uptake and Translocation by Calcium Addition to Culture Medium in *Arabidopsis* and Rice

In *Arabidopsis*, Caesiums-133 concentrations in the shoot decreased with increasing Ca concentrations between 0.5–2.0 mM. The ^{133}Cs concentrations in rice leaves also observed a similar trend in Ca concentration range of 0.2–3.0 mM. These results suggest that Cs root uptake is suppressed by Ca in the growth media or hydroponic solution in young *Arabidopsis* and rice plants.

3.2 Suppression of Caesium-133 Uptake and Translocation by Foliar Application of Calcium During the Vegetative Stage in Rice

A decreasing trend in ^{133}Cs concentration in the brown rice was observed with increasing Ca concentration in the foliar application. The Ca concentration of the spray solution with the highest suppression effect was 30 mM, which decreased the ^{133}Cs concentration in the brown rice by approximately 35% compared to that when a solution without Ca was sprayed on them. This suggests that even foliar-absorbed Cs during the vegetative stage can be suppressed by simultaneous Ca application.

3.3 Suppression of Caesium-133 Translocation to Panicles by Immersion in Calcium Solution During the Ripening Stage in Rice

Caesium-133 concentrations in the brown rice decreased with increasing Ca concentrations in the immersion solution. In particular, Caesium-133 concentration in the brown rice soaked in the immersion solution with a Ca concentration of 20 mM decreased by 20% compared to that in water. This suggests that root-absorbed Cs translocation to panicles during the ripening stage is also suppressed by Ca.

4. CONCLUSIONS

We focus on the Ca applications of root treatment, foliar spraying, and panicle immersion as methods to suppress Cs uptake into roots and leaves, and Cs translocation to brown rice, in *Arabidopsis* and rice. Experiments using young plants and rice during the vegetative stage suggest that both root and foliar Cs uptake are suppressed by Ca. Additionally, experiments during the ripening stage indicate that the translocation of root-absorbed Cs to panicles is also suppressed by Ca.

ACKNOWLEDGMENTS

We would like to express our sincere gratitude to the technical staff at ZAX Co., Ltd. for their assistance with cultivation and sampling, and the analytical team at Entex Co., Ltd. for their assistance with analysis. This study was performed under a contract with the government of Aomori Prefecture, Japan.

References

[1] Kato *et al.*, “Potassium fertilizer and other materials as countermeasures to reduce radiocesium levels in rice: Results of urgent experiments in 2011 responding to the Fukushima Daiichi Nuclear Power Plant accident”, *Soil Sci. Plant Nutr.*, **61**, 179-190 (2015)

[2] Yamagami *et al.*, “Isolation and characterization of *CNGC17* gene from *Arabidopsis thaliana*”, *Proceedings of the international symposium on environmental modeling and radioecology*, Aomori, Japan, 328-331 (2007)

[3] Ashraf *et al.*, “ATP binding cassette proteins ABCG37 and ABCG33 function as potassium-independent cesium uptake carriers in *Arabidopsis* roots”, *Mol. Plant*, **14**, 664-678 (2021)

[4] White *et al.*, “Tansley Review No. 113: Mechanisms of caesium uptake by plants”, *New Phytol.*, **147**, 241-256 (2001)

Copyright on 7th Asia-Pacific Symposium on Radiochemistry 2025 - R7-02 -

ASSESSING POST-REMEDIATION MOBILITY RISKS OF URANIUM(IV) THROUGH COLLOIDAL TRANSPORT AND ISOTOPIC SIGNATURES

Xinyi Shi[2], Xiaoyan Wei[2], Duoqiang Pan[1,2], Wangsuo Wu[1,2]

[1]*Frontiers Science Center for Rare Isotopes, Lanzhou University, Lanzhou 730000, China*
[2]*School of Nuclear Science and Technology, Lanzhou University, Lanzhou 730000, China*

Uranium (U) contamination poses significant challenges to environmental safety and long-term nuclear waste management. In-situ reductive immobilization, a widely adopted strategy for mitigating U migration, relies on converting soluble hexavalent U(VI) to sparingly soluble tetravalent U(IV). However, recent studies highlight that U(IV) species—such as nanoparticulate uraninite (UO_{2+x}) and amorphous U(IV) — exhibit variable stability under environmental conditions, with residual mobility risks mediated by colloids or microbial activity. The long-term stability of U(IV) species—such as nanoparticulate uraninite (UO_{2+x}) and amorphous U(IV)—is undermined by their susceptibility to remobilization via colloid-mediated transport and microbially driven dissolution. This study addresses these parallel risks while advancing uranium isotope fractionation ($\delta^{238}U$) as a novel tool to monitor post-remediation U(IV) mobility, which systematically investigates the mechanisms governing U(IV) migration in reductive porous media and microbial systems, and proposes a novel isotopic tracing approach to monitor U(IV) mobility.

1 NATURAL COLLOID IMPACT

Natural colloidal particles exert a pivotal influence on the facilitation and regulation of contaminant transport processes within environmental matrices, to evaluate the role of colloids in U(IV) mobility under reductive conditions, column experiments were conducted using pyrite (FeS2)-doped quartz sand as a reductive porous medium, bentonite colloids, uranyl nitrate (U(VI)), and humic acid (HA) as a representative material or organic ligand. Experiments varied pH (4.0–6.0) and ionic strength (1–10 mMNaCl), with breakthrough curves and retention profiles analyzed alongside TEM, XPS, and XAFS characterization. Results indicated that pyrite effectively reduced U(VI) to U(IV), with XANES confirming >21% U(IV) formation. However, EXAFS revealed that the dominant product was non stoichiometric UO_{2+x} with particle sizes of 6 – 12 nm, which readily associated with bentonite colloids. Humic acid (HA) reduced U(IV) reduction efficiency but enhanced colloid-facilitated U migration by 10 – 20% via surface complexation. High ionic strength compressed colloidal double layers, reducing U(IV)-colloid mobility, whereas low ionic strength and rising pH promoted colloid stability and U(IV) transport. The stability of U(IV) in pyrite-rich systems is highly dependent on colloid interactions. Organic ligands like HA may paradoxically increase U migration risks despite partial inhibition of reduction, necessitating integrated evaluation of colloid and organic matter impacts in remediation design.

2 BIO-REDUCTIVE IMPACT

RMicrobial reduction by Desulfovibrio vulgaris was studied to assess the mobility of biogenic amorphous U(IV). Shifting focus to microbial systems, dynamic column experiments under varying pH (5.00– 8.20) and ionic strength (0–30 mM NaCl) were coupled with size fractionation (ultrafiltration: 1 kDa – 800 nm), TEM, XPS, and FTIR analyses. Results indicated that D. vulgaris achieved >60% U(VI) reduction, generating amorphous U(IV)-microbe aggregates. Size fractionation showed low mobility for large U(IV)-cell aggregates (>800 nm; <5% transport), while sub-1 kDa dissolved U(IV) and sub– 220 nm colloidal U(IV) exhibited around 40% and 25% mobility, respectively. FTIR and XPS indicated U(IV) binding to microbial extracellular polymeric substances (EPS) via carboxyl, phosphate, and thiol groups. Colloidal U(IV) was associated with Fe/S-rich surface coatings, suggesting microbial Fe(II)/S(-II) metabolites influenced U speciation. The closer pH gets to the zero charge point (5.0) and high ionic strength (30 mM) reduced colloidal stability and U(IV) mobility, whereas pH-away-from 5.00 conditions enhanced colloidal transport by 2– 3 × . Biogenic U(IV) mobility is size-dependent, with nano-scale and dissolved species posing significant risks. Strategies to minimize these fractions—such as optimizing pH or coupling microbial reduction with mineral stabilization—are critical for durable remediation. To address monitoring challenges, uranium isotope fractionation (δ238U) was evaluated as a tracer for U(IV) migration. Column experiments with D. vulgaris were combined with HR-ICP-MS analysis of $\delta^{238}U$ in effluent and retained phases, correlated with U(IV) size distribution and speciation. Results indicated that during U(VI) reduction, light isotopes (235U) preferentially partitioned into the solid phase, resulting in δ238U enrichment in mobile phases (Δ 238Ueffluent-solid = +0.8‰ to +1.2‰). Colloidal U(IV) (＜100 nm) exhibited greater fractionation (Δ238U = +0.6‰) than dissolved U(IV) (Δ 238U = +0.3 ‰), linking isotopic signatures to colloid formation. Under U(IV)-colloid-favorable conditions (pH away form 5.00 , low ionic strength), δ238U strongly correlated with U migration flux (R^2 = 0.92), whereas block in column was observed during U(VI) ion transport. δ238U provides a sensitive, non-invasive tool

to distinguish U(IV) and U(VI) migration pathways, particularly in colloid-dominated systems, enhancing monitoring and risk assessment capabilities.

3. CONCLUSIONS

This study demonstrates that U(IV) mobility in remediated sites is governed by colloid interactions, microbial activity, and isotopic fractionation dynamics. Critical findings include: Bentonite and organic ligands enhance U(IV) transport despite partial reduction, demanding colloid management in barrier design. Biogenic U(IV) stability requires control of nano-scale and dissolved species via environmental conditioning or co-precipitation with Fe/S phases. δ238U offers a robust method to track U(IV) mobility, enabling real-time risk assessment in complex subsurface environments. Future work should focus on field validation of isotopic tracing and multifactorial studies integrating geochemical, microbial, and colloidal variables. These advances will support safer, more predictive strategies for uranium-contaminated site remediation

ACKNOWLEDGMENTS

This work was supported by the National Natural Science Foundation of China (22176077); the Fundamental Research Funds for the Central Universities (lzujbky-2023-stlt01).

Copyright on 7th Asia-Pacific Symposium on Radiochemistry 2025- R7-03* -

7th Asia-Pacific Symposium on Radiochemistry *September 14 ~ 19, 2025 • Kunibiki Messe • Shimane, Japan*

SOIL PROPERTIES: THE CASE STUDY OF THE COFFEE FIELD, AIRID TRAINING CENTER, CHIANG MAI UNIVERSITY, THAILAND.

Khemruthai Kheamsiri[1)], Naofumi Akata[2)], Chutima Kranrod[2)], Hirofumi Tazoe[2)], Tarika Thumwijit[3)], Ilsa Rosianna[1)], Haruka Kuwata[1)], Krit Khetanun[4)], Narit Yimyam[4)], Yusuke Unno[5)], Akira Takeda[5)]

[1]*Graduate School of Health Sciences, Hirosaki University: 66-1 Hon-cho, Hirosaki, Aomori, Japan, 036-8564, h23gg703@hirosaki-u.ac.jp, h24mh202@hirosaki-u.ac.jp, kuwata-07@hirosaki-u.ac.jp*
[2]*Institute of Radiation Emergency Medicine, Hirosaki University: 66-1 Hon-cho, Hirosaki, Aomori, Japan, 036-8564, akata@hirosaki-u.ac.jp, kranrodc@hirosaki-u.ac.jp, tazoe@hirosaki-u.ac.jp*
[3]*Faculty of Associated Medical Sciences, Chiang Mai University, 239 Huay Kaew Road, Muang District, Chiang Mai, Thailand, 50200, Tarika.thumvijit@cmu.ac.th*
[4]*Faculty of Agriculture, Chiang Mai University: 239 Huay Kaew Road, Muang District, Chiang Mai, Thailand, 50200, krit.khet@cmu.ac.th, narit.y@cmu.ac.th*
[5]*Department of Radioecology, Institute for Environmental Sciences: 1-7, Ienomae, Rokkasho, Aomori, Japan, 039-3212, unno@ies.or.jp, takeda@ies.or.jp*

1 BACKGROUND

Chiang Mai was one of the most significant contributors to Thailand's economy, playing a pivotal role in agricultural advancement through its commitment to sustainable farming methods [1]. Therefore, understanding soil conditions is crucial for effective soil management. The objective of this study was to estimate the total element concentrations in soil samples from a coffee field in Chiang Mai province, Thailand. This estimation was achieved using X-ray fluorescence (XRF) spectrometry on glass bead preparations, alongside the determination of radionuclide concentrations via HPGe gamma spectrometry.

2 MATERIALS AND METHODS

The study area, the Agricultural Innovation Research, Integration, Demonstration, and Training Center (AIRID), is located at the Nhong Hoi Highland Agricultural Research Station in Pong Yang Sub-district, Mae Rim District, Chiang Mai Province, Thailand (18°55′ 19.6″ N 98°48′ 55.0″ E). The geography of this area is a high hill landscape at an elevation of 850–900 m above sea level, with an average slope of 18–25°. Chiang Mai is a region characterized by Precambrian and Palaeozoic bedrock with dominant igneous (granite, granodiorite), sedimentary, and metamorphic rocks, leading to predominantly reddish-brown, Brown Lateritic, and red-yellow soils derived from granite [2]. We collected a total of 10 samples from a depth of 30 cm from the surface and 10 samples from a depth of 60 cm on July 14, 2023, respectively.

2.1 Gamma-ray analysis measurement

After drying the soil at 110 ℃ for 24 h, the samples were prepared and stored in pre-weighed polystyrene containers (U8; inner diameter = 50 mm, outer diameter = 56 mm, height = 67 mm), following the method described in Hosoda et al. (2013) [3]. After waiting for the equilibrium, the measurements were conducted using an HPGe detector (EGPC 100-P15, CANBERRA). Each measurement was run for 86,000 s. Radionuclide concentrations were decay-corrected to the sampling date. Calibration was performed using standard gamma volume sources (MX033U8PP; Japan Radioisotope Association, Japan), which contained nine mixed nuclides (^{109}Cd, ^{57}Co, ^{139}Ce, ^{51}Cr, ^{85}Sr, ^{137}Cs, ^{54}Mn, ^{88}Y, and ^{60}Co) with five different thicknesses (5, 10, 20, 30, and 50 mm) according to the Japanese Nuclear Regulation Authority.

2.2 XRF measurement

The soil samples were combusted at 800 ℃ for 8 h to decompose the organic material and carbonates. The sample powder and pure lithium tetraborate flux ($Li_2B_4O_7$/$LiBO_2$ Pure, GL Sciences Inc.) were mixed with 1:10 sample-to-flux ratios. The fused-glass beads used herein were made from lithium tetraborate. A mixture of 0.5 g sample powder and 5.0 g flux was fused and cooled in a crucible made of 95% platinum and 5% gold, using the Bead & Fuse Sampler (TK-4100, AmenaTech). After that, the fused bead samples' major elements were determined by XRF (ZSX Primus IV, Rigaku).

3. RESULTS

Copyright on 7th Asia-Pacific Symposium on Radiochemistry 2025- R7-04* -

The results of ^{40}K from HPGe measurement and the calculated abundance of ^{40}K from K_2O are 1,193.4 to 1,879.5 Bq kg $^{-1}$ and 1,281.0 to 2,029.3 Bq kg $^{-1}$, respectively which higher than the previous study of background radiation in soil of Autsavapromporn et al. (2024) that show the ^{40}K ranged from 195.4 to 1,108.6 Bq kg $^{-1}$ [4]. The Fe content shown in TABLE 1 was low compared to some studies related to soil in Japan, such as Tazaki et al. (2015), who studied the radioactive paddy soils in Fukushima, which shows the content of Fe around 8.9% to 14.3% [5].

TABLE 1. XRF measurement of major elements of the 20 soil samples collected from the ARID coffee plantation.

Sample name	Depth (cm)	Concentration per dried soil weight (%)									
		SiO_2	TiO_2	Al_2O_3	Fe_2O_3	MnO	MgO	CaO	Na_2O	K_2O	P_2O_5
A-30-I	30	66.14	0.33	14.86	4.29	0.13	0.35	0.27	0.31	7.81	0.26
B-30-I		68.78	0.32	14.67	3.97	0.14	0.30	0.17	0.30	7.39	0.22
C-30-I		67.82	0.31	14.84	3.98	0.13	0.29	0.07	0.31	7.56	0.13
D-30-I		66.15	0.35	15.45	4.44	0.16	0.34	0.17	0.31	7.64	0.17
E-30-I		66.94	0.39	15.91	4.66	0.21	0.31	0.28	0.28	6.21	0.16
F-30-I		68.29	0.31	14.17	3.76	0.14	0.28	0.15	0.29	7.05	0.14
G-30-I		68.78	0.36	14.75	3.92	0.15	0.28	0.07	0.29	7.18	0.12
H-30-I		66.66	0.35	15.32	3.63	0.16	0.25	0.25	0.31	6.54	0.14
I-30-I		79.70	0.33	16.55	3.70	0.17	0.34	0.13	0.17	5.56	0.12
J-30-I		72.79	0.35	16.41	3.93	0.18	0.38	0.11	0.18	5.66	0.13
Average		69.21	0.34	15.29	4.03	0.16	0.31	0.17	0.28	6.86	0.16
A-60-I	60	65.91	0.33	14.55	3.84	0.17	0.32	0.10	0.30	7.19	0.14
B-60-I		66.19	0.34	15.25	3.89	0.18	0.34	0.06	0.29	6.96	0.09
C-60-I		65.55	0.35	15.37	3.96	0.22	0.29	0.05	0.29	6.75	0.08
D-60-I		65.00	0.36	15.74	4.22	0.18	0.35	0.07	0.31	7.05	0.08
E-60-I		64.95	0.41	16.38	4.33	0.37	0.34	0.19	0.27	5.93	0.08
F-60-I		66.77	0.33	14.69	4.05	0.15	0.33	0.07	0.29	6.76	0.07
G-60-I		66.50	0.34	15.12	4.09	0.20	0.30	0.05	0.30	6.57	0.07
H-60-I		65.09	0.39	16.63	4.28	0.16	0.33	0.16	0.28	6.23	0.07
I-60-I		64.70	0.42	17.75	4.92	0.14	0.41	0.13	0.23	4.93	0.07
J-60-I		64.52	0.43	17.54	4.83	0.16	0.41	0.10	0.25	5.27	0.07
Average		65.52	0.37	15.90	4.24	0.19	0.34	0.10	0.28	6.36	0.08

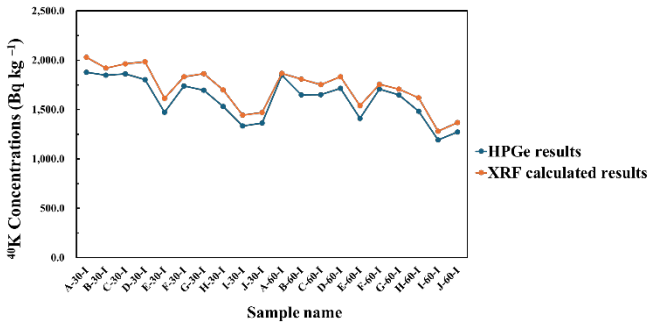


Fig. 1. The figure shows the results of ^{40}K from HPGe measurement and the calculated abundance of ^{40}K from K_2O (XRF) trend of each sample.

ACKNOWLEDGMENTS

This research was supported by the Sasakawa Scientific Research Grant, administered by the Sasakawa Peace Foundation, Grant No. 2024-3026, and by JST SPRING, Grant Number JPMJSP2152. Additionally, the research materials were imported from overseas under the Ministerial Licensing System.

References

[1] Y. Kyaw, T. P. L. Nguyen, E. Winijkul, W. Xue, and S. G. P. Virdis, "The Effect of Climate Variability on Cultivated Crops' Yield and Farm Income in Chiang Mai Province, Thailand," *Climate*, vol. 11, no. 10, 2023, doi: 10.3390/cli11100204.

[2] N. Arunrat, S. Sereenonchai, and R. Hatano, "Effects of fire on soil organic carbon, soil total nitrogen, and soil properties under rotational shifting cultivation in northern Thailand," *J Environ Manage*, vol. 302, p. 113978, 2022, doi: https://doi.org/10.1016/j.jenvman.2021.113978.

[3] M. Hosoda *et al.*, "Activity concentrations of environmental samples collected in Fukushima Prefecture immediately after the Fukushima nuclear accident," *Sci Rep*, vol. 3, no. 1, p. 2283, 2013.

[4] N. Autsavapromporn *et al.*, "Health Impacts of Natural Background Radiation in High Air Pollution Area of Thailand," *Toxics*, vol. 12, no. 6, 2024, doi: 10.3390/toxics12060428.

[5] K. Tazaki, Y. Shimojima, T. Takehara, and M. Nakano, "Formation of Microbial Mats and Salt in Radioactive Paddy Soils in Fukushima, Japan," *Minerals*, vol. 5, no. 4, pp. 849–862, 2015, doi: 10.3390/min5040529.

Copyright on 7th Asia-Pacific Symposium on Radiochemistry 2025- R7-04* -

Invited & Contributed Talk | [R7]Environmental Radiochemistry

Mon. Sep 15, 2025 3:15 PM - 4:25 PM JST | Mon. Sep 15, 2025 6:15 AM - 7:25 AM UTC Hall S(Int'l)

[R7] Environmental Radiochemistry

3:15 PM - 3:45 PM JST | 6:15 AM - 6:45 AM UTC

[R7-05(Invited)]

Environmental Analysis by Accelerator Mass Spectrometry

*Hiroyuki Matsuzaki[1] (1. MALT, The University of Tokyo (Japan))

3:45 PM - 4:05 PM JST | 6:45 AM - 7:05 AM UTC

[R7-06]

Retrospective overview of the results of radionuclide measurements in the liquid radioactive discharges of the Krško Nuclear Power Plant and the Sava River water

*Željko Grahek[1] (1. Ruđer Bošković Institute (Croatia))

4:05 PM - 4:25 PM JST | 7:05 AM - 7:25 AM UTC

[R7-07*]

Study on colloid and radionuclide co-migration model in saturated porous system based on the interaction forces between colloids.

*Qi Tan[1], Xiaoyan Wei[1], Zhen Xu[1], Duoqiang Pan[1], Wangsuo Wu[1] (1. Lanzhou University (China))

©APSORC25

7th Asia-Pacific Symposium on Radiochemistry *September 14 ~ 19, 2025 • Kunibiki Messe • Shimane, Japan*

Environmental Analysis by Accelerator Mass Spectrometry

Hiroyuki Matsuzaki[1]

[1]*Micro Analysis Laboratory, Tandem accelerator, The University Museum, The University of Tokyo: 2-11-16, Yayoi, Bunkyo-ku, Tokyo 113-0032, hmatsu@um.u-tokyo.ac.jp*

Accelerator Mass Spectrometry (AMS) is ultra-sensitive analytical method for extremely rare long-lived isotopes which are produced naturally or anthropogenically. The anthropogenic nuclides mainly produced by nuclear weapon testing, spent fuel nuclear reprocessing plants and nuclear accidents are applied to various environmental analysis studies.

1 Target nuclides of AMS

Accelerator Mass Spectrometry (AMS) is ultra-sensitive analytical method for extremely rare long-lived isotopes. Typical target nuclides (and often used for environmental studies) are ^{10}Be (half life: 1.39E06 yr), ^{14}C (5.7E04 yr), ^{26}Al (7.0E05 yr), ^{36}Cl (3.01E05 yr), ^{129}I (1.57E07 yr) [1]. There are two main sources to produce these nuclides: natural sources and anthropogenic sources. The natural sources include cosmic-ray processes and fission of naturally occurred nuclides (mainly ^{238}U). Comparatively low mass nuclides (^{10}Be, ^{14}C, ^{26}Al ^{36}Cl) are mainly produced by cosmic-ray process. These nuclides are called “Cosmogenic Radio Nuclides” (CRN). Since ^{129}I is a typical fission product of uranium, it is produced both naturally and anthropogenically. Artificial fission phenomena have been occurred in nuclear weapon testing and nuclear reactors. The nuclear weapon testing had been conducted in 1950’s and early 1960’s by the United States, former Soviet Union and other countries. The nuclear weapon testing had produced not only vast amount of fission products but also consequent neutron activated nuclides such as ^{14}C and ^{36}Cl. Those nuclides produced by nuclear weapon testing had been blown up to the stratosphere and expanded all over the globe. These nuclides have been gradually falling onto the ground being called “global fallout”. Next anthropogenic nuclides source is spent nuclear fuel reprocessing plants. Vast amount of fission products, produced in the nuclear fuel during the operation of nuclear reactors, is transported to the reprocessing plants. During reprocessing, volatile nuclides such as ^{129}I are released into the environment. The 3rd source is nuclear accidents. The Fukushima Daiichi Nuclear Power Plant Accident released various kind of fission products into the ambient, among which ^{129}I is a well-analyzed target by AMS. The nuclides released by the nuclear accident is locally highly concentrated around the accident site, but total amount is relatively quite small compared with other two sources.

Though the abundance of these nuclides is quite small, they bring important information of the environment. A significant portion of application studies of AMS is of environmental analysis.

2 Environmental Analysis Studies using AMS

2.1 Environmental Analysis related to the nuclear accident

After the Fukushima Daiichi Nuclear Power Plant Accident, the evaluation of radiation dose for the residents is significantly important issue. The deposition distribution of ^{131}I was recognized as one of important (harmful) nuclides due to the Chernobyl lesson. However it was difficult to measure it due to its short half life (8 days). At this point, ^{129}I attracted attention because ^{129}I is simultaneously produced with ^{131}I in the nuclear reactor and behaves with the same manner with ^{131}I in the environment. We measured systematically ^{129}I in the soil around the accident site and made a distribution map of ^{129}I which traced the distribution of ^{131}I [2].

2.2 Environmental Analysis related to the nuclear weapon testing

Prominent atmospheric nuclear weapon testing was conducted by the United States in 1950’s and by the former Soviet Union in 1960’s. The signals of these weapon testing were recorded as ^{129}I and ^{36}Cl spikes in the ice core of Greenland and Antarctica. The time course profiles of these nuclides and the difference between Greenland and Antarctica (Fig. 1) corresponds the timing and the location of the weapon testing. This kind of nuclides record in natural archives is clear record of human nuclear activities.

2.3 Environmental Analysis related to the reprocessing plant

Copyright on 7th Asia-Pacific Symposium on Radiochemistry 2025

After the Partial Ban Treaty of atmospheric nuclear weapon testing (1963), ^{129}I still increase toward 1990's because it has been released from the reprocessing plant. This enhancement is observed only in Greenland ice core because most of the reprocessing plants are located in the northern hemisphere. There is no enhancement of ^{36}Cl in either Greenland or Antarctica because ^{36}Cl is not a fission product. The time course record of ^{129}I, peaks due to the weapon testing and following increase due to the reprocessing plants is also clearly found in coral, especially of northern hemisphere, samples. There is a clear contrast before and after 1950's in the time course record of ^{129}I in various natural archives. This observational fact suggests that ^{129}I is one of most promising indices for the Anthropocene [3].

In the Arctic Ocean, ^{129}I discharged into the ocean from Sellafield and La Hague reprocessing plants can be used as a good tracer for the dynamics of the water masses. We are now investigating the response of ocean dynamics to the climate change.

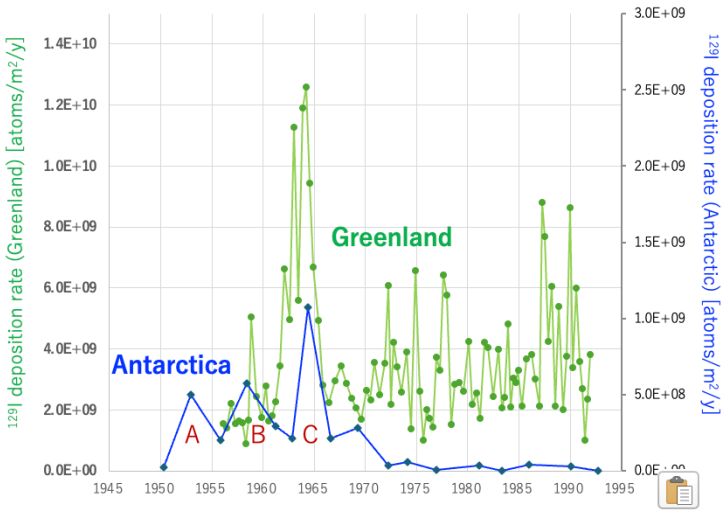


Fig. 1. Time course records of ^{129}I in Greenland/Antarctica ice core

3 Technical principles of AMS and development of detection systems for new nuclides

AMS is a kind of mass spectrometry but with a tandem electrostatic accelerator (Fig. 2) [4]. Utilizing the high kinetic energy of ions provided by the accelerator, interfering isobar can be separated from the interesting ions. One of typical method is to detect the difference of energy loss amounts in the media between isobars. This principle relies on the difference of proton number (i.e. the atomic number Z) between isobars. The relative difference would be smaller as the atomic mass goes larger. For the detection of relatively high mass nuclides various techniques and schemes are introduced. Recently we developed ^{236}U-AMS system using TOF (Time Of Flight). ^{236}U is a quite rare isotope in the natural environment and is produced by the neutron activation of ^{235}U. Since ^{236}U is produced when the nuclear fuel (^{235}U) is burnt, it is a good indicator for the fuel burn-up. ^{236}U is expected to be a significant indicator of the nuclear debris analysis. It can be also used for the environmental impact assessment study during the decommission of the Fukushima Daiichi Nuclear Plant accident.

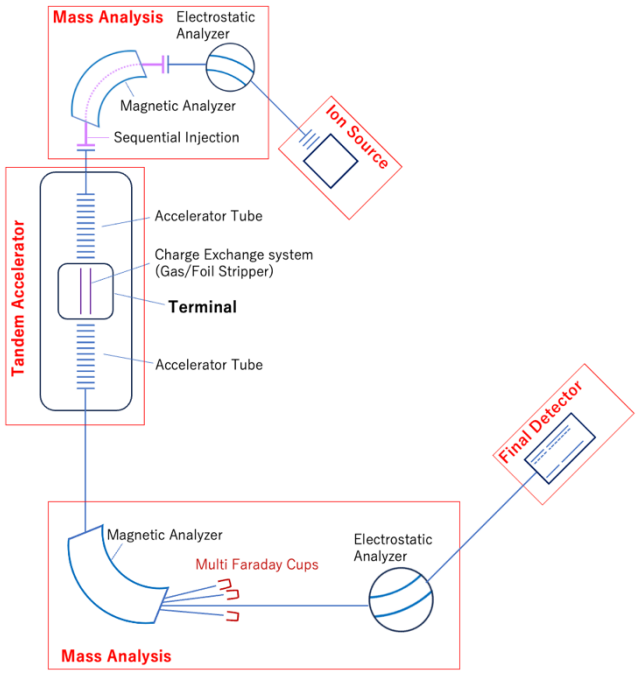


Fig. 2. Fundamental configuration of Accelerator Mass Spectrometry

References

[1] W. Kutchera, et al., Rev. Modern Physics, 95, 035006 (2023).
[2] Y. Muramatsu, et al., J. Environ. Radioactivity, 139, 344-350 (2015).
[3] A.T. Bautista, et al., Sci. Total Environment, 887, 16-4021 (2023).
[4] H. Matsuzaki, et al., Nucl. Instr. Meth. in Physics Research, B463, 55-63 (2020).

Retrospective overview of the results of radionuclide measurements in the liquid radioactive discharges of the Krško Nuclear Power Plant and the Sava River water

[1]Ivana Coha, [1]Gorana Karanović, [2]Marko Štrok, [2]Jasmina Kožar Logar, [2]Benjamin Zorko, [3]Aleš Volčanšek, [3]Jasmina Znidaršić, [3]Danijel Novak, [1]Ivana Tucaković, [1] Željko Grahek

[1]*Ruđer Bošković Institute, Bijenička cesta 54, Zagreb, Croatia*
[2]*Jožef Štefan Institute, Jamova 37, Ljubljana, Slovenia*
[3]*Nuclear power plant Krško, Vrbina 7, Krško Sovenia*

The Krško nuclear power plant (PWR type) is located on the Sava River near densely populated areas with over one million inhabitants, including the city of Zagreb, which is supplied with drinking water from wells near the main stream of the Sava River. Under normal operating conditions, nuclear power plants release small amounts of radiation (radioactive isotopes) into the environment. Therefore, according to the regulations, radiological environmental monitoring programs are required at nuclear power plants. The objectives of the program include: Identifying, measuring and assessing the radionuclides present in the plant environment and the variations in radioactivity levels that may occur; evaluating measurements to determine the impact of operations on the local radiation environment, collecting data to refine transport models, and verifying that radioactive material containment systems are functioning to minimize releases as low as reasonably achievable. In this sense, the main objective of this work is to demonstrate the impact of the Krško Nuclear Power Plant on the environment, especially on the Sava River. For this purpose, the following environmental pathways and sample analyzes are examined: liquid discharges from the NPP, water from the Sava River, drinking water and groundwater. Residual radioactive isotopes remain in the liquid effluents from the Krško Nuclear Power Plant (NEK), which are discharged into the Sava River during the treatment of liquid waste. Most of the released isotopes come from the WMT waste monitoring tanks. This includes monitoring the amount of gamma emitters, ^{3}H, $^{89,90}Sr$ and ^{55}Fe, so that the results of measuring the amount of discharged radionuclides in the Sava River at the Krško NPP in the working period 1982-2022 are presented and compared with the permissible radioactivity limit. Special attention is paid to the monitoring of the amount of tritium discharged into the Sava River. An overview is given of the measurement methods used and the results of tritium measurements in the water of the Sava River at individual locations. It is also shown how advances in the development of liquid scintillation counters have improved the quality of the measurements and the accuracy of the results over time. In this sense, the various results of measurements of tritium (and some other radionuclides) in liquid discharges and in the water of the Sava River are presented, which were performed during the control of NPP operation by the radiochemical laboratory at the Krško Nuclear Power Plant (NEK) and the laboratories of the Ruđer Bošković Institute (RBI) in Zagreb and the Jožef Štefan Institute (JSI) in Ljubljana. Some of the results discussed and shown are presented below.

1 Tritium discharge from NPP Krško in Sava River

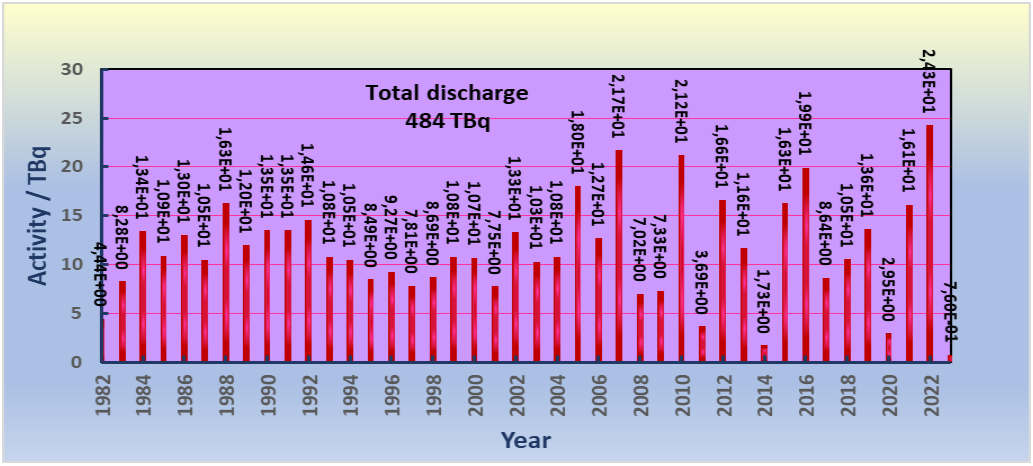


Fig. 1. Annual ^{3}H discharge from NPP Krško to Sava river in period 1982. to 2022.

Copyright on 7th Asia-Pacific Symposium on Radiochemistry 2025 - R7-06 -

1.1 Measurement of tritium in the Sava River during 2019. year at RBI and JSI

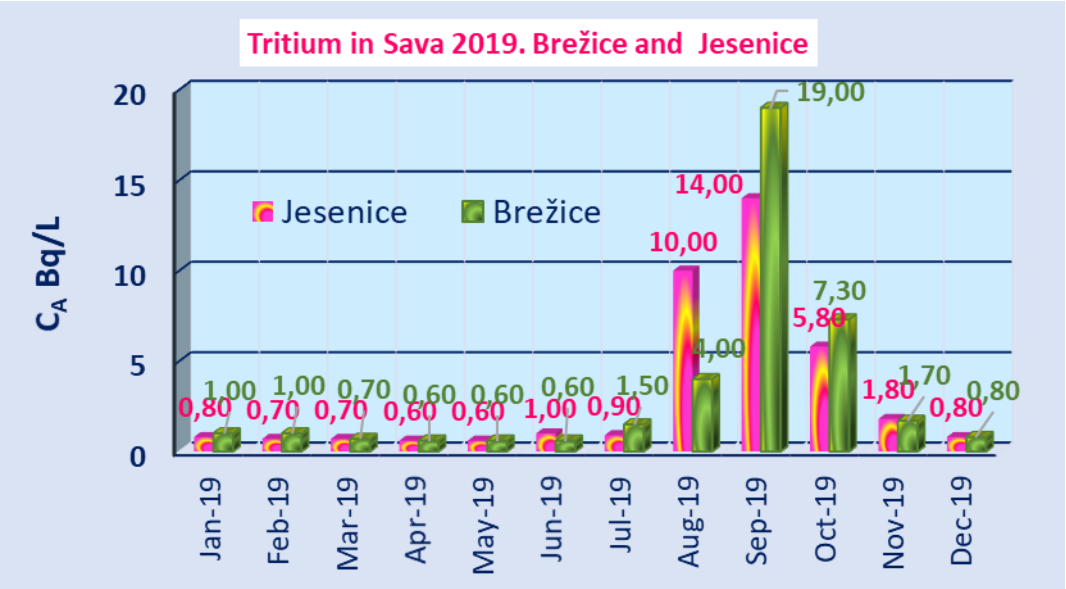


Fig. 2. Result of ^{3}H measurement in monthly sample of the Sava River water at Brežice (5 km downstream NPP, **JSI measurment**) and Jesenice (15 km downstream NPP, **RBI measurment**) locations. Continuous water sampling over 24 hours

1.1.1 Comparative measurements of tritium in liquid discharges from the Krško Nuclear Power Plant

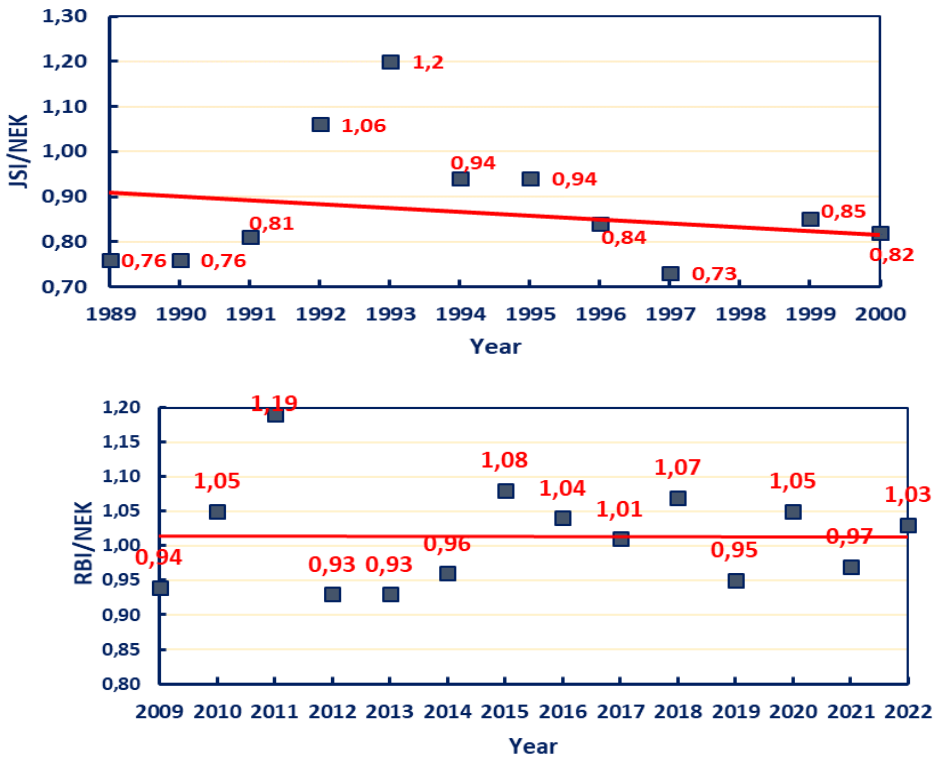


Fig. 3. Interlaboratory comparison of tritium measurement results in liquid discharges from the Krško Nuclear Power Plant during its operation. The figures show the differences in ^{3}H activity measurements on an annual basis. The ratios were obtained as an average of measurements of monthly composite samples in two laboratories, the Laboratory at NPP KRŠKO **(NEK)** and the laboratories at **RBI** or **JSI**.

Copyright on 7th Asia-Pacific Symposium on Radiochemistry 2025 - R7-06 -

7th Asia-Pacific Symposium on Radiochemistry *September 14 ~ 19, 2025 • Kunibiki Messe • Shimane, Japan*

STUDY ON COLLOID AND RADIONUCLIDE CO-MIGRATION MODEL IN SATURATED POROUS SYSTEM BASED ON THE INTERACTION FORCES BETWEEN COLLOIDS

Qi Tan[1], Xiaoyan Wei[1], Zhen Xu[1], Duoqiang Pan[1], Wangsuo Wu[1]

[1]*School of Nuclear Science and Technology (Lanzhou University), Gansu, China, 730000, snst@lzu.edu.cn*

The investigation into the migration behavior of radionuclides is crucial for establishing a long-term and reliable environmental safety evaluation system for these elements. Radionuclides in aqueous environments can significantly change their migration ability by co-migrating with the colloid, making the study of colloid-nuclide co-migration has become an important part of the investigation of nuclide migration. Given that the co-migration process of colloids and nuclides in real-world settings encompasses extensive spatial scales and extended temporal spans, it is imperative to employ models to elucidate the underlying mechanisms of colloid-nuclide co-migration. In the development of the colloid-nuclide co-migration model, primary focus is placed on the migration behavior of colloids and the interaction between nuclides and colloids. Colloidal particles exhibit a more intricate structure compared to free-state nuclides, resulting in diverse migration mechanisms that often dominate the co-migration process. Starting from the migration behavior of colloid, we constructed a co-migration model of ripening/site-blocking mechanism.

1 CO-MIGRATION MODEL OF RIPENING/SITE-BLOCKING MECHANISM

Ripening and site-blocking are two common mechanisms of colloid migration [1]. Under unfavorable conditions, site-blocking usually means that when the intercolloid force is repulsive, the adsorption capacity of the medium to the colloid decreases with the increase of the adsorption amount. The ripening process usually refers to when the intercolloid force is attractive, the adsorption capacity of the medium to the colloid increases with the increase of the adsorption amount. In this work, a finite difference model was constructed to describe the co-migration behavior of radionuclides and colloids in saturated porous media by focusing on the force between colloids.

1.1 Concepts of Models

The proposed model is formulated based on the assumption that the colloid migration is not affected by the presence of nuclides by ignoring the decay process of nuclides in a short period of time. The one-dimensional advection-dispersion migration of nuclides is coupled with the migration of colloid as the pseudo-colloid. The adsorption and desorption process (linear kinetic reactions) of nuclides on host media and mobile or filtered colloid, the ripening in the presence of attractive forces between colloids and the site-blocking in the presence of repulsive forces between colloids, are considered. This model introduced the ripening and adsorption blocking mechanisms in the process of colloid migration into the co-migration model, and had a good fitting effect when the colloid adsorbed nuclides strongly.

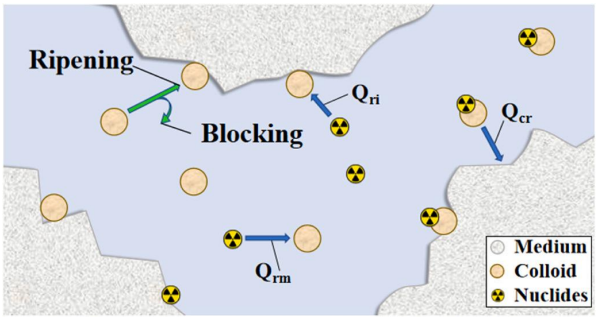


Fig. 1. Schematic diagrams of the mechanisms in a co-migration numerical model.

1.2 Model Verification

The aim of developing the presented model is to provide a tool for describing the migration of nuclides in the presence of colloids in porous media for the long-term safety assessment of deep geological repositories. The model should consider the relevant interactions among nuclides, colloids, and media and be able to describe and explain the key

Copyright on 7th Asia-Pacific Symposium on Radiochemistry 2025- R7-07* -

processes observed in these experiments. By applying the model to an actual laboratory experiment, the feasibility of the model is verified.

By conducting corresponding experiments and combining experimental data from the existing co-migration experiment of the research group [2], the accuracy of the newly established mathematical model in fitting the ripening mechanism is tested. The experimental data and fitting effects are shown in Figure 2-3.

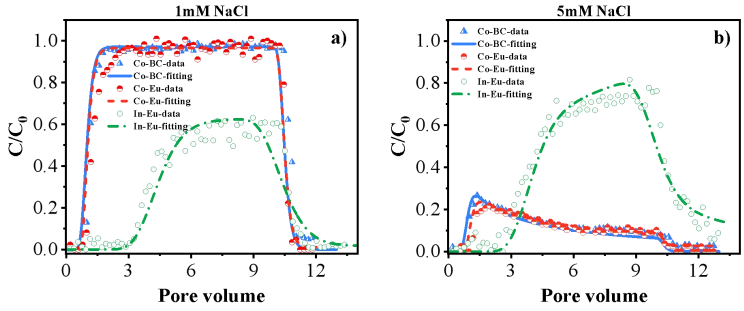


Fig. 2. BC-Eu(III) co-migration experiment breakthrough curve and fitting results of ripening mechanism.

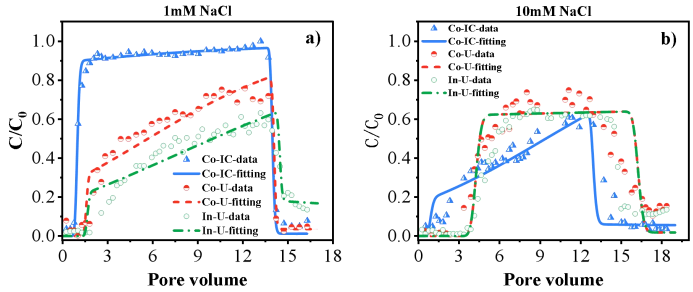


Fig. 3. IC-U(VI) co-migration experiment breakthrough curve and fitting results of site-blocking mechanism.

2. CONCLUSIONS

In this work, a model is developed to simulate the migration of nuclides in saturated porous media in the presence of colloids, which can be applied to fit the experimental data of colloid and nuclide co-migration at the laboratory scale and can help compare and explain the changes of colloid interacting forces, colloid adsorption capacity of nuclide, and colloid retention under different hydrochemical environments. The model explores colloid-nuclide co-migration behavior from the force between colloids, which helps to predict the migration and retention risks of nuclides in porous media under the influence of colloid from different sources.

References

[1] Babakhani, P., Bridge, J., Doong, R.A., Phenrat, T., "Continuum-based models and concepts for the transport of nanoparticles in saturated porous media: A state-of-the-science review." Adv. Colloid Interface Sci. **246**, 75-104 (2017).

[2] Wei, X., Shi, X., Yang, M., Tan, Q., Xu, Z., Ma, B., Wu, W., "Phosphate and illite colloid pose a synergistic risk of enhanced uranium transport in groundwater: A challenge for phosphate immobilization remediation of uranium contaminated environmental water." Water Res. **255,** 121514. (2024).

Copyright on 7th Asia-Pacific Symposium on Radiochemistry 2025- R7-07* -

Contributed Talk | [R6]Radiation and Radioisotopes in Life Science

Mon. Sep 15, 2025 1:30 PM - 3:10 PM JST | Mon. Sep 15, 2025 4:30 AM - 6:10 AM UTC Hall B(Small)

[R6] Radiation and Radioisotopes in Life Science

1:30 PM - 1:50 PM JST | 4:30 AM - 4:50 AM UTC

[R6-01]

MODELING BIOKINETICS OF INSOLUBLE CESIUM-ABSORBED PARTICLES FOLLOWING INTRATRACHEAL ADMINISTRATION IN MICE

*Kentaro Manabe[1], Yutaka Yamada[2], Takamitsu Morioka[2], Kazuhiko Ninomiya[3], Satoru Endo[3], Masatoshi Suzuki[4,5] (1. JAEA (Japan), 2. QST (Japan), 3. Hiroshima University (Japan), 4. Tohoku University (Japan), 5. F-REI (Japan))

1:50 PM - 2:10 PM JST | 4:50 AM - 5:10 AM UTC

[R6-02*]

In Vivo Imaging of ^{95m}Tc-DTPA as a Radiotracer Alternative to Clinical ^{99m}Tc-DTPA Using Electron-Tracking Compton Camera (ETCC)

*Kaiji Tanaka[1], Ryota Iwasaki[1], Ryuta Kiuchi[1], Koya Yoshida[1], Hiroyasu Matsushita[1], Hiroyuki Kimura[2], Masato Asai[3], Yoji Kitamura[4], Takashi Kozaka[4], Hidekazu Kawashima[5], Tsuyoshi Fukuzawa[1], Shigeto Kabuki[1], Kyoshi Nishijima[6], Etsuo Kunieda[7], Junko Kushida[1] (1. Tokai University (Japan), 2. Kyoto University (Japan), 3. Japan Atomic Energy Agency (Japan), 4. Kanazawa University (Japan), 5. Kyoto Pharmaceutical University (Japan), 6. Kanagawa University (Japan), 7. Tokyo General Hospital (Japan))

2:10 PM - 2:30 PM JST | 5:10 AM - 5:30 AM UTC

[R6-03]

Potential involvement of rhizodeposition from white lupin in cesium dynamics in the rhizosphere soil

*Hiroshi Uchibayashi[1], Satoshi Asaeda[1,2], Akiko Maruo[1], Hayato Maruyama[1], Toshihiro Watanabe[1], Yong-Gen Yin[3], Nobuo Suzui[3], Yuta Miyoshi[3], Yusaku Noda[3], Kazuyuki Enomoto[3], Naoki Kawachi[3], Yusuke Unno[4], Takuro Shinano[1] (1. Hokkaido University (Japan), 2. Hiroshima Prefectural Technology Research Institute (Japan), 3. National Institutes for Quantum Science and Technology (QST) (Japan), 4. Institute for Environmental Sciences (Japan))

2:30 PM - 2:50 PM JST | 5:30 AM - 5:50 AM UTC

[R6-04*]

Flexible Scintillator for non-invasive visualization of nutrient transport in plants

*XIAORUI ZHOU[1], Ai Kaiho Soma[1], Yuko Kurita[1], Natsuko Kobayshi[1], Keitaro Tanoi[1,2] (1. Graduate School of Agricultural and Life Science, The University of Tokyo (Japan), 2. Fukushima Institute for Research, Education and Innovation (Japan))

2:50 PM - 3:10 PM JST | 5:50 AM - 6:10 AM UTC

[R6-05]

Sodium-induced dot-like accumulation of ^{137}Cs in rice root grown under low K^+ condition

*Jun FURUKAWA[1], Satomi KANNO[2] (1. Univ. of Tsukuba, CRiES (Japan), 2. Nagoya Univ., IAR (Japan))

©APSORC25

7th Asia-Pacific Symposium on Radiochemistry *September 14 ~ 19, 2025 • Kunibiki Messe • Shimane, Japan*

MODELING BIOKINETICS OF INSOLUBLE CESIUM-ABSORBED PARTICLES FOLLOWING INTRATRACHEAL ADMINISTRATION IN MICE

Kentaro Manabe[1], Yutaka Yamada[2], Takamitsu Morioka[2], Kazuhiko Ninomiya[3], Satoru Endo[4], Masatoshi Suzuki[5, 6]

[1]*Nuclear safety Research Center, Japan Atomic Energy Agency: 2-4 Shirakata, Tokai-mura, Naka-gun, Ibaraki 319-1195, Japan, manabe.kentaro@jaea.go.jp*
[2]*Institute for Radiological Science, National Institutes for Quantum Science and Technology: 4-9-1 Anagawa, Inage-ku, Chiba-shi, Chiba 263-8555, Japan, yamada.yutaka@qst.go.jp*
[3]*Natural Science Center for Basic Research and Development, Hiroshima University: 1-4-2 Kagamiyama, Higashi-Hiroshima-shi, Hiroshima 739-8526, Japan, ninomiya-kazu@hiroshima-u.ac.jp*
[4]*Graduate School of Advanced Science and Engineering, Hiroshima University: 1-4-1 Kagamiyama, Higashi-Hiroshima-shi, Hiroshima 739-8527, Japan, endos@hiroshima-u.ac.jp*
[5]*International Research Institute of Disaster Science, Tohoku University: 519-1176 Aramaki-aza-Aoba, Aoba-ku, Sendai-shi, Miyagi 980-8572, Japan, masatoshi.suzuki.c7@tohoku.ac.jp*
[6]*Regional Environmental Co-Creation Unit, Fukushima Institute for Research, Education and Innovation: 519-1176 Aramaki-aza-Aoba, Aoba-ku, Sendai-shi, Miyagi 980-8572, Japan, masatoshi.suzuki.z5f@research.f-rei.go.jp*

A biokinetic model was developed to assess the clearance and distribution of insoluble micro-particles in the respiratory tract of mice following intratracheal administration. Mice were analyzed at various time points post-administration to determine particle retention. The models incorporated three clearance routes from the respiratory region: rapid clearance, slow clearance and translocation via mediastinal tissues. Transfer coefficients were optimized using experimental data. The model can be used to estimate internal exposure doses due to administrations of radioactive insoluble micro-particles.

1 Introduction

Inhalation of insoluble radioactive particles is a concern because it may cause lung cancer due to internal exposure in the respiratory tracts [1,2]. However, it is not yet clear whether the relationship between internal doses and carcinogenic effects varies depending on the age at the time of exposure. To assess the age-dependent risk of carcinogenesis from insoluble radioactive particles, we are conducting intratracheal administration experiments in mice of various ages which are highly susceptible to lung tumor formation. Here, it is essential to link the cancer risk with internal dose. If exposure doses can be estimated from administered amount using model calculations, this would be highly useful. In this study, we attempted to construct a biokinetic model of clearance from the respiratory tract based on tissue specific accumulation data obtained from particle administration experiments in mice.

2 Materials and methods

The data for model construction were obtained by intratracheal administration of porous silica particles, 2 to 3 micrometers in diameter, absorbed with Cs-137, to female A/J mice, which are highly susceptible to lung tumor formation. The radioactivity absorbed onto the particles was 800 kBq per 60 mg of particles. The mice were 4, 10, or 15 weeks old at the time of administration. The retained activity in lungs were measured at various time points (1–91 days post-administration). Data from all age groups were combined for model construction because no significant age-related differences in retention were observed.

A biphasic clearance pattern was observed in the lungs. Accumulation in the mediastinum was also detected. This pattern resembles the structure used in the ICRP human respiratory tract model for clearance via blood absorption [3]. Accordingly, the structure of the clearance model for insoluble particles was defined as shown in Fig. 1. The transfer coefficients were determined as follows. First, the coefficient for the slow clearance was determined by least-squares fitting, along with the fraction of the administered dose assigned to this slow-clearing component. Subsequently, the coefficient for the rapid clearance was also determined by least-squares fitting. For the transfer to and clearance from the mediastinum, two parameters were required: the transfer rate from the lung and the clearance coefficients to other tissues. These were determined by preparing an ordinary differential equation representing the time course of radioactivity in the mediastinal tissue and manually adjusting the parameters so as to minimize the sum of squared differences between the model output and the measured data.

Copyright on 7th Asia-Pacific Symposium on Radiochemistry 2025 - R6-01 -

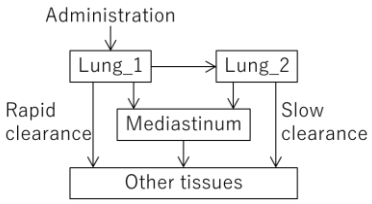


Fig. 1. Structure of the lung clearance model for insoluble micro-particles.

3 Results and discussion

Fig. 2 and Fig. 3 show the comparison between the experimental results and the precited rate by the model constructed in this study. The plots are the experimental data, and the broken lines indicate model prediction. No measurement data were available for the mediastinum beyond 30 days post-administration due to low levels of retention rate. Although variability in the measured values increased with the time after administration, the model constructed in this study well reproduced the observed retention rates of radioactivity.

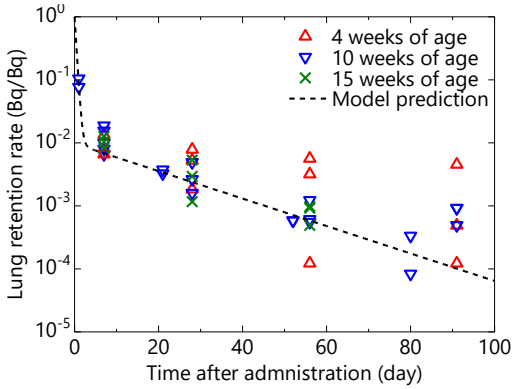


Fig. 2. Lung retention rate

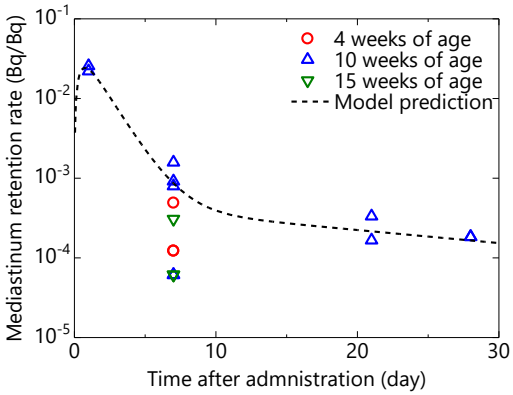


Fig.3. Mediastinum retention rate

This model enables the calculation-based estimation of internal doses to the lungs and mediastinum following intratracheal administration of insoluble micro-particles in mice. It is expected to serve as a useful tool for examining the relationship between radiation dose and carcinogenic risk.

On the other hand, it is known that insoluble particles migrate to various tissues and organs while maintaining their particulate form [4]. Expanding the model by incorporating data on particle accumulation in tissues other than lungs and mediastinum could enhance our understanding of the biological effects of insoluble micro-particles.

4 Conclusions

The biokinetic model was constructed to describe the clearance of insoluble cesium-adsorbed microparticles from the respiratory tract of mice following intratracheal administration. The model incorporating biphasic clearance in the lungs and transfer to the mediastinum reproduced the experimental retention data adequately, and allows for estimation of internal radiation doses to the lungs and mediastinum. It is expected to serve as a valuable tool for evaluating dose response relationships in carcinogenic risk assessment.

ACKNOWLEDGMENTS

This work was supported by Research Project on the Health Effects of Radiation organized by Ministry of the Environment, Japan.

References

[1] Y. OGHISO and Y. YAMADA, “Comparisons of Pulmonary Carcinogenesis in Rats Following Inhalation Exposure to Plutonium Dioxide or X-ray Irradiation,” *J. Radiat. Res.*, **44**, 261 (2003).

[2] K. SHICHIJO, N. FUJIMOTO, D. UZBEKOV, et al., “Internal Exposure to Neutron-activated ^{56}Mn Dioxide Powder in Wistar Rats—Part 2: Pathological Effects,” *Radiat. Environ. Biophys.*, **56**, 55 (2017).

[3] INTERNATIONAL COMMISSION ON RADIOLOGICAL PROTECTION, “Human Respiratory Tract Model for Radiological Protection. Publication 66,” *Ann. ICRP*, **24**, 74 (1994).

[4] L. GERAETS, A.G. OOMEN, J.D. SCHROETER, et al., “Tissue Distribution of Inhaled Micro- and Nano-sized Cerium Oxide Particles in Rats: Results From a 28-Day Exposure Study”, *Toxicol. Sci.*, **127**, 463 (2012).

Copyright on 7th Asia-Pacific Symposium on Radiochemistry 2025 - R6-01 -

7th Asia-Pacific Symposium on Radiochemistry *September 14 ~ 19, 2025 • Kunibiki Messe • Shimane, Japan*

In Vivo Imaging of ^{95m}Tc-DTPA as a Radiotracer Alternative to Clinical ^{99m}Tc-DTPA Using Electron-Tracking Compton Camera (ETCC)

K. Tanaka[1], R. Iwasaki[1], R. Kiuchi[2], K. Yoshida[1], H. Matsushita[1], H. Kimura[4], M. Asai[5], Y. Kitamura[6], T. Kozaka[6], H. Kawashima[7], T. Fukuzawa[2], S. Kabuki[2], K. Nishijima[8], E. Kunieda[9], J. Kushida[3]

[1] *Tokai University, Course of Physics, School of science, Hiratsuka, Japan*
[2] *Tokai University, School of Medicine, Isehara, Japan*
[3] *Tokai University, School of Physics, School of science, Hiratsuka, Japan*
[4] *Kyoto University, Agency for health, Safety and Environment*
[5] *Japan Atomic Energy Agency, Advanced Science Research Center, Ibaraki, Japan*
[6] *Kanazawa University, Research Center for Experimental Modeling of Human Disease, Division of Probe Chemistry for Disease Analysis, Kanazawa, Japan*
[7] *Kyoto Pharmaceutical University, Radioisotope Research Center, Kyoto, Japan*
[8] *Kanagawa University, Department of Applied Physics, Faculty of Engineering, Yokohama, Japan*
[9] *Tokyo General Hospital, Radiotherapy Center, Nakano, Japan*

We evaluated the feasibility of imaging the γ-emitting radioisotope ^{95m}Tc using an electron-tracking Compton camera (ETCC). The ^{95m}Tc was synthesized at the Japan Atomic Energy Agency's tandem accelerator*, and both phantom and in vivo rat imaging studies were conducted. Phantom imaging demonstrated accurate source localization (FWHM ≈ 22 mm), while in vivo imaging with ^{95m}Tc–DTPA revealed renal accumulation consistent with biodistribution data. These results suggest that ETCC can serve as a promising platform for functional imaging with alternative technetium tracers when conventional γ-cameras are inadequate.*

1. PURPOSE

Many countries currently depend on imports of ^{99}Mo, the parent nuclide of ^{99m}Tc used in nuclear medicine diagnostics. Therefore, we are focusing on ^{95}Tc (half-life: 20.0 h; γ-ray energy: 766 keV) and ^{95m}Tc (half-life: 61 d; γ-ray energies: 204, 582, and 835 keV), both of which can be produced domestically using a proton accelerator and investigating their clinical applications. Because these isotopes emit higher-energy γ-rays than ^{99m}Tc, they are incompatible with existing clinical γ-cameras. To address this issue, we are advancing the development of an Electron-Tracking Compton Camera (ETCC) capable of detecting a broad energy range. This study aims to achieve imaging of ^{95m}Tc using the ETCC.

2. METHODS

2.1 Apparatus Configuration

The ETCC consists of a time projection chamber (TPC) filled with an Ar–C_2H_6 gas mixture serving as the scatterer and a GSO scintillator array serving as the absorber. The TPC has a drift length of 150 mm, and orthogonal strip-electrode readout (μ-PIC: micro Pixel Chamber, providing high spatial resolution and fast response) enables three-dimensional (X, Y, Z) reconstruction of electron tracks.

2.2 Radioisotope Synthesis and Imaging Procedure

The ^{95m}Tc was synthesized at the Japan Atomic Energy Agency's tandem accelerator by irradiating natural MoO_3 pellets with a proton beam. The synthesized ^{95m}Tc was used for imaging both phantoms and rats. Imaging studies were conducted at Kanazawa University. In the phantom study, a container loaded with a 1.32 MBq of ^{95m}Tc sample (5 mm in size) was positioned 25.5 mm away from the ETCC detection surface, and imaging was

Copyright on 7th Asia-Pacific Symposium on Radiochemistry 2025- R6-02* -

conducted under both vertical and oblique orientations. Subsequently, ^{95m}Tc-DTPA was administered to rats, and in vivo rat imaging was performed (Fig. 1). The radioactivity of each excised organ was measured using a gamma counter.

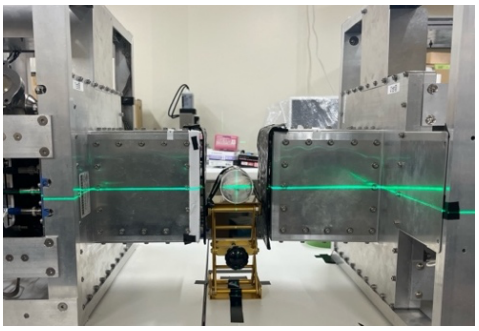


Fig. 1. Experimental setup

3. RESULTS

Events corresponding to the 582 keV and 835 keV peaks were selected using a 10 % energy window. In the phantom study, the reconstructed images clearly reproduced the peak positions matching the actual container arrangement (Fig. 2), with a full width at half maximum (FWHM) of 21.64 mm. In the in vivo rat imaging with ^{95m}Tc-DTPA, two peaks were observed near the kidneys (Fig. 3). Gamma counter measurements indicated that radioactivity was primarily localized in the kidneys, which was consistent with the uptake distribution shown in the reconstructed images.

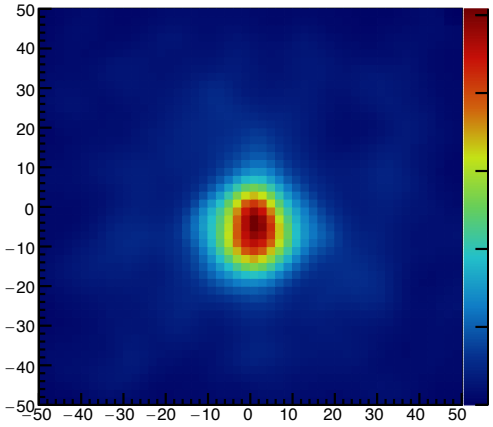


Fig. 2. Imaging of a ^{95m}Tc sample (5 mm in size)

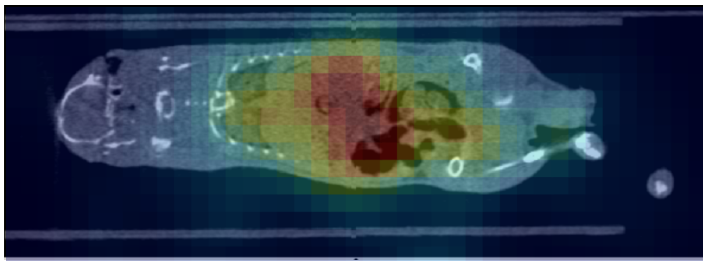


Fig. 3. In vivo rat imaging with ^{95m}Tc-DTPA

4. CONCLUSIONS

In phantom and rat imaging studies with ^{95m}Tc, we successfully acquired functional images that clearly depicted renal accumulation and correlated with the biodistribution patterns measured by gamma counting. These results suggest that the system represents a promising platform for extension to other radioisotopes and clinical diagnostic agents.

ACKNOWLEDGMENTS

The authors thank the Tandem Accelerator Facility team at the Japan Atomic Energy Agency for producing the ^{95m}Tc samples and the Research Center for Experimental Modeling of Human Disease at Kanazawa University for providing imaging facilities and technical support.

Copyright on 7th Asia-Pacific Symposium on Radiochemistry 2025- R6-02* -

7th Asia-Pacific Symposium on Radiochemistry *September 14 ~ 19, 2025 • Kunibiki Messe • Shimane, Japan*

Potential involvement of rhizodeposition from white lupin in cesium dynamics in the rhizosphere soil

Hiroshi Uchibayashi[1], Satoshi Asaeda[1,2], Akiko Maruo[1], Hayato Maruyama[1], Toshihiro Watanabe[1], Yong-Gen Yin[3], Nobuo Suzui[3], Yuta Miyoshi[3], Yusaku Noda[3], Kazuyuki Enomoto[3], Naoki Kawachi[3], Yusuke Unno[4], Takuro Shinano[1]

[1]*Research Faculty of Agriculture, Hokkaido University, Hokkaido, 060-8589, Japan*
[2]*Agricultural Technology Research Center, Hiroshima Prefectural Technology Research Institute, Hiroshima, 739-0151, Japan*
[3]*Takasaki Institute for Advanced Quantum Science, National Institutes for Quantum Science and Technology (QST), Gunma, 370-1292, Japan*
[4]*Department of radio ecology, Institute for Environmental Sciences, Aomori, 039-3212, Japan*

1 Introduction

To mitigate radioactive cesium (RCs) transfer from soil to plant, it is essential to understand the dynamics of cesium in plant rhizosphere. White lupin (*Lupinus albus* L.) is known to form cluster root particularly under phosphorous (P) deficient condition, which releases explosive amount of rhizodeposition (e.g. citric acid, malic acid, etc.) and contributes to nutrient acquisition [1]. Moreover, white lupin is known to have a high capacity of RCs uptake especially under potassium (K) deficient conditions. One possible reason is that rhizodeposition from white lupin may contribute to the mobilization of RCs adsorbed to soil. Here, a pot experiment and a rhizobox experiment were conducted to investigate the possibility of rhizodeposition from white lupin to mobilize cesium (Cs) in soil.

2. Pot experiment

White lupin 'Kievskij mutant' was grown in 4 L pot with K deficient soil (7.1 mg of K_2O kg^{-1} soil) from Fukushima prefecture in a greenhouse. Five treatments of K fertilizer application rates (0, 5, 15, 30, 60 mg of K_2O kg^{-1} soil) were established (n=3). After 42 days of cultivation, shoots and roots of the plants were harvested. Rhizosphere soil was collected by shaking roots in the air to separate the attached soil, while bulk soil was collected from the soil left inside the pot. Dry weight and contents of K and ^{137}Cs of the plants were measured. The soil was extracted with 1.0 M of ammonium acetate solution to measure exchangeable K and ^{137}Cs. Although the dry weight did not significantly differ among the K fertilizer application rates, the ^{137}Cs content in shoot significantly decreased with increasing application rates of K fertilizer. The concentration of the soil exchangeable ^{137}Cs significantly decreased with increasing application rates of K fertilizer. In addition, the concentration of the soil exchangeable ^{137}Cs was higher in planted treatments compared with unplanted treatments, suggesting that white lupine solubilized ^{137}Cs adsorbed to the soil in the rhizosphere.

3. Rhizobox experiment

Eleven-day-old white lupin 'Energy' was grown in a rhizobox, which consisted of a square nylon 48-μm mesh bag and a pair of soil boxes. Each soil box was 160-mm high × 110-mm wide × 14.5-mm deep and filled with K deficient soil from Fukushima prefecture. The test plants were placed in a growth chamber (n=3). After 20 days of cultivation, $^{11}CO_2$ (with a half-life of approximately 20 minutes) was administered, and the translocation of ^{11}C-labeled photosynthates, assimilated in the leaves, to the roots was visualized for 80 minutes using Positron Emitting Tracer Imaging System (PETIS). Immediately after imaging, roots and soil were separated, and the distribution of ^{11}C in the soil alone was imaged for 5 minutes to obtain a two-dimensional visualization of ^{11}C labelled carbon metabolites secreted from the roots into the soil. Subsequently, the rhizobox was divided into 2 × 2 cm sections, and the soil was collected to measure the concentrations of exchangeable elements. In all rhizoboxes, white lupine formed cluster roots. PETIS imaging of ^{11}C distribution in the soil revealed that, in each rhizobox, certain cluster roots formed localized "hotspots" of carbon metabolite secretion into the surrounding soil, which was considered the rhizosphere soil. These results indicate that even under K deficient conditions, white lupine forms cluster roots and actively secretes carbon metabolites into the soil. In one of the rhizoboxes, a positive correlation was observed between ^{11}C intensity in the soil and concentration of the soil exchangeable Cs, which implies that carbon metabolites secreted from cluster roots of white lupin may have mobilized Cs previously adsorbed to soil particles and increased its availability.

4. Conclusion

Based on the results of cultivation experiments under K deficient conditions, white lupine was found to form cluster roots even under K deficiency, and some of these cluster roots actively released carbon metabolites. This suggests that the release of rhizodeposition from cluster roots may have contributed to the elevated exchangeable ^{137}Cs concentrations in the rhizosphere soil of white lupine. On the other hand, the hotspots identified through PETIS imaging represent the instantaneous distribution of carbon metabolites secreted from the roots. Considering that the dynamics of ^{137}Cs in the rhizosphere are influenced cumulatively over time by root activity, further investigation is needed to understand the temporal changes in Cs behavior in the rhizosphere soil.

Copyright on 7th Asia-Pacific Symposium on Radiochemistry 2025

ACKNOWLEDGMENTS

This research was performed by the commissioned research fund provided by F-REI (JPFR25040101).

References

[1] M. W. Shane and H. Lambers, “Cluster Roots: A Curiosity in context”, *Plant and Soil*, **274**, 101-125 (2005).

7th Asia-Pacific Symposium on Radiochemistry *September 14 ~ 19, 2025 • Kunibiki Messe • Shimane, Japan*

Flexible Scintillator for non-invasive visualization of nutrient transport in plants

Xiaorui Zhou[1], Ai Kaiho-Soma[1], Yuko Kurita[1], Natsuko I. Kobayashi[1], Keitaro Tanoi[1,2]

[1]*Graduate School of Agricultural and Life Science, The University of Tokyo: 1-1-1 Yayoi, Bunkyo-ku, Tokyo 113-0032, Japan*

[2] *Fukushima Institute for Research, Education and Innovation: 6-1 Yazawa-machi, Gongendo, Namie town, Futaba County, Fukushima 979-1521, Japan*

Autoradiography as a wide use method for tumor estimation offers high molecular sensitivity and spatial resolution. However conventional autoradiography has been largely applied to animal-related studies, and its application to other organisms remains underexplored, and this method usually requires sectioning the sample which is invasive and labor-consuming. Here we describe a novel autoradiography technique that uses a flexible membrane-like scintillator which conforms to plant leave surface. Imaging with the flexible scintillator enables direct, biocompatible and high sensitivity imaging of the beta particle emission from targeted radiotracers. We show that the flexible autoradiography approach has high potential as a technique for visualization of multiple nutrient elements in various kinds of live plants with a CCD camera. Due to the advantage of conforming specimen, the flexible scintillator showed significantly better image quality in terms of radiotracers signal to whole-body background noise compared to rigid and relatively thick GOS and ZnO:Ag. The sensitivity of the technique means it is suitable for the analysis of plant various physiological phenomena.

1 Introduction

Radiotracers are a powerful tool to visualize element movement in biological samples which can reflect the metabolic and physiological status of the organism [1]. Autoradiography is a technique using scintillator film, beta-imaging system to quantify and localize the radioisotopes, and it offers high molecular sensitivity and spatial resolution [2]. However, conventional autoradiography requires sectioning the sample which is destructive, and labor consuming [3]. Instead, we propose to simplify the process by using a flexible membrane-like scintillator which conforms to the sample surface and enabling a novel application scenario for plant physiological analysis.

2 Material and methods

To make the flexible scintillator, PVA aqueous solution (8wt% in H_2O) was initially spin-coated onto a clean petri dish, acting as a sacrificial layer. The PDMS: A mixed with scintillator powder, prepared as a mixture of the elastomer base and a curing agent PDMS: B as a weight ratio of 10:1, was spin-coated, creating the flexible scintillator. The scintillators are used for testing and considered for the 2000 μm thick GOS, 1000 μm thick ZnO:Ag and a 13μm thick flexible scintillator. Both were estimated to use multiple radioactive sources arranged with a gradient of radioactivity levels.

3 Results and discussion

To monitor plant physiological status in a noninvasive manner, biocompatibility, transparency, stretchability, and conformability are desired simultaneously. Our flexible scintillator meets all these requirements based on the substrate material and the way of dispersing scintillators we chose. The image resolution of 3 mm was achievable and the minimum detectable activity concentration of 3.7 kBq for ^{14}C. The results indicate that this technique has the potential to real-time in situ monitor ion movement in live plant.

Copyright on 7th Asia-Pacific Symposium on Radiochemistry 2025- R6-04* -

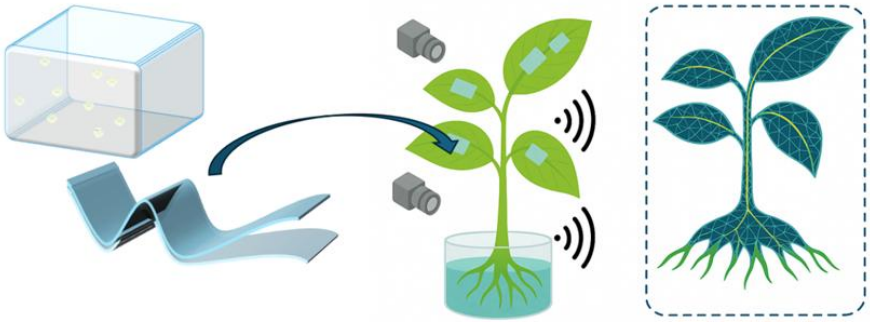


Fig. 1. Non-invasive autoradiographic imaging of plants with flexible scintillation

4 Conclusion

In this study, GOS and ZnO:Ag, respectively offered lower sensitivity in low radioactivity radioisotope than the flexible scintillator. And due to the geometric advantage of conforming to the plant leave surface, the flexible scintillators were predicted to offer better source signal to the background noise for plant.

ACKNOWLEDGMENTS

This work was supported by JSPS KAKENHI Grant Number JP24H00499, and F-REI (JPFR25040101).

References

[1] Seco J, et al., Review on the characteristics of radiation detectors for dosimetry and imaging. Phys Med Biol. 21;59(20):R303-47(2014).
[2] Laniecea, P, et al., “A new high resolution radioimager for the quantitative analysis of radiolabelled molecules in tissue section,” J. Neurosci. Methods 86(1), 1-5 (1998).
[3] Ryohei S, et al., Visualization of Uptake of Mineral Elements and the Dynamics of Photosynthates in Arabidopsis by a Newly Developed Real-Time Radioisotope Imaging System (RRIS), Plant and Cell Physiology, 57(4), 743–753 (2016)

Copyright on 7th Asia-Pacific Symposium on Radiochemistry 2025- R6-04* -

7th Asia-Pacific Symposium on Radiochemistry *September 14 ~ 19, 2025 • Kunibiki Messe • Shimane, Japan*

SODIUM-INDUCED DOT-LIKE ACCUMULATION OF ^{137}Cs IN RICE ROOT GROWN UNDER LOW K^+ CONDITION

Jun Furukawa[1, 2], Satomi Kanno[3]

[1]*Institute of Life and Environmental Sciences, University of Tsukuba:*
Tennodai 1-1-1, Tsukuba, Ibaraki, 305-8572 Japan, furukawa.jun.fn@u.tsukuba.ac.jp
[2]*Center for Research in Radiation, Isotopes, and Earth System Sciences, University of Tsukuba:*
Tennodai 1-1-1, Tsukuba, Ibaraki, 305-8577 Japan
[3]*Institute for Advanced Research, Nagoya University:*
Furo-cho, Chikusa, Nagoya, Aichi, 464-8601 Japan, kanno.satomi@iar.nagoya-u.ac.jp

^{137}Cs diffused into the environment due to a nuclear power plant accident caused serious problems for safe crop production. In plants, Cs^+ is absorbed and transported mainly by the K^+ transport mechanisms, however, the full picture of the genes contributing to Cs^+ transport is still unclear. This study focused on the sodium-induced suppression of Cs^+ transport from root to shoot in rice under low K^+ conditions. Monovalent ions uptake experiments with radioactive tracers ($^{22}Na^+$, $^{43}K^+$, and $^{137}Cs^+$) with different elemental compositions revealed the density of dot-like accumulation of ^{137}Cs in root was induced by the Na^+ absorption. And the density of this accumulation was low in low Na accumulation rice, HKT2;1 mutants. This dot-like accumulation was not observed in ^{22}Na and ^{43}K, therefore, Cs^+ specific transport and accumulation mechanisms might be involved. These findings indicate the possibility of controlling rice shoot ^{137}Cs content by regulating the Na^+ environment during cultivation.

1 INTRODUCTION

The permeability of K^+ transporters to the Cs^+ has been focused due to the problem of radioactive Cs diffused into agricultural lands after the accident at the TEPCO Fukushima nuclear power plant in 2011. There were many researches identified the Cs^+ transport activity of some K^+ transporters, however, the experimental conditions of those transporters are often far from the real plant growing conditions. To identified the Cs behavior related to the other monovalent cations, we conducted the experiment based on the Na^+ and K^+ concentrations of soil solution obtained from real paddy field.

2 MATERIALS AND METHODS

2.1 Plant materials and growth conditions

Rice (*Oryza sativa* L. Nipponbare) was used in this research. The genetic background of two OsHKT2;1 Knock Out lines, KO(NC2534) and KO(ND4057), were Nipponbare, and these rice plants are the same lines as our previous report [1]. After the germination, seedlings were grown under 16-h light/8-h dark cycles at 28°C in the CIRAD nutrient solution with several KCl and NaCl concentrations. Based on the paddy field soil solution [1], K concentration was selected 10 to 100 μM and Na concentration was up to 5 mM.

2.2 Radioisotope tracer ($^{22}Na^+$, $^{43}K^+$, and $^{137}Cs^+$) uptake experiment

For investigating Na^+ effect on the Cs^+ translocation and accumulation, plants grown as described in Section 2.1 were treated for 2 days with 0.01, 0.5, 1.0 and 5.0 mM NaCl with $^{22}Na^+$ (0.03 kBq/ml), 0.01 mM KCl with $^{43}K^+$ (0.5 kBq/ml), or 0.01 mM CsCl with $^{137}Cs^+$ (0.03 kBq/ml). The samples were separated into shoots and roots and the localization of tracers were visualized by IP Scanner (FLA 9500, GE) and then each tissue was weighed, and its γ-radiation was measured with a γ-counter (AccFLEX g7001, Aloka). The amount of total (including radioactive and non-radioactive) Na, K, and Cs were calculated based on the radioactivity and concentration of each solution.

3 RESULTS AND DISCUSSION

3.1 Na^+ absorption mediated by OsHKT2;1 affected Cs^+ translocation from root to shoot

In both HKT2;1 KO lines, Na^+ absorption was drastically suppressed compared to WT throughout investigated Na^+ ranges, suggesting that most of Na^+ absorption was performed by HKT2;1 transporter under those growth conditions. Regarding Cs accumulation, WTs showed Cs decreasing trend in shoots according to the applied Na^+ concentration, however, no similar phenomenon was observed in roots (Fig. 1). In addition to that, both HKT2;1 KO lines remained its Cs accumulation in shoots up to the 5.0 mM Na^+ treatment. These results indicate that the absorbed Na^+, not external Na^+, affected the Cs^+ translocation from root to shoot.

Copyright on 7th Asia-Pacific Symposium on Radiochemistry 2025 - R6-05 -

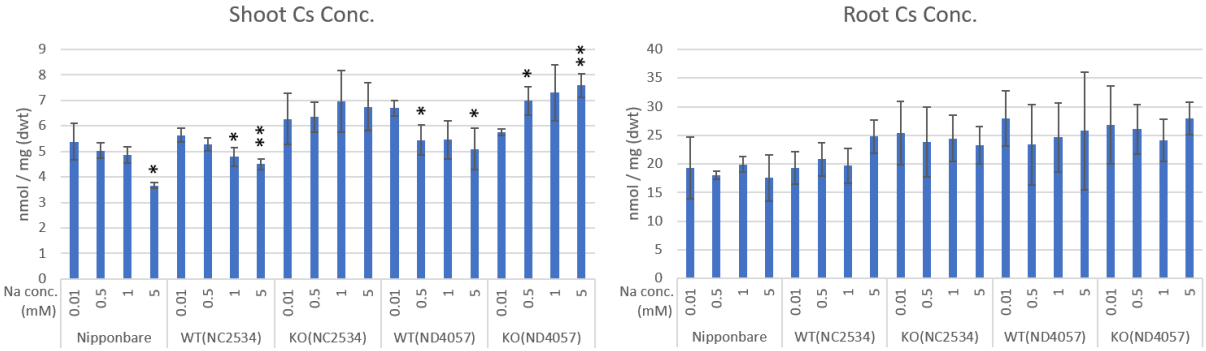


Fig. 1. Comparison of Cs accumulation with different Na^+ treatments.
Cs concentration in shoot and root after 48 h treatment. Data are the mean ± SD (n = 3, three times biologically independent experiments) and (* $p < 0.05$, ** $p < 0.01$; Welch's t-test compared to 0.01 Na^+ treatment of each line).

3.2 Increase of dot-like accumulation of Cs in the Na-treated root

For investigating the mechanisms suppressing Cs translocation from root to shoot, ^{137}Cs localization in root was investigated. According to the Na^+ concentration raised, the density of dot-like accumulation of ^{137}Cs was increased (Fig. 2). And the increase of this dot-like accumulation was not observed in the HKT2;1 KO lines. Based on the photograph of root, the position of this dot is similar to the basal part of root hair. This accumulation pattern was not observed in ^{22}Na and ^{43}K, suggesting the mechanisms for this localization might be Cs^+ specific.

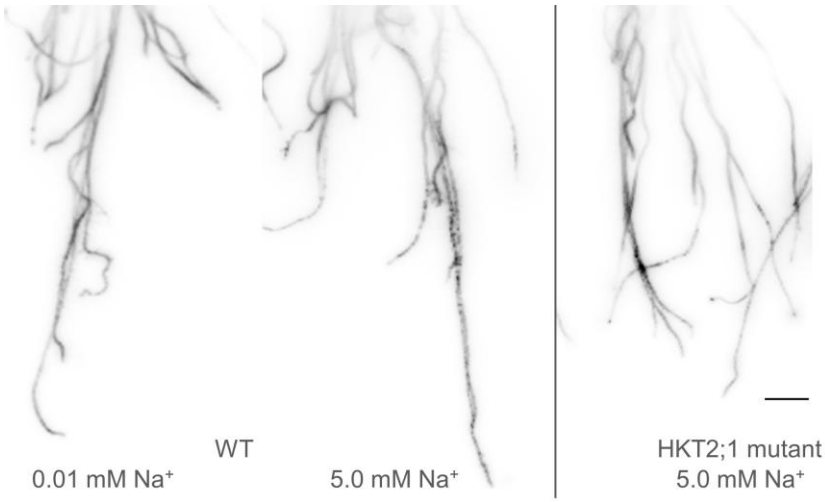


Fig. 2. Comparison of the density of dot-like ^{137}Cs accumulation among several Na^+ treatments.
^{137}Cs localization in root was obtained after 48 h treatment of 0.01 or 5.0 mM Na^+. Bar 1 cm

4 CONCLUSIONS

In these experiments, we identified the Na^+ induced suppression of Cs^+ translocation from root to shoot. And under the same condition, Na^+ induced dot-like ^{137}Cs accumulation was also enhanced in the root. To identify the mechanisms of ^{137}Cs transport in plants, investigation of Cs localization with higher resolution is necessary.

ACKNOWLEDGMENTS

This research was performed by the commissioned research fund provided by F-REI (JPFR25040101).

References

[1] S. KANNO, S. FUJIMURA, J. TAKAHASHI, C. LI, T. SHINANO, S. NAKAMURA, N. LEONHARDT and J. FURUKAWA, "Rice Na^+ absorption mediated by OsHKT2;1 affected Cs^+ translocation from root to shoot under low K^+ environments," *Frontiers in Plant Science*, **15**, 1477223 (2024).

Copyright on 7th Asia-Pacific Symposium on Radiochemistry 2025 - R6-05 -

Contributed Talk | [R1]Nuclear Chemistry

Mon. Sep 15, 2025 3:15 PM - 4:35 PM JST | Mon. Sep 15, 2025 6:15 AM - 7:35 AM UTC Hall A(MP)

[R1] Nuclear Chemistry

3:15 PM - 3:35 PM JST | 6:15 AM - 6:35 AM UTC

[R1-05]

Separation of Sm and Nd from spent fuel powder by pyrochemical process

*Mu Lin[1], Fangli Fan[1], Zhi Lin Qin[1] (1. Institute of Modern Physics, Chinese Academy of Sciences (China))

3:35 PM - 3:55 PM JST | 6:35 AM - 6:55 AM UTC

[R1-06]

High temperature retention of radioactive iodine by silver-loaded zeolite under varying atmospheric conditions

*Haohan Zhang[1], Xuandong Kou[1,2], Robert Eichler[1,2] (1. Paul Scherrer Institut (Switzerland), 2. University of Bern (Switzerland))

3:55 PM - 4:15 PM JST | 6:55 AM - 7:15 AM UTC

[R1-07*]

COPRECIPITATION OF ^{211}At WITH SAMARIUM HYDROXIDE TOWARD IDENTIFICATION OF CHEMICAL SPECIES OF At

*Ryoutarou Masuda[1,2], So Hashiba[1,2], Hiroki Aoto[1], Masashi Kaneko[1], Hiroyuki Kazama[1], Hiromitsu Haba[2], Yousuke Kanayama[2], Yudai Shigekawa[2,3], Akihiro Nambu, Yoshitaka Kasamatsu[1,2] (1. Osaka University (Japan), 2. RIKEN (Japan), 3. Tsukuba University (Japan))

4:15 PM - 4:35 PM JST | 7:15 AM - 7:35 AM UTC

[R1-08*]

Synthesis of UO_2 nanoparticles by microplasma in molten salt

*Junhan Luo[1], Yuexiang Lu[1] (1. Tsinghua University (China))

©APSORC25

7th Asia-Pacific Symposium on Radiochemistry *September 14 ~ 19, 2025 • Kunibiki Messe • Shimane, Japan*

Separation of Sm and Nd from spent fuel powder by pyrochemical process

Mu Lin[1], Fangli Fan[2], Zhi Qin[3]

[1]*Affiliation Information: Nanchang Road/509, Lanzhou, China, 730000, linmu@impcas.ac.cn*
[2]*Affiliation Information: Nanchang Road/509, Lanzhou, China, 730000, fanfangli@impcas.ac.cn*
[3]*Affiliation Information: Nanchang Road/509, Lanzhou, China, 730000, qinzhi@impcas.ac.cn*

The Accelerator-Driven Advanced Nuclear Energy System (ADANES), currently under development at the Institute of Modern Physics, Chinese Academy of Sciences, represents an innovative approach to nuclear waste transmutation and energy production. This system is designed to achieve dual objectives: (1) burning spent nuclear fuel (SNF) to reduce long-lived radioactive waste, and (2) enabling efficient uranium utilization for electricity generation. A critical challenge in this process lies in the removal of fast neutron poisons, particularly samarium (Sm) and neodymium (Nd), which significantly degrade uranium utilization efficiency by fast neutron absorption. To address this challenge, we have developed a pyrochemical separation process targeting Sm and Nd removal from SNF. The experimental protocol involves introducing a chlorination agent to a simulated SNF mixture containing at least U_3O_8, Sm_2O_3, and Nd_2O_3. Selective chlorination occurs at 300°C, converting Sm_2O_3 and Nd_2O_3 into their respective chlorides ($SmCl_3$ and $NdCl_3$). Subsequent thermal treatment at 1200°C under argon flow enables effective evaporation of these chlorides, achieving >50% removal efficiency while retaining uranium oxides. This pyrochemical approach demonstrates significant potential for rapid and effective separation of fast neutron poisons. Future work will focus on process optimization for industrial-scale implementation and validation with actual SNF compositions.

HIGH TEMPERATURE RETENTION OF RADIOACTIVE IODINE BY SILVER-LOADED ZEOLITE UNDER VARYING ATMOSPHERIC CONDITIONS

Haohan Zhang[1], Xuandong Kou[1,2], Robert Eicher[1, 2]

[1]*Laboratory of Radiochemistry, Paul Scherrer Institut (PSI), Forschungsstrasse 111, 5232 Villigen, Switzerland*
[2]*Department of Chemistry, Biochemistry and Pharmaceutical Sciences, University of Bern, Freiestrasse 3, 3012 Bern, Switzerland*

Silver-loaded zeolites are considered promising candidates for the removal of radioactive iodine released from nuclear power plants. To assess their effectiveness under severe accident conditions, it is crucial to assess the iodine retention performance at high temperatures. In this study, the Gas-jet facility at the Swiss Neutron Spallation Source (SINQ) of PSI was used as a reliable source of radioactive iodine that is produced via nuclear fission of enriched ^{235}U. Three commercially available silver-loaded zeolites were tested for iodine adsorption at high temperatures (25–1000°C) under various atmospheric conditions, including inert, oxidizing, and reducing environments. Two of the three tested zeolites demonstrated complete iodine retention up to 1000°C across all tested conditions. Iodine breakthrough was observed only under inert conditions at temperatures over 800°C, which was attributed to the formation of highly mobile iodine compound under inert condition.

1 INTRODUCTION

Following the Fukushima nuclear accident, a new filtered containment venting system (FCVS) has been developed in Japan and applied in several Japanese and French nuclear power plants [1, 2]. Silver-loaded zeolites are being explored as potential adsorbents for iodine removal in FCVS [1]. These materials have demonstrated high efficiency in capturing iodine under various conditions [1-3]. However, their performance at extreme temperatures still requires further evaluation to ensure reliability in severe accident scenarios [1, 4].

This study investigates the performance of three commercially available silver-loaded zeolites (Z1, Z2, and Z3) in removing radioactive gaseous iodine under different atmospheric conditions and temperatures up to 1000°C. A key feature of this study is the direct use of radioactive iodine produced via the nuclear fission of ^{235}U, made possible by the Gas-jet facility at the SINQ, PSI [5]. Gas chromatography experiments were performed under inert, reducing, and oxidizing conditions.

2 RESULTS

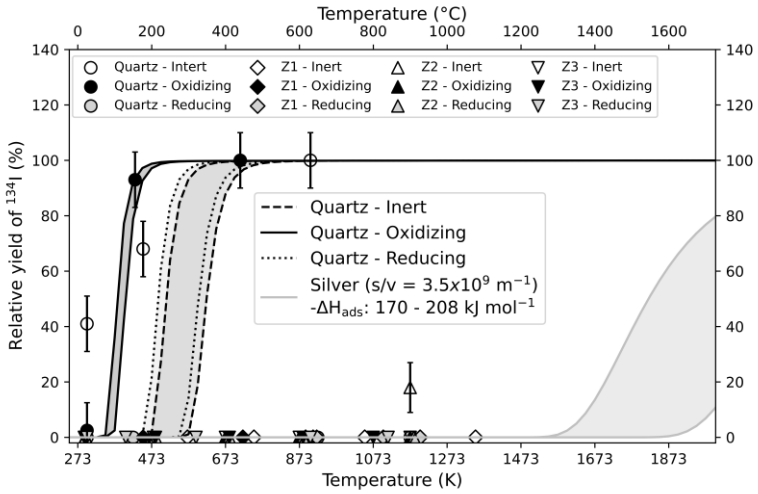


Fig. 1. Percentage of ^{134}I ($T_{1/2}$ ~ 52 mins) passing the empty quartz column with quartz wool or column with different zeolites held in place by quartz wool at different temperatures. The lines and shaded areas represent the expected behavior of iodine assuming experimentally measured adsorption properties on silica and silver metal [6,7] including the surface to volume ratios determined for the zeolites [8]. The symbols represent the experimental data from this work.

Copyright on 7th Asia-Pacific Symposium on Radiochemistry 2025 - R1-06 -

Figure 1 shows iodine retention in empty quartz columns (circles) and in quartz columns containing Z1 (diamonds), Z2 (up triangles), and Z3 (down triangles) under inert (open symbols), oxidizing (black-filled symbols), and reducing (grey-filled symbols) conditions at various temperatures. No iodine breakthrough was observed with Z1 or Z3 under any tested conditions up to 1000°C. Breakthrough occurred only with Z2 at 940°C under inert conditions.

Previous experiments using an empty quartz column under inert conditions indicated the formation of a highly mobile iodine species, resulting in increased iodine transport even at low temperatures. Preliminary analysis suggests that a similar mechanism may be responsible for the iodine breakthrough observed from AgR under inert conditions at elevated temperatures.

The longest experiment lasted for 8 hours, and no iodine (including ^{131}I, ^{133}I, ^{134}I, ^{135}I) breakthrough was observed under oxidizing, reducing, or inert atmospheres up to 800°C. Even at higher temperatures for the most relevant gas-phase compositions, the tested silver-loaded zeolites demonstrated effective iodine retention, showing their potential for application in severe accident conditions.

ACKNOWLEDGMENTS

This study is conducted within the CAESIUM project (Combined Analytical and Experimental Studies of Iodine Uptake Materials), supported by Swissnuclear.

References

[1] Y. Ishikawa *et al*., "Advanced FCVS System Using Silver Zeolite AgX, AgR and XeA," *NURETH-20*, Washington, D.C., August 20-25, 2023, p. 4248-4255, American Nuclear Society (2023).
[2] P. Chantereau *et al*., "Filtration of organic iodine discharges by zeolite adsorbents. Application to French nuclear power plants," *SMiRT 27*, Yokohama, March 3-8, 2024, IASMiRT (2024).
[3] D. Akiyama *et al*., *Journal of Nuclear and Radiochemical Sciences*, **21**, 1-6 (2021).
[4] Y. Ishikawa *et al*., "Advanced Radioactive Material Removal System by Silver Zeolite (9) Performance Evaluation of Silver Zeolite AgX by High Temperature and Atmospheric Pressure Test Equipment," *ICONE31*, Prague, Czech Republic, August 4–8, 2024, Vol. 6, 136295, ASME (2024).
[5] G. Tiebel *et al*., *Nuclear Instruments and Methods in Physics Research Section A: Accelerators, Spectrometers, Detectors and Associated Equipment*,**1041**, 167360 (2022).
[6] E. Karlsson *et al*., *Journal of Radioanalytical and Nuclear Chemistry*, **326**, 1249-1258 (2020).
[7] E. Karlsson *et al*., *Journal of Radioanalytical and Nuclear Chemistry*, **328**, 707-715 (2021).
[8] L. Liu *et al*., *LRC Annual Report 2022*, 16-17 (2023).

Copyright on 7th Asia-Pacific Symposium on Radiochemistry 2025 - R1-06 -

COPRECIPITATION OF ^{211}At WITH SAMARIUM HYDROXIDE TOWARD IDENTIFICATION OF CHEMICAL SPECIES OF At

Ryoutarou Masuda[1,2], So Hashiba[1,2], Hiroki Aoto[1], Masashi Kaneko[1], Hiroyuki Kazama[1], Hiromitsu Haba[2], Yousuke Kanayama[2], Yudai Shigekawa[2, 3], Akihiro Nambu[2] and Yoshitaka Kasamatsu[1, 2].

[1]*Graduate School of Science, The University of Osaka, 1-1 Machikaneyama, Toyonaka, Osaka 560-0043,*

masudar21@chem.sci.osaka-u.ac.jp

[2]*Nishina Center for Accelerator-Based Science, RIKEN, Wako, Saitama 351-0198*

[3]*Institute of Pure and Applied Sciences, University of Tsukuba, 1-1-1 Tennoudai, Tsukuba, Ibaraki 305-8577*

Astatine (At, Z = 85) is predicted to exhibit multiple oxidation state. However, experimental investigations of At are highly challenging, because no stable isotopes exist and only tracer-level quantities are available. The fundamental chemical properties of At remain poorly understood, and no chemical species of At have been definitively identified. Elucidating the basic chemistry of At would lead to advancement of our understanding of relativistic effects in the heavy element region. In this work, a solid precipitate sample of At was successfully produced via coprecipitation with samarium hydroxide method, as a step toward experimental identification of At species using laser ablation and mass spectroscopy. Additionally, quantum chemical calculations were employed to estimate the chemical form of the At sample.

1. INTRODUCTION

The group 17 elements, known as halogen, comprise F, Cl, Br, I, At, and Ts. Halogen typically exists as stable anions due to their high electron affinity and are classified as hard bases according to the HSAB principle. However, the heavier halogen iodine (I, Z = 53) can also form a monovalent cation (I^+) [1]. While halogen ion generally do not form coprecipitate with samarium hydroxide —yielding approximately 0%—a 10–20% precipitate has been reported for iodine, suggesting the formation of IOH (hydroxide) species [2]. In this study, we focus on astatine (At, Z = 85), a heavier homologue of iodine, which is predicted to exist in multiple oxidation states (-1, +1, +3, +5 and +7) [3], making it of significant scientific interest. The At nuclides are typically produced via accelerator-based methods and can only be handled in tracer-scale quantities. Furthermore, the absence of stable isotopes and its radioactivity impose severe limitations on experimental and analytical techniques. As a result, while properties such as ionization potential [4] and electron affinity [5] have been experimentally determined using ion beam methods, no chemical species of At in solution have been identified, and only limited information on its chemistry is available. Given its variable oxidation states depending on the chemical environment, astatine provides a valuable model for evaluating relativistic effects in the heavy element region. Therefore, elucidating its chemical behavior is of fundamental importance. In this study, we successfully produced a solid precipitate sample of At using coprecipitation with samarium hydroxide method, marking a significant step toward the first experimental identification of At species using laser ablation and mass spectroscopy. Furthermore, the chemical form of At in the solid sample was estimated using relativistic quantum chemical calculations, considering spin–orbit coupling, combined with equilibrium simulations.

2. EXPERIMENTAL

We produced ^{211}At ($T_{1/2}$ = 7.2 h) by the ^{209}Bi(α, 2n)^{211}At reaction with the AVF cyclotron at RIKEN and subsequently isolated using a dry distillation method [6]. The collected ^{211}At was prepared as a stock solution in 500 µL of 0.01 M HNO_3. In a polypropylene beaker, 10 µL of At, 20 µL of Sm standard solution (1000 mgL^{-1}, 1 M HNO_3), 200 µL pure water, and 0.1 M perchloric acid (as an oxidizing agent) or 0.6 M ascorbic acid (as a reducing agent) were added and stirred for 1 min. In the solution, 2 mL of the basic solutions: dilute or concentrated aqueous NH_3, or 0.1 or 6.0 M NaOH solutions, was added and was

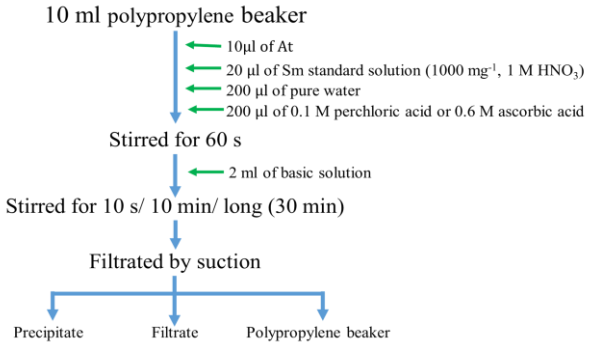


Fig. 1: Experimental scheme.

stirred for 10 s, 10 min, and 30 min (long) at room temperature (Fig. 1). Then, the solution containing the precipitate was filtrated by suction with a PP membrane filter. In addition, we prepared filter-shape standard ^{211}At samples with the same geometry as the precipitated sample to measure γ-ray counts at the same detection efficiency. The precipitate, filtrate, PP beaker, and standard samples were subjected to γ-ray spectrometry with Ge semiconductor detectors. The precipitation yield of ^{211}At was determined using equation (1) by measuring the γ-ray counts of At at 687 keV.

$$Y = \frac{A_{ppt}}{A_{ppt} + A_{fil} + A_{cup}} \times 100 \quad (1)$$

In the above equation, A_{ppt}, A_{fil} and A_{cup} represent the radio activities of the radionuclides in the precipitate, filtrate, and PP beaker, respectively.

3. RESULTS AND DISCUSSION

The coprecipitation yields of ^{211}At exceeded 10% under all conditions, when NaOH was used as the base and either perchloric acid or ascorbic was added as an additive. The maximum yield under the condition of using 0.1 M NaOH, adding perchloric acid, and stirring for 30 min was 60%, which is significantly higher than the reported yields for iodine (10–20%) and shows a trend in which higher base concentrations result in lower precipitation yields. Although for iodine, no clear dependence on base concentration was observed. This result would suggest that At forms precipitate at lower [OH^-], while at higher [OH^-], complex ions may be formed.

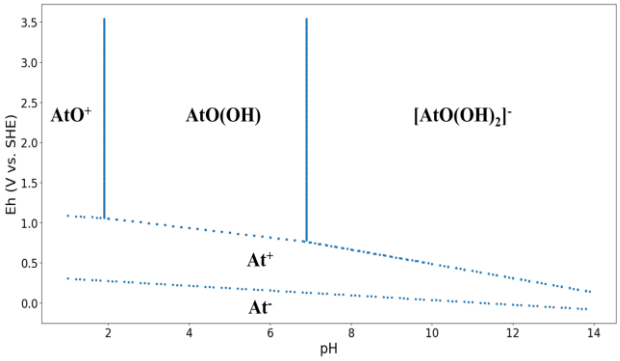


Fig. 2: Pourbaix-diagram of At.

Although the precipitate formed by iodine has been predicted to be IOH, AtOH are not represented in the pourbaix-diagram of At. Therefore, the equilibrium constant for AtOH was extrapolated from those of known XOH species (X = Cl, Br and I) using ionic radius and thermodynamic trends. Based on the estimated value, equilibrium simulations were performed using Chem EQL [7], and a pourbaix-diagram considering AtOH was constructed. However, the pourbaix-diagram does not support the precipitation of AtOH as a dominant species and suggests that the solid species is likely AtO(OH). At higher [$OH]^-$ conditions, the species $[AtO(OH)_2]^-$ is proposed as a soluble complex.

4. CONCLUSIONS

In this work, we conducted coprecipitation experiment of At with samarium hydroxide using ^{211}At and successfully produced the solid precipitate sample of At. The precipitate yield of At was found to increase as the concentration of the basic solution decrease. This trend was not observed for I. We estimated species of the coprecipitate sample of At by pourbaix-diagram as AtO(OH). In the future, we plan to analyze the sample using laser ablation and mass spectroscopy to identify the chemical species.

ACKNOWLEDGMENTS

This work was supported by JSPS KAKENHI (Grant Number: 21K18981 and 21H04473), JST, CREST Grant Number JPMJCR2416, Japan, and JST SPRING, Grant Number JPMJSP2138.

References

[1] G. SCHMITZ, Int. J Chem. Kinetics **36**, 480 (2004).
[2] Y. KASAMATSU *et al*., Applied Radiation and Isotopes. **179**, 110006 (2022).
[3] L. LIU *et al*., Inorg. Chem. **61**, 13462 (2022).
[4] S. ROTHE *et al*., Nat. Commun. **4**, 1835 (2013).
[5] L. DAVID *et al*., Nat. Commun. **11**, 3824 (2020).
[6] X. YIN *et al*., RIKEN Accel. Prog. Rep. **57**, 149 (2024).
[7] ChemEQL ver. 3.1 developed by B. MÜLLER, EAWAG.

Copyright on 7th Asia-Pacific Symposium on Radiochemistry 2025- R1-07* -

7th Asia-Pacific Symposium on Radiochemistry *September 14 ~ 19, 2025 • Kunibiki Messe • Shimane, Japan*

Synthesis of UO_2 nanoparticles by microplasma in molten salt

J. Luo[1], Y. Lu[2]*
[1]*Institute of Nuclear and New Energy Technology, Tsinghua University, Beijing, China, 100084,*
luojh21@mails.tsinghua.edu.cn

Uranium oxides (UO_2, UO_3, U_3O_8) have undergone extensive scientific scrutiny over the past fifty years, owing to their indispensable functions in both traditional nuclear-fuel technologies and cutting-edge catalytic processes. Among these, UO_2 occupies a preeminent position as the standard ceramic matrix for light-water reactor fuel, and in particular within high burn up structures (HBS), by virtue of its outstanding thermal conductivity, chemical inertness under irradiation, and the highest fissile-material density attainable among uranium-oxide compounds. In parallel, U_3O_8 has been firmly established as an effective heterogeneous catalyst for organic transformations, where its multiple oxidation states facilitate redox cycling and substrate activation. It is now well recognized that the structural, optical, and defect-related properties of these oxides are profoundly influenced by particle size, morphology, and surface termination. At the nanoscale, novel phenomena emerge—ranging from enhanced sinter ability and grain-boundary engineering to altered electronic band structure—that are absent in bulk counterparts. Indeed, UO_2 nanoparticles demonstrate markedly lower sintering temperatures, achieve superior burn-up performance when compared to micrometer-sized grains, and exhibit enhanced tolerance to irradiation-induced lattice defects and fission-product segregation. Consequently, the controlled synthesis of nanoscale UO_2, with precise control over morphology, crystallinity, and surface chemistry, has become a paramount research objective for both nuclear-materials science and nano catalysis.

Building on our earlier proof of concept study, which validated the feasibility of microplasma electrode architectures for efficient charge transfer in molten-salt electrolysis, we have developed a novel microplasma assisted electrochemical route for the direct reduction of uranyl ions (UO_2^{2+}) in a chloride-based molten salt medium. Under the influence of a localized plasma sheath at the cathode, uranyl species undergo stepwise electron uptake, yielding dispersed UO_2 nuclei that subsequently grow into monodisperse nanoparticles. By tuning operational parameter, we have achieved fine control over particle size distribution (20–200 nm). Comprehensive characterization by X-ray diffraction (XRD), transmission electron microscopy (TEM), and X-ray photoelectron spectroscopy (XPS) confirms the formation of highly crystalline, stoichiometric UO_2. Furthermore, our approach obviates the use of organic complexing agents or surfactants, thereby eliminating sources of carbonaceous contamination and minimizing wastewater generation. The resultant UO_2 nanoparticles exhibit exceptional resistance to oxidation upon air exposure, underscoring their promise for both advanced fuel-pellet engineering and potential catalytic applications. To the best of our knowledge, this study represents the first demonstration of UO_2 nanoparticle synthesis in molten salts via a microplasma electrolytic cathode, thereby expanding the frontiers of molten-salt electrochemistry into the controlled fabrication of actinide-oxide nanomaterials.

References

[1] J. Luo, Q. Qing, Z. Wang, S. Liu, J. Chen, Y. Lu. *Sep. Purif. Technol*. **332,** 125829 (2024).
[2] J. Luo, Q. Qing, L. Huang, Z. Wang, S. Liu, J. Chen, Y. Lu. *Chin. Chem. Lett.*, **35**, 108483 (2024).
[3] G. Wei, X. Liu, Y. Lu, Z. Wang, S. Liu, G. Ye, J. Chen. *Anal. Chem.*, **90**, 13163-13166 (2018).
[4] C. Ronchi, M. Sheindlin, D. Staicu, M. Kinoshita. *J. Nucl. Mater*., **327**, 58-76 (2004).

Copyright on 7th Asia-Pacific Symposium on Radiochemistry 2025- R1-08* -

Contributed Talk | [R6]Radiation and Radioisotopes in Life Science

Mon. Sep 15, 2025 3:25 PM - 4:45 PM JST | Mon. Sep 15, 2025 6:25 AM - 7:45 AM UTC Hall B(Small)

[R6] Radiation and Radioisotopes in Life Science

3:25 PM - 3:45 PM JST | 6:25 AM - 6:45 AM UTC

[R6-06]

Beta-ray imaging in vivo is a good tool for elucidating nutrient element (phosphate) absorption mechanisms in plant roots

*Satomi Kanno[1], Pascale David[2], Laurent Nussaume[2] (1. Nagoya University IAR (Japan), 2. CEA (France))

3:45 PM - 4:05 PM JST | 6:45 AM - 7:05 AM UTC

[R6-07]

Diverse mechanisms of salt tolerance in the genus *Vigna*

*Yusaku Noda[1], Nobuo Suzui[1], Yong-Gen Yin[1], Yuta Miyoshi[1], Kazuyuki Enomoto[1], Naoki Kawachi[1], Keitaro Tanoi[2], Jun Furukawa[3], Ken Naito[4] (1. QST, Takasaki (Japan), 2. UTokyo (Japan), 3. Tsukuba Univ (Japan), 4. NARO (Japan))

4:05 PM - 4:25 PM JST | 7:05 AM - 7:25 AM UTC

[R6-08]

Plant RI Imaging at Tohoku University: Advancing Plant Science Through Radioisotope Visualization

*Hiroshi Watabe[1], Yohei Kikuchi[1], Shozo Furumoto[1] (1. Tohoku University (Japan))

4:25 PM - 4:45 PM JST | 7:25 AM - 7:45 AM UTC

[R6-09]

Spatiotemporal analysis of Ca transport dynamics in tomato using Ca-45 tracer and compact multiprobe system

*Yusuke Shikanai[1], Takuma Hirashima[1], Yong-Gen Yin[2], Nobuo Suzui[2], Mitsutaka Yamaguchi[2], Yuto Nagao[2], Akihiro Saito[1], Naoki Kawachi[2], Kyoko Higuchi[1] (1. Tokyo University of Agriculture (Japan), 2. Takasaki Institute for Advanced Quantum Science, National Institutes for Quantum Science and Technology (Japan))

©APSORC25

Beta-ray imaging in vivo is a good tool for elucidating nutrient element (phosphate) absorption mechanisms in plant roots

Satomi Kanno[1], Pascale David[4], Laurent Nussaume[5]

[1]Institute for Advanced Research, Nagoya University, Nagoya, 464-8601, Japan, kanno.satomi.h6@f.mail.nagoya-u.ac.jp
[4] CEA, Aix Marseille University, Saint Paul-Lez-Durance, France, pascale.david@cea.fr
[5] CEA, Aix Marseille University, Saint Paul-Lez-Durance, France, laurent.nussaume@cea.fr

Plants absorb elements from their environment to optimally control their growth. In this study, we have improved the spatial resolution of nutrient element (phosphate) radioisotope tracer (Beta ray) imaging by using lenses and image sensors and clarified the absorption and transport of elements in plant organisms from the whole plant to the intercellular level. By combining these tracer imaging techniques with molecular biology, we have evaluated the function of phosphate transporter proteins in vivo and revealed the high contribution of root tip cells to phosphate absorption.

1 Visualize elemental movement in vivo

Plants absorb elements from their environment to optimally regulate their growth. However, the full picture of when, where, and how much of the elements are absorbed and transport regulated is still unknown. These fundamental findings are important for optimizing fertilizer use in crop production. However, to understand them, it is difficult to perform continuous analysis on the same individual plant, especially in microtissues where there are few substances to be analyzed, because the destructive method of collecting and analyzing plants over time is the main method used to understand them. The non-destructive imaging experiment system using radioactive tracers and scintillators established in our previous research has made it possible to analyze isotope behavior in plant organisms by using a camera to acquire light after the scintillator converts radiation emitted from locations where it is taken up and transferred to the plant body (Fig. 1) [1] [3]. Based on this basic principle, the detection sensitivity and spatial resolution have been improved by using objective lenses and image sensors, and the behavior and accumulation patterns of radioisotope tracers at the tissue and intercellular level have been clarified.

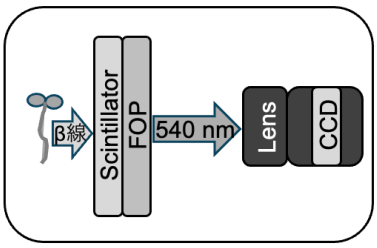


Figure 1. Principle of the first model of Realtime Radioisotope Imaging System (RRIS). Radiation (β-rays) is converted into visible light by phosphor and detected by CCD camera.

1.1 High spatial resolution of radioisotope tracer imaging in combination with microscopy

To obtain magnification of weak scintillation light images, the first approach was to use optical fibers for magnification. Tapered optical fibers allowed magnification up to 5x [2], but were often damaging to soft plant biological samples, limiting the primary observation to sections. Next, by using a combination of an objective lens for low light and a thin scintillator, signals were obtained for magnification with lenses up to 40x (Fig.2) [5].

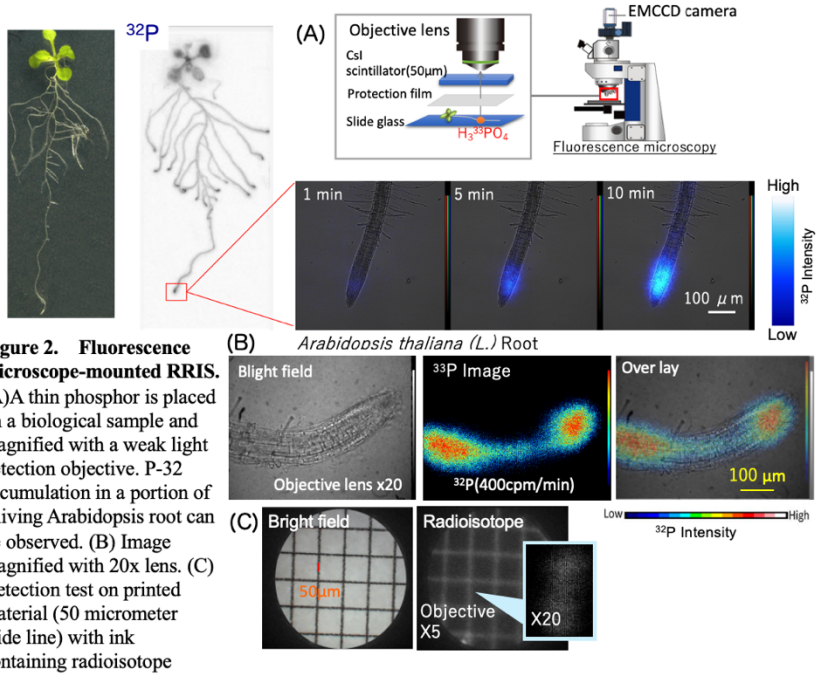


Figure 2. Fluorescence microscope-mounted RRIS. (A)A thin phosphor is placed on a biological sample and magnified with a weak light detection objective. P-32 accumulation in a portion of a living Arabidopsis root can be observed. (B) Image magnified with 20x lens. (C) Detection test on printed material (50 micrometer wide line) with ink containing radioisotope

1.2 High spatial resolution of radioisotope tracer imaging with image sensors

Even with a lens for low light, the signal is reduced through the lens, so we assembled a detection system using only a combination of a scintillator and a CMOS sensor. This system significantly improves sensitivity compared to microscopy, enabling detection in less than a second (100 kBq/500 msec),

Copyright on 7th Asia-Pacific Symposium on Radiochemistry 2025 - R6-06 -

which was difficult to achieve with microscopy systems. This allowed us to observe differences in the accumulation of radioisotope tracer between cells.
However, we also found that the background tends to increase over time due to heat(Fig.3).

1.3 Applications for elucidating the mechanisms of phosphate absorption and its distribution by plants

Phosphate tracer imaging with different localization of phosphate transporter genes was used to estimate the function of phosphate transporters in vivo. This revealed a high uptake contribution of root tip cells to the whole plant. It was shown that root tips alone are responsible for 20% of whole plant absorption and that biomass is restored by functional recovery of root tips only. This indicates the importance of absorption from root tips, especially when growing in low-phosphate environments. [4] [6].

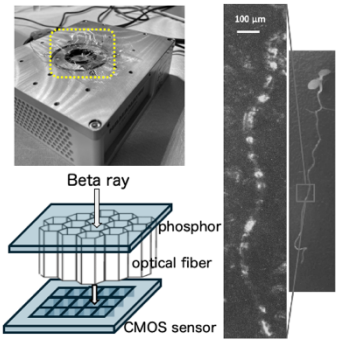


Figure 3. CMOS sensor system with phosphor.
A system of phosphor and CMOS sensor connected by optical fiber. Differences in P-32 accumulation between Arabidopsis root tissues are visible. Detection sensitivity is greatly improved. Spatial resolution is 15 μm.

2. CONCLUSIONS

The combination of a microscope objective and a scintillator or a CMOS sensor and a scintillator can detect up to non-uniform accumulation of radio isotopes between plant cells. In the future, we will continue to investigate the possibility of observing radio isotope localization in plant cells by direct detection using a CMOS image senser with a small pixel size. Combined with plant molecular biology, we were able to elucidate the previously unknown localization of transporters and the actual contribution of absorption to plant growth.

ACKNOWLEDGMENTS

This research was performed by the commissioned research fund provided by F-REI (JPFR25040101), MEXT/JSPS KAKENHI Grant Number JP MEXT/JSPS KAKENHI Grant Number JP23H02338, 22H04807, 20K06318.

References

[1] Kanno et al. “Real-time imaging of radioisotope labeled compounds in a living plant,” Radio Ana Nuc Chem. 272:565-570
[2] Rai et al. “Development of Real-time autoradiography system to analyze the movement of the compounds labeled by β-ray emitting nuclide in a living plant,” Radioisotopes 57(6):287-294, 2007
[3] Yamawaki et al. “The development of real-time RI imaging system for plant under light environment,” Radio Ana Nuc Chem. 282:275-279, 2009
[4] Nussaume et al., “Phosphate import in plants: focus on the PHT1 transporters,” Front Plant Sci 2, 83:1-12, 2011
[5] Kanno et al. “Development of Real-Time radioisotope Imaging Systems for Plant Nutrient Uptake Studies,” Royal Soc Phil Trans B 367:1501-1508,2012
[6] Kanno et al., “A novel role for the root cap in phosphate uptake and homeostasis,” eLife 5;e14577, 2016

Copyright on 7th Asia-Pacific Symposium on Radiochemistry 2025 - R6-06 -

7th Asia-Pacific Symposium on Radiochemistry *September 14 ~ 19, 2025 • Kunibiki Messe • Shimane, Japan*

Diverse mechanisms of salt tolerance in the genus *Vigna*

Yusaku Noda[1], Nobuo Suzui[1], Yong-Gen Yin[1], Yuta Miyoshi[1], Kazuyuki Enomoto[1], Naoki Kawachi[1], Keitaro Tanoi[2], Jun Furukawa[3], Ken Naito[4]

[1] *Takasaki Institute for Advanced Quantum Science, National Institutes for Quantum Science and Technology (QST), Gunma 370-1292, Japan*
[2] *Graduate School of Agricultural and Life Sciences, The University of Tokyo, Tokyo, 113-8657, Japan*
[3] *Faculty of Life and Environmental Sciences, University of Tsukuba, Ibaraki, 305-8572, Japan*
[4] *Research Center of Genetic Resources, National Agriculture and Food Research Organization, Ibaraki, 305-8602, Japan*

Understanding the mechanisms of salt tolerance and the underlying genetics is important for the development of practical salt-tolerant crops, given the increasing problems of soil salinization and freshwater shortage. Wild species of the genus *Vigna* are a great resource for tolerance to various stresses, including salinity. In our studies, we used radio-isotope (RI) imaging to reveal the following unique mechanisms of salt tolerance in the genus *Vigna* 1) Four salt-tolerant species in the genus *Vigna* have developed individual mechanisms of salt tolerance. 2) *V. riukiuensis* has the Na-trapping system by a special starch granule that accumulates in the leaves. 3) Diurnal Na excretion in *V. marina* by high expression of *VmSOS1* and diurnal regulation of *VmSOS2*. As the mechanisms of the tolerant species were different, it would be able to pile up in a single crop via various breeding techniques and would breed the high salt-tolerant crops. This knowledge will be valuable information for future crop development, especially for cropping with saline water and soil.

1 Diversity of Na^+ allocation in four salt-tolerant species

We surveyed Na accumulation and allocation in four salt-tolerant species (*V. nakashimae*, *V. riukiuensis*, *V. luteola* and *V. marina*), which identified as highly salt-tolerant plants [1] using radio-sodium (^{22}Na) and autoradiographic techniques. We performed $^{22}Na^+$ tracer experiment by treating the plants with 100 mM NaCl including $^{22}Na^+$ for 3 days in hydroponic culture. As a result, we revealed the different mechanisms of Na^+ allocation of the salt-tolerant species in the genus *Vigna*. 1) *V. nakashimae* suppresses Na^+ allocation to the leaf and shoot apex. 2) *V. riukiuensis* accumulates a higher amount of Na^+ in the leaves. 3) As new leaves grow and expand, *V. luteola* changes the accumulation of excess Na+ from old to new leaf. 4) V. marina evacuates Na^+ by the root and suppresses Na^+ allocation to the stem and the leaf. As shown in Fig. 1, wild species have acquired various salt-tolerance mechanisms. Identifying one or more of these salt-tolerance-related genes and introducing them into crops will make it possible to increase the salt tolerance of crops and is expected to contribute to the realization of cultivation on saline soils or with saline water [2].

2 Na trapping system by unique starch granule in the leaves of *V. riukiuensis*

As described above, *V. riukiuensis* accumulates a higher amount of Na^+ in the leaves. We first observed vacuoles of the leaf cells to see whether there are any structural differences between *V. riukiuensis* and other species. However, we could not find any characteristic features in the vacuoles (Fig. 2A). Instead, we found an abundance of starch granules in the chloroplast of *V. riukiuensis* leaves. Then, we referred to a report that common reed accumulates starch granules that bind Na at the shoot base [3], we were intrigued to test whether the starch granules in *V. riukiuensis* also have ability to bind Na. We shaded some leaves of *V. riukiuensis* plants for 24 h to have all the starch granules degraded whether starch granules in *V. riukiuensis* positively affected Na allocation to the leaves. The plant with shaded leaves was treated with $^{22}Na^+$ hydroponics solution and the autoradiographic image was taken. It showed that the shaded leaves did not accumulate $^{22}Na^+$, while all other leaves exhibited strong indication of $^{22}Na^+$ allocation. We performed scanning electron microscope-energy dispersive x-ray spectrometry (SEM-EDX) to locate Na in leaf and could detect Na in the cross sections of *V. riukiuensis*, especially in chloroplasts. Moreover, Na was not in the middle of starch granules but was enriched around them**,** suggesting that Na was trapped by starch granules (Fig. 2B).[4]

3 Diurnal Regulation of SOS Pathway and Na Excretion in *V. marina*

V. marina is the most salt-tolerant species in the genus *Vigna*. In our previous study, we revealed *V. marina* allocates the least amount of Na in leaves, stems and roots compared to other species. However, it was unclear whether *V. marina* simply suppresses Na^+ uptake from the root or actively excretes Na^+ that is once loaded to xylem. To observe Na^+ dynamics, we performed the positron-emitting tracer imaging system (PETIS) which enables real-time mapping of sodium in living plants. The imaging revealed that ^{22}Na levels decreased in the root while increasing in the hydroponic culture. Remarkably, we could find that *V. marina* actively excretes ^{22}Na from the root during the light period but not the dark period (Fig. 3). Based on the PETIS results, we conducted transcriptional analysis and confirmed that the SOS1 gene, which encodes one of the most well-known Na^+/H^+ antiporters, was consistently highly expressed in *V. marina*. We also found that the expression level of *VmSOS2*, which is required for activating VmSOS1, was upregulated in the light period and downregulated in the dark period. These findings indicate that the Na^+ excretion ability of *V. marina* is associated with the expression level of *VmSOS1*, and that the presence or absence of diurnal Na^+ excretion is determined by the expression pattern of *VmSOS2*. [5]

Copyright on 7th Asia-Pacific Symposium on Radiochemistry 2025

4 CONCLUSIONS

In addition to Na excretion in *V. marina*, we will identify genes related to salt tolerance, such as Na-binding to starch in *V. riukiuensis*, prevention of Na accumulation in the leaves of *V. nakashimae*, and selective Na accumulation in specific leaves of *V. luteola*. It would probably be possible to develop crop varieties with much higher salt tolerance.

References

[1] Iseki, K *et al*. "Diversity and Evolution of Salt Tolerance in the Genus *Vigna*" *PLoS One* **11**, e0164711 (2016)
[2] Noda, Y *et al*. "Diversity of Na+ Allocation in Salt-Tolerant Species of the Genus *Vigna*" *Breeding Science* **72**, 326-331 (2022)
[3] Kanai M *et al*. "Common reed produces starch granules at the shoot base in response to salt stress" *New Phytologist* **176**, 572-580 (2007)
[4] Noda, Y *et al*. "Starch-dependent sodium accumulation in the leaves of *Vigna riukiuensis*" *Journal of Plant Research* **136**, 705-714 (2023)
[5] Noda, Y *et al*. "Diurnal Regulation of SOS Pathway and Sodium Excretion Underlying Salinity Tolerance of *Vigna marina*" *Plant, Cell & Environment*, DOI: org/10.1111/pce.15402 (2025)

5 ACKNOWLEDGEMENTS

This study was financially supported by JST PRESTO Grant Number JPMJPR11B6, Moonshot R&D Program for Agriculture, Forestry and Fisheries by Cabinet Office, Government of Japan (JPJ009237), JSPS KAKENHI (JP18H02182), NARO Innovation Program, Environmental Radioactivity Research Network Center (Y-19-05), Interdisciplinary Project on Environmental Transfer of Radionuclides (No. Y-1) and the commissioned research fund provided by F-REI (JPFR23040101).

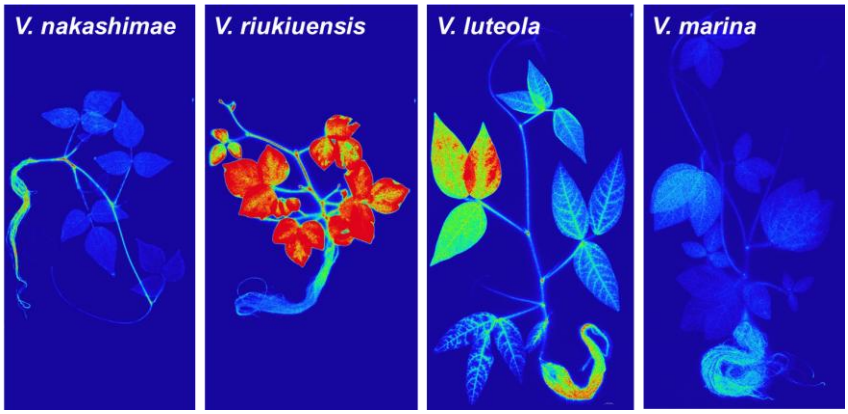


Fig. 1
Autoradiography of ^{22}Na-treated plants. Plants were taken after 72 h treatment with 100 mM NaCl containing $^{22}Na^{+}$

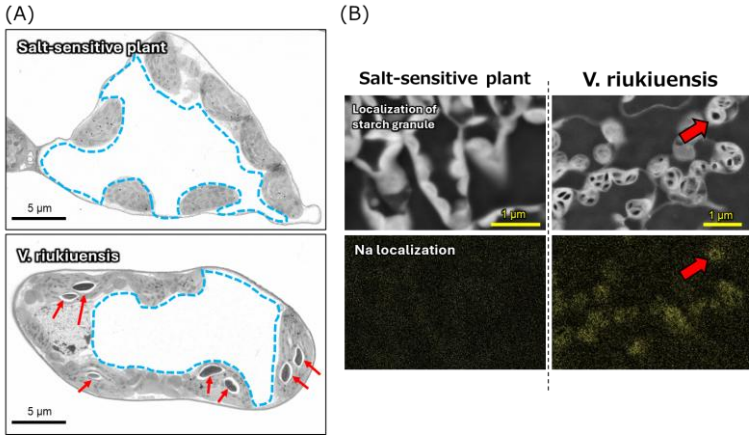


Fig. 2
(A) Electron microscopy images of leaf cells. The region outlined with a blue dotted line indicates the vacuole. Red arrows indicate starch granules. (B) Electron microscopy (Upper) and Na localization (Lower) images. The red arrows indicate representative sites where Na is adsorbed onto starch.

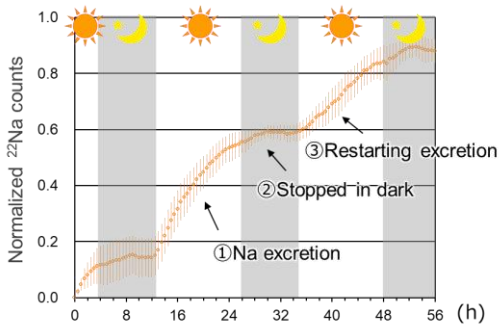


Fig. 3
Time-course of ^{22}Na excretion into the hydroponic solution in *V. marina*. Light and dark periods are indicated by white and gray areas in the plot, respectively.

Copyright on 7th Asia-Pacific Symposium on Radiochemistry 2025 - R6-07 -

7th Asia-Pacific Symposium on Radiochemistry *September 14 ~ 19, 2025 • Kunibiki Messe • Shimane, Japan*

Plant RI Imaging at Tohoku University: Advancing Plant Science Through Radioisotope Visualization

Hiroshi Watabe[1], Yohei Kikuchi[2], Shozo Furumoto[3]

[1]*Research Center for Accelerator and Radioisotope Science, Tohoku University,6-3 Aoba,Aramaki, Aoba, Sendai, 980-8578, hwatabe@tohoku.ac.jp*
[2]*Graduate School of Engineering, Tohoku University, 6-6-1-2 Aoba Aramaki, Aoba, Sendai,980-8579, yohei.kikuchi.e4@tohoku.ac.jp*
[3]*Research Center for Accelerator and Radioisotope Science, Tohoku University,6-3 Aoba,Aramaki, Aoba, Sendai, 980-8578, shozo.furumoto.b6@tohoku.ac.jp*

The Research Center for Accelerator and Radioisotope Science (RARiS) at Tohoku University represents a significant advancement in plant radioisotope imaging capabilities in Japan. Established in April 2024 through the integration of CYRIC and ELPH centers, RARiS builds upon their collaborative work since 2016 as members of the JSPS "Short-lived RI Supply Platform" project. This integration has created a comprehensive research infrastructure that supports nationwide scientific investigations utilizing short-lived radioisotopes.
RARiS houses state-of-the-art imaging equipment including a dedicated PlantPET system(Fig.1), medium/large animal PET/CT (Shimadzu Eminence Sofia), breast-specific PEM (Mirai Imaging) (Fig.2), gamma camera (MIE), and high-resolution fluorescence microscopy (Keyence). This diverse array of imaging modalities enables multifaceted visualization of physiological processes in plant systems at various scales.

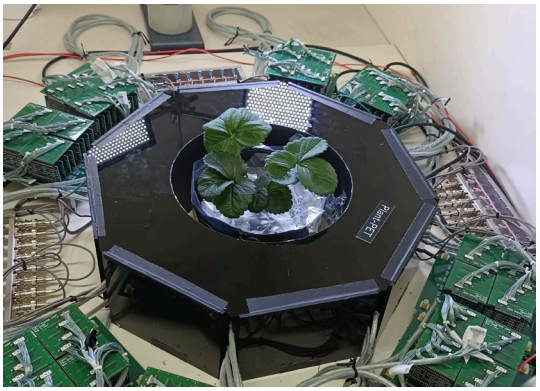


Fig. 1. PlantPET system in RARiS



Fig.2 PEM (positron emission mammography) system for plant imaging

ACKNOWLEDGMENTS

This research was performed by the commissioned research fund provided by F-REI (JPFR23040101)

Copyright on 7th Asia-Pacific Symposium on Radiochemistry 2025 - R6-08 -

7th Asia-Pacific Symposium on Radiochemistry *September 14 ~ 19, 2025 • Kunibiki Messe • Shimane, Japan*

Spatiotemporal analysis of Ca transport dynamics in tomato using Ca-45 tracer and compact multiprobe system

Yusuke Shikanai[1], Takuma Hirashima[1], Yong-Gen Yin[2], Nobuo Suzui[2], Mitsutaka Yamaguchi[2], Yuto Nagao[2], Akihiro Saito[1], Naoki Kawachi[2], Kyoko Higuchi[1]

[1]*Tokyo University of Agriculture: 1-1-1 Sakuragaoka, Setagaya-ku, Tokyo, 156-8502, Japan, ys208202@nodai.ac.jp*
[2]*Takasaki Institute for Advanced Quantum Science, National Institutes for Quantum Science and Technology: Takasaki, Gunma 370-1292, Japan*

1. INTRODUCTION

Calcium (Ca) is one of the essential macronutrients in plants. Ca has roles in stabilizing cell walls and membranes, and as a secondary messenger in signal transduction. Ca transport into plant is driven by transpiration. Therefore, Ca tends to accumulate in high-transpiration tissues (such as older leaves), while low-transpiration tissues (such as young leaves and fruits) often develop Ca deficiency symptoms, even when soil Ca is sufficient.

One of the most serious Ca deficiency disorders in agriculture is blossom-end rot (BER) in tomato, which causes necrosis in the distal part of fruit and significantly reduces its commercial values.

It has been known that the nutrient delivery to fruit largely depends on phloem rather than xylem. However, it remains unclear whether Ca delivery to fruits is directly via xylem as same as leaves or is translocated via phloem from neighboring leaves. To elucidate Ca transport dynamics in fruit, the real-time and non-destructive analysis is essential. So far, few studies are performed in big-fruit tomato cultivars.

2. MATERIALS AND METHODS

To monitor Ca transport dynamics in big-fruit tomato (House momotaro, Takii seeds) in real time manner, we conducted tracer experiments using the radioactive isotope Ca-45 and a compact multi-point detection system under both light and dark conditions (in general, the transpiration is high in light and low in dark) [1] (Fig. 1). The plant was pulse-labeled with Ca-45 at two points on the main stem below the fruit truss, either during the day or at night. Immediately after the pulse, Ca-45 were chased with non-radioactive Ca solution for 2–3 days. During the chase period, radioactivity was monitored over time along the several petioles, a peduncle, fruits and main stem (at several points) above the injection site using compact detectors. In addition, BAS imaging (autoradiograph) was also conducted on plant sections at detection points.

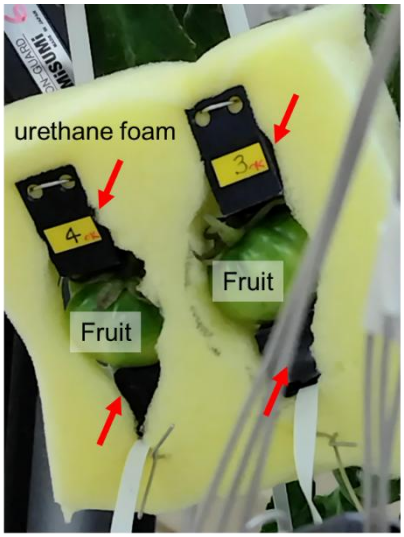


Fig. 1 Installations of compact detectors to fruits
Two fruits were monitored by compact detectors using urethane foam. Arrows indicate compact detectors.

3. RESULTS AND DISCUSSION

We obtained the time-course data with sufficient signal intensity to construct time-activity curves (TACs), successfully recording Ca dynamics reaching the fruit. In our preliminary data, no substantial difference in TAC initiation timing were observed between the peduncle (adjacent to fruit truss) and the neighboring petiole (a leaf), and both showed comparable radioactivity levels in BAS images. These results suggest that, the transport rate and amount of Ca in peduncle and petiole were similar, implying that lower Ca level in fruits compared to leaves is not caused by reduced transport to the peduncle but rather by another factor/structure between the peduncle to the fruits. Further analysis will focus on the slope and inflection points of TACs to determine transport rates and arrival times for each site and to examine the differences between day- night transport. Through these analyses, we expect to obtain new speculation about the dynamics of Ca in fruits which may provide new evidence for preventing BER in future.

In addition, from an economic and practical perspective, we would like to emphasize the usefulness of a compact multi-point detection system for real time monitoring of radio isotope in large plant body, rather than increasing the detector size. This type of detection system is useful to capture the dynamics of radio isotope in complex form plants

Copyright on 7th Asia-Pacific Symposium on Radiochemistry 2025 - R6-09 -

(including tomato), and we believe there is considerable potential demand for such systems in the field of plant science, especially crop and horticultural research.

ACKNOWLEDGMENTS

This research was performed by the commissioned research fund provided by F-REI (JPFR25040101) and supported in part by JSPS KAKENHI Grant Number JP25K09351.

References

[1] Y. Nagao et al. “Development of a compact multiprobe system for monitoring positron-emitting tracers in plant stems,” *Journal of Instrumentation*, 19(04), P04023 (2024).

Contributed Talk | [R7]Environmental Radiochemistry

Mon. Sep 15, 2025 4:45 PM - 6:05 PM JST | Mon. Sep 15, 2025 7:45 AM - 9:05 AM UTC Hall S(Int'l)

[R7] Environmental Radiochemistry

4:45 PM - 5:05 PM JST | 7:45 AM - 8:05 AM UTC

[R7-08]

Comparative Uptake Behavior of Iodide and Iodate by Corals in Seawater

*ZHIYUAN SHI[1], Yuichi Takaku[2], Shinya Yamasaki[2], Yudai Shigekawa[2], Kimikazu Sasa[3], Keisuke Sueki[2], Aya Sakaguchi[2] (1. University of Tsukuba, Environmental Studies (Japan), 2. University of Tsukuba, Institute of Pure and Applied Sciences (Japan), 3. University of Tsukuba (UTTAC), Tandem Accelerator Complex (Japan))

5:05 PM - 5:25 PM JST | 8:05 AM - 8:25 AM UTC

[R7-09]

Development of analytical method for low-level radiostrontium in seawater using strontium sorbent

*Haruka Minowa[1], Yoshimune Ogata[2], Sadao Kojima[2], Yuka Kato[3], Keisuke Sueki[4], Shinji Sugihara[5], Tetsuya Arinobu[2] (1. The Jikei University Shcool of Medicine (Japan), 2. Aichi Medical University School of Medicine (Japan), 3. Aloka Co., Ltd. (Japan), 4. Tokyo Metropolitan University (Japan), 5. Oita University (Japan))

5:25 PM - 5:45 PM JST | 8:25 AM - 8:45 AM UTC

[R7-10]

Effect Analysis of I-129 to the Environment Generated due to the Decay of Te-129m Discharged by the Fukushima Nuclear Accident

*Haruo M Sato[1], Ryo Ikeda[1] (1. Okayama University (Japan))

5:45 PM - 6:05 PM JST | 8:45 AM - 9:05 AM UTC

[R7-11*]

ATMOSPHERIC ^{210}Pb ACTIVITY CONCENTRATIONS IN NORTH KAZAKHSTAN URANIUM MINING AREA

*Assel Aidosovna Bagramova[1], Aya Sakaguchi[2,3], Kohei Sakata[2], Junko Takahashi[3], Aidana Zhumalina[1], Satoru Endo[4], Tsuyoshi Kajimoto[4], Masaharu Hoshi[5], Kassym Zhumadilov[1] (1. Eurasian National University, Department of Nuclear Physics, New Materials and Technologies (Kazakhstan), 2. University of Tsukuba, Institute of Pure and Applied Sciences (Japan), 3. University of Tsukuba, Center for Research in Radiation, Isotopes and Earth System Sciences (Japan), 4. Hiroshima University, Graduate School of Advanced Science and Engineering (Japan), 5. Hiroshima University, The Center for Peace (Japan))

©APSORC25

7th Asia-Pacific Symposium on Radiochemistry *September 14 ~ 19, 2025 • Kunibiki Messe • Shimane, Japan*

Comparative Uptake Behavior of Iodide and Iodate by Corals in Seawater

Zhiyuan Shi[1], Yuichi Takaku[2], Shinya Yamasaki[2], Yudai Shigekawa[2], Kimikazu Sasa[3], Keisuke Sueki[2], Aya Sakaguchi[2]

[1]Univ of Tsukuba, Environmental Studies, 1-1-1 Tennodai, Tsukuba, Ibaraki 305-8572, Japan.
Email: shizy@ied.tsukuba.ac.jp
[2]Univ of Tsukuba, Institute of Pure and Applied Sciences, 1-1-1 Tennodai, Tsukuba, Ibaraki 305-8571, Japan
[3] Univ of Tsukuba (UTTAC), Tandem Accelerator Complex, Tsukuba, Ibaraki 305-0006, Japan

^{129}I is a long-lived anthropogenic radionuclide released from nuclear activities since the 1940s. Owing to its long half-life, solubility in seawater, and well-documented release history, it has attracted attention as a potential oceanic circulation tracer. Coral skeletons, with distinct annual growth bands, are regarded as promising archives to reconstruct the input history of ^{129}I in marine environments. However, iodine in seawater exists mainly as iodide (I^-) and iodate (IO_3^-), and previous research indicates that these species exhibit different $^{129}I/^{127}I$ isotopic ratios. The potential selectivity of coral uptake for different iodine species may influence the reliability of historical reconstructions. This study employed the short-lived isotope ^{125}I as a tracer to evaluate the uptake behaviour of iodate by coral. $^{125}IO_3^-$ and $^{125}I^-$ were prepared separately and purified using anion exchange resin. Uptake experiments were performed with *Galaxea fascicularis* maintained in artificial seawater under controlled light and temperature. As for the tracer production experiments, the recovery of $^{125}IO_3^-$ and $^{125}I^-$ was 89.1 ± 3.2% and 93.3 ± 1.7%, Coral iodine uptake ratio increased during 4 h, uptake ratio reached18.2 ± 8.2% for $^{125}I^-$ and 8.14 ± 3.29% for $^{125}IO_3^-$, suggesting a higher uptake tendency for iodide. These results provide baseline data for understanding coral iodine uptake mechanisms and support future applications in reconstructing ^{129}I input history by using coral cores.

1.INTRODUCTION

^{129}I (half-life: 15.7 Ma) is a long-lived anthropogenic radionuclide that has been continuously released into the environment since the 1940s, mainly come from nuclear weapons testing and nuclear fuel reprocessing. Owing to its long half-life, high solubility in seawater, and clear release history [1], it is regarded as a potential oceanic circulation tracer. Compared to ^{137}Cs, which has been widely used in the past but is limited by its relatively short half-life (30.05 years) [2], ^{129}I allow for longer-term environmental reconstruction. Meanwhile, the development of Accelerator Mass Spectrometry (AMS) has enabled the detection of ^{129}I at ultra-trace levels (as low as 10^{-18} g/g) [3], expanding its applicability in marine studies. To use ^{129}I as an oceanic circulation tracer, it is necessary to clarify its temporal and spatial input history in specific regions. Coral skeletons, which form successive growth bands that can reflect the chemical composition of surrounding seawater [4], are considered one of the most suitable natural archives for this purpose. In seawater, iodine mainly exists in two inorganic forms: iodide (I^-) and iodate (IO_3^-) and their relative abundance as well as isotopic ratio ($^{129}I/^{127}I$) can vary depending on the redox conditions and their sources [5]. These differences in speciation may affect how ^{129}I was recorded in coral skeletons. However, detailed research about how corals uptake different iodine species is still lacking, which introduces uncertainty in interpreting the coral-derived ^{129}I record. In this study, carrier-free ^{125}I tracers were used under laboratory conditions to investigate species-specific uptake behavior of iodine in corals. The results aim to provide a basis for interpreting ^{129}I data from field-collected coral cores.

2. MATERIALS AND METHODS

2.1 Preparation of $^{125}I^-$ and $^{125}IO_3^-$ tracers

Due to the relatively low concentrations of ^{127}I (~5×10^{-5} g/g) and ^{129}I (~10^{-18} g/g) in natural seawater, sample pretreatment is generally required for accurate quantification, making them less convenient for laboratory-scale uptake experiments. Therefore, ^{125}I was used as a substitute, owing to its short half-life and readily detectable NaI detector. According to the equation $A = N\lambda$ (A: radioactivity, N: number of atoms, λ: decay constant), even with the same number of atoms as ^{129}I, the radioactivity of ^{125}I is sufficiently high to allow detection. ^{125}I(NaI) was obtained from the Japan Radioisotope Association (JRA). For $^{125}IO_3^-$ tracer, a ^{125}I standard solution was diluted with MQ water, followed by the addition of NaClO and HNO_3 to oxidize iodide to iodate. After mild heating and drying, the residue was redissolved and passed through an anion exchange column (AG1-×4, NO_3^- form), and MQ water was used as the eluent to collect the iodate fraction. For the preparation of $^{125}I^-$, H_2SO_3 was added to reduce the iodate and ensure complete conversion to iodide.

2.2 Radiotracer-Based Iodine Uptake Experiments with Live Corals

Uptake behavior of iodine was conducted by using *Galaxea fascicularis* (coral species name) fragments (1–2 heads each), cultured in artificial seawater. All experiments were conducted in the Radiation Control Area. In this step of the experiment, $^{125}I^-$ or $^{125}IO_3^-$ in previous step was used to conduct the uptake experiments of iodine species by the coral. Experimental process was: 20 ml of artificial seawater (Pre-warmed to 25 degrees) were added to 20 ml containers, then the coral and stirrer were added, after 4 KBq of $^{125}I^-$ or $^{125}IO_3^-$ (mixed with appropriate amount of $^{127}I^-$ or $^{127}IO_3^-$) were added to the artificial seawater, these groups were placed into a pre-prepared coral rearing system (constant temperature of 25 degrees, special coral lighting). Every hour, 100 μL solution form 20 mL containers were subsampled to observe coral uptake ratio of different iodine species over four hours. Dead coral skeletons were used as a control group to assess non-biological

Copyright on 7th Asia-Pacific Symposium on Radiochemistry 2025 - R7-08 -

adsorption. At the end of each experiment, AG1-X4 resin was used to re-separate iodine species in seawater to confirm that no transformation occurred during the experiments.

3. RESULTS AND DISCUSSION

3.1 Validation of iodine tracer preparation

Carrier-free radioactive tracers of $^{125}IO_3^-$ and $^{125}I^-$ were successfully obtained. For $^{125}IO_3^-$, after oxidation and separation using AG1-X4 anion exchange resin (NO_3^- form), the recovery rate in the eluent remained stable at 80.2% ± 2.3%. For $^{125}I^-$, sodium sulfite was added to reduce iodate to iodide, followed by the same resin separation process. The iodide activity in the effluent was measured using a NaI detector, giving a recovery of 93.3% ± 1.7%. These tracers were well prepared for coral uptake experiments investigating iodine species-specific uptake behavior.

3.2 Coral uptake of iodide and iodate

The coral uptake ratio was calculated by determining the difference between the initial ^{125}I radioactivity and the remaining radioactivity at each time point in the 20 mL seawater after sampling. The uptake behaviors of $^{125}IO_3^-$ and $^{125}I^-$ by each coral is shown in Fig. 1. The x-axis represents experimental time, while the y-axis shows the uptake ratio (%). Each line corresponds to a result of different individual coral. After four hours, iodine chemical species in the 20 mL artificial seawater were separated by AG1-X4 resin (NO_3^- form), confirming that no transformation of iodine chemical species occurred under these experimental conditions. Additionally, the absorption of iodine by coral skeletons was negligible, with the uptake ratio consistently below 1% and confirming no transformation under 4 hours. The uptake ratio results show that, both iodate and iodide groups, the overall uptake ratio of corals increased continuously during the 4-hour experimental period. At the 4-hour point, the average uptake ratio of iodide reached 18.2 ± 8.20%, while that of iodate was 8.14 ± 3.29%. Although most samples followed this increasing variation, some individual variations were observed at specific time points, which might have affected the short-term uptake rate in a few cases.

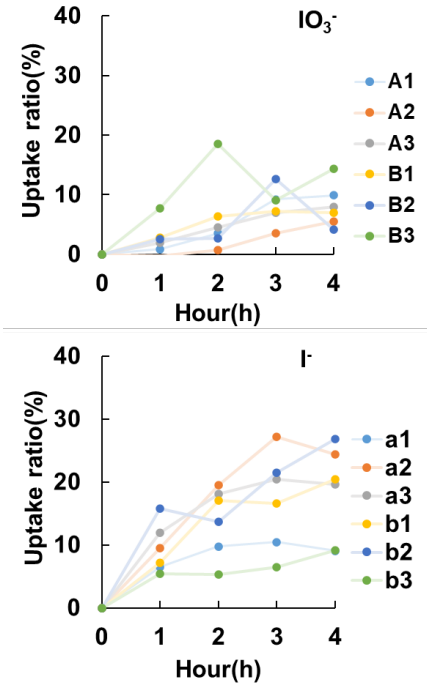


Fig. 1 Variation in uptake ratio of iodine chemical species by corals over time

4. CONCLUSIONS

In this study, carrier-free $^{125}IO_3^-$ and $^{125}I^-$ radiotracers were prepared, and an experimental system was developed at Radio Control area to investigate coral uptake preference of different iodine species. The results showed that corals took up both iodide and iodate, and the uptake ratios generally increased over the 4-hour incubation. The uptake of iodide was higher than that of iodate under the same conditions. Some variation among individual samples was observed. However, unexplained variations in individual samples were also observed. To better understand such variations, additional experimental control parameters need to be introduced in future studies.

ACKNOWLEDGMENTS

This achievement was supported by JST SPRING, Grant Number JPMJSP2124. This work was also supported in part by JSPS KAKENHI (Grant Numbers 22H02001 and 23K23269, PI: Prof. SASA K.).

REFERENCES

[1] U. Fehn, G. Snyder and P. K. Egeberg, “Iodine as a tracer of organic material: ^{129}I results from gas hydrate systems,” *Science*, 289, pp. 2332–2335 (2000).
[2] B. Liu, Z. Wang, X. Zhang and T. Zhang, “Application of ^{137}Cs tracer technique in floodplain deposition research in mesoscale river basins,” *Geoderma*, 439, 117706 (2023).
[3] H. Matsuzaki, C. Nakano, Y. S. Tsuchiya, S. Ito, A. Morita, H. Kusuno, Y. Miyake, M. Honda, A. T. Bautista VII, M. Kawamoto and H. Tokuyama, “The status of the AMS system at MALT in its 20th year,” *Nucl. Instrum. Methods Phys. Res. B*, 361, pp. 63–68 (2015).
[4] A. Sakaguchi, R. Inaba, K. Sasa, T. Matsunaka, S. Hosoya, T. Takahashi, M. Honda, H. Yamano, K. Sasaki, S. Yamasaki, T. Watanabe and K. Sueki, “Reconstruction of anthropogenic ^{129}I temporal variation in the Japan Sea using a coral core sample,” *Marine Environ. Res.,* 142, pp. 91–99 (2018).
[5] X. Hou, A. Aldahan, S. P. Nielsen and G. Possnert, “Time series of ^{129}I and ^{127}I speciation in precipitation from Denmark,” *Environ. Sci. Technol*., 43, pp. 6522–6528 (2009).

Copyright on 7th Asia-Pacific Symposium on Radiochemistry 2025 - R7-08 -

DEVELOPMENT OF ANALYTICAL METHOD FOR LOW-LEVEL RADIOSTRONTIUM IN SEAWATER USING STRONTIUM SORBENT

Haruka Minowa[1], Yoshimune Ogata[2], Sadao Kojima[2], Yuka Kato[3] Keisuke Sueki[4], Shinji Sugihara[5], Tetsuya Arinobu[2]

[1]*The Jikei University School of Medicine: 3-25-8, Nishisinbashi, Minato, Tokyo, Japan, 105-8461, minowa@jikei.ac.jp*
[2]*Aichi Medical University: 1-1 Yazakokarimata, Nagakute, Aichi, Japan, 480-1195, yoshimune.ogata@aichi-med-u.ac.jp*
[3]*Aloka Co. Ltd., 1-20-8 Nakacho, Musashino-shi, Tokyo, Japan, 180-0006, Japan, yuka.kato@aloka.co.jp*
[4]*Tokyo Metropolitan University: 1-1, Minamiosawa, Hachioji, Tokyo, Japan, 192-0364, ksueki727@gmail.com*
[5]*Oita University: 1-1 Idaigaoka, Hasama-machi, Yufu, Oita, Japan, 879-5593, sugihara-shinji@oita-u.ac.jp*

A quantitative analysis method using a Sr sorbent (Pureceram MAq®) was developed for the rapid, simple, and inexpensive analysis of radiostrontium. The sorbent was added at a ratio of 150 mg to 100 mL of seawater sample, and after stirring for 4 hours, the sorbent was separated to be desorbed Sr. The solution containing ^{90}Sr was left until ^{90}Sr-^{90}Y equilibrium, after which ^{90}Y was collected and the β-rays of ^{90}Y were measured with a gas flow counter. This method is effective for the analysis of low-level radioactive Sr in environmental waters.

1 INTRODUCTION

Radiostrontium, ^{90}Sr and ^{89}Sr are the important nuclides for assessment in radioactivity environmental monitoring. The analytical method for radiostrontium is complicated and time-consuming using dangerous chemicals [1], so a simpler and safer method is desired. In this study, we developed an analytical method for radiostrontium at low concentrations, order of mBq L^{-1}, in seawater to separate from Ca and other elements in it. This method can be applied to environmental monitoring around nuclear facilities and to environmental samples in normal times.

A newly developed Sr sorbent, Pureceram MAq® (Nippon Chemical Industrial Co., Ltd.), whose main component is barium silicate, was used. This sorbent specifically sorbs Sr, but hardly sorbs the major elements of seawater, such as Na, K, Ca, and Mg [2]. Sulfate ions are required for Sr sorption [2]. It is presumed that strontium ions precipitate as strontium sulfate, then Sr replace with Ba in the sorbent, and are sorbed as strontium silicate.

2. EXPERIMENTAL

A chemical separation method for Sr and Y was examined using radioactive tracers, ^{85}Sr and ^{90}Sr-^{90}Y. For the tracer experiments, we prepared simulated seawater containing major elements adjusted to the mean elemental composition in the ocean by Nozaki (1997) [3]. The chemical separation procedure was shown in Figure 1. Seawater was adjusted to 0.1M HCl, and Sr sorbent was added and stirred for 4 hours to adsorb Sr to the sorbent. After separation from seawater, Sr was desorbed by heating to 60°C in 2M HCl for 2 hours with stirring. The Sr solution was stored for more than two weeks until in equilibrium to grow up ^{90}Y by the decay of ^{90}Sr. Then, the yttrium hydroxide was precipitated with ammonium hydroxide solution to separate Sr. Finally, Y was collected as oxalate precipitate. The β-ray of ^{90}Y in precipitate was measured with a gas flow counter (LBC-4601, Aloka Co., Ltd.). In the tracer experiment using ^{85}Sr, radioactivity in each fraction were measured by a gamma counter (WIZARD^2, PerkinElmer Japan, G. K.), and in the case of ^{90}Sr or ^{90}Y, measured by a liquid scintillation system (LSC-6100, Aloka Co., Ltd.).

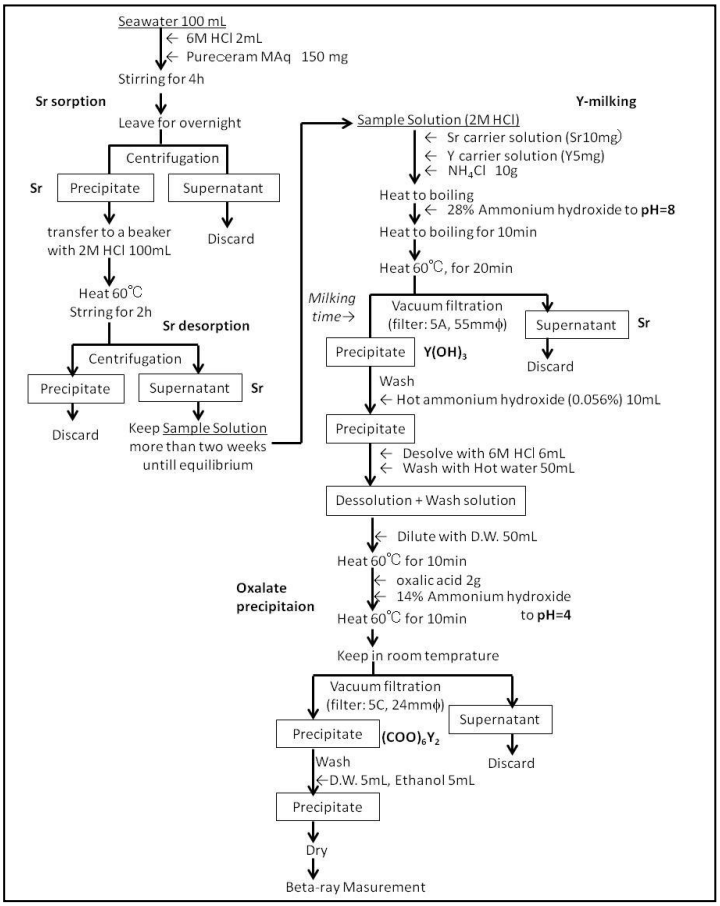


Fig. 1. Chemical separation procedure for Sr in seawater

Copyright on 7th Asia-Pacific Symposium on Radiochemistry 2025 - R7-09 -

3. RESULT AND DISCUSSION

The yields for Sr in Sr sorption, Sr desorption, and Y-milking were determined by experiments using a radioactive tracer. The results of partial and complete experiments are shown in Table 1. The sorption rate of Sr to the sorbent was approximately 90%, and the desorption rate was 70%. The yields for Y by oxalate precipitation in Y-milking were 60-70%, and the total yields were 30-40%. Sr contaminations in final precipitate were under 1%. Experiment of Y collection by carbonate precipitation are in progress. Further improvement is needed in the Y collection method, and it is expected that the Y yield can be increase by improving the precipitation process.

The minimum detectable concentration with this method was 0.23 Bq L^{-1} from 0.1 L of seawater. This method will be applied to enable measurement with a detection limit of approximately 1 mBq L^{-1} from 20 L of seawater. It has been reported that this Sr sorbent also sorbs Ra and radioactive Pb [4], but it is predictable that sorbed elements are not to interfere with the quantitative determination of Sr in this method.

This method requires one day for sorption and desorption of Sr, and one day for Y-milking after two weeks of storage, then total time to analyze for two days. This method can be made using general-purpose measuring equipment and with no dangerous reagents are required. It may be applicable to environmental monitoring of nuclear reactor facilities and to the analysis of trace amounts of radioactive Sr in environmental samples.

TABLE 1. Sr sorption and desorption rate and Y yield

Sample No.	Start solution		Radioactive Tracer	Sr sorption (%) 〈1〉	Sr desorption (%) 〈2〉	Sr yield in Y-milking (%)	Y yield in Y-milking (%) 〈3〉	Total Y yield (%) 〈1 x 2 x 3〉
	Simulated seawater (mL)	Pureceram MAq® (mg)						
J4J-23	98	155.1	^{85}Sr, ^{90}Y	91.2	-	-	-	-
J4J-33	100	148.6	^{85}Sr	91.2	-	-	-	-
J4J-34	100	148.8	^{85}Sr	92.5	-	-	-	-
A4K-23	98	150.0	^{85}Sr	91.4	-	-	-	-
J4K-51	100	148.2	^{85}Sr	90.6	-	-	-	-
J4K-52	100	149.1	^{85}Sr	88.7	70.4	-	-	-
							oxalate	
J5B-11	2M HCl, 100mL		^{85}Sr, ^{90}Y	-	-	0.5	67.9	-
J5B-12	2M HCl, 100mL		^{85}Sr, ^{90}Y	-	-	0.5	72.2	-
J5B-51	100	151.3	^{90}Sr	83.4	70.5	0.3	61.2	36.0
J5B-52	100	150.9	^{90}Sr	89.2	68.0	0.09	54.5	33.1
J5B-53	100	148.9	^{90}Sr	88.4	66.0	0.08	56.9	33.2
J5B-54	100	149.5	^{90}Sr	87.9	69.0	0.09	69.7	42.3

ACKNOWLEDGMENTS

We would like to thank the late Dr. Michio Aoyama for his valuable cooperation and advices. We thank Nippon Chemical Industrial Co., Ltd. for providing Pureceram MAq® for research use. We would like to thank the staff of the radioisotope facilities where this study was carried out. This research was partially supported by the following grants;

(1) Radiation Safety Research Promotion Fund (JPJ007057) 2021, "Development of a safe, rapid, and inexpensive analytical method for strontium in water", Radiation Nuclear Regulation Authority, Japan

(2) Environmental Radioactivity Research Network Center (ERAN), Grant No. F-21-19, F-22-06, P-23-12, P-24-09, and (3) Grants-in-Aid for Scientific Research (KAKENHI) Grant No. 24K08310.

References

[1] Ministry of Education, Culture, Sports, Science and Technology of Japan, “Radioactivity Measurement Series No.2 Radiostrontium Analysis”, Japan Chemical Analysis Center, (2003) (in Japanese)

[2] H. Minowa, Y. Ogata, Y. Kato, S. Kojima, “Characterization of barium silicate-based adsorbent for Sr in seawater and terrestrial water” *Proceedings of the 21st Workshop on Environmental Radioactivity*, *KEK Proceedings* **2020-4**. 176-179 High Energy Accelerator Research Organization (2020) (in Japanese)

[3] Y. Nozaki “Updated (1996 version) Table of the Elements in Seawater and its Remarks” *Bulletin of the Society of Sea Water Science* **51** (5) 302-308 (1997) (in Japanese)

[4] S. Kojima, Y. Ogata, H. Minowa, Y. Kato “Characterization of barium silicate-based adsorbent for Ra and Pb in seawater” *Proceedings of the 21st Workshop on Environmental Radioactivity*, *KEK Proceedings* **2020-4**. 186-191 High Energy Accelerator Research Organization (2020) (in Japanese)

EFFECT ANALYSIS OF I-129 TO THE ENVIROMENT GENERATED DUE TO THE DECAY OF Te-129m DISCHARGED BY THE FUKUSHIMA NUCLEAR ACCIDENT

Haruo Sato[1], Ryo Ikeda[2]

[1]*Okayama Univ.: 3-1-1, Tsushima-naka, Kita-ku, Okayama City, Okayama, 700-8530, sato.haruo@cc.okayama-u.ac.jp*
[2] *Okayama Univ.: 3-1-1, Tsushima-naka, Kita-ku, Okayama City, Okayama, 700-8530, poc988w9@s.okayama-u.ac.jp*

The Fukushima Daiichi Nuclear Power Station accident occurred following the Great East Japan Earthquake in March 2011 led to the release of many kinds of volatile radionuclides, which were deposited on the environment such as soils, forests, residential lands, etc. in the Fukushima prefecture and the neighbouring areas. Te-129m is one of the radionuclides released by the accident, and decays to long-lived I-129. In this study, the radioactivity concentration of I-129 in the environment generated due to the decay of Te-129m was estimated based on the analyzed data of Te-129m in soil. The analysis was conducted for 7 investigation locations in the Fukushima prefecture and neighbouring prefectures. The maximum radioactivity concentration of I-129 was estimated about 1.02E-1Bq/m^2 after 914d even for the maximum deposition amount of Te-129m (2.66MBq/m^2 as of 14 June 2011). This is approximately the same level of radioactivity concentration as in the environment (1.1E-2~1.2E-1Bq/m^2).

1. INTRODUCTION

The Fukushima Daiichi Nuclear Power Station (1F-NPS) accident occurred following the Great East Japan Earthquake on the date of 11 March 2011 led to the release of volatile radionuclides, which were deposited on the environment such as soils, forests, residential lands, etc. in the Fukushima prefecture and the neighbouring prefectures. The amounts of radionuclides discharged into the atmosphere were reported 160PBq for I-131, 18PBq for Cs-134, 15PBq for Cs-137 and 0.14PBq for Sr-90 by the Ministry of the Environment (MOE) [1]. CHINO et al. [2] estimated the total amounts of I-131 and Cs-137 discharged into the atmosphere by April 5, 2011 to be approximately 150PBq and 13PBq, respectively.

From immediately after the accident, air dose rate monitoring and analyses of radionuclides in soils and plants, etc. were conducted in a wide range of area. Consequently, volatile radionuclides such as I-131, Cs-134, Cs-137, Te-129m and Ag-110m were detected in a wide range of area, where was distant over 60km from 1F-NPS, although their concentrations and distributions are different depending on radionuclides [3].

On the other hand, Te-129m, of which radioactivity concentration in soil was approximately the same level as both radiocaesium, was also detected although its half-life is short about 1 month (half-life: 33.6d) [4]. Since very long-lived I-129 (half-life: 1.57E7y) [4] is generated due to the decay of Te-129m, the accumulation of I-129 in the environment by the accident is worried. Te-129m decays to I-129 by the following 2 decay series; Te-129m (64%) → Te-129 → I-129 → Xe-129, Te-129m (36%) → I-129 → Xe-129. Since the half-life of Te-129m is longer than that of Te-129, radioactive equilibrium is established between Te-129m and Te-129, but it is not established between Te-129 and I-129 and between Te-129m and I-129. The radioactivity concentration of I-129 increases due to the decay of Te-129m, but the maximum value of the radioactivity concentration theoretically exists. In this study, we estimated the radioactivity concentration of I-129 in the environment generated due to the decay of Te-129m discharged by the 1F-NPS accident based on the analyzed data (deposition amount) of Te-129m in soil and compared to the radioactivity concentrations of I-129 in the environment.

2. DECAY ANALYSIS OF I-129 FROM Te-129m

2.1 Calculation of the Radioactivity Concentration of I-129 Generated due to the Decay of Te-129m

Te-129m decays to I-129 by the following 2 decay series.

$$^{129m}\mathrm{Te}(64\%) \xrightarrow{\mathrm{IT},\ 33.6\mathrm{d}} {}^{129}\mathrm{Te} \xrightarrow{\beta^-,\ 69.6\mathrm{m}} {}^{129}\mathrm{I} \xrightarrow{\beta^-,\ 1.57\times10^7\mathrm{y}} {}^{129}\mathrm{Xe} \quad (1)$$

$$^{129m}\mathrm{Te}(36\%) \xrightarrow{\beta^-,\ 33.6\mathrm{d}} {}^{129}\mathrm{I} \xrightarrow{\beta^-,\ 1.57\times10^7\mathrm{y}} {}^{129}\mathrm{Xe} \quad (2)$$

For decay series (1) and (2), we derived the following analytical equations.

$$A_1 = \lambda_1 X_0 e^{-\lambda_1 t} \quad (3)$$

$$A_2 = \lambda_2 X_2 = \frac{a X_0 \lambda_1 \lambda_2}{\lambda_2 - \lambda_1}\left(e^{-\lambda_1 t} - e^{-\lambda_2 t}\right) \quad (4)$$

$$A_3 = \lambda_3 X_3 = a X_0 \lambda_1 \lambda_2 \lambda_3 \left\{\frac{e^{-\lambda_1 t}}{(\lambda_2 - \lambda_1)(\lambda_3 - \lambda_1)} + \frac{e^{-\lambda_2 t}}{(\lambda_1 - \lambda_2)(\lambda_3 - \lambda_2)} + \frac{e^{-\lambda_3 t}}{(\lambda_1 - \lambda_3)(\lambda_2 - \lambda_3)}\right\} \quad (5)$$

Copyright on 7th Asia-Pacific Symposium on Radiochemistry 2025 - R7-10 -

$$A_3' = \lambda_3 X_3' = \frac{bX_0\lambda_1\lambda_3}{\lambda_3 - \lambda_1}\left(e^{-\lambda_1 t} - e^{-\lambda_3 t}\right) \quad (6)$$

Where, X_0 is the initial number of nuclei of Te-129m, a and b the proportion of decay to decay series (1) and (2), respectively (a = 64% and b = 36%), λ_1, λ_2 and λ_3 the decay constants (= ln 2/T, T: half-life) of Te-129m, Te-129 and I-129, respectively, t the elapsed time, A_1 the total radioactivity (concentration) of Te-129m, A_2 and A_3 the radioactivities (concentration) of Te-129 and I-129 in decay series (1), respectively, and A_3' the radioactivity of I-129 in decay series (2).

Therefore, the total sum of radioactivity (concentration) of I-129 can be calculated as $A = A_3 + A_3'$ (A: the total sum of radioactivity (concentration) of I-129 generated due to the decay of Te-129m).

2.2 Analytical Condition

The analysis was conducted for 7 investigation locations among the analyzed data (as of 14 June 2011) of soil samples obtained at about 2,200 investigation locations in the Fukushima prefecture and the neighbouring prefectures [3]. The GPS information of the investigation locations and input data of Te-129m for the analysis are shown along with the analysis results.

3. RESULTS AND DISCUSSION

TABLE 1. shows the calculated results of maximum radioactivity concentration of I-129 along with input data of Te-129m (N and E stand for north latitude and east longitude in the Global Positioning System (GPS), respectively). As shown in TABLE 1., the maximum radioactivity concentration of I-129 was estimated about 1.02E-1Bq/m^2 after 914d even for the maximum deposition amount of Te-129m (2.66MBq/m^2 as of 14 June 2011,). The maximum radioactivity concentration of I-129 is equivalent to approximately one of the 1.7E8 of the initial deposition amount of Te-129m. This is approximately the same level as in the environment (1.1E-2~1.1E-1Bq/m^2). Therefore, the effect of I-129 generated due to the decay of Te-129m discharged by the 1F-NPS accident on the environment is considered to be negligible.

TABLE 1. Calculated Results of Maximum Radioactivity Concentration of I-129 along with Input Data of Te-129m

Location	N (north latitude) and E (east longitude) in GPS	Radioactivity Concentration of Te-129m (Bq/m^2) (as of 14 June 2011)	Radioactivity Concentration of Te-129m (Bq/m^2) (as of 15 March 2011)	Maximum Radioactivity Concentration of I-129 (Bq/m^2)
Onami Fukushima City	N37.76, E140.55	1.10E5	7.20E5	4.20E-3
Osuge Tomioka Town	N37.37, E141.01	1.12E6	7.33E6	4.28E-2
Shimokawauchi Kawauchi Village	N37.34, E140.90	1.45E6	9.45E5	5.51E-3
Ottozawa Okuma Town	N37.43, E141.01	2.66E6	1.74E7	1.02E-1
Yamada Futaba Town	N37.43, E140.97	1.54E6	1.01E7	5.87E-2
Ide Namie Town	N37.47, E140.93	1.49E6	9.75E6	5.69E-2
Nagadoro Iitate Village	N37.61, E140.77	2.91E5	1.90E6	1.11E-2

4. CONCLUSIONS

The radioactivity concentration of I-129 in the environment generated due to the decay of Te-129m was estimated based on the analyzed data of Te-129m in soil obtained at about 2,200 locations in the Fukushima prefecture and compared to the radioactivity concentrations of I-129 in the environment all over Japan and some field investigation data of I-129 in soil around 1F-NPS. The maximum radioactivity concentration of I-129 was estimated 1.02E-1Bq/m^2 after 914d for the maximum deposition amount of Te-129m (2.66MBq/m^2 as of 14 June 2011). The maximum radioactivity concentration of I-129 is equivalent to approximately one of the 1.7E8 of the initial deposition amount of Te-129m. This is approximately the same level as in the environment (1.1E-2~1.1E-1Bq/m^2) and the effect of I-129 generated due to the decay of Te-129m discharged by the 1F-NPS accident on the environment is considered to be negligible.

References

[1] Ministry of the Environment (MOE), https://www.env.go.jp/chemi/rhm/h29kisoshiryo/h29kiso-02-02-05.html, accessed on Nov. 1 (2018) [in Japanese].

[2] M. CHINO, H. NAKAYAMA, H. NAGAI, H. TERADA, G. KATATA and H. YAMAZAWA, "Preliminary Estimation of Release Amounts of I-131 and Cs-137 Accidentally Discharged from the Fukushima Daiichi Nuclear Power Plant into the Atmosphere," *Journal of Nuclear Science and Technology*, Vol. 48, No.7, pp.1129−1134 (2011).

[3] Ministry of Educations, Culture, Sports, Science and Technology (MEXT), "Results of the Nuclide Analysis of Soil Sampling at 2,200 Locations in Fukushima Prefecture and Neighbouring Prefectures," https://emdb.jaea.go.jp/emdb/en/portals/1020101001/, accessed on Dec. 7 (2018).

[4] Japan Radioisotope Association, Radioisotope Pocket Data Book, 9th Ed., Maruzen, Tokyo (2000) [in Japanese].

7th Asia-Pacific Symposium on Radiochemistry *September 14 ~ 19, 2025 • Kunibiki Messe • Shimane, Japan*

ATMOSPHERIC ^{210}Pb ACTIVITY CONCENTRATIONS IN NORTH KAZAKHSTAN URANIUM MINING AREA

BAGRAMOVA A[1], SAKAGUCHI A[2,3], SAKATA K[2], TAKAHASHI J[3], ZHUMALINA A[1], ENDO S[4], KAJIMOTO T[4], HOSHI M[5], ZHUMADILOV K[1]

[1]*Eurasian National University, Department of Nuclear physics, New materials and Technologies, 2 Satpayev Str., Astana 010008, Republic of Kazakhstan. Email: assel.yaf.enu@gmail.com*
[2]*University of Tsukuba, Institute of Pure and Applied Sciences, 1-1-1 Tennodai, Tsukuba, Ibaraki 305-8577, Japan*
[3]*University of Tsukuba, Center for Research in Radiation, Isotopes, and Earth System Sciences, 1-1-1 Tennodai, Tsukuba, Ibaraki 305-8572, Japan*
[4]*Hiroshima University, Graduate School of Advanced Science and Engineering, Higashi-Hiroshima City, 1-4-1 Kagamiyama, Hiroshima 739-8527, Japan*
[5]*Hiroshima University, The Center for Peace, 1-1-89 Higashisenda-Machi, Naka-Ku, Hiroshima 730-0053, Japan*

The activity concentrations of lead-210 (^{210}Pb) in size–fractionated aerosol particles were measured using 6-stage cascade impactor in the city of Stepnogorsk, situating in North Kazakhstan uranium province. This study presents the results of samples collected over 12 distinct months during the period 2020–2022. The total ^{210}Pb activity concentrations in the aerosol samples ranged from 0.46 to 2.60 mBq/m^3 (average: 0.86 mBq/m^3). The total ^{210}Pb activity in the air increased with decreasing temperature. The ^{210}Pb was mainly present as fine aerosol particles (smaller than 2.1 μm) and accounted for 95.26±2.33% of the bulk amount. The effective dose through inhalation of the aerosol particles attached with ^{210}Pb was estimated to be 0.88–2.47 μSv/y for different age groups (1-2 y.o., 2-7 y.o., 7-12 y.o., 12-17 y.o., >17 y.o.). The strong correlation between ^{210}Pb and certain major anion concentrations indicates that human activity, particularly high-temperature coal combustion, is a significant contributor to atmospheric ^{210}Pb in the area.

1. INTRODUCTION

Kazakhstan ranks second in the world in uranium (U) mining and the North Kazakhstan uranium province accounts for 12% of the country's uranium reserves [1]. The Stepnogorsk Hydrometallurgical and Chemical Plant (SHCP), located in the North Kazakhstan uranium province, processes uranium ore, with its tailings dump being the region's largest radioactive waste site [2]. Thus, monitoring of uranium and its decay products in nearby residential areas is essential. In this study, we focused on the decay product of ^{238}U, lead-210 (^{210}Pb) ($T_{1/2}$ = 22.3 years), which is important not only for health impact assessment [3,4] but also as a geoscience research tool, and attempted to evaluate the atmospheric concentration of ^{210}Pb in the Northern Kazakhstan uranium province.

2. MATERIALS AND METHODS

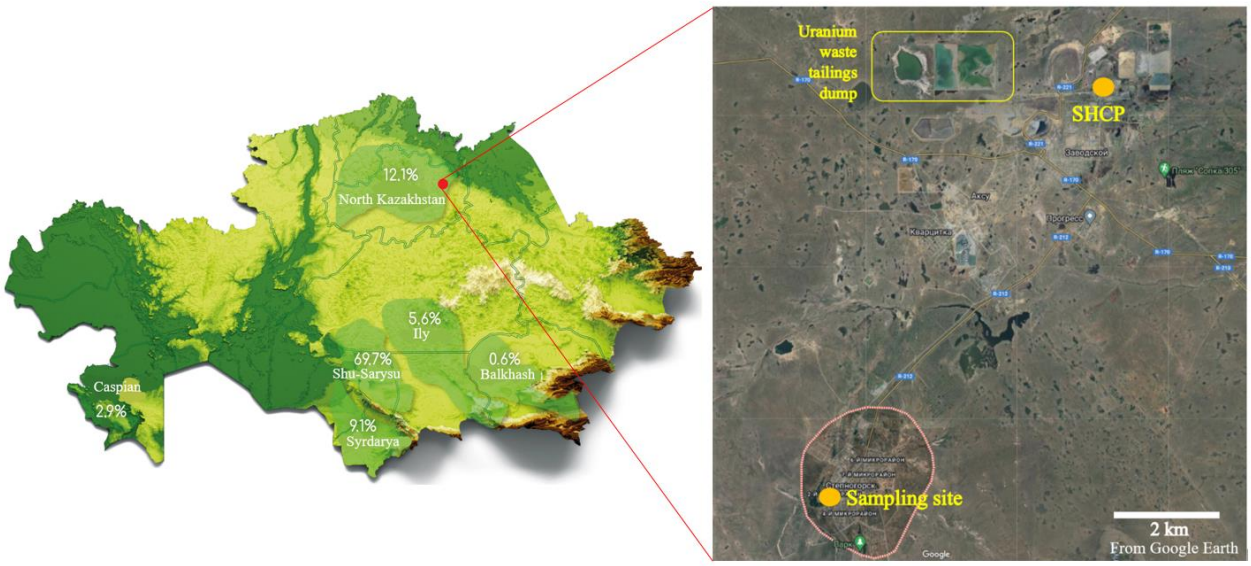


Fig. 1. U reserves (%) in the provinces [1] and sampling site

Copyright on 7th Asia-Pacific Symposium on Radiochemistry 2025- R7-11* -

Aerosol collection was conducted in the city of Stepnogorsk (52°20'43.1"N 71°52'21.5" E), located about 20 km from the SHCP and the tailings dump (Fig. 1). Size-fractionated aerosol particles were collected by a high-volume air sampler equipped with a 6-stage cascade impactor every 2 weeks from 2020 to 2022, excluding the winter season (October to April). The ^{210}Pb on each size filter was measured using a high-purity Ge detector [5]. Major ions were also measured in the samples after extraction with ultrapure water.

3. RESULTS AND DISCUSSION

The total ^{210}Pb activity concentrations in the air ranged from 0.46 to 2.60 mBq/m^3 with a mean of 0.86 mBq/m^3. The negative correlation (R=-0.60) between total activity and average temperature indicated an increase in concentration with decreasing temperature.

The radiation dose from inhaling ^{210}Pb-attached aerosol particles was estimated to be between 0.88 and 2.47 μSv/y for various age groups. These values were about 1.7 times higher than the dose based on the world average ^{210}Pb concentration [6], even though they did not take into account winter values, when ^{210}Pb concentrations are expected to be higher.

The fine fraction(<2.1μm) of aerosols contained 95.26±2.33% of the total activity. The correlation between ^{210}Pb and major anion concentrations, especially secondary species such as sulfate and nitrate, was observed. These results indicate that, although ^{210}Pb is a naturally occurring radionuclide, the major source of atmospheric ^{210}Pb is from human activities such as high-temperature coal combustion rather than uranium mining.

4. CONCLUSIONS

This study focused on atmospheric ^{210}Pb activity in the uranium ore processing and tailings dump area. The results of this study showed that the airborne ^{210}Pb concentration increased during colder periods and the estimated inhalation dose was up to 1.7 times higher than the dose based on the global average ^{210}Pb concentration even though this estimate did not include the data from the winter season. The ^{210}Pb activity was predominantly associated with the fine aerosol fraction, and observed the strong correlation between ^{210}Pb and major anions (sulfate and nitrate) indicated that anthropogenic emissions, such as coal combustion, are a major source of atmospheric ^{210}Pb in the region.

ACKNOWLEDGMENTS

This study was supported by the Science Committee of the Ministry of Science and Higher Education of the Republic of Kazakhstan (Grant No. AP23488651), by JSPS KAKENHI grant no. JP26257501 and 19H01149 and also by the Environmental Radioactivity Research Network Center (ERAN) (F-22-14, F-23-14 and F-24-04).

REFERENCES

[1] Kazatomprom, 2024. URL: https://www.kazatomprom.kz/ru/page/dobicha_prirodnogo_urana
[2] Atomic Energy Agency of the Republic of Kazakhstan. Materials of the work of the commission for the study of the state of the radiation situation at the mine departments of the Tselinny Mining and Chemical Combine. Vol. 20 (1993).
[3] J. G. POUNDS, W.M. BLAKEMORE, “The potential laboratory health hazard of ^{210}Pb and a simple procedure for separation of ^{210}Pb from the daughters ^{210}Bi and ^{210}Po”, *Toxicol Lett*. 9 (1981).
[4] G.R. LAURER et.al., “Skeletal ^{210}Pb levels and lung cancer among radon-exposed tin miners in southern China”, *Health Phys.* 64 (1993)
[5] A. BAGRAMOVA et.al., “Gamma ray registration efficiency simulation of a HPGe detector with PHITS”, *J Radioanal Nucl Chem* 334 (2025)
[6] Compendium of Dose Coefficients based on ICRP Publication 60, ICRP Publication 119 (2012).

Copyright on 7th Asia-Pacific Symposium on Radiochemistry 2025- R7-11* -

Contributed Talk | [R1]Nuclear Chemistry

Mon. Sep 15, 2025 4:50 PM - 6:10 PM JST | Mon. Sep 15, 2025 7:50 AM - 9:10 AM UTC Hall A(MP)

[R1] Nuclear Chemistry

4:50 PM - 5:10 PM JST | 7:50 AM - 8:10 AM UTC

[R1-09*]

Internal Conversion Electron Spectroscopy Using a Silicon Drift Detector (SDD) for Elucidation of Excited-State Structure in Superheavy Nuclei

*Naoto Miyashita[1], Masato Asai[2], Naoyuki Kitagawa[1], Tomoki Fujii[1], Toshitaka Niwase[1], Satoshi Sakaguchi[1] (1. Kyushu University (Japan), 2. Japan Atomic Energy Agency (Japan))

5:10 PM - 5:30 PM JST | 8:10 AM - 8:30 AM UTC

[R1-10*]

Evaluation of radiation tolerance of solar cell detectors using tandem accelerator at Kyushu University

*Hiroto Watanabe[1], Toshitaka Niwase[1], Yuki Yamanouchi[1,2], Tomoki Fujii[1], Naoto Miyashita[1], Naoyuki Kitagawa[1], Yuya Michimoto[1], Ryosuke Shikada[1], Gen Otsuka[1], Satoshi Sakaguchi[1], Takashi Teranishi[1], Hiroyuki Makii[3], Masato Asai[3], Yutaka Watanabe[4] (1. Department of Physics, Kyushu University (Japan), 2. RIKEN Nishina Center for Accelerator-Based Science (Japan), 3. Advanced Science Research Center, Japan Atomic Energy Agency (Japan), 4. Wako Nuclear Science Center, Institute of Particle and Nuclear Studies, High Energy Accelerator Research Organization (KEK) (Japan))

5:30 PM - 5:50 PM JST | 8:30 AM - 8:50 AM UTC

[R1-11*]

Progress for the development of a new detector system for studying the β-delayed fission

*Tomoki Fujii[1], Toshitaka Niwase[1], Yuki Yamanouchi[1], Naoyuki Kitagawa[1], Naoto Miyashita[1], Yusuke Tanaka[1], Satoshi Sakaguchi[1], Yoshikazu Hirayama[2], Yutaka Watanabe[2], Hiroari Miyatake[2] (1. Kyushu University (Japan), 2. Wako Nuclear Science Center, KEK (Japan))

5:50 PM - 6:10 PM JST | 8:50 AM - 9:10 AM UTC

[R1-12*]

Development and performance evaluation of Multi-Sampling Ionization Chamber using intense slow heavy ion beams with mass numbers around 10

*Ryosuke Shikada[1], Masaomi Tanaka[2], Naoyuki Kitagawa[1], Tomoki Fujii[1], Gen Otsuka[1], Hiroto Watanabe[1], Toshitaka Niwase[1], Satoshi Sakaguchi[1] (1. Department of Science, Kyushu University (Japan), 2. Faculty of Arts and Science, Kyushu University (Japan))

©APSORC25

7th Asia-Pacific Symposium on Radiochemistry *September 14 ~ 19, 2025 • Kunibiki Messe • Shimane, Japan*

Internal Conversion Electron Spectroscopy Using a Silicon Drift Detector (SDD) for Elucidation of Excited-State Structure in Superheavy Nuclei

N. Miyashita[1], M. Asai[2], N. Kitagawa[1], T. Fujii[1], T. Niwase[1], S. Sakaguchi[1]

[1] *Department of Physics, Kyushu University, 744 Motooka, Nishi-ku, Fukuoka 819-0395, Japan*
[2] *Advanced Science Research Center, Japan Atomic Energy Agency, Tokai, Ibaraki 319-1195, Japan*

Abstract – To elucidate exited-state structure of superheavy nuclei, we are developing a new nuclear spectroscopy technique using a silicon drift detector (SDD) to measure "internal conversion electrons" which are emitted more abundantly than γ-rays in the case of superheavy nuclei. We tested performance of SDD by measuring γ-rays as well as internal conversion electrons to evaluate energy resolutions, detectable energy range for both low- and high-energy electrons, background characteristics, etc. Our goal is to clarify shell closure at N = 152 and 162. In this presentation, we report current experimental results and discuss prospects.

Keywords – superheavy elements, silicon drift detector, internal conversion electron spectroscopy, shell closure

1. Introduction

1.1 Island of Stability

Atomic nuclei exhibit enhanced stability when the number of protons or neutrons corresponds to certain specific values, known as "Magic number." For example, ^{208}Pb, with 82 protons and 126 neutrons, is well known as a double magic and exceptionally stable nucleus. Theoretical studies have further predicted that, in the superheavy nuclear region, the proton number around between 114 and 126 and the neutron number of 184 may represent new magic numbers. This region is referred to as the "Island of stability" [1]. One of key experimental approaches to elucidate shell structure in this region is the measurement of excited states by means of nuclear spectroscopy.

1.2 Status and Challenges in Spectroscopy of Superheavy Nuclei

One approach to investigating nuclear structure is "α–γ spectroscopy", in which γ-rays emitted following α decay are observed. In nuclei with the atomic number greater than 82, the α decay occurs easily, and the coincident detection of α particles and γ-rays from excited states in the daughter nucleus enables the acquisition of high-resolution and low-background data. However, in the case of superheavy nuclei, excited states populated via the α decays are often located at very low energy, and their de-excitation occurs more often by internal conversion than by γ-ray emission. As a result, the conventional γ-ray spectroscopy technique is ineffective for studying superheavy nuclei, presenting a significant challenge to the investigation of excited-state structure in superheavy nuclei.

1.3 New Method of Nuclear Spectroscopy

To cope this challenge, it is necessary to develop a new nuclear spectroscopy technique that measures internal conversion electrons instead of conventional γ-rays. Traditionally, Si(Li) detector and Si PIN photodiode have been used for the detection of internal conversion electrons [2]. However, these detectors suffer from limited energy resolution, making them inadequate for detailed spectroscopy of internal conversion electrons from superheavy nuclei. In this study, we are working on the development of a new spectroscopic method by employing a silicon drift detector (SDD), which offers higher energy resolution and is better suited for this purpose.

The aim of this study is to establish a new nuclear spectroscopy method using a silicon drift detector (SDD) to enable the measurement of low-lying excited states in superheavy nuclei and to experimentally clarify the existence of deformed shell closures at N = 152 and 162.

2. Silicon Drift Detector

The silicon drift detector (SDD) is a type of detector that has been used in X-ray spectroscopy such as synchrotron radiation experiments and X-ray fluorescence analysis. The SDD consists of concentric ring electrodes patterned on a high-purity silicon substrate, with a small collecting anode located at the center. This structure offers excellent energy resolution for low-energy X-rays (125 eV at 5.9 keV [3]). Furthermore, unlike Ge detectors, the SDD can be operated with the Peltier cooling without using liquid nitrogen, allowing for the construction of more compact and lightweight detection system.

Copyright on 7th Asia-Pacific Symposium on Radiochemistry 2025- R1-09* -

3. Experiment and Results

The aim of this study is to measure the energy resolution of the SDD for low-energy internal conversion electrons and X/γ-rays as part of the development of a new spectroscopy method applicable to superheavy nuclei. For the SDD, we used an XSDD50-01WL manufactured by Techno AP Co., Ltd. This model features a windowless design that allows operation inside a vacuum chamber. We measured energy spectra of X/γ-rays using ^{241}Am, ^{133}Ba, ^{152}Eu and internal conversion electrons using various sources and evaluated the energy resolution (Figs. 1 and 2). This presentation reports on the energy resolution of internal conversion electrons up to several hundred keV, as well as the influence of energy loss due to the detector's dead layer and background radiation. In future work, we plan to measure internal conversion electrons emitted in the decay of short-lived heavy actinide nuclei produced using the tandem accelerator at JAEA. This will enable us to study the excited-state structure and deformed shell closures in heavy actinide nuclei.

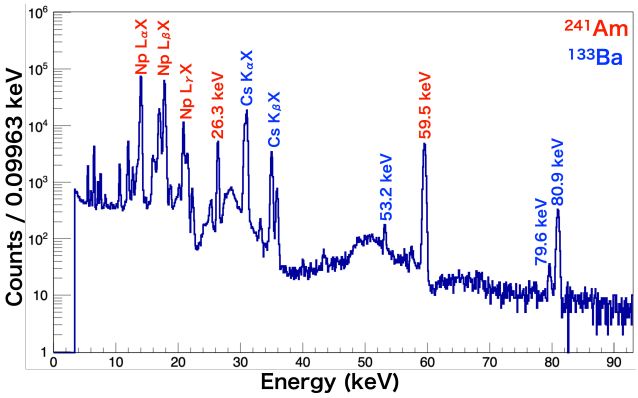


Fig. 1. X/γ-rays Energy Spectrum measured by SDD using ^{241}Am and ^{133}Ba sources.

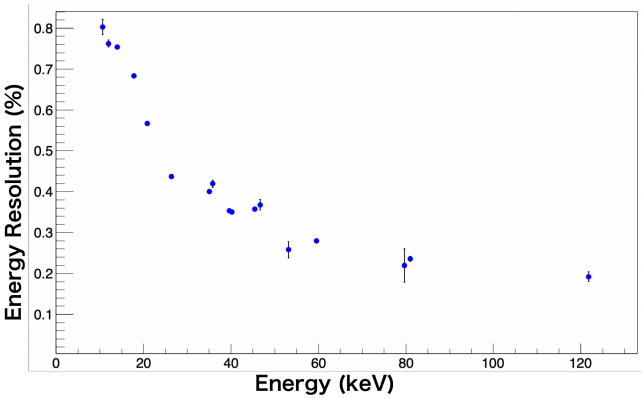


Fig. 2. X/γ-rays Energy Resolution measured by SDD using ^{241}Am, ^{133}Ba and ^{152}Eu sources.

References

[1]: S. Hofmann, Super-heavy nuclei, J. Phys. G: Nucl. Part. Phys. 42, 114001 (2015).

[2]: P. Lechner et al., Silicon drift detectors for high count rate X-ray spectroscopy at room temperature, Nucl. Instrum. Methods Phys. Res. A 458, 281–287 (2001).

[3]: Techno AP Co., Ltd., Technical Report No.09: SDD X-ray Detection Systems, https://www.techno-ap.com/report_no-09.html (accessed April 24, 2025).

Copyright on 7th Asia-Pacific Symposium on Radiochemistry 2025- R1-09* -

7th Asia-Pacific Symposium on Radiochemistry *September 14 ~ 19, 2025 • Kunibiki Messe • Shimane, Japan*

Evaluation of radiation tolerance of solar cell detectors using tandem accelerator at Kyushu University

Hiroto Watanabe[1], Toshitaka Niwase[1], Yuki Yamanouchi[1,2], Tomoki Fujii[1], Naoto Miyashita[1], Naoyuki Kitagawa[1], Yuya Michimoto[1], Ryosuke Shikada[1], Gen Otsuka[1], Satoshi Sakaguchi[1], Takashi Teranishi[1], Hiroyuki Makii[3], Masato Asai[3], Yutaka Watanabe[4]

[1] *Department of Physics, Kyushu Univercity: 744 Motooka, Nishi-ku, Fukuoka 819-0395, Japan*
[2] *RIKEN Nishina Center for Accelerator-Based Science: Wako, Saitama 351-0198, Japan*
[3] *Advanced Science Research Center, Japan Atomic Energy Agency：Tokai, Ibaraki 319-1195, Japan*
[4] *Wako Nuclear Science Center, Institute of Particle and Nuclear Studies, High Energy Accelerator Research Organization (KEK): Wako, Saitama 351-0198, Japan*

1 INTRODUCTION

Semiconductor detectors, such as silicon detector, are used to detect charged particles. Semiconductor detectors identify particles by detecting the electron-hole pairs created by the incident particles. Solar cells are semiconductor devices normally used to generate electricity. Solar cells can also be used as radiation detectors because they work on the same principle as semiconductor detectors [1].

Solar cell detectors are easy to cut for desired size, and very low cost. Although the energy resolution of the solar cell detector is lower than that of the standard Si detector, it has sufficient resolution to separate fission fragments [2]. It has also been suggested that the solar cell detector is more radiation tolerant than the Si detector and is expected to be useful for fission fragment measurements in strong background environments [3].

There are several types for the solar cell, such as *n*-type/*p*-type and single-crystal/poly-crystal semiconductors. It is still unclear which structure is suitable as a heavy ion detector. We performed an experiment to evaluate the radiation tolerance of solar cell detectors of different structures by irradiating the detectors with heavy ion beam using a tandem accelerator.

2 EXPERIMENTAL SETUP

The experiment was carried out using a tandem accelerator at the Center for Accelerator and Beam Applied Science (CABAS), Kyushu University. In this experiment, we used five types of solar cell detectors and a standard Si detector. The beam was ^{127}I accelerated to 66 MeV. The beam intensity was adjusted to 3,000 cps with a mesh installed in the ion source, and the beam was injected directly into the solar cell detectors and Si detector. Beam irradiation time is about 10 hours for the solar cell detectors and about 7 hours for the Si detector.

We used four types of monocrystalline solar cells: *p*-type Aluminum Back Surface Field (Al-BSF), Passivated Emitter and Rear Cell (PERC), *n*-type Tunnel Oxide Passivated Contact (TopCon), and one type of polycrystalline solar cell. A Si PIN diode (Hamamatsu-S3590) was used as a standard Si detector for comparison. The solar cell detectors and Si detector were used without bias voltage. In order to reduce noise, the preamplifier (Cremat CR-110/111) was installed inside a vacuum chamber.

3 RESULT

This experiment provided data on the variation of pulse height with beam dose. An example of the results is shown in Fig 1. Figure 1 (a) shows the experimental results for the *n*-type monocrystalline solar cell detector and Fig 1 (b) shows the experimental results for the Si PIN diode. The horizontal axis shows the beam dose and the vertical axis shows the pulse height. We generated pulse height spectra from these data and analyzed the variation of pulse height and energy resolution as functions of beam dose.

Further analysis is ongoing to evaluate the radiation tolerance of solar cell detectors. The details of the experiment and the results obtained will be reported and discussed in this presentation.

Copyright on 7th Asia-Pacific Symposium on Radiochemistry 2025- R1-10* -

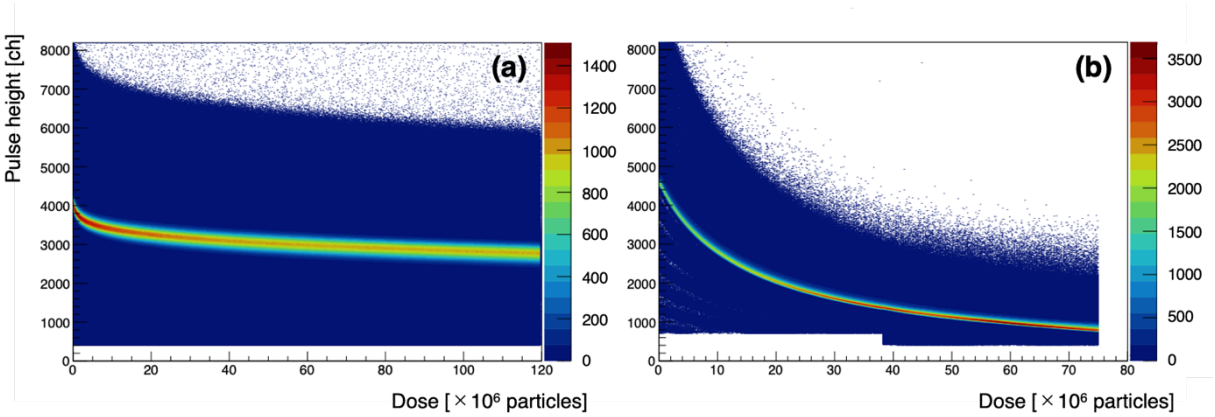


Fig.1. Pulse height variation with beam dose.
(a) *n*-type monocrystalline solar cell detector. (b) Si PIN diode.

References

[1] Gunter siegert, Nuclear Inst. and Methods, **164** (1979) 437.
[2] J. D. Koglin, *et al*., Nuclear Inst. and Methods in Physics Research, A **854** (2017) 64.
[3] A. Henriques, *et al*., Nuclear Inst. and Methods in Physics Research, A **969** (2020) 163941.

Copyright on 7th Asia-Pacific Symposium on Radiochemistry 2025- R1-10* -

Progress for the development of a new detector system for studying the β-delayed fission

Tomoki Fujii[1], Toshitaka Niwase[1], Yuki Yamanouchi[1], Naoyuki Kiatagawa[1], Naoto Miyashita[1], Yusuke Tanaka[1], Satoshi Sakaguchi[1], Yoshikazu Hirayama[2], Yutaka Watanabe[2], Hiroari Miyatake[2]

[1]*Depertment of Physics Kyushu University, 744 Motooka, Nishi-ku, Fukuoka 819-0395, Japan*
[2]*Wako Nuclear Science Center, Institute of Particle and Nuclear Studies, High Energy Accelerator Research Organization (KEK): Wako, Saitama 351-0198, Japan*

We are developing a new detector system using a Ce:GAGG scintillator to study β-delayed fission of neutron-rich actinides in the termination region of the astronomical r-process. To evaluate the detector response to β-ray, we are constructing a monoenergetic β-ray source using a standard β-source, neodymium magnets, and a slit. This presentation reports the development status and future prospects.

INTRODUCTION

Recent observations of gravitational waves and subsequent electromagnetic waves have drawn attention to kilonovae, which occur following binary neutron star mergers, as sites of the *r*-process, which is thought to be one of the origins of elements heavier than iron [1]. The *r*-process occurs in explosive astronomical environments such as neutron star mergers. The *r*-process is expected to terminate with the fission of actinide and transacitnide nuclides. The fission properties of these nuclides, including the fission barrier and fission probability, have a significant influence on the production patterns of heavy elements [2]. However, theoretical predictions of fission properties depend strongly on mass models and astrophysical environments, and are subject to large uncertainties [3]. Therefore, experimental measurements of the decay properties of these nuclides are necessary to understand the origin of heavy elements.

Development of a detector system using GAGG

Our main purpose is to clarify the decay modes of nuclides in the termination area of the *r*-process. We started to develop a new detector system (Fig. 1) to measure the fission barrier and mass distribution of fission fragments. Their nuclides produced by nuclear reactions will undergo *β*-decay. If the excitation energy of the daughter nuclides after *β*-decay is higher than the fission barrier, *β*-delayed fission will occur. The fission barrier can be obtained by subtracting the maximum energy of the *β*-rays in coincidence with fission events from the mass difference between the parent and daughter nuclides [4]. In this study, we used a Ce:GAGG (Ce-doped $Gd_3(Al,Ga)_5O_{12}$) scintillator [5] to measure the energy of *β*-rays. GAGG is sensitive to both *β*-rays and *γ*-rays, so it can simultaneously measure *γ*-rays emitted due to deexcitation following *β*-decay. This makes it possible to determine both the fission barrier and the excitation level transitioned after *β*-decay or fission. In addition, since GAGG crystals are not deliquescent, they can be placed directly in a vacuum without a window. This allows the energy of *β*/*γ*-rays to be measured with high accuracy and precision.

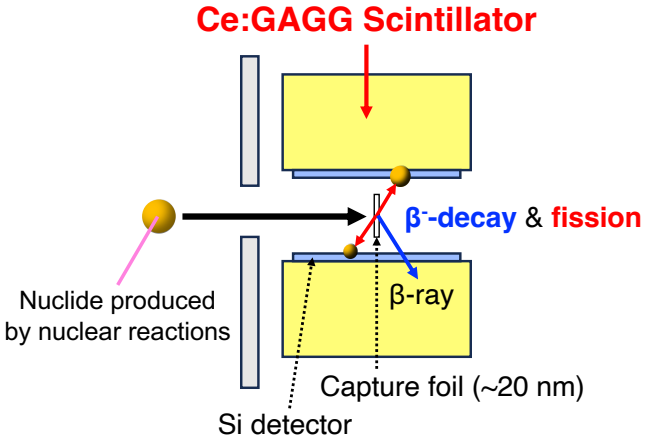


Fig. 1. Detector system to be developed in this study. It consists of Ce:GAGG scintillators (for *β*/*γ*-rays) and Si detectors (for fission fragments).

Copyright on 7th Asia-Pacific Symposium on Radiochemistry 2025- R1-11* -

The GAGG scintillator is undergoing performance evaluation for γ-ray spectroscopy, but its response for β-rays is not fully understood. We plan characterization tests for the energy/time resolution and response functions using a β-ray source and the electron accelerator at the Kyoto University Institute for Integrated Radiation and Nuclear Science (KURNS). Although monoenergetic β-rays are required to measure the energy resolution, standard β-ray sources have continuous energy spectra. Therefore, this study aims to make a β-ray source that emits monoenergetic β-rays (monoenergetic β-ray source, Fig. 2) to evaluate the performance of the GAGG detector for electrons. In this talk, we will report on the progress and prospects of the development of the monoenergetic β-source and the GAGG scintillator.

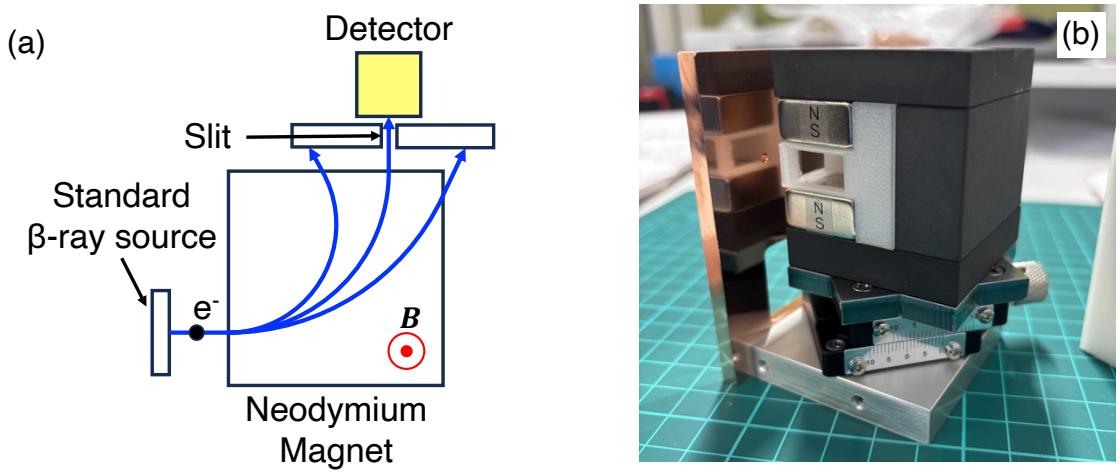


Fig. 2. (a): Schematic view of the monoenergetic β-ray source. (b): Photograph of the source. It consists of a commercially available standard β-ray source, a neodymium magnet, and a slit. The magnetic field of the neodymium magnet bends the trajectory of the electrons and the slit limits their energy entering the detector.

References

[1] M. Tanaka, *et al*., PASJ **69**, 102 (2017).
[2] I. V. Panov, *et al*., Phys. Atom. Nuclei **76**, 88 (2013).
[3] F. Minato, *et al*., Phys. Rev. C. **104**, 044321 (2021).
[4] A. N. Andreyev, *et al*., Rev. Mod. Phys. **85**, 1541–1559 (2013).
[5] T. Yanagida, *et al*., Optical Materials **35**, 2480 (2013).

Copyright on 7th Asia-Pacific Symposium on Radiochemistry 2025- R1-11* -

7th Asia-Pacific Symposium on Radiochemistry *September 14 ~ 19, 2025 • Kunibiki Messe • Shimane, Japan*

Development and performance evaluation of Multi-Sampling Ionization Chamber using intense slow heavy ion beams with mass numbers around 10

R. Shikada[1], M. Tanaka[2], N. Kitagawa[1], N. Miyashita[1], T. Fujii[1],
G. Otsuka[1], H. Watanabe[1], T. Niwase[1], S. Sakaguchi[1]

[1]*Department of Physics, Kyushu Univ.: 744 Motooka, Nishi-ku, Fukuoka, Japan, 819-0395*
[2]*Faculty of Arts and Science, Kyushu Univ: 744 Motooka, Nishi-ku, Fukuoka, Japan, 819-0395*

Radioactive isotope (RI) beams are expected to play an important role in various areas of nuclear research. However, because they often contain unwanted particles and are used at high intensities, a particle identification detector with strong high count-rate capability is required. In this study, we developed a Multi-Sampling Ionization Chamber (MuSIC) and evaluated its performance using intense slow heavy ion beams with mass numbers around 10.

1 INTRODUCTION

1.1 Radioactive Isotope (RI) beam

Radioactive isotope (RI) beams are indispensable tools for the study of unstable nuclei far from the β-stability line. These exotic nuclei play a crucial role in advancing our understanding of nuclear structure and nucleosynthesis. Fusion reactions using neutron-rich RI beams are considered as promising candidates for the synthesis of neutron-rich nuclei. In such reactions, the competition between the fusion hindrance caused by the weak binding nature of RIs and the fusion enhancement due to the presence of excess neutrons is currently under active discussion.[1,2]

However, RI beams often include unwanted particles, making particle identification detectors essential. Furthermore, detectors are operated under the high counting-rate condition.

1.2 Multi-Sampling Ionization Chamber (MuSIC)

Among various detectors, Multi-Sampling Ionization Chamber (MuSIC) is a promising candidate for the particle identification under the high counting-rate condition. It enables particle identification by measuring the energy loss of incident particles in a gaseous medium.

Despite this potential, practical implementations of ionization chambers that combine particle identification resolution and tolerance to high count rates remain limited [3-6]. Therefore, further development and evaluation of ionization chambers under such conditions are required.

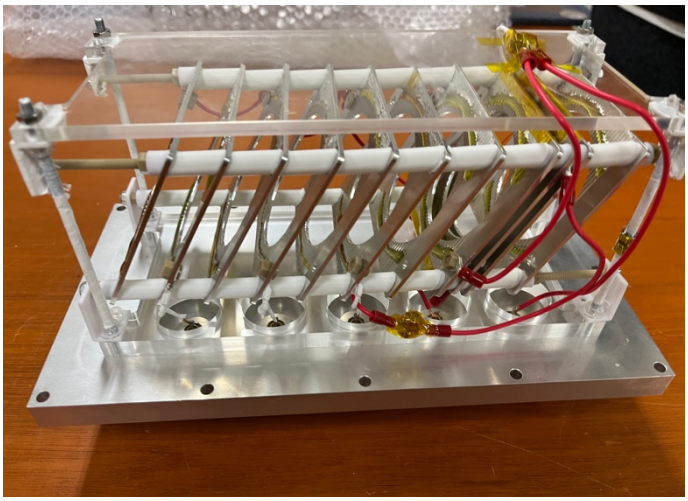


Fig. 1. Picture of electrodes assembled.

Copyright on 7th Asia-Pacific Symposium on Radiochemistry 2025- R1-12* -

2. EXPERIMENTAL SETUP AND RESULTS

Performance tests of the ionization chamber were carried out using ^{10}B, ^{11}B, ^{12}C, and ^{16}O beams, with energies ranging from 18 to 42 MeV and beam intensities up to 300,000 counts per second (cps). The beams were provided by the tandem accelerator at the Center for Accelerator and Beam Applied Science, Kyushu University. The energy loss of the incident particles in the chamber gas was measured to evaluate the response characteristics of the detector.

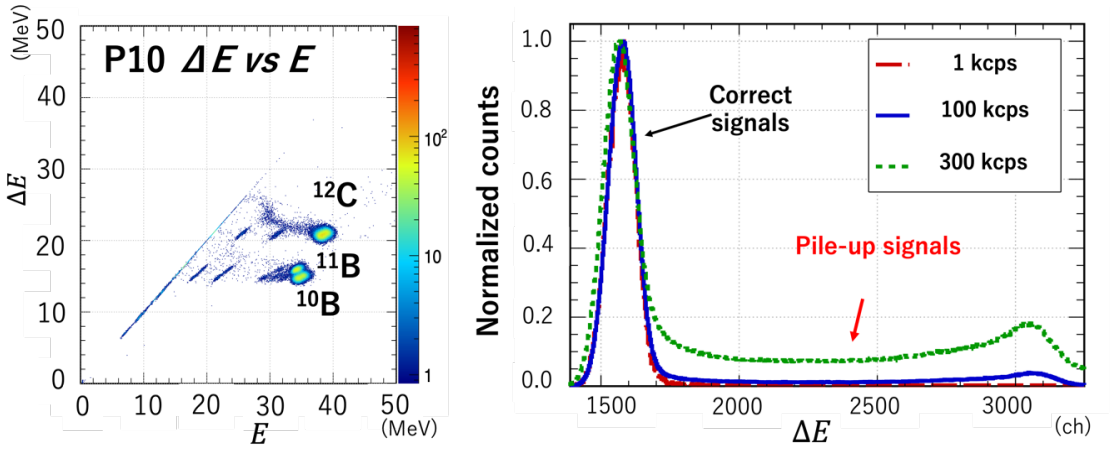


Fig. 2. (a) Two-dimensional distribution of the energy loss ΔE measured at channel 0--1 and total energy E measured at channel 0--4. (b) ΔE spectrum at counting rates of 1k ,100k and 300k cps.

These results demonstrate the feasibility of using this detector in high-intensity RI beam experiments. The detailed results will be presented in the presentation.

References

[1] L.F. Canto *et al*., Phys. Rep. **596**, 1 (2015).
[2] A. Wakhle *et al*., PRC **97**, 021602(R) (2018).
[3] K.Y. Chae *et al*., Nucl. Instrum. Methods Phys. Res. Sect. A **751**, 6 (2014).
[4] J. Lai *et al*., Nucl. Instrum. Methods Phys. Res. Sect. A **851**, 119 (2018).
[5] A. Chester *et al*., Nucl. Instrum. Methods Phys. Res. Sect. A **930**, 1 (2019).
[6] M. S. Kwag *et al*., J. Radioanal. Nucl. Chem. **332**, 579 (2019).

Copyright on 7th Asia-Pacific Symposium on Radiochemistry 2025- R1-12* -

Contributed Talk | [P1]Radiation Safety and Management

Mon. Sep 15, 2025 5:00 PM - 6:00 PM JST | Mon. Sep 15, 2025 8:00 AM - 9:00 AM UTC Hall B(Small)

[P1] Radiation Safety and Management

5:00 PM - 5:20 PM JST | 8:00 AM - 8:20 AM UTC

[P1-01*]

MEASUREMENT OF ^{36}Cl PRODUCTION RATE IN POWER CABLE SHEATHS IRRADIATED AT CERN CHARM FACILITY

*Tatsuhiro Kimura[1], Go Yoshida[2], Hiroshi Matsumura[2], Masumi Matsumura[1], Toshiya Sanami[2], Robert Froeschl[3], Davide Bozzato[3], Arnaud Devienne[3], Masaki Ishida[2], Eisuke Watanabe[2], Kiyokazu Tsugane[2], Eunji Lee[2], Ryoken Shiobara[4], Masahiro Mitsuhashi[4], Hiroshi Yashima[5], Yuuki Hirano[4], Yusuke Nakayashiki[4], Koji Oishi[4], Saori Kurita[6], Miki Nakada[6], Takuya Saze[6], Bui Ngoc Thien[7], Tsutomu Takahashi[1], Tetsuro Yoshida[1], Kimikazu Sasa[1] (1. Tsukuba University (Japan), 2. KEK (Japan), 3. CERN (Switzerland), 4. JER (Japan), 5. Kyoto University (Japan), 6. NIFS (Japan), 7. SOKENDAI (Japan))

5:20 PM - 5:40 PM JST | 8:20 AM - 8:40 AM UTC

[P1-02]

Development of a surface contamination monitor for alpha particles using an outer-layer scintillating fiber

*Sho Toyama[1], Misako Miwa[1], Wataru Kada[1,2], Shigeo Matsuyama[1,2] (1. Department of Quantum Science and Energy Engineering, Graduate School of Engineering, Tohoku University (Japan), 2. Center for Fundamental Research on Nuclear Decommissioning, Tohoku University (Japan))

5:40 PM - 6:00 PM JST | 8:40 AM - 9:00 AM UTC

[P1-03]

THE SHIELDING ABILITY AND RADIOACTIVATION OF NOVEL CERAMICS

*Hiroaki Terato[1], Midori Isobe[1], Hiroyuki Mori[2], Yuriko Mannami[2], Naoyuki Osada[3], Yoshinori Sakurai[3] (1. Okayama University (Japan), 2. Mitsuishi Taika Renga Co. Ltd. (Japan), 3. Kyoto University (Japan))

©APSORC25

7th Asia-Pacific Symposium on Radiochemistry *September 14 ~ 19, 2025 • Kunibiki Messe • Shimane, Japan*

MEASUREMENT OF ^{36}Cl PRODUCTION RATE IN POWER CABLE SHEATHS IRRADIATED AT CERN CHARM FACILITY

Tatsuhiro Kimura[1], Go Yoshida[2], Hiroshi Matsumura[2], Masumi Matsumura[1], Toshiya Sanami[2], Robert Froeschl[3], Davide Bozzato[3], Arnaud Devienne[3] Masaki Ishida[2], Eisuke Watanabe[2], Kiyokazu Tsugane[2], Eunji Lee[2], Ryoken Shiobara[4], Masahiro Mitsuhashi[4], Hiroshi Yashima[5], Yuuki Hirano[4], Yusuke Nakayashiki[4], Koji Oishi[4], Saori Kurita[6], Miki Nakada[6], Takuya Saze[6], Bui Ngoc Thien[7], Tsutomu Takahashi[1], Tetsuro Yoshida[1], Kimikazu Sasa[1]

[1]*University of Tsukuba, 1-1-1 Tennodai, Tsukuba, Ibaraki 305-8577, Japan*
[2]*High Energy Accelerator Research Organization (KEK), 1-1 Oho, Tsukuba, Ibaraki 305-0801, Japan*
[3]*CERN, 1211 Geneva 23, Switzerland*
[4]*Japan Environment Research Co., Ltd., Nishi-shinjyuku Mitui Bldg., 6-24-1, Nishi-Shinjyuku, Shinjyuk-ku, Tokyo 160-0023, Japan*
[5]*Institute for Integrated Radiation and Nuclear Science, Kyoto University 2-1010 Asashiro-nishi, Kumatori, Osaka 590-0494, Japan*
[6]*National Institute for Fusion Science, 322-6 Oroshi-cho, Toki-city, Gifu 509-5292, Japan*
[7]*The Graduate University for Advanced Studies, Shonan Village, Hayama, Kanagawa 240-0193, Japan*
Corresponding author: s2110514@u.tskuba.ac.jp (Tatsuhiro Kimura)

The ^{36}Cl production rate in power cable sheaths irradiated with neutrons was confirmed experimentally at the CERN High-Energy AcceleRator Mixed field (CHARM) facility. A new cable equivalent to the one used at an accelerator facility was adopted for the irradiation sample and installed at several locations in CHARM facility. Gamma-ray spectrometry was conducted to investigate the nuclides produced in the irradiated cables. To determine the generated activity of ^{36}Cl in the irradiated sheath, accelerator mass spectrometry (AMS) was employed. We discussed the ^{36}Cl production amount, comparing it with the previous neutron measurement results by using gold foil activation. Also, Montecarlo simulation was performed to investigate the thermal neutron behavior. The experiment details and the results of the ^{36}Cl production rate will be discussed in the presentation.

1 INTRODUCTION

In accelerator facilities, secondary particles produced by beam collisions activate surrounding materials. Activation becomes more complex at GeV-class proton accelerators due to the variety of secondary particles. Understanding such activation is crucial for planning safe and effective decommissioning. Many power cables are installed in accelerator facilities for power supply, and their activation is a significant issue. Their sheaths contain chlorine, which can capture neutrons and produce ^{36}Cl, a long-lived radionuclide with a half-life of about 300,000 years, leading to long term residual radioactivity. Since ^{36}Cl emits no gamma rays, it is difficult to detect by conventional gamma-ray spectrometry. Thus, precise estimation of its process of production in cable sheaths is essential for radiation management during decommissioning. In this study, we investigated the ^{36}Cl production in cable sheaths irradiated under a well-characterized field at the CERN CHARM facility. Accelerator mass spectrometry (AMS) was used for high-sensitivity quantification of ^{36}Cl, and the applicability of the ^{36}Cl production to thermal neutron fluence estimation in accelerator facilities was also discussed. This study contributes to understanding activation processes and improving neutron monitoring techniques.

2 METHODS

2.1 Cable Irradiation at CHARM Facility

A new power cable equivalent to the one used in the 12GeV-Proton Synchrotron (PS) tunnel at KEK was adopted for the experiment. A 5 cm piece including the copper core and sheath was cut without separation. The irradiation was conducted at the CERN CHARM facility. A 24 GeV proton beam from the synchrotron, with approximately 5×10^{11} protons per 350 ms spill, was directed onto a copper target (8 cm diameter, 50 cm length). The interaction produced a secondary particle field including neutrons via spallation. Figure 1 (a) shows the plane view of the CERN CHARM facility and the sample positions (A to E). All samples were installed at 1.29 m above the floor level (beamline height) and irradiated for three days. As a preliminary investigation, the gamma-ray spectrum of the cable was measured about 10 days after irradiation.

Copyright on 7th Asia-Pacific Symposium on Radiochemistry 2025- P1-01* -

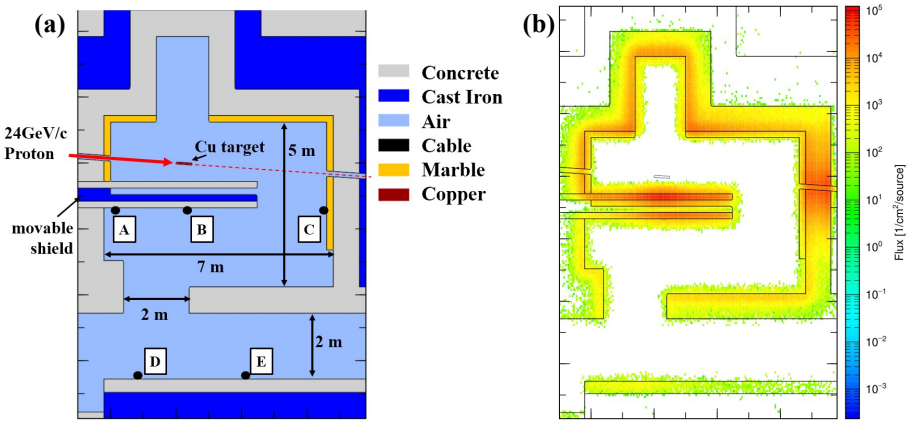


Fig. 1. (a) The plan view of the CERN CHARM facility and the sample positions. (b) low-energy neutron (< 0.1 eV) distribution immediately after irradiation calculated by PHITS simulation.

2.2 Experimental Procedures for AMS of ^{36}Cl

Three irradiated cables (B, C, and D) were used for AMS. Chlorine concentration in the sheath was determined by neutron activation analysis at Kyoto University Research Reactor. Then, 0.35 g of sheath was combusted, and chlorine ions were extracted into water. Cl^- and SO_4^{2-} concentrations in the solution were determined by ion chromatography to evaluate AMS interferences. Finally, chloride carrier was added to the solution to adjust the ^{nat}Cl, followed by $AgNO_3$ to precipitate AgCl. The AgCl was collected by centrifugation, purified by reprecipitation, and then dried for AMS. The ^{36}Cl/^{nat}Cl ratios in the samples were determined using the 6 MV AMS system at the University of Tsukuba [1].

3 RESULTS AND DISCUSSION

The amount of ^{36}Cl in the irradiated cable sheath samples was successfully determined using AMS. A PHITS simulation was performed to investigate how thermal neutrons inducing ^{36}Cl production reached the cable locations. As shown in Figure 1 (b), the simulation revealed that spallation neutrons were moderated in the concrete walls and movable shield, and re-emitted as thermal neutrons into the experimental area. Based on this understanding, the measured ^{36}Cl/^{nat}Cl ratios were used to estimate the thermal neutron fluence using the known cross section. The thermal neutron fluences were higher than those previously estimated by the gold foil activation measurements at the same facility [2]. This was due to the different position of the movable shield in this experiment, which enhanced the neutron moderation in the concrete. In addition, gamma-ray spectrometry confirmed the presence of nuclides produced by nuclear spallation reactions, such as ^{60}Co, in the cable core. Detailed data and interpretations will be presented at the conference.

4 CONCLUSIONS

We successfully determined the amount of ^{36}Cl produced in cable sheaths irradiated at the CERN CHARM facility. A PHITS simulation revealed that thermal neutrons, generated through the moderation of spallation neutrons in the concrete, reached the cable positions. This clarified the neutron transport mechanism leading to ^{36}Cl activation. The thermal neutron fluences estimated from the measured ^{36}Cl/^{nat}Cl ratios were higher than those from gold foil activation measurements at the same facility, likely due to enhanced moderation caused by the position of movable shield. These results demonstrate that ^{36}Cl production can serve as an indicator of thermal neutron fluence in complex fields. However, spatial variations in activation within the cable remain unclear, and the internal activation mechanism requires future investigation. This method could support more reliable activation assessments and deepen the understanding of activation.

ACKNOWLEDGMENTS

I would like to express my deepest gratitude to CHARM operation teams, KUR staff and Tsukuba AMS group members for providing beam time and for their support. This work was supported in part by JSPS KAKENHI 23K23269.

References

[1] K. Sasa et al., Nuclear Instruments and Methods in Physics Research B, 437, 2018, 98-102.
[2] T. Oyama et al., Nuclear Instruments and Methods in Physics Research B, 434, 2018, 29-36.

Copyright on 7th Asia-Pacific Symposium on Radiochemistry 2025- P1-01* -

7th Asia-Pacific Symposium on Radiochemistry *September 14 ~ 19, 2025 • Kunibiki Messe • Shimane, Japan*

Development of a surface contamination monitor for alpha particles using an outer-layer scintillating fiber

Sho Toyama[1], Misako Miwa[1], Wataru Kada[1,2], Shigeo Matsuyama[1,2]

[1]*Department of Quantum Science and Energy Engineering, Tohoku University, 6-6-01-2 Aoba Aramaki-Aza Sendai, Miyagi 980-8579, Japan*
[2]*Center for Fundamental Research on Nuclear Decommissioning, Tohoku University, Sendai, Miyagi 980-8579, Japan*

A surface contamination monitor for alpha particles was developed using an outer-layer scintillating (OLS) fiber. The one-dimensional prototype achieved 160 mm position resolution and ~1 Bq/cm² detection limit. Alpha particles from Am-241 could be identified by utilizing differences in pulse height between Am-241 and Sr-90. These results demonstrate feasibility toward future development of a two-dimensional surface contamination monitor for wide-area applications.

1 Introduction

Surface contamination monitoring plays an essential role in radiation safety management during the operation and decommissioning at radiation facilities. In the early phase of decommissioning, wide-area surface monitoring is required for effective radiation protection planning and cost estimation. In particular, the identification of α-emitting nuclides is essential due to their significant health risks. In Japan, surface contamination density limits are set at 4 Bq/cm² for α-emitters and 40 Bq/cm² for β-emitters. Although ZnS(Ag) and GM survey meters offer high sensitivity, they are limited in area coverage and require selection based on radiation type. Therefore, it is expected that OLS-fiber [1], which is sensitive to both α and β-rays, is a promising sensor for developing wide-area surface contamination monitor. We have previously reported one-dimensional position-sensitive detectors [2] for alpha detection using the OLS-fiber. In this study, we enhanced the basic performance of this detector by improving the fiber characteristics. We will report the resulting improvements in position resolution and detection limits and discuss α/β discrimination based on a pulse-height method. Furthermore, we will also report a two-dimensional contamination monitor and present its performance results.

2 Material and Methods

A single OLS-14-2 fiber was coupled to a SiPM detector module (C13368-3050EA-16; Hamamatsu) and enclosed in dark box. The ends of the fiber were polished and glued with optical grease (EJ-550; Eljen). The output signals from the detector were fed into a digital signal processor (APV8508-14-2PC; Techno AP, 14-bit, 500 MHz) for data acquisition and processing. The radiation sources (Am-241, 8.0 kBq and Sr-90, 10 kBq) were manually scanned along the fiber at regular intervals to evaluate the position resolution across the entire fiber length. Pulse height spectra were also measured to assess the detector's response to α and β-rays. The detection limit of the detector was estimated based on the Currie's equation.

3 Results and discussion

The performance of the one-dimensional position-sensitive detector was evaluated. A linear relationship was confirmed between the time difference and the source position along the entire fiber length, indicating reliable position sensitivity. The position resolution of the detector was approximately 160 mm. Furthermore, under conditions where both α and β-rays are present, α-rays from Am-241 could be identified by utilizing differences in pulse height distributions between Am-241 and Sr-90. The lower detection limit based on Currie's equation was evaluated to be approximately 1 Bq/cm2 with a measurement time of several minutes.

ACKNOWLEDGMENTS

The authors thank Mr. Fujita, Mr. Akari and Ms. Funatsu of Kuraray Co. Ltd. for their assistance in preparing the OLS fiber used in this research. This study was partially conducted under the Joint Research Project "Research and Development for the Decommissioning of Fukushima Daiichi Nuclear Power Plants" a collaboration between Tohoku University and Fukushima Daiichi D&D Engineering Company, TEPCO Holdings, Inc.

References

[1] Sho Toyama, et al., Review of Scientific Instruments **93**.11 (2022).
[2] Sho Toyama, et al., Radiation Measurements **169**.107027 (2023).

THE SHIELDING ABILITY AND RADIOACTIVATION OF NOVEL CERAMICS

Hiroaki Terato[1], Midori Isobe[2], Hiroyuki Mori[3], Yuriko Mannami[4], Naoyuki Osada[5], Yoshinori Sakurai[6]

[1]*Okayama University: 2-5-1 Shikata-Cho, Kita-ku, Okayama, Japan, 700-8558, hiroakiterato@okayama-u.ac.jp*
[2] *Okayama University: 2-5-1 Shikata-Cho, Kita-ku, Okayama, Japan, 700-8558, isobem@okayama-u.ac.jp*
[3]*Mitsuishi Taika Renga Co. Ltd.: 868 Mitsuishi, Bizen, Japan, 705-0132, mtaika-mori@abelia.ocn.ne.jp*
[4]*Mitsuishi Taika Renga Co. Ltd.: 868 Mitsuishi, Bizen, Japan, 705-0132, mtaika-man73@titan.ocn.ne.jp*
[5]*Kyoto University: 2-1010 Asashiro-nishi, Kumatori, Japan, 590-0494, osada.naoyuki.4c@kyoto-u.ac.jp*
[6]*Kyoto University: 2-1010 Asashiro-nishi, Kumatori, Japan, 590-0494, sakurai.yoshinori.8n@kyoto-u.ac.jp*

1. INTRODUCTION

Shielding is essential when handling ionizing radiation and radioactive isotopes to minimize unnecessary exposure. Shielding materials must be carefully selected based on the type and energy of the radiation. Although lead blocks are commonly employed for shielding gamma rays and X-rays, their toxicity has led to a global trend toward minimizing or eliminating their use [1, 2, 3]. As a result, there is a growing demand for alternative shielding materials that are both effective and environmentally safer. In response to this need, a novel iron oxide–based ceramic material has been developed [4]. In this study, the gamma-ray shielding performance of the material was first evaluated using various gamma-ray sources, with the objective of assessing its potential as a substitute for lead (Experiment 1) [5]. Subsequently, considering the prevalent use of lead shielding in nuclear reactors and accelerator facilities, the material's effectiveness against neutron radiation was also investigated (Experiment 2) [6]. Furthermore, since neutron irradiation can induce secondary gamma rays (prompt gamma rays) and material activation, these phenomena were also examined.

2. EXPERIMENT 1

The main component of the ceramic used in this study was iron (III) oxide, and it was manufactured using a previously reported method [4]. A powder containing 99% (w/w) iron oxide was compacted in an iron mold at a pressure of 3 MPa/cm². The compacted material was then sintered at 1,320°C and allowed to cool at room temperature for 10 days. For the shielding capacity experiments, specimens molded into 10 cm × 10 cm plates with a thickness of 1 cm were used. As controls for the evaluation of shielding capacity, lead and iron plates of the same dimensions, as well as concrete blocks with a thickness of 5 cm and dimensions of 10 cm in height and width, were prepared. To evaluate the effect of block stacking, ceramic blocks measuring 5 cm thick, 10 cm high, and 20 cm wide were formed. To assess radiation leakage between blocks, three types of block configurations were created: blocks without gaps, blocks with linear gaps, and blocks with 5 mm offset gaps. The fillers used to fill the gaps in this study were 10 species including epoxy resin, Super3000SW and Fuji Light#10. Three types of gamma-ray sources were used: ^{133}Ba, ^{137}Cs, and ^{60}Co. The radioactivity at the time of the experiment was 1,028.7 kBq, 3,598.0 kBq, and 154.3 kBq, respectively. In the experiments to evaluate shielding performance, the radiation beam from the source was directed at the sample through a square aperture with 2 cm sides formed using lead blocks, and the amount of radiation that passed through was measured. The distance between the radiation source and the detector was 20 cm. The detector used for measurement was a 5 cm diameter NaI (Tl) detector (Universal Scaler TPC-501, Aloka Co., Ltd., Japan). The measurement time was 30 seconds, and each sample was measured 10 times.

The shielding performance against gamma rays was measured using three different gamma-ray sources that emit different energies. As the number of stacked 1 cm thick plates increased, the amount of gamma rays reaching the detector from the source decreased accordingly. This decrease was similar across all radiation types and all shielding materials. Based on the results, the half-value layer (HVL) was calculated, and using these values, the shielding capabilities of each material were compared. The HVLs for each material against each gamma ray showed that lead had the highest shielding capability, followed by iron, then ceramic, and finally concrete. This trend in shielding strength corresponded to the respective material densities. The measured densities of lead, iron, ceramic, and concrete were 1104.8, 798.6, 493.4, and 228.9 kg/m³, respectively. The linear attenuation coefficient (μ) of ^{60}Co gamma rays was 0.162 for ceramic and 0.254 for iron. When divided by their respective densities to obtain the mass attenuation coefficient (μ/ρ), the values were 0.033 for ceramic and 0.032 for iron, which were nearly identical. Lead and concrete blocks used for shielding are typically stacked. In such cases, radiation leakage through the gaps between blocks becomes an issue. The shielding performance against ^{137}Cs gamma rays, relative to 100% for blocks without gaps, was 89.0% for blocks with offset gaps and 67.2% for blocks with linear gaps. This indicates that offset gaps provide better shielding than linear gaps. Regarding fillers used to seal the gaps, their effect on linear gaps was examined, and all types generally improved shielding capacity by a factor of 1.1 to 1.3. These results suggest that linear gaps filled with fillers exhibit nearly the same shielding performance as offset

gaps without fillers. In other words, the use of fillers can substitute for the more labor-intensive process of manufacturing blocks with offset gaps. As described above, the gamma-ray shielding capability of the new iron oxide ceramic material was measured, its performance as a shielding material was discussed, and its precise shielding capability was confirmed. The ceramic material studied in this research was found to be usable as a new, non-toxic, and effective gamma-ray shielding material.

3. EXPERIMENT 2

In Experiment 2, the neutron shielding effectiveness, prompt gamma-ray generation, and activation behavior were investigated. The neutron experiments were conducted using the research reactor at Institute for Integrated Radiation and Nuclear Science, Kyoto University. The evaluation of neutron shielding performance was carried out using the carrying system of the Heavy Water Neutron Irradiation Facility (HWNIF) [6]. The shielding effectiveness of iron oxide ceramics with different thicknesses was assessed using activation foils such as gold foils. The activation characteristics were evaluated by analyzing irradiated samples with an HPGe semiconductor detector, using the rail system of HWNIF. The prompt gamma-ray generation characteristics were examined using the Prompt Gamma-ray Analysis (PGA) system installed in the Neutron Guide Tube (E-3). In all experiments, control tests were conducted using iron and lead samples of the same dimensions for comparison.

The neutron shielding properties of iron oxide ceramics against thermal neutrons were found to be intermediate between those of lead and iron. Conversely, with respect to epithermal neutrons, the material exhibited shielding performance more closely aligned with that of lead than iron. These findings indicate that the ceramic material demonstrates superior neutron shielding capabilities compared to lead, though it remains inferior to iron. Given that the gamma-ray shielding effectiveness of both ceramics and iron generally scales with their respective densities, comparable trends were observed in this context as well. Accordingly, provided that the required shielding performance falls within an acceptable range, the ceramic material offers the potential advantage of weight reduction. Furthermore, the generation characteristics of secondary gamma rays in the ceramic were confirmed to be approximately equivalent to those observed in iron. For thermal neutrons, the measured values were over an order of magnitude higher than those for lead, primarily attributable to the (n,γ) reaction of iron. Regarding activation, the ratio of induced radioactivity was approximately iron : ceramic : lead = 20 : 1 : 0.00003. This is largely ascribed to the production of Mn-56 derived from iron. Collectively, these results suggest that although the ceramic material exhibits a certain degree of neutron shielding efficacy, additional countermeasures may be required to mitigate issues associated with secondary gamma-ray generation and activation.

4. CONCLUSIONS

The results of this study suggest that this ceramic material has the potential to be used as an effective shielding material against gamma rays. It also demonstrated a certain degree of shielding capability against neutron radiation; however, due to the characteristic activation behavior of iron, it was found that measures to address activation would be necessary for its use as a neutron shielding material.

ACKNOWLEDGMENTS

This work was partially supported by the Joint Usage/Research of the Institute for Integrated Radiation and Nuclear Science, Kyoto University (KURNS) (Nos. R6081 and R7169). It was also conducted under the joint research agreement between Okayama University and Mitsuishi Taika Renga Co., Ltd.

References

[1] R. Thoraeus, “Attenuation of gamma radiation from ^{60}Co, ^{137}Cs, ^{192}Ir, and ^{226}Ra in various materials used in radiotherapy,” *Acta Radiol.*, **3**, 81 (1965).
[2] Environmental Health Criteria 85, Lead – Environmental Aspects: World Health Organization (1989).
[3] A. Tajani and M. Maasikas, “Directive (EU) 2017/2102 of the European Parliament and of the Council.” *Off. J. Eur. Union*, 32017L2102 (2017).
[4] H. Mori, Y. Oku, Y. Mannami and T. Kunisada, “Iron (III) oxide-based ceramic material for radiation shielding,” *Ceramics*, **3**, 258 (2020).
[5] M. Isobe, H. Mori, N. Okada, Y. Mannami and H. Terato, “Shielding Ability of a Novel Iron Ceramic Material for Gamma-Rays,” *Radiat. Safety Management*, **22**, 1 (2023).
[6] Y. Sakurai and T. Kobayashi, “Characteristics of the KUR Heavy Water Neutron Irradiation Facility as a neutron irradiation field with variable energy spectra.” *Nucl. Instr. Meth. A*, **453**, 569 (2000).

Poster Presentation | [R7]Environmental Radiochemistry

Mon. Sep 15, 2025 6:30 PM - 8:00 PM JST | Mon. Sep 15, 2025 9:30 AM - 11:00 AM UTC Poster

[Poster] R7

[P-R7-01]

Study on Activity of Cesium-137 in the Coastal and Offshore Waters of Taiwan

*chun hao Chen[1], Jian Wei You[1], Liang Yu Tao[1], Wan Ling Chen[1] (1. Radiation Monitoring Center (Taiwan))

[P-R7-02]

Study on the Activity of Cesium-137 in Surface Soils of Taiwan

*Jian-Wei You[1], Hui-I Lo[1], Wan-Ling Chen[1] (1. Radiation Monitoring Center, Nuclear Safety Commission. (Taiwan))

[P-R7-03]

Research on the environmental behavior of radionuclides released from Rokkasho reprocessing plant at IES

*Shinji Ueda[1], Hidenao Hasegawa[1], Hideki Kakiuchi[1], Yoshihito Ohtsuka[1], Koichi Abe[1] (1. Institute for Environmental Sciences (Japan))

[P-R7-04]

Measurements of hydrogen deposition velocities of forest soil by using D_2 gas

*Masaru Nagai[1], Hideki Kakiuchi[1], Tsuyoshi Masuda[1] (1. Institute for Environmental Sciences (Japan))

[P-R7-05]

Spatial transports of ^{7}Be and ^{22}Na from the Arctic to the Sea of Japan side of Honshu, Japan.

*Keisuke Yoshida[1], Masayuki Umeda[1], Masahiro Yamashita[1], Masanao Nakano[1], Mutsuo Inoue[2] (1. Japan Atomic Energy Agency (Japan), 2. Kanazawa University (Japan))

[P-R7-06]

Trends of ^{129}I/^{127}I ratios and I-129 concentrationsfor environmental samples of Japan

*Sota Nagaoka[1], Noeru Kato[1], Xiaoshui Wang[1], Wataru Nitta[1] (1. Japan Chemical Analysis Center (Japan))

[P-R7-07]

Radon Concentration Measurement in Water Samples using Plastic scintillator pellets: Evaluation of Efficiency and Detection Limit

*Masahiro Hirota[1], Koichi Sakakibara[2], Kazuki Sawahata[3], Yuka Kato[3] (1. Research Center for Advanced Science and Technology, Shinshu University (Japan), 2. Faculty of Science, Shinshu University (Japan), 3. ALOKA Co., Ltd. (Japan))

[P-R7-08]

Experimental method for estimation of ^{210}Pb gamma-ray attenuation in sediment sample using ^{241}Am point source

*Haifeng Shen[1], Satoru Miyata[1], Katsuyuki Suzuki[1], Wataru Nitta[1], Yuji Ohta[1], Hidesuke Itadzu[2] (1. Japan Chemical Analysis Center (Japan), 2. SEIKO EG&G CO.,LTD (Japan))

[P-R7-09]

©APSORC25

Biological Tritium Analysis in Taiwan

HuanChing Huang[1], HueiWen Tsai[1], PingJi Huang[1], *WanJyun Wei[1] (1. National Atomic Research Institute (Taiwan))

[P-R7-10*]

DISTRIBUTION OF ^{137}Cs, ^{90}Sr AND ACTIVITY RATIO OF ^{90}Sr/^{137}Cs IN SOIL AROUND FDNPP

*Riku Kawase[1], Kazuhiko Ninomiya[2], Takashi Yoshimura[1] (1. The University of Osaka (Japan), 2. Hiroshima University (Japan))

[P-R7-11]

Spatiotemporal variations of ^{134}Cs and ^{228}Ra concentrations of surface waters in the off-Doto area (2018-2025)

*Ryoma Arakaki[1], Kaisei Mashita[1], Mutsuo Inoue[1], Yukiko Taniuchi[2], Takuya Nakanowatari[2], Seiya Nagao[1] (1. Kanazawa University (Japan), 2. Japan Fisheries Research and Education Agency (Japan))

[P-R7-12]

EFFECT OF ENVIRONMENTAL CONDITIONS ON STRONTIUM ADSORPTION OF FLUVO-AQUIC SOIL COLLOIDS

*Lingling Ma[1], Yang Shao[1] (1. Institute of High Energy Physics, Chinese Academy of Sciences, (China))

[P-R7-13]

Spatiotemporal variation of FDNPP-derived ^{137}Cs in/around the Bering Sea

*Daichi Koshiishi[1] (1. Kanazawa university (Japan))

[P-R7-14]

RADIOCARBON DATING OF VERDIGRIS ON THE BRONZE FITTINGS ATTACHED TO THE RAFTERS OF THE MAIN HALL, IZUMO TAISHA SHRINE

*Hirotaka Oda[1], Tetsuya Yamada[2], Tsukamoto Toshio[2] (1. ISEE, Nagoya Univ. (Japan), 2. Gangoji Institute Res. Cultural Property (Japan))

[P-R7-15]

A preliminary study- minute-level analysis of environmental gamma dose rate and precipitation

Wei-Min Li[1], *Chi-Wen Hsieh[1], Chuan-Pin Lee[2,3], Yu-Jie Li[4], Chun-Yi Fang[4], Wei-Hsiang Tseng[1], Yu-Cheng Tsai [1] (1. Department of Electrical Engineering, National Chung Cheng University (Taiwan), 2. Center for Energy and Environmental Research, National Tsing Hua University, Hsinchu City 300044, Taiwan (Taiwan), 3. Radioactive Waste Disposal Technology Research and Development Center, National Tsing Hua University, Hsinchu City 300044, Taiwan (Taiwan), 4. Radiation Monitoring Center, Nuclear Safety Commission, Kaohsiung City 833172, Taiwan (Taiwan))

[P-R7-16*]

Measurement of Radioactive Cesium Transfer Factors from Fukushima-Contaminated Soil to Plants

*Yuzuha Mimura[1], Kazuki Daikoku[1], Ayuto Kato[2], Mai Kondo[2], Sawa Ishikawa[1], Mizuki Sumihama[3], Takashi Saito[4], Haruki Minowa[5], Hiroaki Tanigawa[1], Miki Tanigawa[1], Michio Okada[1] (1. Osaka University (Japan), 2. Gifu University (Japan), 3. Osaka University / Gifu University (Japan), 4. Shokei Gakuin University (Japan), 5. Jikei University. Sch. Med. (Japan))

[P-R7-17]

©APSORC25

A comparison between wet-only and total deposition of ^{137}Cs observed in Namie Town, Fukushima Prefecture, Japan

*Hidenao Hasegawa[1], Yoshihito Ohtsuka[1], Naofumi Akata[2], Shinji Ueda[1], Shinji Tokonami[2] (1. Institute for Environmental Sciences (Japan), 2. Hirosaki University (Japan))

[P-R7-18]

Synergistic Coordination-Reduction Interface for Electrochemical Reduction Extraction of Low-Impurity Uranium from Seawater

*Huanhuan Liu[1], Wenkun Zhu[1] (1. Southwest university of science and technology (China))

[P-R7-19]

Self-Absorption Correction Method Validation for Pb-210 quantification using Gamma Spectrometry

*Dante Nakazawa[1], Shigekazu Hirao[2], Kunihiro Sakai[1], Atsuo Suzuki[1] (1. Mirion Technologies (Canberra) KK (Japan), 2. Institute of Environmental Radioactivity at Fukushima University (Japan))

[P-R7-20]

Temporal changes of ^{3}H and ^{129}I in seawater collected at mooring buoy near the marine discharge outlet of the Rokkasho Reprocessing Plant

*Hisaki Kofuji[1], Shinichi Gasa[1], Natsuko Akihama[1] (1. Japan Marine Science Foundation (Japan))

[P-R7-21*]

Depth-Dependent Measurement of Radioactive Cesium Activity Concentration in a 30 cm Soil Core from Fukushima

*Kazuki Daikoku[2], Mizuki Sumihama[2,3], Haruka Minowa[4], Yuzuha Mimura[2], Takeshi Saito[1], Sawa Ishikawa[2], Mai Kondo[3], Ayuto Kato[3], Michio Okada[2] (1. Shokei Gakuin University (Japan), 2. The University of Osaka (Japan), 3. Gifu University (Japan), 4. Jikei Univ. Sch. Med. (Japan))

[P-R7-22]

Efficient Photoassisted Uranium Recovery from Fluorine-Containing Wastewater by Ag/WO_{3-x} with Surface Defect and Heterostructure

*Jia Lei[1], Duo Zhang[2], Shuao Wang[2] (1. Southwest University of Science and Technology (China), 2. Soochow University (China))

[P-R7-23*]

Density of Radioactive Cesium-Rich Microparticles in Contaminated Soils

*Koyo Takeuchi[1], Shinya Yamasaki[1], Satoshi Utsunomiya[2], Yuichi Takaku[1], Keisuke Sueki[1], Yudai Shigekawa[1], Aya Sakaguchi[1] (1. University of Tsukuba (Japan), 2. Kyusyu University (Japan))

[P-R7-24*]

Evaluation of the ability of *Saccharomyces cerevisiae* to reduce U(VI) by anaerobic respiration

*IORI YAMAMOTO[1], Shinya Yamasaki[1], Yuichi Takaku[1], Yudai Shigekawa[1], Aya Sakaguchi[1], Keisuke Sueki[1] (1. University Of Tsukuba (Japan))

[P-R7-25]

Measured and theoretical gamma air dose rates in archived soil samples collected in Japan

*Keiko Tagami[1], Shigeo Uchida[1] (1. National Institutes for Quantum Science and Technology (Japan))

[P-R7-26]

TRITIUM CONCENTRATION IN NATURAL WATER SAMPLES COLLECTED AT TOMIOKA TOWN LOCATED NEARBY FDNPP

*Naofumi Akata[1], Haruka Kuwata[1], Khemruthai Kheamsiri[1], Rosianna Ilsa[1], Yuisa Kitayama[1], Honoka Fukuda[1], Ryohei Yamada[1], William James Stephenson[1,2], Yasuyuki Taira[3], Hideki Saito[4], Noriyuki Takizawa[4] (1. Hirosaki University (Japan), 2. Colorado State University (United States of America), 3. Nagasaki International University (Japan), 4. Tomioka Town Hall (Japan))

[P-R7-27*]

DGT application to study dynamic speciation of uranium in moderately basic environments

*Adrien Constandache[1], Takumi Saito[2] (1. Department of Nuclear Engineering and Management, School of Engineering, the University of Tokyo, 7-3-1 Hongo, Bunkyo-ku, Tokyo 113-8656 (Japan), 2. Nuclear Professional School, School of Engineering, the University of Tokyo, 2-22 Shirakata-Shirane, Tokai-mura, Ibaraki 219-1188 (Japan))

[P-R7-28]

Vertical distribution of ^{129}I, ^{137}Cs, ^{3}H and ^{36}Cl in unsaturated zone observed at Koriyama, Japan

*Tomoko Ohta[1], Keith Fifield[2], László Palcus[3], Stephen G. Tims[2], Stefan Pavetich[2], Hiroyuki Matsuzaki[4], Daisuke Tsumune[5,6], Hiroshi Hayami[6], Yasunori Mahara[7] (1. Nagaoka University of Technology (Japan), 2. The Australian National University (Australia), 3. HUN-REN Institute for Nuclear Research (Hungary), 4. The University of Tokyo (Japan), 5. Tsukuba University (Japan), 6. Waseda University (Japan), 7. Kyoto University (Japan))

[P-R7-29]

Radioactivity of Sulfurous Sinter Deposit from Beitou Hot Spring.

*Takashi Saito[1], Yuto Takahashi[1], Taiga Kaseda[2], Hibiki Shirata[2], Toru Takahashi[2], Shunsuke Hashizume[2], Yuya Koike[3], Mototaka Nakamura[4] (1. Shokei Gakuin University (Japan), 2. Graduate School of Science and Technology, Meiji University (Japan), 3. Meiji University (Japan), 4. Study of European Radon-spa Therapy (Japan))

[P-R7-30*]

Efficient Tritium Enrichment via Direct Seawater Electrolysis: Achieving High Separation Factor and Recovery in a Low-Volume System

*CHIH-YI LAI[1], Mariel Gonzales Tecson[1], Liang-Yu Tao[2], Chun-Hu Chen[1] (1. National Sun Yat-sen University (NSYSU) (Taiwan), 2. Radiation Monitoring Center, Nuclear Safety Commission (Taiwan))

[P-R7-31*]

TRACING RADIONUCLIDES IN THE MARINE ENVIRONMENT USING THE NEW ”MILEA” ACCELERATOR MASS SPECTROMETRY FACILITY, REZ, CZECH REPUBLIC

*Petros Leivadaros[1], Ole Christian Lind[2], Hilde Elise Heldal[3], Christos Tsabaris[4] (1. Czech Technical University in Prague (Czech Republic), 2. Norwegian University of Life Sciences (Norway), 3. Institute of Marine Research (Norway), 4. Hellenic Centre for Marine Research (Greece))

[P-R7-32]

NATURAL RADIOACTIVITY AND RADON INTENSITY IN DIFFERENT TYPES OF ROCK SPECIES AND SOIL IN KOREA

*Kilyong Lee[1], Sungwon Kim[2], Minyong Park[1], Sang-Ok Lee[3], Seung Hwan Lee[2], Jung-Ki Shin[1], Seongjae Jeong[1], Jaeseung Heo[1], Seonghun Choi[1], Sangyong Kim[1] (1. Neosiskorea Co., Ltd

(Korea), 2. Korea Institute of Geoscience and Mineral Resources (Korea), 3. Korea National University of Heritage (Korea))

©APSORC25

7th Asia-Pacific Symposium on Radiochemistry *September 14 ~ 19, 2025 • Kunibiki Messe • Shimane, Japan*

Study on Activity of Cesium-137 in the Coastal and Offshore Waters of Taiwan

C.H, Chen[1], J.W, You[2], L.Y, Tao[3], W.L, Chen[4]

[1] *Radiation Monitoring Center: No.823, Cheng-Qing Rd., Kaohsiung City, Taiwan, 833, nick5030533@nusc.gov.tw*
[2] *Radiation Monitoring Center: No.823, Cheng-Qing Rd., Kaohsiung City, Taiwan, 833, cwyu@nusc.gov.tw*
[3] *Radiation Monitoring Center: No.823, Cheng-Qing Rd., Kaohsiung City, Taiwan, 833, iamtauzi@nusc.gov.tw*
[4] *Radiation Monitoring Center: No.823, Cheng-Qing Rd., Kaohsiung City, Taiwan, 833, chen29@nusc.gov.tw*

Cesium-137, with a half-life of approximately 30 years, is an artificial radionuclide produced as a byproduct of nuclear fission. It is one of the most abundant artificial radionuclides in the marine environment. Its primary sources include nuclear weapon tests conducted between the 1950s and 1960s, reprocessing of spent nuclear fuel, nuclear power plant accidents, and routine discharges from nuclear facilities. International marine radiation pollution investigations often use Cesium-137 as a key radionuclide for monitoring. It is necessary to continuously monitor Cesium-137 levels in the coastal waters of Taiwan and its outlying islands to ensure the safety of seawater radiation levels. In this study, we utilized ammonium phosphomolybdate(AMP) and Polyaluminum Chloride (PAC) to concentrate large-volume seawater samples collected at coastal fishing ports, offshore islands, and deep offshore waters around Taiwan. Seawater samples were collected between 2018 and 2024, with a total of 354 samples. Measurements conducted using a high-purity germanium gamma spectrometer. This method achieves a Minimum Detectable Amount (MDA) of 0.5 mBq/L, making it suitable for background investigation and monitoring of radioactive Cesium-137 in seawater. The research results show that the Cesium-137 activity concentration in surface seawater from coastal fishing ports and offshore islands ranged from 0.52 to 1.95 mBq/L. In deep offshore seawater, cesium-137 activity concentrations ranged from 0.6 to 2.4 mBq/L. No significant changes in Cesium-137 activity concentrations were observed across the years.

1 Introduction

Trace amounts of Cesium-137 persist in the environment, primarily originating from extensive nuclear weapons testing conducted by nuclear-capable nations between 1945 and 1980. The resulting fallout globally dispersed through atmospheric deposition. Additionally, normal operations and accidental incidents at nuclear facilities contribute to increased levels of artificial radionuclides in the environment. Taiwan's coastal waters experienced significant radioactive contamination from 1986 to 1988 due to the Chernobyl nuclear disaster in the Soviet Union. During this period, the activity concentration of Cesium-137 in seawater was slightly elevated compared to routine monitoring values but remained below the investigation standard of 2 Bq/L set by the “Environmental Radiation Monitoring Regulation”. Radioactive substances released into the ocean can disperse via ocean currents and potentially reach the waters surrounding Taiwan, posing risks of widespread marine pollution. Hence, it is necessary to continuously monitor Cesium-137 levels in the coastal waters of Taiwan and its outlying islands, and in deep offshore seawater to ensure the safety of seawater radiation levels.

2 Experimental

We employ AMP to capture Cesium-137 and concentrate large-volume seawater samples collected at coastal fishing ports, offshore islands, and deep offshore waters around Taiwan between 2018 and 2024, with a total of 354 samples, incorporating PAC as a coagulant to accelerate sedimentation. The experimental procedure is illustrated in Figure 1. The MDA for this method is 0.5 mBq/L, making it suitable for environmental background investigations.

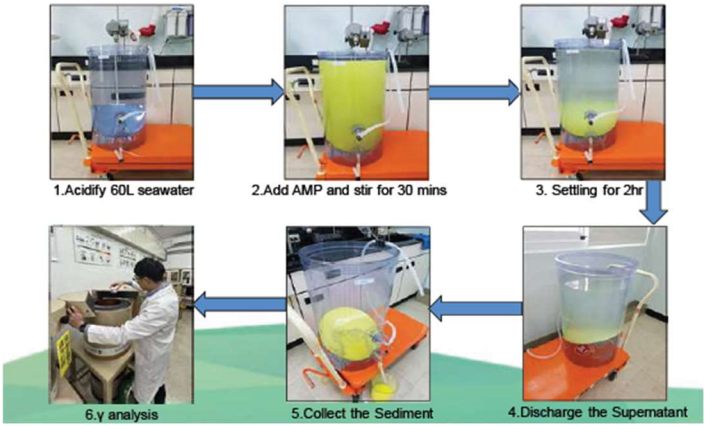


Fig. 1. AMP concentration procedure

Copyright on 7th Asia-Pacific Symposium on Radiochemistry 2025

3 CONCLUSIONS

This study investigated the activity range and trends of Cesium-137 in seawater from 2018 to 2024 at coastal fishing ports, offshore islands, and deep offshore waters around Taiwan, as illustrated in Figure 2 and Figure 3. These results reveal that the activity concentration of Cesium-137 in surface seawater from coastal fishing ports ranged from 0.52 to 1.95 mBq/L, with an average of 1.1 mBq/L. In the waters surrounding the outlying islands, the activity concentration ranged from 0.69 to 1.7 mBq/L, with an average of 1.17 mBq/L. In deep offshore seawater, the activity concentration ranged from 0.6 to 2.4 mBq/L, with an average of 1.52 mBq/L. To sum up, these levels in seawater are similar to the levels recorded in the western North Pacific Ocean (1.0–1.7 mBq/L), as reported in a previous study published in Progress in Oceanography in 2021. No significant changes in Cesium-137 activity concentrations were observed across the years.

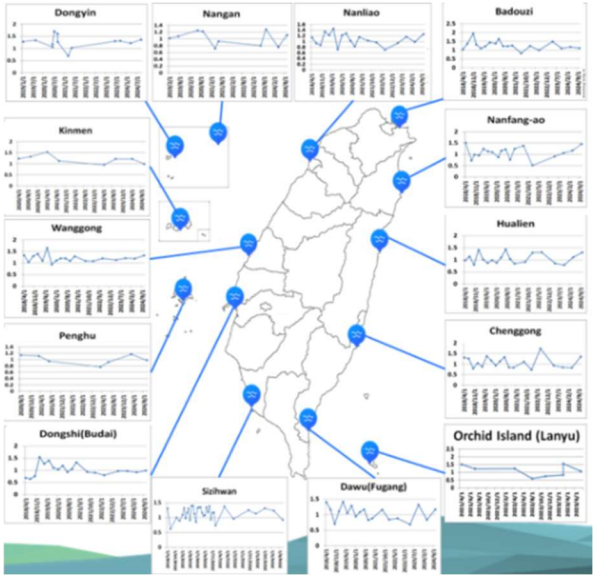


Fig. 2. Monitoring Cesium-137 at Taiwan's coast and its outlying islands

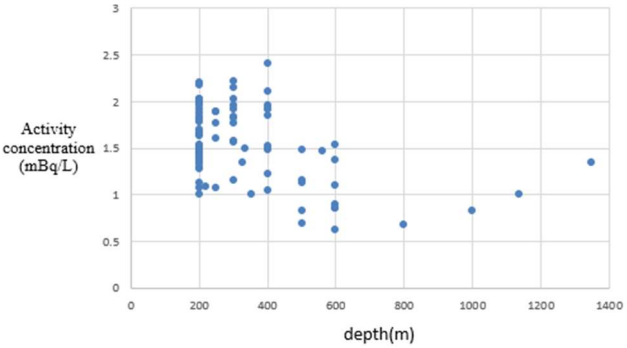


Fig. 3. Monitoring Cesium-137 in deep offshore seawater

ACKNOWLEDGMENTS

This study was funded by the Nuclear Safety Commission, Taiwan, ROC.

References

[1] Kusakabe M, Takata H (2020) Temporal trends of 137Cs concentration in seawaters and bottom sediments in coastal waters around Japan: implications for the Kd concept in the dynamic marine environment. J Radioanal Nucl Chem 323:567–580.

[2] Wei N, Zhang Z, Liu D, Wu Y, Wang J, Wang Q (2015) Coagulation behavior of polyaluminum chloride: effects of pH and coagulant dosage. Chin J Chem Eng 23:1041–1046.

[3] Aoyama M (2018) Long-range transport of radiocaesium derived from global fallout and the Fukushima accident in the Pacific Ocean since 1953 through 2017—part I: source term and surface transport. J Radioanal Nucl Chem 318:1519–1542

[4] Inoue M, Hanaki S, Takehara R, Kofuji H, Matsunaka T, Kuroda H, Taniuchi Y, Kasai H, Morita T, Miki S, Nagao S (2021) Lateral variations of 134Cs and 228Ra concentrations in surface waters in the western North Pacific and its marginal sea (2018–2019): implications for basin-scale and local current circulations. Prog Oceanogr 195:102587

Copyright on 7th Asia-Pacific Symposium on Radiochemistry 2025 P-R7-01 -

7th Asia-Pacific Symposium on Radiochemistry *September 14 ~ 19, 2025 • Kunibiki Messe • Shimane, Japan*

Study on the Activity of ^{137}Cesium in Surface Soils of Taiwan

J.W, You[1], H.I, Lo[2], W.L, Chen[3]

[1] Radiation Monitoring Center: No.823, Cheng-Qing Rd., Kaohsiung City, Taiwan, 833, cwyu@nusc.gov.tw
[2] Radiation Monitoring Center: No.823, Cheng-Qing Rd., Kaohsiung City, Taiwan, 833, lohuii@nusc.gov.tw
[3] Radiation Monitoring Center: No.823, Cheng-Qing Rd., Kaohsiung City, Taiwan, 833, chen29@nusc.gov.tw

^{137}Cesium(^{137}Cs) is an artificial radionuclide with a half-life of 30.2 years, originating from historical nuclear weapons testing, fallout from nuclear accidents, or planned discharges from nuclear facilities. It interacts with environmental, chemical, and biological factors and can persist and accumulate in ecosystems over time. In this study, 659 surface soil samples were collected from various regions in Taiwan between 2020 and 2023. After pretreatment, the samples were filled into standard containers and measured using a high-purity germanium (HPGe) detector. Efficiency calibration was conducted using a mixed radionuclide source, allowing for accurate quantification of ^{137}Cs. The measured concentrations ranged from <MDA (0.3 Bq/kg dry weight) to 157.5 Bq/kg dry weight, with an average of 4.8 Bq/kg dry weight—well below Taiwan's regulatory limit of 740 Bq/kg dry weight. A distribution map created using Geographic Information System (GIS) indicated higher ^{137}Cs levels in northern Taiwan, likely due to rainfall accumulation influenced by the northeast monsoon.

1 Introduction

Background radiation originates from cosmic rays and terrestrial sources. The intensity of terrestrial radiation is influenced by the activity concentrations of radionuclides present in rocks, soil, and sediments. Both naturally occurring radioactive materials (NORM) and artificial radionuclides contribute to the overall radiation dose. Among artificial radionuclides, ^{137}Cs—mainly derived from nuclear fallout or planned discharges from nuclear facilities—exhibits a relatively long half-life of 30.2 years, allowing it to persist and circulate within the environment and ecosystems. Consequently, the monitoring of ^{137}Cs serves as a valuable indicator for assessing regional background radiation and tracing the distribution of anthropogenic radionuclides in the environment. This study aims to assess the presence of ^{137}Cs in surface soils across various regions of Taiwan, including mountainous areas, plains, and zones surrounding nuclear facilities. A comprehensive dataset on environmental background radiation was established, and the spatial distribution of ^{137}Cs was visualized using Geographic Information System (GIS) tools. The findings provide a scientific basis for environmental radiation monitoring, nuclear facility decommissioning, and emergency response planning in the event of future nuclear or radiological incidents.

2 Experimental

The soil samples were dried and filtered to remove large particles (Figure 1), then placed into standard containers at different heights (including 0.5 cm, 1.0 cm, 2.0 cm, 3.0 cm, 4.5 cm). Different radioactive isotopes (including ^{241}Am, ^{109}Cd, ^{57}Co, ^{51}Cr, ^{85}Sr, ^{137}Cs, ^{88}Y, and ^{60}Co.) were mixed and used for efficiency calibration of the high-purity germanium detector, with an energy resolution of less than 2.5 keV at 1332 keV (Figure 2). Subsequently, the soil samples were prepared using the same measurement container and geometric height as the calibration source. All samples were measured for at least 30,000 seconds to ensure sufficient counts. The high-purity germanium semiconductor detector and Genie™ Spectroscopy Software were used to measure the ^{137}Cs content in the soil (Figure 3), and the activity concentration was analyzed using the gamma spectral energy peak at 662 keV within the energy range of 50~2000 keV (Figure 4).



Figure 1. Soil sample pretreatment



Figure 2. Mixed gamma radionuclide standard source



Figure 3. High-purity germanium detector

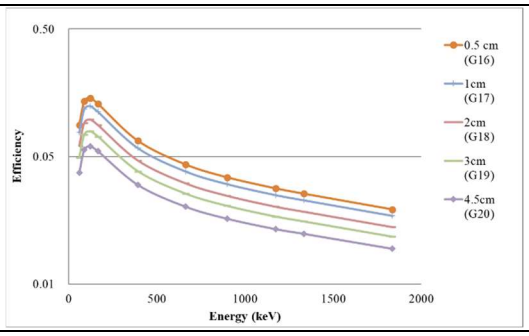


Figure 4. Gamma-ray spectrum absolute efficiency curve

3 CONCLUSIONS

In this study, 659 surface soil samples were collected from various regions in Taiwan between 2020 and 2023. The survey results show that ^{137}Cs was detected in 51% of the soil samples, with activity levels ranging from below the minimum detectable amount (MDA, 0.3 Bq/kg dry weight) to 157.5 Bq/kg dry weight, and an average activity of 4.8 Bq/kg dry weight. Based on the sampling regions, the average ^{137}Cs activity levels from highest to lowest are as follows: northern Taiwan (7.3 Bq/kg dry weight, N = 322), central Taiwan (4.6 Bq/kg dry weight, N = 65), eastern Taiwan (2.8 Bq/kg dry weight, N = 120), and southern Taiwan (1.2 Bq/kg dry weight, N = 152). The above result is similar to the ^{137}Cs activities on average 4.9 Bq/kg dry weight for Japanese soils reported in 2000, but lower than the global average of 51 Bq/kg dry weight reported in a worldwide survey conducted in 2000. The distribution of ^{137}Cs is concentrated in northern Taiwan, with a maximum activity of 157.5 Bq/kg dry weight. Locations with higher ^{137}Cs activity levels receive an average annual rainfall of up to 4,000 mm, with precipitation primarily occurring during the winter. It is speculated that this distribution is due to radioactive fallout from atmospheric nuclear tests in the 1960s, which was deposited through rainfall brought by the northeast monsoon. This hypothesis is indirectly supported by the findings of Chiu et al. (1999), who investigated the levels of radionuclides in soil and plant in northern Taiwan. Their study measured ^{137}Cs activity ranging from 29.2 to 95 Bq/kg in surface soil and the overlying organic layer. The authors attributed the high levels of radioactive fallout in the nature reserve to the region's high annual rainfall (up to 4,000 mm) and its tendency for winter precipitation.

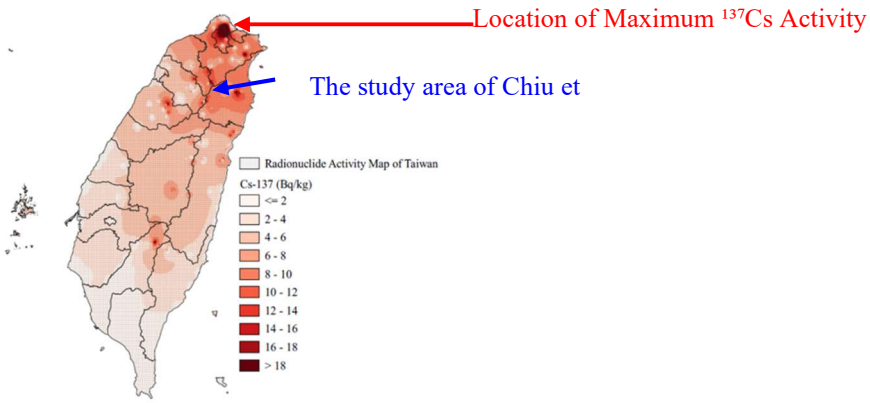


Figure 5. ^{137}Cs Activity Distribution Map in Soil

ACKNOWLEDGMENTS

This study was funded by the Atomic Energy Council, Executive Yuan, Taiwan, ROC.

References

[1]. Aoyama, M. (2018). Long-range transport of radiocaesium derived from global fallout and the Fukushima accident in the Pacific Ocean since 1953 through 2017—Part I: Source term and surface transport. Journal of Radioanalytical and Nuclear Chemistry, 318(3), 1519–1542.

[2]. Chiu, C.-Y., Lai, S.-Y., Lin, Y.-M., & Chiang, H.-C. (1999). Distribution of the radionuclide ^{137}Cs in the soils of a wet mountainous forest in Taiwan. Applied Radiation and Isotopes, 50(6), 1097–1103.

[3]. Komamura, M. (2005). Monitoring ^{90}Sr and ^{137}Cs in rice, wheat, and soil in Japan from 1959 to 2000. Misc. Publ. Natl. Inst. Agro-Environ. Sci., 28, 1–56.

[4]. Masson, O., Bieringer, J., Brattich, E., Dalheimer, A., Estier, S., Penev, I., Ringer, W., Schlosser, C., Steinkopff, T., & Steinmann, P. (2016). Variation in airborne ^{134}Cs, ^{137}Cs, particulate ^{131}I and ^{7}Be maximum activities at high-altitude European locations after the arrival of Fukushima-labeled air masses. Journal of Environmental Radioactivity, 162, 14–22.

[5]. UNSCEAR. (2000). Sources and Effects of Ionizing Radiation, United Nations Scientific Committee on the Effects of Atomic Radiation (UNSCEAR) 2000 Report, Volume I: Report to the General Assembly, with Scientific Annexes—Sources (Appendix-B). United Nations.

7th Asia-Pacific Symposium on Radiochemistry *September 14 ~ 19, 2025 • Kunibiki Messe • Shimane, Japan*

RESAERCH ON THE ENVIRONMENTAL BEHAVIOR OF RADIONUCLIDES RELEASED FROM ROKKASHO REPROCESSING PLANT AT IES

Shinji Ueda[1], Hidenao Hasegawa[1], Hideki Kakiuchi[1], Yoshihito Ohtsuka[1], Koichi Abe[1]

[1]*Department of Radioecology, Institute for Environmental Sciences: Obuchi 1-7,Rokkaho, Aomori, 039-3212, Email Address: sueda@ies.or.jp*

Japan's first commercial spent nuclear fuel reprocessing plant in Rokkasho, Aomori, is currently undergoing final active testing. This paper summarizes the research works of the Institute for Environmental Sciences on the environmental behavior of radionuclides related to the reprocessing plant. Spent fuel rods under active test were sheared and dissolved from 2006 to 2008, and radionuclides such as ^{3}H, ^{14}C, ^{85}Kr and ^{129}I, were released to the atmosphere and ocean. This manuscript summarizes the effects of the active tests using actual spent fuel at the plant on the ambient radiation and radioactivity in environmental samples, based mainly on our research results and previously published literature [1, 2].

1 INTRODUCTION

The Institute for Environmental Sciences (IES) was established in 1990 and has been conducting studies on the environmental behavior of radionuclides (^{3}H, ^{14}C, ^{85}Kr and ^{129}I etc.) released under controlled conditions from the first commercial spent nuclear fuel reprocessing plant at Rokkasho, Aomori, Japan. The reprocessing plant (Fig. 1) is scheduled for completion in FY 2026, and is currently undergoing final testing. The capacity of the reprocessing plant is 800-ton y^{-1} of U_{pr}. Although most of the radioactivity produced during the processing is recovered, a controlled amount of radioactivity is released to the environment as gas and liquid (Table1) [3]. The spent nuclear fuel rods (425 t of total uranium) were cut into segments and chemically processed (testing for dissolution of spent fuel using nitric acid, separation from solutions containing uranium and plutonium, their purification, etc.) between March 2006 and October 2008 (hereafter, the "cutting period"), as part of the test operations of the plant. For example, during the cutting period, approximately 0.019 and 2.2 PBq of ^{3}H, and 0.74 and 0.56 GBq of ^{129}I were discharged from the main stack into the atmosphere, and the pipeline outlet into the Pacific Ocean, respectively [4].

We measured the ambient radiation and radioactivity in various environmental samples collected around the reprocessing plant before/ during/ after the cutting period [5-7]. Continuous monitoring of radionuclides using various environmental samples is an effective means of evaluating their fluctuations. It is also important to understand the extent of the impact of atmospheric and/or oceanic emissions on concentration levels of radionuclides in an environment. At this symposium, we will introduce the research content of the IES and the results of the spatiotemporal changes in radionuclides concentrations in environmental samples around the Rokkasho reprocessing plant before full operation.

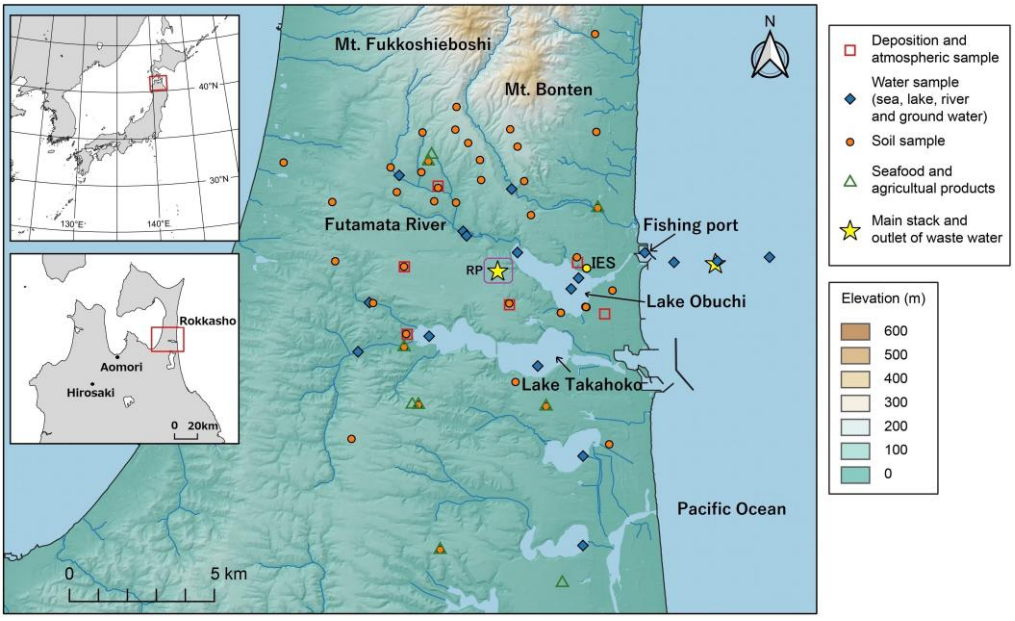


Fig. 1. Map of the spent nuclear fuel reprocessing plant and sampling locations in Rokkasho, Aomori, Japan. RP indicates the fuel reprocessing plant. The star marks indicate the main stack for atmospheric discharge and the outlet for ocean discharge, respectively [1].

Copyright on 7th Asia-Pacific Symposium on Radiochemistry 2025

Table 1. Annual management target value for radionuclides released from spent nuclear fuel reprocessing plant in Rokkasho, Japan [4].

Radionuclide	Amount		Half life
	Gas	Liquid	
^{85}Kr	1.6×10^{17}		10.7 y
Other rare gasses	1.9×10^{14}		
^{3}H	1.0×10^{15}	9.7×10^{15}	12.3 y
^{14}C	5.1×10^{13}		5730 y
^{129}I	1.1×10^{10}	4.3×10^{10}	1.57×10^{7} y
^{131}I	1.0×10^{10}	1.0×10^{11}	8 d
Other iodines	1.7×10^{12}		
Other α	3.1×10^{8}	3.6×10^{9}	
Other β, γ	7.5×10^{9}	9.5×10^{10}	

Assuming that the amount of treatment is max 800-ton y^{-1} of U_{pr} under the New Regulatory Requirements (fuel cooling period: 15y).

2. RESULS

The sampling locations of various environmental samples are shown in Fig. 1. Concentrations, fluctuation and distribution data in various environmental samples were obtained including air, precipitation, lake and river water, groundwater, soil, and agricultural, livestock, and fishery products, respectively.

During cutting period, the concentration of ^{3}H, ^{14}C, ^{85}Kr and ^{129}I in the air increased, whereas that of ^{3}H and ^{129}I increased in several environmental samples. The atmospheric deposition fluxes of ^{129}I largely followed the discharge pattern of ^{129}I from the plant to the atmosphere, and most of the deposited ^{129}I originated from the plant [5]. The background ^{129}I deposition fluxes showed seasonal variation high in winter and low in the other seasons at Rokkasho. The results suggested that reprocessing plants in Europe were the origins of the high ^{129}I flux in winter.

The ^{3}H and ^{129}I concentration in the lake and fishing port water samples gradually increased from 2006 to 2008 [6]. When comparing these concentrations in the lake during the cutting period to those from the later period, the cutting period was found to be approximately 10 - 40 times greater than that of the later period. It is suggested that concentrations of ^{3}H and ^{129}I that flowed into the brackish lake and fishing port through various routes (i.e., from tides, streamflow, and atmospheric deposition) were high because the water bodies in these areas are mostly closed systems. In addition, the ^{129}I inventory in the lake sediments showed traces of ^{129}I from the plant [7], with small amounts still remaining as of 2024.

Thus, increases were observed in air, precipitation, lake water, soil, and sediments etc. due to the effects of radionuclides released during the cutting period at the reprocessing plant. The increases in several environmental samples such as air, precipitation and lake water were temporary, but they quickly decreased to background levels once testing stopped. Meanwhile, traces of ^{129}I from the reprocessing plant were found to remain in the surrounding soil and lake sediments now. The radiation dose due to the test operation was negligible small and would not affect the human body.

ACKNOWLEDGMENTS

This study was performed under a contract with the government of Aomori Prefecture, Japan.

References

[1] S. Ueda, H. Hasegawa, H. Kakiuchi, Y. Ohtsuka, K. Abe, N. Akata, S. Ochiai, Environmental Radioactivity during Active Testing at the Rokkasho Reprocessing Plant —Effects on Environment by Released Radionuclides—. Radioisotopes, **73**, 81–99 (2024).

[2] S. Yoshida, Research on the environmental effects of radionuclides at IES – an overview. Rad. Prot. Dosimetry. 198, 1019–1024 (2022).

[3] Japan Nuclear Fuel Limited: Periodic report based on safety agreement. Rokkasho reprocessing plant in FY 2006-2020. https://www.jnfl.co.jp/ja/business/report/public_archive/safety-agreement-report/2006.html.(in Japanese,11 April 2025, Date accessed).

[4] Japan Nuclear Fuel Limited: https://www.jnfl.co.jp/ja/business/monitoring/periodic/discharge/.(in Japanese,11 April 2025, Date accessed).

[5] H. Hasegawa, H. Kakiuchi, N. Akata, Y. Ohtsuka, S. Hisamatsu, Regional and global contributions of anthropogenic iodine-129 in monthly deposition samples collected in North East Japan between 2006 and 2015. J. Environ. Radioact. **171**, 65-73 (2017).

[6] S. Ueda, H. Kakiuchi, H. Hasegawa, N. Akata, H. Kawamura, S. Hisamatsu, Iodine-129 in water samples collected adjacent to a spent nuclear fuel reprocessing plant in Rokkasho, Japan. J. Radioanal. Nucl. Chem. **303**, 1211-1215 (2015).

[7] S. Ueda, H. Kakiuchi, S. Hisamatsu, Inventory of ^{129}I in brackish lake sediments adjacent to a spent nuclear fuel reprocessing plant in Japan, J. Radioanal. Nucl. Chem., **318**, 89-96 (2018).

7th Asia-Pacific Symposium on Radiochemistry *September 14 ~ 19, 2025 • Kunibiki Messe • Shimane, Japan*

MEASUREMENTS OF HYDROGEN DEPOSITION VELOCITIES OF FOREST SOIL BY USING D_2 GAS

Masaru Nagai[1], Hideki Kakiuchi[2], Tsuyoshi Masuda[2]

[1]Depertment of Radioecology, Institute for Environmental Sciences, 1-7 Ienomae, Obuchi, Rokkasho, Aomori 039-3212 Japan, nagai@ies.or.jp
[2]Tritium Research Center, Institute for Environmental Sciences, 1-7 Ienomae, Obuchi, Rokkasho, Aomori 039-3212 Japan, ckhsd@ies.or.jp, masuda@ies.or.jp

This study investigated the hydrogen deposition velocities of forest soils surrounding a nuclear reprocessing plant located in Rokkasho, Aomori, Japan, using deuterium gas (D_2) as a tracer. To quantify the deposition velocities, closed chambers equipped with fans were installed on forest soils categorized as Japanese cedar forest, Japanese red pine forest, deciduous broadleaf forest, and woodlands. Changes in D_2 concentrations within the chambers were monitored via gas chromatography.

The measured hydrogen deposition velocities across the five soil types ranged from 7.2×10^{-4} to 9.6×10^{-4} m s^{-1}. Post-experiment analyses confirmed the formation of semi-heavy water (HDO) in the soils, indicating the oxidative conversion of D_2 to HDO. Correlations between hydrogen deposition velocity and environmental parameters such as soil temperature, moisture content, and porosity were examined. A statistically significant negative correlation was observed between deposition velocity and soil solid phase fraction ($r=-0.86$, $p < 0.05$).

1 INTRODUCTION

Tritium (^3H) is released into the environment under controlled conditions by a commercial large scale nuclear fuel reprocessing plant in Rokkasho, Aomori, Japan. The main chemical forms of tritium released from nuclear power plants (fission and fusion types) and fuel reprocessing plants are tritiated hydrogen (HT) and tritiated water (HTO). In this study, we investigate the hydrogen deposition velocities of different soil types around a reprocessing plant to clarify the HTO increase in the soil resulting from HT oxidation. The hydrogen deposition velocities in the forest soils around the reprocessing plant are assessed using D_2 as a substrate.

2 METERIALS AND METHODS

2.1 Experimental sites

Hydrogen deposition velocities were measured in five forests near a reprocessing plant. The latitudes, longitudes and soil properties of these sites are listed in Table 1.

TABLE 1. The latitudes, longitudes and soil types of the experimental sites

Site	Forest type	Soil type	Latitude	Longitude
Obuchi 1	Japanese cedar forest	Light clay	40º99'59"	141º32'12"
Obuchi 2	deciduous broadleaf forest	Clay loam	41º01'26"	141º30'89"
Deto	deciduous broadleaf forest	Clay loam	40º99'42"	141º36'51"
Futamata	Japanese red pine forest	Clay loam	40º97'82"	141º29'96"
Sasazaki	woodland	Clay loam	40º88'93"	141º30'63"

2.2 Chamber experiment using D_2 gas

A chamber experiment using D_2 gas was conducted to measure the deposition velocities of D_2 gas. Three exposure chambers (25 × 25 × 25 cm) were each equipped with a fan (to circulate the air inside the chamber) and a lid. The lids of chambers were installed in the forest soils. After single night had passed since the installation, the lids of the chambers were closed and D_2 gas was introduced such that the internal D_2 concentration was 10,000 ppm. Air samples were

Copyright on 7th Asia-Pacific Symposium on Radiochemistry 2025

collected in 1-L aluminum bags (AAK-1, GL-Science, Japan) at five intervals (0, 1, 2, 3, and 4 h post-injection) using a sampling pump (12 L min^{-1}). The gas samples obtained from the chamber experiment were analyzed within 5 h after sampling. Hydrogen was analyzed in a gas chromatograph (Model 8610, SRI) with a molecular sieve-filled stainless steel column (8600-PK3B, SRI) and a HgO-to-Hg conversion detector (RGD, SRI). Following the chamber experiment, soil core samples were collected from inside the chamber using the DIK 1630. The collected soil was well mixed in a polyethylen bag and soil waters were collected using the described by Ayabe et al (2022) [1]. The hydrogen isotope ratio of the soil waters was measured using a stable isotope ratio mass spectrometer (IsoPrime 100, Isoprime, UK).

3 RESULTS AND DISCUSSION

Three chambers were simultaneously established, and changes in D_2 gas concentrations inside the chambers were measured. The hydrogen deposition velocities of five sites were calculated based on the obtained data. The results were shown in Figure 1. The highest value was 9.6 $\times 10^{-4}$ m s^{-1}, which was obtained at Futamata site. The lowest value was 7.2 $\times$ 10^{-4} m s^{-1}, obtained at the Obuchi 2 site. Several studies have measured deposition velocities in forest soils. Lallo et al. (2008) reported that hydrogen deposition velocities in the snow-free season were from 4.0 $\times 10^{-4}$ to 7.0 $\times 10^{-4}$ m s^{-1} in a mixed broadleaf and coniferous forest in southern Finland. Yonemura et al. (2000) reported that the range of annual hydrogen deposition velocities in a forest in Tsukuba, Japan, were from 5.0 $\times 10^{-4}$ to 8.0 $\times 10^{-4}$ m s^{-1} [3]. Our results were comparable.

Soil waters were sampled following the experiments, and the deuterium concentrations were measured. All measured soils had deuterium concentrations higher than those in the control, suggesting that D_2 deposited in the soil was oxidized and converted to HDO.

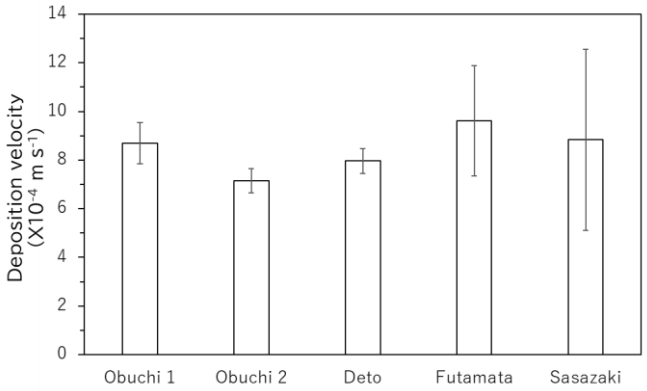


Fig. 1. D_2 deposition velocities measured at five forests.
Error bars indicate standard deviation (n=3).

Many studies have indicated that hydrogen deposition velocity is influenced by various soil environmental factors, including soil temperature, moisture content, and porosity. In the present study, three-phase diagrams and soil temperatures were measured to investigate the relationships between these soil properties and hydrogen deposition velocities.

The solid-phase fraction exhibited a strong negative correlation with hydrogen deposition velocity ($r = -0.86$, $p < 0.05$).

ACKNOWLEDGMENTS

This study was performed under a contract with the government of Aomori Prefecture, Japan.

References

[1] Y. Ayabe, H. Kakiuchi, H. Watanabe, M. Fujii, M. Nagai and T. Tani, “A simple system for extracting water from soil and plant substrates -effects of substrate-derived exchangeable hydrogen on isotope ratios of extracted water-“, *Journal of Forest Research,* **27**, 429-438 (2022)

[2] M. Lallo, T. Aalto and J. Hatakka, “Seasonal variations in hydrogen deposition to forest soil in southern Finland”, *Geophysical Research Letters',* **35**, L04402 (2008).

[3] S. Yonemura, S. Kawashima and H. Tsuruta, “Carbon monoxide, hydrogen, and methane uptake by soils in a temperate arable field and a forest”, *Journal of Geophysical Research*, **105**, 14347–14362 (2000).

Copyright on 7th Asia-Pacific Symposium on Radiochemistry 2025 P-R7-04 -

7th Asia-Pacific Symposium on Radiochemistry *September 14 ~ 19, 2025 • Kunibiki Messe • Shimane, Japan*

Spatial transports of ^{7}Be and ^{22}Na from the Arctic to the Sea of Japan side of Honshu, Japan.

Keisuke Yoshida[1], Masayuki Umeda[1], Masahiro Yamashita[1], Masanao Nakano[1], and Mutsuo Inoue[2]

[1] *Tsuruga Head Office, Japan Atomic Energy Agency: Shiraki 2-1, Tsuruga, Fukui, Japan, 919-1279, yoshida.keisuke@jaea.go.jp, umeda.masayuki47@jaea.go.jp, yamashita.masahiro@jaea.go.jp, nakano.masanao@jaea.go.jp*

[2] *Low Level Radioactivity Laboratory, Institute of Nature and Environmental Technology, Kanazawa University: Wake O-24, Nomi, Ishikawa, Japan, 923-1224, i247811@staff.kanazawa-u.ac.jp*

1 Introduction

^{7}Be (half-life: 53.3 days) and ^{22}Na (half-life: 2.6 years) are cosmogenic radionuclides produced by the reaction of cosmic rays with atmospheric molecules, mainly in the upper troposphere and lower stratosphere. Because the production rates of these radionuclides are high in the upper atmosphere above polar regions, they are often used as tracers to study the transport of air masses. In winter, southeastward monsoons transport ^{7}Be-containing air masses to the Sea of Japan side of Honshu, Japan, resulting in precipitation and an increase in ^{7}Be deposition. Although the lateral transport process of ^{7}Be by monsoons has been clarified[1], spatial transport mechanisms, particularly with respect to altitude, remain obscure. In this study, we elucidated the vertical transport process of air masses from the Arctic region to the Sea of Japan from Honshu, Japan.

2 Experimentals

Deposition samples were collected monthly or during a 10-day period from October 2019 to March 2023 in Tsuruga City, Fukui Prefecture, on the Sea of Japan side of Honshu, Japan (Fig. 1). ^{7}Be and ^{22}Na were collected using an ion-exchange resin and measured by γ-spectrometry, particularly low-background γ-spectrometry for low-level ^{22}Na. Precipitation was measured using a rain gauge installed at the sampling site and snowfall data were obtained from the Japan Meteorological Agency observation station.

3 Results and discussion

During the monsoon season from November to February, ^{7}Be and ^{22}Na deposition increased, and the ^{22}Na/^{7}Be ratio decreased. The low ^{22}Na/^{7}Be ratio is attributed to a large increase in ^{7}Be deposition relative to ^{22}Na deposition. The increase in ^{7}Be and ^{22}Na deposition reflects an upper atmospheric origin of monsoon air masses, whereas the decrease in the ^{22}Na/^{7}Be ratio indicates a small effect of the upper troposphere and stratosphere[2]. ^{7}Be concentration increases with altitude, reaching approximately 10 mBq/m^{3} at 3 km and 20 mBq/m^{3} at 6 km, which is several times higher than surface concentrations (several mBq/m^{3})[3]. These results suggest that an increase in ^{7}Be deposition and a decrease in the ^{22}Na/^{7}Be ratio can occur even when air masses are transported by the monsoon below the upper troposphere. Air masses transported by the monsoon across thousands of kilometers over the Eurasian Continent and the Sea of Japan maintain a low ^{22}Na/^{7}Be ratio, indicating limited mixing with air from the upper troposphere. As the winter atmosphere over Eurasia is stratified, the potential temperature is conserved during southeastward transport[4]. This suggests that air masses originating at high latitudes descend as they move toward the Japanese Archipelago.

Copyright on 7th Asia-Pacific Symposium on Radiochemistry 2025

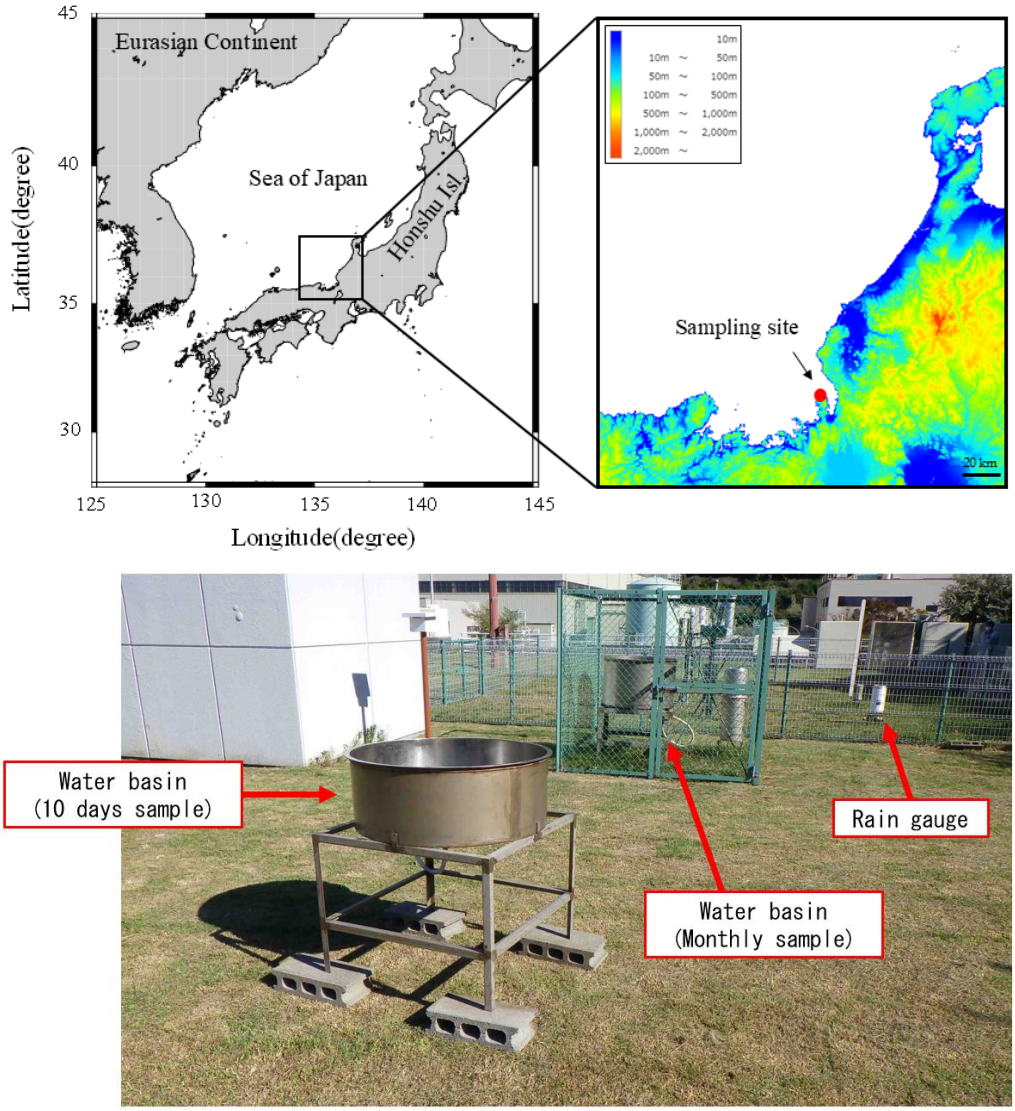


Fig. 1. Sampling site and equipment.

ACKNOWLEDGMENTS

This study was performed under the cooperative research program of the Institute of Nature and Environmental Technology, Kanazawa University ＜no. 22043＞.

References

[1] M. Yamamoto et al., *J. Environ. Radioact.* **2006**, 86, 110–131.
[2] P. Steinmann et al., *J. Environ. Radioact.* **2013**, 124, 68–73.
[3] L. Kownacka, *NUKLEONIKA* **2002**, 47, 79–82.
[4] H. Itoh and Y. Narazaki, *Jpn. J. Health Phys.* **2017**, 52, 122–133.

7th Asia-Pacific Symposium on Radiochemistry *September 14 ~ 19, 2025 • Kunibiki Messe • Shimane, Japan*

Trends of $^{129}I/^{127}I$ ratios and I-129 concentrations for environmental samples of Japan

Sota Nagaoka[1], Noeru Kato[1], Xiaoshui Wang[1], Wataru Nitta[1]

[1]*Japan Chemical Analysis Center: 295-3, Sannocho, Inage-ku, Chiba-shi, Chiba, 263-0051, Japan*
s-nagaoka@jcac.or.jp

To investigate environmental radioactivity levels yearly, nationwide survey for various radioactive concentration was performed by Japan Chemical Analysis Center (abbreviated as JCAC) during the past decades. In this study, we report the $^{129}I/^{127}I$ ratios and I-129(^{129}I) concentrations for samples collected in Hokkaido, Akita, and Chiba since 2011, when the Fukushima Daiichi Nuclear Power Plant(FDNPP) accident occurred. As a result of ^{129}I analysis by accelerator mass spectrometry (abbreviated as AMS), $^{129}I/^{127}I$ ratios were in the order of 10^{-11} to 10^{-8} , and there were no significant differences among the three regions. It was also found that seawater and seaweed have the same level of $^{129}I/^{127}I$ ratio. In addition, ^{129}I in airborne dusts shows the same seasonal trends each year.

1 Introduction

Iodine-129 is a long-lived radionuclide with a half-life of 15.7 million years and is contained in the environment both from natural sources such as cosmic rays and U fission, and from artificial sources such as emissions from nuclear fuel reprocessing plants. JCAC has been analyzing $^{129}I/^{127}I$ ratios and ^{129}I concentrations for environmental samples to clarify the levels and trends of iodine-129 in Japan. In this study, we report the analysis results and trends of six typical environmental samples (soil divided into topsoil(0-5 cm) and subsoil(5-20 cm), milk, seaweeds, vegetables, airborne dusts, and seawater) obtained from three regions in Japan (Hokkaido, Akita, and Chiba) since 2011, when the FDNPP accident occurred, to 2023.

2 Samples and Methods

Environmental samples collected from Hokkaido, Akita, and Chiba in 2011-2023 were all measured for ^{127}I concentration by ICP-MS and $^{129}I/^{127}I$ ratio by AMS. Pretreatment methods for each sample were as follows; [Soils, milk, seaweeds, and vegetables]: After freeze-drying and homogenization, iodine was collected in solution by pyrohydrolysis method[1]. A part of this solution was taken and diluted to measure ^{127}I concentration. The remaining solution was purified by solvent extraction, and AgI precipitate was prepared, which was mixed with Nb powder and used as the AMS measurement sample. [Seawater]: After filtration through a membrane filter, the sample was pretreated in the same method as the above samples. [Airborne dusts]: After homogenization of airborne dust collected on filter paper by Snow White known as a high-volume air sampler, the sample was pretreated in the same method as the above samples.

3 Results and Discussion

The $^{129}I/^{127}I$ ratio and ^{129}I concentration are plotted on each axis for the samples (excluding airborne dust), as shown in Figure 1. The environmental samples contained different levels of ^{129}I, there were no significant differences among Hokkaido, Akita, and Chiba, indicating that the same environmental samples contained approximately the same levels of ^{129}I. In general, surface soil is considered as a major reservoir for anthropogenic ^{129}I, and concentrations in surface soil can be higher than in deeper soil layers. The results of this work were observed as a similar trend, for the samples collected from the same regions. Comparing the results for seawater and seaweeds, the seaweeds had a 10^4-fold higher ^{129}I concentration, but there were no significant differences in the $^{129}I/^{127}I$ ratio. This suggests that seaweeds take up iodine from seawater, but does not show isotope fractionation, such as actively taking up ^{129}I in the process.

Next, the box plot of ^{129}I concentrations of airborne dust sampled monthly from 2017 to 2023 is shown in Figure 2. ^{129}I concentrations presented a similar seasonal trend each year, 1) higher in March, 2) decreased from March to July, and 3) increased from July to October. The same trends were observed for the $^{129}I/^{127}I$ ratio. Meteorological parameters such as temperature may be an important factor for this trend, as temperature and concentration are negatively correlated. On the other hand, the reason for the higher 129I concentration in March was presumed to be due to the re-suspension of radioactive particulate on the surface of ground, and the dispersion of pollen, according to JCAC's previous analysis of pollen collected in Chiba. Furthermore, this trend may be due to the increase in evaporation of seawater with relatively low $^{129}I/^{127}I$ ratios during the summer season when temperatures are high, but the detailed causes need additional data to be proven.

Copyright on 7th Asia-Pacific Symposium on Radiochemistry 2025

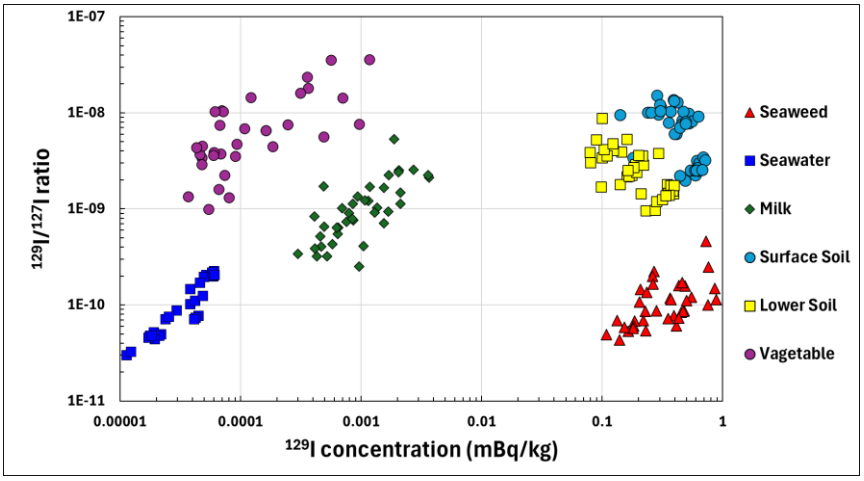


Fig. 1. $^{129}I/^{127}I$ ratios vs ^{129}I concentrations for environmental samples

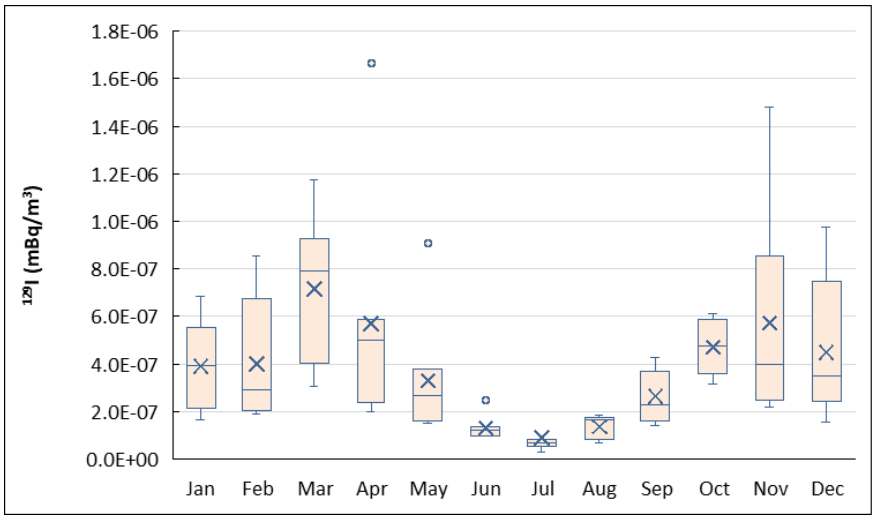


Fig. 2. Seasonal trends for ^{129}I in airborne dusts

4 CONCLUSIONS

The ^{129}I levels in environmental samples in Japan have not changed significantly from 2011 to 2023, and no regional differences were found. In the event of a new nuclear accident in the future, these data will be useful for comparing ^{129}I levels with those in normal times and exploring the impact of such an accident.

ACKNOWLEDGMENTS

Nationwide survey for various radioactive concentration on which the data for this study was based, was obtained as part of an environmental radioactivity monitoring project conducted by JCAC on behalf of the Japanese government.

References

[1] Y. Muramatsu and K. H. Wedepohl, “The distribution of iodine in the Earth’s crust.”, *Chemical Geology*, **147**, 201–216.(1998)

Copyright on 7th Asia-Pacific Symposium on Radiochemistry 2025 P-R7-06 -

7th Asia-Pacific Symposium on Radiochemistry *September 14 ~ 19, 2025 • Kunibiki Messe • Shimane, Japan*

Radon Concentration Measurement in Water Samples using Plastic scintillator pellets: Evaluation of Efficiency and Detection Limit

Masahiro Hirota[1], Koichi Sakakibara[2], Kazuki Sawahata[3], Yuka Kato[4]

[1]*Research Center for Advanced Science and Technology, Shinshu University: 3-1-1 Asahi, Matsumoto city, Nagano, 390-8621, hirota@shinshu-u.ac.jp*
[2] *Faculty of Science, Shinshu University: 3-1-1 Asahi, Matsumoto city, Nagano, 390-8621, k_sakaki@shinshu-u.ac.jp*
[3]*Aloka Co., Ltd.: 3-7-19, Imai, Ome city, Tokyo, 198-0023, kazuki.sawahata@aloka.co.jp*
[4]*Aloka Co., Ltd.: 1-20-8 Nakamachi, Musashino City, Tokyo, 180-0006, yuka.kato@aloka.co.jp*

We investigated a method for measuring radon (Rn) concentration in water samples using plastic scintillator pellets. The method involves introducing Rn-containing water into a vial with the pellets and measuring the scintillation with a liquid scintillation counter. We evaluated the efficiency and detection limit of this method. The efficiency was slightly lower than that of High Efficiency Mineral Oil Scintillator. The detection limit was 1.46 Bq/L. This method offers a potential alternative for Rn measurement in water, with further optimization needed to improve efficiency and reduce measurement error, especially at low Rn concentrations.

1. INTORODUCTION

Radon (^{222}Rn) is widely utilized as a crucial tracer in various fields of hydrological science, including groundwater flow studies [1, 2], hadrochemical process studies, and the evaluation of soil and bedrock water storage functions. In typical hydrological studies, extensive and continuous monitoring is often necessary, which requires the analysis of a large number of samples. Although conventional liquid scintillation counting is a sensitive method for radon measurement, it generates substantial amounts of liquid waste. The acquisition and disposal of liquid scintillation cocktails are costly and pose a significant environmental burden. To mitigate these issues, plastic scintillator pellets offer a potential alternative as they may be reusable. Furthermore, the application of plastic scintillator pellets for the measurement of other radionuclides such as tritium has been proposed [3]. In our previous research, we utilized radon and liquid scintillation counting to evaluate their application as tracers for elucidating hydro-environmental systems in specific contexts. For instance, our studies have clarified radon behavior in a mountainous headwater region of granitic geology, evaluated the outflow of bedrock groundwater [1], and investigated runoff generation processes associated with hydrological interactions among the surface, soil, and bedrock layers in a headwater catchment [2]. In this study, we evaluate the efficiency and detection limit of a radon measurement method using plastic scintillator pellets to assess its potential as a viable alternative to conventional liquid scintillation counting. The cost-effectiveness and environmental benefits of plastic scintillator pellets depend on their reusability, because single-use pellets may not offer significant advantages over traditional methods. Therefore, to fully realize the potential of plastic scintillator pellets as a cost-effective and environmentally friendly alternative, future work will focus on establishing a reliable and efficient method for pellet reuse and evaluating the long-term stability and sensitivity of pellets through repeated use. The current study is a necessary step towards this goal, focusing on the fundamental evaluation of pellet efficiency and detection limit.

2. MATERIAL AND METHOD

Radon-containing water samples were prepared by placing 1.7 kg of a radium hot-spring element in a glass desiccator, by adding 3 L of purified water, sealing the desiccator, and leaving it at room temperature (approximately 20-25°C)for approximately 40 days. The radial hot-spring element consists of granular ceramic balls with diameters of 6–8 mm. The dose rate of the cloth bag containing the ceramic balls was 3.2 μSv/h at a distance of 3 cm from the bag. The ^{226}Ra activity concentration in the ceramic balls, measured using a Ge semiconductor detector with 2 L Marinelli beakers, was 1.06 kBq/kg.

The radon activity concentration of the prepared water was determined by measuring a sample using 20 ml of a high-efficiency mineral oil scintillator (Revvity, High Efficiency Mineral Oil Scintillator, 1 L - Revvity), a method widely used for measuring radon concentration in water. Plastic scintillator pellets (Tokyo Ink Co., Ltd.) were used to measure the radon concentration in water (Figure 1). For each measurement, 15.5 g of the plastic scintillator pellets was added to a 20 ml counting glass vial, followed by the injection of 10 ml (0.01 L) of radon water. The vials were tightly sealed and left to stand for 6 h prior to measurement. After the 6-h equilibration period, the vials were measured for 60 min (3600 s) using a Tri-Carb 2910TR liquid scintillation counter (PerkinElmer, Inc., Waltham, MA, USA). The energy window was initially set from 0 to 2000 keV. The appropriate window width for the analysis was determined based on the measurement results. The efficiency of this method was calculated as follows:



Figure 1. Plastic scintillator pellets and them in a glass vial for radon measurement

Copyright on 7th Asia-Pacific Symposium on Radiochemistry 2025

$$Efficiency(\%) = \frac{C}{R} \times 100$$

Where C (cps) is the total count divided by 3600 seconds, and R (Bq/mL) is the ^{222}Ra activity concentration in the radon water. The detection limit was determined using the Curie method.

3. RESULT AND DISCUSSION

In this study, the significant dependence of both the measurement efficiency and detection limit on the selected energy range (channel range) in the liquid scintillation counting of radon using plastic scintillator pellets was investigated.

The results revealed that the radon detection efficiency varied across all the tested energy ranges (5-2,000 ch, 10-2,000 ch, and 5-700 ch). As shown in Table 1, the 5-700 ch setting consistently yielded the highest efficiency (3.56 %, SD ± 0.22). This finding suggests that limiting the energy window to 5-700 ch effectively optimizes the detection of radon-specific emissions, while minimizing background interference.

Similarly, the detection limit is strongly influenced by the energy range. As presented in Table 1, the lowest detection limit (1.46 Bq/L) was achieved with the 5-700 ch setting. This indicates that this energy range is the most sensitive for detecting low concentrations of radon, likely because of the reduced inclusion of background counts compared with wider energy windows.

Based on these findings, we conclude that the 5-700 ch energy range represents the optimal setting for radon measurements using plastic scintillator pellets under the conditions of this study. This setting maximizes efficiency and minimizes the detection limit, thereby contributing to improved accuracy and sensitivity in radon quantification.

TABLE 1. Radon Measurement Efficiency and Detection Limit at Different Energy Ranges

Energy range	5-2,000	10-2,000	5-700
Efficiency (%)	3.19	3.41	3.56
SD	0.14	0.19	0.22
Detection limit (Bq/L)	1.88	1.61	1.46

4. CONCLUSIONS

In this study, we evaluate the efficiency and detection limit of radon measurements using plastic scintillator pellets. The results demonstrated a significant dependence of both efficiency and detection limit on the selected energy range. Specifically, the 5-700 ch energy range consistently yielded the highest efficiency (3.56 ± 0.22 at 6.7 Bq/L) and the lowest detection limit (1.46 Bq/L), indicating its superiority for radon quantification under the experimental conditions. These findings highlighted the importance of optimizing the energy range for accurate and sensitive radon measurements using plastic scintillator pellets. The 5-700 ch setting provides a promising approach for minimizing background interference and maximizing the detection of radon-specific emissions. Further research is warranted to explore the reusability of pellets and validate these results in diverse environmental settings.

ACKNOWLEDGMENTS

The authors would like to express their gratitude to the Radioisotope Experimental Facilities of the Research Center for Advanced Science and Technology, Shinshu University, for providing the experimental sites. We also thank Aloka Co., Ltd., for generously providing a substantial portion of the plastic scintillator pellets used in this study.

References

[1] Tsubasa Hiramatsu, Koichi Sakakibara, Masahiro Hirota, Yutaro Nagata, Kosuke Tomura, Maki Tsujimura, Yuichi Onda. Bedrock groundwater discharge processes indicated by radioactive radon tracer in a small headwater catchment, Japan. American Geophysical Union (AGU) Fall Meeting 2024, H41P-0742, 2024 (Dec.)

[2] Koichi Sakakibara, Yuichi Onda, Tsubasa Hiramatsu, Ayumi Sugiyama, Masahiro Hirota, Kenji Kato and Maki Tsujimura. Runoff generation processes associated with hydrological interaction among surface, soil, and bedrock layers in a headwater catchment. American Geophysical Union (AGU) Fall Meeting, H41H-1854, 2023 (December).

[3] Etsuko Furuta, R. Ohyama, Shigeaki Yokota, Toshiya Nakajo, Yuka Yamada, Takao Kawano, Tatsuhiko Uda, and Yasuo Watanabe. Measurement of tritium with high efficiency by using liquid scintillation counter with plastic scintillator. Applied Radiation and Isotopes, November 93, 2014, Pages 13-17.

[4] Kazune Tani, Koichi Sakakibara, Masahiro Hirota, Maki Tsujimura, Mayu Fujino and Keisuke Suzuki.

Role of soil and bedrock layers on water storage in a vegetated alpine headwater under the Asian monsoon climate. EGU General Assembly 2025, EGU25-8819, updated April 26, 2025.

7th Asia-Pacific Symposium on Radiochemistry *September 14 ~ 19, 2025 • Kunibiki Messe • Shimane, Japan*

Experimental method for estimation of ^{210}Pb gamma-ray attenuation in sediment sample using ^{241}Am point source

Haifeng Shen[1], Satoru Miyata[1], Katsuyuki Suzuki[1], Wataru Nitta[1], Yuji Ohta[1], Hidesuke Itadzu[2]

[1]*Japan Chemical Analysis Center: 295-3, Sanno-cho, Inage-ku, Chiba city, Chiba, 263-0002, Japan*
[2]*SEIKO EG&G CO., LTD:563, Takatsukashinden, Matsudo city, Chiba, 270-2222, Japan*

Self-attenuation correction is essential in quantifying radioactivity concentrations using low-energy gamma rays (such as ^{210}Pb). In this study, a ^{241}Am point source was used to approximate the material properties of the samples. Based on the results, the gamma-ray counting efficiency for ^{210}Pb was evaluated, and the radioactivity concentration of ^{210}Pb was determined. The results showed good agreement with sediment samples provided by the IAEA Proficiency Test, and the effectiveness of this method was demonstrated.

1. INTRODUCTION

When quantifying radioactivity concentrations using gamma-ray spectrometry with a Ge semiconductor detector, various corrections are required, one of which is the correction for gamma-ray attenuation by the sample itself, commonly referred to as self-attenuation. The extent of self-attenuation depends on the gamma-ray energy, the elemental composition of the sample, and its apparent density. When the gamma-ray energy is several hundred keV or higher, energy and density are the primary influencing factors, and the elemental composition can be reasonably approximated using parameters such as the average atomic number with sufficient accuracy. On the other hand, the influence of the elemental composition becomes more pronounced when the energies are below 100 keV [1]. So, the accurate determination of the chemical composition is necessary and vital. However, many samples, such as soil and marine sediments, are complex to determine the elemental composition accurately. In this study, we use a ^{241}Am point source with a mass attenuation coefficient of gamma ray at 59.5 keV to estimate the sample composition, and then the quantification of ^{210}Pb (gamma-ray energy at 46.5 keV) was performed.

2. EXPERIMENTAL

First, a ^{241}Am point source was placed on the top of a measurement container filled with the sample (cylindrical, 50 mm in diameter, 40 mm filling height) and an empty container, as shown in Figure 1. The mass attenuation coefficient at 59.5 keV was determined through measurement. The sample's composition can be approximately estimated based on the results, and the mass attenuation coefficient at 46.5 keV(^{210}Pb) was evaluated [2]. In this study, a standard radiation source manufactured by Eckert & Ziegler — a multiple gamma-ray emitting large-volume source encapsulated in epoxy and housed in a cylindrical container (50 mm in diameter, 50 mm in height) was used. Next, the counting efficiency of the standard radiation source was transformed to the sample's counting efficiency using Geant4 [3], and the quantification of ^{210}Pb was performed [4–6]. The sample used in this study is the sediment from the IAEA-TERC-2024-01 Worldwide Proficiency Test Exercise. Two samples, Sediment 1 and Sediment 2, were prepared, and a planar-type Ge semiconductor detector (Canberra Industries, Inc., GL0210P) was used for the measurements.

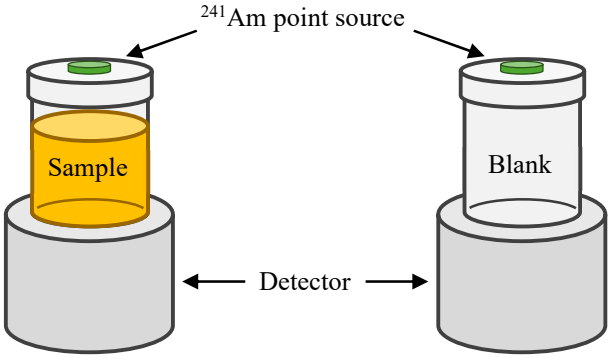


Figure 1. Schematic diagram of the experimental method

Copyright on 7th Asia-Pacific Symposium on Radiochemistry 2025

3. RESULT AND DISCUSSION

As shown in Table 1, the 59.5 keV mass attenuation coefficient was determined from measurements using a ^{241}Am point source, and the sample's elemental composition was initially estimated.

TABLE 1. Estimate Elemental Composition of the Sample

Sample	Mass attenuation coefficient at 59.5 keV (cm^2/g)	Estimate elemental composition of the sample (composition ratio)
Sediment 1	0.2765	O : 0.506 Al : 0.148
Sediment 2	0.2766	Si : 0.318 Fe : 0.028

Based on these results, a conversion factor was derived using Geant4 simulations, and the concentration of ^{210}Pb in the sediment was quantified. The results are shown in Table 2. For both Sediment 1 and Sediment 2, the *En* scores were confirmed to be ≤1, indicating satisfactory agreement with the target values. This method to evaluate the sample material using a ^{241}Am point source was demonstrated to be an effective method for quantifying low-energy gamma rays using a Ge semiconductor detector.

TABLE 2. The Result of ^{210}Pb Measurement

Sample	Target Value (Bq/kg)	Target Uncertainty (k = 1, Bq/kg)	Measurement* (Bq/kg)	*En*
Sediment 1	306.0	17.0	324.4 ± 9.5	0.5
Sediment 2			301.4 ± 9.5	-0.1

*The uncertainty associated with the measured value is the uncertainty related to counting only.

4. CONCLUSIONS

In our study, given that the *En* scores are less than 1, our results are in good agreement with the target values. Thus, this method to evaluate sample material using a ^{241}Am point source was demonstrated to be an effective method for quantifying low-energy gamma rays using a Ge semiconductor detector. The sample's composition can be approximately estimated, this method is expected to suit samples with diverse characteristics.

ACKNOWLEDGMENTS

This research includes results obtained through a project commissioned by the Nuclear Regulation Authority, which is conducted as part of the environmental radioactivity monitoring project carried out by Japan Chemical Analysis Center on behalf of the Japanese government.

References

[1] IAEA Worldwide Proficiency Test Exercise Webinar, “Sample self-attenuation correction,” (2024).
[2] XCOM Photon Cross Sections Database (https://www.nist.gov/pml/xcom-photon-cross-sections-database)
[3] Geant4 Home page (https://geant4.web.cern.ch/)
[4] T. Vidmar, “EFFTRAN—A Monte Carlo efficiency transfer code for gamma-ray spectrometry,” *Nuclear Instruments and Methods in Physics Research A* 550, 603–608 (2005).
[5] T. Vidmar, et al., “Testing efficiency transfer codes for equivalence,” Applied *Radiation and Isotopes*, 68, 355–359 (2010).
[6] S. Chagren, et al., “Efficiency transfer using the GEANT4 code of CERN for HPGe gamma spectrometry,” Applied *Radiation and Isotopes*, 107, 359–365 (2016).

7th Asia-Pacific Symposium on Radiochemistry *September 14 ~ 19, 2025 • Kunibiki Messe • Shimane, Japan*

Biological Tritium Analysis in Taiwan

Wan-Jyun Wei[1], Huei-Wen Tsai[2], Huan-Ching Huang [3], Ping-Ji Huang[4]

[1234]*Affiliation Information: No. 1000, Wenhua Rd., Longtan Dist., Taoyuan City 325207. wanjyun@nari.org.tw*

The Japanese government began discharging ALPS-treated water from the Fukushima nuclear power plant accident on August 24, 2023. The impact of long-term discharge of ALPS-treated water on marine ecology and human ingestion of radiation needs to rely on scientific testing data for relevant assessments. In addition, inter-laboratory capability comparisons are required to ensure the reliability and accuracy of test results from each laboratory. This report compiles the results of bio-tritium analysis of ecosystem samples and coastal fish catches in Taiwan, as well as the results of bio-tritium capability comparison tests among various testing laboratories in Taiwan.

1 INTRODUCTION

In response to Japan‘s long-term practice of discharging ALPS (Advanced Liquid Processing System)-treated water from the Fukushima nuclear power plant into the ocean, the accurate detection and analysis of tritium absorbed and accumulated in marine organisms through metabolism are essential. These efforts provide crucial data for assessing the impact of prolonged discharges on the marine ecosystem and human radiation safety through seafood consumption. Therefore, the NARI (National Atomic Research Institute) established the first biological tritium laboratory in August 2022 to investigate the background baseline of tritium radiation in the country's adjacent sea areas and ecology.

At the same time, to ensure the radiation safety of fishery products consumed by our people and to provide a nationally consistent inspection method, the NARI cooperated with the Office of Food Safety of the Executive Yuan and the Nuclear Safety Commission instructed the development of a two-stage "Method of Test of Tritium in Foods" (1) with reference to international practices to ensure the inspection standards of domestic laboratories and thereby increase the capacity of laboratory inspections. Thus, the NARI convened four domestic laboratories engaged in biological tritium detection to conduct proficiency testing to evaluate whether the testing standards of domestic biological tritium testing laboratories meet relevant regulatory requirements.

1.1 Method of Test of Tritium in Foods

The method of test of tritium in foods is a two-stage detection process, as shown in Fig.1. The first stage involves screening for tissue free water tritium (TFWT). When the radioactivity of TFWT is measured to be more than 10 Bq/L, the second stage, which analyzed organically bound tritium (OBT), will be conducted. This approach can significantly enhance the detection capacity to address Japan's long-term discharge of ALPS-treated water.

1.2 Results of biological tritium detection

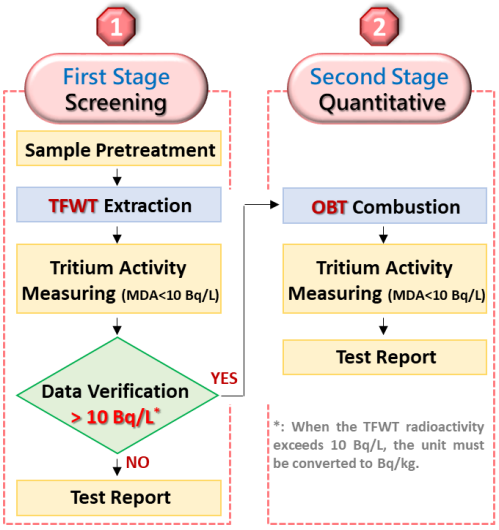
From 2022 to 2024, NARI detected biological tritium content in over 1,000 samples before and after Japan’s discharge, including oceanic fish, imported food, and nearshore ecological species. The analysis results of TFWT were all below the minimum detectable amount (MDA), as shown in Fig. 2.

1.3 Samples preparation and results of TFWT proficiency test

The fish body is cut into equal sizes, and its TFWT is extracted using a freezing dryer to obtain dried fish pieces. The dried fish pieces are rehydrated with a tritium source of known activity to produce fish pieces with a uniform distribution of tritium for the proficiency test.

Results of the inter-laboratory proficiency test for biological tritium: participating laboratories used either the publicly disclosed testing method by the FDA (freeze-drying) or laboratory-developed methods (heat distillation). The tritium (TFWT) activity in fish samples compared to the standard value showed a relative deviation ranging from -8.1% to 2.9%. Additionally, the moisture content in the fish samples compared to the standard value had a relative deviation ranging from -3.8% to 5.7%. The data are shown in Fig. 3. In summary, the analysis results from the four laboratories participating in this proficiency test had $|E_n$(error normalized)$|$ values all below 1.0, meeting the requirements ($|En \leq 1|$) set by the organizing institution.

Copyright on 7th Asia-Pacific Symposium on Radiochemistry 2025



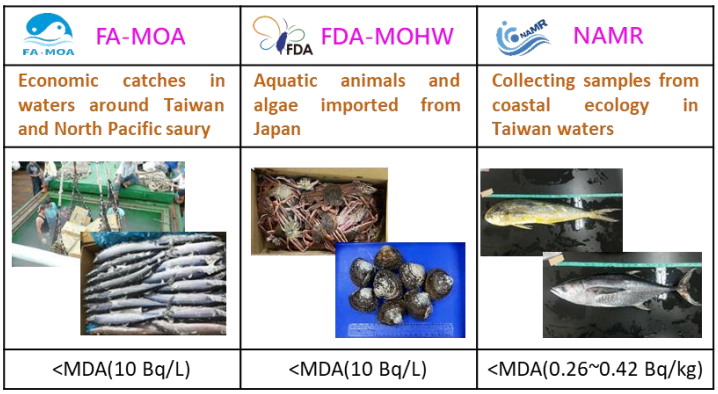


Fig. 2. The results of biological tritium detection.

Fig. 1. Method of Test of Tritium in Foods.

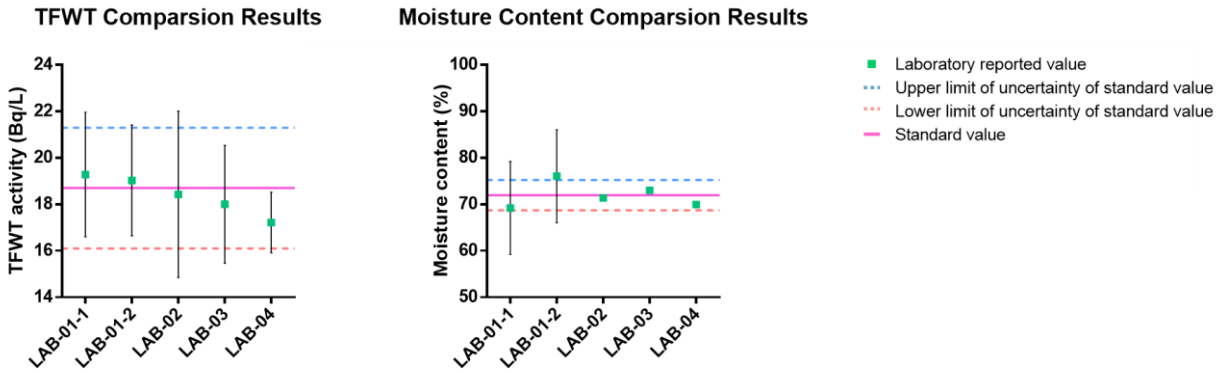


Fig. 3. The results of biological tritium analysis capability comparison test.

2. CONCLUSIONS

In response to the discharge of ALPS-treated water into the ocean over a 30-year period, the NARI Biological Tritium Laboratory continuously monitors the impact on marine ecology and human consumption. It not only provides testing technology services but also assists government agencies in performing tritium content analysis of ecological samples in Taiwan's neighboring seas to conduct long-term assessments of the impact on marine ecological radiation. *Furthermore, NARI has developed electrolytic enrichment technology to conduct background baseline surveys of seawater samples to understand whether the tritium activity in the sea area will be affected before and after Japan's discharge of ALPS-treated water.*

ACKNOWLEDGMENTS

The author gratefully acknowledges the assistance of the Fisheries Agency, the Ministry of Agriculture, the Taiwan Food and Drug Administration, and the National Academy of Marine Research, who contributed to the sampling work in this study.

References

[1] S. B. Kim, C. Shultz, M. Stuart, E. McNamara, A. Festarini and D. P. Bureau, “Organically bound tritium (OBT) formation in rainbow trout (Oncorhynchus mykiss): HTO and OBT-spiked food exposure experiments,” *Appl. Radiat. Isot*, **72**: 114 (2013).
[2] Method of Test of Tritium in Foods (TFDAO0045.00), Food and Drug Administration , Taiwan (2023).
[3] Comprehensive radiation monitoring plan, pp. 15-16., Monitoring Coordination Meeting, Ministry of Environment, Japan (2023).
[4] Rapid tritium analysis method (トリチウム分析法), pp.42-49 and pp.90-92, Nuclear Regulation Authority, Japan(2023).

7th Asia-Pacific Symposium on Radiochemistry *September 14 ~ 19, 2025 • Kunibiki Messe • Shimane, Japan*

DISTRIBUTION OF ^{137}Cs, ^{90}Sr AND ACTIVITY RATIO OF ^{90}Sr/^{137}Cs IN SOIL AROUND FDNPP

Riku Kawase[1], Kazuhiko Ninomiya[2], Takashi Yoshimura[3]

[1]*The University of Osaka: 1-1 Machikaneyama, Toyonaka, Osaka 560-0043, u265929i@ecs.osaka-u.ac.jp*
[2] *Hiroshima University: 1-4-2-Kagamiyama, Higashihiroshima, Hiroshima 739-8526, ninomiya-kazu@hiroshima-u.ac.jp*
[3] *The University of Osaka: 2-4 Yamadaoka, Suita, Osaka 565-0871, tyoshi@rirc.osaka-u.ac.jp*

Distributions of the ^{90}Sr/^{137}Cs ratio in soil around the FDNPP were obtained and the reactor core temperature and release events were identified from the experimental data. The inventories of ^{137}Cs and ^{90}Sr were 811~6560 kBq/m^2 and 118~614 Bq/m^2. The ^{90}Sr/^{137}Cs ratios calculated from these values were obtained in the order of 10^{-5}~10^{-4}, and the reactor core temperature was estimated by the MELCOR code from the distribution of ^{90}Sr/^{137}Cs ratios. The data obtained was then used to identify when the contamination of the contaminated areas was due to the release event.

1 INTRODUCTION

The Fukushima Daiichi Nuclear Power Plant (FDNPP) accident occurred as a result of the Great East Japan Earthquake on March 11, 2011. This accident resulted in a large release of radionuclides into the environment. Among the various radionuclides released, ^{137}Cs and ^{90}Sr are the most remarkable ones because they have long half-lives of 30.1 and 28.7 years respectively and accumulate in the reactor. Therefore, the amount of radionuclides released at that time was also large, and effects remain for long times. Since the amount of released radionuclides is strongly influenced by their volatilities, the temperature of the reactor core and the redox state in the reactor core, the ^{90}Sr/^{137}Cs ratio, the ratio of released radionuclides, can be used to estimate the reactor core state at the time of release. In fact, the reactor core temperature at the time of the accident changed over time.

In this study, we focus on ^{90}Sr as well as ^{137}Cs in order to obtain more details of the contamination caused by the FDNPP accident. ^{90}Sr is a pure β-ray nuclide, and its quantification requires chemical separation process. For this reason, the ^{90}Sr analysis reports have been limited compared to these for ^{137}Cs. The purpose of this study is to obtain the distribution of the ^{90}Sr/^{137}Cs ratio in the soil around the FDNPP and to identify the main source of contamination.

2 MATERIALS AND METHODS

2.1 Sampling Information

The soil samples used in this work were collected in the area surrounding the FDNPP in 2016. The samples were divided into 2 parts of surface (0-2.5 cm) and deep (2.5-5 cm) layers. The samples were dried at room temperature condition.

2.2 Experiments

About 10 g of the soil samples were taken and the radioactivity of ^{137}Cs was determined by 661 keV gamma-ray intensity using a high purity Ge detector. After that, the samples were heated in an electric furnace at 110°C and 400°C for 24 h to remove water and organic matter, respectively. Concentrated nitric acid (50 mL) and 5 mg of ^{88}Sr as a carrier were added, and the solution was heated on a hot plate for 8 hours to extract Sr ions from the sample. After filtration of the sample solution, ^{90}Sr was separated using Sr resin (Eichrom) [1] and growth of Cherenkov light was measured using low background liquid scintillation counter. The chemical yield was determined by comparing ^{88}Sr concentration between before and after separation using ICP-MS.

3 RESULTS AND DISCUSSION

3.1 Inventory Distribution

The inventory of ^{137}Cs in each sample ranged from 811~6560 kBq/m^2, and that of ^{90}Sr ranged from 118~614 Bq/m^2. The distribution of inventories showed that ^{137}Cs was deposited mostly around and to the northwest of the FDNPP. On the other hand, the distribution of ^{90}Sr inventories was different from that of ^{137}Cs; the radiation dose was higher northwest of the FDNPP, whereas from the south to southwest, even near the FDNPP ^{90}Sr was found to be hardly deposited.

Copyright on 7th Asia-Pacific Symposium on Radiochemistry 2025

3.2 $^{90}Sr/^{137}Cs$ Distribution

The $^{90}Sr/^{137}Cs$ ratios calculated from the inventory in each sample were in the order of 10^{-5}~10^{-4}. The $^{90}Sr/^{137}Cs$ ratios were 2~5 times larger in deep layers in most samples, consistent with reports [2] that ^{90}Sr migrates more rapidly to deep layers than ^{137}Cs.

The distribution of the $^{90}Sr/^{137}Cs$ ratios are shown in Fig. 1. In this work, we identified 3 contamination events in terms of $^{90}Sr/^{137}Cs$ ratios; the north to north-west side of the FDNPP area “a”, the west side area “b” and the south to south-west side area “c”. The $^{90}Sr/^{137}Cs$ ratios in contaminated area “a” were mostly in the order of 10^{-4}, in area “b” in the order of 10^{-5} and in area “c” in the range of 5×10^{-5}~5×10^{-4}, respectively. Using The MELCOR code [3], which is commonly used to estimate the release of radionuclides, was used for estimation of temperature of nuclear fuel from experimental $^{90}Sr/^{137}Cs$ ratios in the soil samples.

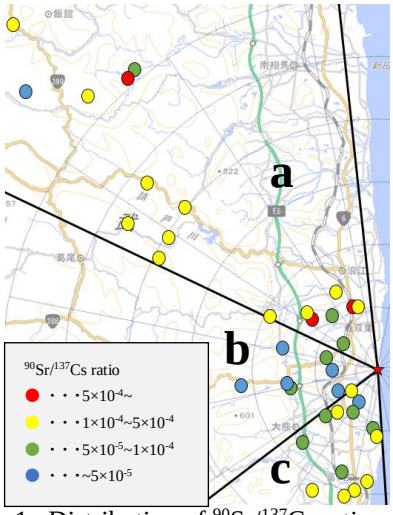


Fig. 1. Distribution of $^{90}Sr/^{137}Cs$ ratios

The $^{90}Sr/^{137}Cs$ ratio was estimated to be more than 5×10^{-4} above 2300 K condition of nuclear fuel, 1×10^{-4}~5×10^{-4} at 1900~2300 K, 5×10^{-5}~1×10^{-4} at 1700~1900 K and less than 5×10^{-5} below 1700 K. In addition to the reactor core temperature information obtained from the MELCOR code, we also investigated the time dependence of temperature changes in each reactor core, the timing of radionuclides release events [4], and wind direction information [5]. From these data, we identified the main source of each contamination area as summarized in Table 1. It was possible to identify which release event caused the contamination in contaminated areas “b” and “c”. The contamination in contaminated area “a” can be attributed to two possible release events, but based on the reactor core temperature, it is considered that the contamination is mainly due to the release at 15:00 on 12 March.

Table 1 Attribution of each release event to the estimated contaminated area

Date of release	Wind direction	Reactor No.	Simulated core temperature	Estimated core temperature	Estimated contaminated area
2011.03.12 15:00	northwest	1	1800~2000	1900~	a
2011.03.15 2:00	south-southwest	2	2000~2400	1700~2300	c
2011.03.15 8:00	southwest	2	1200~1600		
2011.03.15 16:00	west~northwest	3	1100~1200	~1700	b
				1900~	a

References

[1] S. L. Maxwell. et al., “Rapid determination of radiostrontium in large soil samples,” *J. Radioanal Nucl. Chem.*, vol. 295, pp. 965-971, 2013.
[2] M. Herranz. et al. “Inventory and vertical migration of ^{90}Sr fallout and 137Cs/90Sr ratio in Spanish mainland soils,” *J. Environ. Radioact.*, 102, 987-994, 2011.
[3] RM Summers. et al., “MELCOR computer code manuals,” 1995.
[4] Nuclear and Industrial Safety Agency, “東京電力株式会社福島第一原子力発電所の事故に係る 1 号機、2 号機および 3 号機の炉心の状態に関する評価のクロスチェック解析” 2011
[5] National Institute of Informatics, “福島第一原発周辺気象データアーカイブ:2011 年 3 月 11 日～25 日”, 2011

Spatiotemporal variations of ^{134}Cs and ^{228}Ra concentrations of surface waters in the off-Doto area (2018-2025)

*Arakaki, R.[1], Mashita, K.[1], Inoue, M.[1], Taniuchi, Y.[2], Nakanowatari, T.[2], Nagao, S[1].

[1]*Kanazawa University, Wake Nomi, Ishikawa 923-1224, Japan*
[2] *Japan Fisheries Research and Education Agency, 116 Katsurakoi, Kushiro, Hokkaido 085-0805, Japan*

We investigated temporal variations of ^{134}Cs, ^{13}7Cs, and ^{228}Ra concentrations of surface waters in the off-Doto, southeastern Hokkaido during 2018 to 2025. The spatiotemporal variation of ^{134}Cs clarified water circulation systems, and the time-span after the release by the Fukushima Dai-ichi Nuclear Power Plant (FDNPP) accident.

1 Introduction

The FDNPP accident, which occurred on March 11, 2011, led to the release of large amounts of radiocesium (^{134}Cs and ^{137}Cs) into the northwestern North Pacific Ocean, particularly around eastern Japan. The ^{134}Cs detected is believed to have entirely originated from the FDNPP accident owing to its shorter half-life (2.06 years). Therefore, this radionuclide has emerged as a strong chemical tracer of water circulation. Additionally, the lateral distributions of the concentrations of a natural and soluble radionuclide ^{228}Ra (half-life, 5.75 years) have been employed to study the transport patterns of radiocesium in the seas around Japan [1]. In this study, we examine spatiotemporal variations in low-level ^{134}Cs and ^{228}Ra concentrations at the surface off southeastern Hokkaido, Japan (off-Doto region) during 2018–2025 and discussed the subarctic current systems in the northwestern North Pacific Ocean, including the timescale, after the FDNPP accident.

2 Sample and Experimentals

Surface seawater samples were collected from the surface off-Doto, Hokkaido, Japan during the expeditions of R/V Hokko Maru from 2018 to 2025 (Fig. 1). ^{134}Cs was separated quantitatively via co-precipitation by adding ammonium phosphomolybdate (AMP) to ~120 L aliquots of seawater samples. After adjusting the pH of the supernatant to ~1, a minimally radium-contaminated Ba carrier was added, and $BaSO_4$ was precipitated with radium isotopes. Low-background γ-spectrometry was conducted for AMP/Cs and $BaSO_4$ samples using Ge detectors located in Ogoya Underground Laboratory, Japan.

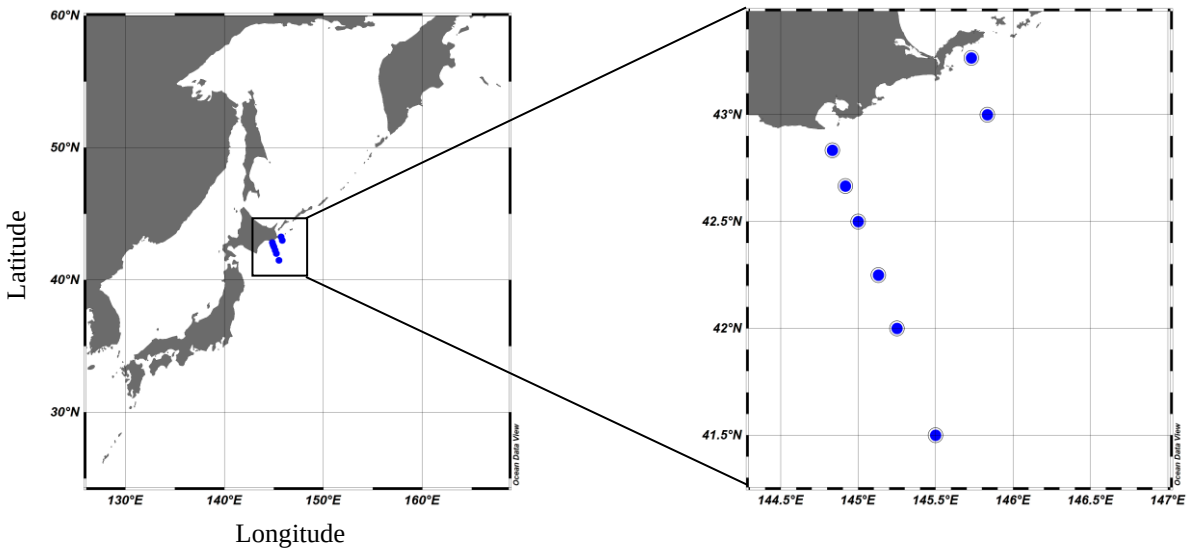


Fig. 1. Surface seawater sampling sites

3 Results and Discussion

The ^{134}Cs concentrations in the off-Doto region, decay-corrected to the date of the FDNPP accident, exhibited wide lateral variation each year (e.g., 0.5–1.1 mBq/L in 2023). From the ^{228}Ra concentrations and salinity, this variation was explained based on the current mixing patterns. Furthermore, the ^{134}Cs concentrations in the waters highly affected by the East Kamchatka - Oyashio Currents gradually increased from 2018 to 2020 [1]. This implies that the water mass maximally contaminated with ^{134}Cs was transported back to the side of the Japanese Islands 10 years after the FDNPP accident along with counter-clockwise currents in the northern North Pacific Ocean. After the gradual decrease from 2020, the ^{134}Cs concentrations increased in 2022. This may indicate the time lag in the transport of ^{134}Cs during the basin scale counter-clockwise current in the Okhotsk Sea (~2 years). In this presentation, based on based on the spatiotemporal variations of ^{134}Cs and ^{228}Ra concentrations, we discuss the subarctic current systems in the northwestern North Pacific Ocean, including water circulation timespans.

ACKNOWLEDGMENTS

We are grateful to the researchers, captain, and crew onboard of the R/V Hokko Maru, for their assistance during sampling.

References

[1] Inoue, M., Mashita, K., Kameyama, H., Mitsunushi, H., Hatakeyama, Y., Taniuchi, Y., Nakanowatari, T., Morita, T., Nagao, S., 2023. Subarctic-scale transport of 134Cs to ocean surface off northeastern Japan in 2020. Sci. Rep. 13, 7524.

EFFECT OF ENVIRONMENTAL CONDITIONS ON STRONTIUM ADSORPTION OF FLUVO-AQUIC SOIL COLLOIDS

Lingling Ma, Yang Shao

Institute of High Energy Physics, Chinese Academy of Sciences, 19B Yuquan Road, Shijingshan District, Beijing, China, 100049, malingling@ihep.ac.cn

1 INTRODUCTON

The environmental fate of radionuclides, particularly $^{90}Sr^{2+}$, has become a critical concern since the 2011 Fukushima nuclear accident. With a 28.5-year half-life and calcium-like biogeochemical behavior, $^{90}Sr^{2+}$ readily infiltrates ecosystems via soil-to-plant transfer, threatening food chains and amplifying long-term ecological risks. Pre-accident Fukushima soils (2005) recorded $^{90}Sr^{2+}$ activity at 3.6 $Bq \cdot kg^{-1}$, escalating to hundreds of $Bq \cdot kg^{-1}$ near reactor sites post-accident. Understanding Sr^{2+} adsorption mechanisms in soil colloids-the nanoscale drivers (1 nm-1000 nm) of contaminant transport-is vital for predicting radionuclide migration and exposure pathways.

Soil colloids are the main components of the root-soil microenvironment. They serve not only as critical carriers for the migration of the radionuclide strontium but also as interactive sites for its morphological transformation.For Fluvo-aquic Soils-a key agricultural type in northern China's alluvial plains-analogous Sr^{2+} studies remain absent. To address this, Sr^{2+} adsorption mechanisms was investigated using natural fluvo-aquic soil colloids through batch experiments. Our findings will offer insights for remediation strategies and ecological risk assessments.

2 EXPERIMENTS AND RESULTS

2.1 Experiments

All experiments were carried out using a batch method on a thermostated oscillator. A centrifuge tube with 4 mg of soil colloids and 100 $mg \cdot L^{-1}$ of Sr $(NO3)_2$ were placed in the water bath thermostated oscillator with a contact time of 12 h at room temperature (25 °C). Then, the solution was filtered through a 0.1 μm filter. The data were measured by ICP-MS (Inductively coupled plasma mass retrospect).

2.2 Results and Discussion

The effects of environmental factors on the adsorption were studied by varying the temperature, pH values and organic matters. As shown in Figure 1, experiments were conducted to investigate the effect of temperature on the adsorption performance of soil colloids under conditions of 15 °C, 20 °C, 25 °C, and 30 °C. At 15 °C and 20 °C, the adsorption performance was nearly identical, with an adsorption rate of approximately 65% and an adsorption capacity of 6.70 $mg \cdot kg^{-1}$. As the temperature increased, the adsorption performance showed a certain decline. This indicates that a low-temperature environment is favorable for the adsorption of strontium by soil colloids. The increase in temperature affects the diffusion rate of strontium ions, thereby influencing their adsorption by soil colloids. At pH 5, the adsorption rate of strontium (Sr) by soil colloids was 52.99%, with an adsorption capacity of 5.43 $mg \cdot g^{-1}$. As the pH increased, both the adsorption rate and capacity rose, reaching 54.73% and 5.64 $mg \cdot g^{-1}$ at pH 9, representing an increase of 1.74% and 0.21 $mg \cdot g^{-1}$, respectively. This demonstrates that soil colloids exhibit enhanced adsorption performance in alkaline environments. The alkaline conditions disrupt the balance of cations and anions present in neutral environments, leading to a predominance of negatively charged sites, which facilitates the adsorption process.

Overall, the adsorption rate increases with rising organic matter concentration. When the concentration increases from 0 to 20 $mg \cdot kg^{-1}$ and from 20 to 40 $mg \cdot L^{-1}$, the adsorption rate rises by approximately 3%, showing a clear upward trend. However, beyond 40 $mg \cdot kg^{-1}$, the adsorption rate exhibits some fluctuations. Soil colloids are not merely organic-inorganic composites but also contain various other substances, which may contribute to the observed variability in adsorption results.Adsorption equilibrium experiments were conducted using soil colloids and organic matter-removed soil colloids at 25°C and pH 7. The results clearly demonstrate that the equilibrium time for strontium (Sr) adsorption by soil colloids is very short, and the presence or absence of organic matter has no effect on the time required to reach adsorption equilibrium. Within the first 10 minutes of adsorption, the adsorption rate of soil colloids reached 71.34%, followed by fluctuations between 61% and 71% over the subsequent 600 minutes. Previous studies report that soil colloids, due to their electric double layer and abundant adsorption sites, typically achieve equilibrium within minutes or tens of minutes, though the adsorption process may exhibit instability. In contrast, after organic matter removal, the Sr

adsorption rate stabilized at approximately 60% post-equilibrium, which is lower than that of untreated soil colloids. This indicates that organic matter in soil enhances Sr adsorption.

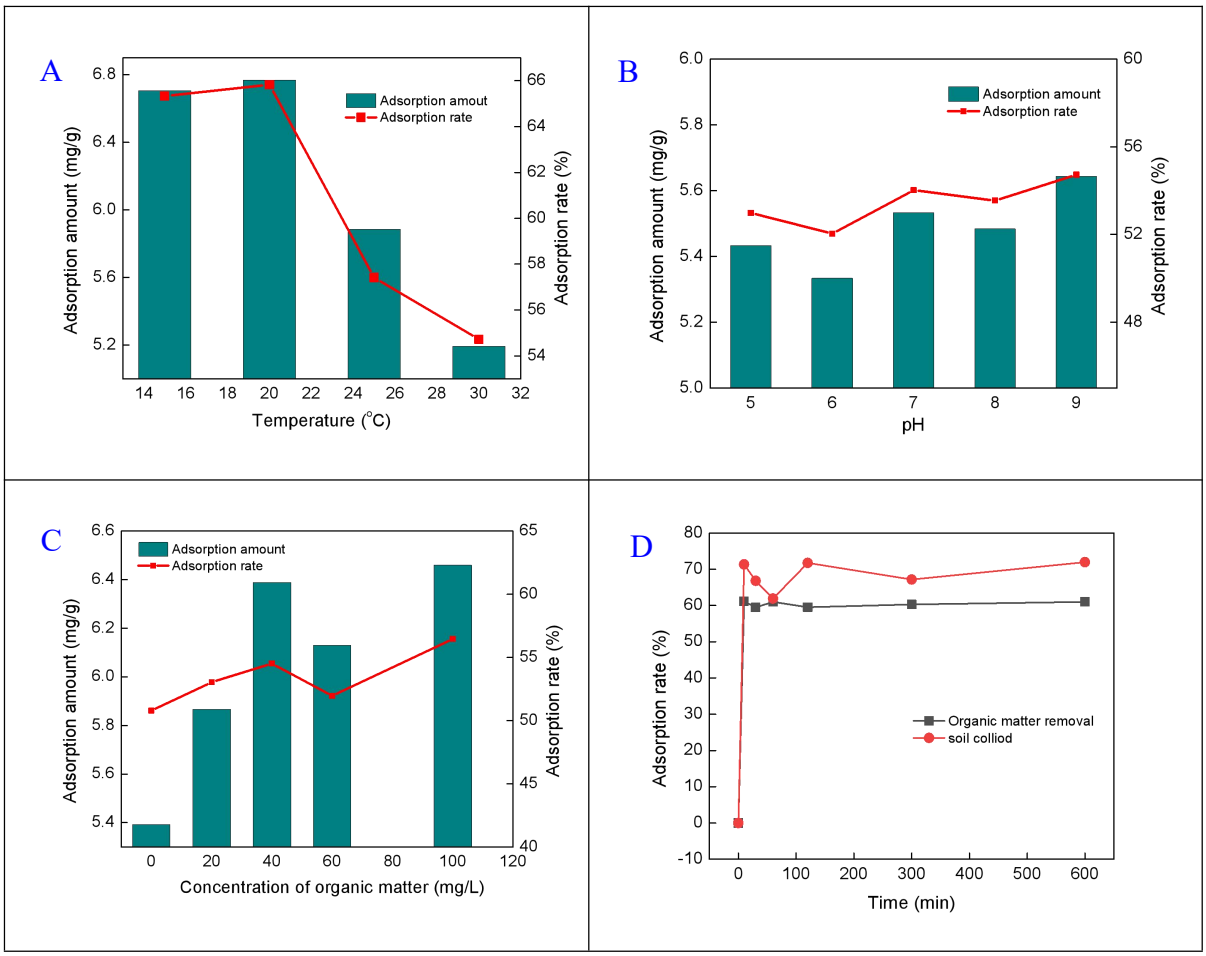


Fig 1 Effect of temperature (A)、pH (B) 、concentration of organic matter (C) and the organic matter removal (D) on the adsorption of Sr^{2+} on soil colloids.

3. CONCLUSIONS

Different environmental conditions exhibit significant effects on strontium adsorption by soil colloids. Rapid adsorption is often attributed to weaker physical adsorption forces, allowing adsorbed substances to easily desorb from soil colloids.The complex composition of soil colloids—including highly mobile metal cations (e.g., Ca^{2+}, which shares chemical similarities with Sr^{2+}) and organic matter—can influence both adsorption and desorption dynamics.

ACKNOWLEDGMENTS

This work is funded by the National Science Foundation of China (Grants 12105311) .

7th Asia-Pacific Symposium on Radiochemistry *September 14 ~ 19, 2025 • Kunibiki Messe • Shimane, Japan*

Spatiotemporal variation of FDNPP-derived ^{137}Cs in/around the Bering Sea

Daichi Koshiishi[1], Hayata Mitsunushi[1], Mutsuo Inoue[1], Seiya Nagao[1], Daiki Nomura[2], Yuichiro Kumamoto[3]

[1]Low Level Radioactivity Laboratory, Kanazawa University, O-24, Nomi, Ishikawa 923-1224, Japan
[2]Faculty of Fisheries Sciences, Hokkaido University, 3-1-1, Minato-cho, Hakodate, Hokkaido 041-8611, Japan
[3]Research and Development Center for Global Change, Japan Agency for Marine-Earth Science and Technology, 2-15 Natushima-cho, Yokosuka, Kanagawa, 237-0061, Japan

Soluble radionuclides are useful tracers for understanding the mechanisms underlying the transport of soluble materials in marine environments. The spatiotemporal variations of the concentrations of ^{137}Cs (half-life of 30.2 y) and ^{228}Ra (5.75 y) in/around the Bering Sea from 2018 to 2024 indicated the transport pattern of the Fukushima Dai-ichi Nuclear Power Plant (FDNPP)-derived ^{137}Cs.

1 Introduction

An anthropogenic ^{137}Cs was introduced into seawater by a global fallout caused by atmospheric nuclear test explosions. Additionally, the FDNPP accident released substantial quantities of ^{137}Cs into the northwestern North Pacific as well as other anthropogenic radionuclides. However, because of the lack of enough ^{137}Cs data, the transport patterns of FDNPP-derived ^{137}Cs in/around the Bering Sea have not been clarified. Natural and soluble ^{228}Ra is generally used to trace the circulation of seawater. Using ^{137}Cs and ^{228}Ra concentrations, we discussed the transport pattern of the FDNPP-derived ^{137}Cs.

2 Materials and Methods

Surface seawater samples were collected in/around the Bering Sea during the expeditions of R/Vs *Mirai and Oshoro Maru* from 2022 to 2024 (Fig. 1). ^{137}Cs was separated quantitatively via co-precipitation by adding ammonium phosphomolybdate (AMP) to ~20–40 L aliquots of samples. Subsequently, a minimally radium-contaminated Ba-carrier was added, and $BaSO_4$ was precipitated with ^{228}Ra. Low-background γ-spectrometry was performed for AMP and $BaSO_4$ samples using Ge-detectors located in Ogoya Underground Laboratory, Japan.

3 Results and discussion

Along with salinity, the ^{228}Ra concentrations distinctively separated the surface in the Bering Sea into the ^{228}Ra-rich eastern shelf and ^{228}Ra-poor western basin areas. In 2022–2024, the concentrations of the FDNPP -derived ^{137}Cs were from 0.4 to 1.5 mBq/L, with the higher values in the eastern Bering Sea than the western Bering Sea and Pacific Ocean side along the Aleutian Islands. Combined with data previously reported [1,2], the temporal variation of the FDNPP-derived ^{137}Cs showed small variation (0.7–1.7 mBq/L) during 2018–2024 after the steep increase in 2018. The spatiotemporal variation of ^{137}Cs concentrations is predominantly ascribed to the continual inflow of the FDNPP-derived ^{137}Cs to the Bering Sea, particularly to the shelf side area, along with the upstream currents.

Copyright on 7th Asia-Pacific Symposium on Radiochemistry 2025

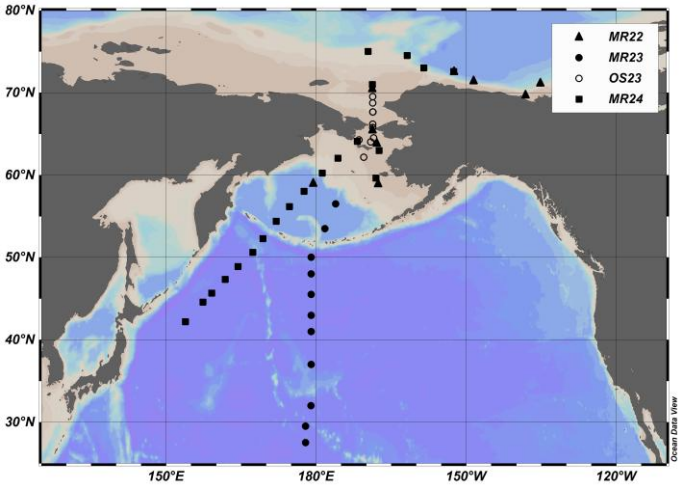


Fig. 1 Seawater sampling sites along the R/Vs *Mirai* (MR22–24 in 2022–2024) and *Oshoro Maru* (OS23 in 2023) expedition routes.

ACKNOWLEDGMENTS

We are grateful to the researchers, captain, and crew onboard of the R/Vs *Mirai* and *Oshoro Maru* for their assistance during sampling.

References

[1] Inoue, M., Takehara, R., Hanaki, S., Kameyama, H., Nishioka, J., Nagao, S., 2020. Distributions of radiocesium and radium isotopes in the western Bering Sea in 2018. *Marine Chemistry*, **225**, 103843.
[2] Kumamoto, Y., Aoyama, M., Hamajima, Y., Inoue, M., Nishino S., Kikuchi, T., Murata, A., Sato, K. (2022) Fukushima-derived radiocesium in the western subarctic area of the North Pacific Ocean, Bering Sea, and Arctic Ocean in 2019 and 2020. *Journal of Environmental Radioactivity* **251-252**, 106949.

RADIOCARBON DATING OF VERDIGRIS ON THE BRONZE FITTINGS ATTACHED TO THE RAFTERS OF THE MAIN HALL, IZUMO TAISHA SHRINE

Hirotaka Oda[1], Tetsuya Yamada[2], Toshio Tsukamoto[3]

[1]*ISEE, Nagoya Univ.: Furo-cho, Chikusa-ku, Nagoya 464-8601, Aichi, oda@nendai.nagoya-u.ac.jp*
[2]*Gangoji Institute Res. Cultural Property: Motomachi2-14-8, Ikoma 630-0257, Nara*

Verdigris is rust generated on bronze implement. It is produced from Cu contained in bronze and CO_2 in the atmosphere. Once verdigris is formed, it has the property which prevents formation of new verdigris more. Radiocarbon age of verdigris indicates period when the rust was formed on the bonze implement. We measured the radiocarbon ages of bronze fittings attached to the end of the rafters of the main hall, Izumo Taisha Shrine in 1953. There is a difference between the historical age when the bronze implement was made and the time when the verdigris formed. By the radiocarbon ages of the rafter end fittings, it was concluded the time gap is only ca. 4 years and shown that the radiocarbon dating is a useful method to estimate the historical age of bronze implement.

1 INTRODUCTION AND PURPOSE

Verdigris is rust generated on bronze implement. It is produced from Cu contained in bronze and CO_2 in the atmosphere. Once verdigris is formed a dense film on the surface of bronze implement, it has the property which prevents formation of new verdigris more. Therefore, radiocarbon dating of the carbon contained in verdigris indicates the age in which the rust was formed and can also estimate the age in which bronze implement was used as a tool. In this study, we measured the radiocarbon ages of bronze fittings attached to the end of the rafters of the main hall, Izumo Taisha Shrine. The bronze fittings were installed during the Showa era relocation of the shrine in 1953, and removed during the Heisei era relocation in 2013.

The age of verdigris, as indicated by radiocarbon dating, should be later than the time of the production of the bronze implement. To clarified the time gap, we measured radiocarbon ages of the verdigris on the bronze rafter end fittings which is known to have been attached in 1953.

2 EXPERIMENTAL

2.1 Samples

The verdigris samples were removed from four bronze rafter end fittings shown in Fig. 1. However, the amount of verdigris collected from the two bronze fittings named ITK2 and ITK4 was too small to measure. These two samples, therefore, were combined into one sample (renamed ITK2&4).



Sample name ITK1 ITK2 ITK3 ITK4

Fig.1 The bronze fittings at the end of the rafters of the main hall, Izumo Taisha Shrin.

2.2 Preparation and Measurement

The verdigris samples were decomposed by heating at 250^{O}C for 2h in evacuated glass tubes. The released CO_2 were purified in a vacuum glass line. Then, they were heated with H_2 at 650^{O}C for 6h to prepare graphite.

Copyright on 7th Asia-Pacific Symposium on Radiochemistry 2025 P-R7-14 -

By accelerator mass spectrometry (AMS), the radiocarbon ages were measured using Compact-AMS (1.5SDH, NEC, U.S.A) at Paleo Labo Co., Ltd., Japan. The radiocarbon ages were calibrated to calendar years using calibration curve OxCal v.4.2

2.3 Results

The results of radiocarbon dating showed in Table 1. The calibrated radiocarbon ages of all three verdigris samples indicated either 1956-1958 or later than the end of the 20th century.

TABLE 1. The results of radiocarbon dating

Sample Name	Radiocarbon age [BP]	Calibrated age [cal AD]
ITK1	-442±18	1956-1957, 2005-2014
ITK2&4	-507±20	1957, 2004-2014
ITK3	-843±20	1957-1958, 1995-1998

3 DISCUSSIONS

When radiocarbon ages are calibrated to calendar ages, multiple candidates may emerge depending on the shape of calibration curve. In this study, all three radiocarbon ages point to two passible periods: one concentrated in the period from 1956-1958, and the other is half a century later, from 2005 own wards or 1995-1998. However, if the latter date is the correct time for the formation of verdigris, it means that no verdigris would have been formed for more than half a century after the bronze fittings were attached to the rafters and exposed to the atmosphere. That is extremely hard to image. It is more natural to think that the verdigris started form immediately after exposure to the atmosphere, and stopped after a certain period when a dense film was formed. The average date for that period in thought to be from 1956 to 1958.

The result indicates that the time gap between the historical age of bronze implement and calibrated radiocarbon age is only ca. 4 years, and radiocarbon dating of verdigris has proven to be useful for dating bronze implement.

ACKNOWLEDGMENTS

We would like to Mr. Kentaro Nakamura and everyone at Paleo Lab, Co., Ltd., for their contribution and helpful discussions with regard to radiocarbon dating. We would also like to thank Izumo Taisha Shrine in Izumo City, Shimane Prefecture, for understanding the purpose of this research and kindly providing us with the verdigris samples. This study was partly supported by JSPS KAKENHI, Grant-in-Aid for Challenging Research (Exploratory), Grant Number JP23K17516.

7th Asia-Pacific Symposium on Radiochemistry *September 14 ~ 19, 2025 • Kunibiki Messe • Shimane, Japan*

A preliminary study- minute-level analysis of environmental gamma dose rate and precipitation

Wei-Min Li,[1] Chi-Wen Hsieh,[1] Chuan-Pin Lee,[2,3] Yu-Jie Li,[4] Chun-Yi Fang,[4] Wei-Hsiang Tseng,[1] Yu-Cheng Tsai [1]*
[1] *Department of Electrical Engineering, National Chung Cheng University, Chiayi County 621301, Taiwan;*
[2] *Center for Energy and Environmental Research, National Tsing Hua University, Hsinchu City 300044, Taiwan*
[3] *Radioactive Waste Disposal Technology Research and Development Center, National Tsing Hua University, Hsinchu City 300044, Taiwan*
[4] *Radiation Monitoring Center, Nuclear Safety Commission, Kaohsiung City 833172, Taiwan*
**chiwenh@ccu.edu.tw*

This study utilized the minute-level environmental gamma dose rate data to correlate with the related short time interval rainfall intensity information acquired from the designed image-based dissipating system, as well as meteorological variables such as ambient temperature, humidity, pressure, and wind speed. The analysis includes time series analysis, dose rate derivative calculation, and discrete Fourier transform. Preliminary results showed that rainfall significantly increases the gamma dose rate, and that gamma dose rate derivative is highly correlated with rainfall intensity profiles. However, the total rainfall during an event does not show a clear relationship with the total dose rate increment. Results suggest a threshold-dependent relationship: significant variations in background gamma dose rate tend to be triggered only when rainfall intensity or accumulation exceeds specific thresholds. And gamma dose rate exhibits strong 24-hour and 12-hour periodicities and demonstrates different patterns in varying precipitation situations.

1 INTRODUCTION

Real-time monitoring of ambient gamma dose rate (GDR) forms the foundation for assessing environmental radiation levels and their fluctuations. Rainfall, particularly short-duration intense precipitation, is widely recognized as a major natural factor causing short-term increases in GDR [1,2,3]. This phenomenon is primarily attributed to the washout and deposition of short-lived progeny of naturally occurring radon (^{222}Rn) in the atmosphere, especially ^{214}Pb and ^{214}Bi, by rainwater—commonly referred to as the "radon washout effect" [2,3,4].

Previous studies have examined this phenomenon from various perspectives. Huang et al. [1] analyzed the correlation between GDR and multiple meteorological parameters using hourly data and discussed the effects under different parameter ranges. Yakovleva et al. [4] focused on using the time derivative of GDR; i.e. dH/dt to estimate rainfall intensity and total precipitation and proposed corresponding models. Livesay et al. [2] investigated the response of radiation portal monitors (RPMs) to rainfall-induced increases in background radiation, confirming that ^{214}Pb and ^{214}Bi are the primary contributing radionuclides. Kumar et al. [5] applied discrete Fourier transform (DFT) to analyze the periodicity of radon activity, which is closely related to GDR fluctuations. However, further exploration is valuable, particularly in specific regions—regarding the fine-scale dynamic response of GDR during intense rainfall events- e.g. typhoons using high temporal resolution data, and its complex interactions with multiple meteorological factors.

This study aims to investigate the detailed observations between rainfall events and ambient GDR during periods of heavy precipitation, using a minute-level GDR data provided by the radiation monitoring station. The analysis is complemented by a proposed micro-second order precipitation observation system [6]. The specific objectives are listed as follows:

(1) To quantify the relationship between rainfall intensity I(t) and the rate of change in GDR, denoted as dH/dt.
(2) To analyze the correlation between total rainfall amount Q and total dose rate increment ΔH during individual rainfall events.
(3) To investigate the temporal dynamics of GDR under different conditions through spectral analysis.
(4) To examine the combined influence of meteorological factors—including temperature, humidity, atmospheric pressure, wind speed, and wind direction—on the diurnal variation of GDR.

Ultimately, this study seeks to enhance the understanding of how background radiation levels in the region are affected by meteorological factors, particularly heavy rainfall, and to provide a scientific basis for future applications.

2 MATERIALS AND METHODS

The ambience GDR, denoted as H(t) data used in this study were obtained from a radiation monitoring station in Chiayi City, Taiwan, covering the period from April 18 to October 22, 2024. The recording frequency was once per minute. Simultaneously, the synchronized precipitation data I(t) were obtained; additional meteorological variables, including temperature T(t), relative humidity RH(t), atmospheric pressure P(t), and wind speed WS(t) were also collected at minute-level resolution over the same period. And the micro-second level with sub-mm diameter of the raindrops observations are acquired in the design system based on the article proposed [6]

3 RESULTS AND DISCUSSIONS

By screening the 10-minute accumulated rainfall data during the study period, several significant rainfall events were identified as case studies. A typical heavy rainfall event that occurred on July 17, 2024, at 17:10, during which the 10-minute accumulated rainfall reached 28.94 mm. We found that the emergence of minute-level rainfall intensity closely coincided with the rapid rise in GDR curve. Typically, the GDR reaches its peak as rainfall intensity begins to decrease

or as the main rainfall episode approaches its end. Subsequently, the GDR exhibits a clear exponential decay trend and generally returns to pre-event background levels within a few hours. This dynamic behavior aligns with the mechanism described in paper proposed [2,3,7], wherein radon progeny are washed down by rain and undergo radioactive decay upon deposition on the ground surface.

To further quantify the real-time impact of rainfall on GDR, we calculated the time derivative of the smoothed GDR, dH/dt (in μSv/h per minute). Basically, this derivative should reflect the shape of the rainfall intensity I(t) [4]. The results reveal a clear similarity in temporal patterns: when rainfall begins or intensifies, dH/dt rapidly becomes positive and increases, indicating that GDR is accelerating; when rainfall weakens or ceases, dH/dt turns negative, suggesting that GDR is declining. In addition, discrete Fourier transform (DFT) is adopted to analyze on hourly-averaged GDR data from the Chiayi station. The result indicated that the spectral peak appears at a frequency of 1 cycle per day (cpd), corresponding to a pronounced 24-hour diurnal cycle. A secondary, yet distinct peak is also observed at 2 cpd, indicating a 12-hour semidiurnal component. To visualize the coupling and phase relationships between GDR and meteorological variables over the diurnal cycle, we plotted the hourly-averaged δγ- the fluctuation factor of GDR relative to its annual mean versus the mean hourly temperature, relative humidity, and air pressure, as shown in Fig. 1.

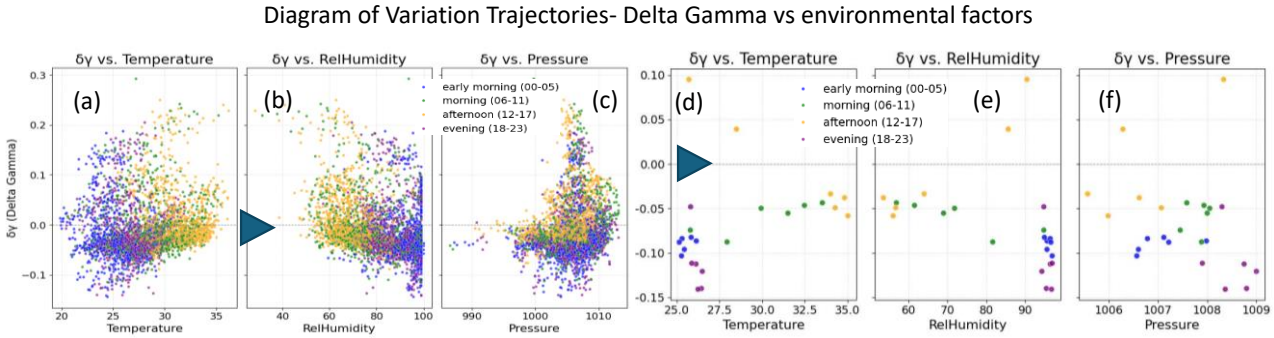


Fig. 1. Scatter plots of hourly δγ versus environmental factors. (a)(b)(c) are no rainfall situations and (d)(e)(f) are heavily rainfall situations. Note that the zero level is marked in triangle sign.

The extensive scatter plots in Fig. 1 also reveal substantial variability in δγ under similar meteorological conditions, suggesting that, beyond the dominant weather factors, other short-term or random influences also affect the gamma dose rate (GDR). Additionally, the color-coded data points by time of day show clear temporal clustering: blue points for early morning hours are in lower temperature and δγ regions, while orange points for the afternoon are in higher temperature and δγ regions. This reflects a discernible migration pattern of δγ along the daily solar cycle.

4 CONCLUSIONS

This study employed high-resolution data to analyze the relationship between rainfall and ambient GDR in Chiayi city, Taiwan. The preliminary findings are as follows: rainfall significantly increases GDR, with its temporal dynamics consistent with the washout and decay mechanism of radon progeny; the shape of the GDR variation rate (dH/dt) is highly correlated with rainfall intensity; and GDR exhibits pronounced 24-hour and 12-hour periodicities that are synchronized with meteorological cycles. These preliminary results indicated that the ambient GDR behaviors are strongly depend on the related environment factors and a super fine time structure could reveal the micro-scopes interpretations.

ACKNOWLEDGEMENTS

The work is supported by NTSC, Taiwan, ROC. ID: NSTC 113-2625-M-194-001

References

[1] Huang, Y. J., et al., (2018). A correlation study of continuously monitored gamma dose rate and meteorological conditions. *Journal of environmental radioactivity*, *192*, 467-477.

[2] Livesay, R. J., et al., (2014). Rain-induced increase in background radiation detected by Radiation Portal Monitors. *Journal of environmental radioactivity*, *137*, 137-141.

[3] Mercier, J. F., et al., (2009). Increased environmental gamma-ray dose rate during precipitation: a strong correlation with contributing air mass. *Journal of environmental radioactivity*, *100*(7), 527-533.

[4] Yakovleva, V., et al., (2021). Rainfall Intensity and Quantity Estimation Method Based on Gamma-Dose Rate Monitoring. *Sensors*, *21*(19), 6411.

[5] Kumar, K. C., et al., (2018). Fast Fourier Transform power spectrum of radon activity. *Radiation Protection and Environment*, *41*(1), 30-36.

[6] Hsieh, C. W., et al., (2019). Automatic precipitation measurement based on raindrop imaging and artificial intelligence. *IEEE Transactions on Geoscience and Remote Sensing*, *57*(12), 10276-10284.

[7] Greenfield, M. B., et al., (2008). Determination of rain age via γ rays from accreted radon progeny. *Journal of Applied Physics*, *104*(7).

Measurement of Radioactive Cesium Transfer Factors from Fukushima-Contaminated Soil to Plants

Yuzuha Mimura[1], Kazuki Daikoku[1], Mizuki Sumihama[1,2], Michio Okada[1], Ayuto Kato[2], Mai Kondo[2], Hiroaki Tanigawa[1], Miki Tanigawa[1], Takashi Saito[3], Haruka Minowa[4] for the Hamadohri Radiation School

[1] *The University of Osaka, 2-1 Yamadaoka, Suita, Osaka 565-0871 Japan, u275041c@ecs.osaka-u.ac.jp*

[2] *Gifu University, 1-1 Yanagido, Gifu, Gifu 501-1193 Japan, sumihama@rcnp.osaka-u.ac.jp*

[3]*Shokei Gakuin University, 4-10-1 Yurigaoka, Natori, Miyagi 981-1295, Japan*

[4]*The Jikei University School of Medicine, 3-25-8 Nishishinbashi, Minato-ku, Tokyo 105-8461, Japan*

We collected various fruits and wild edible plants from multiple locations in Ōkuma Town, Fukushima Prefecture, and measured their radioactive cesium activity concentrations. Soil samples from the respective growing sites were also collected and analyzed for cesium concentrations. Radioactive cesium activity concentrations were measured using a high-purity germanium semiconductor detector. Based on these measurements, transfer factors of radioactive cesium from soil to plants were calculated. The transfer factors varied depending on the plant species. We discuss how environmental conditions, including plant habitat and soil quality, may influence these variations, and outline future challenges for understanding cesium dynamics.

1.Background and Objective and Methods

Since the accident at the Fukushima Daiichi Nuclear Power Plant, environmental contamination by radioactive materials in the surrounding areas has become a serious problem. Okuma Town in Fukushima Prefecture is one of the areas where radioactive cesium has been widely deposited in the soil. I am conducting this research to better understand the transfer of radioactive cesium from contaminated soil into various edible plants still growing wild in this area. I collected yuzu fruits, butterbur sprouts, and soil samples of the respective growing sites from several sites in Okuma Town. I measured the concentration of radioactive cesium in these samples and investigated the relationship between the radioactive cesium concentration in each plant and that in the corresponding soil. All samples were analyzed using a high-purity germanium semiconductor detector capable of measuring gamma-ray emitting nuclides such as radioactive cesium-137 with high precision.

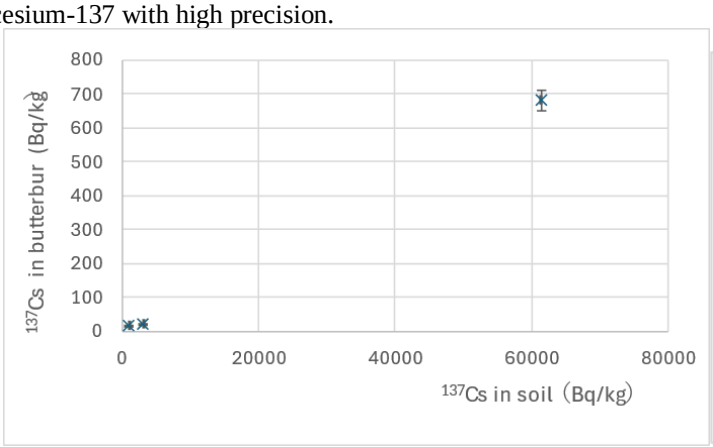


Figure 1 Correlation of Cs-137 between butterbur and soil

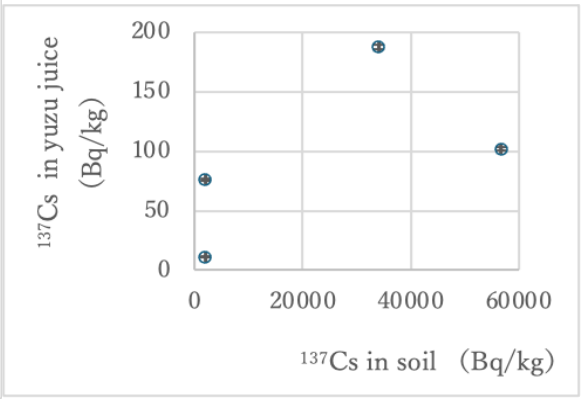


Figure2 Correlation of Cs-137 between yuzu and soil

Figures 1 (2) shows correlations of Cs-137 concentrations between butterbur (yuzu) and soil. The horizontal axis means cesium radioactivity concentrations in butterbur or yuzu soil. The vertical axis means cesium radioactivity concentrations in soil. Comparing plants and soil samples, a correlation was observed between radioactive Cesium concentrations in plants and soil samples for butterbur, but not for yuzu. We hypothesized that this may be due to the chemical form of cesium in the soil. Cesium in soil has two forms: one that is absorbed by plants and one that is not. In addition, potassium is chemically similar to cesium and competes with it in the process of cesium absorption by plants. Therefore, we hypothesized that the concentration of radioactive Cesium in plants may correlate with the amount of cesium and potassium in the form absorbed by plants in soil samples. The small number of samples also makes this data less reliable. Therefore, I would like to increase the number of plant and soil samples and analyze in detail the chemical forms of cesium and potassium in the soil samples. The radioactivity levels of radioactive Cesium in different plant species will then be compared with the amounts of cesium and potassium present in the soil in a form that is easily absorbed by plants in each growing region.

This comparison will provide clues to explain differences in cesium accumulation among soil types and plant species and will contribute to more accurate prediction of cesium transfer from soil to plants in contaminated ecosystems.

ACKNOWLEDGMENTS

This study was conducted as part of the Human Resource Development Program for Building a Foundation Utilizing "Fukkochi" (Knowledge for Reconstruction) of the Fukushima Innovation Coast Framework Promotion Organization and universities, specifically the "Environmental Radiation Training Workshop in the Hamadohri Region of Fukushima Prefecture," as well as the Nuclear Regulation Human Resource Development Project "Human Resource Development Program for Nuclear Regulation through Co-creation with Society." We would like to express our sincere gratitude to everyone involved in the Hamadohri Environmental Radiation Training School.

References

[1] "Decontamination Method for Radioactive Cesium-Contaminated Soil by Water Washing," Regular Meeting of the Atomic Energy Commission, 6th Floor, Central Government Building No. 8, 1-6-1 Nagatacho, Chiyoda-ku, Tokyo, September 6, 2011, 34th Meeting, p. 6–8.

A COMPARISON BETWEEN WET-ONLY AND TOTAL DEPOSITION OF ^{137}Cs OBSERVED IN NAMIE TOWN, FUKUSHIMA PREFECTURE, JAPAN

Hidenao Hasegawa[1], Yoshihito Ohtsuka[1], Naofumi Akata[2], Shinji Ueda[1], Shinji Tokonami[2]

[1]*Department of Radioecology, Institute for Environmental Sciences: 1-7 Ienomae, Obuchi, Rokkasho, Aomori, 039-3212, Japan. hhidenao@ies.or.jp*

[2]*Institute of Radiation Emergency Medicine, Hirosaki University:66-1 Honcho, Hirosaki, Aomori, 036-8564, Japan.*

Total and wet-only ^{137}Cs deposition flux were observed for seventeen months in Namie Town, Fukushima Prefecture. Both tended to be higher from late autumn to spring and lower in summer. The ratio of wet-only ^{137}Cs to total ^{137}Cs deposition flux varied between 0.1 and 0.9, tended to be higher in summer. No clear correlation was found between the ratio of wet-only ^{137}Cs to total ^{137}Cs deposition flux and amount of precipitation.

1 INTRODUCTION

Cesium-137 deposited on the ground as a result of the Fukushima Dai-ichi Nuclear Accident was resuspended and reinjected into the atmosphere, and its influences on the atmospheric concentration of radionuclides was observed for a long time. The removal of ^{137}Cs from the atmosphere can be divided into processes associated with precipitation (wet deposition), and not associated with precipitation (dry deposition). Both processes are important and are incorporated into almost all numerical simulations. Nevertheless, there is limited measurement data to validate the simulation results.

In this study, we measured the concentrations of ^{137}Cs in the total and wet-only deposition samples and estimated the contribution of wet ^{137}Cs deposition flux to the total ^{137}Cs deposition flux.

2 SAMPLES AND METHODS

Monthly total and wet-only deposition were collected at a site in the western part of Namie Town (30.56ºN, 140.75ºE), in the evacuation zone, from November 2019 to March 2021. The sampling site is located at the western edge of the highly contaminated zone. The initial surface contamination (deposition density) of ^{137}Cs (Bq m^{-2}) around the sampling site (10 km radius) was estimated to be 0.1-7 MBq m^{-2}, based on the third airborne survey conducted by the Ministry of Education, Culture, Sports, Science and Technology [1].

Wet-only deposition sample was collected using a handmade wet-only deposition sampler that open automatically at the onset of precipitation by using an optical rain (or snow) sensor, and close at the end after rain or snow has stopped with an opening surface of 0.031 m^2 at heights of approximately 0.5 m (Fig. 1). The total atmospheric deposition samples, each a mixture of wet and dry depositions, were collected in the same interval as the wet-only samples by using a polypropylene basin with an opening surface of 0.18 m^2. Deionized water was poured into the basin at a depth of several centimeters to capture the dry deposition. The collected sample was then passed through a column containing a mixture of Powdex PAO and PCH resins (Ecodyne Co., USA) to separate both ionic and particulate radioactive species from the sample [2]. The homogenized resin was dried in an electric oven at 80°C for over 48 h and then packed into a plastic case (56-mm diameter and 68-mm height) for γ-ray spectrometry. The concentrations of ^{137}Cs in the samples were measured by Ge detectors by using γ-ray 661 keV.

3 RESULTS

Total ^{137}Cs deposition flux ranged from 0.17 to 1.85 (Bq m^{-2} d^{-1}), tended to be higher from late autumn to spring and lower in summer. The seasonal changes in wet-only ^{137}Cs deposition flux were similar to those in total ^{137}Cs deposition flux, with a fluctuation range of 0.05 to 0.50 (Bq m^{-2} d^{-1}). The ratio of wet-only ^{137}Cs to total ^{137}Cs deposition flux ranged from 0.1 to 0.71, tended to be higher in summer. No clear correlation was found between changes in wet-only ^{137}Cs deposition flux and amount of precipitation.

ACKNOWLEDGMENTS

This study was performed under a contract with the government of Aomori Prefecture, Japan.

.

References

[1] MEXT of Japan. Results of the Third Airborne Monitoring Survey by MEXT. (in Japanese) https://radioactivity.nra.go.jp/cont/ja/results/airborne/air-dose/1305819_0708.pdf(date last accessed April 15, 2025).

[2] Kimura, T., Hamada, T. A simple and rapid method of radionuclides in rain water. Radioisotopes 27, 348–349, 1978.

Copyright on 7th Asia-Pacific Symposium on Radiochemistry 2025

Synergistic Coordination-Reduction Interface for Electrochemical Reduction Extraction of Low-Impurity Uranium from Seawater

Huanhuan Liu[1,*], Wenkun Zhu[1,*]

[1]*Southwest University of Science and Technology, Mianyang, 621010, PR China*

[*]E-mail: liuhuanhuan@swust.edu.cn

The “dual carbon” development goal has provided new development opportunities for clean and low-carbon energy sources, including nuclear power. As the most important nuclear fuel resource for nuclear energy development and utilization, the reserves of uranium in land-based uranium mines can only meet the demand for less than a century. Compared with land-based uranium mines, seawater contains approximately 4.5 billion tons of uranium, with a total amount thousands of times that of the known land-based reserves. Electrochemical uranium extraction has emerged as a novel approach in seawater uranium recovery. This method stands out because of its merits, including high efficiency, large extraction volume, and the ability to withstand ion interference. However, the uranium products obtained through electrochemical uranium extraction from seawater are complex and diverse, with a high content of impurity metals, which poses challenges for the subsequent purification of the products. On the one hand, hexavalent uranium (U(VI)) in seawater can participate in the crystallization process of electrochemical uranium extraction from seawater, forming uranate products of uranate anions-alkali metal cations, such as $Na_2O(UO_3 \cdot H_2O)_x$.

Based on this, a synergistic coordination-reduction interface with strong reducing ability for U(VI) was constructed to achieve the stabilization of tetravalent uranium (U(IV)) and the crystallization separation of low-impurity UO_2 in natural seawater. An amorphous-phase derived structural layer (CoMoOS) was in-situ grown on the surface of nickel sulfide (Ni_3S_2) through an in-situ sulfurization process, forming a highly interconnected interface structure and constructing an electrode material (CMOS@NSF) with a synergistic coordination-reduction interface. Research shows that in the structure of CMOS@NSF, on the one hand, the sulfur doping inside CoMoOS adjusts the electron distribution, resulting in the accumulation of electrons on the terminal O, thus forming strong uranyl-ion binding sites. On the other hand, the interface connection between CoMoOS and Ni_3S_2 accelerates electron transfer and enhances the reduction effect. In natural seawater, the electrochemical uranium extraction capacity of CMOS@NSF reaches 2.65 mg g^{-1} d^{-1}, surpassing most uranium extraction adsorbents and electrode materials from seawater. The synergistic coordination-reduction interface enables the formation and stabilization of U(IV), preventing the Co-deposition of alkali metals caused by the participation of U(VI) in crystallization.

Copyright on 7th Asia-Pacific Symposium on Radiochemistry 2025

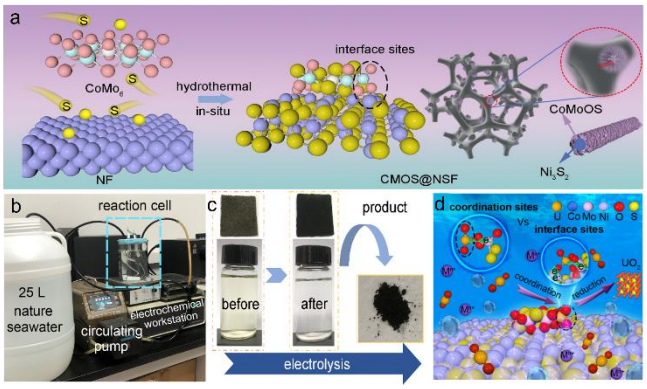


Figure 1: a Scheme of one-step hydrothermal synthesis of materials, b Self-assembled device for electrochemical uranium extraction from seawater, c Photographs of electrodes and solutions before and after the reaction, as well as the collected products, d Schematic mechanism of electrochemical uranium extraction from seawater using CMOS@NSF with a synergistic coordination-reduction interface.

Keywords： Electrochemical; Uranium extraction; Seawater; Structure regulation

[1] Hongliang Guo, Enmin Hu, Yihao Wang, Zhenhong Ou, Bichu Huang, Jia Lei, **Huanhuan Liu***, Rong He, Wenkun Zhu*. A synergistic coordination-reduction interface for electrochemical reductive extraction of uranium with low impurities from seawater [J]. Nat. Commun., 2025, 16, 2021.

[2] **Huanhuan Liu**, Hongliang Guo, Dingping Huang, Li Zhou, Jia Lei,* Yan Liu,* and Wenkun Zhu*. Ultrafast Photoassisted Capture of Uranium over Cu_2O/CuO Heterojunction Enabled by Rapid Interfacial Electron Transfer [J]. ACS Materials Lett., 2025, 7, 295−303.

7th Asia-Pacific Symposium on Radiochemistry *September 14 ~ 19, 2025 • Kunibiki Messe • Shimane, Japan*

Self-Absorption Correction Method Validation for Pb-210 quantification using Gamma Spectrometry

D. Nakazawa[1], S. Hirao[2], K. Sakai[1], A. Suzuki[1]

[1]*Mirion Technologies (Canberra) KK: Asakusabashi Bldg. 4-19-8 Asakusabashi, Taito, Tokyo, 111-0053, Japan*
[2]*Institute of Environmental Radioactivity at Fukushima University: 1 Kanayagawa, Fukushima, Fukushima Prefecture, 960-1296, Japan*

The determination of self-attenuation correction (SAC) factors in gamma spectrometry for the low-energy gamma-ray of 46 keV from Pb-210 presents challenges when the sample composition is unknown. This paper compares the impact of mass attenuation coefficient (MAC) estimations combined with SAC analysis methods using empirical formulas and simulations for cylindrical sample geometries. The sensitivity of any SAC method to the knowledge of the sample composition and its MAC is highlighted, and the validation of empirical SAC calculation methods with reference materials demonstrates their viability for accurate Pb-210 quantification.

1 INTRODUCTION

Quantification of Pb-210 in environmental monitoring of water, soils, and air filters provides useful information of the analysis of harmful radionuclides, as well as soil sedimentation. The main emission from the decay of Pb-210 that is measured with gamma-ray detection systems is the 46.5 keV gamma-ray. A wide variety of techniques and methods are successfully deployed in laboratories and in-situ applications to account for the self-absorption of low energy gamma-rays by the sample and surrounding materials [1-2]. This paper compares different methods of estimating MAC and SAC factors for cylindrical sample geometries. Section 2 describes the full calibration methodology using analytical efficiency transfer, simulation methods for SAC comparison, and transmission-based estimations for MACs. The results of the study are presented in section 3, as well as verification measurements of soil standards obtained from the International Atomic Energy Agency's (IAEA) Terrestrial Environmental Radiochemistry Laboratory.

2. METHODS

The detector system consists of a shielded high-purity germanium detector with a thin entrance window made of carbon composite material. The samples are measured in U8 containers, which are polypropylene with an inner diameter of 48.5 mm and a fill capacity of 49.5 mm. The efficiency calibration of the detector is determined by standards containing mixed nuclides in an alumina matrix with four different fill heights (FH) (5, 10, 20, and 50 mm). A fifth standard of epoxy with a 56.5 mm fill height and consisting of similar nuclides as above, as well as Pb-210. For all calibration measurements, efficiency curves as a function of energy are calculated with air as the matrix, using a SAC factor, true coincidence summing corrections, and background subtraction. The SAC factor is calculated at each photon energy by the following approximation for cylindrical geometries:

$$SAC = \int_0^H \frac{e^{-\mu/\rho \cdot \rho \cdot x}}{(D+x)^2} dx \;/\; \int_0^H \frac{1}{(D+x)^2} dx \;, \qquad (1)$$

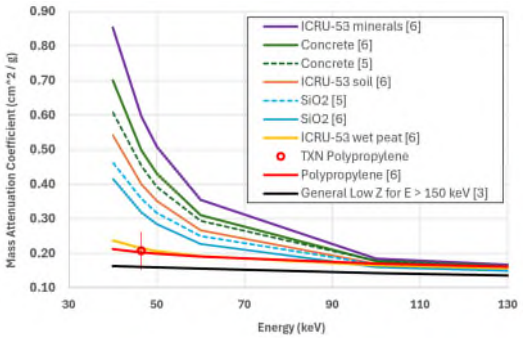
where D is average distance to the active volume of the detector [cm], H is the fill height [cm], μ/ρ is the mass attenuation coefficient (MAC) of the sample [cm^2/g], and ρ is the density of the sample [g/cm^3] [3]. The MACs for materials are either calculated from tables or from empirical formulas [4-5]. To determine the 46.5 keV efficiency in air for the four standards without Pb-210, the average efficiency ratio over all other energies is used as a scaling factor. The air efficiency curves are interpolated from the four fill heights calibrations to the sample height, then the above SAC factor is calculated from the calculated density and the MAC for the sample composition.

First, the MAC values of various materials using tables, empirical formulas [4-5], and transmission-based analysis are compared. For the transmission-based method, standard with the Pb-210 is used as a transmission source, placed above the sample of interest. The MAC for the sample can be estimated directly at 46.5 keV with measurements with and without the sample present, after subtracting contributions from the sample. Next, the efficiency transfer process and the SAC factors of the above method are compared with ISOCS simulations of the measurement setup [6]. Finally, reference standards are measured using the empirical method using best estimates of the sample's MAC.

3. RESULTS

Figure 1 highlights the large range (0.15 to 0.6 cm^2/g) of MAC at 46.5 keV for many materials considered to be low in atomic number and compares the estimations from different sources. Figure 2 shows how this range translates to SAC

for both the analytical method (solid lines) and those based on ISOCS (open circles). When similar materials are used, the SAC factors at 46.5 keV agree to within a few percent using the different methods. Similar comparisons were made with varying densities, fill-heights, and compositions. When the energy increases beyond 150 keV, the MAC and SAC values vary less than in the low energy region. In addition, comparisons between efficiency transfer analysis using Eq. 1 to those determined by simulations show agreement to within a few percent for the FH scaling factors in air.



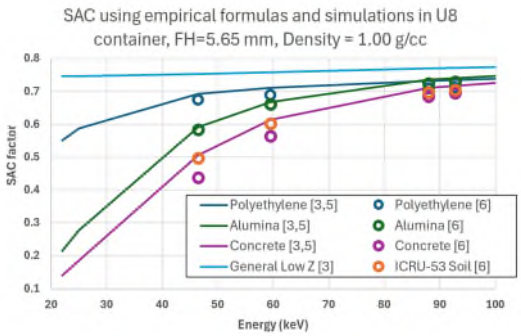
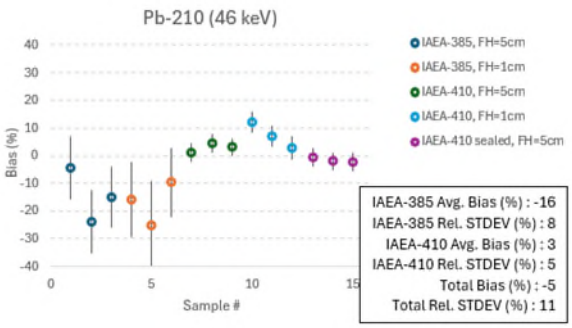


Fig. 1 and 2. The left figure shows mass attenuation coefficients for various materials using different methods. The right figure displays the self-absorption correction factors for materials in the sample geometry using different methods.

IAEA-385 and IAEA-410 soil samples were analyzed with several different compositions. Figures 3 and 4 show the bias of the activity for Pb-210 and Am-241 for three replicate measurements with two fill heights and a common matrix material (concrete from [5]). This matrix closely matched the SAC found by ISOCS using ICRU-53 soil. The expected activities were decay-corrected to the assay dates, and the in-growth of parent nuclides was also considered. The results are consistent with the reference values for both samples and nuclides at a confidence level of 95%. An analysis of K-40 at 1460 keV of all samples yielded an average bias of 2% and relative standard deviation of 9%. Since the SAC factors are much less at this higher gamma-ray energy, this deviation estimates the uncertainty of sampling and preparation.



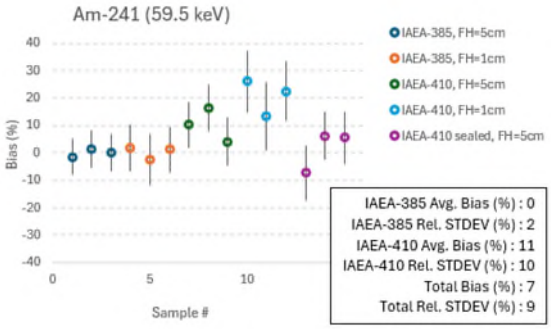


Fig. 3 and 4. The left and right figures are the biases of the empirical method for Pb-210 and Am-241, respectively, for different fill heights. The errors represent the uncertainty at 68% confidence from counting statistics and the certificates.

4. CONCLUSION

Various correction methods for the self-absorption of low energy gamma-rays have been shown to provide similar results for cylindrical geometries. It is critical to select the appropriate sample material or representative matrix, and reference material validation, consistency checks at different energies, or transmission-based measurements can all aid in the sample analysis. Performance at the 10% level at 68% confidence has been demonstrated for the quantification of Pb-210 with gamma spectrometry using empirical formulas and efficiency transfer methods.

References

[1] P. JODLOWSKI. Nukleonika 51, S21-S25 (2006).
[2] M. BONCYZK. Radiat. Phys. Chem. 148, 1-4 (2018).
[3] Gamma-ray Spectroscopy using Germanium Semiconductor Detector, No. 7 of Series of Environmental Radioactivity Measuring Methods, Japan Chemical Analysis Center, (2020).
[4] M. NOGUCHI, T. KOMINE, M. AKIYAMA. Radioisotopes 36, 49-56 (1987).
[5] K. DEBERTIN, R. HELMER, *Gamma- and X-ray Spectrometry with Semiconductor Detectors*, North-Holland, 1988.
[6] R. VENKATARAMAN, et al. Nucl. Instr. Meth. A, 422, p. 450-454 (1999).

Copyright on 7th Asia-Pacific Symposium on Radiochemistry 2025 P-R7-19 -

7th Asia-Pacific Symposium on Radiochemistry *September 14 ~ 19, 2025 • Kunibiki Messe • Shimane, Japan*

Temporal changes of ^{3}H and ^{129}I in seawater collected at mooring buoy near the marine discharge outlet of the Rokkasho Reprocessing Plant

Hisaki Kofuji, Shinichi Gasa, Natsuko Akihama

Japan Marine Science Foundation: Minato-Machi, Mutsu, Aomori, 035-0064, kofuji@jmsfmml.or.jp

To assess short-term variations in the dispersion of radionuclides near the marine discharge outlet of the Rokkasho Reprocessing Plant, seawater samples were collected at several-hour intervals using automated samplers mounted on buoys. The results indicated that elevated ^{3}H concentrations reflecting discharge influence were observed only in 2008. In contrast, increases in ^{129}I concentrations were detected in 2008, 2017, and 2018, with the variations in 2018 corresponding to current fluctuations.

1 Introduction

Japan's first commercial nuclear fuel reprocessing plant, constructed by Japan Nuclear Fuel Limited in Rokkasho Village, Aomori Prefecture, is currently undergoing work in preparation for completion. Since 2006, the plant has conducted active tests using spent nuclear fuel, during which effluents containing radionuclides have been discharged into the ocean through a marine outlet located approximately 2 km offshore. The current around the outlet exhibits complex variability, including changes occurring on an intraday timescale [1]. To assess the advection and diffusion behavior of radionuclides released into the ocean, it is essential to observe changes in their concentrations on a timescale shorter than one day. To obtain such data, seawater was sampled at several-hour intervals using automatic water samplers mounted on moored buoys near the marine outlet, and the concentrations of ^{3}H and ^{129}I (major radionuclides released from the outlet) were measured in the collected samples.

2 Sampling and Analytical Method

Automated water samplers (LYSUM-P or ISCO 6712 Sampler) were mounted on mooring buoys with a diameter of 3.5 meters, located approximately 700 meters north and south of the outlet of the plant. Water was sampled every few hours through inlets placed at depths of 1.0 or 1.5 meters. The collected seawater samples were stored in the samplers and later transported to the laboratory. Up to four samplers were used simultaneously, allowing the collection of up to 96 samples during a single campaign.

Because the amount of sample from the automat of sample obtained from the samplers was limited (900–1000 mL per sample), sequential analysis of ^{129}I and ^{3}H was performed using the same sample. Iodine was extracted from the seawater samples by solvent extraction with hexane, followed by separation and purification, and ^{129}I was measured using accelerator mass spectrometry (AMS) [2]. The concentration of stable iodine in the seawater samples was determined by ion chromatography using a subsample of approximately 25 mL taken from the original sample [3]. For the ^{3}H analysis, the aqueous phase remaining after iodine extraction was used. Organic solvents present in the aqueous phase were removed by heating at temperatures exceeding 70 °C for at least 30 minutes, followed by purification through distillation and concentration via electrolysis. The concentration of ^{3}H was determined using a liquid scintillation counter (ALOKA LSC-LB5).

3 Result and Discussions

3.1 Sequential Analysis of ^{129}I and ^{3}H

In the sequential analysis of ^{129}I and ^{3}H, the procedure for ^{129}I followed the method described in Reference [2], while the analytical procedure for ^{3}H differed from the conventional method. Therefore, an investigation was conducted to determine whether the ^{129}I extraction process affects the ^{3}H analysis, using surface seawater samples collected off the coast of Aomori Prefecture and seawater samples spiked with ^{3}H. For both unspiked samples (^{3}H = 0.07 Bq/L) and spiked samples (^{3}H = 1.25 Bq/L), four replicate analyses were performed with and without the ^{129}I extraction procedure. The results showed that the differences in ^{3}H concentration between samples with and without the ^{129}I extraction process were within the standard deviation range (≤7%) observed in repeated analyses, for both unspiked and spiked samples. These findings confirm that the sequential analytical procedure for ^{129}I and ^{3}H can be applied without issue.

3.2 Temporal changes of ^{129}I and ^{3}H concentration

Copyright on 7th Asia-Pacific Symposium on Radiochemistry 2025

Automated water sampling on the buoy was conducted annually between 2008 and 2019 (except in 2014) for periods ranging from one week to two months. Based on the dates of marine discharge from the reprocessing plant and current data observed in the area by the buoy, analytical samples were selected from the recovered seawater, and the concentrations of ^{3}H and ^{129}I were measured. However, ^{129}I analysis was performed only for samples collected in 2008, 2013, and from 2017 to 2019. The number of analytical samples was 950 for ^{3}H and 450 for ^{129}I. The concentration ranges were 0.04–8.8 Bq/L for ^{3}H and 13–10,100 nBq/L for ^{129}I. The highest concentrations of both nuclides were observed in a sample collected on May 17, 2009, one day after a marine discharge.

A contribution from the reprocessing plant to ^{3}H concentrations was observed only in 2008. In contrast, for ^{129}I, while concentrations in the absence of discharge influence were typically 17–33 nBq/L in surface waters around Aomori Prefecture [4], elevated levels of several hundred nBq/L were also detected in 2017 and 2018. Figure 1 shows the variation in ^{129}I concentration and the current velocity observed by the buoy in 2018. The ^{129}I concentration exhibited periodic fluctuations, ranging from values close to the regional baseline to several hundred nBq/L, with peak concentrations gradually decreasing over time. The current around the discharge outlet is predominantly northward or southward, and previous studies have reported current velocity fluctuations with a cycle of approximately one day [1]. The variations in ^{129}I concentrations in 2018 corresponded to these current fluctuations. On May 21, 2018, wastewater with a ^{129}I concentration of about 0.5 Bq/L was discharged from the outlet. This effluent was rapidly diluted immediately after discharge, temporarily dispersed away from the outlet area, and subsequently returned toward the vicinity of the outlet due to flow reversal. It is considered that the effluent then repeatedly approached and receded from the outlet area, gradually diffusing in the process.

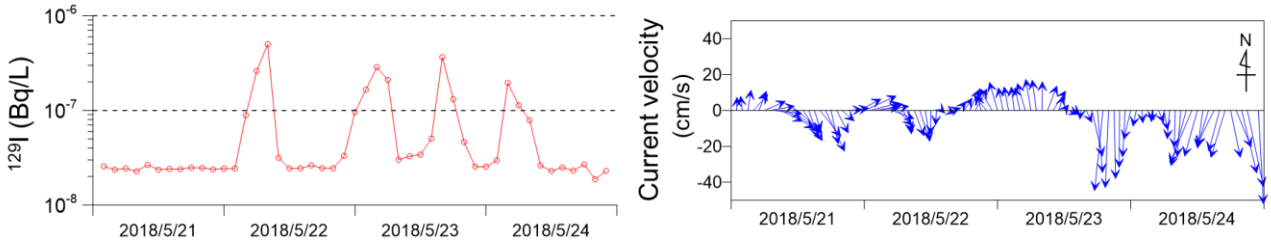


Fig. 1. Temporal changes of ^{129}I concentration in seawater and current velocity.

4. CONCLUSIONS

Seawater sampling conducted near the marine discharge outlet of the Rokkasho Reprocessing Plant using automated samplers mounted on buoys enabled high-frequency monitoring of ^{3}H and ^{129}I. A sequential analysis method for both nuclides using a single sample was established and validated. ^{3}H showed discharge-related increases only in 2008, while ^{129}I exhibited elevated concentrations in 2017 and 2018. In 2018, periodic elevations in ^{129}I corresponded to current fluctuations. These findings demonstrate that buoy-based sampling near the outlet is effective for tracking short-term variations in radionuclide dispersion.

ACKNOWLEDGMENTS

This study was carried out as part of a contract investigation entrusted by the government of Aomori Prefecture, Japan.

References

[1] T. In et al., Diurnal coastal trapped waves propagating along the east coast of the Shimokita Peninsula, Japan, *J. Oceanogr.*, **80**, 21-44 (2024).
[2] S. Gasa et al., Determination of ^{129}I in seawater by accelerator mass spectrometry with solvent extraction method, *Radioisotopes*, **56**, 155-162 (2007). (In Japanese with English abstract)
[3] S. Gasa, M. Kamamoto and H. Kawamura, Determination of stable iodine in seawater by an ion chromatograph, *Proceedings of the 41st Meeting Radioisotopes and Radiation Research*, Tokyo, Japan, July 7-8, 2004. (In Japanese)
[4] S. Gasa, H. Kofuji and T. Kuji, The relationship between distribution of ^{129}I concentration and water masses off the Pacific coast in Aomori Prefecture, Japan, *Radioisotopes*, **68**, 115-123 (2019). (In Japanese with English abstract)

7th Asia-Pacific Symposium on Radiochemistry *September 14 ~ 19, 2025 • Kunibiki Messe • Shimane, Japan*

Depth-Dependent Measurement of Radioactive Cesium Activity Concentration in a 30 cm Soil Core from Fukushima

Kazuki Daikoku[1], Yuzuha Mimura[1], Mizuki Sumihama[1,2], Michio Okada[1], Ayuto Kato[2], Mai Kondo[2], Takashi Saito[3], Haruka Minowa[4] for the Hamadohri Radiation School

[1] *The University of Osaka, 2-1 Yamadaoka, Suita, Osaka 565-0871 Japan, u708261j@ecs.osaka-u.ac.jp*

[2] *Gifu University, 1-1 Yanagido, Gifu, Gifu 501-1193 Japan, sumihama@rcnp.osaka-u.ac.jp*

[3]*Shokei Gakuin University, 4-10-1 Yurigaoka, Natori, Miyagi 981-1295, Japan*

[4]*The Jikei University School of Medicine, 3-25-8 Nishishinbashi, Minato-ku, Tokyo 105-8461, Japan*

It is well known that most radioactive cesium remains in the upper ~10 cm of soil, with a sharp decline in concentration observed beyond that depth. To investigate the depth-dependent distribution of radioactive cesium, we collected 30 cm soil cores from various locations in the Hamadohri region of Fukushima Prefecture using specialized soil sampling equipment. In total, over 70 soil cores were obtained. Radioactive cesium activity concentrations were measured using a high-purity germanium semiconductor detector. Although it is not possible to present all individual data, we analyzed the overall trends, reported the depth-dependent patterns observed in cesium distribution, and discussed possible factors influencing these distribution profiles.

1.1 Background

At Osaka University, a program known as the Hamadohri Environmental Radiation Training Workshop has been established to provide students with hands-on experience in understanding the complex environmental and social issues caused by the Fukushima Daiichi Nuclear Power Plant accident [1]. This workshop is part of a broader effort to develop human resources who can contribute to the long-term reconstruction and revitalization of the affected areas. The Hamadohri region of Fukushima Prefecture—encompassing municipalities such as Iitate, Ōkuma, and Futaba—was heavily impacted by the nuclear accident in 2011. While decontamination and reconstruction efforts have progressed in many areas, significant challenges remain, especially within the Difficult-to-Return Zones where access is still restricted due to high radiation levels. In this workshop, students engage in fieldwork to better understand the current environmental conditions in these areas. One of the key components of the training is the collection and analysis of environmental samples, including soil, vegetation, and ambient radiation measurements. These activities aim to deepen students' understanding of radiological science, measurement techniques, and environmental dynamics. This presentation focuses on the analysis of soil samples collected during the workshop and aims to provide insights into the behavior and distribution of radioactive contaminants in the region more than a decade after the accident.

2. Objectives and Methods

The primary objective of this study was to investigate the vertical distribution and concentration of radio nuclides in soil, and to compare these characteristics across different areas of the Hamadohri region, including both inside and outside the Difficult-to-Return Zones. To achieve this, 30 cm soil cores were collected from three key locations: Iitate, Ōkuma, and Futaba. These areas were selected based on their varying degrees of contamination, geographical distance from the Fukushima Daiichi Nuclear Power Plant, and administrative status regarding return policies. Each soil core was carefully extracted using a stainless‐steel core sampler to minimize contamination. The cores were then sectioned into 2.5 cm intervals, resulting in 12 discrete layers per core. This fine‐scale segmentation allowed for a detailed analysis of radionuclide migration and attenuation with soil depth. Each soil segment was placed in a standardized container and sealed for analysis. The samples were then measured using a high‐purity germanium (HPGe) detector, which offers high resolution and accuracy in identifying and quantifying gamma‐emitting radionuclides such as cesium-137. The use of HPGe detectors is particularly important for distinguishing between isotopes and obtaining reliable data for radiological assessments. Previous studies have suggested that radioactive cesium concentrations in soil often follow an exponential decay pattern with depth, particularly in undisturbed environments [2][3]. This study aimed to evaluate the extent to which that model applies in real‐world conditions within and outside the restricted zones of Fukushima. The results were analyzed to assess regional differences and depth profiles. Generally, radioactive cesium concentrations tend to be higher in the surface soil layers. However, there are locations where this is not the case. This study also considers how frequently such locations occur and discusses possible reasons why the surface concentration may not always be the highest.

Copyright on 7th Asia-Pacific Symposium on Radiochemistry 2025

ACKNOWLEDGMENTS

This study was conducted as part of the Human Resource Development Program for Building a Foundation Utilizing "Fukkochi" (Knowledge for Reconstruction) of the Fukushima Innovation Coast Framework Promotion Organization and universities, specifically the "Environmental Radiation Training Workshop in the Hamadohri Region of Fukushima Prefecture," as well as the Nuclear Regulation Human Resource Development Project "Human Resource Development Program for Nuclear Regulation through Co-creation with Society." We would like to express our sincere gratitude to everyone involved in the Hamadohri Environmental Radiation Training School.

References

[1] M. Takahashi et al.," Environmental radiation workshop held in Iitate village, Fukushima prefecture" Proceedings of the 22nd Workshop on Environmental Radioactivity, KEK proceedings 2021-2, 170-175 (2021)

[2] R. Ohara et al., "Concentration of Cs-137 in soil at Fukaya area, Iitate village, Fukushima prefecture" Proceedings of the 22nd Workshop on Environmental Radioactivity, KEK proceedings 2021-2, 164-169 (2021)

[3] Paddy-field contamination with 134Cs and 137Cs due to Fukushima Dai-ichi Nuclear Power Plant accident and soil-to-rice transfer coefficients, Satoru Endo*, Tsuyoshi Kajimoto, Kiyoshi Shizuma, J. Environ. Radioact. 116, 59-64(2013)

Efficient Photoassisted Uranium Recovery from Fluorine-Containing Wastewater by Ag/WO_{3-x} with Surface Defect and Heterostructure

Jia Lei [1, *], Duo Zhang [2, *], Shuao Wang [2, *]

[1] *Southwest University of Science and Technology, Mianyang, 621010, PR China*

[2] *Soochow University, Suzhou, 215123, PR China*

*E-mail: leijia@suda.edu.cn

The uranium recovery from high concentration fluorine-containing uranium wastewater is a desired research target in the field of environmental radiochemistry but is very challenging due to the formation of stable uranium fluoride complexes that are quite difficult to extract. Photocatalytic reduction of uranium has garnered significant attention due to the advantages of enhanced selectivity, non-toxicity, and mild reaction conditions. For photocatalysis, the separation of photogenerated electrons and holes on the surface of photocatalysts directly affects the photocatalytic efficiency. By constructing spatially separated heterojunction structure, the light-induced electrons and holes would migrate to electron-withdrawing and electron-donating centers, respectively. The resulting δ^--rich/δ^+-rich centers can act as ideal binding sites for U(VI)-F complexes through electrostatic interactions, weakening the U(VI)-F bonds for more facile dissociation. For semiconductors, hot electrons injection arising from the plasmon effect into the semiconductor can effectively decrease the compounding efficiency of high-energy hot electrons with holes. Thus, the combination of plasmonic materials with semiconductors to construct heterojunctions has proven to be an effective approach to enhance the photocatalytic activity. On the one hand, the local electromagnetic field induced by surface plasma accelerates charge separation in semiconductor photocatalysts. On the other hand, plasmonic materials tend to expand the light absorption range of semiconductors and increase the catalytic activity. Additionally, surface defect engineering has emerged as another strategy for improving photocatalytic activity. Primarily, defect engineering facilitates the adsorption of the target species. Secondly, defect engineering tunes the electronic structure and modulates the range and intensity of light absorption. The third aspect is that defect engineering functions as charge separation centers, facilitating the separation of surface charges. As a result, the photogenerated electron-hole pairs can be effectively separated, thereby promoting the utilization efficiency of both holes and electrons for corresponding interfacial redox reactions. Therefore, the heterostructure catalysts combined plasmon effect with defect engineering can efficiently extract uranium from fluorine-containing uranium wastewater through weakening the U(VI)-F bonds, and enhancing the confinement, coordination, and catalytic reduction of uranium.

By employing surface defect engineering and interfacial heterostructure design, we present here the rational design of efficient photocatalyst (Ag/WO_{3-x}) for U(VI) uptake from fluorine-containing uranium wastewater without any sacrificial agents.

The defect-rich surface of Ag/WO_{3-x} facilitates confined adsorption of uranium, while the introduction of Ag nanoparticles enables both efficient electron-hole separation and plasmon effect upon light irradiation. Ag/WO_{3-x} shows high U(VI) removal efficiency of 96.3% at 8 mg/L of U(VI) within 60 minutes. Notably, even when the ratio of F^- to U(VI) is as high as 20:1, the removal efficiency of U(VI) by Ag/WO_{3-x} reaches up to 95%. Additionally, the maximum capture capacity of U(VI) on Ag/WO_{3-x} reaches 676.8 mg/g at 200 mg/L of U(VI) within 60 minutes, which is superior to ever-reported photocatalysts in fluorine-containing uranium wastewater. This work provides an effective way for the uranium capture from fluorine-containing wastewater through the synergy of plasmon effect and defect engineering.

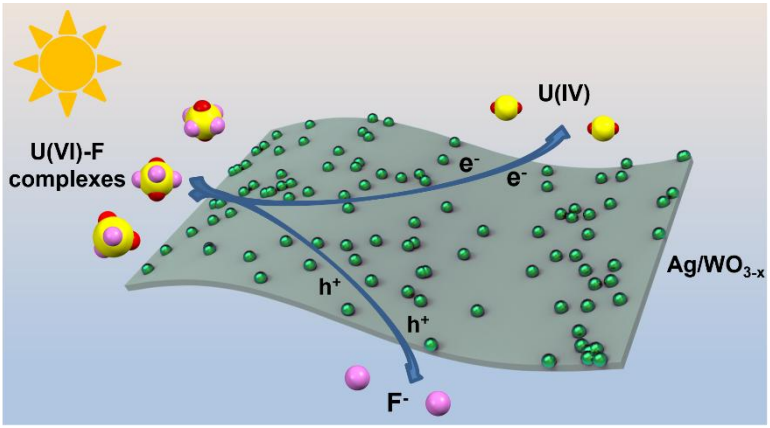


Figure 1. Charge transfer and U(VI) photocatalytic reduction mechanisms by Ag/WO_{3-x} under irradiation.

Keywords: heterostructure; plasmon effect; surface defect; uranium; photoreduction

[1] **Jia Lei**, Yufei Shen, Xueyu Wang, Lixi Chen, Huanhuan Liu, Xiaohui Yu, Duo Zhang*, Shuao Wang*. Record High Uranium Photoassisted Capture Performance from Fluorine-Containing Wastewater by Ag/WO_{3-x} with Surface Defect and Heterostructure. *Inorganic Chemistry*, 2024, 63(41), 19439-19449.

Copyright on 7th Asia-Pacific Symposium on Radiochemistry 2025

7th Asia-Pacific Symposium on Radiochemistry *September 14 ~ 19, 2025 • Kunibiki Messe • Shimane, Japan*

Density of Radioactive Cesium-Rich Microparticles in Contaminated Soils

Koyo Takeuchi[1], Shinya Yamasaki[2], Satoshi Utsunomiya[3], Yuichi Takaku[2], Keisuke Sueki,[2] Yudai Shigekawa,[2] Aya Sakaguchi[2]

[1] *Graduate School of Science and Technology Degree Programs in Pure and Applied Sciences Master's Program in chemistry University of Tsukuba*

[2] *Institute of Pure and Applied Sciences, University of Tsukuba, Japan*

[3] *Department of Chemistry, Kyusyu University, Japan*

Radioactive Cesium-Rich Microparticles (CsMPs) released by the Fukushima Daiichi Nuclear Power Plant accident are highly radioactive and have attracted much attention in terms of their mobility in the environment and biological effects. In this study, heavy-liquid separation of CsMPs in 0.2 g/cm³ increments was performed on soil from Ottozawa, Okuma-machi, Fukushima Prefecture, in order to clarify the density distribution of CsMPs in detail. As a result, a maximum of 7 CsMPs were detected in the 2.2-2.4 g/cm³ fraction and 4 CsMPs in the 2.4-2.6 g/cm³ fraction, with more than 80% of the total concentrated in this range. This is consistent with the density of amorphous silicate glass, the main component of CsMPs. These results suggest that particle density may serve as a critical parameter for the efficient separation of CsMPs from contaminated soils.

1. Introduction

In March 2011, the Fukushima Daiichi Nuclear Power Plant accident released a large amount of radionuclides into the environment, which deposited on terrestrial and marine environments. Among the released radionuclides, the short-lived iodine-131 and cesium-134 decayed rapidly, and cesium-137 with a half-life of about 30 years, became the predominant contributor to ambient radiation. In contaminated soils, radioactive cesium has been reported to be retained mainly in clay minerals and CsMPs [1]. CsMPs retain high radioactivity concentrations and have attracted much attention due to their environmental mobility and biological impact. Therefore, to better understand the behavior and mobility of CsMPs, it is essential to perform separation and analysis based on particle size and density. In previous studies, heavy liquids with a density of 2.4 g/cm^3 were used, and heavy-liquid separation, a separation method utilizing density differences, was performed. Applying the Quantification of Cesium-Rich Microparticles (QCP method) [2], a simplified determination method for CsMPs, to those fractions, 13 CsMPs were found in soils with a density of 2.4 g/cm^3 or lower, and 4 CsMPs were found in fractions with a density of 2.4 g/cm^3 or heavier. However, a more detailed density distribution of CsMPs has yet to be fully characterized. In this study, a more detailed density distribution of CsMPs was determined using heavy-liquid separation.

2. Method

Surface soil samples (<5 cm depth) were collected from Ottozawa, Okuma-machi, Fukushima Prefecture (1.65 km south of the Fukushima Daiichi Nuclear Power Plant). The samples were air dried at room temperature for approximately two months, then subjected to a sequential extraction process to decompose organic matter and amorphous iron oxides. This pretreatment step prevented re-adsorption of dissolved cesium onto the remaining soil matrix. Before and after the successive sequential extraction, γ-ray measurements were performed using a germanium semiconductor detector, and the cesium-137 activity was calculated. The resulting residue was wet classified using a 63 μm sieve to obtain soils of 63 μm or less. A total of seven heavy liquids were prepared using sodium polytungstate in 0.2 g/cm^3 increments from a density of 1.8 g/cm^3 to 3.0 g/cm^3. Heavy-liquid separation was performed by centrifugation and filtration using a 0.45 μm membrane filter for cleaning, and heavy-liquid separation was performed in the order of decreasing density (<1.8, 1.8-2.0, 2.0-2.2, 2.2-2.4, 2.4 -2.6, 2.6-2.8, 2.8-3.0, and >3.0 g/cm³), and different density compartments were obtained. After separation, the particles of each compartment were subjected to γ-ray measurement using a germanium semiconductor detector and the cesium-137 activity was calculated. Particles from each compartment were suspended, lined up on an aluminum plate, dried, and autoradiographed with a cesium-137 standard source at an exposure time of 24 hours. A calibration curve was prepared from the photostimulated luminescence intensity of the cesium-137 standard source, and the cesium-137 activity of each particle was determined; the QCP method was applied, and particles with a cesium-137 activity of 0.0600 Bq or higher, calculated from the calibration curve and decay corrected at 15:36 (JST) on March 12, 2011, were designated CsMPs.

Copyright on 7th Asia-Pacific Symposium on Radiochemistry 2025

3. Results and Discussion

Table 1 shows the number of CsMPs, total weight, total cesium-137 activity, cesium-137 activity of all CsMPs, and radioactive fraction contribution rate. Of the eight fractions separated by density, the highest number of 7 CsMPs was detected in the 2.2-2.4 g/cm^3 fraction, followed by 4 in the 2.4-2.6 g/cm^3 fraction. In terms of proportion of CsMPs by density to total CsMPs, the 2.2-2.4 g/cm^3 fraction accounted for half of the total, and the 2.4-2.6 g/cm^3 fraction accounted for 31%. In the other fractions, the number of detections was small (0 to 1) and the percentage was a few percent. These results demonstrate a pronounced tendency for CsMPs to concentrate within the 2.2–2.6 g/cm^3 density interval. This suggests that CsMPs differ in density from typical clay minerals, and that targeting the 2.2–2.6 g/cm^3 range would enhance separation efficiency.

The 2.2-2.4 g/cm^3 fraction appears to be the most efficient for CsMP isolation and should be prioritized in future separation protocols. Previous studies have reported that CsMPs are composed of silicate glass [2]. Since the generally reported density of amorphous silicate glasses is 2.2-2.5 g/cm^3[3], the density of CsMPs was confirmed to be approximately the same as that of amorphous silicate glass. This may reflect the fact that CsMPs are primarily composed of silicates. Their amorphous structure may also account for their relatively lower density compared to layered silicate minerals, such as weathered vermiculite and illite. X-ray diffraction (XRD) measurements in previous studies have shown that weathered clay minerals are predominantly present in density fractions exceeding 2.4 g/cm^3 [1]. The more frequent detection of CsMPs in lower-density fractions in this study likely reflects differences in crystalline and amorphous structures.

By dividing samples into 0.2 g/cm^3 increments, this study enabled finer resolution of CsMP density distribution. Future work focusing on even more detailed separation within the 2.2–2.6 g/cm^3 range may improve both understanding and recovery efficiency. Furthermore, due to the slow settling velocity of small particles (<1 μm) during heavy liquid separation, accurately estimating their density with the current method is challenging. Therefore, a more thorough investigation of the particle density for such particles is required.

TABLE 1. Results for each density fraction

Density / g cm^{-3}	-1.8	1.8-2.0	2.0-2.2	2.2-2.4	2.4-2.6	2.6-2.8	2.8-3.0	3.0-
Number of CsMPs	0	0	1	7	4	1	0	0
Total Weight / g	0.002	0.017	0.006	0.053	0.109	0.103	0.053	0.026
Total ^{137}Cs Activity / Bq	1.17	1.95	6.23	69.2	63.5	76.0	11.9	2.61
^{137}Cs Activity of all CsMPs / Bq	0	0	0.0815	1.79	0.870	0.122	0	0
Radioactive Fraction Contribution Rate%	0	0	1.3	2.6	1.4	0.16	0	0

4. CONCLUSIONS

This study revealed that CsMPs are predominantly concentrated within the 2.2–2.6 g/cm^3 density range, with the 2.2–2.4 g/cm^3 fraction exhibiting the highest separation efficiency. These findings reflect the intrinsic density characteristics of CsMPs, likely stemming from their amorphous structural composition, and highlight the critical role of optimized density settings in enabling precise isolation and analysis in future studies.

ACKNOWLEDGMENTS

This work was supported by JSPS KAKENHI Grant Number JP24K22345 (S. Yamasaki).

References

[1] S. Yamasaki. *et al.,* "Gravitational separation of ^{137}Cs contaminated soil in Fukushima environment: Density dependence of 137Cs activity and application to volume reduction," *J Environ Radioact* **246**, 106846(10) (2022).
[2] R. Ikehara. *et al.,* "Novel Method of Quantifying Radioactive Cesium-Rich Microparticles (CsMPs) in the Environment from the Fukushima Daiichi Nuclear Power Plant." *Environ Sci Technol* **52**, 6390–6398 (2018).
[3] S. Iizumi, *Chemistry Handbook of Applications*, pp. 375, The Japan Society for Analytical Chemistry, Ed., Maruzen Co., Ltd., Chuo-ku, Tokyo (1980).

7th Asia-Pacific Symposium on Radiochemistry *September 14 ~ 19, 2025 • Kunibiki Messe • Shimane, Japan*

Evaluation of the ability of *Saccharomyces cerevisiae* to reduce U(VI) by anaerobic respiration

Iori Yamamoto[1], Shinya Yamasaki[2], Yuichi Takaku[2], Yudai Shigekawa[2], Keisuke Sueki[2], Aya Sakaguchi[2]

[1] *Graduate School of Science and Technology Degree Programs in Pure and Applied Sciences Master's Program in chemistry, University of Tsukuba, Japan*
[2] *Institute of Pure and Applied Sciences, University of Tsukuba, Japan*

Geological disposal is a promising method for managing radioactive waste, where radionuclides mobility is influenced by their solubility in groundwater. Microbial reduction can alter radionuclides solubility, yet most studies focus on prokaryotes. This study investigates U(VI) reduction by Saccharomyces cerevisiae under anaerobic, fermentative conditions at 37 °C. Our results aim to reveal the potential role of eukaryotes in radionuclides behavior in deep geological environments.

1 Introduction

Geological disposal is being considered as a long-term management method for radioactive waste, including low-level waste containing transuranic elements and high-level waste containing fission products, generated from nuclear fuel reprocessing plants. In assessing the safety and feasibility of geological disposal, it is crucial to accurately understand the migration behavior of radionuclides in the subsurface environment. Dissolution of radionuclides into groundwater, in particular, is one of the key factors governing their mobility; therefore, it is essential to investigate the chemical speciation and solubility of the radionuclides. Recent studies have reported microorganisms capable of reducing radionuclides under anaerobic conditions, thereby altering their solubility through metabolic activity [1]. However, most of these studies have focused on prokaryotic microorganisms with specific reduction capabilities, and research on the reduction of radionuclides by eukaryotic microorganisms remains insufficient. A previous study examined the potential reduction of U(VI) by the eukaryotic microorganism *Saccharomyces cerevisiae* (hereafter referred to as Yeast), but no reduction was observed. This was likely due to insufficient metabolic activity, such as fermentation, under the experimental temperature of 30 °C [2]. In this study, we aimed to evaluate the potential of Yeast to reduce U(VI) under anaerobic conditions by conducting experiments at 37 °C, which promotes fermentation.

2 Method

Yeast was cultivated in sterilized liquid medium at 37 °C for 24 hours under shaking conditions. After cultivation, the cells were washed twice with citrate–sodium citrate buffer (pH 7.0) to obtain microbial suspensions. Experimental samples were prepared under four conditions: (1) Yeast + glucose, (2) Yeast only, (3) glucose only, and (4) control (without Yeast and glucose). All samples contained 1.0 mM U(VI) (as $UO_2(CH_3COO)_2 \cdot 2H_2O$) in citrate–sodium citrate buffer to maintain constant pH and inhibit U(IV) precipitation as UO_2. The vials were sealed with rubber stoppers and aluminum caps, purged with nitrogen gas to ensure anaerobic conditions. Incubation was carried out at 37 °C with shaking at 90 rpm for up to 7 days. Samples were collected on days 0, 1, 4, and 7. The collected solutions were transferred into an anaerobic glove box where the oxygen concentration was reduced to below 0.0% by nitrogen gas purging. Microbial cells were removed by filtration, and the filtrates were then sealed into quartz cells for UV-Vis spectrometry in the globe box. UV–Vis spectra were obtained using a spectrophotometer (HITACHI, U-2910). After baseline correction, the height of the absorbance peak, corresponding to the U(IV)-citrate complex, was measured. The concentration of U(IV)-citrate complex was then calculated using a previously determined molar extinction coefficient of the complex. The conditions (1) and (2) were run in triplicate (n=3) and analyzed statistically.

3. Results and Discussion

In the absence of Yeast (Fig. 1, blue and green), the initial concentration of U(IV) was approximately 0.06 mM and increased over time. These results were attributed to photoreduction of U(VI)-citrate complex. The presence of glucose—a known reducing agent—did not affect the extent of uranium reduction (Fig. 1, blue and green), suggesting that glucose did not directly reduce U(VI).". In contrast, the presence of Yeast led to a significantly greater reduction of U(VI) to U(IV) compared to the control (Fig. 1, yellow). Notably, under the Yeast + glucose condition, approximately 30% of U(VI) was reduced to U(IV) (Fig. 1, red). These results indicate that Yeast can generate sufficient electrons through metabolism under anaerobic conditions to reduce U(VI). In contrast to previous experiments conducted at 30 °C, a clear reduction of uranium was observed in this study. Future research should focus on identifying the specific

Copyright on 7th Asia-Pacific Symposium on Radiochemistry 2025

metabolites generated through Yeast metabolism that contribute to uranium reduction and elucidating the underlying mechanisms, to further clarify the role of eukaryotic organisms in uranium redox reaction.

:

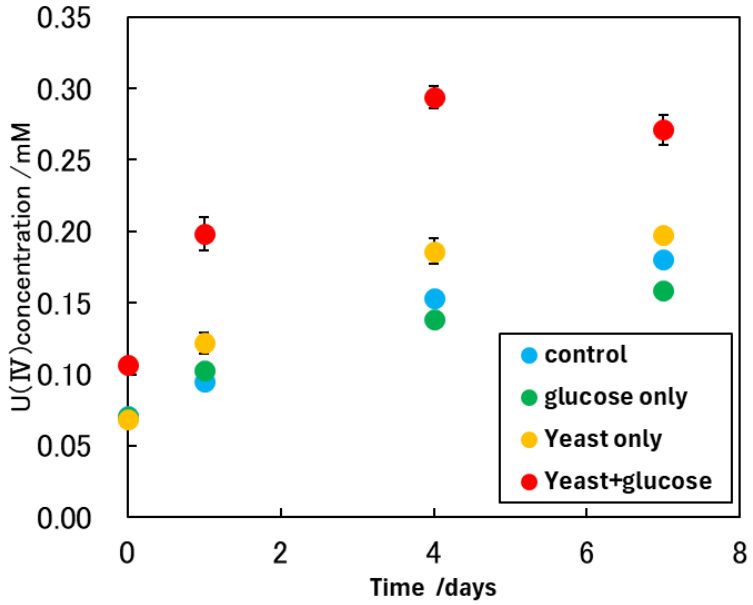


Figure 1 Temporal change in U(IV) concentration by Yeast under anaerobic conditions

4. CONCLUSIONS

This study demonstrated the ability of *Saccharomyces cerevisiae* to reduce U(VI) to U(IV) under anaerobic fermentation conditions. In particular, approximately 30% of U(VI) was reduced in the presence of glucose, suggesting the involvement of electron donation through metabolic processes. The metabolic activity of microorganisms is likely to influence the reduction behavior of radionuclides in the subsurface environment.

References

[1] Chen. S., Gong J, Cheng Y, Guo Y, Li F, Lan T, Yang Y, Yang J, Liu N, & Liao J, "The biochemical behavior and mechanism of uranium(VI) bioreduction induced by natural Bacillus thuringiensis." *Journal of Environmental Sciences*, **136**, 372–381(2024).

[2] Y. Suzuki, "Evaluation of Anaerobic Reduction of Metal Ions by *Saccharomyces cerevisiae*," *Graduate School of Science and Technology Degree Programs in Pure and Applied Sciences Master's Program in chemistry Master's thesis, University of Tsukuba*, (2022).

7th Asia-Pacific Symposium on Radiochemistry September 14 ~ 19, 2025 • Kunibiki Messe • Shimane, Japan

MEASURED AND THEORETICAL GAMMA AIR DOSE RATES IN ARCHIVED SOIL SAMPLES COLLECTED IN JAPAN

Keiko Tagami[1*], Shigeo Uchida[1]

[1] *Institute for Radiological Science, National Institutes for Quantum Science and Technology (QST): Anagawa 4-9-1, Inage-ku, Chiba, 263-8555, Japan, *tagami.keiko@qst.go.jp*

Approximately 1,100 Japanese soil samples collected mostly in the 1970s have been stored in QST. The soil samples were air-dried but not further treated for their gamma-ray activity concentration analysis; the only associated data were gamma air dose rates measured at the sample collection sites. Of these soil samples, about 340 soil samples were selected, sieved to have a soil particle size of ϕ<2 mm, and then their ^{137}Cs, ^{232}Th, ^{238}U, and ^{40}K concentrations were measured using a Ge detection system. Considering the geological differences between eastern and western Japan, 179 and 157 soil samples were used, respectively, to calculate the theoretical gamma air dose rates using the activity concentration data. Then, the calculated and measured air dose rates were compared. The results showed positive correlations in both regions by t-test (p<0.01), with a better correlation factor in eastern Japan. Further analysis of soil apparent density, the percentage of the ϕ<2 mm fraction, and the ^{137}Cs activity concentration could not explain the difference between the theoretical and measured air dose rates.

1 INTORDUCTION

Biosphere safety assessments are necessary for the decision-making steps when selecting a high-level waste geological disposal site decision making steps. One of the important radionuclides for the assessment is uranium (U); however, because the element exists naturally in the environment, the background level of U in the soil must be considered. Not only by using *in-situ* gamma-ray spectrometry, but also by using airborne and/or airborne gamma-ray measurement methods allow us to estimate natural radionuclide concentrations in surface soil [1]. However, it is useful if we could simply apply air dose rates to estimate uranium concentration in soil to map U in the area, although it is not so simple because concentrations of naturally occurring element i.e., ^{40}K, U and Th, in soil from different origins can change with rocks [2]. Yet air dose rates could be a good indicator for rough estimation of U because soil types have been well studied and the information is already available throughout Japan [3].

Although air dose rates can be easily measured, many papers have reported the radioactivity concentrations of naturally occurring ^{40}K, U and Th as well as the anthropogenic ^{137}Cs in soil samples and then calculated air dose rates based on the IAEA method [1] without showing *in-situ* air dose data [4-6]. However, as Pan et al. [7] have shown, there should be variation between the calculated and measured values. If no correlation is found between air dose rates and concentrations of naturally occurring radionuclides, estimating U distribution in open fields should be difficult.

In this study, therefore, we compared air dose rates measured at the soil sampling sites and theoretical air dose rates calculated using ^{40}K, U and Th. In QST, approx. 1100 soil samples collected in Japan, mostly in the 1970s, have been stored after air-dried; these are called as archived soil samples. Of these, ca. 340 samples were used in this study.

2 MATERIALS AND METHODS

Soil samples were selected from eastern and western part of Japan: prefectures for studied soil samples are shown in Fig. 1. We used 179 soil samples from eastern Japan and 157 samples from western Japan; data for 222 samples were already published [8].

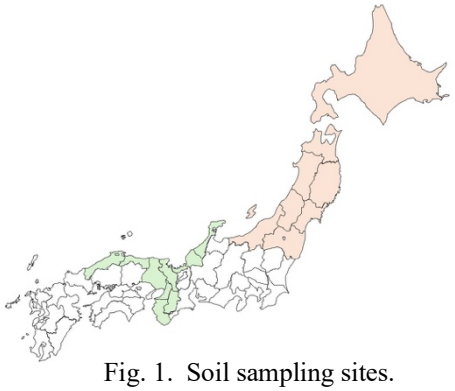


Fig. 1. Soil sampling sites.

Each stored soil sample was sieved to have a soil particle size of ϕ<2 mm; the percentage of this fraction, on a weight basis, was calculated. The sieved sample was then transferred to a U-8 type container and sealed tightly after sample weight and thickness measurements to determine apparent density. The sample was stored at least one month before radiation measurement. Details of the sample treatment method were reported elsewhere [8].

Gamma radionuclides in soil samples were measured with a Ge detection system (Seiko EG&G). Counting times were 80,000 to 250,000s depends on the activities. ^{137}Cs, ^{40}K, ^{238}U (^{214}Bi and ^{214}Pb) and ^{232}Th (^{212}Bi, ^{212}Pb and ^{208}Tl) were used for determination. Because ^{137}Cs contribution to the air dose rate was small, ^{40}K (converted to total K concentration, in g/kg), ^{238}U (converted to total U concentration, mg/kg) and ^{232}Th (mg/kg) were used to obtain

Copyright on 7th Asia-Pacific Symposium on Radiochemistry 2025

theoretical air dose rate using the IAEA method [1]. The in-situ air dose rates were previously reported by Abe et al. [9], and the values were used for comparison.

3 RESULTS AND DISCUSSION

The measured ^{238}U and ^{232}Th concentrations were compared and the results are shown in Fig. 2a. They are correlated well although wider variation was found in Eastern Japan samples. The calculated air dose rates were then compared with reported data [9] and the results showed positive correlations in both regions by t-test ($p<0.01$), but lower correlation factor was observed in Western Japan samples than in Eastern Japan samples (Fig. 2b). Probably soil density or large fragment in soil samples may affect the measured air dose rates; thus we analyzed further using soil apparent density and the percentage of particle size less than 2 mm fraction, but no correlation was found.

Because ^{137}Cs is well adsorbed to soil particles in Japan, but if ^{137}Cs activity concentration was low in a soil sample then the soil ability to fix ^{137}Cs was expected to be low which might affect U and Th series isotope mobility in soil. Thus we also tried to use the ^{137}Cs activity concentration in soil as an indicator of soil particle surface condition, but it could not explain the difference between the theoretical and measured air dose rates. Further analysis is needed to identify what is the main factor affecting the differences.

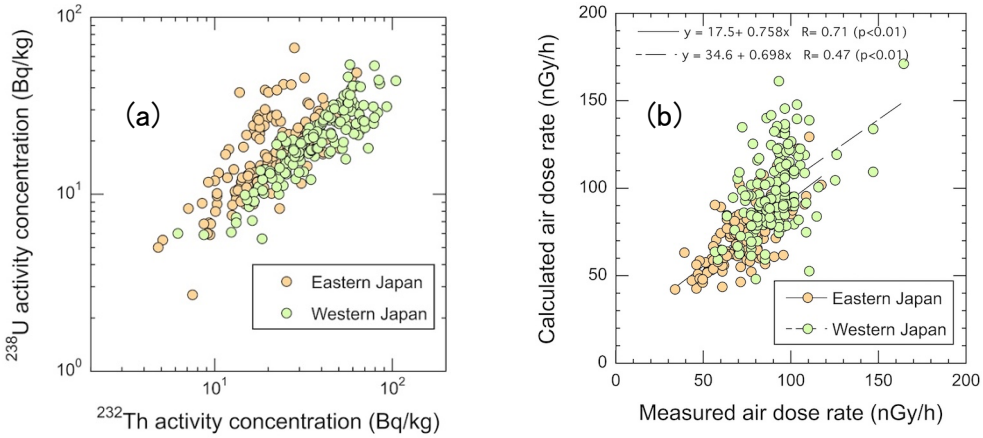


Fig. 2. Comparison of the data for soil samples. (a) activity concentrations of U and Th, and (b) calculated and measured [9] air dose rates.

ACKNOWLEDGMENTS

The study was partially performed under a contract with the Ministry of Economy, Trade and Industry (METI) as part of the R&D supporting program “Project on Research and Development for Validating Safety Assessment of Geological Disposal: Development of the Technology for Integrating Radionuclide Migration Assessments” [Grant Number JPJ007597].

References

[1] IAEA, Guidelines for Radioelement Mapping using Gamma-ray Spectrometry Data, IAEA, Vienna (2003).
[2] S. MINATO, “Uranium, Thorium and Potassium Concentrations in Japanese Soils,” *RADIOISOTOPES*, **54**, 509 (2005).
[3] NATIONAL AGRICULTURE AND FOOD RESEARCH ORGANIZATION, Japanese Soil Inventory, https://soil-inventory.rad.naro.go.jp/index.html (Accessed on 13 May 2025)
[4] G. KARAHAN and A. BAYULKEN, “Assessment of Gamma Dose Rates around Istanbul (Turkey),” *J. Environ. Radioact.* **47**, 213 (2000).
[5] M. TZORTZIS, et al., “A Comprehensive Study of Natural Gamma Radioactivity Levels and Associated Dose Rates from Surface Soils in Cyprus,” *Radiat. Prot. Dos*. **109**, 217 (2004).
[6] E.S. JOEL et al. “In-situ Assessment of Natural Terrestrial-Radioactivity from Uranium-238 (^{238}U), Thorium-232 (^{232}Th) and Potassium-40 (^{40}K) in Coastal Urban-Environment and its Possible Health Implications,” *Scientific Reports*, **11**, 17555 (2021).
[7] Z.-Q. PAN, Y. YANG and M.-Q. GUO, “Natural Radiation and Radioactivity in China,” *Radiat. Prot. Dos*. **24**, 29 (1988).
[8] K. TAGAMI and S. UCHIDA, “Determination of ^{40}K, ^{232}Th and ^{238}U in Easily-Sealed Soil Using a Germanium Detection System and the Comparison with Actually Measured Air Dose Rates,” *RADIOISOTOPES*, **73**, 161 (2024).
[9] S. ABE et al., “Extensive Field Survey of Natural Radiation in Japan,” *J. Nucl. Sic. Technol*. **18**, 21 (1981).

Copyright on 7th Asia-Pacific Symposium on Radiochemistry 2025

TRITIUM CONCENTRATION IN NATURAL WATER SAMPLES COLLECTED AT TOMIOKA TOWN LOCATED NEARBY FDNPP

Naofumi Akata[1], Haruka Kuwata[1], Khemruthai Kheamsiri[1], Rosianna Ilsa[1], Yuisa Kitayama[1], Honoka Fukuda[1], Ryohei Yamada[1], William James Stephenson[2,1], Yasuyuki Taira[3], Hideki Saito[4], Noriyuki Takizawa[4]

[1]*Hirosaki University: 66-1 Hon-cho, Hirosaki, Aomori, 036-8564 Japan, akata@hirosaki-u.ac.jp, kuwata-07@hirosaki-u.ac.jp, h23gg703@hirosaki-u.ac.jp, h24mh202@hirosaki-u.ac.jp, h24mh204@hirosaki-u.ac.jp, fkd.honoka@hirosaki-u.ac.jp, yamada.ryohei@hirosaki-u.ac.jp*

[2]*Colorado State University: Fort Collins, Colorado, 80523 USA, billy.stephenson@colostate.edu*

[3]*Nagasaki International University: 2825-7 Huis Ten Bosch, Sasebo, Nagasaki, 859-3298 Japan, taira@niu.ac.jp*

[4]*Tomioka Town Hall: 622-1 Ozuka, Motooka, Tomioka, Fukushima, 979-1192 Japan, tom1200-003@tomioka-town.jp*

1 INTRODUCTION

Since the Fukushima Dai-ichi Nuclear Power Plant (FDNPP) accident of March 2011, huge amounts of contaminated water have been produced from the decontamination and decommissioning work of the site. Although the contaminated water has been treated by passing it through the multi-nuclide processing system (ALPS), small amounts of radionuclides not removed using ALPS, tritium in particular, are still present [1]. On August 24, 2023, Tokyo Electric Power Company began releasing the treated water through an emission pipeline into the coastal Pacific Ocean as approved by the Japanese government. [2].

Tomioka Town, Fukushima Prefecture is located on the Pacific Ocean side of Fukushima and located between Fukushima Dai-ichi Nuclear Power Plant and Fukushima Dai-ni Nuclear Power Plant. Therefore, the residents have high interest in the treated water. Since tritium concentrations at background level are very low, tritium measurements require special enrichment techniques [3]. In Japan, the Solid Polymer Electrolyte (SPE) system is preferred due to relatively high enrichment factor and safety. Efforts have been made to optimize the process for measuring lower sample concentrations or smaller sample sizes while considering the preparation time. Our laboratory, affiliated with Institute of Radiation Environment Medicine (IREM), Hirosaki University, has developed a simple method for low-level tritium measurement [4]. Since 2022, tritium monitoring of environmental water samples in Tomioka Town was conducted, collaborating with Tomioka Town Government. Here, tritium concentrations before and after the discharge of treated water was reported.

2 MATERIAL AND METHOD

An overview of sampling locations is shown in Figure 1. The 1 liter samples were collected from five points (1-5) in Tomioka town: three at the costal sea and two from the middle of a river. The water temperature was measured before sample collection. Monthly precipitation samples were also collected at Tomioka Town office (6). After sample collection, samples were sent to the laboratory and pH measured by compact pH mater (B-211, Horiba, Japan). River water and precipitation samples were distilled directly, while sea water samples were distilled after Na_2O_2 was added. The distilled sample water was enriched using an improved SPE tritium enrichment system (XZ-001 Tripure, DerNora, Japan), and was distilled again. The 50 mL of re-distilled sample was mixed with scintillation cocktail (UltimaGold LLT, Revvity, Japan) in a 145-mL vial. Tritium activity concentration was measured by low-background liquid scintillation counter (LSC-LB5, Aloka, Japan) after shaking and storing for five days. The counting time was 1,000 min.

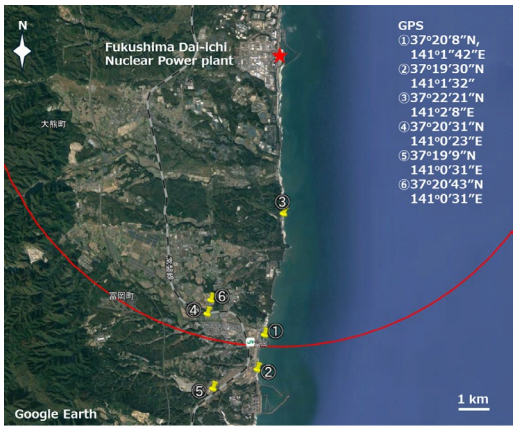


Fig. 1. Overview of sampling location at Tomioka Town, Fukushima Prefecture

2. RESULTS AND DISCUSSION

Tritium concentration in river water samples before the discharge (n = 8) ranged from 0.34 to 0.48 Bq/L, and those of sea water samples (n = 12) ranged from < 0.06 to 0.16 Bq/L, which is normal background level. After the discharge, river water samples (n = 16) ranged from 0.29 to 0.40 Bq/L, but slightly higher tritium concentrations in sea water samples were observed, which ranged from 0.09 to 3.03 Bq/L. Concentrations over 1 Bq/L were found in only 2 samples from point 1 (April 24, 2024) and 3 (October 29, 2024). It is important to note that on the same day of sampling, only 1 of the 3 coastal sea points had elevated tritium concentration, while the other two points were normal. In general, it is well established that tritium concentration in river water is higher than sea water. However, these 2 samples had higher concentration than their respective river samples. Tritium concentration in monthly precipitation on November 2024 was 0.40 ± 0.04 Bq/L, which is lower than those values. Based on these results, it is highly possible that elevated tritium concentrations in sea water samples were a result of treated water being discharged into the ocean. However, these values were below the detection limit for the rapid sea water analysis conducted by Fukushima Prefecture [5]. Tritium concentrations under the detection limit in the environmental water were changing day by day due to the treated water. In 2024, sampling was conducted only during the discharge period. We plan to take samples outside of the discharge period to confirm the return to background level.

ACKNOWLEDGMENTS

This work was partly supported by JSPS KAKENHI Grant Number JP21H03607 and National Institute for Quantum Science and Technology budget titled "Development of assessment model for environment and biological effect assuming dispersion of tritium".

References

[1] Y. Lu et al., “Monitoring long-term ecological impacts from release of Fukushima radiation water into ocean”, *Geography and Sustainability*, 2, 95-98 (2021)
[2] M. F. Ferreira et al., “Controlled release of radioactive water from the Fukushima Daiichi Nuclear Power Plant: Should we be concerned?”, Environmental Science and Technology, 58, 4840-4843 (2024).
[3] H. Kakiuchi, “Electrolytic enrichment technique of tritium in water for environmental analysis”, Journal of Plasma and Fusion Research, 92, 26-30 (2016) in Japanese
[4] N. Akata et al., “Performance test of improved commercially available tritium enrichment system: Toward rapid and high efficiency enrichment”, 13, 60-64 (2024)
[5] Fukushima Prefecture, “Result of Sea Area Monitoring Associated with the Discharge of ALPS Treated Water into the Sea”, https://www.pref.fukushima.lg.jp/site/portal-english/en-moni-k.html, (May 12, 2025)

DGT application to dynamic speciation of U in environments

Adrien Constandache[1], Takumi Saito[2]

[1] *Department of Nuclear Engineering and Management, School of Engineering, the University of Tokyo, 7-3-1 Hongo, Bunkyo-ku, Tokyo 113-8656, JAPAN*
[2] *Nuclear Professional School, School of Engineering, the University of Tokyo, 2-22 Shirakata-Shirane, Tokai-mura, Ibaraki 219-1188, JAPAN*

1 INTRODUCTION

Diffusive Gradients in Thin films (DGT) consists of a membrane, a diffusive gel, and a binding gel, enabling the diffusion of target species while immobilizing them. It acts as a passive in-situ sampler, continuously accumulating labile (i.e. bioavailable) species with minimal environmental disturbance. The accumulated mass obeys the following equation, derived from Fick's law (1):

$$M = D\,S\,t\,\Delta C\,/\,\Delta x \tag{1}$$

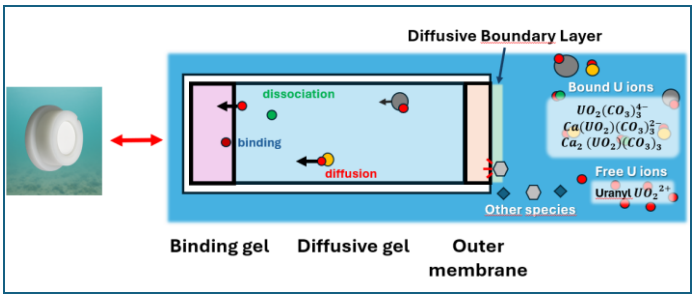
where M is the mass of a target meta ion accumulated on the binding gel (mol or µg), D the diffusion coefficient in the diffusive layer ($m^2\ s^{-1}$), S the exposed sampler area (m^2), t the deployment time (s), ΔC the concentration gradient across the layer—essentially the bulk concentration because the binding gel behaves as an "infinite sink"—and Δx the diffusive-layer thickness (m). With M determined through ICP-MS measurements after extracting it from the binding gel, Eq. (1) can be rearranged to obtain the time-averaged concentration of all labile uranium species trapped in the sampler.

In mildly alkaline waters (pH ≈ 8), uranyl exists as tricarbonate complexes $UO_2(CO_3)_3^{4-}$, $CaUO_2(CO_3)_3^{2-}$ and $Ca_2UO_2(CO_3)_3°$. With a single binding gel such as Chelex, this measurement yields only the bulk value and cannot resolve the relative contributions of individual carbonate and calcium-carbonate complexes. To better discriminate uranium complexes according to their lability—and thus better characterize their bioavailability—we are developing a multi-layer sampler that pairs Chelex with the soft-ligand cation exchanger KMS-1 resin and anchors the design in a reactive-transport model.

2 MULTI-LAYER CONCEPT

The prototype stacks two binding gels beneath a single 0.80 mm polyacrylamide diffusive layer:

- **Chelex-100 (front)** — captures labile (easily exchangeable) UO_2^{2+}.
- **KMS-1 (middle)** — a layered K–Mn–Sn sulfide that captures uranyl from more stable tricarbonate complexes by stripping the carbonate and binding the cation with soft S^{2-} sites.
- **KMS-1 (rear)** — captures uranyl from more stable calcium tricarbonate complexes.



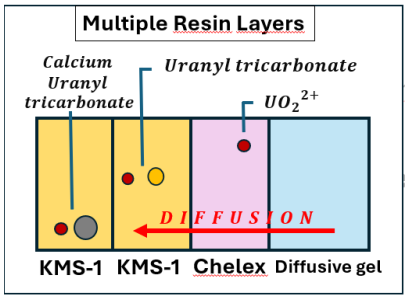


Fig. 1. (left) schematic stretched cross-section of a DGT device in water with key phenomena in each layer
Fig. 2. (right) Presentation of the multi-layer concept applied to Uranyl and its tricarbonate complexes

This arrangement should allow species not retained by Chelex to continue diffusing until they are immobilized by the downstream KMS-1 layers (the KMS-1 sorption mechanism is detailed in (2)). It acts similarly to ion chromatography, where uranium species are separated according to their lability.

3 MATERIALS AND METHODS

3.1 Solution preparation and speciation control

Synthetic test waters were prepared to isolate each target species. PHREEQC speciation calculations guided carbonate and calcium dosing. Total U was 10 µM in all cases. These solutions feed both the diffusion cell and sorption experiments.

3.2 Diffusive gel and diffusion experiments

Polyacrylamide (PAA) diffusive gels were cast according to Zhang & Davison [1]. diffusion coefficients for each species are being measured in a stirred two-compartment cell at 25 °C; the resulting D values provide input for the numerical model.

3.3 Binding gels and sorption kinetics

Chelex-100 beads were suspended in PAA gel discs with 0.50-mm thickness. KMS-1 was synthesized after Manos [2]: Mn 22 mmol, Sn 44 mmol, K_2CO_3 22 mmol, S 132 mmol and H_2O 30 mL were sealed in a 100 mL Teflon-lined autoclave, heated to 200 °C for four days, cooled, filtered, washed (H_2O, CS_2, ethanol) and dried at 60 °C under vacuum. The powder was embedded in 0.50-mm PAA discs. Batch tests follow the disappearance of dissolved U over time from the solution; pseudo-first-order rate constants and Langmuir parameters derived from the measured time-dependent sorption define the kinetic terms in the subsequent modelling part.

3.4 Reactive-transport model

A 2-D axisymmetric “Transport of Diluted Species in Porous Media” setup in COMSOL Multiphysics® incorporates species-specific D, the measured sorption kinetics, and an adjustable diffusive boundary layer. Simulations will help to determine optimal resin gel lengths, predict concentration profiles and time-dependent mass uptake in each layer and guide field deployment time.

4 RESULTS

Free uranyl diffuses at 4.3×10^{-10} $m^2.s^{-1}$ whereas free uranyl complexes diffuse at an average rate of 2.4×10^{-10} $m^2.s^{-1}$.

As for Chelex binding gels, Langmuir fits give an affinity constant $K_{ads} = 1.4 \times 10^6$ $L.mol^{-1}$ and capacity $C_{max} = 1.1 \times 10^{-2}$ $mol.kg^{-1}$ for UO_2^{2+} at pH close to 4; uptake of carbonate complexes is < 5 % at pH close to 8.

5 CONCLUSIONS

Coupling complementary resins within one DGT device and grounding the design in calibrated modelling could be a field tool that quantifies both free uranyl and its dominant carbonate complexes—information essential for evaluating uranium mobility and bioavailability in mild alkaline environments.

References

1. Zhang H. & Davison W., *Anal. Chim. Acta* **398** (1999) 329–340.
2. Manos M. J. & Kanatzidis M. G., *Proc. Natl. Acad. Sci. USA* **105** (2008) 3696–3700.

7th Asia-Pacific Symposium on Radiochemistry *September 14 ~ 19, 2025 • Kunibiki Messe • Shimane, Japan*

Vertical distribution of ^{129}I, ^{137}Cs, ^{3}H and ^{36}Cl in unsaturated zone observed at Koriyama, Japan

Tomoko Ohta[1], L. Keith Fifield[2], László Palcus[3], Stephen G. Tims[2], Stefan Pavetich[2], Hiroyuki Matsuzaki[4], Daisuke Tsumune[5], Hiroshi Hayami[6], Yasunori Mahara[7]

[1]*Nagaoka University of Technology: 1603-1 Kamitomioka-chou, Nagaoka, Niigata, 940-2188, Japan*
tomoohta@vos.nagaokaut.ac.jp
[2]*The Australian National University: Canberra, ACT 2601 Australia,*
[3]*HUN-REN Institute for Nuclear Research,: Bem square 18/c Debrecen, 4026, Hungary*
[4]*The University of Tokyo: Bunkyouku, Tokyo, 113-0032, Japan*
[5]*Tsukuba University: 1-1-1 Tennodai,Tsukuba, Ibaraki, 305-8572, Japa*
[6]*Waseda University: 3-4-1 Okubo, Shinjuku, Tokyo 169-8555, Japan*
[7]*Kyoto University: Kyoto, Kyoto, 606-8501, Japan*

Vertical distribution of ^{129}I, ^{137}Cs ^{3}H and ^{36}Cl in unsaturated zone was obtained in 2012 and 2014 at Koriyama, Fukushima. In the unsaturated layer of the off-site area of the Fukushima Daiichi Nuclear Power Plant in Koriyama, not only ^{137}Cs and ^{129}I but also ^{36}Cl and ^{3}H were detected. Even three years after the accident, vertical movement of ^{129}I in the unsaturated layer was hardly observed.

1 Introduction

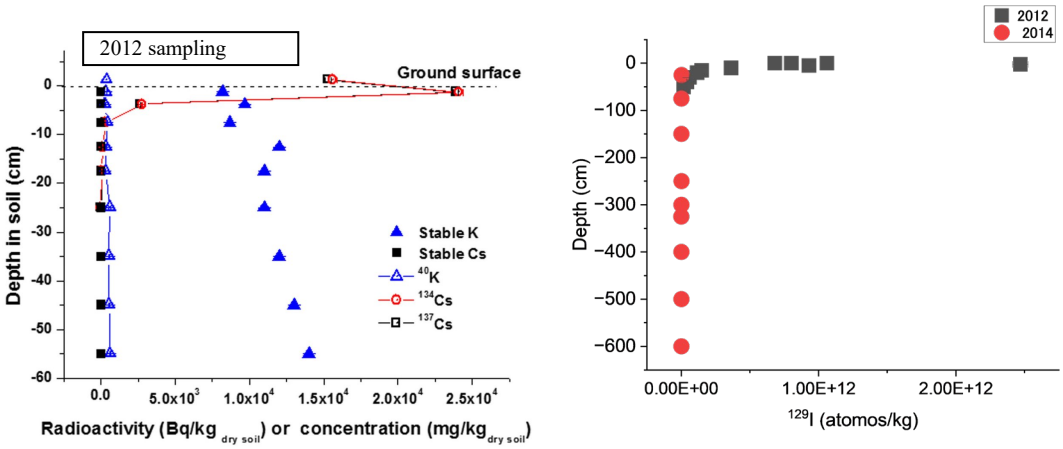
The municipal water supply is derived from two primary sources: river water and groundwater. Surface water flows through forests and into rivers. In this study, soil cores were collected from a depth of 600 cm below the surface in forests outside the Fukushima Daiichi Nuclear Power Plant site to obtain information on radioactive nuclides in the surface and subsurface environment. In Koriyama City, Fukushima Prefecture, the concentrations of ^{3}H, ^{36}Cl, ^{129}I, and ^{137}Cs in soil water and soil were measured at depths ranging from the surface to 600 cm below the surface.

2 Experiment

Soil sample was collected at the site of Koriyama (in the campus of the Fukushima Forestry Research Center), which is 60 km to the west-southwest of the Fukushima nuclear power plant 1 (FNPP1). Two soil cores were collected at the Koriyama site in 2012 and 2014 to depths of 50 cm and 600 cm respectively, and another hole was drilled to 800 cm in 2019 in order to observe fluctuations in the water table. The water level in the latter hole was meticulously monitored at one-minute intervals from January 29, 2019, to December 13, 2021. We measured ^{137}Cs in soil collected in 2012 by HPGe [1]. Tritium in most of the samples was measured by beta-counting using a liquid-scintillation counter (LSC), while 6 samples were measured by the ^{3}He in-growth method. The ^{36}Cl/Cl ratios were measured by accelerator mass spectrometry (AMS) [2]. The ^{129}I/^{127}I ratios were measured by AMS [3, 4].

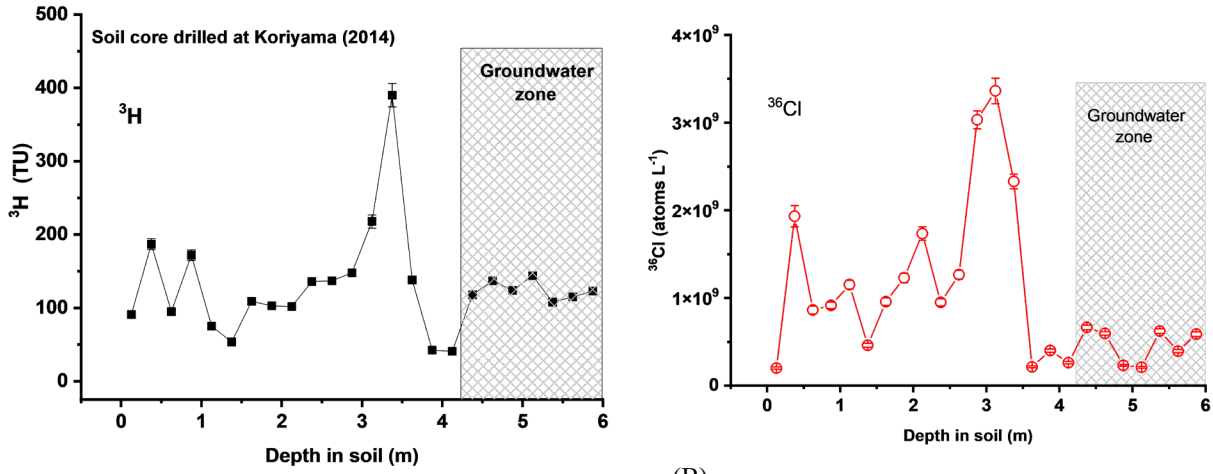
3 Result

Vertical distribution of radionuclides in soil or soil water obtained from the Koriyama are shown in Fig. 1 and Fig. 2.



(A) **(B)**

Fig. 1 Distribution of radionuclides and stable isotopes (^{137}Cs, ^{134}Cs stable Cs, stable K, ^{129}I, ^{127}I) in soil
(A) ^{137}Cs, ^{134}Cs stable Cs, stable K, in soil collected in 2012, (B) ^{129}I and ^{127}I in soil collected in 2012 and 2014



(A) (B)

Fig. 2 Vertical distribution of concentrations of radionuclides (^{3}H and ^{36}Cl) in soil core sample (A): ^{3}H in soil water obtained from 2014 sampling, (B): ^{36}Cl in soil water obtained from 2014 sampling

Both ^{134}Cs and ^{137}Cs in the soil obtained from 2012 are strongly fixed by clay minerals in soil, as shown in Fig. 1(A). More than 99% of the ^{134}Cs and ^{137}Cs deposited from the nuclear accident were trapped in the litter layer and the top 2.5 cm of soil 2.5 years after the accident; their concentrations decrease rapidly with increasing depth. The ^{129}I in soil obtained from 2012 and 2014 was also distributed in shallow depth, as demonstrated in Fig. 1(B). This finding suggests that, even three years post-accident, ^{129}I in the unsaturated layer did not migrate significantly.

The groundwater table in the observation well drilled in 2019 was measured by a water table gauge combined with a barometer for atmospheric pressure compensation. The variation in the groundwater table in the borehole from 2019 to 2021. At this site, the annual variability of the groundwater table ranged between a low in the winter and a high in summer to autumn. The depth of the groundwater table in the well was found to vary over the course of a year by approximately 50 cm from 6.4 to 6.9 m. Therefore, the depth of the groundwater table of 2014 boring was estimated to vary over the course of a year by approximately 50 cm from 4.25 to 4.75 m. Both the ^{3}H and ^{36}Cl concentrations show prominent peaks at a depth of ~ 3.4 m, about 1 m above the water table, although there is some indication that the ^{36}Cl may lag the ^{3}H slightly.

ACKNOWLEDGMENTS

This work was supported by JSPS Grants-in-Aid for Scientific Research (Kakenhi Grant Numbers, 24686098, 17K07024, 20H02674), Ichimura Foundation for New Technology, YESSA (Yanmar shigenjunkan zaidan), Environmental Radioactivity Research Network Center **(**P-24-15**)**. The Heavy Ion Accelerator Facility (HIAF) at ANU is supported by the National Collaborative Research Infrastructure Strategy (NCRIS) of the Australian Government. We are deeply grateful to Dr. Leonard I. Wassenaar and Takuya Matsumoto, the IAEA, HUN-REN, AMS-MALT staff for technical support, and Central Research Institute of Electric Power Industry for financial support for drilling of observation well in 2019.

References

[1] Y. Mahara, T. Ohta, H. Ogawa, A. Kumata, Atmospheric direct uptake and long-term fate of radiocesium in trees after the Fukushima Nuclear accident, Scientific Reports, **4**, Article number: 7121 (2014)

[2] T. Ohta, L. K. Fifield, L. Palcsu, S. G. Tims, S. Pavetich, Y. Mahara, Scientific Reports, **13**, Article number: 19672 (2023)

[3] T. Ohta, T. Hasegawa, W. Jiang, Guo Min Yang, Z.-T. Lu, Y. Mahara. Feasibility of ^{129}I groundwater dating calibrated by both ^{81}Kr and ^{4}He for the assessment of deep geological repositories in Japan. Scientific Reports, **14**, Article number: 15688 (2024)

[4] H. Matsuzaki, Y. Miyake, K. Nakashoji, H. Tokuyama, Y.S. Tsuchiya, H. kusuno, M. Toya, Current status of MALT AMS facility, A report of updated performance and recent achievement, Nuclear Instruments and Methods in Physics Research, B, **463**, 55-63 (2020)

RADIOACTIVITY OF SULFUROUS SINTER DEPOSIT FROM BEITOU HOT SPRING.

Takashi Saito[1], Yuto Takahashi[1], Taiga Kaseda[2], Hibiki Shirata[2], Toru Takahashi[2], Shunsuke Hashizume[2], Yuya Koike[3], Mototaka Nakamura[4],

[1]*Shokei Gakuin University: Yurikaoka 4-10-1, Natori, Miyagi, 981-1295, Japan, t_saito@shokei.ac.jp*
[2]*Graduate School of Science and Technology, Meiji University: Higashi-Mita 1-1-1, Tama-ku, Kawasaki, Kanagawa, 214-8571, Japan.*
[3] *School of Science and Technology, Meiji University: Higashi-Mita 1-1-1, Tama-ku, Kawasaki, Kanagawa, 214-8571, Japan.*
[4]*Study of European Radon-spa Therapy: Yoyogi 1-9-6, Shibuya-ku, Tokyo, 151-0053, Japan.*

This study investigates the source of radioactivity in sulfurous sinter from Beitou Hot Spring, Taiwan, with a focus on the possible presence of hokutolite—a rare radium-bearing mineral. Sinter samples collected in 2023 and 2024 were analyzed using gamma-ray spectrometry, revealing daughter nuclides of ^{226}Ra, ^{228}Ra, and ^{228}Th. The ^{226}Ra concentration ranged from 0.41 to 0.58 Bq/g. Scanning electron microscope analysis identified microcrystalline lead-bearing barite (Ba(Pb)SO$_4$), consistent with hokutolite. Based on measured activity and comparison with known hokutolite radium levels (56.7–68.6 Bq/g), the estimated content of hokutolite in the samples was 6–10 ppm. Assuming that ^{228}Th originated solely from the decay of ^{228}Ra, the age since formation was estimated at 173–450 days, comparable to hokutolite from Tamagawa Hot Spring. These findings suggest that micro-hokutolite forms during the emergence and cooling of hot spring water and becomes incorporated into the sinter, contributing to its radioactivity.

1 Introduction

At Tamagawa Hot Spring in Akita, Japan, and Beitou Hot Spring in Taiwan, it is well known that a very rare mineral called hokutolite—a lead-bearing barite (Ba(Pb)SO$_4$) in which radium is enriched and co-precipitated with barium—forms as a hot spring precipitate. Previous studies have confirmed that the surface of hokutolite from Tamagawa Hot Spring, whose formation age is known, consistently exhibits a nearly constant activity ratio of ^{228}Ra/^{226}Ra. Furthermore, Saito and Nagai [1] reported that the sulfurous sinter (Yu no hana) in Tamagawa Hot Spring water is highly radioactive, and that this radioactivity originates from radium and its daughter nuclides present in microcrystalline hokutolite. However, the presence of hokutolite within the sulfurous sinter of Beitou Hot Spring has not yet been confirmed.

In this study, sulfurous sinter samples were collected from Beitou Hot Spring, and their radioactivity was measured to identify the radionuclides present, determine their activity ratios, and infer their origin.

2 Experimentals

2.1 Sample

In Jun.2023, Nov. 2023 and 2024 as an academic exchange with Taiwan, we had been participated in a survey of around the Xinbeitou hot spring area conducted by the Study of European Radon-spa Therapy and sampled sulfurous sinter.

2.1 Experimental method

After drying each sulfurous sinter sample, the radionuclides were identified using gamma-ray spectrometry. Subsequently, gamma rays emitted from the daughter nuclides of radium isotopes—^{214}Pb (351 keV), ^{228}Ac (911 keV), and ^{208}Tl (583 keV)—were measured to calculate the concentrations of ^{226}Ra ($T_{1/2}$ = 1600 y), ^{228}Ra ($T_{1/2}$ = 5.75 y), and ^{228}Th ($T_{1/2}$ = 1.91 y), respectively.

Furthermore, sulfur in the sulfurous sinter was removed using 2M NaOH sol., and the residue was analyzed by SEM-EDX to confirm the presence or absence of hokutolite.

3 Result and discussions

Based on the results of gamma-ray spectrometry, only daughter nuclides derived from ^{226}Ra, ^{228}Ra, and ^{228}Th were detected in the sulfurous sinter. The calculated radioactivity concentrations and activity ratios are shown in Table 1.

As shown in Table 1, the concentration of ^{226}Ra ranged from 0.41 to 0.58 Bq/g, indicating the presence of radium in the sinter samples.

Table 1 Concentration ^{226}Ra, ^{228}Ra and ^{228}Th, and activity ratios of ^{228}Ra/^{226}Ra and ^{228}Th/^{226}Ra of Sulfurous sinter in Beitou hot spring.

Sample		Concentration (Bq/g)			Activity ratio	
		^{226}Ra	^{228}Ra	^{228}Th	^{228}Ra/^{226}Ra	^{228}Th/^{226}Ra
Sinter A	Nov.2023	0.41±0.01	3.67±0.02	1.42±0.01	8.84±0.39	3.45±0.06
Sinter B	Nov.2024	0.42±0.02	7.40±0.05	1.44±0.01	17.5±1.4	3.39±0.14
Sinter C	Nov.2024	0.41±0.01	7.46±0.05	1.51±0.01	18.1±1.1	3.68±0.10
Sinter D	Nov.2024	0.58±0.01	10.6±0.10	1.97±0.01	18.1±0.8	3.37±0.07

If ^{232}Th ($T_{1/2} = 1.41 \times 10^{10}$ y), ^{228}Ra, and ^{228}Th in the thorium decay series are in secular equilibrium, ^{228}Ra and ^{228}Th should exhibit equal levels of radioactivity. In the absence of ^{232}Th, if ^{228}Ra and ^{228}Th are in transient equilibrium, the radioactivity of ^{228}Th should be 1.5 times that of ^{228}Ra. Since the measured concentration of ^{228}Th was lower than that of ^{228}Ra, and neither ^{232}Th nor other thorium isotopes were detected, it is highly likely that the observed ^{228}Th originated from microcrystalline hokutolite present in the sulfurous sinter. Actually, SEM-EDX analysis revealed the presence of lead-containing barite crystals, several tens of micrometers in size, which appear to be hokutolite. The hokutolite SEM photograph is shown in Fig.1.

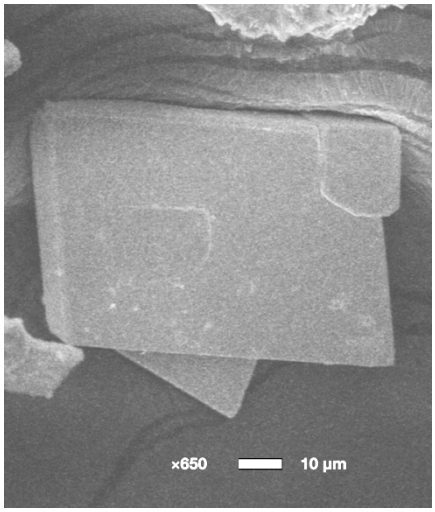


Fig. 1 SEM image of residual solid material in the sulfurous sinter from Beitou hot spring.

Yamamoto *et al.* [2] reported that the radium concentration in hokutolite from Beitou Hot Spring ranges from 56.7 to 68.6 Bq/g. Assuming that all the radioactivity of the sinter is derived from hokutolite, the estimated content of hokutolite in the samples was approximately 6–10 ppm.

The radioactive component found in the sinter is radium incorporated in hokutolite. Assuming that no ^{228}Th was present at the time of hokutolite formation and that the currently detected ^{228}Th was entirely produced through the decay of ^{228}Ra within hokutolite, the elapsed time since hokutolite formation in the sinter samples was estimated to be 173–450 days. This range is comparable to the formation ages of hokutolite in the sulfurous sinter from Tamagawa Hot Spring (91–797 days).

These results suggest that the origin of radioactivity in the sulfurous sinter from Beitou Hot Spring is the incorporation of microcrystalline hokutolite into the precipitate during the emergence and cooling of the hot spring water.

.

References

[1] T. Saito and H. Nagai, Radioactivity of Sulfurous Sinter Depositfrom Tamagawa Hot Spring, *J. Balneol. Soc. Jpn*., **57** 206 (2007).
[2] M. Yamamoto *et al.*, K., Radiochemical aspect of Hokutolite collected recently at Peitou Hot Spring, *Taiwan, Proc. Int. Conf. on Centennial of Discovering Hokutolite and Hot Springs*, 64-69 (2005).

7th Asia-Pacific Symposium on Radiochemistry *September 14 ~ 19, 2025 • Kunibiki Messe • Shimane, Japan*

Efficient Tritium Enrichment via Direct Seawater Electrolysis: Achieving High Separation Factor and Recovery in a Low-Volume System

Lai Chih-Yi[1], Mariel G. Tecson[2], Tao, Liang Yu[3], and Chun-Hu Chen[4]

[1]*Department of Chemistry, National Sun Yat-sen University: No. 70, Lienhai Road, Kaohsiung City, Taiwan, 80424, bernicelai2002@gmail.com*
[2] *Department of Chemistry, National Sun Yat-sen University: No. 70, Lienhai Road, Kaohsiung City, Taiwan, 80424, marieltecson29@gmail.com*
[3] *Radiation Monitoring Center, Nuclear Safety Commission: No. 823, Chengqing Rd., Niaosong Dist., Kaohsiung City, Taiwan, 83347, iamtauzi@nusc.gov.tw*
[4] *Department of Chemistry, National Sun Yat-sen University: No. 70, Lienhai Road, Kaohsiung City, Taiwan, 80424, chunhu.chen@mail.nsysu.edu.tw*

Water electrolysis ($2H_2O \rightarrow O_2 + 2H_2$) is an effective method for tritium enrichment of seawater samples. However, due to the corrosive nature of seawater, distillation becomes a necessary step prior to electrolysis resulting in tritium loss and energy inefficiency. Moreover, the existing technology exhibits large volume reduction to obtain high separation factor and recovery rate which demonstrates the low isotope selectivity of conventional water splitting catalysts. To address this challenge, we utilized an OER catalyst that is resistant to corrosion enabling direct seawater electrolysis. Our result shows a zero change in voltage after twenty-four hours of electrolysis. The catalyst we have developed demonstrated a high separation factor of 5.14 and large recovery rate of around 91% with a volume reduction of less than fifty percent.

1. INTRODUCTION

The amount of tritium in seawater samples are low and below the detection limit of liquid scintillation counter which is around 0.4 Bq/L [1]. Consequently, water electrolysis *($2H_2O \rightarrow O_2 + 2H_2$)* is commonly performed to enrich the amount of tritium. Currently, alkaline and proton exchange water electrolysis are the two commercial methods used for tritium concentration. However, these techniques typically use catalyst that is not suitable for direct seawater electrolysis. For instance, nickel as an oxygen evolution reaction (OER) catalyst corrodes in seawater. As a result, distillation of seawater samples is carried out prior to electrolysis. However, conventional distillation may result in tritium loss. Furthermore, the lengthy pretreatment process can take up to several days to finish, making the overall procedure to be inefficient. Another crucial factor to consider during electrolysis is the catalyst's selectivity for electrolyzing protium instead of tritium. Conventional tritium enrichment process requires a significant volume reduction often 90% to achieve meaningful tritium enrichment which reflects the low isotope selectivity of the electrolysis system. The need for such large reductions in water volume makes the overall enrichment process to be inefficient and energy intensive.

In this study, we utilized an OER catalyst composed of cobalt and manganese that we have previously developed [2] and we utilized it for direct seawater electrolysis. Our study showed that the catalyst we synthesized exhibits good stability and corrosion resistance, maintaining zero voltage degradation after 24 hours of electrolysis in seawater at a high current of 5 A. A high separation factor of 4-5 and recovery rate of around 91% was achieved with a water reduction of around 43% which is significantly smaller compared to conventional that is 90% showing that our catalyst has high isotope selectivity. Our study presents a new approach for efficient tritium enrichment, enabling direct seawater electrolysis while achieving a high separation factor and recovery rate.

2. RESULT: EFFECT OF APPLIED POTENTIAL TO THE TRITIUM ENRICHMENT

The calcium and magnesium from seawater was removed using trisodium phosphate (Na_3PO_4) and sodium (Na_2O) was added carefully in the seawater sample. The alkaline seawater sample was fed into a device electrolyzer shown in Figure 1a. Pt/C and Cobalt Manganese oxy hydroxide (CMOH) with an active area of 25 cm^2 were used as cathode and anode respectively and the electrodes were separated by Anion Exchange Membrane (AEM). Depicted in Figure 1b is the measured potential over time at an applied current of 5 A under seawater electrolysis. The graph shows a very stable electrolysis with a constant voltage during electrolysis. Furthermore, the photograph of the OER catalyst after 24 hours of electrolysis shows no visible signs of corrosion, demonstrating its strong resistance to corrosion.

Copyright on 7th Asia-Pacific Symposium on Radiochemistry 2025

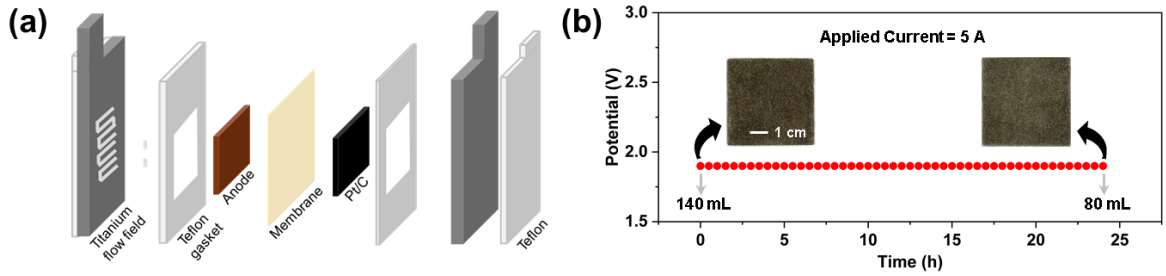


Fig. 1. (a) Device electrolysis set-up using Anion Exchange Membrane (AEM) and (b) Obtained potential at a constant applied current of 5 A, photograph of OER catalyst before and after 24 hours of electrolysis, and the volume of electrolyte before and after electrolysis.

The effect of applied potential was studied and the tritium enrichment factors such as recovery rate, separation, and enrichment were measured (Table 1). A separation factor of 4.29, 5.14, and 2.34 were achieved at the potential of 2.1, 1.9, and 1.7 respectively. The result suggests that for catalyst containing cobalt and manganese, the high separation factor can be obtained at moderate potential which is contrary to most catalysts wherein high separation factor was achieved at lower applied potential.

TABLE 1. Tritium enrichment data for seawater samples electrolyzed at decreasing potential

Potential (V)	Activity (Bq/L)		VRF	RR	β	EF
	Before	After				
2.1	28.8	40.6	1.56	90.63	4.49	1.41
1.9	28.8	45.2	1.75	89.68	5.14	1.57
1.7	28.8	41.5	1.89	76.17	2.34	1.44

*VRF: Volume reduction factor
*RR: Recovery rate
* β: Separation factor
*EF: Enrichment factor

3. CONCLUSIONS

We have developed an OER catalyst suitable for direct seawater electrolysis. The stable potential obtained during electrolysis highlights the excellent corrosion resistance of our catalyst. Additionally, the catalyst demonstrated high separation factor and tritium recovery with less than 50% volume reduction.

ACKNOWLEDGMENTS

We acknowledge the financial support from the Ministry of Science and Technology, Taiwan under grant 1 112-2628-M-110-001-MY4. We also acknowledge the financial support from Radiation Monitoring Center, Nuclear Safety Commission, Taiwan. We also thank all the members of Chun-Hu Chen's laboratory group of National Sun Yat-sen University for their support.

References

[1] Muranaka, Takeshi, and Nagayoshi Shim. 2012. 'Electrolytic Enrichment of Tritium in Water Using SPE Film'. *Electrolysis*. InTech. doi:10.5772/52705.
[2] R. H. Jhang, C. Y. Yang, M. C. Shih, J. Q. Ho, Y. T. Tsai, and C. H. Chen, *Redox-assisted multicomponent deposition of ultrathin amorphous metal oxides on arbitrary substrates: highly durable cobalt manganese oxyhydroxide for efficient oxygen evolution*, J. Mater. Chem. A 6, 17915 (2018).

7th Asia-Pacific Symposium on Radiochemistry *September 14 ~ 19, 2025 • Kunibiki Messe • Shimane, Japan*

TRACING RADIONUCLIDES IN THE MARINE ENVIRONMENT USING THE NEW "MILEA" ACCELERATOR MASS SPECTROMETRY FACILITY, REZ, CZECH REPUBLIC

P. Leivadaros[1], J. John[1], M. Nemec[1], T. Prasek[1], M. Mindova[1], O. Lind[2], H. Teien[2], H.E. Heldal[3], C. Tsabaris[4], E.G. Androulakaki[4], Z. Maniati[4]

[1]*Czech Technical University in Prague, Department of Nuclear Chemistry: Brehova 7, 115 19 Praha 1, Czech Republic (leivapet@fjfi.cvut.cz)*
[2] *Norwegian University of Life Sciences, Environmental Chemistry Section, Postboks 5003, 1432 Ås, Norway (ole-christian.lind@nmbu.no)*
[3] Institute of Marine Research: *Postboks 1870 Nordnes, 5817 Bergen (hilde.elise.heldal@hi.no)*
[4] *Hellenic Centre for Marine Research , Leof. Athinon Souniou Ave 46, 7th km, Anavissos, Greece (tsabaris@hcmr.gr)*

Radionuclides serve as effective tracers in environmental studies, particularly in marine research. Recent advancements in detection methods, such as Accelerator Mass Spectrometry (AMS), enable precise analysis of long-lived radionuclides at ultra-low concentrations. Preliminary findings from studies in Norway's Vefsn fjord and the central-north Aegean Sea demonstrate correlations between isotope ratios and historical events or man-made facilities that act as radionuclide sources. This research enhances our understanding of contamination sources and their impact on marine ecosystems.

1 INTRODUCTION

Radionuclides have been proven to be exceptional tracers for numerous environmental studies, supporting diverse scientific fields such as oceanography, ecotoxicology and climate change including ocean acidification [1]. Recent advancements in radioisotopic tracing and analytical techniques such as Accelerator Mass Spectrometry (AMS) have, in combination with, for example, ICP-MS and gamma-spectrometry, significantly enhanced our ability to detect and trace marine sources of contaminants and radionuclides. Developments such as improved detection efficiency and isobar suppression [2] allow for the analysis of long-lived radionuclides like ^{236}U and ^{129}I at ultra-low environmental concentrations. Using isotopic ratios such as $^{236/238}$U, $^{129/127}$I and $^{135/137}$Cs, and analysing multiple long-lived actinides, including ^{236}U, and ^{239,240}Pu from small ocean water samples, it is possible to identify emission sources, such as the reprocessing facilities of La Hague and Sellafield, and better understand ocean circulation patterns [3]. International initiatives, which focus on the cycling of trace isotopes, are critical for understanding oceanic dynamics, investigating, and identifying the global impact of various sources in the respective ecosystems [4, 5].

In addition, sediment core sampling and analysis can reveal not only the currently established dynamics, but also the historical record of changes that have occurred over time in the respective areas. By examining the above isotopic ratios, and analysing multiple long-lived actinides, in marine sediments, source terms can be identified and spatial distribution patterns better understood.

2 FIELDS OF STUDY

Focusing on marine research here, preliminary results of two ongoing studies will be presented. The first study deals with sediment samples from Vefsn fjord (Norway), an area significantly influenced by historical fallout from the Chernobyl accident and currently also by contamination by the effluents of both the European spent nuclear fuel reprocessing facilities (La Hague, Sellafield). The second study concentrates on the sediment cores from the North Sporades (North Aegean Sea), historically influenced mostly by the discharges from the Black Sea contaminated during the Chernobyl accident. In both cases, the ratios of $^{236/238}$U and $^{129/127}$I isotopes are correlated with ^{137}Cs activity profiles and, in the case of the Aegean sea sediment core, also with ^{210}Pb dating.

3 EXPERIMENTAL

For uranium sample preparation standard method with HNO_3 leaching and UTEVA resin column extraction will be described in more detail, and iodine has been methodologically developed to minimise the losses due to its volatile nature. For iodine, liquid-liquid extraction has been used successfully for the liquid phase, while a comparison of

Copyright on 7th Asia-Pacific Symposium on Radiochemistry 2025 P-R7-31* -

different techniques for the extraction of iodine from the sediment is presented, to showcase the complexity of such a task due to the complicated speciation and nature of iodine.

^{137}Cs and ^{210}Pb have been measured by standard HPGe gamma-spectrometry. The ^{210}Pb data were used for the ^{210}Pb-lead dating of the sediment layers, while ^{137}Cs activity concentrations were correlated with the ^{236}U and ^{129}I to confirm the same origin of the contamination.

The measurements of ^{236}U and ^{129}I and the $^{236/238}$U and $^{129/127}$I isotope ratios were done in the accelerator mass spectrometry (AMS) laboratory in the Czech Republic, located at the Nuclear Physics Institute (NPI) in Řež. The facility is equipped with a 300 kV multi-isotope low-energy AMS system (MILEA).

MILEA is composed of an ion source with a sample changer, a low-energy (LE) part with an injector, a tandem accelerator with a stripper, a high-energy (HE) part for positive ion analysis, and a detector for measuring rare isotopes. The ion source uses caesium sputtering of a sample in a sample holder. The sample changer can measure without interruption because it can be exchanged without losing vacuum. It has a wide spectrum of applications, including almost all AMS measured isotopes with a focus on ^{129}I and actinides [6].

4 RESULTS

For the Vefsn fjord field of study, our measurements so far revealed a first correlation between $^{236/238}$U ratios and earlier measured ^{137}Cs profiles. Two characteristic horizons were identified that can be assigned to major nuclear weapon tests in the North and the Chernobyl accident from 1986.

For the samples from the Aegean basin, the measurements of ^{236}U and ^{129}I and the $^{236/238}$U and $^{129/127}$I isotope ratios are still ongoing. Based on the data from gamma-spectrometry, we can conclude that the ^{137}Cs peak coincides with a sediment layer dated to around 1986.

5 CONCLUSIONS

The characteristic horizon of the Chernobyl incident has been clearly distinguished and characterised in both areas, while the combination of several radioisotopes has proved fruitful for a further integrated analysis of the dynamics in the overall region. The ongoing project, along with others of a similar nature, offers a comprehensive understanding of the fate of various natural and manmade radionuclides in the environment. The combination of techniques used has been demonstrated to be particularly effective in differentiating between the contamination sources related to nuclear weapons, power plant accidents, and reprocessing facility operations.

ACKNOWLEDGMENTS

This work was supported by the MEYS of the Czech Republic grant ´Ultra-trace isotope research in social and environmental studies using accelerator mass spectrometry´ (RAMSES), Project No. CZ.02.1.01 /0.0/0.0/16_019/0000728

References

[1] J. QIAO, N. CASACUBERTA, P. McGINNITY, et al., “Natural and artificial radionuclides as tracers of ocean processes,” *Frontiers in Marine Science*, **10**, 1170408 (2023), https://doi.org/10.3389/fmars.2023.1170408

[2] K. HAIN, M. MARTSCHINI, F. GULCE, M. et al., “Developing Accelerator Mass Spectrometry Capabilities for Anthropogenic Radionuclide Analysis to Extend the Set of Oceanographic Tracers,” *Frontiers in Marine Science*, **9**, 837515 (2022), https://doi.org/10.3389/fmars.2022.837515

[3] K. FENCLOVA, M. NEMEC, T. PRASEK,.“Determination of plutonium and other selected actinides by accelerator mass spectrometry (in Czech),” *Chemické Listy*, **117**, 128 (2023), https://doi.org/10.54779/chl20230128

[4] R. F. ANDERSON, “GEOTRACES Reflections,” *Oceanography*, **37**, 8 (2024), https://doi.org/10.5670/oceanog.2024.405

[5] T. CRESSWELL, M. METIAN, N. S. FISHER, et al., “Exploring New Frontiers in Marine Radioisotope Tracing – Adapting to New Opportunities and Challenges,” *Frontiers in Marine Science*, **7**, 406 (2020), https://doi.org/10.3389/fmars.2020.00406

[6] J. KUCERA, K. P. BRABCOVA, M. NEMEC, et al., “Status report of the first AMS laboratory in the Czech Republic at the Nuclear Physics Institute, Rez,” *Chem. Pap.*, **77**, 7311 (2023), https://doi.org/10.1007/s11696-023-02904-2

Copyright on 7th Asia-Pacific Symposium on Radiochemistry 2025 P-R7-31* -

NATURAL RADIOACTIVITY AND RADON INTENSITY IN DIFFERENT TYPES OF ROCK SPECIES AND SOIL IN KOREA

Kil Yong Lee[1], Sungwon Kim[2], Minyong Park[1], Sang-Ok Lee[3], Seung Hwan Lee[2], Jung-Ki Shin[1], Seongjae Jeong[1], Jaeseung Heo[1], Seonghun Choi[1], Sangyong Kim[1]

[1]*Neosiskorea, Expo-ro 339beon-gil, Yuseong-gu, Daejeon, 34122, Korea, kylee@neosiskorea.com*
[2]*Korea Institute of Geoscience and Mineral Resources. 124 Gwahak-ro, Yuseong-gu, Daejeon, 34132, Korea,*
[3]*Korea National University of Heritage, 367 Baekjemun-ro, Gyuam-myeon, Buyeo-gun, Chungcheongnam-do, 33115, Korea,*

Natural radioactivity and radon emission activity were measured for some rocks and soil collected from various geological sites in Korea. The natural radioactivity of K-40, Ra-226, and Th-2320 were measured in various types of rocks distributed in various geological sites in Korea. Radioactivity of soil in various regions that have been widely used in the construction of traditional Korean houses for a long time were also measured. In addition, the radon (Rn-222) emission activity released from these rocks and soil was measured. Both the natural radioactivity and the radon emission activity were measured using gamma-ray spectroscopy.

I. NTRODUCTION

About 1,000 rock samples were collected in consideration of geological characteristics, and 30 soil samples were collected in consideration of production sites. Rocks and soils are widely used building materials all over the world. Rocks are used directly as building materials, such as stone slabs and interior decorations, and they are also widely used as raw materials for building materials, such as concrete and aggregate. Soil has long been used as the main building material and raw material for traditional Korean houses. Almost all building materials of geological origin, such as rock or soils, cause radiation exposure to residents because they contain natural radionuclides such as K-40, Ra-226 and Th-232. In addition, Rn-222, which is produced by the decay of Ra-226 in building materials, causes internal exposure to residents. To prevent internal and external radiation exposure of indoor residents, it is necessary to assess the radioactivity of natural radionuclides and the radon emission activity of various building materials.

II. NATURAL RADIOACTIVITY

Collected rock samples were crushed and ground and then sealed in a 450 mL marinelli beaker. Soil samples were also sieved and dried, then placed in marinelli beaker and sealed. Activity concentrations of K-40, Ra-226, and Th-232 in rock and soil samples were measured using a high-resolution gamma-ray detector (MIRION-GC6022, Eff; 60%). Since the radioactivity of Ra-226 was obtained by measuring the radioactivity of Pb-214 and Bi-214 which are daughter nuclides of Rn-222, an equilibrium period of approximately 25 days is required for secular equilibrium between Ra-226 ($T_{1/2}$=1600y) and Rn-222 ($T_{1/2}$=3.82d). All rock and soil samples were measured after storage at room temperature for at least 25 days [1].

III. RADON EMANATION ACTIVITY

In this study, the emission activity (EA) of radon released from rocks and soil was calculated using the radon emission coefficient (EC) and the activity concentration of radium (Eq. 1, 2). All rock and soil samples were measured twice on 4 and 25 days after sealing [2].

$$EC = \frac{A2-A1}{A2}. \quad (1)$$

$$EA = EC \times A2. \quad (2)$$

Where, EC is the radon emission coefficient, and A1 and A2 are the radioactive concentrations of radium obtained from the first and second measurements, respectively. EA represents the emission activity of radon released from rocks or soil.

IV. RESULTS

The results revealed that the mean activity concentrations of the rock samples were approximately 910 Bqkg-1, 42 Bqkg-1, and 81 Bqkg-1, respectively, for K-40, Ra-226, and Th-232. The mean activity concentrations of the soil samples were approximately 1070 Bqkg-1, 60 Bqkg-1, and 84 Bqkg-1, respectively, for K-40, Ra-226, and Th-232. The concentration of natural radioactivity in soil was found to be about 10% higher than that in rock. The mean emission coefficients (EC) of radon in rock and soil were 17% and 7%, respectively, and the mean emission activity (EA) of radon in rock and soil were 7.9Bq/kg and 3.1Bq/kg, respectively.

V. **CONCLUSIONS**

These days, people spend more than 80% of their daily lives indoors, so it is important to evaluate the natural radioactivity of building materials. In particular, in the case of radon, a radioactive inert gas, the radon emission activity of indoor building materials is very important as a major factor in the residents' internal exposure. In the future, we believe that there should be systematic and extensive research on natural radioactivity and radon emission activities for various indoor building materials as well as rocks and soils.

References

[1] A. Sakoda, K. Hanamoto, Y. Ishimori, T. Nagamatsu, K. Yamaoka, “Radioactivity and radon emanation fraction of the granites sampled at Misasa and Badgastein,” Appl. Radiat. Isot. **66**, 648–652 (2008).

[2] K. Y. Lee, S. Y. Cho, Y. Y. Yoon, Y. N. Jang, “Determination of the radon emanation fraction from phosphogypsum using LSC,” J. Radioanal. Nucl. Chem. **291**, 197–200 (2012).

Poster Presentation | [P1]Radiation Safety and Management

Mon. Sep 15, 2025 6:30 PM - 8:00 PM JST | Mon. Sep 15, 2025 9:30 AM - 11:00 AM UTC Poster

[Poster] P1

[P-P1-01]

Minor accidents occurred at the Isotope Science Center, the University of Tokyo from FY2020 to FY2025

*Shogo Higaki[1], Naoki Kosaka[1], Atsuko N. Ozeki[1], Masaomi Takahashi[2], Tomokazu Suzuki[2] (1. The University of Tokyo (Japan), 2. The University of Osaka (Japan))

[P-P1-02]

Radiation Safety Issues in the Dose Assessment Building for Advanced Radiation Emergency Medicine at QST Specializing in Radiochemistry and Bioassays

*Kohei Iwaya Iwaya[1], Hatsuho Seno[1], Guosheng Yang[1], Eunjoo Kim[1], Yoshinari Shiino[1], Takeshi Maeda[1], Norihiro Miyaushiro[1], Ktsumi Uzawa[1], Atsushi Kitagawa[1], Munehiko Kowatari[1], Osamu Kurihara[1] (1. National Institutes for Quantum Science and Technology (Japan))

[P-P1-03]

ACTIVATION ASSESSMENT MANUAL FOR ACCELERATOR DECOMMISSIONING: DEVELOPMENT, REVISION, AND CONTRIBUTION TO INTERNATIONAL STANDARDIZATION

*Hiroshi Matsumura[1], Kazuyoshi Masumoto[1], Go Yoshida[1], Akihiro Toyoda[1], Hajime Nakamura[1], Taichi Miura[1], Eisuke Watanabe[1] (1. High Energy Accelerator Research Organization (KEK) (Japan))

[P-P1-04]

DEVELOPMENT OF A METHOD FOR ^{36}Cl ACTIVITY ANALYSIS IN ACTIVATED POWER CABLE SHEATH AT A LARGE-SCALE PROTON ACCELERATOR FACILITY USING ACCELERATOR MASS SPECTROMETRY (AMS)

*Go Yoshida[1], Hiroshi Matsumura[1], Masumi Matsumura[2], Tatsuhiro Kimura[2], Masaki Ishida[1], Eisuke Watanabe[1], Kiyokazu Tsugane[1], Ryoken Shiobara[3], Masahiro Mitsuhashi[3], Masaaki Yamada[3], Koji Oishi[3], Koichi Nishikawa[1], Akihiro Toyoda[1], Hajime Nakamura[1], Taichi Miura[1], Kimikazu Sasa[2], Thien Ngoc Bui[4], Hiroshi Yashima[5] (1. KEK (Japan), 2. University of TSUKUBA (Japan), 3. Japan Environment Research Co., Ltd. (Japan), 4. SOKENDAI (Japan), 5. Kyoto University (Japan))

[P-P1-05]

PRETREATMENT METHOD FOR MEASURING TRITIUM RADIOACTIVITY IN POWER CORD SHEATHS AT A LARGE-SCALE PROTON ACCELERATOR FACILITY

*Ryoken Shiobara[1], Masahiro Mitsuhashi[1], Masaaki Yamada[1], Go Yoshida[2], Akihiro Toyoda[2], Masaki Ishida[2], Kiyokazu Tsugane[2], Hiroshi Matsumura[2], Eisuke Watanabe[2], Hajime Nakamura[2], Taichi Miura[2], Koji Oishi[1] (1. Japan Environment Research (Japan), 2. High Energy Accelerator Research Organization (Japan))

[P-P1-06]

ANALYSIS OF AIRBORNE DUST COLLECTED IN THE J-PARC NEUTRINO EXPERIMENTAL FACILITY

*Eisuke Watanabe[1,2], Eunji Lee[1,2], Kazutoshi Takahashi[1,2], Kiwamu Saito[1,2], Yoshinobu Sakakibara[1,2], Hiroshi Matsumura[1], Go Yoshida[1], Kiyokazu Tsugane[1], Seiji Nagaguro[1,2], Kotaro Bessho[1,2], Hirohito Yamazaki[1,2] (1. KEK (Japan), 2. J-PARC Center (Japan))

©APSORC25

[P-P1-07]

OPTIMIZATION OF PINHOLE COLLIMATORS FOR ACTIVATION IMAGING WITH GEGI5 AND ITS PERFORMANCE VALIDATION AT KEK PHOTON FACTORY

*Kiyokazu Tsugane[1], Go Yoshida[1], Hiroshi Matsumura[1], Akihiro Toyoda[1], Hajime Nakamura[1], Kazuyoshi Masumoto[1], Taichi Miura[1], Eisuke Watanabe[1], Satoshi Shinohara[1], Hiroshi Miyauchi[1] (1. High Energy Accelerator Research Organization (Japan))

[P-P1-08]

MONITORING RADIONUCLIDES IN THE HELIUM GAS CIRCULATING THROUGH THE TARGET CHAMBER AT THE J-PARC HADRON EXPERIMENTAL FACILITY

*Kotaro Bessho[1,2], Hiroaki Watanabe[1,3], Ruri Kurasaki[1,3], Masayuki Hagiwara[1,2,4], Eisuke Watanabe[1,2], Eunji Lee[1,2], Kazutoshi Takahashi[1,2], Yoshimi Kasugai[1], Hirohito Yamazaki[1,2] (1. J-PARC Center (Japan), 2. Radiation Science Center, KEK (Japan), 3. Institute of Particle and Nuclear Physics, KEK (Japan), 4. QST, NanoTerasu Center (Japan))

[P-P1-09*]

NON-DESTRUCTIVE AND ON-SITE ASSESSMENT FOR ACTIVATED CONCRETE IN 500 MeV PROTON BEAMLINE USING GAMMA DETECTORS

*Thien Ngoc Bui[1], Go Yoshida[2], Kotaro Bessho[2], Kiyokazu Tsugane[2], Akihiro Toyoda[2], Ryuki Asakubo[3], Hirokazu Kawamura[3], Fumiyoshi Nobuhara[3], Hiroshi Matsumura[2], Eisuke Watanabe[2], Hajime Nakamura[2], Taichi Miura[2] (1. Accelerator Science Program, SOKENDAI: 1-1 Oho, Tsukuba, Ibaraki, Japan, 305-0801, (Japan), 2. Radiation Science Center, High Energy Accelerator Research Organization (KEK): 1-1 Oho, Tsukuba, Ibaraki, Japan, 305-0801 (Japan), 3. Tokyo Nuclear Service Co. Ltd.: 19-2 Midorigahara 4chome, Tsukuba, Ibaraki, Japan (Japan))

[P-P1-10]

INFORMATION SHARING SYSTEM FOR THE PERSONAL MANAGEMENT OF ITINERANT RADIATION WORKERS

*Kazunori SATO[1], Akihiro Hio[1], Koji Kodama[1], Shunnosuke Takahashi[1], Hiroshi Watabe[1] (1. Tohoku University (Japan))

©APSORC25

7th Asia-Pacific Symposium on Radiochemistry *September 14 ~ 19, 2025 • Kunibiki Messe • Shimane, Japan*

Minor accidents occurred at the Isotope Science Center, the University of Tokyo from FY2020 to FY2025

Shogo Higaki[1], Naoki Kosaka[2], Atsuko N. Ozeki[3], Masaomi Takahashi[4], Tomokazu Suzuki[5]

[1] *Isotope Science Center, the University of Tokyo: 2-11-16 Yayoi, Bunkyo-ku, Tokyo, 113-0032,* shogo@ric.u-tokyo.ac.jp
[2] *Isotope Science Center, the University of Tokyo: 2-11-16 Yayoi, Bunkyo-ku, Tokyo, 113-0032,* kosaka.naoki@ric.u-tokyo.ac.jp
[3] *Isotope Science Center, the University of Tokyo: 2-11-16 Yayoi, Bunkyo-ku, Tokyo, 113-0032,* ozeki@ric.u-tokyo.ac.jp
[4] *The Department for the Administration of Safety and Health, The University of Osaka: 1-1 Yamadaoka, Suita, Osaka 565-0871*, takahashi.masaomi.asp@osaka-u.ac.jp
[5] *Institute for Radiation Sciences, The University of Osaka: 10-1 Mihogaoka, Ibaraki, Osaka 567-0047*, tomokazu@rcnp.osaka-u.ac.jp

1 INTRODUCTION

In Japan, the Act on Regulation of Radioisotopes, etc. is applied as the regulatory system for radiation. Article 31-2 of the act stipulates nine events that require legal reporting under Enforcement Regulation Article 28-3, with the criteria for judgment indicated in the guidelines of the Nuclear Regulation Authority (NRA). Additionally, Article 33, Paragraph 3 of the Act specifies measures to be taken in case of danger, such as fires within controlled areas or accidents during transportation outside the place of business, which may require reporting of measures taken. These radiation-related accidents are published on the NRA's website each time a report is received [1-2]. The number of such incidents is not very high, with 43 cases reported over the 10 years from FY2015 to FY2024. However, there is much to learn from these examples, and "Response to Accidents" is one of the subjects in the periodic training for radiation protection supervisors.

According to Heinrich's Law, there should be many more near-miss incidents behind these legally reportable events. In other fields, efforts are made to collect and share accidents and near-miss incidents within universities for laboratory safety. In the nuclear field, trouble information is published on the Nuclear Facility Information Disclosure Library "NUCIA" website [3], and some cases are horizontally deployed to other facilities. In the medical field, the Japan Council for Quality Health Care conducts a project to collect information on medical accidents [4].

Sharing accidents and near-miss incidents among managers and radiation workers is extremely effective for radiation safety education. Furthermore, improving operations and enhancing education and training as required by Article 38-4 of the Act also contributes to fostering a safety culture in radiation use. On the other hand, in the radiation field, events that are not legally required to be reported may be shared within the place of business but not with managers or radiation workers of other business premises, making it difficult to know many cases. Therefore, a system to collect information on non-reportable events nationwide, from minor accidents to near-miss incidents, is necessary, and if each facility can select events considered effective for use in education and training, it will lead to substantial safety improvement. For this reason, the Education and Training Review Committee of Japanese Society of Radiation Safety Management has been collecting near-miss incidents since 2021 [5-6]. Currently, this activity has been developed into a project funded by Grants-in-Aid for Scientific Research since FY2022.

So far, near-miss incidents that occurred at the Isotope Center from FY2020 to FY2023 have been made public [7]. In our poster presentation, we will show some of minor incidents occurred in Isotope Science Center, the University of Tokyo. In this abstract, we introduce an example.

2. EXAPMLE

2.1 Body Contamination by ^{211}At

In June 2023, after a labeling experiment with ^{211}At, contamination was detected on the right chest and neck of an experimenter's clothing using an alpha/beta survey meter upon exiting the laboratory. No contamination was detected on their skin. A survey meter reading was alpha radiation: 108 cpm (BG: 0 cpm). The cause was presumed to be that the labeling experiment was not conducted within a fume hood, and although the experimenter wore an activated carbon mask and Tyvek suit during the experiment, the neck area was opened.

In July, after another labeling experiment with ^{211}At, contamination was detected on the lower part of the experimenter's left arm using an alpha/beta survey meter upon exiting the laboratory. A survey meter reading was alpha radiation: 149

Copyright on 7th Asia-Pacific Symposium on Radiochemistry 2025

cpm (BG: 0 cpm). In this case, the labeling experiment was conducted within a fume hood. The experimenter wore an activated carbon mask, Tyvek suit, and arm covers during the experiment, but the Tyvek suit was short-sleeved underneath. It is believed that contamination occurred when the experimenter removed the arm covers during work. After washing three times with dish detergent, alpha contamination was no longer detected.
Since At is a halogen with high volatility, it is presumed that contamination occurred due to gaseous ^{211}At compounds. In this experimental operation, ^{211}At was labeled to liquid organic compounds. If contamination were due to liquid, the hands would be the most likely to be contaminated. However, in this case, the experimenter's hands were not contaminated, and contamination was only detected on the neck and lower arm, suggesting that liquid contamination is unlikely. When using ^{211}At, it is strongly recommended to wear a Tyvek suit or similar full-body covering to avoid body contamination.

3. CONCLUSIONS

To prevent recurrence, several examples are introduced in re-education training. However, similar near-miss incidents continue to occur. It is believed that hearing about these incidents only once during training does not make individuals perceive them as something that could happen to them, thus repeated education is necessary.

ACKNOWLEDGMENTS

This work was partly supported by JSPS KAKENHI Grant Number JP22K02944.

References

[1] Nuclear Regulation Authority, Japan, “Reports based on the Act on Regulation of Nuclear Reactors or the Act on Regulation of Radioisotopes, etc.,” https://www.nra.go.jp/activity/bousai/trouble/houkoku/index.html (Accessed in 7 April, 2025). (in Japanese).
[2] Nuclear Regulation Authority, Japan, “Nuclear Regulation Authority Archive Search System, N-ADRES,” https://www.da.nra.go.jp/search?q=group_id+eq+%27%22 放射線防護・原子力防災%22%27&ftxt=1&fuse=1&f.gi=M003_115 (Accessed in 7 April, 2025). (in Japanese).
[3] Japan Nuclear Safety Institute, “Nuclear Facility Information Disclosure Library "NUCIA",” http://www.nucia.jp/ (Accessed in 7 April, 2025). (in Japanese).
[4] Japan Council for Quality Health Care, “Medical Accident Information Collection Project Website,” https://www.med-safe.jp/ (Accessed in 7 April, 2025). (in Japanese).
[5] Education and Training Review Committee of Japanese Society of Radiation Safety Management, “Near-Miss Information Provision Form,” https://forms.gle/xPYDpX9pQizki1RX6 (Accessed in 7 April, 2025). (in Japanese).
[6] T. SUZUKI, S. HIGAKI, and M. TAKAHASHI, “Near-Miss Incident Information Provision Form for Radiation Use,” http://osku.jp/k0486 (Accessed in 7 April, 2025). (in Japanese).
[7] S. HIGAKI, N. KOSAKA, M. TAKAHASHI and T. SUZUKI, “Minor accidents occurred at the Isotope Science Center, the University of Tokyo from FY2020 to FY2023,” *Japanese Journal of Radiation Safety Management*, **23**, 24-28 (2024). (in Japanese).

Copyright on 7th Asia-Pacific Symposium on Radiochemistry 2025

7th Asia-Pacific Symposium on Radiochemistry *September 14 ~ 19, 2025 • Kunibiki Messe • Shimane, Japan*

Radiation Safety Issues in the Dose Assessment Building for Advanced Radiation Emergency Medicine at QST Specializing in Radiochemistry and Bioassays

Kohei Iwaya[1], Hatsuho Seno[1], Guosheng Yang[1], Eunjoo Kim[1], Yoshinari Shiino[1], Takeshi Maeda[1],Norihiro Miyaushiro[1], Katsumi Uzawa[1], Atsushi Kitagawa[1], Munehiko Kowatari[1], Osamu Kurihara[1]

[1] *National Institutes for Quantum Science and Technology (QST), 4-9-1 Anagawa, Inage, 263-8555 Chiba, Japan*
Email Address: iwaya.kohei@qst.go.jp

The Dose Assessment Building for Advanced Radiation Emergency Medicine at QST has been operational since 2021, conducting research and performing dose assessments for internally contaminated patients using bioassays and whole-body counting methods. A key radiation safety challenge involves the segregation of solid/liquid radioactive wastes and the reduction of their volume. This presentation outlines the facility's features and discusses countermeasures for managing radioactive waste generated within it.

1 INTRODUCTION

The National Institutes for Quantum Science and Technology (QST) in Japan was designated by the Nuclear Regulation Authority (NRA) as the core medical support center for radiation emergencies in 2019. To fulfill QST's missions as this core medical support center, the Dose Assessment Building for Advanced Radiation Emergency Medicine (DAB) was established in QST's Chiba research district in 2021, with financial support from the NRA. This presentation discusses the radiation safety aspects of the DAB, including the pre-construction regulatory approval process, operational procedures, and identified radiation safety challenges.

2 Dose Assessment Building for Advanced Radiation Emergency Medicine (DAB) in QST

2.1 Outline of the DAB in QST

The DAB at QST has been operational since 2021. The facility is regulated under both the Act on the Regulation of Nuclear Source Material, Nuclear Fuel Material and Reactors and the Act on the Regulation of Radioisotopes. This dual regulation is necessary because among the actinides used in research at the DAB, Uranium (U), Thorium (Th), and Plutonium (Pu) are classified as nuclear fuel materials, whereas Americium (Am), Curium (Cm), and Neptunium (Np) must be controlled as radioisotopes (RIs). License applications for the use of nuclear fuel materials and RIs were submitted separately during the DAB's construction. The licensing process involved rigorous examination of different aspects for each radioactive or nuclear material type. For nuclear fuel materials, assessments focused on annual handling quantities and measures to prevent dispersion during experiments. For RIs, the evaluation covered the types and quantities of radionuclides to ensure that doses to radiation workers (primarily chemical analysts and researchers) remain below the annual limit of 20 mSv.

The DAB is a four-story building with chemical and biological laboratories on the second and third floors. The first floor houses incineration equipment for radioactively contaminated materials and tanks for radioactive liquid waste treatment. Exhaust air treatment equipment is installed on the fourth floor. Radiation-controlled areas are established on each floor, with appropriate radiation control measures implemented in compliance with both sets of regulations (i.e., for Nuclear Fuel Materials and RIs).

2.2 Activities in the DAB

In addition to performing internal dosimetry for actinide-exposed patients using bioassays [1] and the whole-body counting method [2], the DAB conducts research contributing to the development of internal decontamination materials and the analysis of trace radioactive materials in the environment. A notable feature in radiochemistry is that the DAB holds licenses permitting the use of the widest range of nuclear fuel materials and RIs for bioassay purposes available in Japan. As the core medical support center for radiation emergencies, the DAB plays a significant role in training highly specialized personnel and maintaining the functions and capabilities required for radiation emergency medicine in response to nuclear disasters. Specifically, the DAB offers training courses in nuclear disaster medicine for core personnel, bioassay techniques, and whole-body counting.

3 Radiation Safety Issues in the DAB

3.1 Radiation control implementation

Copyright on 7th Asia-Pacific Symposium on Radiochemistry 2025

Radiation safety practices at the DAB must comply with regulations pertaining to both Nuclear Fuel Materials and RIs. Area monitoring involves measuring and controlling surface contamination density from actinides and other RIs to ensure levels do not exceed the criteria (0.4 Bq/cm² for beta/gamma emitting RIs and 0.04 Bq/cm² for actinides, respectively). Measurements are performed using both ZnS(Ag) scintillation-type and GM-tube-type survey meters. Monthly monitoring, including measurements of dose equivalent rate, surface contamination density, and airborne radioactivity concentration, is conducted. Furthermore, a continuous radiation monitoring system is installed for exhaust air from the DAB's radiation-controlled areas. For individual monitoring, personnel (including analysts, scientists, and radiation protection officers) must wear personal dosimeters when entering radiation-controlled areas. Hand-foot-cloth monitors are installed at exits from these areas to simultaneously measure alpha and beta rays, enabling rapid screening for potential contamination.

Maintaining appropriate humidity levels within the radiation-controlled areas is critical for both laboratory management and radiation safety. Hot and humid summer weather complicates environmental control, sometimes resulting in relative humidity exceeding 90%. Maintaining low humidity, particularly during such periods, increases drainage from dehumidification systems. This increased effluent flows into collection tanks, necessitating more frequent discharge cycles. Prior to each discharge, the radioactivity concentration in the effluent is measured to confirm it is below the regulatory discharge limit.

3.2 Disposal and reduce in volume of waste

Radioactive waste generated from various experiments in the DAB's radiation-controlled areas is stored in the on-site radioactive waste storage facility. According to the license for using nuclear fuel materials, solid radioactive waste must be sorted based on characteristics (e.g., combustible, non-combustible, metal, glass, animal carcasses) and stored appropriately in the radioactive waste storage facility within the QST Chiba district. Prior to sorting, solid radioactive waste is typically washed and dried to remove acidic reagents and moisture, before being categorized as combustible or non-combustible. A muffle furnace is employed to reduce the volume of suitable combustible materials through incineration. This process can reduce the volume of these materials to 10-20% of their original bulk. As of April 2025, the solid radioactive waste stored in the Chiba research district facility reached 67.4% of its maximum capacity; therefore, effective waste treatment and volume reduction are crucial.

In addition to volume reduction, efforts focus on minimizing the generation of both solid and liquid radioactive waste. Analysts and scientists are required to thoroughly wash or rinse glassware, remove residual nuclear fuel material, and strictly segregate effluent streams. Radioactive liquid effluents containing nuclear fuel materials are also temporarily stored in the radioactive waste storage facility prior to further treatment or disposal.

4. SUMMARY

The Dose Assessment Building for Advanced Radiation Emergency Medicine was established in QST's Chiba research district in 2021 with financial support from the NRA. Its purpose is to maintain and enhance QST's capabilities for dose assessment of internally exposed patients, serving as the core medical support center for nuclear emergencies. Sustainable operation of the DAB is essential as a platform supporting radiochemistry research, including bioassays. Key operational and radiation safety challenges include managing humidity control, which impacts liquid effluent generation, and addressing radioactive waste management. Specifically, increased effluent from dehumidification systems requires careful handling as liquid radioactive waste. Furthermore, limited storage capacity for solid radioactive waste necessitates ongoing volume reduction efforts (e.g., incineration) and consideration of future storage and disposal strategies. Minimizing the generation of both solid and liquid waste, through practices like efficient glassware rinsing and effluent segregation, remains a continuous priority.

ACKNOWLEDGMENTS

The authors also thank distinguished researchers and scientists who always comply with regulations and be cooperative with safety personnel in the Dose Assessment Building for Advanced Radiation Emergency Medicine.

References

[1] G. Yang, et al., “The new QST bioassay laboratory in Chiba, Japan”. Radiat. Prot. Dosim. **199**(15-16) 2020-2024. (2023).

[2] Y. Tamakuma, et al., “Development of a new integrated IN-VIVO counting system at the QST”. Radiat. Prot. Dosim. **199**(15-16) 1848-1852. (2023).

7th Asia-Pacific Symposium on Radiochemistry *September 14 ~ 19, 2025 • Kunibiki Messe • Shimane, Japan*

ACTIVATION ASSESSMENT MANUAL FOR ACCELERATOR DECOMMISSIONING: DEVELOPMENT, REVISION, AND CONTRIBUTION TO INTERNATIONAL STANDARDIZATION

Hiroshi Matsumura[1], Kazuyoshi Masumoto[1], Go Yoshida[1], Akihiro Toyoda[1], Hajime Nakamura[1], Taichi Miura[1], Eisuke Watanabe[1]

[1]*High Energy Accelerator Research Organization (KEK), 1-1 Oho, Tsukuba, Ibaraki 305-0801, Japan*
Corresponding author: hiroshi.matsumura@kek.jp

This paper presents the development and international dissemination of a Japanese manual for activation assessment in accelerator facility decommissioning. The manual was initially issued in 2021, and subsequently revised in 2022 and 2024, with an English version released as KEK Report 2024-5. In the manual, systematic methodologies for facility classification and activation assessment are presented based on experimental studies for various types of accelerator facilities. Furthermore, it explains activation determination methods based on the Indistinguishable From Background (IFB) concept, using PET cyclotron facilities as a representative example. Selected methodologies are currently being proposed for inclusion in ISO/DIS 8939 (Decommissioning of Medical Cyclotron), contributing to the international harmonization of radiological safety assessment practices.

1 INTRODUCTION

In preparation for the anticipated decommissioning of accelerator facilities in Japan, a national research project supported by the Nuclear Regulation Authority (NRA) was initiated to develop standardized methods for activation measurement and evaluation. As outcomes, the first edition of the manual was issued in 2021 [1], followed by revisions in 2022 [2] and 2024 [3]. In December 2024, an English version [4] was published to enhance international applicability. Furthermore, selected methodologies from the manual are currently being proposed for inclusion in ISO/DIS 8939 (Decommissioning of Medical Cyclotron).

2 OVERVIEW OF THE MANUAL

2.1 Chapter 2: Measurements and Results for Zoning for Materials Determined to be Not Activated

Chapter 2 summarizes zoning evaluation results generalized by facility type, based on experimental identification of activated areas in electrostatic accelerator facilities, synchrotron radiation facilities, proton therapy facilities, and heavy ion therapy facilities. The evaluation is conducted using thermal neutron fluence during operation, radionuclide analysis with gamma spectrometry, and surface gamma dose rate measurements. Areas with measured values sufficiently below clearance criteria are "determined to be not activated." The manual also describes various thermal neutron measurement methods, including gold foil activation, CR-39 solid-state track detectors, thermoluminescent dosimeters (TLDs), and in-situ gamma spectrometry for Na-24 in concrete, highlighting their respective strengths and limitations.

2.2 Chapter 3: Measurement and Determination Methods for Activation during Decommissioning

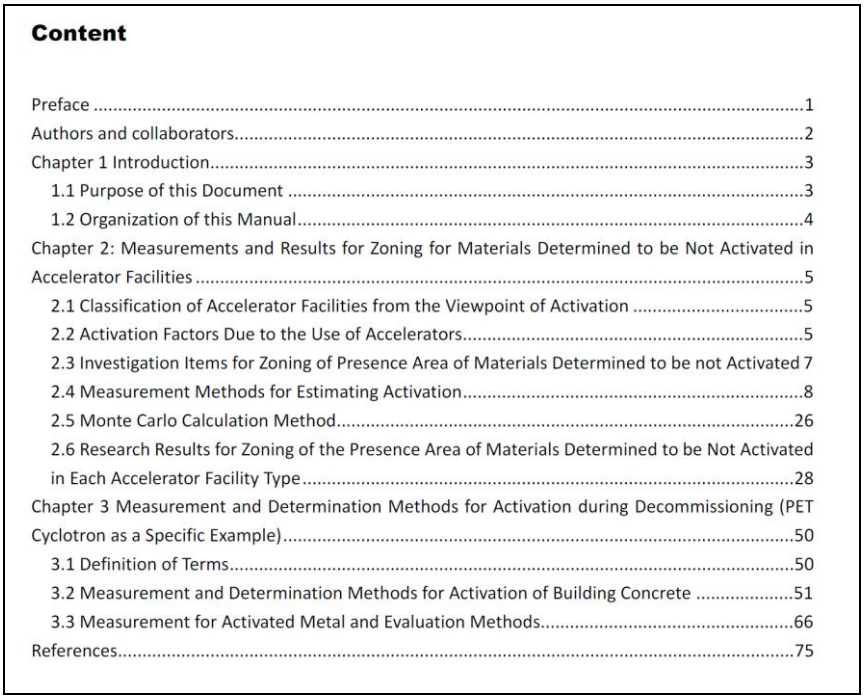
Chapter 3 proposes standardized procedures for evaluating activation in structural materials such as concrete and iron, with PET cyclotron facilities used as representative examples. For example, in the case of concrete, the evaluation can be realized by combining sampling measurements through core boring and surface measurements using a survey meter. The assessment methodology is based on proxy radionuclides and the "Indistinguishable From Background (IFB)" concept. The manual provides practical examples of measurement and evaluation workflows to facilitate objective and effective decision-making during decommissioning.

3 CONTRIBUTION TO ISO/DIS 8939

Although the manual was developed to meet domestic regulatory needs, its methodologies are applicable internationally. We are currently proposing that selected methods from the manual be incorporated into ISO/DIS 8939 (Decommissioning of Medical Cyclotron), which is under development by ISO/TC85/SC5/WG13. These contributions

Copyright on 7th Asia-Pacific Symposium on Radiochemistry 2025

are expected to strengthen the technical foundation of international standards related to the decommissioning of medical cyclotron facilities.



Content

Preface 1
Authors and collaborators....2
Chapter 1 Introduction....3
1.1 Purpose of this Document 3
1.2 Organization of this Manual....4
Chapter 2: Measurements and Results for Zoning for Materials Determined to be Not Activated in Accelerator Facilities 5
2.1 Classification of Accelerator Facilities from the Viewpoint of Activation 5
2.2 Activation Factors Due to the Use of Accelerators....5
2.3 Investigation Items for Zoning of Presence Area of Materials Determined to be not Activated 7
2.4 Measurement Methods for Estimating Activation....8
2.5 Monte Carlo Calculation Method....26
2.6 Research Results for Zoning of the Presence Area of Materials Determined to be Not Activated in Each Accelerator Facility Type....28
Chapter 3 Measurement and Determination Methods for Activation during Decommissioning (PET Cyclotron as a Specific Example)....50
3.1 Definition of Terms....50
3.2 Measurement and Determination Methods for Activation of Building Concrete 51
3.3 Measurement for Activated Metal and Evaluation Methods....66
References....75

Fig. 1. Content of Manual for Measurement and Determination of Activation for the Decommissioning of Accelerators (H. Matsumura et al. KEK Report 2024-5 (2024) [4]).

4 CONCLUSIONS

The 2024 edition of the manual provides a practical and versatile framework for activation assessment applicable to a wide range of accelerator facilities. In addition to supporting domestic standardization efforts, the manual has the potential to contribute significantly to international standardization, particularly through ISO/DIS 8939. Moreover, the methodologies presented in this manual are expected to be further extended and applied to other types of accelerators and materials not specifically covered herein.

ACKNOWLEDGMENTS

The original edition of this manual was developed with support from the Radiation Safety Research Promotion Program (JPJ007057) funded by the Nuclear Regulation Authority of Japan. The manual was created and revised through the cooperation of numerous experts across Japan. We express our sincere appreciation to all who contributed valuable feedback during the revision process.

References

[1] Hiroshi Matsumura (ed.), *Manual of Measurement and Evaluation of Activation for Decommissioning of Accelerator Facilities*, attached as an appendix to the Final Report on the Strategic Promotion Program for Radiation Safety Research funded by the Nuclear Regulation Authority (NRA) of Japan, March 2021 (in Japanese).
[2] H. Matsumura *et al*., *Manual of Measurement and Evaluation of Activation for Decommissioning of Accelerator Facilities*, KEK Report 2022-5 (2022), in Japanese.
[3] H. Matsumura *et al*., *Manual for Measurement and Determination of Activation for the Decommissioning of Accelerators, The 2024 edition*, KEK Report 2024-4 (2024), in Japanese.
[4] H. Matsumura *et al*., *Manual for Measurement and Determination of Activation for the Decommissioning of Accelerators, The 2024 edition English version*, KEK Report 2024-5 (2024).
[5] ISO/DIS 8939, *Decommissioning of Medical Cyclotron*, ISO/TC85/SC5/WG13 (under development).

7th Asia-Pacific Symposium on Radiochemistry *September 14 ~ 19, 2025 • Kunibiki Messe • Shimane, Japan*

DEVELOPMENT OF A METHOD FOR ^{36}Cl ACTIVITY ANALYSIS IN ACTIVATED POWER CABLE SHEATH AT A LARGE-SCALE PROTON ACCELERATOR FACILITY USING ACCELERATOR MASS SPECTROMETRY (AMS)

Go Yoshida[1], Hiroshi Matsumura[1], Masumi Matsumura[2], Tatsuhiro Kimura[2], Masaki Ishida[1], Eisuke Watanabe[1], Kiyokazu Tsugane[1], Ryoken Shiobara[3], Masahiro Mitsuhashi[3], Masaaki Yamada[3], Koji Oishi[3], Koichi Nishikawa[1], Bui Ngoc Thien[4], Hiroshi Yashima[5], Akihiro Toyoda[1], Hajime Nakamura[1], Taichi Miura[1], Kimikazu Sasa[2]

[1]*Radiation Science Center, High Energy Accelerator Research Organization (KEK): 1-1 Oho, Tsukuba, Ibaraki, Japan, 305-0801, yoshigo@post.kek.jp*
[2]*Graduate School of Science and Technology, University of Tsukuba: 1-1-1 Tennodai, Tsukuba, Ibaraki, 305-8577*
[3]*Japan Environment Research Co., Ltd.: 24-1 Shinjuku6chome, Shinjuku, Tokyo, Japan, 160-0023*
[4]*Accelerator Science Program, SOKENDAI: 1-1 Oho, Tsukuba, Ibaraki, Japan, 305-0801*
[5]*Institute for Integrated Radiation and Nuclear Science, Kyoto University: Asashiro 2, Kumatori, Osaka, Japan, 594-0494*

We have conducted a trial study for developing a new method to quantify the long-lived radionuclide ^{36}Cl, produced by activation, in the power cables used in an accelerator room. A cable used in the large Proton Synchrotron facility, was used as sample. We first conducted a neutron activation analysis to determine the chlorine concentration of the cable sheath. Then we combusted the sheath, and trapped the released gases into water to convert covalently bound chlorine into chloride ions, making the samples suitable for accelerator mass spectrometry (AMS). Finally, ^{36}Cl was quantified by AMS. In the presentation, the detailed experimental procedures and the results of ^{36}Cl activity determination will be discussed.

1 INTRODUCTION

The activation of materials in accelerator facilities presents challenges in managing radioactive waste during decommissioning. Previous studies on activation and radioactive waste management have mainly focused on concrete materials and metal components constituting beamlines and magnets, because they occupy a large mass. However, little attention has been given to peripheral equipment such as power supplies.

In large-scale accelerator facilities, various power supply wires, hereafter described as “cable”, are extensively used to supply high voltage or large current to magnets. These cables are typically insulated with plastic sheaths that contain chlorine for incombustibility and electrical insulation. Neutrons generated during accelerator operation can induce nuclear reactions with chlorine, generating the long-lived radionuclide ^{36}Cl. Due to its long half-life (~300,000 years) and the absence of gamma-ray emission, measuring ^{36}Cl is particularly difficult. As a result, its amount and distribution have remained unclear.

To address this, we developed a new analytical method for ^{36}Cl in cables, employing the 12-GeV Proton Synchrotron at KEK (KEK-12GeV-PS), which had finished its operation, as a test site. Accelerator mass spectrometry (AMS), which has demonstrated high sensitivity in trace isotope detection, was used to determine ^{36}Cl activity. As a pretreatment step for AMS, neutron activation analysis, and combustion and gas-trapping experiments are also introduced.

2 METHODS

2.1 Sample for analysis

A cable with a core cross-sectional area of 400 mm², from the KEK-12GeV-PS, was adopted as a sample for ^{36}Cl analysis. This cable had been used to supply power to septum magnets which occurring amounts of beam loss. It can be guessed that the cable sheath had been irradiated with neutrons during beam operation.

2.2 Neutron Activation Analysis to Determine Chlorine Concentration

AMS measures the ratio of radioactive to stable isotopes in a sample. Therefore, to quantify ^{36}Cl activity, it was necessary to determine the stable chlorine concentration in the sheath—information that was not disclosed. We conducted neutron activation analysis at the Kyoto University Research Reactor Institute. The reaction ^{37}Cl(n,γ)^{38}Cl was

Copyright on 7th Asia-Pacific Symposium on Radiochemistry 2025

used for measurement. A 100 mg sample was irradiated with neutrons for 10 seconds at 1 MW thermal output. A standard chlorine-containing plastic sample was also irradiated under the same conditions to create a calibration curve.

2.3 Combustion and Gas Trapping for Chloride Ion Extraction

Chlorine in the cable sheath exists in covalently bound forms and must be converted into chloride ions for AMS. A 0.5 g sample of the sheath was gradually heated in an Ar/O_2 mixture gas stream to gasify the chlorine, which was then trapped in water to form a solution containing chloride ions. Ion chromatography was used to quantify both chloride and interfering sulfate ions (^{36}S) in the trapped solution.

2.4 AMS Measurement of ^{36}Cl Using a 6 MV Tandem Accelerator

Chemical procedures were applied to convert the solution into solid AgCl for AMS target preparation. Stable chlorine standards were added to the trapped water for isotope dilution to a $^{36}Cl/^{nat}Cl$ ratio of 10^{-12}~10^{-11}. $AgNO_3$ was added under nitric acid to form AgCl precipitate, which was centrifuged, washed, redissolved in concentrated NH_3, and reprecipitated for higher purity. The final AgCl (~4 mg) was used for AMS analysis at the 6 MV Tandem Accelerator Facility, University of Tsukuba (UTTAC), as shown in Fig. 1.

Anions generated from the sample pellet in the ion source were accelerated to 6 MV, stripped of electrons in the central stripper, and further accelerated as cations. Bending magnets separated mass numbers, and the target ion was guided to the detector. After the first mass separation, the stable ^{37}Cl was monitored using a Faraday cup, and the $^{36}Cl/^{37}Cl$ ratio was determined at the detector.

3 RESULTS

Representative AMS results are presented. The detector used is a drift ionization chamber with five electrode pairs, where ions lose energy proportionally to Z^2 as they pass through argon gas. This energy loss enables the separation of isobaric ions such as ^{36}Cl and ^{36}S. A two-dimensional plot of energy loss (dE) at different stages was used to distinguish ^{36}Cl from isobaric interferences such as ^{36}S. The ^{36}Cl signal was clearly separated and visually distinguishable. The 1σ region of the ^{36}Cl counts was extracted, and the activity was quantified using the chlorine concentration determined by the neutron activation analysis. Final results will be discussed at the conference.

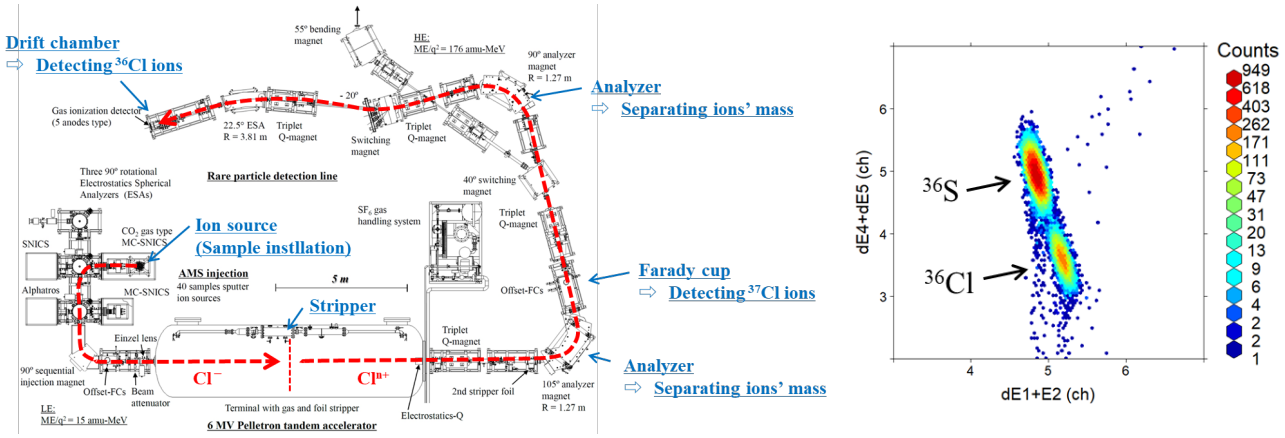


Fig. 1. Overview of UTTAC 6MV-Tandem accelerator (left), AMS spectrum of a cable sheath sample (right).

4. CONCLUSIONS

We developed a method to quantify ^{36}Cl in activated cable sheaths using AMS. By combining neutron activation analysis, combustion-gas trapping, and chemical purification techniques, we successfully prepared samples suitable for AMS measurement. The method enabled clear detection of ^{36}Cl, which had previously been difficult to evaluate due to its long half-life and lack of gamma emissions. This approach would provide a basis for a more accurate assessment of radioactive waste from peripheral components in accelerator facilities.

ACKNOWLEDGMENTS

We would like to express our appreciation to Mr. T. Takahashi and Mr. T. Yoshida for their support in operating the accelerator during the AMS experiments. This research was conducted as a collaborative study between KEK and JER.

7th Asia-Pacific Symposium on Radiochemistry *September 14 ~ 19, 2025 • Kunibiki Messe • Shimane, Japan*

PRETREATMENT METHOD FOR MEASURING TRITIUM RADIOACTIVITY IN POWER CORD SHEATHS AT A LARGE-SCALE PROTON ACCELERATOR FACILITY

Ryoken Shiobara[1], Masahiro Mitsuhashi[1], Masaaki Yamada[1], Go Yoshida[2], Akihiro Toyoda[2], Masaki Ishida[2], Kiyokazu Tsugane[2], Hiroshi Matsumura[2], Eisuke Watanabe[2], Hajime Nakamura[2], Taichi Miura[2], Koji Oishi[1]

[1] *Japan Environment Research Co., Ltd.: Nishi-shinjuku Mitsui Building, 24-1, 6-Chome, Nishi-shinjuku, Shinjuku-ku, Tokyo, Japan, 160-0023, and ryouken-shiobara@jer.tokyo-biso.co.jp*
[2] *Radiation Science Center, High Energy Accelerator Research Organization (KEK): Oho 1-1, Tsukuba, Ibaraki, Japan, 305-0801*

Precise estimation of induced activity at high-energy accelerator facilities is one of the most important issues during closing stage. Previous investigations for residual radio activities have focused mainly on structural materials of accelerator and shielding concrete. Despite the large number of peripheral devices such as power cords existing, studies have not been investigated. The radio activities produced in power cord sheaths are mainly beta-emitters such as tritium and liquid scintillation counting is applied for measurement. However, samples were colored and could not be measured by using conventional methods. In this study, we have developed a pretreatment method for liquid scintillation counting to measure tritium generated by nuclear transmutation in power cord sheaths. Samples were prepared by thermal combustion, and acid gases generated during combustion. These gases were removed using a cold trap placed immediately before the copper oxide bed to prevent its dissolution. As a result, tritium was recovered as transparent liquid and radio activity was successfully determined by liquid scintillation counting method.

1 INTRODUCTION

Accelerators have been used for various purposes, fundamental research, cancer treatment, pharmaceutical manufacturing and so forth. It is well known that the accelerator itself would mainly be activated by secondary neutrons and spallation reactions by high energy particles. Investigations of activation characteristics have been performed on 12 GeV large-scale proton accelerator facility at KEK (KEK-PS). Since it is extensively activated due to the emission of high-energy radiation and prolonged use, the estimation of induced activity should carefully be evaluated during closing stage.

In this study, we focused on the induced activity of power cord sheaths, which have not been investigated. Tritium is produced from the constituent nuclei of power cord sheaths by nuclear spallation reactions. The nuclides which emit beta-ray generated in shielding concrete are pretreated for liquid scintillation measurement [1]. In this method, the tritium is first released from the material as a gas by heating, and the gaseous tritium of unknown chemical form is then oxidized by contact with copper oxide. The collected tritiated water is recovered using cold traps.

$$CuO + HT \rightarrow Cu + HTO \quad (1)$$

However, when this method was applied to the activated power cord sheaths, it failed because the acid gases generated during combustion melted the copper oxide and samples turned blue. This study introduced an improved pretreatment method to solve this issue.

2 EXPERIMENTAL

2.1 Sample Preparation.

Two kinds of power cord were sampled near the beam extraction section of the 12-GeV proton synchrotron at KEK. The contact dose rates of gamma rays were measured using a 1-inch NaI (Tl) scintillation survey meter. The specific activities of ^{22}Na and ^{60}Co in cords were determined by gamma-ray spectrometry using a high-purity germanium semiconductor detector. Since activation of the cords was confirmed by two measurement methods, the copper conductors were removed, and only the sheaths were used as samples for the subsequent analysis.

2.2 Pretreatment Method for Liquid Scintillation Counting

Radioactivity of tritium, a beta emitter, generated in the power cord sheaths was determined by liquid scintillation counting. Liquid scintillation counting requires pretreatment by thermal combustion methods. Each sample was divided into approximately 0.5 g portions and pretreated using the system shown in Fig. 1. In this system, the acid gases

Copyright on 7th Asia-Pacific Symposium on Radiochemistry 2025

generated during combustion were removed by the first cold trap before the gases reached the copper oxide bed. Samples recovered in the cold traps (Steps 1 and 2) were measured by liquid scintillation counting.

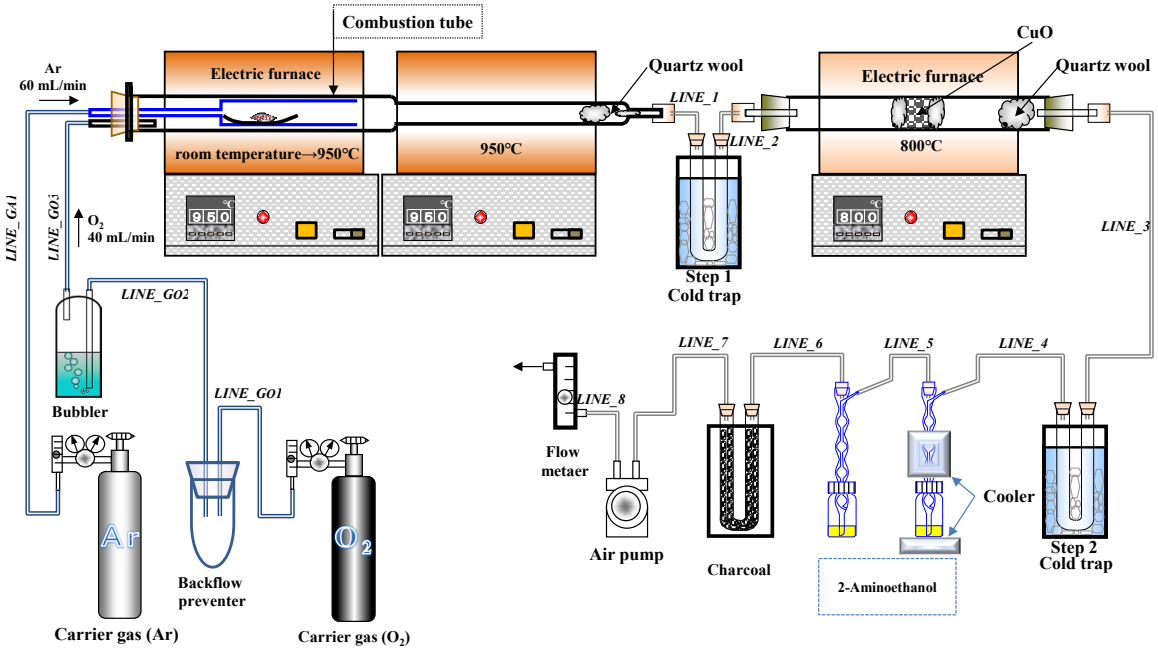


Fig. 1. Pretreatment method for liquid scintillation counting.

3 RESULTS

The samples obtained through the pretreatment method. It became possible to measure tritium by liquid scintillation counting method that they included no solid impurities and yielded colorless and transparent samples.

The measured results by liquid scintillation counting over four times are listed in TABLE 1. The total specific activity determined in Steps 1 and 2 of the cold traps is 49.3 ± 0.5 Bq g^{-1}, 70.3 ± 0.6 Bq g^{-1} on average, respectively. For multiple samples prepared by this method, each specific activity agreed within the statistical error.

TABLE 1. Specific Activities of Tritium in Power Cord Sheaths.

Sample	Experiment number	Specific activity / Bq g^{-1}	Average / Bq g^{-1}	Relative standard deviation / %
A	1	48.6 ± 0.4	49.3 ± 0.5	1.2%
	2	49.1 ± 0.5		
	3	50.2 ± 0.5		
	4	49.1 ± 0.5		
B	1	69.6 ± 0.5	70.3 ± 0.6	0.7%
	2	70.3 ± 0.6		
	3	70.5 ± 0.6		
	4	70.9 ± 0.6		

4 CONCLUSIONS

We have developed a pretreatment method for liquid scintillation counting to measure tritium generated by nuclear transmutation in power cord sheaths. The results demonstrate that samples can be successfully prepared for liquid scintillation counting by using this method. In particular, the cold trap placed before the copper oxide bed effectively removed acid gases generated during combustion, thereby preventing the dissolution of copper oxide.

Future work will focus on confirming the recovery rate of tritium and applying this method to other types of cords.

References

[1] Y. Izumi and Y. Ando *et al.*, "Separation Methods of Radioactive Carbon from Concrete Samples by Thermal Combustion Methods," *Res. Rep. Lab. Nucl. Sci. Tohoku Univ.*, **39**, 47 (2006).

ANALYSIS OF AIRBORNE DUST COLLECTED IN THE J-PARC NEUTRINO EXPERIMENTAL FACILITY

Eisuke Watanabe[1,2], Eunji Lee[2], Kazutoshi Takahashi[3], Kiwamu Saito[1,2], Yoshinobu Sakakibara[1,2], Hiroshi Matsumura[1], Go Yoshida[1], Kiyokazu Tsugane[1], Seiji Nagaguro[1,2], Kotaro Bessho[1,2], and Hirohito Yamazaki[1,2]

[1]*Radiation Science Center, High Energy Accelerator Research Organization (KEK): Oho 1-1, Tsukuba, Ibaraki, 305-0801, ewata@post.kek.jp*
[2]*J-PARC Center: Shirakata 2-4, Tokai, Ibaraki, 319-1195*

In high-energy accelerator facilities, various radioisotopes are observed in dust due to various nuclear reactions, including nuclear spallation reactions. In this study, airborne dust was collected from the machinery room near the target during beam operation at the J-PARC Neutrino Experimental Facility, and the nuclides were determined by gamma-ray spectrometry. Nuclides that were not reported in previous dust studies of high-energy accelerator facilities, such as ^{188}Ir, were observed. The results suggest that the number of nuclides to be monitored is expanding as accelerators become more powerful and experimental facilities become more sophisticated and complex.

1 INTRODUCTION

During the operation of high-energy accelerators, a wide variety of nuclear reaction products are produced when primary and secondary particles strike accelerator components, air, and water. Some nuclides are present as radioactive airborne dust within the accelerator facility and are eventually exhausted outdoors through filters. It is important for accelerator facilities to understand the properties of radioactive dust, not only for assessing the internal exposure of personnel working in the radiation area, but also for monitoring the stable operation of the accelerator and for planning the work in case of anomalies such as target malfunctions. We recently reported on the unprecedented production of radiomercury at the J-PARC Neutrino Experimental Facility and discussed its source [1]. With the increasing intensity of the accelerator, the produced nuclides are becoming more diverse, and further research is needed. In this study, we report on airborne dust samples collected from the machinery room during the operation of the J-PARC Neutrino Experimental Facility.

2 METHODS

In the J-PARC Neutrino Experimental Facility, neutrino beams are produced by extracting pions from 30 GeV protons supplied by the J-PARC Main Ring, using a graphite target. The helium-filled steel vessel containing the target is further shielded by concrete. In the basement of the neutrino target station building, a machinery room for controlling the target cooling system is located close to the He vessel. Airborne dust from the machinery room was collected for this study. During the operation of the neutrino experimental facility in June and December 2024, airborne dust samples were collected from the machinery room at a flow rate of 100 L/min. The dust sample was collected using filter paper (HE-40T, ADVANTEC). The air was also passed through an activated carbon filter (CHC-50-A00, ADVANTEC) to collect some volatile elements such as mercury. Subsequently, gamma-ray spectrometry of the filters was performed using a Ge semiconductor detector.

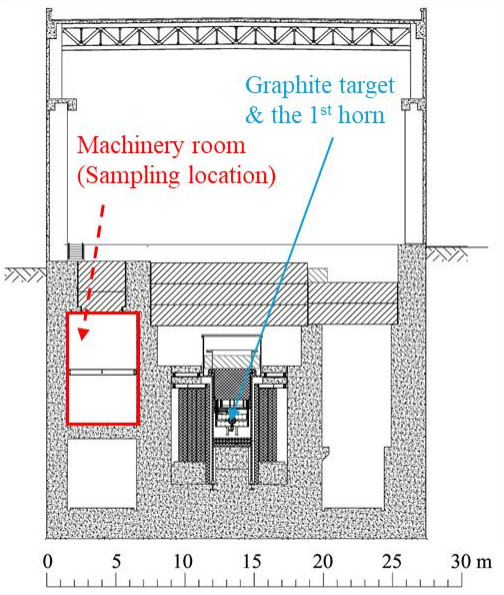


Fig. 1. Cross-sectional view of the neutrino target station building. A pump and collection filters were installed on the ground, and a filter can be removed during beam operation.

3 RESULTS AND DISCUSSION

By the Gamma-ray spectrometry, ^{7}Be, ^{24}Na, ^{28}Mg, ^{42}K, ^{43}K, ^{44g}Sc, ^{44m}Sc, ^{48}V, ^{52}Mn, ^{58}Co, ^{188}Ir, ^{191}Pt and ^{193}Au are detected. Light- and medium-mass nuclides have already been reported in the previous study at the CERN 28 GeV proton synchrotron [2] and at the EP-2 beam line tunnel of KEK 12 GeV proton synchrotron [3]. For example, it is considered that ^{7}Be is produced by reactions such as ^{12}C(p, spal) and ^{16}O(p, spal), and ^{44}Sc is produced by reactions such as ^{48}Ti(p,

Copyright on 7th Asia-Pacific Symposium on Radiochemistry 2025

3p3n) and ^{56}Fe(p, spal). On the other hand, the radioisotopes of Ir, Pt, and Au were not reported in the previous study for the airborne dust sample collected in the high-energy accelerator environments. In this study, radiomercury isotopes with mass numbers A = 192–203 were observed in the activated carbon filter. To elucidate the source of radiomercury production, we have assumed that radiomercury with a wide range of mass numbers is produced in the neutrino target station buildings by spallation reactions targeting Hg and Pb with natural abundance in the air and in accelerator components [1]. It was considered that the radioisotopes of Ir, Pt, and Au observed in the airborne dust in this study are decay products of radiomercury. The increase in beam power of high-energy accelerators suggests the importance of adding previously unknown nuclides to the monitoring targets.

4 CONCLUSIONS

In this study, the airborne dust sample collected in the J-PARC Neutrino Experimental Facility was analyzed. Applying airborne dust analysis insights to high-energy accelerator safety requires quantitative information on adsorbed nuclides and facility-by-facility characterization of dust samples. The presentations will include a quantitative discussion of radioactivity in Neutrino Experimental Facilities and comparisons with airborne dust samples collected preliminarily at the J-PARC Hadron Experimental Facility.

ACKNOWLEDGMENTS

This work was supported by JSPS KAKENHI (grant number JP24K17636). The authors thank Dr. Y. Oyama, Dr. T. Ishida, Dr. T. Sekiguchi, Dr. S. Tada, and Prof. K. Sakashita (Neutrino Group, KEK IPNS) for their support of this study in the J-PARC Neutrino Experimental Facility.

References

[1] E. Watanabe et al., Proc. J-PARC Symp. 2024, accepted.
[2] ST. Charlambus and A. Rindi, Nucl. Instr. Meth. **56**, 125-135 (1967).
[3] H. Muramatsu et al., Appl. Radiat. Isot. **39**, 413-419 (1988).

7th Asia-Pacific Symposium on Radiochemistry *September 14 ~ 19, 2025 • Kunibiki Messe • Shimane, Japan*

OPTIMIZATION OF PINHOLE COLLIMATORS FOR ACTIVATION IMAGING WITH GEGI5 AND ITS PERFORMANCE VALIDATION AT KEK PHOTON FACTORY

Kiyokazu Tsugane[1], Go Yoshida[1], Hiroshi Matsumura[1], Akihiro Toyoda[1], Hajime Nakamura[1], Kazuyoshi Masumoto[1], Taichi Miura[1], Eisuke Watanabe[1], Satoshi Shinohara[1], Hiroshi Miyauchi[1]

[1]*High Energy Accelerator Research Organization (KEK): Oho 1-1, Tsukuba, Ibaraki, Japan, 305-0801*
Corresponding author: kiyokazu.tsugane@kek.jp

We are developing an activation imaging technique using the portable gamma-ray imaging device GeGI5 to visualize weak activation at accelerator facilities. Our studies found that the Pb-Sb alloy collimator with a 5 mm pinhole (5mmPb) equipped with GeGI5 has limitations in shielding performance and detection efficiency for high-energy gamma-rays. To address these issues, we designed and fabricated new tungsten collimators with 5 mm, 7 mm, and 9 mm pinholes (5mmW, 7mmW, 9mmW). The performance of these collimators was evaluated using point sources and in practical conditions at the PF-ring at KEK Photon Factory (PF), focusing on resolution and detection efficiency. In this presentation, we will discuss the evaluation methods and results of the performance of these collimators in detail.

1 INTRODUCTION

In recent years, visualizing weakly activated sources has become essential for radiation management at high-energy accelerator facilities. To address this, we have developed activation imaging techniques using the portable gamma-ray imaging device GeGI5 [1-4], which supports both Compton and pinhole modes; this study focuses on the latter, using a standard 5 mm pinhole Pb-Sb alloy collimator (5mmPb) designed for general gamma-ray imaging. Through these studies, GeGI5 proved effective for visualizing activation at accelerator facilities. However, the 5mmPb showed shielding performance and detection efficiency limitations, especially for high-energy gamma-rays from accelerator activation.

Since the radioactive isotopes produced at accelerator facilities mainly emit high-energy gamma-rays, tungsten, with its higher density, was considered a more suitable material for improving collimation. Moreover, because the activated areas tend to be spatially broad with low surface dose rates (several μSv/h), improving detection efficiency was prioritized over spatial resolution. Thus, we originally designed and fabricated tungsten collimators with enlarged pinholes, specifically a 5 mm, 7 mm, and 9 mm pinhole (5mmW, 7mmW, 9mmW), to enhance imaging efficiency. Their performance was verified using point sources and evaluated at the PF-Ring at KEK Photon Factory (PF) under practical conditions.

2 EXPERIMENTAL

2.1 Basic Structure of GeGI5 and Measurement Principle of Pinhole Mode

The GeGI5 is a gamma-ray detector with an HPGe crystal (90 mm in diameter and 11 mm thick). Sixteen parallel electrodes are placed on the front and rear surfaces in orthogonal directions, forming a 16×16 segment array. GeGI5 operates in Compton or pinhole imaging modes. In the pinhole mode, a lead shield with a pinhole collimator is placed in front of GeGI5, allowing gamma-rays passing through the pinhole to reach the crystal. These gamma-rays ideally undergo the photoelectric effect, producing full-energy events for imaging. However, the system also records single-hit events from incomplete energy depositions, such as Compton scattering with escaping photons, which add noise. Accumulating many such events yields a spatial distribution of counts, thus forming an image of the radiation source.

2.2 Performance Evaluation of Tungsten and Pb-Sb Collimators Using Point Sources

GeGI5, equipped with 5mmPb, 5mmW, 7mmW, and 9mmW, was positioned at 1.0 m from the point source. The point sources used were ^{57}Co, ^{133}Ba, ^{137}Cs, ^{54}Mn, ^{22}Na, and ^{60}Co, and measurements were conducted in pinhole mode. Measurements were taken over 8 hours to 3 days, depending on the source. The performance of the collimators was quantitatively evaluated by fitting the acquired images with a 2D-Gaussian function. FWHM was estimated as the resolution. Detection efficiency was obtained from the net counts obtained in the source region of the visualization image.

2.3 Performance Evaluation of Tungsten Collimators at PF-ring

Copyright on 7th Asia-Pacific Symposium on Radiochemistry 2025

In addition to the evaluation using point sources, measurements were also carried out at the PF-ring, a 2.5 GeV electron accelerator used for materials and life sciences research, using the synchrotron radiation generated by the accelerator. GeGI5 was brought to the PF-Ring, and the Ceramic Chamber integrated Pulse Magnet (CCiPM) was chosen as the measurement target due to expected high activation. GeGI5 was positioned at 1.2 m from the CCiPM. The surface dose rates of the CCiPM before measurement were 23 μSv/h upstream and 8 μSv/h downstream. Measurements were conducted using the 9mmW and 5mmW collimators for 3 and 4 days after 14 and 17 days from accelerator stop, respectively. The performance of the collimators was evaluated based on the resolution and detection efficiency (η) derived from the resulting visualization images.

3 RESULTS AND DISCUSSION

Figure 1(a) shows the spatial resolutions, represented by FWHM values, obtained with the 5mmPb and 5mmW collimators using point sources. Although the resolutions were comparable below 200 keV, the 5mmW collimator exhibited better resolution than 5mmPb above 200 keV. The improvement of approximately 30% was observed above 1000 keV, attributed to the higher-density of tungsten.

The evaluation of detection efficiency using point sources is shown in Fig. 1(b). The number of gamma-rays transmitted through the pinhole increased with the pinhole diameter, resulting in improved detection efficiency at all gamma-ray energies. The detection efficiencies of the 7mmW and 9mmW collimators were approximately 1.5 times and 2 times greater above 600 keV, respectively, than that of the 5mmW collimator. The results demonstrated significant improvements in both resolution and detection efficiency at high gamma-ray energies, supporting the applicability of the original collimators to activation imaging in accelerator facilities.

Figure 1(c) shows the visualization image of the 834.9 keV gamma-ray from ^{54}Mn in the CCiPM, obtained using the 9mmW collimator. The activation at both ends was clearly visualized, confirming that the 9mmW collimator is effective for activation imaging under actual accelerator conditions.

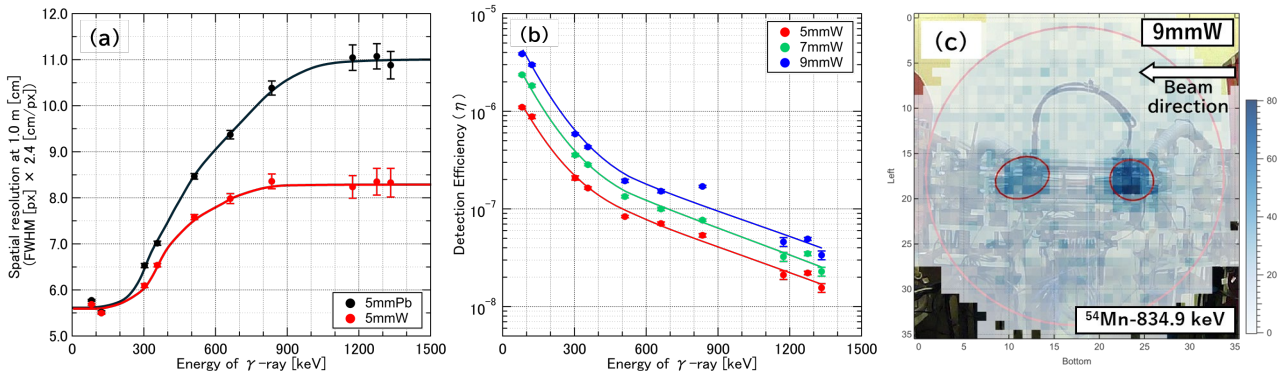


Fig. 1. Comparison of resolution and detection efficiency for each collimator ((a) and (b)), activation imaging of ^{54}Mn (834.9 keV) measured at the CCiPM (c).

4. CONCLUSIONS

The performance of the 5mmW, 7mmW, and 9mmW collimators developed to improve activation imaging efficiency with GeGI5 was evaluated using point sources and under practical conditions at PF-ring with CCiPM. Spatial resolution in the high-energy gamma-ray region was improved by 30% by replacing the Pb-Sb collimator with high-density tungsten. Detection efficiencies of the 7mmW and 9mmW collimators were 1.5 and 2 times greater, respectively, due to their large pinhole diameters. Activation at both ends of the CCiPM was clearly visualized using the 9mmW collimator, demonstrating its effectiveness for practical use in accelerator facilities.

References

[1] G. Yoshida *et al.*, *Environmental Radiochemical Analysis* **VI**, 191 (2019).
[2] Go Yoshida *et al.*, *Proceedings of the 23rd Workshop on Environmental Radioactivity*, 165 (2022).
[3] Go Yoshida *et al.*, *Proceedings of the 34th Meeting for Tandem Accelerators and their Associated Technologies*, 45 (2023).
[4] Kiyokazu Tsugane *et al.*, *Proceedings of the 24th Workshop on Environmental Radioactivity*, 121-125 (2023).

7th Asia-Pacific Symposium on Radiochemistry *September 14 ~ 19, 2025 • Kunibiki Messe • Shimane, Japan*

MONITORING RADIONUCLIDES IN THE HELIUM GAS CIRCULATING THROUGH THE TARGET CHAMBER AT THE J-PARC HADRON EXPERIMENTAL FACILITY

Kotaro Bessho[1,2], Hiroaki Watanabe[1,3], Ruri Kurasaki[1,3], Masayuki Hagiwara[1,2,4], Eisuke Watanabe[1,2], Eunji Lee[1,2], Kazutoshi Takahashi[1,2], Yoshimi Kasugai[1], Hirohito Yamazaki[1,2]

[1] *J-PARC Center, Tokai, Ibaraki 319-1195, Japan, kotaro.bessho@kek.jp*
[2] *Radiation Science Center, KEK, Tsukuba, Ibaraki 305-0801, Japan*
[3] *Institute of Particle and Nuclear Physics, KEK, Tsukuba, Ibaraki 305-0801, Japan*
[4] *QST, NanoTerasu Center, Sendai, Miyagi 980-8579, Japan*

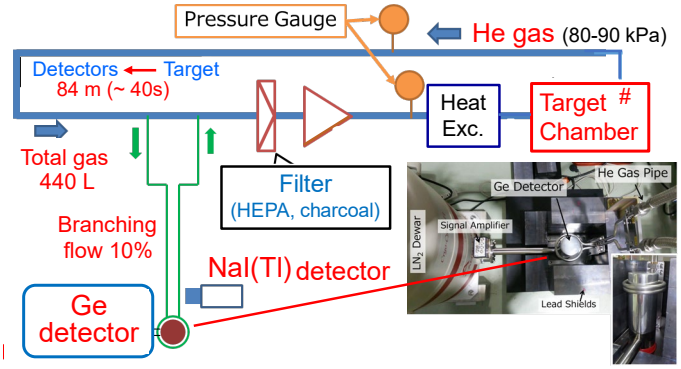
The radiation monitoring system has been utilized to monitor the target soundness at the J-PARC Hadron Experimental Facility since 2015. The target is made of pure gold and is located in a hermetic target chamber filled with helium gas. In the target, large amounts of radionuclides could be produced by irradiating with a 30-GeV high-power proton beam. During beam operation, trace amounts of several γ-emitting nuclides were observed in the circulating helium gas through the target chamber. The behavior of the detected radionuclides could be explained by their chemical states in the gas phase. Significant dependence of Hg nuclide activity on the beam power was observed; it can be expected that γ-rays of Hg nuclides would be sensitive indicators of target abnormalities, such as target damage.

1 INTRODUCTION

At the J-PARC Hadron Experimental Facility (HEF), a secondary-production gold target injected with a 30-GeV proton beam is placed in a hermetic chamber filled with circulating helium gas. After the radioactive material leak incident in 2013 [1], a radiation detector system was specially designed and installed to monitor the soundness of the target [2, 3]. Although the gold target system was upgraded in 2020, the radiation detector system for circulating helium gas has been continuously operated for safe and reliable beam operations since April 2015. The experiences and findings through the operations of the radiation monitoring system for the target at J-PARC HEF are introduced in this report.

2 RADIATION DETECTORS MONITORING RADIONUCLIDES IN CIRCULATING HELIUM GAS

The schematic view of the radiation detector system is shown in Fig. 1. The γ-ray spectra and count rates of the helium gas are continuously monitored by an HPGe detector and a NaI(Tl) detector, which are installed in the helium gas circulation loop. Details of the system were described in the previous reports [2, 3].



Gold target injected with a 30-GeV proton beam of Gaussian shape ($\sigma_{horizontal}$: 2.5 mm, $\sigma_{vertical}$: 1.0 mm)
2nd target system (2015-2019): *W* 15 mm x *H* 11 mm x *L* 66 mm [4]
3rd target system (2020-): *W* 12 mm x *H* 10 mm x *L* 66 mm with a 0.3 mm gap between the top and bottom blocks [5]

Fig. 1. Schematic view of the gas circulating system equipped with radiation detectors (Modified from the reference [2])

3 RESULTS AND DISCUSSION

During normal beam operations, trace amount of γ-emitting nuclides, such as C-10, N-16, O-14, O-19, O-20, F-20, Ne-23, Ne-24, Na-24 (daughter of Ne-24), S-37, Ar-41, Au-192 (daughter of Hg-192), Hg-191m, Hg-192, Hg-193m, Hg-

Copyright on 7th Asia-Pacific Symposium on Radiochemistry 2025

195, and Hg-195m, were continuously detected in the circulating helium gas through the target chamber. These detected nuclides are produced by nuclear reactions originating from the high-energy proton beams in the gold target and the beam windows, then partially transferred to the gaseous phase. On the other hand, calculations on the radionuclide productions revealed that dominant radionuclides induced in the target and the beam windows were Au-196, Au-194, Au-198, Sc-47, Sc-44, Al-28, *etc*., and many kinds of other radionuclides were also produced in these metal components. However, most of these radionuclides were not detected in the gas phase. These results demonstrated that C, N, O, F, Ne, S, Ar, Hg-radionuclides selectively transferred to the gas phase from solid components. The above detected radionuclides may tend to form volatile chemical species.

Figure 2 (a) and (b) show the relationships between the proton beam power and the peak counts for five kinds of radionuclides detected in the helium gas (a) for the 2nd target system used from 2015 to 2019, and (b) for the 3rd target system replaced in 2020. Here, the cooling efficiency for the gold target by cooling water was significantly improved for the 3rd target system [5]. As a result, the temperature of the gold target corresponding to the same beam power became lower in the 3rd target system (b) than in the 2nd target system (a). For C-10 and O-19, the peak counts were nearly proportional to the beam power, and the slopes were similar for the two kinds of target systems. Although the peak counts for Ne-24 and Ar-41 were also proportional to the beam power in the range up to 50 kW, the slope increased in the range above 50 kW for the 3rd target system (b). As for Hg-195m, the data for 50 kW in the 2nd target system (a) and that for 91 kW in the 3rd target system (b) significantly increased compared to the lower beam power trends. Here, the maximum temperatures of the gold target locally and instantaneously reached around 340°C for 50 kW operations in the 2nd system and 91 kW operations in the 3rd system, respectively. A similar sudden increase was also observed for Hg-191m, Hg-192, Hg-193m, and Hg-195. Considering that the boiling point of metallic mercury is 357°C, the temperature around 340°C should correspond to the condition under which the volatility of Hg species begins to increase rapidly. A more systematic and quantitative discussion will be conducted in the presentation.

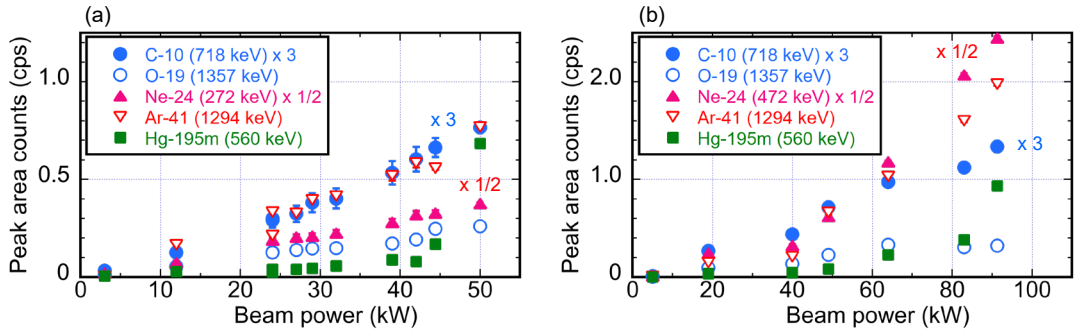


Fig. 2. Relationship between the proton beam power injected into the gold target and the peak counts of several radionuclides detected in the circulating helium gas. (a) 2nd target system (2015-2019); (b) 3rd target system (2020-)

4. CONCLUSIONS

The radiation monitoring system for circulating gas through the target chamber at J-PARC HEF was introduced, and some characteristics concerning the chemical behavior of radionuclides were demonstrated. During normal beam operations, trace amounts of several γ-emitting nuclides were observed in the circulating gas phase, and their behavior could be discussed by considering chemical states and volatility of radionuclides. Especially, the significant dependence of Hg nuclide activity on the beam power was observed, which should be caused by the volatility of Hg species depending on the temperature. Sudden increase of Hg-nuclides in gas phase at high beam-power / high temperature states implies that γ-rays of Hg nuclides would be sensitive indicators of target abnormalities, such as target damage caused by machine troubles. In order to implement reliable safety management at accelerator facilities, understanding the chemical behavior of induced radionuclides is an important issue, and further study is required.

References

[1] M. Hagiwara et al., "Investigation on Radionuclides Released in the Radioactive Material Leak Incident at the J-PARC Hadron Experimental Facility", JPS Conf. Proc., **8**, 051007 (2015).
[2] R. Muto et al., "Monitoring System for the Gold Target by Radiation Detectors in Hadron Experimental Facility at J-PARC", EPJ Web of Conf., **153**, 07004 (2017).
[3] K. Bessho et al., "Analysis of Radionuclides in Helium Gas Circulating Through the Target Chamber at the J-PARC Hadron Experimental Facility", JPS Conf. Proc., **33**, 011143 (2021).
[4] H. Takahashi et al., "Indirectly Water-Cooled Production Target at J-PARC Hadron Facility", J. Radioanal. Nucl. Chem., **3305**, 803 (2015).
[5] M. Saito et al., "Indirectly Cooled Secondary-Particle Production target at J-PARC Hadron Experimental Facility", Phys. Rev. Accel. Beams, **25**, 063001 (2022).

Copyright on 7th Asia-Pacific Symposium on Radiochemistry 2025

7th Asia-Pacific Symposium on Radiochemistry *September 14 ~ 19, 2025 • Kunibiki Messe • Shimane, Japan*

NON-DESTRUCTIVE AND ON-SITE ASSESSMENT FOR ACTIVATED CONCRETE IN 500 MeV PROTON BEAMLINE USING GAMMA DETECTORS

Bui Ngoc Thien[1], Go Yoshida[2], Kotaro Bessho[2], Kiyokazu Tsugane[2], Akihiro Toyoda[2], Ryuki Asakubo[3], Hirokazu Kawamura[3], Fumiyoshi Nobuhara[3], Hiroshi Matsumura[2], Eisuke Watanabe[2], Hajime Nakamura[2], Taichi Miura[2]

[1]*Accelerator Science Program, SOKENDAI: 1-1 Oho, Tsukuba, Ibaraki, Japan, 305-0801, bnthien@post.kek.jp*
[2]*Radiation Science Center, High Energy Accelerator Research Organization (KEK): 1-1 Oho, Tsukuba, Ibaraki, Japan, 305-0801*
[3]*Tokyo Nuclear Service Co. Ltd.: 19-2 Midorigahara 4chome, Tsukuba, Ibaraki, Japan, 300-2646*

Non-destructive assessment using gamma detectors is being developed as an effective method for residual activity measurement conducted during the decommissioning of accelerator facilities. This presentation discusses the first case study applying this method to a large-scale proton accelerator facility for research purposes and its feasibility. As actual field evaluations, contact dose rates and specific activities of residual radionuclides were measured on concrete walls and floors of 500 MeV proton transport beamline in KEK. The results suggested spatially non-uniform neutron distributions, corresponding to the existence of high beam loss areas. A strong correlation was found between dose rate and residual activity. However, variation in the $^{60}Co/^{152}Eu$ ratio across locations suggested that local material composition affects dose-based activity estimates. Accurate conversion from dose rate to activity requires correction factors accounting for nuclide ratio variability due to structural materials.

1 INTRODUCTION

Activation in accelerator facilities refers to the phenomenon in which radionuclides are produced in structural materials of the facility, which is mainly caused by secondary neutrons generated during the accelerator operation. This activation becomes a radioactive waste management issue when the facility is decommissioned. In particular, concrete, which is the largest volume material in such facilities, is significantly affected by activation. Therefore, accurately determining the extent of activation and the resulting activity is essential.

Destructive analysis through core boring can precisely quantify residual radionuclides; however, it is costly, labor-intensive, and limited in spatial coverage. This makes it impractical for large-scale accelerator facilities, such as KEK. We have been developing a non-destructive and simple method for determining residual activity by using a customized scintillation survey meter system, which is specially designed for this application [1].

In this presentation, we report on a field evaluation conducted at a 500 MeV proton beamline in the KEK accelerator facility, which is no longer in operation. This study serves as a feasibility assessment of the proposed method.

2 EXPERIMENTAL

We adopted the Neutron and Meson Science Laboratory (NML) beamline tunnel as a test field for this study. Figure 1 provides an overview of the NML beamline, which was in operation from 1976 to 2006, transporting the 500 MeV proton beam for material researches, particle physics experiments and medical applications. Core drilling for sampling had previously been conducted at five locations within the facility, and in 2024, when the present experiments were conducted, only ^{152}Eu, ^{60}Co, and ^{22}Na were detected, except for natural radionuclides.

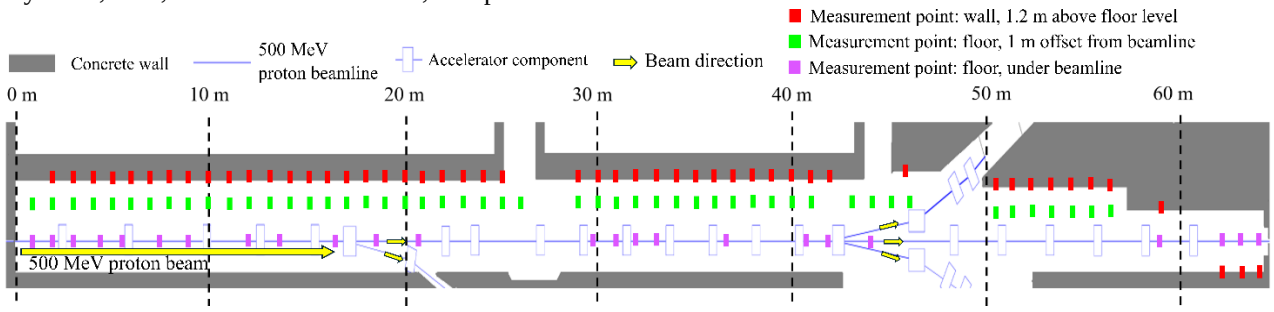


Fig. 1. Horizontal sectional view of Neutron and Meson Science Laboratory beamline tunnel. The dotted vertical lines show 10-m interval along the tunnel. The gray boxes indicate the concrete walls. The blue lines and blue rectangles indicate beamline and accelerator components such as magnets, respectively. The yellow arrows indicate the beam directions. The red, green and purple rectangles indicate the measurement points of contact dose rate and residual activity: wall 1.2 m above floor level, floor 1 m offset from beamline and floor under beamline, respectively.

The field evaluation consists of the following two parts: (1) contact dose rate measurement on concrete floor and walls using a cesium iodide (CsI) scintillation survey meter and (2) quantification of residual activity in concrete using a cerium bromide ($CeBr_3$) scintillation spectrometer. The advantages of these methods have already been demonstrated using some cyclotron facilities for positron emission tomography (PET) (maximum proton energy of 20 MeV), but there are no examples of their application to large-scale facilities such as NML. In (1), a low-cost, portable small detector (customized T-SP2; TAC Co. Ltd.) combined with a 65 mm thick lead radiation shield was used to measure over 100 locations on the

Copyright on 7th Asia-Pacific Symposium on Radiochemistry 2025

floor and walls within the facility. In circumstances such as accelerator tunnels where all walls, floor, and ceiling are activated, a radiation shield that covers the detector crystal completely is essential to suppress background noise. The detector and shield combination used in this study were optimized based on the previous study conducted at the PET cyclotron facility [1]. While (1) offers excellent mobility and rapid results, it does not provide information on residual nuclides and their activity. Therefore, we evaluated residual activity near concrete surfaces by (2). A 2-inch $CeBr_3$ detector (CEBRS-2x2; Mirion Technologies Co. Ltd.) and a specially designed 65 mm thick lead radiation shield were used to measure the same location as in (1). Results consistent with those obtained from core samples of the same facility have been confirmed, indicating that (2) can serve as an alternative to the actual sampling method in the vicinity of the surface.

3 RESULTS AND DISCUSSION

Figure 2 presents the total radioactivity measured along the wall of the NML beamline tunnel. The horizontal axis denotes the distance from the upstream end of the tunnel extending in the downstream direction. The primary detected nuclides were ^{152}Eu and ^{60}Co, both of which are produced via thermal neutron capture reactions, i.e., (n,γ) processes. The activity level of ^{22}Na induced by fast neutron was lower than those of two nuclides.

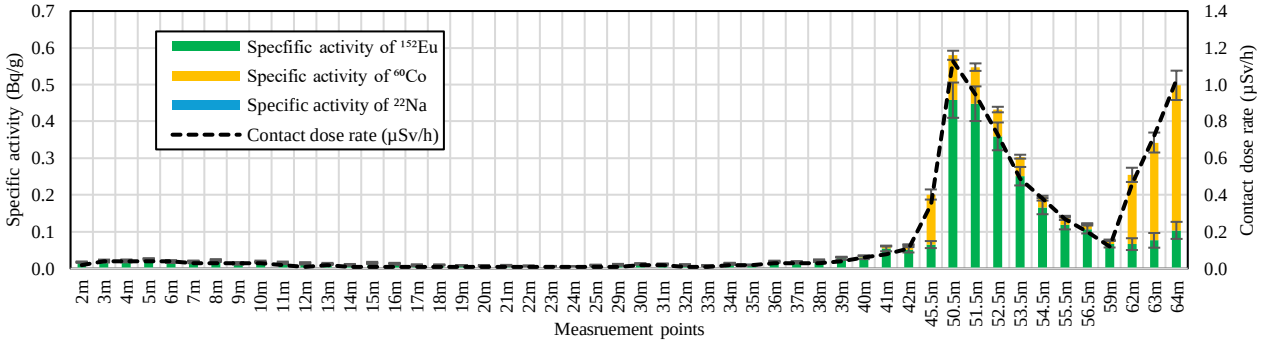


Fig. 2. Spatial distribution of specific activity of ^{152}Eu, ^{60}Co, ^{22}Na and contact dose rate measured along the wall of NML beamline tunnel from 2 m to 64 m in the beam direction. The specific activities of ^{152}Eu, ^{60}Co and ^{22}Na are illustrated in green, yellow and blue stacked columns, respectively, in the units of Bq/g on the left axis. The contact dose rates are illustrated in black dotted lines in the units of μSv/h on the right axis.

The total specific activity of these nuclides remained relatively low, approximately below 0.05 Bq/g, up to a distance of 40 m. A significant increase was observed around 45 m, exceeding 0.5 Bq/g, followed by a rapid decrease with further distance, then the activity sharply increased again beyond 60 m. These fluctuations indicate that the neutron flux within the tunnel is not spatially uniform but instead exhibits localized peaks, likely reflecting areas of substantial beam loss during accelerator operation. A good correlation was observed between the total residual activity and the contact dose rate, as illustrated by the dotted lines in the same figure. However, the activity ratio of ^{152}Eu and ^{60}Co was found to vary with location. This variation suggests the potential presence of reinforcing steel with elevated cobalt content near the concrete surface or the use of heavy concrete with higher cobalt concentrations in certain sections of the structure. Such spatial variation in nuclide composition complicates the estimation of radioactivity based solely on dose rate measurements. Previous studies show that reliable estimation typically assumes a constant nuclide ratio [2]. Therefore, in practical applications, it is essential to apply correction factors that account for differences in local material composition to improve the accuracy of dose-to-activity conversion. The presentation will discuss a detailed analysis of the results and findings.

4 CONCLUSIONS

Non-destructive and on-site assessment for activated concrete of walls and floors in the non-operational 500 MeV proton beamline was performed by using gamma detectors. The fluctuations in contact dose rate indicate that the nonuniform distribution of neutrons in the tunnel, reflects the high beam loss area during accelerator operation. A good correlation was observed between total residual activity and contact dose rate. Spatial variation of activity ratio between ^{152}Eu and ^{60}Co was found along the wall of the beamline. This variation suggests possible elevated cobalt concentration in structural material composition. Correction factors account for the difference in material composition are needed to improve the accuracy of dose-to-activity conversion. As the spatial mapping of activity in NML beamline tunnel was successfully achieved, this non-destructive method has proven to be feasible for determining residual activity which is useful for practical applications such as decommissioning planning of accelerators.

ACKNOWLEDGMENTS

This study was partially funded by TNS as part of a collaborative research agreement

References

[1] H. Matsumura, *et al.*, Environ. Radiochem. Anal., **VI**, 135–147 (2019).
[2] H. Matsumura, *et al.*, J. Phys.: Conf. Ser. **1046** 012016 (2018).

7th Asia-Pacific Symposium on Radiochemistry *September 14 ~ 19, 2025 • Kunibiki Messe • Shimane, Japan*

INFORMATION SHARING SYSTEM FOR THE PERSONAL MANAGEMENT OF ITINERANT RADIATION WORKERS

Kazunori Sato[1,2], Akihiro Hio[2], Koji Kodama[2], Shunnosuke Takahashi[2], Hiroshi Watabe[1]
[1]*Research Center for Accelerator and Radioisotope Science, Tohoku University: 6-3, Aoba, Aramaki, Aoba-ku, Sendai, Miyagi, 980-8578, JAPAN, kns@tohoku.ac.jp*
[2]*Division of Engineering and Technical Staff, Tohoku University: 1-1, Katachira-2-chome, Aoba-ku, Sendai, Miyagi, 980-8577, JAPAN*

An information sharing system for the personal management of itinerant workers was developed. Employers, radiation facilities, and the radiation worker themselves can easily access not only radiation exposure doses, health examination results, safety training results, but also detailed information by using the Personal Management Standard Table. This system is considered useful for the safety management of itinerant workers who work at multiple radiation facilities.

1 INTRODUCTION AND OBJECTIVE

Radiation workers are required to undergo radiation dose measurement, health examinations, and safety education and training from the perspective of preventing radiation hazards. The implementation of these measures and the recording and storage of related information are mandated. Hereinafter, this information will be referred to as "personal management information." In Japan, two laws, the Act on the Regulation of Radioisotopes, etc. (Act No. 167 of 1957) and the Industrial Safety and Health Act (Act No. 57 of 1972), impose obligations for personal management on radiation facilities and employers, respectively.

In recent years, there has been an increase in radiation workers who work at multiple radiation facilities, known as itinerant workers, in the academic field. Under the Japanese legal system, both the employer who dispatches the workers and each radiation facility where the radiation workers work are required to manage the personal information of the radiation workers. However, having employers and each radiation facility separately provide radiation measurement equipment, conduct health examinations, and implement training is burdensome for employers, radiation facilities, and radiation workers themselves. By having either the employer or the radiation facility conduct personal management and sharing the results with the other organization, this inefficiency can be eliminated.
This information sharing has been conducted so far by exchanging paper records by surface mail. In recent years, IT technology has also been used instead of paper documents. [1]

On the other hand, employers who dispatch radiation workers need to know the work content and management status of the radiation facilities where they work in order to ensure their safety. Specifically, this includes an overview of the radiation facility, the types of nuclear materials and radiation used, the expected radiation exposure levels, the types of radiation measurement equipment required (including whether neutron measurement is necessary), internal radiation exposure assessment, and the content of required education and training. Simultaneously, radiation facilities can improve safety at the workplace by knowing what education and training the radiation worker has received from their employer or other radiation facilities. It is important for employers and radiation facilities to share not only the results of radiation exposure measurements and health examinations but also the methods and specific details of these measurements and examinations for safety management purposes.[2] However, to date, such information has not been sufficiently shared yet.

The purpose of this study is to develop an information sharing system for the perosonal management of itinerant workers. This system will allow employers, radiation facilities, and itinerant workers themselves to easily access not only information on radiation exposure doses, health examinations, and the results of safety education and training, but also detailed information on these matters.

2. METHOD

In this system, employers and radiation facilities will be considered separately and registered in the system in advance. An radiation worker who belong to a specific employer submits an application to use a radiation facility where they will work. Each radiation facility pre-registers the information to the system, such as radiation measurements methods, health examinations, and safety training and education which is necessary for those who will work at the facility. These information is called the Personal Management Standard Table. Employers conduct necessary personal management based on this table.

By registering the results of measurements, health examinations, etc., in the system, employers and radiation facilities can access the personal management information of the relevant radiation worker. radiation workers themselves can also access their own information.

Copyright on 7th Asia-Pacific Symposium on Radiochemistry 2025

The Personal Management Standard Table allows PDF files to be attached to provide details of method of radiation exposure measurements, health examinations, and trainings.

3. RESULTS

The system, named MePHISTO, was built on a cloud server and tested at Tohoku University. When an radiation worker submits a usage application, the employer and radiation facility can view the radiation worker's personal records such as radiation exposure measurement results, health examination results, and education and training results, which have been registered in advance. In addition, employers can now refer to the Personal Management Standard Table for each radiation facility, enabling them to understand the necessary management items and details for the radiation worker when using the radiation facility.

4. CONCLUSIONS

We developed an information sharing system for the personal management of itinerant workers. Employers, radiation facilities, and the radiation worker themselves can now easily access radiation exposure doses, health examination results, safety training results, and detailed information. This system is considered useful for the safety management of itinerant workers who work at multiple radiation facilities.

References

[1] FY2021 Nuclear Regulation Authority Radiation Countermeasures Commissioned Expenses (Radiation Safety Regulation Research Strategic Promotion Project Expenses), Radiation Education and Safety Management Network Based on the Isotope Comprehensive Center for the Realization of Sound Radiation Protection: Results Report.
[2] IAEA Safety Standards Series No. GSG-7, Occupational Radiation Protection, General Safety Guide (2018).

Poster Presentation | [P3]Environmental Integrated Knowledge of Radionuclides Dynamics Studied from the Fukushima Accident

Mon. Sep 15, 2025 6:30 PM - 8:00 PM JST | Mon. Sep 15, 2025 9:30 AM - 11:00 AM UTC Poster

[Poster] P3

[P-P3-01*]

Factors controlling dissolved ^{137}Cs activities in Matsukawa-ura lagoon, a semi-closed estuary, after the Fukushima accident

*Takuya Niida[1,2], Hyoe Takata[3], Sho Watanabe[4], Shinya Namura[2], Toshihiro Wada[3] (1. Graduate School of Symbiotic Systems Science and Technology, Fukushima University (Japan), 2. Laboratory for Instrumentation and Analysis, Environmental Engineering Division, KANSO TECHNOS CO., LTD (Japan), 3. Institute of Environmental Radioactivity, Fukushima University (Japan), 4. Fukushima Prefectural Research Institute of Fisheries Resources (Japan))

[P-P3-02*]

OPTIMIZATION OF ^{90}Sr ANALYSIS METHOD FOR THE RESIDUE OF SUSPENDED PARTICULATE MATTER (SPM) SAMPLES AFTER SEPARATION OF ^{129}I

*Shota Morishita[1], Akihito Matsushima[1], Kazuhiko Ninomiya[1] (1. Hiroshima University (Japan))

[P-P3-03]

Cellular effects induced by radiocesium-bearing microparticles (CsMPs)

*Masatoshi Suzuki[1,2], Satoru Endo[3], Kazuhiko Ninomiya[3], Koichi Chida[1], Manabu Fukumoto[1] (1. Tohoku University (Japan), 2. Fukushima Institute for Research, Education and Innovation (Japan), 3. Hiroshima University (Japan))

[P-P3-04]

Fukushima Daiichi NPP-derived radiocesium concentrations in the off-southern Hokkaido, Japan in 2018-2019

*Yuhei Shirotani[1], Shota Kambayashi[1], Naoko Murakami Sugihara[1], Mutsuo Inoue[2] (1. MARINE ECOLOGY RESEARCH INSTITUTE (Japan), 2. Kanazawa University (Japan))

[P-P3-05*]

Comparative Analysis of Canopy Characteristics and Their Influence on ^{137} Cs Migration in Different Fukushima Forest Plots

*Hao Wang[1] (1. University Of Tsukuba (Japan))

[P-P3-06]

Uptake and Elimination of Radiocesium-137 in the Wild Silkmoth *Antheraea yamamai*

*Yusuke YOSHIDA[1], Masaomi TAKAHASHI[1], Akihiro Tohsaki[1], Toshimasa MITAMURA[2], Zenta KAJIURA[3], Risako OHARA[1], Takayuki HONDA[4], Toru TAKAHASHI[4], Satoshi INOSE[4] (1. The University of Osaka (Japan), 2. Fukushima university (Japan), 3. Shinshu University (Japan), 4. Meiji University (Japan))

[P-P3-07]

How the hillslope groundwater discharge controls the dissolved radiocesium concentration of surface water in a forest headwater catchment

*Hiroaki Kato[1], Hiroki Nakada[1], Yuma Niwano[1], Yuichi Onda[1] (1. Center for Research in Radiation, Isotopes, and Earth System Sciences (Japan))

©APSORC25

7th Asia-Pacific Symposium on Radiochemistry *September 14 ~ 19, 2025 • Kunibiki Messe • Shimane, Japan*

Factors controlling dissolved ^{137}Cs activities in Matsukawa-ura lagoon, a semi-closed estuary, after the Fukushima accident

Takuya Niida[1,2], Hyoe Takata[3], Sho Watanabe[4], Shinya Namura[2], Toshihiro Wada[3]

[1] *Graduate School of Symbiotic Systems Science and Technology, Fukushima University, 1 Kanayagawa, Fukushima City, Fukushima 960-1296, Japan, s2571005@ipc.fukushima-u.ac.jp*
[2] *Laboratory for Instrumentation and Analysis, Environmental Engineering Division, KANSO TECHNOS CO., LTD, 3-1-1, Higashikuraji, Katano City, Osaka 576-0061, Japan, niida_takuya@kanso.co.jp*
[3] *Institute of Environmental Radioactivity, Fukushima University, 1 Kanayagawa, Fukushima City, Fukushima 960-1296, Japan*
[4] *Fukushima Prefectural Research Institute of Fisheries Resources, 1-1-14 Koyo, Soma City, Fukushima 970-0005, Japan*

Abstract- The spatial and seasonal dynamics of ^{137}Cs were investigated from 2021 to 2023 in Matsukawa-ura lagoon, a semi-closed estuarine area approximately 40 km north of the Fukushima Daiichi Nuclear Power Plant, Japan. Mass balance calculation suggests that the dissolution of ^{137}Cs from bottom sediments sustained the high dissolved ^{137}Cs concentrations in the estuarine water. Furthermore, dissolved ^{137}Cs concentrations in the lagoon were higher in summer (July) than in winter (February). Quantification of the source revealed that dissolution caused ^{137}Cs concentrations in bottom sediments to decrease by more than 2.4% over 30 days in July, but only by <0.8% over 30 days in February. This finding indicates that warmer waters during the summer accelerate the dissolution of ^{137}Cs from bottom sediments.

1 INTRODUCTION

14 years have passed since the Fukushima Daiichi Nuclear Power Plant (FDNPP) accident on March 11, 2011. Currently, the dissolved ^{137}Cs activity concentration in seawater more than 30 km offshore Fukushima has returned to pre-accident levels, whereas that in coastal waters of Fukushima Prefecture remains above pre-accident levels. Potential sources of dissolved ^{137}Cs in Fukushima coastal waters include direct inflow from the FDNPP, leaching from bottom sediments, and inflow from rivers. However, the completion of impermeable seaside wall in 2016 may have recently limited direct inflow from the FDNPP. On the other hand, previous studies suggest that the leaching of radioactive Cs from bottom sediments to pore water is a ^{137}Cs source in coastal areas. Additionally, studies on rivers have reported that changes in water temperature change the apparent distribution coefficient between dissolved ^{137}Cs and particulate-bound ^{137}Cs, and that in estuaries, particulate-bound ^{137}Cs is desorbed from the particles due to competition with cations such as K^+ and NH_4^+. The relationships between water temperature and dissolved ^{137}Cs concentration in river water and between salinity and dissolved ^{137}Cs in seawater are often discussed, but those in estuarine areas have not been sufficiently addressed. One of the reasons for this is that the dissolved ^{137}Cs transported from land and leached from sediments is immediately diluted and dispersed into large amounts of seawater, making quantitative assessments challenging. However, in semi-closed estuarine areas, quantification is possible by investigating the distribution of ^{137}Cs.

The aim of this study was to investigate the distribution of ^{137}Cs in a semi-closed estuarine area and inflowing rivers in turn allowing us to evaluate the contribution of ^{137}Cs supplied by rivers to estuarine areas, the relationships with salinity and water temperature, and the contribution of dissolution of ^{137}Cs from bottom sediments.

2 MATERIAL AND METHODS

Matsukawa-ura lagoon is a semi-closed estuarine area with an extent of 6.48 km^2 with fluctuating salinity and water temperature conditions and Four rivers flow into Matsukawa-ura lagoon. In this study, we conducted 11 samplings from June 2021 to February 2023 at 13 sites including downstream sites in the four rivers, sites at the mouths of three rivers, five sites within the lagoon (from the southeast to near the lagoon mouth in the north), and a site 800 m offshore along the outer coast of the lagoon. After filtering each water sample, the dissolved and particulate ^{137}Cs concentrations were measured using Ge semiconductor detectors.

3 RESULTS AND DISCUSSION

Time-dependent changes in dissolved ^{137}Cs concentrations in the lagoon are shown in Figure 1a, and the relationship between dissolved ^{137}Cs concentration and water temperature is shown in Figure 1b. Lagoon-wide weighted means dissolved ^{137}Cs concentrations were calculated from the sampling sites using Voronoi partitioning, taking the area of each Voronoi cell as the weight during averaging by area ratio. The dissolved ^{137}Cs concentration in the lagoon tended to be

higher in the summer and lower in the winter (Figure 1a) and showed a significant correlation with water temperature (Figure 1b). Previous studies have revealed that water temperature influences the adsorption and desorption of ^{137}Cs between solutions and particles with high affinities, such as clay minerals having "frayed-edge-sites" (FeS).

The results of the mass balance calculation are shown in Table 1. As a result, 3.4–121 MBq/12 h of dissolved ^{137}Cs was added to the lagoon. However, the fluxes of dissolved and desorbed ^{137}Cs from the river were 0.03–1.23 MBq/12 h and 0.003–0.077 MBq/12 h, respectively, which cannot be explained by the supply from the rivers alone. Therefore, the supply of dissolved ^{137}Cs from seabed sediments must be much greater than that from rivers. Arita et al. (2014) estimated the inventory of ^{137}Cs concentrations in the bottom sediments of the lagoon and the total accumulation of ^{137}Cs in the top 20 cm of sediment to be 220 GBq as of 2013. Quantification of the source revealed that the ^{137}Cs concentration in bottom sediments decreased via dissolution by more than 2.4% in 30 days in July, and by only <0.8% in the same period in February. Thus, we infer that warmer water temperatures during the summer may accelerate the dissolution of ^{137}Cs from bottom sediments. This finding indicates that warmer waters during the summer accelerate the dissolution of ^{137}Cs from bottom sediments.

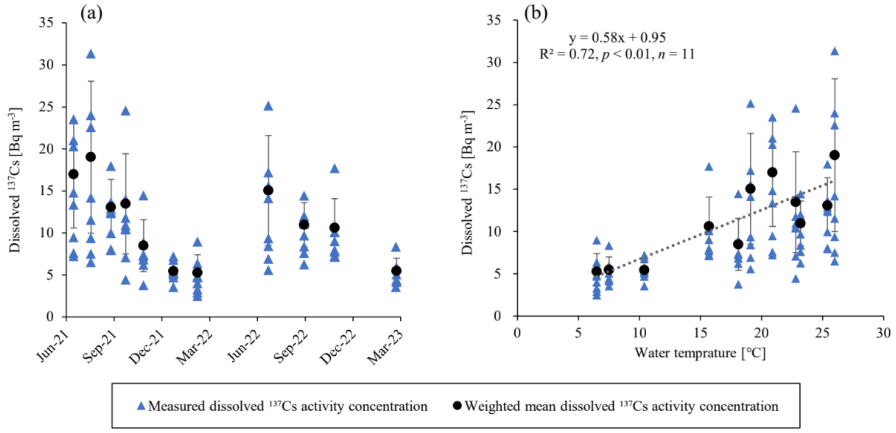


Fig. 1. (a) Temporal variations of dissolved ^{137}Cs concentrations and (b) water temperature versus dissolved ^{137}Cs concentrations in Matsukawa-ura lagoon from June 2021 to February 2023. Black bars represent the standard deviation of the dissolved ^{137}Cs concentrations on each sampling date.

TABLE 1. Mass balance of dissolved ^{137}Cs in Matsukawa-ura lagoon.

	Input of seawater	Mean dissolved ^{137}Cs in lagoon	Flux of riverine dissolved ^{137}Cs	Desorb fraction of riverine particulate ^{137}Cs	Estimated flux of ^{137}Cs desorbed from bottom sediment	Dissolution rate of ^{137}Cs from bottom sediment
	Mm^3/12 h	Bq m^{-3}	MBq/12 h	MBq/12 h	MBq/12 h	%/30 days
Jul-21	7.2	19.0	0.61	0.060	102-120	3.3-3.9
Aug-21	7.2	13.1	1.23	0.077	58-77	1.9-2.5
Feb-22	7.2	5.3	0.03	0.0031	3.3-22	0.1-0.7

ACKNOWLEDGMENTS

This research was funded by an advanced technology deployment project in the agriculture, forestry and fisheries sector of Fukushima Institute for Research, Education and Innovation (F-REI) (JPFR25060109).

References

[1] Arita, K.; Yabe, T.; Hayashi, S. Actual situation of concentration and inventory of radioactive cesium in Matsukawa-ura Lagoon sediment, Fukushima Prefecture. *J. Jpn. Soc. Civ. Eng.Ser. G (Environ. Res.)*. **2014**, 70, III_225–III_231 (in Japanese with English abstract).

[2] Kamo, T.; Suzuki, M.; Wada, T.; Iwasaki, T.; Watanabe, T.; Nishi, R.; Tsurunari, Y. Estimation of freshwater discharge and field observation on aquatic environment around the entrance of Matsukawaura inlet. *J. Jpn. Soc. Civ. Eng. Ser. B3 Ocean. Eng*. **2014**, 70, I_1020–I_1025 (in Japanese with English abstract).

[3] Takata, H.; Wakiyama, Y.; Niida, T.; Igarashi, Y.; Konoplev, A.; Inatomi, N. Importance of desorption process from Abukuma River's suspended particles in increasing dissolved 137Cs in coastal water during river-flood caused by typhoons. *Chemosphere*. **2021**, 281, 130751.

7th Asia-Pacific Symposium on Radiochemistry *September 14 ~ 19, 2025 • Kunibiki Messe • Shimane, Japan*

OPTIMIZATION OF ^{90}Sr ANALYSIS METHOD FOR THE RESIDUE OF SUSPENDED PARTICULATE MATTER (SPM) SAMPLES AFTER SEPARATION OF ^{129}I

Shota Morishita[1], Akihito Matsushima[1], Kazuhiko Ninomiya[1]

[1]*Graduate School of Advanced Science and Engineering Hiroshima University: 1-3-2 Kagamiyama, Higasihiroshima-shi, Hiroshima 739-0046, Japan, m253250@hiroshima-u.ac.jp*

The analysis of time-series of ^{90}Sr emission by the accident of Fukushima Daiichi Nuclear accident provides us the information of the temperature conditions in the reactor. This study focuses on the suspended particulate matter (SPM) filter samples collected just after the accident and developed a procedure to analyze strontium-90 (^{90}Sr) in residue of SPM samples after separation of ^{129}I. The analysis method using solid-state extraction and β-ray measurement by a 2π gas-flow proportional counter was optimized and the reproducibility of the analytical method was confirmed.

1 INTRODUCTION

After the Great East Japan Earthquake on March 11, 2011, a nuclear disaster occurred at the Fukushima Daiichi Nuclear Power Plant, releasing a large amount of radioactive materials into the environment. Long-lived radio nuclides such as ^{137}Cs and ^{90}Sr emitted by the accident still remain in the environment. Although the distribution of radionuclides has been investigated through soil sample measurements, this method only provides integrated values of several radionuclides deposition events in the soil and it is difficult to resolve a time-series analysis of each deposition event.

Experimental studies on the time-series transportion of radionuclides related to Fukushima accident are limited, because air sample analysis taken at the time of release is essential for these studies. Whereas, some studies have been conducted for analyzing radionuclides in suspended particulate matter (SPM) samples collected hourly and regularly by the Japanese air quality monitoring network in eastern Japan [1,2]. These analyses have reported the spherical and temporal variations of radiocesium (^{134}Cs and ^{137}Cs) and radioiodine (^{129}I) in the air.

Here, we focused on ^{90}Sr in the SPM samples. Since ^{90}Sr is not volatile element having a high boiling point compare to radiocesium, its time-series variation may provide information of the temperature conditions in the reactor at the accident. In this study, ^{90}Sr analysis method was developed to quantify ^{90}Sr from the residues of the SPM samples after ^{129}I analysis.

2 EXPERIMENTAL

The analytical method of ^{90}Sr was examined using a soil sample collected in Fukushima Prefecture as a simulated sample of the residue of SPM filter. The soil samples were analyzed using the following procedure. First, a stable strontium isotope was added to the soil as a carrier and strontium ions were extracted with concentrated nitric acid with heating 8 hours. After heating, the soil residue was separated by spontaneous filtration. The solution passed through a strontium resin (Eichrom Technologies) to remove cesium and other interfering elements and strontium fraction with volume of 15 mL was obtained [5]. By adding ammonium carbonate, strontium was collected as a precipitation of strontium carbonate. The precipitation sample was set to a 2π gas-flow proportional counter to β-ray measurement with dilations of 180 min for approximately two weeks to observe the growth of ^{90}Y from ^{90}Sr. Chemical yields were determined by ICP-OES, using aliquots taken before and after the chemical analysis. To verify the reproducibility of the analytical method, the Sr analysis was performed five times under the same conditions.

3 RESULTS AND DISCUSSION

Figure 1 shows the γ-ray spectrum of the soil sample. From the intensity of 661 keV γ-ray, the radioactivity of cesium in the soil was determined as 43.4 Bq/g.

The results of the β-ray measurement using 2π gas-flow proportional counter are shown in Figure 2. The growth curve reaches a saturated value by two-weeks measurement. The growth curve was well fitted by assuming radioactive equilibrium between ^{90}Sr and ^{90}Y that ^{90}Sr have been successfully isolated by the analysis. The chemical yields were determined using the calibration curve method with ICP-OES, and were obtained 88.6 ± 2.2% in average value of 5 time experiments.

The average radioactivity of ^{90}Sr from these measurements was determined to be 0.247 ± 0.044 Bq/g at March 2011. The ^{90}Sr/^{137}Cs ratio in the soil samples was calculated to be 0.00404 ± 0.00078, which is consistent with values reported in previous soil analyses in Fukushima prefecture [3,4].

Copyright on 7th Asia-Pacific Symposium on Radiochemistry 2025

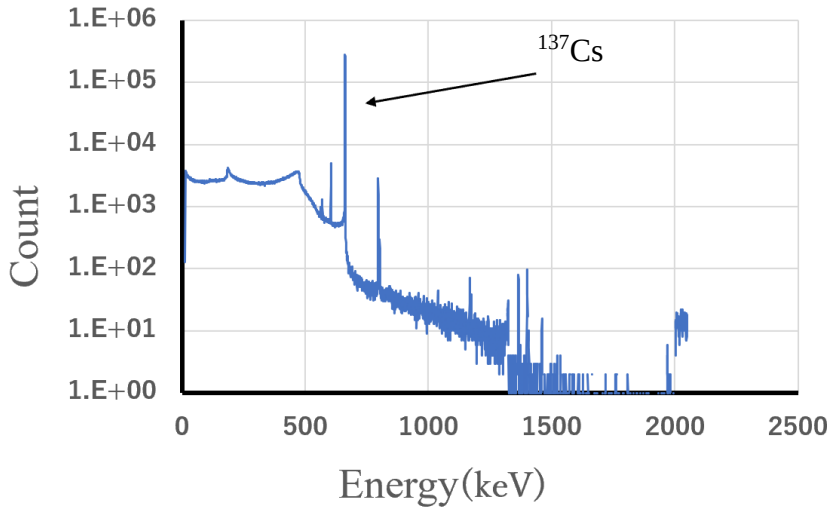


Fig1. Results of γ ray measurement (Soil amount 14.08g, measurement time 24 hours)

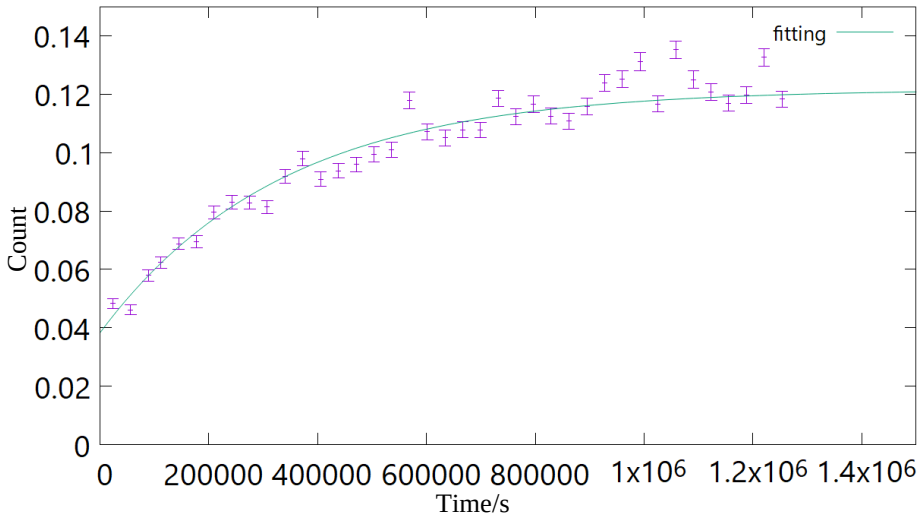


Fig 2. Results of β ray measurement

REFERENCES

[1] Mitsuru Ebihara, Naoki Shirai, Yasuji Oura, Haruo Tsuruta, Hiroyuki Matsuzaki, Yuichi Moriguchi, "Time-series variations in ^{129}I concentrations and ^{129}I/^{137}Cs ratios in suspended particulate matter collected in eastern Japan immediately after the 2011 nuclear accident in Fukushima, Japan," *Journal of Environmental Radioactivity*, 250, 106907, 2022

[2] Mitsuru Ebihara, Naoki Shirai, Yasuji Oura, Haruo Tsuruta, Hiroyuki Matsuzaki, Yuichi Moriguchi, "Detailed deposition density maps constructed by large-scale soil sampling for gamma-ray emitting radioactive nuclides from the Fukushima Dai-ichi Nuclear Power Plant accident," *Journal of Environmental Radioactivity*, 139, 308-319, 2015

[3] Mishra S, Sahoo SK, Arae H, Watanabe Y and Mietelski JW, "Activity Ratio of Caesium, Strontium and Uranium with Site Specific Distribution Coefficients in Contaminated Soil near Vicinity of Fukushima Daiichi Nuclear Power Plant," *Journal of Chromatography & Separation Techniques*, 5, 250, 2014

[4] Sarata Kumar Sahoo, Norbert Kavasi, Atsuyuki Sorimachi, Hideki Arae, Shinji Tokonami, Jerzy Wojciech Mietelski, Edyta Lokas, Satoshi Yoshida, "Strontium-90 activity concentration in soil samples from the exclusion zone of the Fukushima daiichi nuclear power plant," *Scientific Reports*, 6, 23925, 2016

[5] Sherrod L. Maxwell, Brian K. Culligan&Patrick J. Shaw, "Rapid determination of radiostrontium in large soil samples," *Jaurnal of Radioanalytical and Nuclear Chemistry*, 295, 965-971, 2013

Copyright on 7th Asia-Pacific Symposium on Radiochemistry 2025 P-P3-02* -

CELLULAR EFFECTS INDUCED BY RADIOCESIM-BEARING MICROPARTICLES (CsMPs)

Masatoshi Suzuki[1,2,3], Satoru Endo[4], Kazuhiko Ninomiya[5], Koichi Chida[6,7], Manabu Fukumoto[8]

[1]*International Research Institute of Disaster Science, Tohoku University: 519-1176 Aramaki-aza-Aoba, Aoba-ku, Sendai 980-0845, Japan, masatoshi.suzuki.c7@tohoku.ac.jp*
[2]*Regional Environmental Co-Creation Unit, Fukushima Institute for Research, Education and Innovation: 519-1176 Aramaki-aza-Aoba, Aoba-ku, Sendai 980-8572, Japan, masatoshi.suzuki.z5f@research.f-rei.go.jp*
[3]*Course of Radiological Technology, Tohoku University Graduate School of Medicine, 519-1176 Aramaki-aza-Aoba, Aoba-ku, Sendai 980-0845, Japan, masatoshi.suzuki.c7@tohoku.ac.jp*
[4]*Graduate School of Advanced Science and Engineering, Hiroshima University: 1-4-1 Kagamiyama, Higashi-Hiroshima 739-8527, Japan, endos@hiroshima-u.ac.jp*
[5]*Natural Science Center for Basic Research and Development, Hiroshima University: 1-4-2 Kagamiyama, Higashi-Hiroshima-shi 739-8526, Japan, ninomiya-kazu@hiroshima-u.ac.jp*
[6]*International Research Institute of Disaster Science, Tohoku University: 2-1 Seiryo-machi, Aoba-ku, Sendai 980-8575, Japan, koichi.chida.d8@tohoku.ac.jp*
[7]*Course of Radiological Technology, Tohoku University Graduate School of Medicine: 2-1 Seiryo-machi, Aoba-ku, Sendai 980-8575, Japan, koichi.chida.d8@tohoku.ac.jp*
[8]*International Research Institute of Disaster Science, Tohoku University: 519-1176 Aramaki-aza-Aoba, Aoba-ku, Sendai 980-0845, Japan, manabu.fukumoto.a8@tohoku.ac.jp*

1 Introduction

Radioactive particles, so called radiocesium-bearing microparticles (CsMPs), were found in the environment following the Fukushima Daiichi nuclear power plant (FNPP) accident [1,2]. Radioactive particles are expected to enter the body from the environment mainly by inhalation and be deposited in the respiratory tract. The insoluble particles will remain in the body longer than the water-soluble form, contributing to prolonged internal exposure. The physicochemical properties of CsMPs are completely different from those of nuclear fuel fragments. Concentrated radiocesium is the primary source of radiation emitted by CsMPs, but the range of radioactivity possessed by CsMPs is wide. Type A and Type B of CsMPs contain a radioactivity of less than 10 Bq and tens to more than 1 kBq, respectively [3]. In addition, the dose rates in the vicinity of CsMPs are not uniform. Nuclear fuel fragments generated by the accident of Chernobyl nuclear power plant highlighted the hot particle problem, which are more likely to induce biological effects than exposure with a uniform dose-rate distribution [4]. In order to determine cellular effects of CsMPs, we investigated the radiation effects on the induction of DNA double-strand breaks (DSBs) and gene expression in cells co-incubated with CsMPs collected from the soil of Fukushima Prefecture.

2. Materials and methods

Three CsMPs (CsMP-1, -2 and -3), kindly provided by Drs. Sueki and Satou (Tsukuba University, Japan), were isolated from soil collected in the ex-evacuation zone set within a 20-km radius of FNPP. Normal human epithelial cells (RPE1-hTERT) were co-incubated with each three CsMPs. Non-uniform dose-rate distribution was calculated by Monte Carlo simulation with particle and heavy ion transport system (PHITS) code. DSBs were detected in the cells co-incubated with CsMPs for 24 and 72 h and were quantified with the molecular markers of phosphorylated H2AX colocalized with 53BP1. Alteration of gene expression was investigated with the cells co-incubated with a CsMP-1 for 24 h.

3. Results and Discussion

CsMP-1 and -2, but not -3, induced DSBs in the cells located within 1 cm of a CsMP. The induction of DSBs was more effective when the cells were close to a CsMP and when they were co-incubated for a longer time. The number of induced DSBs depended on the radioactivity in CsMPs. No induction of DSBs was observed when the cells were co-incubated with non-radioactive mock particle, indicating that radiation causes DSBs-induction by CsMPs. Monte Carlo simulation evaluated the dose-rate distribution in the area surrounding a CsMP and showed a non-uniform gradation consisting of middle- and low-dose rate. The dose-rate at 1 cm apart from both CsMP-1 and -2 was lower than that at adjacent to CsMP-3, but CsMP-3 did not induce DSBs, although CsMP-1 and -2 were induced in cells in the region with the lower dose-rate.

Copyright on 7th Asia-Pacific Symposium on Radiochemistry 2025

CsMP-1 induced cell death such as the irreversible growth arrest with the phenotype of cellular senescence (senescence-like growth arrest, SLGA) in the adjacent cells. By contrast, the cells away from a CsMP-1 maintained their cell growth. CsMP-1 also altered the gene expression of interferon-stimulated genes (ISGs) due to the radiation emitted by a CsMP-1. ISGs has a function to influence inflammatory response and stress tolerance. Because CsMP-1 induced DSBs in the cells away from a CsMP-1 and these cells maintained the cell growth, stress tolerance-related factors which were activated by the co-incubation with CsMP-1 might be associated with cell growth with DSBs.

4. Conclusion

Here, we investigated cellular effects with CsMPs from environmental samples generated by the FNPP accident. Non-uniform dose-rate distribution may lead to bystander effects, whereby secreted factors derived from cells in which premature senescence is induced by radiation emitted from CsMP-1 may confer an advantage for mutation and cell proliferation to cells away from the CsMP. Based on our findings, animal experiments are needed to clarify whether inhalation of CsMPs affects health impact such as respiratory extra-thoracic cancer or not. Importantly, this study also suggests that type A particles are not carcinogenic.

ACKNOWLEDGMENTS

This work was supported by Research Project on the Health Effects of Radiation organized by Ministry of the Environment, Japan.

References

[1] K. Adachi, M. Kajino, Y. Igarashi, “Emission of spherical cesium-bearing particles from an early stage of the Fukushima nuclear accident.” Sci Rep, **3**, 2554 (2013).
[2] K. Ninomiya, Low-dose radiation effects on animals and ecosystems., pp. 195-204. M. Fukumoto, Ed., Springer Nature, Singapore (2020).
[3] Y. Igarashi, T. Kogure, Y. Kurihara, H. Miura, T. Okumura, Y. Satou, et al. “A review of Cs-bearing microparticles in the environment emitted by the Fukushima Dai-ichi Nuclear Power Plant accident.” J Environ Radioact. **205-206**, 101-18 (2019).
[4] M.W. Charles, A.J. Mill, P.J. Darley, “Carcinogenic risk of hot-particle exposures.” J. Radiol. Prot., **23**, 5-28 (2003).

Fukushima Daiichi NPP-derived radiocesium concentrations in the off-southern Hokkaido, Japan in 2018-2019

Yuhei SHIROTANI[1,2], Shota KAMBAYASHI[1], Naoko MURAKAMI-SUGIHARA[1], Mutsuo INOUE[2]

[1]*Central Laboratory, Marine Ecology Research Institute (MERI), 300 Iwawada, Onjuku, Isumi, Chiba, 299-5105, Japan*
[2]*Low Level Radioactivity Laboratory, Kanazawa University, Nomi, Ishikawa 923-1224, Japan*

In this study, we examined the temporal variation of the concentrations of the Fukushima Daiichi Nuclear Power Plant (FDNPP) accident-derived radiocesium in the off-southern Hokkaido, Japan (2018-2019). Combining with ^{226}Ra and ^{228}Ra data, we discussed radiocesium transported patterns in this complicated current area.

1. Introduction

A large amount of radiocesium was released into the northwestern North Pacific Ocean as a result of the FDNPP accident. ^{134}Cs and ^{137}Cs in seawater were transported over the North Pacific Ocean by water current systems [1,2]. The concentrations of the FDNPP-derived radiocesium increased in Japan Sea in 2013 and in the Bering Sea in 2017-2018 [3-5]. This is plausibly ascribed to the transport around Japan Islands along with the subtropical and subarctic currents, such as the Kuroshio Warm Current and the East Kamchatka Current-Oyashio Current, respectively. In this study, we discussed the transport systems of radiocesium in the off-southern Hokkaido, using salinity, ^{226}Ra and ^{228}Ra in 2018-2019.

2. Seawater samples and methods

Seawater sampling locations are shown in Fig. 1. In June 2018, six samples were collected at sites K2 and E11: 1 m, 250 m, 750 m, 1000 m, 1250 m at the depths, and bottom layer (10-20 m above the seafloor). In June 2019, six samples were also collected at sites K2 and E11 and surface seawater (1 m) at site T2. In October 2019, six samples were collected at site E11 and surface seawater at site T2.

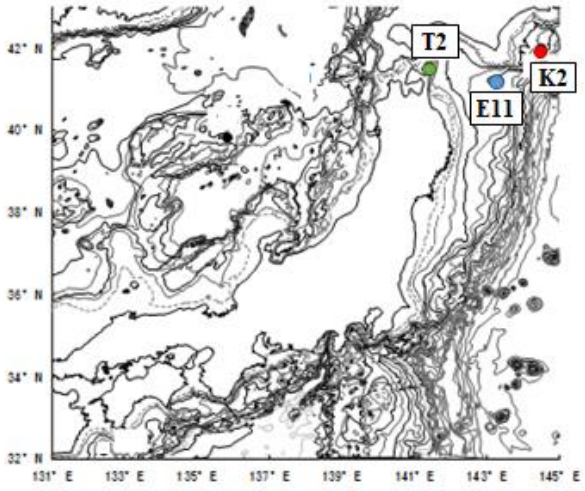


Fig. 1. Sampling Location in the off-southern Hokkaido

^{134}Cs and ^{137}Cs were collected from seawater with ammonium phosphomolybdate (AMP/Cs), and ^{226}Ra and ^{228}Ra were by barium sulfate coprecipitation methods. Low-background γ-spectrometry was conducted to all the AMP/Cs and $BaSO_4$ samples, using Ge detectors completely shielded in the Ogoya Underground Laboratory.

3. Result and discussion

Salinity and ^{228}Ra concentrations at the surface of sites K2, E11, and T2 showed wide variations (32.64-34.61 and 0.09-1.50 mBq/L, respectively) (Fig. 2). This was explained by the mixing of the Tsugaru Warm Current from the Japan Sea, the Soya Warm Current, East Sakhalin Current, and Okhotsk Sea surface water from the Okhotsk Sea, and the Oyashio Current and Kuroshio Warm Current in the Pacific Ocean. The surface ^{134}Cs concentrations corrected radioactive-decay to the FDNPP accident date were from “not detected” to 1 mBq/L. Based on the water masses from salinity and ^{228}Ra concentrations, we discuss the current system of the FDNPP-derived radiocesium in this area, particularly the upstream currents at each site.

Copyright on 7th Asia-Pacific Symposium on Radiochemistry 2025

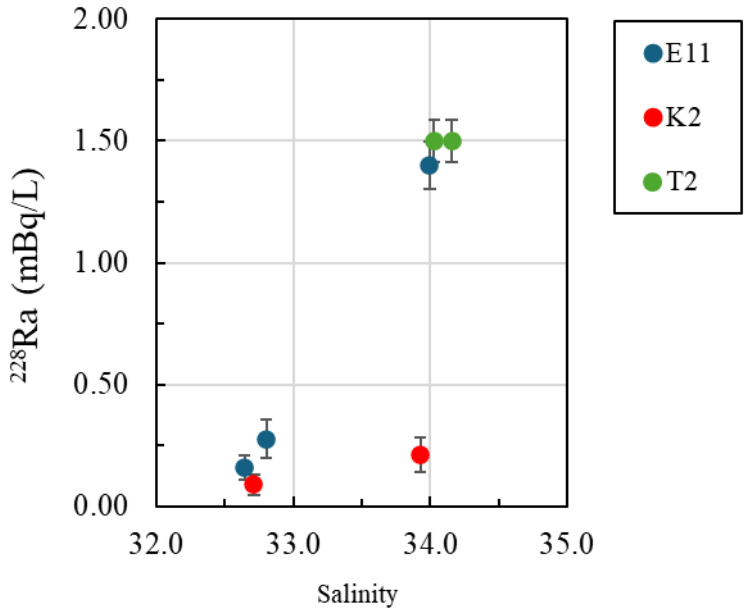


Fig. 2. Relationship between salinity and ^{228}Ra concentrations in surface seawater samples.

ACKNOWLEDGMENTS

The data presented here were obtained during 35 years in a monitoring program, which was initially under contract with the Ministry of Education, Culture, Sports, Science and Technology (1984–2013) and is presently done under the Secretariat of the Nuclear Regulation Authority (2013-present). The authors would like to thank the staff of MERI for helpful discussions and technical assistance. Also, this study was performed under the cooperative research program of Institute of Nature and Environmental Technology, Kanazawa University ＜21041＞.

References

[1] Smith, J. N., Rossi, V., Buesseler, K. O., Cullen, J. T., Cornett, J., Nelson, R., Macdonald, A.M., Robert, M. & Kellogg, J. (2017). Recent transport history of Fukushima radioactivity in the Northeast Pacific Ocean. Environmental science & technology, 51(18), 10494-10502.

[2] Aoyama, M., Hamajima, Y., Inomata, Y., Kumamoto, Y., Oka, E., Tsubono, T., & Tsumune, D. (2018). Radiocaesium derived from the TEPCO Fukushima accident in the North Pacific Ocean: Surface transport processes until 2017. Journal of Environmental Radioactivity, 189, 93-102.

[3] Kumamoto, Y., Aoyama, M., Hamajima, Y., Nishino, S., Murata, A., & Kikuchi, T. (2019). Radiocesium in the western subarctic area of the North Pacific Ocean, Bering Sea, and Arctic Ocean in 2015 and 2017. *Polar Science*, *21*, 228-232.

[4] Inoue, M., Takehara, R., Hanaki, S., Kameyama, H., Nishioka, J., & Nagao, S. (2020). Distributions of radiocesium and radium isotopes in the western Bering Sea in 2018. *Marine Chemistry*, *225*, 103843.

[5] Huang, D., Lin, J., Du, J., & Yu, T. (2020). The detection of Fukushima-derived radiocesium in the Bering Sea and Arctic Ocean six years after the nuclear accident. *Environmental Pollution*, *256*, 113386.

Copyright on 7th Asia-Pacific Symposium on Radiochemistry 2025

7th Asia-Pacific Symposium on Radiochemistry *September 14 ~ 19, 2025 • Kunibiki Messe • Shimane, Japan*

Comparative Analysis of Canopy Characteristics and Their Influence on ^{137}Cs Migration in Different Fukushima Forest Plots

Hao Wang[1], Onda Yuichi[1], Kato Hiroaki[1]

[1] *University of Tsukuba: 1-1-1 Tennodai, Tsukuba-shi, Ibaraki-ken, 305-8577, Japan, S2421150@u.tsukuba.ac.jp*

Following the Fukushima Daiichi nuclear power plant accident, approximately 2.5 PBq of Cesium-137 (^{137}Cs) was deposited in forested regions, with roughly 2,600 km² receiving over 100 kBq/m². In Fukushima, particularly within cedar plantation forests, 60–90% of deposited ^{137}Cs was intercepted by the tree canopy. Previous studies have documented the gradual migration of ^{137}Cs from the canopy to the forest floor. However, these studies typically focus on plot-level trends, often overlooking spatial variability within the canopy itself. Our study aiming to clarify the relationship between canopy characteristics and the distribution of ^{137}Cs within forest ecosystems. Furthermore, we extended our analysis by comparing different forest plots, thereby evaluating how variations in canopy structures influence the distribution and migration of ^{137}Cs across diverse forest conditions.

1 Study Site and Data Collection

The study was conducted primarily at forest plots located in Namie(NC plot)and Yamakiya(MC and YC plot) in Fukushima Prefecture, dominated by cedar plantation forests. LiDAR data were collected using terrestrial laser scanning (TLS) methods. Additionally, concentrations of ^{137}Cs in throughfall (TF), stemflow (SF), and litterfall (LF) were measured approximately once per month to evaluate radiocesium migration.

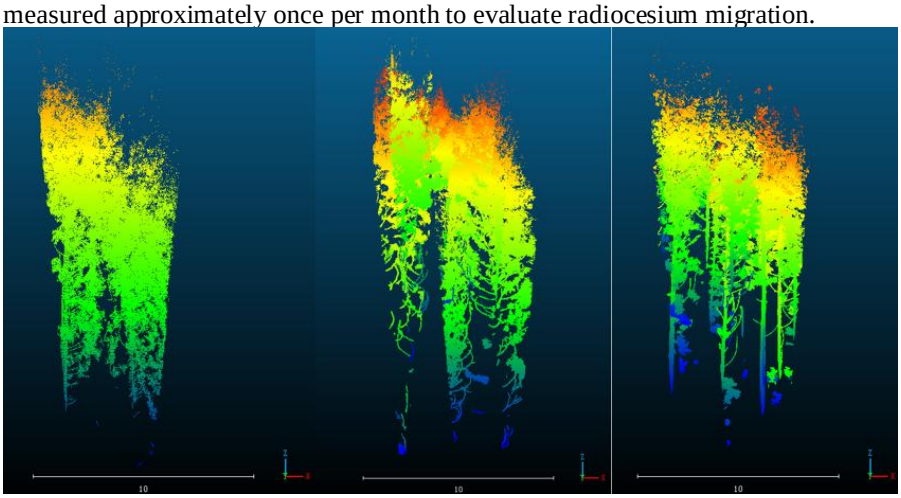


Fig1 Locations of Throughfall Samplers and the point cloud within their corresponding conical effective impact zones(MC YC NC)

Data Processing and Analysis

To assess spatial variability in canopy influence, we first calculated the spatial coefficient of variation (Cv).This analysis confirmed notable spatial heterogeneity in canopy interception within the forest. Subsequently, we quantified canopy structure using a voxel-based approach. The total canopy volume V
V was calculated based on the voxelized point cloud data using the following equation:

$$V = N \times W_{voxel} \times L_{voxel} \times H_{voxel}$$

V is the total volume of the object (m^3),
N is the number of voxels occupied by points, and
$W_{voxel} L_{voxel} H_{voxel}$ represent the width, length, and height of each voxel (m), respectively.

Table1. Canopy information above 3 plots, include number of voxels (5 X 5 X 5 cm), volume, normalized volume

Copyright on 7th Asia-Pacific Symposium on Radiochemistry 2025

	Number of points N(pts)	Volume V m^3	Normalized Volume Vn(m^3/m^2)
NACE	205046	25.631	68.02
MC	310151	38.769	176.38
YC	187970	23.496	106.90

2 CONCLUSIONS.

At the NC plot, the initial deposition of ^{137}Cs was significantly higher than that at both MC and YC, making it the most heavily contaminated of the three plots. Although the canopy volume at NC is smaller than that of MC, it is noticeably larger than that of YC, representing a forest with intermediate canopy density. In terms of rainfall interception, the throughfall ratio at NC also falls between that of MC and YC: compared to MC, the sparser canopy at NC allows more rainfall to reach the forest floor, while compared to YC, its denser canopy enhances interception.

The trend observed at NC is similar to that of MC, showing a negative correlation between canopy volume and throughfall ratio. However, this relationship is more pronounced under high-intensity rainfall events.

Regarding 137Cs migration, despite the smaller canopy volume compared to MC, the higher initial fallout at NC results in consistently elevated 137Cs activity levels in the forest. Notably, vertical heterogeneity in ^{137}Cs distribution is evident at the NC plot: part of the radiocesium likely remains within the canopy, while another portion has been transferred to the forest floor via litterfall and throughfall. In contrast, ^{137}Cs at MC tends to accumulate more stably within the canopy and litter layer, whereas at YC, the sparser canopy may facilitate greater leaching and downward migration of radiocesium.

Additionally, I found that although ^{137}Cs concentrations in the MC canopy have dropped to low, quasi-steady levels, the proportion of ^{137}Cs transferred via throughfall (TF) still rises markedly in years with exceptionally high rainfall—namely 2021 and 2024. By contrast, in other years the transfer is dominated by litterfall (LF), which typically accounts for more than 50 % of the annual flux. These observations imply that intense rainfall events can temporarily activate resuspension or leaching at the canopy–rain interface, causing pulse releases of ^{137}Cs to the forest floor even when overall canopy levels appear stable, whereas under normal rainfall conditions litterfall remains the principal pathway delivering ^{137}Cs to the soil.

At Mc larger canopy tends to amplify the initial wash-off flux of ^{137}Cs per unit of fallout, yet it also lengthens the radionuclide's residence time within the combined canopy–litter compartment. At YC, the open canopy allowed a rapid pulse of ^{137}Cs export in the first few post-accident years, after which concentrations stabilised at low, weakly variable levels. At NC, the intermediate-density canopy and a thick litter layer sequestered much of the fallout early on; consequently, the normalised ^{137}Cs concentrations in throughfall soon became the lowest of the three plots, and subsequent wash-off remained only a minor component of the overall flux—even during heavy-rainfall years. These patterns underscore that canopy architecture governs the timing and magnitude of radionuclide transfer, while the well-developed litter layer at NC acts as a long-term sink that curbs secondary mobilisation.

ACKNOWLEDGMENTS

I would like to express my sincere gratitude to Prof. Onda and Prof. Kato for their invaluable guidance and support throughout this research. Special thanks also go to all members of the laboratory for their kind assistance and encouragement..

References

[1] T. E. Link, M. Unsworth, and D. Marks, "The dynamics of rainfall interception by a seasonal temperate rainforest," *Agric. For. Meteorol.*, **124**, 171 (2004).
[2] Y. Onda, K. Taniguchi, K. Yoshimura, H. Kato, J. Takahashi, Y. Wakiyama, F. Coppin, and H. Smith, "Radionuclides from the Fukushima Daiichi Nuclear Power Plant in terrestrial systems," *Nat. Rev. Earth Environ.*, **1**, 644 (2020).
[3] H. Kato, Y. Onda, K. Hisadome, N. Loffredo, and A. Kawamori, "Temporal changes in radiocesium deposition in various forest stands following the Fukushima Dai-ichi Nuclear Power Plant accident," *J. Environ. Radioact.*, **166**, 449 (2017).
[4] Y. Zhang, H. Wang, Y. Onda, Y. Tan, and H. Kato, "LiDAR-derived canopy structure explains 137Cs concentrations in throughfall in Fukushima plantation forest," *Environ. Pollut.*, **326**, 126262 (2025).

7th Asia-Pacific Symposium on Radiochemistry *September 14 ~ 19, 2025 • Kunibiki Messe • Shimane, Japan*

Uptake and Elimination of Radiocesium-137 in the Wild Silkmoth *Antheraea yamamai*

Yusuke YOSHIDA[1], Masaomi TAKAHASHI[1], Akihiro Tohsaki[1], Toshimasa MITAMURA[2], Zenta KAJIURA[3], Risako OHARA[1], Takayuki HONDA[4], Toru TAKAHASHI[4], Satoshi INOSE[4]
[1]*The University of Osaka (Japan),* [2] *Fukushima university (Japan),*
[3]*Shinshu University (Japan),* [4] *Meiji University (Japan)*

1 INTRODUCTION

This report describes a study on the dynamics of radiocesium in the Japanese oak silkmoth, *Antheraea yamamai*, a representative wild silkworm in Japan.

After the Fukushima Daiichi Nuclear Power Plant accident in 2011, the Research Center for Nuclear Physics at Osaka University promptly initiated a study of radioactive contamination in the soil across Fukushima Prefecture, under the direction of the Ministry of Education, Culture, Sports, Science and Technology. Although decontamination efforts have since progressed in many affected areas, forested regions were largely excluded from these operations. As a result, we have continued to monitor radiation levels in the soil of forests and other locations in the Hamadori district near the power plant. In this context, we have examined the transfer of radioactive cesium from soil to foliage and investigated the circulation of radiocesium within the forest ecosystem.

In addition, sericulture was once a thriving industry in the Hamadori and Nakadori regions before World War II; however, today, very few farmers are still engaged in silkworm cultivation. Over the past two decades, some groups have made efforts to revive sericulture in the area. We aim to utilize silk yarn produced by silkworms as a means of supporting regional reconstruction following the Great East Japan Earthquake and countering harmful rumors related to radiation. However, the potential uptake of radioactive materials by silkworms raised in Fukushima remains a concern. In particular, it is crucial to determine whether radioactive cesium is transferred to cocoon silk.

Our research group aims to elucidate the uptake and internal dynamics of radiocesium in the wild silkmoth *Antheraea yamamai*, which inhabits the forests of the Hamadori and Nakadori regions in Fukushima Prefecture. In particular, our experimental research focuses on determining whether radiocesium is transferred to cocoon silk. In this report, we present the results of our investigation into the transfer of cesium into the cocoon body and its excretion in feces.

2 METHODS

Antheraea yamamai larvae were reared at 25°C until the fifth instar. As feed, leaves of Quercus acutissima (sawtooth oak) obtained from Kyoto Institute of Technology were provided. Seven larvae that molted to the fifth instar on the same day were selected and orally administered 10 μL of water containing 100 Bq of cesium-137. These individuals were then reared at 25°C. The counting rate of gamma rays (662 keV) emitted from cesium-137 within the body was measured using a high-purity germanium detector immediately after administration, and at 5, 24, and 48 hours post-administration. These measurements were used to investigate the accumulation and excretion of cesium-137 in the body.

3 RESULTS

The count rate of gamma rays (662 keV) emitted from cesium-137 within the body was measured from immediately after ingestion up to 48 hours post-administration in *Antheraea yamamai* (Fig. 1). In all seven individuals, the count rate of cesium-137-derived gamma rays decreased to below the detection limit within 48 hours. In all individuals except for specimen B, the count rate had already dropped to less than one-third of the initial level within 5 hours. Specimen B excreted less feces than the others at the 5-hour mark. These findings suggest that cesium-137 is excreted from the body primarily via feces.

Copyright on 7th Asia-Pacific Symposium on Radiochemistry 2025

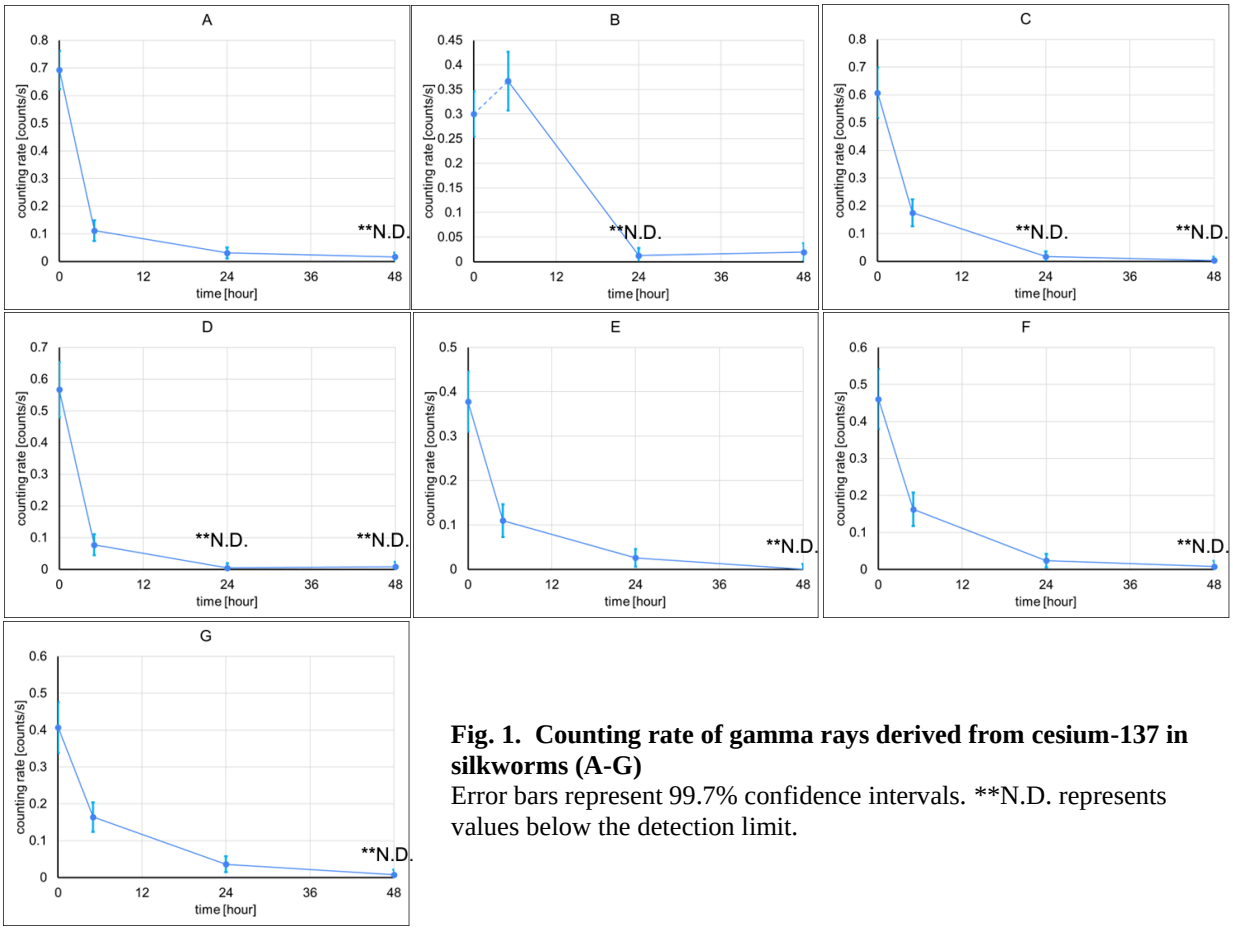


Fig. 1. Counting rate of gamma rays derived from cesium-137 in silkworms (A-G)
Error bars represent 99.7% confidence intervals. **N.D. represents values below the detection limit.

4. CONCLUSIONS

In this study, *Antheraea yamamai* larvae were orally administered a cesium-137 aqueous solution, and the accumulation and excretion of cesium-137 within the body were investigated over a 48-hour period. In all seven specimens, the count rate of gamma rays (662 keV) emitted from cesium-137 decreased to below the detection limit within 48 hours. In six out of the seven individuals, the count rate dropped to less than one-third of the initial level within 5 hours. The one individual that did not exhibit such a decrease had excreted less feces compared to the others at the 5-hour point. These findings suggest that cesium-137 is excreted from the body primarily through feces. Since no detectable radiocesium remained in the body at 48 hours, it is considered unlikely that cesium-137 would be retained in the silk fibers produced.

However, in this experiment, cesium-137 was administered in aqueous form, whereas in actual environmental conditions, it would be ingested as a component of contaminated leaves. The chemical form of cesium-137 may differ in such cases. Future experiments will investigate the accumulation and excretion of cesium-137 by feeding larvae with leaves that have absorbed radiocesium.

ACKNOWLEDGMENTS

We sincerely thank Atsushi Toyoshima, Masashi Murakami, and Kazuhiro Motooka of Osaka University for their invaluable support in conducting measurements using the high-purity germanium detector. We also extend our deep gratitude to Toshiharu Akino, Sumiharu Nagaoka, and Masatoshi Ichida of Kyoto Institute of Technology for kindly providing the sawtooth oak (*Quercus acutissima*) leaves used as feed in this study.

How the hillslope groundwater discharge controls the dissolved radiocesium concentration of surface water in a forest headwater catchment

Hiroaki Kato[1], Haruki Nakada[1], Yuma Niwano[1], Onda Yuichi[1]

[1] *University of Tsukuba: 1-1-1 Tennodai, Tsukuba, Ibaraki, 305-0005, Japan, kato.hiroaki.ka@u.tsukuba.ac.jp*

Understanding radiocesium transport from forested areas after the Fukushima Daiichi accident is essential for assessing its downstream movement, ecological impact, and for developing radiation protection strategies. While previous studies have identified leaching from organic matter as a source, pathways involving forest slope runoff remain poorly understood. This study examined hydrological processes affecting dissolved 137137Cs concentrations in surface water within a forested headwater catchment in Fukushima Prefecture. Field observations included regular sampling of surface water, groundwater, and soil water, alongside monitoring of groundwater flow using piezometers. Results showed that shallow groundwater (0.18–0.94 m depth) contained significantly higher dissolved 137137Cs (0.64 Bq/L) than surface water (0.09 Bq/L). During rainfall events, groundwater levels rose, triggering lateral shallow groundwater flow toward the stream. This flow mixed with surface water and increased its dissolved 137137Cs concentration. The findings highlight shallow groundwater discharge as an important and previously underrecognized pathway for radiocesium export from forest slopes to streams.

1 INTRODUCTION

The 2011 Fukushima Daiichi Nuclear Power Plant accident released large amounts of radiocesium, about 70% of which was deposited in forested areas, particularly in the Abukuma Highlands. Due to limited decontamination efforts in these areas, ^{137}Cs continues to circulate within forest ecosystems and may be transported to aquatic systems via hydrological pathways. While previous studies identified several sources of dissolved ^{137}Cs—such as deep groundwater, soil water, and organic matter—little attention has been given to the role of shallow groundwater. This study, conducted in a forested headwater catchment in Namie Town, investigates how shallow subsurface flow contributes to ^{137}Cs transport, particularly during storm events. The results suggest that shallow groundwater, enriched with dissolved organic carbon, plays a key role in mobilizing ^{137}Cs to streams, highlighting the importance of understanding near-surface flow dynamics in forested slopes affected by radiocesium contamination.

2 METHODOLOGY

2.1 Study Site

To investigate long-term migration and accumulation of ^{137}Cs in forest environments, a study site was established in Akogi, Namie Town, Fukushima Prefecture, approximately 23 km from the Fukushima Daiichi Nuclear Power Plant. Located within the difficult-to-return zone, the site is a government-owned forest with high initial ^{137}Cs deposition (4727 kBq/m²). The total watershed area is 0.008 km², and the dominant vegetation includes Japanese cedar, red pine, and broad-leaved trees. Soil characteristics show high porosity near the surface and a cation exchange capacity of 50 cmol(+)/kg in the top 5 cm. In 2020, 77% of total ^{137}Cs remained in the top 5 cm of soil, with 2.9% in exchangeable form. The site is part of the Ogurasawa tributary of the Ukedo River, where water from a spring infiltrates and re-emerges downstream in a perennial wet zone. Flow monitoring from 2021 to 2023 showed that storm events significantly increased flow rates, with downstream flows reaching up to 10 L/s—about 5.2 times the rate observed upstream. This hydrological behavior suggests substantial subsurface contributions and supports investigations into how water pathways affect the transport of dissolved ^{137}Cs.

1.2 Data Collection and Analysis

From April 2021 to November 2023, surface and subsurface water sampling was conducted to monitor dissolved ^{137}Cs dynamics in a forested catchment in Fukushima. Surface water was sampled at three points: a spring (A1), a V-notch weir 1 m downstream (A2), and the catchment outlet (A3). Automatic samplers at A3 collected water during both stormflow and baseflow. Soil water was collected using zero-tension lysimeters at the slope adjacent to a midstream wet zone, targeting water that passed through litter and topsoil layers rich in ^{137}Cs. Groundwater was sampled from wells and piezometers installed at various depths. Suspended sediments and coarse organic matter were also collected and analyzed for radiocesium. Surface water samples were filtered, and dissolved ^{137}Cs was quantified using gamma spectroscopy. DOC and major cations (Na^+, K^+, NH_4^+, Mg^{2+}, Ca^{2+}) were analyzed to understand mixing effects within organic and mineral soil layers. Flow measurements were conducted using V-notch weirs, a Parshall flume, and water-level loggers, while piezometers and barometric loggers were used to monitor groundwater levels. Hydraulic heads were calculated and visualized using Kriging interpolation. Hydrograph separation was used to estimate baseflow contributions during storm events. Statistical analyses, including ANOVA and correlation tests, assessed relationships among ^{137}Cs, DOC, and K^+ concentrations.

3 RESULTS AND DISCUSSION

From April 2021 to November 2023, baseflow samples were collected to investigate dissolved ^{137}Cs behavior in a forested headwater catchment. Surface water concentrations were lowest (0.064–0.11 Bq/L), while soil infiltration water showed much higher values (up to 5.8 Bq/L). Shallow groundwater had intermediate concentrations, with higher values closer to the surface and farther from the stream. Dissolved ^{137}Cs was strongly correlated with DOC and K^+, particularly in litter layer percolation water. Rainfall-runoff events triggered significant increases in streamflow and dissolved ^{137}Cs concentrations, with peak values during runoff reaching about twice the baseflow levels. Groundwater monitoring during storms showed shifts from vertical to lateral flow toward the stream, indicating increased shallow groundwater discharge as a source of dissolved ^{137}Cs to surface water. These findings highlight the role of organic-rich shallow flow paths in radiocesium mobilization.

3.1 Impact of groundwater discharge on the increase in surface water flow during rainfall events

During rainfall events, hydraulic heads shifted toward the stream, indicating increased groundwater discharge from hillslope soils. This supports earlier findings that rising water tables enhance streamward groundwater flow. A significant correlation ($R^2 = 0.44$, $p < 0.01$) between hydraulic gradient and streamflow at the catchment outlet (A3) confirmed that groundwater contributed to rising surface water flow. In wetter conditions, such as during Events 1 and 2, streamflow increased more rapidly due to enhanced groundwater recharge and discharge. These results demonstrate that hillslope groundwater plays a key role in increasing surface water flow during rainfall in forested catchments.

3.2 Effect of hillslope groundwater discharge on dissolved ^{137}Cs concentrations in surface water

This study examined how hillslope groundwater discharge influences dissolved ^{137}Cs concentrations in surface water during rainfall events in a forested catchment. Hydraulic data showed that increased groundwater flow toward the stream correlates with rising ^{137}Cs levels, though hysteresis patterns suggest mixing of waters from different depths. Peak ^{137}Cs concentrations occurred with rapid shallow groundwater discharge, while deeper groundwater contributions after the peak led to concentration decreases. DOC and K^+ followed similar trends, but decreased more slowly, possibly due to leaching from organic matter in streambeds. The study revealed strong correlations between DOC and ^{137}Cs, highlighting the role of organic-rich soils and riparian zones in mobilizing radiocesium. Shallow hillslope groundwater was identified as a previously underrecognized export pathway, in addition to litter leaching, overland flow, infiltration water, and deep groundwater. These findings emphasize the importance of both hydrological processes and soil chemistry in controlling ^{137}Cs export, and the need for detailed analysis of water sources and interactions within slope soils to better understand contaminant dynamics in forested headwaters.

4 CONCLUSION

This study assessed how shallow groundwater discharge from forest slopes affects dissolved ^{137}Cs concentrations in surface water within a headwater catchment in Namie Town, Fukushima Prefecture—an area with high radiocesium deposition. While prior studies identified key sources of dissolved ^{137}Cs, such as litter leaching, overland flow, infiltration water, and deep groundwater, the role of shallow subsurface groundwater had remained unclear. By integrating hydrological observations and water sampling, the study revealed that dissolved ^{137}Cs concentrations were significantly higher in shallow groundwater (0.64 ± 0.77 Bq/L) than in surface water (0.09 ± 0.02 Bq/L). Rainfall events triggered lateral groundwater flow from soil layers toward the stream, and this flow was closely linked to variations in surface water discharge and radiocesium concentration. These results highlight the importance of shallow groundwater as a transport pathway of ^{137}Cs. The study recommends further investigation of ^{137}Cs mass balance through spring water monitoring and litter leaching experiments to better understand the formation of high-^{137}Cs groundwater and refine estimates of radiocesium export from forested catchments.

ACKNOWLEDGMENTS

This study was supported as a commissioned study of the Japan Atomic Energy Agency (FY2015-2023) and by a Grant-in-Aid for Scientific Research on Innovative Areas (grant number 24110005), a Grant-in-Aid for Scientific Research (A) 22H00556, a Grant-in-Aid for Scientific Research (B) 24K00170, and the Japan Science and Technology Agency as part of the Belmont Forum.

Poster Presentation | [P4]Radionuclide Migration Dynamics: Radioactive Waste Disposal and Environmental Impact Assessment

Mon. Sep 15, 2025 6:30 PM - 8:00 PM JST | Mon. Sep 15, 2025 9:30 AM - 11:00 AM UTC Poster

[Poster] P4

[P-P4-01*]

One-dimensional nanostructure arrays with Schottky Junction enhanced charge separation for the photoelectrocatalytic selective removal of Uranium from wastewater

*Shuyang Li[1] (1. southwest university of science and technology (China))

[P-P4-02]

Unveiling the critical role of the surface hydroxyl groups for electric assisted uranium extraction from the fluorine contained

*Tao Chen[1] (1. Southwest University of Science and Technology (China))

[P-P4-03]

Oxygen vacancy-mediated enhancement of catalytic removal of UO22+ by MOF@COF S-scheme

*Yuqian Zhong[1,2], xinpeng wang[1], liyong yuan[2], weiqun shi[2] (1. Guangxi University (China), 2. The Institute of High Energy Physics of the Chinese Academy of Sciences (China))

[P-P4-04]

The Migration Behavior and Microscopic Mechanisms of Typical Actinides Under the Influence of Environmental Colloids

*Zhen Xu[1], Duoqiang Pan[1], Wangsuo Pan Wu[1] (1. Lanzhou University (China))

[P-P4-05*]

Adsorption and Transport of Te(IV) in Soils Relevant to A Lead-cooled Fast Reactor Environment

*Zhihao Liu[1], Zibo Gao[1], Yujia Lin[1], Huiling Wang[1], Lili Li[2], Muyi Ni[1], Peng Lin[2] (1. Sino-French Institute Nuclear Engineering & Technology (Sun Yat-sen university) (China), 2. China Nuclear Power Technology Research Institute Co., Ltd., Shenzhen, Guangdong (China))

[P-P4-06]

Estimation of nuclide migration behavior considering suspended soil particles in a brackish lake

*Takuma Sawaguchi[1], Toshihisa Sasaki[2], Taro Shimada[1], Seiji Takeda[1] (1. Japan Atomic Energy Agency (Japan), 2. Visible Information Center, Inc. (Japan))

[P-P4-07*]

Mechanism of Eu(III) adsorption and mineral alteration response of Tamusu clay rocks

*Mingwei Wang[1] (1. Sino-French Institute of Nuclear Engineering and Technology, Sun Yat-sen University (China))

[P-P4-08]

Study on the determination of evaluation parameters for assessing radionuclide migration due to surface runoff

*Taro Shimada[1], Naruyuki Ueshima[2], Masakazu Namekawa[2], Shizuka Takai[1], Seiji Takeda[1] (1. Japan Atomic Energy Agency (Japan), 2. NAIS Inc. (Japan))

©APSORC25

[P-P4-09]

Migration of ^{90}Sr and ^{60}Co in the groundwater-soil system surrounding the long-distance effluent pipeline of a proposed NPP: Diffusion experiments and solute transport simulation

*Yu Jia Zhou[1,3], Yuan Chen[2], Li Li Li[3], Pin Chuan Li[5], Yu Han Wu[1,4,6], Liang Ming Kang[1] (1. Sun Yat-sen University (China), 2. State Key Laboratory of Nuclear Power Safety Technology and Equipment, China Nuclear Power Engineering Co., Ltd (China), 3. China Nuclear Power Technology Research Institute Co., Ltd. (China), 4. Guangdong Engineering Technology Research Center of Nuclear Safety & Emergency Response Tech (China), 5. School of Nuclear Science and Engineering, East China University of Technology (China), 6. Key Laboratory of Strategic Mineral Resources of the Upper Yellow River, Ministry of Natural Resources (China))

©APSORC25

One-dimensional nanostructure arrays with Schottky Junction enhanced charge separation for the photoelectrocatalytic selective removal of Uranium from wastewater

Wenbo Zhang, Shuyang Li, Yungui Li, Tao Duan

School of Environment and Resources, Southwest University of Science and Technology, Mianyang 621010, Sichuan *Province, P. R. China*

The photoelectrocatalytic reduction of soluble U(VI) to relatively insoluble U(IV) is a promising method for uranium wastewater treatment. However, the strong reliance on sacrificial agents and an inert atmosphere due to the rapid charge reorganization remains a great challenge. The construction of an inner electrical field at a heterojunction interface accompanied by an external electric field provides a promising strategy for enhancing charge transfer. Herein, a photoelectrode was proposed by in-situ coating nano-TiO_2 cone arrays (NTCA) on a titanium mesh, and used for uranium removal from complex effluents under air conditions without sacrificial agents. The enhanced spatial charge separation driven by the Schottky junction built-in electric field and an external bias voltage, coupled with rapid fluid diffusion, granted the photoelectrode an outstanding photoelectrocatalytic uranium removal performance with photocurrent densities of up to 3 mA cm−2 at − 0.55 $V_{Ag/AgCl}$. The impressive uranium removal performance was maintained in a wide range of chemical conditions, as well as in real seawater and industrial wastewater. Theoretical calculation revealed that uranyl ions were confined on the NTCA surface as $[UO_2(H_2O)_5]^{2+}$, further reduced to UO_2. This work demonstrated a viable route for uranium separation from aqueous solutions with inexhaustible solar energy and minimal electrical energy.

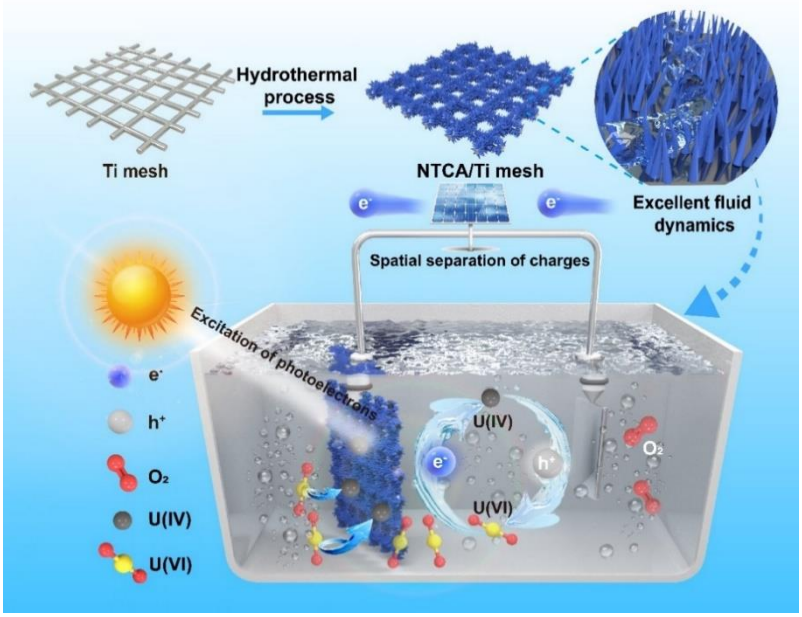


Figure1. Photoelectrocatalytic investigation of uranium immobilization on the NTCA/Ti mesh. Under illumination, the nano-TiO_2 cone arrays grown in situ in the Ti mesh are activated to generate electron-hole pairs. The holes are transferred to the counter electrode (Pt) through an external circuit, while the remaining electrons are used to reduce U(VI) to U(IV) in the air. The system combines the advantages of photocatalysis and electrocatalysis to realize the reduction and immobilization of uranium without the introduction of additional sacrifices.

[1] Shuyang Li, Xiaoyong Yang, Qing Wang, Hewen Shang, Yang Xu, Yinghao Xu, Xiangyu Kong*, Min Zhao, Xuejun, Wangsuo Wu, Duoqiang Pan*, One-dimensional nanostructure arrays with Schottky junction enhanced charge separation for the photoelectrocatalytic selective removal of uranium from wastewater, Nano Energy, 128 (2024) 109866.

Unveiling the critical role of the surface hydroxyl groups for electric assisted uranium extraction from the fluorine contained uranium wastewater

Tao Chen [1,*], Wenkun Zhu [1,*]

[1] *Southwest University of Science and Technology, Mianyang, 621010, PR China*

*E-mail: chent@swust.edu.cn

During the production process of uranium enrichment plants and nuclear fuel plants, a large amount of radioactive wastewater containing fluorine and uranium is generated. In wastewater containing fluorinated and uranium, the competitive coordination between fluorine and uranium will form UO_2F^+, UO_2F_2(aq), $UO_2F_3^-$ and other complexes, resulting in the difficulty of uranium and removal extraction. In the production process, the main method to treat the wastewater fluorine and uranium is to use the anion resin column adsorption method. However, a large number of anions in wastewater will compete with the adsorption sites of resin, which requires multi-stage adsorption column to treat, and the adsorption column is easy to produce saturation, seriously hindering the industrial production. As a new technology, electrically assisted uranium extraction can improve reaction kinetics and exhibit high selectivity towards non reducing coexisting ions by applying an external electric field. However, the uranium coordination sites on traditional electrode materials are separated from the active centers of electrochemical reduction in physical space. The efficiency of electrically assisted uranium extraction is largely limited by the loss of electrons from the active center to the coordination site. Based on the Soft Hard Acid Base (HSAB) theory, defects in the active centers of metal oxides are introduced to construct metal oxygen hydrogen (M-O-H, hard base) metal bonds with specific recognition of uranyl ions (hard acids), which is expected to achieve the unity of surface coordination sites and reducing active sites.

Based on this, this study developed ultra-thin cobalt based oxide (CoO_x) nanosheets rich in hydroxyl groups as electrocatalysts for extracting uranium from fluoride containing uranium wastewater. According to theoretical calculations and other spectroscopic measurements, it has been confirmed that due to the presence of a large number of hydroxyl groups, CoO_x nanosheets can enhance their affinity for uranium and achieve efficient selective capture of uranium in complex environments. Correspondingly, CoO_x nanosheets exhibit excellent U (VI) removal ability (>95%) in the presence of fluoride ions. Using synchrotron radiation X-ray absorption spectroscopy (XAS) measurements, we confirmed that hydroxyl rich CoO_x nanosheets captured free uranyl ions and achieved fluoride uranium separation through electric drive, ultimately forming a stable $2O_{ax}$-1U-$3O_{eq}$ configuration. It is worth noting that for the first time, we have successfully observed the complete reaction process of uranium species on the CoO_x surface, from the initial uranium single atom form being captured by surface hydroxyl dangling bonds, to further undergoing nucleation and growth of uranium nanoclusters, uranium nanoparticles, uranium nanosheets, etc., using techniques such as aberration corrected electron microscopy. This study not only provides a new approach for developing low-cost electrocatalysts to efficiently electrically assist uranium extraction from fluorine-containing uranium wastewater, but also offers a new idea for studying the evolution mechanism of uranium species.。

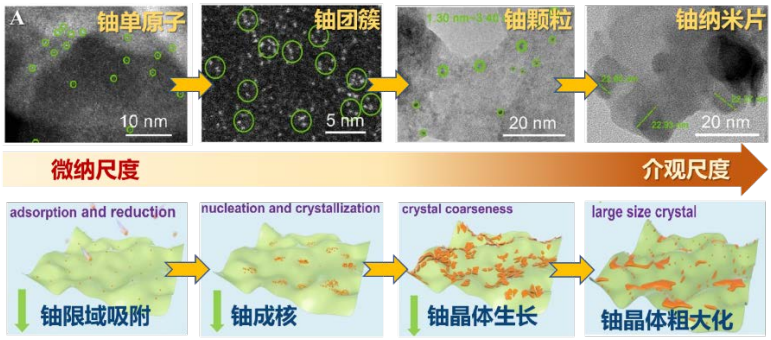


Figure 1: Electron microscopy images and schematic diagrams of uranium nucleation growth at different stages

Keywords: uranium; Fluorine and uranium containing wastewater; Electric assisted separation; Evolution of uranium species;

[1] Li Zhou, Jie Lian, Qiuyang Li, Jin Li, Yuwen Shao, Gang Wu,Tao Ding, Xudong Cui, **Tao Chen**,* and Wenkun Zhu*. Unveiling the critical role of surface hydroxyl groups for electro-assisted uranium extraction from wastewater [J]. Inorganic Chemistry, 2023, 62, 21518-21527.
[2] Li Zhou, Yi Li, Yuwen Shao, Jin Li, Gang Wu, Qiuyang Li, Xi Gong, Jie Lian, Xudong Cui, Wenkun Zhu*, **Tao Chen***. Interface coupling induced built-in electric fields accelerate electro-assisted uranium extraction over Co_3O_4@FeO_x nanosheet arrays[J]. Applied Catalysis B: Environment and Energy, 2024, 353, 124052.
[3] Kaifu Yu, Li Zhou, Linzhen Wu, Changxue Dong, Huanhuan Dong, Jie Lian, Xiaoyong Yang, Rajeev Ahuja*, **Tao Chen***, Wenkun Zhu*. Photo-assisted uranium extraction basedon heterogeneous catalysts[J]. Science Bulletin, 2024, 69(24): 3800-3805.

Oxygen vacancy-mediated enhancement of catalytic removal of UO_2^{2+} by MOF@COF S-scheme

Yuqian Zhong[1,2], Xinpeng Wang[1], Liyong Yuan[2],Weiqun Shi[2]

[1]*School of Resources, Environment and Materials, Guangxi University, State Key Laboratory of Featured Metal Materials and Life-cycle Safety for Composite Structures, Nanning 530004, China*

[2]*Institute of High Energy Physics, Chinese Academy of Sciences, Beijing 100049, China*

* E-mail: wangxinpeng@gxu.edu.cn

Covalent organic framework materials (COFs) exhibit unique advantages for radionuclide management, owing to their tunable pore architectures, high surface areas, and robust chemical stability—properties particularly critical for selective adsorption and photocatalytic reduction of uranium(VI) in nuclear wastewater. However, conventional COFs face inherent limitations, including low carrier mobility and pronounced interfacial charge recombination, which significantly restrict their photocatalytic efficiency and hinder practical deployment under industrial conditions.

Energy band engineering for constructing heterojunctions is usually an effective way to promote photogenerated electron-hole pair separation in single-component materials, but covalent organic framework (COF)-based heterojunctions (e.g., COF/inorganic semiconductors) are often characterized by significant lattice mismatch and weak interfacial bonding (van der Waals interactions predominate), which result in a surge in the density of interfacial defect states and the formation of a carrier mobility barrier, triggering severe nonradiative compositions and ultimately making it difficult to achieve the desired Photocatalytic efficiency.

This work develops an innovative MOF@COF S-scheme heterojunction via covalent interfacial bonding and oxygen vacancy engineering. The covalent MOF-COF linkage enhances lattice compatibility and directional charge transfer, as evidenced by in situ XPS and fs-TAS showing 3.2× improved charge separation and 57% prolonged carrier lifetime. Oxygen vacancies in the MOF matrix, optimized for uranium-specific adsorption (validated by XANES), synergistically enable 98.7% uranium removal in 30 min (4.8× enhancement). This study pioneers precise heterojunction engineering for radionuclide management, offering mechanistic insights into vacancy-mediated adsorption and interfacial charge dynamics for advanced photocatalytic remediation.

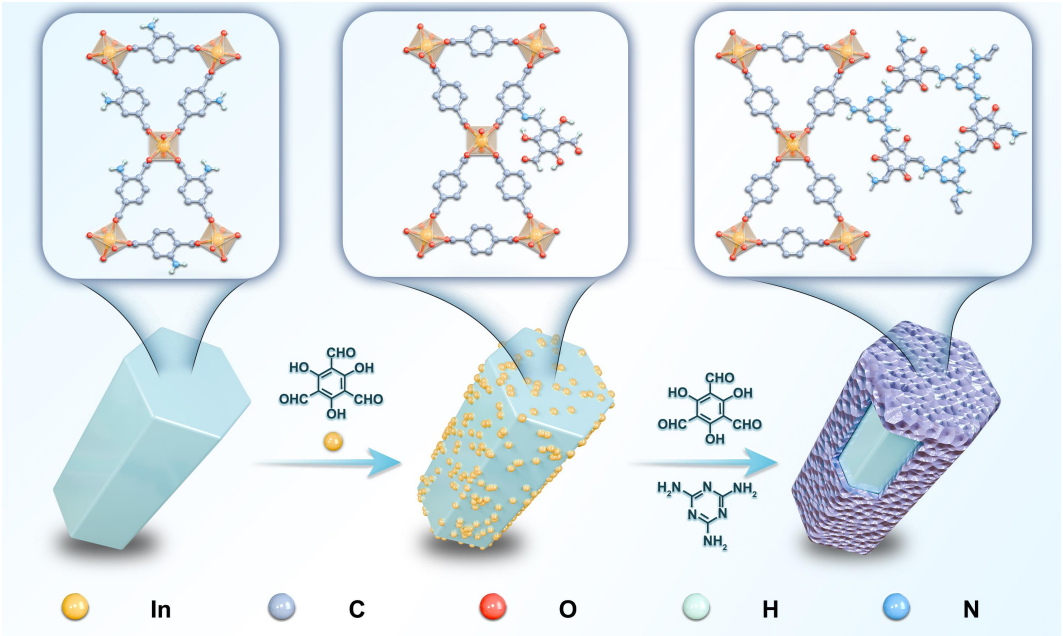


Fig. 1. Schematic illustration of the preparation process of MIL@COF heterojunction structure..

References

[1] Huang Z W, Li X B, Mei L, et al. All-in-one: photo-responsive lanthanide-organic framework for simultaneous sensing, adsorption, and photocatalytic reduction of uranium[J]. *Advanced Functional Materials*, 2024, 34(41): 2404126.
[2] Cai Z, Wang J, Fu H, et al. Designing flexible TiO2/SrTiO3/BiOBr recyclable fiber membrane with spatial dual oxidation sites for photocatalytic uranium extraction under visible light[J]. *Chemical Engineering Journal*, 2024, 500: 156785.
[3] Fu H, Pan Y, Cai Z, et al. Bi2O3/g-C3N4 hollow core–shell Z-scheme heterojunction for photocatalytic uranium extraction[J]. *Nano Research*, 2024, 17(7): 5845-5855.

THE MIGRATION BEHAVIOR AND MICROSCOPIC MECHANISMS OF TYPICAL ACTINIDES UNDER THE INFLUENCE OF ENVIRONMENTAL COLLOIDS

Zhen Xu*, Duoqiang Pan, Wangsuo Wu

[1]*School of Nuclear Science and Technology, Lanzhou University, China*
[2]*Frontiers Science Center for Rare Isotopes, Lanzhou University, China*
**E-mail: xuz@lzu.edu.cn*

The ecological and environmental safety of high-level radioactive waste has always been a worldwide problem, which is as important as nuclear safety. It is also a major issue related to the sustainable development of China's nuclear industry and environmental protection. The existence of environmental colloids can facilitate the transport of environmental contaminants including radionuclides as well as hydrophobic organic compounds. How to effectively control and block the transport of radionuclides in engineering barriers and predict their potential hazards has become an urgent problem. Meanwhile, it is also one of the key scientific problems in the performance and safety evaluation of high-level radioactive waste geological repository. The premise and foundation to solve this problem is to deeply understand and scientifically evaluate the mechanism of environmental colloids on radionuclide transport. Although it has been recognized that bentonite colloids play an important role in the transport of radionuclides[1-4], there are still some limitations in the understanding of the binding properties of composite colloids and radionuclides.

In current study, column experiments were conducted to investigate the co-transport behavior of environmental colloids, such as bentonite colloids (BC), humic acid (HA), and microorganisms, and Eu(III) in saturated porous media. The results showed that under conditions of low ionic strength or high pH, BC exhibits a concentration threshold (150 mg/L) in promoting Eu(III) migration. The synergistic effect of humic acid (HA) and BC on Eu(III) transport demonstrates a non-linear superposition characteristic. The 685 nm $EuPO_4$ intrinsic colloids formed by phosphate influence europium migration through dual mechanisms of colloid stability and physical straining, with their crystal structure capable of being loaded by BC for secondary migration. Notably, when phosphate, BC, and Eu(III) coexist, phosphorus preferentially forms BC-P-Eu(III) ternary pseudo-colloids with BC rather than intrinsic $EuPO_4$ colloids, exhibiting a unique synergistic migration mechanism. This work deepens the theoretical understanding of colloid-mediated radionuclide migration and provides significant scientific insights for the safety assessment of high-level radioactive waste geological repositories and nuclear emergency response.

References

[1] Tang, Q.; Xu, Z.; Tan Q.; Shi X.; Wu, W. and Pan, D. (2024). Insight into impact of phosphate on the cotransport and corelease of Eu(III) with bentonite colloids in saturated quartz columns. J. Hazar. Mater. 461: 132572.
[2] Xu, Z.; Pan, D.; Tang, Q.; Wei, X.; Liu, C.; Li, X.; Chen, X. and Wu, W. (2022). Co-transport and co-release of Eu(III) with bentonite colloids in saturated porous sand columns : Controlling factors and governing mechanisms. Environ. Pollut. 118842.
[3] Xu, Z.; Niu, Z.; Pan, D.; Zhao, X.; Wei, X.; Li, X.; Tan, Z.; Chen, X.; Liu, C. and Wu, W.(2021). Mechanisms of bentonite colloid aggregation, retention, and release in saturated porous media: Role of counter ions and humic acid. Sci. Total Environ. 793, 148545.
[4] Tang, Q.; Xu, Z.; Tan, Q.; Shi, X.; Wu, W.; Pan, D. (2024). Insight into impact of phosphate on the cotransport and corelease of Eu(III) with bentonite colloids in saturated quartz columns. J. Hazard. Mater. 461, 132572.

Adsorption and Transport of Te(IV) in Soils Relevant to A Lead-cooled Fast Reactor Environment

Zhihao Liu[1], Zibo Gao[1], Yujia Lin[1], Huiling Wang[1], Lili Li[2], Muyi Ni[1], Peng Lin[2*]

[1] *Sino-French Institute of Nuclear Engineering and Technology (Sun Yat-sen University), Tangjiawan, Zhuhai, Guangdong Province, P. R. China, 519082*
[2]*China Nuclear Power Technology Research Institute Co., Ltd., Shenzhen, Guangdong, 518000, P. R. China*

[*]*Corresponding author E-mail addresses: lin_peng@cgnpc.com.cn*

Generation IV (Gen-IV) nuclear reactors have been gaining attention due to their potential to meet crucial sustainability, safety, reliability, and economic goals. In these reactors, polonium-210 (^{210}Po) is primarily generated by the neutron activation of bismuth-209 (^{209}Bi) present in the lead-bismuth eutectic (LBE) coolant. The polonium then volatilizes into the cover gas system, where it forms metastable polonium oxides that react with water and eventually migrate into the atmosphere. Over time, water-soluble forms of polonium are deposited into soil through rainfall. Guangdong Province, known for its high annual rainfall, is particularly affected by this process. Polonium predominantly exists in aqueous environments as H_2PoO_3, $HPoO_3^-$, and PoO_3^{2-}, which makes its migration into soils through hydrological pathways more likely. Given that polonium (Po) is highly radiotoxic, its vertical migration through soil poses serious ecological and public health risks. Therefore, understanding the behavior of Po's adsorption and its mobility in soil is essential for accurate environmental assessments and nuclear safety management.

This study investigated the adsorption and transport behavior of tellurium(IV) [Te(IV)], a non-radioactive analogue of polonium (Po), in three distinct soil types—iron oxide-rich, clay-rich, and quartz-rich—collected in proximity to a nuclear power plant. To elucidate the uptake mechanisms of Te(IV) and simulate its subsurface migration, batch adsorption experiments, soil column transport tests, and HYDRUS-1D numerical modeling were employed. The adsorption process was rapid, achieving pseudo-equilibrium within approximately 4 hours. Kinetic analysis revealed that the data conformed to a pseudo-second-order model, indicating chemisorption as the controlling rate process. Equilibrium adsorption data fit well with the Freundlich isotherm, suggesting heterogeneous sorption occurring on multiple active sites. Among the soils tested, the iron oxide- and organic matter-rich soil exhibited the greatest adsorption capacity and strongest retention, with a distribution coefficient (K_d) around 23 mL·g^{-1}, whereas the quartz-rich soil showed considerably lower retention ($K_d \approx 10$ mL·g^{-1}) and earlier breakthrough during column tests. Spectroscopic analyses, including X-ray photoelectron spectroscopy (XPS) and Fourier transform infrared (FTIR) spectroscopy, confirmed the formation of inner-sphere complexes between Te(IV) and both mineral surfaces and organic functional groups, supporting the predominance of chemisorption mechanisms. Correspondingly, soil column results and HYDRUS-1D simulations demonstrated pronounced retardation and limited mobility of Te(IV)/Po(IV) in the iron oxide-rich soil. These findings indicate that under typical environmental conditions, Po(IV) is likely to be effectively immobilized in organic-rich soils, thereby mitigating its potential groundwater migration. This research offers critical insights into the natural attenuation and sorptive capacity of soils for radionuclides, providing valuable guidance for environmental safety assessments and the development of soil remediation strategies around nuclear reactor.

1 Conclusion

The batch experiments revealed that Soil 2 (rich in Fe oxides and organics) had the highest Te(IV) adsorption capacity and efficiency, compared to the more clay-rich Soil 1 and quartz-dominated Soil 3. Adsorption isotherms were better described by the Freundlich model and indicated an endothermic, chemisorption-dominated process, with higher uptake at elevated temperatures (278–308 K) (Fig. 1). Kinetic studies showed that a pseudo-second-order model best fit the data for all soils, highlighting chemisorption as a rate-limiting step, while Weber–Morris analysis identified significant intraparticle diffusion limitations in soils with lower sorptive capacity[1].

Column experiments, combined with HYDRUS-1D modeling, demonstrated that Te(IV) (and by extension Po(IV)) has limited mobility under saturated flow conditions, especially in soils with abundant high-affinity sites (Fig. 2). Post-adsorption spectroscopic analyses (FTIR, XPS) and SEM–EDS mapping confirmed that Te(IV) is retained primarily via inner-sphere complexes at Fe-(hydr)oxide surfaces and on organic-coated minerals, without any change in oxidation state.

These multidisciplinary findings consistently support a mechanism in which Fe oxides provide dominant sorption sites, soil organic matter and clay minerals provide additional capacity, and together these factors govern the strong retention of Te(IV)/Po(IV) in the investigated soil[2].

Copyright on 7th Asia-Pacific Symposium on Radiochemistry 2025

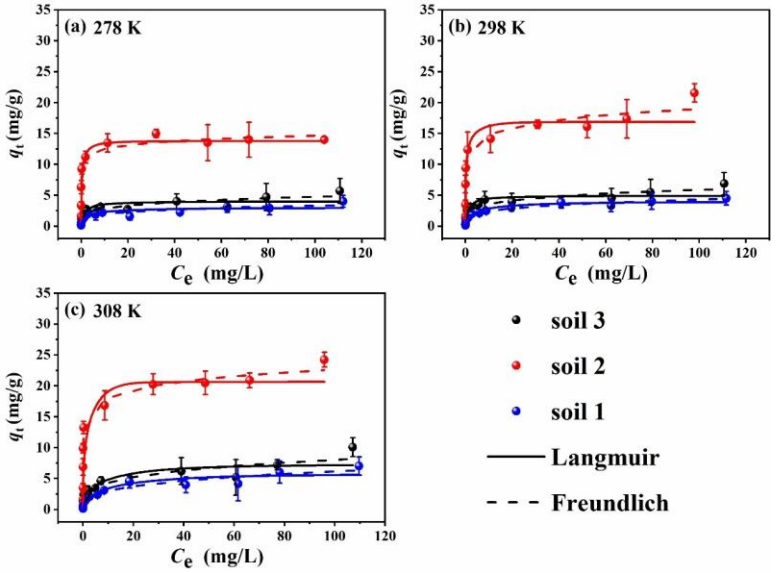


Fig. 1. Adsorption isotherms of Te(IV) with the Langmuir and Freundlich models fitting.
(*s*/*l*= 0.8 g·L^{-1}, *I*= 0.004 mol·L^{-1} NaCl, *t*=48 h)

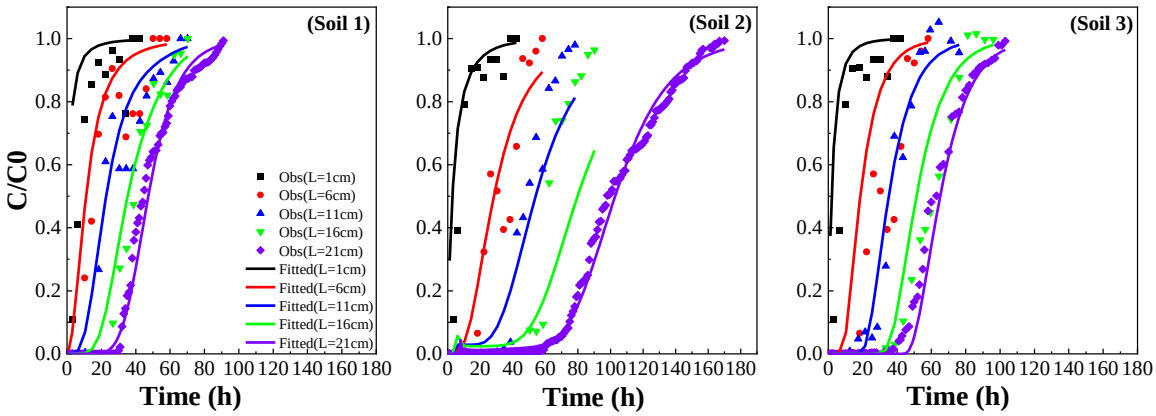


Fig. 2. The observed and simulated breakthrough curves (BTCs) of Te(IV) in soil columns.

ACKNOWLEDGMENTS

This work was supported by the China Nuclear Power Technology Research Institute Co., Ltd. (No. 008-ZB-B-2023-C45-P.T.99-00053).

References

[1]. Neelis S T, et al, Removal of Cr (VI), As (V), Cu (II), and Pb (II) using cellulose biochar supported iron nanoparticles: A kinetic and mechanistic study. *Journal of Environmental Chemical Engineering*, **8**(5), 103886 (2020).

[2]. Kińska K, et al, Interaction of Te (IV) and Te (VI) with the soil matrix–sorption and fractionation as a function of soil composition. *Environmental Pollution*, **361**,124878 (2024).

7th Asia-Pacific Symposium on Radiochemistry *September 14 ~ 19, 2025 • Kunibiki Messe • Shimane, Japan*

Estimation of nuclide migration behavior considering suspended soil particles in a brackish lake

Takuma Sawaguchi[1], Toshihisa Sasaki[2], Taro Shimada[3], Seiji Takeda[4]

[1]*Japan Atomic Energy Agency, Japan: Tokai-mura, Naka-gun, Ibaraki, 319-1195, sawaguchi.takuma@jaea.go.jp*
[2]*Visible Information Center, Inc., Japan: Tokai-mura, Naka-gun, Ibaraki, 319-1112, sasaki@vic.co.jp*
[3]*Japan Atomic Energy Agency, Japan: Tokai-mura, Naka-gun, Ibaraki, 319-1195, shimada.taro@jaea.go.jp*
[4]*Japan Atomic Energy Agency, Japan: Tokai-mura, Naka-gun, Ibaraki, 319-1195, takeda.seiji@jaea.go.jp*

In this study, a three-dimensional nuclide migration analysis for Ni-59 was performed, in order to understand the effect of considering suspended soil particles on the distribution of nuclide concentrations in brackish lakes. The results showed that the main forms of nuclide in brackish lakes were dissolved and sorbed on sediments. Furthermore, there was no significant difference in the amount of dissolved nuclide over time regardless of whether suspended solids particles were considered or not, but the amount of nuclide in sediments was slightly larger in cases where the particles were considered. This is due to the settling and sedimentation of the particles with sorbed nuclide. Therefore, it is important to understand the effects of these phenomena on nuclide concentrations in sediments based on the conditions of suspended soil particle concentration and salinity, and, if necessary, to consider them in the assessment of exposure doses due to contaminated sediments.

1. INTRODUCTION

In the assessment of exposure doses due to nuclides leaking from repository of radioactive wastes, it is important to estimate the migration behavior of nuclides after they reach the living environment (sea, lakes, rivers, etc.) via groundwater. In addition, research on radioactive Cs released into the environment by the Fukushima Daiichi nuclear power plant accident has reported that Cs is concentrated and accumulated in sediments in estuarine coastal areas [1]. This is probably due to the migration of suspended soil particles with sorbed Cs in rivers and their agglomeration and sedimentation in the coastal areas where salinity is high. However, previous safety assessments for radioactive waste disposal [e.g., 2] have not considered the migration of suspended soil particles sorbed with nuclides and the agglomeration/settling/sedimentation of the particles due to salinity changes. In this study, in order to understand the effect of considering suspended soil particles on the distribution of nuclide concentrations in brackish lakes, nuclide migration analysis was performed.

2. ANALYSIS METHODOLOGY

In this study, nuclide migration analysis considering agglomeration/settling/sedimentation of suspended soil particles and sorption/desorption of nuclides on the particles related to the nuclide migration behavior in brackish lakes was performed using 3D-Sea-SPEC [3]. 3D-Sea-SPEC is a code that can not only evaluate the migration of dissolved nuclides and suspended soil particles with sorbed nuclides in three dimensions using advection-diffusion equations but also evaluate changes in salinity in brackish lakes due to tidal fluctuations, and salinity dependent agglomeration/settling of the particles. A simplified brackish lake geometry was assumed in this analysis (Fig. 1). The analysis was first performed considering inflows of salinity from the sea due to the tides and suspended soil particles from the inflow river. Then, after confirming that changes in salinity and suspended soil particle concentration in the brackish lake were stable (the same concentration changes were repeated according to the tidal cycle), the nuclide (Ni-59, which is one of the important nuclides in the safety assessment for intermediate-depth disposal [2]) was supplied along with spring water from the upstream bottom of the lake, and the changes over time of the average amount of nuclide within the divided area were obtained for each form of nuclide presence. In addition, in order to understand the effect of migration of the particles with sorbed nuclide, the analysis was also performed for the case without considering the particles, as in previous evaluations. Since suspended soil particles and sediments were not considered in this case, the amount of nuclide in the sediments was derived from the dissolved nuclide concentration and the sorption distribution coefficient.

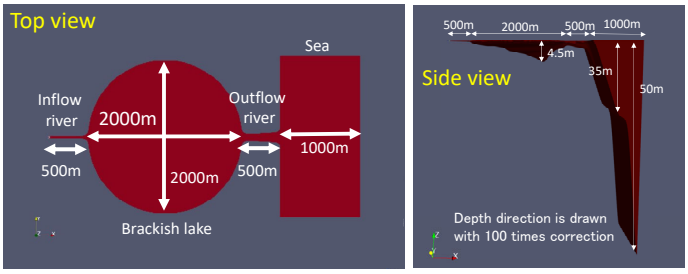


Fig. 1. Analytical geometry for brackish lake in this analysis

3. RESULTS AND DISCUSSION

The analysis results showed that the average values of salinity, suspended soil particle concentration, the amount of dissolved and sorbed on particles nuclide in the same divided area tended to remain within a certain range. On the other hand, the average amount of sediment tended to increase linearly, but the sedimentation rate varied from area to area. Therefore, there were areas where sediments easily accumulated and areas where they were difficult. The amount of nuclide in the sediments also varied with the amount of sediment. Furthermore, it was shown that the main forms of nuclide in brackish lakes were dissolved and sorbed on sediments, and that most of the nuclide supplied from the lake bottom with spring water flowed to the outflow river and sea (Fig. 2). In comparison to the case with or without considering suspended soil particles, there was no significant difference in the change over time of the amount of dissolved nuclide in each divided area. On the other hand, the amount of nuclide in the sediments was approximately 1.3 times larger in the case with considering the particles than without. This is because not only direct nuclide sorption to the sediments but also settling and sedimentation of the particles with sorbed nuclide contribute to the amount of nuclide in the sediments. These results indicate that pathways related to dissolved nuclides in brackish lakes and sorbed nuclides in sediments are important in dose assessment for radioactive waste disposal. Furthermore, although the contribution of settling/sedimentation of suspended soil particles to the amount of nuclide in sediments was slightly in this analysis, the contribution could be larger under some conditions of suspended soil particle concentration and salinity. Therefore, it is important to understand the effects of these phenomena on nuclide concentrations in sediments based on the conditions, and, if necessary, to consider them in the assessment of exposure doses due to contaminated sediments.

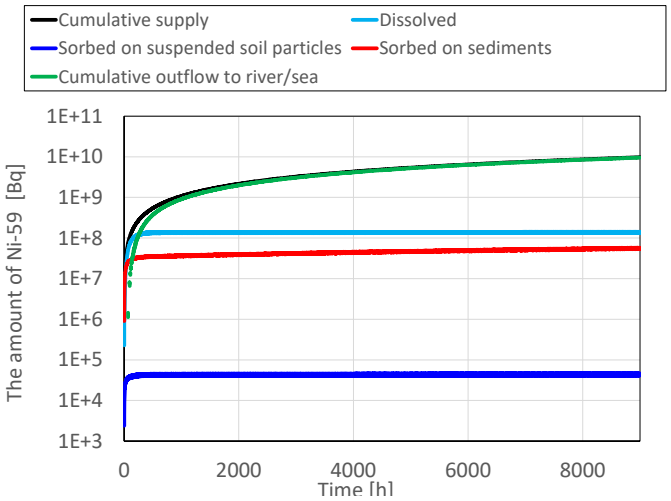


Fig. 2. Change over time in the amount of Ni-59 for each form and in the cumulative supplied/outflowed amount of Ni-59

4. CONCLUSIONS

In this study, in order to understand the effect of considering suspended soil particles on the distribution of nuclide concentrations in brackish lakes, three-dimensional nuclide migration analysis was performed assuming the migration of the particles, salinity-dependent agglomeration/settling/sedimentation, and the sorption of nuclide (Ni-59) supplied from the lake bottom onto suspended soil particles/sediments. The results showed that the main forms of nuclide in brackish lakes were dissolved and sorbed on sediments. Furthermore, there was no significant difference in the amount of dissolved nuclide over time regardless of whether the particles were considered or not, but the amount of nuclide in sediments were larger in cases where the particles were considered. This is due to the settling and sedimentation of the particles with sorbed nuclide. Therefore, it is important to understand the effects of these phenomena on nuclide concentrations in sediments based on the conditions of suspended soil particle concentration and salinity, and, if necessary, to consider them in the assessment of exposure doses due to contaminated sediments. In the future, we will study the effects of organic suspended solids on nuclide migration and develop a long-term estimation method for nuclide migration and exposure dose assessment for brackish lakes.

ACKNOWLEDGMENTS

This research was funded by the Secretariat of Nuclear Regulation Authority, Nuclear Regulation Authority, Japan, and was conducted with the supercomputer HPE SGI8600 in the Japan Atomic Energy Agency.

References

[1] S. Kakehi, et al., Journal of Environmental Radioactivity, 153, 1-9 (2016).
[2] Atomic Energy Society of Japan, AESJ-SC-F012:2023 (2023), [in Japanese].
[3] S. Yamada, et al., Joint International Conference on Supercomputing in Nuclear Applications + Monte Carlo 2020. Proceedings of SNA + MC 2020, pp. 140–146 (2020).

7th Asia-Pacific Symposium on Radiochemistry *September 14 ~ 19, 2025 • Kunibiki Messe • Shimane, Japan*

Mechanism of Eu(III) adsorption and mineral alteration response of Tamusu clay rocks

Mingwei Wang[1], Hongyu Wen[1], Mingliang Kang[1], Hanyu Wu[1,*]

[1] *Sino-French Institute of Nuclear Engineering and Technology, Sun Yat-sen University, Tangjiawan, Zhuhai, P. R. China, 519082*

[*] *Corresponding author E-mail addresses: wuhy76@mail.sysu.edu.cn*

ABSTRACT

With the continuous development of nuclear energy technology, nuclear waste management technology is facing many challenges. Among them, the deep geological disposal method is widely recognized because of its technical feasibility in the field of international nuclear engineering. In China, Tamusu clay rocks from Inner Mongolia are considered to be an ideal host rock for high-level radioactive waste repository due to its high adsorption capacity, self-sealing potential and geochemical buffering capacity. In this study, batch experiments were conducted to systematically study the adsorption behavior of Eu(III) and its mineral alteration process by Tamusu clay rocks in Inner Mongolia. The purpose of this study is to deeply understand the nuclide migration characteristics of clay rocks in a geological disposal environment and the mineral changes under specific conditions, and to provide a scientific basis for the design and safety assessment of the high-level radioactive waste geological disposal repository.

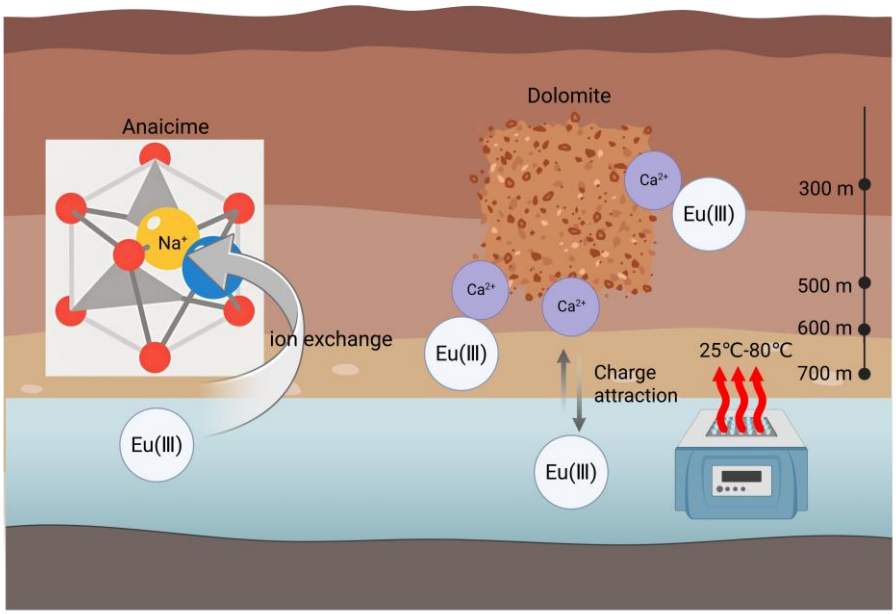
The clay rocks samples from the Tamusu area of Inner Mongolia were used in the experiment. The solid phase samples before and after adsorption were analyzed by advanced characterization techniques such as XRD, SEM-EDS and XPS, and the adsorption behavior and potential mechanism of Eu (III) in the Tamusu area were comprehensively clarified. The experimental results show that the adsorption capacity of clay rocks is closely related to the mineral composition. Among them, Analcime has the most significant contribution to the adsorption of Eu (III), followed by Dolomite and Ankerite. The adsorption data were fitted by Langmuir, Freundlich and Temkin adsorption models. It was found that the Langmuir model had the best fitting effect on all samples at 25°C (R^2 >0.90), and it was speculated that the adsorption process was mainly single-layer uniform adsorption.

Further thermodynamic adsorption experiments showed that as the temperature increased from 25°C to 80°C, the adsorption capacity of the sample TZK1-543 increased significantly, indicating that the process was an endothermic reaction. However, the adsorption behavior of the sample TZK2-516 shows a large temperature dependence, and its adsorption capacity changes little at high temperature, and the conventional adsorption model is difficult to accurately describe its adsorption mechanism. Through XPS analysis, it was found that the binding energy of Eu, Ca and Mg in the sample changed significantly after Eu(III) adsorption, indicating that ion exchange and surface complexation reactions occurred between Eu(III) and the surface of clay minerals. In particular, ion exchange occurred between Na^+ and Eu(III) in analcime, while Ca sites in dolomite promoted the adsorption of Eu(III) through surface complexation.

In addition, the effect of pH change on the alteration was also studied. The results showed that the adsorption capacity of Eu(III) increased significantly with the increase of pH value, especially when pH > 8, the adsorption capacity reached the maximum. At low pH (<6), the solubility of Ca^{2+} and Mg^{2+} increased, resulting in a decrease in adsorption sites, thereby reducing the adsorption efficiency. The SEM-EDS element distribution map further verified the uniform distribution of Eu(III) adsorption sites in clay rocks, indicating that the adsorption of Eu(III) is a multi-mineral synergistic process.

The conclusion of this study is that the adsorption behavior of Tamusu clay rocks on Eu(III) is mainly affected by mineral composition, temperature and pH value. Because of its stable framework structure and ion exchange capacity, analcime plays a leading role in Eu(III) adsorption. The dolomite and ankerite contribute to the adsorption process through surface complexation. The increase in temperature promoted the adsorption of Eu(III), but also accelerated the dissolution of carbonate minerals, resulting in the dynamic change of adsorption sites. Under alkaline conditions, the adsorption efficiency of Eu(III) was significantly improved, while low pH was not conducive to adsorption. These findings provide an important scientific basis for optimizing the design and long-term safety assessment of the high-level radioactive waste geological repository.

Copyright on 7th Asia-Pacific Symposium on Radiochemistry 2025



Graphical Abstract

CONCLUSIONS

This study systematically investigated the adsorption behavior of Eu(III) on Tamusu claystone under simulated geological repository conditions, elucidating the critical roles of mineral composition, temperature, and pH in governing radionuclide retention. Key findings are summarized as follows:

1. The claystone samples (300–800 m depth) were dominated by analcime, dolomite, and ankerite. Adsorption capacity at 25°C followed the order: TZK1-543 > TZK2-516 ≈ TZK1-603 > TZK2-390 > TZK1-747, with analcime contributing most significantly to Eu(III) retention due to its stable framework and ion exchange capability[1]. Dolomite-ankerite aggregates exhibited secondary adsorption contributions, while albite showed minimal affinity.

2. Elevated temperatures (25–80°C) enhanced Eu(III) adsorption on analcime-rich TZK1-543, fitting the Langmuir model (R^2 > 0.99), indicative of monolayer-dominated endothermic processes. In contrast, TZK2-516, with higher dolomite/ankerite content, deviated from conventional models due to temperature-induced carbonate dissolution, highlighting the destabilizing effect of thermal stress on less stable mineral phases[2].

3. Adsorption efficiency increased sharply under alkaline conditions (pH > 8), reaching a maximum capacity of 1.02 $\times 10^{-4}$ mol/g. Low pH (<6) promoted Ca^{2+}/Mg^{2+} dissolution, reducing available adsorption sites. The inverse correlation between ion dissolution and adsorption performance underscores the importance of geochemical stability in barrier materials.

4. Analcime: Eu(III) adsorption occurred primarily via ion exchange with Na^+ in the aluminosilicate framework, as confirmed by XPS and SEM-EDS. Dolomite: Ca sites facilitated Eu(III) retention through surface complexation, though their dissolution at high temperatures compromised adsorption predictability[3].

5. The stability of analcime-rich claystones (TZK1-543) makes them superior candidates for nuclear waste containment, whereas carbonate-rich formations (TZK2-516) may require additional engineering controls to mitigate thermal alteration. These insights are critical for optimizing repository designs and long-term safety assessments.

ACKNOWLEDGMENTS

This work was supported by the National Natural Science Foundation of China [grant number 21906187], the Key Laboratory of Water and Soil Resources Conservation and Restoration in the Middle and Lower Reaches of Yellow River Basin, Ministry of Natural Resources [grant number WSRCR-2023-03], and Key Laboratory of Strategic Mineral Resources of the Upper Yellow River, Ministry of Natural Resources [grant number YSMRKF202211].

References

1. Zeng J, Sastre G, Hong SB Capturing Different Intermediate Phases during Zeolite Synthesis.J AM CHEM SOC 146 (40):27468-27474(2024)
2. Drüppel K, Stober I, Grimmer JC, Mertz-Kraus RExperimental alteration of granitic rocks: Implications for the evolution of geothermal brines in the Upper Rhine Graben, Germany.GEOTHERMICS 88:101903(2020)
3. Liao R, Chen Y, Yu C, Ye W, Wu D, Liu C, Wang QEffect of temperature on mineral evolution and adsorption of Eu3+ by bentonite in hyperalkaline conditions.CLAY CLAY MINER 72:e23(2024)

Study on the determination of evaluation parameters for assessing radionuclide migration due to surface runoff

Taro Shimada[1], Naruyuki Ueshima[2], Masakazu Namekawa[3], Shizuka Takai[4], Seiji Takeda[5]

[1]*Japan Atomic Energy Agency: 2-4 Oaza-Shirakata Tokai-mura, Ibaraki-ken, 319-1195, shimada.taro@jaea.go.jp*

[2]*NAIS: 416-1 Muramatsu Tokai-mura, Ibarakiken, 319-1112, ueshima@nais.co.jp*

[3]*NAIS: 416-1 Muramatsu Tokai-mura, Ibarakiken, 319-1112, namekawa@nais.co.jp*

[4]*Japan Atomic Energy Agency: 2-4 Oaza-Shirakata Tokai-mura, Ibaraki-ken, 319-1195, takai.shizuka@jaea.go.jp*

[5]*Japan Atomic Energy Agency: 2-4 Oaza-Shirakata Tokai-mura, Ibaraki-ken, 319-1195, takeda.seiji@jaea.go.jp*

The authors conducted laboratory experiments for runoff of dust deposited on the ground surfaces—asphalt and concrete in three different aging types—to obtain three parameters required for the CDecom programme developed to evaluate changes in initial radioactivity distribution on the ground surface: equivalent roughness coefficient, transfer rate coefficient due to flow, and suspension coefficient due to raindrop impact. As a result, correlation equations between each parameter and the arithmetic mean roughness obtained by a 3D scanner were derived. A method to set the parameters for CDecom calculation without conducting experiments was suggested.

1 INTRODUCTION

During the decommissioning of nuclear facilities, accidents might occur during dismantling activites, resulting in the release of radioactive substances in the form of dust into the atmosphere, which may be deposited on the ground surface. With rainfall, surface runoff may transport the deposited radionuclides downstream, where they may accumulate in depression. The authors had developed the CDecom programme for termination of decommissioning of nuclear facilities [1]. Recently, we improved the programme to evaluate changes in initial radioactive distribution using a distributed runoff model that divides the watershed into a mesh grid and reflects elevation and land cover conditions. The three parameters used in this evaluation [2] —equivalent roughness coefficient of the ground surface, transfer rate coefficient due to flow, and suspension coefficient due to raindrop impact—usually shouled be determined through experiments based on land cover conditions. The areas covered by concrete slopes, asphalt roads, and other surfaces within and outside sites of nuclear power plants are large, and the aging of these surfaces vary widely at a decommissioning phase. Therefore, it is required to set these parameters using simple indicators without conducting exdperiments on these surfaces. Laboratory experiments were conducted to evaluate dust deposition due to surface runoff associated with rainfall on three types of surfaces with different surface roughness, assuming the aging of asphalt and concrete.

2 METHODOLOGY

Equivalent roughness coefficient N used in CDecom program is that in Manning equation for kinematic wave method [3], is defined as

$$N = (I_b^{1/2} h_s^{5/3})/q_s \quad (1)$$

where h_s is the water depth of overland flow, I_b the gradient of the slope, q_s the flow rate at unit width. The transfer rate coefficient C_g is expressed as

$$C_g = e_h / (C_m - C) A \quad (2)$$

$$C_m = 0.05\ \gamma_s\ \rho\ (\Omega - \Omega_C)\ (I_b h_s / g)^{1/2} \quad (3)$$

$$\Omega = u I_b \quad (4)$$

$$u = (1/N) R^{2/3}\ I_b^{1/2} \quad (5)$$

where e_h is the erosion rate by flow, C_m the equilibrium transport capacity, C the particle conctration in the flow, A the cross section of overland flow, γ_s the density of the particle, ρ the density of waste, Ω the unit stream power, Ω_C the threshold value, g is the gravitational acceleration, u the velocity of overland flow, R the hydraulic radius [4]. Suspension coefficient C_f is expressed as

$$C_f = e_s / B\rho_s exp(-c_h h) P R_q \quad (6)$$

where e_s is the erosion rate by rain drop impact, B the width of overland flow, ρ_s the density of particles, P the rain fall intensity, R_q the run-off rate of overland flow, c_h the damping coefficient for splash erosion.

Data was obtained from experiments and literature, and three parameter values of N, C_g and C_f were determined according to types of material and surface roughness.

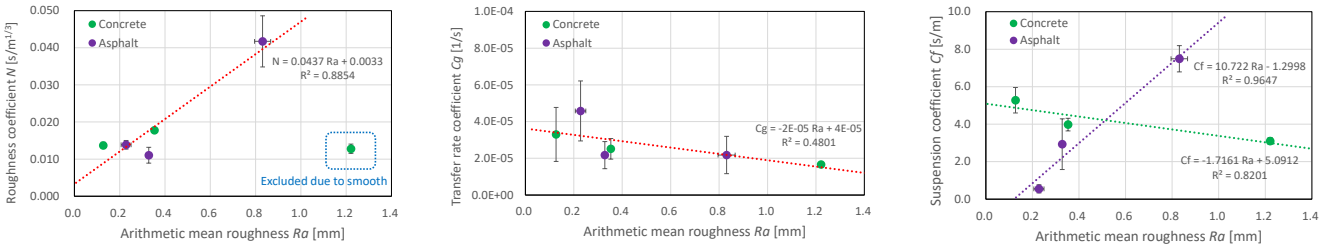
3 EXPERIMENTS

3.1 Experimental Conditions

A slope (1.5 m long, 1.0 m wide) was prepared on a 6% gradient. Iron oxide (Fe_3O_4) powder with D_{50} of 1 μm uniformly dispersed on the slope at 10 g/m² using sieve. Under the surface runoff conditions flowing down from the upstream side, a rain curtain with a median diameter of 2 mm was used to supply rainfall at a rate of 44.4 mm/h [4]. In addition, the depth of the overland flow on the slope was measured by laser coaxial displacement transducer (Keyence CL-P015) at 9 points. Overland flow down the slope including iron oxide powder was collected at the end of the slope. Meanwhile, the arithmetic mean roughness, one of the indicators of surface roughness, was calculated from the elevation distribution obtained using a 3D scanner (SHINING 3D FreeScan Combo) for each pavement condition, and correlations with the parameter values were analysed.

3.2 Experimetal Results

Figure 1 shows the obtained values for three parameters with arithmetic mean roughness. In term of equivalent roughness coefficient *N*, concrete with an arithmetic mean roughness of approximately 1.2 mm was processed for decorative purposes and has artificial depressions on its smooth surface, so it was excluded from the correlation because it was considered to offer no resistance to water flow.The results showed that the equivalent roughness coefficient *N* exhibited a positive correlation with arithmetic mean roughness regardless of material type, while the transfer rate coefficient C_g exhibited a negative correlation with that regardless of material type, both expressed as linear equations. Regarding the suspension coefficient due to raindrop impact C_f, asphalt pavement surfaces exhibited a positive correlation, while concrete surfaces exhibited a negative correlation, both expressed as linear equations. Concrete surfaces have smaller ratio and sizes of coarse aggregate, compared to asphalt pavement surfaces, resulting in smaller indentation volumes that influence raindrop impact on arithmetic mean roughness.



(a) Equivalent roughness coefficient (b) Transfer rate coefficient (c) Suspension coefficient

Fig. 1. Correlation of three parameters with arithmetic mean roughness

4. CONCLUSIONS

Parameter values of equivalent roughness coefficient *N*, transfer rate coefficient C_g and suspension coefficient C_f were obtained by laboratoy experiments using slope of concrete and asphalt pavement with rainfall to evaluate radionuclide migration on the ground surface in and around nuclear facilities. The results indicated that correlations with arithmetic mean roughness for the parameters obtained. A parameter setting method using arithmetic mean roughness as an indicator was suggested, enabling parameter setting without conducting tests involving rainfall and dust deposition.

ACKNOWLEDGMENTS

This study was funded by the Secretariat of Nuclear Regulation Authority, Nuclear Regulation Authority, Japan.

References

[1] K. Miwa, M. Namekawa, T. Shimada and S. Takeda, "Development of dose evaluation method considering radionuclides migration on the surface of the site for confirmation of completion of decommissioning", MRS Advances 7, pp. 165-169, (2022).
[2] T. Kinouchi, K. Yoshimura and T. Omata, "Modeling radiocesium transport from a river catchment based on a physically-based distributed hydrological and sediment erosion model", Journal of Environmental Radioactivity, 139, pp 407-415 (2015).
[3] US Department of Agriculture, USDA-Water Erosion Prediction Project, NSERL Report #10, (1995).
[4] T. Shimada, M. Namekawa, K. Miwa and S. Takeda, "Laboratory experiment on runoff of particles deposited on land surface by rainfall at accidents in the decommissioning stage", Proceedings of Waste Management Symposia 2023 (WM2023) (Internet). (2023).

Migration of ^{90}Sr and ^{60}Co in the groundwater-soil system surrounding the long-distance effluent pipeline of a proposed NPP: Diffusion experiments and solute transport simulation

Jia-yu Zhou[1,3†], Yuan Chen[2†], Li-li Li[3], Chuan-Pin Lee[5], Han-yu Wu[1,4,6,*], Ming-liang Kang[1,*]

[1] *Sino-French Institute of Nuclear Engineering and Technology (Sun Yat-sen University), Tangjiawan, Zhuhai, Guangdong Province, P. R. China, 519082*

[2] *State Key Laboratory of Nuclear Power Safety Technology and Equipment, China Nuclear Power Engineering Co., Ltd., Shenzhen, Guangdong, 518116, P. R. China*

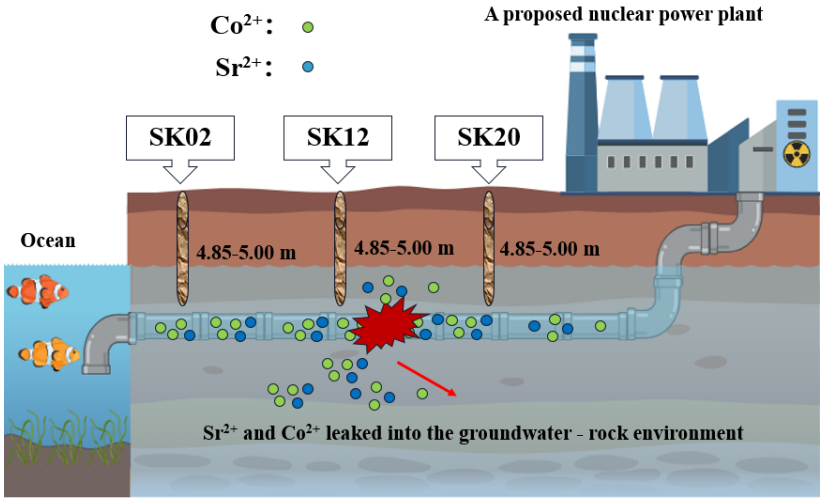
[3] *China Nuclear Power Technology Research Institute Co., Ltd., Shenzhen, Guangdong, 518000, P. R. China*

[4] *Guangdong Engineering Technology Research Center of Nuclear Safety & Emergency Response Tech., Zhuhai, Guangdong, 519082, P.R. China*

[5] *School of Nuclear Science and Engineering, East China University of Technology, Nanchang, Jiangxi, 330013, P. R. China*

[6] *Key Laboratory of Strategic Mineral Resources of the Upper Yellow River, Ministry of Natural Resources, Lanzhou, 730046, P. R. China*

Chinese regulatory authorities are increasingly paying attention to radiation safety at prospective nuclear power plants (NPPs) across their operational lifespan. Therefore, investigating the extent of source item migration and the consequential impact following a potential breach of a long-distance liquid effluent discharge pipeline at an NPP site during the site selection phase is imperative. In this study, soil samples (extracted from a depth of 4.85-5.00 m) from three boreholes near a proposed NPP site were utilized to analyze diffusion behavior under varying environmental conditions and then simulate the solute transport process of ^{90}Sr and ^{60}Co. The results revealed that the decrease of the initial concentration of the source term and the increase of the ionic strength of groundwater lead to the decrease of the capacity factor (α) and the effective diffusion coefficient (D_e) values. Sr(II) and SO_4^{2-} tend to form surface complexes and aggregate at the albite-water interface, whereas Co(II) can diffuse through the pores and interlayer space of montmorillonite. K_d values derived from diffusion experiment fittings do not align with actual adsorption capacities, rendering them unsuitable as solute transport model input parameters. Hence, K_d and D_e parameters from adsorption and through-diffusion experiments, respectively, were used to predict the migration of Sr(II) and Co(II). The study indicates that the radioactive impact of ^{90}Sr and ^{60}Co on groundwater will remain below the drinking-water quality of the World Health Organization (WHO) as long as pipeline rehabilitation is implemented within 60 days of a leakage incident. This research is crucial for the sustainable risk management of the proposed nuclear power plant in China and the preservation of the surrounding environment.



CONCLUSIONS

This study investigated the diffusion behavior of Sr(II) and Co(II) in the groundwater-soil system relevant to a proposed nuclear power plant, considering the influence of initial concentration, ionic strength, and soil composition. As the diffusion process involves the transfer of substance molecules from high- to low- concentration regions, the diffusion rate correlated positively with the concentration gradient of the diffusing substance[1]. Therefore, an increase in source fluid concentration from 540 mg/L to 1000 mg/L nearly doubled the diffusion flux (Fig. 1). As the ionic strength increased, the competitive adsorption effect was enhanced, once dynamic equilibrium was reached due to adsorption and desorption processes, the inhibition of diffusion was related to the decreased adsorption capacity.[2,3]. Soil composition also has a significant influence on the migration of Sr and Co. The enrichment of Sr(II) is related to sulfate complexation, and the enrichment of Co(II) is related to minerals rich in Fe and Mg. (Fig. 2). Meanwhile, Co(II) exhibited a greater

affinity for adsorption onto clay minerals, resulting in enhanced retention in SK12 and SK20 soils compared to SK02. Visual MODFLOW simulations, based on these diffusion parameters, predicted ^{90}Sr and ^{60}Co concentrations under a hypothetical drainage line breach scenario over 30 years. The simulated maximum concentrations of ^{90}Sr and ^{60}Co remained significantly below WHO drinking water guidance levels. These findings highlight the distinct migration behaviors of ^{90}Sr and ^{60}Co in the studied groundwater-soil system and provide critical data for nuclear safety assessments and sustainable risk management strategies for proposed nuclear power plants in China, contributing to the environmental conservation of surrounding regions (Fig. 3).

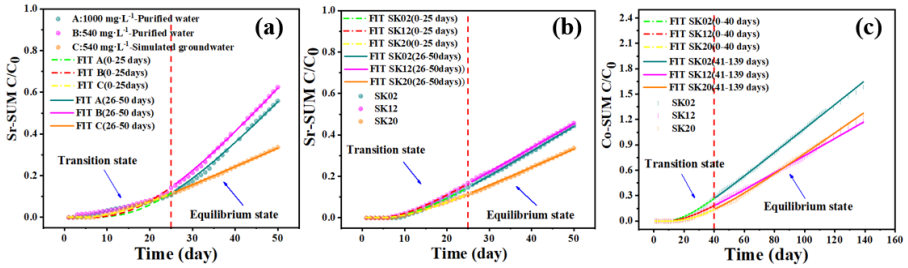


Fig. 1. Cumulative concentration of diffusion in SK02, SK12 and SK20 soils. (a): The diffusion of Sr(II) under different initial concentrations and background electrolyte conditions (soil SK20); (b): Sr(II) diffusion in different groundwater-soil systems. ($[Sr(II)]_{initial}$ = 540 mg/L); (c): Co(II) diffusion in different groundwater-soil systems. ($[Co(II)]_{initial}$ = 164 mg/L).

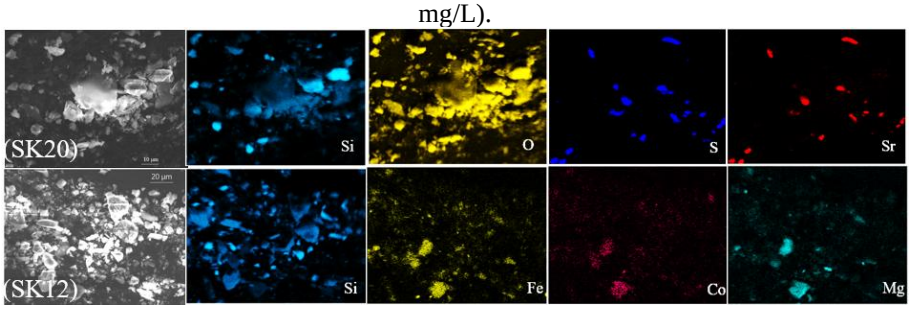


Fig. 2. SEM-EDS images of soil samples after diffusion.

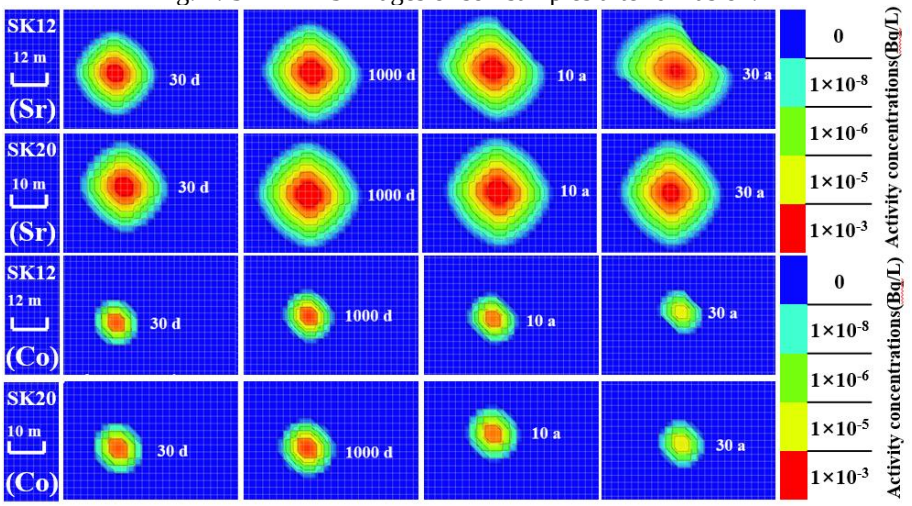


Fig. 3. Simulated spatial distribution of ^{90}Sr and ^{60}Co originating from leak points SK12 and SK20.

ACKNOWLEDGMENTS

This work was supported by the National Natural Science Foundation of China (No. 22341604, 21906187 and 42377218), Key Laboratory of Strategic Mineral Resources of the Upper Yellow River, Ministry of Natural Resources (grant number YSMRKF202211), and Foundation of China General Nuclear Power Corporation (No. K-A2021.561), and Pinnacle project of key technology of seawater cooling tower in nuclear power plant of CGNPC.

References

[1] W. Zhang, B. Ma, J. He et al., Diffusion of ^{125}I in Compacted Beishan Granite Research of Capillary In-Diffusion Method. Journal of Nuclear and Radiochemistry. 37(6), 469-475 (2015). doi.org/10.7538/hhx.2015.37.06.0469 (in Chinese)

[2] T. Melkior, S. Yahiaoui, D. Thoby et al., Diffusion coefficients of alkaline cations in Bure mudrock. Phys. Chem. E art. **32**(1-7), 453-462 (2007). doi.org/10.1016/j.pce.2006.04.035

[3] S. Savoye, C. Beaucaire, B. Grenut et al., Impact of the solution ionic strength on strontium diffusion through the C allovo-Oxfordian clayrocks: An experimental and modeling study. Appl. Geochem. **61**, 41-52 (2015). doi.org/10.10 16/j.apgeochem.2015.05.011

Poster Presentation | [P5]Environmental Radiochemistry Applicable for Nuclear Non-Proliferation, Disarmament, and Nuclear Security

Mon. Sep 15, 2025 6:30 PM - 8:00 PM JST | Mon. Sep 15, 2025 9:30 AM - 11:00 AM UTC Poster

[Poster] P5

[P-P5-01]

Analysis of ^{140}Ba/^{140}La detections at the CTBT Okinawa radionuclide monitoring station in May 2010

*Akiko Furuno[1], Yuichi Kijima[1], Toshiyuki Kurihara[1], Yutaka Tomita[1] (1. Japan Atomic Energy Agency (Japan))

[P-P5-02]

ANALYSIS OF CARBON AND FINE CHARCOAL PARTICLES IN SOIL WITH SOIL PROFILE SURVEY

*Maiko Ikegami[1], Jun Inoue[2], Satoshi Fukutani[1], Koichi Takamiya[1], Hiroshi Yashima[1], Tadashi Mukai[1], Tomonori Adachi[1], Yasuhito Igarashi[1] (1. Institute for Integrated Radiation and Nuclear Science, Kyoto University (Japan), 2. Osaka Metropolitan University (Japan))

[P-P5-03]

Classification of molten particles collected in Hiroshima City based on FIB-TOF-SIMS analysis

*kei nagone[1], yousuke ishii[1], tetsuo sakamoto[1], satoru endo[2], yasuhito igarashi[3] (1. kogakuin univ. (Japan), 2. Hiroshima Univ. (Japan), 3. Kyoto Univ. (Japan))

[P-P5-04]

Vertical profiles of radionuclides and other indices in soil at the site of the remains ofNagasaki Medical College

*Satoshi FUKUTANI[1], Maiko Ikegami[1], Hiroshi Yashima[1], Satoru Endo[2], Naoko Fukuda[3], Sumi Yokoyama[3], Tadashi Mukai[1], Tomonori Adachi[1], Jun Inoue[4], Koichi Takamiya[1], Yasuhito Igarashi[1] (1. Institute for Integrated Radiation and Nuclear Science, Kyoto University (Japan), 2. Graduate School of Advanced Science and Engineering, Hiroshima University (Japan), 3. Atomic Bomb Disease Institute, Nagasaki University (Japan), 4. Department of Geosciences, Graduate School of Science, Osaka Metropolitan University (Japan))

©APSORC25

7th Asia-Pacific Symposium on Radiochemistry *September 14 ~ 19, 2025 • Kunibiki Messe • Shimane, Japan*

Analysis of ^{140}Ba/^{140}La detections at the CTBT Okinawa radionuclide monitoring station in May 2010

Akiko FURUNO[1], Yuichi KIJIMA[1], Toshiyuki KURIHARA[1], Yutaka TOMITA[1]

[1]*Japan Atomic Energy Agency: 2-4 Shirakata, Tokai, Ibaraki, 319-1195 Japan, furuno.akiko@jaea.go.jp*

Abstract The radioactive nuclides ^{140}Ba and ^{140}La, which are not normally detected during routine observations, were detected at the CTBT Radionuclide Monitoring Station in Okinawa from May 15 to 21, 2010. According to previous studies, these are likely to be decadent nuclides of ^{140}Xe produced by nuclear fission reactions, and there is speculation that a nuclear test may have been conducted near the Punggye-ri nuclear test site in North Korea in May 2010. However, there is no consensus on the source of these releases. We estimate the source of these detected events from the perspective of atmospheric dispersion.

1 Introduction

Japan Atomic Energy Agency (JAEA) cooperates in all aspects of work related to radionuclides in the detection of nuclear tests conducted in accordance with the Comprehensive Nuclear-Test-Ban Treaty (CTBT). Radionuclide monitoring stations are located around the world to detect radioactive nuclides released into the atmosphere as a result of nuclear tests. JAEA operates two such stations in Japan; one in Takasaki City, Gunma Prefecture, and the other in Onna Village, Okinawa Prefecture.

^{140}Ba and ^{140}La were detected successively at the Okinawa station from 15 to 21 May 2010. Okinawa Station is located in the centre of Okinawa Island. As there are no nuclear facilities in the area, these radionuclides are likely to have reached the station through long-range dispersion. In addition, ^{140}Ba and ^{140}La are not typically major radionuclides released in nuclear accidents or nuclear tests. The causes of the atmospheric release of these radionuclides and the identification of the facilities responsible have been the subject of numerous previous studies [e.g. 1]. ^{140}Ba and ^{140}La are decadent nuclides of ^{140}Xe, which is produced in nuclear fission reactions. Similar detection events have been reported in Sweden in the past during nuclear tests conducted by the former Soviet Union. There are also reports that artificial seismic waves were detected near the Punggye-ri nuclear test site in North Korea in May 2010 [2, 3]. However, these studies were not reliable, and the question of whether artificial seismic waves have been generated in North Korea remains unanswered. Several source estimation studies from an atmospheric dispersion perspective have been carried out [1, 4], all of which indicate a high probability that the source is the North Korean nuclear test site. However, these studies were carried out in 2013, with low horizontal resolution, and only backtracking analysis was used to trace the dispersion, so it was not possible to accurately identify the source. The aim of this study is to re-estimate the release sources that were not identified in the 2013 study. This will be achieved by conducting an atmospheric dispersion analysis with a higher spatiotemporal resolution than before and using a more accurate estimation method as forward tracking estimation.

2 Materials and Methods

The CTBT particulate radionuclide monitoring stations are planned to be established at 80 locations worldwide, 73 of which are currently operational. As of 2010, in addition to the Takasaki and Okinawa stations managed by Japan, there was also the Ussuriysk station near Vladivostok in Russia. The locations are shown in Figure 1. Figure 2 shows the time series of nuclear species concentrations observed at the Okinawa station.

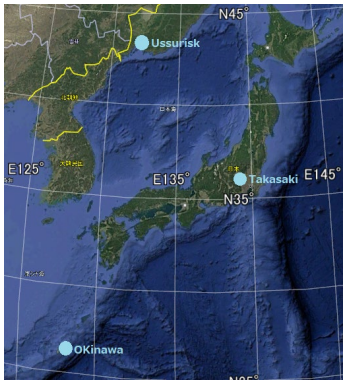


Fig. 1. CTBT Radionuclide Monitoring Stations around Japan

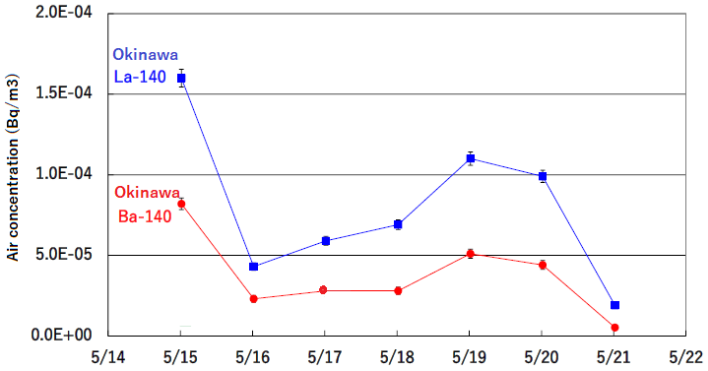


Fig. 2 Time series of air concentrations of radionuclides observed CTBT radionuclide monitoring stations around Japan from May 15 to 21

As shown in Figure 2, ^{140}Ba and ^{140}La were detected simultaneously on 15 May at the Okinawa station, despite not being normally detected there. Although their levels decreased on 16 May, they continued to be detected until 21 May. Additionally, extremely low concentrations of ^{140}La were detected at the Ussuriysk station in Russia on 15, 17, and 18 May. However, the measurements at the Ussuriysk station are highly uncertain. For security reasons, CTBTO analyses may include detections even if the uncertainty is high. ^{140}La was not detected at the Ussuriysk station in our analysis, so the measurements from this station are treated as reference values in this study. Additionally, no particulate nuclides were detected at the Takasaki station during this period.

Several methods can be used to estimate the sources of these radioactive nuclides. Back-trajectory analysis retrospectively traces particle flows from monitoring stations. The 'backtracking method' [5] performs dispersion analysis by reversing the time axis and setting the release points at the locations of high-concentration events. These methods are simple and have low computational costs. However, these methods have a fundamental limitation in that they cannot estimate the sources quantitatively by themselves. Conversely, there is also a method of estimating the release source using forward dispersion simulation. While these methods are computationally intensive, they enable more detailed narrowing down of the release source. In a primitive and simple method [6], multiple candidate sources are first set as initial conditions, and numerous dispersion simulations are performed. Subsequently, statistical methods are used to easily extract the candidate source that best matches the observed results. Back trajectory and backtracking analyses have already been performed on the events targeted in this study. Since these methods did not determine the release points, the method described in [6] will be used to estimate the release sources here. As the release amount is unknown, this study assumes a release rate of 1 Bq/hour. To discuss the agreement between calculations and observations because absolute values are unknown, agreement will be judged using error in rise time in concentration and overlap of detection periods as indicators. The analysis results will be presented at the conference.

References

[1] L.-E De Geer, “Refined evidence of a low-yield nuclear test in North Korea”, *J. Radioanal. Nucl. Chem,* **298,** 2075-2083 (2013).

[2] D. P. Schaff *et al*., “Seismological Constraints on Proposed Low-Yield Nuclear Testing in Particular Regions and Time Periods in the Past, with Comments on “Radionuclide Evidence for Low-Yield Nuclear”, *Science & Global Security,* **20,** 155-171 (2012).

[3] M. Zhang and L. Wen, “Seismological Evidence for a Low-Yield Nuclear Test on 12 May 2010 in North Korea”, *Seismological Research Letters,* **86**, No.1, January/February (2015).

[4] G. Wotawa, “Meteorological analysis of the detection of xenon and barium/ lanthanum isotopes in May 2010 in Eastern Asia”, *J. Radioanal. Nucl. Chem*., DOI 10.1007/s10967-012-2012-7 (2013).

[5] Becker, A. *et al.*, “Global backtracking of anthropogenic radionuclides by means of a receptor oriented ensemble dispersion modelling system in support of Nuclear Test-Ban Treaty verification”, *Atmos. Environ.*, **41**, 4520-4534 (2007)

[6] Furuno, A., et al., “Development of a source term estimation method for nuclear emergency by long range atmospheric dispersion simulations”, *Trans. Atom. Energy Soc. Japan*, **5**, 229–240 (2006) (inJapanese)

7th Asia-Pacific Symposium on Radiochemistry *September 14 ~ 19, 2025 • Kunibiki Messe • Shimane, Japan*

ANALYSIS OF CARBON AND FINE CHARCOAL PARTICLES IN SOIL WITH SOIL PROFILE SURVEY

Maiko Ikegami[1], Jun Inoue[2], Satoshi Fukutani[1], Koichi Takamiya[1],
Hiroshi Yashima[1], Tadashi Mukai[1], Tomonori Adachi[1], Yasuhito Igarashi[1]

[1]*Institute for Integrated Radiation and Nuclear Science, Kyoto University: 2-chome, Asashiro-Nishi, Kumatori, Sennan, Osaka, 590-0494 Japan*
[2]*Department of Geosciences, Graduate School of Science & School of Science, Osaka Metropolitan University: 3-3-138 Sugimoto, Sumiyoshi, Osaka, 558-8585, Japan*

To investigate the deposition of fine charcoal particles derived from urban fires, following the atomic bombing, the carbon concentrations and the number of fine charcoal particles in soil were analyzed as one of the targets in the soil profile survey. The carbon concentration in soil was higher in layers with smaller value (lightness and darkness) + chroma (color intensity) values of the soil. The number of fine charcoal particles was highest in layer A (a humus-rich layer), slightly low in layer LF which is composed of undecomposed plant remains, and low in layers B and C, where humus is less abundant. No relationship was found between the carbon concentration and the number concentration of fine charcoal particles in the soil layers.

1. INTRODUCTION

In the past, various investigation such as analysis of ^{137}Cs, a fission product, in soil was conducted in order to clarify the distribution area of radioactive fallout originating from the atomic bombing in 1945 in Japan. However, the closed-in fallout has not specified. The deposition of fine charcoal particles derived from urban fires, following the atomic bombing, is being analyzed using soil samples.

It is known that soil organic matter affects the behavior of various elements in soil and plays an important role in soil characteristics, so, it is necessary to analyze the carbon content, including organic carbon, in soil. A soil profile survey is necessary to investigate the distribution of fine charcoal particles in soil in more detail.

In this study, total carbon (TC) and total organic carbon (TOC) in soil were measured and a soil profile survey was conducted to examine the relationship between TC, TOC fine, soil properties, and fine charcoal particles.

2. MATERIALS AND METHODS

Soil samples were collected every 1 cm from 0 to 30 cm depth at undisturbed areas using a scraper plate in order to measure TC, TOC, and fine charcoal particles, and soil core samples were obtained for a soil profile survey using a core sampler (5 cm in diameter and 30 cm long) at the same undisturbed areas where the soil samples were collected. In order to determine the TOC concentration, a pretreatment using hydrochloric acid [1] was first performed to remove inorganic carbon from the soil, and the soil samples were dried after the addition of hydrochloric acid. High-performance TOC analyzer (N/C3100+HT1300, analytik jena) was used to measure TC and TOC concentrations in the soil. The soil profile survey and the number concentration of charcoal particles were obtained by a contractor. The soil samples were treated with acid and alkali to extract charcoal particles, which were then counted under an optical microscope.

3. RESULTS AND DISCUSSION

In this study, it was found that TC and TOC concentrations in the soil showed high values in the surface layer, decreasing with depth. A comparison of TC and TOC concentrations showed that they were almost identical at many sampling sites. This result confirmed that the soils contained almost no inorganic carbon. Compared with the results of the soil profile survey, it was shown that carbon concentrations were high or relatively high in the layers L, F, and H (a sedimentary organic matter layer) and layer A (a humus-rich layer), and low in the layer B (a less humus layer). The relationship was determined between carbon concentrations and soil color (value: lightness and darkness; chroma: color intensity). In general, the higher the carbon concentration in soil, the lower value and chroma of the soil [2]. The comparison of carbon concentration and value + chroma values at each sampling site showed that the carbon concentration was higher in layers with smaller value + chroma values, and similar results were obtained in this study.

The overall trend was that the number of fine charcoal particles was highest in layer A, slightly low in layer LF which is composed of undecomposed plant remains, and low in layers B and C, where humus is less abundant. No relationship was found between the carbon concentration and the number concentration of fine charcoal particles in the soil layers.

Copyright on 7th Asia-Pacific Symposium on Radiochemistry 2025

4. CONCLUSIONS

The carbon concentrations and the number of fine charcoal particles were analyzed using the soil profile survey. It was found that detailed soil profile survey would provide the necessary information to analyze the closed-in fallout.

ACKNOWLEDGMENTS

This study was funded by the Ministry of Health, Labour and Welfare (MHLW) under the "FY2025 Study on the Construction of a Meteorological Simulation Model for the Atomic Bombings and the Analysis of Fallout Dispersion."

References

[1] Analytik jena, TOC 0019, Application Note, TOC Solid Analyzer (2019).
[2] Atsushi Torii et al., “How can we estimate soil carbon stock by soil profile description?”, The Japanese Forest Society Congress 119 (2008).

7th Asia-Pacific Symposium on Radiochemistry *September 14 ~ 19, 2025 • Kunibiki Messe • Shimane, Japan*

Classification of molten particles collected in Hiroshima City based on FIB-TOF-SIMS analysis

Kei Nagone[1], Yousuke Ishii[2], Tetsuo Sakamoto[1,2], Satoru Endo[3], Yasuhito Igarashi[4],

[1]*Electrical Engineering and Electronics Program, Graduate School of Engineering, Kogakuin University, 2665-1 Nakano-machi, Hachioji, Tokyo, Japan*
[2]*Department of Applied Physics, School of Advanced Engineering, Kogakuin University, 2665-1 Nakano-machi, Hachioji, Tokyo, Japan*
[3]*Graduate School of Advanced Science and Engineering, Hiroshima University, 3-2, Kagamiyama 1-chome, Higashi-Hiroshima, Hiroshima, Japan*
[4]*Institute for Integrated Radiation and Nuclear Science, Kyoto University, 2 Asashiro-Nishi, Kumatori, Sennan, Osaka, Japan*

In 2019, peculiar glassy particles called "molten particles" were discovered by Wannier et al. on a beach in Hiroshima City. The molten particles are considered to have undergone a high-temperature melting process, and due to their abundance along the coast of Hiroshima Bay, it has been suggested that they may be a part of the so-called "Black Rain." However, the detection of fission products from individual particles is quite difficult, and thus it remains inconclusive whether these particles are of atomic bomb origin. About 80 years have passed after the atomic bombing, and many of the initially produced radionuclides have decayed, therefore analysis with radiation measurements become challenging. To address this issue, the present study focuses on the isotopic ratio anomalies of boron ($^{11}B/^{10}B$) and lithium ($^{7}Li/^{6}Li$), because they are related to boron-neutron-capture reaction. The isotopic measurements were performed using an FIB-TOF-SIMS apparatus. Notably, the molten particles can be classified into four color-based types; black, red, yellow, and silver. We investigated the correlation between particle color and isotopic ratios. As a result, a positive correlation in isotopic anomalies of B and Li was observed in the yellow particles. However, this finding alone is not enough to conclude the particles originated from the atomic bomb. Therefore, we further examined composition of major and trace elements, as well as cross-sectional textures, to identify whether distinct characteristics exist among the particle types. Cross-sectional texture analysis revealed features specific to each color type. These findings are expected to contribute to future comparative studies with molten particles found outside Hiroshima and to investigations aimed at determining their origin.

1 Introduction

Currently, soil surveys are being conducted as part of efforts to redefine the areas affected by the so-called "Black Rain." However, owing to some factors such as reduction in radiation dose over time and soil disturbance, there is a demand for additional indicator that have preserved the original environmental conditions [1]. In this study, attention has been drawn to a group of particles called "molten particles" found in Hiroshima City by Wannier et al. [1]. The molten particles could be originated from a variety of sources other than the atomic bomb, such as meteorites, volcanic activity, or industries. Therefore, the origin of the molten particles should be carefully clarified. We analyzed the molten particles using a focused ion beam time-of-flight secondary ion mass spectrometry (FIB-TOF-SIMS) apparatus developed by the authors[2], which allows simultaneous imaging of all elements and isotopes on both surface and interior of single particles.

2 Method

First, the sand was collected from the beach at Moto-Ujina in Hiroshima City, and particles with high metal content were isolated using magnetic separation. Subsequently, spherical particles, considered to have undergone a melting process, were selected using an optical microscope. These particles were classified into four color types: black, red, yellow, and silver[3] by their appearance. Cross sections of particles were prepared using a cross-section polisher. The cross-sectioned samples were introduced into the FIB-TOF-SIMS system, then elemental and isotopic ratio analysis was performed.

3 Result

3.1 Isotopic Anomalies Due to Neutron Capture Reactions

We focused on isotopic anomalies resulting from neutron capture reactions that could have occurred under neutron flux from the atomic bombing. We selected ^{10}B as an indicator, because it existed in soil and woods, and has a high neutron capture cross section results in the $^{10}B(n,\alpha)^{7}Li$ reaction (also known as the BNC reaction). If this reaction occurred, we would expect deviations in both $^{11}B/^{10}B$ and $^{7}Li/^{6}Li$ isotopic ratios from their natural abundances.

Results of the analysis showed that many of the yellow molten particles exhibited such isotopic anomalies. Moreover, a positive correlation was observed between the anomalies in B and Li isotopic ratios. These deviations were greater than those typically found in natural sources such as meteorites or volcanic materials, suggesting that some of the yellow molten particles may be of atomic bomb origin.

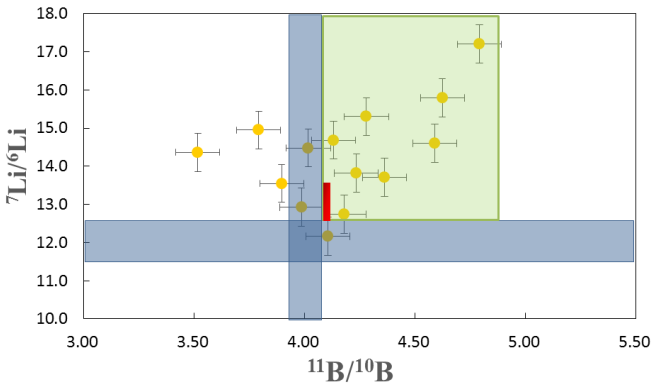


Fig. 1. Isotopic analysis result of yellow molten particles

3.2 Classification and Characteristics of Hiroshima Molten Particles by Color

However, isotopic anomalies alone are insufficient to distinguish these particles from those formed by global fallout due to large-scale nuclear detonations. Therefore, we investigated whether color-dependent differences as classified in previous studies [3]. As a result, the colors are associated with specific compositional or structural features. While no distinct characteristics were found in the elemental composition, cross-sectional texture analysis revealed texture features unique to each color group. In the Future work, we will compare the yellow molten particles, which exhibited isotopic anomalies, with similar particles found in areas outside Hiroshima, such as the Tokyo region.

4. CONCLUSION

This study successfully characterized color-dependent features of Hiroshima molten particles and examined isotopic ratios of elements such as boron, allowing for new insights into the possible influence of the atomic bomb. These results enable comparisons with molten particles from other regions, potentially allowing for the identification of particles unique to Hiroshima and distinguishing them from those produced by global fallout. Such comparative studies will be crucial in exploring the relationship between these molten particles and the "Black Rain," and thus remain an important subject for future investigation.

ACKNOWLEDGMENTS

This study was conducted as part of the project commissioned by the Ministry of Health, Labour and Welfare of Japan, titled *"Study on the Construction of a Meteorological Simulation Model for the Atomic Bombings and the Analysis of Fallout Dispersion."*

References

[1] M. M. A. Wannier *et al.*, *Anthropocene*, **25**, 100196 (2019).
[2] T. Sakamoto *et al.*, *Appl. Surf. Sci.*, **255**, 1617 (2008).
[3] S. Endo *et al. Journal of Nuclear and Radiochemical Sciences*, **23**, 5 (2023)

Vertical profiles of radionuclides and other indices in soil at the site of the remains of Nagasaki Medical College

Satoshi Fukutani[1], Maiko Ikegami[1], Hiroshi Yashima[1], Satoru Endo[2], Naoko Fukuda[3], Sumi Yokoyama[3], Tadashi Mukai[1], Tomonori Adachi[1], Jun Inoue[4], Koichi Takamiya[1], Yasuhito Igarashi[1] and WG Soil

[1] *Institute for Integrated Radiation and Nuclear Science, Kyoto University: 2-1010, Asashiro-Nishi, Kumatori, Osaka, 590-0494, Japan*

[2] *Graduate School of Advanced Science and Engineering, Hiroshima University: 1-4-1 Kagamiyama, Higashi-Hiroshima, Hiroshima, 739-8527, Japan*

[3] *Atomic Bomb Disease Institute, Nagasaki University: 1-12-4, Sakamoto, Nagasaki, 852-8523, Japan*

[4] *Department of Geosciences, Graduate School of Science, Osaka Metropolitan University: 3-3-138 Sugimoto, Sumiyoshi, Osaka, 558-8585, Japan*

In 2023, the remains of the former Nagasaki Medical College were excavated from the current Nagasaki University Sakamoto Campus. Almost all the buildings of the former Nagasaki Medical School were destroyed by the atomic bombing of Nagasaki in 1945. This survey was conducted in the belief that traces of the atomic bombing remained not only in the buildings but also in the soil.
Soil samples were collected at 12 points along the depth direction using soil sections exposed by excavation for the excavation of the remains. Cs-137, Pb-210, and other indices, for example, total carbon (TC), were measured from these samples and their depth profiles were obtained. The results of the analysis were discussed.

1. INTRODUCTION

We are conducting an identification study of the close-in fallout ("Black Rain") from the atomic bombs at Hirosima and Nagasaki. The remains of the former Nagasaki Medical School excavated at the Sakamoto Campus of Nagasaki University are a valuable remnant of the atomic bombing. Almost all of the buildings of the former Nagasaki Medical School were destroyed by the atomic bombing of Nagasaki in 1945. The remains are the remnants of the buildings, but the soil around them is also thought to retain traces of the atomic bombing. We conducted a survey to contribute to the study of closed-in fallout.

2. MATERIALS AND METHODS

Soil samples were collected at 12 points in depth, laterally, using soil sections that were excavated and exposed for the excavation of the remains. These soil samples were taken back to the laboratory, air-dried, and sieved through a 2 mm mesh size sieve to be used as measurement samples. A portion of the measurement sample was taken and the γ rays from the sample were measured with a Ge semiconductor detector (GSW275L, Canberra). And other portion was used for Total Carbon (TC) measurement by a high-performance TOC analyzer (N/C3100+HT1300, Analytik Jena).

3. RESULTS AND DISCUSSION

Cs-137 (662 keV) and Pb-210 (46.5keV) concentration from γ ray spectrometry were shown in Fig. 1, and TC concentration from TOC analyzer was in Fig. 2. Cs-137 is one of typical fallout nuclide from nuclear fission, and Pb -210 is natural radionuclide from Uranium series. In Fig.1, both Cs and Pb show a peak around 46 cm depth. In Fig.2, Similarly, TC concentration increases significantly. One interpretation is that this 46cm depth area was the ground surface in 1945.

Copyright on 7th Asia-Pacific Symposium on Radiochemistry 2025

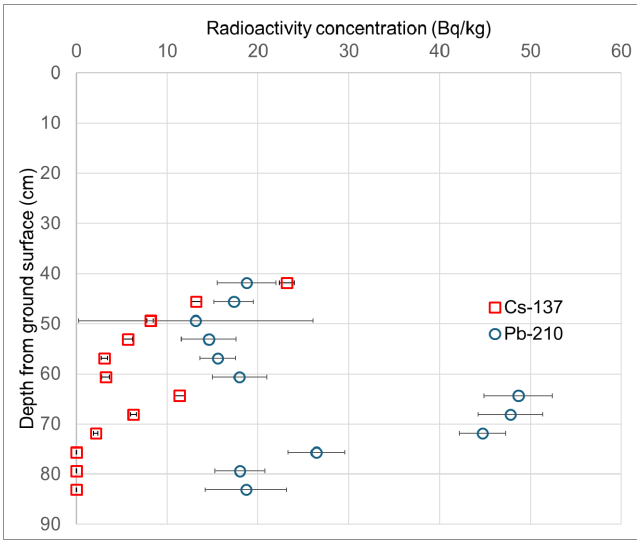


Fig. 1. Vertical distribution of Cs-137 and Pb-210

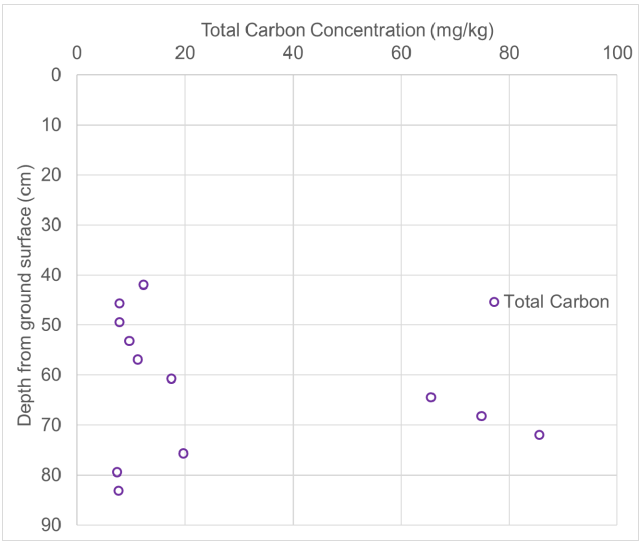


Fig. 2. Vertical distribution of total carbon (TC)

Opening Ceremony

Mon. Sep 15, 2025 8:45 AM - 9:15 AM JST | Sun. Sep 14, 2025 11:45 PM - 12:15 AM UTC Hall S(Int'l)

[OP] Opening Ceremony

8:45 AM - 9:15 AM JST | 11:45 PM - 12:15 AM UTC

Opening Ceremony

©APSORC25

Plenary Talk | Plenary Talk

Tue. Sep 16, 2025 8:45 AM - 9:30 AM JST | Mon. Sep 15, 2025 11:45 PM - 12:30 AM UTC Hall S(Int'l)

[PL2] Pleanary Talk 2 by Chirstoph E. Duellmann

8:45 AM - 9:30 AM JST | 11:45 PM - 12:30 AM UTC

[PL02]

Synthesis and chemical studies of superheavy elements

*Christoph E Duellmann[1,2,3] (1. Johannes Gutenberg University Mainz (Germany), 2. GSI Helmholtzzentrum fuer Schwerionenforschung GmbH, Darmstadt (Germany), 3. Helmholtz Institute Mainz (Germany))

©APSORC25

7th Asia-Pacific Symposium on Radiochemistry *September 14 ~ 19, 2025 • Kunibiki Messe • Shimane, Japan*

SYNTHESIS AND CHEMICAL STUDIES OF SUPERHEAVY ELEMENTS

Christoph E. Düllmann[1,2,3]

[1]*Johannes Gutenberg University Mainz, Fritz-Strassmann-Weg 2, 55128 Mainz, Germany, duellmann@uni-mainz.de*
[2]*GSI Helmholtzzentrum für Schwerionenforschung GmbH, Planckstr. 1, 64291 Darmstadt, Germany*
[3]*Helmholtz Institute Mainz, Staudingerweg 18, 55128 Mainz, Germany*

With the synthesis of elements up to oganesson (Og, element 118) [1], their acceptance as members of the periodic table of the elements [2] and their naming [3], the seventh row of this icon of chemistry is now complete. The now known elements reach well into the realm of the long-sought "island of stability of superheavy nuclei". Long-predicted [4], this is made up of nuclei with long nuclear lifetimes, due to nuclear shell effects associated with the next nuclear shell closures beyond $^{208}_{82}Pb_{126}$, commonly expected around proton number Z ≈ 114-126. Experimental data validate the concept, but the location of the center as well as the extension of the "island" are not yet clear [5]. Stabilizing effects pertaining to this region of enhanced nuclear stability manifest in the known heaviest isotopes, rendering their half-lives long enough for their chemical study.

Electron shells around superheavy nuclei experience a strong Coulomb attraction, accelerating electrons near the nucleus to relativistic velocities, rending atoms of these elements prime laboratories for studying the influence of relativistic effects on atomic and chemical properties [6]. The following topics are thus of prime interest in current superheavy element production and chemistry research:
-optimizing their production in heavy-ion induced fusion-evaporation reactions. Main aims include identifying the most promising routes to produce yet unknown nuclei, including those of elements beyond Og [7];
-their nuclear structure, studied by nuclear spectroscopy [8], by high-precision atomic mass studies [9], and by laser spectroscopic hyperfine structure studies, employing the interaction of electrons with the nucleus [10,11];
-their chemical properties, typically studied by single-atom gas chromatography on hetero-surfaces [12].

After a general introduction to the topic of superheavy element research, I will highlight the experimental progress in the field in the above mentioned areas, centering on work performed at my home institution, GSI Darmstadt [13] and focusing on their chemical study. The current status of such studies is depicted in the periodic table in Fig. 1.

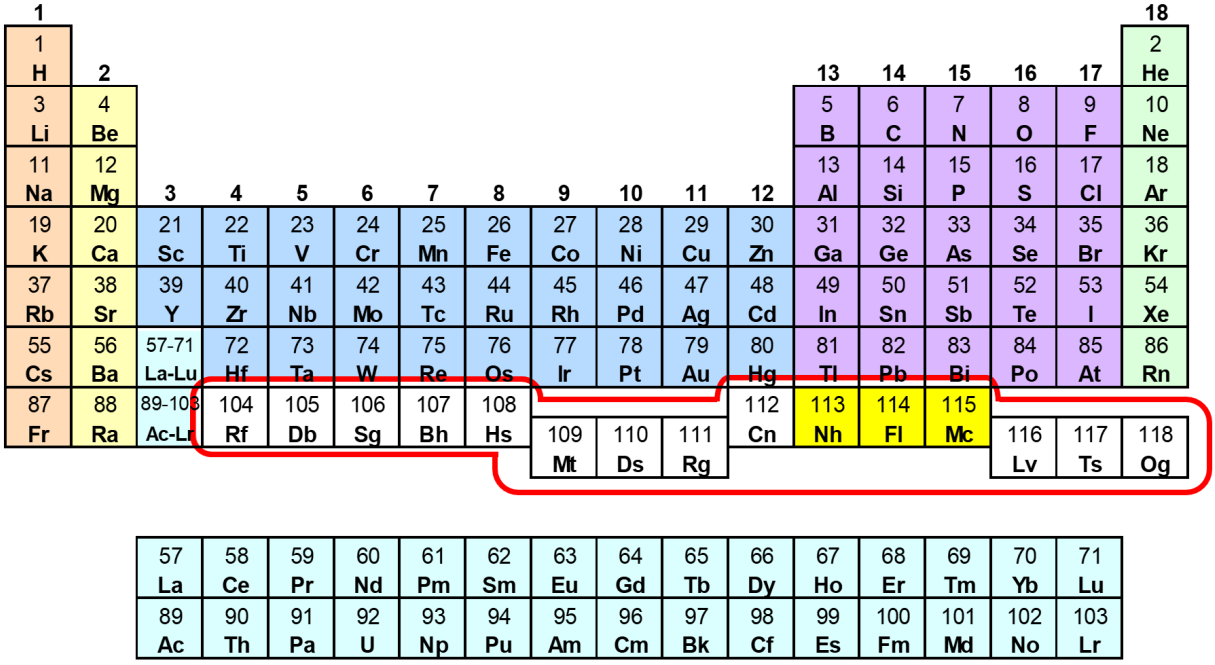


Fig. 1. Current periodic table of the elements. The superheavy elements with atomic numbers ≥104 are located inside the red border. They follow the actinide series, which terminates at Lr, and they thus constitute the transactinide elements. Elements 109 – 111 and 116 – 118 have never been chemically characterized to date and are shown offset. Most recently, chemical properties of the elements 113 – 115, highlighted in yellow, have been determined.

Copyright on 7th Asia-Pacific Symposium on Radiochemistry 2025

Current chemical research at the forefront of the heaviest elements focuses on the 7p elements. The most long-lived known isotopes of these elements feature half-lives of at most a few seconds and can be produced at rates of at most single atoms per day at contemporary experimental facilities. The most successful method for such studies is single-atom gas phase chromatography on hetero-surfaces [12], and the current focus is on the elements from Nh onwards. Fully-relativistic quantum chemical calculations predict these elements to be less reactive than their lighter homologs (e.g. [14-19]) due to relativistic stabilization of the $7s_{1/2}$ and $7p_{1/2}$ orbitals that make up the valence shell of these elements; this also holds for Mc, which accommodates one electron in the $7p_{3/2}$ orbital; density-functional theory-based calculations of their interaction with hetero-surfaces (gold and quartz, as used in the experiment) predict reduced chemical reactivity for Fl, which features a $7s_{1/2}^2 7p_{1/2}^2$ quasi-closed shell electron configuration. Its neighbors with unpaired electrons should exhibit stronger reactivity towards these surfaces, albeit also they are expected to be less reactive than their lighter homologs.

First reports on experimental studies of $_{113}$Nh emerged in 2014 [20], followed by unsuccessful attempts [21,22], which also cast much doubt [22] on the results reported in [20], indicating the need for more efficient setups that were suitable study elements in a wide range of volatility and reactivity. In the past three years, the interaction strength of Nh [23], Fl [24], as well as Mc [23] (where the studied isotope ^{288}Mc has a half-life of only ≈200 ms) with quartz and gold surfaces was measured at GSI and has been reported. Indeed, Fl was shown to exhibit the lowest reactivity, confirming the expected trend and thus validating the decade-old concept of a quite inert element 114 [25], albeit it is less inert than noble gases [23].

Experimental developments towards yet more short-lived elements beyond Mc are already underway [26]. They go hand in hand with advances of actinide target fabrication methods [27], as they are needed in light of ever more powerful accelerators [28]. These shall provide substantially higher beam intensities to reach new elements and isotopes accessible with smaller cross sections; they will also provide higher rates of known nuclei to allow for in-depth next-generation studies.The prospects for experimental reach towards the end of the 7p series and thus the chemical characterization also of Lv, Ts, and Og and the discovery of yet heavier elements are thus excellent.

References

[1] Yu.Ts. OGANESSIAN and V.K. UTYONKOV, *Rep. Prog. Phys.* **78**, 036301 (2015).
[2] P. KAROL *et al*., *Pure Appl. Chem.* **88**, 139 (2016); *ibid.* **88**, 155 (2016).
[3] L. ÖHRSTRÖM and J. REEDIJK, *Pure Appl. Chem.* **88**, 1225 (2016).
[4] A. SOBICZEWSKI *et al*., *Phys. Lett.* **22**, 500 (1966); W.D. MYERS *et al*., *Nucl. Phys*. **81**, 1 (1966).
[5] O. SMITS *et al*., *Nat. Rev. Phys.* **6**, 86 (2024).
[6] P. PYYKKÖ and J.-P. DESCLAUX, *Acc. Chem. Res.* **12**, 276 (1979); V. PERSHINA, *Radiochim. Acta* **107**, 833 (2019).
[7] Ch.E. DÜLLMANN, *EPJWC* **131**, 08004 (2016); H. HABA, *Nat. Chem.* **11**, 10 (2019); J. KHUYAGBAATAR *et al*., *Phys. Rev. C* **102**, 064602 (2020); H.M. ALBERS *et al*., *Phys. Lett. B* **808**, 135626 (2020); J.M. GATES *et al*., *Phys. Rev. Lett.* **133**, 172502 (2024).
[8] D. ACKERMANN and Ch. THEISEN, *Phys. Scr.* **92**, 083002 (2017).
[9] E. MINAYA RAMIREZ *et al*., *Science* **337**, 1207 (2012).
[10] M. BLOCK *et al*., *Prog. Part. Nucl. Phys.* **116**, 103834 (2021).
[11] J. WARBINEK *et al*., *Nature* **634**, 1075 (2024).
[12] A. TÜRLER *et al*., *Nucl. Phys. A* **944**, 640 (2015); A. TÜRLER and V. PERSHINA, *Chem. Rev*. **113**, 1237 (2013).
[13] Ch.E. DÜLLMANN *et al*., *Radiochim. Acta* **110**, 417 (2022).
[14] V. PERSHINA, Inorg. Chem. **57**, 3948 (2018). (Cn, Nh, Fl on Au)
[15] V. PERSHINA and M. ILIAS, *Inorg. Chem.* **58**, 9866 (2019). (Nh Tl on Au)
[16] L. TROMBACH *et al., Phys. Chem. Chem. Phys.* **21**, 18048 (2019).
[17] P. SCHWERDTFEGER *et al*., *Nat. Rev. Chem.* **4**, 359 (2020).
[18] V. PERSHINA *et al*., *Inorg. Chem.* **60**, 9796 (2021) (115 Bi / Nh on quartz)
[19] V. PERSHINA and M. ILIAS, *Dalton. Trans.* **51**, 7321 (2022) (Cn and Fl and oxides on Au and quartz)
[20] S.N. DMITRIEV *et al*., *Mendeleev Comm.* **24**, 253 (2014)
[21] N.V. AKSENOV *et al*., *Eur. Phys. J. A* **53**, 158 (2017).
[22] A. YAKUSHEV *et al*., *Front. Chem.* **9**, 753738 (2021).
[23] A. YAKUSHEV *et al*., *Front. Chem.* **12**, 1474820 (2024).
[24] A. YAKUSHEV *et al*., *Front. Chem.* **10**, 976635 (2022).
[25] K.S. PITZER, *J. Chem. Phys*. **63**, 1032 (1975).
[26] V. VARENTSOV and A. YAKUSHEV, *Nucl. Instrum. Meth. A* **940**, 206 (2019).
[27] Ch.E. DÜLLMANN *et al*., *J. Radioanal. Nucl. Chem*. **332**, 1505 (2023).
[28] Yu.Ts. OGANESSIAN *et al*., *Phys. Rev. C* **106**, L031301 (2022); M. BASTEN *et al*., *Rev. Sci. Instrum.* **93**, 063303 (2022); A. DROUART *et al*., *Nucl. Phys. A* **834**, 747c (2010).

Invited & Contributed Talk | [S1]Evolution of the Periodic Table of the Elements

Tue. Sep 16, 2025 9:35 AM - 10:45 AM JST | Tue. Sep 16, 2025 12:35 AM - 1:45 AM UTC Hall S(Int'l)

[S1] Evolution of the Periodic Table of the Elements

9:35 AM - 10:05 AM JST | 12:35 AM - 1:05 AM UTC

[S1-01(Invited)]

Status and Prospect of the SHE Chemistry at IMP

*Zhi Qin[1], Yang Wang[1] (1. Institute of Modern Physics, CAS (China))

10:05 AM - 10:25 AM JST | 1:05 AM - 1:25 AM UTC

[S1-02]

First results of Cn and Fl chemistry experiments at the Superheavy Element Factory

*Nikolay Aksenov[1] (1. Flerov Laboratory of Nuclear Reactions, Joint Institute for Nuclear Research (Russia))

10:25 AM - 10:45 AM JST | 1:25 AM - 1:45 AM UTC

[S1-03]

Fast Chemistry Experiments Beyond Flerovium

*Patrick Steinegger[1,2], Georg Tiebel[1,2], Annie Bukowski[3], Titeana Cook[3], Rugard Dressler[1], Robert Eichler[1,4], Charles M. Folden III[3], Jenna Garcia[3], Isaac Haynes[3], Dominik Herrmann[1], Yuta Ito[5], Amelia Kirkland[3], Jordan Mildon[3], Tetsuya K. Sato[6], Evgeny Tereshatov[3], Alexander Vögele[1], Vera Zakusilova[3] (1. Paul Scherrer Institut (Switzerland), 2. ETH Zürich (Switzerland), 3. Texas A&M University (United States of America), 4. University of Bern (Switzerland), 5. Wako Nuclear Science Center (Japan), 6. Japan Atomic Energy Agency (Japan))

©APSORC25

7th Asia-Pacific Symposium on Radiochemistry *September 14 ~ 19, 2025 • Kunibiki Messe • Shimane, Japan*

Status and Prospect of the SHE Chemistry at IMP

Z. Qin[1*], Y. Wang[1**]

[1] *Institute of Modern Physics, Chinese Academy of Sciences, Lanzhou 730000, China, *qinzhi@impcas.ac.cn; **wangyang@impcas.ac.cn*

Due to the extremely low production yield and short half-lives, experiments to explore the chemical properties of SHEs (superheavy elements, Z > 103) always rely on state-of-the-art equipment. IMP (Institute of Modern Physics, Chinese Academy of Sciences) has successfully commissioned the China Accelerator Facility for Superheavy elements (CAFE2) and the gas-filled recoil separator SHANS2 [1], which offer us the opportunity to perform experiments on the chemistry of SHEs in China.

Recently, a thermochromatography detection system named LEGEND (on-Line Experiment in Gas-phasE for Nihonium Detector) has been developed in IMP for the chemical study of SHEs [2]. On-line test experiments with short-lived Fr and Tl isotopes have been performed. Rotating 243Am targets with a diameter of 20 cm were successfully prepared. First exploration with a 48Ca beam and 243Am targets at CAFE2 and SHANS2 was performed using the LEGEND with high performance 4H-SiC detectors [3], and one 288Mc (Z=115) event was observed at the high temperature zone (65℃) on a Si3N4 surface. 266Bh (Z=107) is also available in the 243Am(26Mg,3n) reaction at CAFE2 and SHANS2. Based on the above achievements, experimental study on the chemistry of Nh (Z=113) and Mc, as well as the Bh carbonyls will be carried out at IMP in the near future.

References

[1] S. Xu et al., *Nucl. Instrum. Methods phys. Res. A* **1050**, 168113 (2023)
[2] Z. Jia et al., *Nucl. Instrum. Methods phys. Res. A* **1072**, 170166 (2025).
[3] L. Ren et al., *Nucl. Instrum. Methods phys. Res. A* **1072**, 170181 (2025)

Copyright on 7th Asia-Pacific Symposium on Radiochemistry 2025 - S1-01 -

7th Asia-Pacific Symposium on Radiochemistry *September 14 ~ 19, 2025 • Kunibiki Messe • Shimane, Japan*

FIRST RESULTS OF Cn AND Fl CHEMISTRY EXPERIMENTS AT THE SUPERHEAVY ELEMENT FACTORY

N.V. Aksenov, A.S. Madumarov, A.A. Astakhov, A.I. Golczman, G.A. Bozhikov, A.I. Svirikhin, A.Yu. Bodrov, S.N. Dmitriev

Flerov Laboratory of Nuclear Reactions, Joint Institute for Nuclear Research, Joliot-Curie,6, Dubna, Russia, 141980, nikolay.aksenov@jinr.ru

The new JINR basic facility dedicated to study properties of SHE – accelerator complex SuperHeavy Element Factory (SHE Factory) started operating at FLNR in 2019. Nuclear chemistry research is one of the key areas of its fundamental research program. The increased beam intensities at the new DC-280 heavy ion accelerator open up unique possibilities to study the chemical properties of SHE synthesized in fusion reactions with extremely small cross sections at a new statistical level [1]. In this sense, the most important research topic in SHE chemistry is currently considered to be the experimental study of the volatility and adsorption behavior of Cn and Fl [2].

Having started in 2007 at the U-400 accelerator at FLNR [3,4], we continue to study the chemical properties of these elements and its lighter homologues in Periodic Table using gas adsorption thermochromatography in a new round of experiments at the SHE Factory. For this purpose, we have created an experimental complex, including an improved chemical setup for separation and detection of short-lived isotopes of Cn and Fl in the gas phase behind the new gas-filled separator GRAND [5]. The review presents first results on Fl properties obtained at the SHE Factory as well as the theoretical research, a new fast and high-efficient recoil transfer chamber developed using results of studies of stopping ranges in inert gas mixtures and gas flow dynamics of recoils, and adsorption experiments with short-lived radioisotopes of Hg in on-line model thermochromatography studies. The results of the ongoing beam time will be presented at the conference.

ACKNOWLEDGMENTS

References

[1] Yu.Ts. Oganessian, V.K. Utyonkov, D. Ibadullayev et al. “Investigation of ^{48}Ca-induced reactions with ^{242}Pu and ^{238}U targets at the JINR Superheavy Element Factory” *Phys. Rev. C*, **106**, 024612 (2022).

[2] A. Yakushev, L. Lens, Ch. E. Düllmann et al. “On the adsorption and reactivity of element 114, flerovium” *Front. Chem.* **10**:976635 (2022).

[3] R. Eichler, N.V. Aksenov, A.V. Belozerov et al. “Chemical characterization of element 112” *Nature*, **447**, 72 (2007).

[4] R. Eichler, N.V.Aksenov, Yu.V. Albin et al. “Indication for a volatile element 114” *Radiochim. Acta* **98**, 133 (2010).

[5] A.V. Yeremin, A.G. Popeko, A.I. Svirikhin et al. “Universal gas-filled separator GRAND. First experimental results” *Physics of Particles and Nuclei Letters*, **21**, 3 (2024).

Copyright on 7th Asia-Pacific Symposium on Radiochemistry 2025 - S1-02 -

FAST CHEMISTY EXPERIMENTS BEYOND FLEROVIUM

P. Steinegger[1,2], G. Tiebel[1,2], A. M. Bukowski[3,4], T. L. M. Cook[3,5], R. Dressler[1], R. Eichler[1,6], C. M. Folden III.[3,4], J. R. Garcia[3,4], I. W. Haynes[3,4], D. Herrmann[1], Y. Ito[7], A. S. Kirkland[3,4], J. A. Mildon[4,5], T. K. Sato[8], E. E. Tereshatov[3], A. Vögele[1], V. Zakusilova[3]

[1]*PSI Center for Nuclear Engineering and Sciences, 5232 Villigen PSI, AG, Switzerland, patrick.steinegger@psi.ch*
[2]*Department of Chemistry and Applied Biosciences, ETH Zürich, 8093 Zürich, Switzerland*
[3]*Cyclotron Institute, Texas A&M University, College Station, TX 77843, USA*
[4]*Department of Chemistry, Texas A&M University, College Station, TX 77843, USA*
[5]*Department of Nuclear Engineering, Texas A&M University, College Station, TX 77843, USA*
[6]*Department of Chemistry, Biochemistry and Pharmacy, University of Bern, 3012 Bern, Switzerland*
[7]*Wako Nuclear Science Center, IPNS, KEK, Wako, Japan*
[8]*Research Group for Exotic Heavy Element Nuclear Science, Advanced Science Research Center, Nuclear Science Research Institute, Japan Atomic Energy Agency, Tokai-mura, Japan*

How can we chemically characterize the heaviest and newest elements in the periodic table? Among the various techniques, gas-adsorption chromatography has proven to be the most successful. It has allowed experimentalists to derive macroscopic thermochemical properties of these so-called superheavy elements (SHEs), such as standard sublimation enthalpies. However, beyond Fl, any chemistry experiment is confronted with (1) lowest production cross sections for nuclear fusion-evaporation reactions, and (2) half-lives of produced isotopes in the sub-second range. The latter can be addressed by means of (isothermal) vacuum adsorption chromatography connected via a buffer gas cell to a physical preseparator. Here, we report on the status of this development and first off- and online experiments with short-lived radioisotopes of Hg and Po at the Paul Scherrer Institute and at the Cyclotron Institute of Texas A&M University.

1 THE BUFFER GAS CELL AND VACUUM CHROMATOGRAPHY

Chemistry experiments typically occur in the (sub-)eV range. Hence, produced nuclear reaction products (i.e., so-called evaporation residues, EVRs) must be thermalized. In an evacuated environment, the implantation and subsequent thermal release might be employed. However, this strategy proved to be insufficient for enabling stable operation over prolonged period of times [2]. Instead, a buffer gas cell (BGC; see Fig. 1) is a well-established technique to achieve EVR thermalization in low-pressure He (≈ 80 mbar). Stopped ions are subsequently mobilized by means of DC and RF electric fields and are ultimately extracted into vacuum *via* a differential pumping step [3]. From there, the transferred ions can be guided *via* a radiofrequency quadrupole (RFQ) into the isothermal vacuum adsorption chromatography (IVAC) setup. Once within the IVAC column, the injected atoms are transported over the stationary phase (i.e., dehydroxylated fused silica for the herein presented experiments) at different isothermal temperatures. The resulting break-through curve or external chromatogram of the investigated chemical species as a function of the isothermal temperature allows the determination of the adsorption enthalpy of the investigated chemical element on the provided stationary phase.

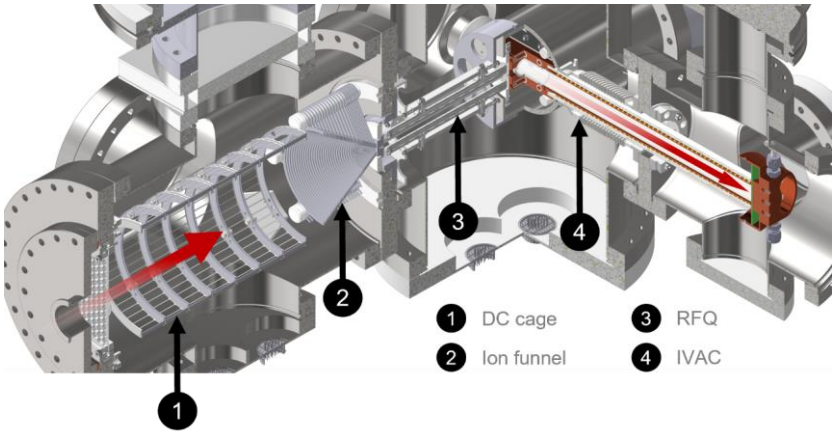


Fig. 1. The buffer gas cell (left side) as interface between the physical preseparator AGGIE (not shown; positioned at the far left) and the isothermal vacuum adsorption chromatography (IVAC) experiment (right side); the progression of the ions/atoms through the experimental setup is indicated (red arrows).

Copyright on 7th Asia-Pacific Symposium on Radiochemistry 2025 - S1-03 -

2 OFF- AND ONLINE EXPERIMENTS WITH SHORT-LIVED RADIONUCLIDES

The developed BGC+IVAC system (see Fig. 1) was tested offline using a ^{232}Th source. The comparably long-lived decay product ^{220}Rn ($t_{1/2}$ = 55.6 s) can be readily transported through the supply line of the He buffer gas to the inside of the BGC. The radioactive disintegration of ^{220}Rn affords short-lived and ionized ^{216}Po ($t_{1/2}$ = 144 ms), which can then be extracted from the BGC and guided into the IVAC setup. Mimicking conditions of an actual SHE experiment, millisecond short-lived isotopes of Hg and Po were produced at the Cyclotron Institute of Texas A&M University, separated from the primary ion beam using the gas-filled recoil separator AGGIE and subsequently injected into the BGC mounted in the focal plane of the separator. These radioisotopes, representative of the short-lived nature of all isotopes of SHEs beyond Fl, were used (1) to validate the employed Monte Carlo (MC) simulation-based transport model, (2) to investigate their adsorption behavior on dehydroxylated fused silica surfaces, and (3) to determine the processing yields.

3 CONCLUSIONS

The presented results show that the envisioned experimental setup is adequate for vacuum adsorption chromatography experiments with elements beyond Fl, all of which feature particularly short-lived isotopes with half-lives markedly below the one second threshold. This conclusion is bolstered further by the successful validation of the applied MC-based transport model. The comparison between off- and online results allows for the assessment of the key differences between the different provision pathways of the short-lived isotopes for chromatographic investigations (i.e., production by decay *vs.* production by nuclear fusion-evaporation reactions). This approach can be further improved by implementing a mass separation step after the chromatography setup, which would enable the identification of the investigated chemical species.

ACKNOWLEDGMENTS

This work has been funded by the Swiss National Science Foundation (project number 200020_196981) and is based upon work supported by the U.S. Department of Energy, Office of Science, Office of Nuclear Physics under Award No. DE-FG02-93ER40773. The authors would like to thank the accelerator staff of the Cyclotron Institute of Texas A&M University providing us with a stable ion beam throughout our experiments.

References

[1] A. Türler and V. Pershina, *Chem. Rev.*, **113** (2013).
[2] P. Steinegger et al., *J. Phys. Chem. C*, **120** (2016).
[3] M. Wada et al., Nucl. Instrum. Methods Phys. Res. Sect. B, **317** (2013).

Invited & Contributed Talk | [P2]ICP-MS Based Radioanalytical Chemistry and Related Applications

Tue. Sep 16, 2025 9:45 AM - 10:55 AM JST | Tue. Sep 16, 2025 12:45 AM - 1:55 AM UTC Hall A(MP)

[P2] ICP-MS Based Radioanalytical Chemistry and Related Applications

9:45 AM - 10:15 AM JST | 12:45 AM - 1:15 AM UTC

[P2-01(Invited)]

In situ Sm-Nd geochronology of xenotime by LA-MC-ICP-MS

*Yueheng YANG[1], Bohang Xie[2], Lei Xu[1], Zhichao Liu[3], Shitou Wu[1], Chao Huang[1], Lie-Wen Xie[1] (1. Institute of Geology and Geophysics, Chinese Academy of Sciences (China), 2. College of Earth and Planetary Science, University of Chinese Academy of Sciences (China), 3. School of Earth Sciences and Engineering, Sun Yat-sen University (China))

10:15 AM - 10:35 AM JST | 1:15 AM - 1:35 AM UTC

[P2-02]

Advances of ICP-MS analysis of actinides at atto-gram levels and its radioecological applications

*Jian Zheng[1], Keiko Tagami[1], Xiang Gu[1], Guosheng Yang[1], Shigeo Uchida[1] (1. National Institutes for Quantum Science and Technology (QST) (Japan))

10:35 AM - 10:55 AM JST | 1:35 AM - 1:55 AM UTC

[P2-03]

Determination of ultra-trace ^{237}Np and Pu isotopes in drinking and surface waters by SF-ICP-MS

*Xiang Gu[1,2], Jian Zheng[1], Guosheng Yang[1], Keiko Tagami[1], Tatsuo Aono[3], Fengchang Wu[2] (1. National Institutes for Quantum Science and Technology (Japan), 2. Institute of Eco-environmental and Soil Sciences, Guangdong Academy of Sciences (China), 3. Fukushima Institute for Research, Education and Innovation (Japan))

©APSORC25

7th Asia-Pacific Symposium on Radiochemistry *September 14 ~ 19, 2025 • Kunibiki Messe • Shimane, Japan*

In situ Sm-Nd geochronology of xenotime by LA-MC-ICP-MS

Yueheng Yang[1], Bohang Xie[2], Lei Xu[1], Zhichao Liu[3], Shitou Wu[1], Chao Huang[1], Liewen Xie[1]

[1] State Key Laboratory of Lithospheric and Environmental Coevolution, *Institute of Geology and Geophysics, Chinese Academy of Sciences, Beijing, China, 100029, and Email Address: yangyueheng@mail.iggcas.ac.cn*
[2] *College of Earth and Planetary Science, University of Chinese Academy of Sciences, Beijing, China, 100049, and Email Address: 15801265636@163.com*
[3] *School of Earth Sciences and Engineering, Sun Yat-sen University, Guangzhou, China, 510275, and Email Address: liuzhch27@mail.sysu.edu.cn*

Your abstract text goes here. Although there are to be no reference citations in abstracts, we take this opportunity to explain the style for references in the main text. References are to be set as square brackets to the text. However, when a reference is placed next to a number, abbreviation, measurement, or acronym, it is written out as square brackets [1-2 or 1,4]. You will find examples below.

Xenotime (YPO4), a commonly occurring mineral across igneous, metamorphic, sedimentary, and hydrothermal environments, offers a valuable information into geological record. Xenotime's characteristically high uranium and thorium content with minimal common lead makes it well-suited for U-Th-Pb dating (Aleinikoff et al., 2012; Andrehs and Heinrich, 1998; Fletcher et al., 2004; Liu et al., 2011; Wasconcelos et al., 2018). Additionally, enriched in heavy rare earth elements (HREEs) with a favorable Sm/Nd ratio, xenotime presents itself as a promising candidate for Sm-Nd dating (Fisher et al., 2011; Foster and Vance, 2006; Hammerli and Kemp, 2021; Xu et al., 2015; Yang et al., 2008). By integrating these dating techniques with xenotime's unique geochemical fingerprint, researchers can glean crucial insights into both the timing of rock formation and the surrounding geological context. While in situ U-Th-Pb dating of xenotime using ion and laser probes is a well-established technique, Sm-Nd isotope dating utilizing LA-MC-ICP-MS for xenotime analysis remains in its nascent stages. In contrast, in situ Sm-Nd isotopic measurements for light rare earth element (LREE)-enriched minerals like apatite, allanite, monazite, and titanite have undergone nearly two decades of development, becoming a routine analytical method with significant applications in geochronology and geochemical tracing. Notably, the application of in situ Sm-Nd isotope dating to heavy rare earth element (HREE)-rich minerals, such as xenotime, gadolinite, aeschynite, and euxenite, is currently understudied, with limited published research on xenotime specifically.

This study presents the development of an analytical protocol for in situ Sm-Nd geochronology of xenotime using LA-MC-ICP-MS. The protocol encompasses the following key steps: 1). Verification of high Sm/Nd ratio for isobaric interference correction: The validity of the high Sm/Nd ratio assumption and the effectiveness of the chosen isobaric interference correction scheme were assessed through standard solution simulations and comparison with Sm-Nd isotope data obtained from xenotime using the isotope dilution method. 2). Evaluation of uncertainty impact on initial Nd isotopes: The influence of uncertainties associated with the $^{147}Sm/^{144}Nd$ ratio on the determination of initial Nd isotopes were quantified. 3). Development of xenotime reference materials (RMs): The establishment of xenotime RMs specifically designed for Sm-Nd isotope dating via microanalysis were undertaken. The consistency of Sm-Nd ages obtained from these RMs with their established U-Pb and Lu-Hf ages were evaluated. 4). Validation of the protocol: The robustness of the developed protocol were verified by comparing the Sm-Nd geochronology results of monazite and xenotime acquired through laser ablation with their corresponding U-Pb ages. 5). Application to established U-Pb xenotime RMs: The first reported Sm-Nd ages and initial Nd isotope data were presented for well-characterized U-Pb xenotime reference materials, such as BS-1, MG-1, and Data XN (Vasconcelos et al., 2018).

In conclusion, the in situ determination of Sm-Nd isotopes in xenotime offers the potential to extract both Sm-Nd ages and initial Nd isotope compositions. When integrated with trace element data and U-Pb ages, this approach provides a comprehensive suite for unraveling the intricacies of fine-scale geological processes. This new analytical protocol for in situ Sm-Nd xenotime geochronology is expected to significantly contribute to the rapid advancement of in situ U-Pb/Lu-Hf geochronology for other HREE-enriched minerals.

ACKNOWLEDGMENTS

This work was financially supported by the Natural Science Foundation of China (42430105 and 42473037), the State Key Laboratory of Lithospheric and Environmental Coevolution (SKL-Z202304), and the Key Research Program of the Institute of Geology and Geophysics, Chinese Academy of Sciences (IGGCAS-202301). We are grateful to

Aleinikoff J.N. for providing MC-1 monazite and xenotime samples and to Wang Y.J. for the mass spectrometric measurements.

References

[1] Aleinikoff J.N., Grauch R.I., Mazdab F.K., Kwak L., Fanning C.M. and Kamo S.L. **2012**. Origin of an unusual monazite–xenotime gneiss, Hudson Highlands, New York: SHRIMP U–Pb geochronology and trace element geochemistry. *American Journal of Science*, 312, 723–765.

[2] Andrehs G. and Heinrich W. **1998**. Experimental determination of REE distributions between monazite and xenotime: potential for temperature–calibrated geochronology. *Chemical Geology*, 149, 83–96.

[3] Fisher C.M., McFarlane C.R.M., Hanchar J.M., Schmitz M.D., Sylvester P.J., Lam R. and Longerich H.P. **2011**. Sm–Nd isotope systematics by laser ablation-multicollector inductively coupled plasma-mass spectrometry: Methods and potential natural and synthetic reference materials. *Chemical Geology*, 284, 1–20.

[4] Fletcher I.R., McNaughton N.J., Aleinikoff J.A., Rasmussen B. and Kamo S.L. **2004**. Improved calibration procedures and new standards for U–Pb and Th–Pb dating of Phanerozoic xenotime by ion microprobe. *Chemical Geology*, 209, 295–314.

[5] Foster G.L. and Vance D. **2006**. In situ Nd isotopic analysis of geological materials by laser ablation MC-ICP-MS. *Journal of Analytical Atomic Spectrometry*, 21, 288–296.

[6] Hammerli J. and Kemp A.I.S. **2021**. Combined Hf and Nd isotope microanalysis of co-existing zircon and REE-rich accessory minerals: High resolution insights into crustal processes, Chemical Geology, 581, 120393.

[7] Liu Z.C., Wu F.Y., Guo C.L., Zhao Z.F., Yang J.H., Sun J.F. **2011**. In situ U–Pb dating of xenotime by laser ablation (LA)–ICP–MS. *Chinese Science Bulletin*, 56, 2948–2956.

[8] Xu L., Hu Z.C., Zhang W., Yang L., Liu Y., Gao S., Luo T. and Hu S.H. **2015**. In situ Nd isotope analyses in geological materials with signal enhancement and non-linear mass dependent fractionation reduction using laser ablation MC-ICP-MS. *Journal of Analytical Atomic Spectrometry*, 30, 232-244.

[9] Yang, Y. H., Sun, J. F., Xie, L. W., Fan, H. R., Wu, F. Y. **2008**. In situ Nd isotopic measurement of geological samples by laser ablation. *Chinese Science Bulletin*, 53, 1062-1070.

[10] Vasconcelos A.D., Gonçalves G.O., Lana C., Buick I.S., Kamo S.L., Corfu F., Scholz R., Alkmim A., Queiroga G. and Nalini H.A. **2018**. Characterization of xenotime from datas (Brazil) as a potential reference material for in situ U–Pb geochronology. *Geochemistry, Geophysics, Geosystems*, 19, 2262–2282.

Copyright on 7th Asia-Pacific Symposium on Radiochemistry 2025 - P2-01 -

Advances of ICP-MS analysis of actinides at atto-gram levels and its radioecological applications

Jian Zheng, Keiko Tagami, Xiang Gu, Guosheng Yang, Shigeo Uchida

Institute for Radiological Sciences,
National Institutes for Quantum Science and Technology (QST), Japan. Email: zheng.jian@qst.go.jp

Various actinides are produced via neutron capture reactions involving uranium in burning uranium fuel in a nuclear reactor. Actinides are highly chemically toxic and have biologically dangerous α-rays. The value of the radiation weighting factor is larger for the types of radiation having larger effects on the human body (α-particles, 20; β-particles and γ-rays, 1). Many actinides that emit α-rays have a long physical half-life, and can exist in various valence states of III to VI. In the case of a nuclear accident, the actinides that had been produced during the normal operation of the reactor could be released into the environment, causing radioactive contamination and posing a radiation risk to humans. In addition, ^{237}Np, ^{239}Pu and ^{240}Pu are also regarded as key long-term dose contributors in certain nuclear waste repositories. Therefore, it is important to study their concentration level, distribution, existence state, environmental behavior and radiation effects.

Mass spectrometry, especially ICP-MS, as an atom-counting approach that counts the atoms themselves, irrespective of their decay mode, specific activity, or half-life, is gradually replacing/has replaced conventional radiometric methods, such alpha spectrometry, LSC etc. as a main-stream technique for hard-to-detect actinides analysis. Due to the strength of argon plasma source of ICP-MS, extremely high, almost 100% ionization efficiency can be achieved for actinides, thus, highly sensitive determination of actinides can be realized. For example, our recent development of sector-field ICP-MS (SF-ICP-MS) techniques has pushed the detection limit for analysis of actinides down to attogram levels [1].

To improve the sensitivity of ICP-MS for ultra-trace radionuclide analysis, two approaches can be considered. First, is the improvement of the sample introduction efficiency of ICP-MS by the hyphenation of a membrane desolvation system to ICP-MS. It has proved to be effective for enhancing actinides analysis sensitivity by a factor of 5 to 10 and lowering the formation of H_2O-origin background species, such as oxides and hydrides (MO^+ and MH^+). Second is the use of larger sample sizes up to several tens of grams to increase the concentration factor of the target radionuclides in low-level environmental samples. With the increase of sample size, however, reducing the enhanced sample matrix effect is a great challenge for the SF-ICP-MS-based method development, which requires a powerful chemical separation capability.

This lecture will discuss the determination of hard-to-detect actinides, Pu isotopes (^{239}Pu, ^{240}Pu, ^{241}Pu), ^{241}Am and ^{237}Np using SF-ICP-MS in different environmental samples, such as soil/sediment, seawater, plants and radioactive Cs particles [2-6]. Chemical separation/purification methods for removal sample matrix (for example, separation of alkali and alkaline earth elements and REEs for ultra-trace ^{241}Am analysis), separation of interfering elements to reduce/eliminate polyatomic and isobaric interferences (for instance, separation of U, Bi, Pb, Tl, Hg, Hf, Pt, Dy for actinides analysis), will be highlighted. Several radioecological application studies on Fukushima accident derived contamination impact of Pu in the environment [7], transfer of Pu from soil to rice [8], and monitoring ^{237}Np activity concentration in seawater before and after the authorized release of contaminated water from Fukushima Daiichi Nuclear Power Plant will be presented.

References

[1] J. Zheng, J. Nucl. Radiochem. Sci. 15(1) 7-13 (2015).
[2] Z. T. Wang, J. Zheng, Y. Ni, W. Men, K. Tagami, S. Uchida, Anal. Chem. 89, 2221-2226 (2017).
[3] Z. T. Wang, J. Zheng, L. G. Cao, K. Tagami, S. Uchida, Anal. Chem. 88, 7387-7394 (2016).
[4] J. Igarashi, K. Ninomiya, J. Zheng, Z. Zhang, M. Fukuda, T. Aono, H. Minowa, H. Yoshikawa, K. Sueki, Y. Satou, A. Shinohara, Environ. Sci. Technol. 58, 14823-14830 (2024).
[5] S. Zhang, Z. Liu, G. Yang, J. Zheng, S. Pan, T. Aono, A. Sakaguchi, Anal. Chem. 95, 16892-16901 (2023).
[6] X. Gu, B. Yang, G. Yang, M. Yamada, F. Wu, J. Zheng, Microchem. J. 208, 112480 (2025).
[7] J. Zheng, K. Tagami, S. Uchida, Environ. Sci. Technol. 47, 9584-9595 (2013).
[8] Y. Y. Ni, J. Zheng, Q. J. Guo, Z. Y. Huang, H. Wang, K. Tagami, S. Uchida, Catena, 210, 105884 (2022).

Copyright on 7th Asia-Pacific Symposium on Radiochemistry 2025 - P2-02 -

7th Asia-Pacific Symposium on Radiochemistry *September 14 ~ 19, 2025 • Kunibiki Messe • Shimane, Japan*

Determination of ultra-trace ^{237}Np and Pu isotopes in drinking and surface waters by SF-ICP-MS

Xiang Gu[1,2], Jian Zheng[1], Guosheng Yang[1], Keiko Tagami[1], Tatsuo Aono[3], Fengchang Wu[2]

[1] *Institute for Radiological Science, National Institutes for Quantum Science and Technology (QST), Japan.*
[2] *Institute of Eco-environmental and Soil Sciences, Guangdong Academy of Sciences, China.*
[3] *Fukushima Institute for Research, Education and Innovation, Japan.*
Email: gu.xiang@qst.go.jp

The Fukushima Daiichi Nuclear Power Plant (FDNPP) accident has raised wide concerns on drinking water contamination by artificial radionuclides. At the early stage of the accident, ^{131}I and radiocaesium (^{134}Cs+^{137}Cs) activity concentrations drew people's attention; however, following stages after releases of radionuclides to the atmosphere, radionuclides entering into drinking water were in concern. Thus, monitoring of radiocaesium in waters of rivers, lakes and groundwater in eight prefectures have been monitored since the accident occurred. The latest monitoring results in January to February 2025 for all the stations, i.e. 324 stations in eight prefectures' terrestrial environment with 386 samples showed that the data were under detection limit for radiocaesium (D.L.= ca.1 Bq/L) [1]. Results for other radionuclides rather than radiocaesium detected were listed in the report of FY 2018 [2]; these isotopes were naturally occurring radionuclides, such as ^{40}K and Th and U series isotopes, and no artificial radionuclides were found in water. Thus, in the freshwater environment, it was not clear the activity concentrations of other artificial long-lived radionuclides originated from the FDNPP accident.

Neptunium-237 (^{237}Np) and plutonium isotopes ($^{239+240}$Pu) have high radiotoxicity and long half-lives, whereas they are rarely determined in drinking or natural waters owing to extremely low abundance. However, to understand the future radiation dose due to long-lived radionuclides released from the FDNPP accident, it would be useful if we could measure the ultra-low levels of these radionuclides with isotope fingerprint for the source identification. Thus, this study established a sequential separation method, including primary $Fe(OH)_2$ co-precipitation, secondary CaF_2/LaF_3 co-precipitation, and anion exchange chromatographic separation, to determine ^{237}Np and $^{239+240}$Pu in drinking and surface water by SF-ICP-MS. The method detection limits of ^{237}Np, ^{239}Pu, and ^{240}Pu were 0.035 fg/L (0.0009 μBq/L), 0.012 fg/L (0.027 μBq/L), and 0.010 fg/L (0.085 μBq/L), respectively for 20 L of water. The method was validated by analyzing the IAEA-443 reference material. Based on the method, ^{237}Np concentrations in 27 tap water and 6 surface samples collected from 9 prefectures of Japan were determined (Fig. 1).

Our measurements showed that the activity concentrations of ^{237}Np ranged from 0.004 to 0.116 μBq/L, with the ^{242}Pu recovery of 70.2-93.8%. However, ^{239}Pu was only determined in 27% of the samples, ranging from 0.080 to 0.111 μBq/L, and ^{240}Pu was not detected at all. The ^{237}Np activity concentrations in drinking waters were close to that in surface waters, indicating that the conventional drinking water treatment techniques cannot effectively remove ^{237}Np from natural waters. Moreover, the significant relationship between the ^{237}Np activity concentrations in drinking water and soil suggested that global fallout was the primary source of ^{237}Np in drinking water. The determined ^{237}Np and ^{239}Pu concentrations in drinking water were far below the guidelines for drinking water quality (1 Bq/L) issued by the World Health Organization. The estimated annual effective dose of ^{237}Np for adults ranged from 3.17×10^{-10} to 9.29×10^{-9} mSv, much lower than the safety threshold. The findings suggested that it is necessary to routinely monitor the ^{237}Np levels in drinking tap water after nuclear accidents to protect the public from excessive internal exposure.

Copyright on 7th Asia-Pacific Symposium on Radiochemistry 2025 - P2-03 -

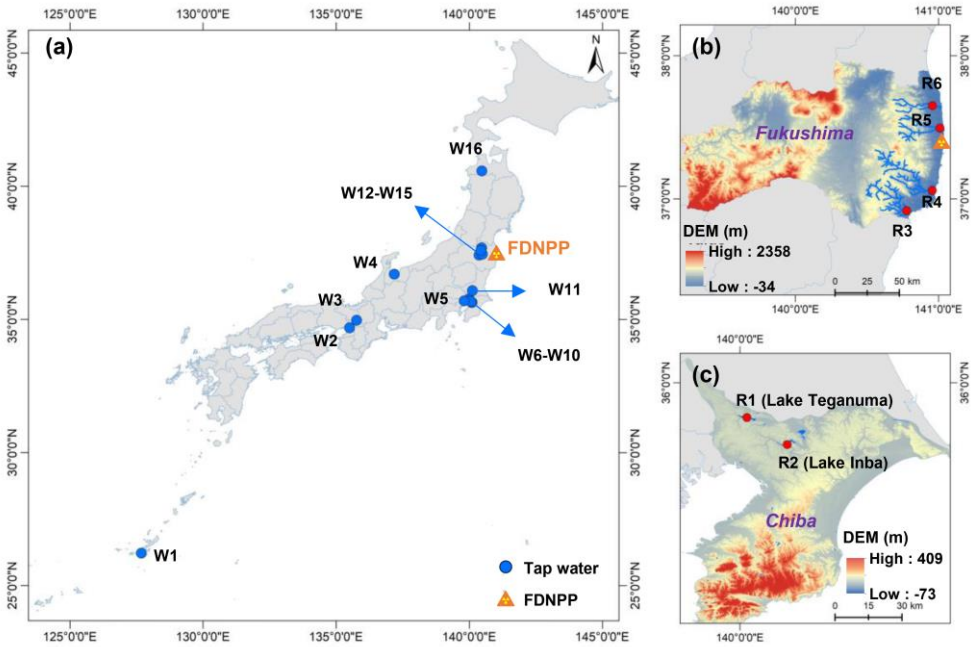


Fig. 1. Location of the tap water samples (a), river water samples in Fukushima (b), and lake water samples in Chiba (c).

Acknowledgement

The authors thank Dr. Nobuyoshi Ishii, Dr. Yanbei Zhu, Dr. Miho Fukuda, Dr. Hirofumi Tazoe, and Dr. Jing Zhang for their assistance in collecting water samples.

References

[1] Ministry of the Environment. Radioactive Material Monitoring Surveys of the Water Environment. https://www.env.go.jp/content/000306912.pdf (Accessed on 18 April 2025).
[2] Ministry of the Environment. FY2018 Resulsts of the Radioactive Material Monitoring in the Water Environment. https://www.env.go.jp/content/900454862.pdf (Accessed on 18 April 2025).

Invited & Contributed Talk | [P2]ICP-MS Based Radioanalytical Chemistry and Related Applications

Tue. Sep 16, 2025 11:10 AM - 12:00 PM JST | Tue. Sep 16, 2025 2:10 AM - 3:00 AM UTC Hall A(MP)

[P2] ICP-MS Based Radioanalytical Chemistry and Related Applications

11:10 AM - 11:40 AM JST | 2:10 AM - 2:40 AM UTC

[P2-04(Invited)]

Application and limitations of MC-ICPMS measured $^{236}U/^{238}U$ as an ocean tracer

Huei-Ting Lin[1], *Chuan-Chou Shen[2,3], Hong-Wei Chiang[4], Jian-Ming Chen[1], Yu-Chen Chou[1] (1. Institute of Oceanography, National Taiwan University (Taiwan), 2. Department of Geosciences, National Taiwan University (Taiwan), 3. Research Center for Future Earth, National Taiwan University (Taiwan), 4. Research Center for Environmental Changes, Academia Sinica (Taiwan))

11:40 AM - 12:00 PM JST | 2:40 AM - 3:00 AM UTC

[P2-05]

Determination of uranium isotope ratios of single uranium particle by multiple collector inductively coupled plasma mass spectrometry

*Jumpei Tomita[1], Ryohei Tomita[1], Takumi Yomogida[1], Daisuke Suzuki[1], Kenichiro Yasuda[1] (1. Japan Atomic Energy Agency (Japan))

©APSORC25

Application and limitations of MC-ICPMS measured $^{236}U/^{238}U$ as an ocean tracer

Huei-Ting Lin[1], Chuan Chou (River) Shen[2,3], Hong-Wei Chiang[4], Jian-Ming Chen[1], Yu-Chen Chou[1]

[1]Institute of Oceanography, National Taiwan University, Taipei, Taiwan, ROC
[2]High-Precision Mass Spectrometry and Environment Change Laboratory (HISPEC), Department of Geosciences, National Taiwan University, Taipei, Taiwan, ROC
[3]Research Center for Future Earth, National Taiwan University, 10617 Taiwan, ROC
[4]Research Center for Environmental Changes, Academia Sinica, Taipei, ROC

Abstract

Analysis of natural $^{236}U/^{238}U$ with only femtogram ^{236}U by a multi-collector high-resolution inductively coupled plasma mass spectrometer (MC-ICPMS) using a secondary electron multiplier (SEM) has allowed us to detect low level anthropogenic ^{236}U enrichment in the environment (Lin et al., 2021, Analytical Chem., 93, 8442-8449). Our methods reduced the abundance sensitivity of ^{238}U tail at 236 atomic mass unit from 10^{-6} to 10^{-10} with the deployment of retarding potential quadrupole (RPQ) lens. Our methods also corrected polyatomic interferences from hydride, nitride, lead, and plutonium and accounted for the non-linear SEM behavior. Measurements on reference materials with $^{236}U/^{238}U$ ratios of 10^{-7} to 10^{-9}, including the IRMM-075 series and the ETH Zurich in-house standard ZUTRI, demonstrate the accuracy of our MC-ICPMS techniques. Our methods were intercalibrated with ETH AMS techniques using seawater near Hawaii. A bi-monthly-resolved coral $^{236}U/^{238}U$ record was analyzed from southern Taiwan. Five $^{236}U/^{238}U$ depth profiles of seawater collected from the northeast, central tropical, and western tropical Pacific Ocean and the offshore of southwestern Taiwan were measured. Results show that $^{236}U/^{238}U$ is sensitive nuclear reaction tracer and that ^{236}U nuclide penetration depths reached 600 m in the tropical Pacific Ocean. Although the overall quantification limit was $^{236}U/^{238}U$ of 4×10^{-10}, the MC-ICPMS method can be the quick screening method for detecting the presence of anthropogenic ^{236}U in environmental samples.

Keywords: $^{236}U/^{238}U$, MC-ICPMS, ocean tracer

7th Asia-Pacific Symposium on Radiochemistry *September 14 ~ 19, 2025 • Kunibiki Messe • Shimane, Japan*

Determination of uranium isotope ratios of single uranium particle by multiple collector inductively coupled plasma mass spectrometry

Jumpei Tomita[1], Ryohei Tomita[2], Takumi Yomogida[3], Daisuke Suzuki[4], Kenichiro Yasuda[5]

[1]*Japan Atomic Energy Agency: 2-4 Shirakata, Tokai-mura, Ibaraki, 319-1195, tomita.jumpei@jaea.go.jp*
[2] *Japan Atomic Energy Agency: 2-4 Shirakata, Tokai-mura, Ibaraki, 319-1195, tomita.ryohei@jaea.go.jp*
[3] *Japan Atomic Energy Agency: 2-4 Shirakata, Tokai-mura, Ibaraki, 319-1195, yomogida.takumi@jaea.go.jp*
[4] *Japan Atomic Energy Agency: 2-4 Shirakata, Tokai-mura, Ibaraki, 319-1195, suzuki.daisuke@jaea.go.jp*
[5] *Japan Atomic Energy Agency: 2-4 Shirakata, Tokai-mura, Ibaraki, 319-1195, yasuda.kenichiro@jaea.go.jp*

1 Introduction

Uranium isotope ratio of each uranium particle in the safeguards environmental samples are usually determined by large-geometry secondary ion mass spectrometry (LG–SIMS) and/or fission-track thermal ionization mass spectrometry (FT–TIMS). Although the LG–SIMS has excellent capability for few micron size uranium particle, the instrument is very expensive. The procedure for picking uranium particles up including neutron irradiation at nuclear reactors is tedious and time-consuming although the multiple collector TIMS instrument is cheaper than that of LG-SIMS. Multiple collector inductively coupled plasma mass spectrometry (MC–ICP–MS), which is cheaper than LG–SIMS, is one of the alternative methods for isotope ratio analysis. This requires chemical treatments for preparing the sample solution, and there is a possibility that the sample is contaminated by uranium and/or other elements, that will interfere with the accurate determination of uranium isotope ratios, during the procedures. In this study, an analytical method for determining uranium isotope ratios of a single uranium particle by MC–ICP–MS was developed. Contamination during chemical treatments was assessed to determine the uranium isotope ratios accurately.

2. Experimental

Each particle containing uranium from NBL CRM U100 was picked up using the manipulator installed in the scanning electron microscopy instrument and placed on a silicon chip (5 × 5 mm) set to a brass holder. The chip was removed from the brass holder and set in a conical PFA jar. After adding 1 mL of ultrapure water to the jar, ultrasonication was conducted for a minute with the jar lid screwed on to transport the particles into the water. The chip was removed from the jar and washed with 1 mL of ultrapure water. After evaporating the solution to dryness, 68% HNO_3 (55.6 µL), 38% HF (5 µL), and ultrapure water (50 µL) were added to the jar. After screwing on the jar lid, the jar was heated at 150°C for 20 min. After the resulting drops of water had collected on the bottom of the jar, the solution was evaporated to dryness. The residue was dissolved in 6–7 mL of 2% HNO_3 solution, and the U isotope ratios were measured using MC–ICP–MS (Neptune–XT, Thermofisher Scientific). The ^{238}U concentration and impurities in the sample solutions were measured using sector field ICP–MS (Element2, Thermofisher Scientific) and quadruple ICP-MS (iCAP–RQ, Thermofisher Scientific), respectively. The particle which was picked up and placed on a silicon chip fixed with carbon tape to the silicon planchet, was also analyzed with the same manner to assess the effect of impurities from the brass holder.

3. Results and discussion

Analytical results of uranium isotope ratios of the particle were shown in Fig. 1. For the particles placed on a silicon chip set to a brass holder, $^{234}U/^{238}U$ and $^{235}U/^{238}U$ ratios obtained agreed with the certified values of CRM U100 within the uncertainties while their $^{236}U/^{238}U$ ratio did not agree with and higher than that of CRM U100. The sample solutions contained 3–4 ng of Pb, indicating that the measurement of ^{236}U was interfered by polyatomic ions such as $^{208}Pb^{14}N_2^+$. The energy dispersive X–ray spectroscopy (EDS) analysis of the brass holder showed that Pb including Pb particles was contained in the holder. To avoid Pb contamination from the brass holder, a silicon planchet was used as a holder of Si chip instead of brass one. As a result, the Pb contamination was decreased to approximately 0.1 ng, and $^{236}U/^{238}U$ ratio determined agreed with certified value of CRM U100. Therefore, an analytical method was developed to accurately determine uranium isotope ratio of a single uranium particle by assessing the origin of contaminants and decreasing the contamination during chemical treatments.

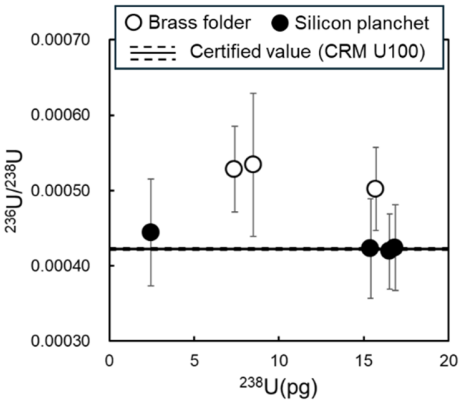


Fig. 1. Analytical results of $^{236}U/^{238}U$ of uranium particle. The horizontal axis and uncertainties show the amount of ^{238}U in a uranium particle and shows 95% confidence intervals.

[Acknowledgement]
This work was financially supported by the Nuclear Regulation Authority of Japan.

Invited & Contributed Talk | [R9]Interdisciplinary and Multidisciplinary Topics

Tue. Sep 16, 2025 1:30 PM - 3:00 PM JST | Tue. Sep 16, 2025 4:30 AM - 6:00 AM UTC Hall S(Int'l)

[R9] Interdisciplinary and Multidisciplinary Topics

1:30 PM - 2:00 PM JST | 4:30 AM - 5:00 AM UTC

[R9-01(Invited)]

Introduction of research activities related to radiochemistry at F-REI

*Tatsuo Aono[1] (1. Fukushima Institute for Research, Education and Innovation (Japan))

2:00 PM - 2:20 PM JST | 5:00 AM - 5:20 AM UTC

[R9-02]

TATTOOS – a future large-scale radionuclide production infrastructure in SWITZERLAND: a status report

*Robert Eichler[1,2], Nicholas van der Meulen[1], Daniela Kiselev[1], Christian Baumgarten[1], Aleksandar Ivanov[1], Sven Jollet[1], Remi Martinie[1,3], Sophie Harzmann[1], Daniel Laube[1], Maryam Mostamand[1], Nils Preiss[1], Thomas Rauber[1], Davide Reggiani[1], Jochem Snuverink[1], Patrick Steinegger[4,1], Stuart Warren[1], Hui Zhang[1] (1. Paul Scherrer Institute (Switzerland), 2. University of Bern (Switzerland), 3. EPF Lausanne (Switzerland), 4. ETH Zurich (Switzerland))

2:20 PM - 2:40 PM JST | 5:20 AM - 5:40 AM UTC

[R9-03]

UV-Vis-NIR spectroscopy combined with Hyperspectral Imaging for Actinide Concentration Determination during Ion Exchange Processes

*Bradley Childs[1], Tsuyoshi A. Kohlgruber[1], Silvina A. Di Pietro[1], Maryline G. Ferrier[1], Scott A. Simpson[1], Emma R. Tardiff[1], Hiroshi H. Saito[1], Saurabh Narain[1], Kiel S. Holliday[1], Lawrence E. Banks[1] (1. Lawrence Livermore National Laboratory (United States of America))

2:40 PM - 3:00 PM JST | 5:40 AM - 6:00 AM UTC

[R9-04*]

Development and Preliminary Experimental Study of an In-Situ Raman-Based High-Temperature and High-Pressure Water Corrosion Testing Platform

*Hu Wen Zhen[1], Li Lili[2], Ouyang Kun [2], Du Yingzhe[2], Yang huan[3], Ling Peng[2], Ni Muyi[1] (1. Sun Yat-sen University (China), 2. CGN Research Institute Co., Ltd (China), 3. Shenzhen Technology University (China))

©APSORC25

Introduction of research activities related to radiochemistry at F-REI

Tatsuo Aono

[1] *Fukushima Institute for Research, Education and Innovation, Japan*
Email:AONO.Tatsuo.t6r@research.f-rei.go.jp

What is F-REI? The Fukushima Institute for Research, Education and Innovation (commonly known as F-REI) is a special corporation established on April 1, 2023 under the Act on Special Measures for the Reconstruction and Revitalization of Fukushima. In addition to providing dreams and hopes for realizing the reconstruction of Fukushima and other prefectures in the Tohoku region, F-REI aims to become a world-renowned "central institute for creative reconstruction" which drives forward with enhancing the scientific capabilities, technological capabilities and industrial competitiveness of Japan and contributes to economic growth and improvement to the daily lives of people living in Japan. F-REI will combine four functions - 1. Research and Development, 2. Industrialization, 3. Human resource development, and 4. Control tower - to create ripple effects both domestically and internationally.

F-REI aims to lead the world in research and development in five research fields unique to Fukushima, a region that has experienced unique experiences of earthquakes, tsunamis, and nuclear accidents (1. Robotics, 2. Agriculture, forestry, and fisheries, 3. Energy, 4. Radiation science, medicine, drug discovery, and industrial use of radiation, and 5. Collection and dissemination of data and knowledge related to nuclear disasters). By forming one of Japan's leading, world-class research centers in this region and making it the core base for creative reconstruction, we will promote research that contributes to solving regional issues and creating new industries. We also aim to further develop the research by integrating and linking the results of each research.

In this fifth research field, perspectives on research and development are to promote multiple efforts and engage in research in natural and social sciences that will contribute to the creative reconstruction of the Fukushima Hamadori region, which experienced a complex disaster. The policy is to investigate and analyze the actual conditions of the natural environment and local communities in the areas affected by the nuclear disaster, and to accumulate and disseminate scientific knowledge to improve the safety of the region. Furthermore, we aim to utilize the results of F-REI's research in revitalizing the region and building consensus among residents, thereby contributing to the creation of a resilient town where people can coexist. (Outline of F-REI, https://www.f-rei.go.jp/english/about/).



Research into environmental radioactivity and dynamics, radiation dose and radioecology following the Fukushima Nuclear Power Station accident has been conducted by various research institutes and universities, and these results are being compiled and published in various formats.

Environmental dynamics research has been carried out by the Regional Environmental Co-Creation Unit in F-REI since spring 2025. It has been confirmed that the activity concentration of cesium-137 in various environmental media is decreasing at a rate exceeding its physical half-life due to effects such as weathering and decontamination.

Ongoing research is important to understand the present circumstances of radionuclide contamination, and it is essential to collect and distribute the acquired information.

Conversely, because of the various regulatory and standard values established for Cs-137, there are restrictions on the shipping and distribution of forest products and freshwater fish, among others, and challenges persist in their management. Furthermore, understanding the transfer mechanism of Cs-137 and predicting future concentration changes requires knowledge. The requirements vary by region, necessitating the incorporation of findings from environmental dynamics research into regional revitalization.

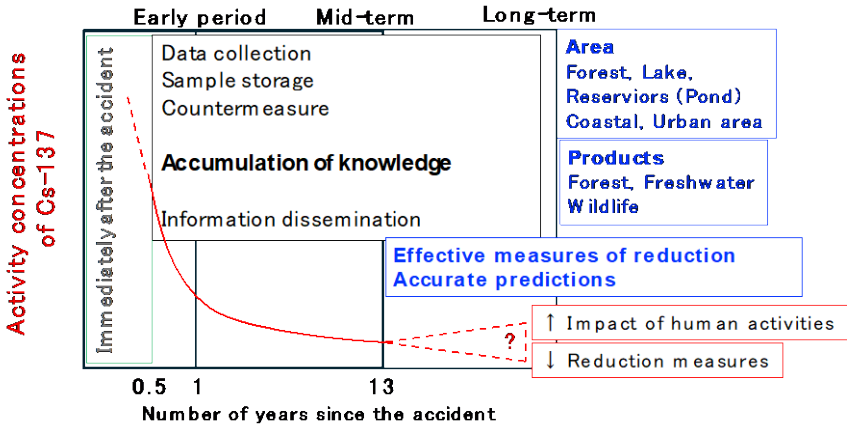


Fig. 1 A typical pattern of the decrease in Cs activity concentration over time scince the Fukushima Nuclear Power Station accident in area and products.

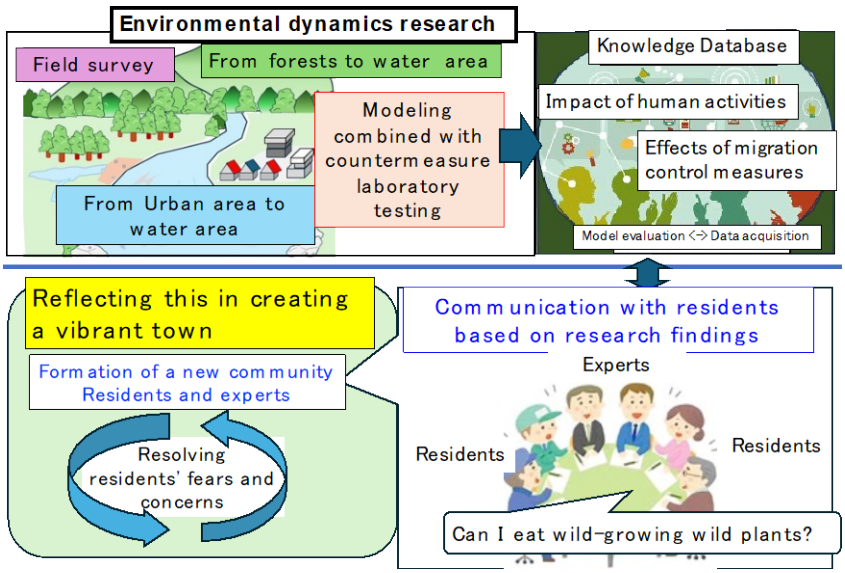


Fig.2 Reflecting the results of environmental dynamics research in town development

F-REI must also deploy effective dose (mainly, Cs-137) reduction strategies based on reliable estimates, including ongoing on-site assessments. Future predictions derived from field survey outcomes and model simulations will be archived in a knowledge database. F-REI will communicate with stakeholders and incorporate the findings into regional revitalization efforts.

The F-REI research history establishes an unbroken link from Fukushima to the future we shape, "Forests as a key link in a rich cycle of natural resources" and "Understanding radiation to put Fukushima's experience to good use"(F-REI Brochure, https://www.f-rei.go.jp/assets/contents/f-rei_brochure_english_202411.pdf). Please refer this information.

Copyright on 7th Asia-Pacific Symposium on Radiochemistry 2025 - R9-01 -

7th Asia-Pacific Symposium on Radiochemistry *September 14 ~ 19, 2025 • Kunibiki Messe • Shimane, Japan*

TATTOOS – A FUTURE LARGE-SCALE RADIONUCLIDE PRODUCTION INFRASTRUCTURE IN SWITZERLAND: A STATUS REPORT

R. Eichler [1,2], N. van der Meulen[1,3], D. Kiselev[4], C. Baumgarten[4], A. Ivanov[4], S. Jollet[4], R. Martinie[4,5], S. Harzmann[6], D. Laube[4], M. Mostamand[3], N. Preiss[4], T. Rauber[4], D. Reggiani[4], J. Snuverink[4], P. Steinegger[1,7], S. Warren[4], H. Zhang[4]

[1]*PSI Center for Nuclear Engineering and Sciences,Paul Scherrer Institute, Forschungsstrasse 111, 5232 Villigen PSI, Switzerland, robert.eichler@psi.ch*
[2]*Department of Chemistry, Biochemistry and Pharmacy. University of Bern, Freiestrasse 3, 3012 Bern, Switzerland*
[3]*PSI Center for Radiopharmaceutical Sciences PSI-ETHZ, Paul Scherrer Institute, 5232 Villigen-PSI, Switzerland*
[4]*PSI Center for Accelerator Sciences and Engineering, Paul Scherrer Institute, 5232 Villigen PSI, Switzerland*
[5]*School of Materials Science and Engineering, Ecole Polytechnique Fédérale de Lausanne EPFL, Rte Cantonale, 1015 Lausanne, Switzerland*
[6]*Department of Radiation Safety and Security, Paul Scherrer Institute, 5232 Villigen PSI, Switzerland*
[7]*Department of Chemistry and Applied Biosciences, Eidgenössiche Technische Hochschule Zürich, Vladimir-Prelog-Weg 1, 8093 Zurich, Switzerland*

Here, we aim at presenting a status report of the Swiss large-scale research infrastructure project IMPACT- TATTOOS.

1 Summary of the IMPACT project

The High Intensity Proton Accelerator (HIPA) facility at the Paul Scherrer Institute (PSI) provides a world-leading continuous proton beam of up to 1.4 MW DC-power. A 70 MCHF proposal named **I**sotope and **M**uon **P**roduction with **A**dvanced **C**yclotron and **T**arget Technology (IMPACT, https://www.psi.ch/en/impact) was approved by the Swiss parliament in December 2024. The proposal focuses on two separate large scale research infrastructures connected to the **H**igh **I**ntensity **P**roton **A**ccelerator (HIPA) facility (see Fig. 1). Firstly, it foresees the upgrade of one of the high-energy proton target stations to produce up to two orders of magnitude more intense muon beams (HIMB - **H**igh-**I**ntensity **M**uon **B**eams, shown in green in Fig.1. Secondly, TATTOOS – (**T**argeted **A**lpha **T**umour **T**herapy and **O**ther **O**ncological **S**olutions, shown in blue in Fig.1 envisages unprecedented radionuclide production rates for radiopharmaceutical as well as other applied and fundamental scientific research. The IMPACT project construction timeline is 2025-2030.

2 The TATTOOS project

The main outline of TATTOOS is sketched in Figure 1 in green. The project aims at the production of radionuclides via high-energy proton-induced spallation. Online selective laser-driven resonance ionization, followed by high resolution online mass separation of produced radionuclides, shall be realized applying the ISOL-technique pioneered at CERN-ISOLDE (https://isolde.cern). The superposition of the mass separation with fast and efficient radiochemical separation, a specialty of the Laboratory of Radiochemistry (LRC) at PSI, will guarantee isotopically and radiochemically pure products. The envisaged production scheme will deliver innovative radionuclides at amounts which will allow for systematic preclinical and clinical studies at the closely collaborating Center for Radiopharmaceutical Sciences (CRS) at PSI, ETH Zurich, University Hospital Zurich (USZ) and University of Zurich (UZH). It is foreseen to provide these radionuclides for fundamental physics and chemistry research as well.

Here, we will present the status of the TATTOOS project with challenges and their envisaged solutions. Some of which are comprising the new building, which will host the installation, the new proton beam line behind the high-energy beam splitter, the high-power target, the extraction and mass separation concepts, as well as the radiochemical laboratory infrastructure together with day-one experimental plans for 2030.

ACKNOWLEDGMENTS

The authors acknowledge the support from the entire IMPACT team at PSI (see Fig. 2) and the financial support through the Swiss State Secretariat for Education, Research, and Innovation (SERI).

Copyright on 7th Asia-Pacific Symposium on Radiochemistry 2025 - R9-02 -

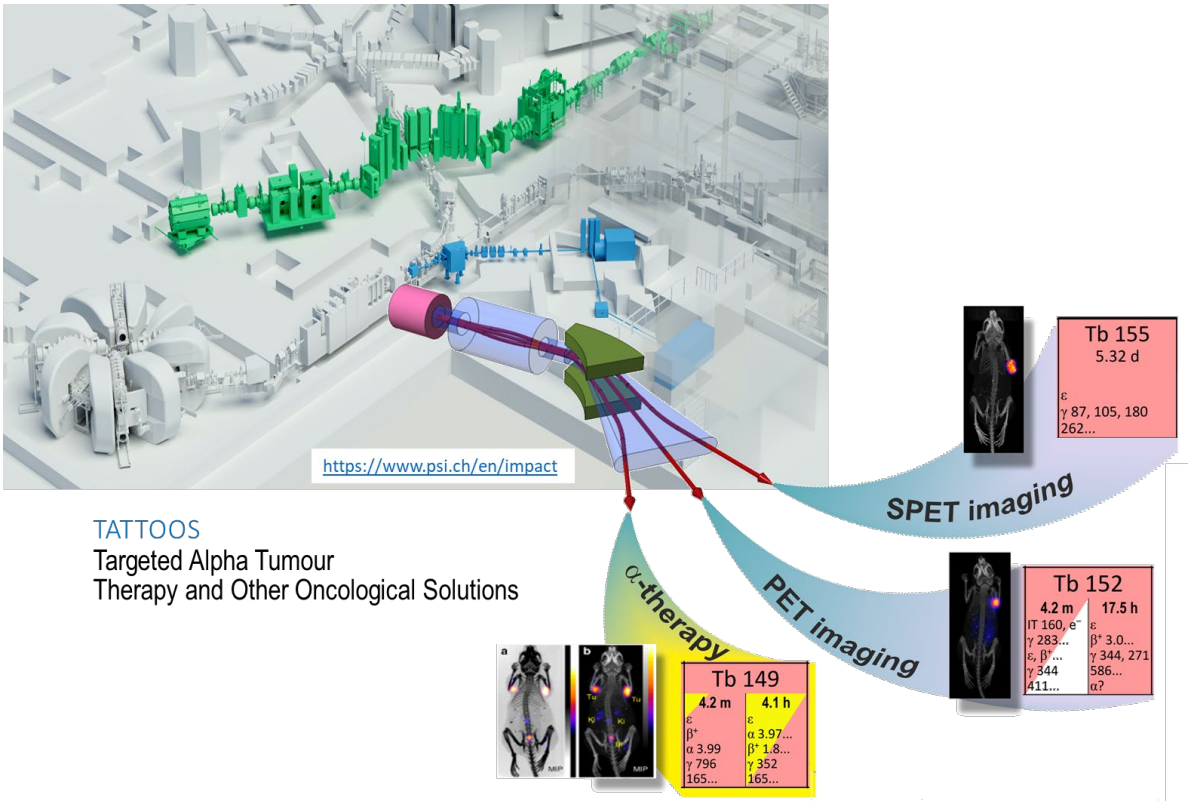


Fig. 1. Overview sketch of the large-scale IMPACT project @ PSI HIPA-facility. Shown in green, is the HIMB (High Intensity Muon Beam) facility with two new muon beam lines, whereas highlighted in blue is TATTOOS. The latter serves the production of radionuclides by 590 MeV proton-induced spallation, which will be mass separated and provided, e.g., the radiopharmaceutical theragnostic "Tb-sisters".



Fig. 2. The PSI-IMPACT team at the IMPACT status information event on March 19, 2025

References

[1] *IMPACT conceptual design report.* R. Eichler, D. Kiselev, A. Koschik, A., A. Knecht, N. van der Meulen, Ed., PSI Report No.: 22-01, Paul Scherrer Institute, Villigen, PSI (2022)

Copyright on 7th Asia-Pacific Symposium on Radiochemistry 2025 - R9-02 -

7th Asia-Pacific Symposium on Radiochemistry *September 14 ~ 19, 2025 • Kunibiki Messe • Shimane, Japan*

UV-Vis-NIR spectroscopy combined with Hyperspectral Imaging for Actinide Concentration Determination during Ion Exchange Processes

Bradley C. Childs[1], Tsuyoshi A. Kohlgruber[1], Silvina A. Di Pietro[1], Maryline G. Ferrier (Kerlin)[1], Scott A. Simpson[1], Emma R. Tardiff[1], Hiroshi H. Saito[1], Saurabh Narain[1], Kiel S. Holliday[1], and Lawrence E. Banks[1]

[1]*Lawrence Livermore National Laboratory: 7000 East Avenue, Livermore, California, 94550, United States of America, and childs4@llnl.gov*

Nuclear materials containing actinides, more specifically uranium and plutonium, are known to exhibit a wide array of colors. This attribute has traditionally been used qualitatively by scientists to make informed decisions on product identity and state. UV-vis-NIR spectroscopy is a tool that can elucidate actinide oxidation states and inform on solution speciation. Through the Nonproliferation Stewardship Program project Simulating Processing of Actinides and Development of Expertise (SPADE), we at LLNL are bolstering our analytical capabilities to further understand actinide aqueous recovery. One method that is currently being studied is the use of hyperspectral imaging (HSI). HSI cameras obtain pixel-level spatial resolution absorbance spectra using over a hundred color sensors, which can extend beyond the visible light region (Figure 1b). Using this technique with actinide material and solution standards to obtain a new set of spectra would increase understanding of speciation during the aqueous separation processes of actinides. Specific attention will be placed on solution interaction with multiple resin (i.e. Dowex, Eichrom) media to observe loading and elution speciation. Here we present how HSI technology combined with UV-Vis spectroscopy provides correlated spectra that can properly inform the status of during separation processes. Images of multiple resins pretreated, conditioned, loaded with actinide solution, partially eluted, and completely eluted will be discussed. In addition to the images, UV-Vis spectroscopy will be taken on all solution in contact with the resin and correlated to known values to determine the effectiveness of HSI.

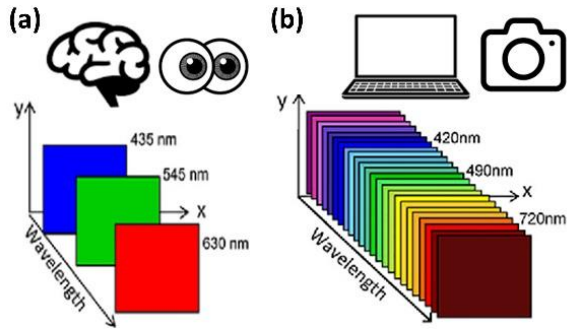


Fig. 1. Above is a display of how a traditional camera functions (a) versus how hyperspectral imaging works (b).

ACKNOWLEDGMENTS

This work was performed under the auspices of the U.S. Department of Energy by Lawrence Livermore National Laboratory under Contract DE-AC52-07NA27344. LLNL-ABS-2005303

Copyright on 7th Asia-Pacific Symposium on Radiochemistry 2025 - R9-03 -

Development and Preliminary Experimental Study of an In-Situ Raman-Based High-Temperature and High-Pressure Water Corrosion Testing Platform

Hu Wenzhen[1], Li Lili[2], Ouyang Kun[2], Du Yingzhe[2], Yang Huan[3], Lin Peng[2], Ni Muyi[1] ([1]Sino-French Institute of Nuclear Engineering and Technology, Sun Yat-sen University, Zhuhai, 519082

[2]China Nuclear Power Technology Research Institute Co., Ltd., Shenzhen, 518031

[3]Sino-German School of Intelligent Manufacturing, Shenzhen Technology University, Shenzhen, 518118)

Abstract

To investigate the corrosion mechanisms of critical structural materials in pressurized water reactor (PWR) primary circuits under in-situ conditions, an autoclave system integrated with in-situ Raman observation windows was designed and constructed. The sealing mechanism of the high-pressure autoclave at 350°C and 20 MPa relies on a sapphire sleeve assembly and a window sleeve assembly, which mutually compress to ensure pressure containment. The system incorporates a slow strain rate tensile (SSRT) control module and a water chemistry circulation loop to simulate the operational environment of nuclear power plant (NPP) structural materials. Preliminary validation experiments were conducted using Zr-4 alloy oxidized for 1 hour. Raman spectra of monoclinic and tetragonal zirconia phases, liquid water, and sapphire components exhibited strong consistency with prior literature, confirming the reliability of the platform. This system enables real-time analysis of material corrosion mechanisms under PWR water chemistry, providing critical insights for optimizing the performance of key nuclear materials.

Keywords: In-situ Raman; high-temperature and high-pressure water corrosion; zirconium alloy Raman spectroscopy

Copyright on 7th Asia-Pacific Symposium on Radiochemistry 2025- R9-04* -

Invited & Contributed Talk | [P5]Environmental Radiochemistry Applicable for Nuclear Non-Proliferation, Disarmament, and Nuclear Security

Tue. Sep 16, 2025 1:30 PM - 3:00 PM JST | Tue. Sep 16, 2025 4:30 AM - 6:00 AM UTC Hall B(Small)

[P5] Environmental Radiochemistry Applicable for Nuclear Non-Proliferation, Disarmament, and Nuclear Security

1:30 PM - 2:00 PM JST | 4:30 AM - 5:00 AM UTC

[P5-01(Invited)]

Characterizing environmental samples for long-lived radionuclides with emphasis on 1940-1950 nuclear events in Japan and Australia

*Mathew P. Johansen[1], D.P. Child[1], M. Peterson[1], E. Young[1], M.A.C. Hotckis[1] (1. Australian Nuclear Science and Technology Organisation (Australia))

2:00 PM - 2:20 PM JST | 5:00 AM - 5:20 AM UTC

[P5-02]

Soil Survey Methodology for Identifying the "Black Rain" Deposition

*Yasuhito Igarashi[1], Satoru Endo[2], Koichi Takamiya[1], Jun Inoue[3], Hiroshi Yashima[1], Maiko Ikegami[1], Yayoi Inomata[4], Satoshi Fukutani[1], Tadashi Mukai[1], Tomonori Adachi[1], Naoko Fukuda[5], Sumi Yokoyama[5], WG Meteorology and Soil (1. Institute for Integrated Radiation and Nuclear Science, Kyoto University (Japan), 2. Graduate School of Advanced Science and Engineering, Hiroshima University (Japan), 3. Osaka Metropolitan University (Japan), 4. Institute of Nature and Environmental Technology, Kanazawa University (Japan), 5. Atomic Bomb Disease Institute, Nagasaki University (Japan))

2:20 PM - 2:40 PM JST | 5:20 AM - 5:40 AM UTC

[P5-03]

THE “BLACK RAIN” GENERATED BY THE HIROSHIMA ATOMIC BOMBWAS ACID RAIN

*Tadashi Mukai[1,2], Tomonori Adachi[3,1], Jun Inoue[2], Hiroshi Yashima[1], Satoshi Fukutani[1], Koichi Takamiya[1], Maiko Ikegami[1], Yasuhito Igarashi[1] (1. Institute for Integrated Radiation and Nuclear Science, Kyoto University (Japan), 2. Graduate School of Science, Osaka Metropolitan University (Japan), 3. ATOX CO.,LTD. (Japan))

2:40 PM - 3:00 PM JST | 5:40 AM - 6:00 AM UTC

[P5-04]

Synchrotron-Based Analysis of Spherical Iron Oxide Particles Found in Hiroshima Bay

*Yukihiko Satou[1], Satoru Endo[2], Ryoga Akaji[2], Takahisa Shobu[1], Aki Tominaga[1], Takehiro Sumita[3] (1. Japan Atomic Energy Agency (Japan), 2. Hiroshima University (Japan), 3. Kyushu University (Japan))

©APSORC25

7th Asia-Pacific Symposium on Radiochemistry *September 14 ~ 19, 2025 • Kunibiki Messe • Shimane, Japan*

CHARACTERIZING ENVIRONMENTAL SAMPLES FOR LONG-LIVED RADIONUCLIDES WITH EMPHASIS ON 1940-1950 NUCLEAR EVENTS IN JAPAN AND AUSTRALIA

Mathew P. Johansen[1], David P. Child[1], Mark Peterson[1], Emma Young[1], and Michael A.C. Hotchkis[1]

[1]*Australian Nuclear Science and Technology Organisation, Lucas Heights 2232, Sydney Australia*

After many decades, long-lived radionuclides from early nuclear detonations (1940s-1950s) continue to persist in worldwide environments and can be elevated in areas near the detonation sites where they pose ongoing challenges for environmental monitoring and safe management [1]. We collected samples originating from both fission and non-fission tests/events, spanning a range of explosive yields (<<1 kt to ~100 kt) and release modes (e.g., accidental scenarios as well as detonations from towers, ground-surface, air-drop, and a ship). Most samples were from legacy sites in Australia from the 1950s British nuclear testing program [2], with additional samples from other world sites such as Palomares, Spain and Nagasaki and Fukushima Japan. We assessed soils and interrogated whole and cross-sectioned particles using conventional radiochemistry, multiple microscopy methods and the VEGA accelerator mass spectrometer at the Australian Nuclear Science and Technology Organisation [3].

Our findings confirm that elevated activity concentrations persist in soils near their original sources, with numerous radioactive particles also present. Particle sizes and emission intensities vary by several orders of magnitude. Particle structures also vary, with many particles exhibiting vitreous surface coatings that provide some resistance to weathering and leaching. However, fissures were present in most particles and many of these formed connection pathways from the interior to the exterior surfaces suggesting a role in facilitating leaching of radionuclides. Greater fracturing occurs in high-Ca content particles and less in Si-dominated particles as distinguished by Ca/Fe and Si/Fe elemental ratios.

In most study soils and particles, the activity concentrations of long-lived ^{239,240}Pu were dominant over those of other radionuclides produced from fission and neutron-activation processes. The highest Pu concentrations were in particles from the Palomares accident site and from the Taranaki accident-simulation test site at Maralinga, Australia. Most of the early fission detonations had distinct ^{240}Pu/^{239}Pu and ^{241}Pu/^{239}Pu atom ratios. For example, the early Australian fission tests and the 1945 Nagasaki fission detonation had similarly low ^{240}Pu/^{239}Pu ratios (0.03-0.05) which contrast with the distinctly higher ratios of later thermonuclear sources as well as nuclear power sources such as the ~0.30 ^{240}Pu/^{239}Pu atom ratio from Fukushima accident fallout [4]. However, the Fukushima residuals contained only minute amounts of ^{239,240}Pu mass and low activities relative to ^{137}Cs.

Currently, a more detailed comparison of Pu and U atom ratios in soils and particles gathered from near the Hiroshima detonation site is being conducted through a collaboration between Australian and Japanese researchers.

References

[1] B. Salbu, V. Kashparov, O.C. Lind, R. Garcia-Tenorio, M.P. Johansen, D.P. Child, P. Roos, C. Sancho. 2018. Challenges associated with the behaviour of radioactive particles in the environment. J. Environ. Radioact. 186, 101-115.

[2] M. P. Johansen, D.P. Child, R. Collins, M. Cook, J. Davis, M.A.C. Hotchkis, D.L Howard, N. Howell, A. Ikeda-Ohno, E. Young. 2022. Radioactive particles from a range of past nuclear events: Challenges posed by highly varied structure and composition. Science of The Total Environment 842, 156755.

[3] M.A.C. Hotchkis, , D/P. Child, M.B. Froehlich, A. Wallner, K. Wilcken, M. Williams. 2019. Actinides AMS on the VEGA accelerator. Nucl. Instrum. Methods Phys. Res., Sect. B 438, 70–76

[4] M.P. Johansen, D. Anderson, D.P. Child, M. A. C. Hotchkis, H. Tsukada, K. Okuda, and T. G. Hinton. 2021. Differentiating Fukushima and Nagasaki plutonium from global fallout using ^{241}Pu/^{239}Pu atom ratios: Pu vs. Cs uptake and dose to biota. Science of the Total Environment 754:141890.

Copyright on 7th Asia-Pacific Symposium on Radiochemistry 2025 - P5-01 -

7th Asia-Pacific Symposium on Radiochemistry *September 14 ~ 19, 2025 • Kunibiki Messe • Shimane, Japan*

Soil Survey Methodology to Identify the "Black Rain" Deposition

Yasuhito Igarashi[1], Satoru Endo[2], Koichi Takamiya[1] Jun Inoue[3], Hiroshi Yashima[1], Maiko Ikegami[1], Yayoi Inomata[4], Satoshi Fukutani[1], Tadashi Mukai[1], Tomonori Adachi[1], Naoko Fukuda[5], Sumi Yokoyama[5], WG Meteorology and Soil

[1] *Institute for Integrated Radiation and Nuclear Science, Kyoto University: 2-chome, Asashiro-Nishi, Kumatori, Sennan, Osaka, 590-0494 Japan*

[2] *Graduate School of Advanced Science and Engineering, Hiroshima University: 1-4-1 Kagamiyama, Higashi-Hiroshima, Hiroshima, 739-8527, Japan*

[3] *Department of Geosciences, Graduate School of Science & School of Science, Osaka Metropolitan University: 3-3-138 Sugimoto, Sumiyoshi, Osaka, 558-8585, Japan*

[4] *Institute of Nature and Environmental Technology, Kanazawa University: Kakuma, Kanazawa, Ishikawa, 920-1192, Japan*

[5] *Atomic Bomb Disease Institute, Nagasaki University: 1-12-4, Sakamoto, Nagasaki, 852-8523, Japan*

To obtain a dataset for verifying the results of atmospheric models for the close-in fallout (CiF) for Hiroshima atomic bombing, undisturbed soil samples were collected at over 100 locations in western Hiroshima prefecture using the scraper-plate method to obtain a 1 cm thick soil layer until a depth of 30 cm. Using these samples, we evaluated the vertical distribution of ^{137}Cs, excess ^{210}Pb, a naturally occurring radionuclide continuously supplied from the air ($^{210}Pb_{ex}$), and fine charcoal particles originating from urban fires after the bombing. In the soil layers the deposition record of ^{137}Cs has been effectively preserved, and its maximum concentration corresponding to the 1963 global fallout maximum was observed. Additionally, the $^{210}Pb_{ex}$ profile in the samples decreased exponentially from the surface layer, and the chronological evaluation of 1963 layer based on the decrease was in good agreement with the layer of maximum ^{137}Cs concentration in 1963.

1 Survey for the identification of the close-in fallout ("Black Rain") in Hiroshima

After the World War II, several surveys and researches for radioactive substances originating from atomic bombing were conducted. These surveys mainly analyzed surface soil samples mixed homogeneously at a depth of 5 to 10 cm for substances such as ^{137}Cs and U isotopes, especially for Hiroshima. However, the traces of these substances were overwhelmed by radioactive materials originating from atmospheric nuclear tests conducted after 1950 (global fallout; GF), which were deposited and fell in large quantities, and thus the close-in fallout ("Black Rain") area remained unclear.

2 Soil samples and analysis for ^{137}Cs, $^{210}Pb_{ex}$ and fine charcoal particles

In this research, the presence/absence of the "Black Rain" deposition was identified based on measurements of ^{137}Cs, $^{210}Pb_{ex}$, and fine charcoal particles. Soil samples from 30 layers at each location were sterilized, dried, sieved, and packed into containers at the Institute for Integrated Radiation and Nuclear Science, Kyoto University and then sent to the respective institutions responsible for measuring radioactive substances. Low-background Ge semiconductor detectors were used to measure ^{137}Cs, ^{210}Pb, and ^{214}Pb. The excess ^{210}Pb value was evaluated by subtracting the quantified ^{214}Pb value from the ^{210}Pb one (the amount of ^{210}Pb originally present in the soil was assessed). Based on the inventory of ^{137}Cs and $^{210}Pb_{ex}$ per unit area and the concentration distribution patterns within each soil column (patterns normalized by dividing the analytical values by the standard deviation of all analytical data for the site), an evaluation of the disturbed and undisturbed status of the site was conducted. For the undisturbed site data, chronological estimation was performed using $^{210}Pb_{ex}$ under the simplest assumption of constant concentration and deposition. In addition, the number concentration of charcoal particles derived from urban fires was obtained for undisturbed sites by Osaka Metropolitan University and a contractor using the same method and standards. Specifically, soil samples were treated with acid and alkali to extract charcoal particles, which were then counted under an optical microscope. The vertical distribution of these analytes in the soil column was plotted over the cumulative areal density (mass depth) and then normalization patterns of ^{137}Cs, $^{210}Pb_{ex}$, and charcoal particles were created. The maximum ^{137}Cs deposition in 1963 was determined as the layer with the highest concentration. In addition, the presence of peaks in the concentrations of ^{137}Cs and charcoal particles in 1945 was examined in the surrounding layer estimated to be 1945 using the $^{210}Pb_{ex}$ method.

3 Vertical distribution of ^{137}Cs, $^{210}Pb_{ex}$ and fine charcoal particles in the soil column from undisturbed site

Copyright on 7th Asia-Pacific Symposium on Radiochemistry 2025

From 1945 to 1980, atmospheric nuclear tests continued, reaching the GF peak in 1963. This resulted in the accumulation of ^{137}Cs (physical half-life approximately 30 years) in the environment. The progeny of ^{222}Rn that escape from the Earth's surface, which are generated in the atmosphere and continuously supplied through precipitation and dry deposition. This radionuclide, excess lead-210 (physical half-life about 22 years, distinguished from soil mineral-derived ^{210}Pb and evaluated as ^{210}Pb$_{ex}$) are used as tracers or chronological indicators in research studies. Both ^{137}Cs and ^{210}Pb$_{ex}$ diffuse and migrate into deeper soil layers due to precipitation, but they also tend to remain in the surface layer by adsorption onto minerals, etc. In addition, conducted a particle number concentration analysis of charcoal particles (size range: about 20 to 100 μm), which are difficult to migrate into the deeper layers, and found cases where the maximum concentration of ^{137}Cs derived from CiF and the maximum charcoal particle number concentration (originated from city fires) coincided (see Fig. 1 as an example) at the 1945 layer.

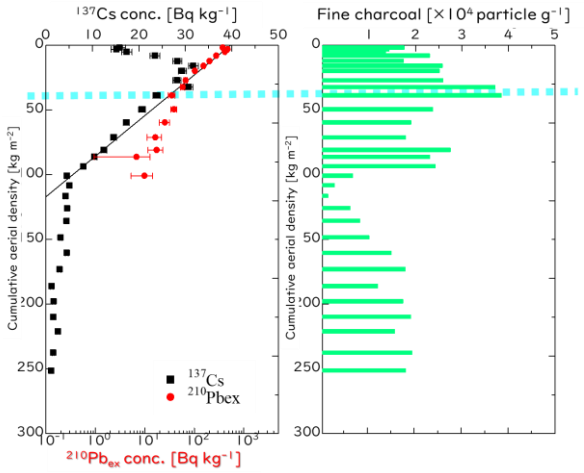


Fig. 1. Vertical distribution of ^{137}Cs, ^{210}Pb$_{ex}$, and charcoal particles at location H-05-03, which was determined to be undisturbed. The chronological estimate based on ^{210}Pb$_{ex}$ (1945) is depicted by the light blue horizontal dotted line. In the layer around 1945, ^{137}Cs and charcoal particles shown maximum concentrations. This location is in an area where the "Black Rain" was reported to have deposited, and the present findings are material evidence of that event.

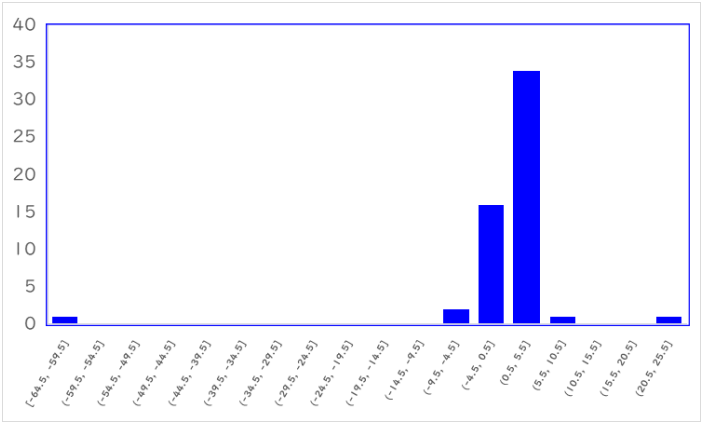


Fig. 2. Frequency distribution of differences (errors) between evaluated and measured GF ^{137}Cs concentration maxima recorded in 1963 (unit in year). Except for two extreme cases at both sides, the differences ranged from a few years to 10 years at most. n=56

We have obtained such soil data from more than 50 sites, where the soil column was not disturbed so far. Excess lead-210 chronological estimation was confirmed its accuracy. For the purpose, we compared estimated 1963 when the GF ^{137}Cs exhibited maximum deposition. So, the difference between 1963 estimated and actually peaked layers was obtained and its thickness accumulated over the past approximately 60 years was calculated by assuming the 1963 GF measurement layer as the reference point and calculating the error (see Fig. 2). As a result, the estimated accuracy of the 1963 layer is quite good (average error of 1.7 years ± 1σ of 2.7 years; n=56), and except for two extreme cases, the error was within a range of a few years to approximately 10 years (see Fig. 2). This suggests that the ^{210}Pb$_{ex}$ method for chronology seems effective. Based on the present methodology we could have identified clear evidence of the "Black Rain" deposition for more than 10 sites among the undisturbed sites. Terrestrial surface soil at undisturbed sites, similar to water sediments, may serve as an archive for changes over the past century.

4 Conclusions

We have almost established a methodology to identify the "Black Rain" in Hiroshima. However, the quantitative nature of the "Black Rain" detection and its detection limits will be future tasks, and the data analysis methods and further exploration of the "Black Rain" tracer substances will also be necessary to reinforce the present results.

ACKNOWLEDGMENTS

This study was funded by the Ministry of Health, Labour and Welfare (MHLW) under the "FY2025 Study on the Construction of a Meteorological Simulation Model for the Atomic Bombings and the Analysis of Fallout Dispersion." We express our gratitude Dr. Tatsuya Shimasaki, Kumamoto University, Mr. Masahira Onoue, Kagoshima University, Prof. Hiroaki Terato, Okayama University, Prof. Yasuji Oura, Tokyo Metropolitan University, Prof. Takahiro Yamada, Kindai University, Prof. Hirokazu Miyoshi of Tokushima University, Ms. Yukari Ito, Tokyo University of Marine Science and Technology, and Prof. Emeritus Sadao Kojima, and Dr. Yoshimune Ogata, Aichi Medical University, all of whom contributed to the measurement of radionuclides in the soil samples, as members of WG Meteorology and Soil.

Copyright on 7th Asia-Pacific Symposium on Radiochemistry 2025 - P5-02 -

7th Asia-Pacific Symposium on Radiochemistry *September 14 ~ 19, 2025 • Kunibiki Messe • Shimane, Japan*

THE "BLACK RAIN" GENERATED BY THE HIROSHIMA ATOMIC BOMB WAS ACID RAIN

Tadashi Mukai[1,2], Tomonori Adachi[1,3], Maiko Ikegami[1], Hiroshi Yashima[1], Satoshi Fukutani[1], Koichi Takamiya[1], Jun Inoue[2], Yasuhito Igarashi[1]

[1] *Institute for Integrated Radiation and Nuclear Science, Kyoto University: 2-chome, Asashiro-Nishi, Kumatori, Sennan, Osaka, 590-0494 Japan*
[2] *Osaka Metropolitan University: 3-3-138 Sugimoto Sumiyoshi-ku, Osaka-shi, 558-8585, Japan*
[3] *ATOX CO. LTD.: Shiba Front Bldg., 4-11-3 Shiba, Minato-ku, Tokyo 108-0014, Japan*

1 INTRODUCTION

The "Black Rain" itself has been studied along with surveys and research on the estimation of the area after the atomic bombings of Hiroshima and Nagasaki in 1945. However, these past researches were mainly from the viewpoint of radioactive substances, and there have been few studies on the main components of rain except for soot [1]. We report the results of our analysis of a) gold folding screen (red copper leaf; copper alloy foil containing zinc) [2] and b) white wall (plaster; calcium carbonate) [3] with traces of the "Black Rain" preserved at Hiroshima Peace Memorial Museum, which provided physical evidence of acid rain.

2 MATERIALS AND METHODS

a) One control area and three black trace areas on the gold folding screen, and b) two control areas and two black trace areas on the white wall were collected to subject the analysis. The analytical methods were observation by optical microscope (SMZ18; Nikon Ltd., Tokyo, Japan), FE/SEM/EDX (JSM122 7900F; JEOL Ltd., Tokyo, Japan) analysis, and compound analysis by XRD (Rigaku SmartLab; Tokyo, Japan). Simulation experiments of model screen and model plaster using inorganic acid solution with China ink were also attempted.

3 RESULTS AND DISCUSSION

a) Observation of the "Black Rain" trace area on the gold folding screen using an optical microscope with reflected and transmitted light revealed that the red copper leaf in this screen area had disappeared and the transmitted light was transparent (Figs. 1 and 2). The SEM/EDX analysis of the leaf fragments remaining in the black traces determined that nitrogen and sulfur, elements derived from the black material, dissolved the porous fragments, suggesting the presence of nitric and sulfuric acids. The XRD analysis revealed no nitric acid compounds, although copper sulfate hydrates were presumed to be mixed. Based on model screen simulation experiments, the possibility of strong acid was found.

The non-detection of nitrate compounds of XRD analysis may be caused by disappearance because of deliquescence.

b) The black traces on the white walls were observed under an optical microscope and found to be black granular on the front surfaces (Figs. 3 and 4). The SEM/EDX analysis showed that no elemental nitrogen (N) was detected in any samples, but elemental sulfur (S) was detected. The difference between the control areas and black trace areas is the distribution of elemental S. The former dendritic form is presumably formed by SOx in the air (gas phase) reacting with calcium carbonate (solid phase), while the latter polygonal form is presumably formed by liquid sulfuric acid (liquid phase) reacting with calcium carbonate (solid phase). The XRD analysis results indicated that the S adherends in all samples were calcium sulfate dihydrate. Based on the above, polygonal calcium sulfate dihydrate crystals were determined to exist on the surface layer of the black trace areas. In the model plaster simulation experiment, elemental S was observed on the surface layer, but calcium sulfate hydrate was undetectable. The cause of this is unknown.

The non-detection of elemental N may be caused by disappearance because of deliquescence or high decomposability.

4 CONCLUSIONS

A novel discovery that copper leaf was dissolved by the "Black Rain" led us to explore the "Black Rain" chemical aspect (highly oxidative) with strong "acid rain". This finding is consistent with the extremely rapid biological effects described by several witnesses after the bombings. The "Black rain" seems to be a complex mixture of chemically reactive and oxidizing (biologically harmful) substances and radioactive substances, rather than simple radioactive fallout. This may provide scientific evidence for the lethal effects on organisms in the A-bomb survivor's testimony. Also, research on the chemical properties of the "Black Rain" is crucial for improving the accuracy of meteorological models. This is because chemicals such as sulfuric acid and nitric acid are major components of aerosols, which has a significant

impact on clouds and precipitation. Incorporating these factors into models is vital for improving the accuracy of estimates of the "Black Rain" occurrence areas.
The sources of nitric acid are NO_X formation from atmospheric nitrogen and oxygen caused by high temperatures during nuclear explosions [4]. In addition, the sources of NO_X and SO_X are the city fires as biomass burning [5] including the sulfur-containing products (rubber, asphalt, paint, etc.), fuels such as coal and oil.

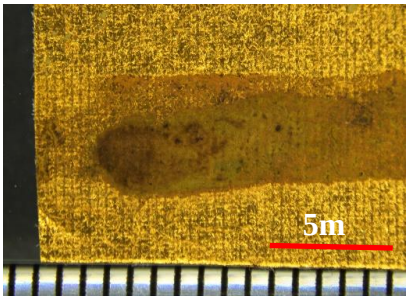


Fig. 1. Black traces on the gold folding screen. (Reflected light image)

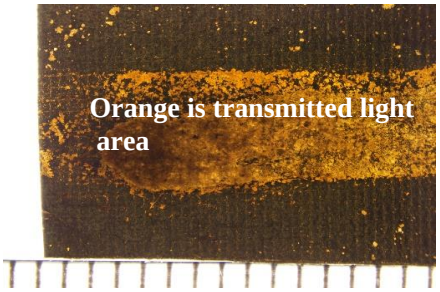


Fig. 2. Black traces on the gold folding screen. (Transmitted light image)

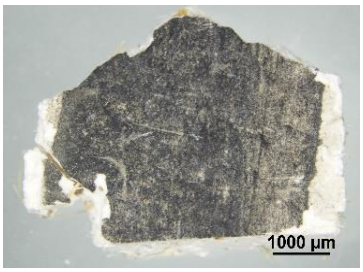


Fig. 3. Black traces on the plaster wall.



Fig. 4. Back of the plaster wall.

ACKNOWLEDGMENTS

This research was funded by the Ministry of Health, Labour and Welfare of Japan and Grant-in-Aid for Scientific Research JP24H00367. We would like to thank the staff of Hiroshima Peace Memorial Museum, especially the curatorial staff, the bereaved family for donating valuable artifacts, Professor Satoru Endo of Hiroshima University for his cooperation in collecting the samples. We thank Rekiseisha Co., Ltd. for model screen, Dr. Tatsuya Katsuno of the Department of Electron Microscopy, Center for General Anatomy, Graduate School of Medicine, Kyoto University, for FE/SEM/EDX analysis, Professor Takuo Okuchi of Institute for Integrated Radiation and Nuclear Science, Kyoto University for XRD analysis, Professor Satoshi Shinoda of Osaka Metropolitan University for laser Raman analysis, Dr. Toshiyuki Tamai, Dr. Motohiro Shizuma, Dr. Hiroshi Hirano, Dr. Toru Nagaoka, Dr. Yoshihisa Kimoto of the Morinomiya Center of Osaka Research Institute of Industrial Science and Technology, Dr. Tsutomu Tanaka, Mr. Masayuki Nezu of the Izumi Center of the Osaka Research Institute of Industrial Science and Technology, Mr. Keita, Takahashi, Mr. Tatsuo Fukui and Dr. Kazuaki Sawada of NIKON SOLUTIONS CO.,LTD, Mr. Syouji Mukuta of HiROX CO.,LTD. for their analysis, Mr. Tetsuji Imanaka of Kyoto University, Specially Appointed Professor Hirohiko Ishikawa of Kyoto University, Dr. Masayuki Takigawa of the National Agency for Marine-Earth Science and Technology for their valuable advice.

References

[1] Fields DE, Cole LL, Summers S, Yalcintas MG, Vaughan GL. "Generation of aerosols by urban fire storm," *Aerosol Sci Technol* **10**:28 –36, (1989).
[2] T Mukai, T Adachi, J Inoue, H Yashima, Y Shibahara, S Fukutani, K Takamiya, M Ikegami, Y Kurihara, N Toe and Y Igarashi. "Gold folding screen (red copper leaf) dissolved by the "Black Rain" generated by the Hiroshima atomic bombing," *Prog Earth Planet Sci* (2025) (to be submitted).
[3] T Mukai, T Adachi, N Toe, Y Shibahara, M Ikegami, H Yashima, S Fukutani, K Takamiya, J Inoue, Y Kurihara and Y Igarashi, "Plaster wall was altered by the "Black Rain" generated by the Hiroshima bombing," *Japan Geoscience Union Meeting* (2025) (submitted).
[4] Gilmore FR "The production of nitrogen oxides by low - altitude nuclear explosions," J Geophys Res 80:4553-4554 (1975).
[5] Akagi SK, Yokelson RJ, Wiedinmyer C, Alvarado MJ, Reid JS, Karl T, Crounse JD, Wennberg PO "Emission factors for open and domestic biomass burning for use in atmospheric models," Atmos Chem Phys 11:4039-4072 (2011).

Synchrotron-Based Analysis of Spherical Iron Oxide Particles Found in Hiroshima Bay

Yukihiko Satou[1], Satoru Endo[2], Ryoga Akaji[2], Takahisa Shobu[1], Aki Tominaga[1], Takehiro Sumita[3]

[1]*Japan Atomic Energy Agency 2-4 Shirakata, Tokai-Mura, Naka-Gun, 319-1195 Japan*
[2]*Hiroshima University, 1-3-2 Kagamiyama, Higashi-Hiroshima City, Hiroshima, 739-8511 Japan*
[3]*Kyushu University, 744 Motooka, Nishi-ku, Fukuoka, 819-0395 Japan*

1 Introduction

In 2019, Wannier *et al.* reported the discovery of approximately 10,000 high-temperature-derived microparticles (Hiroshima Bay particles) on the beaches of Hiroshima Bay [1]. These particles include spherical iron oxides and glassy materials containing vesicles, and their morphological and internal features suggest formation through explosive heating followed by rapid quenching. Their study proposed the Hiroshima atomic bombing as a possible origin.
However, no radioactive nuclides such as cesium-137(^{137}Cs) or uranium have been detected in these particles, leaving the atomic bomb origin hypothesis without decisive evidence. Furthermore, the plausibility of these particles surviving in coastal sands for over 80 years without significant alteration under natural weathering remains questionable.
This study aims to deepen scientific understanding of the formation processes and origin of Hiroshima Bay particles by applying advanced synchrotron radiation-based analytical techniques previously developed for the analysis of Fukushima-derived radioactive particles. We focus on structural and elemental characterization from multiple perspectives.

2. Experimental Methods

Samples were collected from beach sands on Ujina Island, located in Hiroshima Bay, where numerous particles were previously reported in earlier studies. Ujina Island is a key site for particle sampling, as target particles can still be readily collected today. Magnetic separation was first employed to isolate magnetic particles from beach sand. Approximately five spherical particles, each about 500 micrometers in diameter, were then selected based on color and magnetic response. These particles were categorized into three types—Red, Yellow, and Black—based on their external features, and representative particles were analyzed. Synchrotron-based analyses were conducted at the Japan Atomic Energy Agency's dedicated beamline (BL22XU) at SPring-8. First, X-ray computed tomography (XCT) using 17 keV X-rays was performed to visualize the internal 3D structures of the particles. Subsequently, X-ray fluorescence (XRF) analysis using 70keV X-rays was carried out to qualitatively determine the major constituent elements (e.g., Fe, Si, Al). Additionally, surface composition was examined using energy-dispersive X-ray spectroscopy (EDS) attached to a scanning electron microscope (SEM).
For comparison, metal splatter particles from welding rods used in shipbuilding and residues from commercial fireworks were also subjected to XRF analysis to evaluate differences and similarities in morphology and composition with the Hiroshima Bay particles.

3. Results and Discussion

XCT analysis revealed that all analyzed Hiroshima Bay particles (Red, Yellow, and Black types) were spherical and contained prominent internal voids. These cavities likely resulted from gas entrapment during rapid solidification following melt formation at extremely high temperatures. XRF and EDS results showed that the particles predominantly consist of iron (Fe), silicon (Si), and aluminum (Al), with no detectable levels of uranium (U), cesium (Cs), or other radioactive elements typically associated with nuclear materials. While some splatter and firework-derived particles exhibited similar spherical morphologies, they differed significantly in elemental ratios and internal structure.
Notably, industrial-origin particles did not exhibit large internal voids observable by XCT, and their elemental distribution was distinctly different, indicating that morphological resemblance alone is insufficient to assign a common origin with Hiroshima Bay particles. These findings suggest that Hiroshima Bay particles likely formed through unique processes not typical of natural atmospheric particles or common industrial byproducts. XCT analysis of synthetic welding splatter particles is currently underway to further clarify structural and compositional distinctions. Future studies will include crystallographic analysis via X-ray diffraction (XRD) and isotopic analysis using secondary ion mass spectrometry (SIMS) to elucidate the thermal conditions and formation period.

4. Conclusion

This study employed non-destructive synchrotron-based techniques to investigate spherical iron oxide particles collected from Hiroshima Bay. Detailed analysis of their internal structures and elemental compositions revealed characteristics consistent with formation by high-temperature melting followed by rapid cooling, distinct from known industrial or natural particles. Although no radioactive nuclides have been detected, the unique structural features strongly suggest

formation under exceptional thermal conditions. Continued sample collection and further analysis of crystal structures and isotopic ratios are essential for scientifically determining the particles' origin.

ACKNOWLEDGMENTS

The authors gratefully acknowledge the financial support from the Japan Society for the Promotion of Science (JSPS) through a Grant-in-Aid for Scientific Research (KAKENHI), Grant Number JP23K13691. The synchrotron radiation experiments were performed at SPring-8 with the approval of the Japan Atomic Energy Agency (JAEA) as Proposal Nos. 2019B3723, 2019B3724, 2021B3722, 2022A3721, 2022A3723, 2022B3721/BL22XU.

References

[1] Wannier, M. M. A., de Urreiztieta, M., Wenk, H.-R., Stan, C. V., Tamura, N., & Yue, B. (2019). Fallout melt debris and aerodynamically-shaped glasses in beach sands of Hiroshima Bay, Japan. Anthropocene, 25, 100196. https://doi.org/10.1016/j.ancene.2019.100196

Invited & Contributed Talk | [R3]Actinide Chemistry and Nuclear Energy Chemistry

Tue. Sep 16, 2025 3:05 PM - 4:35 PM JST | Tue. Sep 16, 2025 6:05 AM - 7:35 AM UTC Hall A(MP)

[R3] Actinide Chemistry and Nuclear Energy Chemistry

3:05 PM - 3:35 PM JST | 6:05 AM - 6:35 AM UTC

[R3-01(Invited)]

INNOVATIVE APPROACHES TO ACTINIDE HALIDE SPECIATION FOR NUCLEAR FUEL CYCLE ADVANCES

*Ken Ronald Czerwinski[1], Jason Victor[1], Renee Olney[1] (1. University of Nevada, Las Vegas (United States of America))

3:35 PM - 3:55 PM JST | 6:35 AM - 6:55 AM UTC

[R3-02]

SYNTHESIS AND ADSORPTIVITY OF NOVEL BIFUNCTIONAL MONOAMIDE-DIAMIDE RESIN FOR SELECTIVE SEPARATION OF ACTINYL IONS

*Masanobu Nogami[1], Keigo Uchida[1], Shion Matsumoto[1], Chikage Abe[2], Tomoo Yamamura[3] (1. Kindai Univ. (Japan), 2. Tohoku Univ. (Japan), 3. Kyoto Univ. (Japan))

3:55 PM - 4:15 PM JST | 6:55 AM - 7:15 AM UTC

[R3-03]

EFFICIENT SEPARATION of Cs(I) FROM SIMULATED HIGH-LEVEL LIQUID WASTE WITH NEW CALIX[4]-CROWN-6 ETHERS

*Zhijun Guo[1], Tengfei Cui[1], Zhen Xu[1], Haolong Wang[1], Qiang Jin[1], Zongyuan Chen[1] (1. Lanzhou University (China))

4:15 PM - 4:35 PM JST | 7:15 AM - 7:35 AM UTC

[R3-04]

Thiol unit-functionalized ultrastable two-dimensional polymer for adsorption of palladium ions in a nitric acid medium

*Hao WU[1], Naoki Osawa[2], Yan Wu[1], YueZhou Wei[1], WeiQun Shi[1], Seong-Yun Kim[3] (1. Shanghai Jiao Tong University (China), 2. Nagaoka University of Technology (Japan), 3. Tohoku University (Japan))

©APSORC25

7th Asia-Pacific Symposium on Radiochemistry *September 14 ~ 19, 2025 • Kunibiki Messe • Shimane, Japan*

INNOVATIVE APPROACHES TO ACTINIDE HALIDE SPECIATION FOR NUCLEAR FUEL CYCLE ADVANCES

Jason Victor, Renee Olney, and Ken Czerwinski

Radiochemistry Program, University of Nevada Las Vegas 4505Maryland Parkway, Las Vegas, NV USA 89154-4009

Actinide halides are integral to multiple stages of the nuclear fuel cycle, including actinide metal production, separations, uranium enrichment, and fuel fabrication. These compounds also play essential roles in pyrochemical processing, molten salt reactor technology, and the stabilization of nuclear materials. Among the halide systems, uranium fluorides are particularly prominent, especially in the context of expanding high-assay low-enriched uranium (HALEU) fuel development for advanced reactors. In response to the critical role of halide chemistry in fuel cycle operations, this study investigates alternative synthesis pathways and speciation behavior of actinide halides, with a focus on uranium and plutonium compounds.

A central component of this work addresses the deconversion of depleted uranium hexafluoride (UF_6), of which over 700,000 metric tons are stored in the United States. The volatility and chemical reactivity of UF_6 pose long-term management challenges. Conventional deconversion approaches involve hydrolysis, generating uranyl fluoride and releasing hydrogen fluoride. In contrast, the current study examines a novel stabilization method using the ionic liquid 1-methyl-1-propylpiperidinium bis(trifluoromethanesulfonyl)imide. This medium enables controlled hydrolysis of UF_6 and reduction to UF_4 under mild conditions. Key variables investigated include water dosing kinetics, interfacial dynamics, and thermal effects on UF_4 precipitation. Uranium speciation was monitored using UV-vis-NIR spectroscopy, while thermal and structural characterization of the solid phases was conducted via thermogravimetric analysis/differential scanning calorimetry (TGA/DSC) and powder X-ray diffraction (PXRD).

In parallel, this work explores the synthesis of actinide chlorides, emphasizing uranium and plutonium species relevant to pyroprocessing and molten salt reactor applications. Chlorination reactions of actinide oxides with aluminum trichloride ($AlCl_3$) were utilized to form UCl_4 and Pu chlorides via chemical vapor transport, offering a controlled and oxidant-free approach. The reactivity of mixed oxide systems, including $Pu_xU_{1-x}O_2$ and $Ce_xU_{1-x}O_2$, was investigated to assess compositional effects on chlorination efficiency and selectivity. Further experiments using aluminum halides (AlX_3, X = Cl, Br, I) provided insights into the formation and stability of various plutonium halide phases. The resulting materials were characterized using PXRD, TGA/DSC, SEM/EDS, and alpha spectroscopy to determine phase composition, thermal behavior, and elemental distributions.

These findings offer new perspectives on actinide halide chemistry and their relevance to nuclear material conversion, separations, and fuel cycle design. The demonstrated control over fluoride and chloride formation pathways enhances understanding of actinide speciation and provides practical strategies for addressing current and future challenges in nuclear fuel cycle operations.

Copyright on 7th Asia-Pacific Symposium on Radiochemistry 2025 - R3-01 -

SYNTHESIS AND ADSORPTIVITY OF NOVEL BIFUNCTIONAL MONOAMIDE-DIAMIDE RESIN FOR SELECTIVE SEPARATION OF ACTINYL IONS

Masanobu Nogami[1,2*], Keigo Uchida[2], Shion Matsumoto[1], Chikage Abe[3], Tomoo Yamamura[4]

[1]*Graduate School of Science and Engineering Research, Kindai University: 3-4-1 Kowakae, Higashi-Osaka, Osaka, 577-8502, mnogami@emat.kindai.ac.jp*
[2]*Faculty of Science and Engineering, Kindai University: 3-4-1 Kowakae, Higashi-Osaka, Osaka, 577-8502*
[3]*Institute for Materials Research, Tohoku University: 2145-2 Narita-cho, Oarai-machi, Higashiibaraki-gun, Ibaraki, 311-1313*
[4]*Institute for Integrated Radiation and Nuclear Science, Kyoto University : 2, Asashiro-Nishi, Kumatori-cho, Sennan-gun, Osaka 590-0494 JAPAN*

As a part of development of resins for selective separation and higher capacity for actinyl ions (An(VI)) in nitric acid media, novel bifunctional monoamide-diamide resin was synthesized and a preliminary adsorptivity was investigated. As expected, the obtained resins may improve adsorptivity for An(VI) by suppressing the adsorption for lanthanide(III) species.

1 Introduction

Development of highly selective compounds for hexavalent actinide species (actinyl ions, An(VI), AnO_2^{2+}) has been important. We have been focusing on monoamide compounds which coordinate with An(IV) and (VI) species in nitric acid media as promising candidates. However, as reported earlier[1], forming six-coordinated structures where one AnO_2^{2+} ion is surrounded by two carbonyl oxygen atoms of two monoamide molecules might be difficult spatially in case of resins. In order to increase the possibility of these coordinations, we suggested the combined use of monoamide and diamaide compounds as bifunctional groups. Diamide compounds are famous for separating not only An(IV) and (VI) species but also An(III) and lanthanide(III) (Ln(III)) ones. In this study, a preliminary synthesis and adsorptivity of a novel bifunctional monoamide-diamide resin was investigated.

2 Experimental

N,N-dimethylacrylamide (DMMA) and *N,N,N',N'*-tetrapentylmalonamide (TPMA) were used as monoamide and diamide, respectively. The synthetic scheme of the resin has two steps as shown in Fig. 1. DMAA, chloromethylstyrene (CMS), and divinylbenzene (DVB) were firstly copolymerized (8 % crosslinkage) at the mixed ratio of DMAA/CMS = 1 (w/w) with pore producing solvents and a porous silica support similarly to the earlier literatures[2, 3]. Chlorine atoms of poly-CMS were then substituted by TPMA by following the earlier literature[4] and the final resin (Silica DMAA-TPMA) was obtained. Adsorptivity of the resin was examined by a batch method using U(VI) and Ce(III) up to 6 mol/dm^3 (= M) HNO_3 at room temperature.

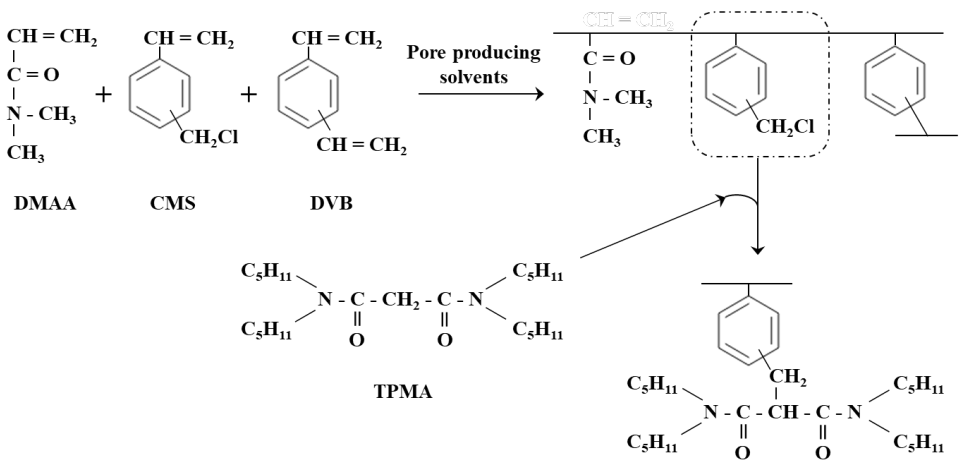


Fig. 1. Synthetic scheme of Silica DMAA-TPMA.

Copyright on 7th Asia-Pacific Symposium on Radiochemistry 2025 - R3-02 -

3 Results and Discussion

The resin showed adsorptivity basically with increasing concentration of HNO_3 for U(VI) and in HNO_3 higher than 3 M for Ce(III), respectively. The K_d values for U(VI) were more than 10 times higher than those for Ce(III). In addition, those for U(VI) of Silica DMAA-TPMA was found to be higher than those of Silica DMAA resins[2] although the direct comparison for experimental conditions would be difficult. This suggests that, as expected, bifunctional monoamide-diamide resins may improve adsorptivity for An(VI) by suppressing the adsorption for Ln(III). It was also revealed that the resin has some points to be improved, *e.g.*, increase in adhesion ratio of the polymers to the silica support.

References

[1] M. Nogami and T. Yamamura, "Consideration of Another Candidate Resins Containing Monoamide Structure with Selectivity for Actinyl Ions," *KURNS Progress Report 2023*, PR5-8 (2024).
[2] M. Nogami, T. Ishihara, K. Suzuki, and Y. Ikeda, "Syntheses and Adsorption Behavior of Monoamide Resins with Porous Silica Support for Selective Recovery of Uranium(VI) from Nitric Acid Media," *J. Radioanal. Nucl. Chem.*, **273**, 37 (2007).
[3] M. Nogami, T. Ishihara, K. Maruyama, and Y. Ikeda, "Effect of Chemical Structure of Monoamide Resins on Adsorptivity to Uranium(VI) in Nitric Acid Media," *Prog. Nucl. Energy*, **50**, 462 (2008).
[4] M. Nogami, I. M. Ismail, M. Yamaguchi, and K. Suzuki, "Synthesis, Characterization and Some Adsorption Properties of TMMA Chelating Resin," *J. Solid State Chem.*, **171**, 353 (2003).

EFFICIENT SEPARATION of Cs(I) FROM SIMULATED HIGH-LEVEL LIQUID WASTE WITH NEW CALIX[4]-CROWN-6 ETHERS

Zhijun Guo[1,2], Tengfei Cui[1], ZhenXu[1], Haolong Wang[1], Qiang Jin[1,2], Zongyuan Chen[1,2]

[1]*Radiochemistry Laboratory, School of Nuclear Science and Technology, Lanzhou University, 730000 Lanzhou, China*
[2]*MOE Frontiers Science Center for Rare Isotopes, Lanzhou University, 730000 Lanzhou, China*

The separation of heat-generating nuclide $^{137}Cs^+$ and long-lived nuclide $^{135}Cs^+$ from high level liquid waste (HLLW) is of great importance for nuclear waste management. In this study, new calix[4]arene-2,4-benzocrown-6 ethers with benzyl substituents, i.e., 25,27- bis(benzyl)calix[4]-benzocrown-6 (L1), 25,27- Bis(4-tert-butylbenzyl)calix[4]-benzocrown-6 (L2) and 25,27- Bis(4-tert-butylbenzyl)calix[4]-4-(tert-butyl)-benzocrown-6 (L3), were synthesized and used as extractants for Cs^+ separation from simulated HLLW. A countercurrent extraction process including 8-stage extraction, 6-stage scrubbing and 6-stage stripping on a simulated HLLW was carried out with L2 and resulted into a decrease of Cs(I) concentration by the order of magnitude of 10^3, a recovery of 99.9% and a purity of 98.1% for final Cs(I) product. The new ligands have good irradiation stability and acid tolerance. Slope analysis, ESI-MS, UV-vis titration and X-ray single crystal studies demonstrated the formation of a 1:1 (M:L) complexes of the ligand with Cs(I).

1 Introduction

The high selectivity of 1,3-alternate calix[4]arene-crown-6 ethers for Cs^+ mainly stems from the synergistic effect of Cs-O_{ether} coordination and Cs cation - π interaction [1, 2]. However, it has been found that the affinity to Cs^+ is also affected by the substituents [3, 4]. The substituted electron-rich aromatic groups (e.g., benzene, naphthalene, and phenol) and electron-donor groups (e.g., amino groups) can strengthen cation-π interactions [5, 6]. In this study, three new 1,3-alternate calix[4]-benzocrown-6 with benzyl substituents were synthesized and used as extractants for Cs^+ separation from simulated HLLW. The coordination chemistry of the ligands with Cs+ was also systematically investigated.

2 Results and Discution

L2 exhibits good Cs^+ selectivity over other elements from the synthetic HLLW (Figure 1). The slight extraction of molybdenum and potassium with D values of 10^{-1} under the condition suggests that Mo and K are possible impurities of the Cs product. The slight extraction of Mo and K can be interpreted by the coextraction of molybdate anions and the similarity between K^+ and Cs^+. The $SF_{Cs/M}$ values for Cs over other metals such as aluminum, nickel, chromium, iron and strontium are high enough with D_M values around 10^{-2}.

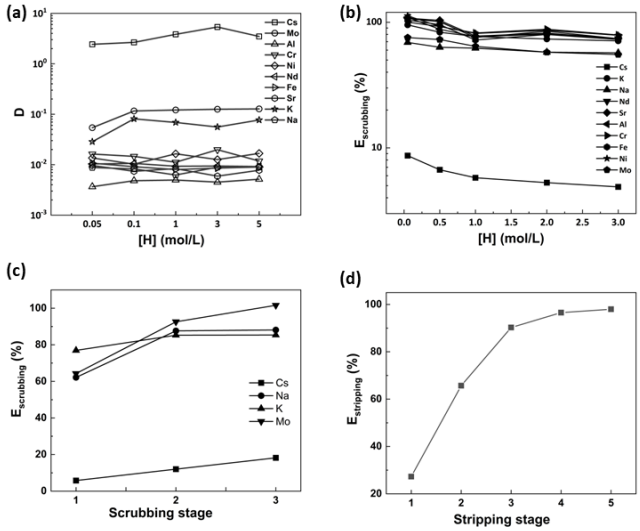


Figure 1. (a) The selectivity of L2 in simulated HLLW ([L]=10.0 mM, [HNO3] = 0.05-5 M); (b) the influence of acidity on scrubbing efficiency ([HNO3] = 0.05-3 M); (c) the effect of scrubbing stage number on scrubbing efficiency; (d) the effect of stripping stage number on stripping efficiency.

Copyright on 7th Asia-Pacific Symposium on Radiochemistry 2025 - R3-03 -

3. CONCLUSIONS

Three calix[4]crown-6 derivatives (L1-3) were synthesized and used to remove Cs^+ from high-level liquid waste (HLLW). Slope analysis indicated the presence of 1:1 (Cs/L) extracted species, which was consistent with the results of ESI-MS, UV-vis titration, and NMR titration. A counter current extraction process including 8-stage extraction, 6-stage scrubbing and 6-stage stripping based on L2 was developed, indicating that Cs^+ can be removed efficiently from the simulated HLLW. The single-crystal structures of [Cs(L1)(NO_3)] and [Cs(L2)(NO_3)] were elucidated by X-ray crystallography. Each central Cs(I) is 8 coordinated with 6 crown-ether oxygen atoms and a bidentate nitrate. The results indicated that 25,27-bis(4-tert-butylbenzyl)calix[4]-benzocrown-6 (L2) is a promising ligand for Cs^+ extraction from acidic HLLW.

ACKNOWLEDGMENTS

This work was supported by the Natural Science Foundation of Gansu Province (21ZD8JA006) and the Fundamental Research Funds for the Central Universities (lzujbky-2022-sp05), China..

References

[1] R. ABIDI, J. M. HARROWFIELD, B. W. SKELTON, A. H. WHITE, Z. ASFARI, J. VICENS, “Synthesis, Structure and Alkali Metal Ion Binding Properties of a Podand Polyether Derived from Calix[4]arene, 5,11,17,23-tetra-tert-butyl-25,27-di(phenylmethoxy)-26,28-di(2‘-methoxyethoxy)-calix[4]arene,” *J. Incl. Phenom. Macrocycl. Chem.* **27**, 291–302 (1997).

[2] R. J. ELLIS, B. REINHART, N. J. WILLIAMS, A. B. MOYERA, V. S. BRYANTSEV, “Capping the calix: how toluene completes cesium(i) coordination with calix[4]pyrrole,” *Chem. Commun.* **53**, 5610-5613(2017).

[3] R. A. SACHLEBEN, A. URVOAS, J. C. BRYAN, T. J. HAVERLOCK, B. P. HAY, B. A. MOYER, “Dideoxygenated calix[4]arene crown-6 ethers enhanced selectivity for caesium over potassium and rubidium,” *Chem. Commun.* 1751–1752 (1999).

[4] J. Y. KIM, I. H. PARK, J. Y. LEE, J. H. LEE, K. M. PARK, S. S. LEE, “Hard and soft metal complexes of calix[4]-bis-monothiacrown-5: X-ray and NMR studies of discrete homodinuclear complexes and a heteromultinuclear network,” *Inorg. Chem.* 52, 10176–10182 (2013).

[5] V. KUMAR, J. N. SHARMA, P. V. ACHUTHAN, D. K. SINGH, S. M. ALI, “A new bisglycolamide substituted calix[4]arene-benzo-crown-6 for the selective removal of cesium ion: combined experimental and density functional theoretical investigation,” *Rsc. Advances* **6**, 47120–47129 (2016).

[6] V. S. TALANOV, G. G. TALANOVA, M. G. GORBUNOVA, R. A. BARTSCH, “Novel caesium-selective,1,3-alternate calix[4]arene-bis(crown-6-ethers) with proton-ionizable groups for enhancedextraction efficiency,” *J. Chem. Soc.-Perkin Trans.* **2**, 209–215 (2002).

Copyright on 7th Asia-Pacific Symposium on Radiochemistry 2025 - R3-03 -

Thiol unit-functionalized ultrastable two-dimensional polymer for adsorption of palladium ions in a nitric acid medium

WU Hao[1*], OSAWA Naoki[2], WU Yan[1], WEI YueZhou[1], SHI WeiQun[1], KIM Seong-Yun[3]

1: Institute of Nuclear Fuel Cycle and Nuclear Materials, Shanghai Jiao Tong University

2: Department of Nuclear Technology, Nagaoka University of Technology

3: Department of Quantum Science and Energy Engineering, Tohoku University

A thiol unit-functionalized amide-linked two-dimensional polymer (DPA-derivatives) platform was constructed in this study via the condensation reaction of trimesyl chloride and melamine, and the subsequent post functionalization of the as-prepared platform was performed by further reacting it with cysteamine etc. to form thiol units around the DPA platform. The adsorption performances of DPA-derivatives towards Pd(II) in nitric acid medium were systematically investigated as an effect of contact time, nitric acid concentration, co-existing metal ions etc. Furthermore, the possible adsorption mechanism and coordination environment were elucidated by X-ray photoelectron spectroscopy (XPS) with the aid of density functional theory (DFT).

Keywords: polymer, thiol unit, amide-linked, Pd(II), XPS, DFT

Introduction

As an important Pt-group metal (PGM), Pd possesses numerous excellent physicochemical properties and has gained increasing research attention in advanced fields, particularly automotive catalytic converters, dental alloys, and corrosion-resistance apparatus. Numerous materials, such as covalent organic frameworks (COFs), metal–organic frameworks, silica-based materials, and ionic liquids, have been investigated for the effective recovery of Pd from HLLW. However, the performance of the most current materials remains unsatisfactory under the aforementioned harsh conditions. Therefore, the development of novel efficient materials possessing high stability and exceptional selective properties is extremely critical. In this study, we employed a rational design approach to prepare a novel thiol unit–functionalized 2D polymer (DPA-BGA).

Experimental

The target DPA-BGA material was prepared via the direct amide condensation of trimesyl chloride and melamine, followed by the postmodification of the thiol units onto the amide-linked DPA platform. The subsequent adsorption performance of DPA-BGA toward Pd(II) was examined using

* Corresponding author. Email: sjtuwuhao123@sjtu.edu.cn

Copyright on 7th Asia-Pacific Symposium on Radiochemistry 2025

the batch method as an effect of contact time, nitric acid concentration, co-existing metal ions etc. The concentration of metal ions in solution were determined via inductively coupled plasma atomic emission spectroscopy (ICP–AES; ICPS-7510, Shimadzu Corporation). Furthermore, the possible adsorption mechanism and coordination environment were elucidated by X-ray photoelectron spectroscopy (XPS) with the aid of density functional theory (DFT) using the Gaussian 09 software at the theory level of B3LYP.

Results and Discussion

The effects of the HNO_3 concentration of DPA-BGA on Pd(II) were determined in an environment containing 0.5–3 M HNO_3, with increasing HNO_3 concentration, the Pd(II) uptake percentage of DPA-BGA was maintained at a relatively high level, exhibiting values of >90% even when the HNO_3 concentration reached 3 M, indicating harsh conditions. The chemical stability of DPA-BGA was investigated via immersion in different concentrations of a nitric acid solution at 25°C for 24 h. The relative peak intensities and peak positions remain nearly unchanged after the HNO_3 treatment, and additional peaks corresponding to the collapse of the structure are not observed, indicating the exceptional chemical stability of DPA-BGA. The considerable resistance of DPA-BGA toward HNO_3 was considered to originate from the stable amide bonds in its main skeleton. On the other hand, from the experimental results of XPS and DFT calculation, it was found that both S and O atoms participate in the coordination with Pd(II).

Conclusion

We have successfully designed and synthesized a 2D polymer (DPA-BGA) that incorporates thiol units around the amide-linked DPA platform. The tailored DPA-BGA exhibits exceptional efficiency for capturing Pd(II) in a nitric acid medium, demonstrating an excellent acid resistance, relatively fast kinetics, and good reusability. The presence of abundant amide bonds ensures the stability of DPA-BGA even under exposure to a high concentration of nitric acid for 24 h. Detailed analysis based on XPS and DFT calculations further confirm that the superior removal performance of DPA-BGA toward Pd(II) can be attributed to the strong binding affinity between the thiol unit and Pd(II), and the possible complexation structures are presented.

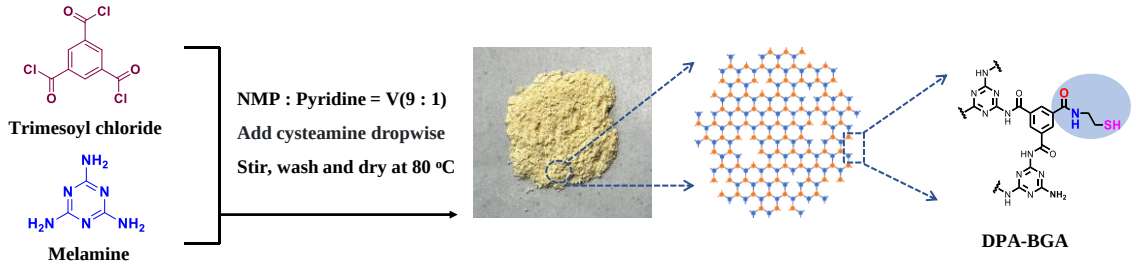


Fig. 1 Schematic of the synthesis of DPA-BGA

Invited & Contributed Talk | [R5]Activation Analysis

Tue. Sep 16, 2025 3:15 PM - 4:25 PM JST | Tue. Sep 16, 2025 6:15 AM - 7:25 AM UTC Hall S(Int'l)

[R5] Activation Analysis

3:15 PM - 3:45 PM JST | 6:15 AM - 6:45 AM UTC

[R5-01(Invited)]

The Role of Prompt γ-ray Analysis in Geology

*Takashi Sano[1], Takahito Osawa[2], Masaya Miyoshi[3], Masataka Kawaguchi[4], Mitsunori Ishimoto[4] (1. National Museum of Nature and Science (Japan), 2. Japan Atomic Energy Agency (Japan), 3. Fukuoka University (Japan), 4. The University of Tokyo (Japan))

3:45 PM - 4:05 PM JST | 6:45 AM - 7:05 AM UTC

[R5-02]

Complete analysis with high-resolution Prompt Gamma Activation

*Zsolt Revay[1] (1. Technical University Munich, Heinz Maier-Leibnitz Center (MLZ) (Germany))

4:05 PM - 4:25 PM JST | 7:05 AM - 7:25 AM UTC

[R5-03]

Machine Learning Methods Applied to Prompt Gamma Activation Analysis

*David Knezevic[1], Daniel Boschmann[2], Christian Stieghorst[1], Dimitrije Maletic[3], Zsolt Révay[1] (1. Heinz Maier Leibnitz Zentrum (MLZ), Technische Universität München (Germany), 2. Institute of Automation Technology Helmut Schmidt University, Hamburg (Germany), 3. Institute of Physics Belgrade (Serbia))

©APSORC25

7th Asia-Pacific Symposium on Radiochemistry September 14 ~ 19, 2025 • Kunibiki Messe • Shimane, Japan

THE ROLE OF PROMPT GAMMA-RAY ANALYSIS IN GEOLOGY

Takashi Sano[1], Takahito Osawa[2], Masaya Miyoshi[3], Masataka Kawaguchi[4], Mitsunori Ishimoto[5]

[1] *National Museum of Nature and Science, 4-1-1 Amakubo, Tsukuba 305-0005, sano@kahaku.go.jp*
[2] *Materials Sciences Research Center, Japan Atomic Energy Agency, 2-4 Shirakata, Tokai-mura, Naka-gun, Ibaraki, 319–1195, osawa.takahito@jaea.go.jp*
[3] *Faculty of Science, Fukuoka University, 8-19-1 Nanakuma, Jonan-ku, Fukuoka 814-0180, miyoshim@fukuoka-u.ac.jp*
[4] *Earthquake Research Institute, The University of Tokyo, 1-1-1 Yayoi, Bunkyo-ku, Tokyo 113-0032, mkawaguchi@eri.u-tokyo.ac.jp*
[5] *Nuclear Professional School, School of Engineering, The University of Tokyo, 2-4 Shirakata, Tokai-mura, Naka-gun, Ibaragi 319-1195, ishimoto@ tokai.t.u-tokyo.ac.jp*

As geologists, we will present the role of the PGA in geology by reviewing our previous research. We have mainly focused on two areas for the use of B, Cl and other trace elements (Ti, K, Gd, Sm): the oceanic crust, which is made up of basaltic rock and covering sediments; and the island arc, where materials recycled from the subduction of an oceanic plate are erupted.

1 PROMPT GAMMA-RAY ANALYSIS

Prompt γ-ray analysis (PGA) is one of the most convenient and accurate methods to determine boron (B) and chlorine (Cl) values in igneous rocks [1-2]. Both B and Cl are powerful elements to discuss material transport in geology. Boron is a useful tracer to evaluate recycling of altered oceanic crust (AOC) and sediments at subduction zones; B is strongly concentrated in marine sediments and the AOC, and parts of these are probably added to island arc magmas [3]. Chlorine is a key element to monitor behaviors of hydrothermal fluids that originated from magma, because Cl is selectively partitioned into aqueous fluids.

Changes in concentrations of B and Cl can monitor magma differentiation processes such as fractional crystallization and crystal accumulation. In order to know initial concentrations in the magma, B and Cl concentrations should be normalized by incompatible elements which show similar incompatibility [4]. Among the incompatible elements, titanium (Ti), potassium (K), samarium (Sm) and gadolinium (Gd) in igneous rocks are readily determined by the PGA [5].

2. GEOLOGICAL APPLICATION

We have mainly focused on two areas for the use of B, Cl and other trace elements: the oceanic crust, which is made up of basaltic rock and covering sediments; and the island arc, where materials recycled from the subduction of an oceanic plate are erupted.

Research into oceanic crust sequences shows that there are stepwise downhole variations: B content and B/K ratio decrease, while Cl content and Cl/K ratio increase with increasing depth. High B content in shallower rocks (extrusive lavas) is probably achieved by low-temperature submarine alteration, and high Cl content in deeper rocks (plutonic section) would show result of high-temperature hydrothermal alteration (Fig.1 [6-7]).

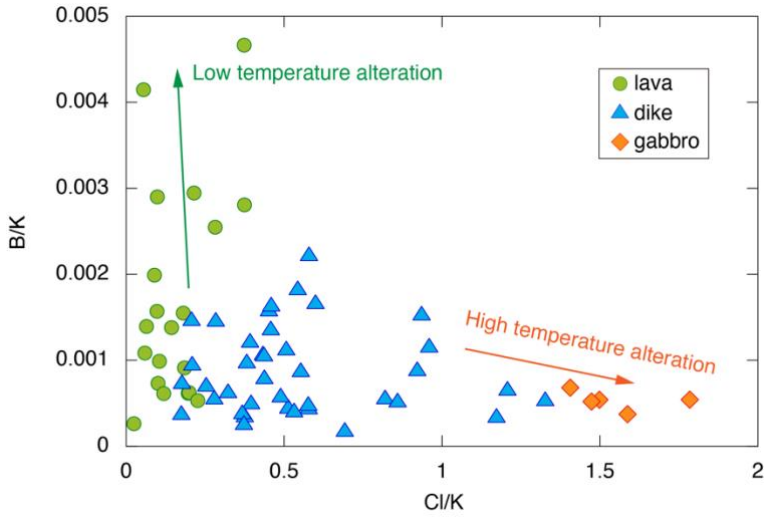


Fig. 1. B/K versus Cl/K for basement rocks in oceanic crust (after [6]).

Copyright on 7th Asia-Pacific Symposium on Radiochemistry 2025 - R5-01 -

Research into island volcanic rocks shows a clear variation in B enrichment across the arc: The B/Nb and B/Sm ratios in frontal arc rocks are high, whereas those in rear arc rocks are low (Fig. 2). This implies that subduction fluids concentrated in the AOC and/or sediments were recycled into magmas beneath the frontal arc more than the rear arc [8-10].

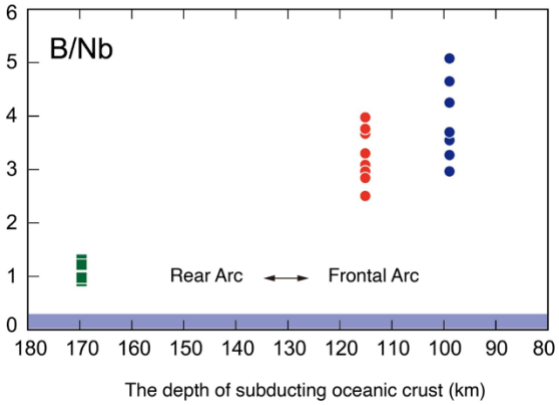


Fig. 2. Across arc variation for volcanic rocks on Kyusyu area, Japan.

ACKNOWLEDGMENTS

We would like to thank staff of Nuclear Professional School, School of Engineering, The University of Tokyo for their support of the PGA.

References

[1] T. SANO, T. FUKUOKA, T. HASENAKA, C. YONEZAWA, H. MATSUE and H. SAWAHATA, "Accurate and efficient determination of boron content in volcanic rocks by neutron induced prompt gamma–ray analysis," *Journal of Radioanalytical and Nuclear Chemistry*, **239**, 613–617 (1999).

[2] T. SANO., T. FUKUOKA and T. HASENAKA, "Determination of chlorine contents in Geological Survey of Japan reference materials by prompt gamma neutron activation analysis", *Geostandards and Geoanalytical Research*, **28**, 443–448 (2004).

[3] T. SANO, T. HASENAKA, A. SHIMAOKA, C. YONEZAWA and T. FUKUOKA, "Boron contents of Japan Trench sediments and Iwate basaltic lavas, Northeast Japan arc: Estimation of sediment–derived fluid contribution in mantle wedge", *Earth and Planetary Science Letters*, **186**, 187–198 (2001).

[4] T. SANO, T. HASENAKA, A. SHIMAOKA, T. FUKUOKA and H. NAGAI, "Low ratio of sediment recycling at Northeast Japan Arc: Constrains from ^{10}Be isotopes and B-Ba-K-Be systematics", *Geochemical Journal*, **51**, 277–291(2017).

[5] T. SANO, T. HASENAKA, H. SAWAHATA and T. FUKUOKA, "Determination of Ti, K, Sm, and Gd Values in Geological Survey of Japan Reference Materials by Prompt Gamma Neutron Activation Analysis", *Geostandards and Geoanalytical Research*, **30**, 31–36 (2006).

[6] T. SANO., M. MIYOSHI, S. INGLE, N.R. BANERJEE, M. ISHIMOTO and T. FUKUOKA, "Boron and Chlorine Contents of Upper Oceanic Crust, Basement Samples from IODP Hole 1256D", *Geochemistry, Geophysics, Geosystems*, **9**, Q12O15, doi:10.1029/2008GC002182 (2008).

[7] M. MIYOSHI, T. SANO, K. SHIMIZU, A. DELACOUR, T. HASENAKA, Y. MORI and T. FUKUOKA, "Boron and chlorine contents of basalts from the Shatsky Rise, IODP Expedition 324: Implications for the alteration of oceanic crust", The *Origin, Evolution, and Environmental Impact of Oceanic Large Igneous Provinces, GSA Special Publications*, **511**, pp. 69–84, C. R. NEAL, W.W. SAGER, T. SANO, E. ERBA, (Eds.) *Geological Society of America* (2015).

[8] M. MIYOSHI T. FUKUOKA, T. SANO and T. HASENAKA, "Subduction influence of Philippine Sea plate on the mantle beneath northern Kyushu, SW Japan: An examination of Boron contents in basaltic rocks", *Journal of Volcanology and Geothermal Research*, **171**, 73–87 (2008).

[9] M. MIYOSHI, M. SHIMONO, T. HASENAKA, T. SANO and T. FUKUOKA, "Determination of boron contents in volcanic rocks by prompt–gamma ray analysis: an implication to magma genesis in Kyushu island, SW Japan", *Journal of Radioanalytical and Nuclear Chemistry*, **278**, 343–347 (2008).

[10] M. MIYOSHI, M. SHIMONO, T. HASENAKA, T. SANO, Y. MORI and T. FUKUOKA, "Boron systematics of Hitatsu and Kirishima basaltic rocks from southern Kyushu, Japan", *Geochemical Journal*, 44, 359–369 (2010).

Copyright on 7th Asia-Pacific Symposium on Radiochemistry 2025 - R5-01 -

7th Asia-Pacific Symposium on Radiochemistry *September 14 ~ 19, 2025 • Kunibiki Messe • Shimane, Japan*

Complete analysis with high-resolution Prompt Gamma Activation Analysis

Zsolt Révay[1]

[1]*Technical University Munich, Heinz Maier-Leibnitz Center (MLZ), Lichtenbergstr. 1., Garching, 85748 Germany, zsolt.revay@frm2.tum.de*

Prompt Gamma Activation Analysis (PGAA) can be best performed at research reactors, especially in cold neutron beams. For the most reliable qualitative and quantitative analysis, the methods need precise energy and efficiency calibration. This high-resolution PGAA enables to detect minor and trace elements in complicated matrices, the complete analysis of samples of all kinds from archaeometry to material science, from minerals to metal alloys, from investigating unknown samples in sealed containers to monitoring chemical processes. The presentation summarizes technical aspects, calibration procedures and applications of high-resolution PGAA.

1 INTRODUCTION

Prompt Gamma Activation Analysis (PGAA) is based on the radiative neutron capture, or the (n,γ) reaction. In the energy range of cold neutrons (less than 10meV), all capture cross sections strictly follow the 1/*v* law, hence the results obtained in cold-neutron beam facilities are always comparable to each other, while thermal beam facilities need a correction for the low-energy resonances (using e.g. Westcott *g* factors) for such elements as Cd, Sm, Lu, and a few other rare-earth elements. Besides that, the reaction rate as calculated from the flux, the composition and the cross sections is very linear. Because of the deep penetration of both neutrons and gamma rays, PGAA is suitable for bulk analysis of all kinds of samples, unique for light elements which are always difficult to determine with other methods, especially H, but also for B. The major problem however is the large number of energy niveaus and transitions due to the high binding energies of the neutrons resulting in rather complicated gamma spectra. The linearity of today's typical spectrometers is far from the precision needed for the reliable identification of characteristic peaks especially in the case of the heavy elements, where thousands of peaks may appear in the finger-print region. [1]

2 METHODOLOGY

The samples are placed in a carefully shielded, evacuated target chamber, and they are irradiated with high-flux cold neutron beam. The gamma spectra are acquired using high-purity germanium (HPGe) detectors and digital spectrometers. [2]

2.1 Spectrum evaluation

Because of the large number of peaks, a special software is used for the evaluation of the spectra based on the Hypermet code of the Naval Research Laboratory, adopted for personal computers in Budapest: Hypermet-PC and Hyperlab. This software family uses a special peak-shape function which proved to describe the peaks even at high energies, where the peaks are highly asymmetric. [3]

2.2 Calibration

A complicated prompt gamma spectrum may contain more than a thousand peaks, whose density especially below 1 MeV may become rather difficult to evaluate. Here, the fitted energy values must have uncertainties of about 0.01 keV, while at high energies, where the occurrence of the peaks are lower, 0.1 keV is enough for the reliable identification of peaks. The nonlinearity of spectrometers is typically about 0.1%, which more than 1 keV for a spectrum up to 11 MeV gamma energies. Using high-precision energy data obtained from crystal-spectrometer measurements of radioactive calibration sources, the (n,γ) reactions from a few elements like chlorine, recently also using the precise atomic mass evaluations, the nonlinearity correction can be established for the spectrometers. The correction function stays valid for a longer time period, we usually determine it at the beginning of each reactor cycle together with the efficiency calibration. [4]

The counting efficiency is also very important, the accuracy of the quantitative analysis is highly dependent on it. One measurement is not enough due to the broad energy range. On the low-energy end, well-known radioactive sources are used, like Eu-152 and Ba-133. For the high energies, the prompt gamma peaks of N (using deuterated urea) and Cl (using PVC) are measured, as their peak intensities are known precisely. They are normalized together and one ortho-

Copyright on 7th Asia-Pacific Symposium on Radiochemistry 2025 - R5-02 -

normal polynomial, typically of the 8th grade is fitted to the points. In principle, all data sets are to be normalized to the source with the most accurate activity, however, we do not use the uncertainty of the activity in our calculations, because the efficiency ratio is used in the determination of concentrations and in the ratio this cancels. [5]

2.3 Data library

The data library was established at the Budapest Neutron Center and is now maintained in MLZ Garching. All stable elements were measured to determine the relative positions and intensities of the peaks using pure elements or simple compounds like oxides as samples. Then the precise energies were determined with interpolating certain peak positions of the element using the peaks of the energy standard: chlorine. The spectra were then calibrated using these lines. Finally, in the standardization stoichiometric compounds were measured to absolutize the peak intensities using cross sections standards: Cl, N, C and ultimately H. This database was first published in 2004, and continuously updated throughout the years. [6]

3 APPLICATIONS

The chemical analysis is based on the comparison of the evaluated peak lists to the spectroscopic library. Based on well-defined statistical quantities, such as internal and external uncertainties (i.e. the standard deviations) as well as using χ^2 fits, the elements forming the sample are then selected and from the mass ratios the composition is calculated. [7]

The method has been applied for tens of thousands of samples in Budapest and in Garching for archeological samples to clarify provenience, to determine the chlorine content of corroded artefacts, for material science to determine hydrogen content of high-purity silicon or deuterated organic compounds, for the determination of trace elements in air filters and plants, also for monitoring chemical reactions in irradiated catalytic reactors.

4 CONCLUSIONS

Prompt Gamma Activation Analysis proved to be a useful analytical tool to determine the composition of large variety of samples. It enables complete analysis based on precise energy and efficiency calibrations using a comprehensive spectroscopy data library including the light and other hard-to-measure elements, major and minor elements, as well as several trace elements.

References

[1] Zs. RÉVAY, T. BELGYA, *Handbook of Prompt Gamma Activation Analysis with Neutron Beams*, pp.1–30. G.L. MOLNÁR, Ed, Kluwer Academic Publishers, Dordrecht/Boston/New York (2004).
[2] Zs. RÉVAY, P. KUDEJOVA, K. KLESZCZ, S. SÖLLRADL, Ch. GENREITH, “In-beam Activation Analysis Facility at MLZ, Garching”, *Nucl. Instrum. Meth.*, **A799,** 114 (2015).
[3] www.hlabsoft.com
[4] B. FAZEKAS, ZS. RÉVAY, J. ÖSTÖR, T. BELGYA, G. MOLNÁR, A. SIMONITS, “A new method for determination of gamma-ray spectrometer nonlinearity” *Nucl. Instr. Meth*. **A422,** 469 (1999).
[5] G.L. MOLNAR, Z. RÉVAY, T. BELGYA, “Wide energy range efficiency calibration method for Ge detectors”, *Nucl. Instrum. Meth.* **A 489,** 140 (2002).
[6] ZS RÉVAY, R.B. FIRESTONE, T. BELGYA, G.L. MOLNÁR, *Handbook of Prompt Gamma Activation Analysis with Neutron Beams,* pp.173–364. G.L. MOLNÁR, Ed., Kluwer Academic Publishers, Dordrecht/Boston/New York, 2004
[7] ZS. RÉVAY, “Determining Elemental Composition Using Prompt Gamma Activation Analysis”, *Anal. Chem.* **81**, 6851 (2009).

Copyright on 7th Asia-Pacific Symposium on Radiochemistry 2025 - R5-02 -

7th Asia-Pacific Symposium on Radiochemistry *September 14 ~ 19, 2025 • Kunibiki Messe • Shimane, Japan*

Machine Learning Methods Applied to Prompt Gamma Activation Analysis

David Knezevic[1], Daniel Boschmann[2], Christian Stieghorst[1], Dimitrije Maletic[3], Zsolt Révay[1]

[1] Heinz Maier-Leibnitz Zentrum (MLZ), Technische Universität München, Lichtenbergstr. 1, 85748 Garching, Germany, david.knezevic@frm2.tum.de / christian.stieghorst@frm2.tum.de / zsolt.revay@frm2.tum.de
[2] Institute of Automation Technology Helmut Schmidt University, Hamburg, Germany, boschmad@hsu-hh.de
[3]Institute of Physics Belgrade, Pregrevica 118, Zemun, 11080, Serbia, maletic@ipb.ac.rs

Machine learning (ML) and deep learning (DL) algorithms can be applied to the Prompt Gamma Activation Analysis (PGAA) in order to automate the analysis process. Biggest challenges in application of the algorithms are number of available spectra and elemental diversity of available spectra. These challenges can be somewhat overcome with creating semi real data sets as well as with simulation. Various approaches and results will be presented.

1 INTRODUCTION

In the recent years, a large number of papers on the application of ML and DL methods to various physics problems are being published. There is a multitude of reasons for this. ML and DL methods are versatile, with many available architectures, and can be used in all aspects of physics experiments, from control of the measurement process to the automation of data analysis.

Analysis of spectra in PGAA is a well-developed method with, in principle, straightforward data treatment. One of the problems that can be mitigated by using ML and DL algorithms is that the process of analysis is time consuming. This is due to large number of gamma rays emitted after neutron capture, the possible interference of the gamma rays from different elements, and the composition of the sample itself (relative ratios of elements) can amplify these problems. Additional complications arise from the fact that the peak shape in PGAA is influenced by several contributions, requiring careful analysis. Even with experts analyzing the data, the analysis can get too complex, and it becomes difficult to achieve the necessary quality in identifying and quantifying the elements present in the target material in a reasonable time.

2 METHODS AND RESULTS

The research is focused on developing ML and DL algorithms for automated analysis of the PGAA spectra. There are two ways to approach this problem with regards to the comparison of the results obtained by algorithms with the results obtained by experts. One way is to have a two-step process, where the first step of automation ends with the algorithm determining the relevant peaks in the spectra, with their areas and errors. After this, the second step would determine the elemental composition of the sample. This would, on one hand, ensure that the results obtained with ML and DL algorithms could always be compared with the results obtained by experts. On the other hand, this would somewhat limit the ML and DL possibilities since the output of the first step would always have to be the same. Second way is to fully automate the analysis of data. Currently the focus is on the full automation of the process, although there are some plans to also investigate the two-step approach.

The first batch of data was tested with multiple algorithms, from the simplest towards more complex. These include Linear Regression (LR), Random Forest (RF), 1D Convolutional Neural Network (1D-CNN), Feed Forward Neural Network (FFNN), and Autoencoder algorithms [1]. The primary goal was to determine the elemental composition of the sample based on the spectra. Some of the results can be seen in Figure 1, while the performance of the various approaches is described by metrics in Table 1. Custom metrics were designed to better reflect the challenging definition of a “good analysis” which includes a relative importance of the quantity of an element. In further algorithm development the metrics are to be improved, and physical knowledge introduced. The basic description of the first iteration of these metrics can be found in Table 1. The first results were promising, showing that Autoencoders and Feed Forward Neural Networks could qualitatively describe the samples rather well, and to a degree describe their quantities over various PGAA spectra. However, a few challenges were identified in the process that had to be resolved in order to improve the results.

One of the main issues in applying the ML and DL algorithms for the PGAA spectra is the necessity for a large amount of data. Although data can be augmented with various methods to a degree, the number of the spectra available at the PGAA facilities is usually relatively small compared to the ones needed to ensure the successful training of the algorithms. In the second, improved, batch of data, the number of spectra was increased but remained comparatively

Copyright on 7th Asia-Pacific Symposium on Radiochemistry 2025 - R5-03 -

small. The algorithm testing for this new data set is currently in progress. The second problem is that the spectra are usually measured with a specific scientific purpose in mind, so not all the elements of interest are equally represented. For this reason, a decision was made to supplement real data with simulations. Since the PGAA spectra are rather complex, and simulations of a large number of isotopes are time consuming, there must be a trade-off between the complexity of simulations and the time required for simulating. The simulation process is currently ongoing and has gone through a few iterations.

New results with the improved data set used to train various ML and DL algorithms will be presented, as well as the results of the simulations and their potential for usage in the algorithms.

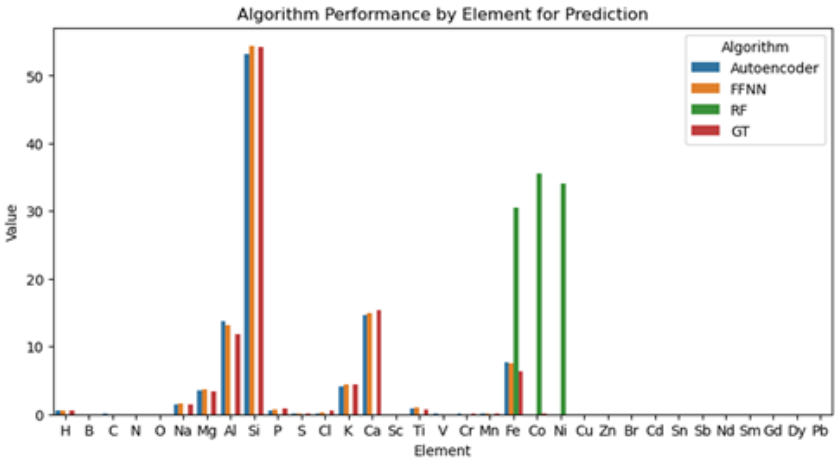


Fig. 1. Example of a prediction of various algorithms. GT represents ground truth, i.e. values obtained by experts.

TABLE 1. Metrics for the used algorithms. MSE and MAE represent Mean squared error and mean absolute error, respectively. MSBE and RP are new metrics introduced to reflect the specifics of the PGAA spectra. MSBE is a metric that penalizes the predictions outside of the uncertainty range, while RP is the average amount of elements that are predicted within their respective uncertainty range.

Algorithm	MSE	MAE	MSBE	RP
Autoencoder	**0.38**	0.06	**1.42**	0.65
1D-CNN	36.08	0.52	37.70	0.88
Linear regression	72.84	1.64	75.94	0.82
FFNN	0.57	**0.05**	1.58	0.91
Random forest	61.05	1.32	63.38	**0.92**

3 CONCLUSIONS

Application of ML and DL algorithms to PGAA data analysis has the potential to automate the process and substantially speed up the analysis time, which can increase the data output in many current and potential applications. Also, these results can be extended to other similar spectral analyses.

ACKNOWLEDGMENTS

This work was done within the “EvalSpek-ML” project funded by the BMBF as part of the ErUM-Data program [Collaborative project 05D2022-EvalSpek-ML, 2023-2026]. We thank the funding organization for the support of our project.

References

[1] Boschmann et al. Automation of PGAA Spectra Analysis with Deep Learning, 2024 IEEE 22nd International Conference on Industrial Informatics (INDIN) (2024)

Copyright on 7th Asia-Pacific Symposium on Radiochemistry 2025 - R5-03 -

Invited & Contributed Talk | [P5]Environmental Radiochemistry Applicable for Nuclear Non-Proliferation, Disarmament, and Nuclear Security

Tue. Sep 16, 2025 3:15 PM - 4:25 PM JST | Tue. Sep 16, 2025 6:15 AM - 7:25 AM UTC Hall B(Small)

[P5] Environmental Radiochemistry Applicable for Nuclear Non-Proliferation, Disarmament, and Nuclear Security

3:15 PM - 3:45 PM JST | 6:15 AM - 6:45 AM UTC

[P5-05(Invited)]

Quality Assurance for a global network

*Nikolaus Hermanspahn[1] (1. CTBTO (Austria))

3:45 PM - 4:05 PM JST | 6:45 AM - 7:05 AM UTC

[P5-06]

EFFICIENCY EVALUATION OF AN AUTOMATED SOLID-PHASE EXTRACTION SYSTEM FOR MONITORING RADIOSTRONTIUM (^{90}Sr) IN SOIL SAMPLES

*Phachirarat Sola[1,3], Hirofumi Tazoe[2], Naofumi Akata[2], Chutima Kranrod[2], Rawiwan Kritsananuwat[3] (1. Thailand Institute of Nuclear Technology (Public Organization) (Thailand), 2. Institute of Radiation Emergency Medicine, Hirosaki University (Japan), 3. Nuclear Engineering, Chulalongkorn University (Thailand))

4:05 PM - 4:25 PM JST | 7:05 AM - 7:25 AM UTC

[P5-07]

ANALYSIS OF FISSILE MATERIAL USING FISSION TRACK METHOD IN NUCLEAR FALLOUT SAMPLES COLLECTED ON DAIGO FUKURYU MARU

*Koichi TAKAMIYA[1], Maiko IKEGAMI[1], Naoyuki OSADA[1], Yasuhito IGARASHI[1] (1. Institute for Integrated Radiation and Nuclear Science, Kyoto University (Japan))

©APSORC25

7th Asia-Pacific Symposium on Radiochemistry *September 14 ~ 19, 2025 • Kunibiki Messe • Shimane, Japan*

Quality Assurance for a global network

Nikolaus Hermanspahn[1]

[1]*Comprehenisve Nuclear Test Ban Treaty Organization (CTBTO),1400 Vienna, Austria, Nikolaus.hermanspahn@ctbto.org*

The international monitoring network that is being operated to monitor compliance with the Comprehensive Nuclear-Test-Ban Treaty (CTBT) is designed to detect nuclear explosions anywhere on earth. Four complementary monitoring technologies are used to ensure that the probability of detecting a nuclear test is maximized. Seismic, infrasound and hydroacoustic technologies can provide fast detection and localization of explosions. The radionuclide component of the network plays an important role in verifying the nuclear nature of the explosion through the detection of fission and activation products. The presentation will provide an overview of test-ban monitoring technologies and their contribution to Treaty Verification. Challenges in providing calibration and quality assurance for radionuclide technologies in a global network will be discussed and highlight opportunities for future research and development.

1 The Comprehensive Nuclear Test Ban Treaty

The Comprehensive Nuclear-Test-Ban Treaty (CTBT) bans all nuclear explosions, whether for military or peaceful purposes.

The CTBT is an essential component of the international nuclear arms control and disarmament framework.

- Nuclear testing is a key step in the development of nuclear weapons. By ending this, the CTBT curbs all nuclear arms proliferation, be it the development of nuclear weapons by countries that do not currently have them, upgrades to current nuclear arsenals or the creation of new, more advanced generations of nuclear weapons.

- The CTBT is fundamental to nuclear disarmament because it establishes trust that any clandestine nuclear test will be detected.

- The CTBT has an intrinsic, complementary relationship with the landmark Treaty on the Non-Proliferation of Nuclear Weapons (NPT), the cornerstone of the global nuclear non-proliferation and disarmament regime, which recognises the crucial importance of ending nuclear test explosions.

- The CTBT prevents the serious health and environmental impacts of nuclear tests.

1.1 The International Monitoring System

The International Monitoring System (IMS) when completed will consist of 321 monitoring stations supported by 16 radionuclide laboratories.

The majority of monitoring stations (241) are seismic, infrasound or hydroacoustic type stations.The radionuclide network is comprised of 80 particulate monitoring stations with additional noble gas (xenon detection) capability planned at 40 stations. For particulate monitoring fission and activation products are detected by gamma spectrometry on the filtration medium. The noble gas collection and measurement systems were specifically developed for CTBT verification monitoring as the requirements for sensitivity and reliability are very high. These monitoring stations are supported by 16 certified laboratories that provide critical quality assurance measurements and provide options to re-analyze network samples for corroboration or results.

Copyright on 7th Asia-Pacific Symposium on Radiochemistry 2025 - P5-05 -

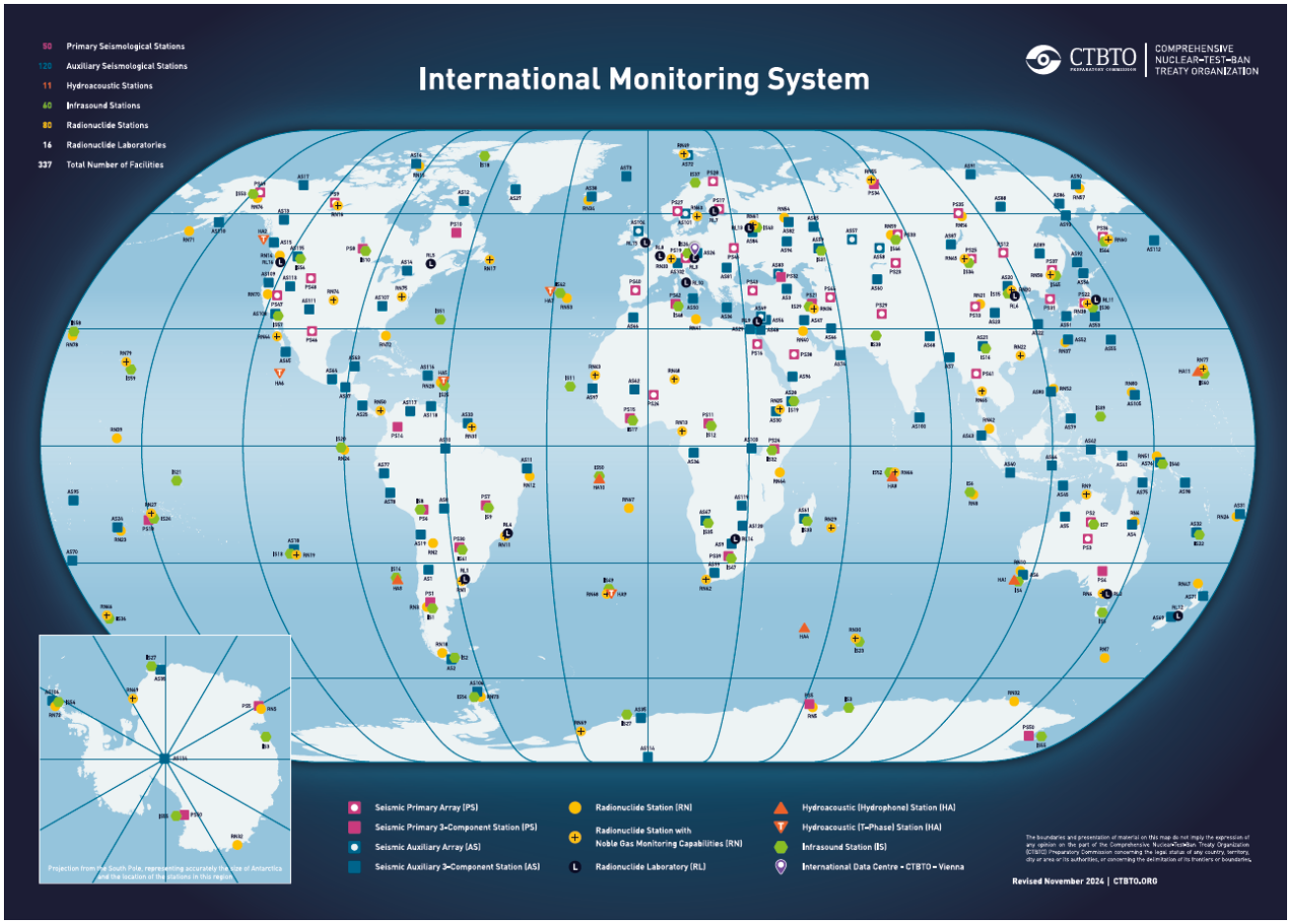


Figure 1 Map of the International Monitoring System. See https://www.ctbto.org/our-work/ims-map

1.1.1 Quality Assurance in a global network

It is essential that State Parties can trust the data they receive from the IMS. Consequently, quality assurance plays an important role in supporting the Verifcation data. In addition to daily (or more frequent) quality assurance measurements of QA sources, supporting measurements by the CTBT laboratories play a critical role in verifying accuracy of the station measurements. The CTBT laboratories are certified for operation for verification measurements. In case of particulate samples, the verification measurements are performed on station samples. In case of noble gas samples, as levels of xenon in the environment are low, the verification measurement is started by the injection of a xenon spike into the noble gas system. The measured sample is then sent to an IMS laboratory for comparison. As part of the on-going certification of the laboratories they are required to meet stringent requirements for performance in proficiency tests. These proficiency test involve the measurement of fresh fission and activation products mimicking as far as possible the signature from a nuclear test. In addition to the logistical challenges posed by a global network, there are additional challenges due to the short-lived nature of the fission/activation products that are of interest for nuclear explosion monitoring.

Copyright on 7th Asia-Pacific Symposium on Radiochemistry 2025 - P5-05 -

7th Asia-Pacific Symposium on Radiochemistry *September 14 ~ 19, 2025 • Kunibiki Messe • Shimane, Japan*

EFFICIENCY EVALUATION OF AN AUTOMATED SOLID-PHASE EXTRACTION SYSTEM FOR MONITORING RADIOSTRONTIUM (^{90}Sr) IN SOIL SAMPLES

Phachirarat Sola[1,3], Hirofumi Tazoe[2*], Naofumi Akata[2], Chutima Kranrod[2], Rawiwan Kritsananuwat[3*]

[1]*Thailand Institute of Nuclear Technology (Public Organization): 9/9 Moo 7 Saimoon, Ongkharak, Nakhon Nayok, Thailand, 26120, and phachirarats@tint.or.th*
[2]*Institute of Radiation Emergency Medicine, Hirosaki University: 66-1, Hon-cho, Hirosaki, Aomori, 036-8564, Japan and tazoe@hirosaki-u.ac.jp*, akata@hirosaki-u.ac.jp, kranrodc@hirosaki-u.ac.jp
[3] *Nuclear Engineering, Chulalongkorn University: 254 Phaya Thai Rd, Wang Mai, Pathum Wan, Bangkok, 10330, and rawiwan.kr@chula.ac.th*

1. INTRODUCTION

Strontium-90 (^{90}Sr) is a long-lived radioactive isotope of concern in environmental monitoring due to its chemical similarity to calcium and tendency to accumulate in bones. Traditionally, ^{90}Sr has been measured using solvent extraction or precipitation methods, which are often time-consuming, labor-intensive, and involve multiple manual steps that can introduce errors and safety risks. To improve selectivity and reduce chemical interferences, the manual solid-phase extraction (SPE) using DGA Resin has been developed, allowing more efficient separation of ^{90}Sr through its daughter nuclide yttrium-90 (^{90}Y) [1]. However, when operated manually, DGA Resin SPE still requires careful handling of strong acids and hydrofluoric acid (HF), precise timing, and repeated manual operations. To address these challenges, this study evaluates an automated DGA Resin SPE system designed to minimize operator exposure, improve consistency, and streamline the analysis of ^{90}Sr in soil samples for long-term environmental monitoring. Although manual SPE using DGA resin has been widely applied due to its quite high selectivity and efficiency for ^{90}Sr analysis, less consistent, and pose safety risks due to handling strong acids. These drawbacks limit their suitability for routine work [2-3]. Both systems are based on the same separation principle. If the performance of the automated SPE system can be improved to match or exceed that of the manual system, it could significantly enhance the analysis of environmental radionuclides by making the process safer and more convenient.

The automated SPE system minimizes human exposure, and improves reproducibility. However, similar advancements have yet to be widely adopted due to certain limitations, such as the limited capacity for simultaneous sample processing and the complexity of the system. This study aims to develop and evaluate an automated SPE system suited to environmental conditions, focusing on technical performance, analytical reliability, and operational efficiency. The overarching goal is to contribute a safer, faster, and more reproducible method for long-term ^{90}Sr monitoring in soil samples.

2. MATERIALS AND METHEDS

2.1 Design of the Automated SPE System

The system was constructed with chemically resistant Teflon components to safely handle corrosive acids, including hydrofluoric acid (HF). Reagent and sample delivery were managed through a 12-port PTFE selector valve and peristaltic pump using PTFE tubing at a fixed flow rate of 2 mL·min^{-1}. Pump activation and rotation direction were controlled via voltage-free external signals.

To ensure uninterrupted and accurate sample delivery, an optical non-contact bubble sensor was installed upstream of the pump to detect liquid depletion. Separation was achieved through a DGA Resin column (50-100 µm particle size, 1 mL bed volume), which selectively retained ^{90}Y for radiochemical analysis with high concentration HNO_3 condition. The fluid paths were further regulated with PTFE three-way solenoid valves, compatible with aggressive solvents.

Programed separation sequence was achieved via the RT731 remote timer controller (GL Sciences), which synchronized the operation of pumps, valves, and the fraction collector. The system supported sequential processing of up to eight soil samples and the automated dispensing of various reagents, including 8 M HCl, 3 M HNO_3/0.3 M HF, 0.02 M HNO_3, and 0.1 M HCl. Final eluates were collected using a fraction collector for subsequent radiometric analysis.

2.1 Validation of System Reliability and Analytical Accuracy

System validation was conducted using certified reference material (IAEA-375, Soil) and multi-elemental standard solutions (XSTC-1 and XSTC-13, SPEX) containing potential interferences such as Cs, Pb, Bi, Th, and U. Soil samples were digested using microwave-assisted acid digestion system (Ethos-1, Milestone), and the resulting solutions were processed through the automated SPE system. Quantification was carried out using a 2π gas flow proportional counter to detect beta emissions.

3. RESULTS AND DISCUSSION

Copyright on 7th Asia-Pacific Symposium on Radiochemistry 2025 - P5-06 -

The performance of the automated SPE system was evaluated through multiple analytical parameters, including yttrium recovery, contamination control for interference radionuclides, reproducibility, and accuracy of ^{90}Sr determination. Across all replicates, yttrium recovery remained consistently high, averaging 93.7%, indicating strong retention efficiency of the DGA Resin column and minimal loss during the separation process. Blank runs confirmed the absence of cross-contamination, demonstrating the system's capability to maintain sample integrity through enclosed, automated flow paths.

To assess long-term operational reliability, 40 simulated samples were processed continuously over extended periods. No degradation in resin performance or mechanical failure was observed, confirming the system's robustness and suitability for routine application. These results affirm that the automated system can sustain performance under repeated use, a critical factor in environmental monitoring programs that demand high throughput and consistent quality.

The system's analytical accuracy was further validated using the certified reference material IAEA-444 (Soil). The measured ^{90}Sr activity was 1120 ± 12 mBq·kg^{-1}, which aligns closely with the certified value of 1090 mBq·kg^{-1}, demonstrating the method's validity for environmental radiostrontium analysis. This agreement supports the system's capability to perform precise quantification, even in complex soil matrices with potential interfering elements.

A comparative evaluation between the automated SPE system and conventional manual methods is demonstrated to key advantages of the automated system include improved safety by minimizing operator exposure to hazardous reagents, enhanced reproducibility due to automated flow control, and reduced contamination risk through closed fluidic pathways. Furthermore, its ability to process multiple samples sequentially enhances overall efficiency, making it particularly well-suited for long-term monitoring programs and emergency response scenarios.

By contrast, conventional methods, though historically reliable, are labor-intensive, pose greater safety risks, and are subject to higher variability due to manual handling. In settings such as Thailand, where traditional approaches still dominate ^{90}Sr analysis, the adoption of automated systems could significantly improve data quality, operational efficiency, and laboratory safety.

4. CONCLUSIONS

The automated solid-phase extraction system using DGA Resin offers a reliable, rapid, and contamination-free approach for the determination of ^{90}Sr in soil samples. Compared to conventional methods, it provides enhanced safety, precision, and efficiency. The performance was validated using certified reference materials and prolonged operation without performance degradation.

This method represents a significant advancement for radiostrontium monitoring, particularly in regions like Thailand, where modernization of analytical techniques is urgently needed. Potential applications include environmental monitoring, nuclear emergency preparedness, waste management, and radiological safety assessments.

ACKNOWLEDGMENTS

The author gratefully acknowledges the Kajima Foundation for travel support enabling international research collaboration, and the Japan Keirin Autorace Foundation (JKA) for funding equipment development support in 2025.

References

[1] H. TAZOE, H. OBATA, T. YAMAGATA, Z. KARUBE, H. NAGAI, and M. YAMADA, "Determination of strontium-90 from direct separation of yttrium-90 by solid phase extraction using DGA Resin for seawater monitoring," *Talanta*, **152**, 219 (2016).

[2] Y. JUNG, H. KIM, J.-M. LIM, and K. H. CHUNG, "Feasibility study of an analytical method for detecting ^{90}Sr in soil using DGA resin and Sr resin," *Journal of Radioanalytical and Nuclear Chemistry*, **313**, 401 (2017).

[3] M. FERDOUS ALAM, Z. A. BEGUM, Y. FURUSHO, H. HASEGAWA, and I. M. M. RAHMAN, "Selective separation of radionuclides from environmental matrices using proprietary solid-phase extraction systems: A review," *Microchemical Journal*, **181**, 107637 (2022).

7th Asia-Pacific Symposium on Radiochemistry *September 14 ~ 19, 2025 • Kunibiki Messe • Shimane, Japan*

ANALYSIS OF FISSILE MATERIAL USING FISSION TRACK METHOD IN NUCLEAR FALLOUT SAMPLES COLLECTED ON DAIGO FUKURYU MARU

K. Takamiya[1], M. Ikegami[2], N. Osada[2], Y. Igarashi[2]

[1]*Integrated Radiation and Nuclear Science, Kyoto University: Asashiro-Nishi-2, Kumatori-cho, Sen-nan-gun, Osaka, 590-0494, takamiya.koichi.2u@kyoto-u.ac.jp*
[2] *Integrated Radiation and Nuclear Science, Kyoto University: Asashiro-Nishi-2, Kumatori-cho, Sen-nan-gun, Osaka, 590-0494*

This study investigated radioactive fallout samples collected on the Daigo Fukuryu Maru to detect fissile material-containing particles from the nuclear test in Bikini Atoll, Marshall Islands in 1954. Building on previous work with soil samples collected in Hiroshima, fission track analysis using a research reactor and autoradiography was applied. Multiple clusters of tracks were detected, similar to those observed in Hiroshima atomic bomb fallout. Based on the track distribution, particle size was estimated to be smaller than several micrometers which was also similar to the sizes estimated for uranium-containing fallout particles delivered from Hiroshima A-bomb.

1 INTRODUCTION

Particles containing fissile materials are formed under conditions of high temperature and high pressure during nuclear disasters or nuclear weapon explosions. These particles can exist in the environment for a long period. During the Fukushima Daiichi Nuclear Power Plant accident in 2011, particles containing high concentrations of radioactive Cs were released from the nuclear plants and discovered in environmental samples [1, 2]. Some of the particles contained uranium originating from the nuclear fuel. Analyzing the properties of the particles provides important information for estimating the conditions inside the reactors. Similarly, particles formed by nuclear explosions contain crucial information for estimating the conditions within a fireball. In a previous study, we developed a method for detecting fissile substance-containing particles in environmental samples, specifically to analyze those formed by the Hiroshima Atomic Bomb [3]. This detection method combines fission track analysis using a research reactor with heavy liquid separation. The present study aims to detect and analyze fallout particles containing fissile material in samples collected from the Daigo Fukuryu Maru which was contaminated by nuclear fallout from the thermonuclear weapon test at Bikini Atoll, Marshall Islands in 1954.

2. EXPERIMENTS

The radioactive fallout particles mixed with iron rust were collected from a drum can placed on the Daigo Fukuryu Maru. The sample was stored in Shizuoka University Campus Museum and a part of the sample was provided for the present analysis. Initially, the sample was spread on a sheet of paper, and distribution of the radioactive isotopes was observed by autoradiography. After autoradiography exposure, most of the sample was recovered into a sample container. Only small particles remained on the surface of the paper and were collected on a paraffin film by pressing the film against it. The fission track detector (BARYOTRAK, Fukuvi Chemical Industry Co. Ltd.) with dimensions of 20 mm × 20 mm was wrapped in the paraffin film so that the collected particles were in contact with the detector. The detector with particles was irradiated with approximately 3×10^{12} or 3×10^{13} n/cm^2 of thermal neutrons using the pneumatic irradiation facility (TC-Pn) at Kyoto University Research Reactor. After neutron irradiation, the track detector was etched with 8M NaOH solution at 70°C for one hour, and the resulting tracks were observed using an optical microscope.

3. RESULTS

The photograph and autoradiography image of the sample are shown in Figure 1. Comparison between the two images indicated that the radioactive fallout in the sample was not homogeneous, as there was no correlation between particle size and radioactivity. As a result of the autoradiograph, observations of the track detector surface revealed multiple clusters of tracks. Figure 2 indicates an example of them. Similar analysis of soil samples collected in Hiroshima also detected clusters of tracks. These clusters are consistent with those produced by fine particles containing high concentrations of enriched uranium derived from the atomic bomb. In this study, the number of tracks in each cluster ranged from tens to hundreds. Furthermore, the ratio of the number of tracks to the irradiated neutron fluence was similar to that observed for Hiroshima soil samples. This indicates that the radioactive fallout collected on the Daigo Fukuryu

Copyright on 7th Asia-Pacific Symposium on Radiochemistry 2025 - P5-07 -

Maru contains fissile material at a level comparable to that in the enriched uranium-containing fallout particles derived from the atomic bomb. Based on the observed track distribution, the particle size is estimated to be smaller than several μm. Future analysis of the samples using SEM/EDX will be conducted to examine their appearance and elemental composition.



Figure 1. The picture (left) and autoradiography image (right) of fallout particles mixed with iron rust collected from the Daigo Fukuryu Maru.

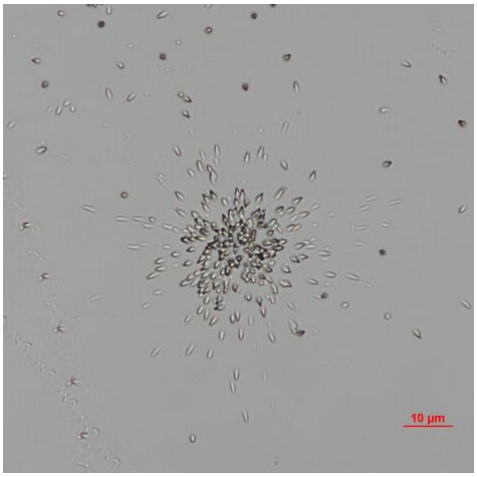


Figure 2. The cluster of fission tracks formed by thermal neutron irradiation (approximately 3×10^{12} n/cm^2) of fallout sample collected from the Daigo Fukuryu Maru.

ACKNOWLEDGMENTS

The authors are grateful to the Shizuoka University Campus Museum for providing the historical samples. This work was partially supported by the Joint Usage/Research of the Institute for Integrated Radiation and Nuclear Science, Kyoto University (KURNS) (No. R6129).

References

[1] K. Adachi et al., Scientific Reports, 3 (2013) 2554.
[2] Y. Satou et al., Geochemical Journal, 52 (2018) 137.
[3] K. Takamiya et al., KURNS Progress Report 2023 (2024) 163.

Invited & Contributed Talk | [R2]Radioanalytical Chemistry and Nuclear Forensics

Tue. Sep 16, 2025 4:40 PM - 6:10 PM JST | Tue. Sep 16, 2025 7:40 AM - 9:10 AM UTC Hall B(Small)

[R2] Radioanalytical Chemistry and Nuclear Forensics

4:40 PM - 5:10 PM JST | 7:40 AM - 8:10 AM UTC

[R2-01(Invited)]

Speciation study on the origin and history of trace amount of uranium in environmental samples

*Takumi Yomogida[1] (1. Japan Atomic Energy Agency (Japan))

5:10 PM - 5:30 PM JST | 8:10 AM - 8:30 AM UTC

[R2-02]

ANALYSIS OF IMPURITIES OF URANIUM ORE CONCENTRATES USING HAND-HELD RAMAN SPECTROSCOPY

*HIROKI NISHIWAKI[1], Yoshiki Kimura[1], Tomoki Yamaguchi[1] (1. Japan Atomic Energy Agency (Japan))

5:30 PM - 5:50 PM JST | 8:30 AM - 8:50 AM UTC

[R2-03]

High-Precision Boron Isotope Ratio and Quantification Analysis at the Picogram Level Using Isotope Dilution Total Evaporation Negative Thermal Ionization Mass-spectrometry

*Zahra Zandvkili[1], Katsuhiko Suzuki[1,2], Junko Kikuchi[2], Yoshitaka Takagai[1] (1. Fukushima university (Japan), 2. Submarine Resources Research Center, Japan Agency for Marine-Earth Science and Technology (JAMSTEC) (Japan))

5:50 PM - 6:10 PM JST | 8:50 AM - 9:10 AM UTC

[R2-04]

EVOLUTION OF RADIOCHEMISTRY FROM THE PERSPECTIVE OF A LABORATORY CHARACTERISING NUCLEAR WASTE

*Christèle COLIN[1], Céline GAUTIER[1], Marina FAURE[1] (1. cea (France))

©APSORC25

7th Asia-Pacific Symposium on Radiochemistry *September 14 ~ 19, 2025 • Kunibiki Messe • Shimane, Japan*

Speciation study on the origin and history of trace amount of uranium in environmental samples

Takumi YOMOGIDA[1]

[1]*Japan Atomic Energy Agency, Nuclear safety Research Center, 2-4 Shirakata Naka Tokai, Ibaraki, 319-1195*
yomogida.takumi@jaea.go.jp

1. Introduction

Uranium (U) is used as a fuel for nuclear power generation, and its migration behavior in the environment is important to understand due to its usefulness as a resource and its chemical toxicity[1]. Since the chemical species of U provide valuable information on the origin and history of uranium, it is important to understand the chemical species of U in environmental samples. However, speciation of U in environmental samples is generally difficult due to trace amounts of U in environmental samples. Analytical methods for precisely determining chemical species in the trace amounts of U are important tools not only for studying the origin of U particles from nuclear facilities, but also for expanding into a wide range of research fields such as geological disposal of radioactive wastes. This study reports on the recent progress of U speciation studies in environmental samples using spectroscopy methods, such as micro-Raman spectrometry[2] and microbeam X-ray absorption spectroscopy(XAS)[3].

2. Experimental

2.1 Micro-Raman spectroscopy

U particles swiped into cotton cloths were deposited on glassy carbon disks (GCD) by a vacuum impactor device. The U particles were identified using a Scanning electron microscopy (JSM 7800F, JEOL Co. Ltd., Japan), which were transferred on the other GCD by using a micromanipulator. The chemical analysis was performed with a micro-Raman spectrometer equipped with a 532 nm diode laser (MicroRAM-300/532A, Lambda Vision, Japan).

2.2 Microbeam X-ray absorption spectroscopy

Experiments using microbeam X-ray were performed at BL37XU, SPring-8. The biotite sample was taken from a boring core of a uranium mine. The biotite thin sample was resin-filled and polished on both sides using lapping films. The thickness of the biotite sample was about 100 μm. A beam size of microbeam X-rays was ca. 1 μm. The distribution of U in biotite was investigated by X-ray fluorescence intensities of U Lα line at an incident energy of 17.2 keV.

3. Results and discussion

3.1 Micro-Raman spectroscopy

Reference particles of UO_2 and U_3O_8 were analyzed. The optimization of the laser power allowed for non-destructive analysis of the U particles with diameters of 1 μm in micro-Raman spectroscopy, which demonstrate that chemical speciation of U could be analyzed at pico-gram level. In addition, we applied the proposed method to the analysis of a real inspection sample collected from a nuclear facility. Some particles had characteristic Raman bands assigned to UO_2. The results indicate the chemical states of UO_2, which is used widely as a nuclear fuel material, could be detected.

3.1 Microbeam X-ray absorption spectroscopy

We used conventional solid-state detector (SDD) and transition edge sensors (TES) for X-ray spectroscopy. With the energy resolution of the SDD detector, it is difficult to detect the fluorescent X-ray of trace amounts of U in the biotite sample. Meanwhile, the fluorescent X-rays of U in the biotite sample were detected by TES because of its high energy-resolution. Micro-XAS measurements successfully identified the chemical state of U in the biotite, revealing that some of the U was reduced to U(IV). It could be a powerful tool for studying the U distribution and speciation in various environmental samples.

ACKNOWLEDGMENTS

Part of this work was financially supported by the Nuclear Regulation Authority of Japan. Part of this work was supported by the Grants-in-Aid for Scientific Research (KAKENHI) from the JSPS (grant no. 19K15606, and 25K08534).

References

[1] Y. Takahashi, A. Yamaguchi, T. Yomogida, “Environmental geochemistry of radionuclides (Environmental radiochemistry)” *Treatise on Geochemistry* (Third Edition), **6**, 105. (2025)

[2] T. Yomogida, F. Esaka, and M. Magara, “Chemical state and isotope ratio analysis of individual uranium particles by a combination of micro-Raman spectroscopy and secondary ion mass spectrometry”. *Anal. Methods*, **9**, 6261 (2017).

[3] T. Yomogida, T. Hashimoto, T. Okumura, S. Yamada, H. Tatsuno, H. Noda, R. Hayakawa, S. Okada, S. Takatori, T. Isobe, T. Hiraki, T. Sato, Y. Toyama, Y. Ichinohe, O. Sekizawa, K. Nitta, Y. Kurihara, S. Fukushima, T. Uruga, Y. Kitatsuji, Y. Takahashi, *Analyst*. **149**, 2932, (2024).

Copyright on 7th Asia-Pacific Symposium on Radiochemistry 2025 - R2-01 -

ANALYSIS OF IMPURITIES OF URANIUM ORE CONCENTRATES USING HAND-HELD RAMAN SPECTROSCOPY

Hiroki Nishiwaki[1], Yoshiki Kimura[2], Tomoki Yamaguchi[3]

[1]: *Japan Atomic Energy Agency:1550, Kagamino-cho Tomata-gun, Okayama, 708-0698, nishiwaki.hiroki@jaea.go.jp*
[2] *Japan Atomic Energy Agency:2-4 Shirane, Shirakata, Tokai-mura, Naka-gun, Ibaraki 319-1195, kimura.yoshiki@zc.iir.isct.ac.jp*
[3] *Japan Atomic Energy Agency:2-4 Shirane, Shirakata, Tokai-mura, Naka-gun, Ibaraki 319-1195, yamaguchi.tomoki@jaea.go.jp*

The spectra of seven types of industrially produced uranium ore concentrates were obtained using a hand-held Raman spectrometer. From the Raman spectra of several ammonium diuranates, the peak in the range of 806-827 cm-1 and around 1010 cm-1 were identified uranyl ions and Sulfate. The sulfates was impurities reflecting the acids used in the manufacturing process. No significant differences were observed in the Raman spectra of two ammonium diuranatse samples made from ore or seawater. Thus, it was suggested that the Raman spectra measured by the hand-held type were more strongly influence by the manufacturing process than raw material.

1 Introduction

Uranium ore concentrate (UOC) is a product of mining and refining processes, and traded in large quantities internationally. This can be a potential target for theft and threaten our social security. Upon the confiscation of unknown UOC, it is important to clarify what kind of substance is and how it was manufactured through some analyses and observations. The information about compounds or impurities in UOC can possibly provide clues to revealing them, also known as nuclear forensic signatures. As part of a joint research effort between the Japan Atomic Energy Agency (JAEA) and the Nuclear Smuggling Detection and Deterrence (NSDD) program of NNSA/US-DOE, we explored nuclear forensic signatures and methodologies for source attribution of uranium-bearing materials.

Raman spectroscopy can be an useful and simple technique to analyze impurities in UOCs, since it is non-destructive, requires no pretreatment, and easily identify chemical species in unknown samples. This analysis can be performed without contacting the sample, reducing the risk of contamination or contact with hazardous materials. In particular, hand-held devices have lower resolution than tabletop devices, but can be analyzed samples at confiscation sites, which is thought to lead to early identification. Therefore, the purpose of this study was to obtain Raman spectra of industrially produced UOCs with a hand-held Raman spectrometer to identify impurities related to the production process and to verify its usefulness in the field of nuclear forensics.

2 Experimental

The hand-held Raman spectrometer, ResQ CQL from RIGAKU was used to analyze UOCs. The excitation wavelength is 1064 nm, which can avoid the influence of fluorescence from the sample. The resolution is 8-11 cm^{-1} and spectral range is 200-2500 cm^{-1}. The laser power was adjusted to 490 mW for measurements. The sample was seven UOCs. Three were dark in color and were thought to be oxides. Four were yellow in color and were ammonium diuranates. Two of these, ammonium duranate, are produced in Japan and are derived from ore and seawater, respectively. The elemental concentrations of UOC were measured by ICP-OES or ICP-MS.

3 Results and discussion

Figure 1 shows the Raman spectra of the UOCs. All dark color samples (sample E~G) could not be analyzed because no clear dark UOCs showed a distinct peak. On the other hand, a clear peak was observed for ammonium diuranate. For all ammonium diuteranate samples (sample A~D), peaks were observed in the 421-486 cm^{-1} and 806-827 cm^{-1} regions, with the 806-827 cm^{-1} region clearly assigned to the symmetric stretching of the uranyl ion. The symmetric uranyl ion stretch is ubiquitous in the region of 750–900 cm^{-1}[1]. In region 970-1460 cm^{-1}, no peak was observed in sample A. This was similar to the spectrum of pure ammonium diuranate synthesized in the laboratory [2]. Thus, this region was attributed to impurities generated during the manufacturing process.

Due to the different elemental compositions of seawater and uranium ore, the impurity composition of UOC also was thought different. While samples of B and C were made from seawater and ore, respectively, the Raman spectra were very similar. Their elemental compositions were also similar, except for trace elements below 10 μg/g. Therefore, it was suggested that the Raman spectra measured by the hand-held type strongly reflects the manufacturing process.

The peak around 1010 cm^{-1} was considered to originate from sulfate. The peaks show similar values with those found in the literature [3]. During the manufacturing process sulfuric acid was used to extract uranium from the ore for

Copyright on 7th Asia-Pacific Symposium on Radiochemistry 2025 - R2-02 -

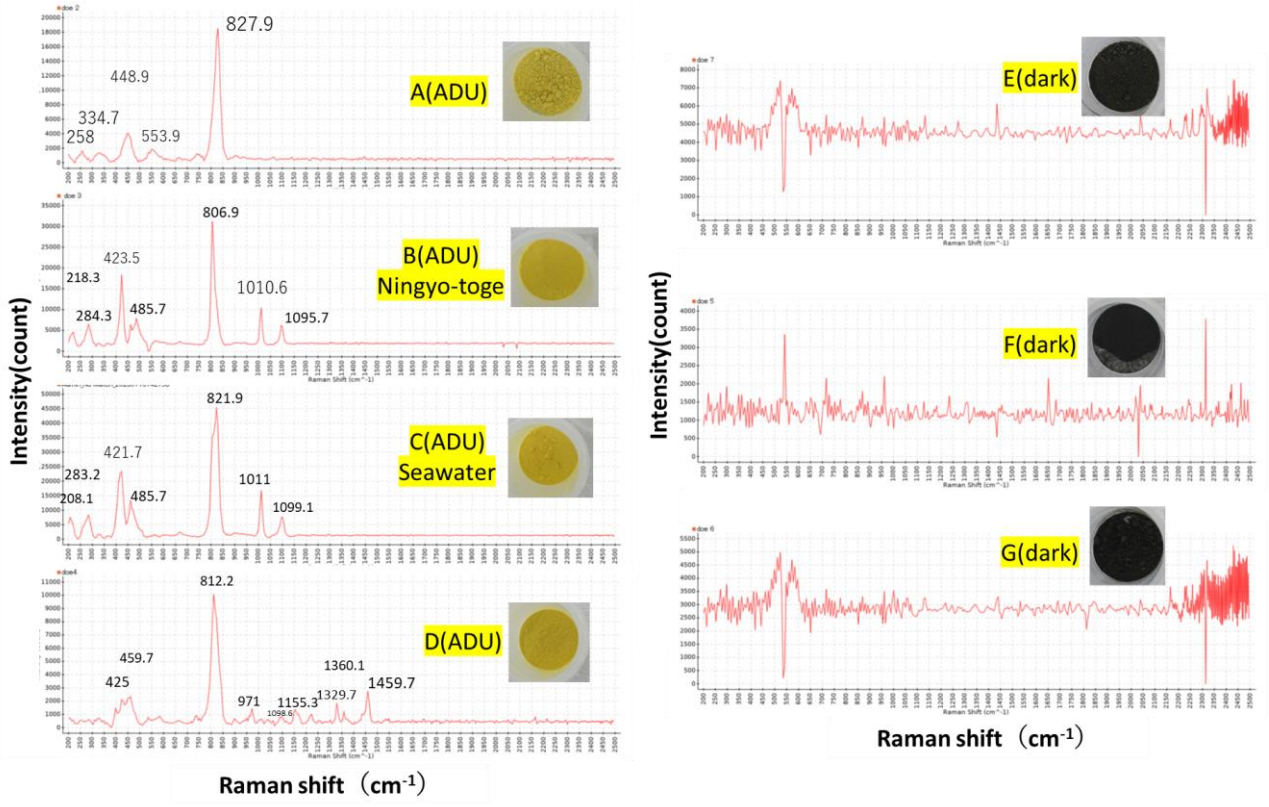


Figure 1. Raman spectra of the UOCs.

sample B and also as a pretreatment for the precipitation step for sample C, respectively. Samples B and C produced contained a lot of sulfur. This suggests that the acid used can be identified from the impurity peaks and that information is helpful in identifying the characteristics of the ore and the ion exchange resins and solvents used in the refining process.

4. SUMMARY

Industrial UOCs were analyzed using hand-held Raman spectroscopy. From the result, no significant differences were observed in the Raman spectra of two ammonium diuranate samples made from different raw materials. Thus, it was suggested that the Raman spectra measured by the hand-held type strongly reflects the manufacturing process. Sulfate was identified as an impurity derived from the manufacturing process. This information helps identify the type of acid used. Therefore, Raman spectroscopy can be an useful in clarifying the manufacturing process for the nuclear forensics.

ACKNOWLEDGMENTS

A subsidy from the Japanese government, MEXT (Ministry of Education, Culture, Sports, Science, and Technology), supports the activity of the Japan Atomic Energy Agency (JAEA) for the "promotion of strengthening nuclear security or the like."

References

[1] D. Ho Mer Lina, D. Manaraa, P. L. Reisc, T. Fanghänela, K. Mayera “The use of different dispersive Raman spectrometers for the analysisof uranium compounds” Vibrational Spectroscopy, 73, 102–110 (2014)
[2] D. Ho Mer Lin1, D. Manara1, Z. Varga1, A. Berlizov, Th. Fanghänel1, and K. Mayer1 “Applicability of Raman spectroscopy as a tool in nuclear forensics for analysis of uranium ore concentrates” Radiochimica Acta, 101, 779–784 (2013)
[3] “Laser Raman spectroscopy as a technique for identification of seafloor hydrothermal and cold seep minerals” Chemical Geology, 259, 240–252(2009)

7th Asia-Pacific Symposium on Radiochemistry *September 14 ~ 19, 2025 • Kunibiki Messe • Shimane, Japan*

High-Precision Boron Isotope Ratio and Quantification Analysis at the Picogram Level Using Isotope Dilution Total Evaporation Negative Thermal Ionization Mass-spectrometry

Zahra Zandvakili[1], Katsuhiko Suzuki[1,2], Junko Kikuchi[2], Yoshitaka Takagai[1]

[1]*Faculty of Symbiotic Systems Science, Fukushima University: 1 Kanayagawa, Fukushima 960-1296, Japan, and E-mail: z.zandvakili@sss.fukushima-u.ac.jp*
[2]*Submarine Resources Research Center, Japan Agency for Marine-Earth Science and Technology (JAMSTEC): 2-15 Natsushima, Yokosuka, Kanagawa 237-0061, Japan, and E-mail: katz@jamstec.go.jp*

1 Introduction

Several analytical techniques have been developed for boron isotope analysis, including negative and/or positive thermal ionization mass spectrometry (NTI-MS and/or PTI-MS), multi-collector inductively coupled plasma mass spectrometry (MC-ICP-MS), laser ablation ICP-MS (LA-ICP-MS), and secondary ion mass spectrometry (SIMS). Among these, NTI-MS is known for its high sensitivity and precision, enabling accurate isotope ratio measurements from nanogram- to picogram-level boron samples, as noted in the literature [1]. For the analysis of wastewater from nuclear power plants under decommissioning, solutions containing low concentrations of boron—leaked from control rods—are discharged, and accurate concentration determination is required. However, even using highly sensitive ICP-MS techniques, it is still difficult to determine such low concentrations of boron, and developing analytical methods for low boron levels remains a challenge. Therefore, in this study, we present a high-precision method for quantifying low concentrations of boron at the picogram level using NTI-MS combined with the isotope dilution–total evaporation (ID-TE) technique.

2 Results and discussion

Boron isotope ratios were measured using negative thermal ionization mass spectrometry (NTI-MS; TRITON, Thermo Fisher Scientific, Germany) through the detection of BO_2^- ions, with ion beams at m/z 42 and 43 corresponding to $^{10}BO_2^-$ and $^{11}BO_2^-$, respectively.

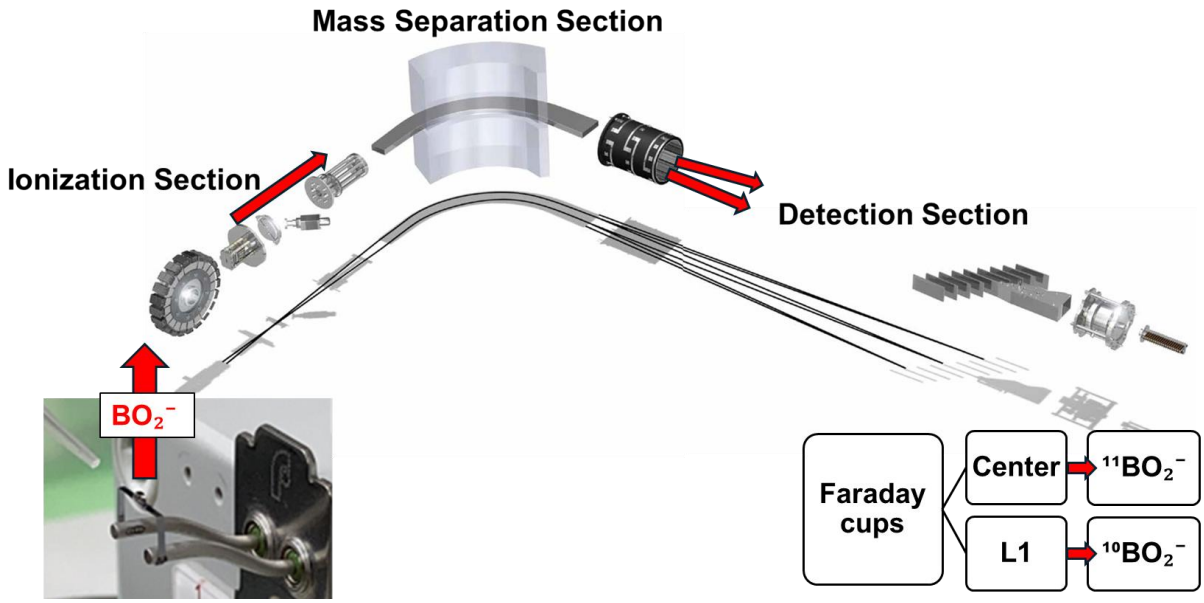


Fig. 1. Schematic of the NTI-MS setup for boron isotope analysis. BO_2^- ions are generated from the heated filament, separated by mass, and detected by Faraday cups—$^{11}BO_2^-$ at the center cup and $^{10}BO_2^-$ at L1—enabling high-precision isotope ratio measurement using NTI-MS technique. Illustrated using the diagram of TIMS in the ThermoFisher leaflet.

Copyright on 7th Asia-Pacific Symposium on Radiochemistry 2025 - R2-03 -

Following the acquisition of a stable thermal emission (TE) profile by NTI-MS, the mean $^{11}B/^{10}B$ ratio obtained showed excellent agreement with the certified value of the ERM-AE101a boron standard, demonstrating high reproducibility (RSD = 0.44%, n = 24). Strong correlations were observed between the loaded boron standard and the quantified standard amount, as well as between the loaded ^{10}B-enriched spike and the spike amount calculated using the ID method (Fig. 2A–B), confirming the validity and accuracy of the ID-TE approach for precise boron quantification. This method was subsequently applied to calculate the background equivalent concentrations (BEC), which were estimated from calibration curves using the added standard and ^{10}B-enriched spike to be 9.8 pg and 4.0 pg respectively. The substantial difference in BEC values is attributed to potential environmental contamination affecting the standard-derived BEC.

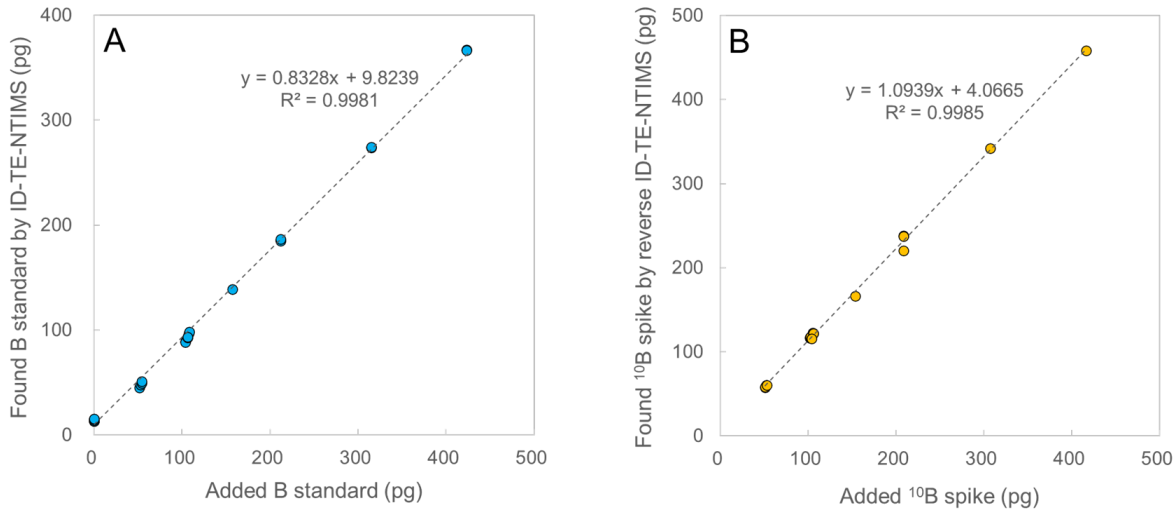


Fig. 2. (A) Comparison between the loaded amounts of the boron standard solution and the corresponding values calculated using the ID-TE method. (B) Comparison between the known loaded amounts of the ^{10}B-enriched spike and the calculated values obtained using the reverse ID-TE method. All values are expressed in picograms per microliter loaded.

The limit of detection (LOD), calculated using the $^{10}BO_2^-/^{11}BO_2$ signal ratio, was determined to be 0.09 pg. This value reflects not only the signal intensity but also the consistency of the response across varying amounts of ^{10}B-enriched spike measurements

These findings highlight the strong potential of the ID-TE-NTI-MS method for precise boron isotope ratio and quantification analysis across diverse sample types—including geological, biological, and environmental materials—and its particular suitability for nuclear-related and low-boron-content studies.

3 CONCLUSIONS

This study demonstrates the effectiveness of the ID-TE-NTI-MS method for ultra-trace boron isotope ratio and concentration analysis. The technique offers high precision, excellent reproducibility, and low detection limits, making it a reliable tool for geological and environmental applications—especially in nuclear studies, where boron may occur across a wide range of amounts, including extremely low concentrations at the picogram level.

.

ACKNOWLEDGMENTS

We would like to express our sincere gratitude to Mr. Nobuyuki Kanazawa, Ms. Mahiro Goto, Ms. Asuka Tnaka for their valuable support and technical assistance for TIMS throughout this study.

References

[1] S. K. AGGARWAL and C. F. YOU, “A review on the determination of isotope ratios of boron with mass spectrometry”. *Mass Spec Rev*, **36**, 499-519 (2017).

Copyright on 7th Asia-Pacific Symposium on Radiochemistry 2025 - R2-03 -

7th Asia-Pacific Symposium on Radiochemistry *September 14 ~ 19, 2025 • Kunibiki Messe • Shimane, Japan*

EVOLUTION OF RADIOCHEMISTRY FROM THE PERSPECTIVE OF A LABORATORY CHARACTERISING NUCLEAR WASTE

COLIN Christèle[1], GAUTIER Céline[1], FAURE Marina[1]

[1]*Université Paris-Saclay, CEA, Service de Physico-Chimie, F-91191, Gif-sur-Yvette Cedex, France, christele.colin@cea.fr*

1. INTRODUCTION

The LASE (Analytical Support to facilities Laboratory) is an analytical chemistry laboratory for the characterisation of radioactive waste from the nuclear industry. Among all the radionuclides present in nuclear waste, it is required to analyse at least ten of them, in particular long-lived radionuclides. To do so, radiochemical methods have been developed in agreement with the requirements of ANDRA (the French national radioactive waste management agency). The laboratory began its development more than 20 years ago, and since then, regulations have changed, such as the European REACH regulation (Registration, Evaluation, Authorisation and Restriction of Chemicals). Consequently, the update of these separation procedures must follow on new safety and performance guidelines.

2. ADAPTATION TO REGULATION

To comply with European regulations, the laboratory has reviewed its radiochemical protocols. The evolutions include replacing liquid-liquid extraction using chloroform with extraction chromatographic resins for separations of Ni-63 [1], Fe-55 [2] and Pd-107 [3]. For the purification of Sr-90, fuming nitric acid was replaced by less concentrated nitric acid [4]. Besides, sample digestion steps have also been re-adapted: a study is currently on going to prevent the use of hydrofluoric acid during sample digestion (for Pd-107, for example).

The presentation will describe the general methodology implemented to update the procedures, including the development and validation steps. The new procedures will be detailed for Ni-63, Fe-55, Pd-107 and Sr-90 with a view to complying with safety and environmental concerns (see Table 1).

TABLE 1. Summary of protocol developments carried out in LASE laboratory

Radionuclide	Previous protocol	New protocol
Ni-63	2 liquid-liquid extractions with chloroform/nitroso 2 naphtol 1 and chloroform/dimethylglyoxime	Anion exchange resin + Ni® resin [1]
Fe-55	Precipitation + anion exchange resin + liquid-liquid extractions with chloroform/N-nitroso-N-phenylhydroxylamine	Anion exchange resin + TRU® Resin [2]
Pd-107	Liquid-liquid extractions with chloroform/dimethylglyoxime + anion exchange resin	Ni® resin + LN® resin [3]
Sr-90	Precipitation with HNO_3 > 85%	Precipitation with HNO_3 69% [4]

3. CONCLUSIONS

The use of extraction chromatographic resins has become essential in radiochemistry within the laboratory to comply with new safety and environmental concerns. Unfortunately, it is not always easy to reduce the number of purification steps since a high separation selectivity and accurate analyses are needed. To meet the demand for lower detection limits, measurement techniques have also been impacted: mass spectrometry is now complementing liquid scintillation measurements for Ca-41, Cl-36, Tc-99 and I-129. Therefore, development of new separation methods is challenging but it is a priority to tackle demands in nuclear waste characterisation so as to support the nuclear revival.

ACKNOWLEDGMENTS

The authors thanks the LA2D/LABOS project for the funding provided and the LASE team for their daily help and advice.

References

[1] C. GAUTIER et al., *Journal of Radioanalytical and Nuclear Chemistry*, **308**, 261 (2016).
[2] C. GAUTIER et al., *Journal of Radioanalytical and Nuclear Chemistry*, **326**, 591 (2020).
[3] M. FAURE et al., *International Conference on Radioanalytical and Nuclear Chemistry RANC 2022*, Budapest, Hungary, May 7-12 (2023).
[4] E. BAUDAT et al., *Journal of Radioanalytical and Nuclear Chemistry*, **328**, 637 (2021).

Copyright on 7th Asia-Pacific Symposium on Radiochemistry 2025 - R2-04 -

Invited & Contributed Talk | [R5]Activation Analysis

Tue. Sep 16, 2025 4:40 PM - 6:10 PM JST | Tue. Sep 16, 2025 7:40 AM - 9:10 AM UTC Hall S(Int'l)

[R5] Activation Analysis

4:40 PM - 5:10 PM JST | 7:40 AM - 8:10 AM UTC

[R5-04(Invited)]

New Research Reactor Project at the Monju site

*Masaji Arai[1] (1. Japan Atomic Energy Agency (Japan))

5:10 PM - 5:30 PM JST | 8:10 AM - 8:30 AM UTC

[R5-05]

ARCHAEOMETRY STUDIES AT MLZ – USING CHEMICAL ANALYSIS WITH NEUTRONS, MULTIVARIATE STATISTICS AND ARTIFICIAL INTELLIGENCE

*Christian Stieghorst[1], Daniel Boschmann[2], Mauro Guerra[3], Daniel Pinheiro[3], Werner G. Häusler[4], Nikola Jovancevic[5], Antonio J.M. Silva[6], Benilde F.O. Costa[7] (1. Heinz Maier-Leibnitz Zentrum (MLZ) - Technical University of Munich (Germany), 2. Institute of Automation Technology Helmut Schmidt University (Germany), 3. LIBPhys-UNL, LA- REAL, Department of Physics, NOVA School of Science and Technology (Portugal), 4. Technical University of Munich, Physics Department (Germany), 5. Department of Physics, Faculty of Science, University of Novi Sad (Serbia), 6. University of Madeira, School of Technologies and Management, CITUR (Portugal), 7. University of Coimbra, CFisUC, Physics Department (Portugal))

5:30 PM - 5:50 PM JST | 8:30 AM - 8:50 AM UTC

[R5-06]

INAA for investigating the causes of colour differentiation of the popular *Haji*-ware in the Japanese Medieval capital

*Makoto TOMII[1], Koichi TAKAMIYA[2], Makoto INAGAKI[2], Yutaka CHIBA[2], Atsushi ITO[2], Masaaki KIDACHI[3], Hideo YOSHII[2] (1. Taisho University (Japan), 2. Kyoto Univeristy (Japan), 3. Ritsumeikan University (Japan))

5:50 PM - 6:10 PM JST | 8:50 AM - 9:10 AM UTC

[R5-07]

SURVEY ON RADIOACTIVE CESIUM MIGRATION BETWEEN ENVIRONMENTAL AND BODY OF WILD BOAR (*Sus scrofa*) LIVING IN FUKUSHIMA PREFECTURE, JAPAN

*MICHIKO FUKUSHIMA[1], Yamato TSUJI[1], Yuto Iinuma[2], Hitoshi KOMATSU[3], Yuuya SUGAWARA[4], Shota MOCHIZUKI[4], Takashi SAKATA[1], Kimie MURAKAMI[3], Kouta KANDA[3] (1. Ishinomaki Senshu University (Japan), 2. Kyoto University (Japan), 3. Fukushima Prefecture Centre for Environmental Creation (Japan), 4. Fukushima University (Japan))

©APSORC25

7th Asia-Pacific Symposium on Radiochemistry *September 14 ~ 19, 2025 • Kunibiki Messe • Shimane, Japan*

New Research Reactor Project at the Monju site

Masaji Arai[1]

[1]*Japan Atomic Energy Agency: 2-4 Shirakata, Tokai-mura, Naka-gun, Ibaraki, 319-1195 arai.masaji@jaea.go.jp*

In 2016, the Japan government decided that the prototype fast breeder reactor "Monju" will be decommissioned. Along with this decision, another decision was made to install a new research reactor in the "Monju" site, aiming to be a core base for R&D and human resource development in the nuclear technology field.

The new research reactor will be a neutron beam reactor capable of irradiation at 10MW. The reactor is expected to contribute to a wide range of basic research, applied research, and industrial use through the R&Ds on neutron beams and radioisotope application, as well as to a continuous development of human resources.

In December 2022, the Japan Atomic Energy Agency (JAEA) was selected as the main implementing body for the detailed design stage. The Agency has been working on a design in cooperation with Kyoto University and the University of Fukui.

Although the main purpose of the new research reactor is to utilize neutron beams, it is also anticipated that it will be used for neutron irradiation, such as activation analysis, material irradiation, and radioisotope production.

During the conceptual design stage, we have interviewed relevant academic communities, and five experimental instruments (small-angle neutron scattering, neutron imaging, neutron powder diffraction, neutron reflectivity, and neutron activation analysis) have been selected as priority facilities for the new research reactor in terms of versatility and broad need. Currently, in addition to the priority instruments, we are also investigating the specifications needed for instruments to be placed near the reactor core in collaboration with an expert task force.

In this presentation, we will give an overview of the new research reactor project as well as introduce the utilization facilities around the core that are currently being considered.

Copyright on 7th Asia-Pacific Symposium on Radiochemistry 2025 - R5-04 -

7th Asia-Pacific Symposium on Radiochemistry *September 14 ~ 19, 2025 • Kunibiki Messe • Shimane, Japan*

ARCHAEOMETRY STUDIES AT MLZ – USING CHEMICAL ANALYSIS WITH NEUTRONS, MULTIVARIATE STATISTICS AND ARTIFICIAL INTELLIGENCE

Christian Stieghorst[1], Daniel Boschmann[2], Mauro Guerra[3], Werner G. Häusler[4], Nikola Jovancevic[5], Daniel Pinheiro[3], António J.M. Silva[6], Benilde F.O. Costa[7]

[1] Heinz Maier-Leibnitz Zentrum (MLZ), Technische Universität München, Lichtenbergstr. 1, 85748 Garching, Germany, christian.stieghorst@frm2.tum.de
[2] Institute of Automation Technology Helmut Schmidt University, Hamburg, Germany, boschmad@hsu-hh.de
[3] LIBPhys-UNL, LA- REAL, Department of Physics, NOVA School of Science and Technology, NOVA University Lisbon, 2829-516 Caparica, Portugal, mguerra@fct.unl.pt / ds.pinheiro@campus.fct.unl.pt
[4] Technical University of Munich, Physics Department, 85747 Garching, Germany, werner.haeusler@tum.de
[5] Department of Physics, Faculty of Science, University of Novi Sad, 21000 Novi Sad, Serbia, nikola.jovancevic@df.uns.ac.rs
[6] University of Madeira, School of Technologies and Management, CITUR, 9020-105, Funchal, Portugal, siljan@sapo.pt
[7] University of Coimbra, CFisUC, Physics Department, 3004-516 Coimbra, Portugal, benilde@uc.pt

Chemical analysis with neutrons is well-suited for archaeometry studies such as provenance analysis. At the Heinz Maier-Leibnitz Zentrum (MLZ) several established and newly-developed methods are available and their capabilities are presented in this paper. The data analysis workflow includes common and advanced multivariate statistical approaches and is exemplarily illustrated for provenance analysis of ancient amphorae.

1 CHEMICAL ANALYSIS WITH NEUTRONS FOR ARCHAEOMETRY AT MLZ

Several methods of chemical analysis with neutrons are available at the Heinz Maier-Leibnitz Zentrum (MLZ). The instrumentation benefits from the comparatively high flux values that can be provided by the FRM II neutron source. Neutron activation analysis (NAA), Prompt gamma activation analysis (PGAA), Prompt gamma-ray activation imaging combined with neutron imaging (PGAI-NT), in-beam NAA (ib-NAA), and the newly developed cyclic in-beam NAA (cib-NAA, see Fig. 1) are well suited for archaeometry studies. We will give a brief overview of these capabilities at the MLZ and show some exemplary applications from the fields of provenance analysis, retro-engineering and conservation/restoration research.

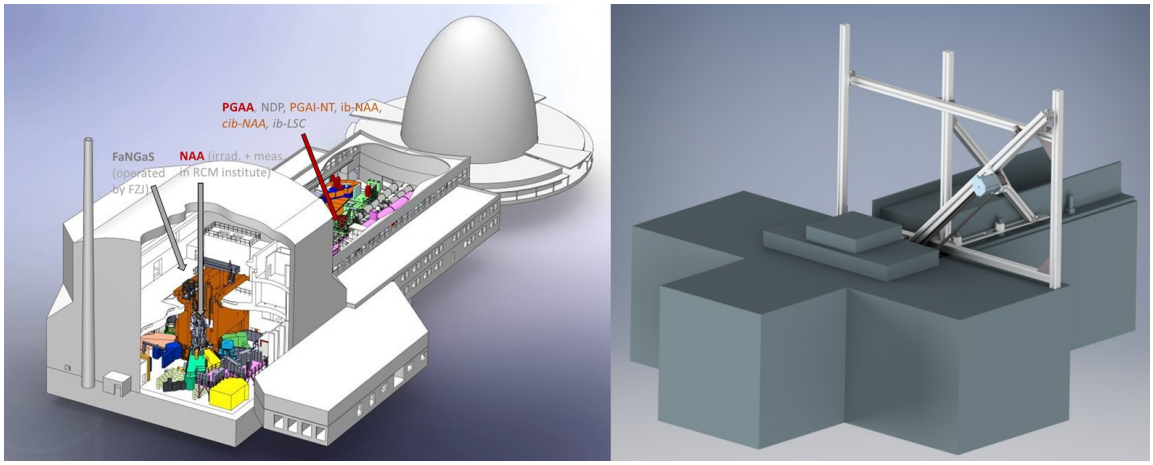


Fig. 1. *Left*: The instruments and setups for chemical analysis with neutrons at MLZ. Setups which are addressed in the presentation are marked in red/orange color. *Right*: Prototype of cyclic in-beam activation analysis setup at the PGAA instrument, the dark gray parts are shielding components of the instrument (drawing).

2 MULTIVARIATE DATA ANALYSIS

Data analysis using multivariate analysis, machine learning (ML) and artificial intelligence (AI) is discussed on the basis of a project to determine the origin of Roman amphorae excavated on the Iberian Peninsula. By comparing the ancient production places (kiln sites) with the finding spots on the former Roman provinces Baetica and Lusitania, it is

Copyright on 7th Asia-Pacific Symposium on Radiochemistry 2025 - R5-05 -

possible to add a part to the puzzle of the complex trade-and-transportation system in the Roman times. As is often the case with comparable provenance projects, the data is too big and complex to obtain results “by hand” using conventional statistical methods in a reasonable amount of time. On the other hand, the amount of data is still too small to be considered a typical “big data” problem, and it is too “sparse” for many modern AI/ML methods, which limits the number of applicable methods. Commonly used multivariate approaches such as principal component analysis (PCA, see Fig. 2) and hierarchical cluster analysis (HCA) show already a clear separation for some data clouds or clusters which are related to the finding spots and kilns sites, but others remain undistinguishable. Therefore, we are currently testing specialized neural networks (auto-encoders), which are working with the given dataset. The latter are advantageous because they can also take non-linear correlations into account. First results are promising. In addition, prior knowledge about the distribution of the data was taken into account in the pre-processing of the data. This included, for example, the statistical distribution of the element mass fractions, which often shows a lognormal characteristic.

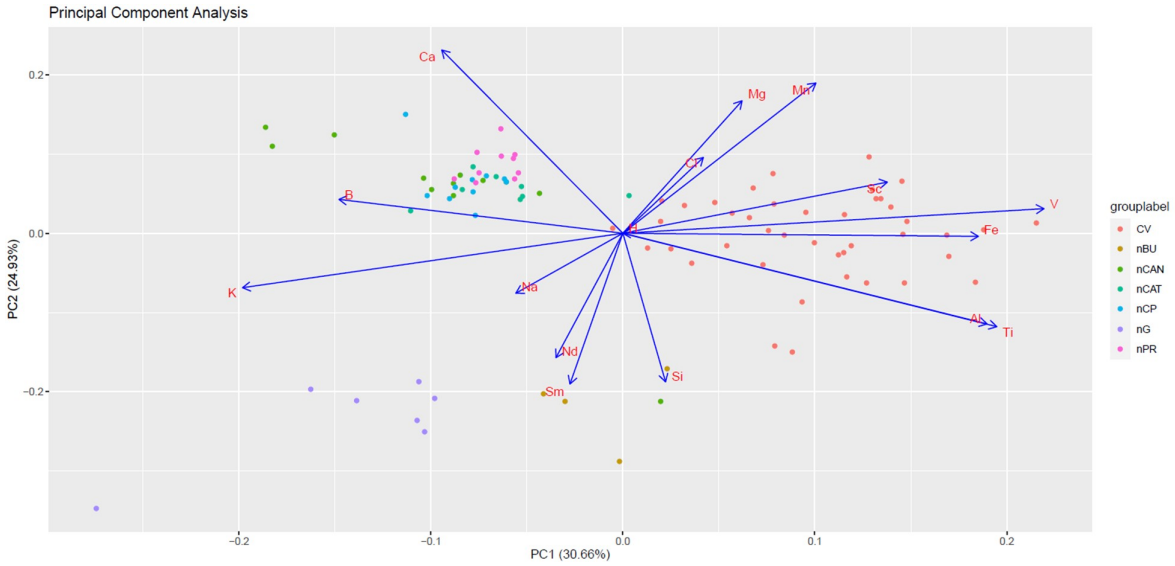


Fig. 2. Classic principal component analysis (PCA) shows that amphorae samples from finding place Castro do Vieito (CV) are clearly different from the kiln sites (nX).

Finally, we bring the activation analysis results into context with previous data analysis performed with XRF, XRD, and Mössbauer results obtained at the University of Coimbra, Portugal, and the physics department in Garching, Germany, see [1][2].

2. CONCLUSIONS

Using multivariate approaches and AI can help to reconstruct ancient transport routes. Advanced techniques like Neural Networks are able to include non-linear dependencies and have the potential to improve the analysis with respect to a better separation of clusters.

ACKNOWLEDGMENTS

Some ideas for applying AI to the archaeometric data in the amphorae project were inspired by our work on the “EvalSpek-ML” project funded by the BMBF as part of the ErUM-Data program and the DAAD-funded project“ SINDA”. We thank the funding organizations for their support of these projects.

We remember Prof. Fritz Wagner, who was a driving force behind several archaeometric projects for many years. We will miss him dearly.

References

[1] B.F.O. Costa, F. Wagner, W. Häusler, C. Stieghorst, A.J.M. Silva, Mössbauer Studies of Haltern 70 Amphorae from Castro do Vieito, Northwest of Portugal. Crystals 2024, 14(9), 786.

[2] Pinheiro, D., Guerra, M., Silva, A. J., Stieghorst, C., & Costa, B. F.O. (2025). X-ray compositional microanalysis and X-ray diffraction of Haltern 70 amphorae sherds. Applied Physics A, 131(4), 231.

Copyright on 7th Asia-Pacific Symposium on Radiochemistry 2025 - R5-05 -

7th Asia-Pacific Symposium on Radiochemistry *September 14 ~ 19, 2025 • Kunibiki Messe • Shimane, Japan*

INAA for investigating the causes of colour differentiation of the popular *Haji*-ware of the fourteenth century in the Japanese Medieval capital

Makoto Tomii[1], Koichi Takamiya[2], Makoto Inagaki[2], Yutaka Chiba[3], Atsushi Ito[3], Masaaki Kidachi[4], and Hideo Yoshii[3]

[1]*Faculty of Literature, Taisho University: 3-20-1, Nishisugamo, Toshima-ku, Tokyo, 170-8470 JAPAN*
m_tomii@mail.tais.ac.jp
[2]*Institute for Integrated Radiation and Nuclear Science, Kyoto University: 2, Asashiro-Nishi, Kumatori-cho, Sennan-gun, Osaka, 590-0494 JAPAN*
[3]*Graduate School of Letters, Kyoto University: Yoshida Honmachi, Sakyo-ku, Kyoto, 606-8501 JAPAN*
[4]*College of Letters, Ritsumeikan University: 56-1 Toji-in Kitamachi, Kita-ku, Kyoto, 603-8577 JAPAN*

We have tackled one of the majour Japanese archaeological questions to be solved; what is the reason of the difference in colour -white or red- of the Japanese medieval popular Haji-ware? To check whether the colour difference was related to the clay material, the concentrations of numerous elements of the texture of both excavated white and red pots were compared through application of INAA in Kyoto University Research Reactor on samples of them respectively. The results indicate the difference in clay texture between the white and red groups.

1 INTRODUCTION

One of the majour Japanese archaeological questions to be solved is the reason of the difference in colour of the medieval low-temperature-fired pottery (*Haji*-ware), so-called White type versus Red type: the White one representing light-grey or ivory in appearance while the Red one representing rather orange. They were popular and used in a ritual or a drinking party especially in thirteenth and fourteenth centuries in and around the old capital, Kyoto. From the results of many excavations, it is evident that the two types were coevally used at the same event, but the manner of rim treatment in production is different between the two. Here the question has arisen, whether they had been produced by the same group of potters or not, and whether they had been produced from the same material of clay or the different one. Some scholars assume that white ones resulted from levigation (water-sieving) of clay to decrease iron oxide while others point out that they could result from the reducing condition of firing. However, the chemical analysis to compare the two types has not been effectively conducted yet, thus we have started the analysis with investigating the clay texture of the two types in detail by INAA.

2 EXPERIMENTS

The pots analysed are selected from two respectively clustered depositions, namely SX2 and SX34, of used *Haji*-ware excavated in the same archaeological site in Kyoto; both dated to fourteenth century, with having the White and Red types [1]. From SX2, the White bowls and cups and the Red medium-sized and small-sized plates were analysed, and from SX34, the White bowls and the Red medium-sized plates were done (Fig. 1). Each of these six groups has seven samples respectively from different pieces.



Fig. 1. The *Haji*-ware pieces excavated from SX34: Red medium-sized plates in the left paper-box and White bowls in the right. The short sides of the box are about 15 cm.

Copyright on 7th Asia-Pacific Symposium on Radiochemistry 2025 - R5-06 -

2.1 Methods

Conventional INAA was applied, to determine each elemental composition of 42 pieces of the *Haji*-ware. Following the majour sampling procedure for INAA on excavated ceramics [2], the main body of every piece had been drilled into fine powder as a sample after removing off the very surface, by an alumina drill, with which only Al might have affected the powder sample in case that contamination occurred during sampling, and then each powder sample had been enclosed in a polyethylene bag. Each of the 42 samples was neutron-irradiated in Kyoto University Research Reactor (KUR), by using Pn-3 (1 MW for 90 seconds) for short-lived nuclides, and Pn-2 (5 MW for 1 hour) for long-lived ones. The gamma-ray spectrometry of the irradiated samples was performed after the irradiation, and the k_0-standardization method for determination of concentration of elements was performed. For the k_0-method, three standard elements were prepared as a comparator: Au, Lu and Zr.

2.2 Results

Except for Al, which might have partly originated from the drill during sampling, concentrations of ten elements (Eu, Ga, K, La, Mg, Mn, Na, Sm, Ti, and V) in most of the 42 samples were determined with irradiation by Pn-3; Mg, Sm, and Ti being slightly less determined than other seven. La, Mn, and Na can divide the 42 samples into two groups, and the groups correspond in general with the colour types though there are a few exceptional samples. As for long-lived nuclides, concentrations of ten elements (Co, Cr, Cs, Fe, Hf, Rb, Sc, Ta, Tb, and Th) in the samples from SX34 were determined while the determination for samples of SX2 irradiated by Pn-2 has not been completed yet. However, the 14 samples can be divided into two groups using Fe concentration as an indicator, which fully corresponds with the colour types.

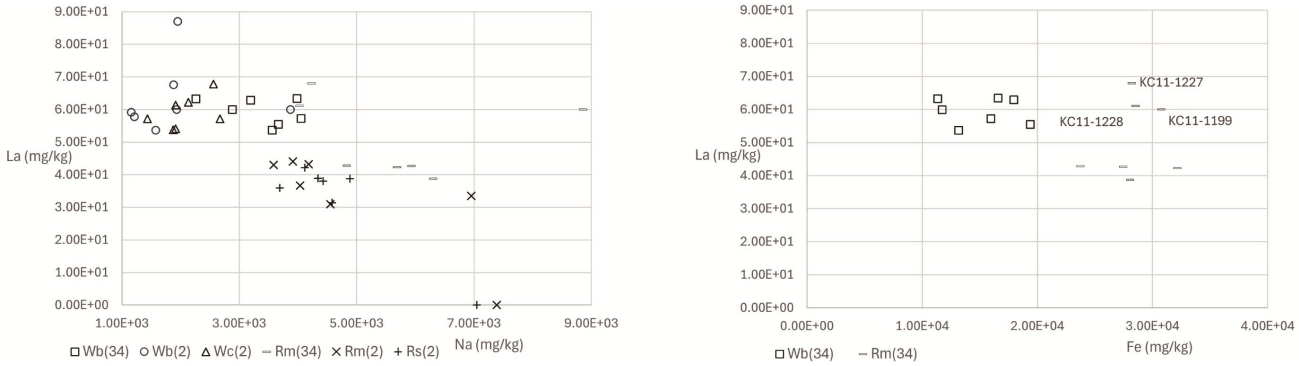


Fig. 2. Distributions of samples on the concentrations combination: Na with La of all 42 samples from SX2 and SX34 on the left, and Fe with La of every of 14 samples from SX34 on the right. Same symbols are valid on both graphs.

3 DISCUSSIONS

Here we can suggest the following three points. Firstly, the correspondence of colour difference with the distribution pattern of Fe concentration, as shown in the right graph of Fig. 2, supports the accepted theory that firing Fe_2O_3-rich clay leads to reddish pottery in appearance. Secondly, as shown in the left graph of Fig. 2, the White type normally contains more La and less Na than the Red type, which indicates that the colour difference might have resulted from the difference of the clay material. Finally, the three samples (KS11-1199, 1227, and 1228) among the seven in the Red type from SX34 which show high concentration of Na might indicate that the White type had had the process of levigation of the original clay material in advance of forming a vessel with the aim of reducing Fe_2O_3, leading to the simultaneous decrease of Na which is quite readily dissoluble in water from a rock among the majour elements in the subsurface (Si, Al, Fe, Ca, Na, K, Mg, and Ti).

ACKNOWLEDGMENTS

This work was supported by JSPS KAKENHI Grant Number 21K18379.

References

[1] M. Tomii et al., *Annu. Rept. of Archaeological Researches in KU sites for 2013*. (2015) 5-122.
[2] J. Sterba, *J. Radio. Nucl. Chem*., 316 (2018) 753-759

Copyright on 7th Asia-Pacific Symposium on Radiochemistry 2025 - R5-06 -

7th Asia-Pacific Symposium on Radiochemistry *September 14 ~ 19, 2025 • Kunibiki Messe • Shimane, Japan*

HERESURVEY ON RADIOACTIVE CESIUM MIGRATION BETWEEN ENVIRONMENTAL AND BODY OF WILD BOAR (*Sus scrofa*) LIVING IN FUKUSHIMA PREFECTURE, JAPAN

M. Fukushima[1], Y. Tsuji[1], Y. Iinuma[2], H. Komatsu[3], H. Sugawara[4], S. Mochizuki[4], T. Sakata[1], K. Murakami[3], K. Kanda[3]

[1]*Ishinomaki Senshu University: 1 Minamisakai, Ishinomaki Miyagi, 986-8580 Japan, neko.fukusima@gmail.com*
[2]*Research Reactor Institute, Kyoto Univeristy*
[3]*Fukushima Prefecture Centre for Environmental Creation*
[4]*Faculty of Food ans Agriculture Sciences, Fukushima Univeristy*

Migration of radioactive cesium caused by Fukushima-Daiichi Reactor accident between environment and several species of wild animals in 2011 has been studied by several groups including Fukushima Prefecture Centre for Environmental Creation. In their results, radioactive cesium levels showed correation between wild boar muscle and stomach contents[1], and it was suggested that radioactive cesuim migrate from diets to wild animal bodies. Wild boar diets show seasonal changes, and it is expected that trace elements levels in wild animals show seasonal changes. For these purposes, stomach contents of wild boars were separated. And stable cesium levels in muscles, blood, and livers of wild boars living in inside of Difficult-to-return Zone were analyzed, and compared with ones from outside of Difficult-to-return Zone in Fukushima Prefecture.

1 INTRODUCTION

Levels of radioactive Cs in wild animals living in Fukushima Prefecture are still high comparing to other areas even after 14 years have passed from Fukushima Daiichi Accident in March 2011. Though chemical form of radioactive Cs in environment after Fukushima Daiichi Accident and stable Cs in nature are thought to be different, it is possible to change chemical form of radioactive Cs by biological metabolism in living matter. For this possibility, wild boar living in Difficult-to return zone in Fukushima Prefecture was chosen. Muscle, blood, and liver of wild boar were collected, radioactivity of Cs-134 and Cs-137 was measured by Ge detector, and stable Cs was analyzed by neutron activation analysis (NAA) in Kyoto University Reactor (KUR), Japan. Also, for the seasonal changes of radioactive Cs in the body of wild boar, the stomach contents of wild boars from both inside and outside of Difficult-to-Return Zone were analyzed.

2. EXPERIMENTS

2.1 Wild boars

Wild boars were trapped in Namie Machi, Futaba Machi, Ohkuma Machi, and Katsurao Mura (inside of Difficult-to-return Zone, n = 25 in total) from May to September 2023, and Nihonmatsu City (outside of Difficult-to-return Zone, n = 21) from December 2021 to February 2023 under the permission of Fukushima Prefecture. After euthanasia by neck shot, musclus quadriceps, contents of the stomach, blood, and the liver were removed from the body, freeze-dried, pulverized, and gamma-ray counting was done for Cs-134 andCs-137 radioactivity. Also, before freeze-drying, some amount of stomach content was kept in 70% ethanol solution and separated each material under optical microscope for estimating wild boar diet; n = 166 and 40 for wild boars from inside and outside of Difficult-to-return Zone, respectively.

2.2 Diet samples of wild boar

Several species of plants were collected from Namie Machi (inside of Difficult-to-return Zone) and Nihonmatsu City (outside of Difficult-to return Zone) as the diet of wild boar in July 2023. Samples were washed with tap water, freeze dried, pulverized, gamma counted before NAA.

2.3 Neutron activation analysis of stable Cs and several other elements

One portion of dried power was supplied for short irradiation in KUR. Eight elements of Ca, Cl, Cu, K, Mg, Mn, Na, and V of wild boar diet were analyzed by the condition of 1.5 min TcPn irradiation, 3 min cooling time, and 10 min gamma counting using germanium detector with Compton suppression system, also eight elements of Co, Cr, Cs, Fe, Rb, Sc, Se, and Zn of muscles, blood, and livers were analyzed by irradiation for 1 hour and gamma counting was done for 20 - 30 min after 1 month cooling time. Four different standard reference materials were used: NIST SRM 1575 Pine Needles, NIST SRM 1577b Bovine Liver, NIST SRM 1573a Tomato Leaves, and NIST SRM 1515 Apple Leaves.

Copyright on 7th Asia-Pacific Symposium on Radiochemistry 2025 - R5-07 -

3. RESULTS

Stomach contents were mainly consisted by leaves, stem, and fleshy fruits for whole study periods. Regarding stomach contents from inside of Difficult-to-return Zone, more than 40% of total contents were roots.

Cs-137 levels of muscles, blood, livers from inside of Difficult-to Return Zone were 1-2 order higher than those from outside. Correation between Cs-137 and stable Cs in muscles, blood, and livers showed strong for all three organs, especially organs from Difficult-to-Return Zone.

References

[1]Y. Nemoto *et al*., Journal of Environmental Radioactivity, **225,** 106342 (2020).

Copyright on 7th Asia-Pacific Symposium on Radiochemistry 2025 - R5-07 -

Invited & Contributed Talk | [R3]Actinide Chemistry and Nuclear Energy Chemistry

Tue. Sep 16, 2025 4:45 PM - 6:15 PM JST | Tue. Sep 16, 2025 7:45 AM - 9:15 AM UTC Hall A(MP)

[R3] Actinide Chemistry and Nuclear Energy Chemistry

4:45 PM - 5:15 PM JST | 7:45 AM - 8:15 AM UTC

[R3-05(Invited)]

Separation of Actinide Elements Based on Molecular Design

*Weiqun Shi[1] (1. Shanghai Jiao Tong University (China))

5:15 PM - 5:35 PM JST | 8:15 AM - 8:35 AM UTC

[R3-06]

Metal phosphonate frameworks (MPFs) for f-block metal separation

*Kai Lv[1], Liangping Xiong[1], Songzhu Qi[1] (1. Institute of Nuclear Physics and Chemistry (INPC), China Academy of Engineering Physics (CAEP) (China))

5:35 PM - 5:55 PM JST | 8:35 AM - 8:55 AM UTC

[R3-07]

Amino Acid Decorated Phenanthroline Diimide as Sustainable Hydrophilic Am(III) Masking Agent with High Acid Resistance

*Bin Li[1] (1. Tsinghua University (China))

5:55 PM - 6:15 PM JST | 8:55 AM - 9:15 AM UTC

[R3-08*]

Adsorption behavior and chemical states of vanadium on iron(II)-bearing clay minerals

*Shiori Morii[1,2], Takumi Yomogida[1,2], Masami Nakada[1], Yoshio Takahashi[2] (1. Japan Atomic Energy Agency (Japan), 2. The University of Tokyo (Japan))

©APSORC25

7th Asia-Pacific Symposium on Radiochemistry *September 14 ~ 19, 2025 • Kunibiki Messe • Shimane, Japan*

Separation of Actinide Elements Based on Molecular Design

Weiqun Shi[1]

[1] *Institute of Nuclear Fuel cycle and Materials, School of Mechanical Engineering, Shanghai Jiao Tong University, Shanghai 200240, China*

Separating actinides from lanthanides is essential for managing nuclear waste and promoting sustainable nuclear energy development. In 2014, we reported a phenanthroline-based tetradentate ligand with hard–soft donors combined in the same molecule, *N*,*N*′-diethyl-*N*,*N*′-ditolyl-2,9-diamide-1,10-phenanthroline (Et-Tol-DAPhen), for the group separation of actinides over lanthanides. The ligand exhibits excellent extraction ability and high selectivity toward hexavalent, tetravalent, and trivalent actinides over lanthanides in highly acidic solution and hence renders huge potential opportunities in high-level liquid waste (HLLW) partitioning. Recently, based on the DAPhen ligand, we proposed a dual strategy to designing covalent organic frameworks (COFs) that skillfully combines molecular rigidity with flexibility, integrating both hard and soft donor atoms in the synthesis of monomers, which results in a specialized COF that efficiently and selectively captures TRUs from acidic aqueous solutions. By utilizing the topological arrangement of rigid ligands to influence the twisting and stretching of flexible ligands, coordination environment featuring nitrogen and oxygen is created, which enhances the separation of transuranium in various oxidation states over lanthanides. In 0.5 M HNO_3 solution, the as-synthesized DAPhen-COF achieves removal rates of 99.1% for Np(V) and 95.8% for Pu(IV). For Am(III), the removal rate reaches 98.6% in 0.01 M HNO_3. DAPhen-COF exhibits remarkable selectivity for Np(V), with a separation factor of over 5000 for Np/Gd, outperforming other solid-phase materials.

On the other hand, traditional solvent extraction and separation of actinide elements generally relies on specific organic ligands. Through the selective complexation of these ligands with the target actinide metal ions, their efficient separation in a mixture of metal ions can be achieved. The separation selectivity mainly depends on the degree of pre-organization of the ligand structure and the complexation between soft/hard complexing atoms and the target ions. Based on years of research on actinide coordination supramolecules, we proposed a new paradigm for the separation of actinide elements (actinide nano-extraction) by using coordinated assembly of nanoclusters as the extracted species state. That is, using macrocyclic pyrogallol[4]arene as an extractant, it captures and chelates uranyl ions at the water phase/organic phase interface and in-situ assembles to form a uranyl coordination nanocage, realizing the efficient extraction and separation of uranyl ions. Studies have shown that each coordination nanocage is assembled from 6 pyrogallol[4]arene macrocycles and 24 uranyl ions. Multiple components exhibit multivalent cooperativity during the assembly process, which can achieve high selectivity and efficiency for uranyl ions. This new idea of actinide separation based on the extracted species of coordinated assembly nanoclusters is an important application of the concept of supramolecular assembly in the fields of radiochemistry and radionuclide separation.

References

[1] L. MEI; P. REN, Q. Y. WU, Y. B. KE, J. S. GENG, K. LIU, X. Q. XING, Z. W. HUANG, K. Q. HU, Y. L. LIU, L. Y. YUAN, G. MO, Z. H. WU, J. K. GIBSON, Z. F. CHAI and W. Q. SHI, "Actinide Separation Inspired by Self-Assembled Metal-Polyphenolic Nanocages," *J. Am. Chem. Soc.*, **142**, 16538 (2020).

[2] R. J. CAO, H. Y. ZHOU, Q. Y. WU, Z. XIAO, T. Y. XIU, J. LI, H. B. TANG, L. Y. YUAN, W. S. WU and W. Q. SHI, "Rigidity-Flexibility Regulation and Hard-Soft Donor Combination: Dual Strategies in Covalent Organic Frameworks Construction for Actinides/lanthanides Separation,"*Adv. Mater.*, **37**, 2414659 (2025).

[3] W. JIN, Q. Y. WU, Y. LOU, Z. W. HUANG, F. LIU, B. W. HU, J. P. YU, K. Q. HU, L. Y. YUAN, W. Q. SHI and L. MEI, "Acyl-Anchored Metal-Organic Cages with Interior Cryptand-Like Recognition Sites for Selective Removal of Radioactive Strontium(II)," *Sci. Bull.*, **70**, 683 (2025).

[4] C. L. XIAO, C. Z. WANG, L. Y. YUAN, B. LI, H. HE, S. WANG, Y. L. ZHAO, Z. F. CHAI and W. Q. SHI, "Excellent Selectivity for Actinides with a Tetradentate 2,9-Diamide-1,10-Phenanthroline Ligand in Highly Acidic Solution: A Hard-Soft Donor Combined Strategy," *Inorg. Chem.*, **53**, 1712 (2014).

[5] X. F. YANG, P. REN, Q. YANG, J. S. GENG, J. Y. ZHANG, L. Y. YUAN, H. B. TANG, Z. F. CHAI and W. Q. SHI, "Strong Periodic Tendency of Trivalent Lanthanides Coordinated with a Phenanthroline-Based Ligand: Cascade Countercurrent Extraction, Spectroscopy, and Crystallography," *Inorg. Chem.*, **60**, 9745 (2021).

[6] Y. LIU, C. Z. WANG, Q. Y. WU, J. H. LAN, Z. F. CHAI, Q. LIU and W. Q. SHI, "Theoretical Prediction of the Potential Applications of Phenanthroline Derivatives in Separation of Transplutonium Elements," *Inorg. Chem.*, **59**, 11469 (2020).

Copyright on 7th Asia-Pacific Symposium on Radiochemistry 2025 - R3-05 -

Metal phosphonate frameworks (MPFs) for f-block metal separation

Kai Lv[1], Liangping Xiong[1], Songzhu Qi[1]

[1]Institute of Nuclear Physics and Chemistry (INPC), China Academy of Engineering Physics (CAEP), *No.64 Mianshan Road, Mianyang, China, 621900, lvkai@caep.cn*

Metal phosphonate frameworks (MPFs) are a category of organic-inorganic hybrid porous materials consisting of single metal ions or metal clusters of different oxidation states bridged by a great variety of organophosphonate ligands. High-valency metal phosphonates (i.e., tri- to hexa-valent metal ions) featuring excellent robustness (e.g., thermal, chemical, radiolytical stability) and intrinsic affinity for f-block metal ions (i.e., lanthanides and actinides) under harsh aqueous conditions represents one of the most potential adsorbent materials for lanthanide and actinide separation since the problems associated with the recovery of spent nuclear fuel have to be tackled. In my presentation, I will start with a concise overview of both actinide separation and MPFs separation chemistry. The current landscape of f-block metal separation chemistry using MPFs will be introduced as follows covering the research work from my group. Lastly, I will offer some future prospects in MPFs chemistry for f-block metal separation.

1 MPFs for lanthanide and actinide separation

We classify MPFs into four sections based the oxidation states of the compositional metal and highlighted the use of highly crystalline arylphosphonate ligand-based MPFs (Figure 1).

1.1 Trivalent MPFs

A new series of light lanthanide arylphosphonate frameworks exhibited superior uptake capacity for UO_2^{2+} at certain pH solution, which was presumably due to the unique binding cavities involving intricate hydrogen bondings.

1.2 Tetravalent MPFs

A few tetravalent metal alkylphosphonate frameworks (M= Sn, Zr, Hf) and a hafnium arylphosphonate framework in the form of powder or polymeric membrane demonstrated large affinity for Ln^{3+}, An in moderate acid solutions[1-3].

1.3 Pentavalent MPFs

A niobium alkylphosphonate framework showed high selectivity for Th^{4+}, UO_2^{2+} in nitric acidic solutions and can be considered as potential chromatographic materials for actinide separation[4].

1.4 Hexavalent MPFs

A new uranyl arylphosphonate framework exhibited appreciable uptake of Eu^{3+} and Am^{3+} in aqueous solutions and unprecedented Eu^{3+}-UO_2^{2+} transmetalation behavior at high Eu concentration[5].

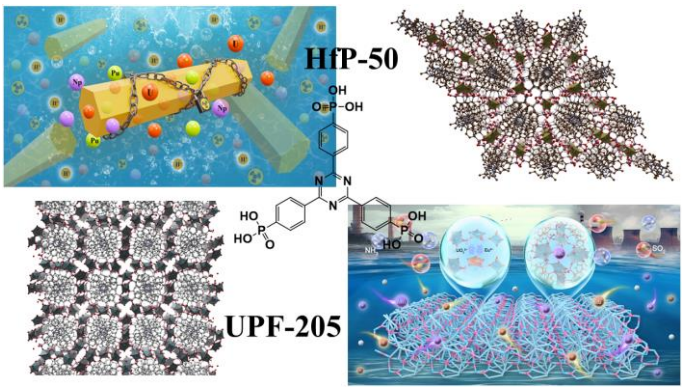


Fig. 1. Tritopic arylphosphonate ligand-based MPFs for f-block metal separation.

2. CONCLUSIONS

We initially married MPFs chemistry with f-block metal separation chemistry and were encouraged by these positive results to dig into the structure-property relationship that remained largely elusive.

ACKNOWLEDGMENTS

This work was supported by the President Fund of CAEP (Grant No. YZJJZQ2023004).

References

[1] S. Z. Qi and K. Lv*, *Inorganic Chemistry*, **62**, 10881 (2023).
[2] L. P. Xiong and K. Lv, *Chemical Engineering Journal*, **355**, 159 (2019).
[3] L. P. Xiong and K. Lv, Journal of Environmental *Chemical Engineering*, **11**, 109619 (2023).
[4] K. Lv, *Journal of Chromatography A*, **1504**, 35 (2017).
[5] S. Z. Qi and K. Lv*, *Chemical Engineering Journal*, **493**, 152818 (2024).

Copyright on 7th Asia-Pacific Symposium on Radiochemistry 2025 - R3-06 -

Amino Acid Decorated Phenanthroline Diimide as Sustainable Hydrophilic Am(III) Masking Agent with High Acid Resistance

Bin Li[1], Li Wang[2], Chao Xu[3]

[1]*Affiliation Information: Shuangqing Road No. 30 of Haidian District, Beijing, China, 100084, Email:Li-b22@mails.tsinghua.edu.cn*
[2]*Affiliation Information: North Third Ring Road West No. 105 of Haidian District, Beijing, China, 100048, Email: liwang862011@gmail.com*
[3]*Affiliation Information: Shuangqing Road No. 30 of Haidian District, Beijing, China, 100084, Email: xuchao@tsinghua.edu.cn*

Hydrophilic actinide masking agents are expected to replace the hazardous organic solvents widely used in liquid - liquid extraction for nuclear waste treatment. However, hydrophilic ligands face challenges in synthesis, purification, and acid resistance. In this study, a phenanthroline diimide framework was combined with a histidine bio - motif to prepare a masking agent capable of effectively separating trivalent lanthanides/actinides (and between actinides) at high acidity above 1 M. This approach utilized the hard - soft coordination properties of *N/O* - hybrid ligands, the imide structure favorable for metal coordination, and the multiple protonation of histidine. The synthesized masking agent has advantages such as easy preparation, high water solubility, high selectivity, and acid resistance. The research indicates that the rational combination of synthetic *N/O* - hybrid ligands and amino acids brings new opportunities for the efficient and sustainable separation of trivalent lanthanides and actinides.

INTRODUCTION AND DISCUSSION

Nuclear energy, as a zero-emission green energy source, holds great potential for addressing environmental protection and energy conservation challenges[1]. However, the handling of associated nuclear waste has long been problematic due to its high radioactivity. Separating minor actinides (mainly Am and Cm) from chemically similar trivalent lanthanides (Lns(III)) in nuclear waste is crucial, with two main approaches explored: oxidation state control and selective recognition by soft donor ligands[2,3]. While oxidation state control is theoretically efficient, it is hindered by unstable oxidized species, corrosive reagents, and incompatibility with industrial settings[2,3]. The soft donor ligand approach, where ligand design is pivotal, has seen advancements but still lacks ideal ligands meeting requirements for high efficiency, easy synthesis/purification, fast kinetics, and stability, with modern recycling processes demanding greener, more sustainable ligand designs[4]. Hydrophilic ligands, despite being promising alternatives, face challenges in synthesis/purification and poor acid resistance.

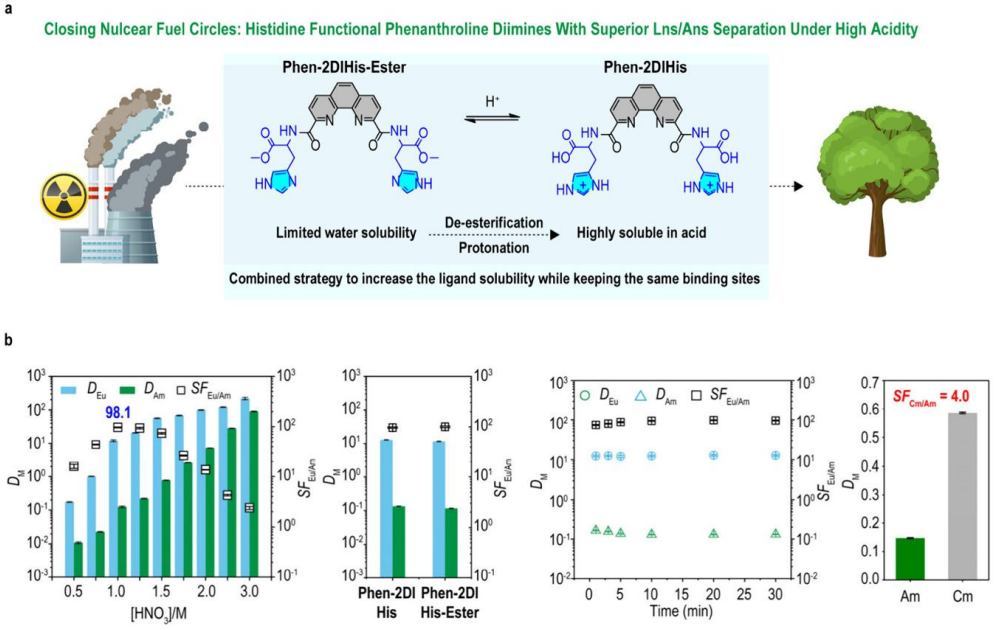


Fig. 1. Ligand structure and separation performance of Eu(III)(Cm(III))/Am(III). (a) Schematic illustration of Phen-2DIHis-Ester and its conversion to highly-soluble Phen-2DIHis for greener nuclear waste management. (b) Separation

performance of Eu(III)(Cm(III))/Am(III). Distribution ratios (D_M, bar graphs) and separation factors (*SF*, boxes) obtained in the extraction experiments of Eu(III)(Cm(III)) and Am(III) by TODGA with Phen-2DIHis(Phen-2DIHis-Ester) under different conditions.

Building on the previous strategies, we demonstrate combining a phenanthroline diimide framework with a histidine bio-motif to create an easily accessible, highly water-soluble, selectively superior, and acid-resistant Am(III) masking agent. This leverages the hard-soft coordination properties of N-heterocyclic ligands, energetically favorable imides for metal coordination, and multiple protonation of histidine, offering new opportunities for efficient, sustainable separation of trivalent lanthanides and actinides.

In this work, we deeply analyzed the role of histidine groups in Phen-2DIHis, the impact of positively charged terminals on coordination, and the driving force for selective actinide masking. Histidine significantly improved the ligand's water solubility under acidic conditions through protonation of the imidazole ring and de-esterification of the ester groups, while evidence from infrared spectroscopy (IR) and electrospray ionization mass spectrometry (ESI-MS) indicated that it did not participate in the inner-sphere coordination of metal ions, potentially only influencing selectivity by modulating the second coordination sphere. Although the protonated imidazole rings carry positive charges that theoretically might cause electrostatic repulsion during metal coordination, experiments showed that the kinetic interactions between the ligand and metal ions were strong enough to enable efficient extraction, proving that charge repulsion can be overcome through rational ligand design (e.g., a rigid phenanthroline diimide skeleton).

The core driving force for selective Am(III) masking stems from the hard-soft acid-base coordination properties of N/O hybrid sites in the ligand with metal ions: density functional theory (DFT) calculations revealed that the bond length between Am(III) and ligand N atoms is shorter than that of Eu(III), with higher electron density at the bond critical points, indicating stronger covalent interactions consistent with the softer Lewis acid nature of actinides due to their more delocalized 5f orbitals. Additionally, this work represents the first combination of a bio-motif (histidine) with a synthetic ligand to construct a hydrophilic system with both high separation efficiency and environmental friendliness, providing new insights for developing more sustainable nuclear waste separation ligands through protein engineering or organic ligand modification. The results not only validate the effectiveness of the "bio-motif + rigid coordination skeleton" design strategy but also offer new solutions to overcome bottlenecks in hydrophilic ligand synthesis, purification, and acid resistance.

CONCLUSIONS

In this study, we successfully prepared an efficient ligand for the separation of Eu(III)/Am(III) and Cm(III)/Am(III) under strong acidic conditions. The ligand was formed by combining a synthetic *N,O* -polydentate ligand with an amino acid. Leveraging the reversibility of the esterification reaction, the histidine-decorated phenanthroline diimide ligand was prepared with high yield and purity through simple precipitation under mild conditions. The multiple protonation of histidine under acidic conditions endowed the ligand with excellent solubility. The extraction performance of the ligand was evaluated in 1.0 M HNO_3 using TODGA as the lipophilic extractant, and the evolution of solution coordination species was investigated by NMR, UV-vis, and TRLFS titrations. The origin of Am(III) selectivity was discussed from the perspectives of bonding nature and electron density combined with DFT calculations. Overall, this study proposed a simple method for constructing water - soluble and efficient trivalent lanthanide/actinide (actinide/actinide) separation ligands. The combination of bio - motifs and synthetic ligands provides ideas for protein engineering and organic ligand modification, which is helpful for developing more sustainable separation ligands to reduce environmental impacts.

ACKNOWLEDGMENTS

C.X. would like to thank National Natural Science Foundation of China (No. U2067213; 22325603); L.Wang would like to thank National Natural Science Foundation of China (22105205) and Beijing Natural Science Foundation (No. 2232002); X. Tang would like to thank the National Natural Science Foundation of China (No. 52173093) for the financial support to this work.

References

[1] Runde, W. H.; Mincher, B. J., Higher Oxidation States of Americium: Preparation, Characterization and Use for Separations. *Chem. Rev.*, **111**, 9, (2011).

[2] Panak, P. J.; Geist, A., Complexation and Extraction of Trivalent Actinides and Lanthanides by Triazinylpyridine N-Donor Ligands. *Chem. Rev.*, **113**, 2, (2013).

[3] Leoncini, A.; Huskens, J.; Verboom, W., Ligands for f-element extraction used in the nuclear fuel cycle. *Chem. Soc. Rev.*, **46**, 23, (2017).

[4] Götzke, L.; Schaper, G.; März, J.; Kaden, P.; Huittinen, N.; Stumpf, T.; Kammerlander, K. K. K.; Brunner, E.; Hahn, P.; Mehnert, A.; Kersting, B.; Henle, T.; Lindoy, L. F.; Zanoni, G.; Weigand, J. J., Coordination chemistry of f-block metal ions with ligands bearing bio-relevant functional groups. *Coord. Chem. Rev.*, **386**, (2019).

Copyright on 7th Asia-Pacific Symposium on Radiochemistry 2025 - R3-07 -

7th Asia-Pacific Symposium on Radiochemistry *September 14 ~ 19, 2025 • Kunibiki Messe • Shimane, Japan*

ADSORPTION BEHAVIOR AND CHEMICAL STATES OF VANADIUM ON IRON(II)-BEARING CLAY MINERALS

Shiori Morii[1,2], Takumi Yomogida[1,2], Masami Nakada[1], and Yoshio Takahashi[2]

[1] *Japan Atomic Energy Agency, 2-4, Shirakata, Nakagun, Tokaimura, Ibaraki, Japan, 319-1195, morii.shiori@jaea.go.jp*
[2] *The University of Tokyo, 7-3-1 Hongo, Bunkyo, Tokyo, Japan, 113-0033, moriishiori@g.ecc.u-tokyo.ac.jp*

This research aimed to understand the redox reaction of Fe-bearing clay minerals and radionuclides. We used vanadium (V) as an analog of radionuclides. The adsorption behavior and chemical states of V on Fe-bearing clay minerals under different pH conditions were investigated by adsorption experiments and XANES measurements. The results of these experiments suggest that V(V) anion complexes adsorbed on the surface of the clay mineral and then reduced to V(IV) cation complexes by the structural Fe(II) in the clay mineral. The structure of XANES spectra indicates that chemical states of V depend on the solution pH. The coordination environments of V on the clay mineral under different pH conditions need to be clarified in the future work.

1 INTRODUCTION

Clay minerals have large adsorption capacity of various elements on their surface, because of their large negative charges in the structure and deprotonated hydroxyl group. Thus, clay minerals can prevent the spreading of harmful elements (mainly cations) in the environment. Under the subsurface condition in the deep geological repository of high-level nuclear waste, bentonite clay mineral will be used as a buffering material which prevents the spreading of radionuclides to the environment. Iron (Fe(II), Fe(III))-bearing clay minerals act as electron donors and have the potential to reduce coexisting elements, altering their mobility [1]. Therefore, it is important to understand the redox reaction of Fe-bearing clay minerals and radionuclides in the deep geological environment. This research aimed to understand the redox reaction of Fe-bearing clay minerals and radionuclides. Because of its similar redox properties, we chose vanadium (V) as an analog of neptunium and plutonium [2]. We investigated the adsorption behavior and chemical states of V on Fe-bearing clay minerals under different pH conditions.

2 EXPERIMENTAL

In this research, we used montmorillonite (SWy-3) which was purchased from the Source Clay Minerals Repository (Purdue University, West Lafayette, IN, USA). The Fe content of SWy-3 is 2 wt % [3]. The suspension of SWy-3 (hereafter, unreduced SWy-3) was prepared by purification, Na^+-saturation, and size-fractionation [3]. The reduced SWy-3 sample was prepared by dithionite reduction of unreduced SWy-3. Oxidation states of Fe in SWy-3 were observed via Fe-57 Mössbauer spectroscopy. The amount of adsorbed V on SWy-3 was investigated under different pH conditions (pH 4, 7, and 9). Unreduced and reduced SWy-3 reacted with V(V) for 20 hours in pH buffered solutions. Those solutions were then filtered to recover SWy-3. The amount of V in the filtrate was measured by inductively coupled plasma optical emission spectrometer (ICP-OES), and the amount of V adsorbed on SWy-3 was determined by the difference of V concentrations in the initial solution and in the filtrate. Oxidation states of V adsorbed on SWy-3 samples were analyzed by V K-edge X-ray absorption near edge structure (XANES) spectra. The XANES measurements were performed using beamline BL-12C, Photon Factory (Tsukuba, Ibaraki, Japan).

3 RESULT AND DISCUSSION

Fe-57 Mössbauer spectra and fitting results of unreduced SWy-3 and reduced SWy-3 are shown in Fig. 1. According to the fitting results of Mössbauer spectra, the amounts of structural Fe(II) in unreduced SWy-3 and reduced SWy-3 were 10 % and 79 %, respectively.

Table 1 shows the results of V adsorption experiments. The adsorption ratio of V on SWy-3 was calculated from the concentration of V in the solutions before and after the adsorption on SWy-3. The adsorption ratio on unreduced SWy-3 sample was high when the solution pH was low. Also, the ratios on reduced SWy-3 were higher than those of unreduced SWy-3. On the other hand, from the structures of the XANES spectra of adsorbed V on reduced SWy-3, a part of the adsorbed V(V) was reduced to V(IV). These results suggest that V(V) anion complexes adsorbed on the surface of reduced SWy-3 and then reduced to V(IV) cation complexes by the structural Fe(II) in reduced SWy-3 [4]. Because of the clay mineral's negative charges in the structure and deprotonated hydroxyl group, V(IV) cation complexes are easily adsorbed on the surface of reduced SWy-3.

Copyright on 7th Asia-Pacific Symposium on Radiochemistry 2025- R3-08* -

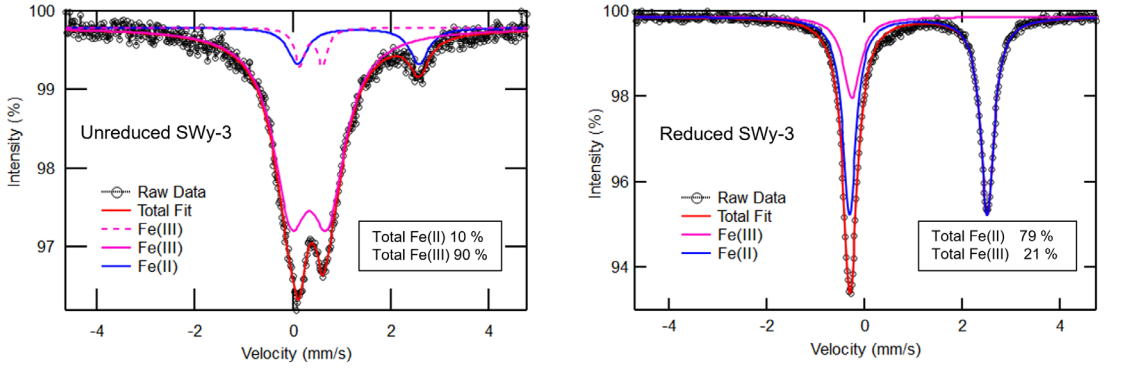


Fig. 1. Fe-57 Mössbauer spectra and fitting results of unreduced SWy-3 (left) and reduced SWy-3 (right).

TABLE 1. The results of V adsorption experiments of unreduced and reduced SWy-3

Sample	pH	Adsorption ratio of V (%)	Adsorption amount of V (mg)	Weight of SWy-3 (g) (Wet condition)
Unreduced SWy-3	4	11	0.026	0.11
	7	0	-	0.17
	9	0	-	0.13
Reduced SWy-3	4	95	0.23	0.16
	7	26	0.062	0.22
	9	10	0.025	0.14

The pre-edge peak energy of the XANES spectrum of V adsorbed at pH 7 was lower than that at pH 4. This result shows the chemical states of V depend on the solution pH. To understand the pH dependence of the redox reaction of SWy-3 and radionuclides, the coordination environment of V on SWy-3 under different pH conditions need to be clarified in the future work. We are planning to investigate those features by extended X-ray absorption fine structure (EXAFS) and Fe-57 Mössbauer spectroscopy.

4 CONCLUSIONS

This research aimed to understand the redox reactions between Fe-bearing clay minerals and V. We investigated the adsorption behavior and chemical states of V on SWy-3 at different pH conditions. The results of these experiments suggest that V(V) anion complexes adsorbed on the surface of reduced SWy-3 and then reduced to V(IV) cation complexes by the structural Fe(II) in reduced SWy-3.The structure of XANES spectra indicates that chemical states of V depend on the solution pH. In the future work, the coordination environments of V on SWy-3 under different pH conditions will be analyzed to understand the pH dependence of the redox reaction of SWy-3 and radionuclides.

ACKNOWLEDGMENTS

This study was performed with the approval of Photon Factory (2024G123). We acknowledge that a part of this work was supported by Grant-in-Aid for Scientific Research (C) (25K00227) from Japan Society for the Promotion of Science (JSPS).

References

[1] D. R. Brookshaw et al., “Redox Interactions of Tc(VII), U(VI), and Np(V) with Microbially Reduced Biotite and Chlorite”, *Environmental Science and Technology,* **49**, 13139 (2015).
[2] H. B. Andrews et al., “Leveraging visible and near-infrared spectroelectrochemistry to calibrate a robust model for Vanadium(IV/V) in varying nitric acid and temperature levels”, *Talanta,* **259**, 124554 (2023).
[3] C. A. Gorski et al., “A Redox properties of structural Fe in clay minerals. 1. Electrochemical quantification of electron-donating and -accepting capacities of smectites”, *Environmental Science and Technology*, **46**, 9360 (2012).
[4] H. Zhu et al., “Adsorption of vanadium (V) on natural kaolinite and montmorillonite: Characteristics and mechanism”, *Applied Clay Science,* **161**, 310 (2018).

Copyright on 7th Asia-Pacific Symposium on Radiochemistry 2025- R3-08* -

Contributed Talk | [R8]Education and Outreach

Tue. Sep 16, 2025 9:45 AM - 10:55 AM JST | Tue. Sep 16, 2025 12:45 AM - 1:55 AM UTC Hall B(Small)

[R8] Education and Outreach

9:45 AM - 10:15 AM JST | 12:45 AM - 1:15 AM UTC

[R8-01]

HUMAN RESOURCE DEVELOPMENT FOR RADIATION SCIENCE AT F-REI

*Hiroshi Watabe[1], Atsushi Toyoshima[2], Hiroki Kanda[2], Shin'ichi Goto[3] (1. Tohoku University (Japan), 2. Osaka University (Japan), 3. Niigata University (Japan))

10:15 AM - 10:35 AM JST | 1:15 AM - 1:35 AM UTC

[R8-02]

LINKING RADIOELEMENT SPECIATION, WORKFORCE DEVELOPMENT, AND GLOBAL COLLABORATION IN RADIOCHEMISTRY FOR EMERGING NUCLEAR TECHNOLOGIES

*Ken Ronald Czerwinski[1] (1. University of Nevada, Las Vegas (United States of America))

10:35 AM - 10:55 AM JST | 1:35 AM - 1:55 AM UTC

[R8-03]

What Can Be Learned from Years of Testing of Education And Training Course for Radiation Workers

*Satoru Nakashima[1], Kuninobu Inada[1], Akihito Matsushima[1], Ryoji Koba[1], Hiroaki Teramoto[1] (1. Hiroshima University (Japan))

©APSORC25

7th Asia-Pacific Symposium on Radiochemistry *September 14 ~ 19, 2025 • Kunibiki Messe • Shimane, Japan*

HUMAN RESOURCE DEVELOPMENT FOR RADIATION SCIENCE AT F-REI

Hiroshi Watabe[1], Atsushi Toyoshima[2], Hiroki Kanda[3], Shin'ichi Goto[4]

[1]*Research Center for Accelerator and Radioisotope Science, Tohoku University,6-3 Aoba,Aramaki, Aoba, Sendai,Japan 980-8578, hwatabe@tohoku.ac.jp*
[2]*Institute for Radiation Sciences, Osaka University, Suita,Japan , 565-0871, toyo@irs.osaka-u.ac.jp*
[3]*Research Center for Nuclear Physics (RCNP),Osaka University,Ibaraki, Japan, 567-0047, kandah@rcnp.osaka-u.ac.jp*
[4]*Department of Chemistry, Niigata University, Niigata, Japan, 950-2181,goto@chem.sc.niigata-u.ac.jp*

The Fukushima International Research Education Institute (F-REI) was established in April 2023 in Namie Town, Fukushima Prefecture, as a cross-ministerial initiative involving the Reconstruction Agency, Ministry of Education, Culture, Sports, Science and Technology, Ministry of Health, Labour and Welfare, Ministry of Agriculture, Forestry and Fisheries, Ministry of Economy, Trade and Industry, and Ministry of Environment. F-REI aims to accelerate research development, industrialization, and human resource development as part of the "creative reconstruction" concept for Fukushima. F-REI focuses on five key areas: robotics, agriculture and forestry, energy, radiation science/pharmaceutical medicine/industrial radiation use, and data collection/dissemination related to nuclear disasters. The radiation science research facility, equipped with cyclotrons, hot laboratories, and controlled areas, is scheduled to begin operation in 2029.

To address the urgent need for skilled personnel in radiation science, F-REI has initiated three human resource development programs:

1.Accelerator Operation Personnel Training: This program develops educational materials including tabletop accelerators and VR tools to provide fundamental understanding of accelerator principles. It also offers on-the-job training at various accelerator facilities to provide diverse operational experience. The program collaborates with technical colleges to recruit graduates and provides rotational training across multiple accelerator facilities

2.Radioisotope Production Personnel Training: This initiative includes workshops and on-the-job training for radioisotope production and separation/purification techniques. The first Training Workshop on Radioisotope Production was successfully held in March 2025 at Osaka University, receiving highly positive evaluations from participants. The program aims to supply useful radioisotopes while training students, researchers, and technicians from both academia and industry.

3.Radiation Management Personnel Training: This program offers basic and advanced courses in radiation management, with special focus on accelerator facilities. It includes training in shielding calculations, radioactive material evaluation, and practical management techniques. The program will establish an "Accelerator Radiation Handling Supervisor" certification and develop international cooperation with IAEA and other organizations.

These initiatives address the declining number of radiation professionals in Japan, as evidenced by decreasing membership in the Japan Radioisotope Association and fewer applicants for radiation handling supervisor examinations. Through these comprehensive training programs, F-REI aims to develop the next generation of radiation science professionals to support sustainable research and development in this critical field.

ACKNOWLEDGMENTS

This research was performed by the commissioned research fund provided by F-REI

Copyright on 7th Asia-Pacific Symposium on Radiochemistry 2025 - R8-01 -

7th Asia-Pacific Symposium on Radiochemistry *September 14 ~ 19, 2025 • Kunibiki Messe • Shimane, Japan*

LINKING RADIOELEMENT SPECIATION, WORKFORCE DEVELOPMENT, AND GLOBAL COLLABORATION IN RADIOCHEMISTRY FOR EMERGING NUCLEAR TECHNOLOGIES

Ken Czerwinski

Radiochemistry Program, University of Nevada Las Vegas 4505Maryland Parkway, Las Vegas, NV USA 89154-4009

The advancement of nuclear technologies across the energy, medical, security, and environmental sectors requires a sound scientific foundation and a skilled, multidisciplinary workforce. Central to these efforts is the detailed understanding of radioelement speciation, defined as the identification of oxidation states, coordination geometries, and the chemical forms of radionuclides in complex systems. Speciation provides critical insight into the reactivity, mobility, and separability of actinides and fission products, impacting key applications including advanced fuel cycle development, radioactive waste management, radiopharmaceutical design, and nuclear forensics. As the nuclear field transitions toward next-generation reactor systems, high-assay low-enriched uranium (HALEU) deployment, and sustainable isotope production methods, the role of precise chemical characterization becomes increasingly vital.

Education is central to this capability. Developing a technically proficient workforce in radiochemistry requires sustained investment in academic programs that combine classroom instruction with hands-on laboratory experience. Speciation techniques, including spectroscopy, electrochemistry, and separation science, must be integrated into curricula and research opportunities at the undergraduate and graduate levels. However, few institutions maintain the infrastructure required for high-level work with radioactive materials. To address this, university-based consortia have emerged as essential models for workforce development, research innovation, and collaborative engagement. These consortia link universities with national laboratories, facilitating access to specialized facilities and expertise. They also promote interdisciplinary research efforts that are essential for training students to address real-world nuclear challenges. The effort expands to all levels of students university systems.

In addition to national coordination, international collaboration in radiochemistry plays a critical role in ensuring global nuclear safety, security, and technological advancement. Programs supported by the International Atomic Energy Agency and bilateral agreements with international partners provide students and researchers with opportunities to participate in cooperative projects, shared training platforms, and policy-oriented engagements. These experiences broaden scientific perspectives and enhance the cultural competency required for working in a global nuclear enterprise. Furthermore, they support the harmonization of standards and practices in nuclear science and technology worldwide.

This presentation will explore the convergence of radioelement speciation, radiochemical education, and international collaboration as foundational elements in advancing both current and future nuclear technology. Examples will be drawn from ongoing research in actinide coordination chemistry, alpha-emitting radiopharmaceutical development, and the forensic characterization of nuclear materials. Emphasis will be placed on the integrative role of academic institutions and university consortia in supporting U.S. and international efforts to train the next generation of nuclear scientists, engineers, and technologists. These efforts are essential for realizing the potential of advanced reactors, closing the fuel cycle, and expanding peaceful uses of nuclear technology through safe, secure, and sustainable approaches.

Copyright on 7th Asia-Pacific Symposium on Radiochemistry 2025 - R8-02 -

7th Asia-Pacific Symposium on Radiochemistry *September 14 ~ 19, 2025 • Kunibiki Messe • Shimane, Japan*

WHAT CAN BE LEARNED FROM YEARS OF TESTING OF EDUCATION AND TRAINING COURSE FOR RADIATION WORKERS

Satoru Nakashima[1], Kuninobu Inada[1], Akihito Matsushima[1], Ryoji Koba[1], Hiroaki Teramoto[1]

[1]*Natural Science Center for Basic Research and Development (N-BARD), Hiroshima University, 1-4-2 Kagamiyama, Higashi-Hiroshima, Hiroshima 739-8526, Japan. E-mail: snaka@hiroshima-u.ac.jp*

A test for checking knowledge about radiation safety treatment is introduced to the education and training course for radiation workers. The participants are guided to solve some questions during the lecture with checking the answers using textbook. It is expected that they could understand more effectively the important points as radiation worker by the test. The results for years of testing were pretty good. Average total score was tracked annually. It was cancelled in 2020 due to COVID-19. The score in 2021 was the best during this overall test, maybe because they were happy to be able to have face-to-face lecture. There were questions with a high correct answer rate regardless of the year, and questions related to average total score. It was found that the score of the test, especially of the multiple answer question, might be related with the attitude and concentration at the lecture.

1 INTRODUCTION

Radiation education and training play a major role in radiation safety treatment. Various efforts are being made to improve the effectiveness of education and training. Content enrichment is a major concern. On-line education also became an important issue. However, it is still important to evaluate the effectiveness of the education and training. We implemented a test to evaluate it [1]. After the report we continued the test from 2005 to 2023. The results of the tests over the years were compiled. In the present study, the trend of scores in the compiled data were investigated.

2 METHOD

2.1 Education and training at N-BARD, Hiroshima University

Education and training at Natural Science Center for Basic Research and Development (N-BARD), Hiroshima University for all radiation workers includes the test. Unsealed radioisotope (RI) has been used in practical training for the third-year undergraduate students in the Department of Biological Science, Hiroshima University. The education and training course for the undergraduate students also includes the test. It is assumed that there will be no significant change in the quality of students throughout this period.

2.2 Test

The questions in the test for the third-year undergraduate students are as follows. Each question is worth 10 points for a total of 100 points.

1. Connect the correct relation with a line based on the properties of ionizing radiation.

Group A	Group B	Group C
α ray	short-wavelength electromagnetic waves	can be shielded with lead blocks and concrete
β ray	high-velocity helium nuclei	stopped by about 1 cm of plastic
γ ray	fast electron	stopped by a piece of paper

2. Connect the correct relation with a line based on the meaning of words.

Group A	Group B	Group C
Exposure dose	Bq	Decay per unit time
Energy of radiation	Sv	Amount of energy imparted to a unit mass of material
Units of radioactivity	Gy	Amount of charge generated in a unit mass of air
Equivalent dose, Effective dose	eV	Effects on the human body
Absorbed dose	C/kg	Energy gained by an electron accelerated by a voltage of 1 V

3. What nuclide is produced when ^{32}P undergoes β^- decay?
Answer the half-life of ^{32}P.

4. State the purpose of the RI act.
Write down the name of prevention regulations of N-BARD, Hiroshima University regarding the RI act.

5. Fill in the brackets with the appropriate word or phrase for the following statement regarding the measurement of personal radiation exposure dose.

Copyright on 7th Asia-Pacific Symposium on Radiochemistry 2025

Badges, pocket dosimeters, etc. are used as personal radiation exposure dosimeters. In the case of uniform exposure to the trunk, wear the badge on your ( ) for men and wear it on your ( ) for women.

6. The effects of ionizing radiation on the human body are classified into stochastic and deterministic effects. Explain these two effects.

7. Which of the following is a correct combination of radiation damage that is thought to have no dose threshold?
(1) Cataracts and Bone marrow death (2) Cataracts and Intestinal death (3) Bone marrow death and Carcinogenesis
(4) Carcinogenesis and Mutations (5) Intestinal death and Mutations

8. Write down the three principles of protection against external exposure to ionizing radiation.

9. List the three main routes by which radioactive substances causing internal exposure are absorbed into the body.

10. Mark with a circle the actions that should not be performed in a laboratory using radioactive isotopes.
(1) During the experiment, you wear laboratory clothing, footwear, gloves, etc.
(2) Eating, drinking and smoking.
(3) You open an unsealed, highly concentrated radioactive isotope on the laboratory bench.
(4) When using radioactive isotopes, you place filter paper inside the hood, place a tray, place absorbent paper inside it, and then conduct the experiment on the tray.

3 RESULTS AND DISCUSSION

Figure 1 shows the change in average total scores over time. The average score is more than 90. This is because the students answered with listening the lecture and looking at the text. This suggests all students understood the contents. The worst score recorded from 2005 to 2023 was 65. There was no need to worry about whether this person should be a radiation worker. The education and training were cancelled in 2020 due to COVID-19. After the cancellation, we restarted the education and training in 2021. The score in 2021 was the best among all tests. It seems that the students experienced the pleasure of attending face-to-face lecture. This might be a corona effect. However, the score became steady state again in 2022 and 2023.

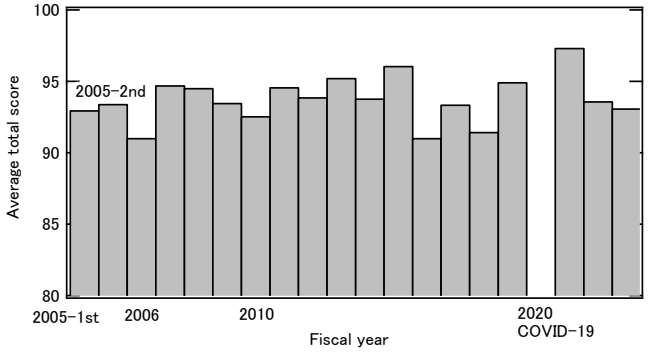


Fig. 1. Change in average total scores over time.

There were some questions with a high correct answer rate and some with a relatively low correct answer rate. Figure 2 shows the typical relation between average total score and average score of each question in each event. The score of Q2 is almost perfect independent of average total score in each event. The score of Q10 shows a relatively good correlation with the average total score in each year. Because students had to choose two answers in Q2. It was found that the score of the test, especially of the multiple answer question, might be related with the attitude and concentration at the lecture. It reflects whether students are attentive to the lecture or not.

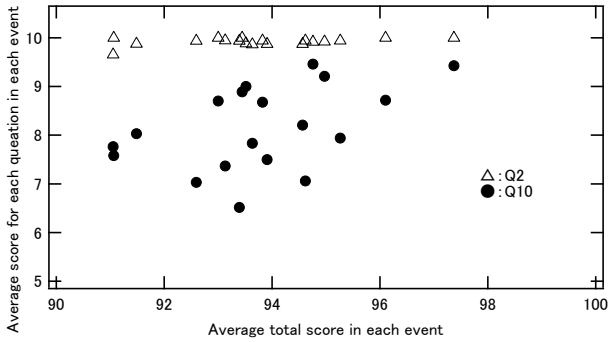


Fig. 2. Relation between average total score and average score of each question for education and training in each event.

4. CONCLUSIONS

Various efforts are being made to improve the effectiveness. At the same time, the effectiveness of education and training must be evaluated. The present results of the test showed a good performance and may suggest the importance of the attitude and concentration.

References

[1] S. Nakashima et al., Japanese J. Rad. Safety Manage., **4**, 39 (2005) (in Japanese).

Contributed Talk | [S1]Evolution of the Periodic Table of the Elements

Tue. Sep 16, 2025 11:00 AM - 12:00 PM JST | Tue. Sep 16, 2025 2:00 AM - 3:00 AM UTC Hall S(Int'l)

[S1] Evolution of the Periodic Table of the Elements

11:00 AM - 11:20 AM JST | 2:00 AM - 2:20 AM UTC

[S1-04]

Isothermal Gas Chromatographic Behavior of Volatile Oxychlorides of Short-lived Molybdenum and Tungsten as a Model of Element 106, Seaborgium

*Tetsuya K. Sato[1,2], Hina Natori[2,1], Ryo Otani[1], Ryota Aoki[2], Kazuaki Tsukada[3], Yuta Ito[4], Masato Asai[1], Minoru Sakama[5], Shinichi Goto[6], Katsuhisa Nishio[1], Hiroyuki Makii[1], Riccardo Orlandi[1], Yuichiro Nagame[1] (1. Japan Atomic Energy Agency (Japan), 2. Ibaraki University (Japan), 3. Tohoku University (Japan), 4. KEK (Japan), 5. Tokushima University (Japan), 6. Niigata University (Japan))

11:20 AM - 11:40 AM JST | 2:20 AM - 2:40 AM UTC

[S1-05]

Towards Next-Generation Techniques for Superheavy Element Detection in Liquids

*Pavel Bartl[1], Lucie Sifnerova[1], Daniela Dvorakova[1], Vaclav Zach[2], Charles M. Folden III[3], Mojmir Nemec[1], Jon Petter Omtvedt[4], Jan John[1] (1. CTU in Prague (Czech Republic), 2. NPI CAS (Czech Republic), 3. TAMU (United States of America), 4. UiO (Norway))

11:40 AM - 12:00 PM JST | 2:40 AM - 3:00 AM UTC

[S1-06*]

SOLVENT EXTRACTION OF Zr AND Hf WITH (O, O-) AND (S, S-) DONOR PHOSPHATE TOWARD CHEMICAL STUDY OF Rf

*Yudai Itakura[1,2], Masashi Kaneko[1], Hiroyuki Kazama[1], Kojiro Nagata[1], Ruilin Wang[1,2], Miyu Konno[1], Enni Khult[1,2], Kyosuke Shibamoto[1,2], Kenta Mori[1], Ryota Kikuchi[1], Kazushi Kawamoto[1], Hiromitsu Haba[2], Yousuke Kanayama[2], Yudai Shigekawa[2], Akihiro Nambu[2], Yoshitaka Kasamatsu[1,2] (1. Department of Chemistry, Graduate School of Science, The University of Osaka (Japan), 2. Nishina Center for Accelerator-based Science, RIKEN (Japan))

©APSORC25

Isothermal Gas Chromatographic Behavior of Volatile Oxychlorides of Short-lived Molybdenum and Tungsten as a Model of Element 106, Seaborgium

Tetsuya K. Sato[1,2], Hina Natori[1,2], Ryo Otani[1], Ryota Aoki[1], Masato Asai[1], Kazuaki Tsukada[3], Yuta Ito[4], Minoru Sakama[5], Shinichi Goto[6], Katsuhisa Nishio[1], Hiroyuki Makii[1], Riccardo Orlandi[1], Yuichiro Nagame[1]

[1]*Japan Atomic Energy Agency: Shirakata 2-4, Tokai-mura, 319-1195, JAPAN*
[2]*Grad. School of Sci. and Eng., Ibaraki Univ.: Bunkyo 2-1-1, Mito, Ibaraki, 310-0056, JAPAN, sato.tetsuya@jaea.go.jp*
[3]*RARiS, Tohoku Univ.: Aoba 6-3, Aramaki, Aoba-ku, Sendai, Miyagi, 980-0845, JAPAN*
[4]*WNSC, KEK: Hirosawa 2-1, Wako, Saitama, 351-0198, JAPAN*
[5]*Grad. School of Biomed. Sci., Tokushima Univ.: Kuramoto 3-18-15, Tokushima, 770-8503, JAPAN*
[6]*Grad. Of School of Sci. and Tech. Niigata Univ.: Igarashi-2 8050, Niigata, 950-2181, JAPAN*

The chemical properties of superheavy elements (Z > 100) may deviate from periodic trends due to strong relativistic effects. As a model study for element 106, seaborgium (Sg), we investigated the volatility of group-6 oxychlorides using isothermal gas chromatography (IGC) with short-lived isotopes of molybdenum (Mo) and tungsten (W). Volatile compounds were synthesized by reaction with chlorinating agents derived from $SOCl_2$ and O_2, and their chromatographic behavior was analyzed. The measured adsorption enthalpies ($-\Delta H_{ads}$) matched the evaluated value for MoO_2Cl_2 suggesting the exclusive formation of MoO_2Cl_2. It was confirmed that tungsten would form volatile oxychlorides as well. These results support future gas-phase studies of Sg.

The chemical properties of superheavy elements with atomic numbers (Z) greater than 100 have been suggested to deviate from periodic trends due to strong relativistic effects. To explore this, we have conducted gas-phase chemical experiments to investigate the volatilities of group-6 element compounds, as a model system for element 106, seaborgium (Sg).

In this study, an isothermal gas chromatographic (IGC) technique was employed for both off-line and on-line investigations of the volatile oxychlorides of the group-6 elements molybdenum (Mo) and tungsten (W). The experimental setup was based on a previously developed on-line apparatus for volatility studies of element 105, dubnium (Db)[1]. The apparatus consists of a recoil chamber, a reaction chamber, an isothermal chromatography column, and a clustering chamber.

For the off-line experiments, short-lived Mo isotopes — ^{104}Mo, ^{105}Mo, and ^{106}Mo ($T_{1/2}$ = 60 s, 36.3 s, and 8.73 s, respectively) — were employed, which were produced from two ^{252}Cf spontaneous fission sources and collected in the N_2 gas in the recoil chamber. For the on-line experiments, the short-lived W isotope ^{173}W ($T_{1/2}$ = 7.6 min) was synthesized using the JAEA tandem accelerator.

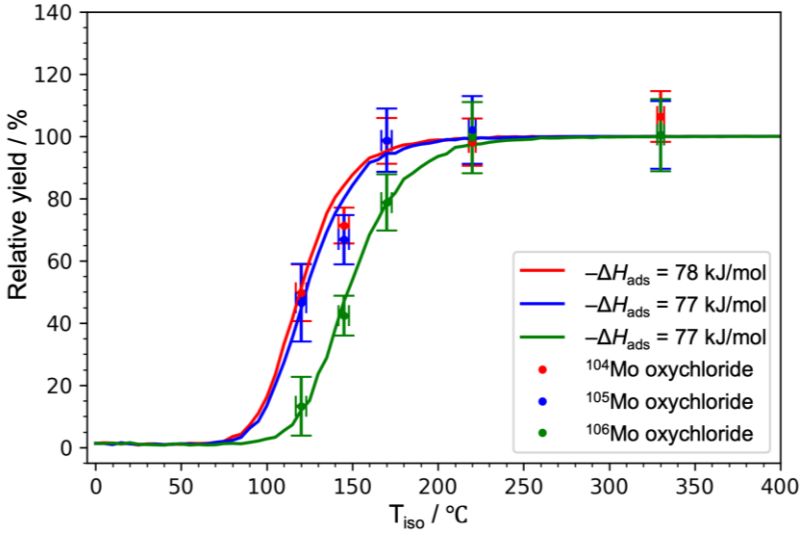


Fig.1 Relative yield of Mo oxychlorides as a function of the isothermal temperature in the chromatography column when the reaction chamber temperature is 550°C and $O_2/SOCl_2$ is used as the chlorinating agents.

Copyright on 7th Asia-Pacific Symposium on Radiochemistry 2025 - S1-04 -

The isotopes were transported by a carrier gas to the reaction chamber, where they reacted with chlorinating agents to form volatile compounds. For the off-line and the on-line experiments, respectively, a N_2 or He/N_2 mixture gas was used as a carrier gas. The chlorinating agents were generated by bubbling pure oxygen or an oxygen–nitrogen gas mixture through thionyl chloride ($SOCl_2$), and the resulting gas was introduced into the reaction chamber. The volatile products were then transferred to the isothermal chromatography column maintained at a fixed temperature. Their migration through the column, which depends on their volatility and the column temperature, was monitored. The amount of compounds eluted from the column was determined via γ-ray spectroscopy.

Using this setup, the formation of volatile oxychlorides of Mo and W was studied under various conditions using their short-lived isotopes. Several isothermal gas chromatograms were obtained. Figure 1 shows typical chromatographic behavior of the short-lived Mo isotopes as a function of the isothermal column temperature. The adsorption enthalpies ($-\Delta H_{ads}$) of Mo oxychlorides were derived from the temperature-yield curves and found to be in good agreement with the value evaluated from literature values for macro amounts of MoO_2Cl_2 ($-\Delta H_{ads} \approx 77$ kJ/mol). Similarly, for ^{173}W, the volatile compounds was successfully observed suggesting a production of volatile oxychlorides such as WO_2Cl_2.

These results suggest that, under the experimental conditions employed, volatile oxychloride compounds were formed, and that the adsorption enthalpy for MoO_2Cl_2 was successfully determined.

In this presentation, we will report the experimental details and results for Mo and W, and discuss the implications for future studies on seaborgium (Sg).

References

[1] N. M. Chiera et al., Angew. Chem. Int. Ed, 60 (2021) 17871-17874.

7th Asia-Pacific Symposium on Radiochemistry *September 14 ~ 19, 2025 • Kunibiki Messe • Shimane, Japan*

TOWARDS NEXT-GENERATION TECHNIQUES FOR SUPERHEAVY ELEMENT DETECTION IN LIQUIDS

Pavel Bartl[1], Lucie Sifnerova[1], Daniela Dvorakova[1], Vaclav Zach[2], Charles M. Folden III[3], Mojmir Nemec[1], Jon Petter Omtvedt[4], Jan John[1]

[1]*Department of Nuclear Chemistry, CTU in Prague: Brehova 7, CZ-11519, Praha, Czechia, pavel.bartl@fjfi.cvut.cz*
[2]*Nuclear Physics Institute, Czech Academy of Sciences: Hlavni 130, CZ-25068, Husinec-Rez, Czechia*
[3]*Cyclotron Institute, Texas A&M University: 400 Bizzell St., US-77840, College Station, TX, USA*
[4]*Department of Chemistry, University of Oslo: P.O. Box 1033 Blindern, NO-0315, Oslo, Norway*

The chemical behavior of superheavy elements is of utmost interest for fundamental research as these elements should evince significant deviation from the periodic law due to the relativistic effects in their electron shells. However, known isotopes of such elements decay almost exclusively via alpha emission or spontaneous fission, which complicates their detection, especially in liquids. Current state-of-the-art methods include classic alpha spectrometry with automated sample preparation or (relatively high-volume) liquid scintillation spectrometry. For years, research on superheavy element chemistry in liquids had been sidelined and only recently has it been slowly regaining attention in the community. This paper deals with the prospect of using novel techniques or modifying the existing ones in order to achieve better superheavy element detection in liquids while using low-volume flow-through techniques, such as microfluidics. More specifically, two examples of such techniques currently under investigation at the CTU in Prague are described in this paper: semiconductor detector surface functionalization for direct alpha spectrometry in an aqueous solution, and liquid scintillation spectrometry in a capillary coupled with a microfluidic mixing system.

1 INTRODUCTION

Currently known isotopes of superheavy elements are all radioactive and decay almost exclusively via alpha emission or spontaneous fission with very short half-lives. From the perspective of liquid-phase chemistry research, this fact complicates their detection directly in the phase of interest as the decay particles/fragments are charged and heavy, i.e., have extremely short range in liquids. The state-of-the-art in the field has utilized two standard detection methods: classic alpha spectrometry with automated sample preparation, e.g., in systems like ARCA [1] or AIDA [2], which benefits from excellent energy resolution of semiconductor detectors but suffers from time-consuming sample preparation and rather low detection efficiency, and relatively high-volume liquid scintillation spectrometry in the SISAK system [3], which, on the other hand, benefits from very high detection efficiency but has worse energy resolution. At the CTU, we have been investigating two novel approaches that are based on said detection methods but utilize different techniques; the compatibility of said techniques with the current experimental setups [4, 5] at the CTU was also taken into consideration.

2 SEMICONDUCTOR DETECTOR SURFACE FUNCTIONALIZATION

One next-generation technique that may significantly improve detection of the superheavy elements is functionalization of semiconductor detector surface to specifically bind chemical species of interest. For this purpose, the so-called self-assembled monolayers (SAMs) are studied at a few institutions worldwide (e.g., [6]). The main advantage of SAMs is that they form a monolayer several atoms “thick” ending with a functional group of choice that can be tuned to bind specific species from the solution. Should this species contain an element of interest, it would be bound in the vicinity of the detector surface; hence, rendering its detection directly in the solution possible. In general, a SAM precursor consists of a tailgroup (the functional group that binds species of interest), a spacer (an aliphatic hydrocarbon chain determining the thickness of the SAM), and a headgroup (surface-specific group that binds to the surface), as shown in Fig. 1 (a). Since the semiconductor detector for alpha spectrometry is typically a gold-coated silicon detector, the headgroup of choice for this application is almost exclusively a thiol (–SH) group, which binds with the gold surface very well via the sulfur bridge. The spacer has an influence on the stability of the SAM and its ability to self-assemble in the first place [7]. Several functional groups are currently under investigation at the CTU in Prague for sorption of different species, e.g., (11-Mercaptoundecyl)-N,N,N-trimethylammonium bromide for sorption of anions (mainly anionic thallium and mercury chlorides) or 11-Mercaptoundecylphosphonic acid for sorption of cations (mainly cationic thallium and lanthanides). The preliminary results show the technique should be suitable for this application (to be published).

3. LIQUID SCINTILLATION SPECTROMETRY IN A CAPILLARY

Another technique with great potential for the detection of superheavy elements is based on liquid scintillation spectrometry (LSS), similar to the one used in [3]. However, the cited technique used large amounts of chemical agents,

Copyright on 7th Asia-Pacific Symposium on Radiochemistry 2025 - S1-05 -

such as acids and scintillation cocktails, and did not, in fact, operate in fully flow-through manner. The approach researched at the CTU aims at developing a fully flow-through detection system coupled with a microfluidic separation system. Therefore, the idea of having a part of a plastic capillary run through a detection chamber with a photomultiplier has arisen, and, surprisingly, the literature research yielded no record of such application making it completely novel. The liquid scintillation spectrometry takes advantage of mixing the scintillation cocktail directly with the aqueous phase or having a custom-made extracting scintillation cocktail to extract certain species from an aqueous solution. The geometry of such a sensitive volume is nearly ideal, as each of the to-be-detected species is directly surrounded by the sensitive molecules capable of producing a detection signal. Integrating the detection volume as part of a capillary connected to a larger microfluidic system introduces, unfortunately, several technological challenges, such as the total internal reflection in the capillary, which may guide interfering light through the, effectively turning it into an optical fiber. Nonetheless, we have shown that several geometry and light shielding techniques may diminish the total internal reflection, making it negligible. On the other hand, the aqueous-to-scintillator ratio has also a significant effect on the measured signal as quenching (non-radiative energy dissipation) occurs. This, however, might be turned into an asset as "some" quenching could help reduce the background while having negligible effect on reduction of the signal originating from the sample. A chemical system for seaborgium and its homologues has been optimized with respect to the parallel extraction experiments performed at the CTU. The developed detection proof-of-concept system based on the commercially available Triathler (Hidex, Finland) LSS system is depicted in Fig. 1 (b).

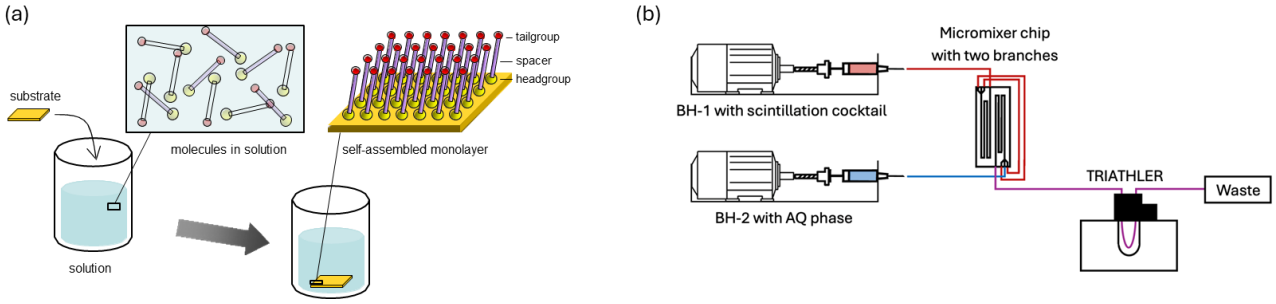


Fig. 1. (a) General schematics of self-assembled monolayer preparation from a precursor; (b) Schematics of the flow-through capillary detection system developed at the CTU in Prague (BH is a syringe pump, the micromixer chip was purchased from Dolomite Microfluidics, USA, and Triathler stands for the Triathler liquid scintillation spectrometer from Hidex, Finland).

4. CONCLUSIONS

Recently, the research interest in the liquid-phase chemistry of superheavy elements has increased highlighting the need to explore more efficient (in terms of both detection and time efficiency) "next-generation" detection techniques sensitive to charged particles directly in liquids. Proof-of-concept work at the CTU in Prague has been conducted on radionuclide sorption using a model semiconductor detector surface functionalized by self-assembled monolayers, and direct liquid scintillation spectrometry in a capillary. Both these techniques showed a great prospect for future applications in the field.

ACKNOWLEDGMENTS

The work has been supported by the large research infrastructure projects, project number LM2023060, and by the Inter-Excellence II program, project number LUAUS25292, both supported by the Ministry of Education, Youth and Sports of the Czech Republic.

References

[1] M. SCHÄDEL et al., *Radiochim. Acta*, **48**, 171–176 (1989).
[2] Y. NAGAME et al., *Radiochim. Acta*, **93**, 519–526 (2005).
[3] J. P. OMTVEDT et al., *J. Nucl. Radiochem. Sci.*, **3(1)**, 121–124 (2002).
[4] P. BARTL et al., *Nucl. Instrum. Methods Phys. Res. A*, **1052**, 168280 (2023).
[5] P. BARTL et al., *Nucl. Instrum. Methods Phys. Res. A*, **1055**, 168500 (2023).
[6] V. ZAKUSILOVA et al., *Appl. Surf. Sci.*, **642**, 158356 (2024).
[7] M. D. PORTER et al., *J. Am. Chem. Soc.*, **109**, 3559–3568 (1987).

SOLVENT EXTRACTION OF Zr AND Hf WITH (O, O-) AND (S, S-) DONOR PHOSPHATE TOWARD CHEMICAL STUDY OF Rf

Yudai Itakura[1,2], Masashi Kaneko[1], Hiroyuki Kazama[1], Kojiro Nagata[1], Ruilin Wang[1,2], Miyu Konno[1], Enni Khult[1,2], Kyosuke Shibamoto[1,2], Kenta Mori[1], Ryota Kikuchi[1], Kazushi Kawamoto[1], Hiromitsu Haba[2], Yousuke Kanayama[2], Yudai Shigekawa[2], Akihiro Nambu[2], Yoshitaka Kasamatsu[1,2].

[1] *Department of Chemistry, Graduate School of Science, The University of Osaka, 1-1 Machikaneyama, Toyonaka, Osaka, 560-0043, itakuray22@chem.sci.osaka-u.ac.jp*
[2] *Nishina Center for Accelerator-based Science, RIKEN, 2-1 Hirosawa, Wako, Saitama, 351-0198*

We performed solvent extraction experiments of Zr and Hf with dibutyl phosphate and diethyl dithiophosphate, and DFT calculations of extracted species of Zr and Hf, and Rf complexes of the same structure toward application of this experimental systems to Rf experiments. The time required for the extraction reactions to reach the equilibrium state was sufficiently short for application to ^{261}Rf experiments by shortening the time using automated extraction apparatus. Calculated K_{ex} values were in good agreement with experimental K_{ex} values in relative value The population analysis explains the higher K_{ex} values of Hf, which indicates that we can discuss the bonding nature of Rf by combining the present extraction experiment and calculation. Predicted distribution ratios of Rf were higher than those of Zr and Hf, which was consistent with the estimation that the interaction of Rf with soft ligands was stronger than those for Zr and Hf.

1. INTRODUCTION

Chemical properties of transactinide elements ($Z \geqq 104$) are expected to deviate from the periodicity of elements in the periodic table due to the relativistic effects on valence electrons. Therefore, it is important to investigate chemical properties of these elements. Transactinide elements can only be synthesized by heavy-ion-introduced nuclear reactions using an accelerator, and almost all nuclides have short half-lives and low production rates. Thus, chemical operations need to be rapid, and we can usually use only one atom of transactinide elements at a time. Rutherfordium (Z = 104, Rf) is the lightest element in transactinide elements. Previous studies on the solution chemistry of Rf have reported that chemical behavior of Rf is similar to that of group 4 elements (Zr and Hf) [1–3], and also that the interaction of Rf with hard bases, such as F^- and OH^-, is weaker than those of its homologues [4,5]. Therefore, we focused on the reactions with soft donors to discuss relativistic effects on Rf through orbital interactions. For this purpose, we focused on dibutyl phosphate ($((CH_3(CH_2)_3O)_2POOH$, HL^O) and diethyl dithiophosphate ($((CH_3CH_2O)_2PSSH$, HL^S) as extractants. In this presentation, we will report solvent extraction of Zr(IV) and Hf(IV) by batch method, population analysis of the extracted species, and prediction of the behavior of Rf.

2. METHODS

Nitric acid aqueous phase containing ^{88}Zr and ^{175}Hf was contacted with CCl_4 organic phase containing extractant and shaken for the specified time. Distribution ratios (D) were obtained from the volume and radioactivity of each phase. Perchloric acid and sodium nitrate were used to adjust pH and [NO_3^-]. Extraction coefficients (K_{ex}) were evaluated from the D values. The complex formation energies and density of states (DOS) of model complexes were calculated by DFT calculation. Model complexes were generated based on experimentally extracted species of Zr and Hf. Vibrational frequencies were calculated to assure that the optimized geometries are local minimum at the potential energy surface.

3. RESULTS AND DISCUSSION

The time dependencies of the D values of Zr and Hf indicates that the reactions reached the equilibrium state in 3-5 min in both cases using HL^O and HL^S, suggesting that the chemical reactions are sufficiently fast for application to ^{261}Rf ($T_{1/2}$ = 68 s) experiments by shortening the time using automated apparatus (flow Injection Solvent Extraction apparatus, ISE). From the dependencies of the D values on extractant and nitrate ion concentrations (Fig. 1), it was estimated that extracted species were $[M(HL^O_2)_n(NO_3)_{4-n}]$ (n = 2-3 for Zr(IV) and n = 3 for Hf(IV)) and $[M(L^S)(NO_3)_3]$ in each system. The K_{ex} values were in the order of Zr < Hf in the HL^O system and Zr ≈ Hf in the HL^S system. The predicted ratios of K_{ex} values of Zr and Hf (K_{ex}(Zr) / K_{ex}(Hf)) from DFT calculation were in good agreement with experimental results. Overlap population DOS analysis indicates that the coordination bonds between Hf ion and HL^O are stronger than those of Zr, which explains the higher K_{ex} values of Hf. Predicted D values for Rf based on calculated K_{ex} value were clearly higher than those of Zr and Hf in both systems. It indicates that the bonds of Rf ion with HL^O and HL^S ligands are more stable than those of Zr and Hf, which is consistent with the estimation that the interaction between Rf and soft ligands is stronger than those of Zr and Hf.

Copyright on 7th Asia-Pacific Symposium on Radiochemistry 2025- S1-06* -

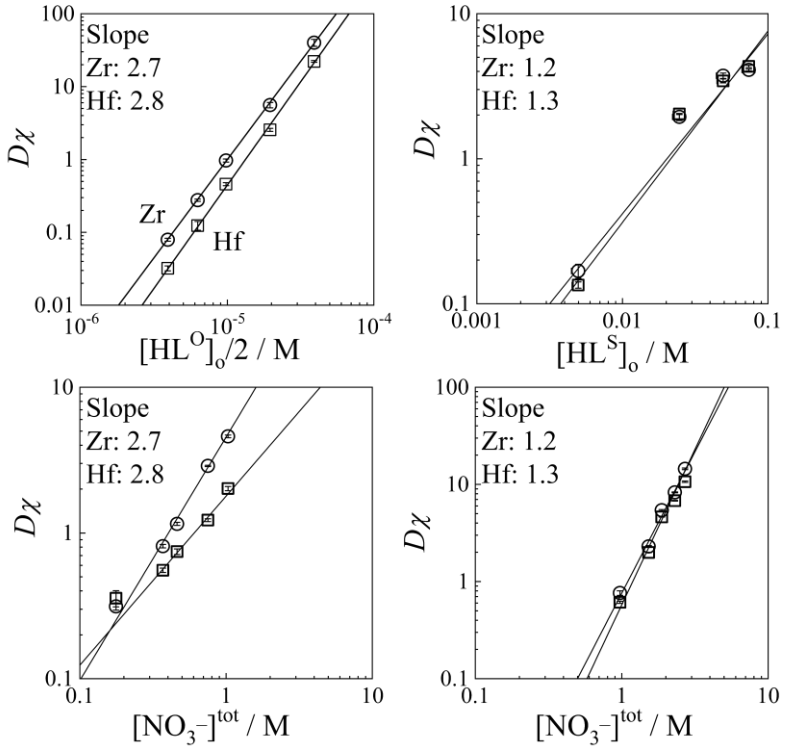


Fig. 1. The dependency of $D\chi$ value on the concentrations of extractant (upper) or nitrate ion (lower) in the HL^O system (left) and HL^S system (right).

4. CONCLUSION

We performed solvent extraction experiments of Zr and Hf with HL^O and HL^S, and DFT calculations of extracted species of Zr, Hf, and Rf complexes of the same structure toward application of this experimental systems to Rf experiments. The time required for the extraction reactions to reach the equilibrium state was short, although it needed to be shortened by automated apparatus. Calculated K_{ex} values were in good agreement with experimental K_{ex} values in relative value, and the stabilities of M-L bonds were obtained from population analysis of extracted species. It was found that we can discuss the bonding nature of Rf by combining the present extraction experiment and calculation. Predicted D values of Rf were higher than those of Zr and Hf, which was consistent with the estimation that the interaction between Rf and soft ligands was stronger than those of Zr and Hf. After determining the experimental conditions with the automated apparatus, we plan to conduct the Rf experiments.

ACKNOWLEDGMENTS

This work was supported by JST SPRING, Grant Number JPMJSP2138.

References

[1] R. SILVA *et al.*, “Chemical separation of rutherfordium”, *Inorg. Nucl. Chem. Letters*, **6**, 12 (1970).
[2] E. K. HULET *et al.*, “Chloride complexation of element 104”, *J. Inorg. Nucl. Chem.*, **42**, 79 (1980).
[3] Z. SZEGLOWSKI *et al.*, “Study of the Solution Chemistry of Element 104 – Kurchatovium”, *Radiochim. Acta* **51**, 71 (1990).
[4] H. HABA *et al.*, “Fluoride Complexation of Element 104, Rutherfordium”, *J. Am. Chem. Soc.*, **126**, 16 (2004).
[5] Y. KASAMATSU *et al.*, “Co-precipitation behavior of single atoms of rutherfordium in basic solutions”, *Nat. Chem.*, **13**, 3 (2021).

Copyright on 7th Asia-Pacific Symposium on Radiochemistry 2025- S1-06* -

Contributed Talk | [S3]Outreach for Education on Radiation and Radioactivity after Fukushima Nuclear Accident

Tue. Sep 16, 2025 11:10 AM - 11:50 AM JST | Tue. Sep 16, 2025 2:10 AM - 2:50 AM UTC Hall B(Small)

[S3] Outreach for Education on Radiation and Radioactivity after Fukushita Nuclear Accident

11:10 AM - 11:30 AM JST | 2:10 AM - 2:30 AM UTC

[S3-01]

FUTURE PERSPECTIVES OF NUCLEAR AND RADIOCHEMISTRY EDUCATION IN THE NEW ERA OF THE SILK ROAD ACCORDING TO CHINESE NUCLEAR ENERGY DEVELOPMENT

*Wangsuo Wu[1] (1. Lanzhou University (China))

11:30 AM - 11:50 AM JST | 2:30 AM - 2:50 AM UTC

[S3-02]

DISSEMINATION OF FOOD REFERENCE MATERIALS FOR MEASUREMENT OF RADIOACTIVITY AFTER FDNPP AND THEIR APPLICATIONS IN PROFESSIONAL TRAINING AND EDUCATION

*Yoshitaka Minai[1], Tsutomu Miura[2], Chushiro Yonezawa[3], Yukiko Okada[4], Fumihiro Arakawa[5], Yoshinobu Uematsu[6], Akira Okada[7], Isao Kojima[8], Takao Osawa[8], Kazutoshi Kakita[8], Shoji Hirai[4] (1. Musashi University and Nedzu Chemical Laboratory (Japan), 2. National Institute of Advanced Industrial Science and Technology (Japan), 3. Japan Institute of International Affairs (Japan), 4. Tokyo City University (Japan), 5. NH Foods Ltd. Research and Development Center (Japan), 6. Japan Accreditation Board (Japan), 7. Toshiba Co. Ltd. (Japan), 8. Japan Society for Analytical Chemistry (Japan))

©APSORC25

7th Asia-Pacific Symposium on Radiochemistry *September 14 ~ 19, 2025 • Kunibiki Messe • Shimane, Japan*

FUTURE PERSPECTIVES OF NUCLEAR AND RADIOCHEMISTRY EDUCATION IN THE NEW ERA OF THE SILK ROAD ACCORDING TO CHINESE NUCLEAR ENERGY DEVELOPMENT

Wangsuo WU

Frontiers Science Center for Rare Isotopes, Lanzhou University: Lanzhou, China, 730000, wuws@lzu.edu.cn

The training of qualified workers through the peaceful development along the New Silk Road is one of our tasks, since our Lab. is located in the capital of Gansu province, Lanzhou, which is now as then located at the Silk Road and closely related to it's development. But, what does nuclear mean? This question can be answered in different ways. In the past, nuclear meant armament, threats and similar things. But in the future, nuclear will stand only for peaceful and sustainable energy. Therefore, I will look about this issue from the perspective of the development of the Silk Road. In Chinese writing, there are two characters which sound alike, but mean different things. But the fact, that they sound alike, demonstrates that they are somehow related, anyway. So, for me, in Chinese language, nuclear energy means peace through development. And that has been, after all, the fundamental idea of the Silk Road in the past, and that is what it will be in the future.

I. CHINA'S FUTURE PERSPECTIVE

By the end of December 2024, China has 57 operational nuclear power units (excluding Taiwan), with a total installed capacity of 59431.7 MWe (~59.43 GW), surpassing the original 2020 target of 58 GW. New reactors are distributed across both coastal and inland regions, exemplified by the Fangchenggang Unit 4 (1188 MWe, Guangxi inland) and Zhangzhou Unit 1 (1212 MWe, Fujian coastal). Nuclear power accounted for 4.73% of national electricity production in 2024 (cumulative generation: 445.175 billion kWh), exceeding the 4% target set for 2020. to 10% by 2035 and, together will renewable energy, to 30%, by 2050. To reach this aim, China needs to build and develop more nuclear power plants.

But, first of all, I want to show why we did choose nuclear energy:

- because we have to re-evaluate, for a number of reasons, coal as an energy source;
- because we do not want to create a conflict, between economic growth and the environment;
- because we will be more able to even out energy prices;
- because we want to overcome the limitations of other energy sources in regards to the availability of resources and their compatibility with the environment;

– because the development of nuclear energy serves to boost productive powers, especially in the area of nuclear power technology.

The challenges we are confronted with, in this endeavour, are

- the safety of the installations;
- the protection of the installations against terrorism as well as the emission of dangerous substances; - the handling of radiation products;
- economic competitivity;

– as well as sustainability.

But, aside from these general challenges we are confronted with, there are some challenges that are specific for China. Among these, there are:

- the availability of nuclear materials and resources in this area;
- competitivity in the construction and installation of nuclear power plants;
- our own capacities for innovation in nuclear technologies;
- the construction of nuclear power plants in the interior parts of China;

– and the training of skilled workers in the area of nuclear technology and nuclear chemistry.

This last challenge for China, concerning the training of skilled workers in the area of nuclear and nuclear and radiochemistry, is a task of our university of the city of Lanzhou, which is located at the Silk Road. How important this area is for China, today, is demonstrated by a look at the past, the present and the future of nuclear and radiochemistry in China.

1895-1942 - The first steps: founding of radiochemistry education and research in China;

Copyright on 7th Asia-Pacific Symposium on Radiochemistry 2025 - S3-01 -

1942-1986: Golden Era: construction and use of nuclear technicians;
1986-2000: Decay;
2000-2011 Renaissance: of nuclear technicians as well as nuclear and radiochemistry;
2011-2020: Fukushima After the incident in Fukushima, it was, at first, not clear how China would proceed, and if China would stick to its plans. Therefore, there were intensive discussions among specialists. They arrived at the conclusion that China will continue to develop its nuclear energy.
2020-2024: Resumed rapid expansion, adding of reactors and increasing of total capacity.
2024- ? : Announced plans to build more new reactors to meet 2035 targets.

II. CURRENT TRAINING IN NUCLEAR AND RADIOCHEMISTRY

While in the last century, our universities hesitated and in some cases stopped some nuclear programs, we have now restarted programs in the areas of radiochemistry, nuclear technology, nuclear physics, nuclear medicine etc. Similar developments occur at a number of institutions outside of universities. We have to recognize, that the number of nuclear workers needed depends on how many nuclear power plants are in use.

Therefore, it is clear that a faster development of nuclear sciences and radiochemistry will enlarges the labour market for skilled workers, there will be a greater demand for skilled workers, and this creates a challenge, weather we will be able provide for this demand. The areas of skills that are affected by this are planning, construction and running of nuclear power plants and the nuclear fuel cycle. If China is to provide for this demand, this would demand a growing workforce in nuclear technology and radiochemistry.

But not only in nuclear technology and nuclear physics, chemistry, we will need skilled workers, because of these development plans, but also in areas like finances, law and protection of the environment.

Thus, the challenge is:
- to provide for the needed skilled workers;
- the lack of teachers;
- laboratories are too old and badly equipped;
– there is not enough done to attract students.

Political decisions can liberate all subordinated institutions. We will need decisions by the People's Congress, to provide for a long-term financing for these programs.

Progress that has already been made:
- The government has decided in favour of a sustainable financing for training programs in the areas of nuclear technology and nuclear physics;
- companies get involved and share their facilities with universities;
– universities work to renew their departments and equipments.

III. CONCLUSIONS

Concluding, I can say that the peaceful use of nuclear energy along the Silk Road will enhance the training of skilled workers in the areas of nuclear and radiochemistry. Chinese people love and hope to set up a peaceful world. We should ensure peaceful use of nuclear energy. We hope everyone in the world enjoy the peaceful development.

Copyright on 7th Asia-Pacific Symposium on Radiochemistry 2025 - S3-01 -

7th Asia-Pacific Symposium on Radiochemistry *September 14 ~ 19, 2025 • Kunibiki Messe • Shimane, Japan*

DISSEMINATION OF FOOD REFERENCE MATERIALS FOR MEASUREMENT OF RADIOACTIVITY AFTER FDNPP AND THEIR APPLICATIONS IN PROFESSIONAL TRAINING AND EDUCATION

Yoshitaka Minai[1], Tsutomu Miura[2], Chushiro Yonezawa[3], Yukiko Okada[4], Fumihiro Arakawa[5], Yoshinobu Uematsu[6], Akira Okada[7], Isao Kojima[8], Takao Osawa[8], Kazutoshi Kakita[8], Shoji Hirai[4]

[1]*Musashi University and Nedzu Chemical Laboratory: 7-3-1 Toyotama-kami, Nerima-ku, Tokyo 176-8534, Japan*
minai@cc.musashi.ac.jp
[2]*National Institute of Advanced Industrial Science and Technology: 1-1-1 Umezono, Tsukuba, Ibaraki 305-8560, Japan*
[3]*Japan Institute of International Affairs: 3-8-1 Kasumigaseki, Chiyoda-ku, Tokyo 100-0013, Japan*
[4]*Tokyo City University: 971 Ozenji, Asao-ku, Kawasaki 215-0013, Japan*
[5]*NH Foods Ltd. Research and Development Center: 3-3 Midorigahara, Tsukuba, Ibaraki 300-2646, Japan*
[6]*Japan Accreditation Board: 2-3 Shiba,4-chome, Minato-ku, Tokyo 108-0014, Japan*
[7]*Formerly, Toshiba Co. Ltd.: 1 Komukai Toshiba-cho, Saiwai-ku, Kawasaki 212-8582, Japan*
[8]*Japan Society for Analytical Chemistry: 1-26-2 Nishigotanda, Shinagawa-ku, Tokyo 141-0031 Japan*

Starting in the spring of 2012, we have been working on the development of environmental radioactivity reference materials for food for four years. This was also an opportunity to see how a group of experts could respond to the social need to ensure the reliability of analytical values for environmental radioactivity thought to be originating from FDNPP.

1 INTRODUCTORY REMARKS

In 2012, one year after FDNPP, brown rice was developed, followed by a series of the food-related radioactivity reference materials using soybeans, shiitake mushrooms, beef, fish meat, and fish bone as matrices. Including the environmental radioactivity reference material for soil, which was developed just before brown rice, distribution to a wide range of users has begun as part of the various reference materials issued by the Japan Society for Analytical Chemistry. Now in 2025, close to fifteen years after FDNPP, these reference materials are still being used in a variety of research and development settings, such as in analytical proficiency tests and as test samples when applying new analytical methods.

This report will note the points to be aware of when developing reference materials for determining radioactivity in foodstuffs, their subsequent use, and the status of follow-up on their development. Reference materials for soil, brown rice, soybeans, shiitake mushrooms, beef, fish meat, and fish bone will be reported, hereafter, focused on usage and contribution of the reference materials to the society.

2 DEVELOPMENT OF REFERENCE MATERIALS

Food-related samples containing radioactivity believed to be from FDNPP were collected and homogenized to prepare candidate reference materials. Radioactivity was measured with the cooperation of many testing and research institutions and evaluated by experts. The step of assigning certified radioactivity values to ^{137}Cs and ^{40}K was taken. These procedures are in accordance with ISO guide line for the development of reference materials with certified values.

3 DISSEMINATION AND USE FOR PROFESSIONAL TRAINING AND EDUCATION

Spreading reference materials to testing and research institutions. We confirmed the progress of the initial goal of improving the reliability of analytical values by observing changes in distribution status (including relationships with industry and region). There were also cases where reference materials were purchased together with analytical equipment. Those materials were used to monitor performance of the equipment and skill of analysts. Education and training of technicians have been a major motivation to purchase reference materials for testing and research institutions.

It was frequently required to explain reliability of radiochemical analysis to people having no scientific basis on nuclear sciences, including radioanalytical chemistry. It was somewhat straight forward for those people to understand the aim of checking radioactivity in foodstuffs having known amounts of radioisotopes. This improved public relations.

To facilitate international comparison of certified values and shorten development time, the participating institutions in the joint experiments related to the certified values were limited to domestic institutions. After that, the equivalence of the certified values was evaluated in joint experiments with overseas testing and research institutions.

Academic and industrial use as environmental samples containing radioactive nuclides originating from FDNPP. Use as trial samples for the analysis of nuclides other than ^{134}Cs, ^{137}Cs, and ^{40}K. Attempts are also being made to analyze them as representative environmental samples related to FDNPP (some long-lived nuclides like ^{135} Cs). These are some of the purposes for which overseas users are looking to use the samples.

Copyright on 7th Asia-Pacific Symposium on Radiochemistry 2025 - S3-02 -

Contributed Talk | [P2]ICP-MS Based Radioanalytical Chemistry and Related Applications

Tue. Sep 16, 2025 1:30 PM - 2:50 PM JST | Tue. Sep 16, 2025 4:30 AM - 5:50 AM UTC Hall A(MP)

[P2] ICP-MS Based Radioanalytical Chemistry and Related Applications

1:30 PM - 1:50 PM JST | 4:30 AM - 4:50 AM UTC

[P2-06]

Radiochemical Analysis of Technetium-99 in Seawater: Resin-Based Preconcentration and Separation with Tracer Validation

*Feng-Yun Jimmy Huang[1], Aya Sakaguchi[2], Ching-Wen Cheng[1], Yuichi Onda[2] (1. Department of Medical Imaging and Radiological Sciences, Central Taiwan University of Science and Technology (Taiwan), 2. Center for Research in Radiation, Isotopes, and Earth System Sciences, University of Tsukuba (Japan))

1:50 PM - 2:10 PM JST | 4:50 AM - 5:10 AM UTC

[P2-07]

Homogeneity and stability testing of carrier-free ^{135}Cs standard solution

*Shiho ASAI[1], Taiyo Tajima[2], Aya Sakaguchi[2], Yasushi Sato[1], Katsuhiro Shirono[1] (1. National Institute of Advanced Industrial Science and Technology (AIST) (Japan), 2. University of Tsukuba (Japan))

2:10 PM - 2:30 PM JST | 5:10 AM - 5:30 AM UTC

[P2-08*]

Investigation of curium isotope measurements by mass spectrometry

*Yuya Kasuga[1], Kazuaki Tsukada[2], Masato Asai[4], Yuichi Takaku[3], Shinya Yamasaki[3], Yudai Shigekawa[3], Keisuke Sueki[3], Aya Sakaguchi[3] (1. Graduate School of Science and Technology Degree Programs in Pure and Applied Sciences Master's Program in chemistry University of Tsukuba (Japan), 2. Research Center for Accelerator and Radioisotope Science (RARiS), Tohoku university (Japan), 3. Institute of Pure and Applied Sciences, University of Tsukuba (Japan), 4. Advanced Science Research Center Japan Atomic Energy Agency (Japan))

2:30 PM - 2:50 PM JST | 5:30 AM - 5:50 AM UTC

[P2-09*]

Synthesis of Neptunium Isotopes via the ^{238}U+p Reaction for the Production of the Np Spike

*Nami Matsuzawa[1], Hayato Ogawa[2], Akihiko Yokoyama[3], Hiromitsu Haba[4], Yudai Shigekawa[4,5], Akihiro Nambu[4], Yousuke Kanayama[4], Hiromichi Shimizu[4], Yuichi Takaku[5], Shinya Yamasaki[5], Keisuke Sueki[5], Aya Sakaguchi[5] (1. Graduate School of Science and Technology, Degree Programs in Pure and Applied Sciences, Master's Program in Chemistry, University of Tsukuba (Japan), 2. Graduate School of Science and Technology, Degree Programs in Life and Earth Sciences, Master's Program in Environmental Sciences, University of Tsukuba (Japan), 3. Institute of Science and Engineering, Kanazawa University (Japan), 4. Nishina Center for Accelerator-Based Science, RIKEN, Wako (Japan), 5. Institute of Pure and Applied Sciences, University of Tsukuba (Japan))

©APSORC25

7th Asia-Pacific Symposium on Radiochemistry *September 14 ~ 19, 2025 • Kunibiki Messe • Shimane, Japan*

Radiochemical Analysis of Technetium-99 in Seawater: Resin-Based Preconcentration and Separation with Tracer Validation

Feng-Yun J. Huang[1], Aya Sakaguchi[2], Ching-Wen Cheng[1], Yuichi Onda[2]

[1]*Department of Medical Imaging and Radiological Sciences, Central Taiwan University of Science and Technology, Taichung 406053, Taiwan. Email: fyhuang@ctust.edu.tw (F.-Y.J.H.); as6167182@gmail.com (C.-W.C.)*
[2]*Center for Research in Radiation, Isotopes, and Earth System Sciences, University of Tsukuba, Ibaraki 305-8572, Japan. Email: ayaskgc@ied.tsukuba.ac.jp (A.S.); onda@geoenv.tsukuba.ac.jp (Y.O.)*

1. PURPOSE

Technetium-99 (^{99}Tc) is a long-lived artificial radionuclide, with a half-life of 2.11×10^5 years, that poses potential risks to both the environment and human health. Numerous radiochemical methods for the determination of ^{99}Tc have been well established, primarily utilizing selective resin-based separation systems followed by measurement using inductively coupled plasma mass spectrometry (ICP-MS) or liquid scintillation counting (LSC) [1–2]. However, few studies have compared the performance of the conventional TEVA resin with the newer TK-201 resin for the preconcentration and separation of ^{99}Tc in seawater, particularly in combination with chemical yield monitoring using different tracers such as ^{99m}Tc and stable rhenium (Re). In this study, the radiochemical determination of ^{99}Tc in seawater was conducted using resin-based preconcentration and separation techniques, validated with tracers including ^{99m}Tc, ^{99}Tc, and Re.

2. MATERIALS & METHODS

The preconcentration and separation of technetium-99 (^{99}Tc) from 1 L of seawater collected from the coastal area of Dongshi Township, Chiayi County, Taiwan, were investigated using different resin combinations, including AG1-X8/TEVA and AG1-X8/TK-201. The separation protocols for ^{99}Tc using TEVA and TK-201 resins were adapted, with minor modifications, from the standard procedures provided by Eichrom Technologies and Triskem International [3]. Tracers including ^{99m}Tc, ^{99}Tc, and stable rhenium (Re) were spiked into the samples to evaluate the chemical yield of ^{99}Tc throughout the preconcentration and separation processes. Standard sources of ^{99m}Tc, ^{99}Tc, and Re were obtained from Global Medical Solutions Taiwan®, Eckert & Ziegler®, and AccuStandard®, respectively. Chemical yields based on ^{99m}Tc, ^{99}Tc, and Re were determined using a gamma counter (Revvity WIZARD2 2470), a LSC (Hidex 300 SL Super Low Level), and inductively coupled plasma optical emission spectrometry (ICP-OES, PerkinElmer Optima 8000), respectively. Decontamination factors (DFs) for interfering nuclides—including Re, Mo, Ru, Co, Ni, Sr, Ag, Sb, Cs, V, Zn, and Pb—were estimated using ICP-OES during the ^{99}Tc separation from seawater. The minimum detectable activity (MDA) of ^{99}Tc by LSC was calculated using the following equation (1). Figure 1 presents the experimental flowchart for the radiochemical analysis of ^{99}Tc from 1 L of seawater via resin-based preconcentration and separation with tracer validation.

$$\mathbf{MDA}\left(\frac{\mathbf{Bq}}{\mathbf{V}}\right) = \frac{\mathbf{4.65 \times \sqrt{B} + 3}}{\mathbf{60 \times E \times R \times V \times T}} \quad (1)$$

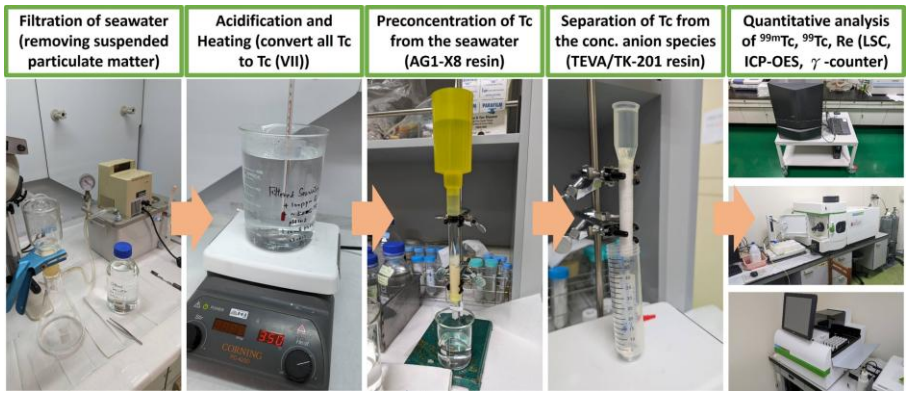


Fig. 1. The experimental flowchart for the radiochemical analysis of ^{99}Tc from 1 L of seawater via resin-based preconcentration and separation.

Copyright on 7th Asia-Pacific Symposium on Radiochemistry 2025 - P2-06 -

3. RESULTS

The radiochemical determination of ^{99}Tc in seawater was conducted using resin-based preconcentration and separation techniques, validated with tracers including ^{99m}Tc, ^{99}Tc, and Re (Fig.2). The chemical yields of ^{99}Tc during the preconcentration step using AG1-X8 resin were 96.9 ± 1.5%, 94.1 ± 2.7%, and 96.9 ± 3.9%, based on ^{99m}Tc, ^{99}Tc, and Re tracers, respectively. When both preconcentration and separation steps were applied, the chemical yields using AG1-X8/TEVA and AG1-X8/TK-201 resin combinations were as follows: 93.0 ± 0.9%, 94.5 ± 2.3%, and 97.7 ± 4.8% for AG1-X8/TEVA; and 90.1 ± 0.2%, 87.3 ± 5.9%, and 100.5 ± 2.8% for AG1-X8/TK-201, based on ^{99m}Tc, ^{99}Tc, and Re, respectively. Decontamination factors (DFs) for interfering nuclides during the preconcentration and separation process were evaluated as DF > 1,000 for Mo, Ru, Co, Ni, Ag, and Sb using AG1-X8; for Mo, Ru, Co, Ni, Ag, and Sb using AG1-X8/TEVA; and for Mo, Ru, Co, Ni, Ag, Sb, V, Zn, and Pb using AG1-X8/TK-201. The MDA of ^{99}Tc measured by LSC were calculated as 0.0342 Bq/L for AG1-X8/TEVA and 0.0378 Bq/L for AG1-X8/TK-201.

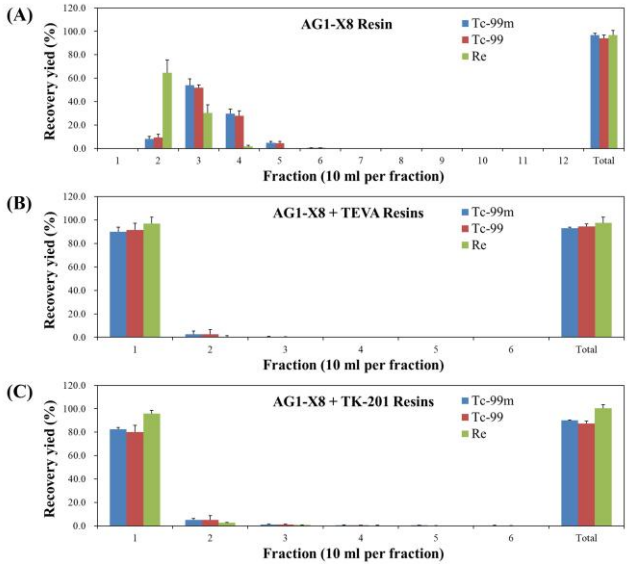


Fig. 2. The chromatograms for chemical yield of ^{99}Tc during the preconcentration and separation in seawater. (A) AG1-X8 resin, (B) AG1-X8/TEVA resin, (C) AG1-X8/TK-201 resin.

4. CONCLUSIONS

In this study, different tracers, including ^{99m}Tc and Re, were used to evaluate the chemical yield of ^{99}Tc during its preconcentration and separation from seawater using various resin systems, including AG1-X8/TEVA and AG1-X8/TK-201. Both tracers provided reliable and high chemical yields (>90%) for monitoring ^{99}Tc throughout the preconcentration and separation process. A radiochemical determination method for ^{99}Tc in seawater was successfully established based on resin-based preconcentration and separation techniques. These preliminary results lay a solid foundation for future large-volume seawater analyses of ^{99}Tc using either ICP-MS or LSC.

ACKNOWLEDGMENTS

This work was financially supported by the Environmental Radioactivity Network Center (ERAN) in Japan for a collaborative researcher grant (ERAN I-24-07) and Central Taiwan University of Science and Technology in Taiwan (CTU113-P003). We sincerely thank Dr. Kayo YANAGISAWA of the Research Group for Nuclear Chemistry, Nuclear Science and Engineering Center, Japan Atomic Energy Agency (JAEA), Ibaraki, Japan, for technical assistance and meaningful discussion.

References

[1] K. Shi, X. Hou, P. Roos, and W. Wu. Analytica Chimica Acta, 709, 1– 20 (2012).
[2] M. Matsueda, K. Yanagisawa, K. Koarai, M. Terashima, K. Fujiwara, H. Abe, A. Kitamura, and Y. Takagai. ACS Omega, 6, 19281−19290 (2021).
[3] Elsje M. van Es, H. Mohamud, B. Russell, O. Kivan, E. Ekebas, F. Falksohn, and A. Bombard. The 64th Conference on Radiobioassay & Radiochemical Measurements / 2019 Eichrom Workshop and Users group Meeting, 28 th October (2019).

Copyright on 7th Asia-Pacific Symposium on Radiochemistry 2025 - P2-06 -

7th Asia-Pacific Symposium on Radiochemistry *September 14 ~ 19, 2025 • Kunibiki Messe • Shimane, Japan*

Homogeneity and stability testing of carrier-free ^{135}Cs standard solution

Shiho Asai[1], Taiyo Tajima[2], Aya Sakaguchi[3], Yasushi Sato[1], and Katsuhiro Shirono[1]

[1] National Metrology Institute of Japan (NMIJ), National Institute of Advanced Industrial Science and Technology (AIST), Umezono 1-1-1, Tsukuba, Ibaraki 305-8563, Japan.
[2] Degree Programs in Pure and Applied Sciences, University of Tsukuba, 1-1-1 Tennodai, Tsukuba, Ibaraki 305-8577, Japan.
3 Center for Research in Isotopes and Environmental Dynamics, University of Tsukuba, 1-1-1 Tennodai, Tsukuba, Ibaraki 305-8577, Japan.

The ^{135}Cs Standard solution was prepared using a commercially available ^{137}Cs solution. The homogeneity and stability of the assigned values were evaluated in accordance with ISO 33405. The evaluation methods discussed here are applicable to a range of long-lived radionuclides.

1 INTRODUCTION

Long-lived radiocesium, ^{135}Cs, is produced alongside ^{137}Cs through uranium fission, and their fission yields are comparable. Notably, the ^{135}Cs/^{137}Cs molar ratio varies characteristically depending on the production source, making it valuable for identifying the origin of radioactivity contamination. However, the absence of reference materials for ^{135}Cs measurement results in insufficient reliability of the measured values. Establishing traceability to SI units is essential to ensure international comparability of these measurements.

This study focused on developing a ^{135}Cs standard solution by measuring Cs isotopes. In our previous work, we determined the mass fractions of Cs isotopes and the ^{135}Cs/^{137}Cs molar ratio in a ^{137}Cs solution that is readily accessible to general users. All assigned values are traceable to SI units, as the measurements were calibrated using certified reference materials, and the associated uncertainties were rigorously evaluated. This value-assigned ^{137}Cs (^{135}Cs) solution is useful for correcting mass discrimination in ^{135}Cs/^{137}Cs measurements performed by mass spectrometry. It can also serve as a calibration standard for quantifying ^{135}Cs.

To adjust the concentration to specifically ICP-MS measurements, the original ^{137}Cs solution was diluted and subdivided into ten separate solutions. Because these ten solutions must be treated equivalently, a between-bottle homogeneity study is crucial. Additionally, assessing the stability of the diluted ^{137}Cs (^{135}Cs) solution in accordance with ISO 33405 is important for determining its shelf life. To evaluate variation, we measured the mass fractions of Cs isotopes (^{133}Cs, ^{135}Cs, ^{137}Cs) and the molar ratios (^{137}Cs/^{133}Cs, ^{135}Cs/^{133}Cs, ^{135}Cs/^{137}Cs) and compared them to the initial values determined approximately one year ago.

2 EXPERIMENTAL

2.1 Determination of mass fractions of Cs isotopes and molar ratios

A solution containing ^{137}Cs (7.0×10^4 Bq/g), purchased from the Japan Radioisotope Association, was selected as the candidate material. This ^{137}Cs solution is characterized by being carrier-free, meaning it does not contain an excessive amount of stable Cs added for preservation purposes—an important feature for accurate Cs isotope ratio measurements by ICP-MS. Ten solutions were prepared from the original ^{137}Cs solution by gravimetric dilution and stored in HDPE bottles. To establish traceability to the SI, the mass fractions of ^{133}Cs and ^{137}Cs were individually determined using the respective certified standards: JCSS-labeled Cs standard solution and ^{137}Cs radioactivity standard solution. The ^{137}Cs radioactivity, approximately 70 Bq/g, in each diluted solution was measured by gamma spectrometry using the high-purity germanium detector (EG&G ORTEC, model GEM40P4-76). The ^{133}Cs mass fractions were determined by ICP-MS/MS (Agilent 8800s) operated in N_2O gas mode, which effectively eliminates isobaric interferences from ^{135}Ba and ^{137}Ba [1].

2.2 Assessment of homogeneity and stability in accordance with ISO 33405

Homogeneity (or inhomogeneity) is one of the major sources of uncertainty in the measurement results for the diluted ^{137}Cs (^{135}Cs) solutions. A one-way analysis of variance (ANOVA) was performed, following the formulas provided in ISO 33405, to evaluate between-bottle variation. The uncertainty of ^{137}Cs radioactivity, being the dominant contributor to overall uncertainty, was used in the ANOVA instead of the ^{135}Cs mass fraction, C_{135} [pg/g], which was calculated using the following equation:

$$C_{135} = C_{133} \times (I_{135}/ I_{133}) \times K_{135/133} \times (m_{135}/ m_{133}) \quad (1)$$

Here, C_{133} is the mass fraction of ^{133}Cs; I and m represent the net counts per second (cps) and the relative atomic mass of the Cs isotopes, respectively. The subscripts indicate the corresponding mass numbers. The mass discrimination correction factor $K_{135/133}$ for the ^{135}Cs/^{133}Cs ratio was estimated using $K_{137/133}$, which was calculated by dividing the molar ratio of ^{137}Cs/^{133}Cs by the net cps ratio of ^{137}Cs/^{133}Cs. The molar ratio of ^{137}Cs/^{133}Cs is equivalent to the ratio of their measured mass fractions. The standard uncertainty of the ^{137}Cs mass fraction (1.6%), which has the highest contribution, indirectly affects the uncertainty of the calculated ^{135}Cs mass fraction.

The initial values may be susceptible to storage conditions, given that the Cs isotope mass fractions range from 20 pg/g

Copyright on 7th Asia-Pacific Symposium on Radiochemistry 2025

to 70 pg/g over approximately one year. Therefore, stability was evaluated by remeasuring the Cs isotopes (^{133}Cs, ^{135}Cs, and ^{137}Cs) by ICP-MS, and the ^{137}Cs radioactivity by gamma spectrometry.

3 Results and Discussion

3.1 Homogeneity of subdivided solutions

ANOVA was performed using the results from two sets of ^{137}Cs radioactivity measurements in the diluted ^{137}Cs (^{135}Cs) solutions as follows:

$$s_{\mathrm{bu}}^2 = (M_{\mathrm{between}} - M_{\mathrm{within}})/n_0 \quad (2)$$

$$u'_{\mathrm{bu}} = \sqrt{M_{\mathrm{within}}/n_0} \cdot \sqrt[4]{2/\nu_{\mathrm{within}}} \quad (3)$$

In these equations, s_{bu}^2 , M_{between}, M_{within}, and n_0, represent the between-bottle component variance, mean square between bottles, mean square within bottles, and the number of replicates (two), respectively. u'_{bb} is the uncertainty associated with inhomogeneity and ν_{within}, denotes the effective degrees of freedom. In this case, M_{between} (68.12) was smaller than M_{within} (212.37) due to the high repeatability standard deviation. According to ISO 33405 (C.6), u'_{bu} was adopted as the upper limit for the between-bottle variation, instead of s_{ub}.

The resulting relative uncertainty associated with inhomogeneity was calculated to be 0.65 %. The between-bottle variation of ^{137}Cs/^{133}Cs molar ratio was also evaluated in the same manner. The relative value of s_{bu} was 0.013 %, which was adopted as homogeneity between bottles of Cs molar ratio.

3.2 Stability for assigned values over one year

The long-term stability of the diluted ^{137}Cs (^{135}Cs) solutions was evaluated by measuring the Cs isotopes approximately one year after the initial value assignment (storage period: 31 January 2024 to 10 December 2024). This was performed to observe significant trends in the measured data by applying the trend analysis described in ISO 33405. The measured ^{135}Cs mass fraction was 21.82 pg/g, which agrees well with the initial value of 21.62 pg/g ± 0.76 pg/g (k=2). The mass fractions of ^{133}Cs and ^{137}Cs are also considered constant over one year. For the ^{135}Cs/^{137}Cs ratio, the measurement results of 1.015 with decay correction remained unchanged from the initial value of 1.008 ± 0.048 (k =2) as of January 31, 2024. Consequently, the mass fraction of ^{135}Cs and the ^{135}Cs/^{137}Cs ratio are considered not to be unstable. This suggests that the effects of contamination and adsorption on the inner walls of the bottle are negligible. The uncertainty budgets are summarized in Tables 1 and 2.

Table 1 Uncertainty budget of ^{135}Cs/^{137}Cs molar ratio

Source of uncertainty	Relative standard uncertainty	Contribution rate
^{135}Cs/^{137}Cs measured molar ratio	2.43 %	93.21 %
Homogeneity	< 0.01 %	< 0.01 %
Stability	0.58 %	5.36 %
Concentration factor	0.30 %	1.43 %
Relative combined standard uncertainty: 2.51 %		
^{135}Cs/^{137}Cs molar ratio 1.008 ± 0.051 (k=2)		

* Reference time: 1200 JST, 31 January, 2024

Table 2 Uncertainty budget of ^{135}Cs mass fraction

Source of uncertainty	Relative standard uncertainty	Contribution rate
^{135}Cs measured mass fraction	1.75 %	70.55 %
Homogeneity	0.65 %	9.58 %
Stability	0.88 %	17.80 %
Concentration factor	0.30 %	2.06 %
Relative combined standard uncertainty: 2.09 %		
^{135}Cs mass fraction 21.62 ± 0.90 pg/g (k=2)		

* Reference time: 1200 JST, 31 January, 2024

4. CONCLUSIONS

Ten Cs isotope standard solutions were prepared for distribution to general users, and property values—including Cs isotope ratios and mass fractions—were assigned. In accordance with ISO 33405, homogeneity was evaluated to ensure that all ten solutions have coherent values. Additionally, the long-term stability of these values was assessed to monitor any variation during the storage period. Measurement results obtained after approximately one year showed no significant changes from the initial values, confirming that the solutions remain sufficiently stable for at least one year. Stability monitoring will continue for at least one more years. The uncertainty evaluation approaches discussed here are not limited to Cs isotope measurement but be applicable to various long-lived radionuclides.

ACKNOWLEDGMENTS

I express my deepest appreciation to Dr. Jin for his invaluable support throughout this study. I would also like to offer special thanks to Dr. Miura, who provided insightful comments and expertise on ^{135}Cs analysis. This work was financially supported by ERAN (Environmental Radioactivity Research Network Center, F21-12, F22-13)

Reference

[1] S. Asai, T. Tajima, A. Sakaguchi, Y. Sato, H. Harano, K. Shirono, SI-traceable quantification of ^{135}Cs in ^{137}Cs solution for ^{135}Cs standardization, *J. Anal. At. Spectrom.*, **40**, 679, 2025.

7th Asia-Pacific Symposium on Radiochemistry *September 14 ~ 19, 2025 • Kunibiki Messe • Shimane, Japan*

Investigation of curium isotope measurements by mass spectrometry

Yuya Kasuga[1], Kazuaki Tsukada[2], Masato Asai[4], Yuichi Takaku[3],
Shinya Yamasaki[3], Yudai Shigekawa[3], Keisuke Sueki[3], Aya Sakaguchi[3]

[1] *Graduate School of Science and Technology Degree Programs in Pure and Applied Sciences Master's Program in chemistry, University of Tsukuba, Japan*
[2] *Research Center for Accelerator and Radioisotope Science (RARiS), Tohoku university*
[3] *Institute of Pure and Applied Sciences, University of Tsukuba, Japan*
[4] *Advanced Science Research Center Japan Atomic Energy Agency Tokai, Ibaraki 319-1195 Japan*

In this study, with the aim of establishing mass spectrometry for curium isotopes in the environment, (1) the production of Cm spike milked from the used neutron source ^{252}Cf and (2) the separation of Am and Cm fractions were addressed. The separation of Cm from Cf was expected to be feasible in real samples, while the complete separation of Am and Cm required further investigation.

1 Introduction

Curium (Cm) isotopes are estimated to be the largest radioactive contribution among the actinides released from the Fukushima Daiichi Nuclear Power Plant accident. However, only one detailed study on Cm from the nuclear accident has been reported [1]. So far, α-spectrometry has been used for the measurement of Cm isotopes in the environment. However, the chemical separation for Cm α-spectrometry is very complicated, and the α-ray energies of ^{243}Cm and ^{244}Cm are so close that they cannot be measured separately. Furthermore, the absence of a Cm spike is another problem. Instead of it, americium (^{243}Am), which is thought to behave similarly to Cm, has been used as a spike for Cm measurements. In this situation, we aimed to establish a mass spectrometry for Cm analysis by developing a Cm spike and a simplified chemical separation method which can be applied to the rapid processing of large numbers of samples, particularly relevant in emergency response scenarios. In this study, we investigated (1) the preparation of the Cm spike for mass spectrometry and (2) the establishment of an efficient chemical separation procedure for Am and Cm.

2 Materials and Method

2.1 Cm spike production

Californium-252 (^{252}Cf, $T_{1/2}$=2.65 y), which is used as a neutron source in various instruments, produces the long half-life nuclide ^{248}Cm ($T_{1/2}$=3.40×10^5 y) by α decay. We focus on the ^{248}Cm as a candidate spike for the measurement of Cm isotopes and attempt to separate and purify ^{248}Cm from the used ^{252}Cf neutron source. Appropriate separation conditions were investigated using Ln® resin (Eichrom Technologies) which is the solid-extraction resin with di(2ethylhexyl) orthophosphoric acid as extractant. In this experiment, Sm and Gd were used as analogue elements of Cm and Cf [2]. The investigations were conducted at room temperature and 50 ℃ using different concentrations of nitric acid (0.3 M, 0.4 M and 0.5 M) of sample and eluent. Based on the results of the analogue experiments, separation experiments for Cm and Cf were carried out using ^{244}Cm and ^{252}Cf radiotracers.

2.2 Separation of Am-Cm

In the mass spectrometry of Cm isotopes, Am isotopes must be separated from the Cm isotope due to the isobaric interference of ^{243}Am with ^{243}Cm. In order to investigate the appropriate conditions for the separation of Am and Cm, Nd and Sm were used as analogue elements [2] and separation experiments were conducted under the same separation system as the Cf–Cm experiments, using Ln resin and nitric acid eluents at concentrations of 0.3 M, 0.4 M, and 0.5 M, at both room temperature and 50 °C. Based on the results of the analogue experiments, separation experiments were conducted using ^{241}Am and ^{244}Cm.

3 Results and Discussion

3.1 Cm spike creation

In the analogue experiments with Sm and Gd, the best separation was achieved under conditions using 0.4 M nitric acid as eluent under room temperature. In the Cm-Cf separation, Cm was completely separated from Cf at all nitric acid concentrations and temperature conditions. Considering the simplicity of the operation and the large difference in elution time between Cm and Cf, the optimum condition was found to be 0.4 M nitric acid at room temperature (Fig.1a). The application of this condition to the separation process suggests the possibility of efficiently obtaining the spike candidate ^{248}Cm from the ^{252}Cf neutron source.

3.2 Separation of Am-Cm

Copyright on 7th Asia-Pacific Symposium on Radiochemistry 2025- P2-08* -

In analogue experiments with Nd and Sm, the most efficient separation was achieved under 0.4 M nitric acid at 50 ℃ using the Ln resin. However, not only the condition under which the separation was successful for these analogue elements (0.4 M nitric acid, 50 ℃), but also any of the other conditions (0.3 M or 0.5 M nitric acid, room temperature or 50 ℃) could not separate Am and Cm. (Fig.1b). This may be because the difference between the distribution coefficients of Am and Cm on the Ln resin was smaller than that expected from the analogue element experiments.

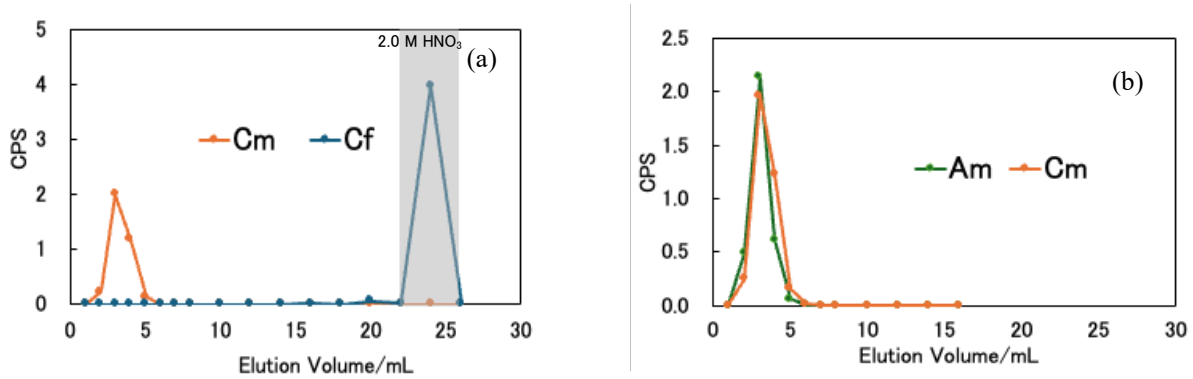


Figure 1 (a) Elution curves of Cm and Cf under the condition of 0.4 M HNO_3 at 50 ℃ (b) Elution curves of Am and Cm under the condition of 0.4 M HNO_3 at 50 ℃

4. CONCLUSIONS

The optimum conditions for the separation of Cm from Cf were found to be 0.4 M nitric acid elution at room temperature, suggesting that ^{248}Cm could be efficiently recovered from a ^{252}Cf neutron source. However, Am and Cm could not be separated under any of the conditions used in this study. Further studies using different resins and eluents are needed to improve the separation of Am and Cm.

ACKNOWLEDGMENTS

This work was partly supported by JST FOREST program, Grant No. JPMJFR231D.

References

[1] M. Yamamoto, et al, J. Environ. Radioact. 132 (2014) 31-46.
[2] E.P. Horwitz and C.A.A. Bloomquist, J. Inorg. Nucl. Chem. 37 (1975) 425.

Copyright on 7th Asia-Pacific Symposium on Radiochemistry 2025- P2-08* -

Synthesis of Neptunium Isotopes via the ^{238}U+p Reaction for the Production of the Np Spike

Nami Matsuzawa[1], Hayato Ogawa[2], Akihiko Yokoyama[3], Hiromitsu Haba[4], Yudai Shigekawa[4,5], Akihiro Nambu[4], Yousuke Kanayama[4], Hiromichi Shimizu[4], Yuichi Takaku[5], Shinya Yamasaki[5], Keisuke Sueki[5], Aya Sakaguchi[5]

[1] Graduate School of Science and Technology, Degree Programs in Pure and Applied Sciences, Master's Program in Chemistry, University of Tsukuba, Japan
[2] Graduate School of Science and Technology, Degree Programs in Life and Earth Sciences, Master's Program in Environmental Sciences, University of Tsukuba, Japan
[3] Institute of Science and Engineering, Kanazawa University, Japan
[4] Nishina Center for Accelerator-Based Science, RIKEN, Wako, Japan
[5] Institute of Pure and Applied Sciences, University of Tsukuba, Japan

The ultimate goal of this study is to produce a "spike" for mass spectrometry of neptunium-237 (^{237}Np). To produce the spike candidate nuclide, ^{236g}Np, an irradiation experiment for the ^{238}U+p reaction was conducted. The byproduct gamma emitter Np nuclides ^{236m}Np, ^{238}Np, and ^{239}Np were measured by gamma-spectrometry after appropriate chemical separation, and the cross sections of these radionuclides were determined. From these results, it can be concluded that the spike candidate ^{236g}Np should be also produced by this reaction.

1 Introduction

The long-lived anthropogenic radionuclide neptunium-237 (^{237}Np, $T_{1/2}$ = 2.14×10^6 years) has been released into the surface environment [1] , due to various human nuclear activities. Recent improvements in mass spectrometry technology and chemical separation techniques have enabled the detection of very low levels of ^{237}Np in the environment. However, accurate/precise quantification of ^{237}Np by mass spectrometry is currently difficult due to the absence of "spike", which is essential for correcting chemical separation yield and instrumental analytical uncertainties. The aim of this study is to produce the long-lived Np isotope ^{236g}Np ($T_{1/2}$ = 1.55×10^5 years), which could serve as a spike for ^{237}Np measurement, using the ^{238}U(p,3n)^{236}Np reaction, with the final goal of establishing an accurate/precise quantification method of ^{237}Np in the environment by mass spectrometry. Here, we focused on quantification of gamma-ray emitting Np isotopes synthesised in the ^{238}U+p reaction in order to investigate the optimal irradiation conditions and to understand the details of the ^{238}U+p nuclear reaction. For this purpose, a chemical separation method for Np from irradiated samples was established, and the nuclear reaction cross section was obtained for each gamma emitting Np isotope produced in the ^{238}U+p reaction.

2 Experiments

2.1 Establishment of Chemical Separation Method

A simulated irradiation sample was prepared by adding a known amount of short-lived ^{239}Np to a nitric acid solution containing 0.78 mg of ^{238}U. After addition of $K_2S_2O_5$ and $TiCl_3$ to the sample for reducing ^{239}Np, U was separated using an anion exchange resin AG® MP-1M. The ^{239}Np adsorbed on the resin was then eluted with a mixture of hydrobromic acid and hydrofluoric acid. The ^{239}Np and ^{238}U in the eluate were measured using a Ge semiconductor detector and ICP-MS, respectively. The recovery rate of Np and the decontamination factor of U were estimated using the measurement results. The above chemical separation method was developed on the basis of the method reported previously [2].

2.2 Irradiation Experiment

^{238}U targets were prepared by the electrodeposition of U from a 2-propanol solution of natural U, containing 0.446 mg/g of ^{238}U, onto an Al foil (400 V, 15 minutes) [3]. A stack target was assembled using the U targets, Al foils, and Ta foils, and irradiated with a proton beam of approximately 30 MeV for one hour at RIKEN. After dissolving the irradiated sample in nitric acid, U and fission products were removed using the method established in this study and the Np isotopes were isolated. The eluate samples were measured using a Ge semiconductor detector to determine the synthesised Np isotopes. The ^{238}Np from the ^{238}U+p reaction was used to correct the recovery rate in the chemical separation of Np isotopes.

3. Results and Discussion

In the established separation method, the recovery rate of ^{239}Np was estimated as 76 ± 12 %, and a high decontamination factor of 10^5 for ^{238}U was achieved.

In the actual irradiation experiment, the recovery rate of Np isotopes in chemical separation ranged from 68.0% to 80.1%. The radioactivity of the Np isotopes produced by the irradiation experiment was identified from the gamma-ray measurement together with the recovery rates. This is the first time we have succeeded in measuring ^{236m}Np gamma rays

Copyright on 7th Asia-Pacific Symposium on Radiochemistry 2025- P2-09* -

directly in the samples obtained from the U+p reaction. The synthesis of ^{238}Np and ^{239}Np by the ^{238}U+p reaction was also observed. The calculated nuclear reaction cross sections were shown in Figure 1.

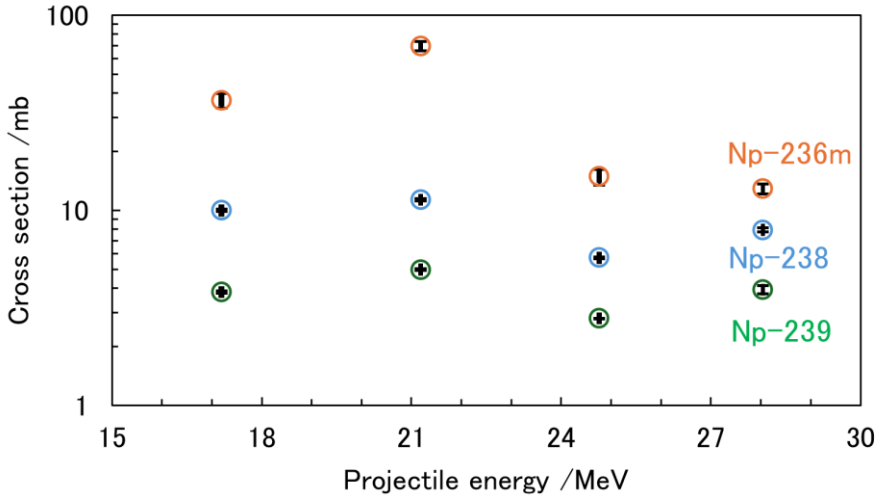


Fig. 1. Nuclear reaction cross sections of gamma-emitting Np isotopes produced by the ^{238}U+p reaction

The cross sections at irradiation energies from 17.2 - 29.6 MeV were 12.9 – 69.5 mb for ^{236m}Np, 5.7 – 11.3 mb for ^{238}Np, and 2.8 – 5.0 mb for ^{239}Np. The isotopic composition of the Np isotopes measured in this study suggests that the spike candidate, ^{236g}Np, may also have been synthesized. For ^{236g}Np and ^{237}Np, which could not be measured by gamma-ray measurements, we plan to measure the samples by ICP-MS after appropriate chemical separations. Their nuclear reaction cross sections will then be obtained from the results.

4. Conclusion

In this study, we succeeded for the first time in directly measuring the gamma-ray-emitting Np isotopes produced in the ^{238}U+p nuclear reaction, and obtained the nuclear reaction cross section.

ACKNOWLEDGMENTS

This work was partly supported by JST FOREST program, Grant No. JPMJFR231D.

References

[1] P. Thakur and G. P. Mulholland, "Determination of ^{237}Np in environmental and nuclear samples: A review of the analytical method," *Applied Radiation and Isotopes*, **70**, 1747–1778 (2012).
[2] S. Zhang *et al.* "Rapid Method To Determine ^{137}Cs, ^{237}Np, and Pu Isotopes in Seawater by SF-ICP-MS," *Anal. Chem.* **95**, 16892–16901 (2023).
[3] W. Parker, H. Bildstein & N. Getoff, "Quantitative Electrodeposition of Thorium and Uranium," *Nature* **200**, 457–458 (1963).

Copyright on 7th Asia-Pacific Symposium on Radiochemistry 2025- P2-09* -

Poster Presentation | [R1]Nuclear Chemistry

Tue. Sep 16, 2025 6:30 PM - 8:00 PM JST | Tue. Sep 16, 2025 9:30 AM - 11:00 AM UTC Poster

[Poster] R1

[P-R1-01*]

Experimental and theoretical study on the coloration of the red uranyl nitrate thiourea complex

*So Hashiba[1], Hiroyuki Kazama[1], Masashi Kaneko[1], Ryoutarou Masuda[1], Kosuke Misawa[1], Yoshitaka Kasamatsu[1] (1. Graduate School of Science, The University of Osaka (Japan))

[P-R1-02]

Design and Synthesis of Tertiary Amine–Bridged Bis(picolinate) Ligands for Chemical State Control of U-235m

*Hiroyuki Kazama[1], So Hashiba[1], Kazushi Kawamoto[1], Kosuke Misawa[1], Ryotaro Masuda[1], Terumi Yokoyama[1], Ryota Kikuchi[1], Masashi Kaneko[1], Yoshitaka Kasamatsu[1] (1. The University of Osaka (Japan))

[P-R1-03*]

Synthesis and structual analysis of $\{(n\text{-}C_mH_{2m+1})_4N\}_2[Th(NO_3)_6]$

*Kosuke Misawa[1], Hiroyuki Kazama[1], Masashi Kaneko[1], Ryoutarou Masuda[1], So Hashiba[1], Koji Yoshimura[2], Yoshitaka Kasamatsu[1] (1. The University of Osaka (Japan), 2. Okayama University (Japan))

[P-R1-04]

Preparation of Simulated MOX Ceramic Nuclear Fuel Microspheres by Microwave-assisted Internal Gelation Process

*WEI TIAN[1], Fangli Fan, Zhi Qin (1. Institute of Modern physics (China))

[P-R1-05]

Radiation-Tolerant Graphene Oxide-Carbon Quantum Dots Composite Membrane for Actinium-225 Solution deacidification

*Jing Bai[1], Baitong Zhang[1], Zhigang Ning[1], Qinggang Huang[1] (1. INSTITUTE OF MODERN PHYSICS, CHINESE ACADEMY OF SCIENCES (China))

[P-R1-06*]

Verification of Excitation Functions in Fast Neutron Induced Reactions Using Activation Method

*Shoma Tsuruta[1], Shinichi Goto[1], Yasuhide Cho[1], Hidetoshi Kikunaga[2] (1. Niigata University (Japan), 2. Tohoku University (Japan))

[P-R1-07]

THICK TARGET YIELD NORMALISED PER ACCELERATED PARTICLE

*Hidetoshi Kikunaga[1], Shin'ichi Goto[2] (1. Research Center for Accelerator and Radioisotope Science, Tohoku University (Japan), 2. Graduate School of Science and Technology, Niigata University (Japan))

[P-R1-08]

Production of carrier-free ^{182}Ta tracer via photonuclear reaction

*Takuya Yokokita[1], Yuki Honda[1], Hidetoshi Kikunaga[1] (1. Tohoku University (Japan))

©APSORC25

[P-R1-09*]

Study of Lu-DOTA using Lu-177 produced by photonuclear reaction

*Miona Tofuku[1], Kazuhiko Akiyama[1], Hidetoshi Kikunaga[2], Shiro Kubuki[1] (1. Tokyo Metropolitan University (Japan), 2. Research Center for Accelerator and Radioisotope Science (Japan))

[P-R1-10]

Production of non-carrier added ^{7}Be by the ^{nat}Li(d,x)^{7}Be reaction

*Akihiro Nambu[1], Hiromichi Shimizu[1], Yousuke Kanayama[1], Yudai Shigekawa[1], Sayantani Mitra[1], Hiromitsu Haba[1] (1. RIKEN Nishina Center for Accelerator-Based Science (Japan))

[P-R1-11*]

Improving the Purity of ^{225}Ac from Thorium Spallation at TRIUMF for Targeted Alpha Therapy Applications

*Elena Timakova[1,2], Eleanor Dunling[1], Justin Bailey[1], Paul Schaffer[1,3,4], Cornelia Hoehr[1,5] (1. Life Sciences, TRIUMF (Canada), 2. Physics, University of British Columbia (Canada), 3. Radiology, University of British Columbia (Canada), 4. Chemistry, Simon Fraser University (Canada), 5. Physics, University of Victoria (Canada))

[P-R1-12]

Optimizing temperature conditions for efficient Zn/Cu thermal separation in ^{64,67}Cu production

*Naoki Takashima[1], Masako Kawabata[1], Akio Ohta[1], Shoji Motoishi[1], Hideya Saeki[1], Yasuki Nagai[1], Yasuhiro Koguchi[1], Kazuyuki Hashimoto[2], Shunsuke Fujino[2], Masatoshi Itoh[3], Hidetoshi Kikunaga[3], Kazuaki Tsukada[3] (1. Chiyoda Technol Corporation (Japan), 2. Japan Atomic Energy Agency (Japan), 3. Tohoku University (Japan))

[P-R1-13*]

Production and separation of ^{149}Tb by the ^{133}Cs + ^{20}Ne reaction

*Yasuhito Kawakami[1], Shin-ichi Goto[1], Masato Asai[2], Tetsuya Kaneko Sato[2], Kazuaki Tsukada[4], Yuta Ito[3], Ichiro Nishinaka[5] (1. Niigata University (Japan), 2. JAEA (Japan), 3. KEK (Japan), 4. RARiS (Japan), 5. QST (Japan))

[P-R1-14]

OPTIMIZING BEAM TRANSPORT AND TARGET THICKNESS FOR 1-30 KEV MUON STOPPING POWER STUDIES

*Ayato Miura[1], Kazuhiko Ninomiya[2], Makoto Inagaki[3], Sohtaro Kanda[4], Yutaka Ikedo[4], Yu Oishi[4], Koichiro Shimomura[4], Yuga Nakazawa[5], Takashi Yoshimura[1] (1. The University of Osaka (Japan), 2. Hiroshima University (Japan), 3. Kyoto University (Japan), 4. Institute of Materials Structure Science, KEK (Japan), 5. Accelerator Laboratory, KEK (Japan))

[P-R1-15*]

ADSORPTION EXPERIMENTS OF MONOVALENT CATIONS ONTO FERROCYANIDE CRYSTALS: TOWARD ELUCIDATING THE CHEMICAL PROPERTIES OF FRANCIUM

*Hiroki Nakada[1], Yoshitaka Kasamatsu[2], Koichi Takamiya[1] (1. Kyoto University (Japan), 2. Osaka University (Japan))

[P-R1-16]

Development of a Functionalized Surface for Alpha-particle Detectors for Use in Liquid Phase

*Ryo Otani[1], Tetsuya K. Sato[1,2], Erina Takeuchi[1], Yuta Miyachi[1,2], Hina Natori[1,2], Maki Honda[1], Yuichiro Nagame[1] (1. Japan Atomic Energy Agency (Japan), 2. Ibaraki University (Japan))

[P-R1-17]

©APSORC25

Detector calibration for Si detector by using a light emitting diode

*Toshitaka Niwase[1], Tomoki Fujii[1] (1. Kyushu University (Japan))

[P-R1-18*]

Determination of γ-ray intensity of ^{196m2}Au and 263.8-keV transition

*Yasuhide Cho[1], Shin-ichi Goto[1], Masato Asai[2], Tetsuya Sato[2], Yuta Ito[3], Kazuaki Tsukada[4], Hidetoshi Kikunaga[4] (1. Graduate School of Science Technology, Niigata University (Japan), 2. JAEA (Japan), 3. WNCS, KEK (Japan), 4. RARiS, Tohoku University (Japan))

©APSORC25

EXPERIMENTAL AND THEORETICAL STUDY ON THE COLORATION OF THE RED URANYL NITRATE THIOUREA COMPLEX

So Hashiba[1], Hiroyuki Kazama[1], Masashi Kaneko[1], Ryoutarou Masuda[1], Kosuke Misawa[1], Yoshitaka Kasamatsu[1]

[1]*Graduate School of Science, The University of Osaka: 1-1 Machikaneyama, Toyonaka, Osaka, 560-0043*
hashibas23@chem.sci.osaka-u.ac.jp

Although color of uranyl (UO_2^{2+}) compounds is typically yellow, that of some compounds is orange or red. The reason for the difference of color has been considered the appearance of new absorption band owing to LMCT transition from equator ligands to uranium 5f orbitals. However, the reason or the condition for the origin of such LMCT bands is not understood theoretically. In this work, a newly synthesized red uranyl nitrate complex with the thiourea derivative was reported. UV-VIS spectra in solution obtained for the thiourea complex and the corresponding urea derivative complex reflected the difference of color between them. TDDFT calculations were conducted for these complexes to elucidate the nature of the absorption. DOS analysis suggests that the specific bonding orbital between uranyl and thiourea causes the peculiar color.

1 INTRODUCTION

Hexavalent uranyl (UO_2^{2+}) complexes consist of a linear uranyl unit and several ligands. The equator plane of uranyl is surrounded by the donor atoms of ligands. Color of uranyl compounds is normally yellow due to an absorption band assigned to ligand-to-metal charge transfer (LMCT) between uranyl oxygen and U 5f orbitals. It is known that the color of some complexes with electron-donating equator ligands is orange or red [1-3]. This coloration is due to the appearance of absorption bands corresponding to LMCT transition between U 5f orbital and equator ligands [1]. However, the origin of these transition was not discussed theoretically. Elucidating the mechanism of the color difference in detail is of interest both from a scientific point of view and the application to the photochemistry of uranium, such as photocatalysis. Understanding the photochemical properties of uranium is expected to lead to new applications of ever-increasing depleted uranium.

In this work, we focused on the complex of uranyl nitrate with thiourea derivatives. Although some of these complexes have been reported to show red or orange colors in the literature [2], their crystal structures or the reason for the peculiar color have not been clarified. In this study, we investigated the structure and absorption spectra of a newly reported complex with thiourea derivatives, 1,3-dimethylpropylenethiourea (DMPT), and a known complex with urea derivatives, 1,3-dimethylpropyleneurea (DMPU) [4], as shown in Figure 1. By comparing the photochemical property of the O-donating complex and the S-donating complex, the mechanism of the color difference is discussed both experimentally and theoretically.

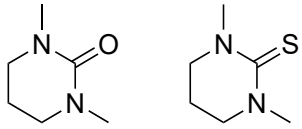


Fig. 1 Structure of DMPU (left) and DMPT (right).

2. EXPERIMENTAL

DMPT was synthesized with the known procedure [5], reacting DMPU with Lawesson's reagent. DMPU and other reagents were purchased and used as received. The complexes were prepared by mixing uranyl nitrate hexahydrate with the corresponding (thio)urea compounds at a 1:3 ratio in ethanol. Then, the solutions were set undisturbed to slowly evaporate solvents. After several days, yellow crystals of $UO_2(NO_3)_2(DMPU)_2$ (**1**) and red crystals of $UO_2(NO_3)_2(DMPT)_2$ (**2**) were obtained. The structures of **1** and **2** were determined by single crystal X-ray diffraction (scXRD). The scXRD measurements were carried out at 173 K using a RIGAKU XtaLAB Synergy Custom spectrometer irradiating Mo Kα X-ray. The structures were solved and refined using SHELX programs through Olex2 software.

The optical properties of the complexes were experimentally investigated via UV-VIS spectroscopy in solutions. Samples were dissolved in 1,2-dichloroethane and filled in glass cells. Spectra were obtained with JASCO V-760 spectrometer.

Theoretical investigations were conducted by density functional theory (DFT) calculations using ORCA version 6.0.0. Geometry optimization and subsequent vibrational frequency calculation of **1** and **2** were performed with PBE0 functional and zeroth-order regular approximation (ZORA) Hamiltonian. SARC-ZORA-TZVP all-electron relativistically contracted basis sets were used for U and ZORA-def2-TZVP basis sets for the other atoms (C, H, O, N, S). Single point and time-dependent DFT (TDDFT) calculations were performed with PBE0 functional and Douglas-Kroll-Hess (DKH2) Hamiltonian with SARC-DKH-TZVPP and DKH-def2-TZVPP basis sets for U and the other atoms, respectively. Solvation effect of 1,2-dichloroethane was considered with conductor like polarizable continuum model (CPCM).

Copyright on 7th Asia-Pacific Symposium on Radiochemistry 2025

3. RESULTS AND DISCUSSION

ORTEP view of a single molecule of **2** is shown in Figure 2. The equator plane of uranyl ion is occupied with four O atoms from two bidentate nitrate and two S atoms from thioureas at the *trans* position. The complex has an inversion center. This is a typical molecular structure for uranyl nitrate with neutral ligands L. Compared to **1**, **2** has a similar structure but the bond angle consisting of U1-S1=C1, 104.46(12)°, is quite different from the corresponding angle of **1**, 139.7(6)° due to the change in the degree of sp^2 hybridization between carbonyl O and thiocarbonyl S.

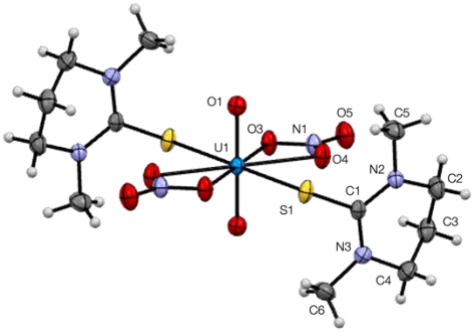


Fig. 2. ORTEP view of **2**

UV-VIS absorption spectra of **1** and **2** in 1,2-dichloroethane are shown in Figure 3. In the spectrum of **2**, there are dull absorption bands between 450 nm to 550 nm while not observed in that of **1**. The difference of color between **1** and **2** is considered to derives from the occurrence of this band in the spectrum of **2**.

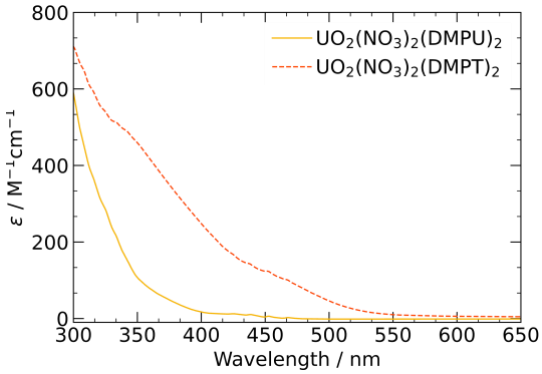


Fig. 3. Experimental UV-VIS absorption spectra of **1** and **2**

Optimized structures of **1** and **2** obtained by DFT calculation were agreed with experimental structures. **2** had no imaginary modes and **1** had weak (<-50 cm^{-1}) imaginary vibrations; however, they were acceptable.

Figure 4 shows calculated UV-VIS spectra with optimized structures using TDDFT calculation. The spectra roughly agree with experimental spectra; only spectrum for **2** has an absorption band at near 450 nm**.** Population analysis revealed that this transition corresponds to LMCT transition from thiocarbonyl π orbital to U 5f, and there was no counterpart in **1**.

To investigate the nature of these orbitals, density of states (DOS) analysis was performed. Partial DOS (PDOS) of U 6d orbitals and overlap population of DOS (OPDOS) between U 6d and carbonyl O or thiocarbonyl S reveals that only **2** has strong bonding orbitals between S and U. The bonding orbitals were distributed in HOMO region and assigned to the initial states of the absorption near 450 nm. The reason why such orbitals only exist in **2** is the energy level of the π orbital of the DMPT ligand was at a higher energy than that of the DMPU ligand, which allowed a covalent interaction with the empty 6d orbital of uranium at higher energy.

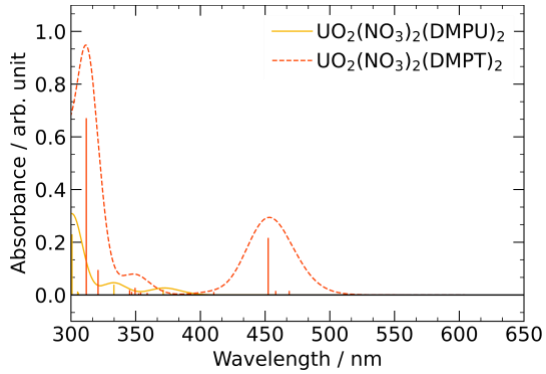


Fig. 4. Calculated UV-VIS absorption spectra of **1** and **2**

4. CONCLUSION

In this study, the molecular structure of "red" uranyl nitrate complex with thiourea derivatives, $UO_2(NO_3)_2(DMPT)_2$ (**2**) has been determined by scXRD measurement. The obtained structure was similar to that of "yellow" urea complex, $UO_2(NO_3)_2(DMPU)_2$ (**1**). The UV-VIS spectrum of **2** reveals that the difference of the color between **1** and **2** was caused by the absorption band near 450 nm, and the result was reproduced theoretically. Population analysis and DOS analysis revealed that the existence of this band in **2** originates from the bonding orbitals between U 6d orbitals and S-donor ligand π orbitals, which is not observed in **1**.

ACKNOWLEDGMENTS

This work was the result of using research equipment shared in MEXT Project for promoting public utilization of advanced research infrastructure（Program for supporting construction of core facilities）Grant Numbers JPMXS0441200024 and JPMXS0441200025. This work was supported by JST, CREST Grant Number JPJCR24I6, Japan and JSPS KAKENHI Grant Number JP21H00473.

References

[1] M. A. SILVER, *et al.*, *Inorg. Chem.*, **54**, 5280 (2015)
[2] A. O. BAGHLAF, *et al.*, *Polyhedron*, **4**, 853 (1985)
[3] S. P. KELLEY, *et al.*, *Inorg. Chem.*, **59**, 2861 (2020)
[4] T. SUZUKI, *et al.*, *Acta Cryst.*, **67**, m18 (2011)
[5] V. IASHIN, *et al., Chem. Eur. J.,* **26**, 13873 (2020)

7th Asia-Pacific Symposium on Radiochemistry *September 14 ~ 19, 2025 • Kunibiki Messe • Shimane, Japan*

Design and Synthesis of Tertiary Amine–Bridged Bis(picolinate) Ligands for Chemical State Control of U-235m

Hiroyuki Kazama[1], So Hashiba[1], Kazushi Kawamoto[1], Kosuke Misawa[1], Ryotaro Masuda[1], Terumi Yokoyama[1], Ryota Kikuchi[1], Masashi Kaneko[1], Yoshitaka Kasamatsu[1]

[1]*Graduate School of Science, The University of Osaka: 1-1 Machikaneyama, Toyonaka, Osaka, 560-0043*
kazama.hiroyuki@chem.sci.osaka-u.ac.jp

U-235m is a nuclear isomer with an exceptionally low excitation energy, and its decay behavior is strongly influenced by the chemical environment. In this study, novel pentadentate bis(picolinate) ligands were synthesized that coordinate in a planar equatorial geometry characteristic of uranyl ions. These ligands were designed to modulate the electronic structure of uranium through coordination and to investigate the resulting effects on nuclear decay.

1 INTRODUCTION

U-235m is a nuclear isomer with an exceptionally low excitation energy of 76.8 eV and primarily decays via internal conversion. Since this deexcitation process involves interactions between the nucleus and outer-shell electrons, the decay constant varies depending on the chemical environment[1]. To better understand the chemical effects on the decay of U-235m, it is crucial to measure its decay constants and internal conversion electron spectra in various chemical states. In this study, we propose a novel approach to controlling the chemical state of U-235m using organic chelating ligands. Focusing on a tertiary amine-based scaffold bearing two picolinate arms and a phenyl substituent, we designed a ligand system suitable for the equatorial pentadentate coordination characteristic of uranyl ions (Fig.1). By varying the electronic properties of the phenyl substituent, the ligands are expected to enable systematic modulation of the electronic structure of the resulting uranium complexes. As a first step, we synthesized a chelating ligand bearing a methyl-substituted phenyl group towards controlling the electronic environment of U-235m through coordination chemistry.

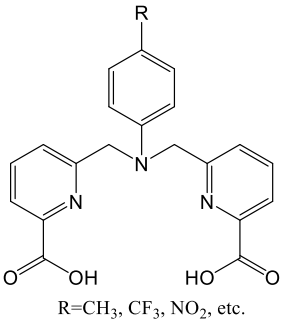


Fig. 1. Schematic structure of new ligand.

1.1 EXPERIMENTAL

Tertiary amine–bridged bis(picolinate) ligands were synthesized in two steps. First, two equivalents of methyl 6-(chloromethyl)picolinate were reacted with one equivalent of *p*-toluidine under basic reflux conditions to afford dimethyl 6,6'-((*p*-tolylazanediyl)bis(methylene))dipicolinate (compound 1). Compound 1 was then hydrolysed under acidic or basic reflux conditions to yield 6,6'-((*p*-tolylazanediyl)bis(methylene))dipicolinic acid (compound 2). The synthesized compounds were characterized by ^{1}H NMR and ESI-MS.

1.2 RESULTS AND DISCUSSION

The precursor, compound 1, was obtained in 88.2% yield. The ^{1}H NMR signals were fully assigned to the expected structure, confirming that the compound was obtained in high purity. The hydrolysed product, compound 2, was found to undergo partial decomposition. Further optimization of the hydrolysis conditions and purification procedures will be carried out to improve the overall synthetic route.

2. CONCLUSIONS

In this study, we proposed a ligand design strategy for controlling the chemical state of U-235m via coordination chemistry. A tertiary amine–bridged bis(picolinate) ligand bearing a methyl-substituted phenyl group was synthesized via a two-step process involving nucleophilic substitution and subsequent ester hydrolysis. The optimized synthetic protocol, detailed characterization of the ligand, and the synthesis and structural elucidation of the corresponding uranium complexes will be presented at the conference.

ACKNOWLEDGMENTS

This work was supported by JST CREST (Grant Number JPMJCR24I6) and by JSPS KAKENHI (Grant Numbers JP21H04473 and JP24K17634), Japan.

References

[1] M. Nève de Mévergnies, *Phys. Rev. Lett.*, **23**, 422 (1969).

7th Asia-Pacific Symposium on Radiochemistry *September 14 ~ 19, 2025 • Kunibiki Messe • Shimane, Japan*

SYNTHESIS AND STRUCTURAL ANALYSIS OF $\{(n\text{-}C_mH_{2m+1})_4N\}_2[Th(NO_3)_6]$

Kosuke Misawa[1], Hiroyuki Kazama[1], Masashi Kaneko[1], Ryoutarou Masuda[1], So Hashiba[1], Koji Yoshimura[2], Yoshitaka Kasamatsu[1]

[1]*Graduate School of Science, The University of Osaka:1-1 Machikaneyama, Toyonaka, Osaka, 560-0043, Japan*
[2]*Research Institute for Interdisciplinary Science (RIIS), Okayama University, Tsushima-naka 3-1-1 Kita-ku, Okayama 700-8530, Japan*
misawak24@chem.sci.osaka-u.ac.jp

We aim to explore the suitable crystals to the observation of ^{229m}Th 8.35 eV γ-ray transition. In this study, we synthesized systematically three-types of thorium compounds with the different counter ions, $\{(n\text{-}C_3H_7)_4N\}_2[Th(NO_3)_6]$ (1), $\{(n\text{-}C_4H_9)_4N\}_2[Th(NO_3)_6]$ (2), and $\{(n\text{-}C_5H_{11})_4N\}_2[Th(NO_3)_6]$ (3), and successfully characterized by single-crystal XRD measurement. The characterization revealed that the hexanitratothorate(IV) anion with 12-fold coordination sphere belongs to the different point group depending in the alkyl chain lengths of the counter cation to give T_h for the complex 2 and D_3 for the complexes 1 and 3. The DFT calculations were carried out to examine the electronic characteristics of the complexes. Also, absorption spectra were simulated in the UV-VUV region to consider for the application of the crystals for observation ^{229m}Th y-ray.

1 INTRODUCTION

Thorium-229 (^{229}Th) has been of great interest due to the presence of a nuclear isomer (^{229m}Th) with an extremely low excitation energy of approximately 8.35 eV [1], which is accessible by direct laser excitation. Because of this small excitation energy, the nuclear decay pathway of ^{229m}Th varies depending on the chemical state. The ^{229m}Th decay pathway is a competing process of internal conversion (IC), γ-ray transitions, and electron bridge (EB). These processes are particularly unique in that they could be influenced by the chemical environment through interactions involving outer-shell electrons.

The γ-ray transitions processes of ^{229m}Th have been successfully observed for ^{229m}Th crystals of CaF_2 and $LiSrAlF_6$ [1][2]. However, the chemical state of thorium in these solid samples remains unclear, and the correlation between structural characteristics, electronic properties, and nuclear decay behavior has not yet been elucidated. If the chemical environment of thorium can be systematically controlled through molecular design, it would become possible to investigate in detail the correlation between structure, electronic properties, and nuclear decay behavior.

In this study, we focused on controlling the coordination symmetry around thorium and attempted the synthesis of hexanitratothorate(IV) complexes ($[Th(NO_3)_6]^{2-}$). Actinide(IV) nitrates, including thorium, are known to form strong coordination bonds with the outer-shell electrons and typically adopt a highly symmetric icosahedral geometry with up to 12 coordination sites. By selecting tetraalkylammonium cations ($\{(n\text{-}C_mH_{2m+1})_4N\}^+$) as counter cation and changing the length of the alkyl chains, it is expected that the symmetry of the $[Th(NO_3)_6]^{2-}$ unit can be controlled.[3][4] Based on the structural analysis and quantum chemical calculations, we discussed the coordination environment may influence the nuclear decay of ^{229}Th.

2 EXPERIMENTAL

Three types of crystals, $\{(n\text{-}C_mH_{2m+1})_4N\}_2[Th(NO_3)_6]$ (m = 3, 4, 5), were synthesized by the solution diffusion method. A solution of 0.780 mol/L of tetraalkylammonium nitrate dissolved in mixed solvent [HNO_3(3 mol/L)/ethanol] and 0.390 mol/L of $Th(NO_3)_4 \cdot 4H_2O$ solution dissolved in solvent [3 mol/L HNO_3] were mixed in layers in a centrifuge tube in 100 μL. Colorless crystals were obtained and analyzed by powder X-ray diffraction (Rigaku MiniFlex 600) and single crystal X-ray diffraction (sc-XRD) (Rigaku XtaLAB Synergy Custom) measurements.

Time-dependent density-functional theory (TD-DFT) calculations were performed for the complex anion moieties, $[Th(NO_3)_6]^{2-}$, based on sc-XRD results of $\{(n\text{-}C_mH_{2m+1})_4N\}_2[Th(NO_3)_6]$. All the DFT calculations were performed using ORCA ver. 6.0 with ZORA-TZVPP/PBE0 level, in which CPCM(water) solvation effect was included. Single point calculations were also performed for the discussion of electronic properties of $[Th(NO_3)_6]^{2-}$ anions.

Copyright on 7th Asia-Pacific Symposium on Radiochemistry 2025

3 RESULT AND DISCUSSION

Sc-XRD analysis confirmed the structures of $\{(n\text{-}C_3H_7)_4N\}_2[Th(NO_3)_6]$ (**1**), $\{(n\text{-}C_4H_9)_4N\}_2[Th(NO_3)_6]$ (**2**), and $\{(n\text{-}C_5H_{11})_4N\}_2[Th(NO_3)_6]$ (**3**). The *R*1 values were 3.84%, 2.93%, and 2.79% for compounds **1, 2** and **3** respectively. The asymmetric units showed a difference in composition. Those of compounds **1** and **3** consist of one Th atom and six nitrate ligands, whereas that of compound **2** consists of one Th atom and three nitrate ligands. This difference indicated that the variation in the symmetry of the anionic moiety arises from the nature of the counter cation. The point group of the anionic moiety in compound **2** was determined to be T_h, whereas those in compounds **1** and **3** were D_3. This demonstrates that compounds with and without inversion symmetry were successfully synthesized. Focusing on the hexanitratothorate(IV) anion, all three compounds consist of six bidentate nitrates coordinated to the thorium center. The averaged bond lengths between Th atom and the nitrate oxygen atoms were 2.562 Å, 2.566 Å, and 2.561 Å for compounds **1**, **2**, and **3**, respectively. The slightly longer bond length was observed for compound **2** than those for compounds **1** and **3**, however, was thought to be a minor effect for discussion of the symmetric difference. The total energies based on TD-DFT calculation also indicated the highly small difference as ca. 2 kJ/mol. The relationship between these symmetry differences and the valence electronic transition properties, as well as their possible implications for nuclear decay behavior, will be discussed based on DFT calculations.

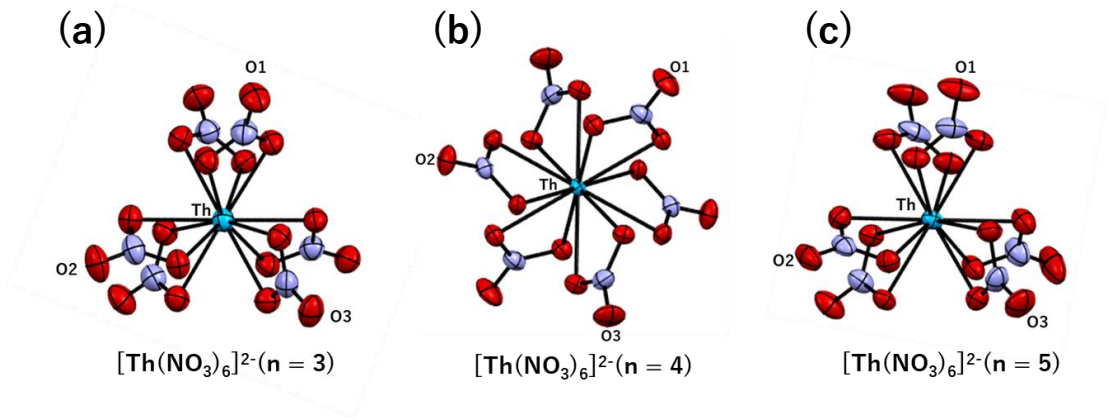


Figure1. Molecular structures of $[Th(NO_3)_6]^{2-}$ units in compounds **1**–**3**; $\{(n\text{-}C_3H_7)_4N\}_2[Th(NO_3)_6]$ (a), $\{(n\text{-}C_4H_9)_4N\}_2[Th(NO_3)_6]$ (b), $\{(n\text{-}C_5H_{11})_4N\}_2[Th(NO_3)_6]$ (c).C

4 CONCLUSIONS

In this study, three different $\{(n\text{-}C_mH_{2m+1})_4N\}_2[Th(NO_3)_6]$ complexes were successfully synthesized. Structural determination revealed that the $[Th(NO_3)_6]^{2-}$ anion adopts either T_h or D_3 symmetry depending on the nature of the counterion. We plan to measure VUV spectra on ^{232}Th samples to evaluate the accuracy of the TD-DFT calculations and to investigate crystals suitable for the application. The relationship between these structural symmetries of thorium is discussed using DFT calculations.

ACKNOWLEDGMENTS

The YANACO CHN Corder MT-6, Rigaku MiniFlex 600 and Rigaku XtaLAB Synergy Custom measurement were performed at the Analytical Instrument Facility, Graduate School of Science, The University of Osaka. This work was supported by JST, CREST Grant Number JPMJCR24I6, Japan. This work was supported by JSPS KAKENHI Grant Number JP21H04473.

References

[1] J. TIEDAU *et al.*, *Phys. Rev. Lett*, **132**, 182501, (2024).
[2] R. ELWELL *et al.*, *Phys. Rev. Lett.*, **133**, 013201, (2024).
[3] G. B. JIN *et al.*, *J. Am. Chem. Soc.*, **139**, 49, 18003–18008, (2017).
[4] G. E. SIGMON *et al.*, *Journal of Solid State Chemistry.*, **183**, 1604-1608, (2010).

Copyright on 7th Asia-Pacific Symposium on Radiochemistry 2025 P-R1-03* -

7th Asia-Pacific Symposium on Radiochemistry *September 14 ~ 19, 2025 • Kunibiki Messe • Shimane, Japan*

Preparation of Simulated MOX Ceramic Nuclear Fuel Microspheres by Microwave-assisted Internal Gelation Process

Wei Tian[1], Fangli Fan[2], Zhi Qin[3,*]
[1]*Affiliation Information: Nanchang Road/509, Lanzhou, China, 730000, linmu@impcas.ac.cn*
[2]*Affiliation Information: Nanchang Road/509, Lanzhou, China, 730000, fanfangli@impcas.ac.cn*
[3]*Affiliation Information: Nanchang Road/509, Lanzhou, China, 730000, qinzhi@impcas.ac.cn*

The rapid development of nuclear power will inevitably produce large amounts of spent nuclear fuels (SNF). In order to improve the utilization rate of uranium resources and achieve the sustainable development of nuclear energy, the closed nuclear fuel cycle must be developed accordingly. Sub-critical Accelerator Driven System (ADS) is a potential way to transmute the minor actinides (MAs) and long-lived fission products (LLFPs) into short-lived or stable nuclides by fast neutrons, and consequently reduce the difficulty of geological disposal. Based on the ADS project, Chinese academy of Sciences proposed an advanced Accelerator Driven closed Nuclear Fuel cycle (ADRUF) concept, which is a process of removing some of the fission products and neutron poisons by an advanced dry head-end processing technology while retaining U, Pu and MAs, and then refabricating the SNF into regenerated nuclear fuels. Therefore, it is of great significance to realize how to reproduce regenerated nuclear fuels from SNF in the ADRUF cycle. Because of high radioactivity and biotoxicity, an improved rapid internal gelation process combining non-cooling instant mixing with microwave-assisted heating is proposed to prepare regenerated ceramic nuclear fuel microspheres from SNF.

In order to simulate the SNF in ADRUF cycle, the preparation of multi-element metal mixed oxides (MOX) ceramic simulated nuclear fuel microspheres is also carried out in this thesis. Under the condition of 3 ℃/min, 1500 ℃ in 4% H2/Ar for 5 h, U+Ce and U+Ce+Nd oxides ceramic microspheres with a density of 95% TD are successfully prepared. The final microspheres are solid solution of faced centered cubic MO2 (M = U, Ce and Nd), and the lattice parameter decreases with increasing content of doped elements. In addition, the oxidation behavior of the ceramic MOX microspheres is also investigated, and it is found that the doped element has certain stabilizing effect on the faced centered cubic MO2 under oxidation ambient. When the content of doped element is less than 10%, the faced centered cubic MO2 can be oxidized to rhombic phase M3O8 and the microspheres are pulverized due to obvious volume expansion above 500 ℃. However, when the content of doped element is more than 20%, the cubic phase MO2 can only be oxidized to the similar cubic phase M4O9 even up to 1000 ℃, and the morphology of the microspheres keeps unchanged during the oxidation process.

Radiation-Tolerant Graphene Oxide-Carbon Quantum Dots Composite Membrane for Actinium-225 Solution deacidification

Baitong Zhang[a,b], Zhigang Ning[a,b], Qinggang Huang[a], Jing Bai[a,b*]
[a] *Institute of Modern Physics, Chinese Academy of Sciences, Lanzhou, 730000, China*
[b] *University of Chinese Academy of Sciences, Beijing, 100049, China*

Abstract

Actinium-225 (^{225}Ac) is a pivotal α-emitting radionuclide for targeted alpha therapy (TAT), while the large-scale production and purification strategy from thorium fissions often result in ^{225}Ac solutions with high acidity and hard for radiopharmaceutical labeling. Considering the conventional acid removal methods from ^{225}Ac solutions face challenges, a radiation-tolerant graphene oxide-carbon quantum dots (GO-CQDs) composite membrane was prepared for $^{225}Ac^{3+}$ solution deacidification. Owing to radioactivity constraints, La^{3+} was used as a non-radioactive surrogate for Ac^{3+} since the chemical similarity and comparable hydrated ionic diameters. Membrane structure was optimized by tuning interlayer spacing (d-spacing) and thickness, the membrane with minimum d-spacing and thickness of 65 nm were achieved to ensure the efficient permeation of H^+ and rejection of La^{3+}. The GO-CQDs membrane demonstrated superior acid removal performance in HNO_3, HCl, and H_2SO_4 media, especially in HNO_3 solution, the highest H^+/La^{3+} separation factor of 55.01 was obtained. Crucially, the membrane not only retained functionality after 100 kGy γ-irradiation, but also compensated for the intrinsic defects of commercial deacidification membrane in nitric acid medium. This work establishes GO-CQDs membrane as a robust, radiation-tolerant technology for trivalent radioisotope solution deacidification.

Keywords: Graphene oxide, Membrane, Deacidification, $^{225}Ac^{3+}$ solution, Radiation

Copyright on 7th Asia-Pacific Symposium on Radiochemistry 2025

7th Asia-Pacific Symposium on Radiochemistry *September 14 ~ 19, 2025 • Kunibiki Messe • Shimane, Japan*

Verification of Excitation Functions in Fast Neutron Induced Reactions Using Activation Method

S. Tsuruta[1], S. Goto[1], Y. Cho[1], H. Kikunaga[2]

[1]*Graduate School of Science and Technology, Niigata University: Niigata, Niigata, 950-2181, Japan*
[2]*RARiS, Tohoku University: Sendai, Miyagi, 980-8587, Japan*

The use of fast neutrons for radioisotope (RI) production is attracting increasing interest, but accurate data on excitation functions and neutron spectra are still limited. This study evaluates the reliability of excitation functions by comparing activation method experiments. Fast neutrons were generated by deuteron irradiation to a graphite converter, and integral cross sections were measured. Good agreement for the ^{58}Ni(n,p)^{58}Co reaction supports the validity of both the PHITS spectrum and TENDL data, confirming the activation method's applicability for such validations.

1. INTRODUCTION

Accurate neutron spectra and excitation functions are essential for reliable estimation of radioisotopes (RIs) production yields. While neutron spectra can be simulated, the validity of theoretical calculations and the accuracy of previously measured excitation functions remain sufficiently verified. In this study, we investigated whether the integral of the excitation function weighted by the neutron spectrum obtained using the activation method (i.e., measuring the radioactivity of a radionuclide obtained by neutron irradiation is measured under various irradiation conditions), could reproduce the calculated value based on the simulated neutron spectrum and the measured excitation function. Fast neutrons were generated by irradiating on deuterons to a graphite converter, a technique previously reported [1-3]. The neutrons were irradiated on various targets, and the integral of the excitation functions weighted by the neutron spectrum, the integral cross section, were obtained.

2 . EXPERIMENTS

Experiments were performed at the Research Center for Accelerator and Radioisotope Science (RARiS) of Tohoku University. In order to generate fast neutrons, deuterons were accelerated using the Model 930 AVF cyclotron and irradiated onto a graphite converter to with energies of 20, 25, 30, and 35 MeV. The deuteron beam current was about 200 nA. Neutrons were irradiated onto different targets which were 0.1 mm thick foils of Ni, Ti, Zr, Mo, In, W, and 0.05 mm Au foil. In addition, oxide pellets of Ni, Ge, and Ce were also used. After irradiation, the produced nuclides were identified and quantified by γ-ray spectrometry using HPGe detector.

3. RESULTS AND DISCUSSION

Nuclides produced by (n,2n), (n,p), and (n,pn) reactions were observed, and their activities at the end of bombardment (EOB) were determined using decay analysis. The activity at EOB, A_{EOB}, for a nuclide with decay constant λ after irradiation for time t is expressed as

$$A_{\mathrm{EOB}} = Nf\left(1 - e^{-\lambda t}\right)\int_0^{E_\mathrm{d}} P(E, E_\mathrm{d})\sigma(E)dE\ , \qquad (1)$$

where N is the number of target atoms per unit area, f is the deuteron flux, $P(E,E_\mathrm{d})$ is the normalized neutron spectrum at deuteron energy E_d, and $\sigma(E)$ is the excitation function. The integral term in this equation is referred to as the "integral cross section". As an example, Figure 1 shows the integral cross sections for the ^{58}Ni(n,p)^{58}Co at different deuteron energies. The line in the figure represents the integral cross sections calculated from the TENDL excitation function and the neutron spectrum simulated by PHITS. The excitation function for this reaction has been measured extensively, exhibits small variations, and is well reproduced by TENDL. The good agreement between the calculated and experimental values suggests that the simulated neutron spectrum is closed to the actual spectrum. In the presentation, the results for the other targets will be presented and discussed.

Copyright on 7th Asia-Pacific Symposium on Radiochemistry 2025

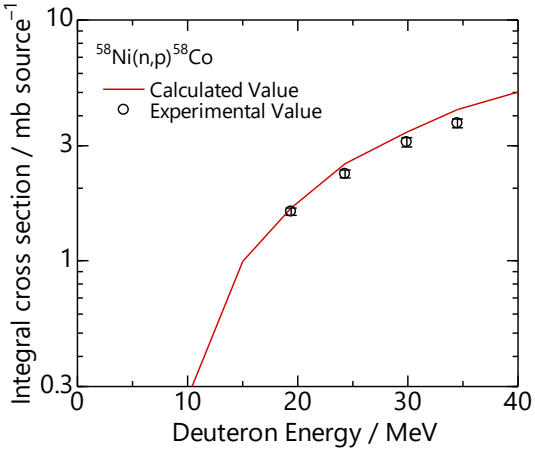


Fig. 1. Comparison of experimental results with the calculation from the TENDL excitation function and PHITS netron spectra

4. CONCLUSIONS

We measured integral cross sections for various nuclides using the activation method to verify the excitation functions of fast neutron-induced nuclear reactions. For the ^{58}Ni(n,p)^{58}Co reaction, our experimental results were close to the values calculated from the TENDL excitation function and PHITS neutron spectrum, confirming the reliability of the simulation. These results demonstrate that the activation methods are effective for validating excitation functions and neutron spectra.

ACKNOWLEDGMENTS

We would like to thank all the operators of the RARiS cyclotron for their cooperation in carrying out this experiment.

References

[1] K. A. Weaver *et al.*, Nucl. Sci. Eng. **52** (1973) 35.
[2] J. P. Meulders *et al.*, Phys. Med. Biol. **20** (1975) 235.
[3] Md K. A. Patwary *et al.*, J. Nucl. Sci. Technol. **58** (2021) 252.

Copyright on 7th Asia-Pacific Symposium on Radiochemistry 2025

THICK TARGET YIELD NORMALISED PER ACCELERATED PARTICLE

Hidetoshi Kikunaga[1], Shin'ichi Goto[2]

[1] *RARiS, Tohoku Univ.: 1-2-1 Mikamine, Taihaku, Sendai, 982-0826, Japan kikunaga@raris.tohoku.ac.jp*
[2] *Grad. School of Sci. Tech., Niigata Univ.: 8050, Ikarashi 2-no-cho, Nishi-ku, Niigata, 950-2181, Japan*

The thick target yields of charged particle induced nuclear reactions and neutral particle induced nuclear reactions have been normalised to values per accelerated particle. This allows direct comparison of the efficiency per beam energy of different nuclear reactions and provides guidelines for the selection of nuclear reaction pathways for the production of radioactive isotopes. The production reaction of Mo-99 is discussed here as an example.

1 INTRODUCTION

When producing radioactive isotopes, the amount produced per beam is a fundamental quantity. In charged hadron injection reactions, this quantity is defined as Thick Target Yield (TTY) [1]. This indicates the amount of radioactivity produced when all the energy of the incident particles is transferred to the target. Correcting for the half-life of the produced radioactivity allows the saturation TTY and physical TTY to be obtained. Similarly, TTY can be defined as the radioactivity generated when all the energy of incident photons or neutrons is transferred to the target. However, in RI production, photons and neutrons are typically obtained as secondary particles. This obscures the quantitative relationship between beam dose and generated radioactivity. In this study, we defined TTY per primary beam for generating photons or neutrons. This can be compared with the TTY of charged hadron injection reactions and can be used to select reaction pathways when producing radioactive isotopes.

2 CALCULATION CONDITIONS

Photons are generated using an electron beam and neutrons using a heavy ion beam. The electron beam either incides directly on the target or through a heavy element converter (such as platinum or tantalum), and the resulting bremsstrahlung radiation incides on the target. In the case of the deuteron beam, beryllium — commonly used to generate fast neutrons — is incident on the target, and the neutrons generated also hit the target. All of the photons' and neutrons' energy is absorbed within the target. To meet these conditions, it was assumed that the target would be a cube with at least 2 m on each side. Calculations were performed using PHITS 3.35[2, 3], with nuclear reaction cross sections obtained from TENDL 2023 [4].

3 RESULTS AND DISCUSSIONS

As an example, the Physical TTY for the ^{100}Mo(g,n), ^{100}Mo(n,2n) and ^{96}Zr(α,n) reactions used to produce ^{99}Mo are shown in Fig. 1. In photonuclear and fast neutron reactions, around 10^{-3} of the beam energy is used for the intended nuclear reaction. By contrast, only around 10^{-6} is utilised for alpha-induced reactions. In sufficiently thick targets, photon- and neutron-induced reactions are more efficient at utilising beam energy for nuclear reactions. Additionally, the production efficiency of a radioactive isotope production system can be evaluated using this Physical TTY as a reference. In an irradiation system containing approximately 50 g of ^{100}Mo metal, photon-induced reactions are more efficient than fast neutron reactions. The presentation will discuss production efficiency in nuclear reactions, as well as other nuclear reactions.

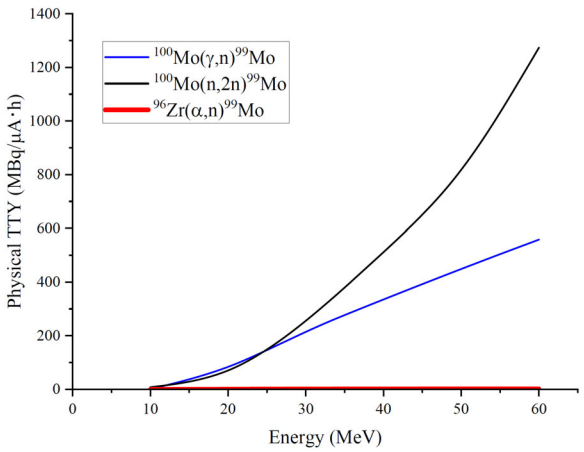


Fig. 1. Comparison of Physical TTY for the ^{99}Mo production reactions

ACKNOWLEDGMENTS

This work is supported by JSPS KAKENHI Grant Number JP22H00123 and JST ERATO Grant Number JPMJER2304.

References

[1] N. Otuka and S. Takács, "Definitions of radioisotope thick target yields", Radiochim. Acta, 103, 1 (2015)/

[2] T. Sato *et al*., "Recent improvements of the Particle and Heavy Ion Transport code System- PHITS version 3.33", J. Nucl. Sci. Technol. 61, 127 (2024).

[3] H. Hirayama et al., SLAC-R-730 (2005) and KEK Report 2005-8 (2005).

[4] TENDL-2023: (release date: December 22, 2023); A.J. Koning *et al*., "TENDL: Complete Nuclear Data Library for Innovative Nuclear Science and Technology", Nuclear Data Sheets, 155, 1 (2019).

7th Asia-Pacific Symposium on Radiochemistry *September 14 ~ 19, 2025 • Kunibiki Messe • Shimane, Japan*

Production of carrier-free ^{182}Ta tracer via photonuclear reaction

Takuya Yokokita[1], Yuki Honda[1], Hidetoshi Kikunaga[1]

[1]*Research Center for Accelerator and Radioisotope Science, Tohoku University: 1-2-1 Mikamine, Taihaku, Sendai, Miyagi 982-0826, Japan, yokokita@raris.tohoku.ac.jp*

Element 105, dubnium (Db), can only be produced in accelerators and exists as single atom. To investigate the chemical properties of Db, it is necessary to obtain comparative data using its lighter homologues, Nb and Ta. However, Nb and Ta are known to readily form polynuclear species. Therefore, for comparison with Db, experiments with Nb and Ta at low concentrations are required, and the use of carrier-free Nb and Ta tracers is preferred. In this study, we produced carrier-free ^{182}Ta using a photonuclear reaction, $^{nat}W(\gamma,x)^{182}Ta$.^{182}Ta has relatively long half-life of 114.74 d, making it suitable for long-term tracer experiments. Furthermore, while ^{179}Ta, which has been used in previous Ta tracer experiments, requires quantification via X-ray spectrometry, ^{182}Ta has the advantage of also being quantifiable by γ-ray spectrometry.

1 INTRODUCTION

The heavy elements with atomic numbers Z ≥ 104 are called superheavy elements (SHEs). In these heavy elements, the influence of relativistic effects on atomic electrons becomes significant, and their chemical properties are expected to deviate from the periodicity of their lighter homologues in the Periodic Table. Thus, it is important and interesting to study the chemical properties of SHEs. SHEs are produced exclusively at accelerator facilities using heavy-ion-induced nuclear fusion reactions. The production rates of SHEs are extremely low, and their half-lives are very short, usually less than one minute. These conditions necessitated rapid chemical experiments on an atom-at-a-time basis. The chemical properties of SHEs have been investigated mainly by partition methods such as chromatography and solvent extraction, based on the comparison of their chemical behavior with that of their lighter homologues in the Periodic Table.[1,2]

Only nine reports on the solution chemistry of element 105, dubnium (Db). [1,2] Additionally, most chemical study of Db has focused on fluoride complexes. Further chemical experiments are needed to elucidate the chemical properties of Db.

Nb and Ta, homologous elements of Db, are known to polymerize readily, except in HF systems. [3] The chemical behavior of Db should be compared with that of mononuclear species of Nb and Ta, because Db exists as single atoms at a time and is therefore not expected to undergo polymerization. Thus, experiments with Nb and Ta are needed using low metal concentration samples (carrier-free radioisotope tracers) to ensure the formation of mononuclear species. In previous Ta tracer experiments, ^{177}Ta and ^{179}Ta have been used [4]. ^{177}Ta has a short half-life (56.36 h), and ^{179}Ta requires quantification by X-ray spectroscopy. Therefore, we focused on ^{182}Ta, which is a relatively long half-life (114.74 d) and γ-ray emitter. In this study, we developed a production method for the carrier-free ^{182}Ta via $^{nat}W(\gamma,x)^{182}Ta$ reaction.

2 EXPERIMENTAL

900 mg of W foils were enclosed in a quartz tube to serve as an irradiation target. The irradiation was performed using a high-intensity electron linear accelerator at the Research Center for Accelerator and Radioisotope Science (RARiS), Tohoku University. An electron beam approximately 132 μA, accelerated to 30 MeV, was converted to bremsstrahlung radiation by a 3 mm thick, water-cooled Ta-based converter. The sample was irradiated for 4 h with continuous water cooling. After irradiation, 240 mg of the W material was analyzed using γ- and X-ray spectrometry with a Ge detector.

The remaining irradiated W (414 mg) was dissolved in a mixture of 2 mL of concentrated HF (c. HF) and 1 mL of c. HNO_3, and the resulting solution was evaporated to dryness. The residue was then dissoved by heating with 1.8 mL of c. HF. Subsequently, the solution was converted to 50 mL of 4 M HCl / 1 M HF by the addition of c. HCl and H_2O. The solution was divided into 50 fractions of 1 mL each and fed into an anion-exchange column (Muromac 1X8 100–200 mesh, 5 mm i.d. × 42 cm height). The resin was washed with 5 mL (5 × 1 mL) of 4 M HCl / 1 M HF and then with 5 mL (5 × 1 mL) of 4 M HCl. To obtain elution curves for ^{182}Ta and ^{181}W, the 1 mL eluent fractions were collected and subjected to γ- and X-ray spectrometry using a Ge detector.

3 RESULTS AND DISCUSSION

Copyright on 7th Asia-Pacific Symposium on Radiochemistry 2025

24 days after the end of irradiation, ^{182}Ta (half-life $T_{1/2}$ = 114.74 d), ^{183}Ta ($T_{1/2}$ = 5.1 d), ^{181}W ($T_{1/2}$ = 121.2 d), and ^{185}W ($T_{1/2}$ = 75.1 d) were detected in 240 mg of irradiated W foil. The activities of ^{182}Ta, ^{183}Ta, ^{181}W, and ^{185}W were 2.0 ± 0.1 kBq, 271.0 ± 3.2 kBq, 234.0 ± 2.6 kBq, and 612.7 ± 7.7 kBq, respectively, at end of bombardment.

The elution curves for the anion-exchange chromatography of ^{182}Ta and ^{181}W are shown in Fig. 1. 86% of the ^{182}Ta was eluted with 5 mL of 4 M HCl. The decontamination factor of W, determined by the measurement of ^{181}W was 6.0 × 10^{-6}.

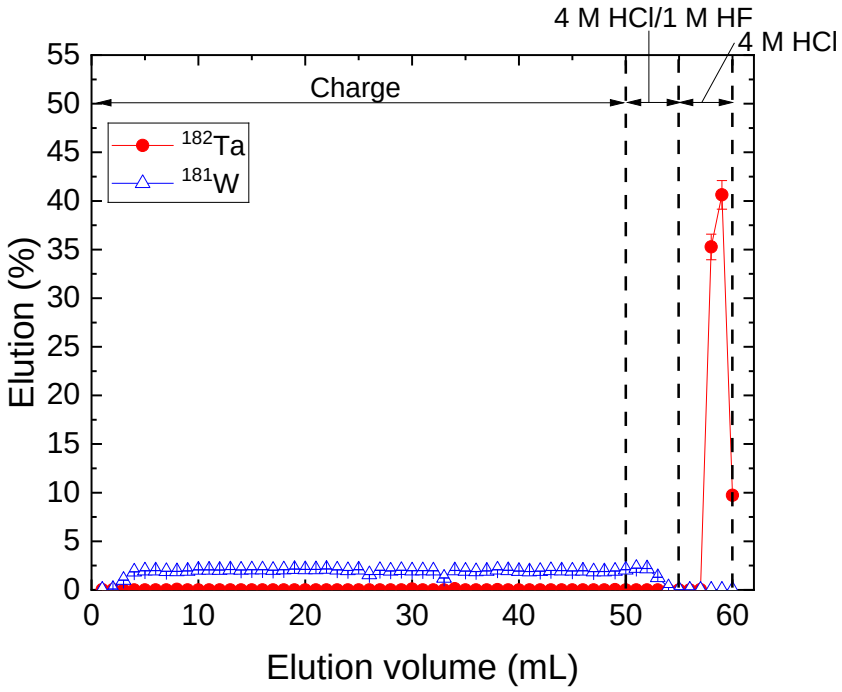


Fig. 1. Elution curves of ^{182}Ta and ^{181}W for the anion-exchange chromatography.

4. CONCLUSIONS

In photonuclear reactions, the high penetrating power of bremsstrahlung radiation allows for an increase in the target material amounts. Therefore, increasing the target amounts could enhance the production yield of ^{182}Ta. The separation scheme used in this study for ^{182}Ta from W involves selectively adsorbing only the desired ^{182}Ta onto an anion-exchange resin while leaving the bulk W target unadsorbed. Therefore, this separation method can be applied when the target amounts of W are increased.

ACKNOWLEDGMENTS

The authors thank to the facility staffs of RARiS in Tohoku University for supplying the high-quality electron beam.

References

[1] *The Chemistry of Superheavy Elements*, 2nd ed., M. Schädel and D. Shaughnessy, Ed., Springer, Heidelberg (2014).
[2] A. Türler and V. Pershina, Advance in the Production and Chemistry of the Heaviest Element, *Chem. Rev.*, **113**, 1237 (2013).
[3] Z. Zhu and C. Y. Chen, Solvent Extraction Technology for the separation and purification of niobium and tantalum: A review, *Hydrometallurgy* **107**, 1 (2011).
[4] Y. Kasamatsu, A. ToyoshimaH. Haba, Toume, K. Tsukada, K. Akiyama, T. Yoshimura, Y. Nagame, Adsorption of Nb, Ta and Pa on anion-exchanger in HF and HF/HNO_3 solutions: Model experiments for the chemical study of Db, *J. Radioanal. Nucl. Chem.* **279**, 371 (2009).

Copyright on 7th Asia-Pacific Symposium on Radiochemistry 2025

Study of Lu-DOTA using Lu-177 produced by photonuclear reaction

Miona Tofuku[1], Kazuhiko Akiyama[1], Hidetoshi Kikunaga[2], Shiro Kubuki[1]

[1]*Tokyo Metropolitan University, 1-1, Minamiosawa, Hachioji-shi, Tokyo, 192-0397*
[2]*Research Center for Accelerator and Radioisotope Science, 1-2-1, Mikamine, Taihaku-ku, Sendai-shi, Miyagi, 982-0826,*

I. INTRODUCTION

Lu-177 has been considered as a promising radioisotope for medical use because of their suitable half-life (6.65 day) for synthesis and practical use as a radiopharmaceutical and their decay properties simultaneously emitting low energy β ray and ideal γ ray for both treatment and diagnosis. Actually, some radiopharmaceuticals employed ^{177}Lu, such as LUTATHERA and Lu-PSMA-617, have been used in clinical sites. Currently, the method generally used to produce this useful RI is known as the indirect method. In this method, ^{177}Lu is obtained as a progeny nuclide of ^{177}Yb produced with the ^{176}Yb(n,γ)^{177}Yb reaction using reactor neutrons. However, there are some problems, such as difficulties in the chemical separation from the target because ^{177}Lu and target material of Yb are homologous elements. Recently, the production of ^{177}Lu by photonuclear reactions: ^{178}Hf(γ,p)^{177}Lu using electron linear accelerators has been noted because ^{177}Lu can be easily separated from target material of Hf by chemical separation.

In this study, we synthesized Lu-DOTA [2], which is the important building block of radiopharmaceuticals, using ^{177}Lu produced in photonuclear reaction and attempted to separate Lu-DOTA from target material of Hf with smaller separation step as possible.

II. EXPERIMENTAL

About 0.1 g HfO_2 was formed into a disk with 9 mm diameter and packaged in high purity Al foil and then sealed into a quartz tube under reduced pressure. The sample was irradiated with bremsstrahlung radiation with a maximum energy of 50 MeV for 1 hour at Research Center for Accelerator and Radioisotope Science, Tohoku University to produce ^{177}Lu. The irradiated samples were dissolved in hydrofluoric acid (HF). The solvent was replaced with two types of ammonium acetate solution including diluted HF or not. Lu-DOTA was directly synthesized by adding DOTA to both solutions from irradiated samples and heating at 95 ^{o}C for 30 minutes. An anion exchange resin was then added and stirred for batch separation. The γ rays emitted from ^{177}Lu in the sample were measured with a Ge semiconductor detector, and the yields of ^{177}Lu DOTA in each solvent were compared. These results were also compared with Lu-DOTA synthesized using isolated ^{177}Lu by extraction chromatography.

III. RESULTS AND DISCUSSION

Figure 1 shows the photo stimulated luminescence of autoradiography (ARG) image of the thin-layer chromatography (TLC) plate on which the sample was loaded and developed after the synthesis. Regardless of the differences in the separation and synthesis method, a spot (Rf=0.33-0.35) derived from a DOTA compound was confirmed in all samples by TLC/ARG. Radioactivity of Lu was observed in the samples recovered from these spots as the results of γ-ray measurement.

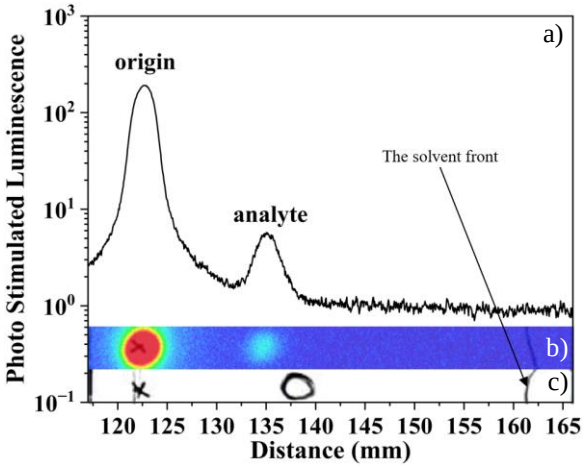


Fig 1. ARG image of TLC plate (TLC/ARG) developing the sample after Lu-DOTA synthesis. a) Photo stimulated luminescence of ARG image. b) ARG image, c) TLC profile.

Table 1 shows the production yield of Lu-DOTA for each separation method. The check mark in the table indicates the presence of diluted HF in the solution. The production yield of Lu-DOTA synthesized followed by the separation for the batch separation without diluted HF is found to be lowest between these separation methods because of the removal of the precipitate produced in the sample. It is considered that this precipitate is produced due to the decrease of fluoride ion in the solution. On the other hand, the yield is found to be increased up to 80.4% with the presence of diluted HF and almost similar to that for using purified ^{177}Lu (97.7%).

Table 1. Comparison of yields with and without dil.HF solvent in the synthesis stage and with different separation methods.

Separation method	With or without dil.HF	Yield of ^{177}Lu	Yield of ^{175}Hf
batch separation		**$26.9_{\pm 8.5}$**	$1.6_{\pm 0.1}$
	✓	**$80.4_{\pm 14.1}$**	$11.5_{\pm 0.4}$
Extraction chromatography		**$97.7_{\pm 0.2}$**	LOD

※Yield(%)=Final$_{Radioactivity}$/Initial$_{Radioactivity}$, LOD: Limit Of Detection.

IV. REFERENCES

[1] Andrey G. Kazakov, *et al.*, *J. Radioanal. Nucl. Chem.*, **317**, 1469 (2018).
[2] Silvio Aime, *et al.*, *Inorg. Chem.*, **36**, 2059 (1997).

Copyright on 7th Asia-Pacific Symposium on Radiochemistry 2025

Production of non-carrier added ^{7}Be by the ^{nat}Li(*d*,*x*)^{7}Be reaction

Akihiro Nambu[1], Hiromichi Shimizu[1], Yousuke Kanayama[1], Yudai Shigekawa[1], Sayantani Mitra[1], and Hiromitsu Haba[1]
[1]*Nishina Center for Accelerator-Based Science, RIKEN, 2-1 Hirosawa, Wako-shi, Saitama 351-0198, Japan*

^{7}Be was produced through the ^{nat}Li$(d, x)^{7}$Be reaction using the RIKEN AVF cyclotron. A chemical separation method of ^{7}Be from ^{nat}Li using an extraction chromatography with LN resin was examined. The production yield, chemical yield, specific radioactivity, and impurities in the purified ^{7}Be were discussed.

1 INTRODUCTION

Diamond is a wide-bandgap semiconductor, which possesses superior electronic properties and whose application to next-generation semiconductor devices has recently been proposed [1]. Although an n-type diamond is expected to be produced by doping Li atoms behaving a shallow donor [2], it is yet to be developed.

Recently, a promising method to produce a Li-doped diamond using ^{7}Be has been suggested [3]. In this method, ^{7}Be (EC, $T_{1/2} = 53$ d, $I_{EC} = 100\%$) is doped into diamond by low-energy implantation ($\sim$20 keV), followed by a thermal diffusion process allowing deep migration into the crystal interior. ^{7}Be subsequently decays to ^{7}Li by electron capture without emitting any strong ionizing radiation, resulting in Li-doped diamond without lattice defects in the interior region of the diamond.

^{7}Be has been produced via the ^{nat}Li$(p, x)^{7}$Be reaction and purified by a cation exchange column chromatography [4, 5]. In this method, a large-scale column with a bed volume of $\sim$7.9 mL was used for a target of only 50 mg [4], or $\sim$1.8 mL for 6 mg [5], which is not preferable to produce a large radioactivity of ^{7}Be from a thick target. Moreover, based on our experience, ^{7}Be purified by a cation exchange column is occasionally contains a small but visible amount of impurities, probably due to the large quantity of resin used in the column.

Recently, the ideal capacity factors (k') was reported for Be with the Eichrom LN resin, impregnated with bis(2-ethyl-1-hexyl) phosphoric acid [6]. In this research, a chemical separation method for ^{7}Be using the LN resin column was examined.

2 MATERIAL AND METHODS

2.1 Target preparation

A ϕ10-mm $^{nat}Li_2CO_3$ pellet target was formed by pressing 276 mg of $^{nat}Li_2CO_3$ powder (chemical purity 99%, KISHIDA CHEMICAL Co., Ltd.) in a ϕ10 mm die under a pressure of 1.6 ton for 3 min, providing a target thickness of 351 mg/cm^2.

2.2 Irradiation

The $^{nat}Li_2CO_3$ pellet target was covered by a 10-μm aluminum foil (99.999%; GoodFellow), placed on a tantalum beam stopper, and irradiated for 30 min with a 24.40-MeV d beam (1 μA) extracted from the RIKEN AVF cyclotron. Incident beam energy was measured by a time of flight method. To avoid damage to the target, a beam wobbling system was used to sweep the beam spot across the target. The beam stopper and the target pellet were cooled with a circulating water (5°C, 2 L/min) and helium gas ($\sim$30 L/min), respectively. Total energy loss in the vacuum window, helium gas, and aluminum cover was estimated using the SRIM code[7], resulting in an incident energy of 24.25 MeV on the target surface.

2.3 Chemical separation

The aluminum foil wrapping the target pellet was removed and the Li_2CO_3 pellet was sank in 5 mL of pure water. Approximately 1 mL of concentrated hydrochloric acid was subsequently added to dissolve the pellet. The solution was heated and evaporated to dryness on a hot plate, and the residue was dissolved with 1 mL of 0.01 M nitric acid (HNO_3): this drying and dissolving procedure was repeated twice to change the chemical form of ^{7}Be from chloride to nitrate.

Because a sufficient radioactivity of ^{7}Be had been produced, only a portion was used to examine the chemical separation method using the LN resin column. Unirradiated target material was mixed with 5% of the target solution to adjust the amount of ^{nat}Li to the irradiated ^{nat}Li. This mixture was dissolved in 4 mL of 0.01 M HNO_3 in a beaker. The entire solution was loaded onto the LN resin column (ϕ5 mm, 50-mm height, LN resin 50–100 μm, Eichrom Technologies, LLC). Under this HNO_3 concentration, ^{7}Be was adsorbed on the resin while Li was not. The beaker was rinsed five times with 200 μL of the same solvent, and all of the rinse solutions were subsequently added to the column. To wash the column, 1 mL of 0.01 M HNO_3 was added ten times. Finally, ^{7}Be was eluted by adding 1 mL of 8 M HNO_3 five times. The flow rate of each solution was $\sim$0.2 mL min^{-1}. Each eluate fraction was collected separately to confirm the elution behavior of ^{7}Be and ^{nat}Li. All of the 8 M HNO_3 fractions containing the majority of ^{7}Be were collected and stored as the purified ^{7}Be sample.

2.4 Measurement

^{7}Be was assayed with its γ ray (477.6 keV, $I_\gamma = 10.4\%$) using a Ge detector. To evaluate the production yield of ^{7}Be, the irradiated target was measured before chemical separation. Each eluate fraction from the LN resin column was measured to inspect the elution behavior of ^{7}Be. After chemical separation, the purified ^{7}Be sample was measured to evaluate the chemical yield.

The amounts of ^{7}Li and ^{9}Be were measured using ICP-MS 7800 (Agilent Technologies). The amount of ^{nat}Li was estimated based on the measured ^{7}Li mass and its natural abundance of 92.4%.

3 RESULTS AND DISCUSSION

The radioactivity of ^{7}Be at the end of bombardment (EOB) was 0.50±0.02 MBq. This result provides a production yield of 0.98±0.03 MBq μA^{-1} h^{-1}, which agrees with 1.06 MBq μA^{-1} h^{-1} calculated from the reported production cross section [8]. ^{7}Be was recovered with the chemical yield of 91±4%. Only the 477.6 keV peak from ^{7}Be was observed in the γ-ray spectrum and any other impurity was below the detection limit.

When the purified ^{7}Be was evaporated to dryness, an almost invisible amount of residual was seen in the bottom of the beaker. Because the impurity is likely to be an organic substance originating from the resin, its amount was not quantified by ICP-MS. However, we visually confirmed that the amount of organic substance was much smaller than that obtained by the conventional cation-exchange method.

The ICP-MS measurement indicated that the amounts of ^{nat}Li and ^{9}Be were 38.9 μg and < 2.0 ng, respectively, which were mainly from the target. Considering that we mixed only 5% of irradiated target with non-irradiated target material before separation, the specific radioactivity of $> 2.5 \times 10^5$ MBq mg^{-1} can be achieved for ^{7}Be in the separation from the whole target amount.

The decontamination factor (DF) of ^{7}Be to ^{nat}Li was 6.5×10^3 according to the definition of eq. (1), where A is the radioactivity and W is the mass of the element. This value was comparable to that of previous method, $(6.9\pm1.0)\times10^3$[5], however, our method appeared more favorable because much more quantity of target material can be purified through it.

$$\mathrm{DF} = \frac{A_{\text{purified, Be}}/A_{\text{target, Be}}}{W_{\text{purified, Li}}/W_{\text{target, Li}}} \,. \tag{1}$$

4 CONCLUSION

A novel chemical separation method of ^{7}Be from ^{nat}Li was developed using extraction chromatography with the LN resin column. ^{7}Be was produced via the ^{nat}Li$(d, x)^{7}$Be reaction followed by chemical separation. The LN resin enabled to use larger amount of target to increase the production yield of ^{7}Be. A decontamination factor, which was nearly comparable to that of the conventional method, was achieved with smaller amount of residual.

References

[1] F. Zhao *et al.*, materials **17**, 3437 (2024).

[2] J. P. Goss *et al.*, Physical Review B **75**, 075202 (2007).

[3] H. Okuno *et al.*, Patent Publication PCT/JP2023/014925.

[4] T. Ohtsuki *et al.*, Applied Radiation and Isotopes **59**, 221 (2003).

[5] N. Gharibyan *et al.*, Applied Radiation and Isotopes **107**, 199 (2016).

[6] D. R. McAlister *et al.*, Solvent Extraction and Ion Exchange **25**, 757 (2007).

[7] J. F. Ziegler *et al.*, Nuclear Instruments and Methods in Physics Research Section B: Beam Interactions with Materials and Atoms **268**, 1818 (2010).

[8] M. Hagiwara *et al.*, Journal of Nuclear Materials **417**, 1267 (2011).

Improving the Purity of ^{225}Ac from Thorium Spallation at TRIUMF for Targeted Alpha Therapy Applications

E. Timakova[1,2], E. Dunling[1], J. Bailey[1], P. Schaffer[1,3,4], C. Hoehr[1,5]

[1] *Life Sciences, TRIUMF, 4004 Wesbrook Mall, Vancouver, BC, V6T 2A3, Canada*
[2] *Physics, University of British Columbia, Vancouver, BC, V6T 1Z4, Canada*
[3] *Radiology, University of British Columbia, Vancouver, BC, V6T 1Z4, Canada*
[4] *Chemistry, Simon Fraser University, Burnaby, BC, V5A 0A7, Canada*
[5] *Physics, University of Victoria, Victoria, BC, V8P 5C2, Canada*

Actinium-225 (^{225}Ac) is a promising radionuclide for targeted alpha therapy (TAT), characterized by the emission of four high-energy alpha particles within a short time period and with high linear-energy transfer, conducive to DNA double-strand breaks. These properties enable highly localized irradiation of tumor cells while minimizing damage to surrounding healthy tissues. Encouraging clinical outcomes in patients with late-stage metastatic cancer have highlighted the potential of ^{225}Ac-based therapies [1], [2]. However, the global supply of ^{225}Ac remains critically limited, hindering its widespread clinical application. ^{225}Ac is primarily sourced through two methods: separation from ^{229}Th obtained from waste stockpiles containing ^{233}U, and isolation from ^{225}Ac and/or ^{225}Ra produced via spallation of ^{232}Th by high-energy proton irradiation (>70 MeV) [3]. At TRIUMF in Vancouver, BC, Canada, the latter method is employed, yielding substantial quantities of ^{225}Ac [4]. Although this method provides large yields, it presents significant radiochemical challenges due to the co-production of hundreds of fission and spallation products [5]. Therefore, efficient and selective purification of ^{225}Ac from radioactive and non-radioactive metal contaminants is essential.

This study aims to enhance the purity and downstream usability of ^{225}Ac produced at TRIUMF by optimizing post-irradiation separation techniques beyond current protocols [5]. We are developing and evaluating separation procedures that incorporate various combinations of extraction resins, including DGA and LN resins, or a stacked column approach using TK221, TEVA, and Sr resins. These methods are adapted from recent advances by groups in Vancouver [6], and Japan [7], with modifications tailored to TRIUMF's processing infrastructure. Key aspects of our study include: (i) implementing a gradient elution scheme using decreasing nitric acid concentrations, starting from 0.7 M with decreasing acid concentration, ending with deionized water on a DGA resin to enhance selective recovery of ^{225}Ac; and (ii) comparing separation efficiencies from freshly irradiated vs. aged thorium targets, and (iii) evaluating the radiolabeling efficiency of purified ^{225}Ac for downstream applications.

Preliminary results will be presented, demonstrating the impact of elution gradients and target age on separation yields and purity profiles. These findings will contribute to increasing the availability and clinical readiness of ^{225}Ac for TAT applications.

References:

[1] C. Kratochwil, F. Bruchertseifer, F. L. Giesel, M. Weis, F. A. Verburg, F. Mottaghy, K. Kopka, C. Apostolidis, U. Haberkorn, A. Morgenstern, "^{225}Ac-PSMA-617 for PSMA-Targeted α-Radiation Therapy of Metastatic Castration-Resistant Prostate Cancer," *J. Nucl. Med.*, vol. 57, no. 12, pp. 1941–1944, Dec. 2016, doi: 10.2967/jnumed.116.178673.

[2] H. Besiroglu and M. Kadihasanoglu, "The Safety and Efficacy of Targeted Alpha Therapy, Ac-225 Prostate-Specific Membrane Antigen, in Patients With Metastatic Castration-Resistant Prostate Cancer: A Systematic Review and Meta-Analysis," *The Prostate*, vol. 85, no. 6, pp. 541–557, May 2025, doi: 10.1002/pros.24857.

[3] A. K. H. Robertson, C. F. Ramogida, P. Schaffer, and V. Radchenko, "Development of ^{225}Ac Radiopharmaceuticals: TRIUMF Perspectives and Experiences," *Curr. Radiopharm.*, vol. 11, no. 3, pp. 156–172, Oct. 2018, doi: 10.2174/1874471011666180416161908.

[4] A. K. H. Robertson, A. Lobbezoo, L. Moskven, P. Schaffer, and C. Hoehr, "Design of a Thorium Metal Target for ^{225}Ac Production at TRIUMF," *Instruments*, vol. 3, no. 1, p. 18, Feb. 2019, doi: 10.3390/instruments3010018.

[5] A. K. H. Robertson, B. L. McNeil, H. Yang, D. Gendron, R. Perron, V. Radchenko, S. Zeisler, P. Causey, P. Schaffer, "^{232}Th-Spallation-Produced ^{225}Ac with Reduced ^{227}Ac Content," *Inorg. Chem.*, vol. 59, no. 17, pp. 12156–12165, Sep. 2020, doi: 10.1021/acs.inorgchem.0c01081.

Copyright on 7th Asia-Pacific Symposium on Radiochemistry 2025

[6] P. Causey, B. Tamboline, M. Wong, A. Lee, R. Riddoch, and P. Schaffer, “Construction of a Scalable Radium Generator from Proton Irradiated Natural Thorium for the Production of 227Ac-free Actinium-225 Supporting Early-Phase Clinical Trials,” *J. Nucl. Med.,* vol. 65, suppl. 2, p. 242392, June 2024.
[7] K. Nagatsu, H. Suzuki, M. Fukada, T. Ito, J. Ichinose, Y. Honda, K. Minegishi, T. Higashi, M. Zhang, “Cyclotron production of ^{225}Ac from an electroplated ^{226}Ra target,” *Eur. J. Nucl. Med. Mol. Imaging*, vol. 49, no. 1, pp. 279–289, Dec. 2021, doi: 10.1007/s00259-021-05460-7.

Optimizing temperature conditions for efficient Zn/Cu thermal separation in ^{64,67}Cu production

Naoki Takashima[1], Masako Kawabata[1], Akio Ohta[1], Shoji Motoishi[1], Hideya Saeki[2], Yasuki Nagai[1], Yasuhiro Koguchi[1], Kazuyuki Hashimoto[3], Shunsuke Fujino[3], Masatoshi Itoh[4], Hidetoshi Kikunaga[4], and Kazuaki Tsukada[4]

[1]*Chiyoda Technol Corporation: Oarai, Ibaraki, 311-1313, Japan, Email Address: takashima-n@c-technol.co.jp*
[2]*Chiyoda Technol Corporation: Tokai, Ibaraki, 319-1106, Japan,*
[3]*Japan Atomic Energy Agency (JAEA): Tokai, Ibaraki, 319-1195, Japan*
[4]*Tohoku University: Sendai, Miyagi, 980-8578, Japan,*

The production of ^{64}Cu or ^{67}Cu involves sublimating and collecting zinc (Zn) through thermal separation, followed by chemical separation to obtain purified copper (Cu). Achieving separation at the optimal sublimation temperature for Zn is crucial to maximize the separation yield of ^{64,67}Cu, ensuring efficient and high-purity production. The radioactivities of ^{67}Cu and ^{65}Zn were monitored as probes of Cu and Zn within the sample when irradiated Zn was heated at 500-600°C during thermal separation. It was found that heating at 500°C better suppresses Cu loss by sublimation and improves the recovery yield through thermal separation.

1 INTRODUCTION

^{64}Cu and ^{67}Cu are gaining attention as promising radionuclides for theranostics, which can be used for both therapy and diagnosis [1]. We have developed a method for producing ^{64}Cu and ^{67}Cu by irradiating metallic ^{64}Zn and ^{68}Zn, respectively, with neutrons generated by an accelerator, followed by purification of the ^{64}Cu and ^{67}Cu using thermal and resin-separation methods [2]. By taking advantage of the difference in vapor pressure between Zn and Cu, Zn can be sublimated or vaporized to isolate Cu under vacuum. In practice, it is possible to produce ^{64,67}Cu with minimal radioactive Zn by using enriched ^{64,68}Zn, however the challenge remains to separate Cu in high yields without monitoring the Zn tracer. In this study, the behavior of ^{67}Cu and ^{65}Zn was evaluated under different heating temperature conditions, aiming to improve the separation efficiency of ^{67}Cu, and automate the separation process for practical use.

2 METHODS

The natural Zn samples were irradiated to generate ^{67}Cu via the ^{68}Zn (n, np) ^{67}Cu or the ^{68}Zn (γ, p) ^{67}Cu reactions using the cyclotron or electron linear accelerator respectively at Research Center for Accelerator and Radioisotope Science (RARiS), Tohoku University. The experimental conditions per production are listed in Table 1. An irradiated sample was placed in the thermal separation device and heated under reduced pressure (~10^{-5} hPa). A schematic diagram of the thermal separation device is shown in Fig. 1. Three heating conditions were tested: (1) 600°C, (2) 600°C followed by cooling to 550°C when approximately 70% of the ^{68}Zn appeared to have sublimated, and (3) 500°C. Gamma rays were measured in real-time using CZT (CdZnTe) detectors installed at two areas: the Zn/Cu sample mounting area and the zinc deposition area. Spectral data were obtained at intervals of 180 or 300 seconds. During heating, the behavior of ^{67}Cu and ^{65}Zn was investigated by monitoring the peak area counts of 185 keV for ^{67}Cu and 1,116 keV for ^{65}Zn at both detection areas. Heating continued until the sublimation of ^{65}Zn was considered complete, or until the gamma ray peak of ^{64,67}Cu in the Zn deposition area was clearly observed indicating the ^{67}Cu transfer to the zinc deposition area.

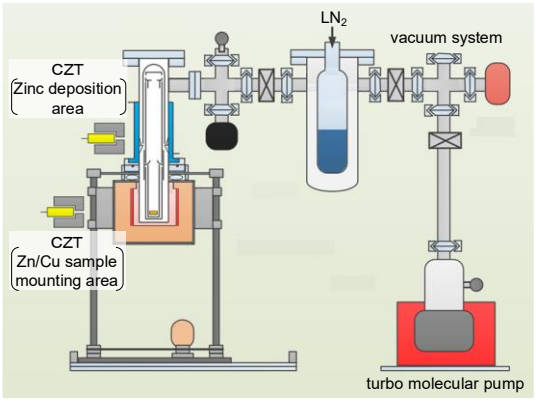


Fig.1. Schematic diagram of thermal separation system

Table 1. Experimental conditions

Production No.	Temperature (°C)	Time (min)	Zn weight (g)	Accelerator
(1)	600	115	15.248	Cyclotron
(2)	600	90	17.384	Cyclotron
(3)	600	123	36.564	Cyclotron
(4)	600-550	115	40.101	Linac
(5)	600-550	124	43.605	Cyclotron
(6)	600-550	120	49.168	Linac
(7)	500	93	5.026	Linac
(8)	500	103	10.770	Cyclotron
(9)	500	171	26.987	Cyclotron
(10)	500	153	35.667	Cyclotron

3 RESULTS AND DISSCUTTIONS

The temporal changes in the peak area counts attributed to ^{65}Zn and ^{67}Cu in the sample mounting areas under heating conditions of 600°C (Nos. (1) – (3)) and 500°C (Nos. (7) – (10)) are shown in Figs.2 and 3, respectively. The peak area counts were normalized based on the initial data in Fig.2, whereas those in Fig.3 were normalized based on the maximum peak area across all time points. Fig.2 shows that Zn begins to sublimate approximately 30-40 minutes after the heating starts, once the temperature has reached to the set value which occurs around 25 minutes. The Zn sublimation rate increased with sample weight, which was more pronounced at 500°C suggesting that the time to complete separation time can be estimated from the sample weight. Note that the sublimation rate may also be influenced by both the weight and the surface area of the sample. The peak area counts for ^{67}Cu in the sample mounting area decreased near the end at 600°C or shortly after the cooling began. This indicates that Cu has transferred or sublimated to the Zn deposition area resulting in yield loss (Fig 3). However, no significant decrease in ^{67}Cu was observed during the experiment at 500°C, suggesting that that ^{67}Cu can be recovered with a high yield while Zn is successfully separated.

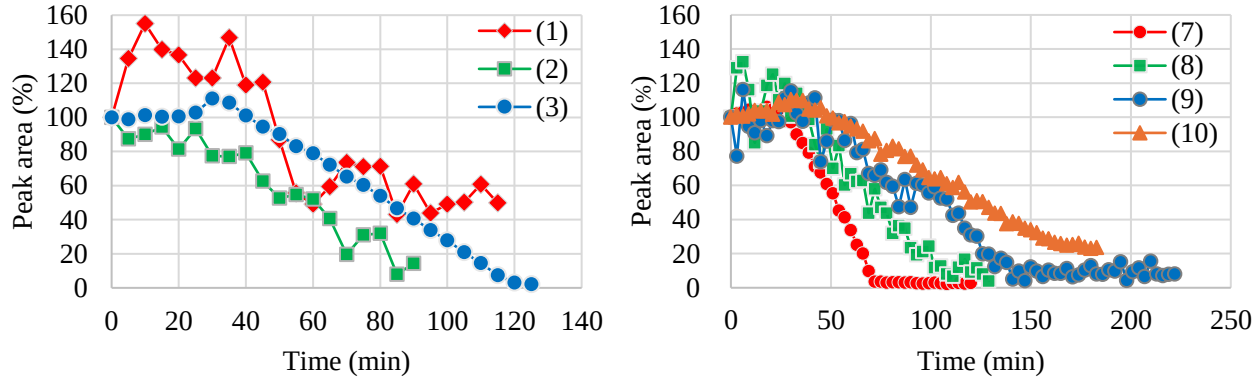


Fig.2. Temporal change in the peak area counts derived from 1116 keV(^{68}Zn) emission in the sample mounting area at heating temperatures of 600°C (left) and 500°C (right)

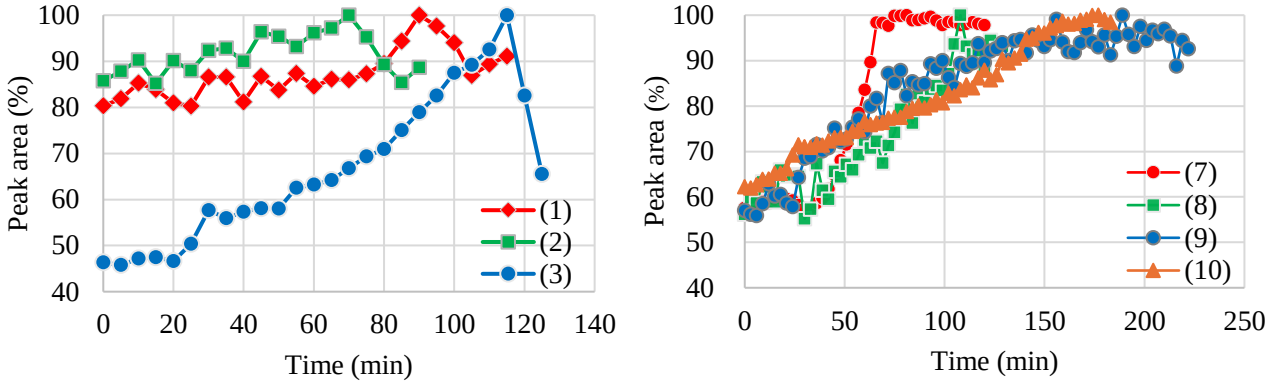


Fig.3. Temporal change in the peak area counts derived from 185 keV(^{67}Cu) emission in the sample mounting area at heating temperatures of 600°C (left) and 500°C (right)

4 CONCLUSIONS

The results suggest that heating at 500°C better optimizes the thermal separation conditions for Zn and Cu, minimizing ^{67}Cu loss and improving the recovery yield. Appropriate separation time can be estimated based on the Zn sublimation rate observed in this study. This separation system can be effectively used for upscale production, ensuring good recovery of Zn and $^{64, 67}$Cu radionuclides.

ACKNOWLEDGMENTS

The radionuclides were supplied by Research Center for Accelerator and Radioisotope Science, Tohoku University and Supply Platform of Short-lived Radioisotopes, supported by JSPS Grant-in-Aid for Scientific Research on Innovative Areas, Grant Number 22H04924.

References

[1] P. Kręcisz et al., J. Med. Chem. 2025 68 (3), 2356-2376
[2] M. Kawabata et. J.Radioanal Nucl. Chem. 2021, 330 (3), 913−922.
[3] A. Ohta et. al., The 68th Annual Meeting of The Japan Society of Nuclear and Radiochemical Sciences, Shizuoka, September 2024

7th Asia-Pacific Symposium on Radiochemistry *September 14 ~ 19, 2025 • Kunibiki Messe • Shimane, Japan*

Production and separation of ^{149}Tb by the ^{133}Cs + ^{20}Ne reaction

Y. Kawakami[1], S. Goto[1], M. Asai[2], T. K. Sato[2], Y. Ito[3], K. Tsukada[4], I. Nishinaka[5],

[1]*Graduate School of Science and Technology, Niigata University: Niigata, Niigata, 950-2181, Japan*
[2]*Avanced Science Research Center, Japan Atomic Energy Agency: Tokai, Ibaraki 319-1195, Japan*
[3]*Wako Nuclear Science Center, KEK : Wako, Saitama, 351-0198, Japan*
[4]*Research of Center for Accelerator and Radioisotope Science, Tohoku University: Sendai, Miyagi, 980-8577, Japan*
[5]*National Institutes for Quantum Science and Technology: Inage, Chiba, 263-8555, Japan*

Alpha-emitting radionuclides, such as ^{149}Tb, are promising agents for targeted alpha therapy (TAT) due to their high cytotoxicity and potential theranostic applications. In this study, ^{149}Tb was produced via the heavy-ion reaction ^{133}Cs + ^{20}Ne, and its separation from target and byproduct elements was achieved using LN resin chromatography. The excitation functions of the produced nuclides were measured, and effective separation of ^{149}Tb from Cs and neighboring lanthanides was demonstrated.

1. INTRODUCTION

Alpha-emitting radionuclides are attracting significant attention in the field of targeted alpha therapy (TAT) for cancer treatment [1]. Among them, ^{211}At and ^{225}Ac are making progress toward clinical application. However, these elements do not have stable isotopes, which makes their handling in drug development difficult. In contrast,^{149g}Tb ($t_{1/2}$ = 4.1 h), a nuclide that decays by EC and alpha emission is a promising candidate for theranostic applications due to the availability of stable terbium isotope, enabling easier experimental handling. Previous studies reported the production of that ^{149}Tb using proton- or heavy-ion-induced reactions using lanthanide targets [1]. However, chemical separation of ^{149}Tb from macroscopic amounts of lanthanide target material remains a significant challenge. In this study, we aimed to produce^{149}Tb by irradiation of ^{20}Ne ions to an alkali metal target, ^{133}Cs. The excitation functions of the produced nuclides were measured, and ^{149}Tb was successfully separated from the target and other lanthanides using extraction chromatography.

2. EXPERIMENTS

The experiment was performed at the 20 MV tandem accelerator facility of JAEA. CsCl was deposited onto 2 μm thick aluminum foil at approximately 400 μg cm^{-2} using vacuum evaporation and covered with another Al foil. Five such targets were stacked to form a target stack. For chemical separation studies, thicker CsCl target (2 mg cm^{-2}) was deposited on 10 μm Al foil. The target stacks were irradiated with ^{20}Ne^{8+} beam accelerated to 105 MeV for 5 hours and 20 minutes at an average beam current of about 100 pnA. After irradiation, each target was sealed in a sachet containing silica gel to avoid deliquescence. The produced nuclides were identified and quantified with γ-ray spectrometry using a HPGe detector.

Chemical separation was performed with extraction chromatography using LN resin [2], a phosphate diester type resin that is effective for rare earth element separation. The irradiated CsCl was dissolved in 1 mL of 0.5 M HNO_3, loaded onto the column, and eluted stepwise with 0.5 M, 1.0 M, and 2.0 M HNO_3. Eluates were collected by 1 mL and each fraction was analyzed for the nuclide contained. The fraction containing the highest yield of ^{149}Tb was evaporated to dryness in a stainless steel dish, and α-ray spectra were measured.

3. RESULTS AND DISCUSSION

The main observed nucludes were ^{132}Cs, ^{138m}Pr, ^{146}Eu, ^{149}Gd, and ^{148,149}Tb. Excitation functions of these nucludes are under analysis. The elution curves obtained as a results of chemical separation is shown in Figure 1. Cs and Pr were eluted with 0.5 M HNO_3, Eu and Gd with 1.0 M, and the objective nuclude^{149}Tb with 2.0 M HNO_3. The target material, Cs, was not detected in fractions other than the initial Cs fraction, demonstrating complete separation from Tb. This separation behavior reproduced the results of preparatory experiments using stable isotopes. The α-ray spectrum of the separated ^{149}Tb showed a sharp peak, indicating effective separation from Cs and other contaminants.

Copyright on 7th Asia-Pacific Symposium on Radiochemistry 2025

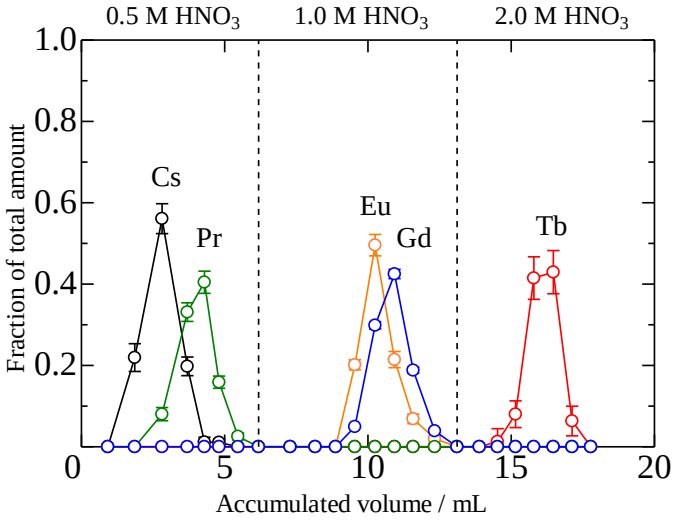


Fig.1 Elution curve of each product nuclide using extraction chromatography with Ln resin.

4. CONCLUSIONS

The ^{133}Cs + ^{20}Ne reaction successfully produced several nuclides,^{149,148}Tb,^{149}Gd and ^{146}Eu. Extraction chromatography using LN regin effectively isoated terbium isotopes from the cesium target material and lanthanide byproducts. This method provides a simple and practical approach for producing ^{149}Tb, offering a promising pathway for the development of alpha-emitters in TAT research.

ACKNOWLEDGMENTS

We would like to thank to the staff on the Tandem Accelerator Facility of JAEA for their support of our experiment.

REFERRENCE

[1] R. Eychenne *et al*., Pharmaceutics **13** (2021) 906.
[2] C. K. Holiski *et al.*, Appl. Radiat. Isot. **214** (2024) 111530.

7th Asia-Pacific Symposium on Radiochemistry *September 14 ~ 19, 2025 • Kunibiki Messe • Shimane, Japan*

OPTIMIZATION OF BEAM TRANSPORTATION AT U-LINE J-PARC MLF FOR MUON STOPPING POWER STUDIES

A Miura[1], K Ninomiya[2], M Inagaki[3], S Kanda[4], Y Ikedo[4], Y Oishi[4], K Shimomura[4], Y Nakazawa[5] and T Yoshimura[1]

[1]*The University of Osaka: 1-1 Machikaneyama, Toyonaka, Osaka 560-0043, Japan, u140944b@ecs.osaka-u.ac.jp*
[2]*Hiroshima University: 1-4-1 Kagamiyama, Higashi-Hiroshima, Hiroshima 739-8527, Japan*
[3]*Kyoto University: 2-chome Asashiro-nishi, Kumatori, Sennan-gun, Osaka 590-0494, Japan*
[4]*Institute of Materials Structure Science, KEK: 1-1 Oho, Tsukuba, Ibaraki 305-0801, Japan*
[5]*Accelerator Laboratory, KEK: 1-1 Oho, Tsukuba, Ibaraki 305-0801, Japan*

This study aims to investigate the stopping power of positive muons in the 1-30 keV range using the Ultra-Slow Muon (USM) from U-line at J-PARC. Stopping power, especially in the intermediate-energy region (several tens of keV), is essential for understanding charged particle deceleration and stopping processes in materials. Beam transportation parameter and optimum target thickness for stopping power measurement were estimated from Monte Carlo simulation. We also performed beam-optics experiments using USMs and laser-ionized hydrogen at the U-line to optimize beam transportation.

1. INTRODUCTION

Stopping power, defined as the energy loss per unit path length when a charged particle passes through a material, is a fundamental parameter for characterizing particle–matter interactions, with applications ranging from radiation shielding design to evaluation of biological effects [1,2]. Since most energy-loss processes are governed by interactions with bound electrons in the material, the stopping power—particularly for heavy charged particles—strongly depends on the incident kinetic energy. In the high-energy region, where the kinetic energy of the incident particle greatly exceeds that of bound electrons, the Bethe–Bloch formula provides an accurate description of energy loss. In the low-energy region, the Lindhard–Scharff–Schiøtt (LSS) theory is commonly used to describe energy losses involving nuclear interactions [3,4]. In the intermediate-energy region, though, semi-empirical formulations developed by Ziegler are widely used, experimental data are essential for accurate evaluation [5]. This energy region is characterized by a peak structure in stopping power as a function of projectile energy, corresponding to the regime in which the particle undergoes rapid deceleration while traversing the material.

A muon is an elementary particle with the same electric charge and spin as the electron, whereas its mass is approximately 207 times greater. Owing to its unique properties, the muon has been widely utilized in fields such as non-destructive elemental analysis using characteristic muonic X-rays and materials science through muon spin rotation/relaxation/resonance (μSR) techniques for probing local magnetic environments [6-8]. Despite these advances in applied muon science, fundamental data such as the stopping power of muons—particularly in the intermediate-energy range (1–100 keV)—remain limited. Some experimental data were reported in 1996 by a research group at the Paul Scherrer Institute in Switzerland [9], but have not been significantly updated since. This is primarily due to the challenges associated with muon production, which typically relies on high-energy proton-induced spallation reactions, and the muon's short mean lifetime of 2.2 μs, which makes it difficult to generate high-quality muon beams.

In this study, we aim to perform measurements of the stopping power of positively charged muons in the 1–30 keV energy range using Ultra-Slow Muons (USMs) available at the U-line of the Materials and Life Science Experimental Facility (MLF) at the Japan Proton Accelerator Research Complex (J-PARC).

2. EXPERIMENTAL SETUP

At the U-line, 4 MeV muons are stopped in a muonium production target, where the resulting thermalized muoniums—bound states of a positive muon and an electron—are emitted into vacuum and ionized by laser excitation to produce USMs with kinetic energies of a few eV [10]. The USMs are then accelerated by electric fields to monochromatic energies in the range 1-30 keV and extracted as a beam with high spatial density. After generation, the USM beam is transported along a linear beamline to two measurement positions—F3 (upstream) and F3D (downstream)—using electric quadrupoles and magnetic and electric bends (Fig. 1).

At both these positions, microchannel-plate with delay-line detectors (MCP-DLD) systems are installed using a linear insertion mechanism. The USM beam parameters, such as profile, intensity and velocity (energy), can be measured the MCP-DLD system. In the stopping power measurement, a thin-foil target was placed the MCP-DLD of the F3 position. By measuring the kinetic energy difference of muons traversing the F3-F3D segment with and without the thin foil, the energy loss within the target—i.e., the stopping power—can be determined.

In the initial experiment, we planned to evaluate the stopping power of 30 keV muons using a carbon thin foil and compared the results with previously reported data to assess the systematic uncertainties associated with the present measurement setup. From time-of-flight measurements without a thin foil, the maximum energy of the USM extracted by the electrostatic field was determined to be 30.5 keV in this case. Additionally, measurements were conducted using laser-ionized hydrogen to validate beam transport simulations and calibrate the detection system at U-line.

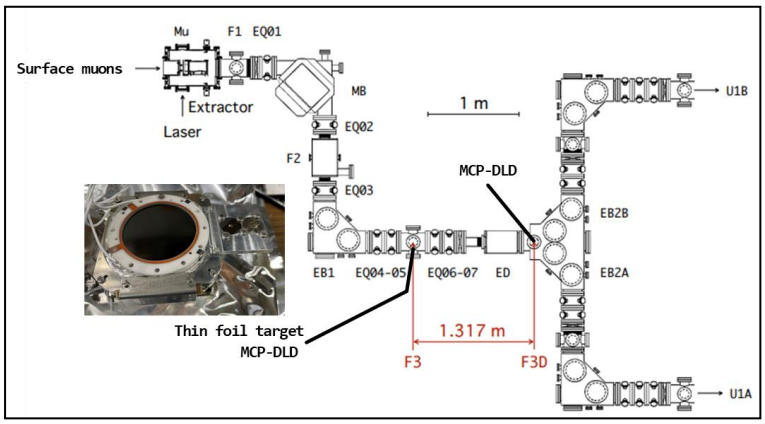


Fig. 1. Layout of the U-line setup and image of the thin-foil target attached to the MCP-DLD detector.

3. OPTIMIZATION OF BEAM TRANSPORTATION

In the present experiment, the GEANT4-based Monte-Carlo simulation program “musrSim” was used to estimate the optimal the beam transport parameters [11]. Simulations were performed using a musrSim executable incorporating the electromagnetic field configuration and geometric structure of the U-line.

During the proton-beam based experiments conducted in beam-off periods, a combination of musrSim simulations and transfer matrix calculations was employed to support the optimization of beam transport. While musrSim enables detailed tracking including nonlinear effects, it is computationally demanding. In contrast, the transfer matrix method, though based on a linear approximation, offers fast evaluation with minimal computational cost. Therefore, in the initial phase, rough estimates of the transport parameters were obtained using matrix calculations, followed by parameter scans using musrSim to achieve high-precision optimization of the final beam transport settings.

4. ESTIMATION OF CARBON THIN-FOIL

At the F3 position in musrSim, carbon foil and its sample holder were implemented, and simulations were executed for the transmission of 30.5 keV muons through the foil. The kinetic energy distributions of the beam at the F3D position were estimated under various foil thickness conditions. Based on these results, the optimal foil thickness under the present experimental setup was determined, and the thin-foil sample and its holder were fabricated accordingly. The constructed target system was then attached to the MCP-DLD at the F3 position on the U-line.

References

[1] T. Kato et al., *IEEE Transactions on Nuclear Science* **68**, 7, 1436 (2021).
[2] D. Atri et al., *Geophys. Res. Lett*. **38**, L19203 (2011).
[3] H. Bethe, *Eur. Phys. J. H* **39**, 537 (2014).
[4] J. Lindhard et al., *Mat.-Fys. Medd. Dan. Vid. Selsk*. **33**, 14 (1963).
[5] D. E. Groom et al., *At. Data Nucl. Data Tables* 76, 2 (2001).
[6] K. S. Takaura et al., *J. Natural Med*. **75**, 532 (2021).
[7] K. Ninomiya et al., *J. Radioanal. Nucl. Chem* **333**, 3445 (2024).
[8] M. Hiraishi et al., *Phys. Rev. Lett*. **132**, 166702 (2024).
[9] F. J. Hartmann et al., *Hyperfine Interactions* 101/102, 623 (1996).
[10] S. Kanda et al., *J. Phys.: Conf. Ser*. **2462**, 012030 (2023).
[11] K. Sedlak et al., *Physics Procedia* **30**, 61 (2012).

7th Asia-Pacific Symposium on Radiochemistry *September 14 ~ 19, 2025 • Kunibiki Messe • Shimane, Japan*

ADSORPTION EXPERIMENTS OF MONOVALENT CATIONS ONTO FERROCYANIDE CRYSTALS: TOWARD ELUCIDATING THE CHEMICAL PROPERTIES OF FRANCIUM

Hiroki Nakada[1], Yoshitaka Kasamatsu[2], Koichi Takamiya[3]

[1]Institute for Integrated Radiation and Nuclear Science, Kyoto University:
2-1010 Asashironishi, Kumatori, Sennan, Osaka 590-0494, Japan,
nakada.hiroki.24n@st.kyoto-u.ac.jp
[2]Graduate School of Science, The University of Osaka:
1-1 Machikaneyama, Toyonaka, Osaka 560-0043, Japan
[3]Institute for Integrated Radiation and Nuclear Science, Kyoto University:
2-1010 Asashironishi, Kumatori, Sennan, Osaka 590-0494, Japan

Francium (Fr), the heaviest known group 1 element, is thought to be strongly influenced by relativistic effects due to its high nuclear charge. This study aims to investigate the influence of relativistic effects on Fr through chemical experiments. We synthesized ferrocyanide crystals, which are known to selectively adsorb cesium (Cs), an element with chemical properties similar to Fr, and determined the absorption ratios of group 1 elements. The influence of relativistic effects can be elucidated by comparing the predicted adsorption behavior based on other group 1 elements with the experimentally observed behavior of Fr. From the results, we assessed the feasibility of future experiments with Fr.

1 INTRODUCTION

Francium (Fr) is known to be the heaviest group 1 element. Fr, an element of the seventh period, has a high nuclear charge and is thought to be strongly affected by the relativistic effects. Fr has one additional electron in the 7s orbital compared to radon, a noble gas with a closed outer electron shell. Relativistic effects cause the 7s orbitals in the outermost shell of Fr to be more tightly bound to the nucleus, and the chemical properties of Fr cannot simply be extrapolated from those of other light homologous elements. On the other hand, if the chemical properties originated from francium's 7s orbital can be experimentally determined, it would provide valuable insight into the influence of relativistic effects on this orbital. In particular, Fr has a simple electronic configuration, with only one electron in the outermost 7s orbital, making it an ideal element for studying these effects.

However, the chemical properties of Fr are investigated in significantly fewer experimental studies because there are no stable isotopes that can be easily used in experiments. Namely, even the most stable isotope of ^{221}Fr has a half-life of only about 22 minutes. Therefore, we developed experimental methods to overcome the limitations associated with studying the chemistry of Fr using homologous elements and aimed to elucidate the influence of relativistic effects on Fr.

2 EXPERIMENTS

In this study, our goal is to understand the chemical properties of Fr from the adsorption behavior of monovalent cations by ferrocyanide salt crystals. Ferrocyanide salt crystals are known to selectively adsorb Cs, a group 1 element with similar chemical properties to Fr, and have been extensively studied for the recovery of ^{134}Cs and ^{137}Cs released during nuclear accidents.

In the present study, the adsorption behavior of monovalent cations on the crystals of ferrocyanide salts was studied by the following methods, and to evaluate the applicability of this system to experiments involving Fr. Zinc ferrocyanide crystals, composed of ferrocyanide ions and zinc ions, were synthesized and mainly used in our experiments. Equal volumes of 0.15 M solution of zinc chloride ($ZnCl_2$) in hydrochloric acid and 0.10 M aqueous potassium ferrocyanide ($K_4Fe(CN)_6$) solution were mixed to form zinc ferrocyanide crystals ($K_2Zn_3[Fe(CN)_6]_2$), with the solution pH adjusted to 2 using hydrochloric acid. (All reagents were products of Wako Pure Chemical Industries Ltd.) The resulting crystals were collected by suction filtration using a polycarbonate membrane filter (pore size: 0.2 μm, ADVANTEC®), dried at 60°C for 24 hours, and stored in a desiccator under dry conditions. Cs^+, Rb^+, and K^+ were employed as representative monovalent cations in the experiments, using their radionuclides: ^{137}Cs, ^{86}Rb, and ^{42}K. The ^{86}Rb and ^{42}K isotopes were produced by neutron irradiation using the pneumatic transport facility of KUR (Kyoto University Research Reactor).

In the monovalent cation adsorption experiments, the synthesized ferrocyanide salt and a solution of the monovalent cation chloride or carbonate were mixed in a test tube and shaken using a mechanical shaker to induce adsorption onto the crystals. After shaking, the crystals and filtrate were separated by suction filtration through a

polycarbonate membrane filter (pore size: 0.2 μm, ADVANTEC®), and γ rays emitted from the crystals, filtrate, wash solution, and experimental apparatus were measured using a germanium semiconductor detector (model: GWL-120230, ORTEC®). The activities of ^{137}Cs, ^{86}Rb, and ^{42}K were estimated by the photo peaks areas at 662 keV, 1077 keV, and 1525 keV, respectively. For ^{86}Rb and ^{42}K, which have relatively short half-lives, activities were corrected with their half-lives.

3 RESULTS AND DISCUSSION

The adsorption ratios of Cs^+, Rb^+, and K^+ onto the zinc ferrocyanide crystals were estimated from the ratio of these activities in the crystals and solutions. Figure 1 shows the relationship between adsorption ratios and shaking time. In the experiments for $^{137}Cs^+$ and $^{86}Rb^+$ under identical conditions, the adsorption ratio of Cs^+ was significantly higher than that of Rb^+, supporting the specific adsorption of Cs^+ on zinc ferrocyanide. Furthermore, it is known that the adsorption of monovalent cations onto zinc ferrocyanide crystals ($K_2Zn_3[Fe(CN)_6]_2$) occurs via an ion-exchange reaction with K^+ ions present in the crystal [3]. The time required to reach equilibrium of the ion-exchange reaction of K^+ in the crystal was investigated, and it was found that equilibrium was achieved within 1 minute for all monovalent cations. The short equilibrium arrival time suggests that the present reaction systems could be applicable to Fr experiments, which require rapid chemical operations due to Fr's short half-life. On the other hand, extremely low concentrations of Fr can be produced and used in actual experiments. However, experiments with trace concentrations of group 1 elements were not conducted in the present study. Therefore, we will conduct experiments using carrier-free group 1 elements at trace concentrations to evaluate the feasibility of this method for Fr and to assess its potential for application under low concentration conditions in the future.

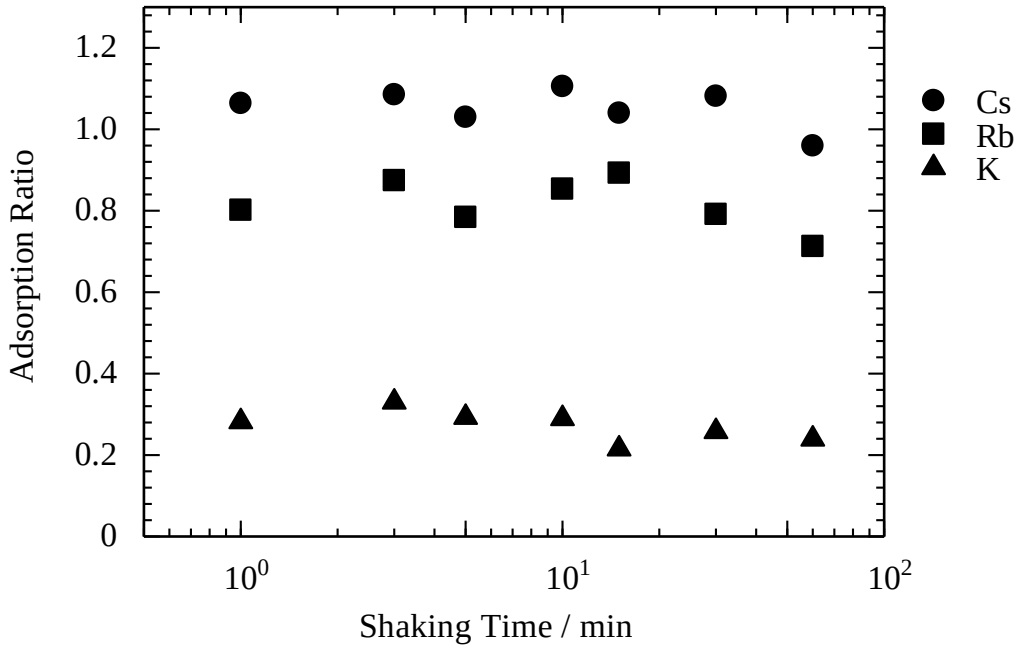


Fig. 1. Dependence of the adsorption ratios of Cs^+, Rb^+, and K^+ onto zinc ferrocyanide crystals on shaking time.

ACKNOWLEDGMENTS

We gratefully acknowledge the cooperation of the KUR staff in the production of radionuclides.

References

[1] K. Shakira, M. Sohsahb, and M. Soliman, "Removal of cesium from aqueous solutions and radioactive waste simulants by coprecipitate flotation" *Separation and Purification Technology*, **54,** 373–381 (2007).
[2] H. Mimura, J. Lehto and R. Harjula, "Ion Exchange of Cesium on Potassium Nickel Hexacyanoferrate (II)s," *Journal of Nuclear Science and Technology*, **Vol. 24, No.5,** 484–489 (1997).
[3] S. Kawamura, H. Kuraku and K. Kurotaki, "Composition and ion-exchange behavior of zinc hexacyanoferrate(II) analogs," *Anal. Chim. Acta*, **49**, 317 (1970).

Copyright on 7th Asia-Pacific Symposium on Radiochemistry 2025

Development of a Functionalized Surface for Alpha-particle Detectors for Use in Liquid Phase

Ryo Otani[1], Tetsuya K. Sato[1,2], Erina Takeuchi[1], Yuta Miyachi[1,2], Hina Natori[1,2], Maki Honda[1], Yuichiro Nagame[1]

[1]*Japan Atomic Energy Agency (JAEA): 2-4, Shirakata, Tokai, Naka, Ibaraki, 319-1195, Japan*
[2]*Graduate School of Science and Engineering, Ibaraki University: 2-1-1, Bunkyo, Mito, Ibaraki, 310-8512, Japan*

For measuring α-emitting nuclides directly in solution, avoiding the pretreatment required by conventional α-spectrometry, LSC, or ICP-MS, we have developed a novel α-particle detector with a functionalized surface enabling selective absorption of elements of interest. As a model experiment, titanium plates were sputter-coated with gold and functionalized with self-assembled monolayers SAMs of sodium 11-mercaptoundecane-1-sulfonate, whose terminal -SO_3^- groups act as strong cation-exchange sites. After conditioning in 1 M HNO_3, the modified surfaces selectively adsorbed $^{88}Zr^{4+}$ and $^{88}Y^{3+}$ from HCl media, exhibiting adsorption behavior consistent with literature ion-exchange data. These results demonstrate that a detector with the SAM surface provides promisingly fast and high-resolution α-particle detection in time-limited radiochemical analyses.

1. Introduction

In general, α-particle spectrometry and liquid scintillation counting (LSC) are the widely used in analytical methods for α emitting nuclides in the liquid phase. Recently, inductivity-coupled plasma mass spectrometry (ICP-MS) is becoming popular for measuring long-lived α-emitters. These techniques require sample pretreatment before measurements, which takes considerable time. Therefore, it is difficult to apply them for α-particle measurements when there is a time limitation, such as short half-lives of nuclides of interest and a restricted measurement time. In some cases, the LSC method requires only a minimal time for pretreatment, but its α-ray resolution is poor, making it difficult to identify nuclides.

For alpha measurements in solution, chemical modification of the detector surface has been proposed to absorb nuclides on the detector [1-2]. Self-assembled monolayers (SAMs) are used for the chemical modification of the gold surface of the detector [3]. The functional groups at the ends of the SAMs are an ion exchange group, which allows ion exchange with elements in solution.

In this work, we attempted to modify the Au surfaces with alkanethiols sputtered onto a Ti foil. We investigated whether it would be possible to measure alpha in a solution by converting the terminal of the alkanethiols into an ion-exchange group.

2. Experiments

As a model of α-particle detector surface, we employed Ti plates. A Ti plate (0.3 mm) was cleaned with methanol, acetone, and ultrapure water in an ultrasonic cleaner. Then it was dried by a dryer, followed by coating with Au by ion sputtering. To perform chemical modification of the Au surface, a thiol agent bearing the SO_3^- groups as strongly acidic ion-exchange sites was used. The thiol agent, HS-$(CH_2)_{11}$-SO_3Na, was purchased from ProChimia Surfaces, Sp.zo.o. For the preparation of a functionalized surface on the Au-coated Ti substrates with the thiol agent, the substrates were immersed in the thiol 1mM ethanol solution for ~24h. The functionalized process is described in [2] as follows:

$$HS\text{-}(CH_2)_{11}\text{-}SO_3Na + Au \rightarrow (HS\text{-}(CH_2)_{11}\text{-}SO_3Na)_{phys}Au \quad (1)$$

$$(HS\text{-}(CH_2)_{11}\text{-}SO_3Na)_{phys}Au \rightarrow Au\text{-}S\text{-}(CH_2)_{11}\text{-}SO_3Na + 1/2H_2 \quad (2)$$

Then, the substrate surfaces were washed with ethanol and ultrapure water. Afterward, they were dried in the air. The functionalized thiol structure of the substrate surface is shown in Fig. 1. The surface was washed with 1M HNO_3 for conditioning.

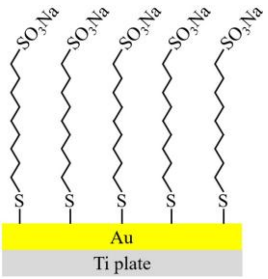


Fig. 1. Schematic diagram of the substrate surface.

To evaluate the cation-exchange property of the conditioned substrates, we measured adsorption efficiencies of Zr and Y on the surface using the ^{88}Zr and ^{88}Y tracers in HCl. After immersing the substrate samples in the solution and washing them with distilled water, the samples were measured to determine the amount of each tracer absorbed on the surface with an HP-Ge semiconductor detector for γ-ray measurement. The obtained HClconcentration dependence of the adsorption efficiencies of Zr and Y was consistent with the literature data [4]. The cation exchange process is described as follows (M = Zr or Y):

$$\text{Au-S-(CH}_2\text{)}_{11}\text{-SO}_3\text{Na} + \text{M}^+ \rightarrow \text{Au-S-(CH}_2\text{)}_{11}\text{-SO}_3\text{M} + \text{Na}^+ \quad (3)$$

3. CONCLUSIONS

We developed the functionalized detector surface that can be applied to the α measurement in the liquid phase. We employed sodium alkanethiol sulfonate to prepare the functionalized surface which is capable of the ion exchange. We prepared the model surface and successfully confirmed that the surface has a capability of the cation exchange using the ^{88}Zr and ^{88}Y tracers in HCl solution.

ACKNOWLEDGMENTS

This study was supported by the Hoga research and development program of JAEA. We thank RIKEN for providing the ^{88}Zr tracer.

References

[1] D. Krupp et al., *Nucl. Instrum. Methods Phys. Res. A*, **897**, 120-128 (2018).
[2] V. Zakusilova et al., *Appl. Surf. Sci.*, **642**, 158356 (2024).
[3] J. Christopher Love et al., *Chem. Rev.*, **105**, 1103-1169 (2005).
[4] F. Nelson et al., *J. Chromatog.*, **13**, 503 (1964).

Detector calibration for Si detector by using a light emitting diode

Toshitaka Niwase[1], Tomoki Fujii[1]
[1]*Department of Physics, Kyushu Univ: 744 Motooka, Nishi-ku, Fukuoka, Japan, 819-0395*

Silicon-based detectors, including silicon photodiode and silicon photomultipliers (SiPM), are widely employed in nuclear physics due to their good energy resolution. SiPMs, with their high quantum efficiency and immunity to magnetic fields, are particularly suitable for scintillation counting. However, their gain is sensitive to temperature variations, requiring regular calibration to maintain measurement accuracy. While charge-sensitive preamplifier systems for silicon detectors can be calibrated using electronic pulser signals, photon detectors like SiPM cannot be calibrated in the same way. To address this, we have developed a novel calibration method using a light-emitting diode (LED). The LED provides precisely controlled pulsed light, enabling gain calibration without using the radioactive sources. This approach offers a simple and repeatable method for evaluating the energy response of photodetectors under varying conditions.

1 Introduction

Silicon semiconductor detectors are widely used for charged particle detection due to their high energy resolution and low noise characteristics. In experiments on superheavy nuclides, silicon detectors play an important role in precisely identifying α-decays and spontaneous fission from background events, and in determining time correlations in decay chains with high accuracy [1]. Silicon photomultiplier (SiPM), or multi-pixel photon counter (MPPC), which are avalanche photodiodes operated in Geiger mode, are based on silicon semiconductors. Compared to conventional photomultiplier tube (PMT), SiPM exhibit higher quantum efficiency and better energy resolution, and are not affected by magnetic fields, making them suitable for use in scintillation counting. In this way, silicon-based particle detectors are extensively utilized in various fields, including nuclear physics and radiochemistry.

However, in nuclear spectroscopic measurements, such as those α- and/or γ- spectroscopy, environmental factors such as long-term temperature variations and gain fluctuations in electronic circuits can distort energy spectra. This issue is particularly pronounced in SiPM, which have a relatively large temperature coefficient of gain, requiring careful calibration to ensure precise measurements.

While the setup of Si detector with a charge-sensitive preamplifier can be calibrated using artificial pulse signals generated by research pulse generator, optical detectors such as SiPM cannot be calibrated in this manner. Therefore, a more conventional approach is necessary for their calibration.

In this study, we have developed a novel calibration method for photodetectors using a light-emitting diode (LED). LEDs can generate pulsed light easily through a control circuit, and both the light intensity and timing of emission can be precisely controlled. By utilizing these features, LEDs can serve as artificial light sources to evaluate the energy response of photodetectors without relying on radioactive sources.

2 Experiment

We have made an LED driver circuit by combining a microcontroller-based rectangular wave generator with a shaping circuit designed to simulate the decay time characteristics of radiation signals. The experimental setup is illustrated in Fig. 1. Even when driven under low voltage and short pulse width conditions, the light emitted from the LED is still too intense for the photodetector. To address this, a neutral density (ND) filter was placed in front of the LED to attenuate the light intensity. In this measurement, we used a general-purpose ND filter that uniformly reduces light intensity across the visible wavelength range (approximately 380 to 700 nm), without selecting a specific wavelength. Although the peak sensitivity of photodetectors varies depending on their type, we used a standard red LED with a peak emission at 625 nm in this work.

The output signal from the detector was processed in the same way as with radiation detection through a preamplifier and shaping amplifier before being sent to a pulse height analyzer to measure the pulse height distribution.

In the conference, we will report in detail on the development process and experimental results of this LED-based calibration method.

Copyright on 7th Asia-Pacific Symposium on Radiochemistry 2025

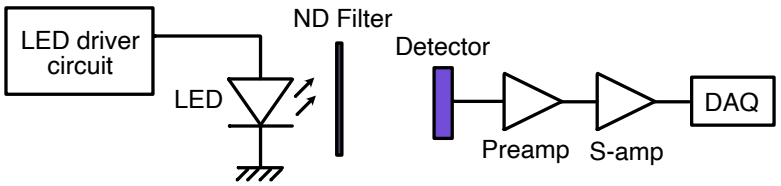


Fig. 1. Experimental setup for the detector calibration of Si detector by using a light emitting diode. The LED is driven by a driver circuit, and the light of LED is attenuated by the ND filter before injection to the detector.

References

[1] K. Morita *et al.*, J. Phys. Soc. Jpn. 81 (2012) 103201.

7th Asia-Pacific Symposium on Radiochemistry *September 14 ~ 19, 2025 • Kunibiki Messe • Shimane, Japan*

Determination of γ-ray intensities of ^{196m2}Au and 263.8-keV transition

Y. Cho[1], S. Goto[1], M. Asai[2], T. K. Sato[2], Y. Ito[3], K. Tsukada[4] ,H. Kikunaga[4]

[1]*Graduate school of Science and Technology, Niigata University : Niigata, Niigata, 950-2181, Japan*
[2]*Advanced Science Research Center, Japan Atomic Energy Agency: Tokai, Ibaraki, 319-1195, Japan*
[3]*Wako Nuclear Science Center, KEK : Wako, Saitama, 351-0198, Japan*
[4]*RARiS, Tohoku University: Sendai, Miyagi, 980-8587, Japan*

Gold is commonly used as a neutron monitor. However, the γ-ray intensities of ^{196m2}Au ($t_{1/2}$ = 9.6 h), produced via the (n,2n) reaction, have previously been reported inaccurately, leading to inconsistencies in radioactivity measurements. In this study, we measured the relative γ-ray intensities of ^{196m2}Au and attempted to determine the absolute intensity of the 188.3-keV γ-ray. In addition, the previously unassigned 263.8-keV transition, which decays with a half-life of 9.6 h, was identified using γ-γ coincidence techniques.

1 INTRODUCTION

Gold is commonly used as a monitor for thermal and fast neutrons due to its single stable isotope, ^{197}Au, and its relatively large neutron activation cross section. Accurate determination of its induced radioactivity is essential for precise neutron flux measurements. However, in experiments involving fast neutron irradiation, the measured radioactivity of ^{196m2}Au varied depending on the γ-ray peak analyzed. This implies that the γ-ray intensities listed in the latest Nuclear Data Sheets 2007 (NDS2007)[1] may be incorrect. The purposes of this study are to obtain high-precision γ-ray intensities of ^{196m2}Au and to assign the 263.8-keV transition, which was observed in decay analysis but no assigned to a specific transition.

2 EXPERIMENTS

The experiment was conducted at the 20 MV tandem accelerator facility of JAEA. Deuterons accelerated to 25 MeV were irradiated to a beryllium converter in order to produce fast neutrons. Gold foils (25 mm × 25 mm) with thickness of 80 μm (four foils, 20 μm each) and 100 μm (two foils, 50 μm each) were irradiated at a beam current of approximately 500 nA for 1 hour, respectively. After irradiation, γ-γ coincidence measurements were performed using one of the 20 μm foils. To determine the radioactivities of the produced nuclides, γ-rays were measured over approximately 10 days using the 50 μm foils.

3. RESULTS AND DISCUSSION

3.1 Determination of γ-ray intensity of ^{196m2}Au

The relative intensities, normalized with 188.3-keV peak (a relatively high intensity γ-ray) were calculated. Table 1 shows the measured relative intensities together with those reported previously. As expected, the values obtained in this study differ from those in NDS2007 and are similar to recent report[2]. The absolute intensity of the 188.3-keV γ-ray is currently being analyzed from the growth and decay of ^{196g}Au radioactivity.

Table 1. Relative γ-ray intensities of ^{196m2}Au normalized with 188.3-keV peak.

Energy / keV	NDS2007 [1]	Moody(2020) [2]	This work
84.7	0.0101 ± 0.0004	0.01535 ± 0.00230	0.00745 ± 0.00030
137.7	0.0435 ± 0.0146	0.04525 ± 0.00115	0.04560 ± 0.00052
147.8	1.449 ± 0.050	1.2614 ± 0.0147	1.2555 ± 0.0122
168.4	0.2609 ± 0.0171	0.1736 ± 0.0018	0.1732 ± 0.0018
174.9	0.01461 ± 0.00057	0.01274 ± 0.00086	0.01289 ± 0.0026
263.8	0.0435 ± 0.0146	0.03021 ± 0.00070	0.03031 ± 0.00032
285.5	0.1478 ± 0.0154	0.11623 ± 0.00172	0.11327 ± 0.00093
316.2	0.0986 ± 0.0094	0.08050 ± 0.00141	0.07772 ± 0.00063

Copyright on 7th Asia-Pacific Symposium on Radiochemistry 2025

3.2 Identification of the 263.8 keV transition by γ-γ coincidence measurement

To identify the 263.8-keV transition, γ-γ coincidence measurements were performed. This method detects cascading γ-rays with transitions occurring within nanoseconds using two Ge detectors. Figure 1 shows the peaks identified in a spectrum correlated with the 263.8-keV γ-rays. Asterisks indicate peaks originated from Compton scattering of intense γ-rays of ^{196g}Au and ^{198}Au. The peaks at 147.8 keV and 188.3 keV were identified as ^{196m2}Au, but they appeared as randomly correlated events due to their high intensity. Peaks at 31 keV, 52 keV, and 175 keV were determined to be truly correlated with the 263.8-keV γ-ray, which is consistent with a 348.4-keV level reported in prompt γ-ray measurements[3].

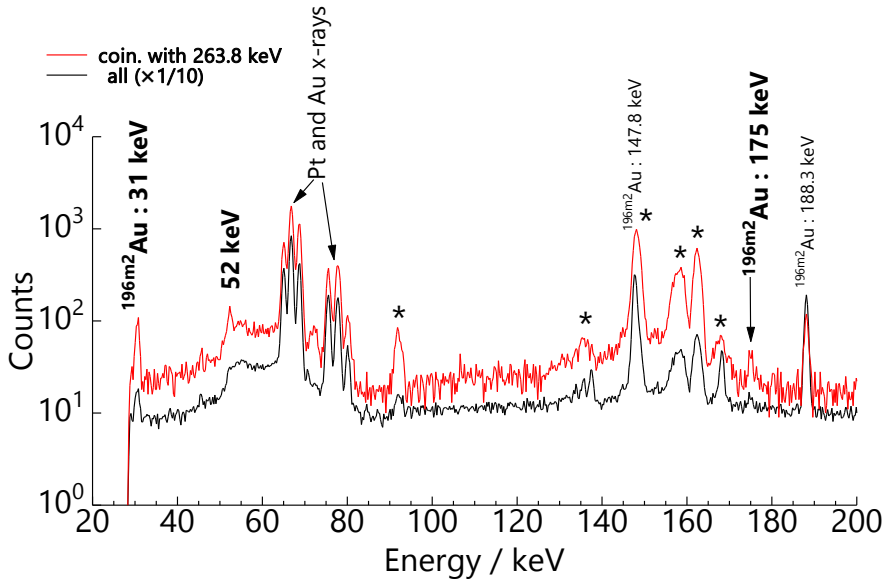


Fig. 1. Peak identification results for spectra of events correlated with 263.8-keV γ-rays. The red line shows the spectrum of correlated events, and the black line is that of all events with counts reduced by a factor of 10.

4 CONCLUSIONS

The relative intensity of γ-rays of ^{196m2}Au was measured with high precision. Absolute intensity determination is ongoing and additional experiments are planned. γ-rays coincident with the 263.8-keV transition were identified using γ-γ coincidence measurements. These results support a consistent interpretation of the ^{196m2}Au γ-ray emission, considering a 348.4-keV level previously observed.

ACKNOWLEDGMENTS

We thank the accelerator operation staff at JAEA and all who supported the γ-ray measurements.

References

[1] X. Hung, Nucl. Data Sheets **108** (2007) 1093.
[2] K. Moody *et al.*, J. Phys. G **47** (2020) 045116.
[3] J. Gröger *et al.*, Phys. Rev. C **62** (2000) 064304.

Copyright on 7th Asia-Pacific Symposium on Radiochemistry 2025

Poster Presentation | [R5]Activation Analysis

Tue. Sep 16, 2025 6:30 PM - 8:00 PM JST | Tue. Sep 16, 2025 9:30 AM - 11:00 AM UTC Poster

[Poster] R5

[P-R5-01]

Precision of simulation for radioactivities produced at a vicinity of nuclear core of KUR

*Norikazu Kinoshita[1], Takuma Noto[1], Kazuaki Kosako[1], Hitoshi Nakashima[1], Yuki Sasaki[1], Kazuyuki Torii[1], Makoto Inagaki[2] (1. Shimizu Corporation (Japan), 2. Kyoto University (Japan))

[P-R5-02]

Evaluation of Total Fluorine Content in the Materials for Laboratory use and Consumer Products Using Instrumental Neutron Activation Analysis

*Yoshiaki Furusho[1], Manabu Takayanagi[1], Tsutomu Miura[2] (1. GL SCIENCES INC. (Japan), 2. AIST (Japan))

[P-R5-03]

Improving the Reliability of Instrumental Neutron Activation Analysis by using the Internal Standard Method

*Tsutomu Miura[1], Hideaki Matsue[2], Koich Takamiya[3], Mitsunori Ishimoto[4] (1. National Institute of Advanced Industrial Science and Technology (Japan), 2. Japan Atomic Energy Agency (Japan), 3. Institute for Integrated Radiation and Nuclear Science, Kyoto University (Japan), 4. Nuclear Professional School, School of Engineering, University of Tokyo (Japan))

[P-R5-04]

Application of INAA to trace metal analysis of polymetallic sulfide ores collected from seafloor massive sulfide deposits

*Jun-ichiro Ishibashi[1], Shin Toyoda[2], Kotaro Yonezu[3], Tatsuo Nozaki[4], Yutaro Takaya[5], Hisao Yoshinaga[6], Koichi Takamiya[6] (1. Kobe Ocean-Bottom Exploration Center, Kobe University (Japan), 2. Institute of Paleontology and Geochronology, Okayama University of Science (Japan), 3. Department of Earth Resources Engineering, Kyushu University (Japan), 4. School of Creative Science and Engineering, Waseda University (Japan), 5. Department of Systems Innovation, The University of Tokyo, Tokyo (Japan), 6. Institute for Integrated Radiation and Nuclear Science, Kyoto University (Japan))

[P-R5-05]

ACTIVATION ANALYSIS OF $PM_{2.5}$ SAMPLES COLLECTED IN HACHIOJI, TOKYO

*Yasuji Oura[1], Shuto Kazama[1], Junya Kaneko[1] (1. Tokyo Metropolitan University (Japan))

[P-R5-06]

PLAN FOR NEUTRON IRRADIATION FACILITIES AND NEUTRON ACTIVATION ANALYSIS INSTRUMENTS IN THE NEW RESEARCH REACTOR AT THE MONJU SITE

*Makoto Inagaki[1], Koichi Takamiya[1], Tsutomu Miura[2], Koshin Washiyama[3], Kazuhiko Akiyama[4], Takahito Osawa[5], Yoshitaka Kasamatsu[6], Naoki Shirai[7], Kunihiko Tsuchiya[8], Go Yoshida[9], Nobuhiro Sato[1] (1. Institute for Integrated Radiation and Nuclear Science, Kyoto University (Japan), 2. Research Institute for Material and Chemical Measurement, National Institute of Advanced Industrial Science and Technology (Japan), 3. Advanced Clinical Research Center, Fukushima Medical University (Japan), 4. Graduate School of Science, Tokyo Metropolitan University (Japan), 5. Nuclear Science Research Institute, Japan Atomic Energy Agency (Japan), 6. Graduate School of Science, The University of Osaka (Japan), 7. Faculty of Science, Kanagawa

©APSORC25

University (Japan), 8. Oarai Nuclear Engineering Institute, Japan Atomic Energy Agency (Japan), 9. Radiation Science Center, High Energy Accelerator Research Organization (KEK) (Japan))

[P-R5-07*]

NON-DESTRUCTIVE DEPTH PROFILE QUANTIFICATION OF CARBON CONTENTS IN JAPANESE SWORD BY MUON LIFETIME ANALYSIS METHOD

*Kousei Yakushi[1], Kenya Kubo[2], Makoto Inagaki[3], Go Yoshida[4], Soshi Takeshita[5], Patrick Strasser[5], Naritoshi Kawamura[5], Yasuhiro Miyake[5], Koichiro Shimomura[5], Tsutomu Saito[6], Kazuhiko Ninomiya[1] (1. Hiroshima University (Japan), 2. International Christian University (Japan), 3. Kyoto University (Japan), 4. KEK Radiation Science Cebter (Japan), 5. KEK IMSS (Japan), 6. National Museum of Japanese History (Japan))

[P-R5-08]

DEVELOPMENT OF A NEW NON-DESTRUCTIVE ELEMENTAL ANALYSIS METHOD FOR TRACE COMPONENTS USING MUON-INDUCED GAMMA RAYS

*Makoto Inagaki[1], Kazuhiko Ninomiya[2], Go Yoshida[3], Kosei Yakushi[2], Eisuke Watanabe[3], Hiroki Nakada[1], Izumi Umegaki[4], Michael Kenya Kubo[5] (1. Institute for Integrated Radiation and Nuclear Science, Kyoto University (Japan), 2. Graduate School of Advanced Science and Engineering, Hiroshima University (Japan), 3. Radiation Science Center, High Energy Accelerator Research Organization (KEK) (Japan), 4. Institute of Materials Structure Science, High Energy Accelerator Research Organization (KEK) (Japan), 5. College of Liberal Arts, International Christian University (Japan))

[P-R5-09*]

ELEMENTAL DEPTH DISTRIBUTION ANALYSIS OF JAPANESE GOLD PRODUCTS FROM LATE 16TH CENTURY USING MUONIC X-RAYS

*Atsuya Yukawa[1], Tsutomu Saito[2], Motonobu Tampo[3], Idumi Umegaki[3], Soshi Takeshita[3], Yasuhiro Miyake[3], Koichiro Shimomura[3], Kazuhiko Ninomiya[1] (1. Hiroshima university (Japan), 2. National Museum of Japanese History (Japan), 3. IMSS KEK (Japan))

©APSORC25

7th Asia-Pacific Symposium on Radiochemistry *September 14 ~ 19, 2025 • Kunibiki Messe • Shimane, Japan*

Precision of simulation for radioactivities produced at a vicinity of nuclear core of KUR

Norikazu Kinoshita[1], Takuma Noto[2], Kazuaki Kosako[3], Hitoshi Nakashima[4],
Yuki Sasaki[5], Kazuyuki Torii[6], Makoto Inagaki[7]

[1] *Institute of Technology, Shimizu Corporation: Koto-ku, Tokyo 135-8530, Japan, norikazu.kinoshita@shimz.co.jp*
[2]*Institute of Technology, Shimizu Corporation: Koto-ku, Tokyo 135-8530, Japan, t.noto@shimz.co.jp*
[3]*Institute of Technology, Shimizu Corporation: Koto-ku, Tokyo 135-8530, Japan, k.kosako@shimz.co.jp*
[4]*Institute of Technology, Shimizu Corporation: Koto-ku, Tokyo 135-8530, Japan, hitoshi.nakashima@shimz.co.jp*
[5]*Nuclear Projects Division, Shimizu Corporation: Chuo-ku, Tokyo 104-8370, Japan, sasaki.yuki@shimz.co.jp*
[6]*Nuclear Projects Division, Shimizu Corporation: Chuo-ku, Tokyo 104-8370, Japan, ka_torii@shimz.co.jp*
[7]*Institute for Integrated Radiation and Nuclear Science, Kyoto University: Sennan, Osaka 590-0494, Japan, inagaki.makoto.2r@kyoto-u.ac.jp*

We compared the specific activities obtained by the activation experiment at KUR with those by the simulation. The simulation applied the detailed geometry that precisely reproduced the structure inside the nuclear research reactor, and three kinds of simplified geometries that homogenized step by step the materials inside the reactor. The calculation time was related to the degree of simplification. We confirmed that the specific activities can be simulated within a precision of approximately 20% at location relatively close to the nuclear core even when the simplified geometries were applied.

1 INTRODUCTION

Decommissioning of aged nuclear power plants is proceeding worldwide. In Japan, decisions have been made to shut down more than ten nuclear power plants. The decommissioning of nuclear reactors proceeds in four phases: planning, removal of spent fuel, demolition of activated facilities around the nuclear core, and demolition of the whole building. The distribution and concentration of radioactivities produced during the operation of a nuclear power plant are important for planning and estimation of costs, etc., for decommissioning.

Generally, the distribution of radioactivities around the reactor is simulated using a combination of Monte Carlo code such as MCNP [1] and radioactivity calculation code such as ORIGEN-S [2] in SCALE-6.2 [3]. A calculation time in the Monte Carlo simulation is longer when the huge and complicated geometry is described in detail. On the other hand, if the geometry is simplified by homogenization, the calculation time is shorter, but the precision would be a problem.

Kyoto University Research Reactor (KUR) of Institute for Integrated Radiation and Nuclear Science, Kyoto University is the best place because the activation experiment and the detailed geometry of the inside of the reactor are available. In the present work, we compared the specific activities obtained by the activation experiment with those obtained by simulation using combination of MCNP and ORIGEN-S codes to confirm the validity for decommissioning of actual nuclear power plants. In the simulation, the complicated geometry was homogenized step by step to investigate the effects on the precision and calculation speed of the simulation.

2 METHODS FOR EXPERIMENT AND SIMULATION

2.1 Activation experiment

Known amounts of standard solutions of Fe, Co, Cs and Eu were individually evaporated on filter papers under an infrared lamp. Each sample was sealed in a polyethylene bag. In addition, known amounts of JCFA-1, JSl-1, and JG-3 were individually sealed in polyethylene bags. The samples were irradiated for 4 hours at Pn-2 of the irradiation port in KUR. The reactor was operated at 1 MW for a thermal power. We analyzed specific activities of ^{46}Sc/Sc, ^{54}Mn/Fe, ^{59}Fe/Fe, ^{60}Co/Co, ^{134}Cs/Cs, ^{152}Eu/Eu, ^{154}Eu/Eu and ^{160}Tb/Tb as of the end of irradiation.

2.2 Simulation of activation

We constructed the detailed geometry (Geometry-A) which reproduces the detailed structure of fuel rods and control rods, and their arrangement. At KUR, uranium silicide (U_3Si_2) with a density of 3.2 gU/cm^3 containing ^{235}U with a 20% enrichment is used as a fuel meat. The fuel meat with a thickness of 0.50 mm is sandwiched by 0.51 mm-thick-aluminum. This 1.52-mm-thick layer is surrounded by layers of water with a thickness of 2.81 mm. As simplified geometry, fuel meat and aluminum were homogenized (Geometry-B). In addition, fuel meat, aluminum and water except inside cells at where control rods are located, were homogenized by maintaining the bulk density and bulk elemental composition (Geometry-

Copyright on 7th Asia-Pacific Symposium on Radiochemistry 2025 P-R5-01 -

C). The fuel meet, aluminum and water inside cells at where control rods are located, are homogenized as well for the simplest geometry (Geometry-D). The list of these geometries is summarized in Table 1. The neutron spectra at location of Pn-2 were obtained for the detailed geometry and simplified geometries using MCNP5 [1]. The specific activities, produced under a thermal power of 1 MW, as of the end of irradiation were simulated with ORIGEN-S code [2] using the neutron spectra obtained by the MCNP calculation.

TABLE 1 Feature of geometry.

Name	Feature of geometry
Geometry-A	detailed geometry
Geometry-B	fuel meats and aluminum layers were homogenized
Geometry-C	fuel meats, aluminum layers, and water were homogenized except the cells of the control rods
Geometry-D	fuel meats, aluminum layers, and water were homogenized in all the cells

3. RESULTS AND DISCUSSION

Single-tread calculation times per 10^6 events on XEON gold 6242R (3.1 GHz) are related to the number of regions (Fig. 1). Significant difference in the memory usage was not observed in the detailed and simplified geometries. If the geometry is huge like actual nuclear power plants, the memory usages would be varied by the degree of simplification of the geometry.

The ratios of calculation/experiment for the specific activities of ^{54}Mn/Fe, ^{60}Co/Co, and ^{152}Eu/Eu simulated using different geometries are shown in Fig. 2 as an example. Averages of some experimental data were applied to the specific activities. Each uncertainty includes the 1σ uncertainties of the specific activities, 10% uncertainty derived from the variation of the neutron flux depending on the location in the capsule, and 1σ statistical uncertainty in the MCNP simulation. The ratios of all the specific activities almost correspond within the uncertainties.

Based on the nuclear reaction data, most of the ^{54}Mn was produced by the ^{54}Fe(n,p)^{54}Mn reaction with neutrons having energies higher than ~1 MeV. The other products were produced by a neutron capture reaction with a thermal energy. In the present work, the specific activities produced by the (n,p) and (n,γ) reactions were simulated within a precision of ~20% even when the simplified geometries were applied.

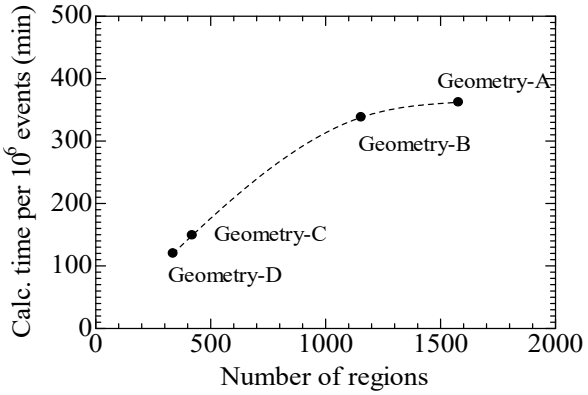


Fig. 1 Calculation time per 10^6 events related with the number of regions. Each data is connected by a spline line.

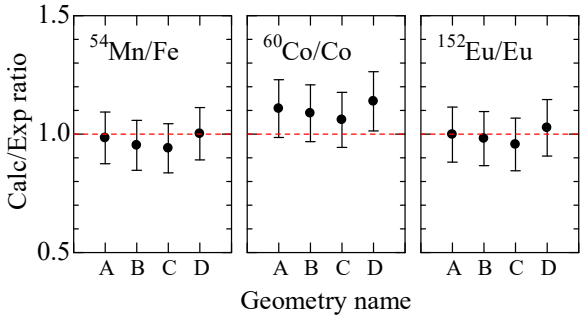


Fig. 2 The calculation/experiment (Calc/Exp) ratios of the specific activities calculated using each geometry.

4. CONCLUSION

The specific activities of eight nuclides produced by the (n,γ) and (n,p) reaction at the activation port Pn-2 of KUR could be simulated with a precision of ~20%. Activation at a location close to the reactor core of actual nuclear power plants would be simulated with the precision same as the present work if the geometry is described in detail. However, further investigation is required to apply the simplified geometry due to the different geometry in the reactor fuel assemblies.

References

[1] X-5 Monte Carlo Team, "MCNP – A General N-Particle Transport Code, Version 5 – Volume I: Overview and Theory," *LA-UR-03-1987*, Los Alamos National Laboratory (April, 2003).

[2] I. Gauld, O. W. Hermann, R. M. Westfall, "Origen-S: Scale system module to calculate fuel depletion, actinide transmutation, fission product buildup and decay, and associated radiation source terms," *ORNL/TM-2005/39 Version 6 Vol. II*, Sect. F7 (2009).

[3] W. A. Wieselquist, R. A. Lefebvre, M. A. Jessee (Eds.), "SCALE Code System," *ORNL/TM-2005/39 Version 6.2.4* (2020).

Copyright on 7th Asia-Pacific Symposium on Radiochemistry 2025 P-R5-01 -

7th Asia-Pacific Symposium on Radiochemistry *September 14 ~ 19, 2025 • Kunibiki Messe • Shimane, Japan*

Evaluation of Total Fluorine Content in the Materials for Laboratory and Consumer Products Using Instrumental Neutron Activation Analysis

Yoshiaki Furusho[1], Manabu Takayanagi[2], Tsutomu Miura[3]

[1]*GL Sciences Inc.: 22-11 Nishisinjuku, Shijuku-ku, Tokyo 163-1130 Japan, furusho@gls.co.jp*
[2]*GL Sciences Inc.: 237-2 Sayamagahara, Saitama, 358-0032, takayanagi@gls.co.jp*
[3]*National Institute of Advanced Industrial Science and Technology (AIST): Tsukuba Central-3, 1-1-1 Umezono, Tsukuba, Ibaraki 305-8563 Japan, t.miura@aist.go.jp*

The application of a non-destructive analytical method using Instrumental Neutron Activation Analysis (INAA) for the quantification of total fluorine (TF) in various products. Conventionally targeted detection techniques, such as LC-MS/MS and the Total Oxidizable Precursor (TOP) assay, have limitations in detecting unknown or structurally complex fluorinated compounds. The mass fraction of total fluorine in a solid sample can be measured directly using INAA. Furthermore, using a cyclic irradiation protocol, the detection limit of total fluorine is 0.2 µg. The reliability of INAA was confirmed by the validation of certified reference materials of silicon carbide ceramics and high-purity organic compounds. Application to 25 types of laboratory and consumer products revealed significant mass fractions of fluorine in water-repellent materials and cosmetics, whereas no fluorine was detected in fast-food packaging. These findings demonstrate that INAA is an effective and comprehensive approach for TF assessment, supporting its integration with conventionally targeted analyses in product safety and environmental monitoring frameworks.

1. Introduction / Objective

Per- and polyfluoroalkyl substances (PFAS) are widely used in modern consumer and industrial products due to their exceptional chemical stability, water and oil repellency, and resistance to heat and degradation. However, their environmental persistence and potential for bioaccumulation and toxicity have raised significant global concerns. As a result, regulatory agencies worldwide have imposed stricter monitoring requirements, necessitating precise and comprehensive fluorine analysis [1].

Although liquid chromatography-tandem mass spectrometry (LC-MS/MS) is effective for quantifying known PFAS, it is limited in detecting unknown or structurally complex fluorinated species. Indirect methods, such as combustion ion chromatography (CIC) for adsorbable organic fluorine (AOF) and the TOP assay described in EPA Method 1621, require complex sample pretreatment and suffer from poor specificity [2,3].

Given these challenges, there is a critical need for a direct, robust, and non-destructive method for sensitive and accurate quantification of total fluorine (TF) with minimal sample preparation. This study aims to establish a reliable analytical framework utilizing INAA [4, 5] for the determination of TF in a wide variety of sample matrices.

2. Experimental

Quantification of fluorine was performed using INAA at the JRR-3 research reactor operated by the Japan Atomic Energy Agency. Samples were heat-sealed in high-purity polyethylene bags and loaded into high-purity polyethylene capsules and irradiated via a pneumatic transport system (PN-3) that enables rapid transporting between the nuclear reactor and the Ge semiconductor detector in the ventilation hood. The thermal neutron fluence rate was 1.5×10^{17} $m^{-2}s^{-1}$, with negligible interference from fast neutrons (fast neutron fluence rate: 4.4×10^{13} $m^{-2}s^{-1}$). (Fig.1)

To measure the short half-life of the induced radioactive nuclide ^{20}F ($T_{1/2} \approx 11$ s), a cyclic irradiation protocol was adopted. Each sample performed five cycles consisting of:

- Neutron irradiation: 5 seconds
- Decay cooling: 10 seconds
- γ -ray measurement: 10 seconds

γ-ray at 1633 keV of ^{20}F, were measured using a Ge semiconductor detector. To compensate for variations in neutron flux and geometry of sample position, ^{46m}Sc was used as an internal standard.

A total of 25 samples, comprising 13 laboratory materials (e.g., SPE cartridges, polypropylene tubes, PEEK tubing) and 12 consumer products (e.g., waterproof paper, food packaging, cosmetics), were selected. The mass fractions of

Copyright on 7th Asia-Pacific Symposium on Radiochemistry 2025

total fluorine were determined by comparing measured count rates with fluorine standards prepared from applying known amounts of F^- standard solution on filter papers, corrected for radioactive decays.

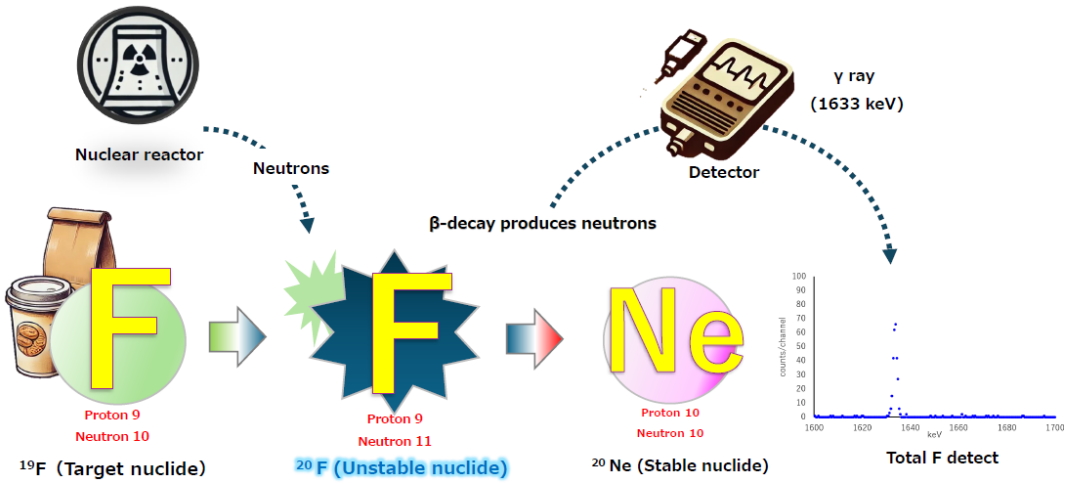


Fig. 1. Conceptual Diagram of Total Fluorine Analysis by Instrumental Neutron Activation Analysis (INAA).

3. Results and Discussions

INAA analysis of the 25 selected samples revealed the following trends:

Among laboratory materials, no detectable fluorine was observed in most components, including polypropylene and glass fiber-based materials. In contrast, high mass fractions of fluorine were found in PEEK components, such as tubing and connectors, likely due to the use of aromatic difluorides as monomers during the synthetic process. This highlights that even high-performance engineering plastics may retain trace fluorine, which could impact TF analysis and chemical recycling.

Among consumer products, substantial fluorine levels were detected in water-proofed paper and food packaging commonly used in supermarkets. These findings suggest the application of organic fluorinated compounds to enhance water repellency. In contrast, fast-food packaging, despite visible surface coatings, exhibited no detectable fluorine, indicating differences in manufacturing processes and regulatory compliance across product types.

Cosmetic products such as sunscreens and foundations often contain fluorinated compounds, including fluorosilicones and fluorphlogopite, which enhance spreadability and water resistance.

The reliability of INAA was confirmed through validation using CRMs based on silicon carbide ceramics and high-purity organic compounds. [4, 5].

4. CONCLUSIONS

This study demonstrates that INAA is a reliable, robust, and non-destructive analytical technique for total fluorine quantification in a broad range of products.

The application to real-world samples revealed diverse fluorine distributions across different materials, supporting the utility of INAA in regulatory compliance, quality control, and environmental monitoring. Furthermore, INAA serves as a complementary technique to targeted methods such as LC-MS/MS, offering a more inclusive approach to fluorine assessment. Future work will focus on expanding the range of applicable matrices and optimizing protocols for field-deployable and high-throughput applications.

References

[1] Laurel A. Schaider et al., Environ. Sci. Technol. Lett. 2017, 4, 105–111.
[2] Jovanović, M. et al., Food Addit. Contam. Part A, 2024, 41, 525–537.
[3] Tsou, K. et al., ACS EST Water, 2023, 3, 2996–3007.
[4] T. Miura, Talanta Open, 2025, 11, 100409.
[5] Hanari, A. et al., BUNSEKI KAGAKU, 2025, 74, 7-11.

7th Asia-Pacific Symposium on Radiochemistry *September 14 ~ 19, 2025 • Kunibiki Messe • Shimane, Japan*

Improving the Reliability of Instrumental Neutron Activation Analysis by using the Internal Standard Method

Tsutomu Miura[1], Hideaki Matsue[2], Koichi Takamiya[3], Mitsunori Ishimoto[4]

[1]*National Institute of Advanced Industrial Science and Technology: Central 3, 1-1-1 Umezono, Tsukuba, Ibaraki, 305-8563, t.miura@aist.go.jp*
[2]*Japan Atomic Energy Agency: 2-4, Shirakata, Tokai, Ibaraki, 319-1195, matsue.hideaki@jaea.go.jp*
[3]*Institute for Integrated Radiation and Nuclear Science, Kyoto University: 2 Asashiro-Nishi, Kumatori, Sennan, Osaka, 591-0494, takaimiya.koichi.2u@kyoto-u.ac.jp*
[4] *Nuclear Professional School, School of Engineering, University of Tokyo: 2-4, Shirakata, Tokai, Ibaraki, 319-1195, ishimoto@tokai.t.u-tokyo.ac.jp*

To improve the reliability of INAA, the internal standard method was employed. An appropriate internal standard was selected for the neutron capture cross section, the half-life and emitted gamma-ray energy of the target nuclide to be measured. This reduced the variability caused by the gradient of the neutron fluence rate in the irradiation capsule and the geometry during gamma-ray measurement, the two main causes of variability in INAA. The validation of developed INAA coupled with internal standard method was performed by comparison with certified values of certified reference material. The developed INAA coupled with internal standard method was applied to the value assignment of candidate certified reference materials, certified reference materials, and industrial materials.

1 Introduction

Instrumental neutron activation analysis (INAA) is an elemental analysis method that enables non-destructive analysis. INAA does not require any chemical pretreatments such as sample decomposition. There is no loss of elements associated with INAA during the sample preparation or measurement procedures and contamination is avoided if proper precautions are taken. However, INAA often has greater uncertainty than other analytical methods. This uncertainty often appears in the correction for the differences in neutron fluence rate among samples and standards, and the sample to-sample measurement repeatability. The most practical way to eliminate the sources of uncertainty is to apply an internal standard method to NAA. This study investigated the applicability of internal standards in INAA to improve analytical reliability.

1.1 Experiments

Neutron irradiation for INAA was performed at KUR at Institute for Integrated Radiation and Nuclear Science, Kyoto University and JRR-3 at Japan Atomic Energy Agency. The internal standard isotopes were selected based on their similarity to the nuclear properties of the target nuclides, as well as the fact that the γ-ray energies emitted by the induced radioactive nuclides do not interfere with each other. For example, ^{198}Au ($T_{1/2}$=2.694 d, 411 keV) was used as the internal standard to measure ^{76}As ($T_{1/2}$=1.097d, 559 keV) [1] and ^{82}Br ($T_{1/2}$=1.471 d, 554 keV) [2]; ^{95}Zr ($T_{1/2}$=64.02 d, 757 keV) was used to measure ^{182}Hf ($T_{1/2}$=42.39 d, 482 keV) [3]; ^{134}Cs ($T_{1/2}$=2.065 y, 796 keV) was used to measure ^{51}Cr ($T_{1/2}$= 27.70 d, 320 keV) and ^{60}Co ($T_{1/2}$=5.271 y, 1332 keV) [4]; and ^{46m}Sc ($T_{1/2}$=18.75 s, 143 keV) was used as the internal standard to measure ^{20}F ($T_{1/2}$=11.01 s, 1633 keV) [5].

1.2 Results and discussions

The application of an internal standard to INAA was very effective in improving the reliability of the measurement. For example, although the sample measurement repetition (n=4) of ^{51}Cr 320 keV γ-ray peak count rate was 3.2 % RSD (relative standard deviation) without using an internal standard. In the same measurement, when the measurement data were normalized to the ^{134}Cs 756 keV γ-ray peak count rate per unit mass using an internal standard, the RSD was improved to 0.42 % [2]. In addition, the day-to-day variation of slopes of calibration plots for ^{76}As using ^{198}Au as internal standard were shown in Table 1. The RSD of slopes on different days was 0.23 %, indicating a reproducible calibration [3].

Copyright on 7th Asia-Pacific Symposium on Radiochemistry 2025

Table 1. Slopes of calibration plots for INAA of ^{76}As using ^{198}Au as internal standard at JAEA JRR-3

Irradiation date	Operation cycles	Slope of calibration plots
2008/12/08	R3-20-5	0.08120
2008/12/15	R3-20-5	0.08140
2009/6/25	R3-21-3	0.08102
	Mean	0.08121
	RSD	0.23 %

Irradiation facility: JAEA JRR-3 PN-1, Thermal neutron fluence rate: $5 \times 10^{17} m^{-2} s^{-1}$, Irradiation time: 20 min, Measured γ-rays: 559 keV for ^{76}As and 411 keV for ^{198}Au, Ge detector: ORTEC GMX 30190.

The developed INAA method coupled with internal standardization was validated by comparing the measured values with certified values of certified reference material or with values obtained using another analytical method [1-6]. The developed method was applied for value assignment of total bromine in the candidate certified reference material (CRM) of plastics for Br analysis [4], As in arsenobetaine standard solution CRM [3], Cr and Co in fine ceramics CRM [2], Hf in high purity Zr metal [1]. Furthermore, the developed method applied precise quantification of total fluorine in the synthetic polymer resins [5], and Ir in the high purity $IrBr_4$ [6].

2. Conclusions

The INAA coupled with internal standardization was developed to enable precise and accurate elemental analysis of solid samples. Although the proposed method requires the prior addition of precisely known quantities of internal standards to the samples and standards, it allows for reliable quantitative analysis. The proposed method is an effective analytical method for the value assignment of certified values of reference materials for which highly accurate measurements are required.

ACKNOWLEDGMENTS

This work was partially supported by Joint Usage/Research of the Institute for Integrated Radiation and Nuclear Science, Kyoto University (KURNS). This study was partially conducted under the Inter-University Program for the Joint use of JAEA/QST Facilities, Nuclear Professional School, School of Engineering, University of Tokyo, at the Research Reactor JRR-3, JAEA.

References

[1] T. Miura, H. Matsue, T. Kuroiwa, *J. Radioanal. Nucl. Chem*., **282**, 49(2009).
[2] T. Miura, H. Matsue, T. Kuroiwa, K. Chiba, *Anal. Sci*., **25**, 881 (2009).
[3] T. Miura, K. Chiba, T. Kuroiwa, T. Narukawa, A. Hioki, H. Matsue, *Talanta*, **82**, 1143 (2010).
[4] T. Miura, R. Okumura, Y. Iinuma, S. Sekimoto, K. Takamiya, M. Ohata, A. Hioki, *J. Radioanal. Nucl. Chem.*, **303**, 1417 (2015).
[5] T. Miura, *Talanta Open.*, **11**, 100409 (2025).
[6] T. Miura, Y. Iinuma, S. Sekimoto, *J. Radioanal. Nucl. Chem.*, **324**, 1007 (2020).

7th Asia-Pacific Symposium on Radiochemistry *September 14 ~ 19, 2025 • Kunibiki Messe • Shimane, Japan*

Application of INAA to trace metal analysis of polymetallic sulfide ores collected from seafloor massive sulfide deposits

Jun-ichiro Ishibashi[1], Shin Toyoda[2], Kotaro Yonezu[3], Tatsuo Nozaki[4], Yutaro Takaya[5], Hisao Yoshinaga[6] and Koichi Takamiya[6]

[1]*KOBEC, Kobe University, Kobe, Japan, 658-0022, E-mail: ishibashi@port.kobe-u.ac.jp*
[2]*Institute of Paleontology and Geochronology, Okayama University of Science, Okayama, Japan, 700-0005*
[3]*Department of Earth Resources Engineering, Kyushu University, Fukuoka, Japan, 810-0395*
[4]*School of Creative Science and Engineering, Waseda University, Tokyo, Japan, 169-8555*
[5]*Department of Systems Innovation, The University of Tokyo, Tokyo, Japan, 113-8656*
[6]*Institute for Integrated Radiation and Nuclear Science, Kyoto University, Kumatori, Japan, 590-0494*

We studied INAA of polymetallic sulfide ores collected from seafloor massive sulfide deposits, with a view to confirm and extend the range of the application. We confirmed cross check between INAA and chemical analysis employing ICP-QMS showed good agreement with exception for some specific cases. Then, we tried to find some interest correlations among concentrations of metal elements in the polymetallic sulfide ores. Together with mineralogical studies, these correlations are interpreted as behavior of rare metal elements with a high affinity for other metal element in sulfide minerals.

1 INTRODUCTION

Seafloor massive sulfide (SMS) deposits are considered as possible future metal resources. Because of complicated mineral assemblage of the polymetallic sulfide ores from SMS deposits, instrumental neutron activation analysis (INAA) takes advantage of multi-elemental analysis without chemical pretreatment. Especially, this technique is useful for preliminary searching of rare metal elements in the ore, which could deliver additional value for the economic estimation. In this study, we applied INAA to polymetallic sulfide ores collected from the seafloor massive sulfide deposits located in the sea areas around Japan.

2 MATERIALS AND METHODS

Polymetallic sulfide ores for this study were collected from Higashi-Aogashima Knoll Caldera located along the Izu-Ogasawara volcanic front, during KS-21-20 cruise using the remotely operated vehicle (ROV) *Hyper-Dolphin* [1]. Sulfide ores and metal-bearing sediment were collected from SMSs associated with active hydrothermal fields in in three areas; CC, SE and E sites. While CC site was located near the central cone, the other two sites, SE and E Sites were along the caldera wall.

INAA was conducted at Institute for Integrated Radiation and Nuclear Science, Kyoto University (KURNS), where the light-water moderated tank-type research reactor is equipped with pneumatic capsule transfer systems for the neutron irradiation. For analysis of short-lived nuclides (Al-28, Mn-56, Cu-66, Ba-139), powdered samples of 10-20 mg were irradiated at Pn-3 (neutron flux = 4.68×10^{12} n/cm^2/sec) for 30 seconds, and the gamma ray spectrum was measured for 3 minutes after adequate cooling time (3-15 minutes). For analysis of medium-lived nuclides (As-76, Sb-122, Au-198), powdered samples of 10-20 mg were irradiated at Pn-2 (neutron flux = 5.50×10^{12} n/cm^2/sec) for 30 minutes and the gamma ray spectrum was measured for 15 minutes after adequate cooling time (25-35 hours). The same irradiated samples were provided for another gamma ray spectrum measurement for 2-3 hours after enough cooling time (3-4 weeks) for analysis of long-lived nuclides (Fe-59, Zn-65, Ag-110m). Irradiation and measurements were conducted in 2021 and 2022 [2][3].

3 CROSS CHECK BETWEEN INAA AND ICP-QMS ANALYSIS

We conducted a cross check analysis of 29 ore and sediment samples to confirm accuracy in a wide range of metal concentrations [2]. Split of the same powdered samples were provided for the INAA and also for ICP-QMS analysis after acid digestion following procedure described in the previous study [4]. Results are shown Fig. 1, where content of 10 elements (Al, Ba, Cu, Mn, Au, As, Sb, Ag, Fe, Zn) determined by INAA is plotted against that by ICP-QMS analysis in logarithmic scales. Contents determined by two analytical techniques basically well agreed, except for the case that determination was difficult due to extremely low content. On the other hand, disagreement in Ba content was attributed to incomplete dissolution during the chemical treatment for ICP-QMS analysis, as noted in the previous study [4].

Copyright on 7th Asia-Pacific Symposium on Radiochemistry 2025

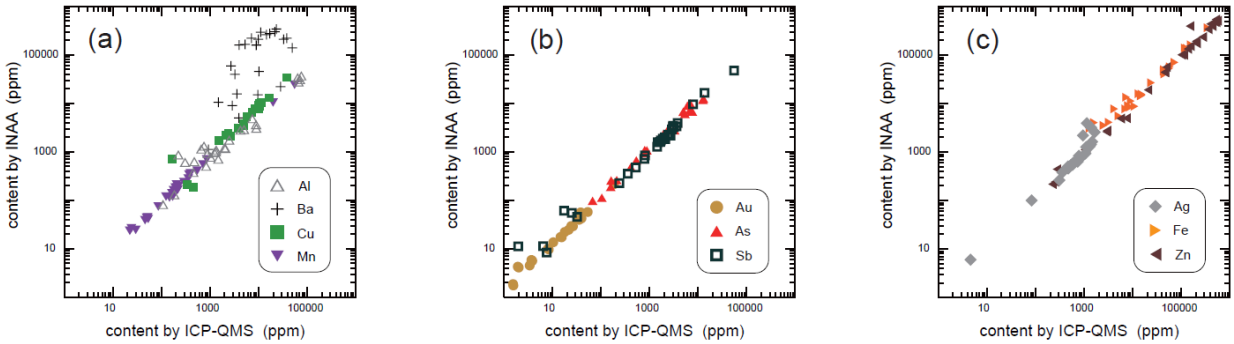


Fig. 1. Results of cross check between INAA and ICP-QMS analysis for the polymetallic sulfide ore samples, shown in 3 panels by elements determined with (a) short-lived nuclides, (b) medium-lived nuclides (c) long-lived nuclides.

4 DISTRIBUTION OF TRACE METAL ELEMENTS IN POLYMETALLIC SULFIDE ORES

We tried to find correlations among content of rare metal elements in the polymetallic ores, with a view to characterize their distribution (Fig. 2). Among the plots of Au content against Zn content, weak correlation was recognized regardless of the sampling sites (Fig. 2a). This result is in accordance with the observation of nanoparticle-mediated growth of native Au [4], which might be fixed with Zn-bearing sulfide minerals dominantly occurred within the polymetallic sulfide ore. Correlation between Ag content and Sb content (Fig. 2b) is attributed to a result of replacement in the tetrahedrite-tennantite system where Cu+As is replaced by Ag+Sb. Indium was detected by INAA only for the ores collected from SE and E Sites, and In content showed correlation with Zn content (Fig. 2c). This correlation is attributed to a result of replacement in sphalerite where Zn+Zn is replaced by In+Cu. The enrichment in Au, Ag at CC Site and in In at SE and E Sites could reflect difference in chemical signature of these sites.

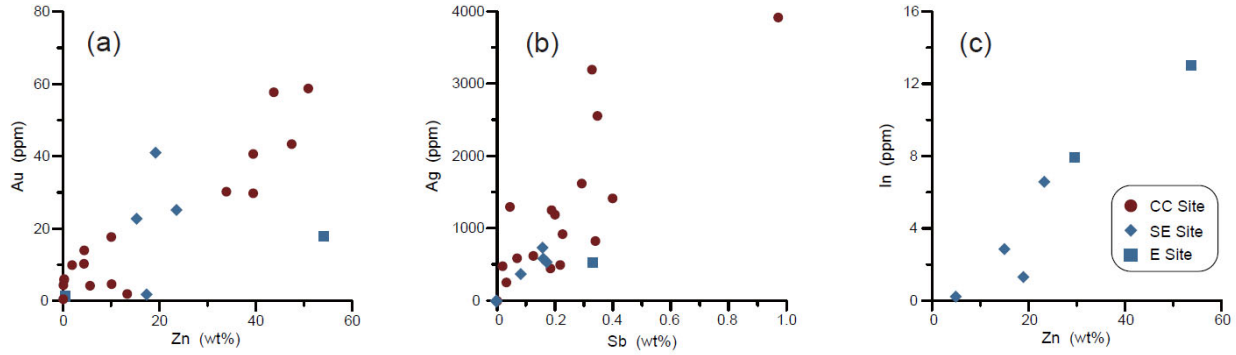


Fig. 2. Relationship between content of metal elements in the polymetallic sulfide ores collected from Higashi-Aogashima Knoll Caldera. Symbols represent sampling sites (circles: CC Site, diamonds: SE Site, squares: E Site)

ACKNOWLEDGMENTS

The authors thank the ROV team, and Captain and crew of Research Vessel *Shinsei-maru* for their support during the KS-21-20 cruise. Irradiation and measurements in this study were conducted by the collaboration research project of KURNS.

References

[1] S. OKADA et al., "Microscopic evidence for nanoparticle-mediated growth of native gold in sulfide deposits at the Higashi–Aogashima Knoll Caldera hydrothermal field". *PLoS ONE*, **20**, e0317220 (2025)

[2] J. ISHIBASHI et al., *KURNS Progress Report 2021*, CO5-16 (2021)

[3] J. ISHIBASHI et al., *KURNS Progress Report 2022*, CO5-9 (2022)

[4] T. NOZAKI et al. "Subseafloor sulphide deposit formed by pumice replacement mineralization", *Science Report*, **11**, 8809 (2021)

Copyright on 7th Asia-Pacific Symposium on Radiochemistry 2025 P-R5-04 -

7th Asia-Pacific Symposium on Radiochemistry September 14 ~ 19, 2025 • Kunibiki Messe • Shimane, Japan

ACTIVATION ANALYSIS OF $PM_{2.5}$ SAMPLES COLLECTED IN HACHIOJI, TOKYO

Yasuji Oura[1], Shuto Kazama[2], Junya Kaneko[3]

[1]*Tokyo Metropolitan University: 1-1 Minami-Osawa, Hachioji, Tokyo, 192-0397, and oura-yasuji@tmu.ac.jp*
[2] *Tokyo Metropolitan University: 1-1 Minami-Osawa, Hachioji, Tokyo, 192-0397*
[3]*Tokyo Metropolitan University: 1-1 Minami-Osawa, Hachioji, Tokyo, 192-0397*

Elemental concentrations in $PM_{2.5}$ samples collected in Hachioji, Tokyo were determined by prompt gamma-ray analysis (PGA), instrumental neutron activation analysis (INAA), and instrumental photon activation analysis (IPAA) which enable to determine the total elemental concentrations regardless of their chemical forms. The variation of many elemental concentrations in $PM_{2.5}$ collected from 2018 to 2024 were revealed. In addition, standard reference materials for aerosols were also analyzed to obtain concentrations of elements not having certified values. This study demonstrates the effectiveness of activation analysis in environmental monitoring of fine particulate pollutants.

1 INTRODUCTION

Air pollution is a major concern because it directly affects our health. One of the air pollutants is suspended particulate matter. Although various sizes of particulate matters suspend in the atmosphere, an influence of very fine particles of less than 2.5 μm of aerodynamic radius ($PM_{2.5}$) on human health has been attracting attention in a recent year. Particles with small diameters settle slowly due to gravity, floating in the air for a while and reaching our lungs through respiration. In the early 1990s, epidemiological data reported in Europe and the United States showed a correlation between the atmospheric concentration of particles with an aerodynamic diameter of 10 μm (PM_{10}) and the daily mortality rate of patients with cardiopulmonary diseases, drawing attention to the characteristics and behavior of PM_{10} particles. Furthermore, it was reported that the concentration of $PM_{2.5}$ particles has a higher correlation with mortality rates. Therefore, research on $PM_{2.5}$ particles has become active worldwide.

Various particles are released into the atmosphere through natural and human activities. These particles contain or adsorb various chemicals. Many of these chemicals affect the human body, and research on organic substances such as polycyclic aromatic hydrocarbons, which are considered to have direct effects, has been particularly active recently. Additionally, many harmful elements are included in particulates, and knowing the elemental composition of the particles is important. Furthermore, the elemental composition provides important information for analyzing the origin of the particles.

Previously, PM10 particulates were collected in Hachioji, Tokyo, from 2002 to 2008 and they were analyzed by activation analysis methods [1]. At present, we have determined elemental composition of $PM_{2.5}$ collected at the same place since 2018. To analyze the origin of the particles, it is desirable to obtain the concentrations of many trace elements. Therefore, the elemental composition of the particles was examined using prompt gamma-ray analysis (PGA), neutron activation analysis (INAA), and photo activation analysis (IPAA). Some elements can exist in multiple chemical forms, but these analytical methods can determine the total concentration regardless of the chemical forms. Variations of elemental compositions are reported as well as technical matters of activation analysis.

2. EXPERIMENTAL

Using a NILU filter holder with successive PM_{10} and $PM_{2.5}$ inlets, $PM_{2.5}$ was collected on a Nuclepore polycarbonate filter with 0.2 μm of pore size or a quartz filter for five weekdays every week at a rooftop of a building in Minami-Osawa campus of Tokyo Metropolitan University. Mass concentration in μg m^{-3} was determined by weighing the filter before and after collection of $PM_{2.5}$.

For analysis by PGA and INAA, the polycarbonate filter was cut in half. The one half was folded into a 10 mm ×10 mm square, sealed in FEP film bag, and irradiated with thermal neutrons for about 6 hours while measuring prompt gamma rays using the JRR-3 prompt gamma-ray analysis system. Then, samples were irradiated for 5 minutes using in Pn-3 at KUR (1 MW operation) or PN3 at JRR-3, and immediately measured for 300 seconds. After cooling, samples were irradiated for 1 hour in Pn-2 at KUR (5 MW operation) or for 20 minutes in PN1 or PN2 at JRR-3. Measurements were performed 4 - 5 times for 3000 - 50000 sec with varying cooling times.

For determination of carbon, $PM_{2.5}$ collected on a quartz filter was used. Two small pieces, each with a diameter of 10 mm, were cut out from a quartz filter and wrapped in aluminum foil. It was irradiated with bremsstrahlung with E_0 = 25 MeV for 20 minutes using the electron linear accelerator at ELPH, Tohoku University. After irradiation, the aluminum foil was removed, and the 511 keV annihilation gamma rays were measured repeatedly with varying cooling times.

Copyright on 7th Asia-Pacific Symposium on Radiochemistry 2025

3. RESULTS AND DISCUSSION

Four standard reference materials, NIST SRM 1632c (bituminous), NIST SRM 1648c (urban particulate matter), NIES CRM No.8 (vehicle exhaust particulates), and NIES CRM No.28 (urban aerosols) were used as a standard sample of a comparative method in INAA. Elements without certified values in these materials were determined by PGA, INAA, and/or IPAA. Tentative determination values for some elements are given in Table 1. For C determination in these SRMs by IPAA, it was found that $^{12}C(\gamma, \alpha n)^{7}Be$ was also applicable, as is $^{12}C(\gamma, n)^{11}C$.

TABLE 1. Analytical results of four SRMs for some elements.

	NIST 1632c	NIST 1648	NIES No.8	NIES No.28
B, mg kg^{-1}	65	164	15	-
C, %	72	17	71	13
Si, %	2.6	13	ND	-
Cl, %	0.15 (0.1139)	0.47	0.093	-
S, %	2.0 (1.462)	6.5	2.8	-

( ) : certified value, - : not determined

Mass concentrations of $PM_{2.5}$ particulates collected on quartz filter and total carbon concentration determined by IPAA are shown in Fig.1. From 2010 to 2023, no collection was conducted using quartz filters. The median mass concentration of $PM_{2.5}$ remained nearly constant from 2006 to 2008, decreased in 2009, and became even lower by 2024. On the other hand, the median of total carbon concentrations has been gradually decreasing since 2006.

Boron concentrations were determined by PGA. Elements other than B could not be determined. Since a peak of boron was not very large, net count value varies significantly depending on how the background count is determined. So, we considered how to determine a net count, that is, how to estimate the background count. Boron concentrations not corrected for filter blank are shown in Fig.2. Only a few significant values were obtained every year, and most were less than detection limit (2 - 4 ng m^{-3}). Concentration values larger than the detection limit were obtained in most of the samples collected in 2023. Since 2020, the median concentration of boron in $PM_{2.5}$ has remained nearly constant, at about half the level observed in 2006.

Suffer concentrations were determined by INAA (irradiation for 5 minutes) with comparison of sulfamic acid reagent. The isotopic abundance of ^{36}S, which is transmuted to ^{37}S to be measured, is very low (0.01%), and gamma-ray energy used for measurement is high (3104 keV), resulting in low sensitivity. Therefore, the count values were not large, and the relative uncertainty of determination values was high. Among the elements that could be determined by INAA, S had the highest concentration. Sulfur concentration gradually decreased from 2008 to 2021, and has remained nearly constant over the past four years.

Fluorine concentration was recently tried to be determined by INAA, in which $^{19}Fe(n, \gamma)^{20}F$ ($T_{1/2}$ = 11 sec) are used. The sample was irradiated for 10 or 20 sec, and approximately 40 sec later, γ-rays were measured for 10 sec together with the irradiation capsule. It was confirmed that ^{20}F in high-purity irradiation capsule, high-purity polyethylene for packaging, and a polycarbonate filter was less than detection limit under our condition. On the other hand, about 250 μg g^{-1} of F was detected in quartz filter. ^{20}F was not detected in $PM_{2.5}$ sample collected on a polycarbonate filter in March 2023 and the upper limit of F concentration was 0.16 μg m^{-3}. On the other hand, ^{20}F was detected in the $PM_{2.5}$ collected on the quartz filter in June 2024 and F concentration corrected for quartz filter blank was found to be 0.19 μg m^{-3} with 94% of relative uncertainty.

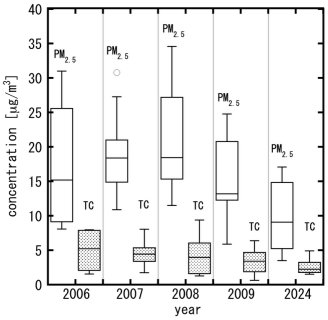


Fig. 1. Box plot of mass concentrations of $PM_{2.5}$ and total carbon concentrations.

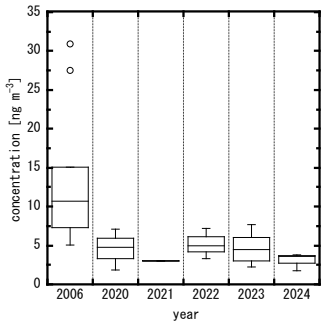


Fig. 2. Box plot of boron concentrations in $PM_{2.5}$ particulates.

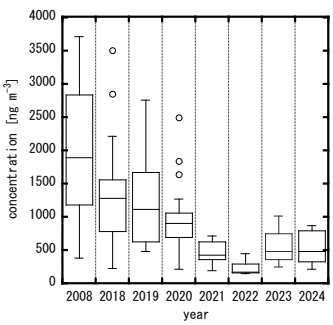


Fig. 3. Box plot of suffer concentrations in $PM_{2.5}$ particulates.

References

[1] M. Ebihara et al., "Application of NAA to air particulate matter collected at thirteen sampling sites in eight Asian countries: A collaborative study", *J. Radioanal. Nucl. Chem.* 278, 463 (2008).

7th Asia-Pacific Symposium on Radiochemistry *September 14 ~ 19, 2025 • Kunibiki Messe • Shimane, Japan*

PLAN FOR NEUTRON IRRADIATION FACILITIES AND NEUTRON ACTIVATION ANALYSIS INSTRUMENTS IN THE NEW RESEARCH REACTOR AT THE MONJU SITE

Makoto Inagaki[1], Koichi Takamiya[1], Tsutomu Miura[2], Kohshin Washiyama[3], Kazuhiko Akiyama[4], Takahito Osawa[5], Yoshitaka Kasamatsu[6], Naoki Shirai[7], Kunihiko Tsuchiya[8], Go Yoshida[9], Nobuhiro Sato[1]

[1]*Institute for Integrated Radiation and Nuclear Science, Kyoto University: 2-1010 Asashironishi, Kumatori, Sennan, Osaka 590-0494, Japan*
[2]*Research Institute for Material and Chemical Measurement, National Institute of Advanced Industrial Science and Technology: 1-1-1 Umezono, Tsukuba, Ibaraki 305-8569, Japan*
[3]*Advanced Clinical Research Center, Fukushima Medical University: 1 Hikarigaoka, Fukushima 960-1295, Japan*
[4]*Graduate School of Science, Tokyo Metropolitan University: 1-1 Minamiosawa, Hachioji, Tokyo 192-0397, Japan*
[5]*Nuclear Science Research Institute, Japan Atomic Energy Agency: 2-4 Shirakata, Tokai, Naka, Ibaraki 319-1195, Japan*
[6]*Graduate School of Science, The University of Osaka: 1-1 Machikaneyama, Toyonaka, Osaka 560-0043, Japan*
[7]*Faculty of Science, Kanagawa University: 3-27-1 Rokkakubashi, Kanagawa-ku, Yokohama, Kanagawa 221-8686, Japan*
[8]*Oarai Nuclear Engineering Institute, Japan Atomic Energy Agency: 4002 Naritacho, Oarai, Higashiibaraki, Ibaraki 311-1393, Japan*
[9]*Radiation Science Center, High Energy Accelerator Research Organization (KEK): 1-1 Oho, Tsukuba, Ibaraki 305-0801, Japan*

A new research reactor with a power of approximately 10 MW is planned to be constructed at the MONJU site in Tsuruga City, Fukui Prefecture, Japan. The reactor facility will include a main reactor facility, a guide hall for neutron beam experiments, a hot laboratory for handling radioactive isotopes, and a reactor management building. This study focuses on the experimental instruments related to neutron activation analysis and research radioisotope production, and the design of the hot laboratory. Three types of irradiation instruments are planned: pneumatic, hydraulic, and hanging irradiation instruments. The hot laboratory is planned as a multistory facility to accommodate irradiation ports, chemical laboratories, measurement rooms, and facilities for additional experimental research spaces, etc. To promote the use of neutron activation analysis at the new research reactor, automation and labor-saving of irradiation, measurement, and analysis are also planned.

1 INTRODUCTION

A new research reactor will be established at the MONJU site in Tsuruga City, Fukui Prefecture [1]. In preparation for its establishment, the Japan Atomic Energy Agency, Kyoto University, and the University of Fukui are collaborating to study the design and utilization of the new research reactor, and Kyoto University has formed a task force to study each experimental instrument to be installed in it. The new research reactor is planned to be a medium-power reactor with approximately 10 MW, which is suitable for neutron beam applications, and will be located on a site of approximately 50 m × 120 m. The reactor will include the main reactor building, a guide hall for neutron beam experiments, a hot laboratory for handling radioactive isotopes (RIs) such as neutron-irradiated samples, and a reactor management building. This study focuses on the experimental instruments for neutron activation analysis and research RI production, and the hot laboratory.

2. DETAILS OF STUDY

The experimental instruments related to neutron activation analysis and research RI production in the new research reactor were discussed. Three types of irradiation instruments were planned: pneumatic, hydraulic, and hanging. For the pneumatic irradiation instrument, the neutron spectrum can be adjusted by changing the distance from the reactor core, and it was estimated that six units (two each for high, medium, and low intensities) would be required. One of the low-intensity units will be used for cyclic irradiation, and one of the high- or medium-intensity units will have a function to cut thermal neutrons by shielding. For the hydraulic irradiation instrument, it was estimated that approximately three units would be dedicated to RI production for industrial use, and approximately two units would be for research use, making a total of five units necessary. The hanging irradiation instrument is designed to irradiate relatively large samples by suspending them from the top of the reactor, and we estimated that one unit would be necessary. This instrument is similar to the slant irradiation instrument of the Kyoto University Research Reactor (KUR).

The design of the hot laboratories in the new research reactor was considered with reference to existing similar facilities. The required area of the hot laboratory was estimated to be approximately 2,000 square meters, based on the type and area of the minimum required laboratory and administrative facilities, with reference to the hot laboratory at KUR. Because the area occupied by the hot laboratory in the current new research reactor facility layout plan is approximately 23 m × 34 m,

Copyright on 7th Asia-Pacific Symposium on Radiochemistry 2025

it is necessary to make the hot laboratory multistory to secure the required area. The hot laboratory requires an irradiation port for loading and unloading samples into and from the reactor for activation analysis and RI production, a laboratory equipped with hoods and glove boxes for handling irradiated materials, and a measurement room equipped with various detectors. Considering the case where short-lived nuclides are quickly chemically processed and measured, the irradiation port, chemical laboratory, and measurement room should be arranged such that users can safely and quickly move or transfer irradiated samples. There is also a demand for a wide range of experimental research, such as basic science research, detector development, irradiation of small amounts of nuclear fuel materials, and tracer production, and the necessary facilities must be provided for such research to be conducted. In addition, non-radiation-controlled rooms are required as rest areas for users and as workspaces for non-radiation work.

To enhance the application of neutron activation analysis in a new research reactor, the automation and labor-saving of irradiation, measurement, and analysis were studied. We plan to develop a comprehensive remote and automated system by introducing the k_0-NAA method, an automatic irradiation system, and an automatic measurement system with an automatic sample changer.

References

[1] Minutes of the 10th Meeting of the Council of Ministers for Atomic Energy, Cabinet Secretariat (in Japanese), https://www.cas.go.jp/jp/seisaku/genshiryoku_kakuryo_kaigi/dai6/gijigaiyou.pdf, 2016-12-21.

7th Asia-Pacific Symposium on Radiochemistry *September 14 ~ 19, 2025 • Kunibiki Messe • Shimane, Japan*

NON-DESTRUCTIVE DEPTH PROFILE QUANTIFICATION OF CARBON CONTENTS IN JAPANESE SWORD BY MUON LIFETIME ANALYSIS METHOD

Kosei Yakushi[1], Kenya Kubo[2], Makoto Inagaki[3], Go Yoshida[4], Soshi Takeshita[5], Patrick Strasser[5], Naritoshi Kawamura[5], Yasushiro Miyake[5], Koichiro Shimomura[5], Tsutomu Saito[6], Kazuhiko Ninomiya[1]

[1]*Hiroshima University: 1-3-2 Kagamiyama, Higashihiroshima-shi, Hiroshima 739-0046, Japan, m256128@hiroshima-u.ac.jp*
[2]*International Christian University: 3-10-2 Osawa, Mitaka-shi, Tokyo 181-8585, Japan*
[3]*Kyoto University: 2-1010 Asashironishi, Kumatori-cho, Sennan-gun, Osaka 590-0494 Japan*
[4]*KEK Radiation Science Center: 1-1 Oho, Tsukuba-shi, Ibaraki 305-0801, Japan*
[5]*KEK IMSS: 1-1 Oho, Tsukuba-shi, Ibaraki 305-0801, Japan*
[6]*National Museum of Japanese History: 117 Jonai-cho, Sakura-shi, Chiba 285-0017, Japan*

Carbon concentration is an important determinant of the mechanical properties of steel. Our group has been developing a novel non-destructive analysis method using lifetime of muon in a material. We applied the muon lifetime analysis method to determine the depth profile of carbon concentration in a Japanese sword. The carbon concentration of the sword was relatively high in the near surface region compare to the deeper side, and we concluded the sword was made by combining two types of iron with different compositions using traditional techniques.

1 INTRODUCTION

The amounts of carbon in steels are known to significantly contribute to their properties. For example, low carbon concentration steels (<0.6%) are soft and tough, while high concentration ones (>0.6%) are hard and brittle. Actually, the composition of steel is controlled according to its intended use, and determination of carbon composition is important in the evaluation of steel properties and in quality control. Generally, a destructive method have been applied to analyze carbon concentration in steel: the amount of carbon dioxide produced according to the amount of carbon when steel is burned is quantified by infrared absorption.

A Japanese sword is a weapon made from steel that also has significant artistic and cultural value. Japanese swords are fabricated by combining steels with different carbon concentrations in the core and outer layers, thereby achieving the seemingly contradictory mechanical properties of high hardness and toughness. However, the carbon content and structural characteristics of these swords vary depending on the historical period, region, and swordsmith. Since destructive analysis methods for carbon quantification never be applied for the valuable Japanese swords, the details of their manufacturing processes remain incompletely understood.

A muon is a negatively charged elementary particle with a mass is approximately 207 times than that of an electron. Due to its large mass, the muon exhibits high penetration capability in matter, and its stopping depth can be controlled by selecting its incident energy. After muon stops in a material, the muon is captured by the atom in proportion to the elemental abundance at the stop position of a material. The captured muon is finally absorbed or decay into electrons, and the lifetime of the muon is different by the muon capturing atom. Therefore, by measuring the muon lifetime, non-destructive and position-selective elemental analysis becomes possible. Our research group has been developing an analytical technique that utilizes muon lifetime spectroscopy to quantify low concentration carbon in steel in a non-destructive manner [1]. In the present study, we applied this technique to a Japanese sword and quantified depth profile of carbon contents.

2 EXPERIMENTAL

The muon experiments were conducted at the D1 area of the MLF (Materials and Life Science Experimental Facility) at J-PARC (Japan Proton Accelerator Research Complex). The D1 area is equipped with a large solid-angle plastic scintillation counter system for μSR (Muon Spin Rotation) experiment for material science, capable of detecting decay electrons with high efficiency [2]. We performed muon irradiation for 3 iron standard samples with carbon contents ranges of 20 ppm to 0.73 %, as well as on a Japanese sword (signed “Kyushu Higo Dotanuki Hyobu”, produced late 16th century). For the Japanese sword analysis, by controlling the incident muon momentum in the range of 30–58 MeV/c, the stopping depth of the muons could be selectively adjusted, enabling the acquisition of lifetime spectra corresponding to specific depths. This momentum range corresponds to analysis depths between approximately 0.26 mm and 2.9 mm. Also, a beam duct and beam slit made by Sn was installed in front of the the Japanese sword to guide the muon beam and limit muon irradiation area with 5 mm × 30 mm.

Copyright on 7th Asia-Pacific Symposium on Radiochemistry 2025

3 RESULTS AND DISCUSSION

The muon decay electron lifetime spectrum obtained by muon irradiation for the Japanese sword with muon momentum of 58 MeV/c is shown in Figure 1. The observed lifetime spectrum is composed of a sum of contributions from different components, depending on which atom the muon is captured. In this study, we considered five components in the analysis of lifetime spectrum: Fe and C originating from the sample; Sn from the duct and slit; Air from the atmosphere inside the duct; and a long-lived background component (BGD). The muon lifetime of each element was taken from the literature value [3]. The intensity of Air was fixed because muon stop behavior in the atmosphere was not influenced by the sample condition. The muon capture ratios between iron and carbon in the samples for all measured conditions were determined by spectrum fitting.

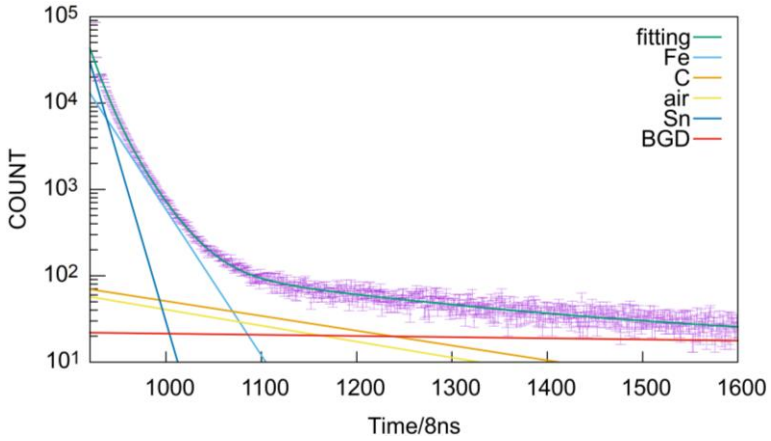


Figure 1. Muon lifetime spectrum obtained from muon irradiation for the Japanese sword with momentum of 58 MeV/c (muon stop depth of 2.9 mm) together with the fitting lines

Based on the results of iron standard samples, the relation between carbon concentration in steel and the muon capture ratio was evaluated. The calibration data showed a linear relationship, and carbon content in the Japanese sword can be determined from the measured muon capture ratios.

Figure 2 shows the depth profile of carbon concentration in the Japanese sword. The carbon concentration is approximately 0.6% near the surface and decreases to around 0.4% with depth greater than 1 mm. Such concentration gradient suggests that the Japanese sword was fabricated by combining steels with different carbon concentrations; high concentration one in the surface and low concentration one in the core. Also, we found that the measured carbon concentrations are generally consistent with those reported for typical traditional Japanese swords [4].

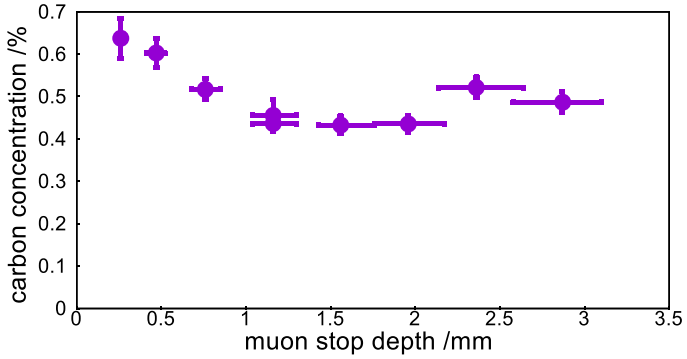


Figure 2. Carbon concentration depth distribution of the Japanese swords

References

[1] Japanese Industrial Standards Committee. “Iron and Steel—Determination of Carbon—Part 3: Infrared Absorption Method after Combustion”. *JIS*. G1211–1213 (2018).

[2] K. Ninomiya et. al., “Development of a non-destructive depth-selective quantification method for sub-percent carbon contents in steel using negative muon lifetime analysis”, *Scientific Reports*, **14**, 1797 (2024)

[3] T. Suzuki et. al., “Total nuclear capture rates for negative muons”, *Phys. Rev. C*, **35**, 2222 (1987)

[4] C. Matsumoto et. al., “Characteristics of Japanese sword produced from tatara steel”, *Journal of Alloys and Compounds*, **577**, S673-S677 (2013)

7th Asia-Pacific Symposium on Radiochemistry *September 14 ~ 19, 2025 • Kunibiki Messe • Shimane, Japan*

DEVELOPMENT OF A NEW NON-DESTRUCTIVE ELEMENTAL ANALYSIS METHOD FOR TRACE COMPONENTS USING MUON-INDUCED GAMMA RAYS

Makoto Inagaki[1], Kazuhiko Ninomiya[2], Go Yoshida[3], Kosei Yakushi[2], Eisuke Watanabe[3], Hiroki Nakada[1], Izumi Umegaki[4], Michael Kenya Kubo[5]

[1]*Institute for Integrated Radiation and Nuclear Science, Kyoto University: 2-1010 Asashironishi, Kumatori, Sennan, Osaka 590-0494, Japan*
[2]*Graduate School of Advanced Science and Engineering, Hiroshima University: 1-4-1 Kagamiyama, Higashihiroshima, Hiroshima 739-8527, Japan*
[3]*Radiation Science Center, High Energy Accelerator Research Organization (KEK): 1-1 Oho, Tsukuba, Ibaraki 305-0801, Japan*
[4]*Institute of Materials Structure Science, High Energy Accelerator Research Organization (KEK): 1-1 Oho, Tsukuba, Ibaraki 305-0801, Japan*
[5]*College of Liberal Arts, International Christian University: 3-10-2 Osawa, Mitaka, Tokyo 181-8585, Japan*

A novel non-destructive elemental analysis method using muon-induced gamma rays was developed to quantify trace components in materials. Conventional muon-based elemental analysis, which relies solely on characteristic muonic X-rays, faces challenges in detecting trace elements owing to interference from X-rays emitted by major components. To overcome this limitation, gamma rays were used in addition to characteristic muonic X-rays. The experiment was conducted at the muon facility MUSE of J-PARC, where standard steel samples containing varying Si concentrations were irradiated with a negative muon beam. The characteristic muonic X-rays and decay γ-rays from nuclides produced by muon nuclear absorption were measured using Ge detectors. The results demonstrated the successful quantification of Si concentrations as low as 0.39 wt% in Fe samples by detecting γ-rays from ^{28}Al, derived from Si, even when Si X-rays were below the detection limit. A calibration curve was constructed by correlating the ratio of the γ-ray intensity from ^{28}Al to the X-ray intensity from Fe with the Si/Fe concentration ratio, which showed good linearity. This study highlights the potential of combining gamma rays with characteristic muonic X-rays to quantify trace components in materials, thereby expanding the capabilities of muon-based elemental analysis.

1 INTRODUCTION

Non-destructive elemental analysis is possible using characteristic muonic X-rays emitted when a material is irradiated with negative muons. Muon-based elemental analysis has been applied to the non-destructive analysis of valuable archaeological materials, samples returned from asteroids, and working batteries, etc., and its use is expanding [1-3].

Because the probability of muon capture by atoms depends approximately on the atomic number, muon-based elemental analysis has approximately the same sensitivity per mass regardless of the element. In other words, it is sensitive to all elements, on average. Although this is an advantage, it is also a disadvantage because the detection of X-rays emitted from trace components is interfered with by X-rays emitted from the major components in the material, making the detection of trace elements difficult.

To overcome this problem, in addition to characteristic muonic X-rays, prompt gamma rays, which are emitted immediately after the muon is absorbed by the nucleus, and decay gamma rays, which are emitted when the nucleus decays, were used in this experiment. Because prompt and decay gamma rays differ from characteristic muonic X-rays in terms of energy and emission timing, the signals of trace components can be detected without interference from characteristic muonic X-rays emitted by the main components. In other words, information on gamma rays emitted between muon beam pulses, which is not currently used for elemental analysis, is useful. Using this new method, we aim to develop a muon-based elemental analysis method that can analyze trace components in samples.

In this study, we succeeded in quantifying less than 1 wt% of silicon in iron samples using characteristic muonic X-rays and decay gamma rays, and demonstrated the feasibility of this method.

2. EXPERIMENTAL

The experiment was performed at the muon facility MUSE of J-PARC. Standard steel samples containing Si were irradiated with a 30 MeV/c negative muon beam. X-rays and γ-rays from nuclides produced by the absorption of muons by nuclei were measured. In the present study, samples with Si relative to Fe concentrations of 3.93, 1.48, and 0.39 wt% were used. X-rays and γ-rays were measured using a Ge detector placed approximately 100 cm and 9 cm from the sample, respectively. The data from the detector were acquired in the form of a list linking the elapsed time from the arrival of the

Copyright on 7th Asia-Pacific Symposium on Radiochemistry 2025

muon pulse beam to the energy of the radiation and analyzed from the beam-synchronous component for the X-rays and the asynchronous component for the γ-rays.

3. RESULTS AND DISCUSSION

X-rays of Fe (1257 keV) were detected in all the samples measured. X-rays of Si (400 keV) were detected in the sample with a Si concentration of 3.93 wt%, but were below the detection limit in samples with Si concentrations of 1.48 wt% and 0.39 wt%. In contrast, γ rays (1779 keV) from ^{28}Al (half-life 2.2 min) derived from Si were detected in all samples, including the sample with a Si concentration of 0.39 wt%. The radioactivity of ^{28}Al, which has a short half-life, saturates within a short time after beam irradiation, and the saturated radioactivity is proportional to the amount of Si in the sample. A calibration curve was constructed by correlating the ratio of the γ-ray intensity from ^{28}Al to the X-ray intensity from Fe with the Si/Fe concentration ratio in the sample, which showed good linearity (Fig. 1).

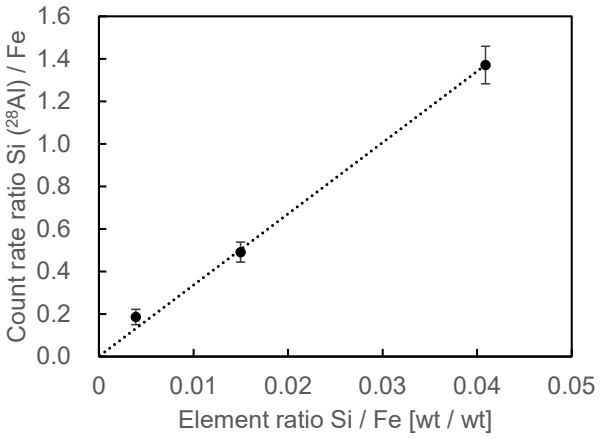


Fig. 1. A calibration curve constructed by correlating the ratio of the γ-ray intensity from ^{28}Al to the X-ray intensity from Fe with the Si/Fe concentration ratio in the sample.

4. CONCLUSION

The results showed that components with a concentration of less than 1 wt%, which are difficult to detect by muon elemental analysis using only X-rays, can be quantified using gamma rays in combination with X-rays. In the future, we will expand this method to other elements and attempt to apply prompt gamma rays to this method.

ACKNOWLEDGMENTS

The muon experiment at the Materials and Life Science Experimental Facility of J-PARC was performed under a user program (Proposal No. 2024A0202).

References

[1] K. Ninomiya *et al.*, "Development of Nondestructive and Quantitative Elemental Analysis Method Using Calibration Curve between Muonic X-ray Intensity and Elemental Composition in Bronze," Bull. Chem. Soc. Jpn., **85**, 228-230 (2012).
[2] T. Nakamura *et al.*, "Formation and evolution of carbonaceous asteroid Ryugu: Direct evidence from returned samples," Science, **379**, eabn8671 (2023).
[3] I. Umegaki *et al.*, "Non-destructive operando measurements of muonic x-rays on Li-ion battery," J. Phys.: Conf. Ser., **2462**, 012018 (2023).

Copyright on 7th Asia-Pacific Symposium on Radiochemistry 2025

7th Asia-Pacific Symposium on Radiochemistry *September 14 ~ 19, 2025 • Kunibiki Messe • Shimane, Japan*

ELEMENTAL DEPTH DISTRIBUTION ANALYSIS OF JAPANESE GOLD PRODUCTS FROM LATE 16TH CENTURY USING MUONIC X-RAYS

Atsuya Yukawa[1], Tsutomu Saito[2], Motonobu Tampo[3], Izumi Umegaki[3], Soshi Takeshita[3], Yasuhiro Miyake[3], Koichiro Shimomura[3], Kazuhiko Ninomiya[1]

[1]*Graduate School of Advanced Science and Engineering, Hiroshima University: 1-3-2, Kagamiyama, Higashihiroshima, Hiroshima, 739-8511, m255489@hiroshima-u.ac.jp*
[2]*National Museum of Japanese History: 117, Jonai, Sakura, Chiba, 285-8502*
[3]*Muon Science Laboratory, IMSS, KEK: 203-1, Shirakata, Tokai, Ibaraki, 319-1106*

During the Edo period, koban coins were made of gold-silver alloy, with their gold concentration varying depending on the era. A surface treatment technique called Irotsuke was used to dissolve and remove silver from the surface, enhancing the gold luster. In this study, to investigate the origin of the Irotsuke technique, we conducted a non-destructive elemental depth-profiling analysis using muons on gold sword ornaments (menuki) produced before the historical period of the koban coins.

1 INTRODUCTION

It is known that the surface treatments were carried out on Japanese gold-silver alloy products around the early modern period. Koban, gold coins from the Edo period, are one of the most commonly made and circulated gold-silver alloy products. The *koban* has a gold rich layer near the surface by a surface treatment technique called "*Irotsuke*" that selectively removes silver from the surface layer, and gives a brilliant gold luster. Although this technique was used in common from the early Edo period, the origin of this technique remains unknown. To investigate the origin, the properties of surface treatments on gold-silver alloys from the same and/or early period should be investigated. However, researches haves been limited because the destructive analysis methods never been applied for these cultural artifacts.

In this study, we focused on a non-destructive elemental analysis technique using muons. Muons are one of the elementary particles having negative charge. The mass of a muon is approximately 207 times than that of an electron. When a muon is injected into a material, the muon losses its kinetic energy and finally stops in the material. After that, the muon forms atomic orbit around a nucleus in a material similar to electrons, resulting in the formation of a muonic atom. The captured muon emits characteristic muonic X-rays (muonic X-rays) in transition of muon atomic levels. These X-rays have unique energies by elements and can easily penetrate through material due to their high energies. Non-destructive and depth-selective elemental analysis can be achieved by muonic X-ray measurement by controlling the muon stopping depth in a material [1].

Production of *koban* coins began in the beginning of 17th century by the person responsible, Goto Shozaburo Mitsutsugu (1571~1625). In this study, to investigate the technological development of the *Irotsuke* technique by examining the surface treatment of a gold products of sword ornaments (*menuki*) were analyzed produced in the 16th century by the master of Mitsutsugu.

2 EXPERIMENTAL

In this study, muon analysis was conducted on two *menuki* produced by metal engravers of the Goto Shirobei family, which has continued since the late Muromachi period in Japan. The first sample is the *Genji Yugao-zu*, created by Joshin (1512–1562), and the second is the *Shachi-zu*, crafted by Tokujo (1548–1631). The photos of the samples are shown in Figure 1. The measurements were performed at the D2 area in MLF (Material and Life science Experimental Facility), J-PARC (Japan Proton Accelerator Research Complex, Ibaraki prefecture, Japan). The experimental setup is shown in Figure 2. The samples were placed in the vacuum chamber and muons were irradiated on the samples. The emitted muonic X-rays were measured using 6 high-purity germanium semiconductor detectors (CANBERRA, GL0110). The incident muon momentum was set to 4.5–13.0 MeV/c for the *Genji Yugao-zu*, and 5.0–14.5 MeV/c for the *Shachi-zu*, corresponding to muon stopping depths of 0.48–11.1 μm and 0.62–15.3 μm, respectively.

For quantitative analysis, muonic X-ray measurements were also conducted on gold-silver standard alloys. For these measurements, the incident muon momentum was fixed at 7.0 MeV/c.

3 RESULTS AND DISCUSSION

From the analysis of the spectra from the gold-silver alloy standard samples, the peak positions originate from gold and silver were investigated. The muonic X-ray spectrum obtained from the *Genji Yugao-zu* is shown in Figure 3. By

Copyright on 7th Asia-Pacific Symposium on Radiochemistry 2025

comparing the spectra from the *menuki* samples with standard samples, all peaks were assigned with gold and silver, indicating that the *menuki* is composed of a gold-silver alloy.

In this study, elemental compositions were determined based on the peak intensities of 41.3 and 130.0 keV for gold, and 45.9 and 140.2 keV for silver. First, the relationship between muonic X-ray intensity ratios and elemental compositions was established using standard samples, and a calibration curve was evaluated. The gold concentration in the *menuki* was then determined by applying this calibration curve. Since consistent results were obtained among all detectors, the averaged values of individual detectors were taken.

The averaged gold concentration in the *Genji Yugao-zu* was 77.2 % and that in *Shachi-zu* was 90.2 %. In both samples, depth dependences on the gold concentration, enrichment of gold contents near surface, were not found and we concluded *irotsuke* were not applied for these samples. From these results, one possibility is that the origin of the *Irotsuke* technique was not came from the Goto Shirobei family and the technique was not passed down to Goto Shozaburo Mitsutsugu, the person responsible of *koban* coins.



Fig. 1. Photos of *Genji Yugao-zu* and *Shachi-zu*

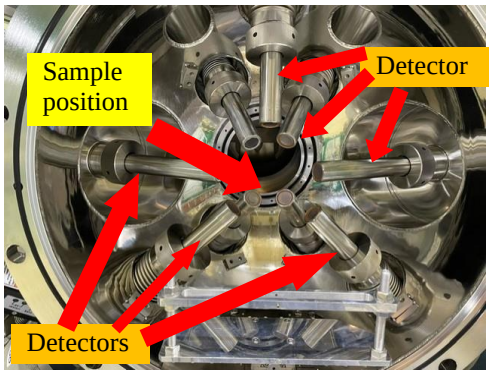


Fig. 2. Muon experiment setup at D2 area, J-PARC MLF.

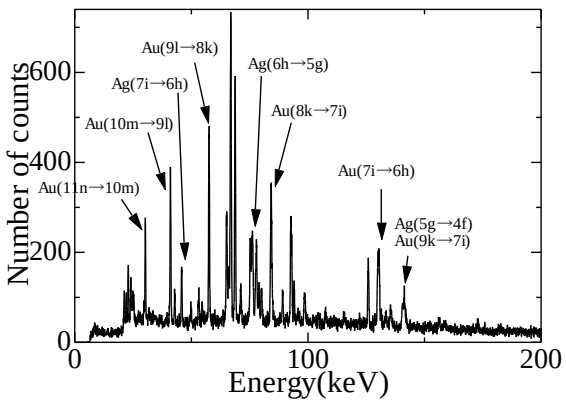


Fig. 3. Muonic X-ray spectrum obtained from the *Genji Yugao-zu*

References

[1] K Ninomiya et. al., “Nondestructive Elemental Depth-Profiling Analysis by Muonic X-ray Measurement,” *Analytical Chemistry*, **87**, 4597 (2015).

Copyright on 7th Asia-Pacific Symposium on Radiochemistry 2025

Poster Presentation | [R8]Education and Outreach

Tue. Sep 16, 2025 6:30 PM - 8:00 PM JST | Tue. Sep 16, 2025 9:30 AM - 11:00 AM UTC Poster

[Poster] R8

[P-R8-01]

THIRTY YEARS OF THE RADIATION EDUCATION FORUM

*Yoshimune Ogata[1], Seiichi Shibata[2], Ryuichi Tanaka[2], Yukio Yoshizawa[2], Tadashi Asakura[2], Sayoko Ohmori[2], Kazuko Ohno[2], Kazuo Sakai[2], Keisuke Sueki[2], Masatune Hatakeyama[2], Soichi Hayashi[2], Tomohiro Watanabe[2] (1. Aichi Medical University (Japan), 2. Radiation Education Forum (Japan))

[P-R8-02]

TERMINOLOGY ON RADIOCHEMISTRY AND NUCLEAR CHEMISTRY IN JAPANESE: HISTORICAL ASPECTS AND PRESENT STATUS

*Yoshitaka Minai[1] (1. Musashi University and Nedzu Chemical Laboratory (Japan))

[P-R8-03]

Activities of the Education Division of the Japan Society of Nuclear and Radiochemical Sciences

*Atsushi Shinohara[1], Mitsuru Ebihara[2], Michiko Fukushima[3], Yasushi Kino[4], Takafumi Kitazawa[5], Yuya Koike[6], Hisaaki Kudo[7], Motoyuki Matsuo[8], Yoshitaka Minai[9], Haruka Minowa[10], Satoru Nakashima[11], Yoshimune Ogata[12], Yasuji Oura[2], Takayuki Sasaki[13], Tsutomu Sekine[4], Keisuke Sueki[14], Tatsuya Suzuki[15], Akihiko Yokoyama[16], Go Yoshida[17] (1. Osaka Aoyama University (Japan), 2. Tokyo Metropolitan University (Japan), 3. Ishinomaki Senshu University (Japan), 4. Tohoku University (Japan), 5. Toho University (Japan), 6. Meiji University (Japan), 7. Nigata University (Japan), 8. The University of Tokyo (Japan), 9. Musashi University (Japan), 10. The Jikei University School of Medicine (Japan), 11. Hiroshima National College of Maritime Technology (Japan), 12. Aichi Medical University (Japan), 13. Kyoto University (Japan), 14. University of Tsukuba (Japan), 15. Nagaoka University of Technology (Japan), 16. Kanazawa University (Japan), 17. High Energy Accelerator Research Organization (Japan))

[P-R8-04]

AN EXAMPLE OF RADIATION EDUCATION IN JAPANESE ELEMENTARY SCHOOLS - MY EXPERIENCES BEFORE AND AFTER THE FDNPP -

*Yukiko Okada[1], Naoto Hagura[2], Takehiro Toda[3] (1. Tokyo City University Atomic Energy Research Laboratory (Japan), 2. Tokyo City University Faculty of Science and Engineering Department of Nuclear Safety Engineering (Japan), 3. RADO Co., Ltd (Japan))

©APSORC25

THIRTY YEARS OF THE RADIATION EDUCATION FORUM

Seiichi Shibata[1], Ryuichi Tanaka[2], Yoshimune Ogata[3], Yukio Yoshizawa[4], Tadashi Asakura[5], Sayoko Ohmori[6] Kazuko Ohno[7], Kazuo Sakai[8], Keisuke Sueki[9], Masatune Hatakeyama[10], Soichi Hayashi[11], Tomohiro Watanabe[12]

[1]*Radiation Education Forum: 6-7-2 Higashi-Ueno, Taito-ku, Tokyo, Japan, 110-0015, shibata3905s@gmail.com*
[2]*Radiation Education Forum: 6-7-2 Higashi-Ueno, Taito-ku, Tokyo, Japan, 110-0015, ryutnk@kra.biglobe.ne.jp*
[3]*Radiation Education Forum: 6-7-2 Higashi-Ueno, Taito-ku, Tokyo, Japan, 110-0015, yoshimune.ogata@aichi-med-u.ac.jp*
[4]*Radiation Education Forum: 6-7-2 Higashi-Ueno, Taito-ku, Tokyo, Japan, 110-0015, yukio.yoshizawa@ymail.ne.jp*
[5]*Radiation Education Forum: 6-7-2 Higashi-Ueno, Taito-ku, Tokyo, Japan, 110-0015, tad_asakura@jikei.ac.jp*
[6]*Radiation Education Forum: 6-7-2 Higashi-Ueno, Taito-ku, Tokyo, Japan, 110-0015, shohmori@outlook.jp*
[7]*Radiation Education Forum: 6-7-2 Higashi-Ueno, Taito-ku, Tokyo, Japan, 110-0015, kakochan@kyoto-msc.jp*
[8]*Radiation Education Forum: 6-7-2 Higashi-Ueno, Taito-ku, Tokyo, Japan, 110-0015, kazsakai0224@outlook.jp*
[9]*Radiation Education Forum: 6-7-2 Higashi-Ueno, Taito-ku, Tokyo, Japan, 110-0015, ksueki727@gmail.com*
[10]*Radiation Education Forum: 6-7-2 Higashi-Ueno, Taito-ku, Tokyo, Japan, 110-0015, hatakeya@hotmail.com*
[11]*Radiation Education Forum: 6-7-2 Higashi-Ueno, Taito-ku, Tokyo, Japan, 110-0015, soichi@fukuoka-u.ac.jp*
[12]*Radiation Education Forum: 6-7-2 Higashi-Ueno, Taito-ku, Tokyo, Japan, 110-0015, tomohiro5131@gmail.com*

The Radiation Education Forum was set up on April 12, 1994, by volunteer researchers and teachers interested in radiation education and the peaceful use of nuclear energy, aiming to improve "radiation literacy" not only of pupils and students but also of the general public in Japan. Here the thirty years of the Radiation Education Forum is reported.

1. EARLY DAYS

It is cause for concern that, despite the fact that people's lives depend on the benefits of scientific progress, young people are turning away from science, and that even people with a high level of knowledge today have excessive anxiety about radiation, which is a major obstacle to the peaceful use of nuclear power. At the time of the establishment of the Radiation Education Forum (hereafter REF), the issue of radiation education in Japan was that no instruction on radiation was included in compulsory education. The REF was founded in 1994 as a voluntary organisation whose aim is to disseminate reliable knowledge on energy, the environment, radiation and nuclear power. The representative founder was Tatsuo Matsuura, Professor Emeritus of Rikkyo University, and the first president was Professor Akito Arima, who had also served as President of the University of Tokyo and Minister of Education. Initially it was a voluntary organization, but in 2000 it obtained certification as an NPO.

The aim of the REF, as a neutral volunteer organization, is to improve radiation education in science and social studies classes through providing solid knowledge of radiation and education on energy and environmental issues, so that the REF is to dispel unfounded fears about radiation. Its focus is on improving elementary, middle and high school education, especially science education.



Fig. 1 Presidents; upper, from left, Prof. Arima, Prof. Fusimi, and Prof. Matsuura, lower, from left, Prof. Hasegawa, Prof. Kudo and Prof. Shibata.

2. ACTIVITIES OF THE RADIATION EDUCATION FORUM

2.1 Submission of a Petition Regarding Radiation Education to the Minister of Education

The word "radiation" was removed from the curriculum guidelines that came into effect in April 1981. Calling for improvements to the curriculum guidelines, we submitted a "Request for Improvement of Radiation Education" to the Minister of Education in 1995, pointing out that the reason knowledge of radiation, radioactivity, and nuclear power among Japanese young people is lower than that of young people in Europe and the United States is because basic knowledge and applications of radiation are not being taught adequately and accurately in schools. The request was submitted to the Minister of Education and the General Director of Science and Technology Agency in 1996. Furthermore, in 2005 we submitted a document entitled "Improving the Curriculum Guidelines to Enhance Energy and Environmental Education" to the Minister of Education, Culture, Sports, Science and Technology. As a result of these activities, the curriculum guidelines were revised in 2008, and the revised curriculum guidelines of 2011 brought radiation back into junior high school science classes for the first time in 30 years. Coincidentally, 2011 was the year that the nuclear disaster occurred at the Fukushima Daiichi Nuclear Power Plant.

Copyright on 7th Asia-Pacific Symposium on Radiochemistry 2025 P-R8-01 -

2.2 Holding Seminars on Energy, Environment and Radiation for School Teachers

The Seminars on energy, environment, and radiation were conducted for nine years from 2001 to 2009 for elementary, junior high, and high school teachers in order to properly incorporate energy, environmental issues, and radiation into school education, while also spreading correct knowledge to students through such programs as the Integrated Study Period that began in 2002. The seminar is held every year in 10 regions across the country (Hokkaido, Tohoku, Hokuriku/Niigata, Northern Kanto/Nagano, Southern Kanto, Shizuoka/Yamanashi, Aichi/Gifu/Mie, Kinki, Chugoku/Shikoku, Kyushu/Okinawa) and is made a success thanks to the dedicated efforts of the many members of our forum from all over the country.

2.3 Holding Study Sessions on Energy, the Environment, and Radiation

The REF held its first study session on energy, environment and radiation in October 1994. Since then, except for a period during the COVID-19 pandemic from 2019 to 2020, study sessions have been held three times a year. Before the COVID-19, all study sessions were held in face-to-face study sessions, but since 2020, we have been holding one in face-to-face study session per year and two online sessions per year. Since the face-to-face study sessions were held in Tokyo, it was difficult for members in rural areas and the general public to participate. On the other hand, online study sessions had the advantage of allowing members from far away to participate. The topics and lecturers from past study sessions can be viewed on the REF website; https://www.ref.or.jp/. Also, Materials from the most recent study sessions are also available to view on the website.

2.4 Periodical Publications

The "Newsletter" began publication in December 1994 and has been published three times a year since then. Since 1997, it has published the peer-reviewed journal "Radiation Education" once a year. Back issues of these publications, except for the most recent ones, are available on the REF website.

2.5 Publication of Radiation Education Materials on the Website

The REF has published radiation education materials on its website that can be used in elementary, junior high and high school classes, including the basics of radiation, experiment guides and lessons learned from the Fukushima nuclear accident.

Furthermore, in 2018, we produced a DVD teaching material on radiation titled "R no Shotai (The Nature of R)" and distributed it free of charge to 10,204 junior high schools nationwide as a Ministry of Education, Culture, Sports, Science and Technology selected teaching material. The DVD will be available on YouTube in 2021. It was later published on Teacher's Net (https://www.teachers-net.com).

2.6 Hosting of an International Conference on Radiation Education

In 1998, the REF held the 1st International Symposium on Radiation Education (ISRE) in Hayama, Kanagawa Prefecture, Japan. After that, the ISRE conferences were held in Hungary in 2002, Nagasaki in 2004, and Taiwan in 2008. In 2016, the event was held in Koriyama City, Fukushima Prefecture, Japan, in light of the nuclear accident, providing an opportunity for school teachers and members of the general public in Fukushima to reaffirm the importance of radiation education. In 2021, ISRE was held online in Taiwan. The proceedings of ISRE can be downloaded from the REF website.



Fig.2 Group photo of the 30th Anniversary Establishment Ceremony

2.6 Current Status of the Radiation Education Forum

The REF holds study sessions once a year face-to-face and twice a year online. The online study sessions conducted as a result of the COVID-19 were welcomed by people living outside the Tokyo metropolitan area, but there are concerns as to whether sufficient time was provided for question and answer sessions. The study sessions are free to attend, even if you are not a member of the forum. Records of past study sessions and how to participate are available on the REF website.

The REF will celebrate its 30th anniversary in 2024. Therefore, on November 17th, a ceremony and celebration to commemorate the company's 30th anniversary was held at the KKR Hotel Tokyo.

The organization also provides a special prize at the Radiation Education Forum, a presentation on radiation education sponsored by the Japan Science and Technology Agency.

3. CONCLUSIONS

Founded in 1994, the Radiation Education Forum is celebrating its 30th anniversary after achieving the milestone of contributing to the inclusion of "radiation" in the curriculum guidelines for compulsory education. The REF will continue to focus on supporting education about radiation in primary, junior high and high schools, in order to dispel excessive anxiety about radiation among the general public and provide them with enough knowledge to "be fearful in the right way."

Copyright on 7th Asia-Pacific Symposium on Radiochemistry 2025 P-R8-01 -

7th Asia-Pacific Symposium on Radiochemistry *September 14 ~ 19, 2025 • Kunibiki Messe • Shimane, Japan*

TERMINOLOGY ON RADIOCHEMISTRY AND NUCLEAR CHEMISTRY IN JAPANESE: HISTORICAL ASPECTS AND PRESENT STATUS

Yoshitaka Minai

Musashi Univesity and Nedzu Chemical Laboratory: 7-3-1 Toyotama-kami, Nerima-ku, Tokyo 176-8534, Japan
minai@cc.musashi.ac.jp

This paper is a communication on how Japanese terminology in radiochemistry and nuclear chemistry was established after the radioactivity discovery in european academia. Various aspects influencing terminology in Japanese academia would be discussed like structure of language using both Chinese characters and phonetic 'kana' alphabet, university system having institutions in pure sciences and other huge institutions in application to technology, governmental control, etc.

1 INTRODUCTORY REMARKS

After discovery of radioactivity at the end of 19th century, many terms and expressions have developed on the road of growth in radiochemistry and nuclear chemistry. The newly born words on radiochemistry were introduced quickly into Japanese academia, where remarkable research activities in physics and chemistry including application grew.

This paper is a communication on how Japanese terminology in radiochemistry and nuclear chemistry was established after the radioactivity discovery in European academia. Are discussed various aspects influencing terminology in Japanese, hereafter.

2 METHOD

Scientific or technical terms on radiochemistry and nuclear chemistry were extracted from some textbooks and reference sources available at present. Those terms were compared with those in English. Such comparison was also made among terms in English, Chinese, and Japanese. Were involved that some booklets translated from the original publication in English. The oldest textbook in this study was published/translated in 1950's.

3 SOCIAL FACTORS INFLUENCING TRANSLATION PROCESSES FROM SCIENTIFIC TERMS IN EUROPEAN LANGUAGES ON RADIOCHEMISTRY AND NUCLEAR CHEMISTRY

3.1 Translation for Promoting Science and Technology to Achieve Quick Industrialization in Japan

Translation of scientific terms is required for education in school systems. When radioactivity was discovered, Japan promoted quick growth of industry based on physics and chemistry under control of the government. Translation was necessary to import science and technology to younger generations who would drive future of industry since foreign languages were not popular in Japan.

3.2 Use of Both Chinese Ideograms and Phonic 'Kana' Characters in Japanese

Traditionally, academic terms were indicated with Chinese 'kanji' ideograms since Japan has been influenced by Chinese 'Kanji'-based culture for nearly fifteen hundred years. It is noteworthy that Japanese language has two sets of phonic 'kana' characters: 'hira-gana' and 'kata-kana' derived from Chinese 'kanji'. Both ideograms and phonic characters compose Japanese characters introduce new terms from foreign culture into Japanese.

As example, Japanese name of element is noted with 'kanji' ideograms or 'kata-kana' phonic characters. Choice of 'kanji' or 'kata-kana' depends on time of discovery of each element. That is very different from Chinese case; new 'kanji' character needs to be created for each discovery of the element.

4 PERSPECTIVES

Our final goal is to develop fundamental educational programs for young scientists interested in radiochemistry and nuclear chemistry. Those specific fields in chemistry have contributed a lot to the modern society in the 20th century and present: for instance, medical applications in both diagnosis and therapy and alternative option for energy production. It is expected that outreach works for public relations would be required as the expert handling radioactivity, in particular. Understanding our roots as radiochemists and nuclear chemists would be a great help for those outreach activities.

Copyright on 7th Asia-Pacific Symposium on Radiochemistry 2025

7th Asia-Pacific Symposium on Radiochemistry *September 14 ~ 19, 2025 • Kunibiki Messe • Shimane, Japan*

Activities of the Education Division of the Japan Society of Nuclear and Radiochemical Sciences

Atsushi Shinohara[1, 2] and Member of steering committee[2]

[1] *Oasaka Aoyama University, 2－11－1、Niina, Minoh, Osaka 562-8580, Japan*

[2] *Education Division, the Japan Society of Nuclear and Radiochemical Sciences*

1 ABOUT EDUCATION DIVISION

As part of a major reform following its incorporation in April 2021, the Japan Society of Nuclear and Radiochemical Sciences established a new Education Division. Its mission is to enhance nuclear and radiochemical education in Japan by exploring current and future directions in teaching methods, organizing educational events, dispatching lecturers, and actively supporting the development of graduate students and early-career researchers in collaboration with the Young Scientists' Group.

2 OUTLINE OF THE EDUCATION DIVISION'S ACTIVITIES

With approximately 70 members (20% of the society members), the division operates under the steering committee of about 20 selected members, who plan and implement specific initiatives. Currently, three main projects are in progress, with additional efforts under consideration, including the development of a radiochemistry certification system, outreach programs and lectures on location, and joint educational events with related academic societies to foster future educators. Below is a brief summary of ongoing initiatives.

2.1 Educational Seminars

These seminars focus on radiochemistry-related topics and have been held in a hybrid format twice annually since 2022, totaling six sessions to date. All have centered on the theme of human resource development, featuring broad discussions on the current status and future plans of five subfields within the society and relevant academic associations. The table below summarizes past seminar topics.

TABLE 1. Summaries of educational seminar

Date	Venue / Format	Theme
May 21, 2022	University of Tokyo / Hybrid	Nurturing the Next Generation and Radiochemistry (Chemical Society of Japan (Kinki), Atomic Energy Society of Japan, Geochemical Society of Japan)
Mar 8, 2023	KEK Kobayashi Hall, Tsukuba / Hybrid	Nurturing the Next Generation and Radiochemistry (JRSM, Pharmaceutical Society of Japan, Japan Radioisotope Association, JAEA)
Sep 23, 2023	Hiroshima University SORC66 / In-person	Communicating Science – Science Communication and Presentation Design –
Mar 13, 2024	KEK Kobayashi Hall, Tsukuba / Hybrid	Nurturing the Next Generation and Division Activities (1) (Alpha-emitting Radionuclides and Environmental Radioactivity, Actinide Chemistry, Young Scientists' Group)
Sep 25, 2024	Shizuoka University SORC67 / In-person	Nurturing the Next Generation and Division Activities (2) (Nuclear Chemistry, Nuclear Probes, Activation Analysis, Young Scientists' Group)
Mar 14, 2025	KEK Kobayashi Hall, Tsukuba / Hybrid	Passing on the Story of "Radiochemistry and Society" – 70 Years since the Bikini Incident –

2.2 Radiochemistry School

Launched last year, this online school-style seminar aims to teach and pass down experimental and technical knowledge in radiochemistry to young researchers. Two sessions have been held so far: "Separation Techniques –

Copyright on 7th Asia-Pacific Symposium on Radiochemistry 2025 P-R8-03 -

Chemical Separation Using Ion-Exchange Resins" (Oct 5, 2023) and "Activation Analysis" (Mar 8, 2025). A session on "Nuclear Reaction Cross-section Measurement" is currently in preparation. Future sessions may also include hands-on training in in-person formats.

2.3 Collection and Sharing of Educational Contents

We are working to collect and, where necessary, develop educational materials related to radiochemistry created or held by society members. The ultimate goal is to make these resources widely accessible. Currently, we are collecting existing materials and preparing for their release within the society.

3 SUMMARY

In the field of radiochemistry, the number of research labs and educational researchers has been declining for many years, making the recruitment and training of university students and young researchers an urgent issue. At the same time, as this conference underscores, solving social issues related to radiation and radioactivity requires trained professionals in this field. Moreover, the demand for the use of radionuclides, especially in medicine, is steadily increasing. Thus, the societal need for radiochemistry experts in Japan is growing.

Moving forward, we aim to strengthen collaboration with the Young Scientists' Group and related academic societies, support graduate education, and raise public awareness. Through these efforts, we hope to broaden the scope and further vitalize our activities. We also look forward to learning about initiatives in other countries during this conference.

Copyright on 7th Asia-Pacific Symposium on Radiochemistry 2025 P-R8-03 -

AN EXAMPLE OF RADIATION EDUCATION IN JAPANESE ELEMENTARY SCHOOLS

- MY EXPERIENCES BEFORE AND AFTER THE FDNPP -

Yukiko Okada[1], Naoto Hagura[2], Takehiro Toda[3]

[1]Tokyo City University Atomic Energy Research Laboratory: *981 Asao-ku, Kawasaki, Kanagawa, 215-0013, Japan.*

[2]Tokyo City University Faculty of Science and Engineering Department of Nuclear Safety Engineering: *1-28-1 Tamazutsumi, Setagaya-ku, Tokyo, 158-8557, Japan.*

[3] RADO Co., Ltd.:*2-4-20 Motomati, Toyama, 930-0033, Japan*

Since Dr. Röntgen discovered artificial radiation in 1895, radiation has been used in many industries, including medicine. Since Dr. Becquerel discovered that radiation is emitted from natural stones in 1896, it has become clear that radiation exists everywhere on Earth. Today, the use of radiation is an indispensable technology. However, for many Japanese people, the word 'radiation' is associated with atomic bombs and is perceived as dangerous and something to be avoided. Radiation brings numerous benefits to our daily lives, but our understanding of it is insufficient. Furthermore, the fact that radiation exists everywhere on Earth and that we are constantly exposed to it is not widely understood. Furthermore, the accident that occurred at the Tokyo Electric Power Company's Fukushima Daiichi Nuclear Power Plant (FDNPP) on 11 March 2011 caused widespread anxiety among the Japanese population.

In this symposium, I will share my experiences in radiation education from before 3.11 to the present and discuss the future direction of such education.

1 Activities up to 11 March 2011

I taught elementary school students (ages 10 to 12) the following three points through experiments. 1. Learn the term 'radiation. 2. Radiation exists everywhere around us. 3. Exposure to large amounts of radiation is dangerous. The amount of radiation in the environment is safe.

2 Activities after 11 March 2011

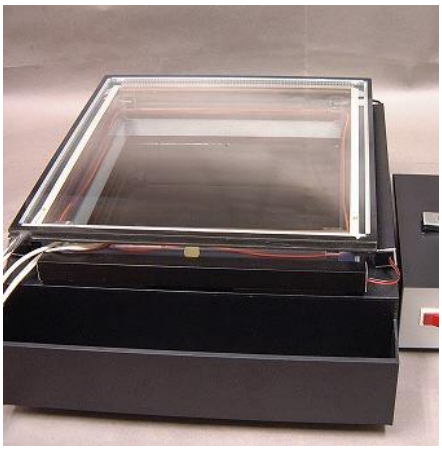
At the request of the Japan Atomic Energy Relations Organization (JAERO), radiation education was conducted at elementary schools in Fukushima Prefecture using the same methods as those implemented prior to 11 March 2011. However, the target age group for this radiation education was expanded to include children aged 6 to 12. Therefore, I had to review the content on the spot as necessary, taking into consideration the ages of the participating children.

2.1 Encountering Excellent Lessons (Case Study of Teachers at Ashizawa Elementary School in Tamura City, 2015)

In 2015, I gave a lecture on radiation at Ashizawa Elementary School in Tamura City, Fukushima Prefecture. After the lecture, I was invited to a classroom with students aged 10 to 12. There were two posters covering the walls with terms related to nuclear power and radiation. However, the students' activities did not stop there. Over the course of a year, they had been deepening their learning across multiple subjects.

2.3. Cloud chamber showing traces of natural radiation

The fact that radiation exists around us is difficult for children to understand. This is true for the general public as well. Generally, in order to observe the traces of radiation, a radiation source is required. However, the cloud chamber I encountered allows you to confirm the traces of radiation without a radiation source. It enables you to observe the traces of alpha particles emitted from radon present in the air. n this cloud chamber experiment, you can observe alpha particles, beta rays, and occasionally radiation from space.



RADO-type Desktop cloud chamber B-112 (Dry ice cooling type)[1)]



Observe the track of natural radioactive rays.

2.4 Future developments in radiation education

Currently, there are several new examples of radiation education. This form of education is very interesting. I will give some examples in my presentation.

3. CONCLUSIONS

The accident at the FDNPP caused confusion among the general public. Similar situations occurred in elementary school education. We learned that basic knowledge about radiation is essential for us. Furthermore, radiation is used in various fields such as energy, medicine, food, and daily necessities.

As children grow, it is important for them to learn about radiation carefully and gradually. And learning about the interesting aspects of science through radiation can also help develop children's scientific abilities.

References

[1] https://kiribako-rado.co.jp/e-goods/

Poster Presentation | [S1]Evolution of the Periodic Table of the Elements

Tue. Sep 16, 2025 6:30 PM - 8:00 PM JST | Tue. Sep 16, 2025 9:30 AM - 11:00 AM UTC Poster

[Poster] S1

[P-S1-01*]

QUANTUM CHEMICAL CALCULATIONS ON COMPLEXES OF No AND ALKALINE EARTH METALS EXTRACTED BY Sr RESIN FROM HDEDTP SOLUTION

*Ruilin Wang[1,2], Eisuke Watanabe[2,3], Takuya Yokokita[2,4], Yudai Itakura[1,2], Miyu Konno[1], Enni Khult[1,2], Kyosuke Shibamoto[1,2], So Hashiba[1,2], Hiromitsu Haba[2], Yudai Shigekawa[2], Akihiro Nambu[2], Yousuke Kanayama[2], Hiromichi Shimizu[2], Masashi Kaneko[1], Hiroyuki Kazama[1], Kojiro Nagata[1], Yoshitaka Kasamatsu[1] (1. Graduate School of Science, OSAKA University (Japan), 2. Nishina Center, RIKEN (Japan), 3. Radiation Science Center, KEK (Japan), 4. RARiS, Tohoku University (Japan))

[P-S1-02]

DEVELOPMENT OF THE LEGEND SYSTEM TOWARDS THE CHEMICAL STUDY OF Nh

*YANG WANG[1], Zimeng Jia[1], Shiwei Cao[1], Yunfei Cui[1], Zhi Qin[1] (1. Institute of Modern Physics,CAS (China))

[P-S1-03*]

Extraction of the group 2 elements and Pb(II) with TODGA-resin towards the chemical experiment with element 102, No

*Enni Khult[1,2], Ruilin Wang[1,2], Masashi Kaneko[1], Hiroyuki Kazama[1], Kyosuke Shibamoto[1,2], Miyu Konno[1,2], Yudai Itakura[1,2], Kenta Mori[1], Ryota Kikuchi[1], Kazushi Kawamoto[1], Ryotaro Masuda[1,2], Hiroki Aoto[1], So Hashiba[1,2], Hiromitsu Haba[2], Akihiro Nambu[2], Koichi Takamiya[3], Makoto Inagaki[3], Eisuke Watanabe[2,4], Takuya Yokokita[2,5], Yousuke Kanayama[2], Hiromichi Shimizu[2], Yudai Shigekawa[2,6], Yoshitaka Kasamatsu[1,2] (1. The University of Osaka (Japan), 2. RIKEN (Japan), 3. KURNS (Japan), 4. KEK (Japan), 5. Tohoku University (Japan), 6. University of Tsukuba (Japan))

©APSORC25

QUANTUM CHEMICAL CALCULATIONS ON COMPLEXES OF No AND ALKALINE EARTH METALS EXTRACTED BY Sr RESIN FROM HDEDTP SOLUTION

Ruilin Wang,[1,2] Eisuke Watanabe,[2,3] Takuya Yokokita,[2,4] Yudai Itakura, [1,2] Miyu Konno, [1] Enni Khult,[1,2]Kyosuke Shibamoto,[1,2] So Hashiba,[1,2] Hiromitsu Haba,[2] Yudai Shigekawa,[2] Akihiro Nambu,[2] Yousuke Kanayama,[2] Hiromichi Shimizu,[2] Masashi Kaneko,[1] Hiroyuki Kazama,[1] Kojiro Nagata,[1] and Yoshitaka Kasamatsu[1,2]

[1]*Graduate School of Science, The University of Osaka, Machikaneyama-cho 1-1, Toyonaka, Osaka 560-0043, Japan,wangr22@chem.sci.osaka-u.ac.jp*
[2] *Nishina Center, RIKEN, Hirosawa 2-1, Wako, Saitama 351-0198, Japan*
[3] *Radiation Science Center, KEK, Oho 1-1, Tsukuba, Ibaraki 305-0801, Japan*
[4] *RARiS, Tohoku University, Mikamine 1-2-1, Taihaku-ku, Sendai, Miyagi 982-0826, Japan*

We performed DFT calculations on the complexes of No and alkaline earth metals extracted from diethyldithiophosphate solution by crown ether resin. The trend in the calculated reaction energies as a function of ionic radius was in excellent agreement with the experimentally observed distribution coefficient (K_d) trends, and the electron density analysis results suggest that No exhibits covalent bonding character in this system. This result shows that No displays softer chemical properties than those of the alkaline earth metals.

1 INTRODUCTION

Element 102, nobelium (No), is the second element to the last of the actinide series. Unlike all other lanthanides and heavy actinides, No exists as a divalent cation rather than trivalent in aqueous solutions. Previous study regarding ion-exchange experiments have reported that No exhibits similar chemical properties to those of alkaline earth metals[1]. Our group has demonstrated that nobelium exhibits different coprecipitation behavior compared to alkaline earth metal ions using the samarium hydroxide coprecipitation method[2]. Subsequently, we concentrated on solid-liquid extraction using a polymer-supported crown ether resin (DtBuCH18C6). A recent online solid-liquid extraction experiment involving ^{255}No in the Sr resin/HNO_3 system was successfully achieved using an automated batch-type solid-liquid extraction apparatus (AMBER)[3], as shown in Fig. 1. It was found that No exhibits similar behaviors to that of Pb, which is softer than alkaline earth metals[4].

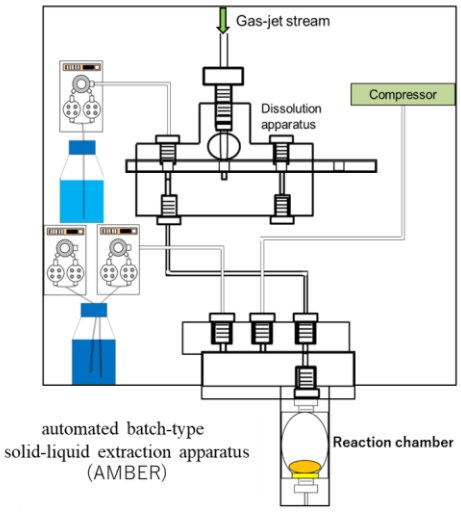


Fig. 1. Automated batch-type solid-liquid extraction apparatus (AMBER)

To further understand the chemical properties of No, we focused on diethyldithiophosphate (HDEDTP) as a new ligand for Sr resin solid-liquid extraction with ^{255}No. We determined the distribution coefficients (K_d) values of No and alkaline earth metals (Ca, Sr, and Ba) in Sr resin/HDEDTP system and found that extraction reactions of all elements reached equilibrium within 1 min of shaking. The K_d values of alkaline earth metals exhibited a positive correlation with their increasing ionic radius, but the K_d values of No were different from the predicted trend from the ionic radius among the alkaline earth metals in this system[5]. In this presentation, we will report quantum chemical calculation results that provide an interpretation of the experimental findings.

2 CALCULATIONS

In this investigation, we discuss the extraction behavior of No based on the comparison of the K_d values with those of alkaline earth metal ions. We conducted theoretical studies on No and alkaline earth metal ions complexes in Sr resin using relativistic quantum chemical calculations (DFT) via ADF 2023.104[6] to gain insights into the electronic characteristics of these complexes. Assuming that No^{2+} adopts a coordination structure analogous to that of the alkaline earth metals, the structures of all complexes were optimized at the B3LYP-DZP level, as depicted in Figure 2. To reduce the optimization cost, the tert-butyl groups were omitted from the models.

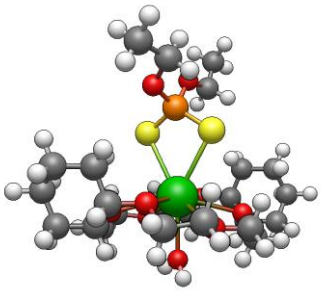


Fig. 2 . Proposed complex structure of No and alkaline earth metals in Sr resin/HDEDTP system

For each structure, single point energy calculation was performed with B3LYP-TZ2P level. To consider solvent effects, the SM12 model was employed. The reaction energy of No^{2+} and alkaline earth metal ions was calculated for the following chemical reaction:

$$[M(H_2O)_8]^{2+}{}_{aq} + DCH18C6_{aq} + DEDTP^{-}{}_{aq} + H_2O_{aq} \rightarrow [M(DCH18C6)(DEDTP)(H_2O)]^{+}{}_{octanol} + 8H_2O_{aq} \quad (1)$$

Covalent interactions between metal ions and dithiophosphate ions were predominantly revealed by quantum atoms in molecules (QTAIM). The chemical bonding and molecular orbital contributions have been calculated from the density of states (DOS), partial density of states (PDOS) and overall population density of states (OPDOS) methods.

3 RESULTS AND DISCUSSION

The correlation between the reaction energy and ionic radius exhibited an agreement in the trend of K_d values. These results confirm the validation of the complex structure. According to QTAIM results, the obtained H(r) calculation results, negative values were observed for only No-S bonds, suggesting covalent interactions. In contrast, the H(r) for other bonds presented positive values, indicating robust electrostatic bonding. Furthermore, the DOS, PDOS and OPDOS have shown bonding interactions between No and sulfur atoms of the dithiophosphate ions in No complex are stronger than those observed in alkaline earth metal complexes. These calculation results show that compared with the alkaline earth metals, No exhibits softer acid characteristics.

References

[1] R. SILVA et al., Inorg. Chem. **13**, 2233 (1974)
[2] H. NINOMIYA et al., RIKEN Accel. Prog. Rep. **52**, 184 (2019).
[3] E.WATANABE, Ph.D. Thesis, The University of Osaka. (2022)
[4] Y. KASAMATSU et al., Radiochim. Acta **103**, 513 (2015)
[5] R. WANG et al., RIKEN Accel Prog. Rep. in press.
[6] G.TE VELDE et al., J.Comput.Chem. **22**, 9 (2001)

7th Asia-Pacific Symposium on Radiochemistry *September 14 ~ 19, 2025 • Kunibiki Messe • Shimane, Japan*

DEVELOPMENT OF THE LEGEND SYSTEM TOWARDS THE CHEMICAL STUDY OF Nh

Yang Wang[1], Zimeng Jia[1], Shiwei Cao[1], Yunfei Cui[1], Zhi Qin[1]

[1] *Institute of Modern Physics, Chinese Academy of Science, Lanzhou, 730000, China, wangyang@impcas.ac.cn*

Superheavy elements (SHE) are defined as elements with Z≥104[1]. Exploring the chemical and physical properties of SHE presents great challenges due to their short lifetimes and low production rates. The study of the chemical properties of Nh (Z=113) is a highly active topic in the field of SHE [2].

To experimentally investigate Nh chemistry, a gas-phase chemical investigation system with the name of LEGEND (on-Line Experiment in Gas-phasE for Nihonium Detector array) was developed at IMP, Lanzhou, China. [3] The whole system mainly contained an RTC, a thermochromatography (TC), and a gas purification equipment. The RTC was optimized regarding to the size of the beam profile at the focal plane of the separator, which could minimize the inner volume and significantly improve the transmission efficiency for radioisotopes with a half-life around 1 s. The TC which comprises of 32 pairs (gap: 0.8mm) of SiC [4] detectors (size: 1×1 cm^2) was directly connected to the RTC, with the temperature from 65 ℃ (inlet) down to -45°C (outlet). Additionally, a gas circulation purification system was developed to remove the impurities moisture and oxygen from the carrier gas to ensure the elemental state of the atoms. With these efforts, offline and online experiments with short-lived Bi, Fr, and Tl isotopes were performed as for the preparation of the future study on Nh.

References

[1] A. Türler, R. Eichler, and A. Yakushev, “Chemical studies of elements with Z≥ 104 in gas phase,” Nuclear Physics A, **944**, 640 (2015).

[2] A. Yakushev, et al., “First Study on Nihonium (Nh, Element 113) Chemistry at TASCA,” Front Chem., **9**, 753738, (2021).

[3] Z. Jia, et al., “A detection system for next-generation gas-adsorption thermochromatography experiments with Nh,” Nuclear Inst. and Methods in Physics Research, A,**1072**, 170166(2025).

7th Asia-Pacific Symposium on Radiochemistry *September 14 ~ 19, 2025 • Kunibiki Messe • Shimane, Japan*

EXTRACTION OF THE GROUP 2 ELEMENTS AND Pb(II) WITH TODGA-RESIN TOWARDS THE CHEMICAL EXPERIMENT WITH ELEMENT 102, No

Enni Khult[1,2], Ruilin Wang[1,2], Masashi Kaneko[1], Hiroyuki Kazama[1], Kyosuke Shibamoto[1,2], Miyu Konno[1,2], Yudai Itakura[1,2], Kenta Mori[1], Ryota Kikuchi[1], Kazushi Kawamoto[1], Ryotaro Masuda[1,2], Hiroki Aoto[1], So Hashiba[1,2], Hiromitsu Haba[2], Akihiro Nambu[2], Koichi Takamiya[3], Makoto Inagaki[3], Eisuke Watanabe[2,4], Takuya Yokokita[2,5], Yousuke Kanayama[2], Hiromichi Shimizu[2], Yudai Shigekawa[2,6], and Yoshitaka Kasamatsu[1,2]

[1]*Graduate School of Science, The University of Osaka: Machikaneyama-cho 1-1, Toyonaka, Osaka 560-0043, Japan, khulte23@chem.sci.osaka-u.ac.jp*
[2]*Nishina Center for Accelerator-Based Science, RIKEN: Hirosawa 2-1, Wako, Saitama 351-0198, Japan,*
[3]*Institute for Integrated Radiation and Nuclear Science, Kyoto University: Asashiro-Nishi 2, Kumatori-cho, Sennan-gun, Osaka 590-0494, Japan,*
[4]*Radiation Science Center, KEK: Oho 1-1, Tsukuba, Ibaraki 305-0801, Japan,*
[5]*RARiS, Tohoku University: Mikamine 1-2-1, Taihaku-ku, Sendai, Miyagi 982-0826, Japan,*
[6]*Institute of Pure and Applied Sciences, University of Tsukuba: Tenodai 1-1-1, Tsukuba, Ibaraki 305-8571, Japan*

Element 102 (No) uniquely exhibits a +2 oxidation state in aqueous solutions within the actinide series. The chemical behavior of No resembles that of group 2 elements, but it may have a softer acidic nature. For a systematic chemical study of No, extraction with DGA ligands is proposed. In this work, we investigated the behavior of group 2 elements and Pb(II) in extraction from nitric acid using TODGA-resin, validated the extraction system's reliability for an online experiment with ^{255}No, and performed relativistic DFT calculations of the extracted M(II)-DGA complexes.

1 INTRODUCTION

Element 102, nobelium (No), presents unique chemical properties within the actinide series, exhibiting a stable +2 oxidation state in aqueous solutions, unlike other actinides that favor +3 or higher states. The chemical behavior of No shows similarities to that of group 2 elements, with an ionic radius intermediate between Ca^{2+} and Sr^{2+} [1]. However, No^{2+} may exhibit a relatively softer acidic nature, in contrast with the hard acid characteristics displayed by group 2 metal ions [2]. Continued research is essential to elucidate the intriguing chemical properties of No, influenced by relativistic effects.

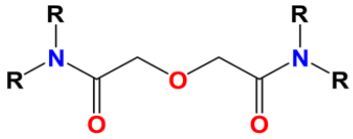


Fig. 1. Diglycolamide (DGA) ligands. TODGA: R = *n*-octyl; TEDGA: R = *n*-ethyl.

For a systematic chemical study of No, we propose extraction with diglycolamide (DGA) ligands (Fig. 1), which allow for various structural modifications to tune their coordination properties and possess good selectivity towards M(II) metal ions [3]. This work investigates the solid-liquid extraction of No's chemical analogues, group 2 elements and Pb(II), from HNO_3 using TODGA-resin as a step towards an online experiment* with ^{255}No. For that, batch extraction experiments of M(II) (M = Ca, Sr, Ba, and Pb) with TODGA-resin were conducted, and relativistic quantum chemical calculations of the extracted M(II)-DGA complexes were performed.

(*) Elements with Z>100 are synthesized in nuclear fusion reactions, have short half-lives, and are available only as single atoms at a time. For this reason, rapid and automated chemical experiments utilizing partition methods are required. These studies, referred to as "online experiments", are conducted at accelerator facilities using the nuclear reaction products [4].

2 METHODS

Solid-liquid extraction experiments were conducted with TODGA (N,N,N',N'-tetraoctyldiglycolamide) resin as solid phase and tracer solutions of Ca(II), Sr(II), Ba(II), and Pb(II), where Pb(II) was chosen as a potential soft-acid analogue of No(II), as liquid phase. The weight distribution ratios K_d were determined as a function of HNO_3 concentration in liquid phase and extraction time. Automated batch solid-liquid extraction experiments were performed using the AMBER apparatus[5] to assess the system's suitability for online experiments with ^{255}No.

Copyright on 7th Asia-Pacific Symposium on Radiochemistry 2025

Relativistic density functional theory (DFT) calculations, using TEDGA (N,N,N',N'-tetraethyldiglycolamide) as a computationally less demanding analogue of TODGA, provided insights into the geometry of the extracted complexes and their relative stabilities, as well as the nature of the formed coordination bonds.

3 RESULTS AND DISCUSSION

The K_d values of Ca(II), Sr(II), Ba(II), and Pb(II) in extraction by TODGA-resin were obtained as a function of HNO_3 concentration. The slope analysis of $\log(K_d)$–$\log([HNO_3])$ dependency suggests that the extracted complexes involve two nitrate ions for charge neutrality. Equilibrium of extraction reactions for Sr and Ba was achieved within 3 min, sufficiently fast for online experiments with ^{255}No ($\tau_{1/2}$ = 3.5 min). The automated extraction experiments using AMBER demonstrated consistent K_d values with those obtained in manual batch experiments and showed good reproducibility in repetitive extraction/re-extraction experiments, validating the system's reliability for the upcoming online experiment ^{255}No.

DFT calculations reveal potential differences between No and group 2 elements in their coordination with TEDGA ligands, particularly highlighting the impact of relativistic effects, including spin-orbit coupling, on the stability of No complexes.

4 CONCLUSIONS

The TODGA-resin/HNO_3 extraction system has been thoroughly evaluated and deemed suitable for online experiments with ^{255}No. The rapid extraction kinetics, consistent performance in automated systems, and insights from DFT calculations pave the way for future studies to probe the unique chemical properties of No.

The forthcoming online experiment with ^{255}No promises to provide valuable data for understanding the behavior of this unique element. It will serve as a crucial first step towards a systematic investigation of No complexation with DGA ligands, enabling a deeper understanding of the relativistic effects at the frontier of the periodic table.

ACKNOWLEDGMENTS

We are grateful to RIKEN Nishina Center accelerator operators and KUR nuclear reactor operators for the help in production of radiotracers.

References

[1] J. MALY, et al, *Science*, **160**, 1114 (1968).
[2] E. WATANABE, PhD Diss., UOsaka (2022).
[3] E. P. HORWITZ, et al, *Solvent Extr. Ion Exch.* **23** 3, 319–344 (2005).
[4] M. SCHÄDEL, *Angew. Chem. Int. Ed.*, **45** 3, 368 (2006).
[5] Y. KASAMATSU, et al, *Radiochim. Acta*, **103** 7, 513–521 (2015).

Poster Presentation | [S2]Radiopharmaceutical Sciences

Tue. Sep 16, 2025 6:30 PM - 8:00 PM JST | Tue. Sep 16, 2025 9:30 AM - 11:00 AM UTC Poster

[Poster] S2

[P-S2-01]

ON-LINE MONITORING OF ^{177}Lu SEPARATION BY EXTRACTION CHROMATOGRAPHY

*Kenji Shirasaki[1], Kohshin Washiyama[2], Tomoo Yamamura[3] (1. Institute for Radiation Science, The University of Osaka (Japan), 2. Advanced Clinical Research Center, Fukushima Global Medical Science Center, Fukushima Medical University (Japan), 3. Institute for Integrated Radiation and Nuclear Science, Kyoto University (Japan))

[P-S2-02]

RECOVERY OF ASTATINE-211 WITH PURE WATER AFTER DRY DISTILLATION SEPARATION

*Kazuhiro Ooe[1], Masashi Murakami[2], Yukiyoshi Kon[2], Atsushi Toyoshima[2], Yoshifumi Shirakami[2] (1. Radioisotope Research Center, Institute for Radiation Sciences, The University of Osaka (Japan), 2. Institute for Radiation Sciences, The University of Osaka (Japan))

[P-S2-03]

Thin-layer chromatography for astatine solutions containing reducing agents

*Ichiro Nishinaka[1], Kazuyuki Hashimoto[2], Akihiko Yokoyama[3] (1. Takasaki Institute for Advanced Quantum Science, National Institutes for Quantum Science and Technology (QST) (Japan), 2. Nuclear Science Research Institute, Japan Atomic Energy Institute (JAEA) (Japan), 3. College and Institute of Science and Engineering, Kanazawa University (Japan))

[P-S2-04*]

Flow-Electrolytic Labeling of ^{211}At for Radiopharmaceutical Synthesis in Targeted Alpha Therapy

*Akina Mitsukai[1], Yoshihumi Shirakami[2], Masashi Murakami[2], Kazuki Kajiyama[2], Sadaaki Kimura[3], Atsushi Toyoshima[2] (1. Graduate school of Science, the University of Osaka (Japan), 2. Institute for Radiation Sciences (Japan), 3. Alpha Fusion Inc. (Japan))

[P-S2-05]

CHROMATOGRAPHIC ANALYSIS OF ASTATINE IN METHANOL SOLUTIONS TOWARD STANDARDIZATION OF THE QUALITY OF ASTATINE SUPPLY SOLUTION

*Shigeki Watanabe[1], Masashi Murakami[2], Ichiro Sasaki[1], Kazuhiro Ooe[2], Yukiyoshi Kon[2], Tomoyuki Ohya[3], Jun Ichinose[3], Katsuyuki Minegishi[3], Kotaro Nagatsu[3], Atsushi Toyoshima[2], Noriko S Ishioka[1] (1. Takasaki Institute for Advanced Quantum Science, National Institutes for Quantum Science and Technology (Japan), 2. Institute for Radiation Sciences, The University of Osaka (Japan), 3. Institute for Quantum Medical Science, National Institute for Quantum Science and Technology (Japan))

[P-S2-06]

CHROMATOGRAPHIC ANALYSIS OF ASTATINE IN AQUEOUS SOLUTIONS FOR STANDARDIZATION OF THE QUALITY OF ASTATINE SUPPLY SOLUTION

*Masashi Murakami[1], Shigeki Watanabe[2], Ichiro Sasaki[2], Kazuhiro Ooe[1], Yukiyoshi Kon[1], Tomoyuki Ohya[2], Jun Ichinose[2], Katsuyuki Minegishi[2], Kotaro Nagatsu[2], Noriko S. Ishioka[2], Atsushi Toyoshima[1] (1. The University of Osaka (Japan), 2. National Institute for Quantum Science and Technology (Japan))

[P-S2-07*]

©APSORC25

SYNTHESIS AND CHARACTERIZATION OF STRONGLY PHOTOLUMINESENCE NITRIDOTECHNETIUM(V) AND RHENIUM(V) COMPLEXES

*Sodai Miyamoto[1], Takashi Yoshimura[2] (1. Department of Chemistry, Graduate School of Science, The University of Osaka (Japan), 2. Radioisotope Research Center, Institute for Radiation Science, The University of Osaka (Japan))

[P-S2-08*]

SYNTHESIS OF CRYPTAND-BASED CHELATING LIGANDS FOR STABLE Pb(II) COMPLEXES IN NUCLEAR MEDICINE APPLICATIONS

*Eishun Kawagishi[1], Kojiro Nagata[2], Masashi Kaneko[1], Hiroyuki Kazama[1], Hiroki Aoto[1], Haruka Maeda[1], Terumi Yokoyama[1], Yoshitaka Kasamatsu[1] (1. Graduate School of Science, The University of Osaka (Japan), 2. Core Facility Center, The University of Osaka (Japan))

[P-S2-09]

Synthesis of Lanthanum, Barium, and Actinuim Complexes with The 15-Membered Cyclic Ligand Having Phosphonate Arms

Kenshin Yamashita[1], Kenta Hamasaki[1], Kenji Shirasaki[1], Takuya Yokokita[2], Hidetoshi Kikunaga[2], Kazuaki Tsukada[2], Tatsuo Yajima[3], *Takashi Yoshimura[1] (1. The University of Osaka (Japan), 2. Tohoku University (Japan), 3. Kansai University (Japan))

[P-S2-10*]

SYNTHESIS OF MACROCYCLIC 1,2-HYDROXYPYRIDINONE-BASE LIGAND FOR ^{227}Th AND ^{89}Zr RADIOPHARMACEUTICALS

*Terumi Yokoyama[1], Hiroyuki Kazama[1], Masashi Kaneko[1], Kojiro Nagata[2], Hiroki Aoto[1], Haruka Maeda[1], Eishun Kawagishi[1], Yoshitaka Kasamatsu[1] (1. Graduate School of Science, The University of Osaka (Japan), 2. Core Facility Center, The University of Osaka (Japan))

[P-S2-11*]

SYNTHESIS AND PROPERTIES OF BARIUM, LANTHANUM, AND ACTINIUM COMPLEXES WITH THE 18-MEMBERED CYCLIC LIGAND WITH PYRIDINE PHOSPHONATE ARMS FOR RADIOPHARMACEUTICALS

*Kaseki Matsuda[1], Kazuaki Baba[1], Kojiro Nagata[1], Kenji Shirasaki[1], Takuya Yokokita[2], Hidetoshi Kikunaga[2], Kazukaki Tsukada[2], Tatsuo Yajima[3], Takashi Yoshimura[1] (1. The University of Osaka (Japan), 2. Tohoku University (Japan), 3. Kansai University (Japan))

[P-S2-12]

Development of an Imaging Probe Targeting Adrenal Aldosterone Synthase (CYP11B2)

*Hiroyuki Kimura[1], Yusuke Yagi[2], Riko Fuseda[3], Takaaki Murakami[4], Marina Omokawa[5], Masakatsu Sone[6], Hiroyuki Yasui[3], Nobuya Inagaki[4], Hideo Saji[7] (1. Agency for Health, Safety and Environment, Kyoto University (Japan), 2. Department of Radiological Technology, Faculty of Medicinal Science, Kyoto University of Medical Science (Japan), 3. Laboratory of Analytical and Bioinorganic Chemistry, Division of Analytical and Physical Sciences, Kyoto Pharmaceutical University (Japan), 4. Department of Diabetes, Endocrinology and Nutrition, Graduate School of Medicine, Kyoto University Hospital (Japan), 5. Faculty of Medicine, Dentistry and Pharmaceutical Sciences, Okayama University (Japan), 6. Department of Metabolism and Endocrinology, St. Marianna University School of Medicine (Japan), 7. Department of Patho-Functional Bioanalysis, Graduate School of Pharmaceutical Sciences, Kyoto University (Japan))

[P-S2-13]

Improved in vivo stability of astatobenzoyl compounds by conjugating with D-oligopeptides

*Hiroyuki Suzuki[1], Mutsuho Murata[1], Kento Kannaka[1], Souma Kitagawa[1], Souta Tatusta[1], Kazuhiro Takahashi[2], Tomoya Uehara[1] (1. Chiba University (Japan), 2. Fukushima Medical

University (Japan))

[P-S2-14*]

Analysis of cell death induced by short-lived alpha-emitting radionuclides

*Soichiro Magara[1], Koki Mayusumi[1], Erina Hilmayanti[1], Kazuhiro Ooe[2,3], Atsushi Toyoshima[2,3], Koichi Fukase[1,2,3], Kazuya Kabayama[1,2,3] (1. Department of Chemistry, Graduate School of Science, The University of Osaka (Japan), 2. Forefront Research Center, Graduate School of Science, The University of Osaka (Japan), 3. Institute for Radiation Sciences, The University of Osaka (Japan))

[P-S2-15*]

Structural Stability of Radio-activated Gold Compounds via Neutron Irradiation

*KAZUKI KAJIYAMA[1], Akina Mitsukai[1], Masashi Murakami[2], Yoshifumi Shirakami[2], Koichi Takamiya[3], Jun Kataoka[4], Atsushi Toyoshima[2] (1. Graduate School of Science, The University of osaka (Japan), 2. Institute for Radiation Sciences, The University of Osaka (Japan), 3. Institute for Integrated Radiation and Nuclear Science, Kyoto University (Japan), 4. Research Institute for Science and Engineering, Waseda University (Japan))

[P-S2-16*]

Development of Dual-Modality Microspheres Containing Gold Nanoparticles for Radioembolization: X-ray CT and SPECT-Visible

*Koino Nakamura[1], Naoyuki Ukon[2], Kohshin Washiyama[2], Daichi Kuroiwa[3], Hirofumi Sekino[3], Hiroshi Ito[3], Yoshitaka Takagai[1] (1. Fukushima University (Japan), 2. Fukushima Medical University Advanced Clinical Research Center (Japan), 3. Fukushima Medical University School of Medicine (Japan))

[P-S2-17]

Synthesis and evaluation of mPEG-modified [^{211}At]AuNP(s): Towards the development of cancer treatment through intratumoral administration

*Yuichiro Kadonaga[1], Hiroki Kato[1], Hiroaki Shimamoto[1], Xuhao Huang[1], Erina Hilmayanti[1], Kazuhiro Ooe[1], Atsushi Shimoyama[1], Kazuya Kabayama[1], Xiaojie Yin[1], Hiromitsu Haba[1], Masashi Murakami[1], Atsushi Toyoshima[1], Koichi Fukase[1] (1. The University of Osaka (Japan))

[P-S2-18*]

Dose-Dependent Cytotoxic Profiling of Astatine-211 for Targeted Alpha Therapy

*Jumpei Ueno[1], Koki Mayusumi[1], Masayuki Takamatsu[1,2], Atsushi Shimoyama[1,2,3], Kazuya Kabayama[1,2,3], Koichi Fukase[1,2,3] (1. Department of Chemistry, Graduate School of Science, The University of Osaka (Japan), 2. Institute for Radiation Science, The University of Osaka (Japan), 3. Forefront Research Center, Graduate School of Science, The University of Osaka (Japan))

[P-S2-19]

Dosimetry in targeted alpha particle therapy with astatine-211 in single cells using Al_2O_3:C, Mg-based fluorescent nuclear track detector

*Jun Hu[1], Tamon Kusumoto[1], Satoshi Kodaira[1] (1. Institute for Radiological Sciences, National Institutes for Quantum Science and Technology (QST), Japan (Japan))

[P-S2-20*]

Development of Astatine-Labeled Functional Proteins for Cancer Therapy

*Koki Mayusumi[1], Kazuya Kabayama[1,2,3], Kazuko Kaneda-Nakashima[1,2,3], Junichi Takagi[4], Hiroaki Suga[5], Kazuhiro Ooe[2,3], Atsushi Toyoshima[2,3], Koichi Fukase[1,2,3] (1. Dept. of Chem., Grad. Sch. of Sci., The University of Osaka (Japan), 2. FRC, Grad. Sch. of Sci., The University of

Osaka (Japan), 3. Inst. for Radiation Sciences, The University of Osaka (Japan), 4. Inst. for Protein Research, The University of Osaka (Japan), 5. Grad. Sch. of Sci., The University of Tokyo (Japan))

[P-S2-21]

Random and Site-Specific Conjugation of TCO to Anti-PD-L1 Monoclonal Antibodies for In Vitro Click Labeling: A Step Toward Pretargeted ImmunoPET Imaging Agents

*Feng-Yun Jimmy Huang[1], Ruey-Jing Huang[2], Ching-Wen Cheng[1], Kuo-Ting Chen[3] (1. Department of Medical Imaging and Radiological Sciences, Central Taiwan University of Science and Technology (Taiwan), 2. Department of Diagnostic Radiology, Hualien Armed Forces General Hospital (Taiwan), 3. Department of Chemistry, National Dong Hwa University (Taiwan))

[P-S2-22]

SYNTHESIS AND EVALUATION OF ASTATINE-211-LABELED FAP-INHIBITOR RADIOPHARMACEUTICALS

*Masayuki Takamatsu[1,2], Atsushi Shimoyama[1,2], Ayaka Aso[1], Taketo Toda[1], Jumpei Ueno[1], Koki Mayusumi[1], Kazuya Kabayama[2], Yuichiro Kadonaga[2], Yoshifumi Shirakami[2], Tadashi Watabe[2,3], Taku Yoshiya[4], Kazuhiro Ooe[2], Atsushi Toyoshima[2], Hiromitsu Haba[5], Jens Cardinale[6], Frederik Lars Giesel[6], Kazuko Kaneda Nakashima[2], Koichi Fukase[1,2] (1. Grad. Sch. Sci., The Univ. of Osaka (Japan), 2. IRS, Osaka Univ., The Univ. of Osaka (Japan), 3. Grad. Sch. Med., The Univ. of Osaka (Japan), 4. Peptide Institute, Inc. (Japan), 5. RIKEN (Japan), 6. University Hospital Düsseldorf (Germany))

[P-S2-23*]

Development of Novel Radioimmunotherapeutic AgentsTargeting Epithelial Cell Adhesion Molecule

*Sato Oshige[1], Takumi Iwasawa[2], Marina Omokawa[3], Yoji Kitamura[4], Takashi Kozaka[4], Yusuke Yagi[5], Takiko Daikoku[6], Kazunori Kato[2], Hiroyuki Kimura[7] (1. Kanazawa University (Japan), 2. Toyo University (Japan), 3. Okayama University (Japan), 4. Division of Animal Disease Model, Kanazawa University (Japan), 5. Kyoto University of Medical Science (Japan), 6. Division of Animal Disease Model, Research Center for Experimental Modeling of Human Disease, Kanazawa University (Japan), 7. Kyoto University (Japan))

[P-S2-24]

Activities of Alpha-tergeted Therapy using astatine-211 at Osaka University in Japan

*Kazuya Kabayama[1], Atsushi Toyoshima[1], Koichi Fukase[1] (1. Institute for Radiation Sciences, University of Osaka (Japan))

[P-S2-25]

Efforts by the Japanese Astatine Community toward clinical application of alpha emitter ^{211}At

*Kohshin Washiyama[1], Takashi Nakano[2], Mikako Ogawa[3], Hiroki Kanda[2], Kazuya Taki[4] (1. Fukushima Medical University (Japan), 2. The University of Osaka (Japan), 3. Hokkaido University (Japan), 4. Sumitomo Heavy Industries, Ltd. (Japan))

©APSORC25

7th Asia-Pacific Symposium on Radiochemistry *September 14 ~ 19, 2025 • Kunibiki Messe • Shimane, Japan*

ON-LINE MONITORING OF ^{177}Lu SEPARATION BY EXTRACTION CHROMATOGRAPHY

Kenji Shirasaki[1], Kohshin Washiyama[2], Tomoo Yamamura[3]

[1]*Institute for Radiation Science, The University of Osaka: 1-1 Machikaneyama, Toyonaka, Osaka, 560-0043, shirasaki@rirc.osaka-u.ac.jp*
[2]*Advanced Clinical Research Center, Fukushima Global Medical Science Center, Fukushima Medical University: 1 Hikarigaoka, Fukushima, 960-1295, kwashi@fmu.ac.jp*
[3]*Institute for Integrated Radiation and Nuclear Science, Kyoto University: 2 Asashiro-Nishi, Kumatori-cho, Sennan-gun, Osaka, 590-0494, yamamura.tomoo.2e@kyoto-u.ac.jp.*

To produce high specific activity ^{177}Lu, the separation and purification of ^{177}Lu from neutron irradiated Yb targets is essential. However, the difficulty lies in the separation of the neighboring lanthanide elements Lu and Yb, the former on the mg to g scale and the latter on the tracer scale. The extraction chromatography, one of the separation techniques have been carried out to solve this critical problem. To accelerate the best condition survey, some technique that allows a faster analysis is desirable. Here, on-line monitoring of the separation of ^{177}Lu was performed using a radiation detector.

1 Introduction

^{177}Lu (half-life: 6.64 d), produced indirectly by neutron irradiation of ^{176}Yb, is a β^- emitter and one of the applicable nuclides for targeted radioisotope therapy (TRT). To date, ^{177}Lu-DOTA-TATE, ^{177}Lu labeled with DOTA-TATE for the treatment of somatostatin-overexpressing tumors [1, 2], and ^{177}Lu-PSMA-617, ^{177}Lu labeled with PSMA-617 for the treatment of castration-resistant prostate cancer [3, 4], have been investigated for TRT use.

In extraction chromatography, bis-2-ethylhexylphosphonric acid (HDEHP) [5] and 2-ethylhexylphosphonic acid (HEH[EHP]) [6] are well known as substrate adsorbed extractants for ^{177}Lu separation, and recently some extractants have explored [7, 8] . In these studies, typically the concentrations of Yb and Lu in the eluate are determined by radiometric or elemental concentration measurements after collecting a certain volume of solution that has passed through the column. However, some technique that allows for faster analysis is desirable for the best condition survey.

Recently, we have demonstrated direct observation of the membrane permeation behavior of active materials through the ion exchange membrane of a vanadium redox flow battery (VRFB) using a real-time monitoring method with radioactive ^{48}V in a solution configuration of a discharged state of the VRFB [9]. In this application, γ-rays emitted from ^{48}V in solution are measured by a radiation detector installed in a lead shield. This time, not only ^{177}Lu, but also ^{169}Yb and ^{175}Yb, radioactive Yb produced by neutron irradiation, are all γ-ray emitters, which has the potential to establish a real-time monitoring system by γ-ray measurement. Actually, this kind of application system was adopted for convenient ^{177}Lu/Yb separation monitoring, especially for the first Yb target removal stage of extraction chromatography separation [7].

In this study, we developed a real-time monitoring technique for ^{177}Lu and radioactive Yb using the on-line γ-ray detector (CZT detector or Ge semiconductor detector) in the separation of ^{177}Lu from neutron irradiated Yb targets by extraction chromatography.

2 Experimental

The experimental apparatus used in this study consists mainly of a pump, a column with a water jacket and a γ-ray detector (CZT detector or Ge semiconductor detector). The solution is pumped up and introduced into the column, which is filled with extraction resin (LN2, Eichrom, 50–100 μm). The column temperature is kept constant by a thermostatic water circulation system. The solution that has passed through the column is introduced into a lead shield with a γ-ray detector installed. Then, the solution is collected in a sample vial as it passes through a bundled flow path in the ring shape for γ-ray measurement. The glass columns used in this study are 5 cm or 30 cm in length (0.5 cm inner diameter), and the total volume of the channel is 3.05 or 7.96 cm^3 when the column is empty. For resin conditioning, 75 mL or 35 mL of 1.5 M HNO_3 or 1.25 M HNO_3/10 w/w% ethanol was passed through.

A certain volume of 0.1 M HNO_3 was taken from the stock solution to be used as the loading solution (the stock solution was prepared by dissolution of irradiated Yb_2O_3 target). After the injection of the loading solution, 1.5 M HNO_3 or 1.25 M HNO_3/10 w/w% ethanol was passed through the column. Subsequently, 4 M or 3.5 M HNO_3 was passed through to complete the ^{177}Lu elution. The flow rate was kept constant during the entire experiment. The γ-ray measurement with the detector was set to repeat the accumulation for 60 s in real-time, starting at the same time as the loading solution began to flow. The measurement was stopped when the last solution was poured.

Copyright on 7th Asia-Pacific Symposium on Radiochemistry 2025

3 Results and Discussion

Figure 1(a) shows an overview of the Lu/Yb separation experiment using enriched ^{176}Yb: the first horizontal axis is the elapsed time, the second is the γ-ray energy, and the vertical axis is the logarithm of the intensity (count rate). This figure shows that the peak energies and their intensities in the γ-ray spectra change with time. To examine in detail, the type of nuclide elution taking place at each stage, the γ-ray energy is evaluated in relation to the elapsed time (Fig. 1(b)). Focusing on the γ-ray energy range above 100 keV, high intensities were detected at around 110, 131, 177, 198, 282, 308, and 396 keV for times between 300 and 400 min. These γ-ray peaks are attributed to ^{169}Yb (110, 131, 177, 198, and 308 keV) and ^{175}Yb (114, 282, and 396 keV), respectively. Thus, Yb is the eluent element at this stage. In the region around 510 min, high intensities were detected at 110 keV as well as 208 keV (which can be distinguished by its obvious shift from 198 keV). Especially at the latter γ-ray energy, the intensity was confirmed only in this region. Since these can be attributed to ^{177}Lu (113 keV and 208 keV), it can be assumed that most of the Yb is leached out by passing 1.5 M HNO_3, and the remaining resin residue, composed mainly of Lu, is leached out by 4 M HNO_3 after 500 min.

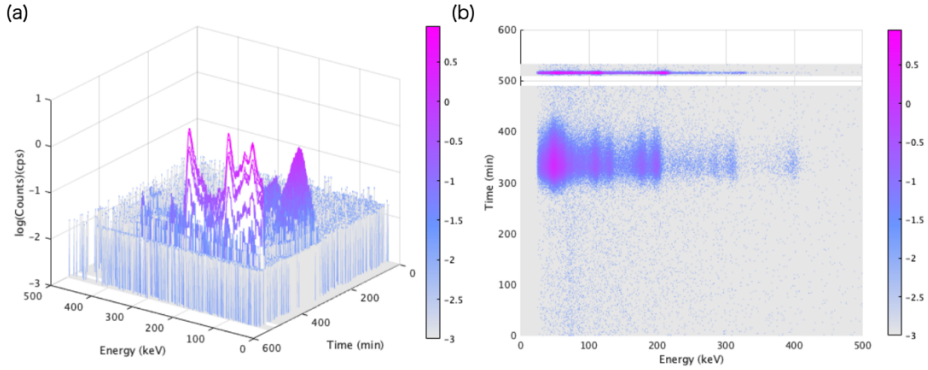


Fig. 1. Overview of the Lu/Yb separation experiment using enriched ^{176}Yb (a) and γ-ray energies relation to time (b).

4 Conclusions

On-line monitoring of the separation of ^{177}Lu, produced by neutron irradiation of enriched ^{176}Yb and radioactive Yb, was performed using an on-line radiation detector. In-situ observation of the Lu/Yb separation behavior was successfully conducted using γ-ray measurements.

ACKNOWLEDGMENTS

This work was supported by MEXT Innovative Nuclear Research and Development Program Grant Number JPMXD0224019804. This work was partially supported by the Joint Usage/Research of the Institute for Integrated Radiation and Nuclear Science, Kyoto University (KURNS) (No. R6P3-4).

References

[1] T. Das, S. Chakraborty, S. Banerjee and M. Venkatesh, Applied Radiation and Isotopes, **65**, 301, (2007).
[2] Y. Zheng, Y. Huh, K. Vetter, N. Nasholm, C. Gustafson and Y. Seo, IEEE Trans Radiat Plasma Med Sci, **7**, 75, (2023).
[3] M. Benesova, M. Schafer, U. Bauder-Wust, A. Afshar-Oromieh, C. Kratochwil, W. Mier, U. Haberkorn, K. Kopka and M. Eder, J Nucl Med, **56**, 914, (2015).
[4] C. Meyer, A. Stuparu, K. Lueckerath, J. Calais, J. Czernin, R. Slavik and M. Dahlbom, J Nucl Med, **64**, 1772, (2023).
[5] F. F. Knapp Jr, S. Mirzadeh, A. L. Beets and M. Du, Journal of Radioanalytical and Nuclear Chemistry, **263**, 503, (2005).
[6] E. P. Horwitz, D. R. McAlister, A. H. Bond, R. E. Barrans and J. M. Williamson, Applied Radiation and Isotopes, **63**, 23, (2005).
[7] U. J. Park, J.-S. Lee, K. H. Choi, S. S. Nam and K. H. Yu, Applied Radiation and Isotopes, **115**, 8, (2016).
[8] X. Fan, G. Ma, H. Peng, J. Gao, Y. Hu, B. Li, J. Liao, Y. Yang, J. Zhang, L. Ma, N. Liu and F. Li, Separation and Purification Technology, **356**, 129802, (2025).
[9] K. Shirasaki and T. Yamamura, Journal of Membrane Science, **592**, 117367, (2019).

Copyright on 7th Asia-Pacific Symposium on Radiochemistry 2025

RECOVERY OF ASTATINE-211 WITH PURE WATER AFTER DRY DISTILLATION SEPARATION

Kazuhiro Ooe[1], Masashi Murakami[2], Yukiyoshi Kon[2], Atsushi Toyoshima[2], Yoshifumi Shirakami[2]

[1]*Radioisotope Research Center, Institute for Radiation Sciences, The University of Osaka: 2-4 Yamadaoka, Suita, Osaka 565-0871, Japan, ooe@rirc.osaka-u.ac.jp*

[2]*Institute for Radiation Sciences, The University of Osaka: 1-1 Machikaneyama, Toyonaka, Osaka 560-0043, Japan*

We report our recent results of dry distillation separation of ^{211}At. The cyclotron irradiated Bi target was placed in the automated dry distillation apparatus, and the evaporated ^{211}At was collected at a cold trap. The trapped ^{211}At was recovered using 100 μL of pure water (non-toxic solution) with an isolation yield of 52%. The isolation yield was increased up to 64% by three times repeated dissolution with 100 μL of pure water.

1. INTRODUCTION

Astatine-211 (^{211}At) is a promising radionuclide for targeted alpha therapy of metastatic cancers. This isotope is produced by the ^{209}Bi(α, 2n)^{211}At reaction using an accelerator. Typically, ^{211}At is isolated from the irradiated Bi target through a dry distillation method and dissolved in various solutions. In many cases, methanol or chloroform is used as solvent for dry distilled ^{211}At. However, these solutions are toxic to living body, and it is desirable to dissolve dry distilled ^{211}At with non-toxic aqueous solution for clinical use of ^{211}At. We have been investigating dry distillation separation for ^{211}At with dissolution by pure water and also constructed the automated dry distillation apparatus for clinical application of ^{211}At. Here, we report on our recent results for the separation of ^{211}At by the automated dry distillation apparatus with dissolution by pure water.

2. EXPERIMENTAL

A schematic diagram of the automated dry distillation apparatus used for the separation of ^{211}At is shown in Fig. 1. This apparatus was designed to fit into the hot cell installed at the University of Osaka Hospital. At-211 was produced in the ^{209}Bi(α, 2n)^{211}At reaction at Research Center for Nuclear Physics at the University of Osaka and transported to Radioisotope Research Center. The irradiated Bi target was put in a quartz column with Cu and quartz boats and heated up to 850°C using an electric furnace. The carrier gas was a mixture of N_2 (30 mL/min) and O_2 (10 mL/min) gas including trace moisture (approximately 3500 ppm) added by passing through a moisture generator, which is a 30 mL glass bottle containing 1 mL of cooled water. The amount of moisture was monitored by a dew point transmitter (Vaisala DMT-143L) set at the front of the quartz column. The evaporated ^{211}At was transported by the carrier gas to a cold trap cooled at -3°C using Peltier element. The accumulating radioactivity of the trapped ^{211}At was monitored by a radiation detector on the cold trap. After the radioactivity of the trapped ^{211}At reached the plateau, the gas flow and heating at quartz column were stopped. Then, 100 μL of pure water (Water for Injection, Otsuka Pharmaceutical Factory, Japan) was injected into the cold trap by a syringe pump. The ^{211}At aqueous solution was received by a 1.5 mL PFA sample vial. The radioactivity of ^{211}At dissolved in pure water was determined by measurement of X-ray from a daughter nuclide, ^{211}Po, with a HPGe detector. The remained ^{211}At in the cold trap after dissolution with pure water was recovered by 6 mL of ethanol. The isolation yield of ^{211}At was calculated from the eluted ^{211}At radioactivity in pure water divided by that in the irradiated Bi target with decay correction.

3. RESULTS

The amount of ^{211}At trapped at the cold trap was 77±7% (n = 29). The isolation yield of dry distilled ^{211}At by dissolution with 100 μL pure water was 52±9%. The undissolved ^{211}At remained in the cold trap was recovered by repeated dissolution with 100 μL of pure water. Three repeated dissolutions resulted in a total isolation yield of 64±6% for ^{211}At. Furthermore, a higher isolation yield for ^{211}At (more than 60%) was observed by dissolution with 100 μL of 7% sodium bicarbonate solution (MEYLON Injection 7%, Otsuka Pharmaceutical Factory, Japan), compared to dissolution with 100 μL of pure water. Because the ^{211}At solution is prepared in non-toxic aqueous solution by the automated dry distillation apparatus, a simple and rapid preparation of radiopharmaceuticals labeled with ^{211}At is possible without a removal step of toxic organic solutions. In clinical use, the isolation yield of ^{211}At should be as high as possible because radioactivity of ^{211}At decreases due to labeling yield and radioactive decay of ^{211}At. For more efficient separation of ^{211}At, the dependence of isolation yield of ^{211}At as a function of the amount of moisture and the ratio of N_2/O_2 in the carrier gas will be investigated.

Copyright on 7th Asia-Pacific Symposium on Radiochemistry 2025

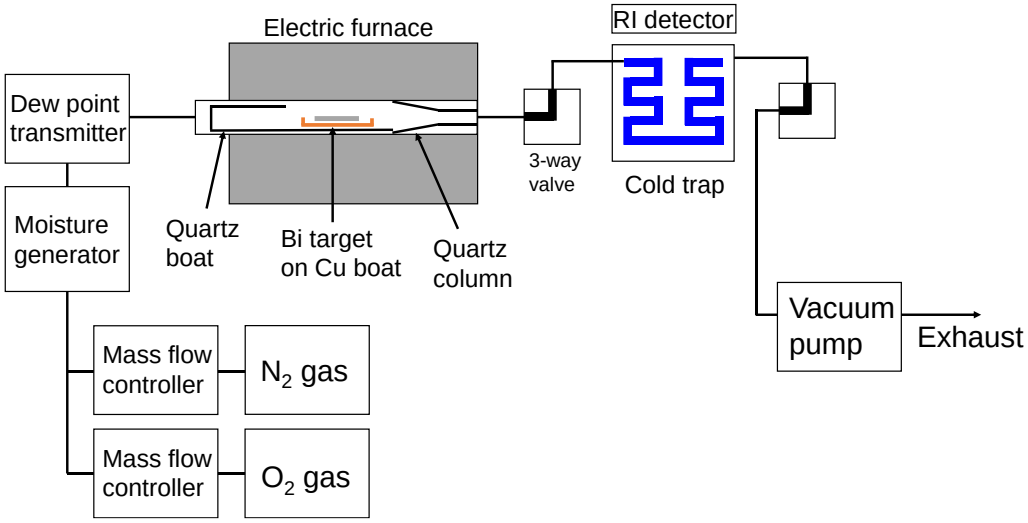


Fig. 1. A schematic diagram of the automated dry distillation apparatus for ^{211}At.

7th Asia-Pacific Symposium on Radiochemistry *September 14 ~ 19, 2025 • Kunibiki Messe • Shimane, Japan*

THIN-LAYER CHROMATOGRAPHY FOR ASTATINE SOLUTIONS CONTAINING REDUCING AGENTS

Ichiro Nishinaka[1], Kazuyuki Hashimoto[2], Akihiko Yokoyama[3]

[1]*Departmemt of Quantum-Applied Bioscience, Takasaki Institute for Advanced Quantum Science, National Institutes for Quantum Science and Technology (QST): Watanuki-machi/1233, Takasaki, Gunma, 370-1292, nishinaka.ichiro@qst.go.jp*
[2]*Department of Research Infrastructure Technology Development, Nuclear Science Research Institute, Japan Atomic Energy Institute (JAEA): Shirakata/2-4, Tokai-mura, Ibaraki, 319-1195, hashimoto.kazuyuki@jaea.go.jp*
[3]*College and Institute of Science and Engineering, Kanazawa University: Kakuma, Kanazawa, Ishikawa, 920-1192, yokoyama@se.kanazawa-u.ac.jp*

Thin-layer chromatography (TLC) was conducted using ^{209,210,211}At radionuclides produced by the irradiation of a stack of lead targets with a ^{7}Li beam. Astatine chemical species were separated and identified as astatide (At^-), astatate (AtO_3^-), perastatate (AtO_4^-) by TLC on silica gel with the mobile phase of ethanol/water. The TLC results exhibited distinct behaviors between the astatine solutions containing the reducing agents. The underlying mechanism is discussed.

1 INTRODUCTION

Alpha-emitting radionuclides have recently garnered attention for use in target alpha therapy (TAT). An α-emitting radionuclide of ^{211}At is a promising candidate for TAT because of its physical and chemical properties. However, astatine exhibits distinct chemical behaviors compared to its homolog iodine. Understanding the fundamental chemical properties of astatine remains challenging due to its limited availability, which can only be produced via accelerators.

In our previous TLC studies [1, 2], the identification of At^-, AtO_3^-, and AtO_4^- was confirmed, and the observed high volatility of astatine was reasonably attributed to the formation of At^0(0) via an oxidation-reduction reaction between At^-(−I) and AtO_3^-(V).

This work presents the TLC experimental results for astatine solutions containing reducing agents (Na_2SO_3, $NH_2NH_2{\cdot}H_2O$, and ascorbic acid) and discusses the underling mechanism.

2. EXPERIMENT

Astatine radionuclides were produced by irradiating stacks of thin targets of lead (Pb) with a 60 MeV $^{7}Li^{3+}$ ion beam supplied from the JAEA tandem accelerator based on the production cross sections for ^{nat}Pb(^{7}Li,xn)$^{207-211}$At [3]. A simple dry distillation method was used to separate and prepare non-carrier-added At aqueous solution.

At solutions containing reducing agents were prepared by adding a portion of the reducing agents (Na_2SO_3, $NH_2NH_2{\cdot}H_2O$, and ascorbic acid) to 0.2 mL of the non-carrier-added At aqueous solution. A 5 μl portion of the At solutions was applied 2 cm from the bottom of a silica gel TLC plate cut into 12 × 2 cm strips. After drying the applied solutions, the plates were developed 8 cm from the start line in the TLC chambers of ethanol/water for approximately 70 min. After drying the plates, they were placed in contact with an imaging plate and irradiated with UV light to obtain images of At and ascorbic acid, respectively.

3. RESUTS AND DISCUSSION

The TLC image for the At solutions containing Na_2SO_3 and $NH_2NH_2{\cdot}H_2O$ have two spot of At^- and AtO_3^-, which show low intensity on the plate compared with the intensity for the At aqueous solution. In contrast, the At solution containing ascorbic acid has a large spot of At^-. These different TLC images were hardly attributed to the results of the reduction with the reducing agents.

The UV images for the At solution containing ascorbic acid have one spot with the same R_f for At^-.

Based on the experimental results in the present and previous studies [1, 2], we will discuss the underling mechanism.

Copyright on 7th Asia-Pacific Symposium on Radiochemistry 2025

ACKNOWLEDGMENTS

The authors thank the JAEA tandem accelerator crew for their assistance with the accelerator operations. This work was supported by JSPS KAKENHI (grant numbers: JP2360013, JP21H03752, and JP23K21835).

References

[1] I. Nishinaka, K. Hashimoto, H. Suzuki, "Thin Layer Chromatography for Astatine and Iodine in Solutions Prepared by Dry Distillation," *J. Radioanal. Nucl. Chem*, **318**, 897-905 (2018).
[2] I. Nishinaka, K. Hashimoto, H. Suzuki, "Speciation of Astatine Reacted with Oxidizing and Reducing Reagents by Thin Layer Chromatography: Formation of volatile Astatine," *J. Radioanal. Nucl. Chem*, **322**, 2003-2009 (2019).
[3] I. Nishinaka, *et al*., "Production and Separation of Astatine Isotopes in The ^{7}Li + ^{nat}Pb Reaction," *J. Radioanal. Nucl. Chem*, **304**, 1077-1083 (2015).

7th Asia-Pacific Symposium on Radiochemistry *September 14 ~ 19, 2025 • Kunibiki Messe • Shimane, Japan*

Flow-Electrolytic Labeling of ^{211}At for Radiopharmaceutical Synthesis in Targeted Alpha Therapy

Akina Mitsukai,[1], Yoshifumi Shirakami[2], Masashi Murakami[2], Kazuki Kajiyama[1], Sadaaki Kimura[3] and Atsushi Toyoshima[2]

[1]*Graduate School of Science, The University of Osaka: 1-1 Machikaneyama, Toyonaka, Osaka, 560 003, Japan*
mitsukai@irs.osaka-u.ac.jp
[2]*Institute for Radiation Sciences, The University of Osaka: 1-1 Machikaneyama, Toyonaka, Osaka, 560 003, Japan*
[3]*Alpha Fusion Inc.: Techno Alliance Building, Room B303, 2-8 Yamadaoka, Suita, Osaka, 565 0871, Japan*

Astatine−211 is a promising radionuclide for Targeted Alpha Therapy. However, conventional labeling methods often suffer from significant limitations. In this study, we investigated a flow-electrolytic labeling of ^{211}At under ambient conditions, without redox/oxidation reagents, employing a bicarbonate/chloride electrolyte. Thin-layer chromatography analysis revealed the formation of At(III) at 800 mV. Subsequent labeling with 3-iodo-L-tyrosine successfully yielded 3-astato-L-tyrosine. This method showed compatibility with a broad pH range and reduced environmental impact.

1 Introduction

Astatine-211 (^{211}At) has attracted considerable attention as a promising radionuclide for Targeted Alpha Therapy. To utilize ^{211}At as a therapeutic drug, it must be efficiently labeled onto molecular targeting vectors such as antibodies or small molecules. Although several labeling methods for ^{211}At have been reported to date, challenges remain including restrictions in solvent conditions and concerns regarding the long-term stability of precursors.

In this study, we focused on flow-electrolytic labeling as an environmentally friendly method that does not require the addition of redox/oxidation reagents and can be applied under ambient conditions. This technique offers compatibility with a wide range of substrates and solvent systems, addressing key limitations of conventional approaches.

2 Experiments

Electrolysis of ^{211}At was conducted using a flow-electrolytic cell [1] with a mixed electrolyte solution containing 833 mM sodium bicarbonate and 167 mM sodium chloride (pH 7.9 - 8.3). The applied potential was varied from -200 to 1000 mV versus an Ag/AgCl reference electrode. To estimate the chemical species of ^{211}At, electrolyzed solutions were collected and analyzed by Thin Layer Chromatography (TLC) using a developing solvent: mixture of MeCN and H_2O with 2:1 ratio. The distribution of ^{211}At was then visualized with an imaging plate (IP). Additionally, labeling was performed by mixing the oxidized ^{211}At-containing solution with a solution of iodotyrosine deviates in a thin tubing.

3 Results and Discussion

Typical results are shown in Figure 1. In the TLC analysis prior to electrolysis (Figure 1a), multiple ^{211}At spots (peaks in the figures) were observed. In contrast, after electrolysis at an applied potential of 800 mV (Figure 1b), a single spot appeared around at R_f value of 0.05. Based on the pH–potential diagram, this species is presumed to be electrochemically oxidized trivalent astatine, At(III). Furthermore, when the oxidized ^{211}At solution was mixed with 3-iodo-L-tyrosine, a new spot emerged around at R_f = 0.58, as shown in Figure 1c. Following measurement, ninhydrin staining of the TLC plate revealed coloration near this spot. This means the presence of a tyrosine derivative. These findings suggest that the observed peak corresponds to 3-astato-L-tyrosine.

At the conference, we will present detailed results obtained under the electrochemical labeling conditions, as well as interpretation of reactive ^{211}At species based on density functional theory calculations.

Copyright on 7th Asia-Pacific Symposium on Radiochemistry 2025

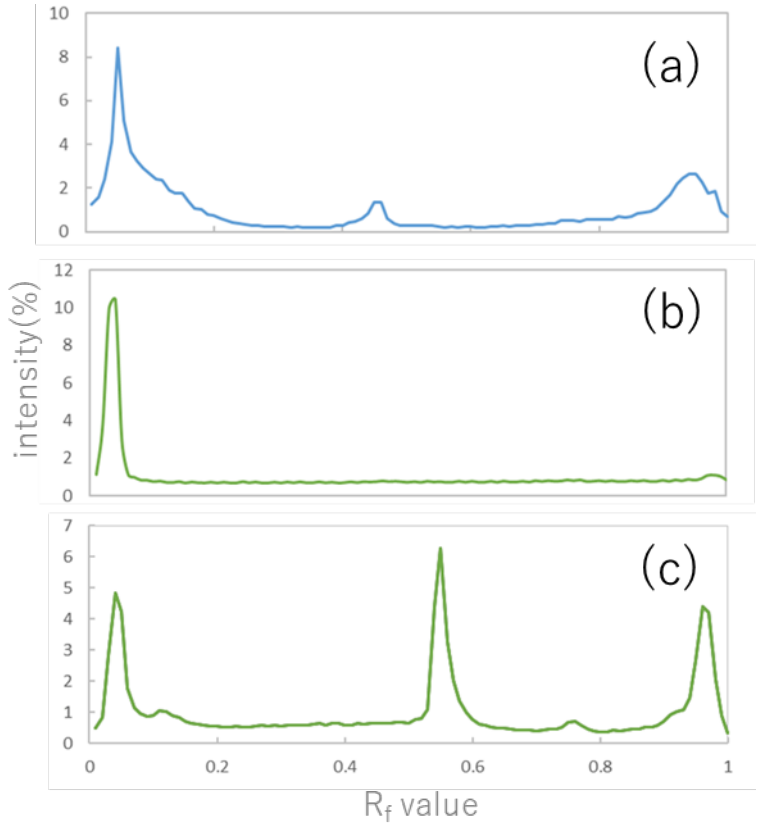


Figure 1. TLC results of ^{211}At species: (a) before electrolysis, (b) after electrolysis, and (c) after labeling with 3-iodo-L-tyrosine. These were obtained at pH 7.9 - 8.3 and at applied potential of 800 mV.

References

[1] A. Toyoshima et al., JACS 131,9180 (2009).

CHROMATOGRAPHIC ANALYSIS OF ASTATINE IN METHANOL SOLUTIONS TOWARD STANDARDIZATION OF THE QUALITY OF ASTATINE SUPPLY SOLUTION

Shigeki Watanabe[1], Masashi Murakami[2], Ichiro Sasaki[1], Kazuhiro Ooe[2], Yukiyoshi Kon[2], Tomoyuki Ohya[3], Jun Ichinose[3], Katsuyuki Minegishi[3], Kotaro Nagatsu[3], Atsushi Toyoshima[2], Noriko S. Ishioka[1]

[1]*Takasaki Institute for Advanced Quantum Science, National Institute for Quantum Science and Technology: 1233 Watanuki, Takasaki, Gunma 370-1292, Japan, watanabe.shigeki@qst.go.jp, sasaki.ichiro@qst.go.jp, ishioka.noriko@qst.go.jp*

[2]*Institute for Radiation Sciences, The University of Osaka: 1-1 Machikaneyama, Toyonaka, Osaka 560-0043, Japan, murakami@irs.osaka-u.ac.jp, toyo@irs.osaka-u.ac.jp*

[3]*Institute for Quantum Medical Science, National Institute for Quantum Science and Technology: 4-9-1 Anagawa, Inage, Chiba 263-8555, Japan*

We have investigated chemical species of ^{211}At produced in methanol solutions by high-performance liquid chromatography (HPLC) analysis. Two major species were consistently observed in the HPLC analyses of ^{211}At produced in four sites, although the contribution of minor components varied depending on the purification method.

1 INTRODUCTION

Astatine-211 (^{211}At) is a promising radionuclide for targeted alpha therapy (TAT), as it can be produced using a cyclotron and bismuth, an inexpensive and readily available target material. However, its clinical application will be constrained by its relatively short half-life of 7.2 hours. To promote the widespread adoption of TAT, it is essential to establish a decentralized production and distribution network for ^{211}At across multiple facilities. In Japan, the high density of cyclotron-equipped institutions and the country's compact geography offer a unique advantage: a well-coordinated supply network can be established to form a comprehensive treatment region despite the short half-life of ^{211}At. However, it has currently revealed that ^{211}At is supplied in varying chemical forms depending on the production facility, due to differences in bismuth target properties, irradiation parameters, and separation and purification methods. Among these, certain variations can alter the chemical species of astatine present in the final product, potentially affecting the efficiency of downstream radiolabeling. To ensure the reproducibility and reliability of radiopharmaceutical synthesis using ^{211}At across different sites, standardization of its chemical quality is therefore indispensable. As an initial step toward this goal, we investigated the impact of irradiation conditions and separation/purification procedures on the chemical species of ^{211}At in methanol solutions supplied by multiple production facilities.

2 EXPERIMENTAL

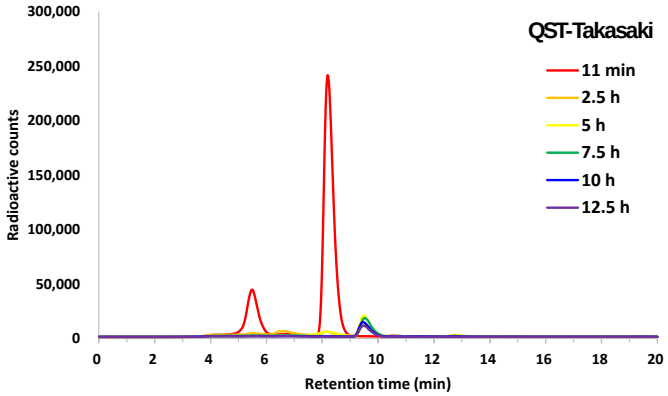
^{211}At was produced by irradiating Bi targets in the Takasaki Institute for Advanced Quantum Science, QST (QST-Takasaki) and the Research Center for Nuclear Physics (RCNP), the University of Osaka. Dry distillation was employed to isolate ^{211}At from the irradiated Bi targets under N_2/O_2 gas, after which it was collected in chloroform ($CHCl_3$). In addition, ^{211}At samples were provided by RIKEN and Fukushima Medical University (FMU), where dry distillation was also employed under O_2 (RIKEN) or N_2/O_2 gas (FMU), followed by shipment as dried residues in glass vials. The chloroform solution was dried and washed with methanol; similarly, the dried residues from RIKEN and FMU were washed with methanol. Aliquots (10 or 20 μL) of the resulting methanol solutions were analyzed by HPLC equipped with a NaI(Tl) detector. A YMC J'sphere ODS-M80 reversed-phase column (4.6 mm i.d. × 250 mm) was used, with a 1:1 (v/v) mixture of 50 mM tetrabutylammonium phosphate (pH 3.7) and MeCN as the mobile phase at a flow rate of 1 mL/min [1]. To elute residual ^{211}At, presumed to be in higher oxidation states, 10 μL of 50 mM $Na_2S_2O_5$ solution was injected after each analysis. Chromatograms were recorded multiple times for each sample to monitor variations in ^{211}At species.

3 RESULTS

Figure 1 shows typical chromatograms of ^{211}At in methanol solutions after collected in $CHCl_3$ prepared from Bi targets irradiated at QST-Takasaki. Separations were performed using N_2/O_2. Two major components with a retention time of approximately 5.6 min and 8.2 min were observed. The proportion of the major component varied depending on experiments but was generally greater than 50%; notably, a predominant peak with a retention time of 9.6 min was observed after more than 5 hours after solution preparation. The elution by column washing with 50 mM $Na_2S_2O_5$ solution typically ranged from 2% to 10%. Two major peaks with retention times of 7.8 min. and 11.8 min were also

observed in HPLC analysis of ^{211}At produced in RCNP at the University of Osaka. Changes on proportion of the major component were different from that produced in QST-Takasaki. We have also analyzed ^{211}At in methanol solutions by the washing residue provided from RIKEN and FMU. Although different separation gases from QST and RNCP, similar chromatograms were obtained for those provided from RIKEN. On the other hand, different chromatograms were obtained for those from FMU. Two major components were observed, but interestingly, no residual ^{211}At in the column was observed in both cases. We will also discuss chemical forms in ^{211}At directly collected by methanol in the section.

(a)



(b)

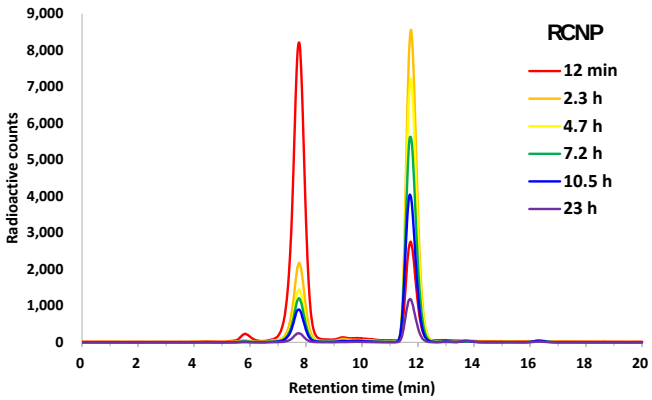


Fig. 1. Typical chromatograms of ^{211}At in methanol solution via $CHCl_3$ prepared from Bi targets irradiated at (a) QST-Takasaki, (b) RCNP at Univ of Osaka. Separations were performed using N_2/O_2 gas.

ACKNOWLEDGMENTS

This research was performed by the commissioned research fund provided by F-REI (JPFR24040203, JPFR25040203). We thank Dr. Haba and Dr. Nambu for supplying ^{211}At produced by the RI Beam Factory, operated by RIKEN Nishina Center and CNS, The University of Tokyo. We also thank to Dr. Takahashi for supplying ^{211}At produced at FMU.

References

[1] E. R. Balkin et al., “Evaluation of a wet chemistry method for isolation of cyclotron produced [211At]astatine,” Appl. Sci., 3, 636–655 (2013)

Copyright on 7th Asia-Pacific Symposium on Radiochemistry 2025

CHROMATOGRAPHIC ANALYSIS OF ASTATINE IN AQUEOUS SOLUTIONS FOR STANDARDIZATION OF THE QUALITY OF ASTATINE SUPPLY SOLUTION

Masashi Murakami[1], Shigeki Watanabe[2], Ichiro Sasaki[2], Kazuhiro Ooe[1], Yukiyoshi Kon[1], Tomoyuki Ohya[3], Jun Ichinose[3], Katsuyuki Minegishi[3], Kotaro Nagatsu[3], Noriko S. Ishioka[2], Atsushi Toyoshima[1]

[1]*Institute for Radiation Sciences, The University of Osaka: 1-1 Machikaneyama, Toyonaka, Osaka 560-0043, Japan, murakami@irs.osaka-u.ac.jp, toyo@irs.osaka-u.ac.jp*

[2]*Takasaki Institute for Advanced Quantum Science, National Institute for Quantum Science and Technology: 1233 Watanuki, Takasaki, Gunma 370-1292, Japan, watanabe.shigeki@qst.go.jp, sasaki.ichiro@qst.go.jp, ishioka.noriko@qst.go.jp*

[3]*Institute for Quantum Medical Science, National Institute for Quantum Science and Technology: 4-9-1 Anagawa, Inage, Chiba 263-8555, Japan*

We investigated the effects of irradiation and separation conditions on the chemical species of ^{211}At in the supplied aqueous solutions by high-performance liquid chromatography (HPLC) analysis. A major component with a retention time of 7.5–7.6 min was consistently observed under various conditions, although the contribution of minor components varied depending on the purification method.

1 INTRODUCTION

Astatine-211, a promising nuclide for targeted alpha therapy (TAT), can be produced by irradiation of bismuth, a relatively inexpensive and readily available element, using an accelerator. However, its distribution area is limited by its relatively short half-life of 7.2 h. The production and supply of ^{211}At at multiple facilities is indispensable for the widespread adoption of TAT. At present, supplied ^{211}At is in various forms depending on the production facilities, which have differences in Bi targets used, irradiation conditions, and separation and purification procedures. Variations among these factors would lead to differences in the chemical species of supplied ^{211}At. This may affect efficiency of labeling reactions to synthesize radiopharmaceuticals. Accordingly, standardizing the quality of the supplied ^{211}At is essential to ensure reliable radiopharmaceutical synthesis across different production facilities. Therefore, for quality standardization of supplied ^{211}At, we investigated the effects of irradiation conditions and separation/purification procedures on the chemical species of ^{211}At in supplied aqueous solutions.

2 EXPERIMENTAL

^{211}At was either supplied as irradiated Bi targets from the Research Center for Nuclear Physics (RCNP) at the University of Osaka, the Takasaki Institute for Advanced Quantum Science, QST (QST-Takasaki), and RIKEN, or produced and purified at Fukushima Medical University (FMU), then provided as a dried residue in a glass vial. For the former, a dry distillation method was used to separate ^{211}At from the Bi target, and the ^{211}At was collected in either distilled water or chloroform. A mixed gas of N_2/O_2, with or without humidification, was flowed during dry distillation. The chloroform solution was subsequently dried, washed with distilled water, and dissolved to obtain an aqueous solution. The dried residue from FMU was also washed with distilled water to prepare an aqueous solution.

After preparation, 10 or 20 μL aliquots of the ^{211}At aqueous solution were injected into a HPLC system equipped with a NaI(Tl) detector. A YMC J'sphere ODS-M80 reversed-phase column (4.6 mm i.d. × 250 mm) was used as the stationary phase, with a 1:1 (v/v) mixture of 50 mM tetrabutylammonium phosphate (pH 3.7) and MeCN as the mobile phase at 1 mL/min flow rate [1]. Subsequently, 10 or 20 μL of 50 mM $Na_2S_2O_5$ solution was injected to reduce and elute any residual ^{211}At, presumably in higher oxidation states, from the column. Chromatograms were obtained several times for each solution to monitor variations in ^{211}At species.

3 RESULTS

Figure 1 shows typical chromatograms of ^{211}At aqueous solutions separated and recovered from Bi targets irradiated at different facilities. Separations were performed using humidified N_2/O_2 gas. Similar chromatograms were obtained regardless of irradiation conditions, and a major component with a retention time of approximately 7.6 min was consistently observed. In repeated experiments, minor additional components occasionally appeared but were not reproducible. The proportion of the main component varied among experiments but was greater than 50%. The eluted fraction obtained by column washing with 50 mM $Na_2S_2O_5$ solution was ranged from 2% to 10%.

Copyright on 7th Asia-Pacific Symposium on Radiochemistry 2025

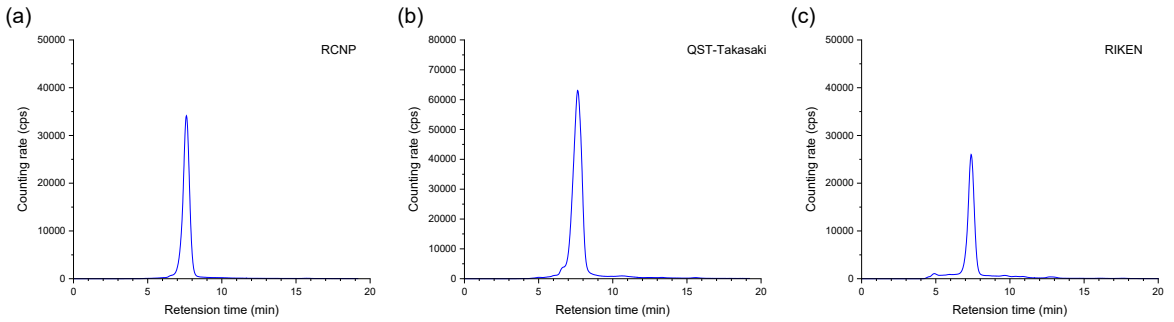


Fig. 1. Typical chromatograms of ^{211}At aqueous solutions separated and recovered from Bi targets irradiated at (a) RCNP, (b) QST-Takasaki, and (c) RIKEN. Separations were performed using humidified N_2/O_2 gas.

Figure 2(a) shows chromatograms of ^{211}At separated using non-humidified N_2/O_2 gas and directly recovered into distilled water. Although the major component at approximately 7.5 min was consistently observed in three replicates of experiments, minor components showed relatively large and irreproducible propotions. Considering the components eluted during the column washing, the proportion of the 7.5-min component was approximately 10%–30%.

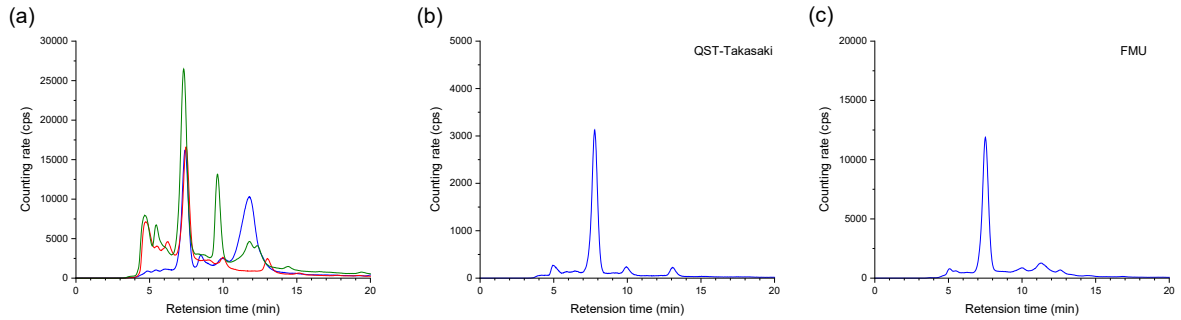


Fig. 2. Chromatograms of ^{211}At aqueous solutions. (a) Solutions obtained after separations using non-humidified N_2/O_2 gas and direct recovery into distilled water. (b) and (c) Solutions obtained after chloroform recovery, drying, and dissolution into distilled water, with Bi targets irradiated at (b) QST-Takasaki and (c) FMU.

In contrast, in the chromatograms of solutions obtained by chloroform recovery, drying, and dissolution into water (Fig. 2(b,c)), the contribution of minor components other than the major component at approximately 7.5 min was small. The proportion of the major component was 30%–50%.

ACKNOWLEDGMENTS

This research was performed by the commissioned research fund provided by F-REI (JPFR24040203, JPFR25040203). The RIKEN ^{211}At was supplied by the RI Beam Factory operated by RIKEN Nishina Center and CNS, University of Tokyo. We thank K. Takahashi of FMU for supplying ^{211}At.

References

[1] E. R. Balkin et al., "Evaluation of a wet chemistry method for isolation of cyclotron produced [^{211}At]astatine," Appl. Sci., **3**, 636–655 (2013).

Copyright on 7th Asia-Pacific Symposium on Radiochemistry 2025

SYNTHESIS AND CHARACTERIZATION OF STRONGLY PHOTOLUMINESENT NITRIDOTECHNETIUM(V) AND RHENIUM(V) COMPLEXES

Sodai Miyamoto[1] and Takashi Yoshimura[2]

[1] *Department of Chemistry, Graduate School of Science, The University of Osaka: 1-1 Machikaneyama, Toyonaka, Osaka, 560-0043, Japan, and miyamoto0904@rirc.osaka-u.ac.jp*
[2] *Radioisotope Research Center, Institute for Radiation Science, The University of Osaka: 2-4 Yamadaoka, Suita, Osaka, 565-0871, Japan, and tyoshi@rirc.osaka-u.ac.jp*

In this study, we synthesized and characterized new nitridotechnetium(V) and nitridorhenium(V) complexes. The structures of all the new complexes were determined by single-crystal X-ray analysis. The complexes exhibited strong photoluminescence in the visible region at room temperature. The new technetium complexes in this study were found to have the highest emission quantum yields and longest emission lifetimes reported to date.

1 INTRODUCTION

Technetium-99m is an important diagnostic nuclide for radiopharmaceutical used in single-photon emission computed tomography (SPECT) imaging. The gamma rays emitted from technetium-99m are monitored in SPECT. The gamma rays are highly penetrating, but insensitive to their surroundings. In contrast, the visible light emitted from a metal complex does not have high transparency but has properties, such as luminescence color, luminescence intensity, and luminescence lifetime that change in response to the surrounding environment. A technetium complex that emits both radiation and visible light is expected to expand the scope of diagnosis. To construct a complex that emits both radiation and photoluminescence from a single complex unit, the complex is required to exhibit strong photoluminescence because the extremely small amount of the complex is used in the diagnosis. In previous reports of the technetium complexes, there is only one data for emission quantum yield (Φ_{em}), and the reported emission quantum yield is small (Φ_{em} = 0.023)[1]. In this study, we have newly synthesized and characterized the strong photoluminescent technetium complex using technetium-99. The isomorphic rhenium complexes have also been synthesized and characterized to compare the structures and chemical properties.

2 EXPERIMENTAL

The new complexes were synthesized by heating the mixture of the silver complex with *N*-heterocyclic carbene ligand (hc) and tetracyanidonitridotechnetium(V) or tetracyanidonitridorenium(V) under reflux in ethanol. The synthesized complexes were characterized by single-crystal X-ray analysis, IR, UV-Vis absorption, and ^{1}H NMR measurements.

3 RESULTS AND DISCCUSION

The new complexes $[MN(CN)_2(hc)]$ (M = Tc and Re) were obtained by the reactions of $[MN(CN)_4]^{2-}$ with $[Ag_2hc]$. Interestingly, only one geometrical isomer (cis isomer) was produced for technetium, whereas two geometrical isomers (cis and trans isomers) were afforded for rhenium. The structures of the complexes were determined by single-crystal X-ray analysis as shown in Fig.1. The new technetium complexes exhibit orange colored photoluminescence in both solid state and solution at room temperature. The isomorphic rhenium complexes also show yellow colored photoemission at

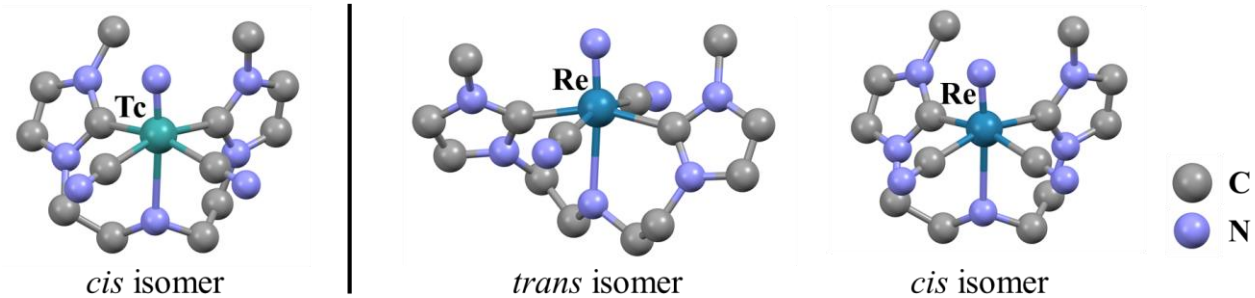


Fig. 1. The molecular structures of technetium and rhenium complexes.

room temperature. The emission quantum yield of the technetium complex is smaller than those of the corresponding rhenium complexes whereas the emission lifetime of technetium complex is longer than those of the rhenium complexes. The new technetium complex in this study is found to have the highest emission quantum yields and longest emission lifetimes reported to date.

4 CONCLUSIONS

The technetium and rhenium complexes with the *N*-heterocyclic carbene ligand were newly synthesized and characterized. The complexes exhibited strong photoluminescence in the visible region at room temperature.

References

[1] Andrew S. Del Negro, Carl J. Seliskar, William R. Heineman, Sean E. Hightower, Samuel A. Bryan, and B. Patrick Sullivan, *J. Am, Chem, Soc*. **2006**, 128, 16494-16495.

SYNTHESIS OF CRYPTAND-BASED CHELATING LIGANDS FOR STABLE Pb(II) COMPLEXES IN NUCLEAR MEDICINE APPLICATIONS

Eishun Kawagishi[1], Kojiro Nagata[2], Masashi Kaneko[1], Hiroyuki Kazama[1], Hiroki Aoto[1], Haruka Maeda[1], Terumi Yokoyama[1], and Yoshitaka Kasamatsu[1]

[1] *Graduate School of Science, The University of Osaka: 1-1 Machikaneyama, Toyonaka, Osaka 560-0043*
kawagishie23@chem.sci.osaka-u.ac.jp
[2] *Core Facility Center, The University of Osaka: 1-1 Machikaneyama, Toyonaka, Osaka 560-0043*

In this study, we aim to develop chelating ligands capable of stably binding Pb for theranostic nuclear medicine applications using $^{203/212}$Pb. To achieve this, we designed and synthesized novel ligands based on cryptands which bear additional coordinating substituents. Quantum chemical calculations revealed that the resulting Pb complexes could accommodate up to ten coordination sites.

1 INTRODUCTION

Targeted alpha therapy (TAT) has recently attracted much attention as a novel strategy for cancer treatment. This approach involves the use of molecularly targeted agents labeled with alpha-emitting radionuclides, which selectively accumulate in tumor tissues by binding to receptors specifically expressed on cancer cells. The emitted alpha particles with short flight range then destroy the tumor cells while minimizing damage to surrounding healthy tissues, offering the potential for highly effective cancer therapy with reduced side effects.

One of the radionuclides used in TAT is lead-212 (^{212}Pb), which undergoes beta decay with a half-life of 10.6 hours, followed by 100% alpha decay. Notably, its isotope, lead-203 (^{203}Pb) is suitable for SPECT imaging due to its electron capture decay properties. The use of radiopharmaceuticals based on the same element allows for both therapeutic and diagnostic applications. This approach represents the concept of theranostics in nuclear medicine.

In the molecular design of radiopharmaceuticals of Pb, it is essential to develop chelating ligands capable of stably coordinating Pb^{2+}, in order to prevent its release *in vivo*. In this study, we focused on cryptands, which are cage-like hard donor ligands. These ligands typically adopt eight-coordinate geometries and exhibit high selectivity and stability for relatively large cations. Since Pb^{2+} can adopt the coordination number of up to 12, improving ligand design to satisfy this coordination capacity is expected to enhance the stability of the resulting complexes.

Here, we aim to develop novel cryptand-based chelating ligands capable of forming stable complexes with Pb^{2+}. This strategy involves synthesis of partial substitution of oxygen atoms in the cryptand framework with nitrogen atoms, along with introduction of additional coordinating substituents such as pyridine moieties. Initially, quantum chemical calculations were conducted to evaluate the structural feasibility of the proposed complexes and support the molecular design of the ligands. Subsequently, the synthesis of a novel ligand (ligand **5**) was carried out according to the scheme shown in Fig. 1.

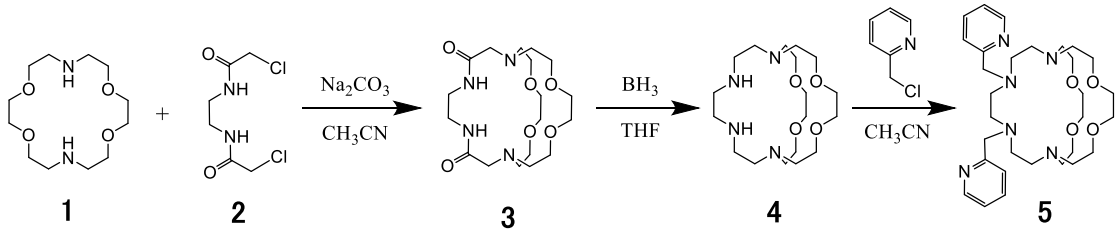


Fig. 1 Synthetic scheme of cryptand analogue ligands

2 EXPERIMENTAL

Based on previously reported structures [1], the Pb complexes $[Pb(\mathbf{4})(H_2O)_2]^{2+}$ and $[Pb(\mathbf{5})]^{2+}$ were modeled. Structural optimization and harmonic vibrational analysis were then performed using ORCA version 6.0 [2]. Calculations were performed using the BP86 functional. The SARC-ZORA-TZVP basis set was applied to lead element, while the ZORA-def2-TZVP basis set was used for all other elements. Scalar relativistic effects were taken into account using the ZORA Hamiltonian, and solvation effects were incorporated via the CPCM model with water as the solvent.

Synthesis of a cryptand analogue (compound **4**) and the novel ligand (compound **5**) were carried out according to the synthetic scheme shown in Fig. 1 [3, 4]. The obtained compounds were characterized by ^{1}H NMR spectra.

3 RESULTS AND DISCUSSION

3.1 Quantum Chemical Calculations

Figure 2 shows the equilibrium structures of the two Pb complexes obtained from geometry optimizations. In both complexes, the imaginary vibrational frequencies were negligibly small, indicating successful convergence of the geometrical optimizations. For ligand **4**, the average distances between the Pb center and the donor atoms were as follows: Pb–N (cryptand) = 3.01(29) Å, Pb–O (cryptand) = 2.79(12) Å, and Pb–O (H_2O) = 2.58 Å and 4.57 Å. In comparison, the sum of the ionic radius of ten-coordinate Pb^{2+} and the van der Waals radii of donor atom are 2.95 Å and 2.92 Å for nitrogen and oxygen atoms, respectively [5, 6]. These results indicate that all heteroatoms of the cryptand framework, as well as one water molecule, are located within the coordination sphere, suggesting that ligand **4** forms a nine-coordinate complex with Pb^{2+}. Similarly, for ligand **5**, the average bond distances were Pb–N (cryptand) = 2.91(19) Å, Pb–O (cryptand) = 3.11(9) Å, and Pb–N (pyridine) = 2.81(7) Å. Compared the bond distances of the complex with ligand **5** to those who ligand **4**, the order of the Pb–N and Pb–O distances are inverted, indicating a stronger interaction between Pb and nitrogen atoms. These findings suggest that the novel cryptand-based ligands have the potential to form stable lead complexes, demonstrating the validity of their molecular design.

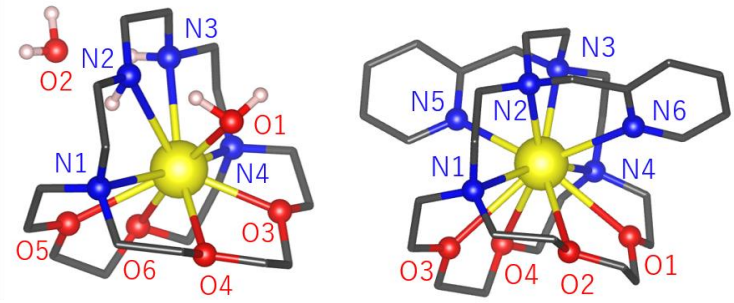


Fig. 2 Optimized structures of $[Pb(\mathbf{4})(H_2O)_2]^2$ and $[Pb(\mathbf{5})]^{2+}$

3.2 Ligand Synthesis

As intermediates, compound **1** was obtained in 12.9% yield, compound **2** in an equimolar amount, and compound **3** in 25% yield. The ^{1}H NMR spectra of each compound showed fully assigned peaks that were consistent with the expected structures and previously reported data [3, 4], indicating that the products were obtained with high purity. Ligand **4** was subsequently synthesized by reduction of the carbonyl group in compound **3** and identified by ^{1}H NMR spectroscopy. Further details regarding the ligand synthesis and spectral analysis will be presented at the conference.

4 CONCLUSION

A cryptand incorporating a pyridine substituent was proposed as a chelating ligand capable of stably coordinating Pb. Quantum chemical calculations predicted that all heteroatoms of the designed cryptand are located within approximately 3 Å of the Pb center, suggesting that the ligand can achieve up to ten-coordinate binding with a single molecule. In addition, the synthesis of a precursor to this ligand was successfully carried out. Complex synthesis, X-ray crystallographic analysis, and electronic structure analysis will be introduced in the presentation.

ACKNOWLEDGMENTS

This work was the result of using research equipment shared in MEXT Project for promoting public utilization of advanced research infrastructure (Program for supporting construction of core facilities) Grant Number [JPMXS0441200023], [JPMXS0441200024], and [JPMXS0441200025].

References

[1] A. N. CHEKHLOV, *Russ. J. Coord. Chem.* **32**, 552–558 (2006).
[2] F. NEESE, *WIREs Comput. Mol. Sci.* **12**, e1606 (2022).
[3] V. J. GATTO and G. W. GOKEL, *J. Am. Chem. Soc.* **106**, 8240-8244 (1984).
[4] W. YAN, *et al.*, *Inorg. Chem. Front.* **9**, 4794-4800 (2022).
[5] R. D. SHANNON, *Acta Crystallographica Section A* **32**, 751–767 (1976).
[6] A. BONDI, *J. Phys. Chem.* **68**, 441–451 (1964).

SYNTHESIS of LANTHANUM, BARIUM, AND ACTINIUM COMPLEXES WITH THE 15-MEMBERED CYCLIC LIGAND HAVING PHOSPHONATE ARMS

Kenshin Yamashita[1], Kenta Hamasaki[1], Kenji Shirasaki[2], Takuya Yokokita[3], Hidetoshi Kikunaga[3], Kazuaki Tsukada[3], Tatsuo Yajima[4], Takashi Yoshimura[2]

[1]*Department of Chemistry, Graduate School Science, The University of Osaka: 1-1 Machikaneyama, Toyonaka, Osaka, 560-0043, Japan*
[2]*Radioisotope Research Center, Institute for Radiation Sciences, The University of Osaka: 2-4 Yamadaoka, Suita, Osaka, 565-0871, Japan, tyoshi@rirc.osaka-u.ac.jp*
[3]*Research Center for Accelerator and Radioisotope Science, Tohoku University: 6-3 Aramaki aza aoba, Aoba, Miyagi 980-8578, Japan*
[4]*Department of Chemistry and Materials Engineering, Faculty of Chemistry, Materials and Bioengineering, Kansai University: 3-3-35 Yamatecho, Suita, Osaka 564-8680, Japan*

The 15-membered triazacrwon ether ligands having pyridinephosphonate and phosphonate were newly synthesized. The La^{3+}, and Ba^{2+} complexes with the ligands were synthesized and characterized. Furthermore, the complex formation of $^{225}Ac^{3+}$ with the new ligand was studied.

1 INTRODUCTION

Targeted alpha therapy (TAT) is one of the most promising approaches to cancer treatment. In this method, a radiopharmaceutical containing an alpha particle emitter such as $^{225}Ac^{3+}$ is administrated into the body, where it accumulates at target sites such as tumors. In this system, a chelating ligand is important to bind an alpha particle emitting radiometal ion and is required to form a highly stable complex. The ligand currently in clinical use is 1,4,7,10-tetraazacyclodecane1,4,7,10-tetraacetic acid (DOTA) which compose a 12-memberd tetraazacrown ether with four carboxy arms. However, the reaction of Ac^{3+} with DOTA is known to be required to heat the reaction solution for the complex formation. Recently, the 18-membered diazacrown ether with two carboxy-pyridine arms (macropa) has been well studied for $^{225}Ac^{3+}$ and $^{223}Ra^{2+}$, while 15-membered cyclic ligands have rarely been developed. It is important to adjust the size of the cyclic moiety in $^{225}Ac^{3+}$ and $^{223}Ra^{2+}$ where electrostatic interaction is dominant in the complex formation. In the present study, new 15-membered N_3O_2 type cyclic ligand have been synthesized in expectation to improve the stability of the ^{225}Ac complex.

2 RESULTS and DISCUSSION

Figure 1 shows the newly synthesized two 15-membered cyclic ligands and with pyridine phosphonate arms (H_6tpp15c5) and phosphonate arms (H_6tp15c5), respectively. The complex formation for TAT is desirable to rapidly proceed at room temperature. In fact, the reactions of La^{3+} with H_3tpp15c5^{3-} and H_3tp15c5^{3-} in 1:1 molar ratios, respectively, were immediately occurred at room temperature to give the 1:1 complexes in the aqueous solutions. The Ba complexes were also synthesized by the similar procedures. The stability constant of the complexes were determined by potentiometric titrations. The stability constants (β) of the Ba complexes in the aqueous solutions are $\log \beta_{BaL} = 7.76$ for H_6tpp15C5 and 8.30 for H_6tp15C5. The $\log \beta_{LaL}$ values in the aqueous solutions are 15.3 for H_6tpp15C5 and 16.3 for H_6tp15C5. The $\log \beta_{LaL}$ values are larger than that with macropa ($\log \beta_{LaL} = 14.99$). The complex formation of $^{225}Ac^{3+}$ with H_6tpp15c5 was also investigated.

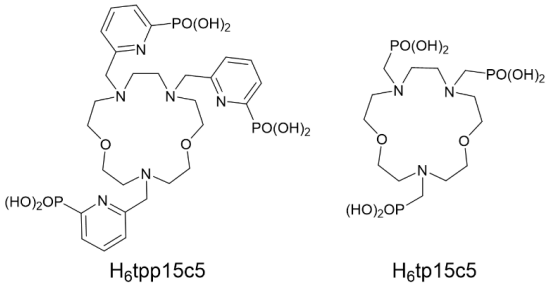


Fig. 1. The structures of H_6tpp15c5 and H_6tp15c5.

3 CONCLUSIONS

In this study, the La^{3+} and Ba^{2+} complexes with the 15-memberd N_3O_2 type cyclic ligands bearing phosphonate or pyridine phosphonate arms were synthesized and characterized. The stability of the La^{3+} complexes are found to be larger than that with macropa.

SYNTHESIS OF MACROCYCLIC 1,2-HYDROXYPYRIDINONE-BASE LIGAND FOR ^{227}Th AND ^{89}Zr RADIOPHARMACEUTICALS

Terumi Yokoyama[1], Hiroyuki Kazama[1], Masashi Kaneko[1], Kojiro Nagata[2], Hiroki Aoto[1], Haruka Maeda[1], Eishun Kawagishi[1], and Yoshitaka Kasamatsu[1]

[1]*Graduate School of Science, The University of Osaka, 1-1 Machikaneyama, Toyonaka, Osaka, 560-0043, Japan.*
Email: yokoyamat24@chem.sci.osaka-u.ac.jp
[2]*Core Facility Center, The University of Osaka, 1-1 Machikaneyama, Toyonaka, Osaka 560-0043, Japan*

A novel macrocyclic ligand bearing 1,2-hydroxypyridinone groups (N_4O_2-HOPO) was synthesized for potential application in thorium-227-based targeted alpha therapy and zirconium-89-based PET imaging. The synthetic pathway was optimized by investigating the influence of different bases on macrocyclization yields. Potassium ions were found to play a crucial role in facilitating macrocycle formation via a template effect, highlighting a key consideration for improving synthetic efficiency. The stability of Th and Zr complexes with the ligand was also evaluated through experimental and quantum chemical approaches.

1 INTRODUCTION

Thorium-227 (^{227}Th) is an α-emitting radionuclide with significant potential for use in targeted alpha therapy (TAT), a treatment that employs high-energy α particles to destroy cancerous lesions. To utilize ^{227}Th in TAT, it is necessary to design ligands that can form highly stable complexes with thorium *in vivo* conditions. Toward this goal, we have focused on 1,2-hydroxypyridinone (1,2-HOPO), an oxygen-donor type ligand known to form stable complexes with tetravalent metal ions, making it a promising chelator for Th^{4+}. Moreover, 1,2-HOPO has also been reported to form stable complexes with zirconium [1]. Zirconium-89 (^{89}Zr) is a positron-emitting radionuclide that can be used in positron emission tomography (PET), a powerful diagnostic imaging technique for cancer. To enable a theranostics approach that combines ^{227}Th-based therapy and ^{89}Zr-based diagnosis it is necessary to design a ligand that can stably chelate both ^{227}Th and ^{89}Zr.

Previous studies have reported the synthesis of 12-membered macrocyclic N_4-type ligands (H_4L) containing 1,2-HOPO and showed the stability constants, $[ML]/([M^{4+}][L^{4-}])$, of $10^{42.9}$ for Zr(IV) and $10^{34.4}$ for Th(IV), indicating lower stability of Th(IV) by eight orders of magnitude compared to Zr(IV). This difference may arise from the disparity in ionic radii between the two metals (r_{Th4+} = 0.94 Å, r_{Zr4+} = 0.72 Å, CN = 6), suggesting challenges in designing a ligand that accommodates both metal centers equally well.

To address this, we propose a novel 18-membered N_4O_2-type azacrown ether ligand bearing 1,2-HOPO moieties (N_4O_2-HOPO). The increased flexibility and cavity size of the macrocyclic scaffold are expected to provide better accommodation for the larger Th(IV) ion, while still enabling effective coordination of Zr(IV). In this study, we established a synthetic method for N_4O_2-HOPO and evaluated its complexation properties and stability through both experimental and quantum chemical approaches.

2 EXPERIMENTAL

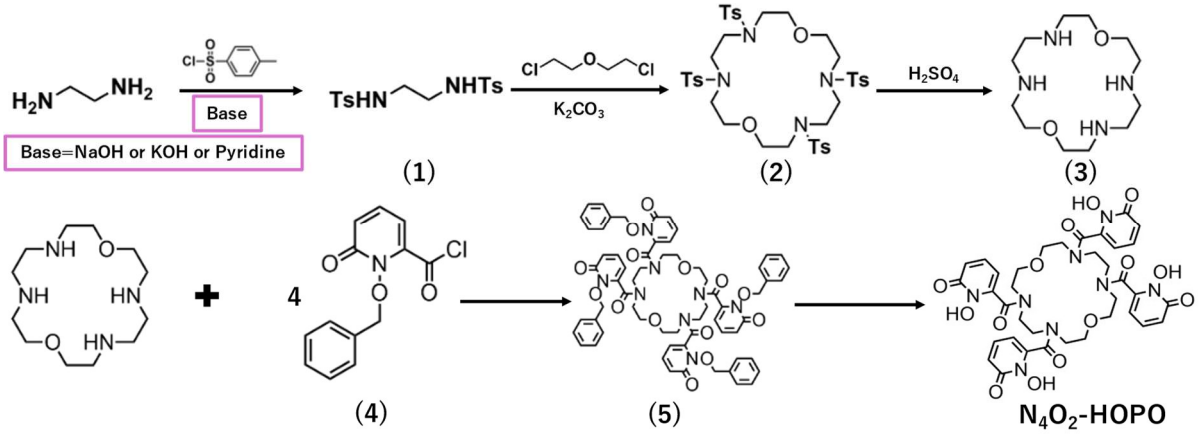


Fig. 1 Synthesis of **N_4O_2-HOPO**

N_4O_2-HOPO was synthesized according to the scheme shown in Figure 1 [2]. *N*,*N*'-Ditosylethylenediamine **(1)** was obtained in 90% yield by stirring ethylenediamine and *p*-toluenesulfonyl chloride under basic conditions (NaOH).

Compound **(1)** was then stirred with bis(2-chloroethyl) ether and K_2CO_3 in DMF at 170 °C for 5 hours, affording 4,7,13,16-tetratosyl-1,10-dioxa-4,7,13,16-tetraazacyclooctadecane **(2)** with a yield of 1.4%. Subsequent deprotection of the tosyl groups from compound **(2)** using concentrated sulfuric acid yielded compound **(3)** with a yield of 18%. The precursor 1-benzyloxy-2(*1H*)-pyridinone-6-carbonyl chloride **(4)** was prepared following the method reported by Deri et al., with a yield of 44% [3]. The introduction of compound **(4)** into the macrocyclic framework was performed following the procedure described by Woods et al. [1]. To evaluate the influence of the base used in the synthesis of compound **(1)** on the macrocyclization yield of compound **(2)**, NaOH, KOH, and pyridine were used as alternative bases, and the resulting yields of compound **(2)** were compared. All products were characterized by ^{1}H NMR, ^{13}C NMR, and ESI-MS.

3 RESULTS AND DISCUSSION

All compounds were unambiguously identified, and the synthesis of N_4O_2-HOPO was completed. The bases used in the synthesis of compound **(1)** and the corresponding yields of compound **(2)** are summarized in Table 1. When KOH or pyridine was used as the base, compound **(2)** was obtained in higher yield compared to the reaction using NaOH. This result suggests that the synthesis of compound **(2)** is strongly influenced by a template effect mediated by potassium ions [4]. In the case where NaOH was used in the synthesis of compound **(1)**, sodium ions were contaminated into the reaction system, which interfered with the potassium-mediated templating process in the subsequent step, thereby lowering the yield. The incorporation of 1,2-HOPO into compound **(3)** was confirmed by ESI-MS, and the synthesis of N_4O_2-HOPO was successfully achieved, establishing a synthetic method.

Table 1. The base used in the synthesis of compound (1) and the reaction yield of compound (2)

Base	Yield of compound **(2)**
NaOH	1.4 %
KOH	10.0 %
Pyridine	8.0 %

4 CONCLUSIONS

We synthesized a new macrocyclic ligand, N_4O_2-HOPO, incorporating 1,2-hydroxypyridinone groups. Through comparative experiments, we demonstrated that the choice of base in the early synthetic steps significantly affects the macrocyclization yield of the intermediate compound. The notably low yield observed when sodium hydroxide was used suggests that the desired reaction is governed by a template effect mediated by potassium ions.

In the presentation, we will also report on the structure and stability of the resulting metal complexes.

ACKNOWLEDGMENTS

This work was the result of using research equipment shared in MEXT Project for promoting public utilization of advanced research infrastructure (Program for supporting construction of core facilities) Grant Number [JPMXS0441200024], and [JPMXS0441200025].

References

[1] WOODS, J. J., *et al., Inorg. Chem.***62**, 50 (2023).
[2] Y. XINHAO. *et al., J. INCL. PHENOM. MACROCYCL. CHEM.*, **33** (1999)
[3] DERI, M. A. *et al. J., Med. Chem.*, **57**, 11 (2014)
[4] KRAKOWIAK, K. E. *et al.*, *Chem. Rev.* **89** (1989)

7th Asia-Pacific Symposium on Radiochemistry *September 14 ~ 19, 2025 • Kunibiki Messe • Shimane, Japan*

SYNTHESIS AND PROPERTIES OF BARIUM, LANTHANUM, AND ACTINIUM COMPLEXES WITH THE 18-MEMBERED CYCLIC LIGAND WITH PYRIDINE PHOSPHONATE ARMS FOR RADIOPHARMACEUTICALS

Kaseki Matsuda[1], Kazuaki Baba[1], Kojiro Nagata[2], Kenji Shirasaki[3], Takuya Yokokita[4], Hidetoshi Kikunaga[4], Kazukaki Tsukada[4], Tatsuo Yajima[5], Takashi Yoshimura[3]

[1] *Department of Chemistry, Graduate School of Science, The University of Osaka, 1-1 Machikaneyama, Toyonaka, Osaka 560-0043, Japan*
[2] *Core Facility Center, The University of Osaka, 1-2 Machikaneyama, Toyonaka, Osaka 560-0043, Japan*
[3] *Radioisotope Research Center, Institute for Radiation Sciences, The University of Osaka, 2-4 Yamadaoka, Suita, Osaka 565-0871, Japan, tyoshi@rirc.osaka-u.ac.jp*
[4] *Research Center for Accelerator and Radioisotope Science, Tohoku University, 6-3 Aramaki aza aoba, Aoba, Miyagi 980-8578, Japan*
[5] *Department of Chemistry and Materials Engineering, Faculty of Chemistry, Materials and Bioengineering Kansai University, 3-3-35 Yamatecho, Suita, Osaka 564-8680, Japan*

The Ba, La and Ac complexes with an 18-membered cyclic ligand, 4,13-diaza-18-crown-6, bearing two pyridine phosphonate arms were synthesized at room temperature. The complex formation reaction of $^{225}Ac^{3+}$ proceeded at 25°C within 5 min at the concentration of the ligand more than 1.0×10^{-4} M

1 INTRODUCTION

Targeted alpha therapy (TAT) has attracted much attention. $^{225}Ac^{3+}$ and $^{223}Ra^{2+}$ are one of radionuclides suitable for TAT. It is desired that the complex formation proceeds at room temperature and the obtained complex is highly stable for TAT. In this study, the Ba^{2+} and La^{3+} complexes with an 18-membered cyclic ligand, 4, 13-diaza-18-crown-6, bearing two pyridine phosphonate arms were synthesized and characterized to obtain their structural information. Furthermore, we report the synthesis of the $^{225}Ac^{3+}$ complexes and their radiolabeling yields.

2 RESULTS AND DISCUSSION

2.1 Synthesis and Characterization of La and Ba Complexes

The Ba^{2+} and La^{3+} complexes with a macropp ligand were synthesized in high yields by the reactions of metal ions with H_4macropp (Fig. 1) at room temperature. The complexes were structurally characterized by the single-crystal X-ray analysis. The La^{3+} complex is a 11-coordinate structure, and the Ba^{2+}complex exhibits a 10-coordinate structure. The acid–base equilibrium and the complex formation reactions of the La^{3+} and Ba^{2+} complexes were tracked by potentiometric titrations to determine the species in the solutions and their stabilities. The speciation of the complexes and pH dependencies of the fractions in the aqueous solutions were determined. We also determined the pM values of La^{3+} and Ba^{2+} for the chemical reactions of macropp ligands. The pM value is the logarithm of the concentration of free metal ions ($-\log[M^{n+}]$) at a pH of 7.4, with a ligand concentration of 10 μM and a metal ion concentration of 1 μM. The pLa^{3+} and pBa^{2+} values are 10.2 and 6.4. The separation conditions of the metal ions and the complexes were investigated by thin layer chromatography (TLC) in order to apply the Ac^{3+} complexes to labeling experiments. The R_f values of La^{3+} ion and the La complex using an alumina TLC plate are 0 and 0.2-0.6, respectively, in phosphate buffer solution (pH 8). The R_f values of Ba^{2+} ion and the Ba^{2+} complex using a cellulose TLC plate are 0 and 0.7 respectively, in HEPES buffer solution (pH 8).

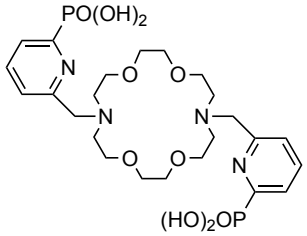


Fig. 1. The H_4macropp ligand.

Copyright on 7th Asia-Pacific Symposium on Radiochemistry 2025

2.2 Complex formation for $^{225}Ac^{3+}$ with macropp

The reaction of $^{225}Ac^{3+}$ with H_4macropp was monitored every 5 minutes for 60 min at 25℃ using TLC. The complex formation reaction of Ac^{3+} with H_4macropp completed at 25℃ within 5 min at the concentration of H_4macropp ranging from 1.0×10^{-3} to 1.0×10^{-7} M. The yield of the Ac complex is found to be decreased with decreasing concentration of H_4macropp.

3 CONCLUSIONS

The La^{3+}, Ba^{2+}, and Ac^{3+} complexes were synthesized by the reactions of metal ions with H_4macropp at room temperature. The structures and stability of the La^{3+} and Ba^{2+} complexes were determined. The condition for separation of the metal ion and the complex using TLC was determined. The complex formation reaction of Ac^{3+} with macropp proceeded at 25℃ within 5 min at the concentration of the ligand more than 1.0×10^{-4} M. The yield of the Ac^{3+} complex was decreased with decreasing the concentration of the ligand.

References

[1] K. Baba, K. Nagata, T. Yajima, and T. Yoshimura, *Bull. Chem. Soc. Jpn*., **95**, 466-475 (2022).

Development of an Imaging Probe Targeting Adrenal Aldosterone Synthase (CYP11B2)

Hiroyuki Kimura[1], Yusuke Yagi[2], Riko Fuseda[3], Takaaki Murakami[4], Marina Omokawa[5], Masakatsu Sone[6], Hiroyuki Yasui[7], Nobuya Inagaki[8], Hideo Saji[9]

[1] Division of Environmental Management, Agency for Health, Safety and Environment, Kyoto University: Yoshida Knoe-cho, Sakyo-ku, Kyoto-City, Kyoto, Japan, 〒606-8501, kimura.hiroyuki.4u@kyoto-u.ac.jp
[2] Department of Radiological Technology, Faculty of Medicinal Science, Kyoto University of Medical Science, 1-3 Imakita, Oyama-higashi, Sonobe, Nantan, Kyoto, Japan, 〒622-0041, y-yagi@kyoto-msc.jp
[3] Laboratory of Analytical and Bioinorganic Chemistry, Division of Analytical and Physical Sciences, Kyoto Pharmaceutical University, 5 Nakauchi-cho, Misasagi, Yamashina-ku, Kyoto, Japan, 〒607-8414, riko.pi8517@gmail.com
[4] Department of Diabetes, Endocrinology and Nutrition, Graduate School of Medicine, Kyoto University Hospital, 54 Shogoin-kawahara-cho, Sakyo-ku, Kyoto, Japan, 〒606-8507, tmurakam@kuhp.kyoto-u.ac.jp
[5] Faculty of Medicine, Dentistry and Pharmaceutical Sciences, Okayama University, 2-5-1 Shikata-cho, Kita-ku, Okayama, Japan, 〒700-8558, m-omokawa@okayama-u.ac.jp
[6] Department of Metabolism and Endocrinology, St. Marianna University School of Medicine, 2-16-1 Sugao, Miyamae-ku, Kawasaki, Kanagawa, Japan, 〒216-8511, sonemasa@marianna-u.ac.jp
[7] Laboratory of Analytical and Bioinorganic Chemistry, Division of Analytical and Physical Sciences, Kyoto Pharmaceutical University, 5 Nakauchi-cho, Misasagi, Yamashina-ku, Kyoto, Japan, 〒607-8414, yasui@mb.kyoto-phu.ac.jp
[8] Department of Diabetes, Endocrinology and Nutrition, Graduate School of Medicine, Kyoto University Hospital, 54 Shogoin-kawahara-cho, Sakyo-ku, Kyoto, Japan, 〒606-8507, inagaki@kuhp.kyoto-u.ac.jp
[9] Department of Patho-Functional Bioanalysis, Graduate School of Pharmaceutical Sciences, Kyoto University, 46-29 Yoshida-shimo-adachi-cho, Sakyo-ku, Kyoto, Japan, 〒606-8501, saji.hideo.4v@kyoto-u.ac.jp

1. INTRODUCTION

Primary aldosteronism (PA) is a form of secondary hypertension caused by excessive aldosterone secretion from the adrenal glands and accounts for approximately 5–10% of all hypertension cases [1]. Currently, adrenal vein sampling (AVS) is the gold standard for the localization of aldosterone-producing lesions in patients with PA (Figure1). However, AVS is technically demanding, limited to specialized centers with high success rates, and places a significant financial and physical burden on patients. Imaging techniques such as computed tomography (CT) and magnetic resonance imaging (MRI) have not yielded satisfactory diagnostic accuracy [2,3], with positive localization rates of only 60–70%. This is largely due to the high prevalence of nonfunctioning adrenal adenomas, which are indistinguishable from aldosterone-producing adenomas (APAs) using conventional imaging. Furthermore, some aldosterone-producing lesions are not detectable on CT, further limiting diagnostic accuracy. Thus, there is a critical need to develop a highly accurate, minimally invasive, and widely accessible method for localizing aldosterone production in PA. We propose that nuclear medicine imaging modalities, such as positron emission tomography (PET) and single photon emission computed tomography (SPECT), could offer a promising solution. Although ^{131}I-adosterol is currently used for adrenocortical scintigraphy to assess cortical function—particularly in conditions such as Cushing's syndrome—it is suboptimal for detecting aldosterone production due to the relatively low concentration of aldosterone compared to other corticosteroids. In this research, we aim to develop a radiolabeled imaging probe that specifically targets CYP11B2 (aldosterone synthase)—an enzyme critical for aldosterone biosynthesis and known to be upregulated in PA. By targeting CYP11B2, we intend to establish a novel, highly specific imaging method for the detection and localization of APAs.

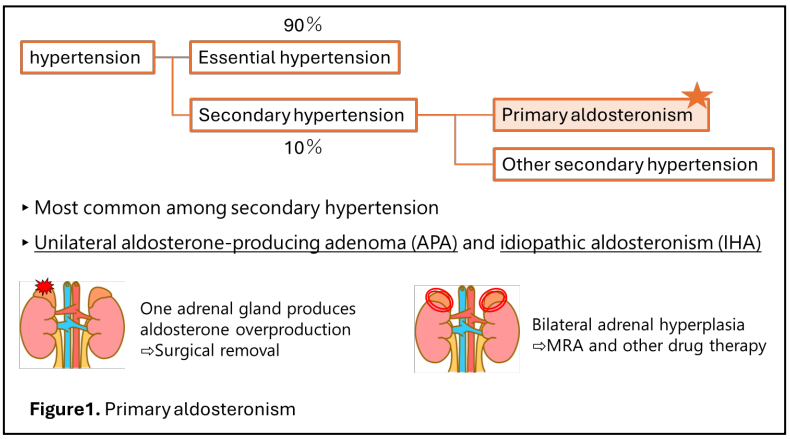


Figure1. Primary aldosteronism

2. METHODS

We developed and synthesized four derivatives of pyridinylbenzimidazole, designated PBI-1 through PBI-4. Their inhibitory effects on CYP11B2, as well as their selectivity relative to CYP11B1, were evaluated using V79 cells transfected with the respective enzymes. The synthesized compounds were subsequently radiolabeled with either iodine-125 (^{125}I) or fluorine-18 (^{18}F), and biodistribution studies of the radiotracers were conducted in ddY mice. Finally, in vitro autoradiography (ARG) was performed using adrenal tissue sections from patients with primary aldosteronism to assess CYP11B2 selectivity over CYP11B1.

3. RESULTS and DISCUSSION

Iodine-labeled PBI-1 and PBI-2 were synthesized for SPECT imaging probes, while fluorine-labeled PBI-3 and PBI-4 were prepared for PET imaging probes, all with relatively high yields. Inhibition assays revealed that PBI-2 and PBI-4—both containing a fluorochlorobenzene moiety—exhibited potent inhibitory activity and high selectivity toward CYP11B2 (IC_{50}: PBI-2 = 0.47 ± 0.19 nM, PBI-4 = 0.25 ± 0.05 nM; selectivity ratio vs. CYP11B1: PBI-2 = 245, PBI-4 = 625). Radiolabeled compounds [^{125}I]PBI-2 and [^{18}F]PBI-4 were successfully obtained. Biodistribution studies of [^{18}F]PBI-4 in ddy mice demonstrated notable accumulation in the adrenal glands (5.76 ± 2.00 %ID/g at 5 minutes post-injection). The low accumulation of radioactivity in bone—an indicator of defluorination—suggests that the [^{18}F]PBI-4 is highly stable in vivo. Conversely, although [^{125}I]PBI-2 rapidly migrates to the adrenal gland following administration, its high accumulation in the stomach and thyroid indicates in vivo instability. In vitro autoradiography (ARG) using human adrenal tissue slices showed greater radioactivity accumulation in CYP11B2-rich regions compared to CYP11B1-dominant regions, consistent with the results from cell-based assays. These findings indicate that [^{18}F]PBI-4 exhibits high selectivity for CYP11B2 and holds significant potential as a PET imaging probe for the localization of aldosterone-producing lesions.

4. CONCLUSIONS

In vitro evaluation of [^{18}F]PBI-4 demonstrated 625-fold greater binding specificity for CYP11B2 over CYP11B1. In vivo biodistribution studies in ddy mice showed notable accumulation of radioactivity in the adrenal glands. The marked difference in uptake between the adrenal glands and kidneys suggests that adrenal tissue can be clearly visualized on PET imaging. Furthermore, low accumulation in bone—an indicator of defluorination—implies that [^{18}F]PBI-4 is highly stable in vivo. To assess its efficacy in human tissue, autoradiography was performed on frozen sections of aldosterone-producing adenomas obtained from patients with primary aldosteronism. [^{18}F]PBI-4 demonstrated high accumulation in areas positively stained for CYP11B2 by immunohistochemistry, whereas minimal uptake was observed in CYP11B1-positive regions. In contrast, compounds with low selectivity for CYP11B1 and CYP11B2 exhibited no specific localization and were uniformly distributed. These findings confirm that [^{18}F]PBI-4 selectively binds to human CYP11B2 and underscore its potential as a novel fluorine-18-labeled PET imaging probe for the detection and localization of aldosterone-producing lesions in primary aldosteronism.

ACKNOWLEDGMENTS

This work was supported by the Research Foundation for Pharmaceutical Sciences, JSPS KAKENHI (Grant Number: JP18K15566, JP20K08061, and JP22K15852), Seeds A of Japan Agency for Medical Research and Development (Grant Number: A134). We would like to thank Nihon Medi-Physics Co., Ltd. (Tokyo, Japan) for their cooperation in the evaluation of IC50 values for CYP11B2 and CYP11B1 activities.

DECLARATIONS

All animal experiments were conducted according to Kyoto University and Kyoto Pharmaceutical University guidelines, and the study protocol was approved by the Institutional Experimental Animal Committee. The study protocol of in vitro ARG using human adrenal sections was reviewed and approved by Kyoto University Graduate School and Faculty of Medicine and Kyoto Pharmaceutical University, Ethics Committee.

REFERENCES

[1] Reincke M, *et al.* Diagnosis and treatment of primary aldosteronism. Lancet Diabetes Endocrinol. 2021;9:876-92.
[2] Kamemura K, *et al.* Significance of adrenal computed tomography in predicting laterality and indicating adrenal vein sampling in primary aldosteronism. J Hum Hypertens. 2017; 31:195-9.
[3] Ladurner R, *et al.* Accuracy of adrenal imaging and adrenal venous sampling in diagnosing unilateral primary aldosteronism. Eur J Clin Invest. 2017; 47:372-7.

7th Asia-Pacific Symposium on Radiochemistry *September 14 ~ 19, 2025 • Kunibiki Messe • Shimane, Japan*

Improved in vivo stability of astatobenzoyl compounds by conjugating with D-oligopeptides

Hiroyuki Suzuki[1], Mutsuho Murata[1], Kento Kannaka[1], Souma Kitagwa[1], Souta Tatsuta[1], Kazuhiro Takahashi[2], Tomoya Uehara[1]

[1]*Graduate School of Pharmaceutical Sciences, Chiba University, 1-8-1 Inohana, Chuo-ku, Chiba 260-8675, h.suzuki@chiba-u.jp*
[2]*Advanced Clinical Research Center, Fukushima Medical University, 1 Hikarigaoka, Fukushima 960-1295, Japan*

1 Introduction

Astatine-211 (^{211}At) is an α-emitting radionuclide appropriate for targeted α-therapy. Astatobenzoyl moieties have been used as the most common astatination moieties to produce ^{211}At-labeled proteins such as antibodies and antibody fragments. However, ^{211}At-labeled proteins prepared by this method show low stability against in vivo deastationation [1]. Because deastationation of ^{211}At-labeled proteins is delayed by slower blood clearance and tissue distribution, in vivo deastatination is considered to occur after tissue accumulation. In our previous studies, alkyl astatide compounds with high stability against in vivo deastatination were produced by using a neopentylglycol moiety that is stable against enzymatic deastatination. We considered that the approach focusing on the stability against enzymatic deastatination may also be effective to produce aryl astatides with high stability against in vivo deastatination. After ^{211}At-labeled proteins are incorporated into the tissues, they are transported into the lysosomes and then degraded. We hypothesized that the radiometabolites fragmented by the lysosomal degradation would undergo enzyme-mediated deastatination. Therefore, we aimed to increase the molecular size to inhibit enzyme recognition of the astatobenzoyl moieties. In the present study, we prepared ^{211}At-labeled oligopeptides consisting of D-amino acids by using a 3-astatobenzoyl moiety, and their in vivo stability against deastatination was assessed.

2. Methods

[^{211}At]3-astatobenzoyl moiety was conjugated with a D-glutamic acid ([^{211}At]At-Bz-e), di-D-glutamic acid ([^{211}At]At-Bz-ee), tri-D-glutamic acid ([^{211}At]At-Bz-eee), tri-L-glutamic acid ([^{211}At]At-Bz-EEE), tri-D-lysine ([^{211}At]At-Bz-kkk), and tri-D-alanine ([^{211}At]At-Bz-aaa) (Fig. 1). Their ^{125}I-labeled counterparts ([^{125}I]I-Bz-e, [^{125}I]I-Bz-ee, [^{125}I]I-Bz-eee, [^{125}I]I-Bz-EEE, [^{125}I]I-Bz-kkk, and [^{125}I]I-Bz-aaa) were also prepared (Fig. 1). These radiohlogenated compounds were injected into six-week-old male ddY mice via the tail vein. At 1 h after the injection, the mice were sacrificed and dissected. The tissues of interest were weighed, and the radioactivity counts in each tissue were determined with an auto-well γ-counter.

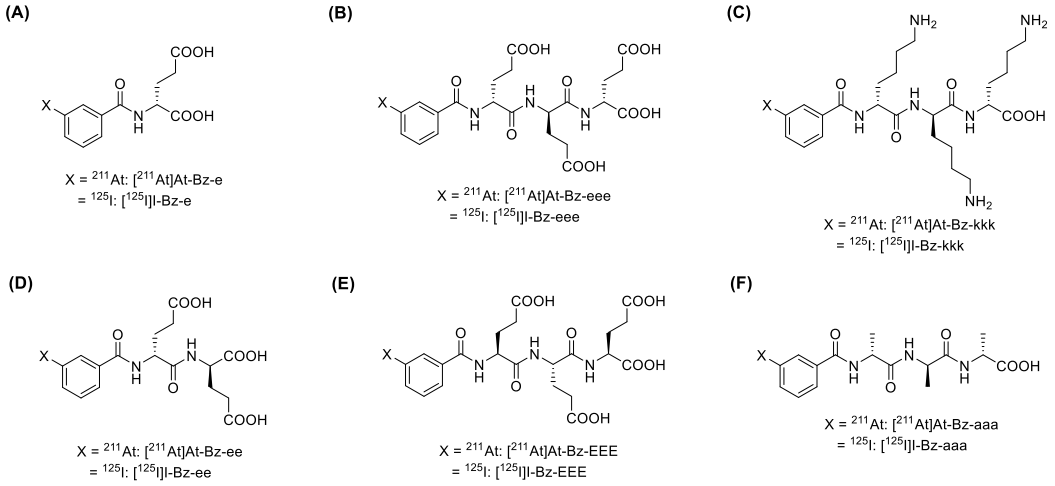


Fig. 1. Structures of ^{211}At- and ^{125}I-labeled compounds evaluated in this study.

3. Results

All ^{125}I-labeled compounds consisting of D/L-glutamic acid(s) showed low accumulation in the stomach and thyroid. Because [^{125}I]I^- and [^{211}At]At^- accumulate in the stomach and thyroid, the results indicate they are stable against in vivo

Copyright on 7th Asia-Pacific Symposium on Radiochemistry 2025

deiodination. Whereas, the radioactivity levels in the stomach after administrating ^{211}At-labeled counterparts decreased as the number of conjugated glutamic acids increased. In addition, [^{211}At]At-Bz-eee showed lower accumulation in the stomach than that of [^{211}At]At-Bz-EEE. Therefore, strategy to increase molecular size by oligopeptides with metabolic resistance would be useful to improve the in vivo stability of astatobenzoyl moieties. Radioactivity level of [^{211}At]At-Bz-eee in the stomach was slightly higher than that of [^{125}I]I-Bz-eee, suggesting that low level of in vivo deastatination occurred. [^{211}At]At-Bz-kkk showed lower radioactivity levels in the stomach and thyroid, which were comparable to those of [^{125}I]I-Bz-kkk. The results indicate that [^{211}At]At-Bz-kkk is highly stable against in vivo deastatination. [^{211}At]At-Bz-aaa showed high accumulation in the stomach, while [^{125}I]I-Bz-aaa showed low accumulation. Hence, the side chain of oligopeptides is also an important factor to stabilize the in vivo stability of astatobenzoyl moieties.

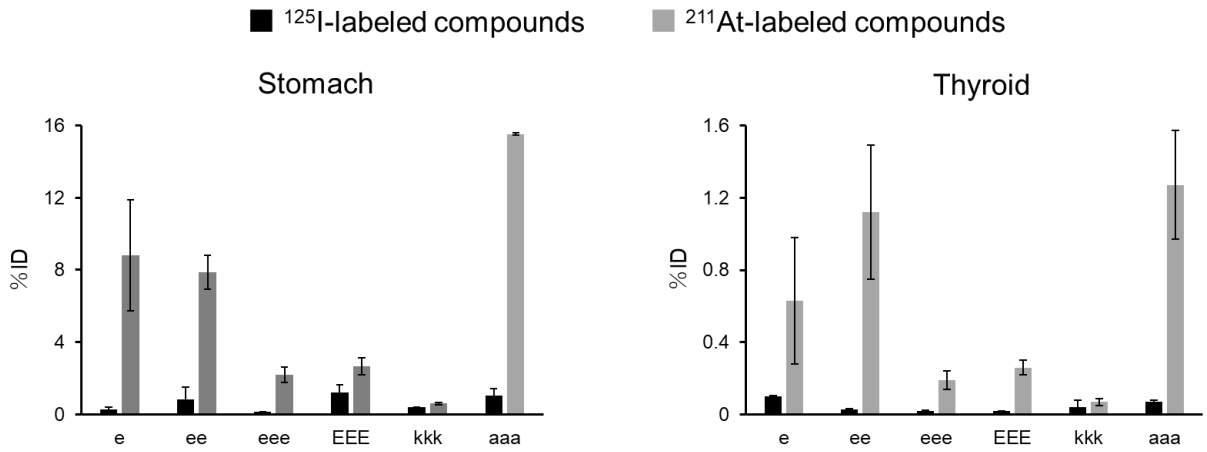


Fig. 2. Accumulation of ^{211}At/^{125}I-labeled compounds in the stomach at 1 h after injection into normal mice.

2. CONCLUSIONS

The results of this study suggest that in vivo stability of ^{211}At-labeled compounds prepared using astatobenzoyl moiety could be improved by increasing the molecular size. Although the choice of constituent amino acids of oligopeptides affected the stability, oligopeptides consisting of D-lysine or D-glutamic acid significantly improved the in vivo stability of the carbon-astatine bond in astatobenzoyl moiety. Because the tripeptide linkers such as kkk and eee can be easily conjugated with astatobenzoyl moieties, the approach introducing the linkers may be useful to produce ^{211}At-labeled proteins with high stability against in vivo deastatination.

ACKNOWLEDGMENTS

This work was supported in part by the Inohana Foundation (Chiba University) Grant-in-Aid (IFCU-2024-01) and a Grant-in-Aid for Fukushima Institute for Research, Education and Innovation.

References

[1] G. Vaidyanathan et al., *Curr. Radiopharm.*, **1**, 177 (2008).
[2] H. Suzuki et al., *J. Med. Chem.*, **65**, 15846 (2021).
[3] Y. Kaizuka et al., *EJNMMI Radiopharm. Chem.*, **9**, 17 (2024).
[4] H. Suzuki et al., *EJNMMI Radiopharm. Chem.*, **9**, 48 (2024).

Copyright on 7th Asia-Pacific Symposium on Radiochemistry 2025

7th Asia-Pacific Symposium on Radiochemistry *September 14 ~ 19, 2025 • Kunibiki Messe • Shimane, Japan*

Analysis of cell death induced by short-lived alpha-emitting radionuclides

Soichiro Magara[1], Koki Mayusumi[1], Erina Hilmayanti[1], Kazuhiro Ooe[2,3], Atsushi Toyoshima[2,3], Koichi Fukase[1,2,3], Kazuya Kabayama[1,2,3]

[1]*Department of Chemistry, Graduate School of Science, The University of Osaka: 1-1Machikaneyama, Toyonaka, Osaka, 560-0043*
[2]*Forefront Research Center, Graduate School of Science, The University of Osaka: 1-1Machikaneyama, Toyonaka, Osaka, 560-0043*
[3]*Institute for Radiation Sciences, The University of Osaka: 1-1Machikaneyama, Toyonaka, Osaka, 560-0043*

Targeted alpha therapy (TAT) is a treatment approach that involves the accumulation of alpha-emitting radionuclides in tumor tissues to induce selective cancer cell killing. In our previous studies, we observed that immunizing mice with cancer cells that were damaged or killed by alpha-emitting radionuclides and subsequently transplanted highly metastatic cancer cells led to a significant suppression of lung metastasis. This suppression is believed to be induced by the activation of immune cells via damage-associated molecular patterns (DAMPs) released by irradiated cancer cells. However, the precise mechanism by which alpha radiation activates immune cell responses remains unclear. In this study, we examined the functional and morphological changes induced by alpha-emitting radionuclides in cancer cells. Our findings suggest that the alpha particles emitted by astatine-211 (^{211}At) induce the dose-dependent expression of senescence-associated β-galactosidase (SA-β-Gal) in B16F10 murine melanoma cells, indicating the potential induction of cellular senescence.

1 Introduction

Radionuclide therapy is one of the cancer treatment modalities that utilizes radioactive isotopes to selectively deliver radiation to tumor tissues, thereby inducing cytotoxic effects [1]. The primary mechanism underlying its therapeutic efficacy involves the induction of DNA damage, particularly single-strand breaks (SSBs) and double-strand breaks (DSBs), which ultimately lead to cancer cell death. [1] In recent years, targeted alpha therapy (TAT), which employs alpha-emitting radionuclides, has garnered significant attention. Among the various forms of ionizing radiation, alpha particles are characterized by their high linear energy transfer (LET) and short path length, enabling them to induce complex and irreparable DNA DSBs within tumor cells while minimizing collateral damage to the surrounding healthy tissues [1, 2].

One of the most promising alpha-emitting radionuclides is astatine-211 (^{211}At), which has a relatively short half-life of 7.2 hours and emits only alpha particles during its decay. Importantly, ^{211}At can be produced without a nuclear reactor, making it readily accessible via cyclotron facilities in Japan. Our previous studies demonstrated that immunizing mice with cancer cells damaged or killed by alpha-emitting radionuclides resulted in marked suppression of pulmonary metastasis upon subsequent challenge with highly metastatic tumor cells. This antimetastatic effect is believed to be mediated by immunogenic cell death (ICD), a form of cell death that activates the immune system through the release of damage-associated molecular patterns (DAMPs) from irradiated cancer cells [3-6]. Despite these promising findings, precise cellular alterations induced by alpha radiation that trigger immune activation remain unclear. In this study, we aimed to characterize the functional and phenotypic changes in cancer cells exposed to alpha-emitting radionuclides to elucidate the mechanisms underlying their immunogenicity.

2 Result

As the alpha-emitting radionuclide used in this study, ^{211}At was selected due to its availability through domestic cyclotron production. ^{211}At is a short-lived nuclide with a half-life of 7.2 hours that emits alpha particles, making it a promising candidate for targeted alpha therapy in nuclear medicine.

To evaluate whether cancer cells damaged by ^{211}At undergo apoptosis or necrosis, we first performed flow cytometric analysis on B16F10 murine melanoma cells treated with either a chemotherapeutic agent or ^{211}At for 24 hours. Our analyses revealed a dose-dependent activation of caspases in response to ^{211}At exposure, suggesting that apoptosis may be partially involved under certain conditions.

Next, we assessed the impact of ^{211}At on cell viability and membrane integrity using the WST-8-based MTT and lactate dehydrogenase (LDH) release assays. The MTT assay indicated a time-dependent decrease in metabolically active cells following ^{211}At treatment, implying the suppression of cell proliferation. Interestingly, however, the LDH assay showed no detectable release of LDH into the culture supernatant under the same conditions, suggesting that the cell membrane integrity was preserved despite the inhibition of cell growth.

These findings implied that ^{211}At may induce a cytostatic effect without causing overt cell membrane disruption under certain conditions. This observation led us to hypothesize that alpha radiation from ^{211}At might induce cellular senescence in B16F10 melanoma cells. Cellular senescence is defined as a state of stable cell cycle arrest in which cells

Copyright on 7th Asia-Pacific Symposium on Radiochemistry 2025

remain metabolically active but no longer proliferate in response to mitogenic stimuli [7]. To test this hypothesis, we examined whether ^{211}At treatment induces a senescent phenotype. We found that ^{211}At exposure led to a dose-dependent expression of senescence-associated β-galactosidase (SA-β-Gal), indicating that cellular senescence was induced under specific conditions.

3 CONCLUSIONS

This study demonstrated that the alpha-emitting radionuclide ^{211}At induced diverse cellular responses, including apoptosis and cellular senescence, in the murine melanoma cell line B16F10. Notably, ^{211}At treatment suppressed cell proliferation without compromising membrane integrity under certain conditions, suggesting induction of cellular senescence. These findings not only contribute to a better understanding of the mechanisms underlying ^{211}At-induced cell death and senescence but also provide a potential basis for the development of novel cancer immunotherapeutic strategies involving immunogenic cell death.

ACKNOWLEDGMENTS

We would like to take this opportunity to thank Dr. Hiromitsu Haba and Dr. Xiaojie Yin (RIKEN Nishina Center for Accelerator Science) for their cooperation in producing and supplying ^{211}At for this study.

References

[1] Hosono M. *Istope News*, **711**, 2 (2013).
[2] Tsuji A. *Drug Deliv. Syst.*, **35**, 121 (2020).
[3] Casares N. *et al. J. Exp. Med.* **202**, 1691 (2005).
[4] Galluzzi L. *et al. Oncoimmunology* **2**, e26536 (2013).
[5] Dmitri V. K. *et al. Nat. Rev. Cancer* **12**, 860 (2012).
[6] Krysko O. *et al. Cell Death and Disease*, **4**, e631 (2013).
[7] Hayflick L, and Moorhead P. S. *Exp Cell Res.* **25**, 585 (1961)

Copyright on 7th Asia-Pacific Symposium on Radiochemistry 2025

7th Asia-Pacific Symposium on Radiochemistry *September 14 ~ 19, 2025 • Kunibiki Messe • Shimane, Japan*

Structural Stability of Radio-activated Gold Compounds via Neutron Irradiation

Kazuki Kajiyama[1], Akina Mitsukai[1], Masashi Murakami[2], Yoshifumi Shirakami[2], Koichi Takamiya[3], Jun Kataoka[4], Atsushi Toyoshima[2]

[1]*Graduate School of Science, The University of Osaka, Osaka, 560-0043, Japan,* kajiyama@irs.osaka-u.ac.jp, mitsukai@irs.osaka-u.ac.jp
[2]*Institute for Radiation Sciences, The University of Osaka, Osaka, 560-0043, Japan,* murakami@irs.osaka-u.ac.jp, yoshifumi_shirakami@irs.osaka-u.ac.jp, toyo@irs.osaka-u.ac.jp
[3]*Institute for Integrated Radiation and Nuclear Science, Kyoto University, Osaka, 590-0494, Japan,* takamiya.koichi.2u@kyoto-u.ac.jp
[4]*Research Institute for Science and Engineering, Waseda University, Tokyo, 169-8050, Japan,* kataoka.jun@waseda.jp

1 Introduction

Radiopharmaceuticals play a crucial role in cancer diagnosis and treatment. These are typically synthesized by chemically labeling a precursor compound with a suitable radioisotope. However, this labeling process is chemically complicated and time-consuming. The present study aims to develop an alternative approach by radioactivating a targeted atom in a pharmaceutical compound via neutron irradiation. When an atom is neutron-activated, it emits prompt gamma rays, which generate recoils on the atom, possibly affecting the molecular structure. In this study, we investigated the structural stability of Auranofin, a gold-containing drug, by neutron irradiation and evaluated molecular degradation caused by recoil energy.

2 Experiments

Neutron irradiation of Auranofin with 0.1 mg vacuum-sealed in a quartz tube was performed at the Kyoto University Research Reactor under the following conditions: thermal power of 5 MW, average thermal neutron flux of 3×10^{13} n/cm²·s, and an irradiation time of 1 hour. The irradiated sample was recovered with 1 mL of acetone, evaporated to dryness, and dissolved in 0.5 mL of acetonitrile.
High performance liquid chromatography (HPLC) was used to assess the stability of the radio-activated Auranofin. The system was equipped with a UV detector for identifying non-activated Auranofin and a NaI detector for detecting ^{198}Au compounds. The non-destroyed fraction of the radio-activated Auranofin was determined by analyzing the radioactivity elution in comparison with the retention time of non-irradiated Auranofin.

3 Results

Radio-activated Auranofin was produced by neutron irradiation with a measured radioactivity of 2.4±0.1 MBq. The recovery rate of ^{198}Au using acetone was 99.5±0.3%. HPLC analysis revealed that the main peak detected by the NaI detector is determined to be 74% of the injected radioactivity. Comparison with the data measured with the UV detector confirmed that this peak is attributed to radio-activated Auranofin. Additionally, a few peaks and non-eluting components, corresponding to approximately 26%, were also observed, which are probably decomposed by-products. This suggests that structural alterations were induced by recoil energy.

4 Conclusion

We studied the synthesis of radio-activated Auranofin by neutron irradiation and evaluated its structural stability. The results confirmed that radio-activated Auranofin can be obtained with high recovery efficiency, although partial degradation occurs due to recoil energy. This provides insights into optimizing the stability of neutron-activated radiopharmaceuticals. In this conference, we will also present experimental results using other gold-based pharmaceuticals and discuss decomposition mechanisms. In the future, the applicability of this method to other gold-containing pharmaceuticals will be explored to expand its potential in nuclear medicine.

ACKNOWLEDGMENTS

This work was supported by JST ERATO (Grant No. JPMJER2102).

7th Asia-Pacific Symposium on Radiochemistry *September 14 ~ 19, 2025 • Kunibiki Messe • Shimane, Japan*

Development of Dual-Modality Microspheres Containing Gold Nanoparticles for Radioembolization: X-ray CT and SPECT-Visible

Koino Nakamura[1], Naoyuki Ukon[2], Kohshin Washiyama[2], Daichi Kuroiwa[3], Hirofumi Sekino[3], Hiroshi Ito[3], Yoshitaka Takagai[1]

[1]*Faculty of Symbiotic Systems Science, Fukushima University: 1 Kanayagawa, Fukushima, Fukushima 960-1296, Japan, and s015@ipc.fukushima-u.ac.jp*
[2] *Advanced Clinical Research Center, Fukushima Medical University: 1 Hikarigaoka, Fukushima, Fukushima, 960-1295, Japan and kwashi@fmu.ac.jp*
[3]*School of medicine, Fukushima Medical University: 1 Hikarigaoka, Fukushima, Fukushima, 960-1295, Japan and h-ito@fmu.ac.jp*

Radioembolization using radioactive microspheres has been expected in the treatment of liver cancer. Single-photon emission computed tomography (SPECT) is commonly used to localize the distribution of these particles post-injection. However, once radioactivity decays, visualization becomes difficult. To overcome this limitation, microspheres that are visible in both SPECT and X-ray computed tomography (CT) are required - such dual-modality systems have been challenging. In this study, we developed microspheres containing gold nanoparticle (AuNPs-MS) adsorbed with an iodinated X-ray contrast agent. The adsorption conditions were optimized, and the microspheres were evaluated for X-ray visibility and quantitative imaging performance. The iodine loading was quantified using X-ray fluorescence (XRF) analysis in the points of both CT and radioactive imaging modalities.

1. INTRODUCTION

Radioembolization with radioisotope-labeled microspheres has emerged as a targeted therapeutic approach for hepatic tumors. While SPECT enables post-administration tracking of these particles, the imaging is no longer feasible after radionuclide decay. Thus, enabling visibility via X-ray CT is a critical requirement. In this study, we developed AuNPs-MS with enhanced CT visibility by incorporating an iodinated contrast agent. We aimed to evaluate their imaging performance and establish a quantification method for iodine loading.

2. EXPERIMENTS

The base material, spherical polymeric microspheres (average particle size: 60 μm), were zwitterionized via organic synthesis. The synthesized resins were evaluated using Fourier transform infrared spectrophotometer (FT-IR). Gold nanoparticles were encapsulated within the synthesized amphoteric ion-exchange microspheres. The gold nanoparticles were prepared by reducing gold (III) chloride trihydrate with trisodium citrate. The resulting gold nanoparticle-containing microspheres were thinned using a focused ion beam (FIB) and observed by scanning transmission electron microscopy (STEM). The adsorption of an X-ray contrast agent onto the AuNPs-MS was investigated. In this study, Lipiodol, a hydrophobic iodine-based contrast agent, was used. AuNPs-MS and the X-ray contrast agent solution were placed in microtubes, shaken at room temperature, and the supernatant was collected. The supernatant was dropped onto filter paper, dried, and the iodine content was measured using an XRF. The adsorption rate and amount were calculated based on the X-ray intensity of the solution before and after adsorption. AuNPs-MS samples containing different amounts of the X-ray contrast agent were prepared and sealed in 1 cm-square plastic cells. These samples were imaged using X-ray CT. A positron emission tomography (PET)/SPECT/CT system for small animals was used to evaluate the visibility of the samples at radioisotope laboratory rooms of Fukushima Medical University.

3. RESULTS AND DISCUSSION

The zwitterionized microspheres were measured by FT-IR to confirm their binding. The synthesized AuNPs-MS was visually pink. Observation of the interior of the AuNPs-MS using TEM revealed spherical gold nanoparticles monodispersed in microspheres. The size of the encapsulated gold nanoparticles was 6.8 ± 2.4 nm (n=83), indicating that the concentration of gold nanoparticles was uniform from the surface layer to the inner 4 μm. In the adsorption experiment of X-ray contrast agent on AuNPs-MS, more X-ray contrast agent was adsorbed when gold nanoparticles were present. This is thought to be because the presence of gold nanoparticles is essential for encapsulation of the X-ray contrast agent and because of the high affinity between gold and the iodine atoms in the X-ray contrast agent. Quantitative evaluation of visibility by X-ray CT showed that CT values increased in proportion to the increase in X-ray contrast agent content, resulting in improved visibility.

Copyright on 7th Asia-Pacific Symposium on Radiochemistry 2025

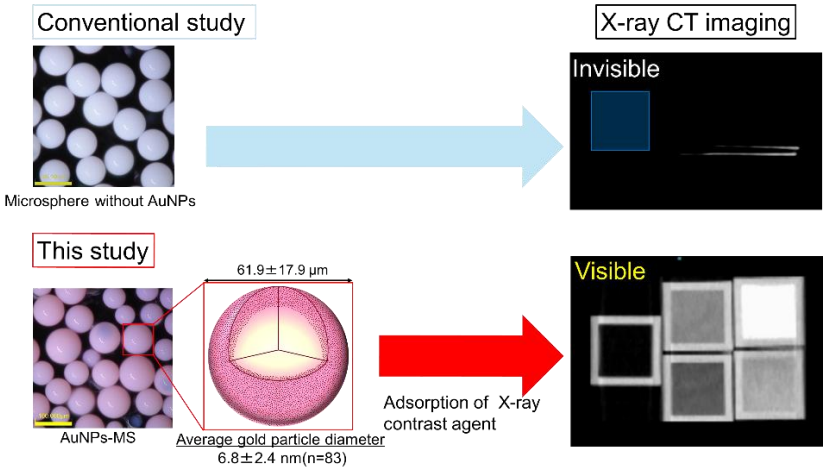


Figure 1 Conceptual diagram comparing X-ray visibility of previously reported and present microspheres

4. CONCLUSION

AuNPs-MS was synthesized and evaluated on the surface and from the inside of it. The adsorption of lipiodol on AuNPs-MS was investigated, and the adsorption rate and amount were calculated from the X-ray intensity obtained from XRF measurements. The results showed that lipiodol can be quantitatively included in AuNPs-MS. X-ray CT imaging showed that the inclusion of iodine contrast agent in AuNPs-MS improved the visibility of AuNPs-MS compared to the case without the inclusion of iodine contrast agent.

ACKNOWLEDGMENTS

This research was supported by Japan Agency for Medical Research and Development (AMED) under Grant Number JP23ama221605 and JP24ama221605.

Synthesis and evaluation of mPEG-modified [^{211}At]AuNP(s) :Towards the development of cancer treatment through intratumoral administration

Yuichiro Kadonaga[1], Hiroki Kato[1], Hiroaki Shimamoto[2], Xuhao Huang[3], Erina Hilmayanti[4], Kazuhiro Ooe[5], Atsushi Shimoyama[6], Kazuya Kabayama[4], Xiaojie Yin[7], Hiromitsu Haba[7], Masashi Murakami[4], Atsushi Toyoshima[4], Koichi Fukase[4]

[1]*Department of Advanced Radioisotope Medicine, Institute for Radiation Sciences, The University of Osaka, 2-4 Yamadaoka, Suita 565-0871, Osaka, Japan, kadonaga.yuuichirou.med@osaka-u.ac.jp, kato.hiroki.med@osaka-u.ac.jp*
[2]*Department of Oral and Maxillofacial Radiology, Graduate School of Dentistry, The University of Osaka, 1-8 Yamadaoka, Suita, Osaka 565-0871, JAPAN, shimamoto.hiroaki.dent@osaka-u.ac.jp*
[3]*The University of Osaka, Immunology Frontier Research Center (IFReC), 3-1 Yamadaoka, Suita, Osaka 565-0871, Japan, huang@biken.osaka-u.ac.jp*
[4]*Interdisciplinary Research Center for Radiation Sciences, Institute for Radiation Sciences,The University of Osaka, 2-4 Yamadaoka, Suita 565-0871, Osaka, Japan, hilmayantie22@chem.sci.osaka-u.ac.jp, kaba@irs.osaka-u.ac.jp, murakami@irs.osaka-u.ac.jp, toyo@irs.osaka-u.ac.jp, koichi@chem.sci.osaka-u.ac.jp*
[5]*Radioisotope Research Center, Institute for Radiation Sciences, The University of Osaka, 2-4 Yamadaoka, Suita 565-0871, Osaka, Japan, ooe@rirc.osaka-u.ac.jp*
[6]*Department of Chemistry, Graduate School of Science, The University of Osaka, 1-1, Machikaneyama, Toyonaka, Osaka 560-0043, Japan, ashimo@chem.sci.osaka-u.ac.jp*
[7]*Nuclear Chemistry Group, Nishina Center for Accelerator-Based Science, RIKEN 2-1 Hirosawa, Wako 351-0198, Saitama, Japan, yinxj04@impcas.ac.cn, haba@riken.jp*

1. Introduction

Radionuclide therapy by using astatine-211 (^{211}At) attracts attention due to its high therapeutic efficacy and low side effects. ^{211}At can induce DNA double-strand break by emission of alpha particles with a high linier transfer (LET). Therefore, ^{211}At should effectively destroy tumor. Additionally, alpha particle irradiates tumor tissues without damaging normal tissues if cancer-selective accumulation of ^{211}At is enabled. As other characteristics, ^{211}At rapidly decays after accumulating cancer cells due to its short half-life (7.2 h), and tiny amount of daughter nuclides (^{207}Bi and ^{207}Pb) show negligible toxicity. Hence, outpatient treatment can be possible and improve the quality of life (QOL) for cancer patients. We previously reported sodium astatide ([^{211}At]NaAt) as a thyroid cancer treatment agent [1]. Since 2021, the clinical trial of [^{211}At]NaAt has been on-going. Although ^{211}At selectively accumulates thyroid due to a halogen, its property must be counteracted when targeting other cancers. Therefore, we employed to support ^{211}At on gold nanoparticles (AuNP). In 2021, we disclosed significant anti-tumor activity by intratumoral administration of pegylated [^{211}At]AuNP ([^{211}At]AuNP-S-mPEG) with C6-glioma (brain tumor) xenograft rats and PANC-1 (Pancreatic cancer) xenograft mice [2]. In this demonstration, we revealed the high potential of [^{211}At]AuNP for cancer treatment. Thus, we next evaluated the therapeutic effect for tongue cancer.

2. Experiment

We first synthesized various sizes of AuNP-S-mPEG(s) by using 2-30 nm of AuNP and different length of mPEG-SH (Mn. 1k-20k). Briefly, a solution of methoxypolyethylene glycol thiol (mPEG-SH) in H_2O was added to a solution of AuNP in H_2O at room temperature. The reaction mixture was stirred at the same temperature for 2 h. After 2 h, the resulting mixture was purified by ultrafiltration with H_2O for 10 min, repeated several times. The purified AuNP-S-mPEG(s) were diluted with H_2O. Next, a solution of ^{211}At in H_2O was added to AuNP-S-mPEG and stirred at room temperature for 15 min. After that, ^{211}At-labeled AuNP-S-mPEG ([^{211}At]AuNP-S-mPEG) were locally administered them to SAS (tongue cancer) xenograft mice.

3. Results

^{211}At-labeling of all AuNP-S-mPEG(s) smoothly proceeded in >95% RCY(s) (Fig. 1). For in vivo experiments, significant anti-tumor activities were shown. Additionally, Noticeable weight loss was not observed in the mice, suggesting that the side effects of the [^{211}At]AuNP-S-mPEG(s) were low.

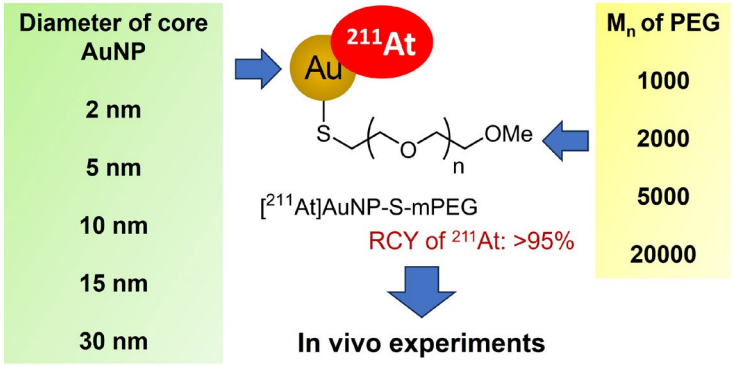


Fig. 1. Preparation of [^{211}At]AuNP-S-mPEG(s).

ACKNOWLEDGMENTS

This work was supported by JSPS KAKENHI, grant numbers JP23K06049 and JP24H00804, and JST ERATO Grant Number JPMJER2102

References

[1] Watabe, T.; Kaneda-Nakashima, K.; Liu, Y.; Shirakami, Y.; Ooe, K.; Toyoshima, A.; Shimosegawa, E.; Fukuda, M.; Shinohara, A.; Hatazawa, J. Enhancement of ^{211}At Uptake via the Sodium Iodide Symporter by the Addition of Ascorbic Acid in Targeted α-Therapy of Thyroid Cancer. *J. Nucl. Med.* **2019**, *60*, 1301-1307.

[2] Kato, H.; Huang, X.; Kadonaga, Y.; Katayama, D.; Ooe, K.; Shimoyama, A.; Kabayama, K.; Toyoshima, A.; Shinohara, A.; Hatazawa, J.; Fukase, K. Intratumoral administration of astatine-211-labeled gold nanoparticle for alpha therapy. *J. Nanobiotechnology* **2021**, *19*, 223.

Copyright on 7th Asia-Pacific Symposium on Radiochemistry 2025

Dose-Dependent Cytotoxic Profiling of Astatine-211 for Targeted Alpha Therapy

Jumpei Ueno[1], Koki Mayusumi[1], Masayuki Takamatsu[1,2], Atsushi Shimoyama[1,2,3], Koichi Fukase[1,2,3], Kazuya Kabayama[1,2,3]

[1] *Depertment of Chemistry, Graduate School of Science, The University of Osaka: 1-1Machikaneyama, Toyonaka, Osaka, 560-0043*
[2] *Institute for Radiation Science, The University of Osaka: 1-1Machikaneyama, Toyonaka, Osaka, 560-0043*
[3] *Forefront Research Center, Graduate School of Science, The University of Osaka: 1-1Machikaneyama, Toyonaka, Osaka, 560-0043*

Targeted Alpha Therapy is a therapy in which α-ray emitting nucleus are combined with the targeting ligand to selectively accumulate on cancer cells. Astatine-211 (^{211}At), a type of α-ray emitting nuclei, has attracted attention as an excellent alpha-particle emitter. However, evaluation of the basic potency of ^{211}At and exploration of its evaluation methods are currently insufficient. Therefore, we developed a system to determine the median cytotoxic concentration of ^{211}At and to compare At-labelled drugs with existing anti-cancer drugs.

1 INTRODUCTION

Astatine-211 (^{211}At), an α-emitting radionuclide, exhibits superior therapeutic potential in targeted alpha therapy (TAT) because of its high linear energy transfer (LET) and short particle range (<70 μm), enabling precise tumor cell killing while sparing the surrounding healthy tissues. With a half-life of 7.2 hours and stable daughter nuclides, ^{211}At minimizes long-term radiation exposure risks, making it ideal for clinical application.

Despite ongoing trials for differentiated thyroid and castration-resistant prostate cancers, differentiated thyroid cancer treatment [^{211}At]NaAt[1] and castration-resistant prostate cancer treatment [^{211}At]PSMA-5[2] are being conducted at Osaka University Hospital. However, quantitative methods to evaluate its efficacy remain underdeveloped, hindering direct comparison with conventional anticancer drugs.

At present, the basic potency of ^{211}At has not been adequately assessed. Therefore, we established data and methods to quantitatively compare the efficacy of ^{211}At in vitro. Generally, IC_{50} and EC_{50} are used to evaluate anti-cancer drugs, but since ^{211}At decays unlike conventional drugs, a method to quantitatively compare the efficacy of ^{211}At that takes this into account is needed. To solve this problem, we propose to use a parameter we call “total dose”, which is obtained by integrating the decay curve of ^{211}At.

1.1 Purpose

This study aimed to (1) establish a robust in vitro system for quantifying ^{211}At potency using a novel “total dose” parameter integrating radioactive decay, (2) determine the median cytotoxic concentration (CC_{50}) of free ^{211}At, and (3) enable cross-comparison between ^{211}At-labeled compounds and non-radioactive therapeutics using standardized concentration units.

1.2 Method

Mouse Lewis lung carcinoma (LLC) cells, selected for high radiosensitivity, were seeded in 96-well plates and exposed to ^{211}At under two conditions: continuous exposure or removal after 2 hours. Cell viability was assessed 72 hours post-treatment using Cell Counting Kit-8. The “total dose” (Bq·s/mL) was calculated by integrating ^{211}At’s decay curve ($t_{1/2}$ = 7.2 h) over exposure duration, accounting for physical decay and intracellular retention(Fig.1). Dose-response curves were analyzed to derive CC_{50} values in radioactivity (kBq/mL) units.

$$T.D. = \int A_0 \exp(-\lambda t)\, dt \quad (1)$$

In Formula(1), *T.D.* represents total dose,
A_0 represents initial dose,
λ represents half-life and t represents time.

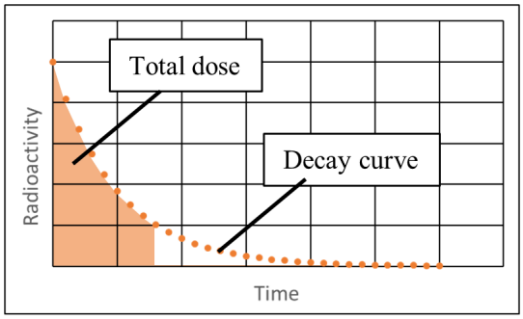
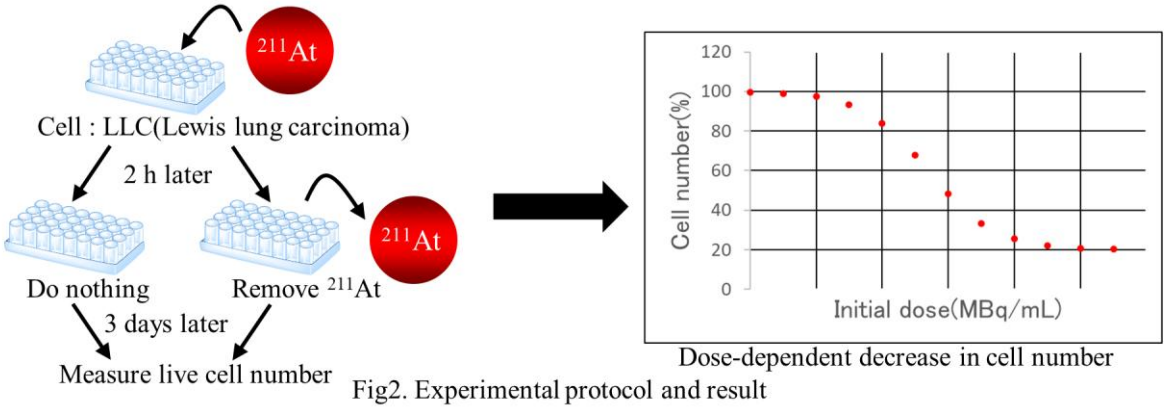


Fig1. Method for calculating total dose

1.3 Result

Free ^{211}At induced dose-dependent cytotoxicity, with an CC_{50} of 125 kBq/mL. Total dose analysis revealed that cell viability correlated exclusively with cumulative energy deposition, independent of initial activity concentration or exposure duration (Fig2). Notably, cells exposed transiently (2-hour exposure) showed equivalent lethality to

continuously irradiated cells when total doses were matched, contrasting sharply with β-emitters, where prolonged low-dose exposure enhances survival. We analyzed the results using the total dose and obtained a value for the total dose with a cell viability of 50%, using the unit as Bq·s/mL. This value could be converted into mol/L and compared with existing anticancer drugs. Furthermore, comparison of the results for wells in which ^{211}At was removed midway and those in which it was not, showed that cell viability was independent of the concentration of ^{211}At and depended on the total dose.



Dose-dependent decrease in cell number

Fig2. Experimental protocol and result

1.4 Discussion

The total dose model successfully decouples ^{211}At's efficacy from temporal administration variables, a critical advancement for standardizing TAT dosimetry. Similar experiments with β-ray-emitting radionuclides in previous studies have shown that the lower the intensity of the β-rays, the higher the cell survival rate, even when the total dose of β-rays to the cells is the same.[3] Unlike β-emitters, where dose rate effects dominate, ^{211}At's high-LET α-particles induce irreparable DNA damage regardless of the exposure time, validating its unique radiobiological profile. The conversion of CC_{50} to molar units enables direct benchmarking against small-molecule anticancer agents, addressing a longstanding barrier in translational research.

2. CONCLUSIONS

We determined the median cytotoxic concentration of ^{211}At by measuring the viability of At-treated cells and constructed a system that allowed us to compare At-labelled drugs with existing anti-cancer drugs.By comparing the number of cells in wells in which ^{211}At was removed during the process with those in which it was left in, we found the total dose of ^{211}At that its cell number depends on the total dose.

ACKNOWLEDGMENTS

We are grateful to Dr. T. Watabe, Dr. K. Kaneda, Dr. A. Toyoshima and all members in Institute for Radiation Science in The University of Osaka for collaboration of this work. We wish to thank Dr. T. Sato in JAEA for advice on experimental analysis. This work is supported by JSPS KAKENHI (20H05675, 24K23086, 25H00006).

We would like to take this opportunity to thank Dr. Hiromitsu Haba (RIKEN Nishina Center for Accelerator Science) for their cooperation in producing and supplying ^{211}At for this study.

References

[1] Watabe, T., Nakashima, K., Liu, Y., Shirakami, Y., Ooe, K., Toyoshima, A., Shimosegawa, E., Fukuda, M., Shinohara, A., Hatazawa, J. "Enhancement of ^{211}At Uptake via the Sodium Iodide Symporter by the Addition of Ascorbic Acid in Targeted α-Therapy of Thyroid Cancer", *The Journal of Nuclear Medicine*, **60**, 1301 (2019).

[2] Watabe, T., Nakashima, K., Shirakami, Y., Kadonaga, Y., Ooe, K., Wang, Y., Haba, H., Toyoshima, A., Cardinale, J., Giesel, F. L., Tomiyama, N., Fukase, K. "Targeted α-therapy using astatine (^{211}At)-labeled PSMA1, 5, and 6: a preclinical evaluation as a novel compound", *European Journal of Nuclear Medicine and Molecular Imaging*, **50**, 849, (2023).

[3] Soroko, S. S., Skamnitskiy, D. V., Gorshkova, E. N., Kutova, O. M., Seriev, I. R., Maslennikova, A. V., Guryev, E. L., Gudkov, S. V., Vodeneev, V. A., Balalaeva, I. V., Shilyagina , N. Y. "The Dose Rate of Corpuscular Ionizing Radiation Strongly Influences the Severity of DNA Damage, Cell Cycle Progression and Cellular Senescence in Human Epidermoid Carcinoma Cells", *current issues in molecular biology*, **46**, 12, (2024).

Dosimetry in targeted alpha particle therapy with astatine-211 in single cells using Al_2O_3:C, Mg-based fluorescent nuclear track detector

Jun Hu[1], Tamon Kusumoto[1], Satoshi Kodaira[1]

[1] *Institute for Radiological Sciences, National Institutes for Quantum Science and Technology (QST), Japan.*

Alpha emitters offer the potential to deliver high linear energy transfer (LET) radiation directly to tumors, primarily due to their short path length in biological tissues (<100 μm in water). This property has garnered increasing interest in its application for targeted radionuclide therapy[1], which is currently under active investigation in clinical trials. Among these, astatine-211 (^{211}At) stands out due to its favorable radiophysical characteristics[2]. It emits a single alpha particle per decay with 100% alpha emission, minimizing the risk of unpredictable dose distribution that can result from the release of radioactive daughter nuclides—a common issue with other alpha emitters such as thorium-227, radium-223, lead-212, bismuth-212, and actinium-225, which undergo complex decay chains and may suffer from recoil-induced daughter release. In addition to its decay simplicity, ^{211}At possesses a half-life ($t_{1/2}$) of 7.2 hours, which offers a practical balance between physical decay and logistical considerations. Less than 1% of its radioactivity remains after 48 hours, potentially reducing off-target radiation exposure to normal tissues. Simultaneously, the half-life is sufficient to allow for transportation (up to approximately 3 hours) and subsequent radiolabeling procedures, with adequate activity remaining for clinical application. Due to its high LET, ^{211}At is expected to exhibit potent cytotoxicity within targeted cells. Accurate estimation of the absorbed radiation dose in the targeted area is therefore essential for evaluating the therapeutic efficacy of ^{211}At-labeled antibodies. Moreover, the overall effectiveness of treatment is influenced by the binding affinity and biological distribution of the targeting antibody, which determines the amount of radioactivity delivered to the tumor site. Because multiple alpha particle traversals are generally required to induce cell death, the number of effective "hits" per cell—and their corresponding energy deposition—varies depending on both the specific cell type and the physical characteristics of the emitted particles[3]. Thus, quantifying both the spatial energy deposition and the number of cellular hits is critical for assessing the safety, pharmacokinetics, and therapeutic potential of targeted alpha particle therapy using ^{211}At.

Aluminum oxide doped with carbon and magnesium (Al_2O_3:C,Mg)- based fluorescent nuclear track detector (FNTD) is a highly promising dosimeter for this application. It offers superior particle identification capabilities, along with high energy and spatial resolutions, and enables in situ measurement under a fluorescent microscope. It has the ability to measure and distinguish individual alpha tracks with high density, yielding a rich amount of information regarding the planar distribution, incident angle, alpha energy, and LET of individual particles[4]. In this study, we employed the FNTDs to record the 3D trajectories of alpha particle emission and estimate the residual energy deposition within single cells.

References

[1] J. Tranel, F. Y. Feng, S. S. James, and T. A. Hope, “Effect of microdistribution of alpha and beta-emitters in targeted radionuclide therapies on delivered absorbed dose in a GATE model of bone marrow,” *Phys. Med. Biol.*, 66, 3 (2021), doi: 10.1088/1361-6560/abd3ef.

[2] P. Albertsson *et al.*, “Astatine-211 based radionuclide therapy: Current clinical trial landscape,” *Front. Med.*, 9, 1076210 (2023), doi: 10.3389/fmed.2022.1076210.

[3] S. Kodaira, H. K. Li, T. Konishi, H. Kitamura, M. Kurano, and S. Hasegawa, “Validating α-particle emission from ^{211}At-labeled antibodies in single cells for cancer radioimmunotherapy using CR-39 plastic nuclear track detectors,” *PLOS ONE*, 12, 6 (2017), doi: 10.1371/journal.pone.0178472.

[4] J. Hu, T. Kusumoto, M. Janik, and S. Kodaira, “Alpha particle spectrometry in fluorescent nuclear track detectors with an automatic 3D track reanalysis algorithm,” *Radiat. Meas.*, 170, 107051 (2024), doi: 10.1016/j.radmeas.2023.107051.

Development of Astatine-Labeled Functional Proteins for Cancer Therapy

Koki Mayusumi[1], Kazuya Kabayama[1,2,3], Kazuko Kaneda-Nakashima[1,2,3], Junichi Takagi[4], Hiroaki Suga[5], Kazuhiro Ooe[2,3], Atsushi Toyoshima[2,3], Koichi Fukase[1,2,3]
[1]*Dept. of Chem., Grad. Sch. of Sci., The University of Osaka, Toyonaka, Japan, 560-0043*
[2]*FRC, Grad. Sch. of Sci., The University of Osaka, Toyonaka, Japan, 560-0043*
[3]*Inst. for Radiation Sciences, The University of Osaka, Toyonaka, Japan, 560-0043*
[4]*Inst. for Protein Research, The University of Osaka, Suita, Japan, 565-0871*
[5]*Grad. Sch. of Sci., The University of Tokyo, Bunkyo, Japan, 113-0033*

Targeted alpha therapy (TAT) is a promising approach for treating refractory cancers. We developed a novel TAT agent using astatine-211 (^{211}At), a short-lived alpha-emitter, conjugated to Mirabody (aMD4-MB), a small functional protein targeting hepatocyte growth factor receptor (HGFR), overexpressed in pancreatic cancer cells (Fig. 1).

aMD4-MB showed high binding affinity and rapid internalization into PANC-1 cells. The ^{211}At-labeled form, ^{211}At-aMD4-MB, retained binding ability and induced DNA double-strand breaks and calreticulin expression in a radiation dose-dependent manner, indicating potent cytotoxicity and immunogenic effects. In a xenograft mouse model, ^{211}At-aMD4-MB showed limited tumor accumulation but tumor growth inhibition. This suggests that rapid and efficient intracellular delivery compensates for the short half-life and limited tissue penetration of ^{211}At. Our findings highlight ^{211}At-aMD4-MB as a promising TAT agent with potential for broader application in HGFR-positive cancers.

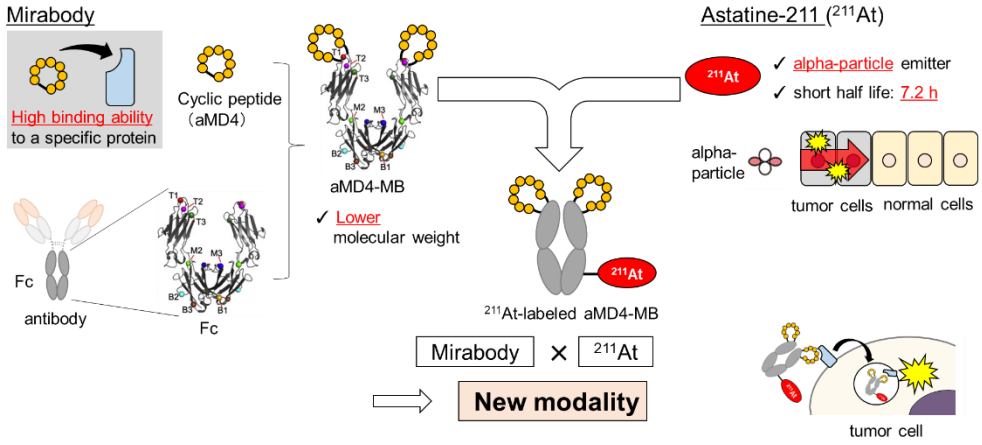


Fig. 1. Concept of this study (^{211}At-labeled aMD4-MB)

1. Introduction

In recent years, the survival rate of cancer patients has increased due to the development of cancer treatment methods. However, some cancers, such as pancreatic cancer, still have a low response rate to treatment, and there is a need to develop effective treatments. Targeted alpha therapy (TAT), in which alpha-particle emitting radionuclides administered into the body are accumulated in the tumor, is currently attracting attention. Representative alpha- particle emitting radionuclides are ^{225}Ac ($T_{1/2}$: 10 days) and ^{223}Ra ($T_{1/2}$: 11.4 days).

We use astatine-211 (^{211}At) as an alpha- particle emitter. ^{211}At is a short-lived nuclide with a half-life of 7.2 hours that emits alpha- particles and can be produced using a cyclotron. We have previously demonstrated that ^{211}At-labeled antibodies can inhibit tumor growth in mice with carcinoma, and that internalization into cells and retention in the vicinity of DNA can enhance the killing effect. However, due to the short half-life of ^{211}At, a lower molecular weight of the carrier molecule was required to improve tissue penetration for quick cancer delivery. Therefore, in this study, we used a functional protein of lower molecular weight to evaluate its ^{211}At labeling and the cytotoxic activity of the labeled entity.

2. Results

The functional protein used in this study was Mirabody, a functional molecule consisting of a cyclic peptide with high binding ability to a specific target introduced into the Fc region of an antibody, with a molecular weight about one-

Copyright on 7th Asia-Pacific Symposium on Radiochemistry 2025

third that of an antibody [1-2]. In this study, we used Mirabody (aMD4-MB), which contains a cyclic peptide (aMD4) that binds to the hepatocyte growth factor receptor (HGFR), which is highly expressed in cancer cells.

First, the high binding ability of aMD4-MB to PANC-1 cells, a human pancreatic cancer cell line, was confirmed by flow cytometry (FCM). Furthermore, the internalization ability of aMD4-MB was evaluated by FCM and live cell imaging, and it was found that aMD4-MB was rapidly internalized in as short a time as 5 minutes, indicating the high internalization ability of aMD4-MB and its usefulness as a ^{211}At carrier molecule.

Next, aMD4-MB-B_{10}, labeled with a decaborane (B_{10}) linker for binding ^{211}At to the above molecule, was prepared. This labeled form was confirmed by flow cytometry to have the same cell-binding capacity.

^{211}At was bound to aMD4-MB-B_{10} with a reaction time of 10 min, and purified by gel filtration to yield ^{211}At-aMD4-MB. The ^{211}At-labeled aMD4-MB was used to evaluate DNA double-strand breaks (DSBs) against PANC-1, and the induction of DSBs was confirmed in a radiation dose-dependent manner. Using this ^{211}At-labeled aMD4-MB, we evaluated DNA double-strand breaks (DSBs) against PANC-1 and found a radiation dose-dependent induction of DSBs. We further evaluated the plasma membrane expression of calreticulin, a type of damage-associated molecular patterns (DAMPs), and confirmed a dose-dependent expression of CRT.

Finally, in vivo ^{211}At-aMD4-MB kinetics and therapeutic effects were evaluated. ^{211}At-aMD4-MB was administered to a PANC-1-bearing xenograft mouse model, and its biodistribution was evaluated at 0.5 and 3 hours. Although accumulation in tumors was confirmed, sufficient accumulation was not observed. On the other hand, the therapeutic effect of ^{211}At-aMD4-MB on the xenograft mouse model was confirmed by tumor growth inhibition, despite the low level of tumor accumulation in the biodistribution. This may be due to the effective tumor-killing effect of aMD4-MB, which was demonstrated in vitro by its high binding capacity and rapid internalization.

3. CONCLUSIONS

In this study, we used Mirabody (aMD4-MB) as an ideal carrier molecule for TAT. Rapid and precise intracellular targeting of cancer cells is necessary to take full advantage of the short-lived and short-range properties of ^{211}At. aMD4-MB was shown to be a useful carrier for ^{211}At due to its rapid binding and internalization ability to MET-high expressing cancer cells. Furthermore, ^{211}At-aMD4-MB showed cytotoxic effects via dose-dependent DNA double-strand breaks and DAMPs induction in vitro, and rapid accumulation in tumor tissues and tumor growth inhibition in vivo. Based on these results, ^{211}At-labeled Mirabody is a new modality for TAT and is expected to be applied to a variety of cancer types in the future.

ACKNOWLEDGMENTS

This research was supported by the Consortium for Quantum Application Co-Creation (QiSS) under the Joint Research Promotion Program for Industry-Academia Co-Creation Platform (JST-OPERA). We would also like to take this opportunity to thank Dr. Hiromitsu Haba, Dr. Yang Wang and Dr. Xiaojie Yin (RIKEN Nishina Center for Accelerator Science) for their cooperation in manufacturing and supplying ^{211}At for this research.

References

[1] Mihara E, *et al*. Lasso-grafting of macrocyclic peptide pharmacophores yields multi-functional proteins *Nat. Commun*. **2021**.12, 1543
[2] Ito K, *et al*. Artificial human Met agonists based on macrocycle scaffolds *Nat. Commun*. **2015**. 6, 6373

Random and Site-Specific Conjugation of TCO to Anti-PD-L1 Monoclonal Antibodies for In Vitro Click Labeling: A Step Toward Pretargeted ImmunoPET Imaging Agents

Feng-Yun J. Huang[1], Ruey-Jing Huang[2,3], Ching-Wen Cheng[1], Kuo-Ting Chen[4]

[1]*Department of Medical Imaging and Radiological Sciences, Central Taiwan University of Science and Technology, Taichung 406053, Taiwan. Email: fyhuang@ctust.edu.tw (F.-Y.J.H.); as6167182@gmail.com (C.-W.C.)*
[2]*Department of Diagnostic Radiology, Hualien Armed Forces General Hospital, Hualien 971051, Taiwan (R.O.C.). Email: hrj0713@gmail.com (R.-J.H.)*
[3]*Hualien Hsien Association of Radiological Technologists, Hualien 97002, Taiwan (R.O.C.). Email: hrj0713@gmail.com (R.-J.H)*
[4]*Department of Chemistry, National Dong Hwa University, Hualien 974301, Taiwan. Email: ktchen26@gms.ndhu.edu.tw (K.-T.C)*

1. PURPOSE

ImmunoPET has become a critical tool for evaluating the clinical applications of immunotherapy. However, conventional immunoPET tracers, such as those labeled with zirconium-89 (^{89}Zr), have notable limitations, including high internal radiation doses and elevated background radioactivity in patients. These issues primarily stem from the relatively long half-life of ^{89}Zr and the use of direct radiolabeling methods. In recent years, pretargeted immunoPET tracers utilizing inverse electron demand Diels–Alder (IEDDA) bioorthogonal click chemistry between trans-cyclooctene (TCO) and tetrazine (Tz) have emerged as a promising strategy to overcome these drawbacks. In this study, both random and site-specific conjugation of TCO to anti-PD-L1 monoclonal antibodies (mAbs) will be performed to develop pretargeted immunoPET imaging agents based on the TCO–Tz click reaction. As the radioligand, ^{68}Ga-NOTA-Tz will be synthesized and employed in in vitro TCO–Tz click labeling experiments to validate the feasibility of this pretargeted immunoPET imaging approach.

2. MATERIALS & METHODS

Random conjugation of TCO to anti-PD-L1-mAb was performed using a lysine-based method with slight modifications from prior studies [1,2], employing a 20-fold molar excess of TCO (Fig. 1). Site-specific conjugation was achieved via enzymatic glycan modification to yield TCO–anti-PD-L1-mAb with a defined DAR of 2 (Fig. 1) [2]. Both conjugates were assessed by HPLC for chemical yield and concentration, and DAR was determined by ESI LC-MS. For the radioligand, aliquot of NOTA-Tz (10 mg/mL in DMSO) was radiolabeled with ^{68}Ga (37–370 MBq; GalliaPharm, Eckert & Ziegler) in 1 M ammonium acetate (pH 5), using a 10^5–10^6 molar excess of NOTA-Tz. The reaction was performed at room temperature with shaking (500 rpm, 20 min) [3]. Radiochemical purity and yield were analyzed by ITLC/SG and Radio-SE-HPLC (Zenix-C SEC-300; PBS; 1 mL/min). The in vitro click reaction between TCO–anti-PD-L1-mAb and ^{68}Ga-NOTA-Tz was carried out in PBS under optimized TCO:Tz ratios (500 rpm, 40 min). The resulting complex was purified using a 40 kDa Zeba spin column and analyzed by Radio-SE-HPLC.

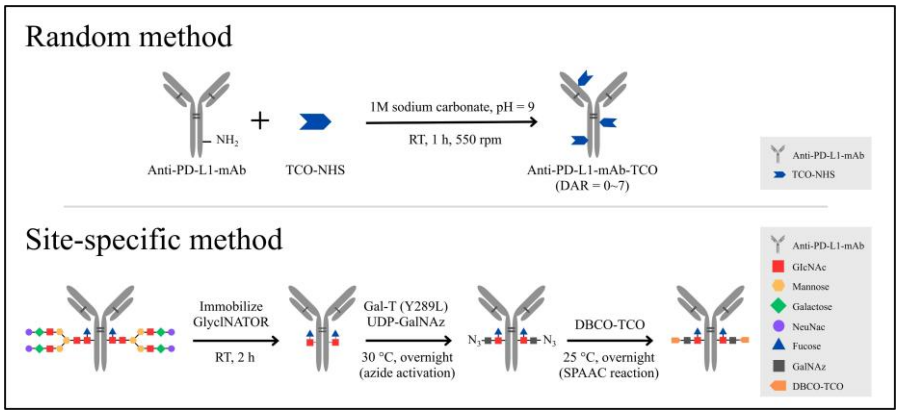


Fig. 1. Experimental flowchart for the preparation of random and site-specific TCO–anti-PD-L1-mAb conjugates.

3. RESULTS

Both random and site-specific TCO–anti-PD-L1-mAb conjugates were successfully synthesized, appearing as clear, transparent, non-aggregated solutions, with chemical yields approaching 100% as determined by HPLC. The drug-to-

antibody ratio (DAR) was measured by LC-MS and found to be 2.97 for the random conjugate (Fig. 2A, 2B) and 2.01 for the site-specific conjugate (Fig. 2C, 2D, 2E). The radiochemical yield of ^{68}Ga-NOTA-Tz exceeded 90%. Results from the in vitro IEDDA TCO–Tz click radiolabeling demonstrated rapid and efficient reactivity between TCO–anti-PD-L1-mAb and ^{68}Ga-NOTA-Tz. HPLC chromatograms confirmed the formation of the ^{68}Ga-NOTA-Tz–TCO–anti-PD-L1-mAb complex (radiochemical purity larger than 95.3%), as the radio signal from ^{68}Ga-NOTA-Tz (NaI detector) overlapped with the UV signal (280 nm) of the antibody conjugate following the click reaction (Fig. 3).

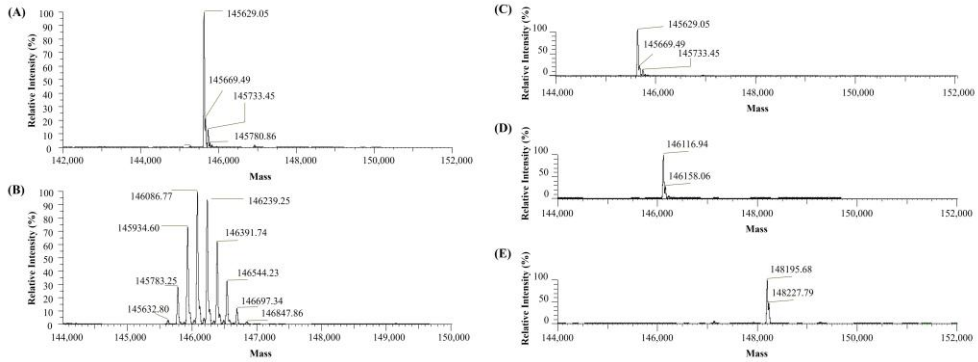


Fig. 2. LC-MS spectra of random and site-specific TCO–anti–PD–L1–mAb conjugates. (A) Unmodified anti-PD-L1-mAb (control), (B) Randomly conjugated TCO–anti-PD-L1-mAb (20× molar excess), (C) Unmodified anti-PD-L1-mAb (control), (D) Azide-modified anti-PD-L1-mAb-N_3 (site-specific, DAR = 2), (E) Site-specifically conjugated anti-PD-L1-mAb-N_3–DBCO–TCO (DAR = 2).

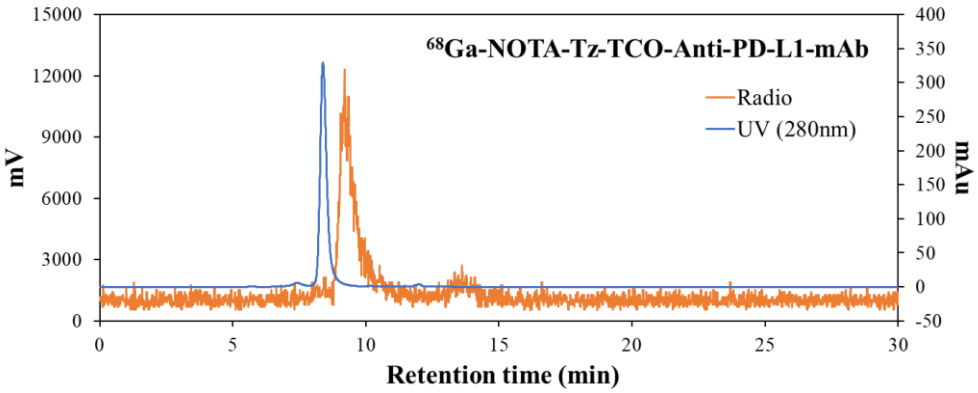


Fig. 3. Radio-SE-HPLC chromatograms of the ^{68}Ga-NOTA-Tz–TCO–anti-PD-L1-mAb complex.

4. CONCLUSIONS

In this study, random and site-specific TCO–anti-PD-L1-mAb conjugates were successfully prepared, with drug-to-antibody ratios (DARs) of 2.97 and 2.01, respectively. The in vitro click radiolabeling reaction between the TCO–anti-PD-L1-mAb conjugate and ^{68}Ga-NOTA-Tz confirmed the high reactivity and rapid kinetics of the TCO–Tz bioorthogonal system. These findings support the potential for further in vivo evaluation of pretargeted immunoPET imaging agents.

ACKNOWLEDGMENTS

This work was financially supported by the Hualien Armed Forces General Hospital in Taiwan (grant numbers: HAFGH_A_112002 and HAFGH_A_113001) and Taichung Veterans General Hospital/Central Taiwan University of Science and Technology Joint Research Program in Taiwan (grant numbers: TCVGH-CTUST1127701 and TCVGH-CTUST1137701).

References

[1] S. C. Tsai et al. MDPI, IJMS, 2023, 24, 17132 (2023)
[2] Y. C. Chen et al. Springer, JRNC, 333, 5997-6005 (2024)
[3] P. E. Edem et al. MDPI, Molecules, 25, 463 (2020)

7th Asia-Pacific Symposium on Radiochemistry *September 14 ~ 19, 2025 • Kunibiki Messe • Shimane, Japan*

SYNTHESIS AND EVALUATION OF ASTATINE-211-LABELED FAP-INHIBITOR RADIOPHARMACEUTICALS

Masayuki Takamatsu[1,2], Atsushi Shimoyama[1,2,3], Ayaka Aso[1], Taketo Toda[1], Jumpei Ueno[1], Koki Mayusumi[1], Kazuya Kabayama[2,3], Yuichiro Kadonaga[2], Yoshifumi Shirakami[2], Tadashi Watabe[2,3], Taku Yoshiya[4], Kazuhiro Ooe[3], Atsushi Toyoshima[3], Hiromitsu Haba[5], Jens Cardinale[6], Frederik Lars Giesel[6], Kazuko Kaneda-Nakashima[1,2], Koichi Fukase[1,2]

[1]*The University of Osaka Graduate School of Science: 1-1Machikaneyama, Toyonaka, Osaka, 560-0043*
[2]*The University of Osaka Institute for Radiation Science: 1-1Machikaneyama, Toyonaka, Osaka, 560-0043*
[3]*The University of Osaka Graduate School of Medicine: 1-1Machikaneyama, Toyonaka, Osaka, 560-0043*
[4]*Peptide Institute, Inc., 7-2-9 Saito-asagi, Ibaraki, Osaka, 567-0085*
[5]*RIKEN Nishina Center for Accelerator-Based Science, 2-1 Hirosawa, Wako, Saitama, 351-0198*
[6]*University Hospital Düsseldorf, Moorenstr. 5, Düsseldorf, Germany, 40225*

Targeted alpha therapy, a cancer therapeutic method using alpha-particle emitting radionuclides, received considerable attention recently (Fig.1). Alpha-particles have a high linear energy transfer over a short path length (only a few cells). Thus, the accumulation of the labeled molecules to cancer tissue enables cancer treatment with low side effects. Fibroblast activation proteins (FAP) are overexpressed in tumor stroma and have received attention in radionuclide therapy as target molecule. FAP inhibitor (FAPI) is used as probe to deliver the nuclide to cancer tissues.

In this study, we designed and synthesized astatine-211-labeled FAPIs with a polyethylene glycol (PEG) linker or piperazine (PIP) linker between the FAP targeting site and the astatine-211 binding site (Fig.2). Dihydroxyboryl-astatine substitution reaction was employed for the astatine labeling of FAPI derivatives. We evaluated the effect of linker structure in FAP selectivity by using FAPα-overexpressing HEK293 cells and the lung cancer cell line A549, observing similar trends in both cases. On the other hand, elongation of the PEG linker tended to decrease FAP selectivity. In mice model, antitumor effect was nearly identical between PEG and PIP linker. While most of the currently synthesized FAPIs feature PIP linkers, our study revealed that PEG linkers show comparable performance. PEG linkers are also anticipated to serve as linkers in FAPI derivatives, given their widespread use due to their high biocompatibility and hydrophilicity.

1 INTRODUCTION

A Fibroblast activation protein (FAP), overexpressed in tumor stroma, serves as a critical target for molecular cancer therapies, facilitating specific delivery while minimizing adverse effects. FAP inhibitors (FAPIs) selectively accumulate in tumor stroma and have shown utility in cancer imaging and therapy. Recent advancements in radionuclide-based FAPIs, such as ^{68}Ga- and ^{18}F-labeled variants for PET imaging and ^{177}Lu- and ^{225}Ac-labeled compounds for therapy, highlight their clinical potential. Among α-emitters, ^{211}At offers advantages due to its short half-life (7.2 h) and decay chain simplicity, improving therapeutic outcomes and patient quality of life. This study synthesizes and evaluates 211At-labeled FAPI derivatives for their potential in targeted α-particle radiotherapy, focusing on their antitumor efficacy, biodistribution, and safety.

1.1 Method

^{211}At was produced using the ^{209}Bi(α, 2n)211At reaction, followed by dry distillation purification. Five FAPI precursors with dihydroxyboryl groups (B-FAPI) were labeled with ^{211}At via substitution reactions, yielding derivatives (^{211}At-FAPI1 to ^{211}At-FAPI5) with radiochemical yields (RCYs) ranging from 15% to 100% and purities exceeding 78%. In vitro assays assessed cellular uptake of the compounds in HEK293 and A549 cells and their FAPα-overexpressing derivatives, confirmed through flow cytometry. Biodistribution studies evaluated tumor and organ uptake of ^{211}At-FAPI1 and ^{211}At-FAPI5 in mice at 1 and 3 hours post-injection. Therapeutic efficacy was tested using PANC-1 xenograft mice, divided into control and treatment groups, with tumor growth and body weights monitored for four weeks.

1.2 Result and Discussion

^{211}At-labeled FAPI derivatives were synthesized with high yields and purities. Cellular uptake studies demonstrated significant selectivity for FAPα-overexpressing cells compared to parental cells, confirming target specificity. Biodistribution analysis revealed favorable tumor uptake and minimal off-target accumulation for ^{211}At-FAPI1 and ^{211}At-FAPI5, with ^{211}At-FAPI5 showing slightly superior retention. Therapeutic experiments showed that both compounds

significantly inhibited tumor growth in PANC-1 xenograft mice compared to controls. No significant toxicity or adverse effects were observed, as indicated by stable body weights and normal behavior.

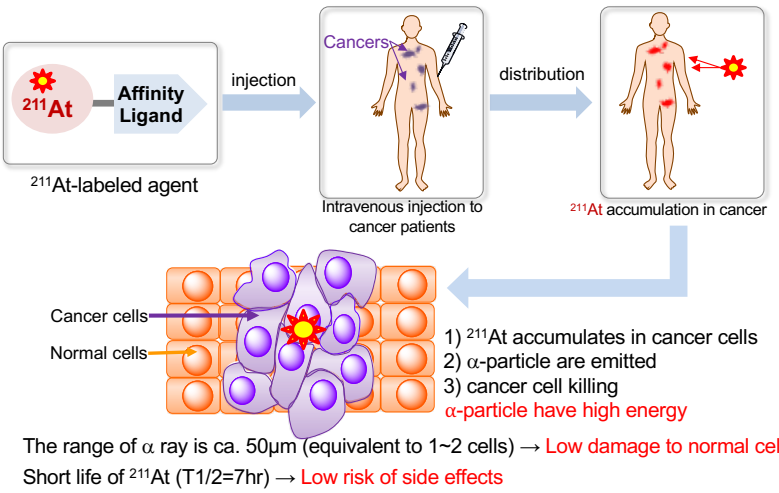


Figure 1. Concept of nuclear medicine with ^{211}At-labeled agent

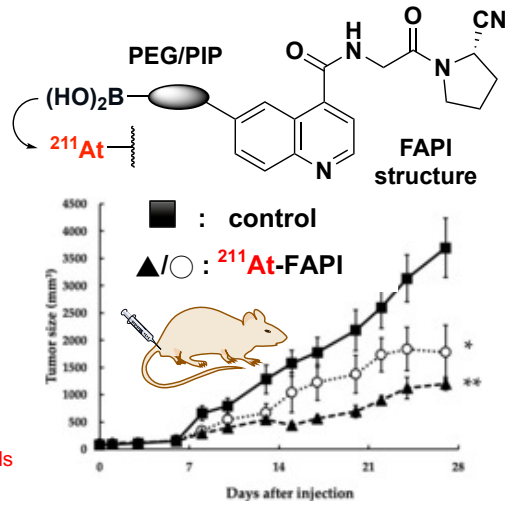


Figure 2. ^{211}At-labelled FAPI

2. CONCLUSIONS

^{211}At-labeled FAPI compounds demonstrate excellent specificity for FAPα, favorable biodistribution, and significant antitumor efficacy with minimal toxicity, positioning them as promising candidates for targeted α-particle radiotherapy. Future work will focus on optimizing synthesis, enhancing tumor retention, and advancing clinical translation to further establish their therapeutic potential.

ACKNOWLEDGMENTS

We are grateful to all members in Institute for Radiation Science in The University of Osaka for collaboration in this work. This work is supported by JSPS KAKENHI (20H05675, 24K23086, 25H00006).

References

[1] A. Aso, K. Kaneda-Nakashima, H. Nabetani, Y. Kadonaga, Y. Shirakami,* T. Watabe, T. Yoshiya, M. Mochizuki, Y. Koshino, K. Ooe, A. Kawakami, N. Jinno, A. Toyoshima, H. Haba, Y. Wang, J. Cardinale, F. L. Giesel, A. Shimoyama, K. Fukase, "Substrate Study for Dihydroxyboryl Astatine Substitution Reaction with Fibroblast Activation Protein Inhibitor (FAPI)" *Chem. Lett. 51*, 1091 (2022)

[2] A. Aso, H. Nabetani, Y. Matsuura, Y. Kadonaga, Y. Shirakami, T. Watabe,* T. Yoshiya, M. Mochizuki, K. Ooe, A. Kawakami, N. Jinno, A. Toyoshima, H. Haba, Y. Wang, J. Cardinale, F. L. Giesel, A. Shimoyama, K. Kaneda-Nakashima, K. Fukase "Evaluation of Astatine-211-Labeled Fibroblast Activation Protein Inhibitor (FAPI): Comparison of Different Linkers with Polyethylene Glycol and Piperazine" *Int. J. Mol. Sci. 24*(10), 8701 (2023)

7th Asia-Pacific Symposium on Radiochemistry *September 14 ~ 19, 2025 • Kunibiki Messe • Shimane, Japan*

Development of Novel Radioimmunotherapeutic Agents Targeting Epithelial Cell Adhesion Molecule

Sato Oshige[1], Takumi Iwasawa[2], Marina Omokawa[3], Yoji Kitamura[4], Takashi Kozaka[5], Yusuke Yagi[6], Takiko Daikoku[7], Kazunori Kato[8], Hiroyuki Kimura[9]

[1]*Graduate School of Medical Sciences, Kanazawa University, Takara-machi 13-1, Kanazawa, Ishikawa, Japan, 〒920-8640, o2153030902@stu.kanazawa-u.ac.jp*

[2]*Institute of Life Innovation Studies, Toyo University: Akabane-dai 1-7-11, Kita-ku, Tokyo, Japan, 〒115-8650 , iwasawa@toyo.jp*

[3] *Faculty of Medicine, Dentistry and Pharmaceutical Sciences, Okayama University, 2-5-1 Shikata-cho, Kita-ku, Okayama, Japan, 〒700-8558, m-omokawa@okayama-u.ac.jp*

[4] *Division of Probe Chemistry for Disease Analysis, Research Center for Experimental Modeling of Human Disease, Kanazawa University, 13-1 Takara-machi, Kanazawa, Ishikawa, Japan, 〒920-8640, ykitamu@staff.kanazawa-u.ac.jp*

[5] *Division of Probe Chemistry for Disease Analysis, Research Center for Experimental Modeling of Human Disease, Kanazawa University, 13-1 Takara-machi, Kanazawa, Ishikawa, Japan, 〒920-8640, t-kozaka@staff.kanazawa-u.ac.jp*

[6] *Department of Radiological Technology, Faculty of Medicinal Science, Kyoto University of Medical Science, 1-3 Imakita, Oyama-higashi, Sonobe, Nantan, Kyoto, Japan, 〒622-0041, y-yagi@kyoto-msc.jp*

[7] *Division of Animal Disease Model, Research Center for Experimental Modeling of Human Disease, Kanazawa University, 13-1 Takara-machi, Kanazawa, Ishikawa, Japan, 〒920-8640, takiko.daikoku@gmail.com*

[8]*Guraduate School of Health and Sports Sciences, Toyo University: Akabane-dai 1-7-11, Kita-ku, Tokyo, Japan, 〒115-8650 , k-kato@toyo.jp*

[9]*Division of Environmental Management, Agency for Health, Safety and Environment, Kyoto University: Yoshida Knoe-cho, Sakyo-ku, Kyoto-City, Kyoto, Japan, 〒606-8501, kimura.hiroyuki.4u@kyoto-u.ac.jp,*

1. OBJECTIVE

Cancer is the leading cause of death in Japan, and the current lifetime risk of developing cancer is approximately 50% [1]. Although there have been remarkable advances in cancer treatment in recent years, such as targeted therapy and immunotherapy, a major challenge is that treatment often cannot be completed due to the development of drug resistance during the therapeutic process. Therefore, we turned our attention to radioimmunotherapy, which is less prone to inducing drug resistance. Epithelial cell adhesion molecules (EpCAM) are highly expressed in various epithelial tumors [2], and we hypothesized that it could be an optimal target for cancer therapy. We have cloned several antibodies that bind to EpCAM and evaluated their functionality. Among these, we focused on the anti-EpCAM antibody (Ep4-1), which is suitable for use in radioimmunotherapy. In previous studies, we successfully conjugated approximately two molecules of a chelating agent to Ep4-1 and obtained ^{111}In-labeled Ep4-1 (^{111}In-Ep4-1) with high radiochemical yield and radiochemical purity. Furthermore, the synthesized ^{111}In-Ep4-1 was found to be highly stable in both mouse plasma and human plasma. In this study, we evaluated the binding affinity of ^{111}In-Ep4-1 to EpCAM and its contribution using EpCAM-high–expressing cell lines (DLD-1).

2. METHODS

First, a novel monoclonal antibody (Ep4-1) targeting the epithelial cell adhesion molecule EpCAM was successfully and stably developed. A chelating agent, *p*-SCN-Bn-DTPA, was conjugated to Ep4-1 to synthesize the *p*-Bn-DTPA-Ep4-1 antibody. Subsequently, ^{111}In-Ep4-1 was synthesized by radiolabeling *p*-Bn-DTPA-Ep4-1 with $^{111}InCl_3$ (Figure 1). The number of *p*-SCN-Bn-DTPA molecules conjugated to the antibody was determined using Matrix-Assisted Laser Desorption/Ionization Time-of-Flight Mass Spectrometry (MALDI-TOF MS). The radiochemical yield (RCY) of the resulting ^{111}In-Ep4-1 was determined by thin layer chromatography. Additionally, unreacted ^{111}In was separated using an ultrafiltration spin column, and the radiochemical purity (RCP) was calculated using the same method. For *in vitro* cellular experiments, we used wild-type (EpCAM (+)) and EpCAM knockout cells (EpCAM (-)) human colon

adenocarcinoma cells (DLD-1), a cell line with high EpCAM expression. DLD-1 cells were seeded 2 x 10^5 cells per well in 12-well plates and incubated for 2 days before being treated with the labeled antibody. We administered ^{111}In-Ep4-1 to the cells and measured the accumulation and internalization over time using a γ-counter.

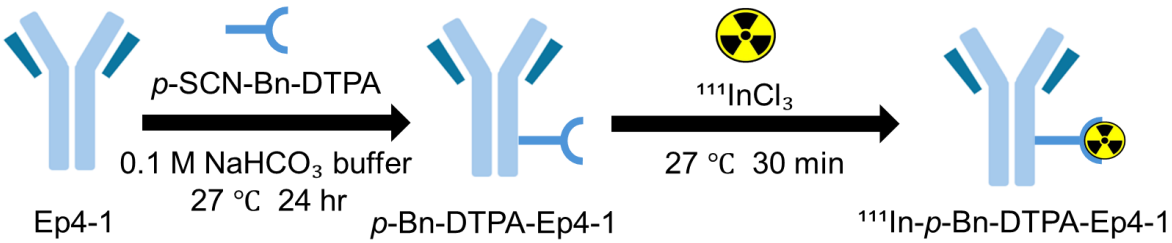


Figure. 1 The synthetic procedure for ^{111}In-Ep4-1

3. RESULTS

The number of DTPA molecules conjugated to the synthesized DTPA-Ep4-1 was approximately 2. ^{111}In-Ep4-1 was obtained with a radiochemical yield of 85% and radiochemical purity of 90%. Additionally, it was confirmed that the accumulation of ^{111}In-Ep4-1 increased up to 4 hours after the start of uptake. Furthermore, at all-time points, the internalization rate exceeded 68%. The accumulation of ^{111}In-Ep4-1 in EpCAM (-) cells was inhibited by 95% at 4 hours post-administration compared to EpCAM (+) cells (Figure. 2).

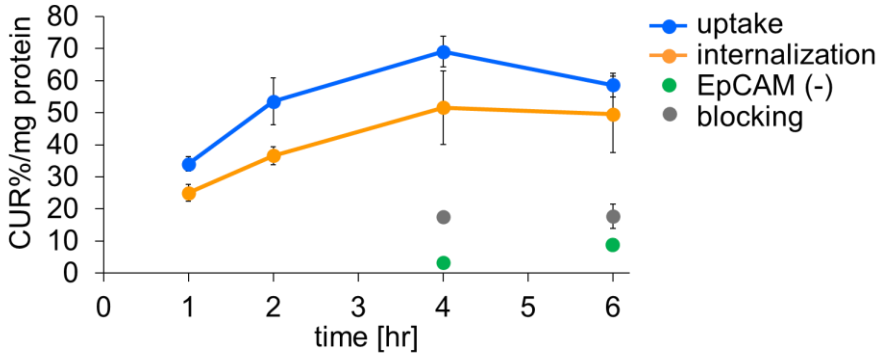


Figure. 2 Evaluation of ^{111}In-Ep4-1 accumulation in DLD-1

4. CONCLUSIONS

^{111}In-Ep4-1 has a strong binding affinity to EpCAM and can be efficiently internalized by cells through EpCAM. Although further validation in animal models is required, these results suggest that ^{111}In-Ep4-1 could be utilized in radioimmunotherapy when labeled with therapeutic radionuclides.

ACKNOWLEDGMENTS

This work was supported by JSPS KAKENHI (JP22H02928 and JP24K02395).

REFERENCES

[1] National Cancer Center Cancer Information Service “Latest Cancer Statistics”. National Cancer Center. 2024-12-16, https://ganjoho.jp/reg_stat/statistics/stat/summary.html, (referenced 2025-04-24).
[2] Gires, O., Pan, M., Schinke, H. *et al.* Expression and function of epithelial cell adhesion molecule EpCAM: where are we after 40 years?. *Cancer Metastasis Rev* 39, 969–987 (2020).

Activities of Targeted Alpha Therapy using astatine-211 at Osaka University in Japan

Kazuya Kabayama[1,2,3], Atsushi Toyoshima[1,2,3], Koichi Fukase[1,2,3]

[1] *Institute for Radiation Sciences, The University of Osaka: 1-1Machikaneyama, Toyonaka, Osaka, 560-0043*
[2] *Forefront Research Center, Graduate School of Science, The University of Osaka: 1-1Machikaneyama, Toyonaka, Osaka, 560-0043*
[3] *Department of Chemistry, Graduate School of Science, The University of Osaka: 1-1Machikaneyama, Toyonaka, Osaka, 560-0043*

At Osaka University, a collaborative project with multiple pipelines aimed at conquering cancer using alpha particles is underway, primarily led by the Graduate School of Science, the Graduate School of Medicine, the Research Center for Nuclear Physics, and the Institute for Radiation Sciences. In this talk, we will present an overview of these interdisciplinary studies.

1 INTRODUCTION

Alpha particles transfer high energy over a short distance and induce DNA double-strand breaks more efficiently than conventional beta particles. If alpha emitters can be successfully concentrated at the tumor site, they can precisely destroy cancer cells. Moreover, since radiation exposure to surrounding individuals is minimal, there is no need for a special hospital room, making it possible to perform the treatment as a one-day outpatient procedure. We have focused on astatine-211 (^{211}At), a short-lived alpha-emitting radionuclide. ^{211}At is a halogen element with a half-life of 7.2 hours and can be covalently bound to drug molecules. It also emits characteristic X-rays that allow for imaging, making it a promising candidate for theranostic applications that combine therapy and diagnosis.

2 RESEARCH ACTIVITIES

We are currently developing a range of ^{211}At-labeled agents for various types of cancer: [^{211}At]-NaAt for differentiated thyroid cancer, [^{211}At]-PSMA5 for prostate cancer, ^{211}At-labeled gold nanoparticles for brachytherapy, and ^{211}At-labeled amino acid derivatives targeting cancer-specific amino acid transporter LAT1. The results of these studies have already been published in scientific journals and announced through press releases. We have also reported successful outcomes from a study applying ^{225}Ac-labeled FAPI (fibroblast activation protein inhibitor), another alpha-emitting radionuclide, to pancreatic cancer.

Furthermore, Osaka University Hospital launched an investigator-initiated clinical trial of [^{211}At]-NaAt for refractory thyroid cancer in the period of 2023 - 2025. In 2024, we also began a clinical trial of [^{211}At]-PSMA5 for patients with metastatic prostate cancer.

All researchers involved in this project are fully committed to developing breakthrough therapies—"dream drugs"—through innovative medical advances born from the integration of science and medicine.

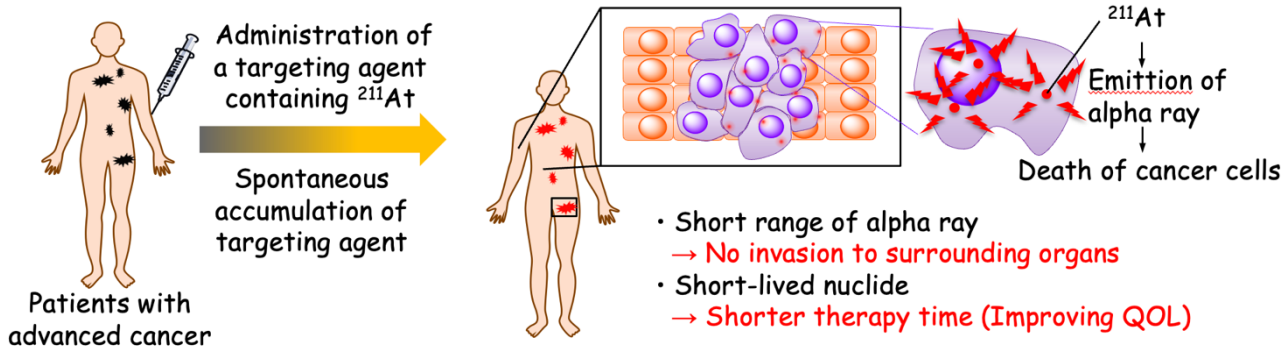


Fig. 1. Targeted Alpha Therapy using ^{211}At

Copyright on 7th Asia-Pacific Symposium on Radiochemistry 2025

ACKNOWLEDGMENTS

We are grateful to Dr. T. Watabe, Dr. K. Kaneda, and all members in Institute for Radiation Science of The University of Osaka for collaboration of this work. We also thank to RIKEN Nishina Center for Accelerator-Based Sciences and Supply Platform of Short-lived Radioisotopes, supported by JSPS Grant-in-Aid for Transformative Research Areas, Grant Number 22H04924 for the stable supply of ^{211}At.

Efforts by the Japanese Astatine Community toward clinical application of alpha emitter ^{211}At

Kohshin Washiyama[1], Takashi Nakano[2], Mikako Ogawa[3], Hiroki Kanda[2], Kazuya Taki[4],
and members of the Japan Astatine Community

[1] *Advanced Clinical Research Center, Fukushima Medical University: 1 Hikarigaoka, Fukushima, Fukushima, 960-1295, Japan and kwashi@fmu.ac.jp*
[2] *Research Center for Nuclear Physics, The University of Osaka: 10-1, Mihogaoka, Ibaraki, Osaka, 567-0047, Japan and nakano@rcnp.osaka-u.ac.jp, kanda@rcnp.osaka-u.ac.jp*
[3] *Graduate School of Pharmaceutical Sciences, Hokkaido University: N12 W6, Kita-ku, Sapporo, Hokkaido 060-0812, Japan and kwashi@fmu.ac.jp*
[4] *Sumitomo Heavy Industries, Ltd.: 2-1-1 Osaki, Shinagawa-ku, Tokyo 141-6025, Japan and kazuya.taki@shi-g.com*

Radiotheranostics, a combination of diagnosis and treatment using radionuclides, is currently developing rapidly in the medical field. The construction of a supply chain for radionuclides and a stable supply are important factors for making radiotheranostics sustainable medical treatment. Astatine-211 (^{211}At) is an alpha-emitting radionuclide that can be produced by using a cyclotron and has been recognized for its potential worldwide. The Japan Astatine Community (JAC), which consists of universities, research institutes, and companies, will promote research and development and clinical application of ^{211}At in Japan through information exchange and events among community members.

1. Background

Radionuclides are widely used in various fields such as industry, agriculture, space, and health care due to their radioactivity and radiation characteristics. In particular, in the field of health care, applications were immediately sought after the discovery of X-rays by Dr. W. C. Röntgen in 1895, radioactivity by Dr. H. Becquerel in 1896, and radium by the Curies (1898), and they are still indispensable for the treatment of cancer and infectious diseases, sterilization of medical equipment, etc. In recent years, advances in molecular biology and innovative developments in imaging equipment have made remarkable progress in imaging diagnosis and treatment using radiopharmaceuticals, and even prostate cancer that has metastasized throughout the body can now be completely treated with drugs labeled with novel radionuclides such as ^{68}Ga, ^{177}Lu, and ^{225}Ac. Hence, radiotheranostics is positioned as an important pillar of future healthcare.

Such technological innovation has been supported by radionuclides, which are the essence of diagnosis and treatment. Generally, radionuclides are mainly produced in three ways: nuclear reactors, accelerators, and generators, and the nuclides that are the source of generators are derived from nuclear reactors or accelerators. Due to their characteristics, nuclear reactors are advantageous for producing β^- emitters and fission products. The production of ^{177}Lu, the world's most widely used β^- emitter, is controlled within a global network to keep a sustainable supply. On the other hand, α-emitters have high atomic numbers and no stable isotopes, so accelerator-based production is preferable. One of the promising alpha emitters for cancer treatment, ^{225}Ac, can be produced from ^{226}Ra or ^{232}Th but requires advanced chemical separation technology. However, many of these nuclides are very difficult to manufacture in Japan from the viewpoint of securing materials, hindering research and development progress. Therefore, we focused on another α-emitter, astatine-211 (^{211}At), which can be produced by accelerators in Japan.

2. Astatine-211

Astatine was first synthesized by Corson, MacKenzie, and Segrè at the University of California, Berkeley, in 1940[1], and since then, researchers have been studying the chemical properties of this element and its application in nuclear medicine. In 1987[2], the Astatine Workshop was held at the Central Research Institute of Physics of the Hungarian Academy of Sciences in Budapest. We have gradually come to understand astatine through the mutual exchange of scientific insights accumulated by individual research facilities, but since the longest half-live of astatine is only 8 hours, all of these are based on research conducted mainly by research facilities with cyclotrons that can accelerate alpha particles[3]. Some of the highly advanced research groups at Duke University in the United States and the University of Gothenburg in Sweden conducted clinical trials in the 2000s [4,5] and reached the milestone of the first application. This achievement is due to applying the established general manufacturing method of radioimmunoconjugates to astatine, however it is not necessarily the result of understanding astatine itself. Hence, we have not yet been able to advance more clinical trials and realize the true potential of astatine by 2017.

The production of ^{211}At requires α-beams for incident particles to make ^{209}Bi(α, 2n)^{211}At nuclear reaction, however, the raw material bismuth is easy to obtain, and the chemical separation of the irradiated target is relatively easy. Japan has been actively promoting the production and supply of ^{211}At for about a decade, and six research institutes and universities have established a stable supply of ^{211}At through academic cooperation (Figure 1). By providing ^{211}At to many researchers, which has improved the skills of handling ^{211}At and promoted the sharing of various knowledge found in the process of drug development using astatine, leading to the ability to conduct human clinical trials. To further strengthen this effort, we established the Japan Astatine Community (JAC) as an organization to promote the use and R&D of this nuclide and to support its subsequent clinical use.

Manufacturing sites		Production route and Separation method	History	Map location
Research Center for Nuclear Physics(RCNP), Osaka University		^{209}Bi(α,2n)^{211}At Dry distillation	1980~ Medical use 2015~	
Takasaki Ion Accelerators for Advanced Radiation Application(**TIARA**), Takasaki Advanced Radiation Research Institute, National Institutes for Quantum and Radiological Science and Technology(QST) or QST(Takasaki)	QST	^{209}Bi(α,2n)^{211}At Dry &Wet chemistry	Since **2012**	
Quantum Medical Science Directorate, National Institute of Radiological Sciences(NIRS), National Institutes for Quantum and Radiological Science and Technology(QST) or QST(Chiba)	QST	^{209}Bi(α,2n)^{211}At Dry distillation	Sine **2013**	
Nishina Center for Accelerator-Based Science, Institute of Physical and Chemical Research(RIKEN)	RIKEN	^{209}Bi(α,2n)^{211}At Dry distillation	Since **2015**	
Advanced Clinical Research Center(ACRC), Fukushima Medical University(FMU)	FMU	^{209}Bi(α,2n)^{211}At Dry distillation	Since **2016**	
The tandem accelerator facility, Nuclear Science Research Institute, Japan Atomic Energy Agency(JAEA)	JAEA	^{209}Bi(^{7}Li,5n)^{211}Rn/^{211}At Dry & Wet chemistry	Since **2011**	

Fig. 1. Production sites of ^{211}At in Japan

3. The Japan Astatine Community (JAC)

The JAC is working to become a hub for the systematic collaboration of stakeholders in industry, academia, and government for the social implementation of targeted radionuclide therapy using ^{211}At by sharing actions necessary for the early realization of this goal. Our activities are ultimately to obtain the following five outcomes:

1. establish and strengthen the astatine supply network
2. provision of up-to-date technical and professional information on astatine to nuclear medicine professionals
3. study towards international standardization of astatine-labeled drug production
4. access to an international network centered on the WAC
5. promotion of rapid transfer of innovations from scientific societies to industry

The JAC is a member of the Worldwide Astatine Community (WAC) and operates the WAC with 1) the Network for Optimized Astatine labeled Radiopharmaceuticals (NOAR) in Europe, 2) the Astatine User's Community developed by the Department of Energy's Isotope Program in the United States, 3) the Korea Institute of Radiological and Medical Sciences (KIRAMS) in South Korea, 5) Chinese Astatine Community and 5) various industrial partners, which share the same goals to explore the full potential of the ^{211}At in targeted radionuclide therapy. Membership in the WAC is open to all [6].

4. Conclusion

Conclusion: The JAC, in liaison with the WAC, will facilitate the use and research and development of ^{211}At and support its clinical use in Japan as a hub for skills and knowledge of astatine.

References

[1] D. R. Corson, K. R. MacKenzie, and E. Segrè, Astatine : The Element of Atomic Number 85 , (1947) *Nature*, **159**, 24.
[2] Preface (1989) *Radiochim Acta*, **47**, I.
[3] D. S. Wilbur, Enigmatic astatine, (2013) *Nature Chem*, **5**, 246.
[4] M. R. Zalutsky, D. A. Reardon, G. Akabani, R. E. Coleman, A. H. Friedman, H. S. Friedman, R. E. McLendon, T. Z. Wong, and D. D. Bigner, Clinical experience with alpha-particle emitting 211At: treatment of recurrent brain tumor patients with 211At-labeled chimeric antitenascin monoclonal antibody 81C6, (2008) *J Nucl Med*, **49**, 30.
[5] H. Andersson, E. Cederkrantz, T. Bäck, C. Divgi, J. Elgqvist, J. Himmelman, G. Horvath, L. Jacobsson, H. Jensen, S. Lindegren, S. Palm, and R Hultborn, ntraperitoneal α-Particle Radioimmunotherapy of Ovarian Cancer Patients: Pharmacokinetics and Dosimetry of ^{211}At-MX35 F(ab')$_2$ - A Phase I Study, (2009) *J Nucl Med*, **50**, 1153.
[6] J. F. Gestin, K. Washiyama, Kyo Chul Lee, and E. R.Balkin, The World Astatine Community: the global network for sharing experience and knowledge of astatine-211, (2024) *WCI Newsletter*, **13**, 1.

Poster Presentation | [S3]Outreach for Education on Radiation and Radioactivity after Fukushima Nuclear Accident

Tue. Sep 16, 2025 6:30 PM - 8:00 PM JST | Tue. Sep 16, 2025 9:30 AM - 11:00 AM UTC Poster

[Poster] S3

[P-S3-01]

Unique educational materials for social outreach related to low-level radionuclides

*Mutsuo Inoue[1], Shinya Ochiai[1] (1. LLRL K-INET Kanazawa Univ. (Japan))

©APSORC25

7th Asia-Pacific Symposium on Radiochemistry *September 14 ~ 19, 2025 • Kunibiki Messe • Shimane, Japan*

Unique educational materials for social outreach related to low-level radionuclides

Mutsuo Inoue[1], Shinya Ochiai[1]

[1]*Low Level Radioactivity Laboratory, Institute of Nature and Environmental Technology, Kanazawa University*

Interestingly, to establish low-level radioactivity (γ-ray) systems without the help of cutting-edge technology, it has been effective to use lead roof tiles from an old castle refined in the Edo period, iron from a battleship built in the Taisho period, and an old tunnel in the former copper mine.

Artificial (e.g., ^{134}Cs and ^{137}Cs) and natural (e.g., ^{226}Ra, ^{228}Ra, ^{228}Th, ^{234}Th, ^{210}Pb, and ^{7}Be) γ-ray-emitting radionuclides, which have been used as strong tracers to study environmental radioactivity, geochemistry, and radioactive dating, generally have low activity. The measurement of low-level radionuclides in environmental samples is affected by the environmental radioactivity. Therefore, it is necessary to decrease the background-level of γ-spectra.

After the Fukushima Dai-ichi Nuclear Power Plant (FDNPP) accident, interest in environmental radioactivity has grown, and outreach activities are required. In social lectures, we use unique educational materials to explain low-background γ-measurements easily and interestingly (Fig. 1). In this presentation, we introduce a cosmic-ray sensor, ^{210}Pb-free lead roof tiles from Kanazawa Castle, ^{60}Co-free iron from the old battleship Mutsu, and least ^{226}Ra- and ^{228}Ra-contaminated natural minerals (barite) used in our social lectures on low-background γ-spectrometry (Fig. 1). This content is based on a sense that is completely opposite to the notion that conventional “radioactivity is always dangerous” and can bring new insight to environmental radioactivity. The effective use of such old materials has invited the interest of various participants regarding the unexpected relationship with radioactivity research.

a



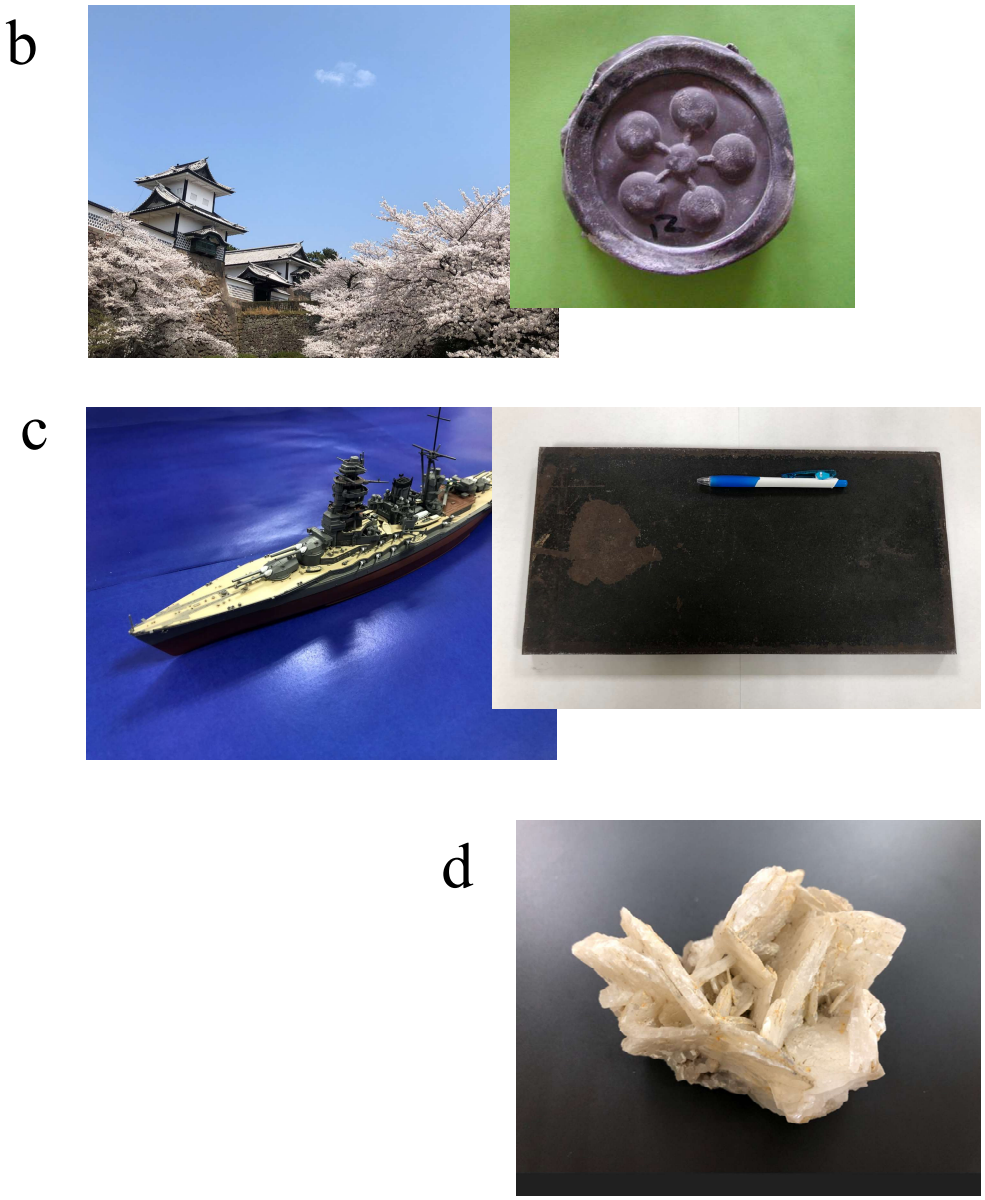


Fig. 1: Educational materials for social lectures; a) Ogoya Tunnel (interior) and a cosmic-ray sensor, b) Kanazawa Castle and a roof tile from the castle, c) the battleship Mutsu and an iron plate from Mutsu, and d) barite ($BaSO_4$).

Plenary Talk | Plenary Talk

Wed. Sep 17, 2025 8:45 AM - 9:30 AM JST | Tue. Sep 16, 2025 11:45 PM - 12:30 AM UTC Hall S(Int'l)

[PL3] Plenary Talk 3 by François Guérard

8:45 AM - 9:30 AM JST | 11:45 PM - 12:30 AM UTC

[PL03]

^{211}At-radiolabeling chemistry for targeted alpha therapy: recent progress and remaining challenges

*François Guérard[1] (1. Nantes Université (France))

©APSORC25

^{211}At-radiolabeling chemistry for targeted alpha therapy: recent progress and remaining challenges

François Guérard[1]

[1] Nantes Université, Inserm, CNRS, Université d'Angers, CRCI^{2}NA, Nantes, France
francois.guerard@univ-nantes.fr

Astatine-211 is considered as one of the main three alpha emitters for broad application in the therapy of cancers in the next few years and could become the preferred one in the coming decade.[1] This growing interest finds its origin in the favorable physical characteristics of this radionuclide: a short half-life of 7.2 h, both decay branches leading to a single high energy alpha particle, the absence of a cascade of daughter radionuclides and the 72-97 keV X-rays that could be used for imaging.[2] The inexpensive starting material required for its production (^{209}Bi) is also a clear advantage, and several industrial actors have recently initiated the installation of dedicated particle accelerators to cover upcoming demand. With this expected production upscale, the number of clinical studies should rapidly rise, but if ^{211}At supply is expected to improve, challenges remain regarding radiolabeling chemistry with this still quite unknown radioelement. Because astatine exists only as short-lived radionuclides and can be used only in trace amounts for experimentation, most spectroscopic tools cannot be used to investigate its chemical characteristics, which has long limited the development of appropriate radiosynthetic procedures.[3]

In this context, this lecture will introduce how key finding made in recent years at Nantes Université by combining experimental data and theoretical chemistry were used to address challenges in developing ^{211}At-radiotracers. In particular, the limited number of available approaches to produce ^{211}At-aryl compounds was expanded by using the more favorable nucleophilic astatine species, giving access to simpler, less toxic and/or more robust approaches for preclinical therapy studies and for the preparation of clinical trials. On the other hand, latest studies have focused on developing ^{211}At-labeled compounds with improved in vivo stability. Considering astatine not only as a halogen but also as a metal will also be discussed in the perspective of developing new chemical approaches.

ACKNOWLEDGMENTS

This work was supported by the French National Agency for Research, grants ANR-19-CE07-0036 (ExPAt), ANR-11-LABX-18-01(Labex IRON), INCa-DGOS-INSERM-ITMO Cancer_18011. Co-funded by the European Union (ERC, SAt-Radio,101087175).

References

[1] R. Zimmermann, « Is ^{211}At Really Happening? », *J. Nucl. Med.*, 2025, doi: 10.2967/jnumed.125.269699.
[2] S. Lindegren, P. Albertsson, T. Bäck, H. Jensen, S. Palm, et E. Aneheim, « Realizing Clinical Trials with Astatine-211: The Chemistry Infrastructure », *Cancer Biother Radiopharm*, vol. 35, nº 6, p. 425-436, 2020, doi: 10.1089/cbr.2019.3055.
[3] F. Guérard *et al.*, « Advances in the Chemistry of Astatine and Implications for the Development of Radiopharmaceuticals », *Acc. Chem. Res.*, vol. 54, nº 16, p. 3264-3275, 2021, doi: 10.1021/acs.accounts.1c00327.

Copyright on 7th Asia-Pacific Symposium on Radiochemistry 2025

Invited & Contributed Talk | [S2]Radiopharmaceutical Sciences

Wed. Sep 17, 2025 9:35 AM - 10:45 AM JST | Wed. Sep 17, 2025 12:35 AM - 1:45 AM UTC Hall S(Int'l)

[S2] Radiopharmaceutical Sciences

9:35 AM - 10:05 AM JST | 12:35 AM - 1:05 AM UTC

[S2-01(Invited)]

Isotope Mass Separation at CERN-MEDICIS :clinical research with High Molar Activity radiotherapeutics

*Thierry Stora[1] (1. CERN (Switzerland))

10:05 AM - 10:25 AM JST | 1:05 AM - 1:25 AM UTC

[S2-02]

Production of ^{155}Tb via α-particle induced reaction on ^{153}Eu

*Yudai Shigekawa[1,2], Ryotaro Masuda[3], Sayantani Mitra[1], Akihoro Nambu[1], Yoshitaka Kasamatsu[3], Hiromitsu Haba[1] (1. RIKEN (Japan), 2. University of Tsukuba (Japan), 3. Osaka University (Japan))

10:25 AM - 10:45 AM JST | 1:25 AM - 1:45 AM UTC

[S2-03*]

Developing robust targetry and radiochemistry of antimony-119 for pre-clinical applications in radioligand therapy

*Aivija Grundmane[1,2], Caterina F Ramogida[1,2], Valery Radchenko[2,3] (1. Simon Fraser University (Canada), 2. TRIUMF (Canada), 3. University of British Columbia (Canada))

©APSORC25

7th Asia-Pacific Symposium on Radiochemistry *September 14 ~ 19, 2025 • Kunibiki Messe • Shimane, Japan*

Isotope Mass Separation at CERN-MEDICIS :clinical research with High Molar Activity radiotherapeutics

Thierry Stora[1]

[1]*CERN, 1 Esplanade des particules, CH-1217 Meyrin, Switzerland, Thierry.Stora@cern.ch*

1 ABSTRACT

CERN-MEDICIS is an isotope mass separation facility dedicated to the production of innovative radionuclides used for translational biomedical research and dispatch to partner institutes. Radionuclides are used in the synthesis of radiopharmaceuticals in nuclear medicine and in particular for the emerging field of theranostics – combining therapy and diagnostics in a single vector. Translational research has indeed recently witnessed an impressive boost in nuclear medicine when diagnostics could be combined with targeted treatment using radiotherapeutics. Translational biomedical research at MEDICIS is done within a collaboration of 21 external institutes, including large university hospitals. Hosted in the class A nuclear laboratory of ISOLDE at CERN, the facility produces batches of non-conventional radionuclides from targets irradiated by the proton beam delivered at PSBooster in dedicated irradiation stations. It also receives irradiated targets from MEDICIS partner institutes for purification by mass separation. This complementary and diverse production capacity of the collaboration allows to offer complementary radionuclides, at the heart of the success of theranostics. With world expert laboratories, such as metrology or radiochemistry laboratories, the collaboration had been able to aggregate a highly multidisciplinary translational board, capable of providing highly innovative isotopes, and an associated translational biomedical research programme. MEDICIS, by pushing the techniques of isotope mass separation, aims to enhance the landscape of medical isotopes available for diagnostics and therapeutic applications across Europe and beyond, and aims at the development of a new generation of theranostics drugs based on a better match of innovative radionuclides combined with new targeting vectors. [1].

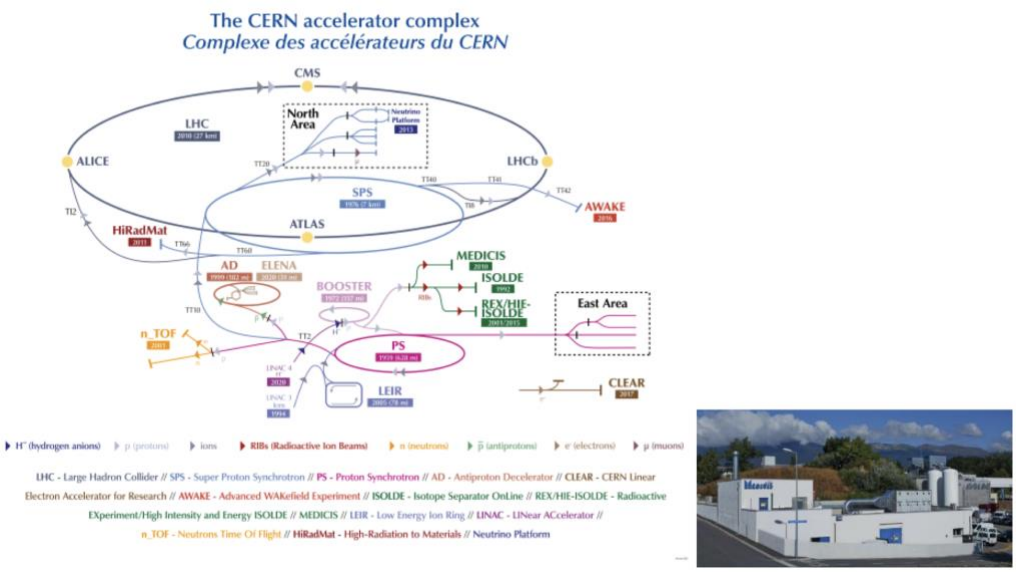


Fig. 1. MEDICIS facility hosted in the nuclear class A laboratory, and the CERN accelerator complex in 2025

The goals of the MEDICIS project encompass several key areas:

Production of novel radionuclides: MEDICIS aims to produce non-conventional radionuclides that are pivotal for translational medical research, utilizing advanced isotope mass separation techniques. For instance, projects such as the production of actinium-225 (Ac-225), a promising agent for targeted alpha therapy, have been initiated under MEDICIS by mass separation. Extremely high separation performance could be achieved through accelerator and beam developments, leading to the capacity to supply doses relevant for clinical research treatments on a weekly basis.

Copyright on 7th Asia-Pacific Symposium on Radiochemistry 2025 - S2-01 -

Support Translational Medical Research: By producing radionuclides like high molar activity samarium-153 (Sm-153) uniquely available thanks to the purification by mass available at MEDICIS, and of Thulium/Erbium-165 (Tm/Er-165), MEDICIS seeks to facilitate clinical studies and enhance treatment protocols for various cancers. It also networks with national metrology institutes to determine precise nuclear data and properties required for their application in nuclear medicine.

Foster Collaborative Research: Engage with academic and clinical institutions, including university hospitals, to translate research findings into clinical applications, fostering innovation in nuclear medicine. The MEDICIS collaboration includes notable partners from a variety of institutions, including leading universities and university hospitals across Europe, facilitating a multi-disciplinary approach to radionuclide research and clinical application. Furthermore, it is a cornerstone of PRISMAP, the European Medical Radionuclide Programme, and a major stakeholder in the European Radioisotope Valley Initiative (ERVI) of the European Commission. The ERVI programme, and the inclusion of a sustainable PRISMAP consortium for the years to come were included in the recommendation 9912/24 from the Conseil de 'Union Européenne in June 2024 [2].

In 2025, CERN Council approved the use of the mass separated radionuclides from MEDICIS for clinical experimental trials, and the operation is approved until 2030. As MEDICIS has already demonstrated, its programme can proceed allowing for further development of clinical applications for radionuclides in hospital settings, relying on external sources from partner institutions, notably in 2026 and 2027 during CERN Long Shutdown LS3. This is notably the case for the approved project Sm153-[Sm]-FAPI46 radioligand therapy with High Molar Activity HMA Sm-153, submitted by Kratochwil et al. [3].

ACKNOWLEDGMENTS

This project has received funding from the European Union's Horizon 2020 research and innovation programme under grant agreement No 101008571 (PRISMAP).

References

[1] https://Medicis.cern/, accessed May 2025
[2] https://www.radionuclides.eu, accessed May 2025
[3] https://cds.cern.ch/record/2853121, accessed May 2025

Production of ^{155}Tb via α-particle induced reaction on ^{153}Eu

Yudai Shigekawa[1,2], Ryotaro Masuda[3], Sayantani Mitra[1], Akihiro Nambu[1], Yoshitaka Kasamatsu[3], and Hiromitsu Haba[1]

[1]*Nishina Center for Accelerator-Based Science, RIKEN: 2-1 Hirosawa, Wako, Saitama, 351-0198, Japan, yshigekawa@ied.tsukuba.ac.jp*
[2]*Institute of Pure and Applied Sciences, University of Tsukuba: 1-1-1 Tennodai, Ibaraki, 305-8577, Japan*
[3]*Graduate School of Science, Osaka University: 1-1 Machikaneyama, Toyonaka, Osaka, 560-0043, Japan*

^{155}Tb is a promising radioisotope for single photon emission computed tomography (SPECT). Toward large-scale production of ^{155}Tb, we developed a method to produce it via an α-particle induced reaction on ^{153}Eu. We first measured the production cross sections of terbium radioisotopes by 51-MeV α-particle irradiation of stacked ^{nat}Eu targets. Next, we produced ^{155}Tb by irradiating an enriched ^{153}Eu target with a 28-MeV α-particle beam and performed chemical separation. The production and chemical yields of ^{155}Tb were sufficiently high for large-scale production. We also evaluated the radionuclidic and chemical purities of the obtained ^{155}Tb sample.

1 Introduction

^{155}Tb ($T_{1/2}$ = 5.32 d) is a radioisotope that decays by electron capture, accompanied by the emission of low-energy γ rays (e.g., 87 and 105 keV). This isotope is considered promising for single photon emission computed tomography (SPECT), which will be combined with cancer therapies using the radioisotopes of rare-earth elements (e.g., ^{177}Lu, ^{149}Tb, and ^{161}Tb) [1]. Additionally, ^{155}Tb is expected to be applicable to γ-ray perturbed angular correlation spectroscopy, potentially realizing novel imaging techniques capable of probing local chemical environments in the human body [2].

Previous studies have utilized two methods for the production of ^{155}Tb: (1) proton-induced spallation followed by on-line mass separation and chemical separation at CERN [3], and (2) proton-induced nuclear fusion reactions on ^{155}Gd and ^{156}Gd targets [1]. The latter method is feasible at small cyclotrons, although there are several problems. For example, the chemical separation of ^{155}Tb from a bulk amount of Gd is challenging due to their similar chemical properties. Moreover, the enrichment levels of the normally available ^{155}Gd and ^{156}Gd are not very high (~93%), which have limited the radionuclidic purity of ^{155}Tb to ~93% [1].

To address these issues, we aim to produce ^{155}Tb through the ^{153}Eu(α,2n)^{155}Tb reaction. The advantage of this method is that the chemical separation of ^{155}Tb from the bulk amount of Eu is easier than that from Gd because Eu can be reduced from 3+ to 2+ in aqueous conditions [4]. Moreover, ^{153}Eu with an enrichment level of >99% is commercially available, potentially improving the radionuclidic purity. The primary radionuclidic impurity in this method is ^{156}Tb ($T_{1/2}$ = 5.35 d) produced in the ^{153}Eu(α,n)^{156}Tb reaction. In this study, we first measured the production cross sections of ^{155}Tb and ^{156}Tb via the α-particle induced reactions on ^{nat}Eu, which have never been reported thus far. Furthermore, we produced ^{155}Tb by the α-beam irradiation of an enriched ^{153}Eu target and performed chemical separation.

2 Cross-section measurement

We prepared 16 pieces of ^{nat}Eu targets (^{153}Eu 52%, ^{151}Eu 48%; 0.60–0.85 mg/cm^2) on thin ^{27}Al foils (Al_a, 2.95 mg/cm^2, 99.999% purity) by the electrodeposition method. The deposition yields, required to determine the thickness of each ^{nat}Eu target, were monitored with an ^{88}Y tracer. We used ^{nat}Ti foils (2.35 mg/cm^2, 99.6% purity) for the ^{nat}Ti(α,x)^{51}Cr monitor reaction and thick ^{27}Al foils (Al_b, 13.13 mg/cm^2, >99% purity) as energy degraders. We stacked 5 sets of Al_a-Eu-Al_a-Ti-Ti-Al_b and 11 sets of Al_a-Eu-Al_a-Ti-Ti onto a target holder. The stacked target was irradiated with an α-particle beam of 50.9(1) MeV at the RIKEN AVF cyclotron. The average beam current was 100 particle nA (pnA), and the irradiation time was 1 h. After irradiation, we performed γ-ray spectroscopy of each foil with high-purity Ge detectors. The cross sections of ^{51}Cr, ^{155}Tb, and ^{156}Tb were determined from the γ rays of 320, 105, and 534 keV, respectively.

First, we confirmed that the cross sections of the ^{nat}Ti(α,x)^{51}Cr reaction were consistent with the IAEA recommended values [5] within error, supporting the accuracy of the beam energy, the beam current, and the target thickness. Next, we evaluated the cross sections of the ^{153}Eu(α,2n)^{155}Tb and ^{153}Eu(α,n)^{156}Tb reactions as a function of the beam energy. The maximum cross section of ^{155}Tb was 900(120) mb at 28.5(5) MeV, which was sufficiently high for the large-scale production. The maximum cross section of ^{156}Tb was 100(20) mb at 20.2(8) MeV. If we irradiate an $^{153}Eu_2O_3$ target (35 mg/cm^2) with a 30-MeV α beam (energy in the target: 26.3–30.0 MeV), which is below the threshold of the production of ^{153}Tb ($T_{1/2}$ = 2.34 d), the production yield of ^{155}Tb is estimated to be 3.2(4) MBq/(pμA·h) and the radioactivity ratio of ^{156}Tb to ^{155}Tb is ~2%, which is better than the case for the Gd targets (~7%) [1].

Copyright on 7th Asia-Pacific Symposium on Radiochemistry 2025 - S2-02 -

3 Production of ^{155}Tb by α-particle bombardment of ^{153}Eu target

We prepared the ^{153}Eu target using ^{153}Eu oxide powder purchased from ISOFLEX (USA), which had a ^{153}Eu enrichment level of 99.8(1)%. The powder was first heated at 900 °C for 20 h and then pressed into a $^{153}Eu_2O_3$ pellet with a thickness of 73.4 mg/cm^2 and a diameter of 7 mm. The ^{153}Eu target was irradiated with an α-particle beam of 27.8 MeV at the RIKEN AVF cyclotron. The average beam current was 2.1 pμA, and the irradiation time was 77 min. After irradiation, the target was subjected to γ-ray spectroscopy, where only the γ-ray peaks of ^{155}Tb and ^{156}Tb were observed. The radioactivity of ^{155}Tb at the end of bombardment (EOB) was determined to be 13.1(4) MBq, corresponding to a production yield of 4.9(2) MBq/(pμA·h). This is consistent with 4.7(6) MBq/(pμA·h) calculated from our experimental cross sections. The ratio of ^{156}Tb to ^{155}Tb was evaluated to be 8.3(4)%. This ratio is estimated to be reduced by decreasing the thickness of the $^{153}Eu_2O_3$ target.

4 Chemical separation of ^{155}Tb

We first dissolved the $^{153}Eu_2O_3$ target (24.4 mg as ^{153}Eu) with concentrated HCl and then performed a three-step separation. In the first step, Eu^{3+} was reduced to Eu^{2+} by zinc powder in the presence of SO_4^{2-}, which formed the precipitate of $EuSO_4$ [4]. The precipitate was removed using a filter paper (Millipore RAWP02500) by suction. The yield of ^{155}Tb in the filtrate was 90(4)%. In our preparatory experiment, we measured the precipitation yield of Eu to be 92(1)% using a ^{148}Eu tracer. Therefore, in this study, the amount of ^{153}Eu in the filtrate was estimated to be ~2 mg. After we evaporated the filtrate and dissolved the residue in 0.3 M HNO_3, we performed extraction chromatography using a column of Ln resin (Eichrom). Zinc was eluted from the column with 0.3 M HNO_3, followed by the elution of Eu and Gd (potentially contained in the target material) with 0.75 M HNO_3. ^{155}Tb was then eluted from the column with 3 M HNO_3. The chemical yield of ^{155}Tb for this column chromatography was 82(4)%. For further purification, the 3 M HNO_3 eluate was loaded onto a column of DGA resin (Eichrom). After rinsing the column with 3 M HNO_3, ^{155}Tb was eluted with 0.05 M HCl. The chemical yield for this column purification was ~100%.

The radioactivity of the purified ^{155}Tb was 10.3 MBq at EOB and the overall chemical yield was 76(3)%. Hence, by a 27.8-MeV α-particle beam irradiation at 2 pμA for 14 h, 100 MBq of purified ^{155}Tb at EOB can be obtained, which is sufficiently high for imaging experiments. The purified sample was subjected to inductively coupled plasma mass spectrometry (ICP-MS). The amount of ^{159}Tb was measured to be 0.4 ng, yielding a ^{155}Tb specific radioactivity of 28.5(8) MBq/ng at EOB. The amount of ^{153}Eu in the purified sample was 110 ng, indicating that the chemical separation process performed in this study reduced the ^{153}Eu content by a factor of ~10^5.

5 Conclusions

We measured the excitation functions of the ^{153}Eu(α,2n)^{155}Tb and ^{153}Eu(α,n)^{156}Tb reactions by irradiating stacked ^{nat}Eu targets with a 51-MeV α-particle beam. We produced ^{155}Tb by irradiating an enriched ^{153}Eu target with a 28-MeV α-particle beam and performed chemical separation. The developed method demonstrated high production and chemical yields of ^{155}Tb for future large-scale production.

ACKNOWLEDGMENTS

This work was supported by JSPS KAKENHI Grant Number JP 22H05024.

References

[1] C. Favaretto *et al.*, "Cyclotron production and radiochemical purification of terbium-155 for SPECT imaging," *EJNMMI Radiopharm. Chem.*, **6**, 37 (2021).
[2] K. Shimazoe *et al.*, "Imaging and sensing of pH and chemical state with nuclear-spin-correlated cascade gamma rays via radioactive tracer," *Commun. Phys.*, **5**, 24 (2022).
[3] B. Webster *et al.*, "Chemical Purification of Terbium-155 from Pseudo-Isobaric Impurities in a Mass Separated Source Produced at CERN," *Sci. Rep.*, **9**, 10884 (2019).
[4] A. G. Kazakov *et al.*, "Separation of radioisotopes of terbium from a europium target irradiated by 27 MeV α-particles," *Radiochim. Acta*, **106**, 135 (2018).
[5] A. Hermanne *et al.*, "Reference Cross Sections for Charged-particle Monitor Reactions," *Nucl. Data Sheets*, **148**, 338 (2018).

Copyright on 7th Asia-Pacific Symposium on Radiochemistry 2025 - S2-02 -

DEVELOPING ROBUST TARGETRY AND RADIOCHEMISTRY OF ANTIMONY-119 FOR PRE-CLINICAL APPLICATIONS IN RADIOLIGAND THERAPY

Aivija Grundmane[1,2], Caterina F. Ramogida[1,2], Valery Radchenko[2,3]

[1]*Simon Fraser University, Department of Chemistry: 8888 University Dr W, Burnaby, British Columbia, V5A 1S6, aivija_grundmane@sfu.ca, caterina_ramogida@sfu.ca*
[2]*TRIUMF, Life Sciences Division: 4004 Wesbrook Mall, Vancouver, British Columbia, V6T 2A3, vradchenko@triumf.ca*
[3]*University of British Columbia, Department of Chemistry: Vancouver, British Columbia, V6T 1Z4.*

Antimony-119 (^{119}Sb) is a radionuclide of interest for radioligand therapy using Auger electrons. The suggested cyclotron production route by proton bombardment of tin-119 (^{119}Sn) requires expensive enriched material, which must be recovered after purification and reused. Previously, we were able to establish a robust purification method for separating ^{119}Sb from Sn by designing new extraction chromatography resins. In this work, we aimed to find a suitable method of recycling the enriched ^{119}Sn material compatible with the improved purification method. Two new methods of electroplating Sn for cyclotron target preparation and irradiation were developed, one of which was found to be capable of near-quantitative (96 ± 3%) recycling of the recovered Sn. The method's compatibility with the developed purification system establishes a new, improved approach for ^{119}Sb production.

1 INTRODUCTION

Antimony-119 (^{119}Sb, $t_{1/2}$ = 38.19 h) is a radionuclide of therapeutic interest, predominantly emitting Auger (range in tissue < 0.5 μm) and conversion (range in tissue < 10 μm) electrons, accompanied by low energy (< 30 keV) X-rays and gamma rays. Due to the low path-length in tissue, ^{119}Sb can be applied to target cancer on a cellular basis, provided a sufficiently selective delivery mechanism can be attained. To date, no suitable delivery mechanisms have been developed, due to several factors, including a lack of robust purification method for isolating ^{119}Sb in a suitable oxidation state, species, and matrix for further application pre-clinically. Moreover, the suggested production route by proton bombardment of tin-119 (^{119}Sn) (^{119}Sn(p,n)^{119}Sb) using a conventional low energy cyclotron requires expensive enriched material, which should be recycled and reused for ^{119}Sb radiopharmaceuticals to be viable. Some of these efforts were addressed in prior work, in which we were able to establish a robust production of ^{119}Sb by designing new ether functionalized extraction chromatography resins [1,2]. These resins showed improved purification of ^{119}Sb in a suitable matrix compatible with further applications in radiopharmaceutical synthesis. The proposed separation system was also able to quantitatively recover the Sn target material in a small volume. In this work, we report an electroplating method capable of near-quantitative recycling of the recovered Sn. Initial testing shows the method's compatibility with the developed purification system, establishing a new, improved approach for ^{119}Sb production.

2 METHODS

To establish methodology natural Sn was used instead of enriched ^{119}Sn. For ^{119}Sb production by cyclotron irradiation, Sn target material needs to be electroplated on a metal cathode (e.g., silver (Ag)) that doubles as the solid support called target backing. After irradiation, the targets are dissolved in concentrated hydrochloric acid (HCl) and the ^{119}Sb is separated from the bulk Sn target material by purification using dibutyl ether resin, where Sn is recovered as Sn(IV) in 2 mL conc. HCl [1,2]. From this starting matrix, two electroplating methods (Method 1 and Method 2) were investigated for suitability of Sn recycling, while a third method (Method 3), known as the gold standard in the field was used as a reference for target quality. Method 1 involved the preparation of Sn(IV) sols as per Wang et al. and was first adapted from the source material for electroplating on Ag target backing, keeping the molar ratio of Sn(IV) chloride pentahydrate, ammonium hydroxide, and acetylacetone as 1:1.85:0.35 in 1:1 ethanol and water [3]. Once reproducibility was achieved, recycling was attempted using this method, using the Sn(IV) chloride in conc. HCl as the starting material instead. Method 2 involved the use of copper (Cu) target backing and simply required dilution of the starting matrix to a lower concentration of HCl (~ 4.5 M). Method 3 is a conventional Sn(II) sulfate bath, electroplated on Ag target backings as per Olson et al. [4]. This method could not be used for target recycling testing, as it requires Sn(II) as the starting oxidation state but was used as a reference for surface morphology, which was investigated using scanning electron microscopy (SEM) and energy dispersive X-ray (EDX) analysis. The integrity of Ag and Cu target backings in HCl was tested by subjecting them to typical dissolution conditions and measuring trace metal contents in HCl by ICP-MS.

3 RESULTS

All three methods of electroplating were implemented successfully using various Sn containing starting materials (method 1: Sn(IV) chloride pentahydrate, method 2: Sn(IV) chloride in conc. HCl, method 3: Sn(II) sulfate). Only method 2 was found to be compatible with Sn recycling from the developed purification method, recovering 96 ± 3% (n = 5) of

Copyright on 7th Asia-Pacific Symposium on Radiochemistry 2025- S2-03* -

the Sn. Not only is the Sn recovery near-quantitative, but the surface morphology was also found to be much more homogeneous compared to the noticeable heterogeneity and the formation of different crystals/clusters of contaminants on the surface of Sn targets electroplated using methods 1 and 3 (Figure 1). However, it should be noted that method 2 requires the use of a Cu cathode/target backing, which has lower durability in HCl than Ag (Table 1).

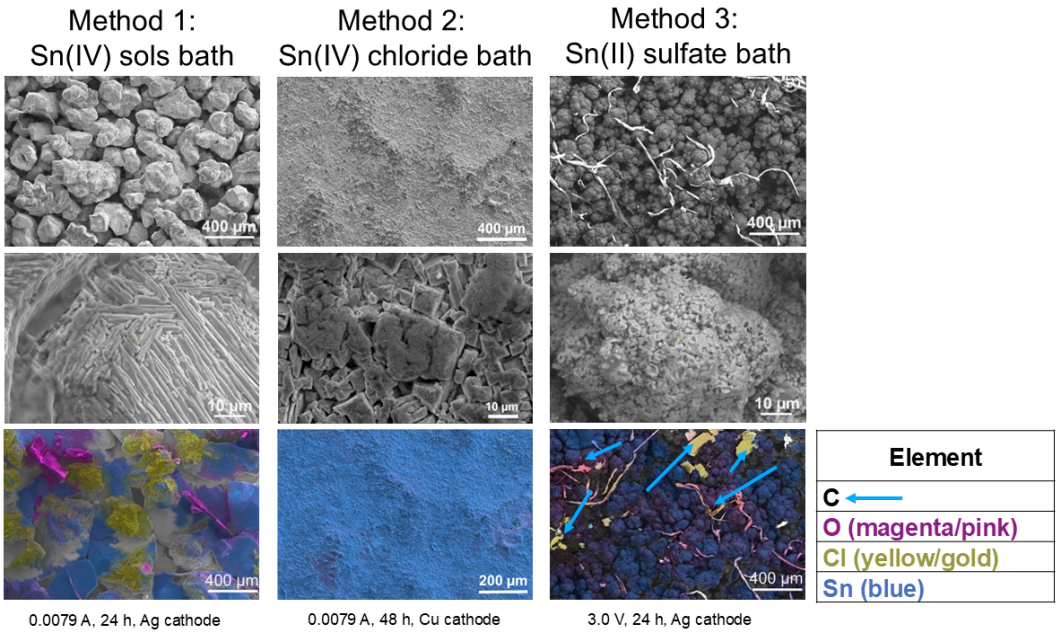


Fig. 1. Surface morphology of Sn targets electroplated using methods 1, 2, and 3. SEM images shown in greyscale, with EDX elemental analysis overlayed in color.

TABLE 1. Trace metal composition of select elements after target dissolution of Cu and Ag backed targets in HCl (n=3).

Element	Method 2: Cu target backing (µg)	Methods 1,3: Ag target backing (µg)
Copper (Cu)	1200 ± 400	5 ± 2
Silver (Ag)	To be measured.	100 ± 9

4. CONCLUSIONS

All electroplating methods implemented in this work were found to successfully electrodeposit Sn for cyclotron irradiation applications. Method 2 was the only method found to be compatible with Sn recycling from the developed purification method, boasting near-quantitative Sn recovery of 96 ± 3% (n = 5) and high surface homogeneity. Although elevated amounts of Cu were observed after target dissolution of Cu backed targets, this contamination should not affect the separation chemistry, as Cu does not have any affinity for the dibutyl ether resin [2]. However, the Cu will be recovered alongside Sn, and the effect of presence of Cu for further Sn recycling cycles is currently being investigated.

ACKNOWLEDGMENTS

This work was supported by the CIHR, NSERC via Discovery Grants, as well as the NFRF-T Grant. TRIUMF receives funding via a contribution agreement with the NRC. We would like to thank Dr. Xin Zhang and Nathanael Sieb for acquiring SEM/EDX images, as well as Dr. Aeli Olson and Dr. Brooke McNeil for all of their contributions.

References

[1] A. GRUNDMANE, C. F. RAMOGIDA and V. RADCHENKO, “Novel dibutyl ether resin for the purification of the Auger emitter antimony-119 from tin targets,” *Nuclear Medicine and Biology*, **146-147**, 109022 (2025).
[2] A. GRUNDMANE, I. DOVHYI, L. ABURTO-KUNG, S. HAPPEL, C. F. RAMOGIDA and V. RADCHENKO, *EJNMMI Radiopharmacy and Chemistry*, submitted April 24, 2025.
[3] Y. WANG, L. ZHU, R. CAO, W. LI and H. LIU, *Surface and Coatings Technology*, **331**, 90-96 (2017).
[4] A. P. OLSON, L. MA, Y. FENG, F. NAJAFI KHOSROSHAHI, S. P. KELLEY, E. ALUICIO-SARDUY, T. E, BARNHART, H. M. HENNKENS, P. A. ELLISON, S. S. JURISSON and J. W. ENGLE, *Inorganic Chemistry*, **60**, 15223-15232 (2021).

Copyright on 7th Asia-Pacific Symposium on Radiochemistry 2025- S2-03* -

Invited & Contributed Talk | [P4]Radionuclide Migration Dynamics: Radioactive Waste Disposal and Environmental Impact Assessment

Wed. Sep 17, 2025 9:45 AM - 10:55 AM JST | Wed. Sep 17, 2025 12:45 AM - 1:55 AM UTC Hall B(Small)

[P4] Radionuclide Migration Dynamics: Radioactive Waste Disposal and Environmental Impact Assesment

9:45 AM - 10:15 AM JST | 12:45 AM - 1:15 AM UTC

[P4-01(Invited)]

In Situ Measurement of Tritium behavior in Lead-Bismuth Reactor

*Muyi Ni[1,3], Yingwu Jiang[1], Junkang Yang[1], Peng Lin[2,3], Shiying Li[2], Xiajie Liu[2,3] (1. Sun Yat-sen University (China), 2. China Nuclear Power Technology Research Institute Co. (China), 3. CNPRI-SYSU Joint Research Center for Coolant Chemistry of Nuclear Reactor (China))

10:15 AM - 10:35 AM JST | 1:15 AM - 1:35 AM UTC

[P4-02]

Migration and Deposition of Radioactive Liquid Effluents in the Soil-Groundwater System Surrounding Terrestrial Discharge Pipelines

*Yuan CHEN[1], Han-yu WU[2], Le-wen SUN[2], Qiao-ya LIN[2], Jie YANG[1], Ming-liang KANG[2] (1. State Key Laboratory of Nuclear Power Safety Technology and Equipment, China Nuclear Power Engineering Co., Ltd. (China), 2. Sino-French Institute of Nuclear Engineering and Technology, Sun Yat-sen University (China))

10:35 AM - 10:55 AM JST | 1:35 AM - 1:55 AM UTC

[P4-03]

A Study on Application AI-Enhanced Multivariate Association Analysis for Environmental Radiation Monitoring Prediction Model in Taiwan

*Wei-Hsiang Tseng[1], Chuan-Pin Lee[2,3], Yu-Jie Li[4], Chin-Yi Fang[4], Yu-Cheng Tsai[1], Wei-Min Li [1], Zih-Shiuan Chiou[1], Yu-Hung Wang[3], Shih-Chin Tsai[5,3], Tzu-Chen Liao[3], Chi-Wen Hsieh[1] (1. Department of Electrical Engineering, National Chung Cheng University (Taiwan), 2. Center for Energy and Environmental Research, National Tsing Hua University (Taiwan), 3. Radioactive Waste Disposal Technology Research and Development Center, National Tsing Hua University (Taiwan), 4. Radiation Monitoring Center, Nuclear Safety Commission (Taiwan), 5. Nuclear Science and Technology Development Center, National Tsing Hua University (Taiwan))

©APSORC25

7th Asia-Pacific Symposium on Radiochemistry *September 14 ~ 19, 2025 • Kunibiki Messe • Shimane, Japan*

In Situ Measurement of Tritium behavior in Lead-Bismuth Reactor

Ni Muyi[1,3], Jiang Yingwu[1], Yang Junkang[1], Lin Peng[2,3], Li Shiying[2], Liu Xiajie[2,3]

[1]*Sino-French Institute of Nuclear Engineering & Technology, Sun Yat-sen University, Zhuhai, 519082, China*
[2]*China Nuclear Power Technology Research Institute Co., Ltd, Shenzhen, 518000, China*
[3]*CNPRI-SYSU Joint Research Center for Coolant Chemistry of Nuclear Reactor, Zhuhai, 519082, China*

The Lead-Bismuth Fast Reactor (LFR) represents a promising concept, characterized by its excellent neutron economy, chemical stability, and thermal properties. From a nuclear safety perspective, significant attention has primarily been directed towards understanding the behavior of 210Po and other fission products. Simultaneously, the issue of tritium in LFR remains inadequately addressed due to the challenges associated with conducting tritium experiments.

Formation of tritium/helium bubbles induces significant local stress and volume expansion, leading to hardening and embrittlement of structural materials, thus expediting their degradation through irradiation effects. Current understanding of tritium transport within liquid Lead-Bismuth Eutectic (LBE) remains incomplete. To bridge this gap, a novel device employing the "permeation pot" method has been developed for the first experimental quantification of diffusivity, permeability, and solubility of hydrogen isotopes in liquid LBE. Notably, hydrogen diffusivity in this medium is found to be three to four orders of magnitude greater than in conventional 316L stainless steel structural material. Furthermore, the temperature-dependence of diffusivity in liquid metals is minimal compared to solids, as indicated by the activation energy. Conversely, solubility in 316L significantly surpasses that in LBE by three to four orders of magnitude. This discrepancy accelerates the tritium release from LBE to structural material, leading to the failure of the structural material.

In addition, tritium not only poses a risk of hydrogen embrittlement to structural materials but also represents a potential hazard to operators due to radionuclide leakage from the cover gas. Basing on the existing "permeation pot" has been upgraded to integrate with a gaseous oxygen control device. An innovative approach was utilized to regulate the oxygen balance in lead bismuth eutectic (LBE), while deuterium—acting as a surrogate for tritium—simulates the migration of tritium from LBE to the cover gas. This setup enables in-situ measurement of tritium composition in the cover gas. The results indicate that the corrosion layer formed on structural materials by LBE not only protects the base material from further corrosion but also serves as a hydrogen permeation barrier, limiting the infiltration of hydrogen isotopes. Consequently, the majority of tritium is released into the cover gas due to its low solubility in LBE, primarily existing in the form of HTO, regardless of temperature, oxygen content, or tritium source. This finding underscores the need for the purification system in the cover gas to account for HTO

Copyright on 7th Asia-Pacific Symposium on Radiochemistry 2025 - P4-01 -

Migration and Deposition of Radioactive Liquid Effluents in the Soil-Groundwater System Surrounding Terrestrial Discharge Pipelines

Yuan Chen[1], Han-yu Wu[2*], Le-wen Sun[2], Qiao-ya Lin[2], Jie Yang[1], Ming-liang Kang[2*]

[1]*State Key Laboratory of Nuclear Power Safety Technology and Equipment, China Nuclear Power Engineering Co., Ltd., Baolong Rd. Nr. 3, Shenzhen, Guangdong, 518116, P. R. China, chenyuan2016@cgnpc.com.cn*
[2]*Sino-French Institute of Nuclear Engineering and Technology, Sun Yat-sen University, Zhuhai, Guangdong, 519082, P.R. China*

Radiation safety of nuclear power plants (NPPs) throughout the entire operational lifespan is increasingly gaining attention. Currently, all operational NPPs in China are coastal, with the treated liquid effluents being directly discharged into the ocean. In recent years, China has also begun constructing its first batch of coastal nuclear power projects located at a certain distance from the shore, where the treated liquid effluents are discharged into the ocean via long-distance terrestrial pipelines. This study focuses on Co-60, Sr-90, Cs-137, I-131, and H-3 in the liquid effluents of a proposed nuclear power plant as representative radionuclides, investigating their deposition and migration behaviors in the soil-groundwater system surrounding the terrestrial discharge pipelines.

Taking into account the hydrogeological conditions around the pipelines, locations susceptible to leakage (such as joints), and areas involving sensitive aquatic environments, seven sampling points were set up along the 13km pipeline to collect soil and groundwater samples. Adsorption-desorption experiments of radionuclides in the soil-groundwater system were conducted under different environmental conditions. Experimental results showed that the solid-liquid distribution coefficient (K_d) of radionuclides at different sampling points all followed the pattern Cs > Co > I > Sr. The lowest K_d value for Sr was mainly due to the high background concentration of Sr(II) in the native groundwater, and Sr-90 has a greater propensity to migrate with groundwater. Based on the experimental results and in combination with the liquid effluent source terms of the nuclear power plant, the adsorption deposition amounts and residual concentrations in the soil of four radionuclides (Cs-137, Sr-90, Co-60, and I-131) were calculated. It was found that the deposition amounts of radionuclides in the soil at all sampling points were within the acceptable concentration limits specified by the Interim Regulation for Acceptable Levels of Residual Radionuclides in Soil of Site Considered for Release (HJ 53-2000) in China.

H-3 primarily exists in groundwater in the form of tritiated water (HTO) and has an extremely strong migration ability in the environment. The diffusion experiment results showed that the properties of HTO are very similar to those of H_2O, with its α (capacity factor) value being equal to the ε (porosity) value. This indicates that HTO is not adsorbed by the soil but rather flows through the pores, with limited soil retention capacity and the fastest diffusion rate. Except for HTO, the apparent diffusion coefficients (D_a) of radionuclides in different soil samples all followed the pattern I(-I) > Sr(II) > Co(II) > Cs(I). This suggests that in the event of a long-distance discharge pipeline leak, H-3 would be the first to diffuse into the groundwater, followed by I-131 primarily in the anionic form. Among the radionuclides primarily in the cationic form, Sr-90 would be the first to diffuse into the groundwater.

In the event of a shear fracture accident of the pipeline, with a leakage time of 150 seconds, H-3 had the largest migration and diffusion range reaching 7.42E+03 m^2 among the studied radionuclides. The activity peaks of Sr-90, Co-60, I-131, Cs-137, and H-3 were 1.48E-05 Bq/L, 1.92E-03 Bq/L, 3.52E-02 Bq/L, 2.64E-02 Bq/L, and 3.25E+03 Bq/L, respectively, all of which were below the WHO Guidelines for Drinking-water Quality.

This study is crucial for the site selection of proposed nuclear power plants, sustainable risk management, and the protection of the surrounding environment, contributing to the overall safety and sustainability of nuclear power plants.

ACKNOWLEDGMENTS

This work was supported by the Foundation of China General Nuclear Power Corporation (No. K-A2021.561) and the China General Nuclear Power Group Research Project on the Research and Development of Key Technologies in Seawater Cooling Towers.

Application AI-Enhanced Multivariate Association Analysis for Radiation Monitoring Prediction Model in Taiwan

Wei-Hsiang Tseng[1], Yu-Jie Li[2], Chuan-Pin Lee[3,4], Chin-Yi Fang[2], Yu-Cheng Tsai[1], Wei-Min Li[1], Zih-Shiuan Chiou[1], Yu-Hung Wang[4], Shih-Chin Tsai[4], Tzu-Chen Liao[4], Chi-Wen Hsieh[1]

[1]*Department of Electrical Engineering, National Chung Cheng University, Chiayi County 621301, Taiwan; hot0213338@gmail.com (W.-H.T.); abc8520085@gmail.com (Y.-C.T.); gilbertli1206@gmail.com (W.-M.L.); a067213121@gmail.com (Z.-S.C.); chiwenh@ccu.edu.tw (C.-W.H.)*

[2] *Radiation Monitoring Center, Nuclear Safety Commission, Kaohsiung City 833172, Taiwan; yjkex@nusc.gov.tw (Y.-J.L.); cyfang@nusc.gov.tw (C.-Y.F.)*

[3]*Center for Energy and Environmental Research, National Tsing Hua University, Hsinchu City 300044, Taiwan*

[4] *Radioactive Waste Disposal Technology Research and Development Center, National Tsing Hua University, Hsinchu City 300044, Taiwan; bennis6723@gmail.com (C.-P.L.)*

Nuclear power is considered one of the key energy sources for sustainable development, making environmental radiation monitoring increasingly important. This study integrates environmental dose rate data from 63 monitoring stations managed by Taiwan's Radiation Monitoring Center. By incorporating spatial correlations between stations and weather-related factors, we employ artificial intelligence (AI) techniques—specifically, the Variational Autoencoder (VAE) architecture—to forecast future dose rates at each monitoring site. Using approximately 300 days of full-time data collected in 2024 as the dataset, preliminary results show that when forecasting dose rates 7 minutes ahead based on the current 10-minute radiation spatial dose rate data, about 70% of the stations achieved a Mean Absolute Error (MAE) of less than 0.005, indicating meaningful predictive performance. The study also found that the model is sensitive to threshold values in the data; when monitoring data is too low, the predicted values tend to exhibit periodic oscillations with significantly larger errors.

Keyword: Nuclear energy, Environmental radiation monitoring, Artificial intelligence, Variational Autoencoder

1. INTRODUCTION

Taiwan's last nuclear power plant is scheduled to cease operations by the end of May 2025. However, nuclear safety continues to be a key public concern, making environmental radiation monitoring even more critical. In recent years, the development of artificial intelligence (AI) has gradually extended into scientific domains [1–2]. In the nuclear energy sector, AI has been applied to tasks such as monitoring system optimization and fault diagnosis [3–4]. Among various AI techniques, models based on the Transformer architecture and Multi-Head Self-Attention mechanism have demonstrated excellent performance in capturing complex patterns in spatiotemporal data and have been effectively utilized in related research [5]. Motivated by these advancements, this study aims to apply AI techniques to predict future radiation dose rates at 63 environmental radiation monitoring stations across Taiwan.

2. MATERIALS AND METHODS

In this study, we applied the radiation monitoring instruments surround the Taiwan island is the SERVCOMPUTING INC. MERM-PE-HDBM model and adopt a Transformer-based architecture incorporating Multi-Head Self-Attention as the core model framework. We reference the Air Former model proposed by Liang, Y. in 2023 [6], which introduces a Variational Autoencoder (VAE)-based architecture capable of capturing both spatial and temporal associations for air pollution prediction. Inspired by this approach, we aim to apply the model to forecast future environmental radiation dose rates to enable systematic monitoring. Considering that weather conditions may influence fluctuations in radiation dose rates, this study specifically includes rainfall data as an input feature for prediction [7]. In Fig. 1, radiation dose rate and rainfall data collected from each monitoring station are aggregated. The overall dataset is normalized based on its calculated mean (0.049) and standard deviation (0.017). Subsequently, the data undergo spatial and temporal association analysis before being fed into the neural network for training. Finally, the model's output is evaluated to interpret the performance of the trained neural network.

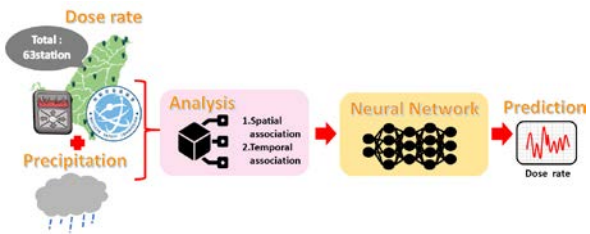


Fig. 1. Main Architecture

3. RESULTS

The results show that the training loss, reconstruction loss (rec loss), and KL divergence loss (kl loss) all effectively converge within one standard deviation (0.017), while the validation loss also demonstrates good convergence. When the radiation dose rate at a given monitoring station is higher than the dataset's mean value (0.049), the model performs well in prediction, as shown in Fig. 2(a). However, when the average dose rate at a station is lower than the dataset's mean, the prediction exhibits periodic oscillations, as illustrated in Fig. 2(b). Stations with average dose rates below the dataset mean are the minority, primarily located on offshore islands. These regions are more susceptible to external interferences such as instrumentation noise and environmental variability, making the radiation dose rate patterns less distinct and harder for the model to capture, which in turn results in poorer predictive performance.

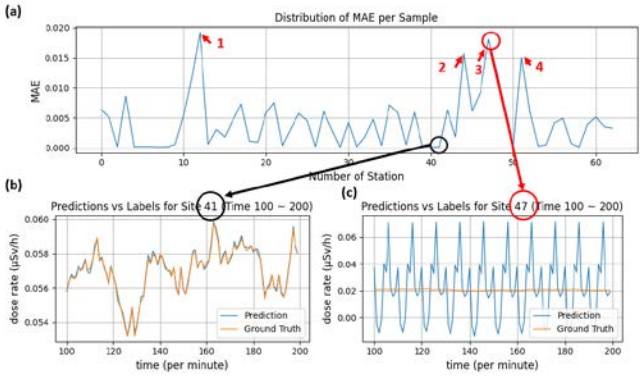


Fig. 2. Model Predictions of Environmental Radiation Monitoring Values: (a) MAE loss across all stations; arrows 1, 2, 3, and 4 indicate offshore island locations. (b) Prediction result for a station where the environmental radiation dose rate is higher than the dataset mean (0.049). (c) Prediction result for a station where the dose rate is lower than the dataset mean. The actual measured radiation dose rates (yellow line) and the model's predicted values (blue line) show good alignment.

4. CONCLUSIONS

This study demonstrates the feasibility of integrating artificial intelligence with environmental radiation monitoring using a Variational Autoencoder (VAE) model architecture. By incorporating rainfall as an additional feature alongside the radiation dose rate at each station, the model successfully predicts the dose rate for the next 7 minutes. By leveraging spatial associations from neighboring stations and temporal associations from historical data at each site, the prediction error was effectively reduced to within one standard deviation (0.017).Compared to conventional Transformer models, the proposed model shows improved capability in handling long-term temporal dependencies. Future work will focus on further refining the model architecture and conducting experiments to optimize its performance, particularly in scenarios where radiation levels are lower than the overall dataset mean. The goal is to establish a more robust and comprehensive radiation monitoring system.

ACKNOWLEDGMENTS

This study was mainly supported by the Taiwan Radiation Monitoring Center of the Nuclear Safety Commission for the development of an environmental radiation dose monitoring model (Project No. 1131226) and the National Science and Technology Council (NSTC, Taiwan R.O.C) through a mutual fund program under grant number NSTC 114-2623-E-007 -001-NU.. All relevant data and information were provided by the Radiation Monitoring Center. We sincerely thank the Center for their strong support and assistance throughout the project.

References

[1] Fatima Ezzahra Arhouni, Maged Ahmed Saleh Abdo, Saad Ouakkas, Mohamed Lhadi Bouhssa, Aziz Boukhair, Artificial intelligence-driven advances in nuclear technology: Exploring innovations, applications, and future prospects, Annals of Nuclear Energy, 2025, ISSN 0306-4549, https://doi.org/10.1016/j.anucene.2024.111151.
[2] Brown, David. "Artificial Intelligence for Accelerating Nuclear Applications, Science, and Technology." , Jul. 2022. https://doi.org/10.2172/1913826
[3] Jendoubi, C., & Asad, A. (2024). A Survey of Artificial Intelligence Applications in Nuclear Power Plants. IoT, 5(4), 666-691. https://doi.org/10.3390/iot5040030

[4] Fu Wang, Tangfan Xiahou, Xian Zhang, Pan He, Taibo Yang, Jiang Niu, Caixue Liu, Yu Liu, Convolutional preprocessing Transformer-based fault diagnosis for rectifier-filter circuits in nuclear power plants, Reliability Engineering & System Safety, Volume 249, 2024, ISSN 0951-8320, https://doi.org/10.1016/j.ress.2024.110198.
[5] Tuo, Y, & Liu, X. "Enhancing Nuclear Power Plant Operational Forecasting With Transformer Neural Networks: a Time-Series Data Approach." August 4–8, 2024. V001T01A037. ASME. https://doi.org/10.1115/ICONE31-135879
[6] Lau, W. K. M., & Tao, W. (2020). Precipitation–Radiation–Circulation Feedback Processes Associated with Structural Changes of the ITCZ in a Warming Climate during 1980–2014: An Observational Portrayal. Journal of Climate, 33(20), 8737-8749. https://doi.org/10.1175/JCLI-D-20-0068.1
[7] Liang, Y., Xia, Y., Ke, S., Wang, Y., Wen, Q., Zhang, J., Zheng, Y., & Zimmermann, R. (2023). AirFormer: Predicting Nationwide Air Quality in China with Transformers. Proceedings of the AAAI Conference on Artificial Intelligence, 37(12), 14329-14337. https://doi.org/10.1609/aaai.v37i12.26676

Invited & Contributed Talk | [S2]Radiopharmaceutical Sciences

Wed. Sep 17, 2025 3:00 PM - 4:30 PM JST | Wed. Sep 17, 2025 6:00 AM - 7:30 AM UTC Hall S(Int'l)

[S2] Radiopharmaceutical Sciences

3:00 PM - 3:30 PM JST | 6:00 AM - 6:30 AM UTC

[S2-07(Invited)]

Development of At-211 YF2, a PSMA-targeted agent: from bench to bedside, and academia to industry

*Yutian Feng Feng[1] (1. Duke University Medical Center (United States of America))

3:30 PM - 3:50 PM JST | 6:30 AM - 6:50 AM UTC

[S2-08]

Production of ^{211}At/^{18}F-labeled PSMA compounds for radiotheranostics under Investigational GMP

*Sadahiro Naka[1,2], Yoshifumi Shirakami[3], Kazuhiro Ooe[3], Kenta Kurimoto[1,2], Toshihiro Sakai[1], Masashi Murakami[3], Yukiyoshi Kon[3], Hiromitsu Haba[4], Atsushi Toyoshima[3], Tadashi Watabe[1,3], Noriyuki Tomiyama[1,3] (1. Department of Radiology, Graduate School of Medicine, The University of Osaka (Japan), 2. Department of Pharmacy, The University of Osaka Hospital (Japan), 3. Institute for Radiation Sciences, The University of Osaka (Japan), 4. Nishina Center for Accelerator-Based Science, RIKEN (Japan))

3:50 PM - 4:10 PM JST | 6:50 AM - 7:10 AM UTC

[S2-09*]

Astatine dry distillation: evaluating co-distillation of radionuclidic impurities and target starting material.

*Ellinor Hansson[1,2], Charlotte Ytterbrink[1], Tom Bäck[1], Erik Leidermark[1,4], Holger Jensen[3], Björn Eriksson[2], Sture Lindegren[1], Emma Aneheim[1,4] (1. Gothenburg University (Sweden), 2. Atley Solutions (Sweden), 3. Copenhagen University Hospital (Denmark), 4. Sahlgrenska University Hospital (Sweden))

4:10 PM - 4:30 PM JST | 7:10 AM - 7:30 AM UTC

[S2-10*]

Neutron activation of gold nanoparticles for imaging of pharmacokinetics

*Nanase Koshikawa[1], Yuka Kikuchi[1], Jun Kataoka[1], Kazuo Skipjack Tanaka[1], Katsuyuki Tokoi[2], Akina Mitsukai[2], Hiroki Aoto[2], Masashi Murakami[2], Yuichiro Kadonaga[2], Atsushi Toyoshima[2], Hiroki Kato[2], Kazuhiro Ooe[2], Koichi Takamiya[3] (1. Waseda Univ. (Japan), 2. Osaka Univ. (Japan), 3. Kyoto Univ. (Japan))

©APSORC25

Development of ^{211}At YF2, a PSMA-targeted agent: from bench to bedside, and academia to industry

Yutian Feng
Duke University Medical Center
Co-Founder and CEO, Alpha Nuclide Inc.

Objectives: We have developed the low-molecular-weight PSMA-targeted agent [^{211}At]YF2 for targeted α-particle therapy (TAT) of prostate cancer. Preclinical evaluations showed promising results, and results from an early stage clinical study were consistent. Although these promising results warrant full-scale clinical evaluation, supply of At-211 becomes the bottleneck.

Methods: The tin precursor (Sn-YF2) and unlabeled iodo standard (I-YF2) of [^{211}At]YF2 were synthesized and fully characterized. A one-step labeling method was developed to produce [^{211}At]YF2 from this tin precursor, and the RCY and RCP were determined using RP-HPLC. Cell uptake, internalization and in vitro cell-killing (MTT) assays were performed on PSMA+ PC-3 PIP cells. Biodistribution of [^{211}At]YF2 was performed using athymic mice bearing s.c. PSMA+ PC-3 PIP xenografts. Therapeutic efficacy of [^{211}At]YF2 was determined using the same xenograft model (170 mm^3 tumor volume). Co-administration of iodinated YF2 resulted in a 5-fold increase in tumor-to-kidney dose ratio for [^{211}At]YF2. Significant tumor growth inhibition (TGI) and survival benefit were seen for mice treated with [^{211}At]YF2. A single dose of 2.2 MBq led to a 3.6-fold increase in median survival. In a second study, a dose-dependent TGI and survival benefit was observed for the treatment groups, with 8 MBq of [^{211}At]YF2 inducing a 4.5-fold increase in median survival. Radiation toxicity was seen in mice treated with 9 or 12 MBq [^{211}At]YF2, indicating an MTD of 8 MBq. The biodistribution and dosimetry of ^{211}At-YF2 first was evaluated in healthy CD-1 mice and converted to human-equivalent values using standardized adult phantoms. Human radiation dosimetry and estimated dosage were calculated using Rapid 3D-Rd software. The murine dosimetry and the first-in-human clinical dosimetry and imaging results for ^{211}At-YF2 were performed to assess its safety and tolerability in three patients with mCRPC. An innovative ^{211}At

production, drug product manufacture, and distribution model was developed and commercialized.

Results: Sn-YF2 and I-YF2 were synthesized in overall yields of 16% and 28%, respectively. The average RCY for [^{211}At]YF2 was 78 ± 5% (n=8) and RCP was >99%. A maximum of 684 MBq of [^{211}At]YF2 was produced in one step in 1 h. Significantly higher cell uptake, internalization and cell-killing efficacy was seen for [^{211}At]YF2 compared with [^{211}At]VK-02-90-Lu. Similar tumor uptake in vivo was observed for [^{211}At]YF2 and [^{211}At]VK-02-90-Lu at 1 and 4 h, while tumor uptake was higher for [^{211}At]YF2 at 24 h, with 16.16 ± 2.06% ID/g versus that of [^{211}At]VK-02-90-Lu 9.72 ± 1.89% ID/g (P=0.0009). Higher kidney levels were observed for [^{211}At]YF2 at all time points. Low uptake was observed in the salivary glands and lacrimal glands for both agents. A single dose of [^{211}At]YF2 showed significant antitumor efficacy and survival benefit, with several long-term survivors. A single dose of 8 MBq [^{211}At]YF2 was well tolerated. Clinical translation showed that ^{211}At-YF2 was well tolerated in all patients, with all adverse events (AEs) being ≤ Grade 2 in severity. High initial uptake of ^{211}At-YF2 was observed in the kidneys, urinary bladder, salivary glands, and thyroid, followed by rapid clearance. Pronounced uptake of ^{211}At-YF2 in tumor sites identified by PSMA-PET was observed in all patients even at 24 h.

Conclusions: [^{211}At]YF2 exhibited more cellular uptake, internalization and cytotoxicity than [^{211}At]VK-02-90-Lu on PSMA+ PC3 PIP cells. In a single-dose therapy study, mice treated with [^{211}At]YF2 showed significant tumor growth inhibition and survival benefit. ^{211}At-YF2 demonstrated selective and prolonged tumor uptake, an unremarkable safety profile, and appropriate biodistribution in mCRPC patients. These findings suggest that ^{211}At-YF2 is a promising TAT agent for treating PSMA-positive mCRPC and warrants further clinical development. We successfully developed a commercial supply model for global access of ^{211}At, which laid the foundation for ^{211}At-containing TAT agents to reach their full potential.

Copyright on 7th Asia-Pacific Symposium on Radiochemistry 2025 - S2-07 -

7th Asia-Pacific Symposium on Radiochemistry *September 14 ~ 19, 2025 • Kunibiki Messe • Shimane, Japan*

Production of ^{211}At/^{18}F-labeled PSMA compounds for radiotheranostics under Investigational GMP.

Sadahiro Naka[1,2], Yoshifumi Shirakami[3], Kazuhiro Ooe[3], Kenta Kurimoto[1,2], Toshihiro Sakai[1], Masashi Murakami[3], Yukiyoshi Kon[3], Hiromitsu Haba[4], Atsushi Toyoshima[3], Tadashi Watabe[1,3], Noriyuki Tomiyama[1,3],

[1]*Department of Radiology, Graduate School of Medicine, The University of Osaka: 2-2 Yamadaoka, Suita, Osaka, Japan*
naka-s@office.osaka-u.ac.jp
[2]*Department of Pharmacy, The University of Osaka Hospital: 2-15 Yamadaoka, Suita, Osaka, Japan*
[3]*Institute for Radiation Sciences, The University of Osaka: 2-4 Yamadaoka, Suita, Osaka, Japan,*
[4]*Nishina Center for Accelerator-Based Science, RIKEN, 2-1 Hirosawa, Wako, Saitama, Japam*

1. INTRODUCTION

The prostate-specific membrane antigen (PSMA) is a major target for the theragnostics in prostate cancer. [^{211}At]PSMA-5 was developed at Osaka University as an alpha-therapy drug targeting PSMA based on ^{18}F-PSMA-1007, which was already widely used as an excellent diagnostic agent. It has shown excellent tumor growth inhibition in a model mouse of prostate cancer with minimal side effects in normal organs and is expected to be a new targeted alpha therapy, especially metastatic castration-resistant prostate cancer [1]. In this study, we describe the investigational GMP manufacturing of ^{211}At-PSMA-5 for investigator-initiated clinical trials and ^{18}F-PSMA-1007 as a companion diagnostic agent in pre-treatment patient screening at the University of Osaka Hospital.

2. EXPERIMENTAL

Production of labeled compounds was performed at the short-lived radiopharmaceutical manufacturing facility of the University of Osaka Hospital in compliance with the investigational GMP.

^{211}At was produced with the nuclear reaction of ^{209}Bi(^{4}He, 2n) using AVF Cyclotron at RIKEN or Research Center for Nuclear Physics, the University of Osaka. ^{211}At in irradiated Bi target was purified by an automated dry distillation apparatus (Cosmic mini, NMP Business Support). The procedure for recovery of purified ^{211}At from the trap tube to the reaction vessel and reaction condition were investigated. Using an optimized synthesis procedure, six lot tests of [^{211}At]PSMA-5 solution were performed (three times by each target) using an automated synthesizer as a process validation.

The radiosynthesis of [^{18}F]PSMA-1007 was carried out using a MPS-200 cassette types of multipurpose synthesizer (Sumitomo Heavy Industries). The precursor for direct radio-labelling was the acetate salt of the precursor compound bearing trimethyl ammonium as leaving group. The [^{18}F]fluoride obtained from the nuclear reaction in ^{18}O(p, n)^{18}F using a medical cyclotron Cypris HM-18 (Sumitomo Heavy Industries) was trapped on an anion-exchange cartridge and eluted by $TBAHCO_3$ solution. After the solvent removed, the precursor/DMSO solution was added to the reaction vessel and radio-fluorination was carried out. The purification and recovery of [^{18}F]PSMA-1007 were done using SPE cartridges and ethanol solutions. Final production of [^{18}F]PSMA-1007 was ethanol/phosphate buffered saline including 400 mg sodium ascorbate as a stabilizing agent.

3. RESULTS AND DISCUSSION

More than 90% of the purified ^{211}At was recovered by allowing 700 µL mL of 7% sodium bicarbonate injection solution to keep for 5 min into the trap tube. Using a glass vial as the reaction vessel, the labeling rate of [^{211}At]PSMA-5 was over 70% in a 45-minute reaction at 95 ^{0}C with 1 mL of reaction solution (700 µL of ^{211}At soluton, 10 µL of 1 mg/mL PSMA-5 precursor and 290 µL of 0.1 M potassium iodide a.q. solution), and the residual radioactivity in the reaction vessel was less than 5%. In the six-lot tests, [^{211}At]PSMA-5 solution was obtained in a synthesis time of approximately 130 minutes with a radiochemical yield of 29±3% (after decay collection). Radiochemical purity was 96±1% at the end of synthesis, and it was remained above 90% after 6 hours of synthesis.

In the result of [^{18}F]PSMA-1007 synthesis, the radiochemical yield of [^{18}F]PSMA-1007 with 1.6 mg precursor was 40±2% within 45 min and the radiochemical purity was 97±0%. In addition, radiochemical purity was constant at least for 8 hr. Acetonitrile and DMSO as residual solvents and residual TBA could not be observed, and ethanol portion of injection solution was approximately 6%. And then, all other quality test items in both productions were also confirmed to meet the specification criteria.

4. CONCLUSIONS

In this study, [^{211}At]PSMA-5 and [^{18}F]PSMA-1007 was obtained stably in a process validation, meeting all quality specification criteria. We have already started supplying [^{211}At]PSMA-5 and [^{18}F]PSMA-1007 for investigator-initiated clinical trials (NCT06441994).

ACKNOWLEDGMENTS

This work was supported by the staff of SHI Accelerator Service.

References

[1] Eur J Nucl Med Mol Imaging, Watabe T et al, 2023. doi: 10.2967/jnumed.120.245084.

7th Asia-Pacific Symposium on Radiochemistry *September 14 ~ 19, 2025 • Kunibiki Messe • Shimane, Japan*

Astatine dry distillation: evaluating co-distillation of radionuclidic impurities and target starting material.

Ellinor Hansson[1,2 *], Tom Bäck[1], Charlotte Ytterbrink[1], Erik Leidermark[1], Holger Jensen[3], Björn Eriksson[2] Sture Lindegren[1], Emma Aneheim[1,4]

[1] *Department of Medical Radiation Sciences, Institute of Clinical Sciences, Sahlgrenska Academy, University of Gothenburg, 41345 Gothenburg, Sweden.*
[2] *Atley Solutions AB, 41327 Gothenburg, Sweden.*
[3] *Department of Clinical Physiology and Nuclear Medicine, Cyclotron and Radiochemistry unit, Copenhagen University Hospital, 2100 Copenhagen, Denmark.*
[4] *Department of Oncology, Region Västra Götaland, Sahlgrenska University Hospital, 41345 Gothenburg, Sweden.*

Introdution

The medical isotope astatine-211 (At-211) is cyclotron produced using the 209Bi(α,2n)211At nuclear reaction. As global demand for At-211 continues to rise, increasing incidence energy of the alpha particles from circa 28 to above 30 MeV would enhance production efficiency. However, this strategy may also elevate the co-production of undesirable radionuclides, most notably Polonium-210 (Po-210).

For At-211 to be used safely and effectively in radiopharmaceutical production, it is critical to achieve efficient separation of Po-210 and other radionuclide impurities in the work up procedure after cyclotron production. This study investigates the efficacy of reduced pressure dry distillation in isolation of At-211 from the bismuth target with focus on analyzing breakthrough of impurities in the distillation process.

Methods

At-211 was produced using the MC32 Scanditronix cylotron at Copenhagen University Hospital, Denmark, using an <30 MeV incidence energy on the Bi-target. After production the target contain co-produced nuclides and decaying products including Po-210, Bismuth-207 (Bi-207), Sodium-24 (Na-24) and Gallium-66 (Ga-66). The irradiated targets underwent one of two protocols: (1) direct (< 6 hours after EOB) low pressure dry distillation on an Atley C100 system followed by high-purity germanium (HPGe) spectrometry of the eluate and the remaining target material; or (2) a delayed analysis was performed to determine Po-210 in the eluate i.e. after > 10 half-lives of At-211. Po-210 content was quantified via alpha spectrometry and alpha camera analysis, both before and after low pressure dry distillation.

The co-distillation of non-radioactive Bi-209 and Al-27 was determined using inductively coupled plasma mass spectrometry (ICP-MS). Additionally, from the decay of At-211, Bi-207 levels in the dry distillation eluate were assessed via HPGe and compared to theoretical post-distillation levels.

Results

Dry distillation of the target resulted in isolated yields of At-211 exceeding 80% (non-decay corrected). In the distillation process a reduced pressure of 600 mBar at 720 °C with a low-flow nitrogen stream. While Na-24 and Ga-66 were detectable by HPGe in the irradiated target material, they were absent in the dry distillation eluate, indicating complete removal from the levels produced.

An initial evaluation of Po-210 indicated near complete removal of Po-210 directly produced in the cyclotron irradiation. Po-210 may also result from the decay of co-produced At-210. This part of Po-210 was analysed by measuring purified eluate after 10 half-lives of At-210. Measurements were made via both alpha camera and alpha spectrometry.

ICP-MS analysis did not show any co-distillation of natural bismuth or aluminum above ambient levels. This result was confirmed by Bi-207 quantification that indicated a near complete removal of Bi-207 at the distillation, further supporting the selectivity of this purification method.

Discussion

This study demonstrates the effectiveness in isolation of At-211 using dry distillation of irradiated bismuth targets. In the distillation process both the target starting material and radionuclide impurities are effectively removed. Given the clinical importance of minimizing Po-210 levels, these results underscore dry distillation as a robust method for At-211 purification.

Copyright on 7th Asia-Pacific Symposium on Radiochemistry 2025- S2-09* -

Neutron activation of gold nanoparticles for imaging of pharmacokinetics

Nanase Koshikawa[1], Yuka Kikuchi[1], Jun Kataoka[1], Kazuo S. Tanaka[1], Katsuyuki Tokoi[2], Akina Mitsukai[2], Hiroki Aoto[2], Masashi Murakami[3], Yuichiro Kadonaga[3], Atsushi Toyoshima[3], Hiroki Kato[3], Kazuhiro Ooe[3], Koichi Takamiya[4]

[1]*Graduate School of Advanced Science and Engineering, Waseda University: 3-4-1 Okubo, Shinjuku-ku, Tokyo, Japan* [2]*Department of Chemistry, Graduate School of Science, Osaka University, 1-1 Machikaneyama, Toyonaka, Osaka, Japan* [3]*Institute for Radiation Sciences, Osaka University, 1-1, Machikaneyama-cho, Toyonaka, Osaka, Japan* [4]*Institute for Integrated Radiation and Nuclear Science, Kyoto University, 2, Asashiro-Nishi, Kumatori-cho, Sennan-gun, Osaka, Japan*

Gold nanoparticles (AuNPs) have been attracting attention as promising drug carriers. However, direct and highly sensitive method to visualize AuNPs has not yet been established. In this study, we propose and demonstrate "activation imaging" of AuNPs. Stable gold atom, ^{197}Au, changes to radioactive ^{198}Au when irradiated with low-energy neutrons. ^{198}Au emits 412-keV gamma rays and has 2.7-days half-life. These gamma rays allows imaging of AuNPs from outside the body, and relatively long half-life enables the investigation of long-term pharmacokinetics over several days. We injected radioactive AuNPs to tumor-bearing mice and performed imaging with Compton camera. The distribution of AuNPs was successfully visualized even 4 days after injection. Moreover, ^{211}At, which is a promising alpha-emitting nuclear medicine, was labeled on radioactive AuNPs and injected to the mice. Simultaneous imaging of ^{211}At and AuNPs was achieved using 79-keV X-rays from ^{211}At and 412-keV gamma rays from ^{198}Au. Although we successfully visualized AuNPs, spatial resolution of Compton camera ($\sim$10 mm) was insufficient to investigate pharmacokinetics in detail. Therefore, we are now developing novel SPECT (single photon emission computed tomography) system for high energy gamma rays to visualize radioactive AuNPs with high spatial resolution.

1 Introduction

Delivering drugs to tumors is essential for effective cancer therapy with minimal side effects. Gold nanoparticles (AuNPs) are promising drug carriers due to their tumor accumulation and ease of functionalization. However, their in vivo distribution changes with various factors such as size and shape[1], making imaging crucial for optimizing delivery. While tracers like fluorescent dyes, radioisotopes, and contrast agents have been used[2], they may detach from AuNPs and accumulate differently. Imaging with computed tomography (CT) by using AuNPs as contrast agents has also been proposed[3], but it requires high doses due to limited sensitivity[3]. Therefore, we propose "activation imaging" of AuNPs as a direct method with high sensitivity. Activation imaging activates materials via neutron irradiation and performs visualization using X-rays and/or gamma rays emitted from the activated atoms.

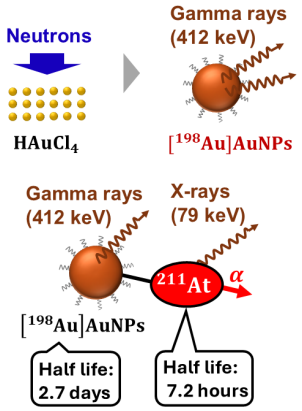


Fig. 1. $[^{198}Au]AuNPs$ (*top*) and $[^{211}At/^{198}Au]$-AuNPs (*bottom*)

In this study, we synthesized radioactive gold nanoparticles ($[^{198}Au]AuNPs$) (Fig. 1 (*top*)), injected them into tumor-bearing mice, and performed in vivo imaging. Moreover, we conjugated ^{211}At with $[^{198}Au]AuNPs$ (Fig. 1 (*bottom*)). ^{211}At is a promising therapeutic drug that emits alpha particles and 79-keV X-rays during decay. The distributions of ^{211}At and AuNPs can be visualized individually using 79-keV X-rays and 412-keV gamma rays, respectively, enabling the investigation of in vivo retention of conjugation. Furthermore, the relatively long half-life of ^{198}Au, 2.7 days, allows the long-term tracking of ^{211}At-labeled AuNPs, which has been challenging because of the short half-life of ^{211}At, 7.2 h. Mice injected with $[^{211}At/^{198}Au]AuNPs$ were imaged 2 days after administration to demonstrate long-term tracking.

2 In vivo imaging of AuNPs

Imaging was performed with hybrid Comtpon camera (HCC) that can perform broadbandband X-rays and gamma-rays imaging. The HCC consists of two pixelated Ce-doped $Gd_3Al_2Ga_3O_{12}$ (Ce: GAGG) scintillators, a scatterer and an absorber, and the scatterer has a pinhole in the center. The pixel pitch is 1×1 mm^2. The scatterer works as an active shield, and low-energy (< 200 keV) X-rays and gamma rays can be visualized based on the principle of pinhole cameras (pinhole mode), as shown in Fig. 2 (a) (*left*). For high-energy gamma rays, imaging based on the principle of Compton cameras can be performed as shown in Fig. 2 (a) (*right*) (Compton mode). In Compton mode, gamma rays that are scattered at the scatterer and absorbed at the absorber are used for image reconstruction. The scattering angle is calculated by using the energy deposit at the scatterer and absorber, and the source position is limited to the conical surface. The source is visualized by repeating this process. Pinhole and Compton mode allow imaging using wide-band X-rays and gamma rays with energies ranging from tens of keV to approximately 1 MeV.

Copyright on 7th Asia-Pacific Symposium on Radiochemistry 2025- S2-10* -

Tetrachloroauric(Ⅲ) acid tetrahydrate ($HAuCl_4 \cdot 4H_2O$) was irradiated with low-energy (primarily thermal) neutrons using Kyoto University Research Reactor (KUR)[4]. After that, AuNPs were synthesized by mixing with trisodium citrate followed by reduction with $NaBH_4$. [^{198}Au]AuNPs was then purified by ultrafiltration. Tumor-bearing mice were intratumorally injected with [^{198}Au]-AuNPs. We performed imaging at 9 min and 4 days after injection. Moreover, we labeled ^{211}At with [^{198}Au]AuNPs. Tumor-bearing mice were injected with [^{211}At/^{198}Au]AuNPs via the tail vein. Imaging was performed at 9 min and 2 days after injection. Visualization of ^{211}At and ^{198}Au was performed using the same measurement data and setting energy windows at 79 ± 10 keV (pinhole mode) and 412 ± 30 keV (Compton mode), respectively.

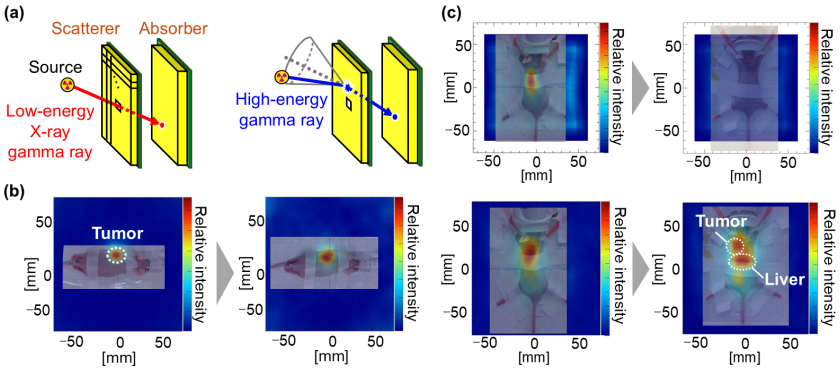


Fig. 2. (a) Pinhole-mode (*left*) and and Compton-mode (*right*) imaging using HCC. (b) Images of the mouse injected with [^{198}Au]AuNPs obtained at 9 min (*left*) and 4 days (*right*) after administration. (c) Images of the mouse injected with [^{211}At/^{198}Au]AuNPs. *Top left* and *top right*: Images of ^{211}At obtained at 9 min and 2 days after administration, respectively. *Bottom left* and *bottom right*: Images of ^{198}Au obtained at 9 min and 2 days after administration, respectively.

Fig. 2 (b) shows images of mice intratumorally injected with [^{198}Au]AuNPs. Left and right images were obtained at 9 min and 4 days after administration, respectively. Even 4 days after injection, [^{198}Au]AuNPs remaining in the tumor were imaged successfully. Fig. 2 (c) shows images of mice intravenously injected with [^{211}At/^{198}Au]AuNPs. Figs. 2 (c) (*top left*) and (*top right*) show images of ^{211}At obtained at 9 min and 2 days after administration, respectively. Figs. 2 (*bottom left*) and (*bottom right*) show images of ^{198}Au obtained at 9 min and 2 days after administration, respectively. In images (*top left*) and (*bottom left*), accumulation of ^{211}At and ^{198}Au in the same area was observed, suggesting successful conjugation. Two days later, imaging of ^{211}At became impossible because of its decay (*bottom right*), but we could still image [^{211}At/^{198}Au]AuNPs using 412-keV gamma rays from ^{198}Au with a longer half-life (*bottom right*).

3 Development of high-contrast SPECT

Although [^{198}Au]AuNPs and [^{211}At/^{198}Au]-AuNPs in mice's body were successfully visualized with HCC, spatial resolution of HCC (∼10 mm) was insufficient for detailed investigation of pharmacokinetics. Therefore, we developed a SPECT (single photon emission computed tomography) system for high energy gamma rays, aiming to achieve the few-millimeter spatial resolution required for imaging in small animals such as mice. SPECT is a X-ray/gamma-ray imaging device equipped with a collimator that limits the arrival direction of X-rays and gamma rays. Although SPECT can provide high spatial resolution, conventional SPECT systems are limited to imaging gamma rays below 200 keV, as higher-energy gamma rays can penetrate the collimator walls, reducing image contrast. Thicker collimator walls can block high-energy gamma rays more effectively, but they also reduce detection efficiency.

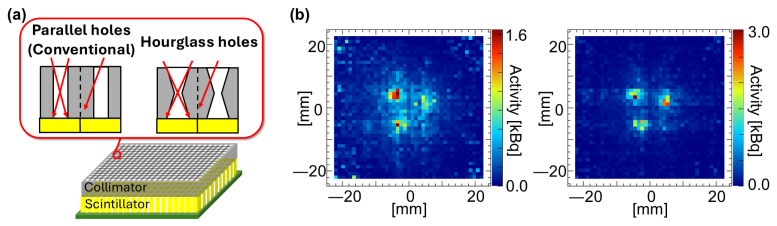


Fig. 3. (a) Parallel-hole collimator and hourglass-hole collimator. (b) Images of ^{198}Au sources (ϕ3 mm) obtained with parallel-hole SPECT (*left*) and hourglass-hole SPECT (*right*).

Therefore, we developed a novel SPECT capable of high-resolution and high-contrast imaging using high-energy gamma rays. we developed a novel collimator with an array of hourglass-shaped holes as shown in Fig. 3 (a). This hole shape offers thick collimator walls while maintaining high sensitivity compared to the conventional parallel shape. The 1-mm pitch array of Ce: GAGG was used as the detector. we visualized ^{198}Au in a Derenzo phantom using 412-keV gamma rays with this high-constrast SPECT system. As a result, ϕ2-mm sources were successfully separated. Moreover, imaging of three ϕ3-mm sources spaced 1 cm apart was performed using both hourglass-hole and conventional parallel-hole collimators. The image obtained with the hourglass-hole collimator showed higher contrast than that obtained with the parallel-hole collimator (Fig. 3(b)).

References

[1] B. D. Chithrani, A. A. Ghazani, and W. C. Chan, Nano Lett. 6, 662–668 (2006).
[2] J. Zhu, J. Chin, C. Wangler, B. Wangler, R. B. Lennox, and R. Schirrmacher, Bioconjugate Chem. 25, 1143–1150 (2014).
[3] R. Popovtzer, A. Agrawal, N. A. Kotov, A. Popovtzer, J. Balter, T. E. Carey, and R. Kopelman, Nano Lett. 8, 4593–4596 (2008).
[4] R. Matsushita, M. Koyama, S. Yamada, M. Kobayashi, and H. Moriyama, J. Radioanal. Nucl. Chem. 216, 95–99 (1997).

Copyright on 7th Asia-Pacific Symposium on Radiochemistry 2025- S2-10* -

Invited & Contributed Talk | [R3]Actinide Chemistry and Nuclear Energy Chemistry

Wed. Sep 17, 2025 3:00 PM - 4:30 PM JST | Wed. Sep 17, 2025 6:00 AM - 7:30 AM UTC Hall A(MP)

[R3] Actinide Chemistry and Nuclear Energy Chemistry

3:00 PM - 3:30 PM JST | 6:00 AM - 6:30 AM UTC

[R3-15(Invited)]

URANYL COORDINATION WITH BIOLOGICAL LIGANDS ANALYZED BY HERFD-XANES SPECTROSCOPY

*Akihiro Uehara[1], Daiju Matsumura[2], Daisuke Akiyama[3], Akira Kirishima[3], Shino Homma-Takeda[1], Teruaki Konishi[1], Kenji Ishii[4] (1. Institute for Radiological Science, National Institutes for Quantum Science and Technology (QST) (Japan), 2. Materials Sciences Research Center, Japan Atomic Energy Agency (Japan), 3. Institute of Multidisciplinary Research for Advanced Materials, Tohoku University (Japan), 4. Synchrotron Radiation Research Center, National Institutes for Quantum Science and Technology (QST) (Japan))

3:30 PM - 3:50 PM JST | 6:30 AM - 6:50 AM UTC

[R3-16*]

Structure Elucidation of Uranyl Complexes using DOSY

*Christian Urbank[1,2], Koichiro Takao[2], Lisa Vondung[1] (1. University of Hamburg (Germany), 2. Tokyo Institute of Science (Japan))

3:50 PM - 4:10 PM JST | 6:50 AM - 7:10 AM UTC

[R3-17*]

Development of synthetic method for partially oxidized phthalocyanine complexes extensible to minor actinides

*Takumi Saito[1], Miki Harigai[1], Hisao Yoshinaga[1], Takashi Shimada[1], Tomoo Yamamura[1] (1. Kyoto University (Japan))

4:10 PM - 4:30 PM JST | 7:10 AM - 7:30 AM UTC

[R3-18*]

Coordination-Driven In-situ Reduction and Extraction of Neptunium

*Huaixin Hao[1], Shuyun Zhang[2], Jin Chen[1], Jing Su[2], Zhipeng Wang[1], Chao Xu[1] (1. Tsinghua University (China), 2. Sichuan University (China))

©APSORC25

7th Asia-Pacific Symposium on Radiochemistry *September 14 ~ 19, 2025 • Kunibiki Messe • Shimane, Japan*

URANYL COORDINATION WITH BIOLOGICAL LIGANDS ANALYZED BY HERFD-XANES SPECTROSCOPY

Akihiro Uehara[1], Daiju Matsumura[2], Daisuke Akiyama[3], Akira Kirishima[4], Shino, Homma-Takeda[5], Teruaki Konishi[6], Kenji Ishii[7]

[1]*Institute for Radiological Science, National Institutes for Quantum Science and Technology (QST), 4-9-1 Anagawa, Inage, Chiba, 263-8555, Japan, uehara.akihiro@qst.go.jp*
[2]*Materials Sciences Research Center, Japan Atomic Energy Agency, 1-1-1 Kouto, Sayo, Hyogo 679-5148, Japan, daiju@spring8.or.jp*
[3]*Institute of Multidisciplinary Research for Advanced Materials, Tohoku University, 1-1 Katahira, 2, Aoba, Sendai, 980-8577, Japan, d.akiyam@tohoku.ac.jp*
[4]*Institute of Multidisciplinary Research for Advanced Materials, Tohoku University, 1-1 Katahira, 2, Aoba, Sendai, 980-8577, Japan, kiri@tohoku.ac.jp*
[5]*Institute for Radiological Science, National Institutes for Quantum Science and Technology (QST), 4-9-1 Anagawa, Inage, Chiba, Japan, 263-8555, takeda.shino@qst.go.jp*
[6]*Institute for Radiological Science, National Institutes for Quantum Science and Technology (QST), 4-9-1 Anagawa, Inage, Chiba, Japan, 263-8555, konishi.teruaki@qst.go.jp*
[7]*Synchrotron Radiation Research Center, National Institutes for Quantum Science and Technology (QST), 1-1-1 Kouto, Sayo, Hyogo, 679-5148, Japan, ishii.kenji@qst.go.jp*

Uranium (U) has the potential to form complexes with biological ligands in body fluids resulting in the deposition in tissue at the internal exposure. In the present study, the coordination of U with biological ligands was analyzed by using high-energy-resolution fluorescence detected X-ray absorption near edge structure (HERFD-XANES) spectroscopy. Spectra of uranyl compounds, such as uranium oxide, uranyl hydroxide, uranyl phosphate, uranyl carbonate were measured as standard samples. Acetate, cysteine, and oxalate were used as representative ligands for biological samples. The pre-edge peak of HERFD-XANES spectra in U hexavalent samples was observed though this was not observed in normal XANES spectra.

1. INTRODUCTION

A fundamental approach on mechanism analyses of the interaction between actinides and biological substances leads to dose assessment of the internal exposure at nuclear disaster and decorporation with chelating agents. Analytical method of X-ray absorption near edge structure (XANES) has been used in the structural analysis of actinides coordinated with biological ligands and organic compounds for the decorporation because local structural information such as bond distance and coordination number can be obtained in either solid or liquid samples [1,2]. However, the compounds which actinides are coordinated with similar organic ligands were not clearly distinguished based on the normal XANES. Recently, high-energy-resolution fluorescence detected X-ray absorption near edge structure (HERFD-XANES) has been applied to the analysis of actinide compounds [3,4]. In HERFD-XANES, the spectral broadening caused by the core-hole lifetime in normal XANES is suppressed, allowing for the acquisition of XANES spectra with better energy resolution. Oxidation state of U inorganic compounds revealed on the comparison of HERFD-XANES spectra at the U L3 edge[5-10]. Detail information on electronic transition and elemental valence states are obtained by further splitting the X-ray fluorescence to distinguish even minute structural changes. In the present study, HERFD-XANES spectrum of uranium compounds coordinated by bio-ligands were measured, and their local structure of uranium was compared with normal XANES spectra.

2. EXPERIMENTAL

HERFD-XANES spectra were measured at BL11XU beamline of SPring-8, Japan. The X-ray beam was monochromatized with a Si (311) double-crystal monochromator. The X-ray fluorescence (U Lα1 line (13.614 keV)) emitted from the sample in the hutch was dispersed by three vertically placed Si (880) spherical curved crystals (10 cmϕ, crystal spacing 17.5 cm) and then measured with a silicon microstrip detector. The sample, the curved crystal, and the detector were all on the same Rowland circle (radius 1 m). The spherically curved crystal and the silicon microstrip detector were moved on a rotation stage to maximize the intensity of the U Lα1 line. The horizontal and vertical beam sizes were 1- and 0.3 mm, respectively. For the comparison with HERFD-XANES, normal XANES spectra was also measured at BL14B1 beamline. U samples were prepared at QST and Tohoku University.

3. RESULTS AND DISCUSSION

HERFD-XANES spectra of U standard samples, uranium dioxide, uranyl carbonate, uranyl hydroxide, and uranyl phosphate were measured (some examples were shown in Figure 1). Top and shoulder peaks of the spectra were clearly

Copyright on 7th Asia-Pacific Symposium on Radiochemistry 2025 - R3-15 -

observed compared with normal XANES spectra. The pre-edge peak at 17.166 keV was observed in HERFD-XANES spectra of U(VI) samples depending on the symmetry of the coordination structure which was not observed in normal XANES spectra. Spectrum of uranyl cysteine complex was similar to that of uranyl acetate. On the other hand, the spectrum of uranyl oxalate was similar to that of uranyl hydroxide. Finally, by refining shape of the spectra, it becomes possible to obtain peak shifts accompanying the formation in detail.

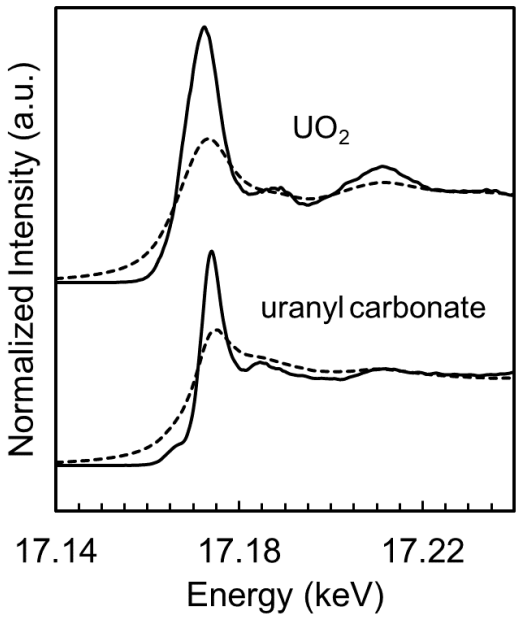


Figure 1. HERFD-XANES (solid line) and normal XANES (dotted line) spectra of UO_2 and uranyl carbonate samples at U L3 edge.

4. REFERENCES

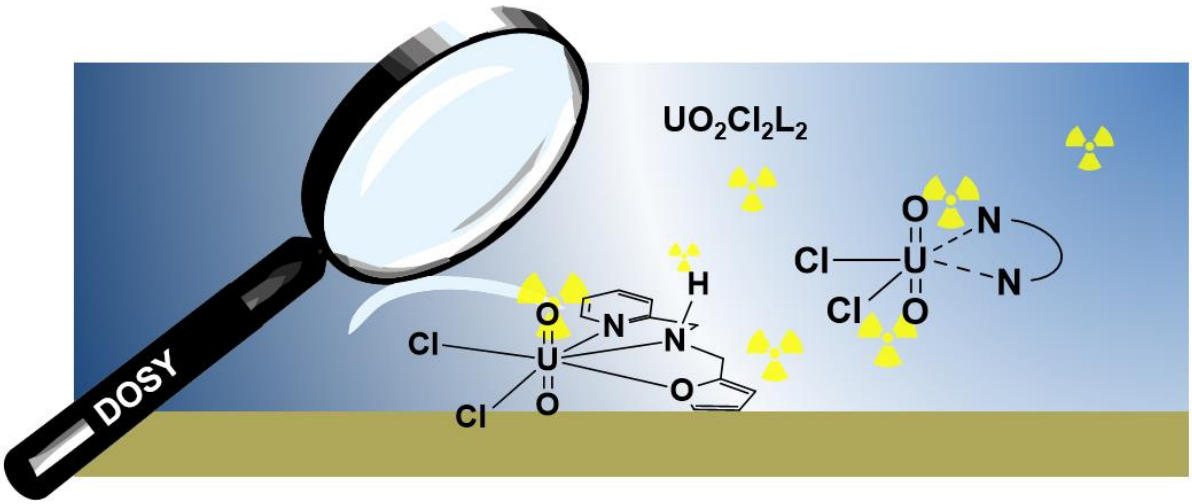
[1] A. Uehara, et al., *Anal. Methods.*, 14 (2022) 2439-2445.
[2] A. Uehara, et al., *J. Toxicol. Sci.*, 49 (2024) 543-548.
[3] K.O. Kvashnina, et al., *Chem. Comm.*, 58 (2022) 327-342.
[4] R. Caciuffo, et al., *Rev. Modern Phys.*, 95 (2023) 015001, 1-52.
[5] R. Bes, et al., *Inorg. Chem.*, 55 (2016) 4260-4270.
[6] G. Leinders, et al., *Inorg. Chem.*, 56 (2017) 6784-6787.
[7] N. Kawamura, et al., *JPS Conf. Proc.*, 30 (2020) 011172.
[8] C. Dewey, et al., *Environ. Sci. Technol.*, 54 (2020) 6021-6030.
[9] M.O.J.Y. Hunault, et al., *Crystals*, 11 (2021) 56.
[10] T. Yomogida, et al., *Inorg. Chem.*, 61 (2022) 20206-20210.

Structure Elucidation of Uranyl Complexes using DOSY

Christian Urbank[1,2], Koichiro Takao[2], Lisa Vondung[1]

[1]*University of Hamburg; Martin-Luther-King-Platz 6, 20146 Hamburg, Germany*
[2]*Institute of Science Tokyo: 2-12-1 N1-32, O-okayama, Meguro-ku, Tokyo 152-8550, Japan*

In the last few decades, the utilization of diffusion-ordered NMR spectroscopy (DOSY) has become an increasingly important component of the standard toolkit of coordination chemistry. Using the relation between the diffusion coefficient (*D*) and the molecular weight (*M*), external calibration curves could be derived, allowing for the non-destructive approximation of M in solution. [1]
The field of actinide chemistry was thus far the exception to this rule, as it was presumed that points of high density would negatively influence the experiments. A recently published study has shown that certain correction factors can be included, opening the pathway for the analysis of systems with heavier elements. [2]
In our work, we tested the accuracy of the most common DOSY interpretation methods and could show the limits in their general applicability. Therefore, we developed an improved method for interpreting DOSY data. We demonstrated the robustness of this new method for a large set of organic and inorganic molecules and used it to elucidate the structures of several uranyl complexes in solution. Originating from our research on the reactivity of uranyl coordination compounds, this work could be used to illuminate the complex nature of questions regarding environmental remediation and the migration behavior of actinides. [3]



Graphic inspired by Stalke et. al.

ACKNOWLEDGMENTS

We thank the *Fonds der Chemischen Industrie* and the *German Academic Exchange Service* for their generous financial support.

References

[1] R. Neufeld, D. Stalke, *Chem. Sci*., **6**, 3354 (2015).
[2] A. Kreyenschmidt, M. John, D. Stalke, *Organometallics*, **42**, 2957 (2023).
[3] R. Selvakumar, G. Ramadoss, Mridula P. Menon, K. Rajendran, P. Thavamani, Ravi Naidu, M. Megharaj, J. Environ. Radioact., **192**, 592 (2018).

Copyright on 7th Asia-Pacific Symposium on Radiochemistry 2025- R3-16* -

7th Asia-Pacific Symposium on Radiochemistry *September 14 ~ 19, 2025 • Kunibiki Messe • Shimane, Japan*

Development of synthetic method for partially oxidized phthalocyanine complexes extensible to minor actinides

Takumi Saito[1], Miiki Harigai[1], Hisao Yoshinaga[1], Takashi Shimada[1], Tomoo Yamamura[1]

[1] *Kyoto univ. Nuclear Radiation Physics Lab.: 2-1010 Asashiro-Nishi, Kumatori-cho, Sennan-gun, Osaka, 590-0494,*
Saitou.takkumi.88e@st.kyoto-u.ac.jp
harigai.miki.2k@kyoto-u.ac.jp
yoshinaga.hisao.4n@kyoto-u.ac.jp
shimada.takashi.6w@kyoto-u.ac.jp
yamamura.tomoo.2e@kyoto-u.ac.jp

1 Introduction

Phthalocyanine (Pc) complexes can be partially oxidized by triiodide ions (I_3^-), anions with high electron affinity, leading to unique electronic and magnetic properties [1][2]. In transition metal and lanthanide Pc systems, such partially oxidized complexes have shown excellent electrical conductivity and magnetic characteristics [2,3].

Actinide-based Pc complexes, which exhibit intermediate electronic behavior between 3d and 4f elements, represent promising targets for further exploration. For uranium, partially oxidized Pc complexes with iodide counterions have been synthesized, displaying a tetragonal crystal system with a similar separated stacking structure as observed in dysprosium (Dy) analogues [3-5].

However, the synthesis of these actinide complexes often requires pure metal starting materials. While pure metals can be obtained via methods such as the Van Arkel–de Boer process (thermal decomposition of metal iodides) [6] or polarography [7], these approaches have limitations: the former becomes impractical for elements beyond neptunium due to high vapor pressure, and the latter involves mercury, raising environmental concerns. Consequently, synthetic strategies relying on pure metal powders are limited in scope.

To overcome these challenges, we have explored a pyrochemical synthesis approach using uranium tetraiodide (UI_4) as an alternative precursor. In this study, we aim to develop a general pyrochemical method applicable to uranium and other actinides. As a first step, we investigate the synthesis of bilayer, partially oxidized Pc complexes using alternative metal iodides and iodine-based oxidants. On the day, we will present the apparatus for synthesizing metal iodides and the results of the synthesis.

2 Consideration of synthesis method

The partially oxidized uranium Pc complexes were synthesized by heating pellets of uranium powder, iodide powder, and phthalonitrile that had been sealed under vacuum in ampules [4, 5]. This reaction process, firstly, UI_4 was generated by uranium powder and iodide gas [6]. And then, the uranium Pc complex was synthesized by intermolecular reaction of UI_4 and phthalonitrile [1]. The uranium Pc complex was partially oxidized by I_3^-, produced by the chemical equilibrium between I_2 and I^- in the gas phase. Therefore, the starting material doesn't need to be pure powder but can be substituted with UI_4.

Laboratory-scale synthesis of UI_4 has long been known using dioxide and aluminum iodide. In this method, metal dioxide and aluminum iodide are synthesized in a solid-gas reaction at 350°C in a vacuum. The UI_4 and aluminum iodide can be purified by sublimation from the unreacted metal dioxide using a temperature gradient [8, 9]. This method can be applied to metals after Np, which have higher vapor pressure, although the temperature during purification is higher than that of UI_4 [10][11].

3 Selection of alternative actinides

Zirconium (Zr) and Cerium (Ce) were selected as the respective alternative metals to simulate uranium and actinides after Np. The selected metals take the same chemical forms as actinides, MI_4 and MI_3, and the vapor pressures of the alternative metals are known [12, 13]; the standard enthalpy and standard entropy of CeI_3 show similar trends to those of the post-Np metal iodides [14]. For these reasons, Zr and Ce were selected as simulated actinide elements. Based on the above background, this study investigates a dry method for the synthesis of iodine complexes, which is expected to be applied to uranium and other actinides. As a first step, we will synthesize iodine-based bilayered partially oxidized complexes using alternative metal iodides.

References

[1] Jianzhuang. Jiang, springer, Springer Heidelberg Dordrecht London New York, (2010)
[2] Tamotsu Inabe, Chem. Rev., 104 (2004) 5503.
[3] Tetsu Sato, et al., Angew. Chem. Int. Ed., 60 (2021) 21179.
[4] Jan Janczak, et al., Polyhedron, 18 (1999) 1621.
[5] Jan Janczak, et al., Inorg. Chim. Acta, 304 (2000) 150.

Copyright on 7th Asia-Pacific Symposium on Radiochemistry 2025- R3-17* -

[6] J.C. Spirlet, In , Vol.31, Academic Press, New York, 31 (1987) p.11.
[7] Y. Shiokawa, et al., J. Alloys Compd., 255 (1996) 98.
[8] Stefan S. Rudel, et al., Dalton Trans., 46 (2017) 5835.
[9] Marcel CHAIGNEAU., Bull. Soc. Chim. Fr., (1957) 886.
[10] Sherman Feted, et al., J. Am. Chem. Soc., 70 (1948) 3539.
[11] Fried, Sherman, J. Am. Chem. Soc., 73 (1951) 416.
[12] Stull, Daniel R, Industrial \& Engineering Chemistry, 39 (1947) 517.
[13] Anna Rita Villani, et al., J. Chem. Eng. Data, 45 (2000) 823.
[14] Lester R. Morss, et al., THE CHEMISTRY OF THE ACTINIDE AND TRANSACTINIDE ELEMENTS. Vol4. Chapter19. p.2175.

Copyright on 7th Asia-Pacific Symposium on Radiochemistry 2025- R3-17* -

Coordination-Driven In-situ Reduction and Extraction of Neptunium

Huaixin Hao[1†], Shuyun Zhang[2†], Jing Chen[1], Jing Su[2*], Zhipeng Wang[1*], Chao Xu[1*]

[1]*Institute of Nuclear and New Energy Technology, Tsinghua University, Beijing 100084, China*
[2]*College of Chemistry, Sichuan University, Chengdu 610064, China*
[*]*E-mail: wangzhipeng@mail.tsinghua.edu.cn (Z.P. Wang), xuchao@tsinghua.edu.cn (C. Xu), jingsu@scu.edu.cn (J. Su)*

The recycling of neptunium (Np) from nuclear wastes is crucial for the sustainable development of nuclear energy, yet it is still a challenging task owing to the complexity of Np chemistry. Precise control of oxidation state is highly desirable for the effective recovery of Np. In this study, we report an innovative strategy for Np recovery through in-situ coordination and reduction of Np(V) in a biphasic extraction system. By leveraging the synergistic effects of coordination by a P=O donating ligand (trialkyl phosphine oxide, TRPO) and reduction by hydroquinone (HQ) in the organic phase, efficient Np(V)-to-Np(IV) conversion and high distribution ratio (D) of Np were achieved in a single extraction contact. The reduction mechanism of Np was elucidated through spectroscopic and theoretical analyses. This work enriches the redox chemistry of Np and provides a novel pathway for Np-recovery in advanced nuclear fuel cycles.

Keywords: *Neptunium, Coordination, Reduction, Extraction*

1 INTRODUCTION

Np-237, a long-lived minor actinide in spent nuclear fuel, poses a serious environmental threat due to its high radiotoxicity and mobility, yet holds strategic value as a precursor for producing plutonium-238 used in space exploration.[1] In nitric acid-based reprocessing streams, Np predominantly exists as poorly extractable pentavalent neptunyl ions ($Np^{V}O_2^+$), which needs to be converted into more highly charged Np^{4+} for efficient recovery.[2] Traditional reduction methods, such as using low-valent metal ions (Fe(II), U(IV)) or salt-free organic reductants, often suffer from low efficiency, secondary waste generation, or safety concerns.[3] For actinide ions, its abundant valence electrons are susceptible to the coordination environment, which in turn governs the ionic reactivity and redox chemistry. Several actinide complexes with atypical oxidation state and unique structures have been synthesized through modification of the coordination sphere of the cation. Notably, even rare and disproportionation-prone pentavalent species like plutonium(V) and americium(V) have been stabilized via non-aqueous coordination strategies.[4-6] These findings inspired our search for more efficient Np(IV) generation and separation methods.

2 RESULTS AND DISCUSSION

In this work, we present a novel strategy for in-situ reduction of Np(V) in a biphasic extraction system (Fig. 1). Unlike the traditional stepwise procedure of first reducing Np(V) to Np(IV) in the aqueous phase and then extracting Np(IV) by the organic solvent, we incorporate hydroquinone (HQ) into an organic solvent containing the P=O donating TRPO ligand (trialkyl phosphine oxide) to create a unique "coordination-reduction-extraction" system, which enables simultaneous Np(V)-to-Np(IV) reduction and extraction, achieving >99% Np recovery under ambient conditions.

Furthermore, the reaction pathway and mechanism of Np in the “coordination–reduction–extraction” system were systematically elucidated through combined spectroscopic characterization and theoretical calculations (Fig. 2). It should be emphasized that such an in-situ reduction and extraction of Np is basically driven by the coordination of TRPO in the organic phase. Specifically, when the two phases are contacted, Np(V) in the aqueous phase distributes partially into the organic phase and then disproportionates to Np(IV) and Np(VI) through the coordination of TRPO. Subsequently, with the synergistic effect of TRPO coordination and HQ reduction in the organic phase, Np(VI) is reduced to Np(V) and Np(IV) successively while Np(V) converts to Np(IV) directly. Theoretical calculations further reveal that the presence of TMPO (trimethylphosphine oxide, a structural analogue of TRPO) significantly enhances the interaction between HQ and NpO_2^+, lowers the energy barriers along the reduction pathway, accelerates the reaction kinetics, and promotes the release of reaction intermediates, thereby advancing the efficient reduction of Np(V) to Np(IV). Finally, owing to the strong Np(IV)-TRPO coordination, the generated Np(IV) stays in the organic phase and the transfer of Np from the aqueous phase to the organic phase follows the same “coordination-reduction-extraction” cycle, thereby achieving efficient recovery of Np.

Copyright on 7th Asia-Pacific Symposium on Radiochemistry 2025- R3-18* -

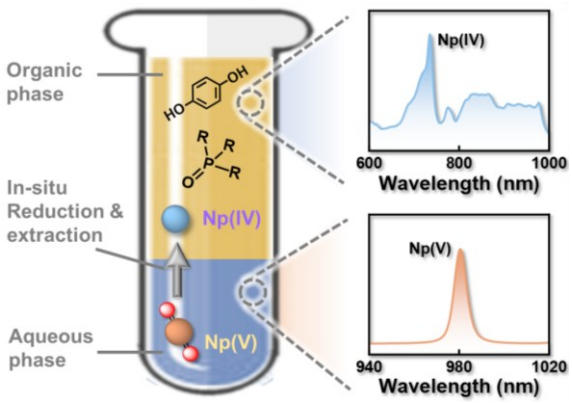


Fig. 1. Scheme for incorporation of HQ in TRPO-containing organic solution and in-situ generation of Np(IV) in a biphasic system in the present work.

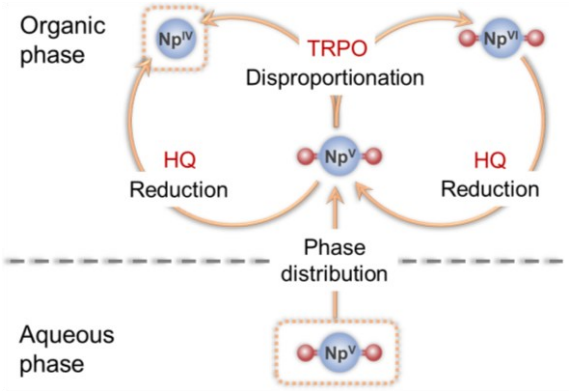


Fig. 2. Oxidation state variation and distribution of Np in the in-situ "coordination-reduction-extraction" system.

3. CONCLUSIONS

In summary, we have demonstrated that incorporating reductive HQ in the TRPO/n-dodecane solution can effectively promote Np(V)-Np(IV) conversion either in the organic phase or in a biphasic system. The synergy between coordination and reduction drives >99% Np recovery from high-acidity solutions under ambient conditions, offering a robust strategy for nuclear waste treatment. The findings in this work not only provide a promising Np recovery strategy, but also enriches the limited knowledge on Np redox chemistry.

ACKNOWLEDGMENTS

C. Xu acknowledges the financial support from National Natural Science Foundation of China (22325603). Z.P. Wang acknowledges the financial support from National Natural Science Foundation of China (22376116) and Young Elite Scientists Sponsorship Program by CAST (2023QNRC001). J. Su acknowledges the financial support from National Natural Science Foundation of China (22076130), the Fundamental Research Funds for the Central Universities (20826041D4117) and the Natural Science Foundation of Sichuan (2025ZNSFSC0109).

References

[1] B. Acevedo, K. Van Hecke, T. Cardinaels and M. Verwerft, *Radiochim. Acta*, 2023, **111**, 857-885.
[2] P. K. Verma and P. K. Mohapatra, *Radiochim. Acta*, 2022, **110**, 527-548.
[3] H. Hao, Y. Liu, H. Cao, Z. Wang, C. Xu and J. Chen, *Dalton Trans.*, 2024, **53**, 17909-17917.
[4] Y. Wang, S.-X. Hu, L. Cheng, C. Liang, X. Yin, H. Zhang, A. Li, D. Sheng, J. Diwu, X. Wang, J. Li, Z. Chai and S. Wang, *CCS Chem.*, 2020, **2**, 425-431.
[5] Z. Wang, J.-B. Lu, X. Dong, Q. Yan, X. Feng, H.-S. Hu, S. Wang, J. Chen, J. Li and C. Xu, *J. Am. Chem. Soc.*, 2022, **144**, 6383-6389.
[6] X. Dong, H. Hao, J. Chen, Z. Wang and C. Xu, *Chem. Sci.*, 2024, **15**, 2118-2122.

Copyright on 7th Asia-Pacific Symposium on Radiochemistry 2025- R3-18* -

Invited & Contributed Talk | [P4]Radionuclide Migration Dynamics: Radioactive Waste Disposal and Environmental Impact Assessment

Wed. Sep 17, 2025 3:00 PM - 4:30 PM JST | Wed. Sep 17, 2025 6:00 AM - 7:30 AM UTC Hall B(Small)

[P4] Radionuclide Migration Dynamics: Radioactive Waste Disposal and Environmental Impact Assesment

3:00 PM - 3:30 PM JST | 6:00 AM - 6:30 AM UTC

[P4-06(Invited)]

Enhanced Uranium Mobility via Colloidal Transport: Implications for Remediation Strategies in Contaminated Sites

*Duoqiang Pan[1], Xiaoyan Wei[1], Xinyi Shi[1], Wangsuo Wu[1] (1. Lanzhou University (China))

3:30 PM - 3:50 PM JST | 6:30 AM - 6:50 AM UTC

[P4-07]

Stability and transport of Ce(IV)-Borate intrinsic colloid

*Zongyuan CHEN[1,2], Ganlin Zu[2], Kang Chen[2], Qiang Jin[1,2], Zhijun Guo[1], Wangsuo Wu[1,2] (1. MOE Frontiers Science Center for Rare Isotopes, Lanzhou University (China), 2. school of nuclear science and technology, Lanzhou University (China))

3:50 PM - 4:10 PM JST | 6:50 AM - 7:10 AM UTC

[P4-08*]

Study on the Adsorption and Migration Behavior of Radioactive ^{210}Po in Lead–Bismuth Reactors

*Yuqing Wang[1], Chenyu Liu[1], Hanyu Wu[1], Shengqing Wang[1], Muyi Ni[1] (1. Sun Yat-sen University (China))

4:10 PM - 4:30 PM JST | 7:10 AM - 7:30 AM UTC

[P4-09]

The adsorption of U(VI) on chlorite: Batch, modeling and XPS study

*Qiang Jin[1], Zongyuan Chen[1], Zhijun Guo[1], Wangsuo Wu[1] (1. Lanzhou University (China))

©APSORC25

7th Asia-Pacific Symposium on Radiochemistry *September 14 ~ 19, 2025 • Kunibiki Messe • Shimane, Japan*

ENHANCED URANIUM MOBILITY VIA COLLOIDAL TRANSPORT: IMPLICATIONS FOR REMEDIATION STRATEGIES IN CONTAMINATED SITES

Duoqiang Pan[1,2], Xiaoyan Wei[2], Xinyi Shi[2], Wangsuo Wu[1,2]

[1]*Frontiers Science Center for Rare Isotopes, Lanzhou University, Lanzhou 730000, China*
[2]*School of Nuclear Science and Technology, Lanzhou University, Lanzhou 730000, China*

The occurrence forms and migration behaviors of uranium in the environment are crucial for the environmental safety assessment around nuclear facilities. Based on the geochemical process of uranium in the environment, remediation strategies including phosphoric agents, reductive agents, as well as reductive bacteria treatment, have been proposed to immobilize uranium in the contaminated sites. The solutes migration models have been constructed to describe and predict the uranium migration ability and then evaluate the effectiveness of immobilization remediation. However, the migration distance of on-site monitoring is often greater than the predicted migration distance, studies have revealed that the colloids mediated transport contribute an important role in radionuclide migration. Uranium, on the one hand, is prone to form the intrinsic colloids under groundwater conditions due to its nucleation and crystallization process; on the other hand, it easily associates with the widely existed environmental colloids to form the pseudo colloids. The existence of colloidal stated uranium significantly affects the transport patterns and the environmental risk, which should be given critical consideration when assessing the remediation effectiveness on a uranium contaminated site. In this presentation, aiming at the environmental risk and the immobilization effectiveness adjacent to uranium contaminated sites, the uranium transport abilities under the phosphoric or reductive media were investigated at the absence and presence of environmental colloids, the transport occurrence and mechanism of uranium were clarified with the aid of advanced spectroscopic evidences as well as theoretical calculation, the role of colloidal state uranium, including both intrinsic and pseudo uranium colloids, were identified and described.

1 PHOSPHORUS IMMOBILIZATION

The phosphorus-containing agents have been proposed to remediate the uranium contaminated sites due to the formation of insoluble uranyl phosphate mineralization products. However, the colloids, including both pseudo and intrinsic uranium colloids, could disturb the environmental fate of uranium due to its nonnegligible mobility. The transport pattern and micro-mechanism of uranium coupled to phosphate and illite colloid (IC) showed that uranium transport was facilitated in granular media by forming the intrinsic uranyl phosphate colloid (such as Na-autunite) when the pH > 3.5 and CNa^{+} < 10 mM. Meanwhile, the mobility of uranium depended greatly on the typical water chemistry parameters governing the aggregation and deposit of intrinsic uranium colloids. However, the attachment of phosphate on illite granule increased the repulsive force and enhanced the dispersion stability of IC in the IC-U(VI)-phosphate ternary system. The non-preequilibrium transport and retention profiles, HRTEM-mapping, as well as TRLFS spectra revealed that the IC enhanced uranium mobility by forming the ternary IC-uranyl phosphate hybrid, and acted as the coagulation preventing agent for uranyl phosphate particles.

2 REDUCTIVE IMMOBILIZATION

Reduction-mediated immobilization is also widely considered a reliable strategy for remediation uranium contaminated sites. However, the potential role of environmental colloids on the effectiveness and application of the strategy has been overlooked. Therefore, the effect of environmental colloids on the environmental behaviors of uranium in the reducing media with varying ambient conditions was examined. In the zero valent iron (ZVI) contained porous media, the illite colloids (IC) facilitated uranium transport in the reductive media, and the uranium transported depending on ionic strength and flow rate. At low ionic strength, uranium transport was facilitated as U(VI) species, whereas the co-transport of U(IV) emerged at the high ionic strength, and the U(IV) species was predominantly transported with decreasing flow rate at high ionic strength. The spectroscopic analysis revealed the unique mechanism of IC enhancing the U(IV) transport. The co-transported U(IV) was driven by U(VI) reduction on IC surface or solution rather than ZVI surface due to the galvanic coupling between IC and ZVI, in which the transfer accelerating effect of Fe^{2+} and electron at high ionic strength induced the formation of a stable U(IV)-IC colloid. However, in the sets of pyrite (FeS_2) doped quartz sand columns, the transport pattern of uranium with bentonite colloids (BC) indicated that uranium also showed considerable mobility as the tetravalent state in the reductive media. BC greatly facilitated the transport of U(IV) by providing an efficient ride, high resolution transmission electron microscope (HRTEM) revealed that the crystalline uranium particles distributed between 6-12 nm tended to attach onto BC particles, X-ray photoelectron spectroscopy (XPS) and extended X-ray absorption fine structure (EXAFS) clarified that the migration products of uranium existed as

Copyright on 7th Asia-Pacific Symposium on Radiochemistry 2025 - P4-06 -

the form of both non-crystalline and crystalline UO_{2+x}. The reduction process of uranium was inhibited in the presence of HA since the chelating and enwrapping of HA to uranium blocked the electron transfer process. .

3. CONCLUSIONS

In summary, the observed facilitation of uranium transport resulted from the formation of both intrinsic and pseudo uranyl colloids, the enhanced uranium transport arising from perturbation of environmental granules, including bentonite colloids, illite colloid, and humic acid colloids et al., should be taken into consideration when evaluating the potential migration risk of uranium and optimizing the in-situ immobilization remediation strategy for the uranium contaminated sites. Relevant achievements provide theoretical basis and support for the reliable assessment on nuclear environmental safety around uranium contaminated sites.

ACKNOWLEDGMENTS

This work was supported by the National Natural Science Foundation of China (22176077); the Fundamental Research Funds for the Central Universities (lzujbky-2023-stlt01).

References

[1] Wei, X., Shi, X., Yang, M., Tan, Q., Xu, Z., Ma, B., Wu, W. (2024). Phosphate and illite colloid pose a synergistic risk of enhanced uranium transport in groundwater: A challenge for phosphate immobilization remediation of uranium contaminated environmental water. Water Res., 255, 121514.

[2] Tang, Q., Xu, Z., Tan, Q., Shi, X., Wu, W., Pan, D. (2024). Insight into impact of phosphate on the cotransport and corelease of Eu(III) with bentonite colloids in saturated quartz columns. J. Hazard. Mater., 461, 132572.

[3] Wei, X., Pan, D., Xu, Z., Xian, D., Li, X., Tan, Z., Liu, C., Wu, W. (2021). Colloidal stability and correlated migration of illite in the aquatic environment: the roles of pH, temperature, multiple cations and humic acid. Sci. Total Environ., 768: 144174.

7th Asia-Pacific Symposium on Radiochemistry *September 14 ~ 19, 2025 • Kunibiki Messe • Shimane, Japan*

STABILITY AND TRANSPORT OF CE(IV)-BORATE INTRINSIC COLLOID

Zongyuan Chen[1,2], Kang Chen[2], Ganlin Zu[2], Qiang Jin[1,2], Zhijun Guo[1,2], Wangsuo Wu[1,2]

[1]*Frontiers Science Center for Rare Isotopes, Lanzhou University, No.222 South Tianshui road, 730000 Lanzhou, China*
[2]*Radiochemistry Laboratory, School of Nuclear Science and Technology, Lanzhou University, No.222 South Tianshui road, 730000 Lanzhou, China*

Tetravalent actinides, An(IV), are usually assumed to be immobile in the subsurface. However, there are certain geochemical scenarios that An(IV) could occur as intrinsic colloids and become mobile. B_2O_3 is one of the major components of high-level radioactive waste (HLW) glass, and the erosion of HLW glass may lead to the leakage of An(IV) with $B_4O_7^{2-}$ [1] and formation of An(IV)-borate intrinsic colloids. The colloidal stability and transport behavior of such colloid is unknown so far. In this study, Ce(IV) was used as an analogue of tetravalent actinides, the stability of Ce(IV)-borate colloids was investigated by aggregation kinetics experiments as a function of pH, electrolytes, and colloidal humic acid (HA), and the effect of Ce(IV)-borate colloid formation on Ce(IV) transport was studied at varying Ce(IV) concentration, ionic strength (I), pH and HA.

Ce(IV) can form stable Ce(IV)-borate colloid with borax, and Ce(IV)-borate colloid aggregated when pH closed to pH_{IEP} 7.8. The critical coagulation concentrations (CCCs) were followed an order of NaCl>KCl>$MgCl_2$>$NaNO_3$> $CaCl_2$>Na_2SO_4. Effect of negatively-charged HA on the stability of Ce(IV)-borate colloid was HA concentration-dependent. At low HA concentration (0.1-1.0 mg/L), the surface charge of Ce(IV)-borate colloids was neutralized, resulting in a lower CCC, whereas Ce(IV)-borate colloid stability was improved at higher concentration HA (2.5-25 mg/L).

The transport behavior of Ce(IV)-borate colloid was completely different to that of soluble Ce(IV) (Figure 1). The transport of Ce(IV)-borate colloid was favored at pH 8.9 and *I* 6.5mM, a condition close to the underground water condition in China's Beishan area (a site for China's HLW repository), suggesting that An(IV) could be mobile in the geological disposal system by forming An(IV)-borate colloids. Because of their strong interaction at pH 5.0, Ce(IV)-borate colloid transport was facilitated with high HA concentration (10-25 mg/L), whereas it was impeded with low HA concentration (0.1-1 mg/L). Under same conditions, soluble Ce(IV) was always impeded by HA.

These findings emphasize the potential role of An(IV)-borate colloid formation in altering Ce(IV) transport behaviors, and provide important references to better predict the fate and transport of An(IV) in the context of HLW geological disposal.

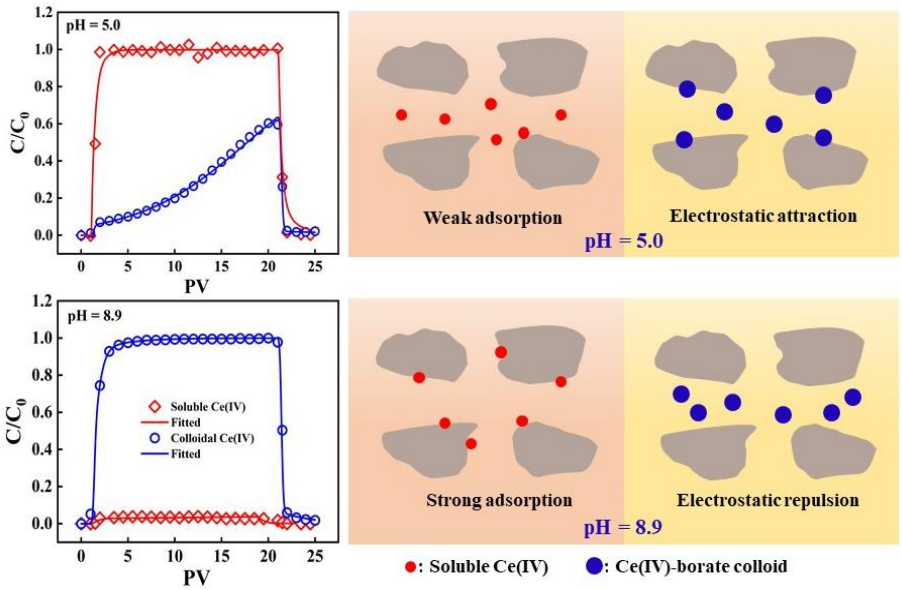


Fig. 1. This is the APSORC 25 logo (this is for example only; do not reproduce this logo).

References

[1] [1] Strachan D., Neeway JJ., Pederson L., Schreiber DK., Mitroshkov A., Zhu ZH., Ryan, JV., (2022). On the dissolution of a borosilicate glass with the use of isotopic tracing-insights into the mechanism for the long-term dissolution rate. Geochim. Cosmochim. Acta 318: 213-229.

Copyright on 7th Asia-Pacific Symposium on Radiochemistry 2025 - P4-07 -

Study on the Adsorption and Migration Behavior of Radioactive ^{210}Po in Lead-Bismuth Reactors

Yuqing Wang[1], Chenyu Liu[1], Hanyu Wu[1], Shengqing Wang[1], Muyi Ni[1,*]

[1]Sun Yat-sen University, No. 2, Daxue Road, Xiangzhou District, Zhuhai City, Guangdong, China 519085

*Email: nimuyi@mail.sysu.edu.cn

Lead-bismuth eutectic (LBE) has been selected as the primary coolant for lead-cooled fast reactors (LFRs) due to its good neutron economy and thermohydraulic properties. However, LBE generates volatile and radiotoxic polonium-210 (^{210}Po), posing significant radiological safety concerns. During normal operation, ^{210}Po may react with moisture to form polonium hydride (H_2Po), which could leak into the containment and deposit on containment structures or equipment surfaces, increasing occupational exposure risk. Under severe accident conditions, radioactive H_2Po aerosols may escape into the environment, causing radiological hazards to the public and the environment.

This study developed an experimental platform to investigate the adsorption and aerosol migration behavior of radioactive ^{210}Po-doped LBE under various operating conditions, based on actual LFR operational parameters. Experiments were conducted to analyze ^{210}Po-doped LBE across a temperature gradient of 1073 K to 293 K on different adsorbent materials. Alpha spectrometry and liquid scintillation counting (LSC) results indicate significant ^{210}Po-doped LBE adsorption on SiO_2 and SS316L substrates within the 870~960 K range. XRD, TEM, and EDS analyses confirmed that the adsorbed species on SiO_2 remained as Po and PbBi forming crystalline structures on the surfaces, the adsorbed species on SS316L remained as Po and Bi without crystalline structures. The particle size of the peak ^{210}Po-doped LBE aerosol concentration is 38nm, while the aerosol particles size within 10 nm to 85nm. 85 percent of ^{210}Po-doped LBE aerosol preferentially reacted with NaOH, only 0.6 percent of ^{210}Po-doped LBE aerosol deposit on the Fe foils.

This study systematically investigated the adsorption and migration behavior of ^{210}Po in the LBE reactor, achieving accurate activity quantification, and providing technical support for the development of aerosol purification systems. These findings provide a reference for optimizing radiation protection in LBE reactors.

Keywords: LBE, Polonium, Aerosols, Adsorption, LSC

Copyright on 7th Asia-Pacific Symposium on Radiochemistry 2025- P4-08* -

The adsorption of U(VI) on chlorite: Batch, modeling and XPS study

Qiang Jin[1,2], Zongyuan Chen[1,2], Zhijun Guo[1,2], Wangsuo Wu[1,2]
[1] *Frontiers Science Center for Rare Isotopes, Lanzhou University, 730000 Lanzhou, China*
[2]) *Radiochemistry Laboratory, School of Nuclear Science and Technology, Lanzhou University, 730000 Lanzhou, China*

A mechanistic modelling of the adsorption processes onto individual minerals presenting in the near- and far-fields can greatly enhance the credibility of long-term safety assessments of granite-based geological repositories. In this study, the titration and U(VI) adsorption characteristics of chlorite, one of the major minerals of rock fractures, have been studied. Potentiometric titration curves at two ionic strengths (0.1 and 0.4 mol/L NaCl) are successfully interpreted by considering protonation/deprotonation reactions on generic edge sites (≡SOH) in the framework of a non-electrostatic surface complexation model (SCM). The adsorption of U(VI) on chlorite was reached after 24 hours, the adsorption kinetics can be described by a pseudo-second-order model. A non-electrostatic SCM with three surface complexes ($\equiv SOUO_2^+$, $\equiv SO(UO_2)_3(OH)_5$ and $\equiv SO(UO_2)_3(OH)_7^{2-}$) was set up based on pH edges of U(VI) at adsorption equilibrium in the absence of CO_2. Additional, experimental data measured as a function of U(VI) concentration, solid-to-liquid ratio and carbonate concentration were well reproduced by the proposed model. Finally, parallel experiments were conducted using X-ray photoelectron spectroscopy (XPS) to analyze the variation of U(VI) surface species speciation at different pH values. The good agreement between SCM prediction and XPS analysis demonstrates the reliability of the model in predicting and quantifying the radionuclides retention by chlorite.

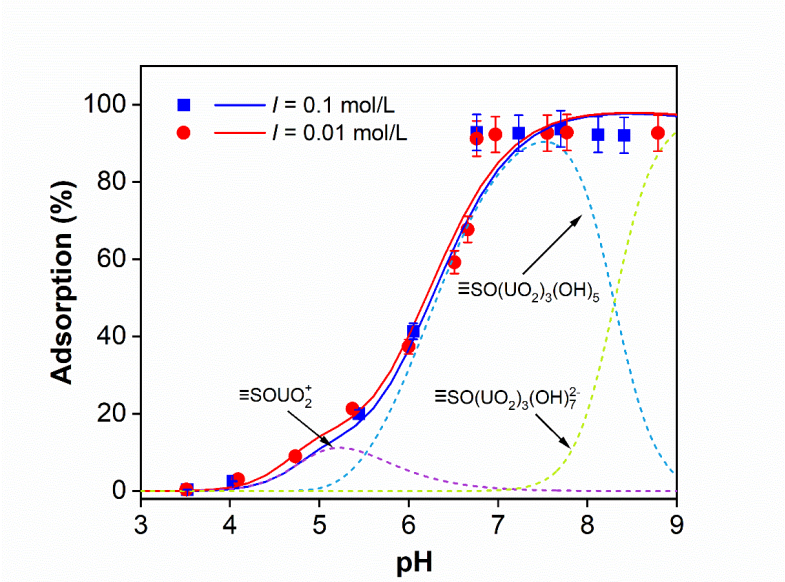


Fig. 1. Adsorption edge of U(VI) on chlorite at different ionic strengths (I). $C_{U(VI)}$ = 5.2 × 10^{-5} mol/L, m/V = 5. 0 g/L, p_{CO2} = 0 atm. The points are experimental data and the lines are modeling results. The dashed lines illustrate the modeled contributions of different surface species to U(VI) adsorption at I = 0.1 mol/L.

ACKNOWLEDGMENTS

This work funded by the National Natural Science Foundation of China (Grant Nos. 12175094, 22176079), the Natural Science Foundation of Gansu Province, China (No. 22JR5RA480) and the Fundamental Research Funds for the Central Universities (lzujbky-2022-sp05, lzujbky-2023-stlt01).

Invited & Contributed Talk | [R3]Actinide Chemistry and Nuclear Energy Chemistry

Wed. Sep 17, 2025 4:45 PM - 6:15 PM JST | Wed. Sep 17, 2025 7:45 AM - 9:15 AM UTC Hall A(MP)

[R3] Actinide Chemistry and Nuclear Energy Chemistry

4:45 PM - 5:15 PM JST | 7:45 AM - 8:15 AM UTC

[R3-19(Invited)]

Study on Consolidation Behavior and Radionuclides Immobilization Mechanism of Radioactive Wastes by Cold Sintering Process

*Xiangbiao Yin[1], Yuezhou Wei[1] (1. University of South China (China))

5:15 PM - 5:35 PM JST | 8:15 AM - 8:35 AM UTC

[R3-20]

RECENT PROGRESS IN SOLIDIFICATION AND CONDITIONING OF HIGH-/INTERMEDIATE-LEVEL AND LONG-LIVED RADIONUCLIDE-BEARING LIQUID WASTE IN CHINA: A PATRIAL REVIEW

*Yumeng Hou[1], meng Wei[1] (1. CNNC Long' an Co., Ltd. (China))

5:35 PM - 5:55 PM JST | 8:35 AM - 8:55 AM UTC

[R3-21]

DEVELOPMENT OF A LOW-TEMPERATURE DECONTAMINATION MEDIUM

*Katerina Cubova Cubova[1], Jan Houzar[1], Mojmir Nemec[1] (1. Czech Technical University in Prague, Dpt of Nuclear Chemistry (Czech Republic))

5:55 PM - 6:15 PM JST | 8:55 AM - 9:15 AM UTC

[R3-22*]

Study on removal of the nuclear fuel materials from waste liquid using flocculation and precipitation method

*Lucie Šifnerová[1], Fuminori Honda[2], Yu Tachibana[2], Takeru Matsuishi[2], Toshiaki Hiyama[2] (1. Czech Technical University (Czech Republic), 2. Kyushu University (Japan))

©APSORC25

Study on the Consolidation Behavior and Radionuclides Immobilization Mechanism of Radioactive Wastes by Cold Sintering Process

Xiangbiao Yin[1,*], Yuezhou Wei[1]

1. School of Nuclear Science and Technology, University of South China, Hengyang 421001, China

Current solidification methods for radioactive waste, such as high-temperature sintering and encapsulation, often face challenges including significant volume increase, high sintering energy consumption, low waste loading capacity, Cs volatilization, and high radionuclide leaching rates. This study aims to develop low-temperature solidification methods for different types of cesium (Cs) and strontium (Sr) waste adsorbents. We propose the use of cold sintering to solidify secondary waste forms, such as Cs/Sr-laden zeolites, ammonium phosphomolybdate (AMP), and titanates, establishing an efficient cold-sintering approach for waste forms. The results demonstrate that by selecting suitable transient liquid phases, highly densified waste forms can be prepared at a sintering temperature of 200 °C, a uniaxial pressure of 500 MPa, and a sintering duration of 5 minutes. The obtained waste forms achieve densities exceeding 95% of their theoretical values, with a compressive strength of 382 MPa. After 14 days, the normalized leaching rates of Cs and Sr are below 10^{-5} $g \cdot cm^{-2} \cdot d^{-1}$, indicating that cold sintering technology holds great potential for volume reduction and solidification of radioactive solid waste.

Keywords:
Radioactive wastes treatment; Radionuclides immobilization; Cold sintering process; Solidification; Volume reduction

Copyright on 7th Asia-Pacific Symposium on Radiochemistry 2025

7th Asia-Pacific Symposium on Radiochemistry *September 14 ~ 19, 2025 • Kunibiki Messe • Shimane, Japan*

RECENT PROGRESS IN SOLIDIFICATION AND CONDITIONING OF HIGH/INTERMEDIATE-LEVEL AND LONG-LIVED RADIONUCLIDE-BEARING LIQUID WASTE IN CHINA: A PATRIAL REVIEW

Yumeng Hou, Meng Wei

CNNC Long' an Co., Ltd. ,Beijing, China, 100000

Radioactive waste refers to the waste that contains radioactive nuclides and poses hazards to organisms and the environment. To ensure the safety of the waste and human health and minimize its environmental impact, countries manage radioactive waste in accordance with the generation and hazard level of the waste. For low-activity waste (~98% of total volume), including low-level (LLW), very low-level (VLLW), and very short-lived (VSLW) radioactive waste, established management strategies are operationally effective. In contrast, for the most radioactive waste (~2% of the total) generated by spent fuel reprocessing plants, namely, intermediate/high-level waste (HLW, ILW) and long-lived radionuclide-bearing waste, the solidification and conditioning plans, as well as the long-term management plans, have not yet been fully determined. This review reports recent advancements in solidification and conditioning techniques for ILW/HLW liquid waste and long-lived radionuclide-bearing streams in China. Key methodologies involve utilizing geologically stable granite substrates for sintering high-level liquid waste, stabilizing tritiated wastewater via highdensity cement matrices combined with multilayer encapsulation systems, and immobilizing high-molybdenum-content streams using low-temperature borosilicate glass. Novel approaches also include iron phosphate glass matrices (with enhanced chemical stability, low melting points, and corrosion resistance) for high-level waste separation streams, integrating high-level waste into gadolinium zirconate pyrochlore ceramic lattices, and long-term fixation of ^{129}I (AgI) through hot isostatic pressing (HIP) technology. Additionally, the review will also explore and analyze the potential applications of these new technologies in industrial settings, along with the current challenges and difficulties encountered.

1 Introduction

China is advancing the development of large-scale commercial reprocessing plants (LCRPs). To improve their economic viability and safety, the process flows and waste management strategies in LCRPs differ fundamentally from those of military reprocessing facilities. The key distinctions include: 1. Separation of high-level liquid waste (HLLW) – This not only enables recovery of high-value isotopes (e.g., ^{237}Np, ^{241}Am, and ^{90}Sr) but also reduces the volume of high-level solid waste requiring deep geological disposal. 2. Immobilization of ^{129}I – Advanced iodine adsorbents are designed to ensure the long-term stability of ^{129}I within waste matrices. 3. Treatment of tritium-enriched waste liquids – Novel methods are being developed to safely manage high tritium activity (e.g., isotopic separation and ceramic encapsulation). Compared to existing reprocessing plants in China, LCRPs generate unique waste streams that challenge conventional treatment technologies. For this end, we surveyed several universities and research academies in China. From their research findings, we gleaned some insights into the treatment or conditioning of the above-mentioned novel liquid waste/solid waste source terms. [1]

2 Solidification and Conditioning Technique

2.1 The solidification of iodine wastes

In China's reprocessing plants, ^{129}I is primarily adsorbed via silver-functionalized silica gel (Ag/SG) as silver iodide (AgI) or silver iodate ($AgIO_3$), then compacted and encapsulated in UC-C type waste containers. However, AgI and $AgIO_3$ exhibit phase instability under geological reducing conditions. To address this, >95 vol% of ^{129}I must be immobilized in a waste matrix capable of confinement integrity for over 100,000 years. [2]

The China Institute of Atomic Energy (CIAE), in collaboration with Southwest University of Science and Technology (SWUST), has immobilized ^{129}I using low-temperature borosilicate glass matrices via hot isostatic pressing (HIP). SWUST's optimized formulation employs B_2O_3 as the base flux, supplemented with Bi_2O_3, ZnO and SiO_2 to enhance glass network stability. CIAE's certified process involves: (1) slurry preparation through sequential conveying, batching, mixing, and grinding of iodine waste, solidifiers, and deionized water; (2) hydrothermal treatment of the slurry in sealed metal containers to generate partially amorphous sodalite precursors (XRD-confirmed); (3) HIP sintering to form sodalite. MCC-1 leaching tests demonstrated exceptional chemical durability: iodine release rates ranged from 3.767×10^{-9} to 1.254×10^{-7} g/(m^2·d) over 168 days, normalized to geometric surface area.

Copyright on 7th Asia-Pacific Symposium on Radiochemistry 2025 - R3-20 -

2.2 The solidification of tritium-containing waste liquid

Tritiated wastewater resists effective separation or removal via conventional water treatment methods due to its strong concealment, persistent internal radiation hazards, and limited disposal options. To address this challenge, Southwest University of Science and Technology developed a containment strategy combining high-density concrete solidification with a multi-barrier encapsulation system. The procedure includes: (1) pouring concrete into a steel drum, (2) inserting a primary barrier layer of tritium-impermeable materials, (3) overlaying additional concrete, and (4) hermetically sealing the drum. Experimental validation demonstrated a normalized standard leaching rate of 1×10^{-5} g/(m^2·d), confirming the system's effectiveness in immobilizing radioactive tritium.

2.3 Iron phosphate glass solidification technology

The Shanghai Institute of Optics and Fine Mechanics has developed iron phosphate glass formulations for solidifying two types of high-level radioactive waste: liquid waste generated from reprocessing spent fuel of high-burnup power reactors, and actinide-rich waste streams obtained after separating strontium and cesium from the original liquid waste.The resulting vitrified products exhibit a waste metal inclusion rate of $20-22\%$, with performance metrics (including chemical stability) surpassing those of conventional borosilicate glass. Furthermore, a 127-hour continuous melting trial was successfully conducted on a Φ550 mm cold crucible platform at pilot scale. All batches of solidified glass met the required standards for chemical stability and waste oxide encapsulation efficiency, with no signs of equipment corrosion observed.

Due to its significantly higher solubility for MoO_3 compared to borosilicate glass systems, iron phosphate glass vitrification is a promising candidate for immobilizing Zr-Mo precipitates (characterized by exceptionally high molybdenum content) generated during the pretreatment of high-level radioactive liquid waste.

2.4 Rock-mineral immobilization technology

Rock-mineral immobilization utilizes natural substrates such as zircon, monazite, and granite. This technology has internationally pioneered a ceramic non-occupying-design direct solidification approach, transcending the limitations of traditional host-guest architectures. It enables holistic immobilization of complex metallic matrices while reducing ceramic consolidation time from several hours to minutes. Particularly applicable to secondary actinide waste streams (containing Am and Cm) derived from high-level radioactive liquid waste partitioning, this method achieves exceptional inclusion rates (>20 wt%). In the resultant glass-ceramic matrices, highly radioactive minor actinides are predominantly sequestered within the crystalline ceramic phase, exhibiting chemical stability significantly superior to the vitreous matrix.

3. Conclusion

The development of Large-scale Commercial Reprocessing Plants (LCRPs) in China necessitates advanced waste management strategies distinct from historical approaches. This survey highlights significant progress in solidification and conditioning technologies tailored to LCRP-specific waste streams. Key advancements include the successful immobilization of volatile **^{129}I** within durable low-temperature glass or sodalite matrices via HIP, demonstrating exceptional long-term stability. For challenging **tritiated waste**, a robust multi-barrier concrete encapsulation system has proven effective for containment. **Iron phosphate glass** emerges as a superior alternative to borosilicate glass, particularly for high-Mo waste streams, showcasing high waste loading and successful pilot-scale production. Furthermore, innovative **rock-mineral immobilization** techniques offer rapid, high-capacity solidification for complex actinide wastes. Collectively, these advanced technologies represent crucial steps towards enhancing the safety, efficiency, and long-term viability of radioactive waste management in China's future commercial reprocessing endeavors.

References

[1] Darda S A, Gabbar H A, Damideh V, et al. A comprehensive review on radioactive waste cycle from generation to disposal[J]. Journal of Radioanalytical and Nuclear Chemistry, 2021, 329(1): 15-31.

[2] Development of New Waste Forms to Immobilize Iodine-129 Released from aSpent Fuel Reprocessing Plant [J]. Advances in Science and Technology, 2010, 73158-170.

Copyright on 7th Asia-Pacific Symposium on Radiochemistry 2025 - R3-20 -

7th Asia-Pacific Symposium on Radiochemistry *September 14 ~ 19, 2025 • Kunibiki Messe • Shimane, Japan*

DEVELOPMENT OF A LOW-TEMPERATURE DECONTAMINATION MEDIUM

Katerina Cubova[1], Jan Houzar[2], Mojmír Němec[3]

[1]*Czech technical University in Prague, Department of Nuclear Chemistry, Brehova 7, 115 19 Prague 1, Czech Republic, katerina.cubova@fjfi.cvut.cz*
[2] *Czech technical University in Prague, Department of Nuclear Chemistry, Brehova 7, 115 19 Prague 1, Czech Republic, houzajan@fjfi.cvut.cz*
[3] *Czech technical University in Prague, Department of Nuclear Chemistry, Brehova 7, 115 19 Prague 1, Czech Republic, mojmir.nemec@fjfi.cvut.cz*

One of the key activities for the safe operation and also decommissioning of nuclear power plants is the decontamination of equipment. Decontamination consists of removing radionuclides from the contaminated material and treating the resulting waste. Decontamination for decommissioning aims at reduction of the activity of radionuclides below clearance levels so that the materials can be further treated as non-active and released or re-used. Operational decontamination is carried out to ensure safe operation for staff and minimal damage to the decontaminated surface. In both cases, decontamination of primary circuit focuses in the first step mainly on removal of inner corrosion layers containing activated corrosion products adsorbed and/or incorporated during the NPP operation and very often also immobilized fission products coming from microcracks in fuel cladding. However, the large volume of secondary waste is generated and must be treated. In this context, there is a strong demand from nuclear operators for new solutions to replace or improve currently used technologies. The current trend in development of new decontamination methods is therefore to minimize amount of waste, maximize recycling opportunities and reduce energy consumption.

The aim of this work is development and verification of the low temperature recyclable decontamination medium to be applicable in specific conditions of Czech NPPs. Additionally, the research emphasizes the possibility of recycling the developed medium after its use, which would not only reduce the energy consumption but also the volume of generated secondary radioactive waste. This research follows the recently patented medium [1] originally developed for the purpose of decommissioning application. This medium was based on peroxodisulfate anion activated by silver ions in sulphuric acid environment and allows efficient disruption and dissolution of the surface corrosion layer in temperatures below 60°C. The requirement is up-scaling of the already existing process and parallel modifications in its chemistry to make it applicable for operational decontamination of primary circuit components in a circuit and bath decontamination. Results from testing persulfate media modifications and further optimizations of the parameters of the most suitable medium will be presented. Data from a regeneration study will also be included.

ACKNOWLEDGMENTS

This work was supported by Center for Advanced Nuclear Technology II (CANUT II) – TN02000012; Technology Agency of the Czech Republic.

References

[1] Czech Technical university in Prague, Prague 6, Dejvice, CZ; ÚJV Řež, a.s., Husinec, Řež, CZ. CHEMCOMEX, a.s., Prague 5, Zbraslav, CZ. Method of decontamination of internal surfaces of the primary circuit of a nuclear power plant and decontamination solution. Inventors: Němec M, Čubová K, et al. Czech Republic. Patent CZ308870. 2021-07-15

Copyright on 7th Asia-Pacific Symposium on Radiochemistry 2025 - R3-21 -

7th Asia-Pacific Symposium on Radiochemistry *September 14 ~ 19, 2025 • Kunibiki Messe • Shimane, Japan*

Study on removal of the nuclear fuel materials from waste liquid using flocculation and precipitation method

Lucie Sifnerova[1,*], Takeru Matsuishi[2], Yu Tachibana[2], Toshiaki Hiyama[2], Fuminori Honda[2,†]

[1]*Department of Nuclear Chemistry, CTU in Prague: Brehova 7, CZ-11519, Praha, Czechia, sifneluc@fjfi.cvut.cz*
[2] *Central Institute of Radioisotope Science and Safety, Kyusyu University, Motooka 744, Fukuoka Nishi, Fukuoka, 819-0395, Japan, † honda.fuminori.790@m.kyushu-u.ac.jp*

The large volume and inherent risks of handling radioactive liquid waste, including potential spills, present significant challenges in nuclear waste management. This study explores the removal of nuclear fuel materials from such waste using flocculation and precipitation methods. Poly-silicate iron (PSI), a coagulant commonly applied in water treatment, was evaluated for its potential in nuclear waste solution treatment.

1 Introduction

Uranium, a radioactive element, is an essential fuel used in nuclear power generation. After being mined from uranium ore, it undergoes refining and an enrichment process to increase the concentration of uranium-235 (^{235}U) for use as nuclear fuel. These processes, as well as the use of uranium as fuel, generate various types of waste containing uranium. Such waste often includes uranium and other actinides, and due to the potential radiation exposure to humans and other living organisms, as well as environmental impacts, strict and systematic management of the waste's quantity, storage methods, and storage locations is required. However, due to the high radioactivity and long half-lives of these materials, the disposal, storage, and final management of the waste remain significant challenges.

Although not to the same extent as in nuclear power generation, uranium is also widely used in industrial products, glassware, and in laboratory settings for purposes such as chemical processing research and negative staining in electron microscopy. While the amount of uranium used in laboratories is minimal, the resulting waste takes various forms, including aqueous or acidic liquid waste. In Japan, there is currently no public organization responsible for accepting such small-scale radioactive waste, and as a result, facilities that use even small amounts of nuclear materials have been storing these liquid and solid wastes in on-site storage facilities for extended periods.

Liquid waste is typically stored in sealed glass or plastic containers; however, as these containers age, degradation can lead to breakage and leakage of radioactive solutions. Compared to solid waste, leakage of liquid waste poses a more serious problem as it can spread over a larger area, seep into flooring materials, and require extensive decontamination efforts, resulting in a significant increase in secondary waste.

An effective initial countermeasure is to separate and solidify the radioactive materials, such as uranium, from the liquid waste. This process can significantly reduce the effort required for waste management, limit the risk of leakage due to container failure, and lower the overall risk potential.

Common methods for separating uranium from inorganic liquid waste include solvent extraction and ion exchange. While these methods are effective, they are often time-consuming and generate large volumes of secondary waste, making them less suitable for treating large volumes of low-concentration liquid waste containing small amounts of nuclear material, as typically encountered in laboratory settings.

To address this issue, we are investigating the application of a coagulation–sedimentation treatment method using poly-silicate iron (PSI) coagulants as a stabilization technique for such low-concentration radioactive liquid waste. PSI is a coagulant composed of iron (Fe) and silica (SiO_2), primarily used in water treatment due to its high coagulation and sedimentation efficiency. While polyaluminum chloride (PAC) coagulants have been widely used in traditional water treatment, concerns regarding the environmental impact of aluminum and the establishment of discharge standards have prompted a shift toward PSI, which is increasingly being adopted for its lower environmental burden.

In the treatment of uranium-containing liquid waste, ensuring that the effluent meets water quality standards is also a key requirement. PSI has demonstrated the capability to meet these standards, making it a promising material for the effective and environmentally responsible treatment of such waste [1].

In this study, to optimize the coagulation performance of poly-silicate iron (PSI) coagulants for actinide elements, we first conducted cold tests using non-radioactive cerium compounds—specifically, cerium acetate and cerium nitrate aqueous solutions. Subsequently, hot tests were performed using uranium-containing liquid waste. The pH of the solutions was adjusted using a sodium hydroxide solution.

Copyright on 7th Asia-Pacific Symposium on Radiochemistry 2025- R3-22* -

2 Experimental Procedure

In the cold tests, the cerium concentration in the test solutions was determined by the calibration curve method using an energy-dispersive X-ray fluorescence analyzer (EDX-7000, Shimadzu Corporation). For the hot samples, the radioactivity concentration of the solution was measured using a scintillation-type α/β radiation detector (JDC-5300, Hitachi Aloka Medical, Ltd.). Two types of poly-silicate iron coagulants were used, differing in their iron and silica content: PSI-010 (Fe 4 wt%) and PSI-025 (Fe 6 wt%). As a pretreatment before coagulation and sedimentation, the solutions were mixed thoroughly using a shaker for 24 hours to ensure homogeneity.

3. Experimental Results

Figure 1(a) shows the formation of precipitates in a cerium nitrate solution as a function of pH adjustment. Precipitation of cerium hydroxide was observed at pH 7.5, and when the pH exceeded 12, the concentration of cerium in the solution fell below the detection limit. PSI-010 and PSI-025 were each added to the test solution at 1 vol.%, followed by pH adjustment. After thorough mixing and centrifugation, the cerium concentration in the supernatant was measured. Figure 1(b) presents photographs of the appearance of each test solution.

As a result, precipitation was observed even at pH values below 7. Notably, around pH 7.5—considered suitable for wastewater treatment—PSI-025 showed a higher cerium removal efficiency compared to PSI-010. Similar results were obtained using a cerium acetate solution. Precipitate formation began at pH 10.9, and at pH values above 11.5, cerium was nearly undetectable in the solution. The coagulation–sedimentation treatment using PSI showed comparable trends to those observed with the cerium nitrate solution.

Figure 1(c) summarizes the results of the coagulation–sedimentation tests using different PSI coagulants on cerium-containing solutions. These results suggest that PSI-025 has a higher cerium removal capacity than PSI-010. Furthermore, a comparison of the floc particle sizes showed that PSI-010 tended to form finer particles than PSI-025. While PSI-010 may require longer treatment times when using gravitational settling or filtration with filter paper, centrifugation was found to significantly reduce separation time for both coagulants.

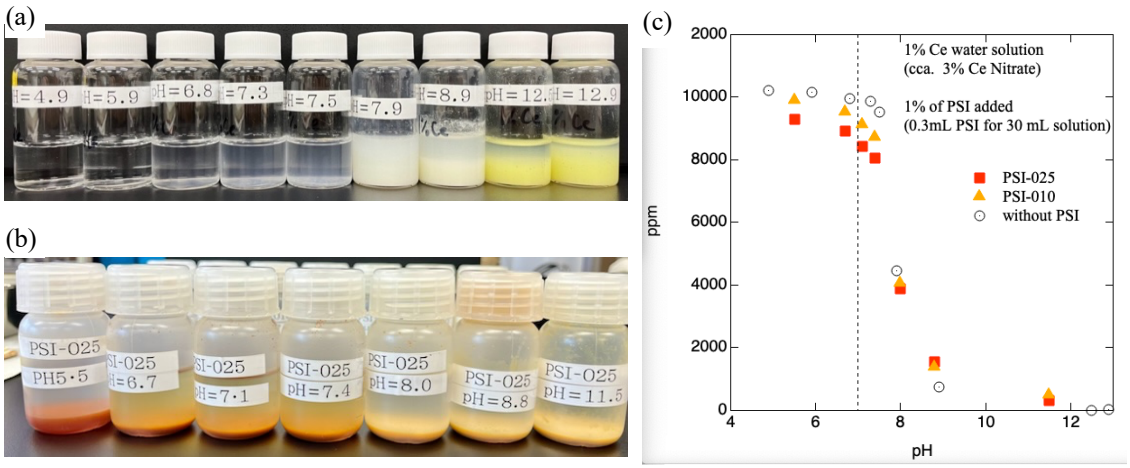


Fig.1 Precipitation of cerium nitrate by adjusting pH (a) without PSI and (b) with PSI-025, and (c) the comparison of the Ce concentration by pH adjustment alone and flocculation precipitation with adding PSI.

In the conference, we will present results of the application of the coagulation–sedimentation treatment method for uranium waste liquid.

ACKNOWLEDGMENTS

This work is financially supported by the Nuclear Energy System Research and Development Project (Gensiryoku System Kaihatsu Jigyo). The authors acknowledge valuable discussion with Drs. Sakasegawa and Nishiwaki, Japan Atomic Energy Agency.

References

[1] K. AKASHI, J. TANAKA, T. MATSUISHI, AND T. HIYAMA, “Waste solution treatment of uranyl acetate using poly-silicate iron (PSI) flocculant,” *Nippon Hoshasen Anzen Kanri Gakkai-shi (Online)*, 20 (1), 2–5 (2021).

Copyright on 7th Asia-Pacific Symposium on Radiochemistry 2025- R3-22* -

Contributed Talk | [R3]Actinide Chemistry and Nuclear Energy Chemistry

Wed. Sep 17, 2025 9:45 AM - 10:45 AM JST | Wed. Sep 17, 2025 12:45 AM - 1:45 AM UTC Hall A(MP)

[R3] Actinide Chemistry and Nuclear Energy Chemistry

9:45 AM - 10:05 AM JST | 12:45 AM - 1:05 AM UTC

[R3-09]

Measurement of Sr-90/Cs-137 ratios of smear samples collected in reactor buildings of the Fukushima Daiichi Nuclear Power Station using beta-ray spectrometry

*Asako Shimada[1], Yoshihisa Iida[1], Yu Maruyama[1] (1. Japan Atomic Energy Agency (Japan))

10:05 AM - 10:25 AM JST | 1:05 AM - 1:25 AM UTC

[R3-10]

Studies of Cerium Oxide Nanoparticles Aggregation and Dissolution Mechanisms from Nuclear Fuel Debris

*Cong Chao[1], Yiwei Zhang[2], Miguel Pineda[1], Eric S Fraga[1], Naokazu Idota[2], Takehiko Tsukahara[2], Panagiota Angeli[1] (1. Department of Chemical Engineering, University College London (UK), 2. Laboratory for Zero-Carbon Energy, Institute of Integrated Research, Institute of Science Tokyo (Japan))

10:25 AM - 10:45 AM JST | 1:25 AM - 1:45 AM UTC

[R3-11*]

Uranium Dissolution Behavior from Fuel Debris Pellets and Micro-Nanoparticles

*Tongyu XU[1], Naokazu IDOTA[1], Yuma DOTSUTA[2], Yukihiko SATOU[2], Toru KITAGAKI[2], Takehiko TSUKAHARA[1] (1. Institute of Science Tokyo (Japan), 2. Japan Atomic Energy Agency (Japan))

©APSORC25

7th Asia-Pacific Symposium on Radiochemistry *September 14 ~ 19, 2025 • Kunibiki Messe • Shimane, Japan*

MEASUREMENT OF Sr-90/Cs-137 RATIOS OF SMEAR SAMPLES COLLECTED IN REACTOR BUILDINGS OF THE FUKUSHIMA DAIICHI NUCLEAR POWER STATION USING β-RAY SPECTROMETRY

Asako Shimada[1], Yoshihisa Iida[1], Yu Maruyama[1]

[1]*Japan Atomic Energy Agency: 2-4 Shirakata, Tokai-mura, Naka-gun, Ibaraki, 319-1195, shimada.asako@jaea.go.jp*

Smear samples were collected inside of reactor buildings at the Fukushima Daiichi Nuclear Power Station. Dominant γ-ray emitting nuclides were Cs-137 and Cs-134. In addition, Co-60 and Sb-125 were detected for some samples although their radioactivities were 1/1000 ~ 1/100000 compared to that of Cs-137. Simple and rapid analytical method using β-ray spectrometry were developed to analyze Sr-90. The Sr-90/Cs-137 mole ratios for smear samples collected in Units 1 and 2 were 0.0017±0.0013 and 0.0077±0.0044, respectively. This results agreed with the reported Sr-90/Cs-137 ratio for rubble samples collected inside Units 1 and 2.

1 INTRODUCTION

It is expected to obtain information about the progression of the accident, chemical forms of released radionuclides, and source terms from the contamination distribution within reactor buildings of the Fukushima Daiichi Nuclear Power Station (1F). Therefore, smear samples were collected inside reactor buildings at the 1F. Sr-90 is one of the target nuclides because Sr is easily released in a reducing atmospheric condition and can use as an indicator for estimating the atmospheric condition during core melt. Usually, radiochemical analysis of Sr-90 is complicated and time-consuming. Therefore, rapid and simple analytical method using β-ray spectrometry for Sr-90 in the smear samples were developed. Sr-90 radioactivity in the smear samples were analyzed using the developed method and mole numbers of Sr-90 were calculated. The mole numbers of Sr-90 were normalized by dividing the mole numbers of Cs-137 to compare the Units.

2 Experimental

γ-Ray emitting nuclides in the smear samples were measured using Ge semiconductor detector (BE3830-CP5-PLUS-SL-iPA-SL10, Mirion Technologies Canberra Industries, Inc.). Energy and efficiency were calibrated using mixed radioactivity standard planar source (MX421, Cd-109, Co-57, Ce-139, Cr-51, Sr-85, Cs-137, Mn-54, Y-88, Co-60, Japan Radioisotope Association). β-ray spectra were measured using low background β-ray spectrometer (picobeta, NC7153, Fuji Electric Co., Ltd.). Standard smear samples for β-ray spectrometry were prepared using radioactivity standard solutions of Cs-137 and Sr-90 purchased from Japan Radioisotope Association. Briefly, smear filters were stocked in plastic bags, then, 5000 Bq of Cs-137 and 0-50 Bq of Sr-90 were added.

3 Results and discussions

Figure 1 shows one example of γ-ray spectrum of smear sample collected inside of the reactor buildings at the 1F. Dominant γ-ray emitting nuclides were Cs-137 and Cs-134. In addition, Co-60 and Sb-125 were detected in some samples, and their radioactivity were 1/1000 ~ 1/10000 to that of Cs-137.

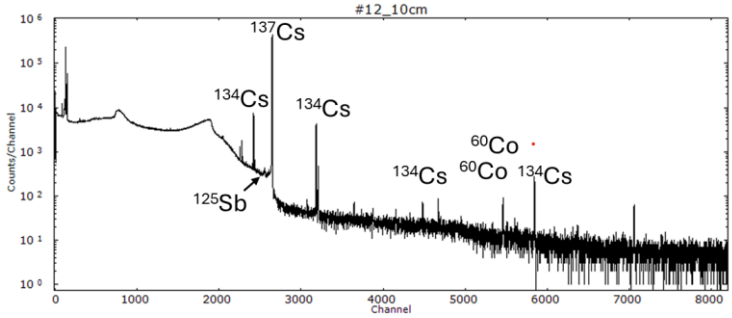


FIGURE 1. γ-Ray spectrum of smear sample collected inside reactor building at the 1F

Copyright on 7th Asia-Pacific Symposium on Radiochemistry 2025 - R3-09 -

Because 14 years after the accident, secular equilibrium between Sr-90 and Y-90 was reached. The maximum β-ray energy of all detected γ-ray mitting nuclides are lower than that of Y-90. Although only β-ray emitting nuclides such as H-3, C-14, Ni-63, Tc-99, I-129 possibly existed in the smear sample, these maximum β-ray energy also lower than that of Y-90. Therefore, we developed an analytical method of Sr-90 using higher energy region only related to Y-90.

Calculated Sr-90/Cs-137 mole ratios at the time of March 11, 2011, in smear samples were summarized in Table 1. The Sr-90/Cs-137 mole ratios for Units 1 and 2 were 0.0017±0.0013 (0.00031-0.0047) and 0.0077±0.0044 (0.0024-0.012), respectively, and that for Unit 1 is lower than that for Unit 2. It is expected that the atmospheric condition of Unit 1 might not reach drastic reducing condition. In addition, these results agreed with the Sr-90/Cs-137 radioactivity ratios (decay corrected to March 11, 2011) obtained for rubble samples collected in Units 1 (0.0035±0.0015) and 2 (0.019) [1]. When the applicability of scaling factor method was evaluated to estimate inventory of Sr-90, it is possible to measure Sr-90 using smear samples instead of rubble samples. Measuring smear samples without dissolution and chemical separation make shorten the analysis time from approximately 3 weeks to 80 minutes.

Smear samples were divided into plural pieces for destructive analysis. For example, the smear sample, 4th floor, north, wall, 1m, was divided into 5 pieces. For 2 pieces of them, their Sr-90 radioactivity were less than detection limit. The Sr-90/Cs-137 mole ratios were obtained for the remaining 3 pieces. The Sr-90/Cs-137 mole ratios varied within 25%, therefore, nuclides contents in a smear sample are roughly homogeneous.

TABLE 1 Calculated Sr-90/Cs-137 mole ratios in smear samples (decay corrected to March 11, 2011)

Unit 1		Unit 2	
Sampling point	Sr-90/Cs-137	Sampling point	Sr-90/Cs-137
2nd floor, steps	0.0012	1st floor, wall	0.0079
2nd floor, floor	0.00031	2nd floor, wall	0.012
2nd floor, wall, 1 m	0.00094	3rd floor, wall	0.0024
2nd floor, wall, 20 cm	0.0021	4th floor, wall	0.0024
3rd floor, floor	0.00077	5th floor, floor	0.0092, 0.012
4th floor, steps	0.0012		
4th floor, north, wall, 1 m	0.0031		
4th floor, north, wall, 1 m (divided pieces)	0.0039 0.0045 0.0028 Avg. = 0.0037±0.0009		
4th floor, north, wall, 20 cm	0.0047		
4th floor, north, floor	0.0024		
4th floor, east, wall 1 m	0.0010		
4th floor, east, wall 20 cm	0.00070		
average	0.0017±0.0013	average	0.0077±0.0044

4. CONCLUSIONS

Rapid and simple analytical method for Sr-90 was developed and applied to smear samples collected at Units 1 and 2 of the 1F. The measuring time was decreased from 3 weeks to 2 hours. The calculated Sr-90/Cs-137 mole ratios for Unit 1and 2 were agreed with those obtained for rubble samples collected inside the Units 1 and 2.

ACKNOWLEDGMENTS

This work was supported by Nuclear Regulation Authority. The authors extend their sincere appreciation to Mr. Masanori Hayashi, Ms. Keiko Kamohara, and Ms. Yasuko Sekisawa for their invaluable assistance with the radiochemical analysis.

References

[1] Y. Sato, K. Tanaka, T. Ueno, K. Ishimori, Y. Kameo, “Radiochemical Analysis of Rubble Collected from Fukushima Daiichi Nuclear Power Station”, Jpn. J. Health Phys., **51**(4), 209 (2016).

Copyright on 7th Asia-Pacific Symposium on Radiochemistry 2025 - R3-09 -

7th Asia-Pacific Symposium on Radiochemistry *September 14 ~ 19, 2025 • Kunibiki Messe • Shimane, Japan*

Studies of Cerium Oxide Nanoparticles Aggregation and Dissolution Mechanisms from Nuclear Fuel Debris

Cong Chao[1], Yiwei Zhang[2], Miguel Pineda[1], Eric S Fraga[1], Naokazu Idota[2], Takehiko Tsukahara[2], and Panagiota Angeli[1]

[1] *ThAMeS Multiphase and Sargent CPSE, Department of Chemical Engineering, University College London, Torrington Place, London WC1E 7JE, UK,*
[2] *Laboratory for Zero-Carbon Energy, Institute of Integrated Research, Institute of Science Tokyo, N1-6 2-12-1, Ookayama, Meguro-ku, Tokyo, 152-8550, Japan*

Understanding the properties and behaviors of aerosols generating in the Fukushima nuclear plant is significant for its evacuation. This work aimed to focus on the aggregation and dissolution of nanoparticles generating from the Fukushima nuclear plant decommissioning. To investigate the impacts of different chemical components on nanoparticles, redox-dissolution experiments were carried out in batch-type reactors and microchannels. We found that CeO_2 nanoparticles tend to agglomerate when exposed to substances like H_2O_2, HNO_3. Moreover, nanoparticle denaturation behaviors highly depend on the surrounding environment, and they perform different dissolution kinetics in H_2O_2 and HNO_3 solutions. These results suggest that specific interfacial reactions occur on the nanoparticle surfaces.
***Keywords**: Cerium Oxide nanoparticles, fuel debris, microfluidics, particle aggregation, Fukushima decommissioning, surface reactions*

1 Introduction

The significance of size effects in nanoparticles have been noticed in various applications, such as environmental remediation and catalysts [1]. In the Fukushima nuclear accident, large amounts of particles were generated during the retrieval of nuclear fuel debris, posing serious risks to both the environment and human health [2]. Our previous research has identified certain metal species that hinder the dissolution of MOX fuel, leading to disruption in the retrieval process [3]. Therefore, understanding the physicochemical properties and behaviours of these generated particles is very significant. Cerium oxide is widely recognized as plutonium oxide surrogate due to their similar properties, and zirconium, abundant in the plant, were chosen as representatives in this study. We aimed to evaluate their dissolution and denaturation behaviour in simulated chemical environments in the Fukushima nuclear plant and investigate their impacts on the fuel debris. To gain a fundamental understanding of the thermodynamic behaviours and mechanisms underlying nanoparticle denaturation, we characterized the structural variations of nanoparticles after mixing, and quantitively evaluated the dissolved metals.

2 Experimental

To investigate nanoparticle behaviours and reactions occurring during debris decommissioning, we conducted experiments using both batch and continuous systems (Figure 1). In batch experiment, CeO_2, ZrO_2 and $(Ce, Zr)O_2$ suspension were prepared, with reaction solvents such as H_2O_2, HNO_3, deferoxamine B (DFB), etc. were selected. These suspensions were then mixed with the reaction solvent in a batch-type reactor under constant agitation via a stirrer for several days, respectively. H_2O_2 concentrations ranged from $1*10^{-4}$ M to 1.2 M, corresponding to the ionizing irradiated aerated water in the Fukushima nuclear plant. Supernatant was collected under centrifugation using an ultrafiltration tube (Amicon® Ultra Centrifugal Filter, 100 kDa MWCO) for concentration measurement. The separated suspension was then dried to investigate their physicochemical property changes. In the continuous system, continuous syringe pumps were employed to precisely control the flow rates of the reaction solvent and nanoparticle suspension. These solutions were introduced into the main circular microchannel through a T-junction inlet configuration. Upon collision within the microchannel, reactions were induced. Similar post-treatment was applied in the continuous system.

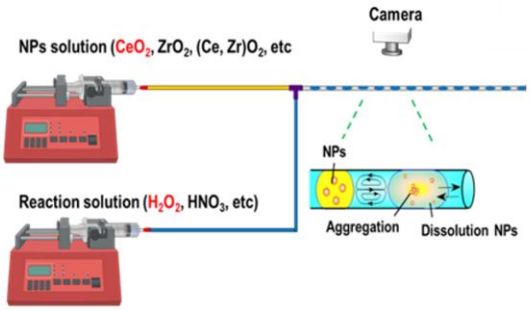


Figure 1. Schematics illustration of and continuous system set up.

3 Results and Discussion

In this study, we evaluated the individual effects of

different chemical components on various size groups of nanoparticles and monitored changes in dissolution rates under different residence times, including tracking particle size changes, crystal structure deformations, valences transformations and dissolved metal concentrations. Dynamic light scattering (DLS) results indicated that CeO_2 suspension remained stable in deionized (DI) water, but there was an increase in the average particle size following treatment of H_2O_2 and HNO_3. Moreover, the proportion of larger particles (particle size >1000nm) increased with longer contact time, indicating significant aggregation of nanoparticles. Additionally, we found different degrees in microfluidic experiments compared to batch experiments, with particles aggregating rapidly within seconds. High-resolution images of CeO_2 nanoparticles revealed that initial particles suspended in DI water exhibited needle-like shapes, while particle aggregation was evident after contact with reaction solvents, consistent with DLS results.

Concentration measurements indicated that few CeO_2 nanoparticles can dissolve under 1.2 M H_2O_2 treatment (Figure 2), while they showed better dissolution performances when surrounded by nitric acid, contributing to lower surface charge and smaller electrostatic repulsive forces among particles. This likely contributed to higher degrees of CeO_2 nanoparticles, potentially hindering redox-dissolution reactions due to decreased specific surface areas. Experiments conducted in microchannel proved effective in removing the negative impacts stemming from the low surface-are-to-volume ratio resulting from aggregation in traditional batch experiments.

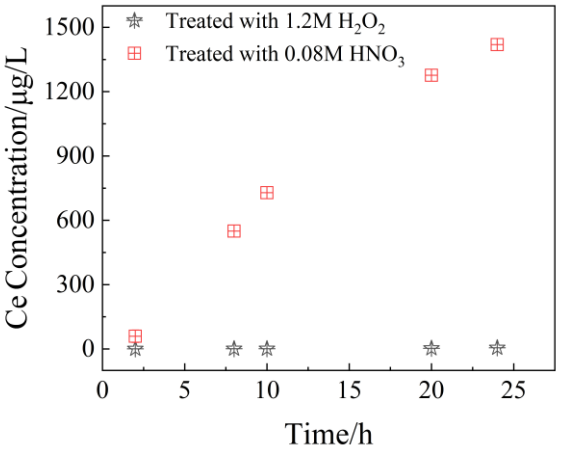


Figure 2. CeO_2 dissolution performances under treatment with H_2O_2 and HNO_3

4. Conclusions

We successfully developed a novel method using a microchannel reactor to measure the kinetics of nanoparticles dissolution accurately and continuously. This approach allowed for real-time monitoring of dissolution rates. The study indicated that the dissolution rate of cerium oxide and zirconium oxide nanoparticles in the microscale environment was higher than that in the bulk scale as expected. These findings suggested that specific reactions may occur at nano-scale interfaces of colloidal particles formed during the retrieval of nuclear fuel debris. Such changes at the nanoscale interfaces may have negative impacts on waste management in nuclear development. This research clarifies the microscopic interfacial behaviour and reaction mechanisms between nanoparticles and environments.

ACKNOWLEDGMENTS

This work was financially supported by the by the Engineering and Physical Sciences Research Council (ESPRC), project number EP/X022218/1, JAEA Nuclear Energy S&T and Human Resource Development Project Grant Number JPJA22F22717857 and Secretariat of the Nuclear Regulation Authority, Japan.

References

[1] J. Dolai, K. Mandal and N R. Nanoparticle size effects in biomedical applications. ACS Applied Nano Materials, 4(7), 6471-6496 (2021).
[2] T. Ohnuki, S. Yukihiko, U. Satoshi. Formation of radioactive cesium microparticles originating from the Fukushima Daiichi Nuclear Power Plant accident: characteristics and perspectives. Journal of Nuclear Science and Technology, 56(9-10), 790-800 (2019).
[3] D K. Hwang, T. Tsukahara, K. Kosuke, O. Masahiko, and Y. Ikeda. Studies on supercritical hydrothermal syntheses of uranium and lanthanide oxide particles and their reaction mechanisms. Journal of Nuclear Materials, 466, 134-141 (2015).

7th Asia-Pacific Symposium on Radiochemistry *September 14 ~ 19, 2025 • Kunibiki Messe • Shimane, Japan*

Uranium Dissolution Behavior from Fuel Debris Pellets and Micro-Nanoparticles

Tongyu Xu[1], Naokazu Idota[2], Yuma Dotsuta[3], Yukihiko Satou[3], Toru Kitagaki[3], Takehiko Tsukahara[1,2]

[1] *Department of Chemical Science and Engineering, Institute of Science Tokyo*
[2] *Laboratory for Zero-Carbon Energy, Institute of Integrated Research, Institute of Science Tokyo, 2-12-1-N1-6, Ookayama, Meguro-ku, Tokyo, 152-8550; tsukahara.t.ab@m.titech.ac.jp*
[3]*Japan Atomic Energy Agency, 2-4 Shirakata, Tokai-mura, Ibaraki, 319-1195, Japan*

To understand the dissolution and denaturation mechanisms of fuel debris into cooling seawater, this study conducted experiments of simulated fuel debris dissolution under various conditions, focusing on the thermodynamic and kinetic behavior of uranium, with application of a novel microfluidic approach. The results revealed that uranium dissolution behavior under microscale differed significantly from conventional batch experiments, and the presence of zirconium (Zr) and hydrogen peroxide (H_2O_2) markedly influenced dissolution kinetics. Moreover, since micro-nanoparticle generation was observed during microfluidic dissolution, further investigation into dissolution mechanisms and behavior of fuel debris nanoparticles was in progress.

1 INTRODUCTION

Having been immersed and cooled by seawater over a decade, fuel debris has undergone long-term denaturation and dissolution. Previous studies have shown that H_2O_2, produced by radiolysis of cooling water, can oxidize low-solubility U(IV) to more soluble U(VI), thereby accelerating uranium dissolution [1]. For fuel debris retrieval, a feasible approach involves cutting the debris into smaller pieces for removal. During cutting operations, such as laser or thermal cutting, nanoparticles would be generated from the exposed surfaces. With larger specific surface area and distinctive behavior of nanoparticles [2], understanding their dissolution mechanisms is essential for fuel debris retrieval management.

In this study, fuel debris dissolution experiments were conducted under a variety of conditions to investigate uranium dissolution behavior and mechanisms. In addition to conventional batch dissolution tests, a microfluidic approach—offering a powerful means to observe complex interfacial reactions [3–4] was utilized to examine dissolution under dynamic surface conditions. The study discusses differences in dissolution mechanisms between static batch conditions and dynamic microfluidic environments, providing insights critical for understanding and managing uranium behavior. Moreover, further investigation into nanoparticle dissolution characteristics was carried out.

2 EXPERIMENTAL

For microfluidic dissolution experiments, a novel microfluidic device for solid–liquid reaction systems was fabricated using a transparent polydimethylsiloxane (PDMS) body, with its framework illustrated in Fig.1. Simulated solid fuel samples—UO_2 and $(U_{0.7},Zr_{0.3})O_2$ pellets (φ10 mm, cylindrical)—synthesized by a sintering method, were embedded within a microchannel formed on the PDMS substrate. This design allowed continuous solution flow to directly contact and react with the pellet surfaces under microscale. Constant solution flow at 0.001 mL/min was provided by syringe or HPLC pumps connected via capillary tubes. Various solution conditions were tested, including pure water, 0.01M HNO_3, 0.15mM H_2O_2, and 0.1mM deferoxamine B solutions.

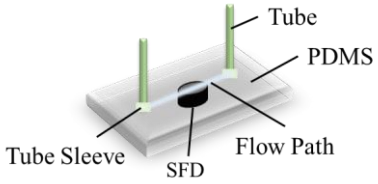


Fig.1 Framework of microfluidic device

For comparison, static batch experiments were also conducted using similar pellets and solution compositions, with pellets immersed in 100 mL of static solution for up to 100 days. At specified intervals, solution samples were collected, and dissolved uranium concentrations were analyzed using ICP-MS. Material composition, crystal structure, and surface structure before and after dissolution were characterized by Laser Raman spectroscopy, X-ray diffraction (XRD), and scanning electron microscopy (SEM), respectively. To account for the potential influence of H_2O_2 spontaneous decomposition, weekly monitoring of H_2O_2 concentration changes was performed during the microfluidic experiments.

Additionally, aqueous suspensions of UO_2 and $(Zr,U)O_2$ nanoparticles were prepared at concentrations ranging from 1 wt% to 4 wt%. Batch dissolution experiments into H_2O_2 solutions at concentrations of 0.15 mM, 0.015 mM, and 0.0015 mM were carried out. Particle size, zeta potential and dissolved U concentration in solution were monitored at certain time intervals.

Copyright on 7th Asia-Pacific Symposium on Radiochemistry 2025- R3-11* -

3 RESULTS AND DISCUSSION

Raman spectroscopy confirmed that the surfaces of the initial fuel debris pellets consisted of UO_2, UO_{2+x}, and ZrO_2 phases. Uranium exhibited the highest solubility in H_2O_2 solution, followed by deferoxamine-B, HNO_3, and pure water.

To evaluate uranium dissolution kinetics, time-dependent dissolution rates per surface area of fuel debris in the microchannel were calculated and compared with those under batch conditions, as shown in Fig.2. In all solution environments, the uranium dissolution rates in microfluidic reactions were faster than those in batch systems. Moreover, dissolution rates remained nearly constant over time in all solutions except for H_2O_2 under microfluidic conditions. This finding suggests that a rapid and pronounced uranium dissolution occurs at the initial stage when fuel debris surfaces contact with H_2O_2 in the microchannel. Small fluctuations in dissolution rates were also detected under microfluidic conditions.

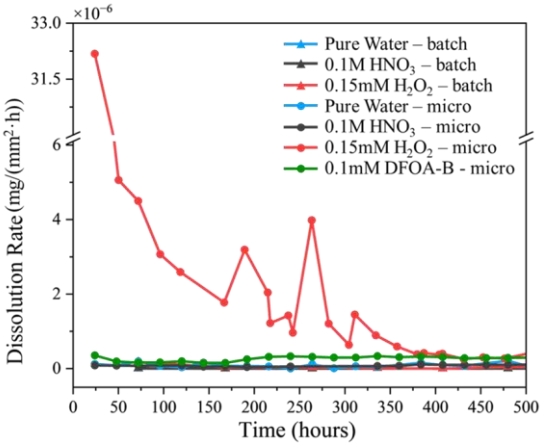


Fig.2 Time-dependence uranium dissolution rates pre surface area

Raman spectroscopy and XRD analysis before and after dissolution indicated no significant changes in the crystalline structures of the debris surfaces. However, SEM observations revealed that pinhole-shaped damage appeared on pellet surfaces after microfluidic dissolution. Furthermore, laser camera imaging captured the movement of particles under an electric potential, suggesting that micro-scale dissolution may be driven by particle detachment from the surface.

In the nanoparticle dissolution experiments, particle aggregation was initially observed as particle sizes increased upon contact with H_2O_2 solutions. As dissolution consists, disaggregation occurred, together with direct reaction on particle surface, reflected by a gradual decrease in particle diameter until reaching a stable size.

4 CONCLUSIONS

Uranium exhibited greater solubility in H_2O_2 solution compared to other solution conditions; however, the presence of zirconium inhibited uranium dissolution by catalyzing the decomposition of H_2O_2. Under microfluidic conditions, uranium dissolution rates were significantly higher, driven by multiple simultaneous processes, including direct surface reactions and particle release from the debris. Nanoparticles demonstrated distinct dissolution behaviors, such as aggregation and disaggregation, intense surface reactions, and dynamic dispersion and sedimentation.

ACKNOWLEDGMENTS

This work was financially supported by the Secretariat of the Nuclear Regulation Authority, Japa, and partially supported by JAEA Nuclear Energy S&T and Human Resource Development. Project Grant Number JPJA22F22717857.

References

[1] Kumagai Y, Takano M, Watanabe M. Reaction of hydrogen peroxide with uranium zirconium oxide solid solution–Zirconium hinders oxidative uranium dissolution. 2017, J. Nucl. Mater., 497, 54-59.
[2] Hedberg J, Blomberg E, and Wallinder O I. In the Search for Nanospecific Effects of Dissolution of Metallic Nanoparticles at Freshwater-Like Conditions: A Critical Review. **2019** *53* (8), 4030-4044
[3] Neuville A, Renaud L, Luu T T, et al. Xurography for microfluidics on a reactive solid.2017, Lab on a Chip, 17, 293-303.
[4] Brandt A and Tsukahara T. Development of Real-Time Analysis System of Selenium Ion in Solutions by Using Microextraction and Fluorescence Microscopy. 2021, ACS Earth and Space Chem., 5, 558-595.

Copyright on 7th Asia-Pacific Symposium on Radiochemistry 2025- R3-11* -

Contributed Talk | [S2]Radiopharmaceutical Sciences

Wed. Sep 17, 2025 11:00 AM - 12:00 PM JST | Wed. Sep 17, 2025 2:00 AM - 3:00 AM UTC Hall S(Int'l)

[S2] Radiopharmaceutical Sciences

11:00 AM - 11:20 AM JST | 2:00 AM - 2:20 AM UTC

[S2-04*]

THE REACTIONS OF RARE EARTH ELEMENTS AND ACTINIUM WITH THE TWELVE-MEMBERED AZA-MACROCYCLIC LIGAND HAVING PHOSPHONIC PYRIDINE ARMS

*Kenta Hamasaki[1], Kazuaki Baba[1], Kojiro Nagata[2], Kenji Shirasaki[3], Takuya Yokokita[4], Hidetoshi Kikunaga[4], Kazuaki Tsukada[4], Tatsuo Yajima[5], Takashi Yoshimura[3] (1. Department of Chemistry, Graduate School of Science, The University of Osaka (Japan), 2. Core Facility Center, The University of Osaka (Japan), 3. Radioisotope Research Center, Institute for Radiation Sciences, The University of Osaka (Japan), 4. Research Center for Accelerator and Radioisotope Science, Tohoku University (Japan), 5. Department of Chemistry and Materials Engineering, Faculty of Chemistry, Materials and Bioengineering, Kansai University (Japan))

11:20 AM - 11:40 AM JST | 2:20 AM - 2:40 AM UTC

[S2-05*]

CORRELATION BETWEEN COORDINATION STRUCTURES AND ELECTRONIC PROPERTIES OF CYCLEN-BASED COMPLEXES WITH HEAVY P-BLOCK ELEMENTS

*Hiroki Aoto[1], Hiroyuki Kazama[1], Masashi Kaneko[1], Kojiro Nagata[2], Haruka Maeda[1], Eishun Kawagishi[1], Terumi Yokoyama[1], Yoshitaka Kasamatsu[1] (1. Graduate School of Science, The University of Osaka (Japan), 2. Core Facility Center, The University of Osaka (Japan))

11:40 AM - 12:00 PM JST | 2:40 AM - 3:00 AM UTC

[S2-06*]

Basic Performance Evaluation of an Electron-tracking Compton Camera Using Multiple Radionuclide Point Sources and Multi-Source Imaging with 18F-FDG

*Ryota Iwasaki[1], Kaiji Tanaka[1], Ryuta Kiuchi[1], Shigeto Kabuki[1], Hiroyasu Matsushita[1], Koya Yoshida[1], Hiroyuki Kimura[2], Yoji Kitamura[3], Takashi Kozaka[3], Masato Asai[4], Hidekazu Kawashima[5], Kyoshi Nishijima[6], Tsuyoshi Fukuzawa[1], Yoshio Kunieda[7], Junko Kushida[1] (1. Tokai University (Japan), 2. Kyoto University (Japan), 3. Kanazawa University (Japan), 4. Japan Atomic Energy Agency (Japan), 5. Kyoto Pharmaceutical University (Japan), 6. Kanagawa University (Japan), 7. Tokyo General Hospital (Japan))

©APSORC25

7th Asia-Pacific Symposium on Radiochemistry *September 14 ~ 19, 2025 • Kunibiki Messe • Shimane, Japan*

THE REACTIONS OF RARE EARTH ELEMENTS AND ACTINIUM WITH THE TWELVE- MEMBERED AZA-MACROCYCLIC LIGAND HAVING PHOSPHONIC PYRIDINE ARMS

Kenta Hamasaki[1], Kazuaki Baba[1], Kojiro Nagata[2], Kenji Shirasaki[3], Takuya Yokokita[4], Hidetoshi Kikunaga[4], Kazuaki Tsukada[4], Tatsuo Yajima[5], Takashi Yoshimura[3]

[1]*Department of Chemistry, Graduate School of Science, The University of Osaka: 1-1 Machikaneyama, Toyanaka, Osaka 560-0043, Japan*
[2]*Core Facility Center, The University of Osaka: 1-1 Machikaneyama, Toyonaka, Osaka 560-0043, Japan*
[3]*Radioisotope Research Center, Institute for Radiation Sciences, The University of Osaka: 2-4 Yamadaoka, Suita, Osaka 565-0871, Japan, tyoshi@rirc.osaka-u.ac.jp*
[4]*Research Center for Accelerator and Radioisotope Science, Tohoku University: 6-3 Aramaki aza aoba, Aoba, Miyagi 980-8578, Japan*
[5]*Department of Chemistry and Materials Engineering, Faculty of Chemistry, Materials and Bioengineering, Kansai University: 3-3-35 Yamatecho, Suita, Osaka 564-8680, Japan*

Yttrium, lanthanoids (REE), and actinium (Ac) are important in radiopharmaceuticals. In this study, we designed a novel twelve-membered aza-macrocyclic ligand with phosphonic pyridine arms, and synthesized REE complexes by the reactions of macro amounts of stable REE isotopes with the ligand. Single-crystal X-ray structure analysis was successfully conducted for all the REE complexes except for the radioactive element promethium. The complex formation reactions of macro amounts of Y, La, Lu with the ligand were monitored by ^{1}H NMR spectroscopy, and the complex formations were found to be completed within 3 minutes at room temperature. The potentiometric titration of the REE complexes revealed that the stability constants of the Y and late lanthanide complexes are sufficient for in vivo use as radiopharmaceuticals. In addition, we performed radiochemical labeling using ^{152}Eu and ^{225}Ac to investigate reactivities at tracer conditions.

1 INTRODUCTION

Nuclear medicine is important as an effective means for cancer therapy. In this therapy, it is important to deliver and accumulate radiometals specifically to cancer cells by using radiopharmaceuticals, which can minimize unintended damage to normal cells. Radiopharmaceuticals have cancer-selective molecules, such as peptides and antibodies with high specificity for targeted cancer cells. As such molecules are often heat sensitive, it is required to synthesize radiopharmaceuticals under mild conditions such as room temperature. It is also crucial for rapid complex formation because many of the radiometals used in this therapy have short half-lives. Currently, there is growing clinical interest in radioactive REE and ^{225}Ac for the therapeutic and diagnostic purposes, but there are very few chelating ligands that rapidly form stable complexes with these metals at room temperature. In this study, we synthesized a novel twelve-membered aza-macrocyclic ligand with phosphonic pyridine arms, and we investigated its chelation behavior with REE and ^{225}Ac using macro amounts of stable isotopes and tracer amounts of radioisotopes.

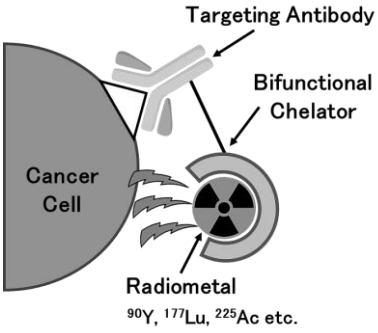


Fig. 1. The concept of nuclear therapy using radiopharmaceutical.

2 RESULTS and DISCUSSION

The new REE complexes were synthesized by the reactions of REE triflate salts with the ligand in water at room temperature. Single-crystals suitable for X-ray diffraction analysis were obtained by adding acetone to the reaction solutions. The crystal structures of the obtained REE complexes are the 10-coordinate dimer for La, the 9-coordinate dimer for Pr-Tb, and the 8-coordinate monomer for Y and Er-Lu. The reactions between Y, La, Lu, and the ligand were monitored by ^{1}H NMR spectroscopy, and it was found that the complexing was completed within 3 minutes at room temperature. The potentiometric titration of the complexes revealed that the stability constants of the complexes with the ligand are larger in the heavier lanthanides, and the stability constants of the Y and late lanthanide complexes are sufficient for *in vivo* use. We subsequently investigated the reactivity of tracer concentrations of ^{152}Eu and ^{225}Ac with the ligand by radio-thin-layer-chromatography. The radio labeling yields in the ligand concentrations of 10^{-3}~10^{-7} M were also investigated.

Copyright on 7th Asia-Pacific Symposium on Radiochemistry 2025- S2-04* -

7th Asia-Pacific Symposium on Radiochemistry *September 14 ~ 19, 2025 • Kunibiki Messe • Shimane, Japan*

CORRELATION BETWEEN COORDINATION STRUCTURES AND ELECTRONIC PROPERTIES OF CYCLEN-BASED COMPLEXES WITH HEAVY P-BLOCK ELEMENTS

Hiroki Aoto[1], Hiroyuki Kazama[1], Masashi Kaneko[1], Kojiro Nagata[2], Haruka Maeda[1], Eishun Kawagishi[1], Terumi Yokoyama[1], Yoshitaka Kasamatsu[1]

[1]*Graduate School of Science, The University of Osaka: 1-1 Machikaneyama, Toyonaka, Osaka, 560-0043, aotoh22@chem.sci.osaka-u.ac.jp*
[2]*Core Facility Center, The University of Osaka: 1-1 Machikaneyama, Toyonaka, Osaka, 560-0043*

Stable complexes are essential for the applications of ^{212}Pb and ^{212}Bi to targeted alpha therapy. To understand the factors of stability of ^{212}Pb and ^{212}Bi complexes, we synthesized and characterized DOTAM and H_2PSC complexes with the heavy p-block elements using crystallography, spectroscopy, and density functional theory calculation. *The characteristic coordination structures of these complexes were found to be influenced by the interaction between Pb 6p orbitals and the 2p orbitals of coordinated N and O atoms. The 6p orbitals of Pb^{2+} were found to be hybridized in the HOMO region by the analysis of UV-vis absorption and time-dependent density functional theory calculation.*

1. INTRODUCTION

Targeted alpha therapy (TAT) is an efficient cancer therapy that minimize side effects by using short range and high liner energy transfer of alpha particles well [1]. The heavy p-block element lead-212 (^{212}Pb, $t_{1/2}$ = 10.6 h) is expected to be used in TAT and be sustainably supplied without accelerators or nuclear reactors, as its parent nuclide, thorium-232, is an abundant natural resource. For the application of ^{212}Pb to TAT, a chelator forming a stable ^{212}Pb complex is required to deliver ^{212}Pb to cancer. The chelating ligand 1,4,7,10-tetraazacyclododecane-1,7-diacetic amide-4,10-diacetic acid (H_2PSC), as shown in Fig. 1, has been investigated for TAT application to ^{212}Pb. The H_2PSC ligand was developed by modifying the chemical structure of 1,4,7,10-tetraazacyclododecane-1,4,7,10-tetraacetic amide (DOTAM), which is a well-known chelator exhibiting high stability toward $^{212}Pb^{2+}$. H_2PSC has indicated stable *in vivo* behavior not only with ^{212}Pb but also with ^{212}Bi [2], which is the daughter nuclide of ^{212}Pb. Revealing the characteristics of H_2PSC complexes with heavy p-block elements can potentially elucidate the stability of H_2PSC complexes toward ^{212}Pb and ^{212}Bi.

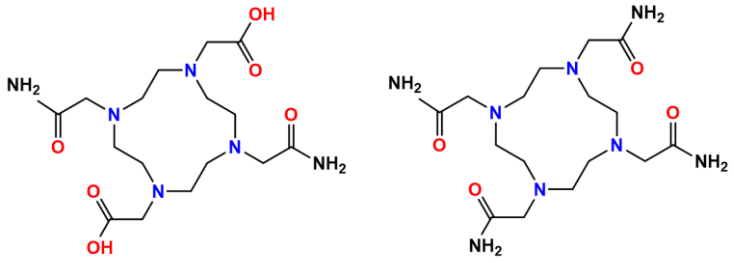


Fig. 1. The chemical structural formula of H_2PSC and DOTAM

This study aims to reveal the characteristics of heavy p-block element complexes with DOTAM and H_2PSC. The Tl^+, Pb^{2+}, Bi^{3+}, and Sn^{2+} complexes with DOTAM and H_2PSC were synthesized and characterized using crystallography, spectroscopy, and density functional theory (DFT) calculation.

2. EXPERIMENTAL

DOTAM was prepared according to a reported procedure [3]. H_2PSC was synthesized and identified by ^{1}H NMR, FT-IR, CHN elemental analysis, and single crystal X-ray diffraction (scXRD) analysis. Heavy p-block elements, Tl^+, Pb^{2+}, Bi^{3+}, and Sn^{2+} complexes with DOTAM and H_2PSC were synthesized and characterized by FT-IR and UV-vis analysis. The crystal and coordination structures were evaluated by scXRD and the coordination bond lengths were analyzed.

Optimization of ground state was obtained using ωB97/def2-TZVP level by TURBOMOLE ver. 7.7 software. Single-point energy calculations and time-dependent (TD-)DFT calculations were performed using ωB97/ZORA-def2-TZVPP level for C, H, O, N atoms and ωB97/SARC-ZORA-TZVPP level for Tl. Pb. Bi, and Sn by ORCA ver. 6.0.0 software. The equilibrium structures of DOTAM and H_2PSC complexes were obtained using geometry optimization based on DFT calculation. The electronic properties of heavy p-block ions in the complexes were investigated by electrostatic potential maps, natural bond orbital (NBO), and density of state (DOS) analysis. TD-DFT calculations were performed to characterize the electronic absorption spectra observed in the UV-vis experiment.

Copyright on 7th Asia-Pacific Symposium on Radiochemistry 2025- S2-05* -

3. RESULTS AND DISCUSSION

Heavy p-block element complexes with DOTAM $[M(DOTAM)]^{n+}$ (where M^{n+} = Tl^{+}, Pb^{2+}, Bi^{3+}, Sn^{2+}) and Pb^{2+} complex with H_2PSC $[Pb(HPSC)]^{+}$ and [Pb(PSC)] were successfully synthesized with a 1:1 p-block metal-to-ligand stoichiometry. The coordination structures of all synthesized complexes were found to adopt an 8-coordinated square antiprismatic geometry. The p-block elements were coordinated by 4 nitrogen atoms and 4 oxygen atoms from the DOTAM and H_2PSC. In non-p-block element complexes with DOTAM, the metal-oxygen bond (M-O) lengths are regularly shorter than the metal-nitrogen bond (M-N) lengths reflecting the smaller van der Waals radius of oxygen atoms compared to nitrogen atoms. However, the M-O lengths in heavy p-block elements complexes with DOTAM were observed to be longer than the M-N lengths. The DOS analysis indicated that antibonding orbitals were formed in the interactions between valence *p* orbitals of heavy p-block elements and O 2*p* orbitals in HOMO region. It was proposed that the empty valence *p* orbitals in the free heavy p-block element ions were partially occupied by electron donation from the N donor atoms of the cyclen ring. These interactions are considered to contribute to the formation of the characteristic coordination structures of $[M(DOTAM)]^{n+}$.

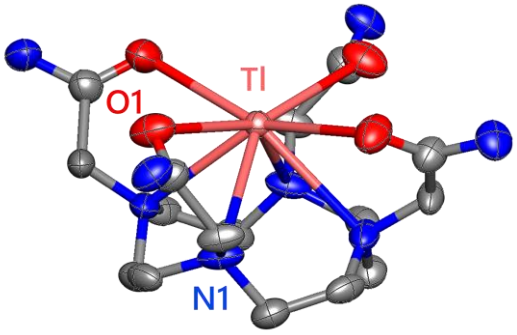


Fig. 2. The molecular structure of $[Tl(DOTAM)]NO_3$

Comparison of the coordination structures of $[Pb(HPSC)]NO_3$ and [Pb(PSC)] with that of $[Pb(DOTAM)](NO_3)_2$, the Pb-O bond lengths in PSC complexes were observed to be longer than the Pb-N bond lengths, contrary to the expectation that the electrostatic interaction of the Pb^{2+} ion and the carboxyl arms would shorten the Pb-O bonds.

UV-vis absorption spectra of Pb^{2+} ion, $[Pb(DOTAM)](NO_3)_2$, and [Pb(PSC)] in aqueous solution indicated a red-shift of the absorption band corresponding to the Pb $6s^2 \rightarrow 6sp$ transition by coordination of Pb^{2+} with DOTAM and PSC. The degree of the red-shifts were larger than those observed in the previously reported Pb^{2+} complexes [4]. These large shifts suggest that the greater hybridization of 6*p* orbitals of Pb^{2+} into the HOMO region results in the lowering the transition energies. This origin will be discussed in detail using TD-DFT calculations

4. CONCLUSIONS

In this study, heavy p-block element complexes with DOTAM and H_2PSC were successfully synthesized and their coordination structures were determined. The Pb-O and Pb-N bond lengths in these complexes were found to be influenced by the orbital interactions between Pb 6*p* orbitals and 2*p* orbitals of O and N donor atoms. The UV-vis absorption spectra revealed the large red-shifts. These shifts suggest the hybridization of 6*p* orbitals of Pb^{2+} in the HOMO region. These structural and electronic characteristics are considered to influence the stability of the complexes and this knowledge will contribute to ^{212}Pb TAT application.

ACKNOWLEDGMENTS

This work was the result of using research equipment shared in MEXT Project for promoting public utilization of advanced research infrastructure (Program for supporting construction of core facilities) Grant Number [JPMXS0441200022], [JPMXS0441200023], [JPMXS0441200024], and [JPMXS0441200025].

This work was supported by JST SPRING, Grant Number JPMJSP2138.

References

[1] C. KRATOCHWIL, *et al*., *The Journal of Nuclear Medicine*, **57**, 12 (2016).
[2] M. LI, *et al*., *Pharmaceutics*, **15**, 2 (2023).
[3] H. MAUMELA, *et al*., *Journal of the American Chemical Society*, **117**, 25, (1995).
[4] J. W. NUGENT, *et al*., *Polyhedron*, **91**, (2015).

Copyright on 7th Asia-Pacific Symposium on Radiochemistry 2025- S2-05* -

7th Asia-Pacific Symposium on Radiochemistry *September 14 ~ 19, 2025 • Kunibiki Messe • Shimane, Japan*

Basic Performance Evaluation of an Electron-tracking Compton Camera Using Multiple Radionuclide Point Sources and Multi-Source Imaging with ^{18}F-FDG

R. Iwasaki[1], K. Tanaka[1], R. Kiuchi[2], S. Kabuki[2], H. Matsushita[1], K. Yoshida[1], H. Kimura[3], Y. Kitamura[4], T. Kozaka[4], M. Asai[5], H. Kawashima[6], K. Nishijima[7], T. Fukuzawa[2], E. Kunieda[8], J. Kushida[9]

1 Tokai University, Course of Physics, School of Science, Hiratsuka, Japan
2 Tokai University, School of Medicine, Isehara, Japan
3 Kyoto University, Agency for Health, Safety and Environment, Kyoto, Japan
4 Kanazawa University, Division of Probe Chemistry for Disease Analysis, Research Center for Experimental Modeling of Human Disease, Kanazawa, Japan
5 Japan Atomic Energy Agency, Advanced Science Research Center, Tokai, Japan
6 Kyoto Pharmaceutical University, Radioisotope Research Center, Kyoto, Japan
7 Kanagawa University, Department of Applied Physics, Faculty of Engineering, Yokohama, Japan
8 Tokyo General Hospital, Radiotherapy Center, Nakano, Japan
9 Tokai University, School of Science, Hiratsuka, Japan

This study evaluated the basic performance of an electron-tracking Compton camera (ETCC), focusing on its ability to distinguish multiple radionuclide sources and reconstruct images. Using ^{133}Ba, ^{22}Na, ^{137}Cs, and ^{54}Mn point sources, spatial and energy resolution were assessed. A multi-source imaging test with ^{18}F-FDG demonstrated that the ETCC can clearly identify 511 keV sources, indicating its potential for applications in nuclear medicine, including PET imaging.

1 . PURPOSE

This study aims to evaluate the fundamental performance of the electron-tracking Compton camera (ETCC) and to clarify its capability for distinguishing different and multiple radiation sources, as well as its image reconstruction performance. First, point sources of ^{133}Ba, ^{22}Na, ^{137}Cs, and ^{54}Mn are used to systematically assess the ETCC's energy and spatial resolution, thereby verifying its ability to handle high-energy gamma rays. Furthermore, a multi-source experiment was conducted using ^{18}F-FDG (511 keV) as a simulated source and a disk phantom to image three-point sources simultaneously, aiming to evaluate the ETCC's applicability in real environments. In particular, this study aims to evaluate the quality of reconstructed images and the reliability of source identification for 511 keV gamma rays detected by the ETCC, thereby laying the groundwork for future biomedical and clinical applications.

2 . METHODS

The ETCC consists of a scatter detector and an absorber detector, which employs a Time Projection Chamber (TPC)(Fig. 1). The absorber detector is a gas-based tracking detector (μ-TPC) employing a micro pixel chamber (μ-PIC) as its core component, while the scatter detector uses GSO(Ce) scintillators.
For the basic performance evaluation of the ETCC, point sources of ^{133}Ba (356 keV), ^{22}Na (511 keV), ^{137}Cs (662 keV), and ^{54}Mn (835 keV) were used. Each source was positioned at the center of the ETCC's field of view for imaging. The acquired event data were reconstructed to evaluate spatial.
Next, ^{18}F-FDG point sources (diameter : 6.25 mm) were arranged at 25 mm intervals and placed such that their center aligned with the center of the ETCC's field of view. This setup was used to assess spatial resolution and quantitative capability.

Copyright on 7th Asia-Pacific Symposium on Radiochemistry 2025- S2-06* -

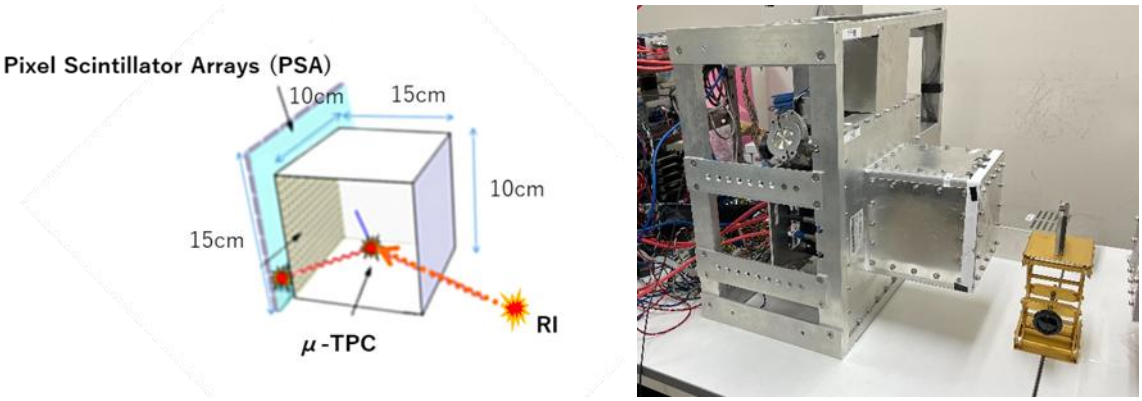


Fig. 1. ETCC schematics

3 . RESULTS

In the experiment using multiple radionuclide point sources, gamma-ray events were extracted within an energy window of ±10% around each source's energy peak (356 keV, 511 keV, 662 keV, and 835 keV), and image reconstruction was performed under the same conditions. As shown in Figure 2, the full width at half maximum (FWHM) decreased with increasing gamma-ray energy, indicating an improvement in spatial resolution. This trend is attributed to the fact that higher-energy gamma rays producing clearer electron tracks following Compton scattering, thereby enhancing reconstruction accuracy. These results demonstrate that while the ETCC exhibits energy dependence, it maintains stable reconstruction performance in the medium-to-high energy range (~835 keV).

Figure 3 shows the reconstructed image from the multi-source imaging test using ^{18}F-FDG point sources. Reconstruction was performed using an energy window of ±10% centered at 511 keV. The radiation intensity was approximately 1.1 MBq, and 80,000 events were employed for image reconstruction. As seen in Figure 3, multiple 511 keV radiation sources were successfully identified, confirming the effectiveness of the ETCC for multi-source imaging.

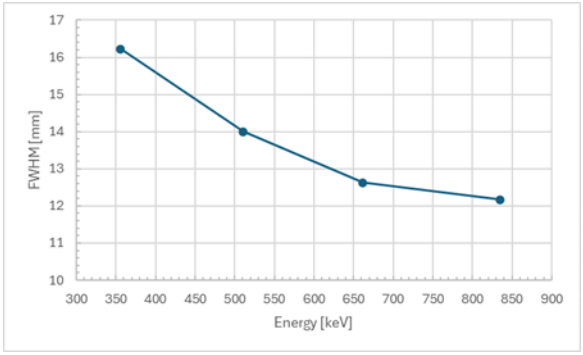


Fig. 2. Energy dependence of spatial resolution in ETCC

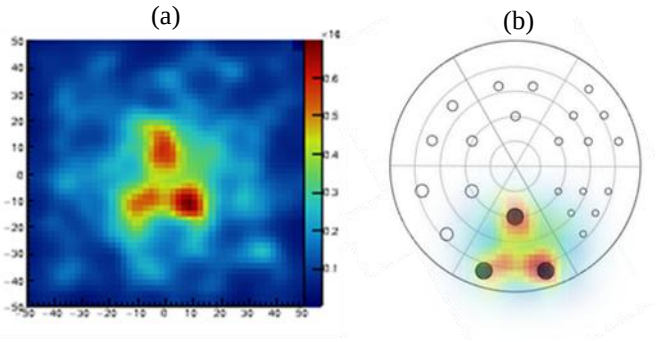


Fig. 3. Reconstructed image of the three ^{18}F-FDG point sources (a), and its overlay with the experimental setup

4. CONCLUSIONS

In the multi-nuclide experiment, spatial resolutions ware found to improve with increasing gamma-ray energy, confirming that the ETCC demonstrates stable performance in the medium-to-high energy range. Furthermore, in the multi-source imaging experiment using ^{18}F-FDG, multiple 511 keV sources were clearly identified, indicating that the ETCC can effectively function with radiopharmaceuticals commonly used in PET. These findings suggest that the ETCC has strong potential as a high-sensitivity, wide field-of-view imaging device for future applications in nuclear medicine diagnostics.

ACKNOWLEDGMENTS

This research was supported through the collaboration of Tokai University, Kanazawa University, and affiliated institutions. We sincerely thank all contributors for their valuable assistance with the experiments and data analysis. We are also grateful to the Research Center for Experimental Modeling of Human Disease at Kanazawa University for providing the ^{18}F-FDG used in this study.

Copyright on 7th Asia-Pacific Symposium on Radiochemistry 2025- S2-06* -

Contributed Talk | [P4]Radionuclide Migration Dynamics: Radioactive Waste Disposal and Environmental Impact Assessment

Wed. Sep 17, 2025 11:10 AM - 11:50 AM JST | Wed. Sep 17, 2025 2:10 AM - 2:50 AM UTC Hall B(Small)

[P4] Radionuclide Migration Dynamics: Radioactive Waste Disposal and Environmental Impact Assesment

11:10 AM - 11:30 AM JST | 2:10 AM - 2:30 AM UTC

[P4-04*]

Simulation of Tritium Multi-Medium Transport and Food Chain Transfer in Marine Environments with Human Dose Assessment

*Junyang Zeng[1], Lili Li[2], Yingzhe Du[2], Ziliang Hou[2], Youting Wu[3], Shiying Li[2], Hanyu Wu[1], Zhihao Liu[1], Peng Lin[2], Muyi Ni[1], Xiajie Liu[2] (1. Sun Yat-sen University (China), 2. China Nuclear Power Technology Research Institute (China), 3. Ocean University of China (China))

11:30 AM - 11:50 AM JST | 2:30 AM - 2:50 AM UTC

[P4-05*]

Shelf sea sediments as a dynamic sink for strontium, cesium, and cobalt: Redox-sensitive trapping mechanisms mediated by iron-clay synergy

*Lewen Sun[1], Qiaoya Lin[1], Xiaobo Zhang[2], Maoran Wang[1], Yu Zhang[1], Zezu Chen[1], Mingliang Kang[1] (1. Sun Yat-sen University (China), 2. Southern Marine Science and Engineering Guangdong Laboratory (Zhuhai) (China))

©APSORC25

Simulation of Tritium Multi-Medium Transport and Food Chain Transfer in Marine Environments with Human Dose Assessment

Junyang Zeng[1], Lili Li[2], Yingzhe Du[2], Ziliang Hou[2], Youting Wu[3], Shiying Li[2], Hanyu Wu[1], Zhihao Liu[1], Peng Lin[2],*, Muyi Ni[1],*, Xiajie Liu[2]

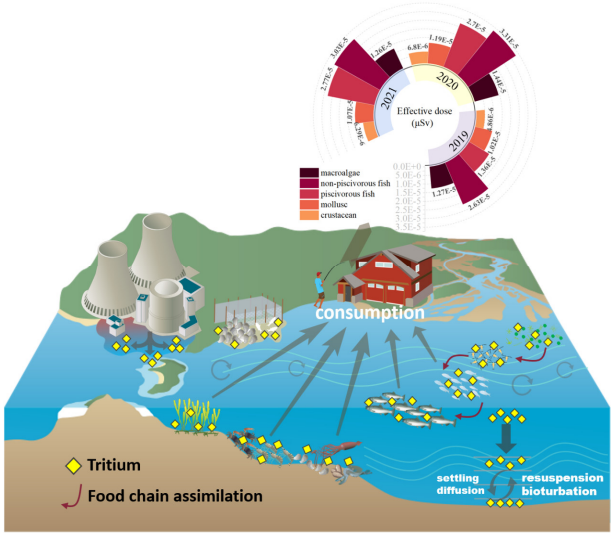
[1] *Sino-French Institute of Nuclear Engineering and Technology, Sun Yat-sen University, Zhuhai, 519082, China*
2China Nuclear Power Technology Research Institute Co., Ltd, China General Nuclear Power Corporation, Shenzhen, 518000, China
3 Frontiers Science Center for Deep Ocean Multispheres and Earth System and Key Laboratory of Physical Oceanography, Ocean University of China, Qingdao, 266100, China

During both normal operation and accident scenarios of nuclear power plants (NPPs), liquid effluents are discharged. Considering that most NPPs worldwide are located along coastlines, a large amount of radionuclides, including tritium, are released into the ocean with these effluents. Tritium in the ocean undergoes long-distance transport with seawater, interacts between water columns and sediments, transfers through the food chain, and ultimately enters the human body via seafood consumption. Given the distinct transport mechanisms of radionuclides in different media, separate investigations for each medium are necessary.

In this study, the multi-medium transport of tritium in the marine environment from 2019 to 2021 is simulated, considering decay reactions, tidal effects, flow fields, temperature-salinity fields, atmospheric driving fields, and different release patterns of radionuclides. The model includes a tritium water column transport sub-model, a tritium water-sediment transfer sub-model, a food chain transfer sub-model, and a dose assessment sub-model. It calculates the spatiotemporal variation of tritium concentration, analyzes the interactions between water and sediments, tracks dynamic transfer processes in different marine organisms, and evaluates the dose risk to humans from seafood consumption.

Concentration distribution results show that under quarterly discharge, tritium from effluents affects the entire South China Sea after four months, with strong seasonal transport patterns. In summer, influenced by the southwest monsoon, tritium migrates northeastward from the release point; in autumn and winter, the prevailing northeast monsoon causes high-concentration tritium to accumulate mainly in the Beibu Gulf and waters near the release point. Tritium distribution in sediments is negligible, approximately one order of magnitude lower than that in the near-bottom water layer, indicating no sediment enrichment. Organically bound tritium (OBT) in marine organisms is the form of tritium transfer through the food chain: higher-trophic-level aquatic species show weaker dependence of OBT concentration on seawater tritium (HTO) concentration, and fish exhibit stronger tritium enrichment capacity compared to mollusks and crustaceans. Over the simulated three years, the committed effective dose to humans from seafood consumption is 2.49×10-4 μSv, far below the international public dose limit of 1 mSv.

Keywords: *Radionuclide; Tritium; Ocean modelling; Marine multi-medium transport; Food chain transfer; Dose assessment*



Graphic Abstract

Copyright on 7th Asia-Pacific Symposium on Radiochemistry 2025- P4-04* -

CONCLUSIONS

(1) Tritium transport exhibits distinct seasonal variations, with high tritium concentrations primarily observed in the Beibu Gulf and along the coast of Guangdong.

(2) Tritium radioactivity in near-bottom waters was approximately ten times higher than in sediments, with no significant enrichment in the sediments.

(3) Fish have a higher tritium enrichment capacity than macroalgae, molluscs, and crustaceans. Simulations show that OBT levels in piscivorous fish did not reach equilibrium, indicating a strong tritium enrichment potential.

(4) The estimated tritium effective dose to the public from seafood consumption was estimated at 2.49×10-4 μSv, significantly below international dose limits.

ACKNOWLEDGMENTS

This work was supported by the funding from the National Natural Science Foundation of China (No. U2230109, U24B20194), China Nuclear Power Technology Research Institute Co., Ltd. (No. 008-ZB-B-2023-C45-P.T.99-00053).

Copyright on 7th Asia-Pacific Symposium on Radiochemistry 2025- P4-04* -

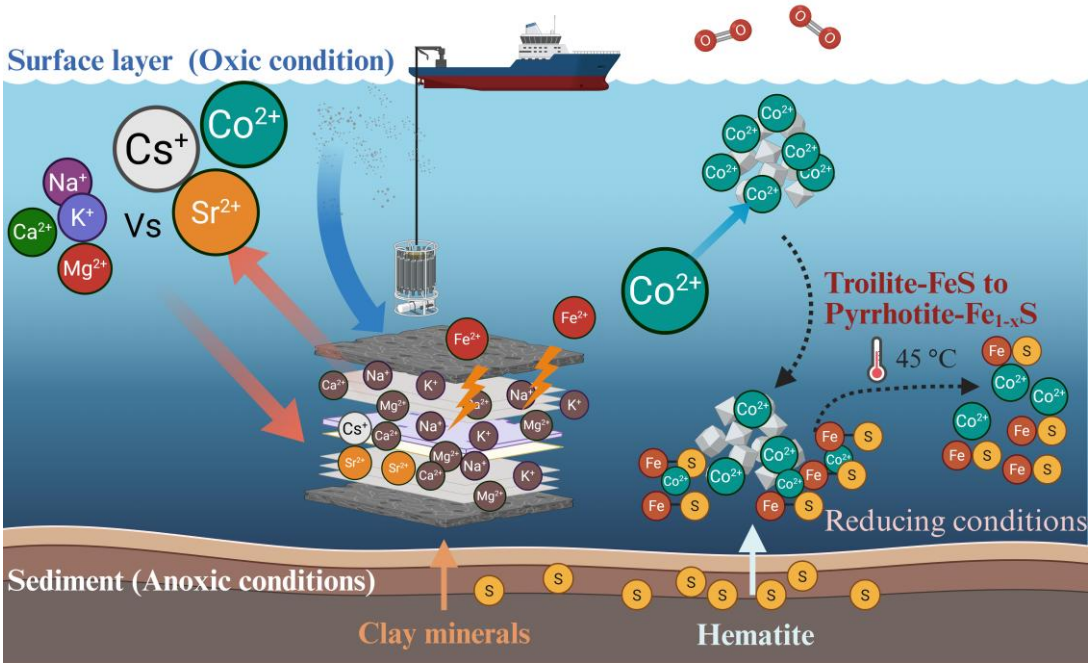
Shelf sea sediments as a dynamic sink for strontium, cesium, and cobalt: Redox-sensitive trapping mechanisms mediated by iron-clay synergy

Lewen Sun[1], Qiaoya Lin[1], Xiaobo Zhang[2], Maoran Wang[1], Yu Zhang[1], Zezu Chen[1], Mingliang Kang[1,*]

[1] *Sino-French Institute of Nuclear Engineering and Technology (Sun Yat-sen University), Tangjiawan, Zhuhai, Guangdong Province, P. R. China, 519082*
[2] *Southern Marine Science and Engineering Guangdong Laboratory (Zhuhai), Tangjiawan, Zhuhai, Guangdong Province, P. R. China, 519082*
[*] *Corresponding author E-mail addresses: kangml3@mail.sysu.edu.cn*

Human activities, such as nuclear tests, the use of nuclear energy, nuclear accidents, and the disposal of radioactively contaminated water into the ocean, have led to increasingly diverse pathways for the introduction of artificial radionuclides such as Sr-90 ($T_{1/2}$ = 28.8 y), Cs-137 ($T_{1/2}$ = 30.2 y), and Co-60 ($T_{1/2}$ = 5.27 y) into marine environments. These radionuclides, with long half-lives, significant biological toxicity, and the potential for bioaccumulation through the food chain, pose long-term risks to marine ecosystems. As key sinks for land-derived pollutants and sensitive ecological zones, shelf seas are particularly vulnerable. The dynamic hydrodynamic conditions and frequent sediment-water exchanges in shelf seas may facilitate the remobilization of radionuclides previously accumulated in sediments, exacerbating secondary pollutant diffusion and ecological exposure. This study examines the adsorption mechanisms of Sr(II), Cs(I), and Co(II) in the seawater-sediment system, focusing on how redox conditions influence their behavior. In kinetic experiments, the adsorption equilibrium for all radionuclides was reached within 48 hours, with the equilibrium adsorption capacities (q_e) under anoxic conditions at 25°C and low initial concentrations (~10 ppm) following the order: Co (0.4315 mg/g) > Cs (0.2850 mg/g) > Sr (0.0553 mg/g). Thermodynamic results reveal that Sr(II) and Cs(I) adsorption is primarily controlled by physical adsorption and influenced by ion exchange with clay minerals in the sediment. The adsorption of Co(II) on sediments is not only governed by ion exchange with clay minerals but is also significantly influenced by iron (Fe) oxides in the marine environment. Under oxic conditions, Sr(II) and Cs(I) primarily undergo ion exchange at the sediment-water interface, facilitated by clay minerals, while Co(II) deposition on sediments may be influenced by iron oxide interactions. In anoxic conditions, enhanced cation exchange capacity (*CEC*) of clay minerals further promotes Sr(II) and Cs(I) adsorption, while Co(II) becomes enriched around iron sulfides in reduced sediments. Additionally, elevated temperatures (＞40°C) induce the transformation of troilite-FeS to pyrrhotite-$Fe_{1-x}S$, which may reduce the Co(II) fixation capacity due to the formation of more compact magnetite. This research provides insights into the factors controlling the fate and transport of these radionuclides in marine sediments, with implications for environmental monitoring and coastal ecosystem management.

Key words: Radionuclides; Redox conditions; Adsorption mechanism; Sediment-water system.



Graphical Abstract

Copyright on 7th Asia-Pacific Symposium on Radiochemistry 2025- P4-05* -

1 Conclusion

The comparative investigation of radionuclide (Co, Sr, Cs) adsorption behaviors in seawater-sediment systems versus seawater-only systems under oxic/anoxic conditions revealed distinct deposition mechanisms. To mitigate radiation-related risks, stable isotopes (^{88}Sr, ^{133}Cs and ^{59}Co) were employed as non-radioactive substitutes for their radioactive counterparts (^{90}Sr, ^{137}Cs, ^{60}Co, etc.) in the adsorption experiments. Systematic analysis of adsorption kinetics demonstrated that anoxic conditions enhanced adsorption capacities for all target radionuclides (Co > Cs > Sr), with equilibrium attainment occurring within 48 h.

In the single seawater system, adsorption efficiency was used to evaluate deposition potential, and pH changes over time were monitored. The adsorption capacities of all three radionuclides were consistently higher under anoxic conditions. For Sr(II) and Cs(I), the increase in sediment adsorption under anoxic conditions is likely due to enhanced *CEC* [1, 2]. Co deposition appears to be primarily influenced by sediment composition, particularly interactions with iron oxides and sulfides. Specifically, under oxic conditions, Co(II) deposition on sediments may be affected by Fe oxides, while under anoxic conditions, enrichment around Fe sulfides is observed. Elevated temperatures (45°C) facilitate the transformation of FeS to $Fe_{1-x}S$, reducing Co(II) fixation due to the formation of more compact magnetite [3].

Establishing the relationship between physicochemical parameters of seawater and radionuclide adsorption (Fig.1). Notably, the adsorption of Co(II) showed a strong positive correlation with pH (r = 0.94 in oxic and r = 0.72 in anoxic conditions), likely mediated through Co–Fe oxide coprecipitation rather than direct pH control. This interpretation aligns with FeOOH phase transformations observed under variable redox environments [4]. Sediment composition exerted dominant control on Co(II) partitioning, while Sr(II) exhibited weak sediment interaction, detectable only under anoxic conditions. The inverse correlation between Sr adsorption and sulfate concentration (r = -0.99) suggests potential Sr–S complexation in sulfidic conditions. In contrast, under oxic conditions, Sr(II) adsorption was negatively correlated with Na^+ (r = -0.79), indicating ion-exchange competition within clay interlayers. Cs(I) showed no dominant single correlation, implying its sorption is governed by a complex interplay of multiple ions. These mechanistic insights offer key parameters for predicting radionuclide behavior in anoxic marine sediments and improving environmental risk models.

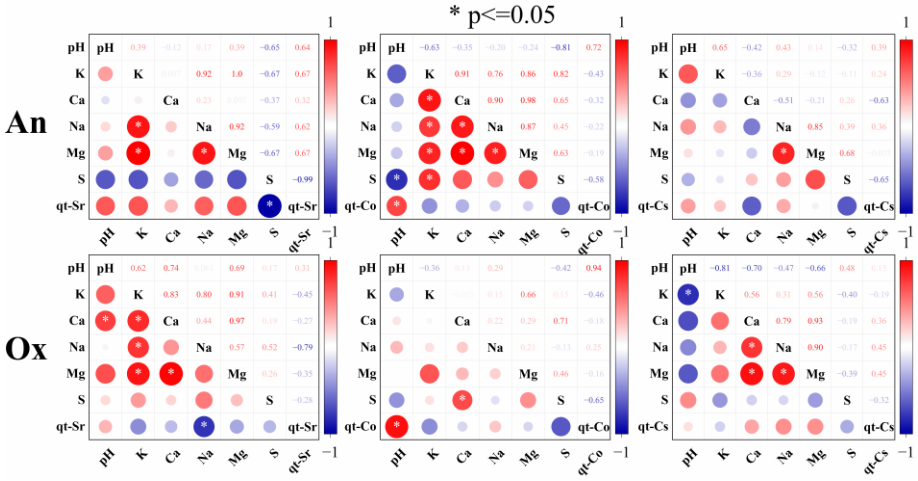


Fig.1. Correlation between adsorption capacity and seawater physicochemical parameters over time.

ACKNOWLEDGMENTS

This work was supported by the National Natural Science Foundation of China [Grant number 45000-41030072].

References

[1] Renault, P., et al., Variations in the cation exchange capacity of a ferralsol supplied with vinasse, under changing aeration conditions: Comparison between CEC measuring methods. Geoderma. 154(1): p. 101-110 (2009).
[2] Su, Y., et al., Reduction of precious metal ions in aqueous solutions by contact-electro-catalysis. Nature Communications. 15(1): p. 4196 (2024).
[3] Pohl, H.A., Solubility of Iron Sulfides. Journal of Chemical and Engineering Data. 7(2): p. 295-306 (1962).
[4] Rickard, D. and G.W. Luther, Chemistry of Iron Sulfides. Chemical Reviews. 107(2): p. 514-562 (2007).

Copyright on 7th Asia-Pacific Symposium on Radiochemistry 2025- P4-05* -

Contributed Talk | [P4]Radionuclide Migration Dynamics: Radioactive Waste Disposal and Environmental Impact Assessment

Wed. Sep 17, 2025 4:45 PM - 5:25 PM JST | Wed. Sep 17, 2025 7:45 AM - 8:25 AM UTC Hall B(Small)

[P4] Radionuclide Migration Dynamics: Radioactive Waste Disposal and Environmental Impact Assesment

4:45 PM - 5:05 PM JST | 7:45 AM - 8:05 AM UTC

[P4-10*]

Radionuclide behavior in bedrock for safe disposal of nuclear waste

*Noora Pakkanen[1], Marja Siitari-Kauppi[1] (1. University of Helsinki (Finland))

5:05 PM - 5:25 PM JST | 8:05 AM - 8:25 AM UTC

[P4-11*]

ANTIMONY MIGRATION IN COASTAL ENVIRONMENT: SYNERGISTIC ADSORPTION MECHANISM OF ORGANIC MATTER AND MINERAL PARTICLES UNDER UV-C IRRADIATION

*Qiaoya lin[1], lewen sun[1], xiaobo zhang[2], mingliang kang[1] (1. Sun Yat-sen University (China), 2. Southern Marine Science and Engineering Guangdong Laboratory (China))

©APSORC25

7th Asia-Pacific Symposium on Radiochemistry *September 14 ~ 19, 2025 • Kunibiki Messe • Shimane, Japan*

RADIONUCLIDE BEHAVIOR IN BEDROCK FOR SAFE DISPOSAL OF NUCLEAR WASTE

Noora Pakkanen[1], Marja Siitari-Kauppi[1]

[1]*Department of Chemistry, A.I. Virtasen aukio 1, Helsinki, Finland, 00560, noora.m.pakkanen@helsinki.fi / marja.siitari-kauppi@helsinki.fi*

Currently, nuclear energy accounts for 9 % of the global electricity production [1]. The production of this low-emission energy generates low-, intermediate-, and high-level radioactive waste. The spent nuclear fuel´s (SNF) final disposal strategy varies from country to country depending on the country´s geographical location. For example, in Finland the disposal of spent nuclear fuel (SNF) in the deep geological repository is planned to begin in the 2020s [2]. The disposal of SNF follows the Swedish KBS-3V safety concept of multiple barriers, in which the disposed SNF is protected by several engineered and natural barriers. These barriers are the copper canister, the bentonite buffer, the tunnel backfill material, and the surrounding bedrock [2]. The main purpose of the multiple barrier principle is to prevent the migration of harmful radionuclides into the surrounding groundwater system if radionuclides are released from the repository. Thus, when multiple barriers are used, the failure of one barrier does not compromise the containment of radionuclides. The disposal continues for a hundred years before the repository is sealed, and it will no longer be possible to recover the SNF for later use. After this, the deep geological repository is meant to protect the SNF for at least 100,000 years [2].

The long-term functionality of the repository has been assessed by a safety assessment consisting of conceptual and mathematical models. The safety assessment also requires an estimate of a situation in which radionuclides originating from nuclear waste migrate in the surrounding geosphere [3]. Through the geosphere, radionuclides can, in the worst case, end up in the food chain and ultimately lead to an uptake in humans. In particular, the highly radiotoxic actinides of SNF are considered to be very harmful to humans and the environment [4]. This highlights the fact that to perform reliable safety case, the behavior of SNF radionuclides and especially actinides in the geosphere must be thoroughly studied and understood.

The mobility of a radionuclide in the rock depends on three factors: retention, diffusion and the structure of the surrounding porous material [5-6]. These key processes have been extensively investigated in laboratories: **1)** Retention and distribution of radionuclides between the solid and liquid phases have been studied with batch sorption experiments to determine the distribution coefficient (K_d), **2)** core scale diffusion experiments have been used to determine the diffusion coefficients (D_a), and **3)** the porosity (ε) of the studied medium has been investigated, among other things, by water gravimetry. All these parameters are important and necessary for the safety case calculations.

There is one method in radiochemistry that can determine all these key parameters. The autoradiography method (AG) has emerged alongside more conventional radiochemical measurement technologies for analyzing the results of the laboratory tests (e.g. batch sorption and through-diffusion experiments). AG is based on measuring the radiation coming from within a sample. Some of the first radioactivity measurements were completed using AG; for example, Henri Becquerel determined the radioactivity of uranium through photography in 1896.

AG is a versatile method that allows, for example, the digital analysis of the tracer´s distribution on the imaged surface (**Fig. 1**). Combined with X-ray fluorescence generated by the rock surface elements (after being excited by a primary X-ray source), it is possible to determine the mineral-specific sorption and the diffusion depth of the tracer from the sample surfaces [7]. In addition, the total connected porosity of the studied sample can be determined with ^{14}C-polymethylmethacrylate autoradiography (PMMA) technique. The new developments in the AG techniques, like gaseous detector Beaquant^{TM} technique that couples a micro-patterned gaseous detector (MPGD) and a parallel ionization multiplier (PIM) device, allow count-to-count detection of radiation emitted from the sample surfaces [8].

Copyright on 7th Asia-Pacific Symposium on Radiochemistry 2025- P4-10* -

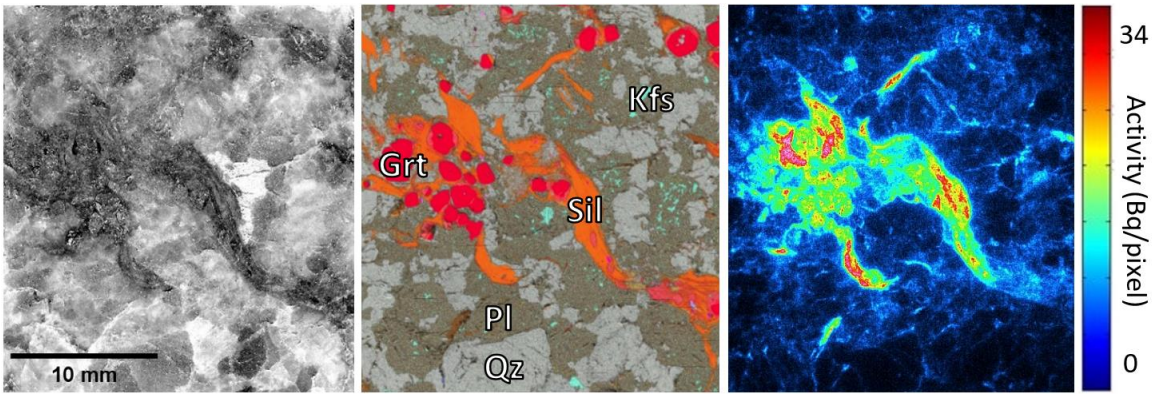


Fig. 1. Spatial distribution of ^{152}Eu on granitic rock´s surface. From left to right: Tabletop scanned image of the surface, µXRF mineral map (Grt = Garnet, Sil = Sillimanite, Kfs = K-feldspar, Pl = Plagioclase, Qz = Quartz) and Beaquant™ autoradiography (AG) image with Bq/pixel scale. Visual inspection of AG shows that sillimanite binds ^{152}Eu the strongest, whereas quartz is the weakest sorbing mineral on the rock surface.

The successful disposal of SNF requires scientific and technical knowledge of radionuclide´s behavior in the rock matrix. Radiochemical methods, for example the AG method pointed out in this work, are well suited to generating this knowledge. The presentation discusses the role of radiochemistry in determining parameters for the safety assessment of nuclear waste disposal. Different radiochemical methods used to produce parameters will be considered while reflecting on the Olkiluoto-related case study, which investigates the sorption behavior and transport of the actinide analogue europium in heterogeneous crystalline bedrock.

References

[1] IEA, *World Energy Outlook 2023.* OECD Publishing, Paris (2023)
[2] POSIVA, *Safety Case Plan for the Operating License Application.* Posiva Oy, Eurajoki, Finland (2017).
[3] NEA, *International Features, Events and Processes (IFEP) list for the deep geological disposal of radioactive waste.* Version 3.1, NEA/RWM/R(2024)2. OECD Publishing, Paris (2024)
[4] R. EWING, "Long-term storage of spent nuclear fuel", *Nature Materials*, **14**(3), pp. 252 – 257 (2015).
[5] I. NERETNIEKS, "Diffusion in the rock matrix: An important factor in radionuclide retardation?" *Journal of Geophysical Research: Solid Earth*, **85**(B8), pp. 4379 – 4397 (1980).
[6] POSIVA, *Retention Properties of Rock Matrix (REPRO) - Final report.* Posiva Oy, Eurajoki, Finland (2022).
[7] J.W.L. Ang, A. Bongrand, S. Duval, *et al.* "Detecting radioactive particles in complex environmental samples using real-time autoradiography", *Sci. Rep.*, **14** (2024)
[8] C. DELAYRE, J. SAMMALJÄRVI, S. BILLON, E. MUURI, P. SARDINI, and M. SIITARI-KAUPPI," Comparison of phosphor screen autoradiography and micro-pattern gas detector based autoradiography for the porosity of altered rocks", *Sci. Rep.*, **10** (2020).

Copyright on 7th Asia-Pacific Symposium on Radiochemistry 2025- P4-10* -

7th Asia-Pacific Symposium on Radiochemistry *September 14 ~ 19, 2025 • Kunibiki Messe • Shimane, Japan*

ANTIMONY MIGRATION IN COASTAL ENVIRONMENT: SYNERGISTIC ADSORPTION MECHANISM OF ORGANIC MATTER AND MINERAL PARTICLES UNDER UV-C IRRADIATION

Qiaoya Lin[1], Lewen Sun[1], Xiaobo Zhang[2] , Mingliang Kang[1,*]

[1] *Sino-French Institute of Nuclear Engineering and Technology (Sun Yat-sen University), Tangjiawan, Zhuhai, Guangdong Province, P. R. China, 519082*
[2] *Southern Marine Science and Engineering Guangdong Laboratory (Zhuhai), Tangjiawan, Zhuhai, Guangdong Province, P. R. China, 519082*
[*] *Corresponding author E-mail addresses: kangml3@mail.sysu.edu.cn*

This study investigates the photochemical transformation effects on natural organic matter (NOM) and its subsequent impacts on antimony (Sb) speciation in sediment-seawater systems under UV-C irradiation. Controlled 23-day laboratory experiments were performed in UV-C irradiation with parallel dark controls. The experimental design focused on two key drivers of Sb migration: (i) sediment resuspension induced by internal solitary waves and anthropogenic activities (marine fisheries and aquaculture), and (ii) UV-C exposure associated with mariculture wastewater treatment. Our results demonstrate that NOM in sediments existed as three phases: dissolved organic matter (DOM), particulate organic matter (POM) and colloidal organo-mineral associations, and UV-C irradiation accelerated significant photodegradation, liberating POM and colloidal organo-mineral associations and transforming them to DOM in seawater. Notably, Sb exhibited preferential adsorption onto coarse-grained mineral fractions (> 3 μm) rather than remaining in dissolved ionic forms (<3 kDa) after the photodegradation process. This study elucidates the critical role of particle-mediated processes in controlling Sb behavior under UV-C exposure, with particular emphasis on the dominance of large particle-size sediments (>3 μm) in controlling Sb migration. The findings establish a mechanism framework linking photochemically enhanced NOM-mineral interactions to Sb adsorption dynamics, which are particularly relevant under scenarios of UV-C radiation associated with wastewater treatment. Furthermore, this work underscores the necessity of incorporating particle-size-resolved adsorption models into marine contaminant fate assessments, while providing novel insights for predicting Sb migration patterns in coastal environments subjected to nuclear power plant (NPP) accidents.

Keywords: natural organic matter; UV-C irradiation; antimony; sediment-seawater systems.

1 INTRODUCTION

Radioactive Sb has garnered significant research attention as a priority pollutant due to its high toxicity and environmental persistence. The isotope with the highest half-life (^{125}Sb; $T_{1/2}$ = 2.76 years) demonstrated concerning migration capacity, with post-Chernobyl studies detecting its presence in molluscs and soil as early as one month and up to 6.5 years, respectively [1]. Therefore, the Sb migration capacity in the coastal system should be further discussed due to the coastal NPP. This mobility underscores Sb behavior in coastal systems, particularly given the Sb global migration.

Coastal systems face compounded environmental and anthropogenic drivers. Photochemical transformation critically regulates the solubility and mobility of heavy metals in aquatic systems through phase transformations of NOM. The solar radiation facilitated the NOM photochemical transformation and mainly occur in DOM and POM photodegradation [2]. Conventional laboratory simulations have focused on UV-A wavelengths (315-400 nm), given the stratospheric ozone attenuation of shorter UV-C radiation (100-280 nm) [3], It is worth noting that the UV-C disinfection has been a wildly applied technology in mariculture wastewater treatment [4], for our study, Guishan Island is one of the most important areas for mariculture industry in China, Therefore, the study of UV-C irradiation in marine environment should be taken seriously like solar radiation, however, the influence of UV-C irradiation between Sb and coastal systems after the NPP accident has rarely been discussed.

Concurrently, the internal solitary waves has been demonstrated to induce sediment resuspension in coastal regions of South China Sea [5], and the anthropogenic activities (e.g., marine fisheries /aquaculture [6]) are important contributors to sediment resuspension, thus, the mariculture wastewater existed as a mixture of sediments and seawater rather than only seawater, recent study has found the NOM could further assemble into colloidal organo–mineral associations and occur in water-dispersible colloids or building units of soil microaggregates [7], the interaction between photodegradable colloidal organo–mineral associations and Sb speciation remains poorly understanding, creating critical uncertainties in predicting Sb fate under UV-C irradiation.

2. CONCLUSIONS

The sediments (G1, G2, G3) and seawater were collected near Guishan Island, Guangdong Province, China. The samples were subjected to laboratory-based photochemical experiments. In Fig. 1, after 23 days of UV-C irradiation, the

Copyright on 7th Asia-Pacific Symposium on Radiochemistry 2025- P4-11* -

results demonstrated that the equilibrium concentration (C_e) of Sb in particles <3 μm was lower than that in dark controls across all sites. Significant C_e increases occurred in >3 μm particles from G1 and G2 under UV-C exposure. Furthermore, in Fig. 2, after 23 days of UV-C irradiation, the UV-Vis spectral analysis revealed distinct sedimentary organic matter (SOM) responses, G1 exhibited stable DOM content and increased ion concentrations of seawater. The results suggested that the UV-C liberated SOM from colloidal organo-mineral complexes and dissolved Sb ions were immobilized on >3 μm particles, the encapsulated ions of sediment microaggregates are released simultaneously. G2 and G3 showed minimal ionic concentration fluctuations, but G3 showed that the content of DOM in dark control samples was lower than G3 in UV-C irradiation, which indicated POM of sediments transformed to DOM in seawater in G3. Therefore, the demonstrated particle-size mediated Sb control mechanisms necessitate refined adsorption models for coastal nuclear contaminant management, especially UV-C-exposed mariculture wastewater conditions.

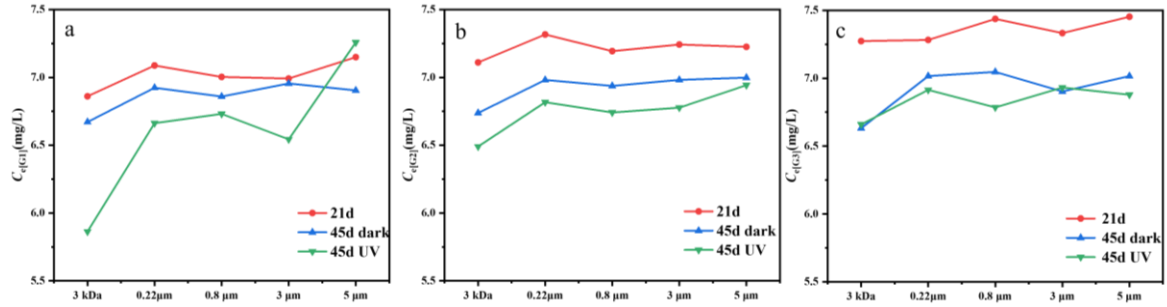


Fig. 1 Sb equilibrium concentration of different size particles in G1 (a), G2 (b) and G3 (c) samples

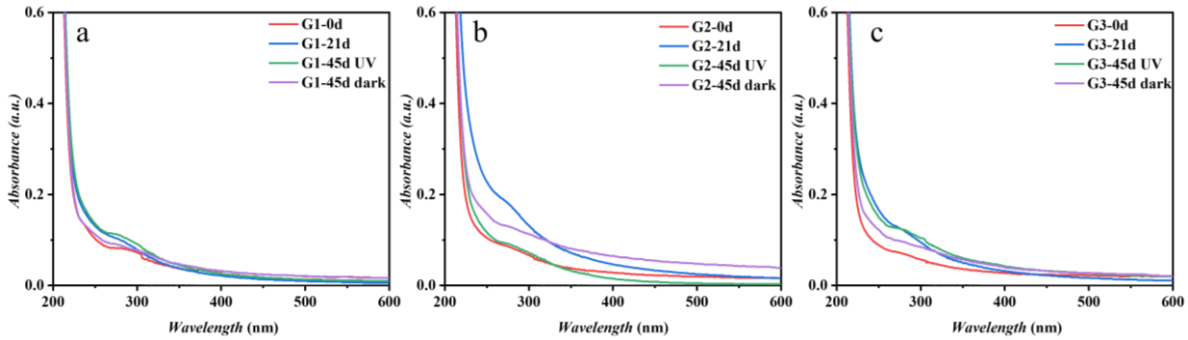


Fig. 2 UV–vis spectra of G1 (a), G2 (b) and G3 (c) samples

ACKNOWLEDGMENTS

This work was supported by the National Natural Science Foundation of China [Grant number 45000-41030072].

References

[1] GIL-DíAZ T, SCHäFER J, POUGNET F, et al. “Distribution and geochemical behaviour of antimony in the Gironde Estuary: A first qualitative approach to regional nuclear accident scenarios,” *Marine Chemistry*, **185,** 65-73 (2016).

[2] SHANK G C, EVANS A, YAMASHITA Y, et al. “Solar radiation–enhanced dissolution of particulate organic matter from coastal marine sediments,” *Limnology and Oceanography*, **562**, 577-88 (2011).

[3] WILLIAMSON C E, ZEPP R G, LUCAS R M, et al. “Solar ultraviolet radiation in a changing climate,” *Nature Climate Change*, **46**, 434-41 (2014).

[4] SHEN J, ZHENG X, LIU M, et al. “Targeted cultivation of diatoms in mariculture wastewater by nutrient regulation and UV-C irradiation,” *Frontiers in Microbiology*, **15,** 1371855 (2024).

[5] BOEGMAN L, STASTNA M. “Sediment resuspension and transport by internal solitary waves,” *Annual review of fluid mechanics*, **511**, 129-54 (2019).

[6] RAY N E, BONAGLIA S, CAVAN E L, et al. “Biogeochemical consequences of marine fisheries and aquaculture,” *Nature Reviews Earth & Environment*, **63**, 163-77 (2025).

[7] TANG N, SIEBERS N, LEINWEBER P, et al. “Implications of Free and Occluded Fine Colloids for Organic Matter Preservation in Arable Soils,” *Environmental Science & Technology*, **5619**, 14133-45 (2022).

Copyright on 7th Asia-Pacific Symposium on Radiochemistry 2025- P4-11* -

Contributed Talk | [S2]Radiopharmaceutical Sciences

Wed. Sep 17, 2025 4:45 PM - 6:05 PM JST | Wed. Sep 17, 2025 7:45 AM - 9:05 AM UTC Hall S(Int'l)

[S2] Radiopharmaceutical Sciences

4:45 PM - 5:05 PM JST | 7:45 AM - 8:05 AM UTC

[S2-11]

Preparation of Tc Medical Solution Dissolved with Minute Amount of Pure Water or Saline Solution

*Masato Asai[1], Hiroyuki Kimura[2], Shigeto Kabuki[3], Tetsuya Sato[1], Kazuaki Tsukada[1,4], Yuta Ito[1,5] (1. Japan Atomic Energy Agency (Japan), 2. Kyoto University (Japan), 3. Tokai University (Japan), 4. Tohoku University (Japan), 5. KEK (Japan))

5:05 PM - 5:25 PM JST | 8:05 AM - 8:25 AM UTC

[S2-12]

Separation of trace medical isotopes from natural thorium decay chain

*Lifeng Chen[1], Yuezhou Wei[1], Xuexiang He[1], Wannian Feng[1] (1. University of South China (China))

5:25 PM - 5:45 PM JST | 8:25 AM - 8:45 AM UTC

[S2-13]

PREPARATION OF SCANDIUM-47 LABELLED PSMA-617 FOR RADIOTHERANOSTIC APPLICATION

*Yoshifumi Shirakami[1], Masashi Murakami[1], Akina Mitsukai[1], Kazuki Kajiyama[1], Kazuko Kaneda Nakashima[1], Yuichiro Kadonaga[1], Atsuko Saito[1], Sadahiro Naka[1], Tadashi Watabe[1], Kenji Shirasaki[1], Takuya Yokokita[2], Hidetoshi Kikunaga[2], Atsushi Toyoshima[1] (1. The University of Osaka (Japan), 2. Tohoku University (Japan))

5:45 PM - 6:05 PM JST | 8:45 AM - 9:05 AM UTC

[S2-14]

Development of automatic synthesis system of [^{18}F]FBPA synthesis from[^{18}F]HF ([$^{18}F^-$]) and basic evaluation.

*Yasukazu Kanai[1], Yoshihide Hattori[2], Sadahiro Naka[3], Toshihiro Sakai[4], Koji Ono[1], Mitsunori Kirihata[2] (1. Osaka Medical and Pharmaceutical University (Japan), 2. Osaka Metroplitan University (Japan), 3. The University of Osaka (Japan), 4. Hanwa Intelligent Medical Center (Japan))

©APSORC25

Preparation of Tc Medical Solution Dissolved with Minute Amount of Pure Water or Saline Solution

Masato Asai[1], Hiroyuki Kimura[2], Shigeto Kabuki[3], Tetsuya Sato[1], Kazuaki Tsukada[1,4], Yuta Ito[1,5]

[1]*Advanced Science Research Center, Japan Atomic Energy Agency, Tokai, Ibaraki 319-1195, Japan*
[2]*Agency for Health, Safety and Environment, Kyoto University, Kyoto 606-8501, Japan*
[3]*School of Medicine, Tokai University, Isehara, Kanagawa 259-1193, Japan*
[4]*Research Center for Accelerator and Radioisotope Science (RARiS), Tohoku University, Sendai 980-8578, Japan*
[5]*Wako Nuclear Science Center, KEK, Wako, Saitama 351-0198, Japan*

We have developed a new technique to prepare minute amount of Tc medical solution from irradiated MoO_3 samples. The sublimation and thermochromatography technique was used to separate Tc from MoO_3 where the Tc were deposited at low-temperature part of the chromatography column. We have succeeded in recovering 80-90% of the deposited Tc with only 300 μL of pure water or saline solution without using any acid and alkali. This enables us to prepare the highly-concentrated Tc medical solution in the easiest and simplest way.

1. Introduction

Technetium-99m (^{99m}Tc) is one of the most widely used radioisotopes in medical diagnostic imaging tests. The ^{99m}Tc are produced through the β^- decay of ^{99}Mo which are produced in thermal neutron induced fission of highly-enriched ^{235}U in nuclear reactors. In Japan, most of ^{99m}Tc are imported from overseas, which sometimes causes supply shortage. To overcome this problem, other production routes are considered, e.g., the ^{98}Mo(n,γ)^{99}Mo reaction using domestic research reactors, the ^{98}Mo(n,2n)^{99}Mo reaction using accelerator neutrons (high-energy neutrons generated by accelerators), the ^{98}Mo(γ,n)^{99}Mo reaction using electron accelerators, the direct production of ^{99m}Tc through the ^{100}Mo(p,2n)^{99m}Tc reaction, etc. We have proposed another method to use ^{95}Tc ($T_{1/2}$ = 20 h) and ^{96}Tc (4.2 d) in combination with the Electron Tracking Compton Camera (ETCC) [1-3]. These isotopes are easily produced in the ^{95}Mo(p,n)^{95}Tc and ^{96}Mo(p,n)^{96}Tc reactions using small accelerators, while they emit only high-energy γ rays whose images cannot be measured by SPECT which is dedicated to detect low-energy γ rays such as 140 keV ones emitted from ^{99m}Tc. On the other hand, the ETCC is suited to take images of high-energy γ rays ranging from 160 to 2000 keV and has a wide field of view (3 str). We are developing this novel method by constructing a new ETCC system and testing it by taking functional images of small animals using ^{95}Tc, ^{96}Tc, and ^{95m}Tc-labeled radiopharmaceuticals.

One of difficulties we are facing in this study is a preparation of minute amount of Tc radiopharmaceutical solution from limited amount of Tc nuclear reaction products. We typically inject 200 μL of Tc radiopharmaceutical solution into a mouse. If the total radioactivity of Tc is limited, we have to prepare the Tc medical solution by dissolving most of the chemically purified Tc with only a few hundreds of μL of saline solution. In addition, the chemical separation, purification, and dissolution efficiencies should be as high as possible, the final Tc solution should not contain any acid, alkali, and toxic impurities, the Tc should be dissolved as a form of TcO_4^-, and all the processes should be completed within a few hours. It is challenging, but if it is possible, this technique is very useful not only for animal testing but also to prepare the highly concentrated Tc medical solution for human testing even though the total radioactivity of Tc available is limited. The aim of the present study is to establish a useful method to chemically separate Tc from an irradiated MoO_3 target and to prepare minute amount of highly concentrated Tc medical solution.

2. Methods

The Tc isotopes ^{95}Tc, ^{96}Tc, and ^{95m}Tc are produced in the (p,n) reactions with the 10-14 MeV proton beam and the MoO_3 target. To prepare the Tc medical solution, the Tc have to be chemically separated from the irradiated MoO_3 target, purified, and finally dissolved in saline solution. One of the methods is based on the aqueous chemistry where the MoO_3 is dissolved in NH_4OH solution and then precipitated to separate Tc from MoO_3 [4]. Then, the supernatant containing Tc is passed through an alumina column and an anion exchange column (or the TEVA@ resin column) to further purify the Tc, and the Tc retained in the column are stripped with 10 mL of 6M HNO_3 solution [4]. However, to prepare the Tc saline solution, we have to convert 6M HNO_3 solution into 0.9% NaCl solution. We carried out this conversion by evaporating the HNO_3 solution to dryness, dissolving the residue in HCl solution, evaporating it again to dryness, and finally dissolving it in pure water or saline solution. However, this process was very time-consuming, the dissolution efficiency for Tc in pure water or saline solution was not high enough, part of the Tc were lost during the evaporation of

Copyright on 7th Asia-Pacific Symposium on Radiochemistry 2025 - S2-11 -

the HCl solution, and about a half of the Tc dissolved in the final solution had a form different from TcO_4^-, all of which are inappropriate to be applied to this study. Another method is based on the sublimation and thermochromatography technique where the Tc contained in the irradiated MoO_3 are sublimated in a quartz tube heated in an electric furnace, and the Tc are separated from MoO_3 with the thermochromatography technique [5]. Then, the Tc deposited on the quartz surface are dissolved with 0.1 M NaOH solution, and the solution is passed through a cation exchange column to remove Na^+ and through an alumina column to retain Tc in it [5]. Finally, the Tc are stripped with 10 mL of saline solution. This method is appropriate to prepare the Tc medical solution, but the 10 mL of stripping solution is too much to prepare the 200 μL solution. We adopted this sublimation and thermochromatography technique but improved its deposition and dissolution processes to reduce the volume of solution, where the sublimated Tc were collected on small pieces of gold surface, and the gold pieces were washed with 300 μL of pure water or saline solution to remove the deposited Tc.

3. Experiments and Results

The ^{95m}Tc were produced in the ^{95}Mo(p,n)^{95m}Tc reaction by bombarding the $^{95}MoO_3$ target with the 14 MeV proton beam at the JAEA tandem accelerator facility. The irradiated $^{95}MoO_3$ target was heated at 840 °C in a quartz tube in which the moist O_2 gas was flowing at 50 mL/min. The sublimated ^{95m}Tc were deposited at the temperature range of 100-300 °C where we set small pieces of gold foil inside the quartz column to catch the ^{95m}Tc on their surface. After the thermochromatography separation, the gold foil was taken out of the column and put in 300 μL of pure water or saline solution.

In this thermochromatography experiment, we succeeded in depositing 98% of ^{95m}Tc on the small pieces of gold surface, and accomplished that 80% or 90% of the deposited ^{95m}Tc were dissolved with only 300 μL of pure water or saline solution, respectively. We could also synthesize the ^{95m}Tc-DTPA with this Tc saline solution, and succeeded in taking functional images of mouses with the ETCC.

4. Conclusions

We have developed a new technique to prepare minute amount of Tc medical solution from irradiated MoO_3 samples. The sublimation and thermochromatography technique was applied to separate and purify the Tc. We have succeeded in recovering 80-90% of the Tc with only 300 μL of pure water or saline solution without using any acid and alkali. This enables us to prepare the highly-concentrated Tc medical solution in the easiest and simplest way.

References

[1] Y. Hatsukawa et al., Pros One **13**, e0208909 (2018).
[2] T. Hayakawa et al., Heliyon **4**, e00497 (2018).
[3] S. Kabuki and Y. Hatsukawa, Nucl. Med. in Clinic **53**, 53 (2020) (in Japanese).
[4] M. Izumo et al., JAERI-M 90-156 (1990).
[5] Y. Nagai et al., J. Phys. Soc. Jpn. **86**, 053202 (2017).

Separation of trace medical isotopes from natural thorium decay chains

Lifeng Chen[1], Yuezhou Wei[2], Xuexiang He[3], Wannian Feng[4]

[1] School of Nuclear Science and Technology, University of South China, Hengyang, 421001, P.R. China, chenlf@usc.edu.cn
[2] School of Nuclear Science and Technology, University of South China, Hengyang, 421001, P.R. China, yzwei@usc.edu.cn
[3] School of Nuclear Science and Technology, University of South China, Hengyang, 421001, P.R. China, hexx@usc.edu.cn
[4] School of Nuclear Science and Technology, University of South China, Hengyang, 421001, P.R. China, fengwn@usc.edu.cn

Targeted alpha nuclide therapy (TAT) shows great promise in the treatment of malignant tumors. Based on the advantages of short penetration distance and high linear energy transfer density of alpha nuclides in human tissues, TAT can not only cause serious damage to malignant tumor tissues and cells, but also significantly reduce the damage to normal tissues and cells. $^{212}Pb/^{212}Bi$ are two of the few alpha nuclides that can be applied to TAT, which have good efficacy in the treatment of malignant tumors such as prostate cancer, breast cancer and pancreatic cancer. However, the resources are very scarce in the world. The separation of ^{212}Pb and ^{212}Bi from the natural thorium decay chain is an important method to solve the shortage of $^{212}Pb/^{212}Bi$ supply. In this work, a novel and advanced method was developed for the direct and selective separation of ^{212}Pb and ^{212}Bi from natural thorium based on anion exchange. It was demonstrated the first case in the world that reports the direct and selective separation of ^{212}Pb and ^{212}Bi from natural thorium using the anion exchange chromatography. Experimental results showed that a silica-based anion exchange resin functionalized with 1-methylpyridine had high adsorption selectivity toward lead and bismuth ions in halogen medium such as chloride, bromine or iodine ion medium, but did not adsorb thorium and other nuclide ions in the decay chain of natural thorium. In the halogen (X) medium, Pb^{2+} and Bi^{3+} have a strong affinity with the halogen ion X^-, and can form stable complex anions such as $[PbX_4]^{2-}$ and $[BiX_5]^{2-}$, so that they could be fixed by the anion exchange resin during the experiments. In contrast, the parent nuclides Th^{4+} and its decay daughters Ac^{3+} and Ra^{2+} almost could not bind with X^-, so that they existed in cationic form and were not adsorbed by the anion exchange resin. The novel silica-based anion exchange resin used in the separation was exclusively developed by the team of Professor Yuezhou Wei, which has the advantages of fast adsorption/desorption speed, high separation efficiency, small equipment scale, and low amount of secondary waste, etc. It is demonstrated especially suitable for the efficient and rapid extraction of ^{212}Pb and ^{212}Bi and other short-lived radionuclides, which can significantly reduce the decay loss of these nuclides. Fig. 1 shows the experimental results on the separation of lead and bismuth from the simulated decay chain of natural thorium, and Fig. 2 shows the gamma energy spectrum of the natural thorium, the separated ^{212}Pb sample and the separated ^{212}Bi sample. This method effectively overcomes the problems of high material cost, water solubility and waste of ^{212}Bi for commercial crown ether materials reported, which has a good application prospect in the future.

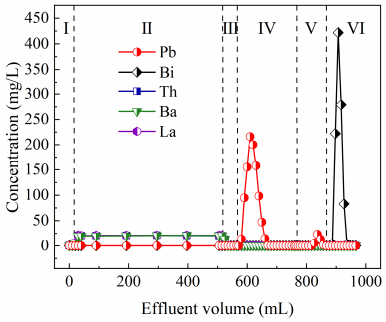


Fig.1 Separation of Pb and Bi from the simulated decay chain of natural thorium

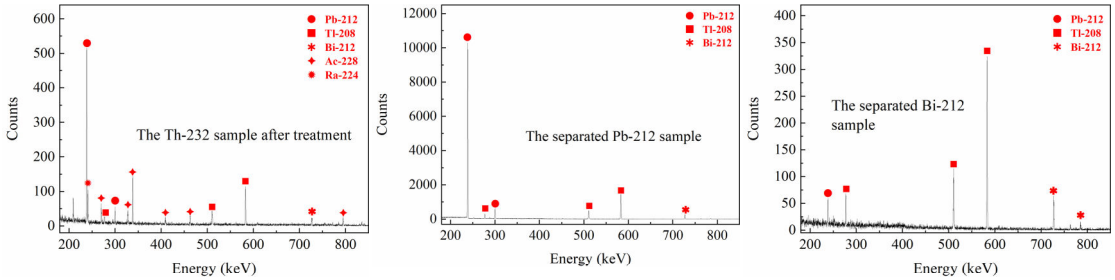


Fig.2 γ-energy spectrum of natural thorium(left), the separated ^{212}Pb sample (middle) and the separated ^{212}Bi sample

PREPARATION OF SCANDIUM-47 LABELLED PSMA-617 FOR RADIOTHERANOSTIC APPLICATION

Yoshifumi Shirakami[1], Masashi Murakami[1], Akina Mitsukai[2], Kazuki Kajiyama[2], Kazuko Kaneda-Nakashima[1], Yuichiro Kadonaga[1], Atsuko Saito[3], Sadahiro Naka[4], Tadashi Watabe[4], Kenji Shirasaki[1], Takuya Yokokita[5], Hidetoshi Kikunaga[5], Atsushi Toyoshima[1]

[1]*Institute for Radiation Sciences, The University of Osaka: 2-4 Yamadaoka, Suita, Osaka 565-0871, Japan, yoshifumi_shirakami@irs.osaka-u.ac.jp; murakami@irs.osaka-u.ac.jp; kkaneda@irs.osaka-u.ac.jp; kadonagay19@irs.osaka-u.ac.jp; shirasaki@rirc.osaka-u.ac.jp; toyo@irs.osaka-u.ac.jp*
[2]*Graduate School of Science, the University of Osaka: 1-1 Machikaneyama, Toyonaka, Osaka 560-0043, Japan mitsukai@irs.osaka-u.ac.jp; kajiyama@irs.osaka-u.ac.jp;*
[3]*Research Center for Ultra-High Voltage Electron Microscopy, The University of Osaka, 7-1 Mihogaoka, Ibaraki 567-0047, Osaka, Japan; saito@uhvem.osaka-u.ac.jp*
[4]*Department of Radiology, Graduate School of Medicine, The University of Osaka, 2-2 Yamadaoka, Suita, Osaka 565-0871, Japan; naka@tracer.med.osaka-u.ac.jp; watabe.tadashi.med@osaka-u.ac.jp*
[5]*Research Center for Accelerator and Radioisotope Science, Tohoku University, 1-2-1 Mikamine, Taihakuku, Sendai, Miyagi, 982-0826, Japan, takuya.yokokita.a5@tohoku.ac.jp; kikunaga@lns.tohoku.ac.jp*

Scandium-47 (^{47}Sc) is a promising radioactive metal nuclide for nuclear medicine therapy and diagnosis. We have established a method for preparing [^{47}Sc]PSMA-617 with a high radiochemical yield (>95%), and the product remained stable for 24 hours after labeling. The optimized reaction conditions involve heating at 80°C for 1 hour in a buffer solution of ammonium acetate adjusted to pH 5.0.

1. INTRODUCTION

Scandium-47 (^{47}Sc) is a promising radioactive metal nuclide for nuclear medicine therapy and diagnosis due to its half-life of 3.3 days and emission of beta rays (average energy: 162 keV) and gamma rays (159.4 keV). However, there are very few literature reports on the production and medical use of ^{47}Sc [1]. We produced ^{47}Sc using an electron beam accelerator and investigated the selection of chelating agents suitable for labeling ^{47}Sc and the optimal labeling conditions. Furthermore, we synthesized [^{47}Sc]PSMA-617 (Fig.1) using the ligand PSMA-617, which is widely used in the treatment of prostate cancer, and report the results of comparing its physicochemical properties with those of [^{177}Lu]PSMA-617 and [^{225}Ac]PSMA-617, which are already in clinical use.

2. EXPERIMENTAL

Using 5 g of titanium metal with natural isotopic composition as the target material, it was sealed in a quartz tube and irradiated for 3 hours with bremsstrahlung radiation up to 30 MeV generated by a High Intensity Electron LINAC. Scandium-47 was produced through the photon nuclear reaction ^{nat}Ti(γ, x)^{47}Sc. After irradiation, the titanium metal was dissolved in acid, separated and purified using ion exchange resin, and $^{47}ScCl_3$ was obtained as a 1 mmol/L hydrochloric acid solution (yield: >100 MBq, radionuclide purity: 87.5%). PSMA-617 was purchased from MedChemExpress (Monmouth Junction, USA) and dissolved in water (1 mg/mL). In a polypropylene vial, the PSMA-617 aqueous solution (1 mg/mL), 100 µL of water, 50 µL of 1 mol/L ammonium acetate buffer, and 30 µL of $^{47}ScCl_3$ solution (1-20 MBq) were added and heated at 80°C for 1 hour. A small amount of this reaction solution was taken and analyzed by cellulose acetate membrane electrophoresis (electrolyte: 0.06 mol/L barbital buffer, pH8.6, voltage 133 V, current 1 mA/cm) and HPLC (Column: Cosmosil MSII, 150×4.6 mm; Eluent: Water/MeCN; Flow rate: 1 mL/min; Detector: UV & RI).

3. RESULTS AND DISCUSSION

When the reaction mixture of PSMA-617 and ^{47}Sc was analyzed by the electrophoresis, [^{47}Sc]PSMA-617 was detected at +30 mm of migration distance with a high radiochemical yield (RCY: 96.7%) (Figure 2, left). Meanwhile [^{47}Sc]PSMA-617 was eluted at 16.9 minutes by HPLC analysis (Figure 2, right). To achieve not less than 90% RCY, 20 mmol of ligand was enough for labeling at pH 5.0, whereas 300 mmol of ligand was required at pH 6.5. The chemical characteristics and biological behavior of this agent was comparable to those of [^{177}Lu] and [^{225}Ac]PSMA-617 [2]. This radiolabeling technique can be expanded to peptides, antibodies, and small-molecule drugs.

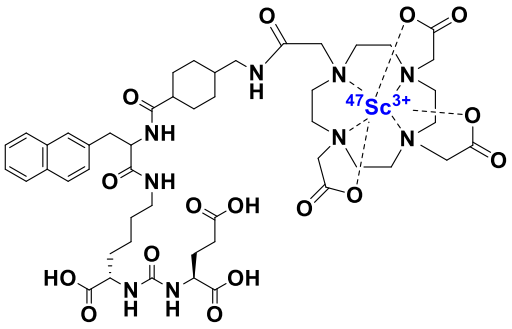
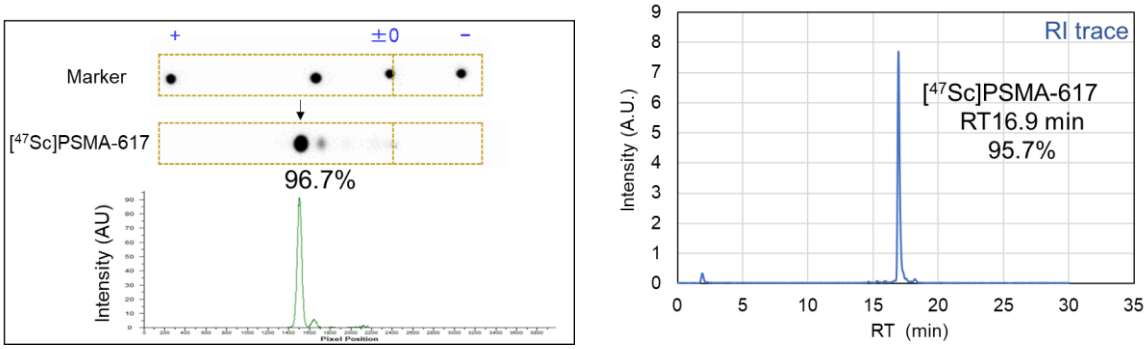


Fig. 1. Chemical structure of [^{47}Sc]PSMA-617.



Electrophoresis HPLC

Fig. 2. Analysis of [^{47}Sc]PSMA-617 by electrophoresis and HPLC.

4. CONCLUSIONS

We have established optimized conditions for the preparation of [^{47}Sc]PSMA-617, enabling its application in radiotheranostics for the treatment of patients with prostate cancer.

ACKNOWLEDGMENTS

This work was supported by the Research Program in Research Center for Election Photon Science, Tohoku University (Proposal No. 3071).

Ac-225 is provided by the U-233 cooperation project between JAEA and the Inter-University Cooperative Research Program of the Institute for Materials Research, Tohoku University. Proposal No. 202011-RDKGE-0001

References

[1] M. Yagi, K. Kondo, “Preparation of Carrier-free 47Sc by the ^{48}Ti (γ, p) Reaction,” Int. J. App.l Radiat. Isot, **28**, 463-468 (1977).

[2] K. Kaneda-Nakashima, Y. Shirakami, Y. Kadonaga, T. Watabe, K. Ooe, X. Yin, H. Haba, K. Shirasaki, H. Kikunaga, K. Tsukada, A. Toyoshima, J. Cardinale, F. L. Giesel, K. Fukase, “Comparison of Nuclear Medicine Therapeutics Targeting PSMA among Alpha-Emitting Nuclides,” Int. J. Mol. Sci. **25**, 933 (2024).

Copyright on 7th Asia-Pacific Symposium on Radiochemistry 2025 - S2-13 -

Development of automatic synthesis system of [^{18}F]FBPA synthesis from[^{18}F]HF ([^{18}F^{-}]) and basic evaluation.

Y. Kanai[1], Y. Hattori[2], S. Naka[3], T. Sakai[4], K. Ono[1], M. Kirihata[2]

[1]*Kansai BNCT Medical Center/BNCT Joint Clinical Institute, Osaka Medical and Pharmaceutical University,2-7, Daigakumachi, Takatsuki, Osaka, JAPAN, 569-8686, e-mail: yasukazu.kanai@ompu.ac.jp*
[2]*BNCT Research center, Osaka Metroplitan University, 1-1. Gakuenmaghi, Naka-ku, Sakai, Osaka, JAPAN, 599-8531*
[3]*The University of Osaka Hospital, 2-15, Yamadaoka, Suita, Osaka, Japan, 565-0871*
[4]*Hanwa Intelligent Medical Center, 3176, Fukai-Kitamachi, naka-ku, Sakai, Osaka, Japan, 599-8271*

Aim/Introduction: 2-[^{18}F]Fluoro-4-borono-phenylalanine (FBPA, Figure 1) is an important PET tracer for the determination of Boron Neutron Capture Therapy (BNCT) applicability. FBPA is a derivative of 4-borono-phenylalanine (BPA, Figure 1), a compound used in BNCT as a boron source (Figure 1). Nowadays [^{18}F]FBPA is mostly produced from [^{18}F]F_2 gas produced by ^{20}Ne (d, α)^{18}F nuclear reaction. This method is a simple and reliable . But this method produces only 1~2 GBq of [^{18}F]FBPA. A BNCT system that using cyclotron neutron generation system was recently established. Due to this change, BNCT has possibility to expanding all over the world. As BNCT expands, we need more [^{18}F]FBPA radioactivity in one synthesis. Since nuclear reaction yield is larger in ^{18}O(p, n)^{18}F nuclear reaction than ^{20}Ne (d, α)^{18}F. We previously reported a novel [^{18}F]FBPA synthesis from [^{18}F]HF which is produced by ^{18}O(p, n)^{18}F nuclear reaction (Scheme 2). In this study, we tried improve of this method for high radiochemical yield and attempt to adopt for automatic synthesizer.

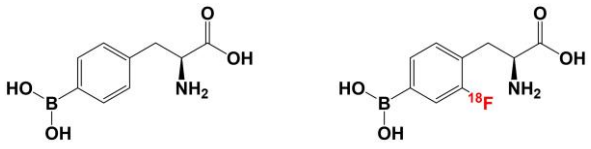
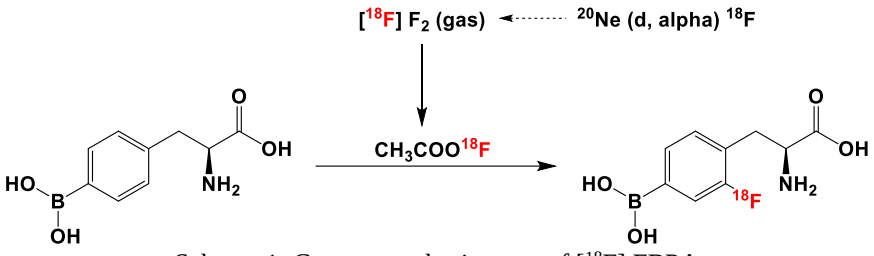
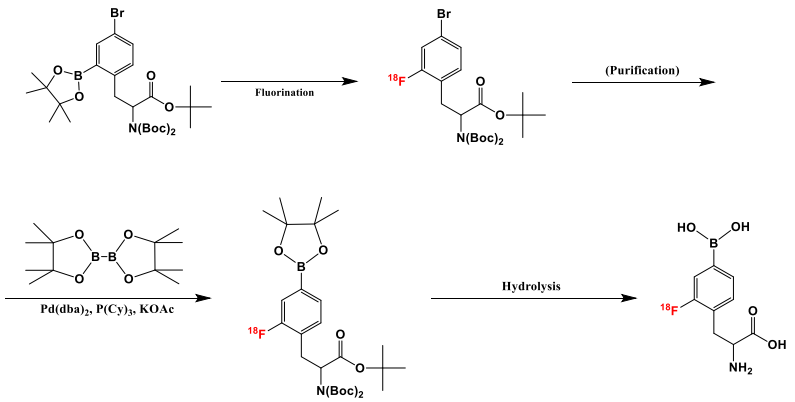


Figure 1: Chemical Structure of BPA and [^{18}F]FBPA



Scheme 1: Current synthesis route of [^{18}F] FBPA



Scheme 2: Novel synthesis route of [^{18}F] FBPA (From [^{18}F] HF)

Materials and Methods: Our synthesis method is consisted with 3 steps as show in scheme 2 and Figure 2. The first step is ^{18}F-fluorination reaction. In this step, pinacol borane precursor and copper reagent were used. In this step we investigated amount of precursor and copper reagent. Furthermore, we optimize reaction condition. The reaction solvent was a mixture (1/2 v/v) of n-butanol (n-BuOH) and dimethyl acetamide (DMA) mixture. After the fluorination reaction, the reaction mixture was passed through cartridge column to remove the copper reagent and purification. The second step is C-B bond formation (borylation) step, we used bis (pinacolato)diboron, bis(dibenzylidene acetone)palladium(0), tricyclohexyl phosphine and potassium acetate in dimethy formamide (DMF). In this step, we investigated the optimal combination of these reagents and reaction conditions. After the second step reaction, the reaction mixture was passed through a tC18 cartridge for purification. In the third step, acid was added to reaction mixture for deprotection. A crude mixture was purified by HPLC. Finally, [^{18}F]FBPA fraction was collected after HPLC purification of the crude mixture. Radiochemical purity (RCP) and molar activity (MA) were determined by HPLC. Finally, we tried to adopt this method for the automatic synthesizer (modified type of MPS-200 Aβ made by Sumitomo Heavy Industry, Figure 3).

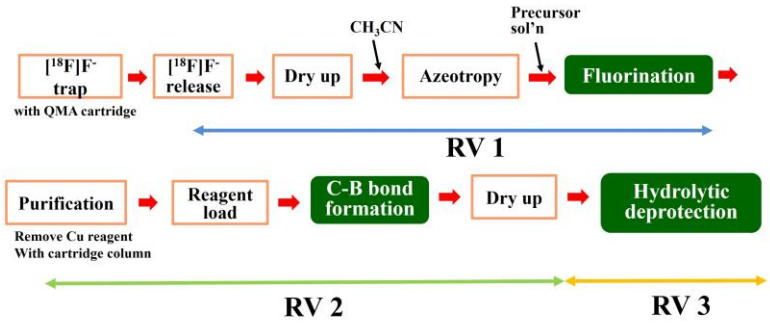


Figure 2: Synthesis step of [^{18}F]FBPA

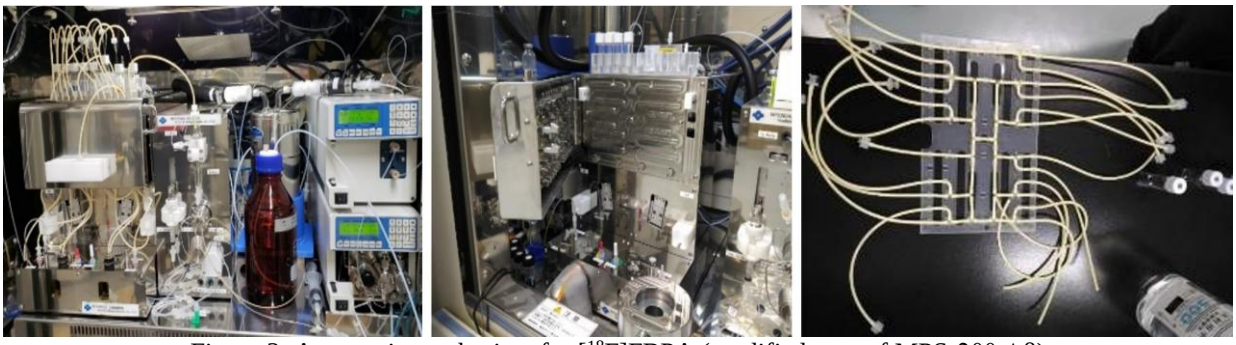


Figure 3: Automatic synthesizer for [^{18}F]FBPA (modified type of MPS-200 Aβ)

Result: Optimized reaction condition in each step are shown in Figure 4. The radiochemical yield of [^{18}F]FBPA from [18F]Fluoride ion was more than 10% (non-decay collected). The total synthesis time from the end of bombardment was about 110 min. The radiochemical purity of [^{18}F]FBPA was more than 90%, and mollar activity was about 1,000 GBq/μmol. About 9 GBq of [^{18}F]FBPA was produced by our method with 60 min and 50 μA irradiation using a 12 MeV cyclotron. Using the automatic synthesis module (improved CFN MPS-200), we established new and efficient [^{18}F]FBPA synthesis by the "F-minus method" with nucleophilic aromaticsubstitution reaction as the key reaction. The total synthesis time was 110 minutes and the radiochemical yield was approx. 10%. These results indicate that this synthetic method has high promising for medical use.



Figure 4: Optimized reaction condition in each step

Conclusion: We succeeded to improve the radiochemical yield of [^{18}F]FBPA from [^{18}F]HF and adopt to our method for automatic synthesizer. In this study, we find the suitable synthesis condition of [^{18}F] FBPA with high radiochemical yield and optical purity. We will develop and establish the synthesis method for clinical use of [^{18}F] FBPA in near future.

Poster Presentation | [R2]Radioanalytical Chemistry and Nuclear Forensics

Wed. Sep 17, 2025 6:30 PM - 8:00 PM JST | Wed. Sep 17, 2025 9:30 AM - 11:00 AM UTC Poster

[Poster] R2

[P-R2-01]

Non-Spectrometric Identification of Alpha Emitters Using TPX-3CAM

*Mariko Segawa[1], Ichiro Nishinaka[2], Makoto Maeda[1], Patwary M.D Kawchar[1,3], Yosuke Toh[1] (1. Japan Atomic Energy Agency (Japan), 2. National Institutes for Quantum Science and Technology (Japan), 3. Comilla University (Bangladesh))

[P-R2-02]

COMPARISON OF AGE DATING USING THERMAL IONIZATION MASS SPECTROMETER WITH ALPHA SPECTROMETER

*Erlina Noerpitasari[1], Yoshiki Kimura[2], Umino Yuji[2], Tomoki Yamaguchi[2] (1. National Research and Innovation Agency of Indonesia (Indonesia), 2. Japan Atomic Energy Agency (Japan))

[P-R2-03]

Efficiency Calibration Method of Ge Semiconductor Detectors for Determination of Low-Energy γ-Ray Emitting Nuclides and Validation of the Method

*Takumi Ono[1], Hidesuke Itadzu[1], Masayuki Mizui[1] (1. SEIKO EG&G (Japan))

[P-R2-04*]

ENERGY CONVERSION OF γ-RAY USING SOLID MATERIALS

*Hikaru Yamabe[1], Jun Kumagai[1], Yoshiyuki Hirano[1], Muneaki Yamamoto[1], Tetsuo Tanabe[1], Tomoko Yoshida[1] (1. Nagoya University (Japan))

[P-R2-05]

DEVELOPMENT OF LOW-VOLUME ELECTROLYTIC ENRICHMENT BY SPE MEMBRANE FOR TRITIUM IN WATER SAMPLES

*Yoshihito Ohtsuka[1] (1. Institute for Environmental Scieneces (Japan))

[P-R2-06]

TLC plates containing fluorescent indicators are useful for analysis of alpha-particles and beta$^+$-rays

*Kento Kannaka[1], Hiroyuki Suzuki[1], Kazuhiro Takahashi[2], Tomoya Uehara[1] (1. Chiba University (Japan), 2. Fukushima Medical University (Japan))

[P-R2-07*]

Concentration of Radioactive Iodine Using Forward Osmosis Membrane

*ZHAOYANG SI[1], Tamao Tanji[1], Yoshitaka Takagai[1], Takahiro Osaki[2], Yuji Katayama[2] (1. Fukushima University (Japan), 2. Asahi Kasei (Japan))

©APSORC25

7th Asia-Pacific Symposium on Radiochemistry *September 14 ~ 19, 2025 • Kunibiki Messe • Shimane, Japan*

Non-Spectrometric Identification of Alpha Emitters Using TPX-3CAM

Mariko Segawa[1], Ichiro Nishinaka[2], Makoto Maeda[1], Patwary. K. M. Kawchar[1], Yosuke Toh[1]
[1] *Japan Atomic Energy Agency (JAEA), Shirane 2-4, Tokai, Ibaraki, 319-1195, Japan*
[2]*National Institutes for Quantum Science and Technology (QST), Takasaki, Gunma 370-1292, Japan*

A pixel-level time-resolved detection system based on TPX-3CAM has been developed for identifying alpha-emitting radionuclides. By utilizing time-of-arrival (ToA) and time-over-threshold (ToT) information, we demonstrate a non-spectrometric particle classification approach, which distinguishes alpha particles from background radiation using spatial and temporal statistics.

1. Introduction

Alpha-emitting radionuclides such as ^{211}At are increasingly important in targeted alpha therapy. However, detecting and identifying these particles based on conventional imaging coupled with energy spectrometry remains challenging due to their short range in matter, high ionization density, and the presence of β-rays and X-rays that are co-emitted from the same radionuclide. These radiation backgrounds hinder precise classification, especially in low-activity conditions. Conventional camera type imaging coupled with spectrometry-based techniques require accurate energy calibration and is often hard to distinguish radiation types in complex or low-dose environments.

To address these limitations, we introduce a "non-spectrometric particle identification" approach. Instead of utilizing the energy spectra, this method classifies particles by analyzing spatial clustering, temporal structure features recorded at the pixel level. These differences in ionization track structure and timing have potential to allow for reliable separation of particle species without requiring energy spectrum measurements. This study aims to demonstrate that the method can reliably identify alpha emissions from short-lived radionuclides using a real-time sensor equipped in a TPX-3CAM camera [1].

2. Methods and Experiments

The TPX-3CAM camera, equipped with a sensor of 256×256 pixels with a 55 μm pitch, was mounted above a planar ^{211}At source with an air gap of approximately 2 mm, optimized by PHITS simulation [2]. The experimental setup and the detector-source configuration are shown in **Fig. 1**. The spatial coordinates, ToA (time-of-arrival), and ToT (time-over-threshold, proxy pulse-height) were recorded for each event at each pixel. Measurements were performed at the JAEA-Tokai tandem accelerator using a drop deposited ^{211}At sample of 192 Bq/5 μL [3]. Data were processed using custom GUI implementing a method of Density-Based Spatial Clustering of Applications with Noise (DBSCAN) clustering [4] and ΔToA (differential time-of-arrival) based coincidence filtering. Radiation classification was performed by analyzing both cluster geometry and statistical time correlations.

3. Results and Discussion

Alpha particles formed compact clusters (< 10 pixels) with high ToT values, reflecting their high linear energy transfer (LET). The spatial distribution of these clusters, visualized in X–Y coordinates with ToT, is shown in **Fig. 2**. Alpha events appeared as dense and localized signals, whereas background events (e.g., X-rays) were sparsely distributed. The DBSCAN clustering was applied using spatial and ΔToA parameters to classify these events. The resulting classification color-map in **Fig. 2** displays eleven clusters (Cluster 0-10) clearly separated from background events, which are labeled as "Noise". To validate the result, a comparative measurement with β- and X-ray sources was performed. The ToT spectrum for these sources agreed well with those of the background events in the ^{211}At data, as shown in Fig.2. This agreement shows that the system's capability to discriminate radiation types based on their spatiotemporal features.

4. Conclusion

We demonstrated that the non-spectrometric particle identification method using TPX-3CAM enables discrimination of alpha radiation in complex fields. By focusing on the spatial and timing data instead of absolute energy spectra, this method provides a calibration-light alternative to conventional camera-system combined with spectrometric techniques. Potential applications include real-time monitoring of alpha-emitting radionuclides and automated isotope characterization in radiopharmaceutical development.

ACKNOWLEDGMENTS

This work was supported in part by the Japan Society for the Promotion of Science (JSPS) KAKENHI Grant Number 25K15769 and 23K07219.

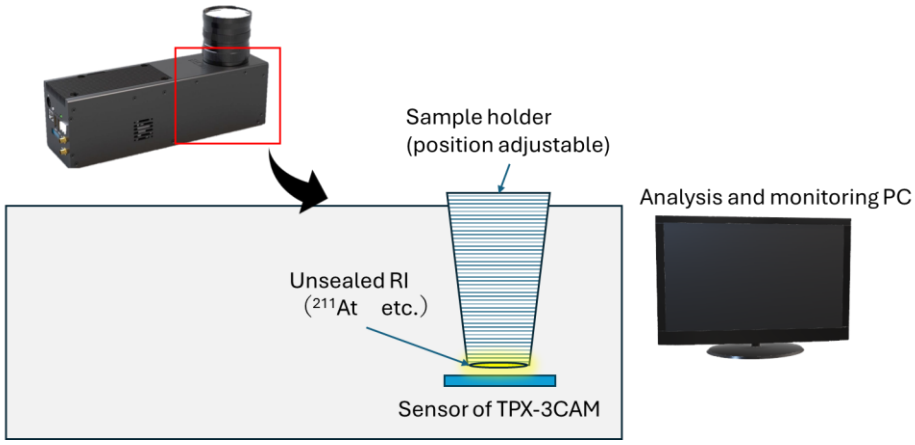


Fig. 1. Schematic of TPX-3CAM imaging setup with geometry optimized via PHITS simulation.

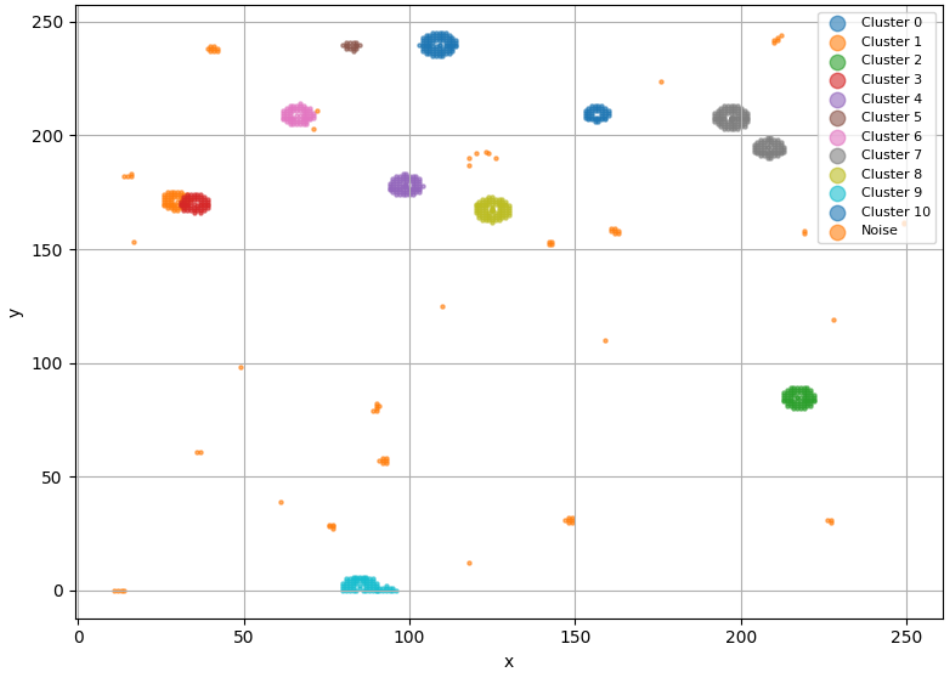


Fig. 2. Spatial distribution and classification of radiation events measured by TPX-3CAM
Alpha-particle events form compact elliptical clusters due to their high LET, while background events appear as sparsely distributed signals. The DBSCAN classification results ("Cluster 0–10" for alpha, "Noise" for background) are shown in color map in the X–Y coordinate space.

References

[1] T. Poikela, *et. al.*, "Timepix3 a 65k channel hybrid pixel readout chip with simultaneous ToA/ToT and sparse readout," Journal of instrumentation 9(05), C05013 (2014).
[2] T. Sato, *et. al.*, "Recent improvements of the Particle and Heavy Ion Transport code System - PHITS version 3.33," Journal of Nuclear Science and Technology, vol. 61, pp. 127–135, 2024.
[3] I. Nishinaka, *et. al.*, "Astatine-211 tracer studies by thin-layer chromatography and solvent extraction using cyclotron-produced At-211," Radiochim. Acta, 108(3), 157–164 (2020).
[4] M. Ester, *et. al.*, "A density-based algorithm for discovering clusters in large spatial databases with noise," Proc. KDD'96, pp. 226–231, 1996.

Copyright on 7th Asia-Pacific Symposium on Radiochemistry 2025 P-R2-01 -

7th Asia-Pacific Symposium on Radiochemistry *September 14 ~ 19, 2025 • Kunibiki Messe • Shimane, Japan*

COMPARISON OF AGE DATING USING THERMAL IONIZATION MASS SPECTROMETER WITH ALPHA SPECTROMETER

Erlina Noerpitasari[1], Yoshiki Kimura[2], Umino Yuji[2], Tomoki Yamaguchi[2]

[1]*Indonesian National Research and Innovation Agency, B.J. Habibie Science Techno Center, Building No. 720, South Tangerang, 15138, Indonesia, erli002@brin.go.id*
[2] *Integrated Support Center for Nuclear Non-proliferation and Nuclear Security, Japan Atomic Energy Agency, 2-4 Shirakata, Tokai-mura, Ibaraki 3191195, Japan*

Nuclear forensics plays a crucial role in determining the origin of nuclear or radioactive materials found outside regulatory control, utilizing the unique signatures inherent to such materials. These signatures are classified as comparative and predictive, with predictive signatures being particularly valuable for estimating the age of the material. Determining the age of nuclear materials provides insight into the production facilities and processes involved. $^{230}Th/^{234}U$ radiochronometers are widely used for this purpose. Using mass spectrometry techniques, such as Thermal Ionization Mass Spectrometry (TIMS), providing high sensitivity and accuracy. However, mass spectrometry techniques are expensive and not accessible in all countries, prompting interest in cheaper alternative methods such as alpha spectrometry. This research works on a comparison of age dating using TIMS and alpha spectrometry.

1 INTRODUCTION

Nuclear forensics is the science of uncovering the origin of nuclear or radioactive materials found outside regulatory control. The special characteristics of the material are called signatures, there are two types of signatures, namely comparative and predictive signatures. One of the predictive signatures is the determination of the age of the material. This value is very useful for knowing the production facilities of the material. The radiochronometer that is widely used is $^{230}Th/^{234}U$. Several researchers from several countries use mass spectrometry techniques to determine the age of nuclear materials with $^{230}Th/^{234}U$ radiochronometers using Inductively Coupled Plasma-Mass Spectrometer/ICP-MS [1-3], Thermal Ionization Mass Spectrometer/TIMS [4-5], Laser Ablation-ICP-MS/LA-ICP-MS [6]. Although they have high sensitivity and good accuracy, mass spectrometry methods are methods that require high costs. Few researchers, although they have used mass spectrometry methods, the bias in the age calculation results obtained is quite significant or not close to the known age value [6].

In addition to sophisticated or advanced methods, low-cost methods that still produce accurate data are also quite interesting for researchers. Some researchers conducted age determination of enriched uranium material using non-destructive techniques using a gamma spectrometer [7-8]. Ravi *et al.* (2022) [9] and Wallenius *et al.* [10] had conducted age determination of nuclear material for nuclear forensics using the Isotope Dilution-Alpha Spectrometry (ID-AS) technique with good results, the age value obtained is close to the known age value. The ID-AS technique is still a technique with a fairly high cost because it requires a tracer/isotope standard to correct for imperfections in the chemical separation carried out.

2. METHODOLOGY

Before measurement, separation of thorium and uranium is required. Thorium was separated using CAO8-P gel, separation is carried out twice to obtain purer thorium. Uranium was separated using Uteva resin. After each fraction were collected, the solution was baked into the filament for further TIMS measurement, and evaporated to the surface of stainless-steel plate for further alpha spectrometer measurement. The following equation was used to calculate the age of the material,

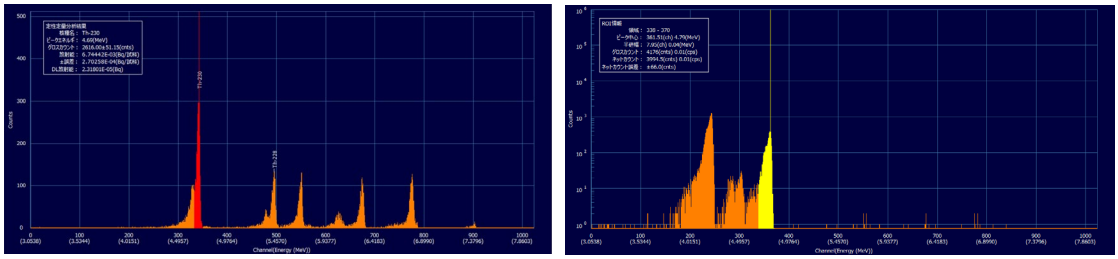
$$t = \frac{1}{\lambda_{234U} - \lambda_{230Th}} * ln\left[1 + \frac{R(\lambda_{234U} - \lambda_{230Th})}{\lambda_{234U}}\right] \quad (1)$$

where λ are the decay constants, and R is $^{230}Th/^{234}U$ atom ratio at time t, the ratio was provided from the TIMS and alpha spectrometer measurement.

2. RESULT AND DISCUSSION

Figure 1 presents the spectra of thorium and uranium following the separation process. The results clearly indicate that thorium was successfully separated from uranium, as evidenced by the distinct and non-overlapping peaks corresponding to each element. This demonstrates the effectiveness of the separation technique employed. Figure 2 compares the age determination results obtained using TIMS and alpha spectrometry. Both methods yielded age

estimates that significantly deviate from the known age of the sample. Further investigation is necessary to identify the source of the inconsistencies and to improve the accuracy of age determination in future analyses.



(a) (b)

Fig. 1. Alpha spectra of thorium (a) and uranium (b) fraction

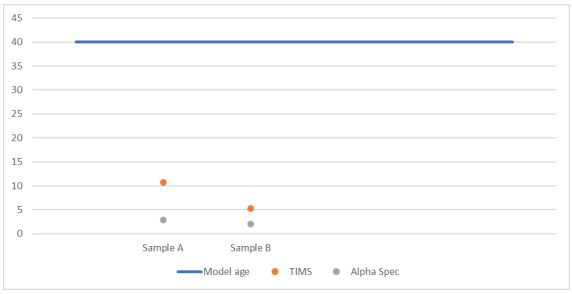


Fig. 2. Age comparison using TIMS and Alpha Spectrometer.

3. CONCLUSIONS

Thorium separation was successful but the result for age dating by alpha spectrometer and TIMS were differs significantly from the model age (about 40 years). It needs further improvement to get better result.

ACKNOWLEDGEMENTS

The authors would like to thank Integrated Support Center for Nuclear Nonproliferation and Nuclear Security (ISCN)-Japan Atomic Energy Agency (JAEA) for their kind support in this research on the visiting scholar in the field of nuclear forensics program.

References

[1] Z. VARGA and G. SURANYI, “Production date determination of uranium-oxide materials by inductively coupled plasma mass spectrometry”, *Analytica Chimica Acta*, **599**, 16-23 (2007).

[2] K. TREINEN *et al.*, “Evaluating uranium radiochronometry by single-collector mass spectrometry for nuclear forensics: a multi-instrument investigation”, *Journal of Radioanalytical and Nuclear Chemistry*, **322**, 1627-1640 (2019).

[3] A. SERBAN *et al.*, “Determination of age, isotopic ratios, and elemental impurities in nuclear materials by single quadrupole ICP-MS”, *Journal of Radioanalytical and Nuclear Chemistry*, **333**, 165-173 (2024).

[4] A. OKUBO, N. SHINOHARA, and M. MAGARA, “Uranium age-dating using in-situ isotope ratios by thermal ionization mass spectrometry for nuclear forensics”, *Journal of Radioanalytical and Nuclear Chemistry*, **314**, 231-234 (2017).

[5] S. P. LAMONT and G. HALL, “Uranium age determination by measuring the $^{230}Th/^{234}U$ ratio”, *Journal of Radioanalytical and Nuclear Chemistry*, **264**, 423-427 (2005).

[6] T. J. KELL and S. V. JOVANOVIC, “^{230}Th heterogeneity in a CMX-7 depleted uranium metal sample”, *Journal of Radioanalytical and Nuclear Chemistry*, **333**, 3565-3570 (2024).

[7] C. T. NGUYEN and J. ZSIGRAI, “Gamma-spectrometric uranium age-dating using intrinsic efficiency calibration”, *Nuclear Instruments and Methods in Physics Research B*, **243**, 187-192 (2006).

[8] A.I. APOSTOL *et al.*, “Isotopic composition analysis and age dating of uranium samples by high resolution gamma ray spectrometry”, *Nuclear Instruments and Methods in Physics Research B*, **383**, 103-108 (2016).

[9] P. RAVI K. *et al.*, “Application of radio-analytical technique for determination of “Age” of nuclear materials for nuclear forensics”, *Journal of Radiation Research and Applied Sciences*, **15**, 213-218 (2022).

[10] M. WALLENIUS *et al.*, “Determination of the age of highly enriched uranium”, *Analytical and Bioanalytical Chemistry*, **374**, 379-384 (2002).

Copyright on 7th Asia-Pacific Symposium on Radiochemistry 2025

Efficiency Calibration Method of High Purity Ge Detectors for Determination of Low-Energy γ-Ray Emitting Nuclides and Validation of the Method

Takumi Ono[1], Hidesuke Itadzu[2], Masayuki Mizui[3]

[1]SEIKO EG&G Co.,Ltd., 563, Takatsukashinden, Matsudo-shi, Chiba, Japan, 270-2222, takumi.ono@sii.co.jp
[2]SEIKO EG&G Co.,Ltd., 563, Takatsukashinden, Matsudo-shi, Chiba, Japan, 270-2222, hidesuke.itadzu@sii.co.jp
[3]SEIKO EG&G Co.,Ltd., 563, Takatsukashinden, Matsudo-shi, Chiba, Japan, 270-2222, masayuki.mizui@sii.co.jp

We have obtained an efficiency curve for high purity Ge detectors for the analysis of low energy γ-ray emitting nuclides such as Pb-210 and Am-241. By applying two corrections to the efficiencies obtained from standard source measurements, we obtained efficiency curves covering the range from 39.6 keV to 1836 keV. The validity of this method was confirmed through the quantitative analysis of Pb-210 and Am-241 standard sources.

1 INTRODCTION

High purity Ge (HPGe) detectors are widely used for the quantitative analysis of nuclides that emit gamma rays. Calibration of HPGe detectors typically involves multinuclide standard sources that emit gamma rays of various energies. However, calibration sources generally do not include nuclides emitting gamma rays below 88 keV. To quantify nuclides such as Pb-210 (46.5 keV) and Am-241 (59.5 keV), which emit gamma rays below 88 keV, it is necessary to obtain efficiency curves that covered low energies as low as 40 keV. Therefore, in this study, efficiency curves covering the energy range from 39.6 keV to 1836 keV were obtained by combining the efficiencies obtained from measurements of multiple multinuclide sources and I-129 (39.6 keV) sources. The validity of the obtained efficiency curves was confirmed by comparing the quantified values obtained from measuring the Pb-210 sources and Am-241 sources with the calibrated values of radioactivity.

2 METHODS

All the measurement samples were nuclides filled in cylindrical 'U-8' containers (ϕ =55mm) with various volumes. We measured two types of sources for calibration using a Ge detector (ORTEC GMX-30200-S). One type is 'U-8 Mix' source that contains multinuclide emitting gamma rays with energies range from 88keV to 1836 keV, and another type is I-129 source that emits gamma rays with energy of 39.6 keV. The efficiency curves were obtained based on the measurement results of these sources. However, since the actual filling height and density of U-8 Mix sources and I-129 sources differ, the efficiencies cannot be simply combined. This is because efficiency is affected by density and filling height. Therefore, two corrections were applied to combine the efficiencies: self-absorption correction considering the density and height adjustment correction. After applying these corrections, the efficiencies were combined to create an efficiency curve covering the energy range from 39.6 keV to 1836 keV.

2.1 Source for Efficiency Calibration

As standard sources, we used the U-8 Mix sources containing nine nuclides emitting gamma rays from 88 keV to 1836 keV and I-129 sources. Both sources were used at five different heights: 5, 10, 20, 30, and 50 mm. The density and actual filling height of sources are shown in Table 1.

Table.1 Density and actual filling height of the sources.

Filling Height of Sources	Density [g/cm^3]		'Actual' Filling Height [mm]	
	U-8 Mix	I-129	U-8 Mix	I-129
5mm	1.03	1.03	5.0	5.0
10mm	1.00	0.99	10.3	10.4
20mm	1.00	0.99	20.6	20.8
30mm	1.00	1.01	30.9	30.8
50mm	1.03	1.03	50.0	50.0

2.2 Combine the Efficiency Curves

Self-absorption correction was calculated using Eq. (1) to obtain the efficiency (ε_{void}) without self-absorption from the measured efficiency ($\varepsilon_{measured}$). In Eq. (1), Eff(ξ) is the efficiency at distance ξ from the detector, and μ is the linear attenuation coefficient (mm^{-1}) of the material filled in the sample.

$$\varepsilon_{measured} = \frac{\int_0^h Eff(\xi) e^{-\mu\xi} d\xi}{\int_0^h Eff(\xi) d\xi} \varepsilon_{void} \quad (1)$$

Height adjustment correction was performed as follows. The relationship between the height (h) of the I-129 source and the efficiency ($\varepsilon_{void}^{I\text{-}129}$ (h)) was approximated by quadratic formula, and the efficiency $\varepsilon_{void}^{I\text{-}129}$ (h') at the height (h') of the U-8 mixed source was calculated. This allowed the combination of the efficiencies ε_{void}^{Mix}(h') and $\varepsilon_{void}^{I\text{-}129}$(h') of the U-8 mixed source. By combining the efficiency curves of various heights, the efficiency of samples with arbitrary energy, height, and density can be calculated. The obtained efficiency curve is shown in Fig. 1.

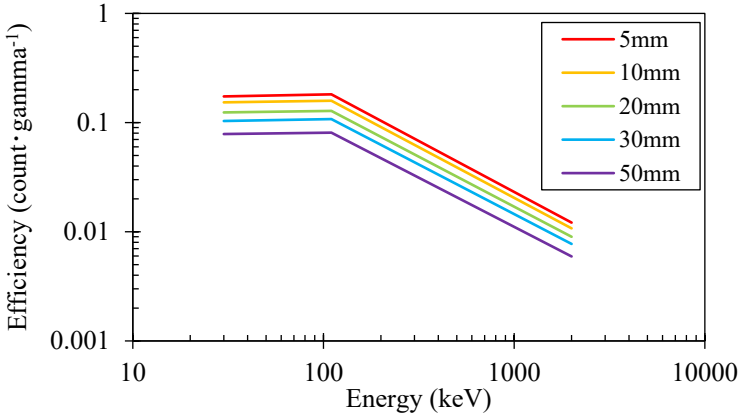


Fig.1 Efficiency curves covering energies from 39.6 keV to 1836 keV.

2.3 Quantitative Analysis of Radioactivity

Using the obtained efficiency curve, we measured and quantified standard sources. The sources used were Am-241 sources at specified filling heights of 5, 10, 20, 30, and 50 mm, and Pb-210 sources at specified filling heights of 5 and 50 mm in U-8 containers.

3 RESULTS AND DISCUSSION

The analysis results of the Am-241 and Pb-210 sources are shown in Table 2. The expanded uncertainties of the quantified and calibrated values are given for *k*=2. There is good agreement between quantified and calibrated radioactivity. These quantitative results indicate that the method is valid.

Table.2 Results of measurement and analysis of standard sources. Expanded uncertainty is the value at *k*=2.

Nuclide	Filling Height[mm]	Quantified Radioactivity [Bq]	Calibrated Radioactivity [Bq]
Am-241	5	60.9 ± 3.6	59.8 ± 1.9
	10	120 ± 7	119 ± 4
	20	240 ± 14	238 ± 7
	30	352 ± 21	357 ± 11
	50	593 ± 35	595 ± 18
Pb-210	5	240 ± 14	232 ± 26
	50	2360 ± 140	2310 ± 260

4 CONCLUSION

By measuring the standard sources containing gamma-ray emitting nuclides from 88 keV to 1836 keV along with the I-129 source and applying various corrections, we were able to obtain an efficiency curve covering low energies around 40 keV. Furthermore, the analysis of Am-241 and Pb-210 standard sources showed good agreement between quantified and calibrated radioactivity, confirming the validity of this method.

Copyright on 7th Asia-Pacific Symposium on Radiochemistry 2025

7th Asia-Pacific Symposium on Radiochemistry *September 14 ~ 19, 2025 • Kunibiki Messe • Shimane, Japan*

ENERGY CONVERSION OF γ -RAY USING SOLID MATERIALS

Hikaru Yamabe[1], Jun Kumagai [2], Yoshiyuki Hirano [3], Muneaki Yamamoto [4], Tetsuo Tanabe [5], Tomoko Yoshida [6]

[1] *Graduate School of Engineering, Nagoya University, Nagoya 464-8603, Japan, yamabe.hikaru.y7@s.mail.nagoya-u.ac.jp*
[2] *Institute of Materials and Systems for Sustainability, Nagoya University, Nagoya, 464-8603, Japan, kumagai@imass.nagoya-u.ac.jp*
[3] *Graduate School of Medicine, Nagoya University, Nagoya 464-8603, Japan, hirano.yoshiyuki.n6@f.mail.nagoya-u.ac.jp*
[4] *Institute of Materials and Systems for Sustainability, Nagoya University, Nagoya, 464-8603, Japan, m-yamamoto@energy.nagoya-u.ac.jp*
[5] *Graduate School of Engineering, Nagoya University, Nagoya 464-8603, Japan, tanabet311211@jcom.zaq.ne.jp*
[6] *Graduate School of Engineering, Nagoya University, Nagoya 464-8603, Japan, yoshida.tomoko.h9@f.mail.nagoya-u.ac.jp*

In this study, we aimed to convert the energy of γ-rays into electrical energy using solid materials as the medium. To achieve this, we fabricated a parallel-plate type radiation battery using two metal plates of different types or thicknesses, and measured the output generated by actual γ-irradiation. We conducted experiments by varying the type and thickness of the electrodes as well as the insulating material between the plates, with the goal of improving output. Furthermore, we predicted the output current using PHITS and Geant4 simulations and compared the results with experimental values to further enhance the output.

1 BACKGROUND AND OBJECTIVE

Recently, the use of nuclear power is expected to contribute to saving fossil fuels and mitigating CO_2 emission, while the disposal of large amounts of radioactive waste is a concern with its increasing use. In this study, aiming at the effective conversion of energy emitted from the radioactive wastes into electric energy, we have tried to develop a parallel-plate type radiation battery which will work as a power source giving a constant current as shown in Fig.1[1]. It is based on electron emission from a metal plate under γ-ray irradiation, i.e., when two parallel metal plates made of different metals or thicknesses are irradiated with γ-rays, electrons are emitted from the plates with different fluxes from each plate. This induces an electric potential difference between them. Then, a constant current will be obtained in a resistance load connecting both plates.

Since an electron flux emitted from a metal plate under γ-ray irradiation varies depending on the metal and its thickness, there should be an optimum combination of metals and their thicknesses to give the maximum electric potential difference. In addition, the selection of an insulator set between the plates should influence the output power because it absorbs or emits electrons. This energy conversion method relies solely on radiation and metal, making it a power source that does not generate additional waste.

However, in practice, the electrons emitted from the metal plates interact with the air or insulator between the plates, leading to additional electron generation or absorption. As a result, the resulting potential difference does not simply correspond to the difference in the number of electrons emitted from the two metal plates.

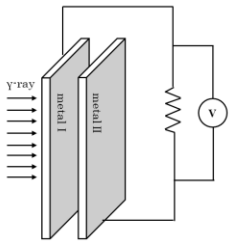


Fig.1 The parallel-plate type radiation battery

1.1 EXPERIMENTAL

In this study, a parallel-plate type radiation battery with each plate of a different metal and thickness was constructed, and the output power when a resistance was connected between the two plates was measured under γ-irradiation using a Co60 source at Nagoya University. Emitted electron fluxes for the geometries of a metal plate and two metal plates with an insulator under γ-irradiation were calculated using simulation codes of PHITS[2] and GEANT-4 [3], by changing the metal and the thickness of the plates and the insulator.

1.1.1 RESULTS AND DISCUSSION

Fig. 2 shows electron fluxes emitted from the single metal plate of Pb and Al under γ-irradiation calculated using PHITS. The figure shows that in order to get the large difference in electron fluxes emitted from the two metal plates, it is better to select different kinds of metals and/or the combination of thin and thick ones.

Copyright on 7th Asia-Pacific Symposium on Radiochemistry 2025

Under the γ-irradiation, the parallel-plates type radiation battery worked as a constant current power source. Fig.3 shows the changes in the output current for a multilayered plates-type radiation battery with increasing the number of plates. Although the output currents increased with the number of plates, the increasing manner was different depending on the order of the layers, because of the large difference in the emitted electron fluxes between Pb and Al, and the injection of electrons emitted from a plate into neighboring plates. Additionally, it was found that significant interactions involving high-energy electrons generated between the metal plates, indicating that the output current is not solely determined by the difference in electron flux emitted from a single metal plate. Furthermore, the output current varied significantly depending on the choice of insulating layer, suggesting that low-energy electron flux contributes substantially to the overall output.

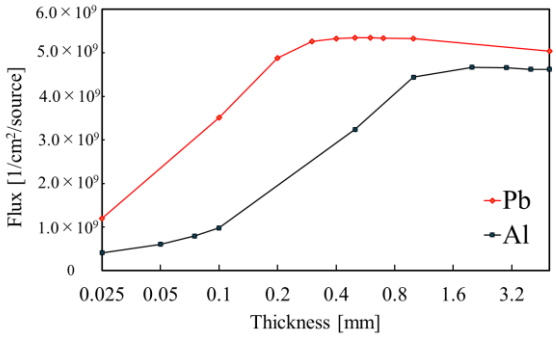


Fig. 2. Electron fluxes emitted from the single metal plate of Pb and Al under the γ -irradiation calculated with PHITS.

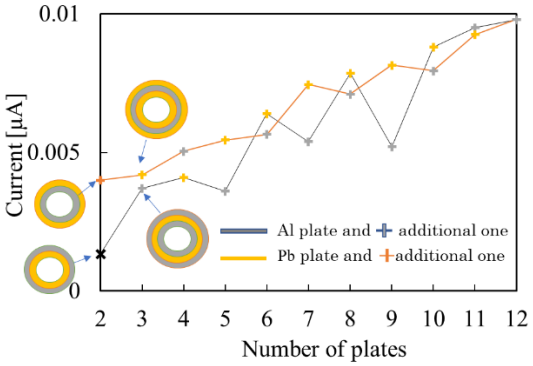


Fig. 3. Changes in output currents with increasing the number of metal plates. Yellow line: a Pb plate was set nearest to the γ -source then overlaid with the order of Al, Pb, Al and Al plate, nearest.

2. CONCLUSIONS

We aimed to utilize radioactive waste by converting γ-rays energy into electric energy by fabricating a parallel-plate type radiation battery using two metal plates of different types or thicknesses. Simulations using PHITS and Geant4 determined the optimal metal combinations based on electron flux emitted from single-plate irradiation, and a constant current was successfully obtained in a parallel-plate radiation battery. In a cylindrical-type radiation battery using Pb and Al plates, output current changed with the order of the layers and the kind of insulating material, suggesting that the inter-plate electron interactions, as well as low-energy electrons flux, significantly affect the overall output current.

References

[1] **Chen, A. Y. K., Yoshida, T., & Tanabe, T.** (2005). Enhanced gamma-ray energy conversion in water vessels—Part I: Physical mechanisms. *Nuclear Science and Engineering, 150*(3), 349–356.
[2] **Shikaze, Y.** (2024). Evaluation of radiation dose caused by bremsstrahlung photons generated by high-energy beta rays using the PHITS and GEANT4 simulation codes. *Journal of Nuclear Science and Technology, 61*(7), 894–910.
[3] **Pandola, L., Andenna, C., & Caccia, B.** (2015). Validation of the Geant4 simulation of bremsstrahlung from thick targets below 3 MeV. *Nucl. Instrum. Meth. B*, 350, 41-48

Copyright on 7th Asia-Pacific Symposium on Radiochemistry 2025

7th Asia-Pacific Symposium on Radiochemistry *September 14 ~ 19, 2025 • Kunibiki Messe • Shimane, Japan*

DEVELOPMENT OF LOW-VOLUME ELECTROLYTIC ENRICHMENT BY SPE MEMBRANE FOR TRITIUM IN WATER SAMPLES

Yoshihito Ohtsuka[1]

[1]*Department of Radioecology, Institute for Environmental Sciences: Obuchi 1-7, Rokkaho, Aomori, 039-3212, Email Address: ohtsuka@ies.or.jp*

A low-volume tritium electrolytic enrichment system is developed for water sample using a solid polymer electrolyte (SPE). Because this system does not have a cooling function for the sample, the tritium separation factor is not larger than previous reports, but it is practical for enriching tritium in 50-100 mL of samples. In the future, it is expected that the system will be equipped with a cooling function, making tritium enrichment more efficient.

1 INTRODUCTION

Japan's first commercial spent nuclear fuel reprocessing plant is scheduled to begin operation in Rokkasho, Aomori Prefecture in 2026, and the plant will release tritium into the atmosphere and ocean even during normal operation. Release of ALPS (Advanced Liquid Processing System)-treated water containing tritium from the Fukushima Daiichi nuclear power plant, Japan to ocean began in August 2023. For these reasons, determination of tritium in the environment and food is important for evaluating an internal dose assessment and for social concerns.

It is common to enrich the tritium in environmental and food stuff samples by several times or more before measuring them because tritium concentration in the general environment is smaller than the limit of detection of 0.3 – 0.6 Bq L^{-1} [1] by liquid scintillation counter (LSC) in recent years. Tritium enrichment method was developed alkaline electrolytic enrichment and solid polymer electrolyte (SPE) system. The former method is a conventional tritium enrichment method, but it has the disadvantages of the risk of explosion due to the evolution of hydrogen, and of the enrichment limit due to the increase in concentration of alkaline electrolyte as electrolysis progresses [2]. In the latter method using the SPE, evolved gases are separated by an SPE membrane, so there is little risk of an explosion. Although there is commercially available electrolytic tritium enrichment equipment, such as TRIPURE (De Nora Permelec Ltd.), this system requires an initial sample volume of about 1 L of water. For example, approximately 2 kg-dw of sample is required to obtain 1 L of combustion water for OBT measurement, so a tritium enrichment system with a small initial sample volume is practically indispensable to evaluate tritium level in the environment. Therefore, a low-volume electrolytic enrichment system using the SPE method is developed. This system is expected to be safer and easier to operate than the alkaline electrolytic enrichment method.

2 Experimental

In this system, platinum foil was pressed onto each side of the SPE to create an electrode in the cell. The SPE selected Nafion® (N–115, DuPont), which is often used for tritium electrolytic enrichment. The effective reaction area is approximately 4.5 cm^2. Considering the rapid diffusion of oxygen and hydrogen gas generated from surface of the electrode and efficient electric power supply to the SPE, electricity was supplied to the platinum foil by passing an electric current from the stainless-steel plate through the gas diffusion layer (SIGRACET®, GDL29AA, SGL Carbon AG) to the platinum foil. A conceptual diagram of the SPE membrane and electrodes of this device is shown in Fig. 1. A 15 mL of enrichment cell and two 50 mL of water reservoirs are made from commercial centrifuge tubes. The area around the electrodes becomes hot because the electrolysis of water is an exothermic reaction. Therefore, these gases were passed through the sample water in water vessels to recover some of the water vapor and reduce sample loss.

3 RESULTS

A 100 mL of the reference sea water IAEA-443 was purified by distillation and adjusted to approximately 1 Bq L^{-1} is concentrated to 22 mL using the system. During the two enrichments, mean current and voltage is 1.3 and 1.5 A (2.9 and 3.3 mA mm^{-2}) and approximately 10 V, respectively, and volumetric concentration ratio is about 4.4. A 10 mL of the solution enriched tritium is mixed with a 10 mL of scintillator (Ultima Gold LLT, Revvity). The tritium activity concentration of the enrichment solution is found to be 2.7 and 3.1 Bq L^{-1} by using Quantulus GCT 6220 (Revvity) for 1,000 min. measurement.

Tritium separation factor, β can be calculated by the following formula (1):

$$\frac{V_f}{V_i} = \left(\frac{T_f \cdot V_f}{T_i \cdot V_i}\right)^{\beta} \quad (1)$$

Copyright on 7th Asia-Pacific Symposium on Radiochemistry 2025

Where V_i and V_f are the initial and final sample volume, T_i and T_f are the initial and final tritium activity concentration, respectively. In this system, the values of β range are 2.2 and 2.6.
The value of β has been reported to be 4 – 15 by various combinations of SPE and metal electrodes [3 – 7], and the β of this system is smaller than them. In many cases of tritium enrichment, the sample water has been cooled to 2 – 20°C to reduce the amount of water vapor generated from the sample. Because this system does not have a cooling function, it seems that a large amount of water vapor is generated, resulting in a small β value.

Although the separation factor of this system is smaller than the β value of commercially tritium enrichment equipment TRIPURE (De Nora Permelec Ltd.) when concentrating an 800 mL of water sample to 50 mL, but it is still a practical value. In the future, this system will have the sample cooling function and will be a more efficient tritium enrichment device.

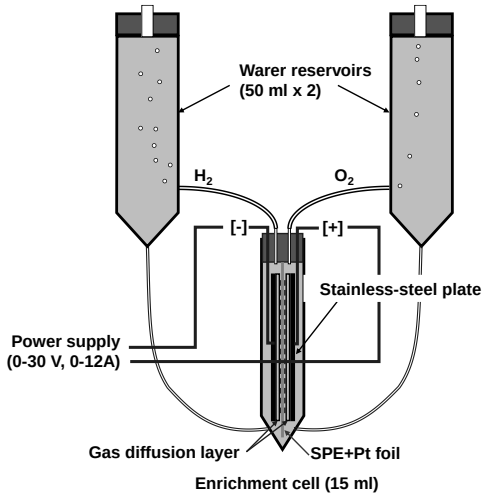


Fig. 1. A conceptual diagram of the tritium enrichment system.

ACKNOWLEDGMENTS

This study was performed under a contract with the government of Aomori Prefecture, Japan. The author thanks for technical support of this system for Dr. H. Kakiuchi. The author is grateful to the staff of Entex Co. Ltd for tritium analysis.

References

[1] H. Kakiuchi, N. Akata, *Recent studies on environmental monitoring of tritium in the adjacent nuclear facilities. J. Plasma and Fusion Research*, **89**, 645 (2013).
[2] N. Akata, C. Iwata, A. Kato, M. Tanaka, H. Tazoe, N. Shima, K. Ichiyanagi, M. Hegedűs, G. Bátor, T. Kovács and H. Kakiuchi, *Low-volume electrolytic enrichment for tritium measurement using improved solid polymer electrolyte system at NIFS and its application*, Radiation Environment and Medicine, **9**, 93 (2020).
[3] K. Uematsu, H. Yamazaki and M. Sato, Tritium enrichment by electrolysis using solid polymer electrolyte. *Radioisotopes*, **45**, 375 (1996).
[4] T. Muranaka, N. Shima, H. Sato, A study to estimate tritium concentrations of 1 Bq/L or lower in water samples. *Fusion Sci. Technol*., **48**, 516 (2005).
[5] Y. Ogata, Y. Sakuma, N. Ohtani, M. Kotake, Tritium separation by electrolysis using solid polymer electrolyte, *Fusion Sci. Technol*., **48**, 136 (2005).
[6] S. Sugihara, A. Hirose, N. Momoshima, Y. Maeda, Background tritium concentrations of river and lake waters in Japan, *Fusion Sci. Technol*., **54**, 289 (2008).
[7] A. M. Soreefan and T. A. DeVol, Determination of tritium enrichment parameters of a commercially available PEM electrolyzer: a comparison with conventional enrichment electrolysis, *J. Radioanal. Nucl. Chem.*, **282**, 511 (2009).

7th Asia-Pacific Symposium on Radiochemistry *September 14 ~ 19, 2025 • Kunibiki Messe • Shimane, Japan*

TLC plates containing fluorescent indicators are useful for analysis of alpha-particles and beta$^+$-rays

Kento Kannaka[1], Hiroyuki Suzuki[1], Kazuhiro Takahashi[2], Tomoya Uehara[1]

[1]*Laboratory of Molecular Imaging and Radiotherapy, Graduate School of Pharmaceutical Sciences, Chiba University, 1-8-1 Inohana, Chuo-ku, Chiba 260-0856, Japan, kannaka@chiba-u.jp*
[2] *Advanced Clinical Research Center, Fukushima Global Medical Science Center, Fukushima Medical University, Fukushima 960-1295, Japan*

1. Introduction

In recent years, development of therapeutic radiopharmaceuticals using α-particles emitting radionuclides and diagnostic radiopharmaceuticals using β^+-rays emitting radionuclides has been actively pursued. Thin-layer chromatography (TLC), which is an inexpensive and quick separation method, is widely used for the synthesis and verification of these radiopharmaceuticals. To detect these radiations developed on TLC, TLC analyzers or autoradiography are widely used. However, these detection systems are expensive and require long detection times. In addition, the room where these devices are installed must have low background radioactivity. These characteristics make them unsuitable for busy laboratories and clinical settings. Therefore, the development of a simple and cost-effective method for detecting α- and β^+-rays would be useful for rapid radiopharmaceutical development. In this study, we developed a new α- and β^+-rays detection system that can inexpensively and efficiently convert radiation into light.

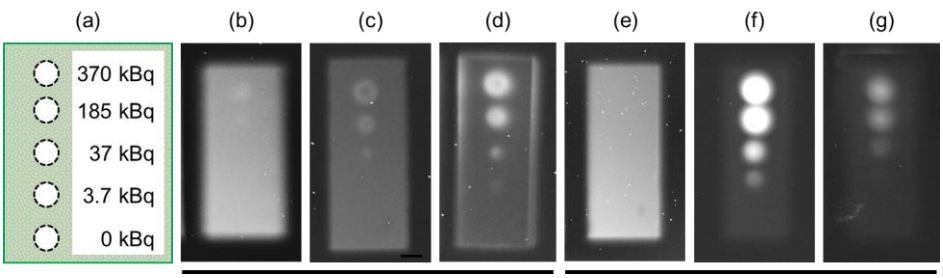
2. Method

The imaging system consisting of CMOS (Complementary Metal Oxide Semiconductor, BITRAN) camera and a black box was assembled. The f-value of lens attached to the camera was set to 0.95, and the exposure time was 1-5 minutes. TLC plates were prepared with and without fluorescent indicators (F_{254} or F_{254S}). Radioactive compounds containing astatine-211 (^{211}At) or fluorine-18 (^{18}F) were used as the α and β^+ sources. To evaluate whether the photo-conversion was due to α- and β^+-rays, we also evaluated iodine-125 (^{125}I) and indium-111 (^{111}In) as X- and γ-rays, respectively. In addition, a plastic scintillator (PS) made of polyvinyltoluene was placed on the TLC plates for comparison with F_{254}. Finally, the camera-based optical imaging system developed in this study was compared with the existing TLC analyzer by analyzing the ^{18}F-labeled and ^{211}At-labeled model compounds.

3. Results and discussion

First, each RI-labeled compound was applied to a TLC plate without fluorescent indicator and imaged by the camera. ^{211}At-labeled compound was not detectable, but ^{18}F-labeled compound was slightly detectable. This was thought to be Cherenkov light generated by the interaction with silica gel. Using PS, which is expensive, overlaid on the TLC plates, strong emission was observed for both RIs. In addition, using various types of glass plate, which are not expensive, overlaid in the TLC plates, a slight enhancement of luminescence was observed and both RIs were detectable, but the luminescent intensities were lower than with PS. Furthermore, each RI-labeled compound was applied to a TLC plate containing fluorescent indicator, F_{254}, which is not expensive and commonly used in organic synthesis, and imaged by the camera. Figure 1 shows luminescence images of ^{18}F-labeled and ^{211}At-labeled compounds applied to TLC plates with F_{254} or without F_{254}, and compared with and without PS. For each RI, strong luminescence was observed on the TLC plates with F_{254}. In particular, in the case of ^{211}At, higher luminescence intensity was observed than when PS was placed on a TLC plate without F_{254}. On the other hand, the luminescence intensity of ^{125}I and ^{111}In, which emit X- and γ-rays, were very weak when measured under same conditions. These results suggested that the high luminescence intensity of ^{18}F and ^{211}At were due to the α- and β^+-rays. In addition, there was a correlation between radioactivity and luminescence intensity. Finally, ^{18}F-labeled and ^{211}At-labeled model compounds were analyzed by the TLC analyzer and the camera-based optical imaging system after development using TLC with $F_{254/254S}$, and there is no difference between the two detection methods.

Copyright on 7th Asia-Pacific Symposium on Radiochemistry 2025



	(b)	(c)	(d)	(e)	(f)	(g)
TLC plate fluorescent indicator	−	+	−	−	+	−
Plastic scintillator	−	−	+	−	−	+

Figure 1. Illustration of radioactivity applied on a TLC plate (a). Luminescence images of ^{18}F-labeled compound (b, c, d) and ^{211}At-labeled compound on TLC plates (e, f, g).

4. CONCLUSIONS

In this study, the camera-based optical imaging system was developed and combined with the TLC plate containing fluorescent indicator to achieve optical detection of α-particles and β^+-rays. This analytical system using TLC with the fluorescent indicator is an inexpensive and convenient method for the analysis of radiopharmaceuticals using RIs emitting short range radiation.

ACKNOWLEDGMENTS

This study was supported by the Shimadzu Science Foundation and the Sasakawa Scientific Research Grant from Japan Science Society.

7th Asia-Pacific Symposium on Radiochemistry *September 14 ~ 19, 2025 • Kunibiki Messe • Shimane, Japan*

Concentration of Radioactive Iodine Using Forward Osmosis Membrane

Zhaoyang Si[1], Tamao Tanji[1], Ayako Yanagihori[1], Takahiro Osaki[2], Yuji Katayama[2], Masato Mikawa[2], Yoshitaka Takagai[1]

[1] Fukushima University*: 1 Kanayagawa, Fukushima, Fukushima 960-1296 JAPAN,* and *s015@ipc.fukushima-u.ac.jp*
[2] Asahi Kasei Corporation*: 2-1 Samejima, Fuji, Shizuoka 416-8501 JAPAN, and osaki.tf@om.asahi-kasei.co.jp*

Following the accident at the Fukushima Daiichi Nuclear Power Plant, large amounts of ^{129}I were released into the environment. ^{129}I (with a half-life of 15.7 million years) accumulates in seaweed and organic matter on the surface of the ground for long periods of time. Its ingestion by humans often causes thyroid exposure. It is necessary to accurately determine and analyze the radioactive iodine in the environment in order to understand the dynamics and/or its effects on living organisms. Since the amount of ^{129}I in environmental water is extremely low, the determination is difficult even to use inductively coupled plasma mass spectrometry (ICP-MS). Iodine is also required concentrating special chemical method due to its highly volatile chemical properties. Thus, in this study, a forward osmosis (FO) membrane which was not required any heating, was used for the enhancement of the concentration of iodine. Here, a stable iodine ^{127}I and ^{131}I were used for the evaluation of the FO membrane and spike recovery tests were conducted using environmental samples.

1. INTRODUCTION

Hollow-fiber forward osmosis (FO) membranes use osmotic pressure, generated by the difference in salt concentration between the two sides of the membrane, as the driving force for concentration. Reverse osmosis (RO) requires higher pressure than osmotic pressure, whereas FO membranes do not require any heating or pressurization, so it is expected that the concentration will be facilitated. Meanwhile, as far, FO membranes have been challenging to be available to a concentration system of trace materials for the trace analysis. In this study, we focused on radioiodine ^{129}I as a model substance and examined the possibility of using FO membrane systems for the concentration of ^{129}I in the environment. Iodine is difficult to concentrate chemically with heating due to its high volatility, which requires concentration under conditions of room temperature and pressure. The aim of this study was to evaluate the performance of FO membranes in concentrating trace concentrations of $^{129}I^-$. In this study, ^{131}I has been used and verified as a model substance for concentration by FO membranes.

2. EXPERIMENT

For the enrichment experiments, a solution containing low concentrations of iodine was used for feed solution (FS) as a sample and 1 M magnesium chloride solution for draw solution (DS). The flow path used in the concentration experiment was constructed as shown in Fig. 1. To obtain changes in the concentration behavior over time, the FS solution to be concentrated was aliquoted after a certain time and the FS was weighed. FS and DS are pumped and circulated using pumps. Stable isotope of iodine (sodium iodide) was measured by ion chromatography, and radioisotope ^{131}I was determined using a germanium semiconductor detector. As a basic verification for concentrating environmental samples, iodine was concentrated while taking into account the effects of pH and the effects of coexisting salt (KNO_3) in the FS. Next, we carried out a concentration test of ^{131}I to verify whether the FO system could concentrate radioactive iodine. In the FO enrichment using radioactive iodine, the presence or absence of remaining ^{131}I in the flow path was also checked, and the recovery rate was calculated.

Copyright on 7th Asia-Pacific Symposium on Radiochemistry 2025

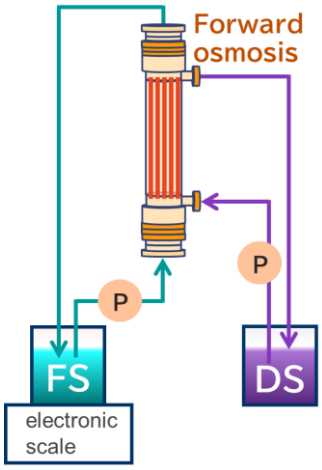


Fig. 1. The overview of the FO membrane system.

3. RESULTS ANS DISCUSSION

Figure 2 shows the results of concentration of I ions using the FO system. The concentrations of I were increased with the time. In addition, the enrichment efficiency can be evaluated by plotting the relationship between the weight ratio of FS (on x-axis) and the concentration ratio of I^- (on y-axis). It was found that the enrichment efficiency was slightly decreased as the enrichment of I^- progressed. In subsequent verifications, the enrichment behavior and enrichment efficiency will be evaluated as shown in Fig. 2. The condition of pH was not impacted on the enrichment using FS. The addition of $^{131}I^-$ to environmental waters exhibited a similar enrichment pattern as that observed in ultrapure water. Conversely, the various environmental waters exhibited elevated levels of radioactivity. Furthermore, no leakage of $^{131}I^-$ from FS to DS was observed in the concentration of $^{131}I^-$ using environmental water, in comparison to ultrapure water. From the considerations in those results, it is anticipated that FO membranes have the potential to be utilized for the expeditious concentration of radioactive iodine in environmental water, yielding substantial results.

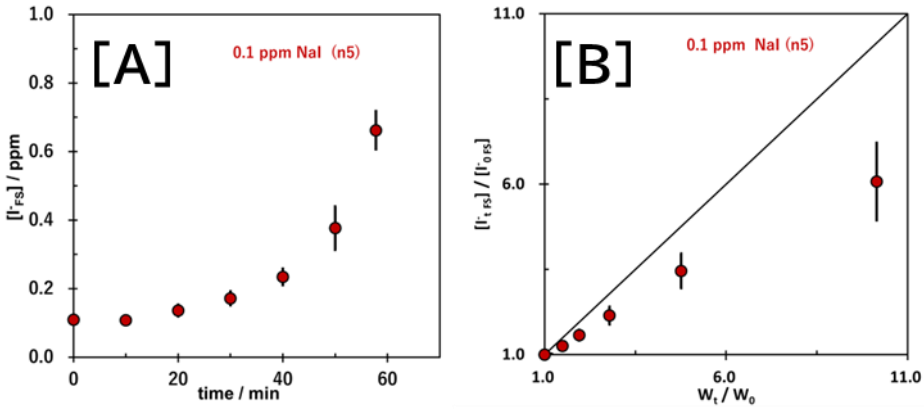


Fig. 2. The plotting in enrichment efficiency of iodine in the relationship between time vs. concentration [A], and between the weight ratio of FS and the concentration ratio of iodine in FS [B].

4. CONCLUSION

In this study, it was revealed that the FO membrane enrichment system can efficiently enrich not only stable iodine but also radioactive iodine in environmental water. We believe that this will greatly contribute to the analysis of very small amounts of radioactive iodine in the environment.

Copyright on 7th Asia-Pacific Symposium on Radiochemistry 2025 P-R2-07* -

Poster Presentation | [R3]Actinide Chemistry and Nuclear Energy Chemistry

Wed. Sep 17, 2025 6:30 PM - 8:00 PM JST | Wed. Sep 17, 2025 9:30 AM - 11:00 AM UTC Poster

[Poster] R3

[P-R3-01]

Elution of Sr and Cs from geopolymers under radiation environments

*Norikazu Kinoshita[1], Yuki Sasaki[1], Kazuyuki Torii[1], Makoto Inagaki[2] (1. Shimizu Corporation (Japan), 2. Kyoto University (Japan))

[P-R3-02]

MEASUREMENT OF SPECTROSCOPIC PROPERTIES OF U(VI) HYDROXO COMPLEXES USING TIME-RESOLVED LASER LUMINESCENCE SPECTROSCOPY

*Euo Chang Jung[1], Hee-Kyung Kim[1], Wansik Cha[1], Hye-Ryun Cho[1], Sang-Ho Lee[1] (1. Korea Atomic Energy Research Institute (Korea))

[P-R3-03]

Study on cost optimization of geological disposal of high level solid waste containing Am and Cm under high-level liquid waste partitioning strategy

*Xiantao Meng[1], Meng Wei[1], Meilan Jia[2] (1. CNNC Long'an Co. Ltd. (China), 2. China Institute for Radioation Protection (China))

[P-R3-04*]

Redox Stabilization of Am(V) in a Biphasic Extraction System Boosts Americium/Lanthanides Separation Efficiency

*Huaixin Hao[1], Xue Dong[1], Jing Chen[1], Zhipeng Wang[1], Chao Xu[1] (1. Tsinghua University (China))

[P-R3-05]

Generation and Accumulation Behavior of I-131 in Spent Fuel Reprocessing Plant

*Duo Ma[1], Shuai Liu[1], Long Cao[1], Zongqing Bao[1], Lingling Kong[1] (1. CNNC Longan Co., Ltd. (China))

[P-R3-06*]

GAS-PHASE REACTION OF Th, U, Np, Pu, Am, AND Cm IONS WITH O_2 IN A REACTION CELL IN ICP-MS/MS

*Kazushi Kawamoto[1], Hiroyuki Kazama[1], Masashi Kaneko[1], Ruilin Wang[1], Yudai Itakura[1], Enni Khult[1], So Hashiba[1], Kyosuke Shibamoto[1], Kenta Mori[1], Ryota Kikuchi[1], Tatsuya Suzuki[2], Kenji Konashi[3], Chikage Abe[3], Yoshitaka Kasamatsu[1] (1. Graduate school of science, the university of Osaka (Japan), 2. Department of Nuclear Technology, Nagaoka University of Technology (Japan), 3. International Research Center for Nuclear Materials Science, Institute for Materials Research, Tohoku University (Japan))

[P-R3-07]

Solvent extraction of trivalent actinides and lanthanides with high concentrations of tri-*n*-butyl phosphate and nitrate ion from high-level radioactive liquid waste using multistage centrifugal contactor

*Masaumi Nakahara[1], Yuichi Sano[1] (1. Japan Atomic Energy Agency (Japan))

[P-R3-08*]

©APSORC25

SYNTHESIS AND REDOX PROPERTIES OF DINUCLEAR U(IV) COMPLEXES WITH SCHIFF BASE MULTIDENTATE LIGANDS

*Nao Yoshida[1], Keisuke Morimoto[1], Kenji Shirasaki[1], Atsushi Shinohara[1], Takashi Yoshimura[1] (1. The University of Osaka (Japan))

[P-R3-09]

Novel Continuous Decomposition Technology for Radioactive Organic Liquid Waste Based on a Modified Emulsion Flow Device

Takanori Hoshino[1], *Yoichi Arai[1], Sou Watanabe[1], Masahiro Nakamura[1], Hideya Suzuki[2], Yasutoshi Ban[1] (1. Japan Atomic Energy Agency (Japan), 2. Emulsion Flow Technologies Ltd. (Japan))

[P-R3-10*]

Effect of substituents on the solvent extraction of lanthanides using diglycolamide ligands

*Kenta Mori[1], Hiroyuki Kazama[1], Masashi Kaneko[1], Ruilin Wang[1], Yudai Itakura[1], Miyu Konno[1], Enni Khult[1], Kyosuke Shibamoto[1], Ryota Kikuchi[1], Kazushi Kawamoto[1], Yoshitaka Kasamatsu[1] (1. The University of Osaka (Japan))

[P-R3-11]

DFT Study of Substituent Effect on MA/Ln Separation Using BTPhen-type Ligands

*Yuto Fukasawa[1], Satoru Nakashima[1] (1. Hiroshima University (Japan))

[P-R3-12]

Dissolution Behavior of UTi_2O_6 Solid Phase in Aqueous Media

Takuma Koyama[1], Daisuke Akiyama[2], Akira Kirishima[2], Taishi Kobayashi[1], *Takayuki Sasaki[1] (1. Kyoto University (Japan), 2. Tohoku University (Japan))

[P-R3-13*]

Enhanced Uranium Adsorption via Sulfonation of Polyether Ether Ketone

*xin Yu Song[1], Peng Liu[1] (1. Harbin Engineering University (China))

[P-R3-14]

Estimation of tritium amount in activated charcoal by the soaking and burning method

*Miki Nakada[1], Chie Iwata[1], Masahiro Tanaka[1] (1. NIFS (Japan))

[P-R3-15*]

Exploration of uranium adsorption properties of polyimide dixime-based uranium adsorption membrane materials

*Yanxin Jiang[1], Peng Liu[1] (1. Harbin Engineering University (China))

[P-R3-16]

All-in-One: Photo-Responsive Lanthanide-Organic Framework for Simultaneous Sensing, Adsorption, and Photocatalytic Reduction of Uranium

*zhiwei huang[1,2], KongQiu Hu[2], Lei Mei[2], WangSuo Wu[1], WeiQun Shi[2,3] (1. Lanzhou University (China), 2. Institute of High Energy Physics, Chinese Academy of Sciences (China), 3. Shanghai Jiao Tong University (China))

[P-R3-17*]

Chemical characterization of Platinum group alloys in fused borosilicate glasses

*Mizuki Kato[1], Haruaki Matsuura[1], Isamu Sato[1], Yuki Oiwa[1], Sayaka Chiba[1], Haruka Tada[2], Hiroki Izumi[2] (1. TOKYO CITY UNIVERSITY (Japan), 2. IHI Corporation (Japan))

©APSORC25

[P-R3-18]

Influence of Actinide Radiotoxicity on Nuclear Waste Disposal Frameworks in Spent Nuclear Fuel Reprocessing Systems

*Shuai Liu[1], Meng Wei[1], Jianquan Liu[1] (1. CNNC Long'an Co. Ltd. (China))

[P-R3-19*]

Adsorption and separation performance of platinum group metals using a novel MPE-TDGA/SiO_2-P adsorbent

*Mai Tanaka[1,2], Naoki Osawa[3], Hao Wu[4], Seong-Yun Kim[1] (1. Tohoku university (Japan), 2. JNFL (Japan), 3. Nagaoka university (Japan), 4. Shanghai Jiao Tong University (China))

[P-R3-20]

Analytical Strategy for Evaluating High-Specific-Activity ^{177}Lu in Theranostic Radiopharmaceutical Production

*Miki Harigai[1], Kazumi Nakano[2], Kenji Shirasaki[3], Hiroyuki Kimura[4], Tomoo Yamamura[1] (1. Institute for Integrated Radiation and Nuclear Science, Kyoto University (Japan), 2. Agilent Technologies, Inc. (Japan), 3. Institute for Radiation Science, The University of Osaka (Japan), 4. Institute for Environmental Safety and Health, Kyoto University (Japan))

[P-R3-21*]

Separation behavior of MA(III) from simulated high-level liquid waste using TEHDGA and HONTA impregnated XAD7-HP adsorbents

*Masahiko Kubota[1,2], Seong-Yun Kim[1], Tsuyoshi Arai[3], Sou Watanabe[4], Tatsuya Ito[5], Ryuji Nagaishi[5] (1. Tohoku University (Japan), 2. Japan Nuclear Fuel Chemical Analysis Co., Ltd (Japan), 3. Shibaura Institute of Technology (Japan), 4. Nuclear Fuel Cycle Engineering Laboratories, Japan Atomic Energy Agency (Japan), 5. Collaborative Laboratories for Advanced Decommissioning Science (CLADS), Japan Atomic Energy Agency (Japan))

[P-R3-22]

Synthesis of simulated radioactive waste containing ^{241}Am for evaluation of hydrogen generation

*Riko Ikarugi[1] (1. Japan Atomic Energy Agency (Japan))

[P-R3-23]

Adsorption behavior of fission product elements on synthesized tungsten oxide type inorganic adsorbent supported in silica beads

*HanYu Wang[1], Xianwei Wang[1], Wenzun Luo[1], Naoki Osawa[1], Tatsuya Suzuki[1] (1. Nagaoka University of Technology (Japan))

[P-R3-24]

Chemical stability of sulfur-containing functionalized silica-based adsorbents under nitric acid conditions for platinum group metals adsorption

*Naoki Osawa[1], Mai Tanaka[2], Hao Wu[3], Tatsuya Suzuki[1], Seong-Yun Kim[2] (1. Nagaoka University of Technology (Japan), 2. Tohoku University (Japan), 3. Shanghai Jiao Tong University (China))

[P-R3-25]

Establishment of a multi-element ICP-MS/MS quantitative method for quality assurance of high-specific-activity Lu-177 preparations

Miki Harigai[1], Kazumi Nakano[2], Kenji Shirasaki[3], Hiroyuki Kimura[4], *Tomoo Yamamura[1] (1. Institute for Integrated Radiation and Nuclear Science, Kyoto University (Japan), 2. Agilent Technologies, Inc. (Japan), 3. Institute for Radiation Science, The University of Osaka (Japan), 4. Agency for Health, Safety and Environment, Kyoto University (Japan))

©APSORC25

[P-R3-26*]

Adsorption and separation performance of minor actinides and lanthanides using MPEDGA/SiO_2-P adsorbent

*Riho Okajima[1,2], Masahiko Kubota[1], Seong-Yun Kim[1] (1. Department of Quantum Science and Energy Engineering, Graduate School of Engineering, Tohoku University (Japan), 2. Japan Nuclear Fuel Limited (Japan))

[P-R3-27]

Spent Nuclear Fuel Reprocessing and Regeneration in Accelerator Driven Advanced Nuclear Energy System

*Fangli Fan[1] (1. Institute of Modern Physics, Chinese Academy of Sciences (China))

[P-R3-28*]

ADSORPTIVITY OF TRIPHOSPHINE TRIOXIDE-IMPREGNATED
ANION EXCHANGE RESINS FOR RECOVERY OF URANIUM FROM SEAWATER

*Shion Matsumoto[1], Yukito Tounai[1], Masanobu Nogami[1], Chikage Abe[2] (1. KINDAI University (Japan), 2. TOHOKU University (Japan))

[P-R3-29]

Solidification and Stabilization Treatment of Liquid Nuclear Fuel Waste Containing Oil

Takeru Matsuishi[1], Toshiaki Hiyama[1], *Fuminori Honda[1] (1. RIC, Kyushu University (Japan))

[P-R3-30*]

A Study on the Preliminary Evaluation of the Nuclide Monitoring for Modelling at High-Level Radioactive Waste Disposal Site

*WooBeom Ha[1], DoWon Hyun[1], SangHeon Lee[1], JongSoon Song[1] (1. chosun university (Korea))

©APSORC25

7th Asia-Pacific Symposium on Radiochemistry *September 14 ~ 19, 2025 • Kunibiki Messe • Shimane, Japan*

Elution of Sr and Cs from geopolymers under radiation environments

Norikazu Kinoshita[1], Yuki Sasaki[2], Kazuyuki Torii[3], Makoto Inagaki[4]

[1]*Institute of Technology, Shimizu Corporation: Koto-ku, Tokyo 135-8530, Japan, norikazu.kinoshita@shimz.co.jp*
[2]*Nuclear Projects Division, Building Construction Headquarters, Shimizu Corporation: Chuo-ku, Tokyo 104-8370, Japan, sasaki.yuki@shimz.co.jp*
[3]*Nuclear Projects Division, Building Construction Headquarters, Shimizu Corporation: Chuo-ku, Tokyo 104-8370, Japan, ka_torii@shimz.co.jp*
[4]*Institute for Integrated Radiation and Nuclear Science, Kyoto University: Kumatori, Sennan, Osaka 590-0494, Japan, inagaki.makoto.2r@kyoto-u.ac.jp*

Geopolymers are believed to be promising materials for immobilization of radioactive wastes because of greater K_ds to Sr and Cs etc. We obtained elution rates of Sr and Cs from the geopolymer immobilizing a simulated waste at high dose environment and time variation of elution rates at natural radiation environment. The present work showed trends of elution from the geopolymers immobilizing actual wastes and long-term elution when the wastes are immersed by water.

1. INTRODUCTION

Low-level radioactive wastes discharged from nuclear power plants, such as filters, metals, spent resin, and sludge, are immobilized with cement in metal drums or containers. These wastes contain radioisotopes such as ^{90}Sr and ^{137}Cs. Low elution rates for the radionuclides are critical for immobilization of these wastes. Compared with cement, geopolymers are believed to have lower elution rates, greater compressive strength, and greater resistance to heat, among other advantages. Our group has previously reported on the trends of the K_ds for Sr and Cs ions on geopolymers prepared using 1–5 M NaOH solutions [1]. In addition, we elucidated the adsorption mechanism affecting K_ds of Sr and Cs [2]. The K_ds of both elements increased with the NaOH concentration. The elements were encapsulated in the pores of the geopolymers by the Coulomb interaction between ionic charges of the elements and the surface pores.

On the other hand, radiation environment is known to promote corrosion in water by radiation effect [3]. Therefore, radiation from the radioactive wastes would increase elution rates of the radioisotopes from the geopolymers immobilizing the radioactive wastes. In the present work, we investigated the elution rates of Sr and Cs from the geopolymers under different radiation doses to ensure the stability by the radiation.

2. METHODS

Geopolymer samples were prepared by kneading ingredients of fly ash (FA), blast-furnace slag (BFS), NaOH solution with a concentration of 1–5 M, and municipal solid waste incineration ash (MSWIA) in a weight ratio of 7.0 : 3.0 : 10.0 : 24.4. In the present work, the non-radioactive MSWIA was regarded as a radioactive waste. The samples were cured for 3 months at room temperature, and then pulverized into less than 1 mm. The pulverized samples were used for the elution experiment.

Each geopolymer sample mixed with its 10 times weight of water was stirred for 2 hours under different radiation doses in the ^{60}Co irradiation facility, Institute for Integrated Radiation and Nuclear Science, Kyoto University. Then, supernatants were collected by centrifugation and filtration using a 0.22 μm PTFE filter. Sr and Cs concentrations in the supernatants were determined using an ICP-MS. We obtained elution rates at dose rates from the natural environment of ~3×10^{-8} Gy/h to 15 Gy/h. In addition, the similar elution experiments were carried out under natural radiation environment to obtain the time variation of the elution rates in 1 week.

3. RESULTS AND DISCUSSION

Fig. 1 shows elution rates of Sr and Cs at different doses and time variation in natural radiation environment. We have reported that the geopolymers had greater K_d by using NaOH solution with higher concentration. Elution should be suppressed in materials with greater K_d. Even the geopolymers immobilizing the simulated waste showed the same trend as the geopolymers reported previously. On the other hand, significant difference was not observed in the elution rates between ~3×10^{-8} Gy/h and 15 Gy/h. The elution rates of both Sr and Cs increased gradually with an elution time. The time variation of the elution rates at 2 h approximately reproduced the elution carried out under radiation environments.

Copyright on 7th Asia-Pacific Symposium on Radiochemistry 2025

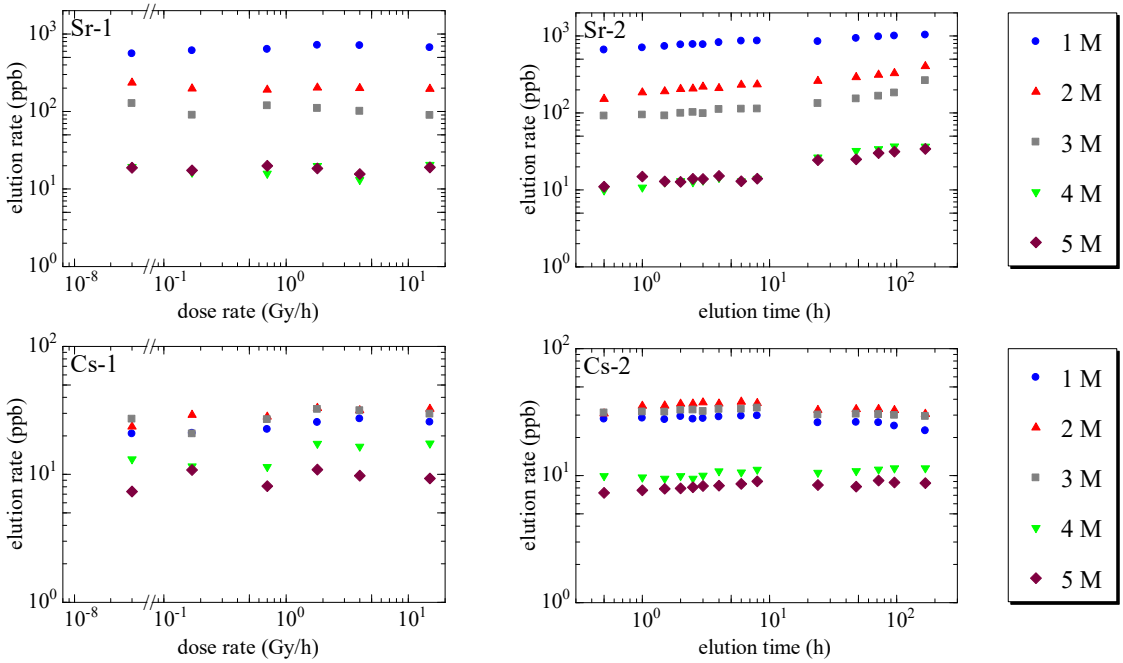


Fig. 1 Elution rates for Sr and Cs at different dose rates (Sr-1 and Cs-1) and time variation of elution rates for Sr and Cs in 1 week under natural radiation environment (Sr-2 and Cs-2).

For example, the geopolymers containing ^{90}Sr and ^{137}Cs have absorbed doses of 0.49–0.54 MeV/Bq and 0.35–0.38 MeV/Bq, respectively, assuming a density of 2.1–2.3 g/cm^3, based on simulation using PHITS code [4]. In the present work, we investigated the elution rates at dose rates from ~3×10^{-8} to 15 Gy/h. The doses correspond to concentrations of 64–5.3×10^7 Bq/g for ^{90}Sr and 92–7.5×10^7 Bq/g for ^{137}Cs in the geopolymer immobilizing the radioactive waste. These concentrations are equivalent to L3 and part of L2 waste in the classification of the low-level radioactive waste. The present work showed that the elution rates were not varied by the concentrations of radioactive nuclide in L3 waste. On the other hand, the geopolymer should not be applied to the wastes with higher than L2 because of hydrogen production by radiolysis of water. In addition, we should note the elution of radioactive nuclides in water from the immobilized waste although the geopolymer has greater K_ds.

4. CONCLUSION

We investigated elution of Sr and Cs from the geopolymers immobilizing MSWIA. The elution rates showed the similar trends expected from the previous work even in the samples that the simulated waste was immobilized. The elution rates were not varied by the dose rates below 15 Gy/h. On the other hand, the rates increased gradually with an elution time in 1 week.

ACKNOWLEDGMENTS

The authors wish to thank the staff of Institute for Integrated Radiation and Nuclear Science, Kyoto University for operation of the ^{60}Co irradiation facility.

References

[1] N. Kinoshita, Y. Yoda, H. Nakashima, M. Asada, S. Kiyomura, Y. Sasaki, K. Torii, K. Sueki, "Physical and adsorption characteristics of geopolymers prepared using 1–5 M NaOH solution for immobilization of radioactive wastes," *J. Nucl. Radiochem. Sci.*, **22**, 7-13 (2022).

[2] N. Kinoshita, M. Hotta, H. Nakashima, K. Torii, Y. Sasaki, "Impact of NaOH concentrations on the structure of geopolymers and thus changing the adsorption mechanism of Sr^{2+} and Cs^+ ions," Tot. Environ. Eng. **2**, 100007 (2025).

[3] K. Bessho, Y. Oki, N. Akimune, H. Matsumura, K. Masumoto, S. Sekimoto, N. Osada, N. Kinoshita, H. Monjushiro, S. Shibata, "Corrosion of copper in water and colloid formation under intense radiation field," *J. Radioanal. Nucl. Chem.* **303**, 1117-1121 (2015).

[4] T. Sato, Y. Iwamoto, S. Hashimoto, T. Ogawa, T. Furuta, S. Abe, T. Kai, Y. Matsuya, N. Matsuda, Y. Hirata, T. Sekikawa, L. Yao, P.E. Tsai, H.N. Hunter, H. Iwase, Y. Sakaki, K. Sugihara, N. Shigyo, L. Sihver, K. Niita, "Recent improvements of the Particle and Heavy Ion Transport code System - PHITS version 3.33," *J. Nucl. Sci. Technol.* **61**, 127-135 (2024).

Copyright on 7th Asia-Pacific Symposium on Radiochemistry 2025 P-R3-01 -

7th Asia-Pacific Symposium on Radiochemistry *September 14 ~ 19, 2025 • Kunibiki Messe • Shimane, Japan*

MEASUREMENT OF SPECTROSCOPIC PROPERTIES OF U(VI) HYDROXO COMPLEXES USING TIME-RESOLVED LASER LUMINESCENCE SPECTROSCOPY

Euo Chang Jung, Hee-Kyung Kim, Wansik Cha, Hye-Ryun Cho, Sang-Ho Lee

Korea Atomic Energy Research Institute: 989-111 Daedeok-daero, Yuseong-gu, Daejeon 305-353, Republic of Korea
ecjung@kaeri.re.kr

The chemical speciation of U(VI) hydroxo complexes has been studied for decades using time-resolved laser luminescence spectroscopy, however, there are several inconsistencies in the data reporting their spectroscopic properties. Samples containing major components of U(VI) hydroxo complexes, such as UO_2OH^+, $UO_2(OH)_2$, $UO_2(OH)_3^-$, $(UO_2)_2(OH)_2^{2+}$, $(UO_2)_3(OH)_5^+$, and $(UO_2)_3(OH)_7^-$, were prepared with different U(VI) concentration and pHs. Their spectroscopic properties measured at 1 ℃ and 25 ℃ were compared with previously reported data, and some corrected values are presented.

1 INTRODUCTION

Due to its relevance to the long-term safety assessment of nuclear waste repositories, numerous studies have been conducted on the complexation of U(VI) with inorganic and organic ligands. Among the various techniques, time-resolved laser luminescence spectroscopy has proven to be a sensitive and selective technique for the chemical speciation of U(VI) complexes. Prior to determining the thermodynamic constants of ternary U(VI) species composed of U(VI) hydroxo complexes and other ligands, many experimental results on the luminescence characteristics of U(VI) hydroxo complexes were reported first. However, the reason for the discrepancies in the spectral data (spectral shape and lifetime) reported in the literature remains an open question. A recent round-robin test on the aqueous U(VI) system pointed out differences in the luminescence lifetimes, which are particularly due to difference in the experimental conditions and algorithms for spectral analysis [1,2]. For example, luminescence lifetimes of UO_2OH^+ and $(UO_2)_3(OH)_7^-$ species vary greatly in the literature. There are relatively few studies investigating the spectral properties of the $UO_2(OH)_2$, $UO_2(OH)_3^-$ and $(UO_2)_3(OH)_7^-$ species under basic pH conditions, and the data supplementation is needed.

In this study, spectral properties were measured by considering the following two observations. First, when a high-pulse energy laser beam of ultraviolet wavelength is incident on the aqueous sample, the luminescence intensity of the U(VI) hydroxo species is observed to change over irradiation time. Second, we found that luminescence of the cuvette itself and the luminescence arising from U(VI) adsorbed on the cuvette walls could act as major interference factors in determining the spectral properties of dissolved U(VI) species under basic pH conditions. The spectral properties of U(VI) hydroxo complexes measured under experimental conditions excluding these interference factors were compared with values previously reported in the literature.

2 EXPERIMENT AND RESULTS

Three laser beams of different wavelengths (266, 355, 430 nm) were used as light sources, and the luminescence spectra were recorded using an intensified charge-coupled device attached to the exit port of the spectrometer. The detailed experimental setup is described in Reference [3]. For samples with U(VI) concentrations below 1 x 10^{-7} M, a 266 nm laser beam with high luminescence quantum efficiency is widely used as an excitation light source.

Figure 1(a) shows the well-known luminescence spectra of UO_2^{2+} and UO_2OH^+ measured from samples with U(VI) concentration of 1 x 10^{-8} M, pH 4.8 and temperature of 1 ℃. These spectra were measured under gate delay times of 1 μs and 120 μs, respectively. The peak wavelengths of UO_2^{2+} and UO_2OH^+ spectra are 488−509−533 nm and 497−519−542 nm, respectively.

Figure 1(b) shows the variation of luminescence intensity as a function of gate delay time, measured from the sample used in Fig. 1(a). The luminescence intensities were obtained by integrating the signal from 475 to 600 nm in the luminescence spectrum. The data show two straight lines with different slopes. The luminescence lifetimes of UO_2^{2+} and UO_2OH^+, determined from the slopes of the lines, are 13.6 and 115.2 μs, respectively. In these experiments, changes in luminescence intensity were observed under conditions of high laser pulse energy at 266 nm. As the laser irradiation time elapsed, the luminescence intensity of free uranyl ion hardly changed, while the luminescence intensity of U(VI) hydroxo species decreased rapidly and then tended to recover. The cause of this phenomenon is not clearly known. However, the laser pulse energy-dependent luminescence intensity change may affect the determination of the luminescence lifetime. No decrease in luminescence intensity was observed when the laser pulse energy was 0.1 mJ at 266 nm. Additionally, no

decrease in luminescence intensity was observed even when the laser pulse energy was higher than 1.0 mJ for 355 and 430 nm.

Figure 1(c) shows the luminescence spectra measured in empty quartz cells without aqueous solutions. These two spectra are the most commonly observed spectral shapes in many cells, and have luminescence lifetimes of tens of microseconds. In low concentration samples where the luminescence intensity of the U(VI) species is not strong, the interference of this background signal cannot be ignored to determine the spectral characteristics of U(VI) species. Similarly, trace amounts of U(VI) adsorbed on the quartz walls also generate a non-negligible luminescence signal that can act as an interference factor.

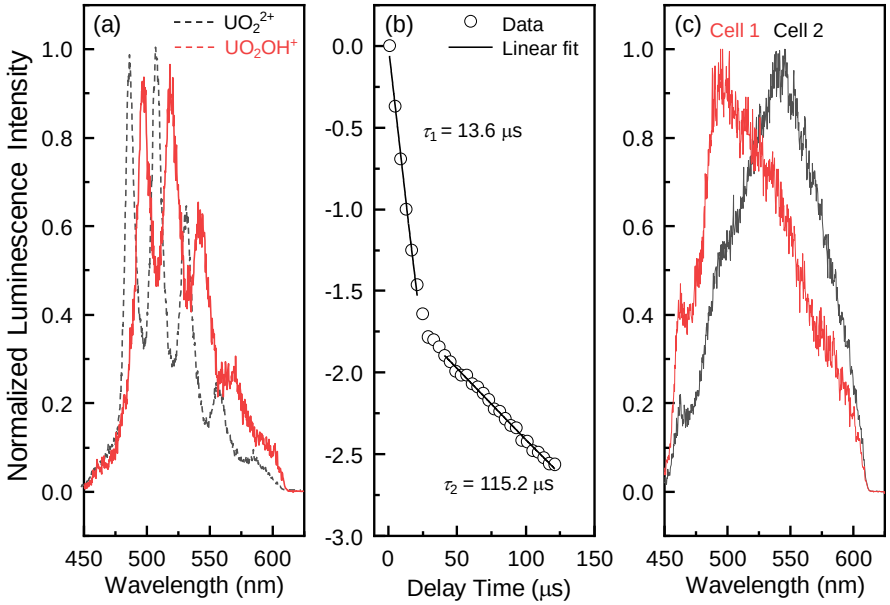


Fig. 1. The experiment was carried out at a laser pulse energy of 1.0 mJ (266 nm). (a) Luminescence spectra of UO_2^{2+} and UO_2OH^+ measured from sample with a U(VI) concentration of 1 x 10^{-8} M, pH 4.8 and temperature of 1 ℃. (b) Changes in luminescence intensity as a function of gate delay time measured from the sample used in Fig. 1(a). (c) Representative background spectral shapes observed in several empty quartz cells without U(VI) aqueous solution.

3 SUMMARY

The luminescence spectral shapes and lifetimes of the UO_2OH^+, $UO_2(OH)_2$, $UO_2(OH)_3^-$, $(UO_2)_2(OH)_2^{2+}$, $(UO_2)_3(OH)_5^+$, and $(UO_2)_3(OH)_7^-$ species measured in this experiment were compared with the results summarized in literature [4-6].

ACKNOWLEDGMENTS

This work was supported by the Institute for Korea Spent Nuclear Fuel (iKSNF) and National Research Foundation of Korea (NRF) grant funded by the Korea government (Ministry of Science and ICT, MSIT) (No 2021M2E1A1085202).

References

[1] I. Billard et al., “Aqueous Solutions of Uranium(VI) as Atudied by Time-Resolved Emission Spectroscopy: A Round-Robin Test,” *Appl. Spectrosc.* **57**, 1027 (2003).
[2] K. Müller et al., “Interdisciplinary Round-Robin Test on Molecular Spectroscopy of the U(VI) Acetate System,” ACS Omega, **4**, 8167 (2019).
[3] Euo Chang Jung, Tae-Hyeong Kim, Hee-Kyung Kim, Hye-Ryun Cho, and Wansik Cha, “Excitation and Emission Properties of Adsorbed U(VI) on Amorphous Silica Surface,” JNFCWT, **18**, 497 (2020).
[4] C. Moulin, I. Laszak, V. Moulin, and C. Tondre, “Time-Resolved Laser-Induced Fluorescence as a Unique Tool for Low-level Uranium Speciation,” *Appl. Spectrosc.* **52**, 528 (1998).
[5] B. Drobot, A. Bauer, R. Steudtner, S. Tsushima, F. Bok, M. Patzschke, J. Raff, and V. Brendler, “Speciation Studies of Metals in Trace Concentrations: The Mononuclear Uranyl(VI) Hydroxo Complexes,” *Anal. Chem.* **88**, 3548, 2016.
[6] B. Drobot, R. Steudtner, J. Raff, G. Geipel, V. Brendler and S. Tsushima, “Combining luminescence spectroscopy, parallel factor analysis and quantum chemistry to reveal metal speciation – a case study of uranyl(VI) hydrolysis,” *Chem. Sci.* **6**, 964 (2015).

7th Asia-Pacific Symposium on Radiochemistry *September 14 ~ 19, 2025 • Kunibiki Messe • Shimane, Japan*

STUDY ON COST OPTIMIZATION OF GEOLOGICAL DISPOSAL OF HIGH LEVEL SOLID WASTE CONTAINING AM AND CM UNDER HIGH-LEVEL LIQUID WASTE PARTITIONING STRATEGY

Xiantao Meng [1], Meng Wei [1], Meilan Jia [2]

[1] *CNNC Long'an Co., Ltd., Beijing, China*
[2] *China Institute for Radioation Protection, Taiyuan, China*

Under the high-level liquid waste (HLLW) partitioning strategy, the amount of high-level solid waste requiring deep geological disposal generated by spent fuel reprocessing plants will be significantly reduced. If neptunium (Np) in the HLLW is recovered as a product, then the high-level solid waste containing americium (Am) and curium (Cm) (with borosilicate glass-based waste forms as the focus of this study) will become the primary waste source item requiring deep geological disposal after HLLW separation. Therefore, investigating the disposal costs of these Am-Cm solid wastes will be the most important part of the work in analyzing the impact of HLLW separation technology on the waste disposal costs of reprocessing plants. Based on the disposal unit model (horizontal tunnel + vertical borehole) of the high-level waste disposal underground laboratory in the Beishan area of China, this study analyzes the impact of various variables, such as the amount of Am-Cm glass solid waste, the temporary storage time before disposal, the spacing between disposal tunnels, and the spacing between vertical boreholes, on the temperature of the filling material in vertical boreholes and the surrounding rock. Furthermore, based on the safety principles of the disposal unit design, a series of layout schemes for Am-Cm waste packages in the disposal repository are proposed. Finally, by comparing the engineering and management costs of various disposal schemes, the most economical Am-Cm waste management strategy is proposed.

Keywords: Partitioning of high-level liquid waste, Am, Cm, vitrification, temporary storage, disposal, cost, temperature field simulation

7th Asia-Pacific Symposium on Radiochemistry *September 14 ~ 19, 2025 • Kunibiki Messe • Shimane, Japan*

Redox Stabilization of Am(V) in a Biphasic Extraction System Boosts Americium/Lanthanides Separation Efficiency

Xue Dong, Huaixin Hao, Jing Chen, Zhipeng Wang*, Chao Xu*

Institute of Nuclear and New Energy Technology, Tsinghua University, Beijing 100084, China
**E-mail: wangzhipeng@mail.tsinghua.edu.cn (Z.P. Wang), xuchao@tsinghua.edu.cn (C. Xu)*

Americium (Am) is a key radioactive element in consideration in nuclear waste treatment. Separation of Am from the fission products, lanthanides, is a prerequisite to minimize the hazardous impact of Am and make utilization of rare Am isotopes, but it represents a great challenge due to the chemical similarity between the two groups of elements. Herein, we realize the separation by first oxidizing Am(III) to high valent Am(VI) and then converting it to Am(V) in situ in a biphasic extraction system with Bi(V) oxidant incorporated in an organic phase. Am(V) is highly stabilized during the separation process and this leads to record high Ln/Am separation factors (>10^5) in a single contact over a wide range of acidities.

Keywords: *Americium(V), Redox Chemistry, Am/Ln separation*

1 INTRODUCTION

Americium (Am), a highly radiotoxic minor actinide in spent nuclear fuel, poses a significant challenge to nuclear waste management. The efficient separation of Am from chemically similar lanthanides (Ln) is crucial for enabling Am transmutation and reducing long-term radiological hazards. Conventional separation strategies primarily rely on the design of ligands bearing soft N and S donor atoms, which preferentially bind to the relatively softer Am(III) over the harder Ln(III). However, such approaches suffer from limitations including slow kinetics, ligand instability, and narrow operation acidities.[1] An alternative yet less explored strategy involves exploiting the different redox properties between Am and lanthanides, as well as the notable differences in steric configuration and charge density between linear americyl ion and spherical Ln ion.[2] Despite the theoretical advantage, high-valent Am species, such as Am(V) and Am(VI), are highly susceptible to rapid reduction upon contact with organic extractants, which severely compromises the Am/Ln separation efficiency.[3] Therefore, achieving and maintaining the stability of high-valent Am during solvent extraction remains a key challenge in the development of effective Am/Ln separation processes.

2 RESULTS AND DISCUSSION

Recently, we proved that the incorporation of oxidative Bi(V) species in an organic solvent containing TODGA (*N*,*N*,*N*′,*N*′-tetraoctyl diglycolamide) would greatly overcome the reduction issue by oxidizing Am(III) to Am(V) in the organic solvent and result in efficient separation of Am from lanthanides and curium (Cm).[4,5] High Ln/Am separation factors have been maintained for a few hours during the extraction and then decreased gradually. We attribute the decrease in Ln/Am separation factors to the persistent consumption of Bi(V) by Am(III) and other reducing products in the solution. The consumption of Bi(V) and decrease of Ln/Am separation factors become more significant when relatively high concentrations of Am are present, and this might be problematic when dealing with real waste containing Am at the mM level.[4] To slow down the consumption rate of Bi(V) and the reducing rate of Am(V) and thus to improve the applicability of this separation method in dealing with high concentrations of Am, herein we demonstrated a new strategy for more efficient generation and stabilization of Am(V) in a biphasic system by first oxidizing Am(III) to Am(VI) in an aqueous solution and then contacting it with a Bi(V)-incorporating organic solvent (Fig. 1).[6] Am(VI) will be reduced to Am(V) and Am(III) in the biphasic system, but any Am(III) will be extracted by TODGA and oxidized to Am(V) by Bi(V) in the organic phase immediately and then Am(V) will transfer back to the aqueous phase. Apparently, much less Bi(V) will be consumed by starting with Am(VI) solution than with Am(III) solution, thereby enhancing the stability of Am(V) over a long duration. Accordingly, record high Ln/Am separation efficiency was achieved over a wide range of acidities.

Copyright on 7th Asia-Pacific Symposium on Radiochemistry 2025 P-R3-04* -

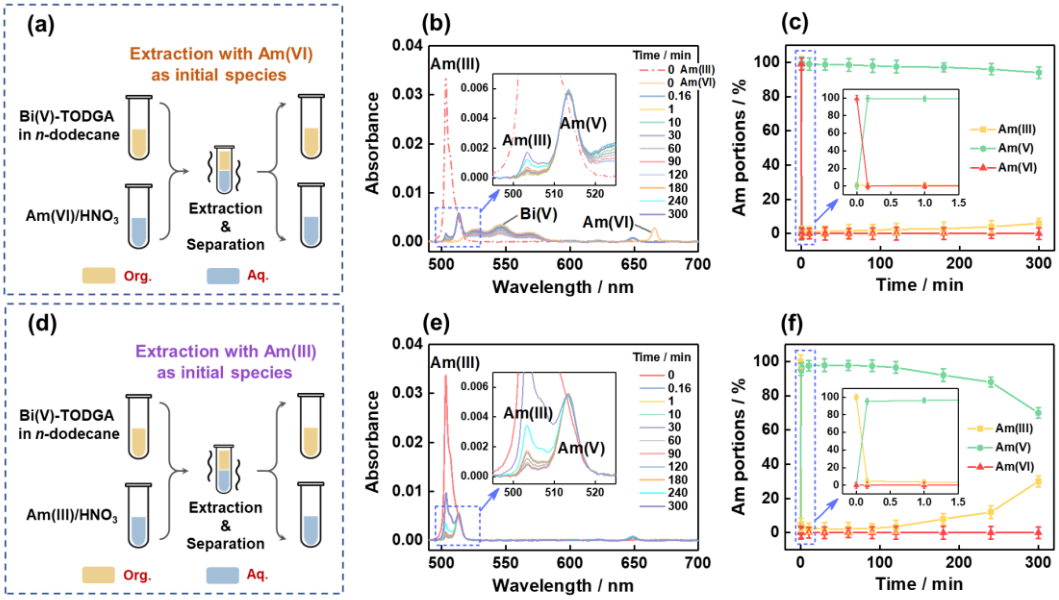


Fig. 1. Comparison of Am(V) formation through two different paths. (a) The scheme for generation of Am(V) in a biphasic system with Am(VI) as the initial Am species. (b) Variation of absorption spectra and (c) time-dependent change of portions of Am in different oxidation states in the nitric acid aqueous solution after mixing Am(VI)/HNO_3 with the Bi(V)-incorporating TODGA/*n*-dodecane organic solution. (d–f) Corresponding scheme and results with Am(III) as the initial Am species.

3. CONCLUSIONS

In conclusion, by exploiting the unique properties of Am(VI) reduction and Am(III) oxidation in a deliberately designed biphasic extraction system with Bi(V) incorporated in the organic phase, Am(V) was efficiently generated, stabilized, and separated from lanthanides with record high efficiency. The findings from this work not only provide an extremely efficient Am/Ln separation method to support the advanced nuclear fuel cycle, but also enrich our understanding of the less-explored redox chemistry of the highly radioactive element Am.

ACKNOWLEDGMENTS

C. X. is thankful for the financial support from the National Natural Science Foundation of China (22325603) and Beijing Natural Science Foundation (JQ20041). Z. W. is thankful for the financial support from the National Natural Science Foundation of China (22006090 and 22376116).

References

[1] Leoncini, J. Huskens and W. Verboom, *Chem. Soc. Rev.*, 2017, **46**, 7229-7273.
[2] C. J. Dares, A. M. Lapides, B. J. Mincher and T. J. Meyer, *Science*, 2015, **350**, 652-655.
[3] B. J. Mincher, L. R. Martin and N. C. Schmitt, *Inorg. Chem.*, 2008, **47**, 6984-6989.
[4] Z. Wang, J.-B. Lu, X. Dong, Q. Yan, X. Feng, H.-S. Hu, S. Wang, J. Chen, J. Li and C. Xu, *J. Am. Chem. Soc.*, 2022, **144**, 6383-6389.
[5] Z. Wang, X. Dong, Q. Yan, J. Chen and C. Xu, *Anal. Chem.*, 2022, **94**, 7743-7746.
[6] X. Dong, H. Hao, J. Chen, Z. Wang and C. Xu, *Chem. Sci.*, 2024, **15**, 2118-2122.

Copyright on 7th Asia-Pacific Symposium on Radiochemistry 2025 P-R3-04* -

7th Asia-Pacific Symposium on Radiochemistry *September 14 ~ 19, 2025 • Kunibiki Messe • Shimane, Japan*

Generation and Accumulation Behavior of I-131 in Spent Fuel Reprocessing Plant

Duo Ma[1], Shuai Liu[1], Longhao Cao[1], Zongqing Bao[1], Lingling Kong[1]

[1]*CNNC Longan Co., Ltd.: Beijing, China*

Iodine is an important fission product produced during the irradiation of nuclear fuel in reactors with high yields (U-235 thermal neutron fission: I-129 yield is 0.84%, I-131 yield is 2.82%). Radioiodine is a widely concerned radionuclide in the nuclear industry because it is easy to accumulate in thyroid gland, resulting in obvious internal exposure.Among them, I-131 is a radioactive gas nuclide with a short half-life of 8.02 and a high specific activity, so it is a key concern in nuclear power plants.In spent fuel reprocessing plants, I-131 has basically decayed during the cooling process of spent fuel for several years, so I-129 with a longer half-life (half-life of 1.57×107 years) is a radionuclide focused on in reprocessing plants. Generally, during the dissolution process of spent fuel, it will be driven into the atmosphere for adsorption and solidification.But it is worth noting that Cm-244 and other nuclides in spent fuel will still produce I-131 even after iodine removal in dissolution process. In order to evaluate the impact of newly produced I-131 on reprocessing plants and whether it is necessary to control it, the production and accumulation of I-131 in reprocessing plants are calculated and studied in this paper. The potential influence is analyzed, and I-131 control and management scheme for reprocessing plant is proposed.

Keyword: Spent fuel reprocessing, Iodine-131, Radioactive iodine management

GAS-PHASE REACTION OF Th, U, Np, Pu, Am, AND Cm IONS WITH O_2 IN A REACTION CELL IN ICP-MS/MS

Kazushi Kawamoto[1], Hiroyuki Kazama[1], Masashi Kaneko[1], Ruilin Wang[1], Yudai Itakura[1], Enni Khult[1], So Hashiba[1], Kyosuke Shibamoto[1], Kenta Mori[1], Ryota Kikuchi[1], Tatsuya Suzuki[2], Kenji Konashi[3], Chikage Abe[3], Yoshitaka Kasamatsu[1].

[1] *Graduate School of Science, The University of Osaka, 1-1, Machikaneyama-cho, Toyonaka, Osaka, 560-0043, Japan; kawamotok24@chem.sci.osaka-u.ac.jp*

[2] *Department of Nuclear Technology, Nagaoka University of Technology, 1603-1, Kamitomioka-machi, Nagaoka, Niigata, 940-2188, Japan*

[3] *International Research Center for Nuclear Materials Science, Institute for Materials Research, Tohoku University, 2145-2, Narita-cho, Oarai-machi, Higashiibaraki-gun, Ibaraki, 311-1313, Japan*

The gas-phase reactions of actinide (An, An =Th, U, Np, Pu, Am, and Cm) ions with O_2 were investigated using ICP-MS/MS method. AnO^+ and AnO_2^+ were observed as reaction products. Based on the experimental results, the reaction constant for the reaction $An^+ + O_2 \rightarrow AnO^+ + O$ was evaluated. The negative correlation of the reaction constant with the promotion energy to the $6d^2$ electronic state of An^+ suggests that the 6d orbital is involved in the bonding of AnO^+.

1 INTRODUCTION

Fuel debris of Fukushima Daiichi Nuclear Power Station contains actinide nuclides with high radiotoxicity. In the analysis of these actinides, triple quadrupole inductively coupled plasma mass spectrometry (ICP-MS/MS), a rapid and highly sensitive analytical technique, is expected to be utilized. ICP-MS/MS can reduce the isobaric interference (such as $^{238}U/^{238}Pu$ and $^{243}Am/^{243}Cm$) by introducing reaction gases into a reaction cell located between two mass filters arranged in tandem. For isobaric discrimination, it is important to understand the gas-phase reaction between actinide ions (An^+) and the reaction gas in the cell. The purpose of this study is to clarify the reactivity of An^+ and reaction gases in ICP-MS/MS both experimentally and theoretically. We focus on the reaction of An^+ with O_2, which is the simplest reaction. In this presentation, we report the modeling of the reaction behavior of An^+ with O_2 and the evaluation of the reaction constant by numerical analysis.

2 METHOD OF EXPERIMENTATION

A 5 wt.% HNO_3 solution containing ^{232}Th, ^{238}U, ^{237}Np, ^{241}Am, ^{244}Cm or ^{240}Pu (1 ppb except Pu, 0.1 ppb for Pu) was prepared. ICP-MS/MS measurements were conducted using Agilent 8900 (Agilent Technologies, Japan). O_2 was introduced into the reaction cell at flow rate 0 to 0.90 mL min^{-1} as reaction gas. In the first quadrupole mass filter (Q1), only singly charged actinide ions (An^+) were allowed to pass. After reaction with O_2 in the reaction cell, the product ions (An^+, AnO^+, and AnO_2^+) were discriminated in the second quadrupole mass filter (Q2) to investigate the flow rate effects on the molecular ion formation.

3 RESULTS AND DISCUSSION

An^+, AnO^+, and AnO_2^+ were observed for all actinides studied except Cm. The intensity of An^+ decreased with increasing O_2 flow rate. At lower O_2 flow rates, AnO^+ ions were detected, whereas AnO_2^+ became predominant at higher flow rates. This trend suggests that the sequential reactions $An^+ + O_2 \rightarrow AnO^+ + O$ and $AnO^+ + O_2 \rightarrow AnO_2^+ + O$ proceeded in the reaction cell. The reaction constant k_1 and k_2 based on collision theory was evaluated by establishing the simultaneous equation shown in Eqs. (1)-(3)[1] and fitting them to the experimental values, with the detected An^+, AnO^+, and AnO_2^+ concentration as n_A, n_B, and n_C, respectively, and the O_2 flow rate (mL min^{-1}) as Φ. For model validation, the reaction constants of Th^+, U^+, Pu^+, Am^+ and Cm^+ were normalized relative to Np^+, and the resulting ratios were compared with previous gas-phase reaction studies, showing good agreement (TABLE 1).

$$\begin{cases} \frac{dn_A(\phi)}{d\phi} = -k_1 n_A(\phi) & (1) \\ \frac{dn_B(\phi)}{d\phi} = k_1 n_A(\phi) - k_2 n_B(\phi) & (2) \\ \frac{dn_C(\phi)}{d\phi} = k_2 n_B(\phi) & (3) \end{cases}$$

TABLE 1. The reaction constants of An^+ normalized relative to Np^+

	Th	U	Pu	Am	Cm
$k_1(An^+)/ k_1(Np^+)$	1.28(1)	1.16(2)	0.885(8)	0.565(4)	0.65(2)
ref. [2]	1.3(9)	1.1(7)	0.4(3)	0.4(3)	0.5(4)
$k_2(An^+)/ k_2(Np^+)$	0.350(1)	1.533(8)	0.522(2)	0.00365(2)	—
ref. [3]	<0.004	1.6	0.25	<0.004	—

As discussed in the previous study regarding to gas phase reaction of lanthanoid or actinoid ions with O_2 gas [2], plotting k_1 against $E_P(6d^2)$, which is the energy difference between the ground state and the electronic state occupying two 6d electrons of An^+ reveals a negative correlation (Fig. 1). This indicates that the lower the $6d^2$ excited state of An^+ is, the higher the reactivity of An^+ with O_2 becomes. Thus, the 6d orbital of An^+ is thought to be involved in the An^+-O bonding. This interpretation was further supported by DFT calculations. Overlap population density of state analysis of An^+-O bonding qualitatively suggested that the 6d orbitals of An^+ contribute to the bonding interactions with oxygen.

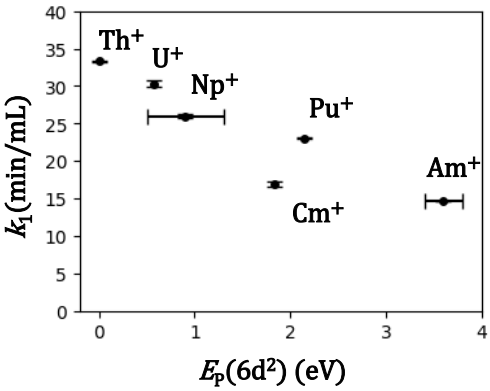


Fig. 1. Plotting of k_1 against $E_P(6d^2)$

4 CONCLUSIONS

We have studied the gas-phase reaction of An^+ with O_2 using ICP-MS/MS. By constructing a reaction model, the reaction constants k_1 and k_2 were successfully evaluated. The negative correlation of k_1 with $E_P(6d^2)$ suggests that the 6d orbital of An^+ is involved in the An^+-O bonding.

ACKNOWLEDGMENTS

This work was performed under the GIMRT Program of the International Research Center for Nuclear Materials Science, Institute for Materials Research, Tohoku University (Proposal No. 202312-IRKAC-0026).

This work was supported by JSPS KAKENHI Grant Number JP24K17634.

References

[1] H. KAZAMA. *et al.*, "Reaction of Np, Am, and Cm ions with CO_2 and O_2 in a reaction cell in triple quadrupole inductively coupled plasma mass spectrometry", *J. Anal. At. Spectrom.*, **38**, 1676 (2023)

[2] R. M. COX *et al.*, "Activation of CO_2 by Actinide Cations (Th^+, U^+, Pu^+, and Am^+) as studied by Guided Ion Beam and Triple Quadrupole Mass Spectrometry", *Inorg. Chem.* **61**, 8168 (2022)

[3] J. K. GIBSON and J. MARÇALO, "New developments in gas-phase actinide ion chemistry", *Coord. Chem. Rev.*, **250**, 776 (2006)

7th Asia-Pacific Symposium on Radiochemistry *September 14 ~ 19, 2025 • Kunibiki Messe • Shimane, Japan*

SOLVENT EXTRACTION OF TRIVALENT ACTINIDES AND LANTHANIDES WITH HIGH CONCENTRATIONS OF TRI-*N*-BUTYL PHOSPHATE AND NITRATE ION FROM HIGH-LEVEL RADIOACTIVE LIQUID WASTE USING MULTISTAGE CENTRIFUGAL CONTACTOR

Masaumi Nakahara[1], Yuichi Sano[2]

[1]*Japan Atomic Energy Agency: 4-33 Muramatsu Tokai-mura, Naka-gun, Ibaraki, 319-1194, and nakahara.masaumi@jaea.go.jp*
[2]*Japan Atomic Energy Agency: 4-33 Muramatsu Tokai-mura, Naka-gun, Ibaraki, 319-1194, and sano.yuichi@jaea.go.jp*

To recover minor actinides (MA) from high-level radioactive liquid waste, a hybrid MA recovery process combining solvent extraction and low-pressure loss extraction chromatography has been developed. In this study, the countercurrent experiment for trivalent actinides and lanthanides recovery in the solvent extraction process was performed with high-level radioactive liquid waste in the hot cell.

1. INTRODUCTION

Minor actinides (MA) such as Np, Am, and Cm are supposed to recover for reducing the volume and potential radiotoxicity of high-level radioactive liquid wastes in nuclear fuel reprocessing. Among MA, Np is co-extracted with U and Pu using tri-*n*-butyl phosphate (TBP) in the solvent extraction method [1]. On the other hand, Am and Cm are transferred to raffinate in the solvent extraction process. Various extractants such as *n*-octyl(phenyl)-*N,N*-diisobutylcarbamoylmethylphosphine oxide (CMPO) and bis(2-ethylhexyl) hydrogen phosphate (HDEHP) are developed to recover trivalent MA from the raffinate in the world [2,3]. Solvent extraction and extraction chromatography using CMPO and HDEHP as extractants have been generally studied for the MA recovery process. Japan Atomic Energy Agency (JAEA) proposed a novel hybrid MA recovery process combining solvent extraction and low-pressure loss extraction chromatography [4]. In the hybrid MA recovery process, MA and lanthanides are firstly recovered from raffinate by solvent extraction using higher TBP and NO_3^- concentrations than the Plutonium Uranium Reduction Extraction (PUREX) process. High TBP and NO_3^- concentrations increase the distribution ratios of MA and lanthanides in the HNO_3–TBP system. As the next step, MA is mutually separated from lanthanides by extraction chromatography with large SiO_2-based adsorbents to decrease the pressure loss in a column. The low-pressure loss enables the supply of liquid to the column by gravity.

In this study, countercurrent experiment was performed to evaluate the extraction behavior of Am and lanthanides from high-level radioactive liquid waste. In addition, the decontamination performance of the fission product (FP) was investigated. The experiment was conducted in a hot cell at the Chemical Processing Facility (CPF) in the Nuclear Fuel Cycle Engineering Laboratories in the JAEA.

2. EXPERIMENTAL

The feed solution composition was determined by reference to concentrated high-level radioactive liquid waste. A portion of the raffinate in the solvent extraction process using an irradiated fast reactor “Joyo” fuel is mixed with some reagents to adjust the concentration of FP. 50% TBP diluted *n*-dodecane was used as an extractant. The NO_3^- concentration was adjusted with $NaNO_3$.

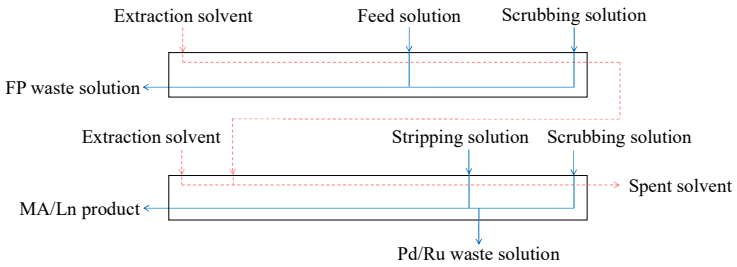


Fig. 1. Conceptual flowsheet for the solvent extraction process in the hybrid MA recovery process.

Copyright on 7th Asia-Pacific Symposium on Radiochemistry 2025

Figure 1 shows the flowsheet concept for the solvent extraction process in the hybrid MA recovery process. 16 stages of the centrifugal contactor was used as an extractor. Before supplying the feed solution, HNO_3 solutions and 50% TBP/*n*-dodecane were provided to fill the centrifugal contactor.

The H^+ concentration was analyzed with a titrator. The NO_3^- concentration was measured by ion chromatography. Nuclides were detected by gamma-ray spectrometry. The metal concentrations were analyzed by inductively coupled plasma atomic emission spectrometry.

3. RESULTS AND DISCUSSION

The reagents and feed solution containing radioactive materials were pumped to the centrifugal contactor, and the flow rate of the solutions was constant in the countercurrent experiment. The centrifugal contactor was stably operated during the experiment, and the aqueous phase entrainment was not observed in the organic phase outlet. ^{137}Cs was transferred to FP waste solution, and the decontamination factor of ^{137}Cs was over 10^3. Am and lanthanides were extracted into the loaded solvent. The leakages of ^{241}Am and ^{154}Eu to the FP waste solution were under the lower detection limit of gamma-ray spectroscopy, and ^{241}Am and ^{154}Eu with high TBP and NO_3^- concentrations were extracted using the raffinate derived from the irradiated fast reactor fuel in the hot cell.

4. CONCLUSIONS

The countercurrent experiment was carried out with high concentrations of TBP and NO_3^- to evaluate the extraction behavior of Am and lanthanides and the decontamination performance of FP in the solvent extraction process in the hybrid MA recovery process. The extraction of Am and lanthanides with high concentrations of TBP and NO_3^- was demonstrated with the high-level radioactive liquid waste derived from the irradiated fast reactor. Further investigation for optimizing the flowsheet should be required.

ACKNOWLEDGMENTS

This work was supported by the Ministry of Education, Culture, Sports, Science and Technology of Japan (MEXT) Innovative Nuclear Research and Development Program.

References

[1] M. NAKAHARA, Y. SANO, Y. KOMA, M. KAMIYA, A. SHIBATA, T. KOIZUMI and T. KOYAMA, "Separation of Actinide Elements by Solvent Extraction Using Centrifugal Contactors in the NEXT Process," *Journal of Nuclear Science and Technology*, **44**, 373 (2007).

[2] E. P. HORWITZ, D. G. KALINA, H. DIAMOND, G. F. VANDEGRIFT, and W. W. SCHULZ, "The TRUEX Process – A Process for the Extraction of the Transuranic Elements from Nitric Acid Wastes Utilizing Modified PUREX Solvent," *Solvent Extraction and Ion Exchange*, **3**, 75 (1985).

[3] B. WEAVER and F. A. KAPPELMANN, *Talspeak: A New Method of Separating Americium and Curium from the Lanthanides by Extraction from an Aqueous Solution of an Aminopolyacetic Acid Complex with a Monoacidic Organophosphate or Phosphonate*, ORNL-3559, Oak Ridge National Laboratory, Oak Ridge, Tennessee (1964).

[4] Y. SANO, A. SAKAMOTO, Y. MIYAZAKI, S. WATANABE, K. MORITA, T. EMORI, Y. BAN, T. ARAI, K. NAKATANI, H. MATSUURA and S. KUNII, "Hybrid Process Combining Solvent Extraction / Low Pressure Loss Extraction Chromatography for a Reasonable MA(III) recovery Process," *Proc. International Conference on Nuclear Fuel Cycle | New Nuclear Perspectives in the Energy Supply Crisis and Climate Emergency (GLOBAL 2022)*, Reims, France, July 6–8, 2022, No. 044, French Nuclear Society (2022).

Copyright on 7th Asia-Pacific Symposium on Radiochemistry 2025

7th Asia-Pacific Symposium on Radiochemistry *September 14 ~ 19, 2025 • Kunibiki Messe • Shimane, Japan*

SYNTHESIS AND REDOX PROPERTIES OF DINUCLEAR U(IV) COMPLEXES WITH SCHIFF BASE MULTIDENTATE LIGANDS

Nao Yoshida[1], Keisuke Morimoto[1], Kenji Shirasaki[2], Atsushi Shinohara[1], Takashi Yoshimura[2]

[1] *Department of Chemistry, Graduate School of Science, The University of Osaka: 1-1 Machikaneyama, Toyonaka, Osaka, 560-0043, Japan, and yoshidan@rirc.osaka-u.ac.jp*
[2] *Radioisotope Research Center, Institute for Radiation Sciences, The University of Osaka: 2-4 Yamadaoka, Suita, Osaka, 565-0871, Japan, and tyoshi@rirc.osaka-u.ac.jp*

In this work, we synthesized and characterized new dinuclear U(IV) complexes with three different substituents on the Schiff base ligands. The complexes showed two-step of one-electron redox processes attributed to U_2(IV,V)/U_2(IV,IV) and U_2(V,V)/U_2(IV,V).

1 INTRODUCTION

Electronic interactions between metal centers have been a focus of research for several decades and remain a topic of high importance. The interactions occur between two or more redox-active metal centers linked by a bridging ligand in chemically identical environments, a phenomenon that has been well studied in various metal complexes. The extent of the electronic interaction is generally influenced by the distance between the metal centers, the structure and conformation of the bridging ligand, and the coordination environment of the metal ion. As f-electrons are localized on the inner shells, electronic interactions between lanthanide ions are small, whereas valence electrons in actinides are known to extend to the outer shells. Therefore, the stronger electronic interactions are expected between the actinide centers. In this study, we have synthesized dinuclear U(IV) complexes and investigated the redox interactions between two uranium centers.

2 RESULTS AND DISCUSSION

The U(IV) dinuclear complexes **1**-**3** with both tetradentate Salophen^{Me} and tridentate ligands (Sap^{Me} **1**, Sap: **2**, and Sap^{Cl}: **3**) were synthesized by the reactions of UCl_4 with the ligands. The structures of the complexes **1** and **2** were determined by the single-crystal X-ray analysis. The two uranium ions are coordinated by Salophen^{Me} and tridentate ligands and are sandwiched by the two types of the ligands. In addition, the oxygen atoms of the adjacent sap-type ligands bridge two uranium ions to form the dinuclear U(IV) complexes. The uranium ions have an eight-coordinate distorted square antiprism geometry. The U-O and U-N bond distances are in the ranges of 2.203(2) − 2.443(1) Å and 2.634(2) − 2.556(2) Å, respectively.

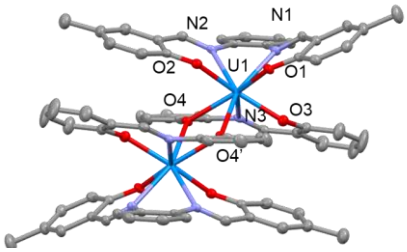


Fig. 1. The molecular structure of **2**.

The redox potentials of the complexes were determined by cyclic voltammetry in 0.1 M (n-$C_4H_9)_4NPF_6$-CH_2Cl_2. Two-step of one-electron redox waves were observed. The redox potentials are listed in Table 1. These redox processes are assignable to U_2(IV,V)/U_2(IV,IV) and U_2(V,V)/U_2(IV,V). The potentials are negative in the order of **1** < **2** < **3**. This indicates that the substituent on the sap influences the redox potentials of the U_2(IV,V)/U_2(IV,IV) and U_2(V,V)/U_2(IV,V) processes, and the potentials shift negative with the ligand bearing the stronger electron-donating ability of the substituents. The comproportionation constant (K_{com}) is derived from the equation (1), which represents the stability of the mixed valence state of the complex and the strength of the metal-metal interaction.

$$[U^{4+}, U^{4+}] + [U^{5+}, U^{5+}] \leftrightarrows 2[U^{4+}, U^{5+}]$$

$$K_{com} = \frac{[U^{4+}, U^{5+}]^2}{[U^{4+}, U^{4+}][U^{5+}, U^{5+}]} \quad \cdots (1)$$

The values of K_{com} are also shown in Table 1. The values of 10^6 indicate that there are electronic interactions between two uranium centers in the complexes. The K_{com} values are less dependent on the nature of the substituents on the sap ligands. Therefore, the substituent on the sap ligand is found to have less influenced on the electronic interaction between the uranium centers.

TABLE 1. The redox potentials and K_{com} values of **1**, **2**, and **3**

$E_{1/2}$ (V vs Fc^+/Fc)			K_{com}
	$U_2(IV,V)/U_2(IV,IV)$	$U_2(V,V)/U_2(IV,V)$	
1	−0.26	+0.12	2.7×10^6
2	−0.23	+0.16	4.0×10^6
3	−0.17	+0.20	1.8×10^6

3 CONCLUSION

The new dinuclear uranium (IV) complexes were synthesized and characterized. The two-step of one-electron redox processes were observed in all the new complexes. This indicates that the dinuclear uranium complex with Schiff base ligands exhibits electronic interactions between the uranium centers.

Copyright on 7th Asia-Pacific Symposium on Radiochemistry 2025 P-R3-08* -

7th Asia-Pacific Symposium on Radiochemistry *September 14 ~ 19, 2025 • Kunibiki Messe • Shimane, Japan*

Novel Continuous Decomposition Technology for Radioactive Organic Liquid Waste Based on a Modified Emulsion Flow Device

Takanori Hoshino[1], Yoichi Arai[2*], Sou Watanabe[3], Masahiro Nakamura[4], Hideya Suzuki[5] and Yasutoshi Ban[6]

[1] *Nuclear Fuel Cycle Engineering Laboratories, Japan Atomic Energy Agency 4-33, Muramatsu, Tokai-mura, Naka-gun Ibaraki 319-1194, Japan, hoshino.takanori@jaea.go.jp*
[2] *Nuclear Fuel Cycle Engineering Laboratories, Japan Atomic Energy Agency 4-33, Muramatsu, Tokai-mura, Naka-gun Ibaraki 319-1194, Japan, arai.yoichi@jaea.go.jp*
[3] *Nuclear Fuel Cycle Engineering Laboratories, Japan Atomic Energy Agency 4-33, Muramatsu, Tokai-mura, Naka-gun Ibaraki 319-1194, Japan, watanabe.sou@jaea.go.jp*
[4] *Nuclear Fuel Cycle Engineering Laboratories, Japan Atomic Energy Agency 4-33, Muramatsu, Tokai-mura, Naka-gun Ibaraki 319-1194, Japan, nakamura.masahiro22@jaea.go.jp*
[5] *Emulsion Flow Technologies Ltd., 7-5 Shirakata, Tokai-mura, Naka-gun, Ibaraki 319-1106 Japan, suzuki.hideya@emulsion-flow.tech*
[6] *Nuclear Science Research Institute, Japan Atomic Energy Agency 2-4 Shirakata, Tokai-mura, Naka-gun, Ibaraki 319-1195, Japan, ban.yasutoshi@jaea.go.jp*

In order to safely process organic solvents containing radioactive materials, a continuous degradation process using an emulsion flow device was investigated. It was found that circulating a nitric acid solution containing Ag^{2+} ions enables the degradation of PUREX and TEHDGA solvents.

1 Introduction

Radioactive liquid wastes are generated through various experiments and/or analyses in nuclear facilities. These liquid wastes containing both radioactive elements and chemical reagents have been stored in nuclear facilities due to a lack of efficient treatment procedures. The Japan Atomic Energy Agency (JAEA), in collaboration with several organizations, started the Systematic Treatment of RAdioactive Liquid Wastes for Decommissioning (STRAD) project to develop appropriate treatment procedures for such radioactive liquid waste [1]. Radioactive aqueous and organic liquid wastes, which contain radioactive materials, are generated through solvent extraction experiments on nuclear fuel materials. Treatment of liquid wastes generated from the reprocessing experiments is one of the important tasks of this project, and technologies to recover nuclear materials from aqueous and spent solvents have been developed. Our research team has successfully developed and utilized adsorbents incorporating iminodiacetic acid groups onto polymer-coated porous silica, along with fluorine-containing ligands, for the recovery of radionuclides from organic solvents [2-5]. After removing the nuclear fuel material from the solvent, volume reduction and stabilization treatment of the organic solvent is required. Although one of the promising treatment techniques for disposal of the spent solvent is solidification, complete mineralization of organic compounds is ideal.

To achieve complete mineralization of organic solvents, we initiated the development of decomposition technologies. We have devised a novel approach combining the oxidative reaction of Ag^{2+} with emulsion flow technology. Emulsion flow technology is a method of solvent extraction by mixing and separating organic and aqueous phases continuously in one vessel. In this study, we investigated the applicability of an emulsion flow technology that has been developed for efficient solvent extraction by mixing and separating an organic solvent and an aqueous solution continuously. To confirm the decomposition performance inside the emulsion flow apparatus, decomposition tests of the PUREX solvent (30% TBP in n-dodecane) and N,N,N',N'-tetra(2-ethylhexyl)diglycolamide (TEHDGA) were carried out, where Ag^{2+} ions were generated by electrolysis of Ag^{+} ions in $AgNO_3$ solution.

2. Experimental

The emulsion flow apparatus consists of a column in which an emulsion state is generated and pumps for supplying organic and aqueous solutions. The two phases are supplied into the column from opposite ends, and the counter-current forms an emulsion state inside the column. The supplied liquids go out from the column from different ends. A part of the organic compounds supplied into the column are decomposed inside the column, and residual organic compounds are discharged from the column. Thus, circulating an organic liquid and an aqueous solution containing Ag^{2+} is expected to achieve semi-continuous treatment. After a defined digestion period, the solution was sampled, and the concentrations of carbon and phosphorus were determined by Total Organic Carbon (TOC) and Inductively Coupled Plasma Atomic Emission Spectroscopy (ICP-AES), respectively. Furthermore, hydrophilic degradation products in the aqueous solution were investigated using Time of Flight Mass Spectrometry (TOF-MS).

3. Results and Discussion

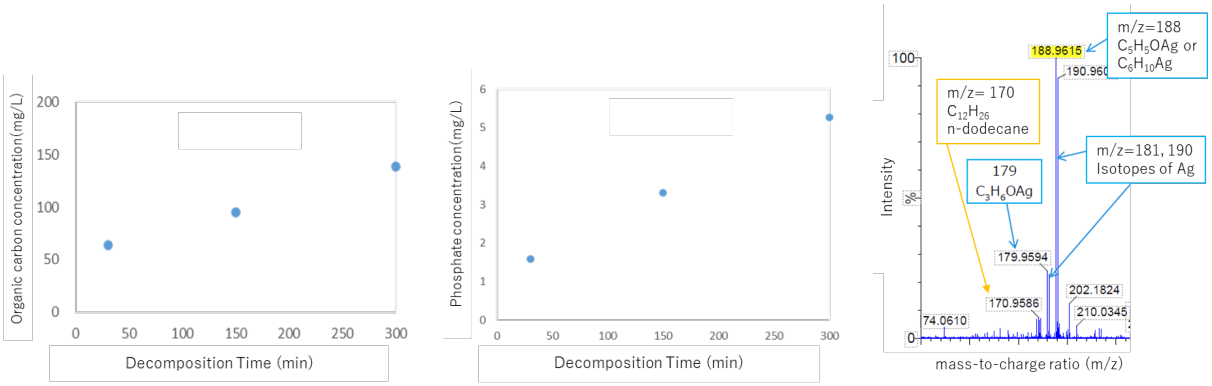
Copyright on 7th Asia-Pacific Symposium on Radiochemistry 2025

The ability of the emulsion flow device to degrade organic solvent was assessed by analyzing the degradation products present in the aqueous solution. The analytical results are shown in Fig. 1. The concentration of degradation products in the aqueous phase increased with time, indicating degradation of the organic solvent. The increase in phosphorus concentration in the aqueous solution after the decomposition test indicates that TBP has been transformed into water-soluble decomposition products and further into phosphate. In addition, analysis of the TOF-MS revealed intermediates such as C_3H_6OAg, which are thought to be formed by an oxidation reaction with Ag^{2+} during the decomposition of n-dodecane. The use of an emulsion flow device demonstrated the feasibility of continuous Ag^{2+} decomposition, suggesting the applicability of this technology to the treatment of organic liquid wastes. The reaction equations for the complete oxidation and mineralization of n-dodecane and TBP are known as equations (1) and (2), respectively [6]. It is speculated that the decomposition reaction of TEHDGA proceeds according to equation (3).

$$CH_3(CH_2)_{10}CH_3 + 74Ag^{2+} + 24H_2O \rightarrow 12CO_2 + 74Ag^{+} + 74H^{+} \quad (1)$$

$$(C_4H_9)_3PO_4 + 72Ag^{2+} + 24H_2O \rightarrow 12CO_2 + H_3PO_4 + 72Ag^{+} + 72H^{+} \quad (2)$$

$$C_{36}H_{72}N_2O_3 + 210Ag^{2+} + 69H_2O \rightarrow 36CO_2 + 210Ag^{+} + 210H^{+} \quad (3)$$



(a) (b) (c)

Fig. 1. Results of analysis of aqueous solutions after degradation tests.
(a) TOC analysis after PUREX solvent decomposition (b) ICP-AES analysis after PUREX solvent decomposition (c) Mass analysis after n-dodecane decomposition

4. CONCLUSIONS

This study demonstrates that employing an emulsion flow device enables the continuous degradation of organic solvents via silver oxidation. However, further improvements in the apparatus are essential for practical application. The presentation will detail the performance evaluation of the improved emulsion flow device and the performance of the device when processing simulated radioactive liquid waste.

ACKNOWLEDGMENTS

The authors are grateful to Ms. Christian Tabak Leela and Mr. Toshihiro Iwamoto of JAEA, Mr. Masahiro Sekikawa and Mr. Shuichi Shoji of Inspection Development Company Ltd. in Japan for their cooperation in tests and analyses.

References

[1] S. Watanabe, H. Ogi, Y. Arai, H. Aihara, Y. Takahatake, A. Shibata, K. Nomura, Y. Kamiya, N. Asanuma, H. Matsuura, T. Kubota, N. Seko, T. Arai, T. Moriguchi, "STRAD project for systematic treatments of radioactive liquid wastes generated in nuclear facilities," *Progress Nuclear Energy*, **117**, 103090 (2019).
[2] Y. Arai, S. Watanabe, T. Kubota, K. Nomura, "Radioactive nuclides recovery from spent solvent in STRAD project (1) Zr recovered by alkaline solutions," Proc. DEM-2018, Oct. 22-24, 2018, Avignon, France, 206, (2018).
[3] F. Nakamura, R. Abe, T. Arai, N. Seko, H. Hoshina, Y. Arai, S. Watanabe, K. Nomura, "Radioactive nuclides recovery from spent solvent in STRAD project (2) Zr adsorption onto ion exchange resins," Proc. DEM-2018, Oct. 22-24, 2018, Avignon, France, 195, (2018).
[4] Y. Arai, S. Watanabe, S. Ohno, K. Nomura, F. Nakamura, T. Arai, N. Seko, H. Hoshina, N. Hagura, T. Kubota, "Microscopic analyses on Zr adsorbed IDA chelating resin by PIXE and EXAFS," Nuclear Instruments and Methods in Physics Research Section B: Beam Interactions with Materials and Atoms, 477, 54-59 (2020).
[5] Y. Arai, S. Watanabe, S. Ohno, M. Nakamura, A. Shibata, F. Nakamura, T. Arai, N. Seko, H. Hoshina, N. Hagura, T. Kubota, "Analysis on adsorbent for spent solvent treatment by micro-PIXE and EXAFS," International Journal of PIXE, 29[01n02], 17-31, (2019).
[6] F. Kobayashi, J. Ishii, K. Shirahashi, M. Umeda, K. Sakuraba, "Basic Study on the Mineralization of Organic Solvents by the Silver Mediated Electrochemical Oxidation Process with the Ultrasound Agitation," Japan Atomic Energy Agency, JAEA-Technology 2009-056, (2009). [in Japanese].

7th Asia-Pacific Symposium on Radiochemistry *September 14 ~ 19, 2025 • Kunibiki Messe • Shimane, Japan*

EFFECT OF SUBSTITUENTS ON THE SOLVENT EXTRACTION OF LANTHANIDES USING DIGLYCOLAMIDE LIGANDS

Kenta Mori[1], Hiroyuki Kazama[1], Masashi Kaneko[1], Ruilin Wang[1], Yudai Itakura[1], Miyu Konno[1], Enni Khult[1], Kyosuke Shibamoto[1], Ryota Kikuchi[1], Kazushi Kawamoto[1], Yoshitaka Kasamatsu[1].

[1]*Graduate School of Science, The University of Osaka: 1-1 Machikaneyama, Toyonaka, Osaka 560-0043, Japan, morik24@chem.sci.osaka-u.ac.jp*

We synthesized the novel diglycolamide (DGA) ligand with a trifluoromethyl group, which functions as electron-withdrawing substituent. The separation mechanism was investigated through solvent extraction experiments with lanthanides, combined with DFT calculations. The distribution ratios obtained from solvent extraction experiments were compared with those obtained with the unsubstituted DGA, and a clear difference was observed. In addition, the structures of the extracted chemical species were optimized by DFT calculations, and there is no difference in structure between the two complexes.

1. INTRODUTION

Spent nuclear fuel and high-level radioactive liquid waste (HLLW) generated from nuclear energy systems contain a variety of metals. The separation and recovery of these metals are important not only for the reuse of resources, but also for reducing the radiotoxicity and volume of the remaining waste. However, the main metal ions; lanthanides (Ln), americium (Am), and curium (Cm), all stably exist as trivalent ions in aqueous solutions, and their chemical properties are very similar, making them difficult to separate from each other. Solvent extraction is mainly used for the separation of metal ions in HLLW, and various ligands have been developed so far. In particular, diglycolamide (DGA) has been widely used in the nuclear power field as an excellent extractant for recovery and mutual separation of Ln, Am, and Cm [1]. However, the details of the factors governing selectivity remain to be fully investigated [2]. DGAs are synthetically accessible, and the molecular framework can be modified to incorporate different substituents for tuning its coordination properties. Therefore, in this study, we synthesized a new DGA ligand in which a trifluoromethyl group was introduced into the phenyl ring. Solvent extraction experiments were conducted with lanthanides using this ligand. The distribution ratios (*D*) were compared with those obtained using the unsubstituted DGA ligand; *N*,*N*'-dimethyl-*N*,*N*'-diphenyl-diglycolamide (DMDPhDGA) (Fig. 1) [3], to investigate the effect of the substituent on extraction efficiency.

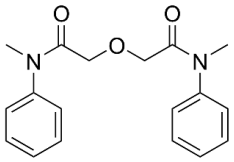


Fig. 1. The structure of DMDPhDGA.

2. EXPERIMENT

DMDPhDGA having methyl and phenyl group in the side chain of the amide parts and CF_3DMDPhDGA which is a novel DGA having a trifluoromethyl group in the phenyl moiety were synthesized following the scheme shown in Fig. 2. The products were identified by ^{1}H NMR and elemental analysis. The aqueous phase containing ^{152}Eu in 4 M HNO_3 and the organic phase containing the DGA ligands in chloroform were shaken for several minutes, and the *D* values were determined by γ-ray measurement. ICP-MS was also used to determine the *D* values using stable lanthanide isotopes. The extracted species were assumed to be complexes with three DGA ligands coordinated with the metal, and the structures were optimized using DFT calculations. Then, the complexation energy was calculated by single point calculation.

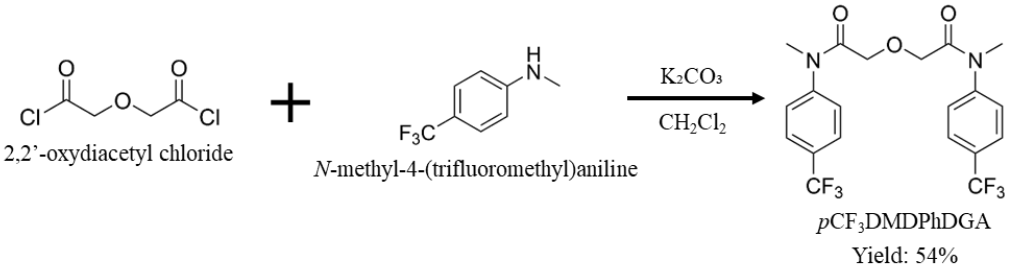


Fig. 2. The scheme of synthesis of *p*CF_3DMDPhDGA.

3. RESULTS AND DISCUSSION

The new ligands were successfully synthesized at high purity. In the extraction using *p*CF_3DMDPhDGA, the time dependence of the *D* values was constant after approximately 10 minutes of shaking, indicating that equilibrium of extract reactions was reached (Fig. 3). The *D* values obtained with *p*CF_3DMDPhDGA were slightly different from those obtained with DMDPhDGA. The structures of the model complexes for both ligands optimized by DFT calculation were similar to each other, suggesting that the factors other than the structures affect the difference in the *D* values. The presentation will also discuss the thermodynamic stability of the extracted species.

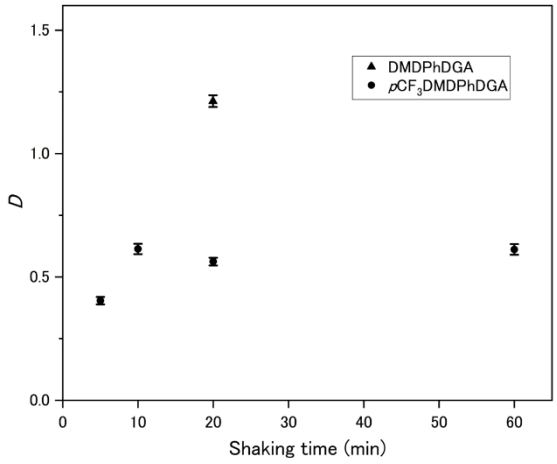


Fig. 3. The distribution ratios in the extraction with DMDPhDGA (triangle, n=3) and *p*CF_3DMDPhDGA (circle, n=1). Organic phase is 0.05 M DGA in chloroform and aqueous phase is 4 M HNO_3.

4. CONCLUSIONS

A new DGA ligand, CF_3DMDPhDGA was successfully synthesized and the extraction performance was compared with that of unsubstituted analogue, DMDPhDGA. A clear difference in the *D* values of ^{152}Eu using the two ligands was observed. The optimized structures of the extracted species derived by the DFT calculation were similar for these complexes. This study provides clues to reveal the DGA separation mechanism of Ln.

ACKNOWLEDGMENTS

The ^{1}H NMR, XRD and elemental analysis measurements were performed at the Analytical Instrument Facility, Graduate School of Science, The University of Osaka.

References

[1] Y. BAN *et al.*, “Extraction of Trivalent Rare Earths and Minor Actinides from Nitric Acid with N,N,N’,N’ Tetradodecyldiglycolamide (TDdDGA) by Using Mixer-Settler Extractors in a Hot Cell”, *Solvent Extr. Ion Exch.*, **37**, 27-37 (2019).
[2] M. KANEKO *et al.*, “Theoretical Elucidation of Am(III)/Cm(III) Separation Mechanism with Diamide-type Ligands Using Relativistic Density Functional Theory Calculation”, *Inorg. Chem.*, **57**, 14513-14523 (2018).
[3] H. NARITA *et al*., “Solvent Extraction of Trivalent Lanthanoid Ions with N,N’-Dimethyl-N,N’-Diphenyl-3-Oxapentanediamide”, *Radiochim. Acta*, **81**, 223-226 (1998).

7th Asia-Pacific Symposium on Radiochemistry *September 14 ~ 19, 2025 • Kunibiki Messe • Shimane, Japan*

DFT STUDY OF SUBSTITUENT EFFECT ON MA/Ln SEPARATION USING BTPHEN-TYPE LIGANDS

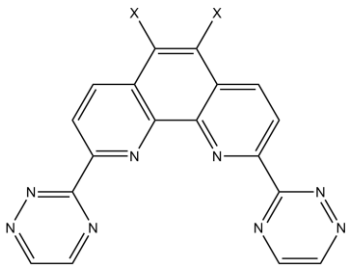
Yuto FUKASAWA[1], Satoru NAKASHIMA[1,2]

[1] *Chemistry Program, Graduate School of Advanced Science and Engineering, Hiroshima University, 1-3-1 Kagamiyama, Higashi-Hiroshima, Hiroshima 739-8526, Japan. E-mail: yupon.hydroxide@gmail.com*
[2] *Natural Science Center for Basic Research and Development (N-BARD), Hiroshima University, 1-4-2 Kagamiyama, Higashi-Hiroshima, Hiroshima 739-8526, Japan. E-mail: snaka@hiroshima-u.ac.jp*

BTPhen ligand shows useful minor actinide separation from lanthanide for solvent extraction. To know the effect of substituent on extraction and separation, we performed analysis using computational chemistry method for the BTPhen-type ligands with various types of substituents (X = F, CN, CH_3, NH_2), which have different electron donating/withdrawing effect toward the ligand. When an electron-withdrawing group was introduced, the selectivity was improved due to the difference in the destabilization between the Eu and Am complexes. When an electron-donating group was introduced, the selectivity was also improved due to the difference in the stabilization between the Eu and Am complexes. The introduction of NH_2 substituent with withdrawing inductive effect and much donating resonance effect suggested the best distribution coefficient from the water phase to organic phase and the best Am selectivity.

1 INTRODUCTION

The liquid waste generated from the reprocessing of spent nuclear fuel (SNF) came from nuclear power plant, called high-level liquid waste (HLLW), contains minor actinides (MA). MAs are nuclides with high radiation toxicity and long radioactive half-lives, which becomes the reason for the extended storage period of the HLLW. The partitioning and transmutation (P&T) strategy has been proposed to deal with MA elements, thereby changing the MAs to short-lived or stable nuclides and then reducing the risk of HLLW. However, before the P&T process, the lanthanide elements must be separated from the HLLW, because lanthanide elements have a large neutron capture cross section. The separation is challenge due to the similar chemical properties between lanthanides and MAs. Therefore, a lot of research has been conducted to selectively remove only MA from HLLW by solvent extraction. The separation factor was explained from hard and soft character of the coordinating element [1,2]. In the study of solvent extraction, various types of organic ligands called extractants have been developed, and among them, extractants with 2,9-bis(1,3,4-triazinyl)-1,10-phenanthroline (BTPhen, Scheme 1) as the basic skeleton have been shown to exhibit high MA extraction and separation abilities. A previous study [3] reported that the extraction ability was further improved by replacing the hydrogen at the 5- and 6- positions of the phenanthroline ring of the BTPhen with bromine. It was also shown that the Am selectivity was improved as the number of bromine substitutions increased [3]. The effect of bromine was explained using DFT calculation [4]. In addition, when halogens (F, Cl, I) other than bromine were substituted in the DFT calculation, it was suggested that the electronic state of the extractant was affected and then the separation factor was improved by the F substituent [4]. In the present study, to further investigate the effect of the substituent on extraction and separation, we performed analysis using computational chemistry method for the cases where various types of substituents (X = F, CN, CH_3, NH_2) having different electron donating/withdrawing effect toward the ligand were introduced.



Scheme 1 X_2BTPhen (X = H, F, CN, CH_3, NH_2) without side chain.

2 METHOD

All calculation processes were performed using the DFT calculation program ORCA (ver. 4.1.0). The calculation model was created based on the crystal structure of the complex formed by the BTPhen-type ligand and lanthanide recorded in the crystal structure database (CSD). The side chain was removed from BTPhen for the computational cost. Americium (Am^{3+}), a representative MA, and europium (Eu^{3+}), a lanthanide of the same group with Am, were used to evaluate the separation ability. The relativistic effect was considered using ZORA-SARC, and the functional BP86/SVP was applied for the structure optimization calculation and the functional B2PLYP/TZVP was applied for the single-point energy calculation. The Gibbs energy of complex formation was calculated from the results of the energy calculation. Bond critical point (BCP) analysis and natural population analysis (NPA) were also performed.

3 RESULTS AND DISCUSSION

Table 1 summarizes the substituent effect. Donating/withdrawing of electrons via σ-bonds is caused by a difference in electronegativity (inductive effect). Donating/withdrawing of electron via π-bonds is caused by resonance of lone-pair electrons to π-bonds (resonance effect).

Copyright on 7th Asia-Pacific Symposium on Radiochemistry 2025

Table 1. Electronic character of substituent to the aromatic ring

	Halogen (-F)	Cyano (-CN)	Methyl (-CH_3)	Amino (-NH_2)
Inductive effect	Much withdrawing	Withdrawing	Donating	Withdrawing
Resonance effect	Donating	Withdrawing	Donating	Much donating

$[M(H_2O)_9]^{3+}$ combines with the BTPhen ligand and the obtained complex is extracted to organic phase as is shown in (1). The change of Gibbs free energy is shown in eq. (2). The Am selectivity is evaluated by $\Delta\Delta G$ in eq. (3)

$$[M(H_2O)_9]^{3+} + X_2BTPhen + 3\ NO_3^- \rightarrow 9\ H_2O + [M(X_2BTPhen)(NO_3^-)_3] \cdots (1)$$

$$\Delta G(M)(X) = \{9G(\ H_2O\ ) + G(\ [M(X_2BTPhen)(NO_3^-)_3]\ )\ \} - \{G(\ [M(H_2O)_9]^{3+}\ ) + G(X_2BTPhen\ ) + 3G(\ NO_3^-)\ \} \cdots (2)$$

$$\Delta\Delta G = \Delta G(Am) - \Delta G(Eu) \cdots (3)$$

Table 2. Complex formation Gibbs energy

Ligand	ΔG / kJ mol^{-1}		ΔΔG kJ mol^{-1}
	Eu	Am	
X = H	-30.8	-39.1	-8.3
X = F	-20.5	-31.1	-10.5
X = CN	-13.3	-23.2	-9.9
X = CH_3	-35.3	-44.5	-9.2
X = NH_2	-32.3	-47.7	-15.4

Table 2 shows the results from complexation Gibbs energy analysis. Regardless of its metal center, for the cases of X = F or CN, the ΔG values move to the positive direction compared with X = H. Eu complexes moved to the more positive direction than Am complexes. The results suggest that the substitution with F and CN makes less stable complex with Am and Eu. On the other hand, the ΔG values for X = CH_3 and NH_2 moved to the negative direction compared with X = H. Am complexes moved to the more negative direction than Eu complexes. The results suggest that substitution by CH_3 and NH_2 makes more stable complex with Am and Eu. $\Delta\Delta G$ values indicated that all substituted cases show higher selectivity than X = H. Obviously higher selectivity was shown for X = NH_2.

From the BCP analysis, the electron density at BCP (ρ_{BCP}) of Am complexes were larger than those of Eu complexes for all ligands, suggesting that all the present ligands show Am selectivity. Regardless of the metal center, the ρ_{BCP} values became smaller for X = F and CN cases, while the values became larger for CH_3 and NH_2 cases. From the ρ_{BCP} values between Am and Eu complexes ($\Delta\rho_{BCP}$), substituted cases indicate larger values than X = H case. $\Delta\rho_{BCP}$ results corresponded to the results from energy calculation.

The natural electron population (ρ_{atom}) values of Am were systematically larger than those of Eu independent of the substituent. This also suggests the Am selectivity of BTPhen-type ligands. The ρ_{atom}(Eu) values became larger for X = F and NH_2 than X = H, while the values became smaller for X = CN and CH_3. The F and NH_2 group show electron withdrawing inductive effect and electron donating resonance effect.

From MOOP diagrams, bonding contribution between metal d-orbital and donor atom is observed at -5 to -15 eV region and the bonding contribution seems to be highest for X = NH_2 and lowest for X = CN. The anti-bonding contribution is also observed at -15 to -20 eV region, and the anti-bonding contribution obviously decrease for X = NH_2 while almost no change was observed for the other cases compared to X = H. Concerning the contribution of metal f-orbital and donor atom, for M = Eu, anti-bonding contribution was only found at -10 to -20 eV region. The anti-bonding contribution became smallest for X = NH_2 and largest for X = CN. On the other hand, for M = Am case, there are bonding and anti-bonding contribution. Relatively larger bonding contribution was observed for X = NH_2, while almost no change was found for anti-bonding contribution. These results suggest the relation between MOOP diagrams and energy calculation, that is, X = NH_2 complex showing largest bonding affinity in MOOP diagram forms the most stable complex as is suggested from the complexation Gibbs energy calculation.

4 Conclusion

The substitution effect on the Am/Eu separation using BTPhen ligand was studied. When an electron-withdrawing group was introduced, the selectivity was improved due to the difference in the destabilization of the Eu and Am complexes, while when an electron-donating group was introduced, the selectivity was also improved due to the difference in the stabilization of the Eu and Am complexes. The NH_2 substituent with withdrawing inductive effect and much donating resonance effect is the best substituent for the Am selectivity.

References

[1] M. Kaneko, S. Miyashita, and S. Nakashima, *Inorg. Chem.*, **54**, 7103-7109 (2015).
[2] T. Kimura, M. Kaneko, M. Watanabe, S. Miyashita, and S. Nakashima, *Dalton Trans.*, **47**, 14924-14931 (2018).
[3] A. Aster, D. M. Laventine, L. M. Harwood, M. J. Hudson, and A. Geist, *Chem. Commun.*, **49**, 8534-8536 (2013).
[4] Y. Fukasawa and S. Nakashima, *RSC Advances*, **13**, 2476-2482 (2023).

7th Asia-Pacific Symposium on Radiochemistry *September 14 ~ 19, 2025 • Kunibiki Messe • Shimane, Japan*

Dissolution Behavior of UTi_2O_6 Solid Phase in Aqueous Media

Takuma KOYAMA[1], Daisuke AKIYAMA[2], Akira KIRISHIMA[2], Taishi KOBAYASHI[1], Takayuki SASAKI[1,*]

[1] *Department of Nuclear Engineering, Kyoto University, Kyoto Daigaku-Katsura, Nishikyo, Kyoto, 615-8540, Japan, sasaki.takayuki.2a@kyoto-u.ac.jp*
[2] *Institute of Multidisciplinary Research for Advanced Materials, Tohoku University, 1-1 Katahira, Aoba, Sendai, 980-8577, Japan*

The chemically diverse fuel debris at Fukushima Daiichi NPS presents unprecedented challenges for long-term disposal, and conventional waste forms such as cement and vitrified glass are unlikely to deal with this complexity. We synthesized uranium titanate (UTi_2O_6, brannerite) via a low-temperature mechanochemical treatment, and examined its leaching behavior in acidic solutions. UTi_2O_6 dissolved far less uranium than UO_2, owing to a stable Ti-containing lattice and the formation of amorphous Ti hydroxide shielding layer on the surface. These results highlight mechanochemically produced UTi_2O_6 as a durable, corrosion-resistant waste form for 1F debris.

1. Introduction

The hydrogen explosions and core meltdowns at Fukushima Daiichi Nuclear Power Station (1F) produced vast quantities of highly radioactive fuel debris, adding unprecedented complexity to nuclear waste inventory in Japan. Conventional treatment pathways—cementation for low-level solids and vitrification for high-level wastes—are not readily adaptable to the chemical heterogeneity and radioactivity levels of these mixed debris forms. As utilities prepare for fuel-debris retrieval and disposal, additional waste-form options would be needed to ensure long-term containment and disposal.

Titanium-based matrices have emerged as a promising candidate [1-3]: titanium is known to coexist with uranium in natural ores and synthetic "synroc" analogues, exhibits low aqueous solubility, and forms corrosion-resistant crystallinity capable of incorporating radionuclides. However conventional titanate synthesis typically requires prolonged high temperature processing and risks losing volatile fission products during titanate formation. Therefore, this study aimed to develop and evaluate a lower-temperature mechanochemical synthesis method for uranium titanate (UTi_2O_6) [4], and to assess its suitability as a durable waste form for uranium in heterogeneous fuel debris.

2. Experimental

U_3O_8 powder was reduced to UO_2 by heating at 1000°C for 6 h in an Ar–10% H_2 atmosphere. In the mechanochemical process, stoichiometric UO_2 and TiO_2 mixtures were milled under Ar in a planetary ball mill. Then, the mixture was pressed into 7 × 10 mm pellets, and heat-treated at 1300°C in Ar to yield phase-UTi_2O_6. The XRD patterns of the prepared samples were obtained using an X-ray diffractometer. The microstructure and elemental composition of samples were evaluated using SEM instrument equipped with EDX apparatus. BET surface-area analyzer was used to measure surface area and pore size distribution of solids.

Solid-phase titanium uranate samples were immersed in solutions (Fig. 1). Batch leaching tests were carried out at 25 °C under ambient pressure in 0.1 M $NaClO_4$ over a pH range of 1.0 to 4.0, adjusted in 0.25-unit increments. Solid-to-liquid ratios, pH, and ionic strength were optimized based on prior dissolution and kinetics data. At defined time points a 0.5 mL aliquot of each immersion medium was pipetted for pH measurement and passed through a 0.45 µm PTFE syringe filter to remove particulates. At those same time points, an additional 0.5 mL aliquot was pipetted and subjected to ultrafiltration (3 kDa MWCO) by centrifugation at 13,000 rpm for 20 minutes. All filtrates were then analyzed by ICP-MS (using indium and bismuth as internal standards) to quantify the uranium and titanium species dissolved into solutions.

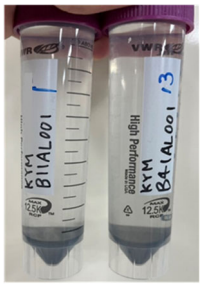


Fig. 1 UTi_2O_6 powder samples for leaching tests

3. Results and Discussion

Fig. 2 shows that XRD confirmed the quantitative formation of the UTi_2O_6 phase, while SEM-EDX mapping revealed a uniform distribution of uranium and titanium with no segregation. In the pH 1 leaching test, the dissolved Ti:U atomic ratio was 2:1— consistent with the stoichiometry of UTi_2O_6 (Fig. 3). As pH increased, however, titanium concentration dropped significantly compared to uranium, and UTi_2O_6 released far less uranium than UO_2 controls [5]. These results demonstrate that the UTi_2O_6 lattice effectively inhibits the oxidation of U(IV) to the more soluble U(VI). Moreover, surface hydrolysis of Ti(IV) likely produces an amorphous $Ti(OH)_4$ that "chemically armors" against uranium oxidation and leaching. Together, these findings highlight mechanochemically synthesized UTi_2O_6 as a corrosion-resistant waste form for the heterogeneous debris expected from 1F. Future work will examine its stability under reducing, deep-groundwater conditions and assess the impact of iron and zirconium impurities typical of real fuel-debris compositions.

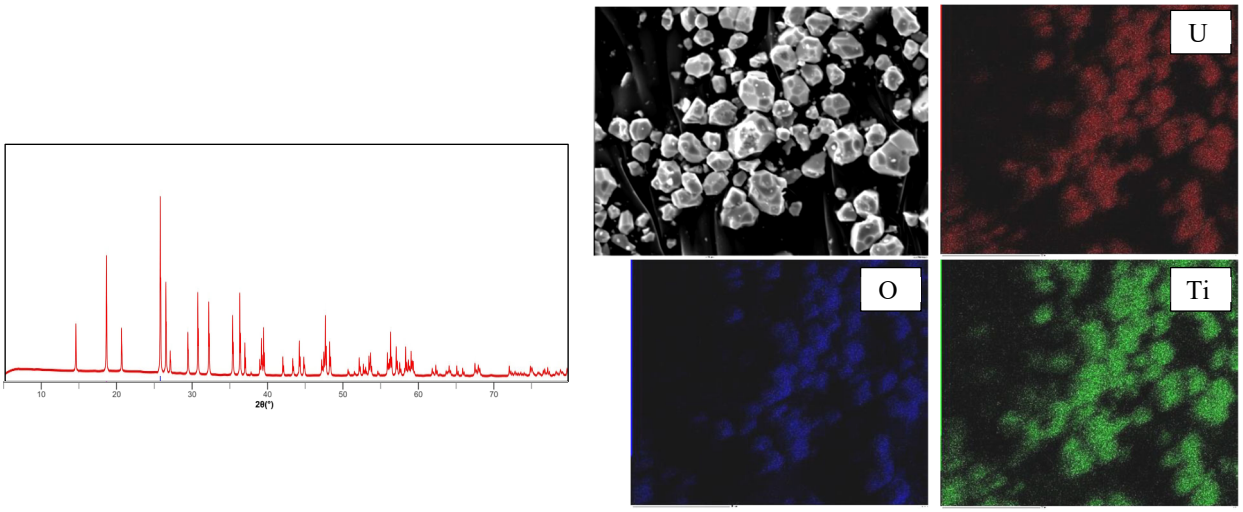


Fig. 2 XRD pattern, and SEM-EDX analysis of uranium titanate: top-left, SEM micrograph; top-right, uranium (U) elemental map; bottom-left, oxygen (O) map; bottom-right, titanium (Ti) map.

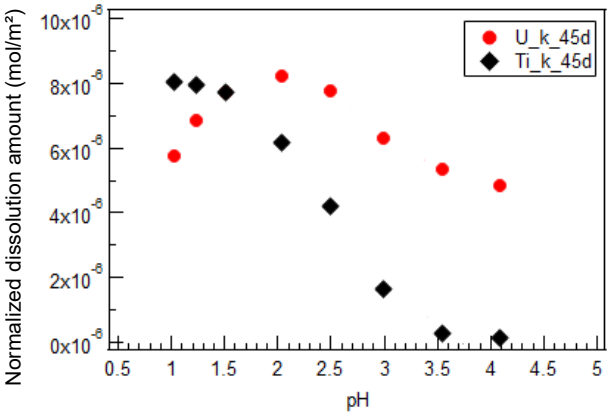


Fig. 3 pH dependence of the normalized dissolution amounts of uranium and titanium after a 45-day immersion of UTi_2O_6.

Acknowledgments
This work was supported by JAEA Nuclear Energy S&T and Human Resource Development Project Grant Number JPJA24H24020125.

References

[1] S.V. Yudintsev, S.V. Stefanovsky, M.S. Nikol'skii, O.I. Stefanovskaya, B.S. Nikonov. Brannerite, UTi_2O_6: Crystal Chemistry, Synthesis, Properties, and Use for Actinide Waste Immobilization, Radiochemistry (New York, N.Y.), Vol. 58, pp. 333-348 (2016).
[2] F.A. Charalambous, R. Ram, M. I. Pownceby, J. Tardio, S. K. Bhargava. Chemical and microstructural characterization studies on natural and heat treated brannerite samples, Minerals Engineering, Vol. 39, pp. 276–288, (2012)
[3] Y. Zhang, G. R. Lumpkin, H. Li, M. G. Blackford, M. Colella, M. L. Carter, et al, Recrystallisation of amorphous natural brannerite through annealing: The effect of radiation damage on the chemical durability of brannerite, Journal of Nuclear Materials, Vol. 350, pp. 293–300 (2006).
[4] D. Akiyama, T. Mishima, Y. Okamoto, A. Kirishima, Dry synthesis of brannerite (UTi_2O_6) by mechanochemical treatment, High temperature materials and processes, Vol. 42, pp. 172-176, (2023).
[5] R. Tonna, T. Sasaki, Y. Okamoto, T. Kobayashi, Interpretation of dissolution behavior at the surface of uranium-zirconium oxide solid solutions, Journal of Nuclear Materials, Vol. 612, 155820 (2025).

7th Asia-Pacific Symposium on Radiochemistry *September 14 ~ 19, 2025 • Kunibiki Messe • Shimane, Japan*

Enhanced Uranium Adsorption via Sulfonation of Polyether Ether Ketone

Song Yiuxin[1], Liu Peng[*2]

[1]*Affiliation Information: Yantai Research Institute and Graduate School, Harbin Engineering University, Yantai 264006, China*

[2]*College of Nuclear Science and Technology, Harbin Engineering University, Harbin 150001, China*

[*] Corresponding Author：liup@hrbeu.edu.com

Copyright on 7th Asia-Pacific Symposium on Radiochemistry 2025 P-R3-13* -

Polyetheretherketone (PEEK) features excellent chemical stability, irradiation stability and mechanical strength, making it an ideal engineering plastic. However, its adsorption capacity under acidic conditions is limited.To solve this problem, we sulfonated PEEK with concentrated sulfuric acid and introduced sulfonic acid groups to synthesize sulfonated polyetheretherketone (SPEEK). The adsorption mechanism of uranium by SPEEK includes electrostatic attraction and adsorption to the surface of SPEEK through the interaction between uranyl ions in the solution and O atoms on sulfonic acid groups. The grafting of sulfonic acid groups significantly improved the adsorption performance of SPEEK in acidic environments, broadening its applicability for the treatment of radioactive wastewater.

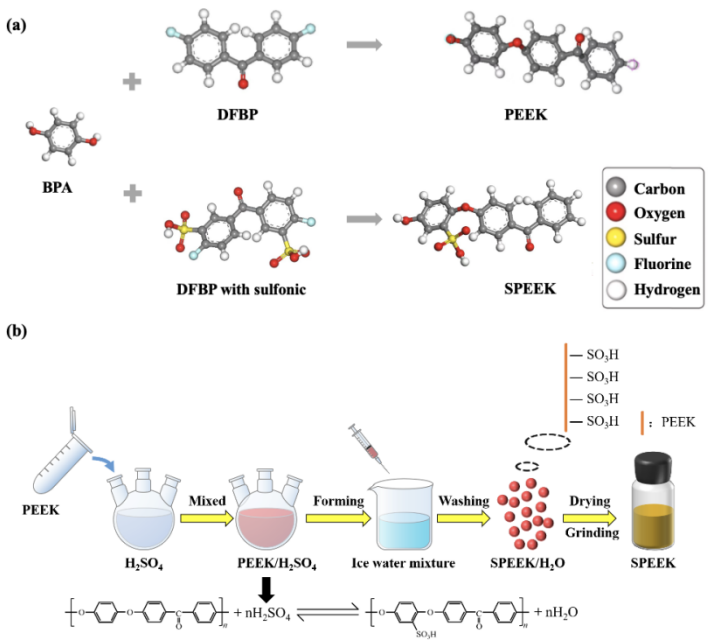


Fig. 1.(a) The atomic models of PEEK, SPEEK ;(b) Synthesis process of sulfonated polyether ether ketone.

1 Experimental Methods

A full characterization of the material was done by Fourier transform infrared spectroscopy, X-ray diffraction, scanning electron microscopy, thermogravimetric analysis, and X-ray photoelectron spectroscopy. In this work, a SPEEK material was prepared by post-sulfonation and its adsorption properties were evaluated (Fig. 1). This was done by varying the sulfonation temperature (50-90 °C), sulfonation time (2-8 h), and molecular weight of the polymer. The results were fitted to the pseudo-second order and Langmuir isotherm equations, respectively, and FT-IR, SEM, and XPS analyses were used to verify the mechanisms. Batch experiments were used to determine the effects of pH, adsorbent dose, contact time, ionic strength, temperature, initial uranium concentration, and competing ions.

2 Results

The adsorption followed the monolayer chemisorption process (R^2>0.99) with a spontaneous (G_0) and endothermic (ΔH=+28.4 kJ/mol) characteristic. The sulfonation temperature was found to be the main influencing factor in the adsorption performance of SPEEK. At an optimum temperature of 50 °C and 4 h, the PEEK exhibited a remarkable adsorption capacity of 181 mg/g at 298.15 K, exceeding 85% of the reported uranium adsorbents. "More than 80 percent of the heavy metals were removed by the method of adsorption at a pH of 2; and more than 97 percent at a pH of more than 3".

In conclusion, the sulfonation modification can effectively inhibit interparticle agglomeration and improve the adsorption performance of SPEEK.The high adsorption capacity (181.76 mg/g) and fast kinetics of SPEEK (enhanced uranium sorption within 120 min) provide a new strategy for the design of high-performance uranium adsorbents, which has great potential for application in nuclear wastewater treatment and uranium resource recovery.

Keywords: Sulfonated Polyether Ether Ketone (SPEEK)；Uranium Adsorption；Radioactive Wastewater Treatment

7th Asia-Pacific Symposium on Radiochemistry September 14 ~ 19, 2025 • Kunibiki Messe • Shimane, Japan

Estimation of tritium amount in activated charcoal by the soaking and burning method

Nakada Miki[1], Iwata Chie[2], Tanaka Masahiro[3]

[1]*National Institute for Fusion Science: 322-6 Oroshi-cho, Toki-shi, Gifu, 509-5292, nakada.miki@nifs.ac.jp*
[2] *National Institute for Fusion Science: 322-6 Oroshi-cho, Toki-shi, Gifu, 509-5292, iwata.chie@nifs.ac.jp*
[3] *National Institute for Fusion Science: 322-6 Oroshi-cho, Toki-shi, Gifu, 509-5292, tanaka.masahiro@nifs.ac.jp*

The soaking method for the tritium analysis in activated charcoal used in the cryosorption pump of a fusion test device was proposed. To determine the extraction efficiency of the soaking method, the amount of tritium in the sample after the soaking evaluation was evaluated using the combustion method. As a result, the extraction efficiency was found to be approximately 55 percent. However, the extraction rate of some samples was low at approximately 13 percent.

1 Introduction

Various research and much effort are being conducted for the realization of a fusion reactor. First generation fusion reactors use the fusion reaction between deuterium and tritium. Here, tritium is a radioactive nuclide with a half-life of 12.3 years and is a beta emitter with a maximum energy of 18.6 keV. Therefore, it is important to know where and how much tritium remains in the fusion device from the viewpoints of not only radiation safety management but also decommissioning of a fusion device. This study reports the preliminary results of an estimate of the tritium inventory in activated charcoal used in the cryosorption pump by the soaking method

2 Materials and methods

Among various measurement methods of tritium in materials, we applied the soaking method for tritium analysis in activated charcoal. The soaking method has some advantages: 1) non-destructive, 2) simple operation procedure, 3). No special analytical system is required. Details of the analysis method by soaking are described below.

2.1 Sample collection

Large Helical Device (LHD) [1], in which a plasma experiment involving a deuterium fusion reaction was conducted, uses various cryosorption pumps as a vacuum pumping device to achieve a high vacuum. The cryosorption pump uses activated charcoal as an absorbent. In this study, activated charcoal striped from the cryosorption pump of the Neutral Beam Injection [NBI] system [2], which is one of the auxiliary plasma heating devices in the LHD, was used as a sample.

2.2 Preprocessing and measurement

A procedure of the soaking method is shown in Figure 1. In the soaking method, activated charcoal is soaked in deionized water for a certain period, and tritium in the activated charcoal is extracted into the sample water using an isotope exchange reaction. To confirm the change in tritium release velocity during immersion, tritium was extracted using the following steps.

(1) Divide the activated charcoal into approximately 0.6 g.
(2) Prepare 5 vials (20 ml, vials (a), (b), (c), and (d)) to which 10 cm^3 of pure water has been added.
(3) Put the activated charcoal fractionated in (1) into a vial (a) and allow it to stand for 1h.
(4) Remove the activated charcoal from vial (a) and transfer it to vial (b).
(5) Perform the same procedure as (3) and (4) for vials (b), (c), and (d), changing the leaving time to 2 h, 3 h, and 18 h, respectively.
(6) Sample water in each vial was mixed with the scintillator (10 cm^3, ULTIMA Gold LLT, Revvity), and then tritium activity was measured by a liquid scintillation counter (Tri-Carb4910TR, Revvity) for 50 minutes.

For the evaluation of the remaining tritium in the activated charcoal after the procedure of vial (d), the burning method was applied. A schematic diagram of the burning apparatus is shown in Figure 2. Activated charcoal removed from the vial (d) was taken out into a sample plate made of alumina and heated at about 950°C for about 10 minutes under a moist air atmosphere for complete burnup [3]. Tritiated water vapor in the air after the burning process is collected by three water bubblers at the downstream. Then the tritium activity in the water bubbler was determined by a liquid scintillation counter in the same manner as the soaking method.

Copyright on 7th Asia-Pacific Symposium on Radiochemistry 2025

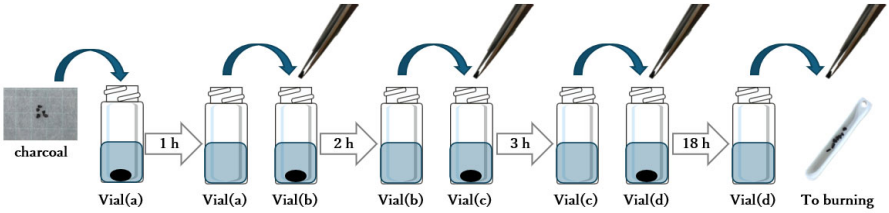


Fig. 1. A procedure of the soaking method.

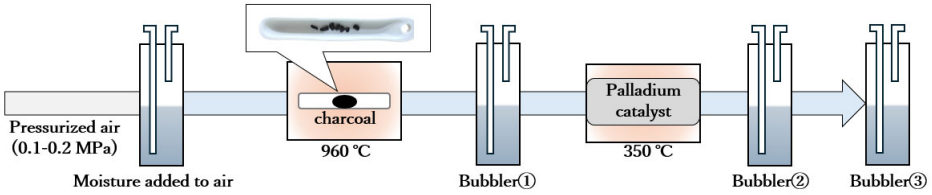


Fig. 2. A schematic diagram of the burning apparatus.

3 Results

The release velocity of tritium by the soaking method is shown in Figure 3. It was found that the tritium release velocity was the fastest in the first hour, and that the tritium exchange progressed after that, although the release velocity became smaller. Figure 4 shows a comparison of tritium released by the soaking method to the total tritium released by the soaking and burning method. The amount of tritium in activated charcoal was estimated to be from 5.8 to 32 Bq/g. The extraction rate of tritium by the soaking method was approximately 55%, although some samples, such as sample number 23, had an extraction rate of about 13%. To investigate the reasons for the significantly low extraction rate, we plan to continue conducting more tests.

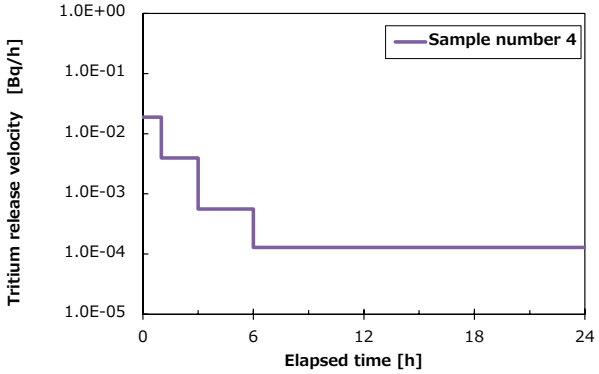


Fig. 3. The release velocity of tritium by the soaking method.

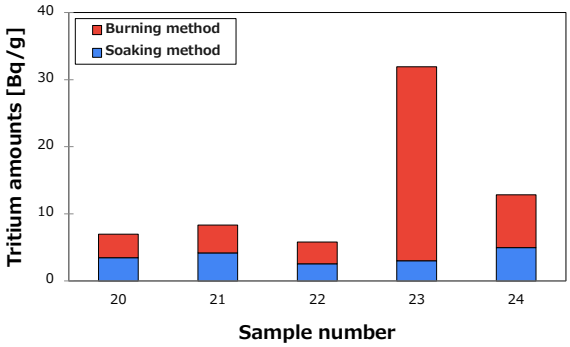


Fig. 4. Tritium amounts in activated charcoal.

4. CONCLUSIONS

Using activated charcoal collected from the LHD, the remaining amount of tritium produced in the plasma experiment was evaluated to be from 5.8 to 32 Bq/g in the pump. The radioactivity was estimated by comparing the results of the soaking method with those of the burning method, which were multiplied by 2 times with exceptions.

ACKNOWLEDGMENTS

The activated charcoal samples were provided by Mr. Masayuki Shibuya and Mr. Mamoru Sato of the National Institute for Fusion Science. The burning of activated charcoal was conducted with the help of Prof. Masuzaki Suguru and Mr. Yonezu Hiroaki.

References

[1] M. Osakabe, *et al*., Fusion Science and Technology, 72, 199-210, (2017).
[2] O. Kaneko, *et al*., Fusion Engineering and Design, 20, 519-524 (1993).
[3] S. Masuzaki, *et al*., Nuclear Materials and Energy, 26, (2021).

Copyright on 7th Asia-Pacific Symposium on Radiochemistry 2025 P-R3-14 -

Exploration of uranium adsorption properties of polyimide dixime-based uranium adsorption membrane materials

Jiang Yanxin[1], Liu Peng[*2]

[1]*Affiliation Information: Yantai Research Institute and Graduate School, Harbin Engineering University, Yantai 264006, China*

[2]*College of Nuclear Science and Technology, Harbin Engineering University, Harbin 150001, China*

The adsorption method has the advantages of high selectivity, low cost and simple preparation, and is the most promising technology for uranium extraction from seawater. Among them, amidoxime-based membrane adsorbent materials have high selectivity and adsorption capacity for uranium. Studies have shown that uranium selectivity is provided by the cyclic imide dixime functional group in it. In this study, polyimide dixime hydrogel (PIDOH) membrane material was successfully prepared by adjusting the temperature, and its uranium adsorption mechanism was explored, which provided a theoretical basis for further exploration.

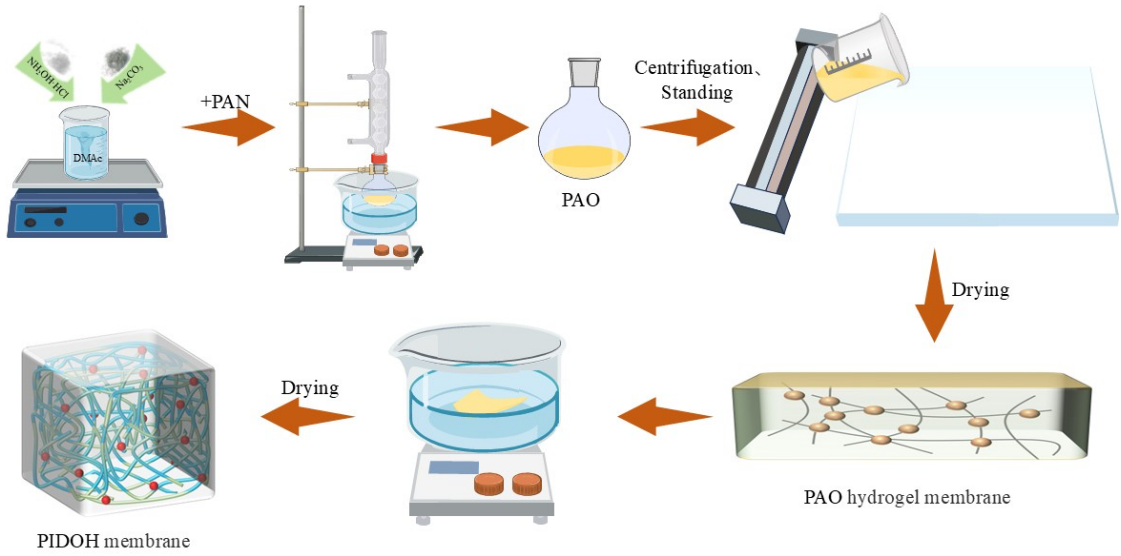
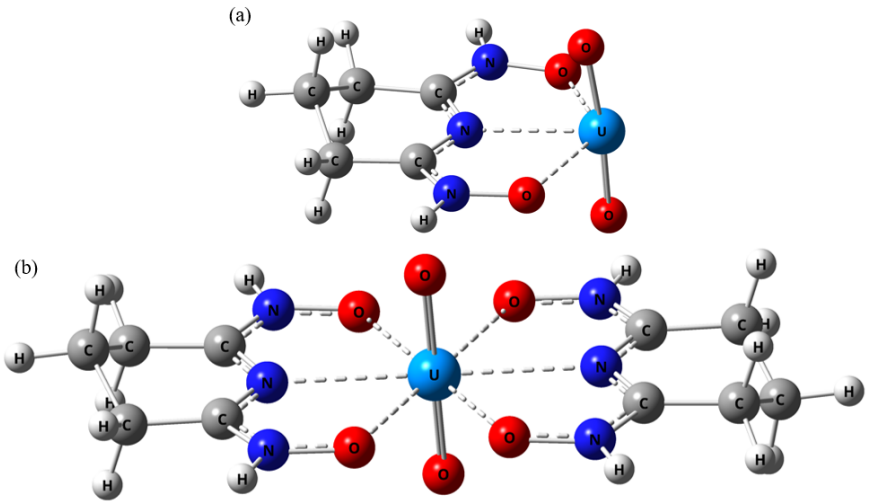


Fig. 1. Flow chart of preparation of PIDOH membrane



* Corresponding Author：liup@hrbeu.edu.com

Fig. 2. Simulated structural diagram of the binding of acylimide oxime functional group with uranium: (a) PIDO:UO_2^{2+}=1:1; (b) PIDO:UO_2^{2+}=2:1

Table 1 Binding energy calculation results

System	Energy(E)/Hartree	Acting Energy/Hartree	Acting Energy/kcal·mol^{-1}	Acting Energy/eV
UO_2^{2+}	-627.3481439	/	/	/
PIDO	-510.1321908	/	/	/
PIDO+UO_2^{2+}	-1137.59822	-0.118	-73.974	-3.208
2PIDO+UO_2^{2+}	-1647.798971	-0.186	-116.997	-5.073

1 Experimental Methods

Fourier transform infrared spectroscopy, X-ray diffraction, scanning electron microscopy and X-ray photoelectron spectroscopy were used to characterize the materials. In this study, PIDOH membrane material was successfully prepared, its uranium adsorption properties were explored (Fig. 1), and the experimental results were analyzed, and it was found that the uranium adsorption experimental results were in line with the quasi-second-order kinetic equation. FT-IR and XPS were used to explore the uranium adsorption mechanism of PIDOH membranes, and the chelation mechanism of imide dixime functional groups and uranium was explored by theoretical calculations.

2 Results

Under the optimal treatment conditions of 7 h of hydrothermal time and 60°C and 90 min of alkali treatment, PIDOH membrane can effectively avoid the interference of competing ions, and the removal rate of uranium is higher than that of other common metal ions (such as iron, chromium, etc.), the removal rate of uranium in the solution reaches 88% after 24 h adsorption, and the PIDOH membrane has good selective uranium adsorption performance, and PIDOH membrane has good chemical stability and recycling performance, and the removal rate of uranium in the solution is still 95% after 4 uranium adsorption cycles Above, the desorption rate is close to 100%. Simulation calculations revealed the uranium adsorption mechanism of PIDOH membranes, and proved the stability and evidence of the 2:1 coordination model of imide dixime functional group and uranyl ion(Fig. 2 and Table 1), which provided a solid theoretical basis for the design and optimization of imide dixime-based membrane materials for uranium extraction from seawater.

Keywords: Uranium extraction from seawater; Hydrogel Membrane; Adsorption; Imide dioxime

All-in-One: Photo-Responsive Lanthanide-Organic Framework for Simultaneous Sensing, Adsorption, and Photocatalytic Reduction of Uranium

Zhi-Wei Huang,[1,2] Kong-Qiu Hu,[2] Lei Mei,[2] Wang-Suo Wu,[1] Wei-Qun Shi [2,3]

[1] *School of Nuclear Science and Technology, Lanzhou University, Gansu 730000, China*
[2] *Institute of High Energy Physics, Chinese Academy of Sciences, Beijing 100049, China*
[3]*School of Mechanical Engineering, Shanghai Jiao Tong University, Shanghai, 200240, China*

The detection, separation, and recovery of uranyl ions in radioactive wastewater have long posed significant challenges in environmental fields. Given the designable nature of metal-organic frameworks (MOFs), constructing multifunctional MOFs shows promise for achieving simultaneous fluorescence detection, selective adsorption, and photocatalytic reduction of uranyl ions, thereby addressing potential pollution issues.

In this work, a novel photo-responsive MOF material (IHEP-24) was successfully synthesized by integrating viologen ligands with lanthanide metal clusters. This material exhibits excellent photoluminescent properties and demonstrates high sensitivity and selectivity for uranyl ion fluorescence detection. Leveraging the precise recognition sites within its framework, IHEP-24 enables selective adsorption of uranyl ions. Furthermore, the presence of photoactive viologen radical ligands facilitates the photocatalytic reduction of adsorbed uranyl ions to U(IV), achieving thorough decontamination of uranyl in aqueous solutions. Batch experiments, photoelectrochemical characterization, and theoretical calculations were systematically employed to elucidate the adsorption and photocatalytic mechanisms.

This work provides guidance for the precise construction of robust multifunctional MOF materials. The investigation of structure-performance relationships enhances the understanding of uranyl adsorption and photocatalytic reduction processes, paving the way for developing novel high-efficiency materials for radionuclide separation and enrichment.

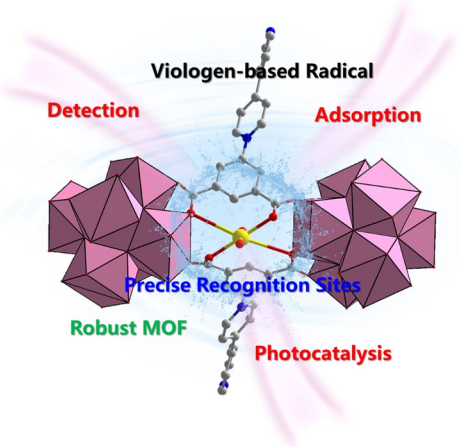


Fig. 1. Photo-Responsive Lanthanide-Organic Framework for Simultaneous Sensing, Adsorption, and Photocatalytic Reduction of Uranium

ACKNOWLEDGMENTS

The authors are thankful for support from the National Science Fund for Distinguished Young Scholars (Grant No. 21925603). The authors are also thankful for support from the National Natural Science Foundation of China (22076187, 22076186, and 22122609).

References

[1] Zhi-Wei Huang, Wang-Suo Wu,* Wei-Qun Shi* et. al. All in One: Photo-Responsive Lanthanide-Organic Framework for Simultaneous Sensing, Adsorption, and Photocatalytic Reduction of Uranium. *Adv. Funct. Mater.*, **34**, 2404126 (2024).

[2] Zhi-Wei Huang, Kong-Qiu Hu, Wei-Qun Shi* et. al. Thermally Induced Orderly Alignment of Porphyrin Photoactive Motifs in Metal-Organic Frameworks for Boosting Photocatalytic CO_2 Reduction. *J. Am. Chem. Soc.* **145**, 18148-18159 (2023).

[3] Zhi-Wei Huang, Kong-Qiu Hu,* Wei-Qun Shi.* et. al. Modulating the Coordination Microenvironment of Uranyl Compounds to Enhance Photocatalytic CO_2 Reduction. *Inorg. Chem. Front.* **10**, 4754-4762 (2023).

[4] Zhi-Wei Huang, Wang-Suo Wu,* Wei-Qun Shi.* et. al. Encapsulation of Polymetallic Oxygen Clusters in a Mesoporous/Microporous Thorium-Based Porphyrin Metal-Organic Framework for Enhanced Photocatalytic CO_2 Reduction. *Inorg. Chem.* **61**, 3368-3373 (2022).

7th Asia-Pacific Symposium on Radiochemistry *September 14 ~ 19, 2025 • Kunibiki Messe • Shimane, Japan*

Chemical characterization of Platinum group alloys plate in fused borosilicate glasses

Mizuki Kato[1], Haruaki Matuura[1], Isamu Sato[1], Yuuki Oiwa[1], Sayaka Chiba[1], Haruka Tada[2], Hiroki Izumi[2]

[1]*Tokyo City University, 1-28-1 Tamazutsumi, Setagaya-ku, Tokyo, 158-8557, Japan*
[2]*IHI Corporation, TOYOSU IHI BUILDING., 1-1, Toyosu 3-chome, Koto-ku, Tokyo, 135-8710, Japan*

Platinum group alloys (Mo, Ru, Rh, Pd, and Tc) present in insoluble residue waste in spent fuel reprocessing processes are expected to change in composition with changes in fuel specifications and irradiation conditions, and flexible responses are necessary. Therefore, the phase states of platinum group alloys and glass were confirmed and their chemical morphology and migration behavior were evaluated by mixing and heating tests of borosilicate glass, waste liquid components, and plate-type platinum group alloys. It was found that an increase in Mo in the platinum group alloys changed the amount of consumed oxygen, resulting in a change in the Ru chemical form.

1 Introduction

In the spent fuel reprocessing process, platinum group alloys (Mo-Ru-Rh-Pd-Tc) contained in the insoluble residue wastes are mixed with other wastes and fed to the glass melting furnace [1]. It is important to understand the behavior of the platinum group alloys in the vitrification process because the platinum group alloys affect the flowability of the glass in the glass melter due to the state of the cold cap in the initial stage of melting and settling to the bottom of the furnace. The platinum group alloys are expected to change in composition of the waste liquid due to changes in fuel specifications and irradiation conditions, so flexible measures are necessary in the vitrification process. Therefore, in this study, heating tests and various analyses using plate-type Platinum group alloys were conducted to elucidate the chemical states of Platinum group alloys, glass, and waste liquid components in a simulated vitrified product after heating in accordance with changes in spent fuel.

2 Methods

TABLE 1. Sample Conditions and Measurements

Heating conditions				Analysis		
Alloy	Oxygen	Temp	Other	SEM-EDS glass	SEM-EDS interface	EXAFS glass
R6-2	20%	900℃	Temp rise rate10℃/min Hold for 3h Room temperature slow cooling	○	○	○
	5%	1150℃		○	○	○
R6-3	20%	900℃		○	○	○
	5%	1150℃		○	-	○
R6-4	20%	900℃		○	○	○
	5%	1150℃		○	○	○

Simulated alloys were prepared by weighing and mixing Mo, Ru, Rh, and Pd powders as R6-2 (Mo:15,Ru:65,Rh:10,Pd:10wt%), R6-3 (Mo:20,Ru:60,Rh:10,Pd:10wt%), which is equivalent to current fuel, and R6-4 (Mo:30 R6-4 (Mo:30, Ru:50, Rh:10, Pd:10wt%), in which Mo was overestimated, were weighed and mixed with each other to make mock alloys. These alloys were heated to simulate the vitrification process, borosilicate glass, and simulated waste liquid components. To simulate the upper and lower parts of a glass melting furnace, the upper part was heated at a temperature increase of 10°C/min, oxygen concentration of 20%, and holding time of 3 hours at 900°C. The lower part was heated at a temperature increase of 10°C/min, oxygen concentration of 5%, and holding time of 3 hours at 1150°C. A simulated vitrified product was prepared. After heating, the glass alloy was cooled at room temperature, cut, and the cut surface was analyzed by SEM-EDS and local structure analysis by fluorescence XAFS.

Copyright on 7th Asia-Pacific Symposium on Radiochemistry 2025

3 Results & Discussion

The prepared simulated vitrified glass was observed by SEM-EDS. The white areas at the interface between the alloy and glass are considered to be the unoxidized metallic phase, while the gray areas are considered to be the depleted Mo phase. Pd is partially separated from the alloy, suggesting that after the oxidation transition of Mo, a ternary system of Ru-Rh-Pd is formed and Pd is not oxidized but separated. For further clarification of the oxidation state, XAFS analysis was performed, showing that the Mo oxides were molybdenum oxide and molybdate, while the Ru oxides remained as metal or ruthenium oxide, suggesting the effect of the amount of oxygen consumed on oxidation. The EXAFS radial structure function of the simulated vitrified glass shown in Figure 2 indicates that the oxides near Mo are close to molybdate. On the other hand, the structure near Ru is similar to either ruthenium oxide or metal, depending on the alloying ratio of Mo and heating conditions.

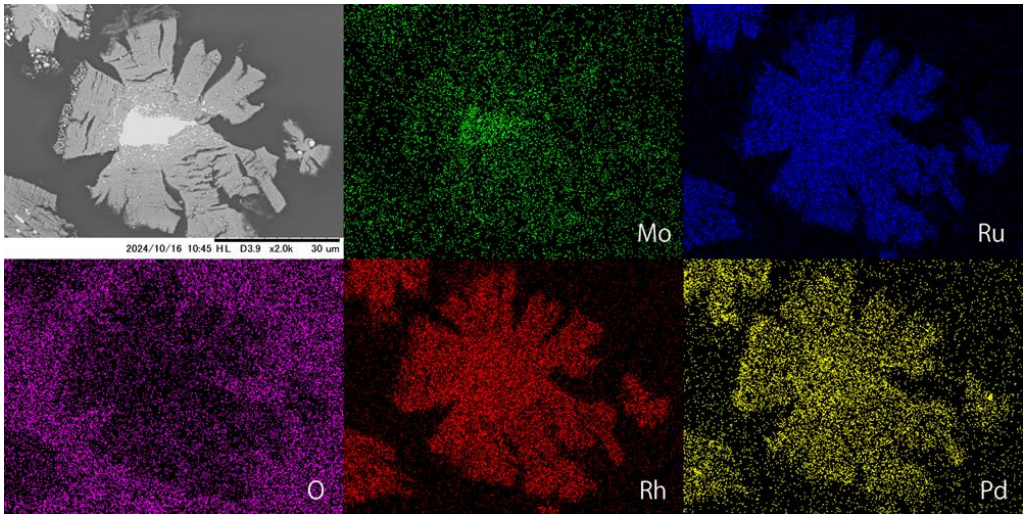


Fig. 1. SEM-EDS of R6-2 upper simulated vitrified body.

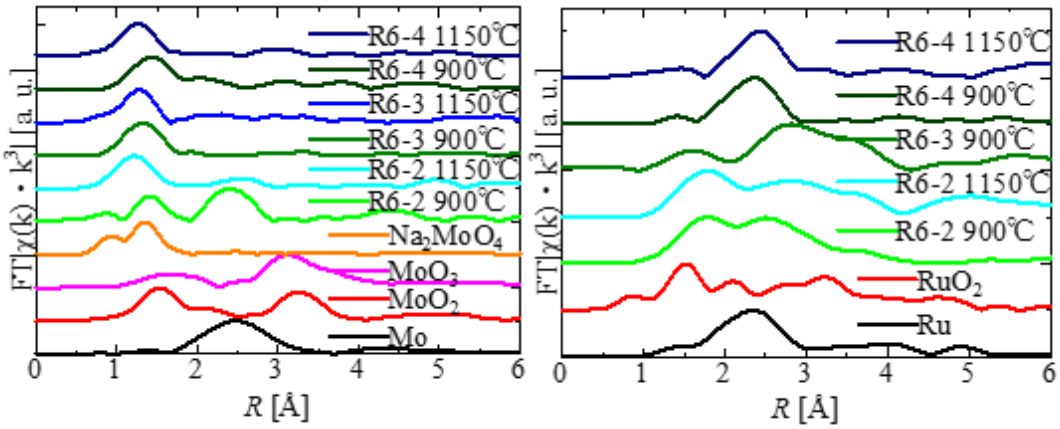


Fig. 2. EXAFS radial structure functions (left: near Mo, right: near Ru)

ACKNOWLEDGMENTS

This research is a part of the results of the "FY2024 Basic Research Project on Vitrification Technology for Volume Reduction of Radioactive Waste (JPJ010599)" of the Agency for Natural Resources and Energy, Ministry of Economy, Trade, and Industry.

References

[1] JAPAN NUCLEAR FUEL LIMITED. (n.d.). Activity, Technology Development
URL: https://www.jnfl.co.jp/en/activity/technology/
Last viewed:2025/05/11

Influence of Actinide Radiotoxicity on Nuclear Waste Disposal Frameworks in Spent Nuclear Fuel Reprocessing Systems

Shuai Liu [1], Meng Wei [1], Jianquan Liu [1]

[1] *CNNC Long'an Co. Ltd: B3 Huayuan Road, Haidian District, Beijing, China, 100080, liushuailzu@foxmail.com*
[1] *CNNC Long'an Co. Ltd: B3 Huayuan Road, Haidian District, Beijing, China, 100080, weim@cnla.cn*
[1] *CNNC Long'an Co. Ltd: B3 Huayuan Road, Haidian District, Beijing, China, 100080, liujq@cnla.cn*

Radiotoxicity, representing the Radiological hazard potential associated with internal exposure to radioactive isotopes, serves as a fundamental parameter for assessing geological repository safety. This hazard metric offers superior radiobiological risk characterization compared to conventional radioactivity measurements alone when managing spent nuclear fuel. Current research lacks systematic investigations into temporal evolution patterns of actinide-specific radiological hazards across diverse waste matrices, particularly regarding their implications for advanced partitioning technologies and repository optimization. Addressing this knowledge gap could iterate waste form design through enhanced actinide segregation protocols and disposal matrix selection.

This investigation employs depletion analysis software to quantify millennial-scale radiological hazard profiles in five distinct waste streams derived from uranium oxide fuel (initial enrichment: 4.95% U-235, discharge burnup: 55 GW/tU, 8-year cooling period) processed through advanced separation techniques (TRPO method). The analyzed matrices include: (1) spent fuel, (2) uranium/plutonium-containing HLLW, (3) Am-Cm stream, (4) neptunium-plutonium stream, and (5) uranium product. Our findings reveal distinct temporal hazard patterns: neptunium demonstrates minimal long-term radiological impact, whereas plutonium and americium exhibit millennial-scale persistence. Curium's hazard potential shows marked attenuation beyond three centuries post-disposal.

Non-partitioned vitrified HLLW requires approximately three hundred millennia to achieve radiologically benign levels. Advanced actinide segregation reduces vitrified waste hazards by orders of magnitude, with residual plutonium concentrations decreasing to 0.1% of initial values. However, the remaining plutonium inventory maintains 150 times the reference uranium toxicity, necessitating improved recovery processes. Strategic management of HLLW residues reveals potential disposal pathway optimization: neptunium extraction combined with plutonium minimization could enable intermediate-depth disposal of Np-Pu concentrates. Implementing Np/Pu separation would permit co-vitrification of plutonium with Am-Cm fractions.

Notably, Am-Cm glass matrices exhibit extraordinary radiological hazards (10^4×natural uranium equivalence). While interim storage (century-scale) reduces their thermal output and specific activity to intermediate-level waste transport standards, radiotoxicity decay analysis confirms these matrices require millennium-scale isolation - exceeding current intermediate-depth repository specifications. This temporal disparity highlights critical challenges in developing compatible disposal solutions for separated actinide streams.

Keywords: Radiotoxicity; Naturel uranium in equilibrium; Spent Fuel Reprocessing; Pu recovery; HLLW Partitioning; Long-lived Minor Actinides; Disposal.

7th Asia-Pacific Symposium on Radiochemistry *September 14 ~ 19, 2025 • Kunibiki Messe • Shimane, Japan*

Adsorption and separation performance of platinum group metals using a novel MPE-TDGA/SiO_2-P adsorbent

Mai Tanaka[1,2], Naoki Osawa[3], Hao Wu[4], Seong-Yun Kim[1]

[1] *Department of Quantum Science and Energy Engineering, Graduate School of Engineering, Tohoku University, 6-6-01-2 Aza-Aoba-Aramaki, Aoba-ku, Sendai, Miyagi 980-8579 Japan, sonyun.kimu.d7@tohoku.ac.jp*
[2] *Japan Nuclear Fuel Limited, 4-108 Aza-Okitsuke, Oaza Obuchi, Rokkasyo-mura, Aomori, 039-3212 Japan*
[3] *Department of Nuclear Technology, Nagaoka University of Technology, Nagaoka, Niigata 940-2188, Japan*
[4] *School of Nuclear Science and Engineering, Shanghai Jiao Tong University, Shanghai 200240, China*

To develop an efficient separation process for platinum group metals (PGMs), contained in high-level radioactive liquid waste (HLLW), a novel N,N'-dimethyl -N,N'-di-(2-phenylethyl)-thiodiglycolamide (MPE-TDGA) extractant impregnated adsorbent, for instance MPE-TDGA/SiO_2-P adsorbent was prepared, and its adsorption and separation performance toward PGMs from simulated HLLW were evaluated.

1. INTRODUCTION

To establish the nuclear fuel cycle, spent nuclear fuel generated by nuclear power generation is to be reprocessed to reduce the amount of nuclear waste [1]. High-level radioactive liquid waste (HLLW), generated during the reprocessing of spent nuclear fuel via the PUREX method, contains platinum group metals (PGMs), including Ru, Rh, and Pd. The presence of PGMs is known to interfere with the vitrification process of HLLW.[2]. To solve this problem, the separation of PGMs from HLLW using extractant impregnated macroporous silica-based adsorbents, has been proposed [3]. In this study, a novel MPE-TDGA/SiO_2-P adsorbent was prepared to develop an efficient separation process for PGMs. The MPE-TDGA/SiO_2-P adsorbent was characterized using SEM, TG, and N_2 gas adsorption/desorption. Furthermore, the adsorption and separation performance of PGMs from simulated HLLW was evaluated using this adsorbent.

2. EXPERIMENTAL

A novel extractant of N,N'-dimethyl -N,N'-di-(2-phenylethyl)-thiodiglycolamide (MPE-TDGA) was synthesized by dehydrative condensation using N-methyl-2 phenylethylamine and thiodiglycolic acid. MPE-TDGA/SiO_2-P adsorbent was prepared by impregnating MPE-TDGA into a silica/polymer composite support (SiO_2-P). The effect of nitric acid concentration ([HNO_3] = 0.5 M ― 5 M) was evaluated in batch tests using simulated HLLW prepared with 14 representative metal ions at a concentration of 5 mM each in 5 h contact time at 298 K. Furthermore, column test was conducted to obtain its separation performance, using 5 mL of the feed solution containing 5 mM of 14 types of metal ions, 50 mL of 2 M HNO_3 as the washing solution, 40 mL of 0.2 M thiourea in 0.1 M HNO_3 and 20 mL of the 0.01 M EDTA solution.

3. RESULTS AND DISCUSSION

The result of the effect of nitric acid concentration is shown in Figure 1. The Pd(II) uptake ratio was close to 100%, although it showed a slight tendency to decrease with increasing nitric acid concentration. On the other hand, the uptake ratio of Ru(III) showed a maximum at a nitric acid concentration of 3 M. Also, the uptake ratio of Rh(III) showed a slight tendency to increase with increasing nitric acid concentration.

Furthermore, the result of the column test is shown in Figure 2. First, most of the Ru(III) and Rh(III) were eluted with non-adsorbed metal ions after the washing solution of 2 M HNO_3 flushing. Next, almost 99% of Pd(II) was eluted by 0.2 M thiourea in 0.1 M HNO_3. At the same time, the slight amount of Ru(III) remaining in the column was eluted.

According to these results, it is thought that MPE-TDGA/SiO_2-P adsorbent showed high adsorption performance of Pd(II) owing to the affinity between Pd(II) and sulfur donor of MPE-TDGA extractant based on the hard and soft acid–base (HSAB) theory. On the other hand, Ru(III) and Rh(III) are slow to undergo the ligand displacement reaction and require more time for adsorption [4]. Therefore, the adsorption and separation performance of Ru(III) and Rh(III) could be improved by optimizing the experimental conditions.

Copyright on 7th Asia-Pacific Symposium on Radiochemistry 2025

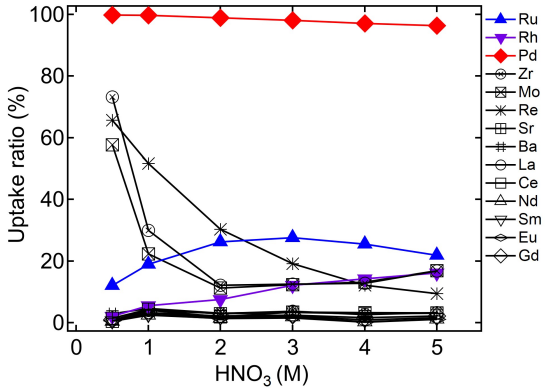


Fig. 1. Effect of concentration of nitric acid on the adsorption of 14 metal ions on the MPE-TDGA/SiO_2-P.
Metal ions: 5 mM, [HNO_3]: 0.5-5 M, phase ratio: 4 mL/0.2 g, shaking speed: 160 rpm, shaking time: 5 h, temperature: 298 K.

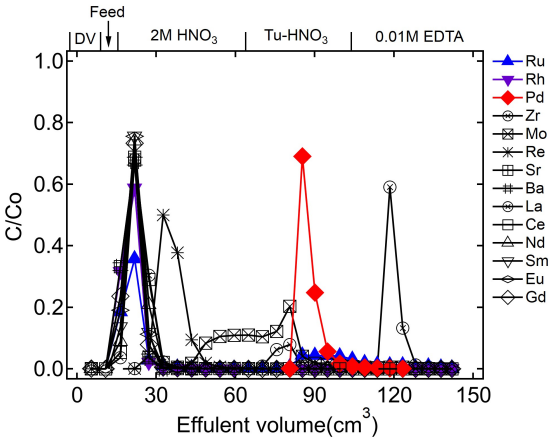


Fig.2. Chromatographic separation on the MPE-TDGA/SiO_2-P column.
Flow rate: 0.5 cm^3 min^{-1}, height: 15 mm, inner diameter of the column: 10 mm, temperature: 298 K

4. CONCLUSIONS

From the above-mentioned results, the prepared MPE-TDGA/SiO_2-P adsorbent was evaluated to have a high adsorption performance toward Pd(II). Furthermore, the efficient elution of most of the Pd(II) using the MPE-TDGA/SiO_2-P adsorbent was confirmed by the column test. Therefore, MPE-TDGA/SiO_2-P adsorbent is considered as a promising adsorbent for the efficient separation of Pd(II) from HLLW.

References

[1] S.M. Woo, S.S. Chirayath, et al., "Nuclear fuel reprocessing: Can pyro-processing reduce nuclear proliferation risk?", *EnergyPolicy*, 144 (2020).
[2] B. Luckscheiter and M. Nesovic, "Development of glasses for the vitrification of high level liquid waste (HLLW) in a joule heated ceramic melter", *Waste Management*, **16**, 571 (1996).
[3] S.-Y. Kim, Y. Xu, et al., "A novel partitioning process for treatment of high level liquid waste using macroporous silica-based adsorbents", *J Radioanal Nucl Chem*, **295**, 1043 (2013).
[4] T. Ito, S.-Y. Kim, et al., "Adsorption Behaviors of Platinum Group Metals in Simulated High Level Liquid Waste Using Macroporous (MOTDGA-TOA)/SiO_2-P Silica-based Absorbent", *Separation Science and Technology*, **48**, 2616 (2013).

7th Asia-Pacific Symposium on Radiochemistry *September 14 ~ 19, 2025 • Kunibiki Messe • Shimane, Japan*

Analytical Strategy for Evaluating High-Specific-Activity ^{177}Lu in Theranostic Radiopharmaceutical Production

Miki Harigai[1], Kazumi Nakano[2], Kenji Shirasaki[3], Hiroyuki Kimura[4], Tomoo Yamamura[1]

[1]*Institute for Integrated Radiation and Nuclear Science, Kyoto University: 2, Asashiro-Nishi, Kumatori-cho, Sennan-gun, Osaka, 590-0494, harigai.miki.2k@kyoto-u.ac.jp, yamamura.tomoo.2e@kyoto-u.ac.jp*
[2]*Agilent Technologies, Inc.: 9-1 Takakura-cho, Hachioji, Tokyo, 192-8510, kazumi_nakano@agilent.com*
[3] *Institute for Radiation Science, The University of Osaka: 1-1 Machikaneyama, Toyonaka, Osaka, 560-0043, shirasaki@rirc.osaka-u.ac.jp*
[4] *Institute for Environmental Safety and Health, Kyoto University: Yoshida-Konoe-cho, Sakyo-ku, Kyoto, 606-8315, kimura.hiroyuki.4u@kyoto-u.ac.jp*

Direct determination of ^{177}Lu by inductively coupled plasma mass spectrometry (ICP-MS) is hampered by its low concentration and 6.65-day half-life. For radiopharmaceutical production, however, rigorous impurity profiling is indispensable and ICP-MS offers unrivalled elemental sensitivity. We demonstrate an indirect, yet robust, approach for evaluating the specific activity of reactor-produced ^{177}Lu through precise measurement of its decay progeny ^{177}Hf by triple-quadrupole ICP-MS (ICP-QQQ).

1 Introduction

The β-emitter ^{177}Lu has become a cornerstone of theranostic radiopharmacy, with growing clinical use in peptide receptor radionuclide therapy and prostate cancer treatment. Manufacturing medical-grade ^{177}Lu demands strict control of radiochemical purity and exact quantification of both product and co-generated nuclides. Conventional ICP-MS quantification of ^{177}Lu is severely affected by isobaric and polyatomic interferences, notably from ^{177}Yb and ^{177}Hf produced during neutron irradiation of enriched ^{176}Yb targets. Reaction-cell mass-shift techniques with ICP-QQQ have recently resolved these interferences across a wide elemental range [1], enabling accurate assays of other therapeutic radionuclides such as ^{161}Tb. Building on this progress [3], we propose to infer ^{177}Lu specific activity from the activity of its daughter ^{177}Hf, determined after chemical purification, combined with precise characterization of the ^{176}Yb starting material.

2. Experimental

Analyses were performed on an Agilent 8900 ICP-QQQ operated with 10 % NH_3 in He as the reaction gas. For target-material characterization, Q1 was set to m/z 176 to quantify ^{176}Hf and ^{176}Lu across the full Q2 mass range. Irradiated and chemically purified samples prepared at our institute were measured at Q1 = 177; appropriate product-ion transitions were selected to obtain interference-free ^{177}Hf signals. Specific activity of ^{177}Lu was then calculated from the measured ^{177}Hf concentration, decay-corrected to end of bombardment, and the isotopic abundance of ^{176}Yb.

3. Results

The NH_3/He reaction gas efficiently eliminated overlapping contributions from Yb and Lu isobars, yielding single-digit ng kg^{-1} detection limits for both elements. Isotope-ratio measurements confirmed that the enrichment of ^{176}Yb in the target material (97.1 ± 0.2 %) agreed with supplier specifications. In purified samples, ^{177}Hf was quantified with relative standard deviations below 3 %. The derived specific activities of ^{177}Lu ranged from 3.9 to 4.2 TBq mg^{-1}, consistent with theoretical values for indirect (^{176}Yb(n,γ) ^{177}Yb→^{177}Lu) production under the applied irradiation conditions. Detailed numerical data and uncertainty budgets will be presented.

ACKNOWLEDGMENTS

This work was supported by MEXT Innovative Nuclear Research and Development Program Grant Number JPMXD0224019804.

References

[1] N. Sugiyama and K. Nakano, Technical note: Reaction data for 70 elements using O_2, NH_3 and H_2 gases with the Agilent 8800 Triple Quadrupole ICP-MS, *Agilent Technologies, Inc.* (2014)
[2] G. Woods, Application note: Resolution of ^{176}Yb and ^{176}Lu interferences on ^{176}Hf to enable accurate ^{176}Hf/^{177}Hf isotope ratio analysis using ICP-QQQ with MS/MS, Agilent Technologies, Inc. (2017)
[3] S. W. McNeil, et al., A simple and automated method for ^{161}Tb purification and ICP-MS analysis of ^{161}Tb, EJNMMI Radiopharmacy and Chemistry, 7,31 (2022)

Separation behavior of MA(III) from simulated high-level liquid waste using TEHDGA and HONTA impregnated XAD7-HP adsorbents

Masahiko Kubota[1,2], Seong-Yun Kim[1], Tsuyoshi Arai[3], Sou Watanabe[4], Tatsuya Ito[5], Ryuji Nagaishi[5]

[1] *Department of Quantum Science and Energy Engineering, Graduate School of Engineering, Tohoku University, Aramaki-Aza-Aoba 6-6-01-2, Sendai, 980-8579, Japan, sonyun.kimu.d7@tohoku.ac.jp*
[2] *Japan Nuclear Fuel Chemical Analysis Co., Ltd. 4-91 Okitsuki Obuchi, Rokkasho, Aomori, 039-3212, Japan*
[3] *Materials Science and Engineering, Shibaura Institute of Technology, Koutou-ku, Tokyo, 135-8548, Japan*
[4] *Nuclear Fuel Cycle Engineering Laboratories, Japan Atomic Energy Agency,Tokai-mura, Ibaraki 319-1194, Japan*
[5] *Collaborative Laboratories for Advanced Decommissioning Science (CLADS), Japan Atomic Energy Agency, 2-4 Shirakata, Tokai, Naka, Ibaraki, 319-1195, Japan*

In the treatment of high-level liquid waste (HLLW), the separation of minor actinides (MA) and lanthanides (Ln) is an important process. However, due to their similar chemical properties, the separation of MA alone is a difficult challenge. In this study, we report on the separation of MA(III) and Ln(III) using a two-stage separation column employing XAD7-HP adsorbent. Separation tests were conducted using a solution containing radioisotopes (^{241}Am and ^{152}Eu) added to simulated HLLW in a column packed with TEHDGA/XAD7-HP adsorbent, successfully achieving simultaneous recovery of MA(III) and Ln(III). In the second column using HONTA/XAD7-HP adsorbent, MA (III) showed the possibility of being separated from a mixture of MA (III) and Ln (III) solutions.

1. INTRODUCTION

High-level liquid waste (HLLW) generated through the reprocessing of spent nuclear fuel contains significant amounts of lanthanides (Ln) and actinides (MA) as fission products.[1] If these elements can be separated from one another, it is expected that the reduction of long-lived nuclides and heat-generating nuclides within glass solidification bodies can be achieved, contributing to the long-term reduction of radiation risks and the reduction of the area required for storage facilities. However, since MA and Ln have very similar ionic radius and coordination chemistry, it is extremely difficult and challenging to separate them from each other.

Our research group has investigated a two-stage separation process using adsorbents containing *N*,*N*,*N*',*N*'-tetra(2-ethylhexyl)diglycolamide (TEHDGA) and hexaoctylnitriloteroacetamide (HONTA).[2] We evaluated the separation process using adsorbents with the aim of achieving two-stage separation of MA(III) and Ln(III). While evaluations of the co-separation of MA(III) and Ln(III) in the TEHDGA column and the mutual separation of MA(III) and Ln(III) in the HONTA column are underway, fundamental research is necessary to establish a more effective process for the mutual separation of MA and Ln using extraction chromatography. We focused on Amberlite (XAD7-HP) as the adsorbent material for this study. XAD7-HP is a white spherical material with a macroporous structure composed of cross-linked copolymers, and has a large specific surface area. Compared to ion exchange resins, it has excellent properties such as chemical stability due to the absence of functional groups. XAD7-HP is mainly used in adsorption and separation fields, but research on separating Ln(III) and MA(III) from HLLW has been limited to date.

In this study, the separation of MA(III) from simulated HLLW solutions using TEHDGA/XAD7-HP and HONTA/XAD7-HP adsorbent was investigated. Specifically, the characterization of TEHDGA/XAD7-HP and HONTA/XAD7-HP adsorbent were evaluated using SEM, XRD, TG, and N_2 gas adsorption/desorption. Next, we evaluated the adsorbent by investigating the effects of HNO_3 concentration, contact time, chemical stability, and γ-ray irradiation under HNO_3 solution conditions. Finally, to investigate the dynamic adsorption and separation behavior, column tests were conducted using simulated HLLW solutions spiked with ^{241}Am and ^{152}Eu.

2. EXPERIMENTS

The adsorbents were prepared by impregnating TEHDGA and HONTA extractants into XAD7-HP using the impregnation method, resulting in TEHDGA/XAD7-HP adsorbent and HONTA/XAD-7HP adsorbent containing 20% extractants. To investigate the dynamic adsorption behavior of ^{241}Am, ^{152}Eu, and other metal ions toward the adsorbents, separation tests were conducted using the column method. The column test apparatus consisted of a Pyrex glass column (TEHDGA/XAD7-HP: 10 mm (Φ) × 150 mm (H), HONTA/XAD7-HP: 10 mm (Φ) × 100 mm (H)), a hot water circulation jacket, a metering pump, a fraction collector, and a constant-temperature hot water circulation system. In the column separation test, simulated HLLW solution (feed solution) spiked with tracer amounts of ^{241}Am and ^{152}Eu was used.

As eluents and washing solutions, 7 M nitric acid and distilled water were used for the TEHDGA/XAD7-HP column, and 0.2 M nitric acid and 1 M nitric acid were used for the HONTA/XAD7-HP column. The concentrations of ^{241}Am and

^{152}Eu in the aqueous phase were measured using a γ-ray spectrometer, and the concentrations of other metals were measured using ICP-AES.

3. RESULTS AND DISCUSSION

The results of the column test using TEHDGA/XAD7-HP adsorbent (flow rate: 3 cm^3 min^{-1}) are shown in Figure 1. First, all metal ions except ^{241}Am, Ln(III) were eluted with the washing solution (7 M nitric acid), followed by the target metal ions ^{241}Am, ^{152}Eu, and Ln(III) being eluted with the eluent (distilled water). This demonstrates that the TEHDGA/XAD7-HP adsorbent column can co-separate ^{241}Am and Ln(III) from a solution containing various metal ions including ^{241}Am. This indicates that separation is possible even at relatively high flow rates due to the rapid reaction between the metal ions and the extractant.

Next, the results of column tests using HONTA/XAD7-HP adsorbent are shown in Figure 2 at a flow rate of 1 cm^3 min^{-1}. After passing the feed solution and washing solution, the non-adsorbed components Ln(III) and ^{152}Eu were quickly eluted. Following the elution of the non-adsorbed components, ^{241}Am was eluted. This demonstrated that the HONTA adsorbent column can separate ^{241}Am and Ln(III) from a solution containing ^{241}Am and various metal ions. However, the peaks of Ln(III) and MA(III) were closely spaced, suggesting that the adsorption/desorption reactions between the metal ions and the extractant were slow, and the contact time required for adsorption onto the adsorbent was insufficient. Therefore, to achieve complete separation, it is necessary to extend the column length and optimize the flow rate.

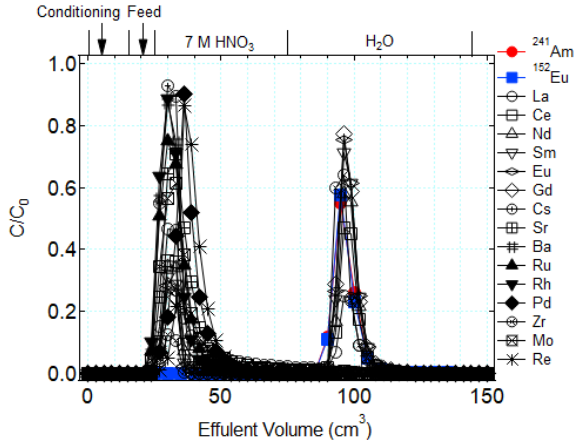


Fig.1 Chromatographic separation results for using TEHDGA/XAD7-HP. Flow rate: 3 cm^3 min^{-1}, height : 150 mm, inner diameter of the column: 10 mm, and temperature: 323 K

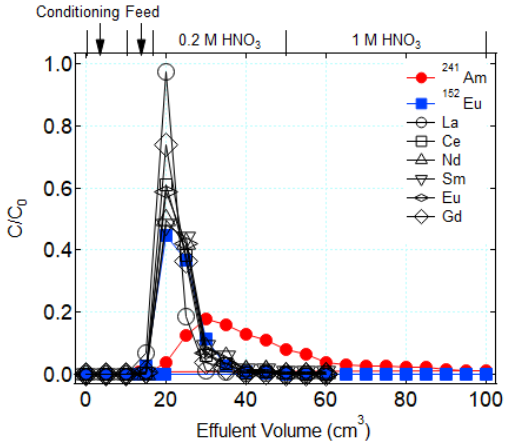


Fig.2 Chromatographic separation results for using HONTA/XAD7-HP. Flow rate: 1 cm^3 min^{-1}, height: 100mm, inner diameter of the column: 10 mm, and temperature: 298 K

4. CONCLUSIONS

To separation of MA(III) from solutions containing Ln(III) with similar chemical properties, we evaluated TEHDGA/XAD7-HP and HONTA/XAD7-HP columns using a solution spiked with ^{241}Am and ^{152}Eu in simulated HLLW. In column tests using TEHDGA/XAD7-HP adsorbent, simultaneous elution of Ln(III) and Am(III) was confirmed. In the subsequent separation process, HONTA/XAD7-HP adsorbent column was used, it was confirmed that ^{241}Am eluted after the rare earth elements. Thus, the possibility of separating and recovering MA(III) using a two-step separation flow was demonstrated.

References

[1] L. Xu, X. Yang, A. Zhang, C. Xu, C. Xiao, “Separation and complexation of f-block elements using hard-soft donors combined phenanthroline extractants”, *Coord Chem Rev.*, **496**, 215404 (2023).
[2] M. Kubota, S.-Y. Kim, H. Wu, T. Arai, S. Watanabe, Y. Sano, M. Takeuchi, “Study on the development of flow sheet for the separation of MA(III) and Ln(III) fission products using two-step process with impregnated adsorbents”, *Prog Nucl Sci Technol.*, in press (2025).

Copyright on 7th Asia-Pacific Symposium on Radiochemistry 2025

7th Asia-Pacific Symposium on Radiochemistry *September 14 ~ 19, 2025 • Kunibiki Messe • Shimane, Japan*

Synthesis of simulated radioactive waste containing ^{241}Am for evaluation of hydrogen generation

Ikarugi Riko, Kitatsuji Yoshihiro, Kumagai Yuta

Japan Atomic Energy Agency

1 Introduction

An adsorbent and sludge generated in The ALPS (Advanced Liquid Processing System) process for removing radionuclides are highly radioactive, and there is a need to develop technology to safely store and dispose of them at 1F decommissioning site. In the management of highly radioactive waste, the risk of hydrogen generation due to radiolysis is a concern. To rationalize the risk management of hydrogen generation, we are developing a technique to easily measure the amount of hydrogen generation from radioactive waste containing α-nuclides and clarifying the mechanism of hydrogen generation by radiolysis of hydrous solid.

Previous studies have shown that the stagnant water in the nuclear reactor buildings of 1F containing α-nuclides derived from nuclear fuel, most of which are sorbed onto fine particles, which are solid composed mainly of iron [1,2]. Therefore, we attempted to synthesize iron oxide particles containing ^{241}Am as simulated α-nuclides waste. In this presentation, we will describe the synthesis method of the simulated α-nuclide waste, the analysis of its chemical form, and the results of confirming the distribution state of ^{241}Am in the particles. In addition, the result of an attempt to measure the hydrogen generation of hydrous solid using synthesized simulated α-nuclides waste will also be reported.

2 Synthesis of simulated α-nuclide waste

Synthesis of simulated α-nuclide waste was performed by mixing a water solution of $FeCl_3 \cdot 6H_2O$ and $FeSO_4 \cdot 7H_2O$, adding 92.5 kBq of ^{241}Am, and then gradually adding ammonium hydroxide in an Ar atmosphere to form deposits by hydrolysis reaction. The resulting black precipitate was filtered and dried under reduced pressure. The radioactivity of precipitate and filtrate was measured, and it was confirmed that 99% of the added ^{241}Am was contained in the precipitate. The ^{241}Am content in the solid portion was estimated to be 107.7 kBq/g.

3 Analysis of simulated α-nuclide waste

To check the chemical state of simulated α-nuclide waste, X-ray diffraction and Raman spectroscopy were performed. The results revealed that the chemical form of simulated α-nuclide waste sample is the iron oxide γ-Fe_2O_3 shown in Fig. 1 and Fig.2[3,4]. To confirm the homogeneity of the synthesized simulated α-nuclide waste, a certain amount of the sample was aliquoted, and gamma ray was measured using Ge semiconductor detector to determine the amount of radioactivity per simulated waste sample weight. As a result, a strong correlation (R^2=0.9998) was observed between the weight and the radioactivity. From this result, it was confirmed that ^{241}Am was uniformly contained in the simulated α-nuclide waste.

Copyright on 7th Asia-Pacific Symposium on Radiochemistry 2025

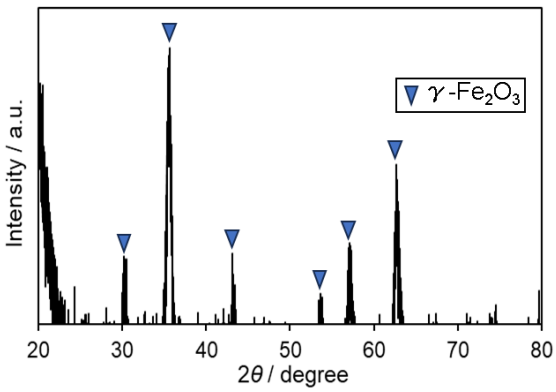


Fig1.XRD spectrum of product

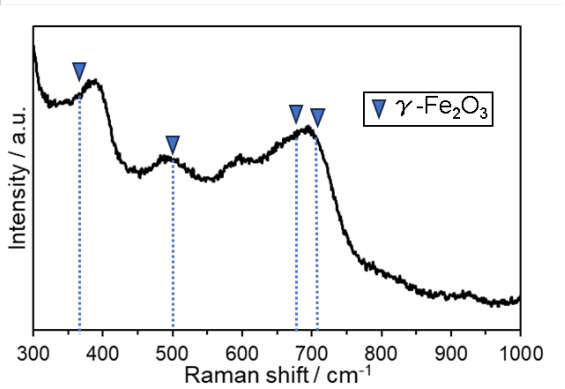


Fig2.Raman spectrum of product

4 Evaluation of hydrogen generation using simulated α nuclide waste

Using the synthesized simulated α-nuclide waste, the amount of hydrogen generating was measured by a hydrogen actual survey evaluation system. Two samples were prepared by dispensing approximately 100 mg of simulated α-nuclide waste into test tubes. One of the samples was made hydrous by adding pure water (10% of the sample weight), and the other was made dry. The change of the amount of H_2 generation in the test tube was examined. As shown in Fig 3, the amount of hydrogen generation increased with time. Compared to the dry sample, the hydrous sample showed an increasing trend in hydrogen generation. The synthesized simulated α-nuclide waste is applicable for the actual measurement of hydrogen production under various conditions.

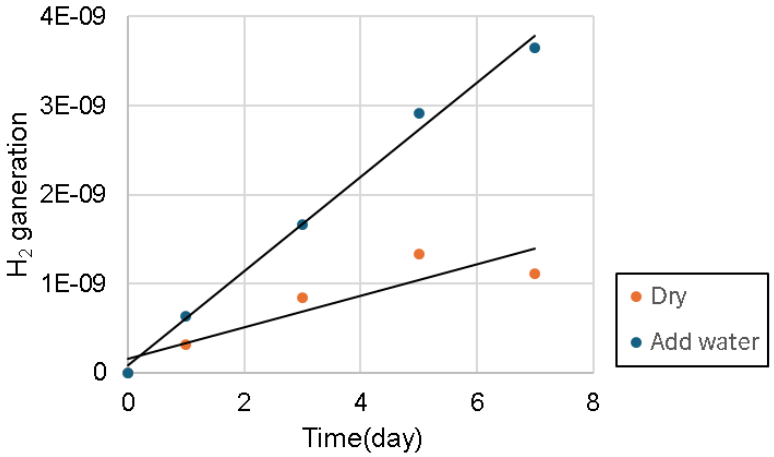


Fig3. The amount of generated H_2 by the time progress

ACKNOWLEDGMENTS

I would like to thank M. Kawai for supporting the Evaluation of hydrogen generation section.

References

[1] T. Yomigida et al., Analysis of particles containing alpha-emitters in stagnant water at torus room of Fukushima Dai-ichi Nuclear Power Station's Unit 2 reactor. *Sci. Rep.* 12, 7191 (2022).

[2] T. Yomigida et al., Analysis of particles containing alpha emitters in stagnant water in Fukushima Daiichi Nuclear Power Station's Unit 3 reactor building, *Sci. Rep.*, 14, 14945 (2024).

[3] P.P.C. Sartoratto et al., The thermal stability of maghemite-silica nanocomposites: An investigation using X-ray diffraction and Raman spectroscopy"Journal of Alloys and Compounds 434-435 (2007) 650-654.

[4] Guilherme V.M et al., Surface-enhanced Raman spectra of magnetic nanoparticles adsorbed on a silver electrode" Journal of Electroanalytical Chemistry 603 (2007) 27–34

7th Asia-Pacific Symposium on Radiochemistry *September 14 ~ 19, 2025 • Kunibiki Messe • Shimane, Japan*

Adsorption behavior of fission product elements on synthesized tungsten oxide type inorganic adsorbent supported in silica beads

Hanyu Wang, Xianwei Wang, Wenzun Luo, Naoki Osawa, Tatsuya Suzuki[1]

Nagaoka University of Technology, Kamitomiokamchi 1603-1, Nagaoka, Niigata,940-2137

As a commonly used material in separation technologies, inorganic adsorbents demonstrate significant application potential in radiochemical separation. They can be employed both for recovering valuable elements from fission products and for removing environmentally hazardous radioactive elements. In this study, batch experiments were conducted to evaluate the adsorption performance of a synthetic silicate-supported tungsten oxide hydrate (W-Si) toward representative elements under simulated high-level liquid waste (HLLW) conditions. The experimental results showed that W-Si exhibited markedly different adsorption capacities for the various representative elements in the simulated HLLW environment.

1 Introduction

Since the early twentieth century, in an effort to reduce over-reliance on fossil fuels and to meet the growing demand for affordable energy, nuclear energy programs have regained widespread global attention and momentum [1]. Against this backdrop, nuclear facilities—such as power reactors and spent fuel reprocessing plants—inevitably generate large volumes of radioactive liquid waste during operation. These waste streams contain various toxic and hazardous substances, particularly fission products with long half-lives and high radiotoxicity [2], such as strontium and cesium, as well as valuable noble metals like ruthenium, rhodium, and palladium.

Ion separation techniques commonly applied in the treatment of radioactive liquid waste include precipitation, ion exchange, solvent extraction, and chromatographic separation. Among these, ion exchange is widely adopted due to its excellent physical stability and high selectivity.

To address the critical challenge of efficiently separating and recovering valuable fission products or removing environmentally hazardous radioactive elements, this study aims to develop an efficient and environmentally friendly inorganic ion exchange material. Batch adsorption experiments were conducted to systematically investigate the adsorption behavior of a synthetic silicate-supported tungsten oxide hydrate (W-Si) toward various representative fission products under different nitric acid concentrations. The findings are expected to support the removal of radioactive elements and the recovery of noble metals, thereby providing a more optimized pretreatment strategy for radioactive waste management.

2 Experimental

2.1 Synthetic Experiment

The inorganic adsorbent was synthesized via vacuum impregnation using a rotary evaporator set to a rotational speed of 40° per second. First, about 19.8g of WCl_6 (Based on previous experimental results, the synthetic yield of the inorganic ion exchanger was determined to be around 80% under standard preparation conditions) and twice the volume of silicon dioxide (about 15g) were added to the pear-shaped flask. The reactor was heated to 100°C, and air was evacuated using a vacuum pump until the solution began to boil. The temperature was then lowered to 80°C and maintained for 24 hours. After this period, the silicone oil bath temperature was increased to 120°C under reduced pressure conditions to evaporate water. The resulting solids were repeatedly rinsed with ultrapure water until the filtrate reached a neutral pH of 7. Finally, the solids were placed in an evaporation unit and dried at 100°C for 2 hours to remove any remaining surface moisture.

2.2 Characterization

In order to further understand and confirm the composition and characteristics of the inorganic adsorbent, the XRD method was used to investigate the structure of the inorganic adsorbent by X-ray diffractometer (XRD, MiniFlex600, Rigaku, Japan).

2.3 Bath experiment

The simulated solution containing nearly every element at a concentration of 4 mg/L (strontium, zirconium, molybdenum, rhodium, palladium, cesium, barium, cerium) were prepared in 5 mL of nitric acid solution (0.01, 0.1, 0.5,

Copyright on 7th Asia-Pacific Symposium on Radiochemistry 2025

1, 2, 3, 4 mol/L). 0.1 grams (The inorganic adsorbent constituted 51.3% of the total mass) of the synthesized inorganic ion exchange resin was added to 4 mL of these simulated solutions. The mixed of W-Si and simulated solution were stirred at room temperature for about 24 hours. The solutions before and after the bath experiment were diluted, and the concentration of elements was measured using ICP-MS (Agilent 7700, Agilent, America).

3. Results and Conclusions

As shown in Figure 1, the synthesized inorganic adsorbent without silicon dioxide ($WO_3 \cdot H_2O$) predominantly consists of the tungstite phase. The characteristic peaks at 16.456° and 25.605° are consistent with the standard XRD pattern for tungstite, and the remaining minor peaks also match well with those in the reference card, further confirming the successful formation of tungstite.

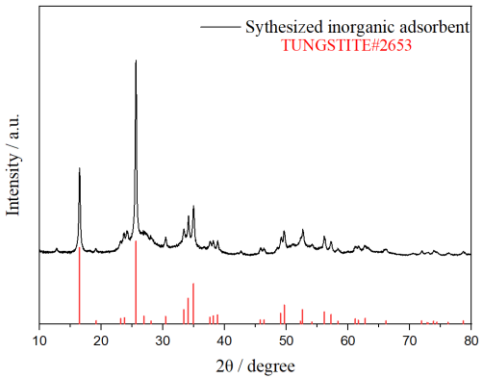


Fig.1. XRD patterns of inorganic adsorbent, SiO_2 and PDF cards

Figure 2 presents the batch experiments results for nine elements in simulated HLLW, focusing on the adsorption behavior of the W–Si under varying nitric acid concentrations. The results show that within the nitric acid concentration range of 0.01 to 4 mol/L, the W–Si adsorbent exhibits high distribution coefficients (Kd) for zirconium, cesium, and cerium. In contrast, the Kd values for barium and ruthenium decrease significantly with increasing acid concentration. For strontium, palladium, rhodium, and molybdenum, the Kd values remain low across the entire concentration range, showing weak Kd to nitric acid concentration.

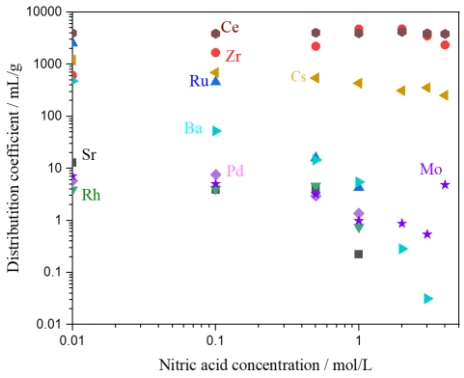


Fig.2. The result of bath experiment in HNO_3 environment

ACKNOWLEDGMENTS

This study was partially supported by the subsidy program “Project of Decommissioning, Contaminated Water and Treated Water Management” conducted by the Ministry of Economy, Trade and Industry of Japan.

References

[1] S. Inan, Y. Altas, Preparation of zirconium–manganese oxide/ polyacrylonitrile (Zr Mn oxide/PAN) composite spheres and the investigation of Sr(II) sorption by experimental design, Chem. Eng. J. 168 (2011) 1263–1271.

[2] Y. Park, Y.C. Lee, W.S. Shin, S.J. Choi, Removal of cobalt, strontium and cesium from radioactive laundry wastewater by ammonium molybdophosphate-polyacrylonitrile (AMP-PAN), Chem. Eng. J. 162 (2010) 685–695.

Chemical stability of sulfur-containing functionalized silica-based adsorbents under nitric acid conditions for platinum group metals adsorption

Naoki Osawa[1], Mai Tanaka[2], Hao Wu[3], Tatsuya Suzuki[1], Seong-Yun Kim[2]

[1]*Department of Nuclear Technology, Nagaoka University of Technology, Nagaoka, Niigata, 940-2188, Japan*
[2]*Department of Quantum Science and Energy Engineering, Tohoku University, Sendai, Miyagi, 980-8579, Japan*
[3]*School of Nuclear Science and Engineering, Shanghai Jiao Tong University, Shanghai, 200240, China*

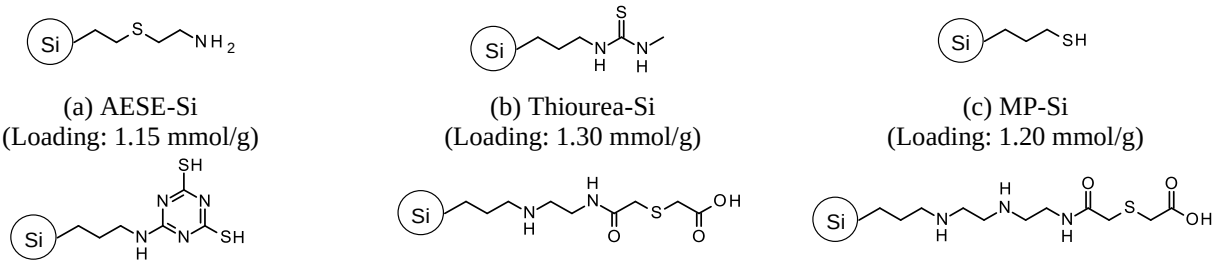
Chemical stability of adsorbents in nitric acid is essential for the separation of nuclides from high-level liquid waste (HLLW) when using the extraction chromatography method. Through batch adsorption experiments, this study investigates the adsorption performance of two types of sulfur-containing functionalized silica-based adsorbents to evaluate their effectiveness in adsorbing Pd(II). The chemical stability of the sulfur-containing groups in nitric acid solution is summarized based on nitric acid concentration, contact time, and reaction temperature. Results indicate that the sulfide function, which is incorporated into thiodiglycolamide type extractants for the adsorption of platinum group metals from HLLW, demonstrates chemical stability against nitric acid.

1 INTRODUCTION

Nuclide separation from high-level liquid waste (HLLW) involves various elements that contribute to the reduction of radioactive waste and the recovery of valuable materials. Recently, extraction chromatography has gained attention due to its use of less harmful organic solvents, simplified apparatus facilitating easy solid–liquid separation, and enhanced operability. The recovery of platinum group metals from HLLW can meet the rising demand in the catalysis industry and secure resources without dependence on specific production regions. The thiodiglycolamic (TDGA)-type extractant is considered a promising candidate for platinum group metal recovery due to the strong affinity between sulfur donors and platinum group metals in accordance with the Hard and Soft Acids and Bases Theory [1]. In the fields of ore smelting and catalyst recycling, platinum group metals are primarily treated as chloride complexes in hydrochloric acid solutions [2]. To successfully recover these metals from HLLW, stable adsorption performance in nitric acid solution must be achieved. This study utilizes two types of sulfur-containing functionalized silica-based adsorbents to investigate the effects of sulfur-containing groups on adsorption performance in nitric acid. The chemical stability of the sulfur-containing groups in relation to nitric acid is then evaluated by investigating sulfur leakage from six different types of adsorbents [3].

2 EXPERIMENTAL

Figure 1 illustrates the structures of sulfur-containing silica-based adsorbents. The effects of sulfur-containing functional groups are examined using two types of silica-based adsorbents: 2-aminoethyl sulfide-ethyl-functionalized silica gel (AESE-Si) and Thiourea- (Thiourea-Si). A batch adsorption experiment is conducted with simulated HLLW containing 5 mM of 15 different metal ions. The chemical stability of the sulfur-containing functional groups is then evaluated using four types of functionalized silica-based adsorbents: 3-mercaptopropyl- (MP-Si), 2,4,6-trimercaptotriazine- (DMT-Si), and TDGA acid derivatives (TDGAA2-Si, TDGAA3-Si). This evaluation considers nitric acid concentration, contact time, and reaction temperature by measuring the amount of sulfur that leaks into the solution following the batch adsorption experiment.



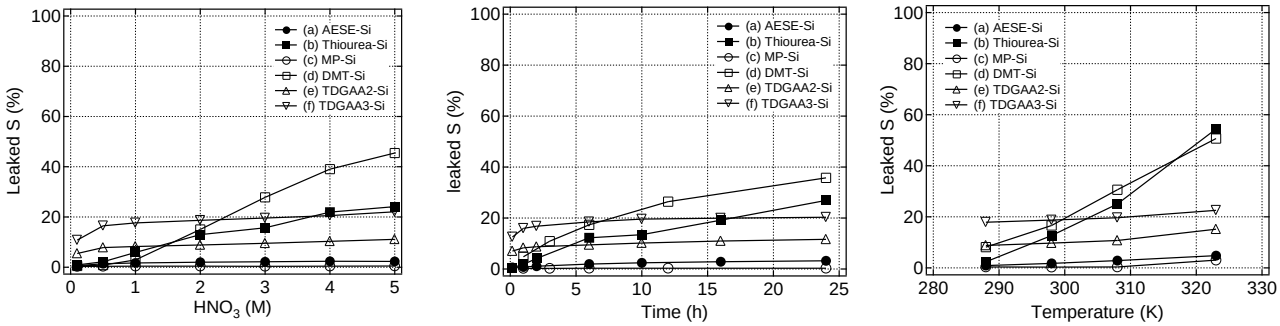
(a) AESE-Si (Loading: 1.15 mmol/g)
(b) Thiourea-Si (Loading: 1.30 mmol/g)
(c) MP-Si (Loading: 1.20 mmol/g)
(d) DMT-Si (Loading: 0.63 mmol/g)
(e) TDGAA2-Si (Loading: 1.53 mmol/g)
(f) TDGAA3-Si (Loading: 1.25 mmol/g)

Fig. 1. Structures of sulfur-containing functionalized silica-based adsorbent

Copyright on 7th Asia-Pacific Symposium on Radiochemistry 2025

3 RESULTS AND DISCUSSION

Results from batch adsorption experiments conducted over a contact time of 5 h at 298 K showed that the sulfide in AESE-Si and the thioketone in Thiourea-Si exhibited a high distribution coefficient for Pd(II), exceeding 10^3 cm^3/g within a nitric acid concentration range of 0.1 to 5 M. The ratio of sulfur leakage from the functional groups of the adsorbents is presented in Figure 2 and reflects variations in nitric acid concentration, contact time, and reaction temperature. AESE-Si, MP-Si, TDGAA2-Si, and TDGAA3-Si demonstrated chemical stability under nitric acid conditions. The sulfur leakage ratios from these adsorbents were largely unaffected by adsorption conditions, whereas Thiourea-Si and DMT-Si showed gradual effects. The results for TDGAA2-Si and TDGAA3-Si suggest that the secondary amine is resistant to nitric acid, whereas the deterioration of Thiourea-Si is primarily attributed to the decomposition of the thioketone. These findings indicates that the TDGA structure not only can provide selective adsorption for platinum group metals from HLLW, it can also maintain chemical stability under nitric acid conditions.



(a) Nitric acid concentration (contact time: 5 h, reaction temperature: 298 K)

(b) Contact time (HNO_3 concentration: 2 M, reaction temperature: 298 K)

(c) Reaction temperature (HNO_3 concentration: 2 M, contact time: 5 h)

Fig. 2. Ratios of Sulfur leakage from sulfur-containing functions

4 CONCLUSIONS

This study evaluated the adsorption performance and chemical stability of sulfur-containing functionalized silica-based adsorbents for the recovery of platinum group metals from HLLW. The sulfide function in AESE-Si and the thioketone function in Thiourea-Si demonstrated significant adsorption selectivity for Pd(II). The chemical stability of the TDGA structure was assessed by measuring the sulfur leakage from various types of sulfur-containing functionalized silica-based adsorbents.

References

[1] Naoki Osawa, Masahiko Kubota, Hao Wu, and Seong-Yun Kim, "Development of *N,N,N',N'*-tetra-2-ethylhexyl-thiodiglycolamide silica-based adsorbent to separate useful metals from simulated high-level liquid waste", *Journal of Chromatography A*, **1678**, 463353 (2022).

[2] Yu-Ki Taninouchi and Toru H. Okabe, "Technological development trends in platinum group metal recycling – Chemical pretreatment for efficient leaching-", *Journal of MMIJ*, **139**, 29-38 (2023).

[3] Naoki Osawa, "Fundamental study on separation characteristics of platinum-group metals and co-existing metals from high-level liquid waste using sulfur-containing amide-type silica-based adsorbent", *Doctoral Thesis (Tohoku University)* (2024).

Copyright on 7th Asia-Pacific Symposium on Radiochemistry 2025

Establishment of a multi-element ICP-MS/MS quantitative method for quality assurance of high-specific-activity Lu-177 preparations

Miki Harigai[1], Kazumi Nakano[3], Kenji Shirasaki[2], Hiroyuki Kimura[4], Tomoo Yamamura[1]

[1]*Institute for Integrated Radiation and Nuclear Science, Kyoto University: 2, Asashiro-Nishi, Kumatori-cho, Sennan-gun, Osaka, 590-0494, harigai.miki.2k@kyoto-u.ac.jp*

[2] *Institute for Radiation Science, The University of Osaka: 1-1 Machikaneyama, Toyonaka, Osaka, 560-0043, shirasaki@rirc.osaka-u.ac.jp*

[3]*Agilent Technologies, Inc.: 9-1 Takakura-cho, Hachioji, Tokyo, 192-8510, kazumi_nakano@agilent.com*

[4] *Agency for Health, Safety and Environment, Kyoto University: Yoshida-Konoe-cho, Sakyo-ku, Kyoto, 606-8315 , Kyoto, , kimura.hiroyuki.4u@kyoto-u.ac.jp*

High-specific-activity ^{177}Lu used in theranostic radiopharmaceuticals is acutely vulnerable to trace metal contaminants: sub-ppm Zn^{2+}, Fe^{3+} and Cu^{2+} can reduce radiochemical yield (RCY) and effective molar activity (EMA) by ≥ 30–60 % [1, 2]. Routine quality control with ICP-OES reaches a detection limit (DL) of only ~100 ppb for Fe, leaving ten + potentially critical elements unmanaged at the ppt scale [3]. We therefore established a triple-quadrupole ICP-MS/MS procedure that simultaneously quantifies fourteen elements (Na→Pb) at sub-ppb concentrations, directly supporting Good-Manufacturing-Practice (GMP) batch release.

Using an Agilent 8900 ICP-MS/MS, we systematically optimized cell-gas chemistries (He, H_2, O_2, NH_3) and Q_1/Q_2 isolation windows. External calibration (1–50 µg L^{-1}) generated element-specific DLs and background-equivalent concentrations (BECs). The method was applied to ten API lots of reactor-produced ^{177}Lu (2022–2024, Kyoto University Research Reactor Institute), and impurity profiles were correlated with DOTATATE labelling RCY and EMA.

All elements were quantified with DLs of 5–30 ppt and BECs of 4–35 ppt. Reactive-cell operation suppressed polyatomic interferences, lowering 56Fe and 78Se BECs from ≥ 0.1 ppb (no-gas) to ≤ 0.02 ppb. Day-to-day repeatability was excellent (sensitivity RSD ≤ 3 %, DL variability ≤ 10 %). Lot analysis revealed process-dependent fluctuations in Yb, Al, Fe and Ca; samples containing Fe > 20 ppb showed a drop in DOTATATE RCY from 70 % to 45 % and an almost 50 % reduction in EMA.

The protocol is 10^2–10^3-fold more sensitive than ICP-OES, enabling ppt-level metal specifications. When integrated with UPLC titration [4] and PCTA challenge testing [2], it delivers end-to-end impurity control that underpins the reliable, clinically reproducible supply of high-specific-activity ^{177}Lu and ^{90}Y radiopharmaceuticals.

1 Introduction

^{177}Lu and ^{90}Y are essential radionuclides for peptide receptor radionuclide therapy (PRRT) and PSMA-targeted therapy, with rapidly growing clinical demand [1]. However, when Zn^{2+} is present at a chelate/metal ratio of 0.10 (≈ 10 µM), the RCY of ^{177}Lu–DOTATATE decreases from 70% to 40%, and at 5 ppm Fe^{3+}, the p SCN Bn PCTA/^{90}Y labeling drops sharply to less than 20%, It has been reported that sub-ppm levels of multivalent metal ions significantly inhibit high-radioactivity labeling [1][2].

The composition of metal impurities depends on the manufacturing route. In ^{177}Lu, carrier Lu residues associated with the direct method (n,γ) and Yb, Al, Fe from the indirect method (Yb → Lu), as well as Ca and Cu derived from quartz fragment dissolution after irradiation, are of concern [3]. On the other hand, Al, Cu, Fe, and Zn residues are present in the solution of the ^{90}Sr/^{90}Y generator, with Fe^{3+} reaching up to 5 ppm in some cases [2].

The ICP OES method (Fe DL ≈ 100 ppb), which is currently mainstream in existing QC, has insufficient sensitivity and cannot ignore the effects of polyatomic interference [3]. Methods such as UPLC titration using DOTA peptides/metal complexes [4] and Fe screening utilizing the sensitivity of p SCN Bn PCTA [2] have been proposed; however, QC methods capable of simultaneously quantifying multiple elements at the ppt level and directly linking them to labeling quality indicators (RCY, EMA) have yet to be established.

The objectives of this study are to use the Agilent 8900 ICP MS/MS to (i) quantify 14 elements from Na to Pb at the ppt level and achieve management that exceeds international acceptable concentrations (Fe, Zn ≤ 5 ppb) by two orders of magnitude, (ii) clarify the quantitative correlation between impurity concentrations and RCY/EMA, and (iii) to provide operational guidelines directly linked to GMP batch release testing.

2 Experimental

2.1 Instrumentation and Tuning

An Agilent 8900 ICP MS/MS (installed in October 2024) was used, and routine inspections were conducted to confirm the mass axis (±0.1 amu), peak width (0.6–0.8 amu at –10 %), oxide ratio (CeO^+/Ce^+ < 1.5 %), and divalent ratio (Ce^{2+}/Ce^+

< 10%) during routine inspections. Q_1 was set to transmission mode or single isolation, and cell gas flow rates were set to He 4 mL min^{-1}, H_2 7 mL min^{-1}, O_2 0.35 mL min^{-1}, and NH_3 0.50 mL min^{-1}.

2.2 Calibration and Detection Limits

W II/W X mixed standard solutions and Na standard solutions were diluted with 1% HNO_3, and calibration curves were prepared in the concentration range of 1–50 μg L^{-1}. The sensitivity, DL, and BEC for each element were calculated based on standard guidelines (3σ criterion). Repeatability was evaluated over three days, confirming that the ^{89}Y sensitivity RSD ≤ 3% and DL variation ≤ 10%.

2.3 Application to Production Lots

Samples from 10 lots of ^{177}Lu raw material manufactured at the Kyoto University Research Reactor (KUR) from 2022 to 2024 were measured, and the results were compared with peptide purity [4] determined by UPLC titration, RCP/EMA [5] determined by HPLC UV, and PCTA sensitivity test [2].

3 Results and Discussion

3.1 Detection Limits and Backgrounds

The detection limits (DL) for 14 elements were 5–30 ppt (median 12 ppt), and the background concentrations (BEC) were 4–35 ppt, with all elements falling within the sub-ppb range (Table 3-1). Using MS/MS mode with cell gas, 56Fe, which is interfered by $^{40}Ar^{16}O^+$, ^{78}Se, which is interfered by $^{38}Ar^{40}Ar^+$, and 40Ca interfered by $^{40}Ar^+/^{40}K^+$ were reduced by more than one order of magnitude to ≤ 0.02 ppb (Fe, Se) and ≤ 0.05 ppb (Ca) [3].

3.2 Analysis of Production Lots

Analysis of 10 lots manufactured at KUR revealed variations in Yb, Al, Fe, and Ca concentrations due to irradiation methods (direct vs. indirect) and separation processes. In two lots where Fe concentrations exceeded 20 ppb, DOTATATE-labeled RCY decreased from 70% to 45%, EMA also decreased from 15 GBq $μmol^{-1}$ to 8 GBq $μmol^{-1}$.

3.3 Implications for GMP Release Testing

This method demonstrates sensitivity 10^2–10^3 times higher than ICP-OES, enabling a significant enhancement of ppb management standards to ppt. Additionally, by combining the UPLC titration method [4] and PCTA sensitivity test [2], consistent metal impurity monitoring from raw materials to final formulations can be achieved, providing a robust QC platform to support GMP batch release of high-ratio radioactivity $^{177}Lu/^{90}Y$ formulations.

Acknowledgments

This work was supported by the MEXT Innovative Nuclear Research and Development Program (Grant JPMXD0224019804).

References

[4] W. A. P. Breeman, H. S. Chan, E. de Blois, J. Radioanal. Nucl. Chem. 302 (2014) 825–830.
[3] D. Pawlak, J. L. Parus, I. Sasinowska, R. Mikolajczak, J. Radioanal. Nucl. Chem. 261 (2004) 469–476.
[1] M. Asti et al., Nucl. Med. Biol. 39 (2012) 509–517.
[5] M. Radzik et al., Nucl. Med. Biol. 93 (2021) 63–73.
[2] U. Pandey et al., Radiochim. Acta 102 (2014) 947–955.

7th Asia-Pacific Symposium on Radiochemistry *September 14 ~ 19, 2025 • Kunibiki Messe • Shimane, Japan*

Adsorption and separation performance of minor actinides and lanthanides using MPEDGA/SiO_2-P adsorbent

Riho Okajima[1,2], Masahiko Kubota[1], Seong-Yun Kim[1]

[1] *Department of Quantum Science and Energy Engineering, Graduate School of Engineering, Tohoku University, 6-6-01-2 Aza-Aoba-Aramaki, Aoba-ku, Sendai, Miyagi 980-8579 Japan, sonyun.kimu.d7@tohoku.ac.jp*
[2] *Japan Nuclear Fuel Limited, 4-108 Okitsuki Obuchi, Rokkasho, Aomori, 039-3212, Japan*

The separation of minor actinides (MA(III)) and lanthanides (Ln(III)) from high-level liquid waste was the purpose of synthesizing N,N′-Dimethyl-N,N′-di-2-phenylethyl diglycolamide (MPEDGA). The synthesized MPEDGA was impregnated into microporous silica particles to prepare an adsorbent, and its adsorption and separation properties were systematically evaluated through a series of experiments.

1 INTRODUCTION

The separation of fission products from high-level liquid waste (HLLW) remains a significant challenge throughout the nuclear fuel cycle. To address these issues, a partitioning process for the treatment of HLLW based on extraction chromatography using macroporous silica-based adsorbents has been investigated [1]. In particular, the separation of long-lived minor actinides (MA(III)) from HLLW generated during spent nuclear fuel reprocessing is essential to reduce the burden of waste disposal and mitigate environmental impacts [2]. As an extractant for the separation of MA(III) and lanthanides (Ln(III)) from HLLW, N,N′-Dimethyl-N,N′-di-2-phenylethyl-diglycolamide (MPEDGA) has demonstrated the ability to extract both MA(III) and Ln(III) by liquid-liquid extraction. However, there has been no systematic investigation of its adsorption characteristics in the solid phase and performance based on column methods. Therefore, it is necessary to collect fundamental data for the development of a practical process design. In the present study, we synthesized MPEDGA and prepared MPEDGA/SiO_2-P. The MPEDGA/SiO_2-P impregnation and composition were evaluated using a scanning electron microscope (SEM), and thermogravimetric analysis (TG). Batch experiments were used to examine the adsorption behavior of metal ions, and the adsorption distribution of Eu(III) and Nd(III) on the MPEDGA/SiO_2-P was confirmed by particle-induced X-ray emission (PIXE). Slope analysis was used to estimate the number of MPEDGA coordinated with Eu(III) and Nd(III). Column experiments were also conducted to evaluate the separation performance using a simulated HLLW.

2 EXPERIMENTAL

MPEDGA (Fig.1. (a)) was synthesized according to a previously reported reaction flow [3]. The MPEDGA/ SiO_2-P adsorbent was prepared by impregnating MPEDGA into SiO_2-P particles, as detailed in previous studies. The surface morphology was examined using SEM, and TG was conducted under a nitrogen atmosphere. Batch experiments were performed to evaluate the adsorption properties, using a simulated HLLW solution containing 15 different metal ions, as well as a solution containing 14 Ln(III) ions. A solid state study of the behavior of the MPEDGA/SiO_2-P adsorbent before and after the adsorption experiments was performed using PIXE. The number of MPEDGA coordinated with Eu(III) and Nd(III) was estimated using slope analysis. Additionally, column experiments were performed to assess the separation of metal ions. Metal ion concentrations before and after adsorption and separation were analyzed by ICP-AES and AAS.

3 RESULTS AND DISCUSSION

Figures 1(b) and 1(c) show SEM images of SiO_2-P and MPEDGA/SiO_2-P. The smooth surface and lack of visible MPEDGA deposits suggest successful impregnated into the SiO_2-P particles. Figure 1(d) presents the TG curves of SiO_2-P and MPEDGA/SiO_2-P. The weight loss derived from the divinylbenzene copolymer and MPEDGA was estimated from the TG results. In turn, the composition of the adsorbent was found to be 19.3 wt.% MPEDGA and 80.7 wt.% SiO_2-P. Furthermore, as shown in Figure 2, which presents the adsorption ratios of Ln(III) in a 2 M nitric acid solution, it was observed that Ln(III) with higher atomic numbers exhibited greater adsorption. In addition, the batch experiments demonstrated significant selectivity for other metal ions, particularly Zr(IV) and Re(VII). In column experiments using MPEDGA/SiO_2-P with simulated HLLW, Ln(III) were completely adsorbed from the feed solution. Subsequently, Ln(III) were eluted when pure water was passed through the column. Finally, Zr(IV) was selectively eluted using an $H_2C_2O_4$ solution. The results of the separation process demonstrate the effectiveness and selectivity of the MPEDGA/SiO_2-P adsorbent in separating Ln(III) from simulated HLLW. MA(III), which exhibits similar properties to Ln(III), is also predicted to undergo a comparable separation process.

Copyright on 7th Asia-Pacific Symposium on Radiochemistry 2025

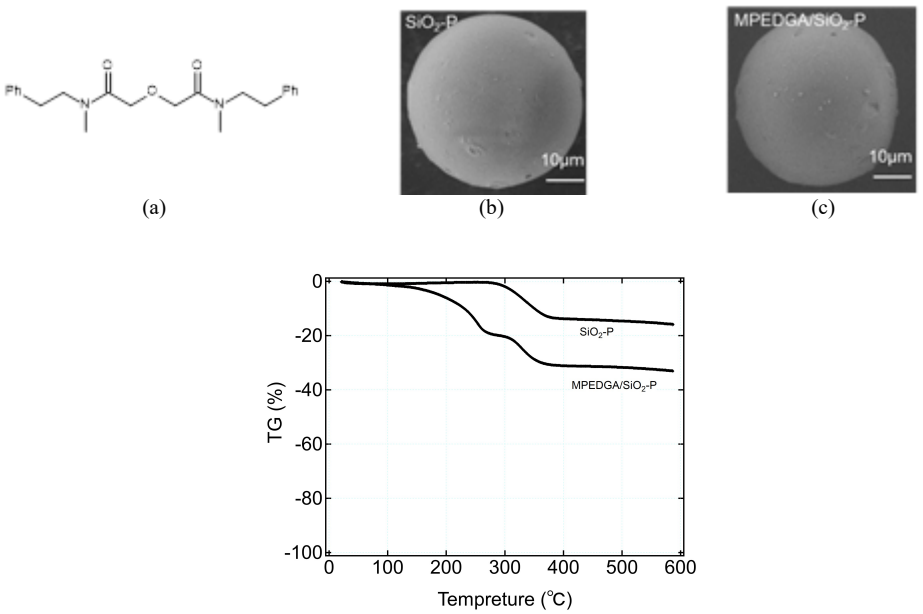


Fig.1. Characterization of the MPEDGA/SiO_2-P.
(a) Structural formula of MPEDGA, (b) SEM of SiO_2-P, (c) SEM of MPEDGA/SiO_2-P and (d) TG curves.

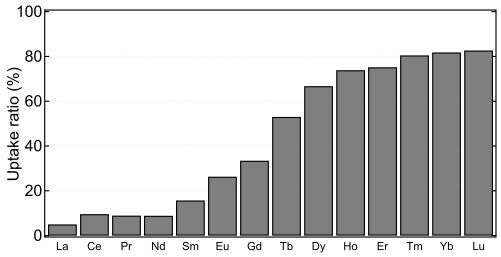


Fig.2. 2M HNO_3 Concentration on uptake ratio of 14 metal ions onto MPEDGA/SiO_2–P.
[Metal]: 1 mM for the 14 metal ions, [HNO_3]: 2M, temperature: 25°C, contact time: 5 h.

4. CONCLUSIONS

MPEDGA was synthesised and impregnated into SiO_2-P. Its adsorption and separation properties were then evaluated through a series of systematic experiments. The impregnation and composition of the MPEDGA on the SiO_2-P were confirmed using SEM and TG analyses. Batch experiments revealed that Ln(III) with a higher atomic number exhibited greater adsorption ratio. Column experiments confirmed the separation behavior of Ln(III) eluted water. These results indicate that MPEDGA/SiO_2-P may be a promising adsorbent for the separation of MA(III) and Ln(III).

References

[1] S.-Y. Kim, Y. Xu, T. Ito, Y. Wu, T. Tada, K. Hitomi, E. Kuraoka and K. Ishii, “A novel partitioning process for treatment of high level liquid waste using macroporous silica-based adsorbents”, *Journal of Radioanalytical and Nuclear Chemistry*, **295**, 1043-1050 (2013)
[2] J Veliscek-Carolan, “Separation of actinides from spent nuclear fuel: A review”, Journal of Hazardous Materials , **318**, 266-281 (2016)
[3] S.-Y. Kim, T. Takahashi, T. Ito and Y. Wu, “Selective Separation of Trivalent Europium(III) from Americium(III) using N,N’Dimethyl-N,N’-di-2-phenylethyl-diglycol Amide (MPEDGA) Extractant in Ionic Liquid”, *Solvent Extraction Research and Development, Japan*, **28**, 49-57. (2021)

Copyright on 7th Asia-Pacific Symposium on Radiochemistry 2025

Spent Nuclear Fuel Reprocessing and Regeneration in Accelerator Driven Advanced Nuclear Energy System

Fang-Li Fan, De-Sheng Chen, Cun-Min Tan, Mu-Lin, Wei Tian, Qing-Gang Huang, Jing Bai, Zhi Qin

Institute of Modern Physics, Chinese Academy of Sciences, Lanzhou 730000, China

Nuclear energy as clean energy has become an effective technology to deal with the global energy crisis and climate change. However, a drawback of nuclear energy is the disposal of spent nuclear fuel, due to the long-term and high radiotoxicity generated by the minor actinides (MAs) and plutonium. Therefore, reprocessing and regeneration of spent nuclear fuel became the key issues for the environmentally friendly and sustainable development of nuclear energy. A successful approach involved in recycle of spent nuclear fuel is needed to maximize energy utilization of the fuel by recovering actinide (An) species present while also minimizing the waste destined for geologic storage and simultaneously meeting nonproliferation standards. Currently, about 99.5% uranium and plutonium have been recovered in aqueous reprocessing by PUREX process. However, PUREX process generates a large volume of high level radioactive liquid wastes still possessing significant amounts of long-lived and highly radioactive minor actinides (neptunium, americium and curium).

For the development of nuclear energy requirements, the concept of an accelerator-driven advanced nuclear energy system (ADANES) has been proposed in China. ADANES consists of a burner system and a fuel recycle system. By taking the powerful exogenous neutrons of ADANES, transmutation, proliferation and power generation will be implemented in the burner. For the spent nuclear fuel reprocessing, only some volatile/semi-volatile fission products and metal fission products with relatively high fast neutron absorption cross-section are need to remove. The rest spent nuclear fuel will be refabricated to new nuclear fuel and burned in the accelerator driven advanced nuclear energy system. Due to the operation control of accelerator, is has inherent safety.

The spent nuclear fuel reprocessing and regeneration for accelerator driven advanced nuclear energy system have been studied in our laboratory. Here, high temperature dry reprocessing was the main technology. For those volatiles and semi-volatile fission products (^{3}H, ^{14}C, Kr, I, Xe, Mo, Tc, Ru, Te and so on) can be easily removed through high temperature oxidation/reduction processes. For some metal fission products (Sm, Nd, Ru, Rh, et al) with relatively high fast neutron absorption cross-section, anhydrous separation processes are being developed. Moreover, this reprocessing procedure is not necessary to separate the long-lived minor actinides Np, Am and Cm finely. These rest spent nuclear fuel including some fission products would be refabricated as new nuclear fuels referring to the preparation technologies of UO_2 fuel. Current research work focuses on the simulated spent nuclear fuel. Further research about spent nuclear fuel reprocessing and regeneration will continue to be conducted.

Copyright on 7th Asia-Pacific Symposium on Radiochemistry 2025

7th Asia-Pacific Symposium on Radiochemistry *September 14 ~ 19, 2025 • Kunibiki Messe • Shimane, Japan*

ADSORPTIVITY OF TRIPHOSPHINE TRIOXIDE-IMPREGNATED ANION EXCHANGE RESINS FOR RECOVERY OF URANIUM FROM SEAWATER

Shion Matsumoto[1], Yukito Tonai[2], Chikage Abe[3], Masanobu Nogami[1,2]

[1]*Graduate School of Science and Engineering Research, Kindai University: 3-4-1 Kowakae, Higashi-Osaka, Osaka, 577-8502, mnogami@emat.kindai.ac.jp*
[2]*Faculty of Science and Engineering, Kindai University: 3-4-1 Kowakae, Higashi-Osaka, Osaka, 577-8502*
[3]*Institute for Materials Research, Tohoku University: 2145-2 Narita-cho, Oarai-machi, Higashiibaraki-gun, Ibaraki, 311-1313*

Adsorbents for recovery of uranium from seawater, more preferably concentrated seawater, were prepared by impregnating a triphosphine trioxide into two types of anion exchange resins. Investigation on adsorptivity of these adsorbents to U(VI) in NaCl solutions revealed that the adsorptivity of both adsorbents decreased with increasing NaCl concentrations, and that the adsorptivity under higher NaCl concentrations was high enough.

1 Introduction

We have previously found that PPTPT-(Poly-CMS), an adsorbent prepared by impregnating 1,1,3,5,5-pentaphenyl-1,3,5-triphosphapentane trioxide (PPTPT : Fig. 1(a)) into porous silica support coated with a copolymer of chloromethylstyrene (CMS) and divinylbenzene (DVB), indicates unusually high selectivity for uranium (VI) in low-concentration nitric acid [1]. This property suggests that this adsorbent may be capable of adsorbing U(VI) in neutral aqueous solutions such as seawater. We are also aiming to apply this adsorbent for the separation of U(VI) from concentrated seawater which is emitted from desalination plants of seawater. However, adsorptivity of this adsorbent in salt solutions is reduced due to its hydrophobic nature [1]. To overcome the problem, use of polar polymer supports has been explored. In the previous study [2], the adsorbent combining PPTPT with a candidate polar polymer support, dihydroxyphosphono resin (RCSPO : Fig. 1(b)) (PPTPT-RCSPO), exhibited adsorption to U(VI) in high-concentration NaCl solutions.

In this study, in order to explore alternative polar polymer supports to RCSPO, the adsorptivity of adsorbents combining PPTPT with anion exchange resins to U(VI) was investigated in NaCl solutions.

2 Experimental

A strongly-basic anion exchange resin of quaternary ammonium type (AER : Fig. 1(c)) and a weakly-basic anion exchange resin of tertiary pyridine type (PyAER : Fig. 1(d)) were used as candidate polar polymer supports. AER was synthesized by the conventional manner, *i.e.*, by reacting trimethylamine with Poly-CMS [1], and PyAER was synthesized by following Ref. [3]. PPTPT-AER and PPTPT-PyAER were prepared by impregnating PPTPT into AER and PyAER, respectively. As test solutions, 0.17-1.71 mol/dm^3 (= M) NaCl (0.51 M for seawater) containing 1 mg/dm^3 (= ppm) U(VI) were used. They were prepared by 100-fold dilution of an ICP-MS standard solution containing U(VI) and other 17 kinds of metal ions (100 ppm each) in 5% HNO_3, followed by adjusting pH to 7.9-8.1 using Na_2CO_3 solutions. Precipitated metal ions caused by pH adjustment were removed by filtration. For the adsorption procedure, the samples were prepared by mixing each adsorbent (0.15 g) with the test solution (3 cm^3) at room temperature for 24 h. Concentrations of U in the liquid phase were then measured using ICP-MS. The adsorptivity was evaluated by distribution ratio (K_d).

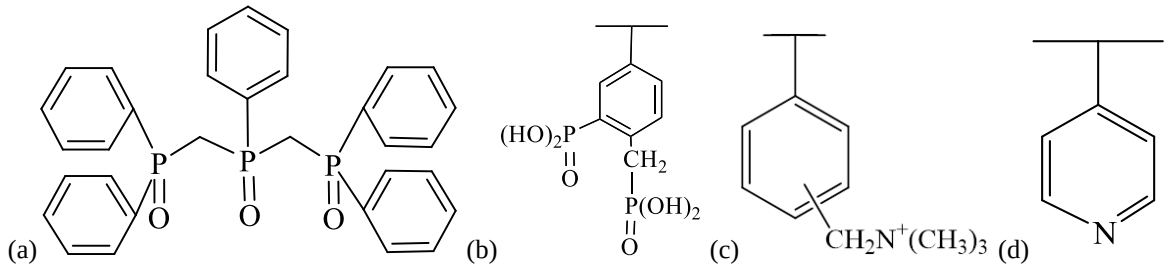


Fig. 1. Chemical structures of (a) PPTPT, (b) RCSPO, (c) AER, and (d) PyAER.

Copyright on 7th Asia-Pacific Symposium on Radiochemistry 2025 P-R3-28* -

3 Results and Discussion

Figure 2 shows adsorptivity of each adsorbent to U(VI) in NaCl solutions. The K_d values for PPTPT-AER, PPTPT-PyAER, and AER decrease with increasing NaCl concentrations. While, no adsorptions are observed for PyAER. Similarly, no significant adsorptions are observed for AER in the range of 0.51-1.71 M NaCl. The adsorptivity of both PPTPT-impregnated adsorbents shows no significant difference between AER and PyAER. These results indicate that the adsorption of PPTPT-AER (in 0.51-1.71 M NaCl) and PPTPT-PyAER (in all examined NaCl concentrations) to U(VI) is attributed solely to the impregnated PPTPT. The reason for the decrease in K_d values with increasing NaCl concentrations for PPTPT-AER and PPTPT-PyAER is expected to be interference by Na^+ ions. On the other hand, the opposite tendency was observed for PPTPT-RCSPO where the K_d values increased with increasing NaCl concentrations [2]. The difference in the above trend will be investigated in the near future. Comparing the absolute K_d values for PPTPT-RCSPO [2], those for PPTPT-AER and PPTPT-PyAER are improved, suggesting that AER and PyAER may be more suitable for enhancing the adsorptivity of PPTPT than RCSPO.

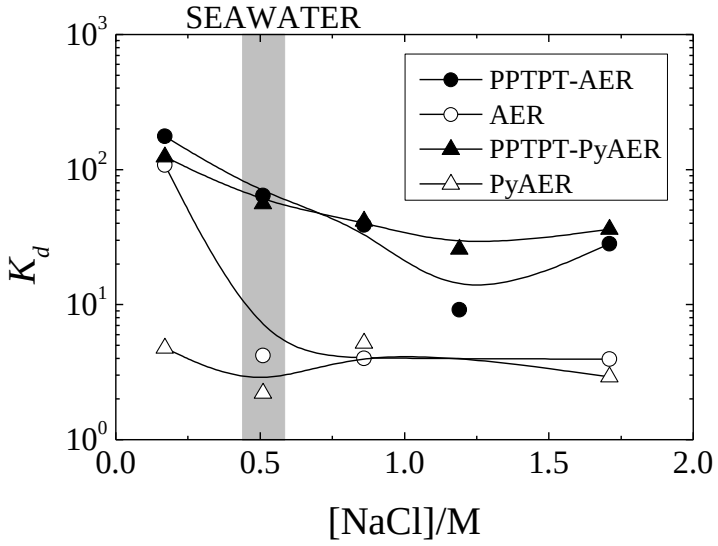


Fig. 2. Adsorptivity of each adsorbent to U(VI) in NaCl solutions.

References

[1] M. Nogami, Y. Sugiyama, and Y. Ikeda, "Adsorptivity of silica-supported adsorbents impregnated with polyphosphine polyoxides to U(VI) and some other metal ions in nitric acid media," J. Radioanal. Nucl. Chem., **284**, 195(2010).

[2] K. Hashimoto, M. Nogami, M. Harada, and Y. Ikeda, "Synthesis and Adsorptivity of Novel Bifunctional Chelating Adsorbent for Recovery of Uranium from Seawater," Abst. ASNFC 2015, Tokyo, Japan, 2015 Dec, 2B-24.

[3] M. Nogami, M. Aida, Y. Fujii, A. Maekawa, S. Ohe, H. Kawai, and M. Yoneda, "Ion-exchange selectivity of tertiary pyridine-type anion-exchange resin for treatment of spent nuclear fuels," Nucl. Technol., **115**, 293(1996).

Copyright on 7th Asia-Pacific Symposium on Radiochemistry 2025 P-R3-28* -

7th Asia-Pacific Symposium on Radiochemistry *September 14 ~ 19, 2025 • Kunibiki Messe • Shimane, Japan*

Solidification and Stabilization Treatment of Liquid Nuclear Fuel Waste Containing Oil

Takeru Matsuishi, Toshiaki Hiyama[1], Fuminori Honda[†]

[1] *Central Institute of Radioisotope Science and Safety, Kyusyu University, Motooka 744, Fukuoka Nishi, Fukuoka, 819-0395, Japan,* [†] *honda.fuminori.790@m.kyushu-u.ac.jp*

A wide variety of nuclear fuel materials are stored in universities, research institutions, and companies, often in diverse chemical forms and under conditions posing significant management risks. Furthermore, long-term disposal strategies for such waste remain unclear. This study investigates the solidification and stabilization of oily liquid waste containing particulate nuclear fuel materials such as uranium. Using commercially available polymer-based solidification agents, solidification was achieved by applying amounts exceeding standard dosage guidelines, thus providing a pathway for managing liquid radioactive waste in solid form. Additionally, centrifugation techniques were employed to sediment fine particles within the oil, enabling separation into low- and high-concentration fractions. This method has the potential to reduce the risk of leakage significantly by minimizing particulate content in the waste.

1 Introduction

Uranium is used not only as nuclear fuel but also in industrial applications, and in fundamental and applied research fields such as magnetism, novel superconductors, and spintronics, owing to the unique properties of its 5*f* electrons. In Japan, uranium is legally classified as a nuclear fuel material. Because uranium emits alpha radiation and has an extremely long half-life, its handling and storage require strict caution. At the small-scale nuclear fuel handling facilities (hereinafter referred to as "KLOFs"), only small quantities of uranium are used. However, because these facilities are often engaged in research and development, they generate a variety of materials that must be rigorously controlled—including products, research samples, waste, and contaminated items that contact nuclear fuel materials during handling.

Currently, Japan lacks public disposal facilities for nuclear fuel-containing waste. As a result, such waste is stored long-term at individual facilities. A major concern during long-term storage is the degradation of container integrity. In fact, leakage incidents involving liquid waste containing radioactive materials have occurred due to container deterioration, troubling facility managers. Liquid waste poses greater contamination and decontamination challenges than solid waste, often seeping into flooring and significantly increasing secondary waste volume.

Liquid waste must be classified and treated based on whether it is organic or inorganic, acidic or basic, and its flammability or explosiveness. One strategy for safer management is solidification. Solidification methods include solvent extraction, ion exchange, evaporation and drying, and high-temperature oxidation. However, KLOFs typically do not have permission to implement such methods, resulting in long-term storage of liquid waste in sealed plastic or glass containers.

Organic liquid waste requires careful treatment due to toxicity and risks of fire or explosion. Oil-based waste is particularly problematic due to its large volume and flammability. Cutting, grinding, or electrical discharge machining (EDM) of uranium or thorium intermetallic compounds often uses paraffin or mineral oils, leading to contamination. Uranium particles can also be found in rotary pump oils used for vacuum operations. Studies confirm the presence of substantial amounts of oil-based waste containing significant trace nuclear fuel materials at domestic research facilities. Establishing a processing flow for stabilizing such waste is urgently needed.

In our presentation we report stabilization trials targeting oil contaminated with uranium, focusing on (1) direct solidification using polymer materials and (2) particle-oil separation via centrifugation.

2 Experimental Procedure

2.1 Direct Solidification Using Polymer Materials:

Cold tests were conducted using actual EDM oil (ENEOS, METALWORK EDF-K2), cutting oil (Refinetec Co. Ltd., Lubricant Q), and rotary pump oil (MORESCO, MR-200). Commercial polymer-based solidifying agents primarily composed of vegetable-based materials were used. 100 mL of each oil sample was heated to 100 °C and mixed with an excess amount of solidifying agent, followed by cooling to room temperature. Figures 1(a) and 1(b) show the oils and solidifier used in this study, respectively.

Copyright on 7th Asia-Pacific Symposium on Radiochemistry 2025

2.2 Centrifugal Separation of Oil and Particles:

Simulated waste was created by cutting a cerium metal rod with Lubricant Q, generating an oil suspension containing cerium and cerium oxide particles. This suspension was centrifuged at 2500 rpm for 15 minutes using a Kokusan H-80α centrifuge. Residual cerium in the supernatant was measured with an EDX-7000 fluorescence X-ray analyzer (Shimadu Co. Ltd.).

3. Experimental Results

3.1 Direct Solidification Using Polymer Materials:

As shown in Fig. 1(c), partial solidification was achieved when heating oils to 100 °C and mixing with 3-4 g of solidifier. Solidification was incomplete with the standard dose of solidifier. Nearly complete solidification resembling wax or soap was achieved at five times the standard dose. However, re-softening occurred above 50 °C, indicating that controlled storage temperatures and sealing are necessary to prevent leakage.

3.2 Centrifugal Separation of Oil and Particles:

The cerium-laden oil suspension, obtained by cutting the cerium metal rod was visually turbid as shown in Fig. 2(a). Using quantitative filter paper, about 200 mL of the suspension was filtered within several hours. Particles settled naturally after 1-2 days of static storage. Centrifugation significantly accelerated this process. Figure 2(b) shows the suspension after centrifugation at 2500 rpm for 15 min. Note that the right bottle in Fig. 2(b) is a reference one, which was left for 20 minutes without centrifugation. As can be seen, centrifugation works well for sedimentation and clarification of the supernatant, indicating its practicality for processing large volumes.

4. Conclusion:

We explored two stabilization strategies for uranium-contaminated oil waste: direct solidification using polymer materials and particle-oil separation via centrifugation. Cold tests were conducted using actual EDM and cutting oils. Preliminary analyses of elemental content in oil-based waste were performed. We also developed simulated oily waste and assessed its separation via centrifugation, evaluating methods to quantify and manage particulate uranium in oil. These findings contribute to safe and practical waste stabilization procedures for small-scale nuclear facilities.

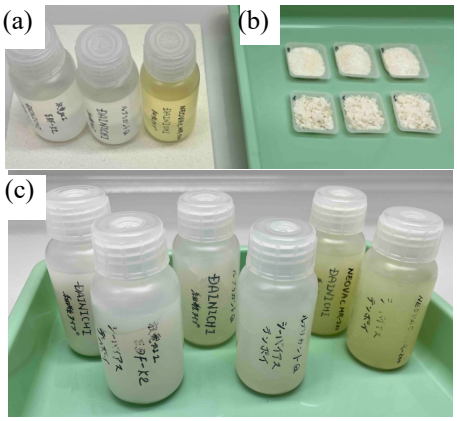


Fig.1 (a) Test oils for solidification and (b) polymer-based solidifying agents, and (c) direct solidification using polymer materials.

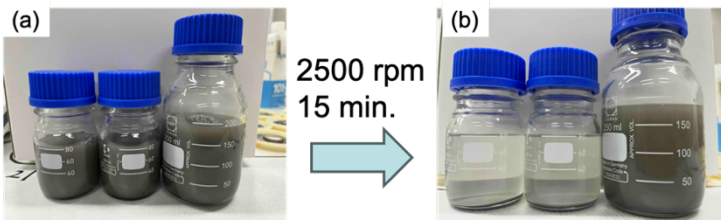


Fig.2 The Lubricant Q oil (a) after cutting the cerium metal rod and (b) after centrifuge 2500 rpm for 15 min. The right bottle in (b) is a reference bottle that was left uncentrifuged for 20 min.

In the conference, we will present results of the application of the coagulation–sedimentation treatment method for uranium waste liquid.

ACKNOWLEDGMENTS

This work is financially supported by the Nuclear Energy System Research and Development Project (Gensiryoku System Kaihatsu Jigyo). The authors acknowledge technical support with Dr. Homma and valuable discussions with Drs. Shirasaki (Tohoku U.), Yamamura (Kyoto U.), and Tachibana (Kyushu U.).

7th Asia-Pacific Symposium on Radiochemistry *September 14 ~ 19, 2025 • Kunibiki Messe • Shimane, Japan*

A Study on the Preliminary Evaluation of the Nuclide Monitoring for Modelling at High-Level Radioactive Waste Disposal Site

Woo-Beom Ha[1], Do-Won Hyun[1], Sang-Hoen Lee[1], Jong-Soon Song[1]

[1]*Chosun University, 309 Pilmun-daero, Dong-gu, Gwangju, Republic of Korea, and jssong@chosun.ac.kr*

This study aimed to develop a radionuclide migration monitoring technique to ensure the long-term safety of a high-level radioactive waste disposal facility. Using the RESRAD-OFFSITE code, a preliminary evaluation was conducted to assess the migration behavior of actinide series radionuclides in groundwater pathways in a deep subsurface environment. Preliminary results indicate that some long-lived radionuclides may reach external exposure points after tens of thousands of years, and the study confirmed the potential to establish criteria for selecting radionuclides and determining the start of monitoring for the establishment of a long-term monitoring system.

1. Establishment of evaluation methods and input factors

In this study, the RESRAD-OFFSITE program was used to evaluate long half-life and highly toxic nuclides such as U-233, U-238, Np-237, and Am-241. The model utilized for the assessment was the Exponential Release Model, which can effectively reproduce long-term release scenarios. To reflect the deep disposal environment, conservative parameters were set to determine the reachability of nuclides through the groundwater pathway, including hydraulic conductivity (1 m/y), hydraulic gradient (0.02), and effective porosity (0.2), which govern groundwater flow within the subsurface rock media. The distance to the well was set to 100 m and the simulation period to 100,000 years. Based on the conservative settings of the key parameters, the time to well location and concentration evolution of each nuclide was predicted over time. [1-4]

2. Interpretation of results

The results of simulating the concentration changes of U-233 in well water over time, based on its movement through the groundwater pathway, are shown in Figure 1. During the initial tens of thousands of years, U-233 did not reach the well location, maintaining a concentration level close to '0'. After approximately 70,000 years, U-233 began to gradually move along the saturated zone pathway and reach the well location, resulting in a slow increase in concentration. In particular, after approximately 80,000 years, the concentration in well water rose sharply, reaching approximately 6.5×10^{4} pCi/L at the 100,000-year time point. This is interpreted as being due to the slow groundwater movement speed of the radionuclide, low hydraulic conductivity, and strong adsorption characteristics. In other words, U-233 tends to remain at the contamination source for extended periods, or its movement is delayed due to interactions with the geological medium, resulting in gradual accumulation over tens of thousands of years before being released externally.

3. CONCLUSIONS

This study utilized the RESRAD-OFFSITE code to predict the long-term groundwater migration of U-233, a representative nuclide suitable for setting long-term monitoring criteria due to its long half-life and delayed migration characteristics in deep disposal environments, and to quantitatively evaluate the concentration changes at external exposure points. The simulation results showed that key nuclides such as U-233 and U-238 reached the well water location after a time lapse of tens of thousands of years or more, followed by a rapid concentration increase. This is due to the low water mobility and long-term accumulation characteristics of these nuclides, which are important factors to be considered in the design of groundwater monitoring systems outside the repository.

In particular, this study is significant as a preliminary approach to evaluate the predictability of long-term concentration changes in the deep environment from the perspective of 'nuclide mobility monitoring' and can be used as a basis for future detailed modeling studies with detailed numerical analysis and parameter sensitivity analysis.

Copyright on 7th Asia-Pacific Symposium on Radiochemistry 2025

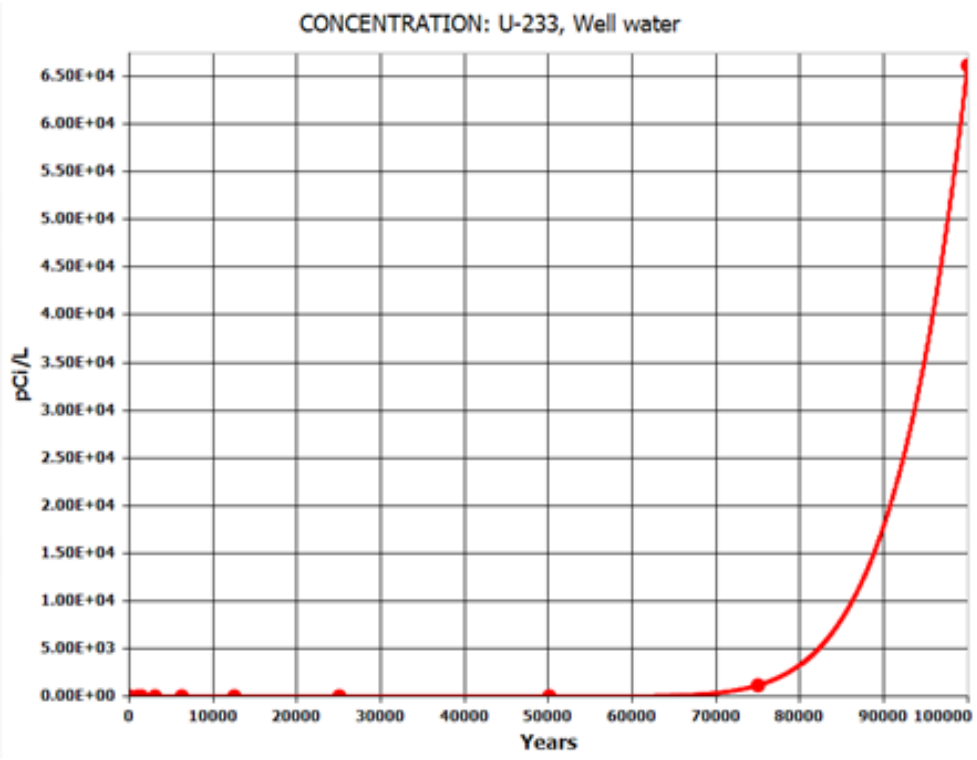


Fig. 1. Spill concentration of U-233 over time

ACKNOWLEDGMENTS

This work was supported by the Korea Institute of Energy Technology Evaluation and Planning(KETEP) and the Ministry of Trade, Industry & Energy(MOTIE) of the Republic of Korea (No. RS-2024-00419806).

References

[1] S. G. KIM and C. H. KANG and Y. M. LEE and Y. S. HWANG, Performance Assessment for Radionuclides Transport from HLW Repository, *Proceedings of the Korean Society of Soil and Groundwater Environment Conference*, pp.41-46 (2001).

[2] S. J. PARK and B. S. SHIN and S. Y. AHN and J. Y. LEE, Safety assessment of second-phase disposal facility in Gyeongju low- and intermediate level radioactive waste (LILW) repository using RESRAD-OFFSITE code, *Journal of Nuclear Science and Technology*, 58, 11 (2021)

[3] T. Y. NA and B. G. CHAE and E. S. PARK and M. J. KIM, Comparative Analysis of Siting Criteria of High-Level Radioactive Waste Disposal in Leading Countries. *The Journal of Engineering Geology*. (2024)

[4] Paul Wersin, et al. Sulphide Fluxes and Concentrations in the Spent Nuclear Fuel Repository at Olkiluoto. POSIVA 2014-01

Copyright on 7th Asia-Pacific Symposium on Radiochemistry 2025 P-R3-30* -

Poster Presentation | [R4]Nuclear Probe in Chemistry

Wed. Sep 17, 2025 6:30 PM - 8:00 PM JST | Wed. Sep 17, 2025 9:30 AM - 11:00 AM UTC Poster

[Poster] R4

[P-R4-01*]

MEASUREMENT AND FIRST-PRINCIPLES CALCULATION OF LOCAL FIELDS AT THE NUCLEI OF In/Cd DOPANTS IN ANATASE TiO_2

*Hiiro Amaike[1], Hokuto Shinmei[1], Wataru Sato[1], Tomonori Ida[1] (1. Kanazawa University (Japan))

[P-R4-02*]

Synthesis and ^{61}Ni Mössbauer measurements of Hofmann-Type Supramolecular Complex Using 3-Fluoropyridine

*Yayoi Shinohara[1], Kosuke Kitase[1], Shinji Kitao[4], Takumi Kubota[5], Yasuhiro Kobayashi[4], Makoto Seto[4], Daisuke Akahoshi[2,3], Takahumi Kitazawa[1,3] (1. Department of Chemistry, Faculty of Science, Toho University (Japan), 2. Department of Physics, Faculty of Science, Toho Univercity (Japan), 3. Research Centre for Materials with Integrated Properties, Toho University (Japan), 4. Institute for Integrated Radiation and Nuclear Science, Kyoto University (Japan), 5. Agency for Health, Safety and E nvironment, Kyoto University (Japan))

[P-R4-03*]

MAGNETIC PROPERTIES OF Zn FERRITE $Zn_xFe_{3-x}O_4$

*Hibiki Hirahara[1], Taisuke Ito[1], Wataru Sato[1,2] (1. Graduate School of Natural Science and Technology, Kanazawa University (Japan), 2. Institute of Science and Engineering, Kanazawa University (Japan))

[P-R4-04*]

^{61}Ni Mössbauer Spectroscopic and Chemical Characterization for Supramolecular Fe(4-cyanopyridine)$_2$[Ni(CN)$_4$] Host Framework Materials

*Tamaki Chiba[1], Kosuke Kitase[1], Shinji Kitao[4], Yasuhiro Kobayashi[4], Takumi Kubota[5], Makoto Seto[4], Daisuke Akahoshi[1,3], Takahumi Kitazawa[3,2] (1. Department of Chemistry, Faculty of Science, Toho University (Japan), 2. Department of Physics, Faculty of Science, Toho University (Japan), 3. Research Centre for Materials with Integrated Properties, Toho University (Japan), 4. Institute for Integrated Radiation and Nuclear Science, Kyoto University (Japan), 5. Agency for Health, Safety and Environment, Kyoto University (Japan))

[P-R4-05*]

EFFECT OF INDIUM CONCENTRATION ON THE PHOTOCATALYTIC PERFORMANCE AND LOCAL STRUCTURE OF $SrTiO_3$

*Ibuki Ejiri[1] (1. Graduated school of Natural Science and Technology, Kanazawa University (Japan))

[P-R4-06*]

INITIAL STATE OF CAPTURED MUON IN COPPER ATOM AND CHEMICAL ENVIRONMENTAL DEPENDENCE ON MUON CAPTURE

*Miu Nomura[1], Satoaki Den[1], Naoko Nishino[1], Kazuhiko Ninomiya[1], I-Huan Chiu[2], Shunsuke Asari[3], Akira Sato[3], Takashi Yoshimura[3], Alex Amato[4], Sayato Biswas[4], Lars Frieder Gerchow[4], Carlos Vigo[4], Chennan Wang[4], Charles Hillis Mielke III[4], Debarchan Das[4], Fabian Hotz[4], Gianluca Janka[5], Hubertus Luetkens[4], Katharina von Schoeler[4], Narongrit Ritjoho[6], Thomas Prokscha[4], Toni Shiroka[4], Zaher Salman[4], Zurab Guguchia[4] (1. Hiroshima University (Japan), 2. Japan

©APSORC25

Atomic Energy Agency (Japan), 3. Osaka University (Japan), 4. Paul Scherrer Institute (Switzerland), 5. ETH Zürich (Switzerland), 6. Suranaree University of Technology (Thailand))

©APSORC25

7th Asia-Pacific Symposium on Radiochemistry *September 14 ~ 19, 2025 • Kunibiki Messe • Shimane, Japan*

MEASUREMENT AND FIRST-PRINCIPLES CALCULATION OF LOCAL FIELDS AT THE NUCLEI OF In/Cd DOPANTS IN ANATASE TiO_2

H. Amaike[1], H. Shimmei[1], T. Ida[1,2], W. Sato[1,2]

[1]*Graduate School of Natural Science and Technology, Kanazawa University: Kanazawa, Ishikawa 920-1164, Japan*
[2]*Institute of Science and Engineering, Kanazawa University: Kanazawa, Ishikawa 920-1192, Japan*

In the present research, we have worked on doping of donor indium ions (In^{3+}) into the lattice of anatase TiO_2 by means of a sol-gel method followed by a solid-state reaction. The formation of anatase was confirmed by the X-ray diffraction (XRD) patterns. Perturbed angular correlation (PAC) measurements with the $^{111}Cd(\leftarrow {}^{111}In)$ probe introduced in anatase TiO_2 revealed that the probe occupies a site exhibiting an explicit electric quadrupole frequency of 17.9 Mrad/s, and density functional theory (DFT) calculation demonstrates that the above position occupied by the probe is a substitutional Ti site. These results signify successful doping of donor In into anatase.

1 INTRODUCTION

Titanium dioxide (TiO_2) doped with various metal ions has been attracting attention as promising semiconductors. Anatase is known to be a metastable TiO_2 with the widest band gap of 3.2 eV of all TiO_2 structures, leading to applications in materials for power devices or sensors. However, information on the local structure of impurity-doped anatase is limited because of the lack of its thermal stability for doping. In this study, we investigated the appropriate temperature conditions for doping of trivalent indium ions (In^{3+}) as impurities into anatase TiO_2 based on powder X-ray diffraction (XRD) patterns. In addition to the bulk structural information, the electric field gradients at the impurity nuclei were measured by the perturbed angular correlation (PAC) method using ^{111}Cd ($\leftarrow {}^{111}In$) as a probe, and the local structure around the probe was identified by comparing the experimental results with density functional theory (DFT) calculation results for a crystal model shown in Fig. 1.

2 EXPERIMENTS AND CALCULATIONS

Anatase TiO_2 was prepared by a solid-state reaction of precursors synthesized by the sol-gel method using titanium(IV) isopropoxide, acetic acid, and isopropanol as starting reagents [1]. After each sample was calcined in air, the synthesis of anatase TiO_2 was confirmed by XRD. After adding a droplet of $^{111}Cd(\leftarrow {}^{111}In)$ HCl solution, the same sample was again heat treated in air for the diffusion of the probe. Then, PAC measurements were performed at room temperature.

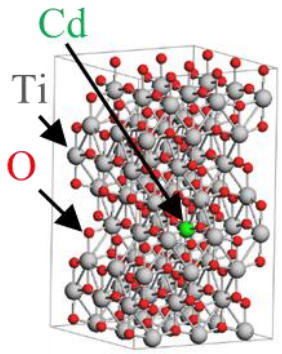


Fig. 1. The Structure of anatase TiO_2 doped with a Cd ion.

For first-principles calculations, the TiO_2 crystal model was constructed based on a crystal structure consisting of 72 Ti atoms and 144 O atoms determined by X-ray structural analysis, with one Ti atom replaced by a Cd atom (Fig. 1). For DFT calculation conditions, the PAW method was employed as a pseudopotential and the GGA-WC was employed as an exchange-correlation functional. The electric field gradient at the Cd nucleus was calculated taking structural relaxation into account. All calculations were performed with Quantum ESPRESSO [2].

Copyright on 7th Asia-Pacific Symposium on Radiochemistry 2025

3 RESULTS & DISCUSSION

Fig. 2 is the XRD pattern obtained for a sample calcined in air at 823 K for 16 hours. The synthesized crystal has a single phase of anatase. We found from the experiment that rutile is grown when precursor powder is calcined longer than 16 hours. The PAC spectrum for the anatase sample is shown in Fig. 3. The quadrupole frequency for the probe was found to be 17.9 Mrad/s. This value is in good agreement with that obtained by the DFT calculation as listed in TABLE 1.

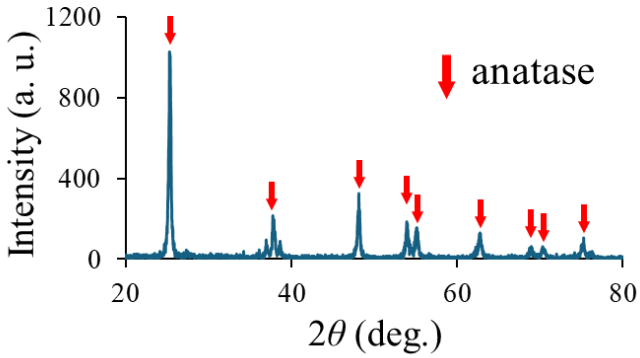


Fig. 2. XRD pattern obtained for a sample calcined at 823 K for 16 h.

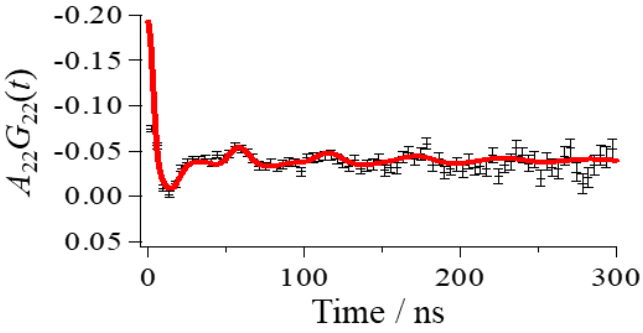


Fig. 3. PAC spectrum of the ^{111}Cd (← ^{111}In) probe in anatase.

TABLE 1. Electric quadrupole interaction parameters at impurity ^{111}Cd nuclei in TiO_2 obtained by PAC measurements and DFT calculations

Crystal		Dopant	ω_Q (Mrad/s)	η
Rutile	Exp. (this work)	^{111}Cd(← ^{111}In)	16.8(7)	0.18(1)
	Calc. (this work)	Cd^{2+}	13.5	0.20
Anatase	Exp. (this work)	^{111}Cd(← ^{111}In)	17.9(3)	0.08(1)
	Calc. (this work)	Cd^{2+}	14.3	0.00

References

[1] M. Tahir et al., *Appl. Catalysis B: Envi*. **162**, 99 (2015).
[2] P. Giannozzi et al., *J. Phys. Condens. Matter* **21**, 39550 (2009).

Copyright on 7th Asia-Pacific Symposium on Radiochemistry 2025 P-R4-01* -

Synthesis and ^{61}Ni Mössbauer measurements of Hofmann-Type Supramolecular Complex Using 3-Fluoropyridine

Yayoi Shinohara[1], Kosuke Kitase[1], Shinji Kitao[4], Yasuhiro Kobayashi[4], Takumi Kubota[5], Makoto Seto[4], Daisuke Akahoshi[2,3], Takafumi Kitazawa[1, 3]

[1]1 - Department of Chemistry, Faculty of Science, Toho University, 2-2-1 Miyama, Funabashi, Chiba, 274-8510, Japan
2 - Department of Physics, Faculty of Science, Toho University, 2-2-1 Miyama, Funabashi, Chiba, 274-8510, Japan
3 - Research Centre for Materials with Integrated Properties, Toho University, 2-2-1 Miyama, Funabashi, Chiba, 274-8510, Japan
4 - Institute for Integrated Radiation and Nuclear Science, Kyoto University, 2 Asashiro-nishi, Kumatori, Sennan-gun, Osaka, 590-0494, Japan
5 - Agency for Health, Safety and Environment, Kyoto University, Gokasho, Uji, Kyoto 611-0011, Japan

Proto-type of Hofmann-type spin crossover (SCO) coordination compound, Fe(pyridine)$_2$[Ni(CN)$_4$], was found in 1996.[1] Hofmann-type supramolecular complexes are a class of two- or three-dimensional coordination polymer frameworks composed of Fe(II) centers linked by square-planar $[Ni(CN)_4]^{2-}$ metalloligands and axial organic ligands such as pyridine and 3-fluoropyridine.[2],[3] SCO Hofmann-type compound are one of most sophisticated switchable coordination complexes associated with the potential applications in memories, molecule switches, sensors, and artificial muscles.

We have synthesized a Hofmann-type supramolecular complex, Fe(3-fluoropyridine)$_2$[Ni(CN)$_4$], using a direct method, with the goal of obtaining novel Mössbauer parameters for ^{61}Ni and investigating its spin crossover (SCO) behavior. The complex was characterized using CHN elemental analysis, infrared spectroscopy, thermogravimetric (TG) analysis, SQUID magnetometry, and ^{61}Ni Mössbauer spectroscopy.

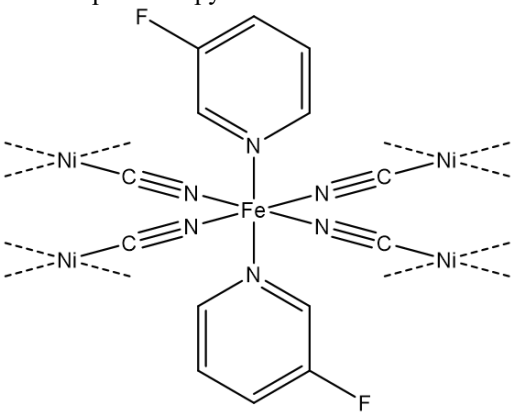


Figure 1: Estimated structure of Fe(3-fluoropyridine)$_2$[Ni(CN)$_4$]

^{61}Ni Mössbauer measurements have been carried out because there were few studies. Natural abundance(%) of ^{61}Ni is 1.25%. The nuclear γ -resonance effect in ^{61}Ni was first observed in 1960 by Obenshain and Wegener.[4] A key achievement in the ^{61}Ni Mössbauer spectroscopy was the successful preparation of a ^{61}Co Mössbauer source via the photonuclear reaction ^{62}Ni(γ, p)^{61}Co. The source was produced by irradiating a ^{62}Ni–14at%V alloy target with 31 MeV bremsstrahlung X-rays generated by the linear accelerator (LINAC) at Kyoto University's Institute for Integrated Radiation and Nuclear Science (KURNS). The resulting ^{61}Co ($T_{1/2} \approx 99$ minutes) was used for Mössbauer emission spectroscopy at 21 K. ^{61}Ni Mössbauer spectroscopy using the 67.4keV γ -ray emission line showed partially spilt lines due to the electric quadrupole interaction. The analysis was fitted in Lorentz distribution.

The Mössbauer spectra of the synthesized complex exhibited an isomer shift of –0.03 mm/s relative to a Ni-14at%V reference alloy, indicating that Ni(II) exists in a divalent low-spin state. While the FWHM of Ni-14at%V was 0.48 mm/s, it of the synthesized complex was 2.05 mm/s. Quadrupole splitting was also appeared, suggesting that the Ni(II) center adopts a square-planar coordination geometry.

Copyright on 7th Asia-Pacific Symposium on Radiochemistry 2025 P-R4-02* -

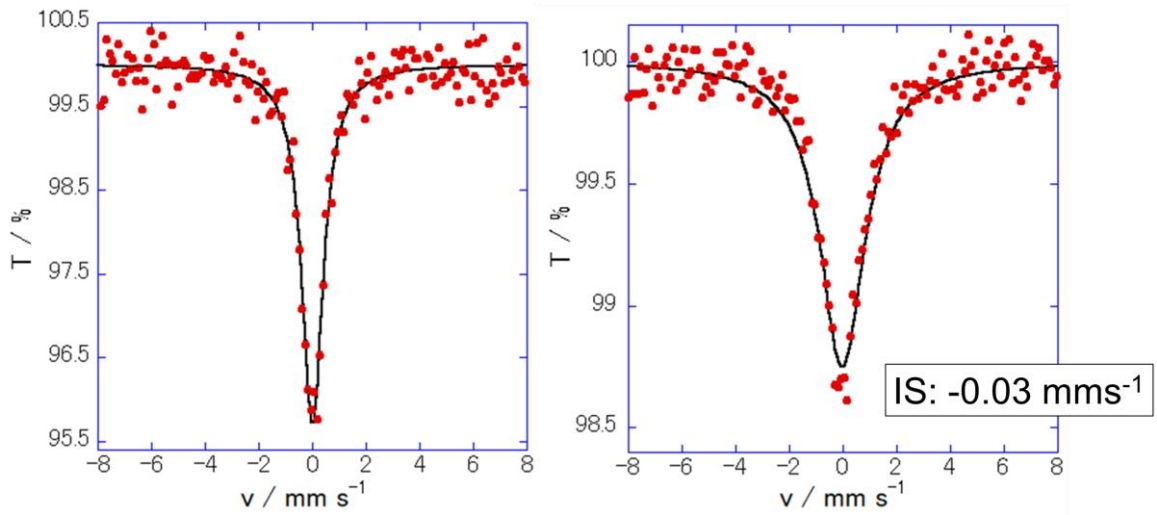


Figure 2: ^{61}Ni Mössbauer measurement results of (left)Standard sample Ni-14at%V and (right) Fe(3-fluoropyridine)$_2$[Ni(CN)$_4$]

Furthermore, the reversible color change from yellow to orange was observed between room temperature and 80 K, indicating SCO behavior. The SQUID data as shown in Figure 3 revealed an abrupt spin transition between high-spin and low-spin states, with a hysteresis width (ΔT) of 10 K and a spin transition rate of 81%. Notably, the hysteresis width was narrower than previously reported for nanoparticle forms of the same complex, suggesting differences in particle size or surface conditions.[2],[3]

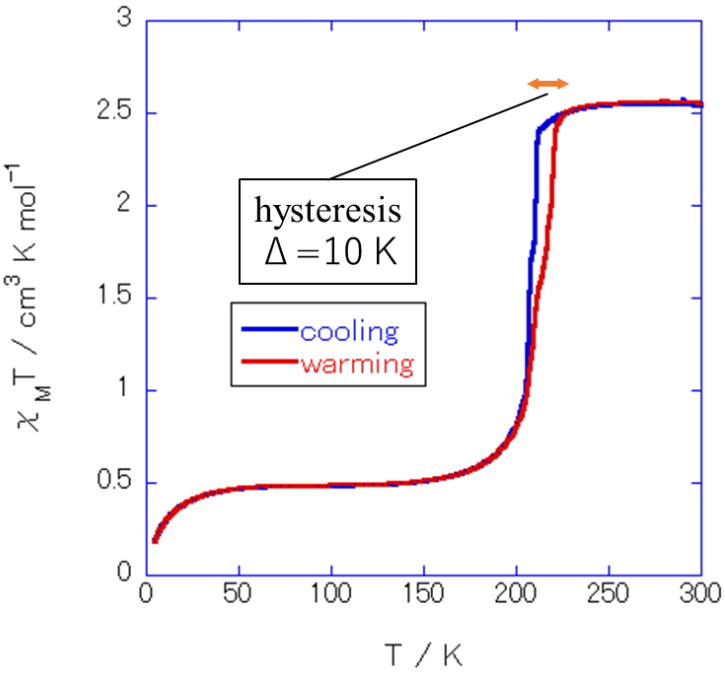


Figure 3: SQUID measurement results of Fe(3-fluoropyridine)$_2$[Ni(CN)$_4$]

References

1. T. Kitazawa, Y. Gomi, M. Takahashi, M. Takeda,M. Enomoto, A. Miyazaki and T. Enoki, J. Mater. Chem.,1996, 6, 119–121;
2. V. Martínez, A.B. Gaspar, M.C. Muñoz, G.V. Bikini, G. Levchenko, and J.A. Real. Chem. 2009.Eur. 15.10960-10971
3. V. Martínez, I. Boldog, A.B. Gaspar, V. Ksenofontov, A. Bhattacharjee, P. Gütlich and J.A. Real. Chem.Mater. 2010.22. 4271-4281
4. F.E.Obenshain and H.H.F.Wegener. :Phys. Rev. 1961. 121,1344

Copyright on 7th Asia-Pacific Symposium on Radiochemistry 2025 P-R4-02* -

7th Asia-Pacific Symposium on Radiochemistry *September 14 ~ 19, 2025 • Kunibiki Messe • Shimane, Japan*

MAGNETIC PROPERTIES OF Zn FERRITE $Zn_xFe_{3-x}O_4$

Hibiki Hirahara[1], Taisuke Ito[1], Wataru Sato[1, 2]

[1]*Graduate School of Natural Science and Technology, Kanazawa University, Kanazawa, Ishikawa 920-1192, Japan*
[2]*Institute of Science and Engineering, Kanazawa University, Kanazawa, Ishikawa 920-1192, Japan*

Magnetic properties of Zn ferrite $Zn_xFe_{3-x}O_4$ with a normal spinel structure were investigated by means of Mössbauer spectroscopy. Low-temperature spectra suggest that the superexchange interaction between the B-site Fe ions is ferromagnetic, which is different from antiferromagnetic interaction in Cd ferrite with a similar structure.

1. INTRODUCTION

Spinel ferrites have received high interest for application to a wide range of spintronic devices because of the variation of their electrical and magnetic properties depending on the type of constituent cations and their occupied sites. $CdFe_2O_4$ and $ZnFe_2O_4$ are well known normal spinel ferrites; however, their crystal structure and superexchange interactions make their magnetic properties very complex [1-3]. As for partially *A*-site substituted Cd ferrite, $Cd_{0.75}Fe_{2.25}O_4$, spin glass behavior with very long relaxation time has been observed in our previous research. In this study, we investigated magnetism in $Zn_xFe_{3-x}O_4$, an isomorphic compound of $ZnFe_2O_4$, by ^{57}Fe transmission Mössbauer spectroscopy; comparative and contrastive observations for different *x* are discussed.

2. EXPERIMENTS

Stoichiometric amounts of ZnO, Fe_2O_3, and Fe_3O_4 powders were mixed in a mortar for 1 hour. After pressing into pellets, they were calcined at 1100 °C for 45 minutes in vacuum. Powder X-ray diffraction patterns were obtained for each sample to confirm the synthesis of the target compounds. Mössbauer spectroscopy measurements were performed in the temperature range of 10 to 298 K to investigate the temperature and thermal profile dependences of their magnetic properties.

3. RESULTS AND DISCUSSION

Fig. 1 shows the ^{57}Fe Mössbauer spectra of $ZnFe_2O_4$ measured at 298 K and 10 K. It was found that $ZnFe_2O_4$ is in a paramagnetic state at 298 K and 10 K. Fig. 2 shows the ^{57}Fe Mössbauer spectra of $Zn_{0.9}Fe_{2.1}O_4$ measured at 298 K and 10 K. For $Zn_{0.9}Fe_{2.1}O_4$, in contrast to $ZnFe_2O_4$, the Mössbauer spectrum at 10 K clearly shows magnetic components, signifying the growth of magnetic domains, despite the presence of only a small fraction of Fe^{3+} ions in the *A* site.

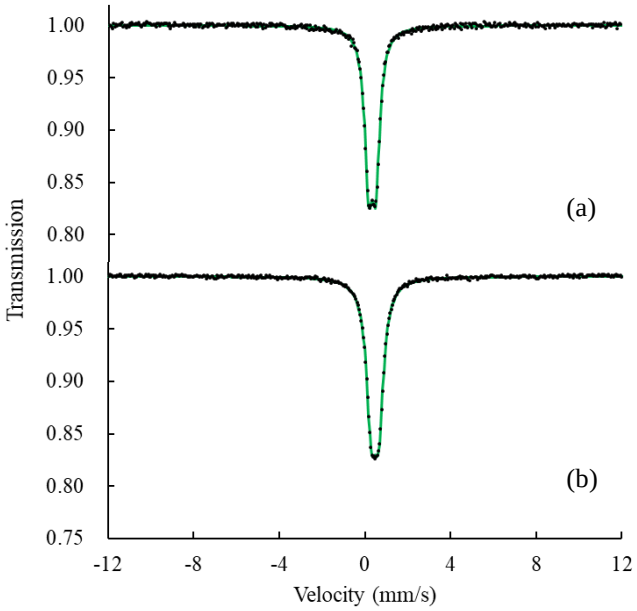


Fig. 1. ^{57}Fe Mössbauer spectra of $ZnFe_2O_4$ measured (a) at 298 K and (b) at 10 K.

Copyright on 7th Asia-Pacific Symposium on Radiochemistry 2025

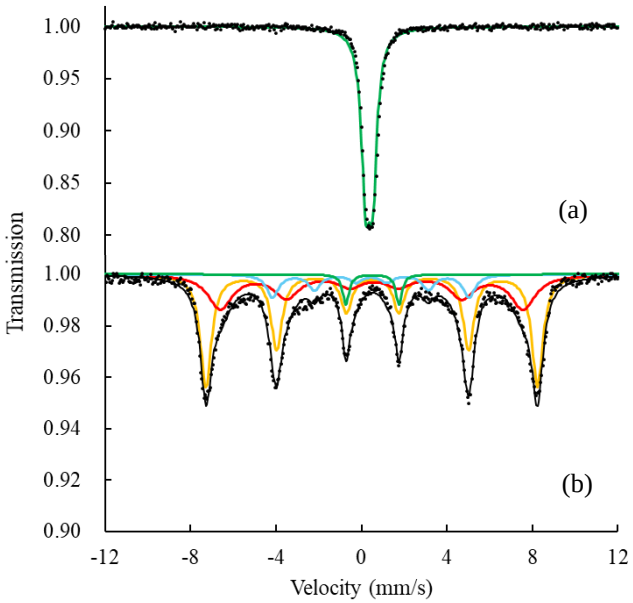


Fig. 2. ^{57}Fe Mössbauer spectra of $Zn_{0.9}Fe_{2.1}O_4$ measured (a) at 298 K and (b) at 10 K.

The *B* sites in the spinel structure have a pyrochlore lattice, and if the superexchange interactions between the *B*-site Fe ions cause antiferromagnetic coupling, magnetic frustration arises and prevent spin ordering as has been observed in our previous work for $Cd_{0.75}Fe_{2.25}O_4$. The low-temperature spectrum of $Zn_{0.9}Fe_{2.1}O_4$ signifies that spins in Fe^{3+} are well ordered, suggesting that the superexchange interaction between *B*-site Fe ions of $Zn_{0.9}Fe_{2.1}O_4$ is ferromagnetically correlated.

References

[1] Y. Yamada, K. Kamazawa and Y. Tsunoda, Phys. Rev. B **66**, 064401 (2002).
[2] K. Kamazawa and Y. Tsunoda, Phys. Rev. B **68**, 024412 (2003).
[3] T. Usa, K. Kamazawa, H. Sekiya, S. Nakamura, Y. Tsunoda, K. Kohn and M. Tanaka, J. Phys. Soc. Jpn. **73**, 2834 (2004).

7th Asia-Pacific Symposium on Radiochemistry *September 14 ~ 19, 2025 • Kunibiki Messe • Shimane, Japan*

^{61}Ni Mössbauer Spectroscopic and Chemical Characterization for Supramolecular Fe(4-cyanopyridine)$_2$[Ni(CN)$_4$] Host Framework Materials

Tamaki Chiba[1], Kosuke Kitase[1], Shinji Kitao[4], Yasuhiro Kobayashi[4], Takumi Kubota[5], Makoto Seto[4], Daisuke Akahoshi[2,3], Takafumi Kitazawa[1, 3],

1 - Department of Chemistry, Faculty of Science, Toho University, 2-2-1 Miyama, Funabashi, Chiba, 274-8510, Japan
2 - Department of Physics, Faculty of Science, Toho University, 2-2-1 Miyama, Funabashi, Chiba, 274-8510, Japan
3 - Research Centre for Materials with Integrated Properties, Toho University, 2-2-1 Miyama, Funabashi, Chiba, 274-8510, Japan
4 - Institute for Integrated Radiation and Nuclear Science, Kyoto University, 2 Asashiro-nishi, Kumatori, Sennan-gun, Osaka, 590-0494, Japan
5 - Agency for Health, Safety and Environment, Kyoto University, Gokasho, Uji, Kyoto 611-0011, Japan

Fe(4-cyanopyridine)$_2$[Ni(CN)$_4$] framework belonging to two-dimensional Hofmann-type coordination polymer is one of the magnetic functional MOF materials. Mössbauer spectroscopy is a powerful tool for the investigation of elucidating fine structures around specific elements. However, Mössbauer spectroscopy on Hofmann-type complexes primarily focus on ^{57}Fe. Herein, we synthesized Ni(II) contained Hofmann-type coordination polymer compounds and investigated them using ^{61}Ni Mössbauer spectroscopy.

The spin-crossover (SCO) phenomenon is a reversible spin switching in metal ions between high-spin (HS) and low-spin (LS) states triggering by external stimuli such as temperature, pressure and, guest molecule inclusion and release, and light The Hofmann-type SCO compounds which was found to act SCO behavior of the original Fe(pyridine)$_2$[Ni(CN)$_4$] in 1996 [1] is coordination polymer with metal ion and cyanometalate, and another ligand such as pyridine or pyrazine-type ligand as shown Figure 1.

^{57}Fe Mössbauer spectroscopy is a very powerful tool for iron(II) SCO materials because I.S. and Q.S. parameters are very sensitive to iron(II) spin states. Hence, ^{57}Fe Mössbauer spectroscopy has been extensively used to study Hofmann complexes which has been used to study Fe-type SCO Hofmann complexes [1−3]. In contrast, ^{61}Ni Mössbauer spectroscopy has been only very few reported due to very short life time of source ^{61}Co.

Now we have researched three Hofmann-type complexes Fe(4-cyanopyridine)$_2$[Ni(CN)$_4$]n Benzene/m 4-cyanopyridine, Fe(4-cyanopyridine)$_2$[Ni(CN)$_4$] m 4-cyanopyridine with ^{61}Ni Mössbauer spectroscopy it using ^{61}Ni Mössbauer spectroscopy with a 67.4 keV γ–ray probe because of the transition of nuclear spin from I = 5/2 (excited state) to 3/2 (ground state).

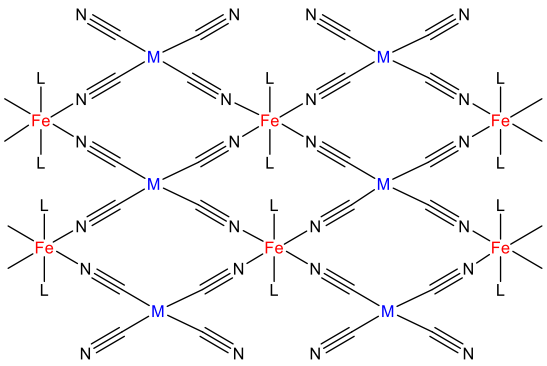


Figure 1 Structure of FeL$_2$M(CN)$_4$

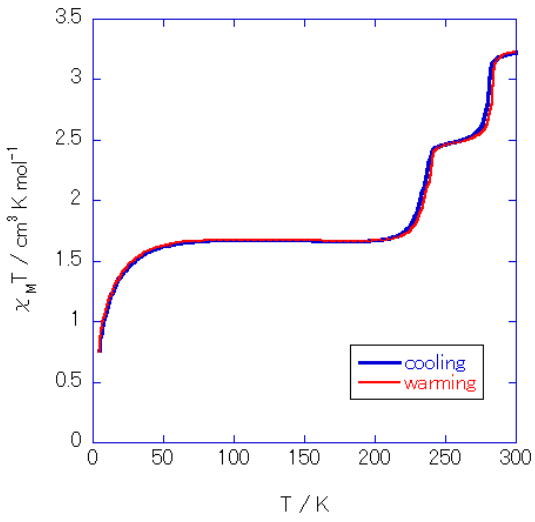


Figure 2 SQUID data for **(1)**

We freshly have synthesized Fe(4-cyanopyridine)$_2$[Ni(CN)$_4$][{0.9Benzene}{1.6H$_2$O}] **(1)**, Fe(4-cyanopyridine)$_2$[Ni(CN)$_4$] 1.75(4-cyanopyridine)nH$_2$O **(2).** Figure 2 indicates compound **(1)** acts as a spin crossover with 2-step behaviors between 225 K and 280 K, remaining about 50% high spin states at low temperatures. Crystal structure of Fe(4-cyanopyridine)$_2$[Pd(CN)$_4$]{2(4-cyanopyridine)} has been determined using the suitable single crystal obtained by diffusion method for x-ray diffraction method.

Ni-61 source production associated with ^{62}Ni(γ, p)^{61}Co was done using activation with Bremsstrahlung from the Electron beam of the KURNS-LINAC. Ni-61Mössbauer measurements were carried out conventional methods, Since the half-life of Co-61 is about100 minutes, about three hours measurements were done for one cycle. For one SCO compound sample, three times cycles are carried out in order to get suitable Mössbauer spectra. All spectra were obtained at 20 K. Obtained spectra have been fitted Moss Winn program aiming to become the standard reference PC software for Mossbauer spectrum analysis. Line shapes for Mössbauer spectra arrowed by Lorentzian line. As shown in Figure 3, Isomer shift of (1) and (2) are – 0.037(30) and -0.041(39) mm/s, and line width of (1) and(2) are 1.53(9) and 1.33(12) mm/s.

IS values of **(1)** and **(2)** are in the ranges of Ni(II) oxidation states, indicating square-planer Ni(II) coordination environments with diamagnetisms. Slight differences in Mössbauer parameters might be associated with guest molecules accommodating in the host Fe(4-cyanopyridine)$_2$[Ni(CN)$_4$] framework.

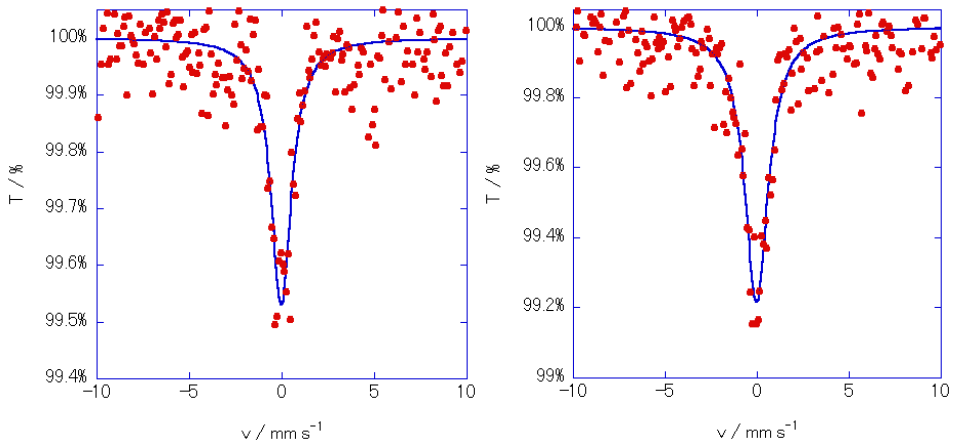


Figure3.Ni-61 Mössbauer spectra for **(1), left** and **(2),right**

ACKNOWLEDGMENTS

This work was partially supported by the Joint Usage/Research of the Institute for Integrated Radiation and Nuclear Science, Kyoto University (KURNS) (No. R4P3-7, R5P1-2, R6P1-2). We thank to Ms. Myhanh Matsushita for preparation single crystal of Fe(4-cyanopyridine)$_2$[Pd(CN)$_4$]{2(4-cyanopyridine)}/

References

[1] Kitazawa, T.; Gomi, Y.; Takahashi, M.; Takeda, M.;Enomoto, M.; Miyazaki, A.; Enoki, *J. Mater. Chem.* 1996, 6(1) 119-121, DOI:10.1039/JM9960600119.

[2] G. Molnár, T. Guillon, N. O. Moussa, L. Rechignat, T. Kitazawa, M. Nardone, A. Bousseksou, *Chem. Phys. Lett.*, 423, 152 (2006).

[3] T, Kitazawa, T. Kishida, T. Kawasaki, M, Takahashi, *Hyperfine Interact.*, 238(1), 1 (2017).

7th Asia-Pacific Symposium on Radiochemistry *September 14 ~ 19, 2025 • Kunibiki Messe • Shimane, Japan*

EFFECT OF INDIUM CONCENTRATION ON THE PHOTOCATALYTIC PERFORMANCE AND LOCAL STRUCTURE OF $SrTiO_3$

I. Ejiri[1], S. Komatsuda[2], W. Sato[1,3]

[1]*Graduated School of Natural Science and Technology*, *Kanazawa University: / Kanazawa, Ishikawa, 920-1192*
[2]*Institute of Human and Social Sciences*, *Kanazawa University: / Kanazawa, Ishikawa, 920-1192*
[3]*Institute of Science and Engineering*, *Kanazawa University: / Kanazawa, Ishikawa, 920-1192*

Strontium titanate ($SrTiO_3$) is a promising photocatalyst whose performance is raised by cation doping. In this study, $SrTiO_3$ doped with In of various concentrations was synthesized to determine the optimal doping level for photocatalytic activity. It was found that the photocatalytic activity peak reaches its peak with 0.5 at.% In^{3+} doping, and turns down beyond this point. Time-differential perturbed angular correlation (TDPAC) measurements with the $^{111}In(\leftarrow^{111}Cd)$ probe indicated that this reduction was due to the formation of the secondary phase of In_2O_3. The secondary phase may interfere with charge transportation, reducing photocatalytic efficiency.

1 INTRODUCTION

Strontium Titanate ($SrTiO_3$, STO), a cubic ABO_3-type perovskite, is a metal oxide semiconductor widely utilized as a photocatalyst for water splitting. Recent studies on STO have demonstrated that the substitution of Ti^{4+} sites with a small concentration of low-valence dopant ions can enhance its photocatalytic performance [1]. Previous studies confirmed that photocatalytic activity of In-doped STO was enhanced with In^{3+} occupying the Ti^{4+} sites [2, 3]. However, we found that in the doping concentration range of 0.1 to 1 at.%, part of the dopants form a secondary phase, leading to the reduction of photocatalytic activity. For more detailed investigation in the present study, we investigated the local structure at In impurities and its relation to the photocatalytic activity of STO by means of the time-differential perturbed angular correlation (TDPAC) method with a $^{111}Cd(\leftarrow^{111}In)$ probe and, the photocatalytic activity measurement.

2 EXPERIMENTAL

In-doped STO was synthesized via a conventional solid-state reaction. $In(NO_3)_3$ $3H_2O$(99.99%) was dissolved in ethanol, and then, Stoichiometric amounts of $SrCO_3$(99.9%) and TiO_2(99.99%) were mixed in the solution. The mixtures were stirred until dryness. The resulting powder was groundand pelletized. The pellets were calcinated at 1473 K for 24h. Each calcined disk was then ground into powder, and the crystal structures of In-doped STO were evaluated by X-ray diffraction (XRD) patterns. The photocatalytic activity was measured by degradation rate of methylene blue (MB) under UV light (365 nm) irradiation. For TDPAC measurements, droplets of radioactive probe of ^{111}In HCl solution was added onto pellets of In-doped STO precursor, obtained by the same method described above. The pellets were calcinated at 1473 K for 24h, then ground into powder and sealed in a Pyrex tube. TDPAC measurements were carried out for the 171-245 KeV cascade γ-rays of the $^{111}Cd(\leftarrow^{111}In)$ probe with the intermediate state of I=5/2.

3 RESULTS

Figure 1 shows the MB degradation rate as a function of UV irradiation time for STO samples with different In concentrations. As shown in Fig.1, photocatalytic activity was the best enhanced by 0.5 at.% doping among the present samples. At a concentration of 0.7 at.%, however, the photocatalytic activity decreased despite the increase in the amount of In. This observation might be due to the effect of the local structural change of In on the photocatalytic activity.

Copyright on 7th Asia-Pacific Symposium on Radiochemistry 2025

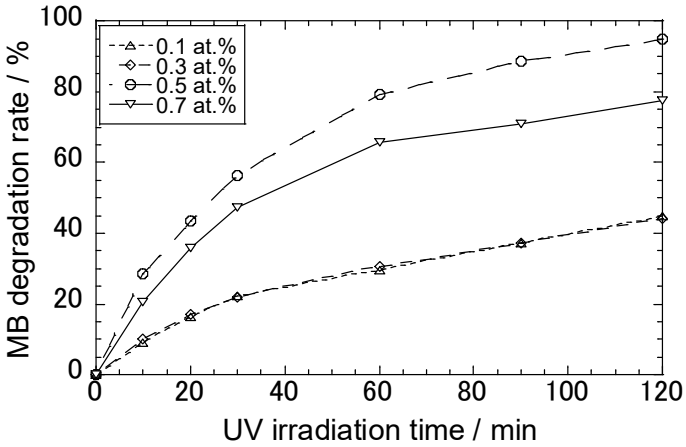


Fig. 1. MB degradation rate as a function of UV irradiation time.

The TDPAC measurements revealed that the local structures at the probe in 0.1 to 0.5 at.% In-doped STO were similar to those observed in undoped STO sample, indicating that dopant In^{3+} ions occupy the substitutional Ti sites and they are distributed uniformly in the samples. On the other hand, it was found that in samples doped with 0.7 at.% or more In, some In ions aggregated to form In_2O_3 secondary phase. These results suggest that minute aggregations of indium oxide, which are undetectable by XRD, are responsible for the suppression of photocatalytic activity at higher indium concentration. Such aggregations might enhance the recombination of photo-generated charge carriers or hinder their transport, thereby reducing overall photocatalytic efficiency.

4 CONCLUSIONS

In this study, the relation between the In^{3+} concentration and the photocatalytic activity of STO was investigated. The results revealed that the photocatalytic activity increases with increasing In concentration up to 0.5 at.%, but decreases at concentrations of 0.7 at.% or higher. The results of TDPAC measurements suggest that this decrease in photocatalytic activity at high concentrations of In is attributed to the formation of the secondary phase of In_2O_3.

ACKNOWLEDGMENTS

The present work was supported by the Grant-in-Aid for Early-Career Scientists (JSPS) Grant Number 21K17993. This work was accomplished as part of the Visiting Researcher's Program of Institute for Integrated Radiation and Nuclear Science, Kyoto University (KURNS).

References

[1] Tsuyoshi Takata and Kazunari Domen, "Defect Engineering of Photocatalysts by Doping of Aliovalent Metal Cations for Efficient Water Splitting", *J. Phys. Chem. C, **113**,* 19387 (2009).
[2] M. Kitta et al., "Direct confirmation of the dopant site in indium-doped photocatalyst via atomic-scale analytical transmission electron microscopy imaging", *Appl. Phys. Lett*. **118**, 153901 (2021).
[3] S. Komatsuda et al., "Investigation of doping effect on the local structure and photocatalytic activity of $SrTiO_3$", *Interactions* **245**:37(2024).

Copyright on 7th Asia-Pacific Symposium on Radiochemistry 2025 P-R4-05* -

7th Asia-Pacific Symposium on Radiochemistry *September 14 ~ 19, 2025 • Kunibiki Messe • Shimane, Japan*

INITIAL STATE OF CAPTURED MUON IN COPPER ATOM AND CHEMICAL ENVIRONMENTAL DEPENDENCE ON MUON CAPTURE

Miu Nomura[1], Satoaki Den[1], Naoko Nishino[1], Kazuhiko Ninomiya[1], I-Huan Chiu[2], Shunsuke Asari[3], Akira Sato[3], Takashi Yoshimura[3], Alex Amato[4], Sayani Biswas[4], Lars Frieder Gerchow[4], Carlos Vigo[4], Chennan Wang[4], Charles Hillis Mielke III[4], Debarchan Das[4], Fabian Hotz[4], Gianluca Janka[5], Hubertus Luetkens[4], Katharina von Schoeler[4], Narongrit Ritjoho[6], Thomas Prokscha[4], Toni Shiroka[4], Zaher Salman[4], Zurab Guguchia[4]

[1]*Graduate School of Advanced Science and Engineering, Hiroshima University, 1-4-2, Kagamiyama, Higashi-Hiroshima, Hiroshima, 739-8526, Japan*
[2]*Materials Sciences Research Center, Japan Atomic Energy Agency, Tokaimura, Ibaraki, 319-1195, Japan*
[3]*Graduate School of Science, Osaka University, 1-1 Machikaneyama, Toyonaka, Osaka 560-0043, Japan*
[4]*Paul Scherrer Institute, Forschungsstrasse 111, CH-5232, Villigen PSI, Switzerland*
[5]*Institute for Particle Physics and Astrophysics, ETH Zürich, 8093, Zürich, Switzerland*
[6]*School of Physics, Institute of Science, Suranaree University of Technology, 111 University Avenue Muang, Nakhon Ratchasima, 30000, Thailand*

In the formation process of a muonic atom chemical effect is known; muon capture probability and initial state of captured muon differ by the chemical environment of muon capturing atom. Using this property, chemical state of an atom can be investigated by observing muonic atom formation process. In this paper, muon capture processes for copper compounds of CuO, CuS, CuSe and CuTe were revealed by muonic X-ray measurements.

1 INTRODUCTION

An atomic system that contains charged particles other than proton and electrons is called an exotic atom. A muonic atom is an atomic system consisting a nucleus, electrons and a negatively charged muon in a muon atomic orbit around the nucleus. A muon has 207 times larger than that of an electron. When a muon is irradiated on and stopped in a material, the muon forms a muon atomic orbit around a nucleus, and a muonic atom forms. Since the captured muon exists excited muon atomic levels in initial, the captured muon immediately deexcites to muonic 1s state by emitting characteristic muonic X-rays (muonic X-rays). In recent years, non-destructive elemental analysis methods using muon has been developed [1]. This technique is based on the measurement of muonic X-rays emitted after muon introduction in the sample. Due to high energies of muonic X-rays, this method can quantify elemental composition deeply inside of the material, including light elements, depth selectively. For example, muon elemental analysis has been conducted for asteroid sample [2], and this method also applied for archeological artifacts [3].

Although the muon atomic orbit is far from the valance electrons due to large mass of the muon and small radius of muon atomic orbit, muon capture processes are strongly influenced by the chemical environment of the muon capturing atom. The muon capture probability for each element and quantum level of captured muon is changed by the chemical state. For example, in muon capture processes for CO and CO_2, per atom muon capture ratios of A(C/O) were about 40 % different between two compounds and muonic X-ray intensity patterns, such as 3p-1s/2p-1s were completely different each other [4]. The existence of such a “Chemical environmental effects” on muon capture indicates the possibility of a novel chemical state analysis method using muonic X-ray measurements. Actually, we have demonstrated that the composition of iron sand can be determined from muonic X-ray intensities [5]. However, it remains unclear what chemical state is reflected such chemical effects.

In this work, to investigate chemical environmental effects on muon capture processes, systematic studies for copper compound have been conducted. Muon capture ratio and initial state of capture muon for each element were evaluated from muonic X-ray intensities.

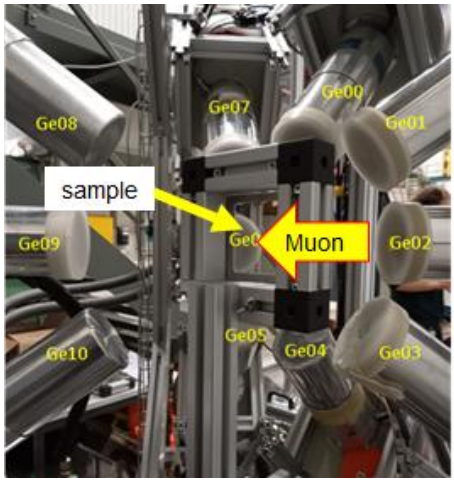


Fig. 1. Photo of experimental setup at πE1 beamline.

2 EXPERIMENTAL

Copyright on 7th Asia-Pacific Symposium on Radiochemistry 2025

The muon irradiation experiments were conducted at πE1 beamline in Paul Scherrer Institute (PSI), Switzerland. The photograph of the experimental setup is shown in Figure 1. The muon beam generated at muon production target was transported in the vacuum beam duct, passed through a plastic scintillation counter and titanium vacuum window, and irradiated on the sample. The momentum of incident muon was set 33 MeV/c. Muonic X-rays emitted after muon stop in the samples were measured by high-purity germanium detectors. The details of the experimental setup were shown in elsewhere [6].

In this study, we prepared copper compound samples, CuO, CuS, CuSe and CuTe. The powder samples were filled in aluminum case with a diameter of 37 mm and thickness of 3 mm. We also performed muon irradiation for copper and aluminum metal samples for estimation of background. The duration of muon irradiation was about 1.5 hours for each sample.

2 RESULTS AND DISCUSSION

Figure 2 shows the muonic X-ray spectra for copper compounds. Muonic X-rays originated from muon capture in copper, oxygen, sulfur, selenium and tellurium were clearly observed. The intensity patterns of muonic copper, such as 3p-1s/2p-1s and 4p-1s/2p-1s were evaluated for the measured samples.

The intensity patterns of muonic X-rays were different each other. For example, the ratio of 3p-1s/2p-1s of CuO sample were 20 % higher than that of CuS sample. This difference indicates that the muons captured in Cu atoms for CuO have relatively higher angular momentum quantum number states compare to those for CuS if muons exist in the same principal quantum number states. We estimated initial state of captured muon from muonic X-ray intensity patterns for each sample using the muon cascade code [7]. The details will be presented in the session.

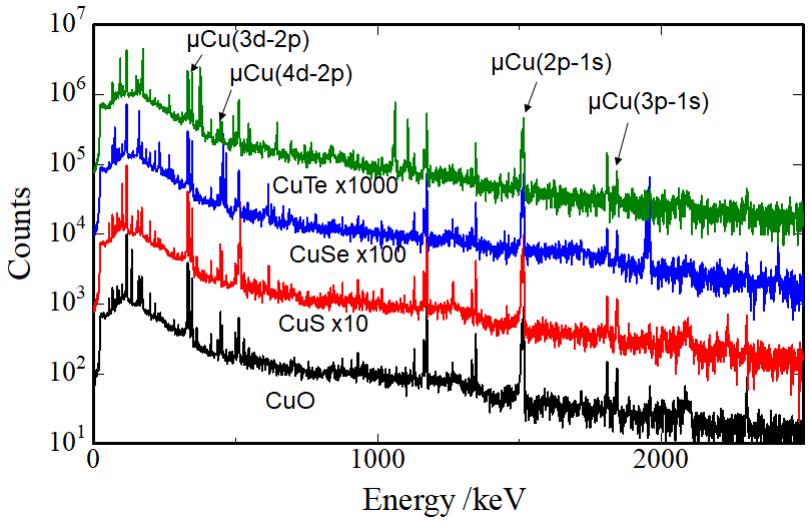


Fig.2. Muonic X-ray spectra for copper compounds.

References

[1] K. NINOMIYA, "Non-destructive, position-selective, and multi-elemental analysis method involving negative muons" *Journal of Nuclear and Radiochemical Sciences*, **19**, 8 (2019).
[2] T. NAKAMURA et al, "Formation and evolution of carbonaceous asteroid Ryugu: Direct evidence from returned samples" *Science*, **379**, eabn8671 (2023).
[3] K. SHIMADA-TAKAURA et al, "A novel challenge of nondestructive analysis on OGATA Koan's sealed medicine by muonic X-ray analysis" *Journal of Natural Medicines*, **75**, 532 (2021).
[4] G. YOSHIDA et al, "Muon capture probability of carbon and oxygen for CO, CO_2, and COS under low-pressure gas conditions" *Journal of Radioanalytical and Nuclear Chemistry*, **303**, 1277 (2015).
[5] K. NINOMIYA et al, "Non-Destructive Composition Identification for Mixtures of Iron Compounds Using a Chemical Environmental Effect on a Muon Capture Process" *Bulletin of the Chemical Society of Japan*, **95**, 1769 (2022).
[6] S. BISWAS et al, "The non-destructive investigation of a late antique knob bow fibula (Bugelknopffibel) from Kaiseraugst/CH using Muon Induced X-ray Emission (MIXE)" *Heritage Science*, **11**, 43 (2023).
[7] V. R. AKYLAS and P. VOGEL "Muonic atom cascade program" *Computer Physics Communications*, **15**, 291 (1978).

Copyright on 7th Asia-Pacific Symposium on Radiochemistry 2025 P-R4-06* -

Poster Presentation | [R6]Radiation and Radioisotopes in Life Science

Wed. Sep 17, 2025 6:30 PM - 8:00 PM JST | Wed. Sep 17, 2025 9:30 AM - 11:00 AM UTC Poster

[Poster] R6

[P-R6-01]

HETEROGENEOUS DISTRIBUTION OF HTO IN ORGANISMS

*Tsuyoshi Masuda[1], Takahito Moriwaki[1] (1. Institute for Environmental Sciences (Japan))

[P-R6-02]

Glutathione, applied to roots site-specifically, inhibits the movement of cadmium in roots of oilseed rape plants (*Brassica napus*)

*Shin-ichi Nakamura[1], Taku Yuzawa[1], Tianyi Zhou[1], Ryotaro Iida[1], Nobuo Suzui[2], Yonggen Yin[2], Yuta Miyoshi[2], Yusaku Noda[2], Kazuyuki Enomoto[2], Ryohei Yamagaya[2], Takahiro Sato[2], Yasuyuki Ishii[2], Naoki Kawachi[2], Akihisa Shinozawa[1], Kanna Sato-Izawa[1] (1. Tokyo University of Agriculture (Japan), 2. National Institutes for Quantum Science and Technology (Japan))

[P-R6-03]

Characteristics of Tritium, Hydrogen, and Oxygen Isotope Compositions in Surface Water Across Thailand

*Chonlada Pitakchaianan[1], Kanyanan Kosinarkaranun[1], Pantiwa Kumsut[1], Tatsuhide Hamasaki[1], Ryuta Hazama[1], Anawat Rittirong, Koichi Sakakibara, Yoshiyuki Hirano, Koki Kashiwaya, Yoshimune Ogata, Yuka Kato, Wanwisa Sudprasert, Kiadtisak Saenboonruang, Kanokwan Khamanek, Soontree Khuntong, Donruedee Toyen, Archara Phattanasub, Monthon Yongprawat, Chakrit Saengkorakot, Piyawan Krisanangkura, Chittranuch Chantarot (1. Osaka Sangyo University (Japan))

[P-R6-04]

Characteristics of ^{7}Be and ^{210}Pb in the Atmosphere of Bangkok, Thailand

*Kanyanan Kosinarkaranun[1], Chonlada Pitakchaianan[1], Pantiwa Kumsut[1], Ryuta Hazama[1], Tatsuhide Hamasaki[1], Anawat Rittirong[2], Hisakazu Muramatsu[3], Pannipa Noithong[4], Wanwisa Sudprasert[5] (1. Osaka Sangyo University (Japan), 2. Osaka University (Japan), 3. Shinshu University (Japan), 4. Roi Et Provincial Office of Learning Encouragement, DOLE (Thailand), 5. Kasetsart University (Thailand))

[P-R6-05*]

Analysis of leaf position-dependent phosphorus allocation in a deciduous woody plant *Populus alba* L.

*Aoi Hirata[1], Yuko Kurita[1], Ryohei Sugita[2], Natsuko Kobayashi[1], Keitaro Tanoi[1,3] (1. Graduate School of Agricultural and Life Science, The University of Tokyo (Japan), 2. Radioisotope Research Center, Nagoya University (Japan), 3. Fukushima Institute for Research, Education and Innovation (Japan))

[P-R6-06]

Photosynthate Allocation in Soybean: Influence of Sink-Source spatial Relationships

Ai Kaiho-Soma[1], Yuko Kurita[1], Natsuko I. Kobayashi[1], Tomoko M. Nakanishi[1,2], *Keitaro Tanoi[1,2] (1. Graduate School of Agricultural and Life Sciences, The University of Tokyo (Japan), 2. Fukushima Institute for Research, Education and Innovation (Japan))

[P-R6-07]

©APSORC25

BIOIMAGING AND XPDT TREATMENT USING HIGHLY LUMINESCENT NANOCOMPOSITE SCINTILLATORS

*Václav Čuba[1], Xenie Lytvynenko[1], Lenka Prouzová[1], Jan Bárta[1] (1. Czech Technical University in Prague (Czech Republic))

[P-R6-08]

Experimental systems for the internal and external exposure of silkworms to radioactive cesium for evaluating biological effects.

Sota Tanaka[1], Sho Amano[2], *Tadatoshi Kinouchi[3] (1. Faculty of Bioresource Sciences, Akita Prefectural University (Japan), 2. Oita University Faculty of Medicine (Japan), 3. Institute for Integrated Radiation and Nuclear Science, Kyoto University (Japan))

©APSORC25

7th Asia-Pacific Symposium on Radiochemistry *September 14 ~ 19, 2025 • Kunibiki Messe • Shimane, Japan*

HETEROGENEOUS DISTRIBUTION OF HTO IN ORGANISMS

Takahito Moriwaki[1], Tsuyoshi Masuda[2]

[1]*Institute for Environmental Sciences: 1-7 Ienomae, Obuchi, Kamikita, Aomori, 039-3212, Japan, moriwaki@ies.or.jp*
[2]*Institute for Environmental Sciences: 1-7 Ienomae, Obuchi, Kamikita, Aomori, 039-3212, Japan, masuda@ies.or.jp*

To investigate the possibility of heterogeneous distribution of HTO in organisms, we conducted two types of experiments. First, cells were cultured in the medium containing HTO and tritiated lysine. After 24 hours, the tritium activity concentrations in evaporated water, which were separately recovered from intracellular water and culture medium supernatant, were measured. The estimated tritium activity concentration of HTO from intracellular water was lower than that from the supernatant in the experiment group administered HTO in culture medium, while that from intracellular water was higher than that from supernatant for the group administered tritiated lysine. Next, mice were administered HTO continuously by drinking water. After that the tissue free water sample from each of the organs were collected by evaporation. The tritium activity concentrations in HTO varied among organs. The International Commission on Radiological Protection assumes uniform distribution of HTO in their metabolic model to calculate dose coefficients for tritium. Contrary to that, these results suggested that heterogeneous distribution of HTO occurs in cultured cells and mice. Therefore, we concluded that a new dosimetry framework taking heterogeneous distribution of HTO into consideration is needed to ensure the safety for tritium intakes.

1 INTRODUCTION

Tritium is a radionuclide of hydrogen with half-life of 12.3 years. Since the average range of β-rays from tritium in water (0.56 μm) is two orders of magnitude shorter than the typical cell size of 20 μm, β-rays from tritium in extracellular fluid give little energy into cell nucleus and other organelles. Therefore, it is essential to estimate tritium activity in cells for research to investigate biological effects of tritium. However, most of research assumes uniform tritium activity concentration for intracellular water and extracellular water, such as culture medium supernatant in cell experiments and extracellular fluid in animal experiments.

To investigate the possibility of heterogeneous tritium activity concentration between inner and outer cells, in this paper, we estimated those values from cells cultured in tritiated media.

In addition to that, the International Commission of Radiological Protection has adopted the assumption of uniform distribution of HTO among organs and tissues to calculate the dose coefficients for tritium [1]. However, experimental data for activity concentrations of HTO in tissue free water after the administration of HTO have been scarcely reported. Therefore, to validate the assumption, it is necessary to measure activity concentrations of HTO in tissue free water in each organ. Here we provide the tritium activity concentration data of HTO in organs obtained from mice administered HTO continuously by drinking water.

2 METHODS

For cultured cell experiment, human retinal pigment epithelial cells hTERT RPE-1 cells were cultured on 12-mm-diameter cover glass coated with Cellmatrix Type I-C (Fujifilm Wako) in DMEM, high glucose, GlutaMAX Supplement, HEPES (Gibco) supplemented with 5% fetal bovine serum (Serena Europe). For HTO and tritiated (^{3}H-) lysine treatment, cells were plated at 80% confluency. After the cell adhesion, 16 cover glasses were placed in a flask filled with 3 mL of the medium containing 200 kBq/mL HTO and ^{3}H-lysine, respectively, and then cultured for 24 hours. HTO in culture medium supernatant was collected by rapid tissue water collection system [2] as following steps: evaporation of water from 1 mL of supernatant and 4 mL of career pure water at 120°C in 50 mL heating tube; and condensation in another 50 mL tube adjacent to and separated from heating tube by moisture permeable membrane. Water in cells was also collected by the system as follows: picking up cover glass, removing residual medium carefully using waste paper, setting 16 cover glasses in a heating tube, adding 5 mL of pure water as career, evaporating the career and extracted water, and condensing them. The tritium activity was measured by liquid scintillation counter LSC-6000 (Aloka CO., Ltd) with Ecoscint Ultra (National Diagnostics, USA). The tritium activity concentration in cells was calculated from the measured tritium activities, assuming a cell layer thickness of 10 μm and a water content of 50% to estimate water volume in cells.

For animal experiment, B6C3F1 mice were administered HTO continuously by drinking water. The mice were sacrificed over time and dissected brain, eye-lens, thymus, lung, heart, liver, kidney, spleen, small intestine, skeletal muscle, adipose tissue, and ovary. The tissue free water in those samples were evaporated at 120°C and distilled water

were collected by condensation by using the rapid tissue water collection system [2]. The tritium activity concentrations were measured by liquid scintillation counter as described above.

3 RESULTS

In the experiment group administered ^{3}H-lysine, the activity concentrations both in supernatant and cellular water were elevated suggesting that production of HTO from ^{3}H-lysine in RPE-1 cells and leakage of HTO to supernatant, while the elevation of cellular water HTO in the experiment group administered HTO indicates infiltration of HTO from culture medium (Table 1). The estimated activity concentration of HTO from intracellular water was lower than that from the supernatant in the experiment group administered HTO in culture medium, while that from intracellular water was higher than that from supernatant for the group administered ^{3}H-lysine (Figure 1). These results indicated that both the extracellular administration of HTO and intracellular production of HTO resulted in a heterogeneous distribution of HTO between intra and extra cellular waters after 24 hours, though the values were dependent on the assumption relevant to the water volume in cells.

In animal experiment, the activity concentrations of tritium in tissue free water varied among the organs. For example, these were lower in liver than the other organs. The differences of the concentration between cell free water and culture medium were observed.

Table 1. Tritium activities in HTO (kBq/flask)

	HTO	^{3}H-Lysine
Medium supernatant	584	52
Cellular water	0.19	0.52

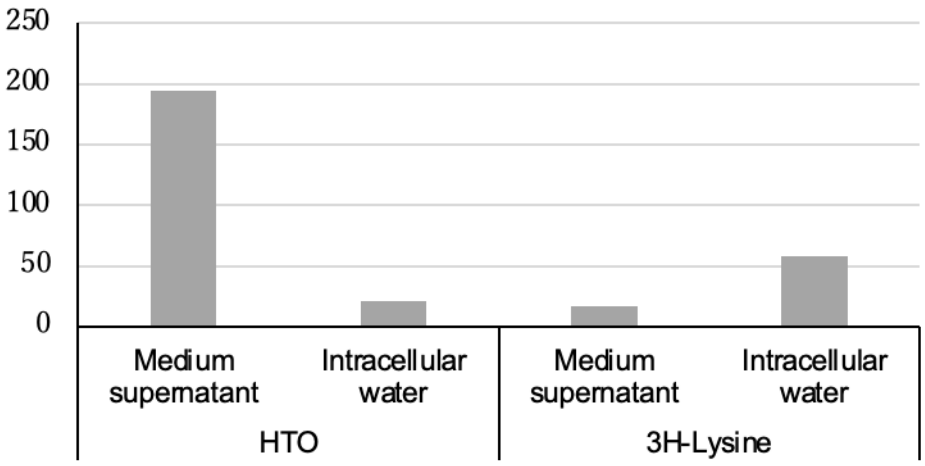


Fig. 1. Tritium activity concentrations (kBq/mL)

4. CONCLUSIONS

The difference between intracellular water and culture media supernatant in cell culture and the variations of the activity concentrations of HTO among organs in mice were demonstrated. Therefore, the necessity of a new dosimetry framework considering heterogenous distribution of HTO was suggested.

ACKNOWLEDGMENTS

This study was performed under a contract with the Aomori Prefectural Government, Japan. We extend our gratitude to Akiko Abe for technical assistance. The authors also would like to thank Naijou for assistance with animal care.

References

[1] International Commission on Radiological Protection, ICRP Publication 134: Occupational intakes of radionuclides: Part 2, Annual ICRP, 45(3-4), 7-349 (2016).
[2] Masuda et al., Estimation of the ratio of exchangeable organically bound hydrogen to total organically bound hydrogen in flatfish fresh. Radiation Protection Dosimetry, 200(16-18), 1813-1817.

7th Asia-Pacific Symposium on Radiochemistry *September 14 ~ 19, 2025 • Kunibiki Messe • Shimane, Japan*

Glutathione, applied to roots site-specifically, inhibits the movement of cadmium in roots of oilseed rape plants (*Brassica napus*)

Shin-ichi Nakamura[1], Taku Yuzawa[1], Tianyi Zhou[1], Ryotaro Iida[1], Nobuo Suzui[2], Yonggen Yin[2], Yuta Miyoshi[2], Yusaku Noda[2], Kazuyuki Enomoto[2], Ryohei Yamagaya[2], Takahiro Sato[2], Yasuyuki Ishii[2], Naoki Kawachi[2], Akihisa Shinozawa[1], Kanna Sato-Izawa[1]

[1]*Department of Bioscience, Tokyo University of Agriculture, 1-1-1 Sakuragaoka Setagaya-ku, Tokyo, Japan, 1568502*
[2]*Department of Quantum-Applied Biosciences, National Institutes for Quantum Science and Technology, 1233 Watanukimachi, Takasaki-shi, Gunma, Japan, 3701292*

1 INTRODUCTION

Cadmium (Cd) is one of the toxic heavy metal elements. A portion of Cd released into the environment is absorbed by agricultural crops. Crops with high Cd level are detrimental to our health. There is an urgent need to establish novel cultivation techniques for safe crops with low Cd level. Our previous studies have demonstrated that glutathione (GSH), applied to roots of oilseed rape plants site-specifically, inhibits Cd transport from roots to shoots selectively [1]. GSH is a bioactive peptide composed of three amino acids: glutamic acid, cysteine, and glycine. GSH is known to have a variety of physiological activities, including removal of reactive oxygen species and serving as a precursor to phytochelatins, among other functions [2]. Elucidation of the molecular mechanism governing the Cd movement triggered by GSH will contribute to reducing the amount of Cd accumulation in crop plants.

1.1 EXPERIMENTAL METHODS

Oilseed rape plants (*Brassica napus* L. var. Nourin No. 16 and Westar) were used as test plants in our studies. These plants were grown hydroponically in a growth chamber with fully controllable growth conditions according to the method of Nakamura et al. [3]. The cultivation period for oilseed rape plants was four weeks after sowing. Test plants were subjected to Cd and Cd + GSH treatments prior to harvest to determine the effect of GSH on Cd movements in the crucifer varieties Nourin No.16 and Westar. Cd content in test plants was calculated from analytical results using an atomic absorption spectrophotometer (AA-7000, Shimadzu, Kyoto, Japan). In-air micro-PIXE (Particle Induced X-ray Emission) analysis enables us to visualize tissue distribution of various elements in prepared samples [4]. Through this analysis, we attempted to visualize Cd distribution in the roots of the test plants.

1.1.1 RESULTS

GSH, applied to roots, also reduced Cd accumulation in shoot in the Westar variety. On the other hand, GSH treatment did not result in a reduction of Cd accumulation in the roots. These experimental results suggest that GSH inhibits Cd transport from roots to shoots and reduced Cd accumulation in shoots in the Westar variety as well as in the Nourin No.16 variety. Visualization of Cd distribution in roots of oilseed rape plants was successfully achieved by micro-PIXE analysis. This analysis revealed that GSH, applied to roots, increased the amount of Cd accumulated in the epidermal portion of the roots. Additionally, we will present the results of an experimental visualization of effects of GSH treatment on the condition of *Brassica* roots, including the generation of reactive oxygen species.

2. CONCLUSIONS

Root applied GSH also inhibits Cd transport from roots to shoot in the Westar variety. The Westar variety is transformable and could be a powerful tool to elucidate control mechanisms of Cd movement in oilseed rape plants. The results of the micro-PIXE experiment suggested that GSH inhibited Cd movement in the roots by confining Cd to the epidermal layer of the roots.

ACKNOWLEDGMENTS

A part of this research was performed by the commissioned research fund provided by F-REI (JPFR24040101) and a Grant-in-Aid for Scientific Research (KAKENHI B; 22H02480).

References

[1] S. NAKAMURA et al., "Application of glutathione to roots selectively inhibits cadmium transport from roots to shoots in oilseed rape," *J. Exp. Bot.*, **64**, 1073-1081 (2013).
[2] G. NOCTOR et al., "Glutathione," *The arabidopsis book*, **9**, e0142 (2011).
[3] S. NAKAMURA et al., "Effect of cadmium on the chemical composition of xylem exudate from oilseed rape plants (*Brassica napus* L.)," *Soil Science and Plant Nutrition*, **54**, 118-127 (2008).
[4] T. SAKAI et al., "JAERI Takasaki in-air micro-PIXE system for various applications," *Nuclear Instruments and Methods in Physics Research Section B: Beam Interactions with Materials and Atoms*, **190**, 271-275 (2002).

Copyright on 7th Asia-Pacific Symposium on Radiochemistry 2025

Characteristics of Tritium, Hydrogen, and Oxygen Isotope Compositions in Surface Water Across Thailand

Chonlada PITAKCHAIANAN[1)], Kanyanan KOSINARKARANAN[1)], Pantiwa KUMSUT[1)], Tatsuhide HAMASAKI[1)], Ryuta HAZAMA[1)], Anawat RITTIRONG[2)], Koichi SAKAKIBARA[3)], Yoshiyuki HIRANO[4)], Koki KASHIWAYA[5)], Yoshimune OGATA[6)], Yuka KATO[7)], Wanwisa SUDPRASERT[8)], Kiadtisak SAENBOONRUANG[8)], Chittranuch CHANTAROT[8)], Kanokwan KHAMANEK[8)], Soontree KHUNTONG[9)], Donruedee TOYEN[10)], Archara PHATTANASUB[11)], Monthon YONGPRAWAT[12)], Chakrit SAENGKORAKOT[11)], Piyawan KRISANANGKURA[12)]

Graduate School of Human Environment, Osaka Sangyo University [1)], Research Center for Nuclear Physics, Osaka University[2)], Faculty of Science, Shinshu University[3)], Department of Radiological Sciences, Nagoya University Graduate School of Medicine[4)], Graduate School of Engineering, Kyoto University[5)], Department of Chemistry, Aichi Medical University[6)], Aloka Co., Ltd.[7)], Department of Applied Radiation and Isotopes, Kasetsart University[8)], Faculty of Science at Sriracha, Kasetsart University[9)], Department of Materials Science, Kasetsart University[10)], Thailand Institute of Nuclear Technology[11)], Office of Atoms for Peace[12)]

Tritium is a natural radionuclide that is constantly produced by nuclear reactions between atmospheric constituent elements and secondary cosmic rays in the upper atmosphere. Tritium then moves down to the troposphere and is transported into the environment through the hydrological cycle. This study aims to measure tritium activity concentrations in freshwater across Thailand to establish baseline levels before any future developments of nuclear facilities such as nuclear power plant, fusion reactor, or additional research reactor. In earlier studies, nationwide tap water samples, primarily sourced from reservoirs or dams and treated in municipal systems, were collected in July 2021, while rainwater samples were collected from Sriracha, Chonburi province (2020-2022), and Chiang Mai province (2021-2022). To comprehensively represent Thailand's natural water sources, the study in 2023 expanded to include surface water samples from 14 large reservoirs during the wet season in October 2023 and the dry season in February 2024, providing a total of 28 samples. This inclusion of dam and reservoir samples provides critical insights into tritium levels in surface waters that serve as primary tap water sources and are influenced by direct atmospheric deposition. The study also evaluated tritium concentrations across different water types, comparing them against global averages and standards, and examined relationships between tritium levels, geographical factors, and meteorological characteristics. Measurements of tritium activity concentrations were conducted by Osaka Sangyo University (OSU) using electrolytic enrichment (solid polymer electrolyte film) and a low- background liquid scintillation counter (AccuFLEX LSC-LB7). Collaborations with Shinshu University and Kyoto University allowed for additional measurements of oxygen/hydrogen isotope compositions and chemical compositions using a water isotope analyzer (Picarro L-2130i), an automatic titration system, a cation analyzer (IC (Thermo) ICS-1500), and an anion analyzer (IC (Thermo) ICS-2100). These measurements aimed to understand sources and circulation regimes of the water samples. The results showed that tritium concentrations in surface water samples ranged from 0.14±0.02 - 0.33±0.05 Bq L^{-1} with a mean concentration of 0.23±0.05 Bq L^{-1}. The highest concentrations were observed in the north (0.27 ± 0.04 TU), followed by the northeast (0.25 ± 0.06 Bq L^{-1}), central (0.23 ± 0.02 Bq L^{-1}), east (0.19 ± 0.03 Bq L^{-1}), and south (0.18 ± 0.03 Bq L^{-1}), with a correlation coefficient (CC) of 0.85 between tritium concentration and latitude. All measured tritium levels were below the natural background. A strong negative correlation between $\delta^{18}O$, δD, and latitude was observed, with $\delta^{18}O$ (CC = −0.82) ranging from −9.03‰ in the north to −4.43‰ in the south, and δD (CC = −0.86) ranging from −72.55‰ to −27.27‰. d-excess values ranged from -2.13 to 10.46‰. The high d-excess values were observed in the coastal basins, suggesting that marine moisture from the surrounding seas contributes to precipitation in these areas. This study provides baseline tritium levels for each region in Thailand, contributing to the advancement of nuclear safety and safeguards in preparation for future developments. This research was conducted under an international joint research project between Thailand and Japan: JSPS Bilateral Program, Grant number JPJSBP120209203.

Characteristics of ^{7}Be and ^{210}Pb in the Atmosphere of Bangkok, Thailand

Kanyanan Kosinarkaranun[1, *], Chonlada Pitakchaianan[1], Pantiwa Kumsut[1], Ryuta Hazama[1], Tatsuhide Hamasaki[1], Anawat Rittirong[2], Hisakazu Muramatsu[3], Pannipa Noithong[4], Wanwisa Sudprasert[5]

[1]Osaka Sangyo University, [2]Osaka University, [3]Shinshu University, [4]Roi Et Provincial Office of Learning Encouragement, DOLE, [5]Kasetsart University

Air pollution from PM2.5 is a major contributor to environmental issues in Thailand. The study of radionuclides such as ^{7}Be and ^{210}Pb is crucial for understanding their atmospheric behavior, deposition processes, and implications for radiation protection. ^{7}Be, with a half-life of 53.3 days, is a cosmogenic radionuclide continuously produced in the upper atmosphere region. In contrast, ^{210}Pb, with a half-life of 22.3 years, is a naturally present radionuclide found within the decay chain of ^{238}U. A previous study in Bangkok, Thailand (13.765° N, 100.526° E) by Suzuki *et al*. 2017 reported seasonal variation of ^{7}Be concentration from June 2014 to December 2016, with higher concentration was observed from January to May, while lower concentration was observed from in June to December, respectively. However, there is a lack of published data on ^{210}Pb concentrations in the atmosphere in Bangkok using high-volume air samplers. Therefore, the present study examines a short-term variation of ^{7}Be and ^{210}Pb concentrations, providing insight into their vertical distribution behavior and addressing the gap in atmospheric radionuclide data for Bangkok.

Atmospheric concentrations of ^{7}Be and ^{210}Pb have been continuously monitored at the Office of Atoms for Peace in Bangkok, Thailand, from May to September 2022. The sampling location is at 13.85 °N, 100.57 ºE, and at a height of 30 m above ground level. Aerosol samples were collected using a high-volume air sampler (HV-1000F, SIBATA Co., Ltd.) operating at a flow rate of 1000 L/min. The measurement of ^{7}Be and ^{210}Pb in aerosol samples were conducted at Osaka Sangyo University, Osaka, Japan, using an HPGe detector (GX2018, CANBERRA) connected to a data acquisition device (APU8002 and DSA1000). Gamma-ray signals were analyzed at 46 keV (^{210}Pb) and 477 keV (^{7}Be).

Monthly variations from May to September 2022 showed that ^{7}Be concentrations were highest in June and lowest in August, while ^{210}Pb concentrations peaked in August and were lowest in July. In comparison, observations in Osaka revealed a typical double-peak pattern for both ^{7}Be and ^{210}Pb, with higher concentrations in spring (March–May) and autumn (September–November), and lower in summer (June–August). The differences in seasonal patterns may be attributed to distinct air mass origins: in Thailand, air masses during the rainy season predominantly originate from Indian Ocean, while in Osaka, they primarily come from the Pacific Ocean.

This study was supported by the international joint research project between Japan and Thailand: JSPS-NRCT Bilateral Joint Research Project, Grant number JPJSB120209203.

Copyright on 7th Asia-Pacific Symposium on Radiochemistry 2025

7th Asia-Pacific Symposium on Radiochemistry *September 14 ~ 19, 2025 • Kunibiki Messe • Shimane, Japan*

Analysis of leaf position-dependent phosphorus allocation in a deciduous woody plant *Populus alba* L.

Aoi Hirata[1], Yuko Kurita[1], Ryohei Sugita[2], Natsuko Kobayashi[1], Keitaro Tanoi[1,3]

[1]*Graduate School of Agricultural and Life Science, The University of Tokyo: 1-1-1 Yayoi, Bunkyo-ku, Tokyo 113-0032, Japan*
[2] *Radioisotope Research Center, Nagoya University: Furo-cho, Chikusa-ku, Nagoya, Aichi 464-8601, Japan*
[3]*Fukushima Institute for Research, Education and Innovation: 6-1 Yazawa-machi, Gongendo, Namie town, Futaba County, Fukushima 979-1521, Japan*

Woody plants sustain their growth by allocating phosphorus (P) to meet the demands of each organ. In plants, P is efficiently utilized by being preferentially transported to young leaves and the shoot apex, but the mechanisms that regulate this allocation are not yet well understood. In this study, we established an observation system to analyze the dynamics of radioisotope (RI)-labeled P (^{32}P) absorbed from roots in poplar and used this system to quantify P allocation. Within 1 h after ^{32}P application, the ^{32}P activity per unit leaf area was nearly uniform across all leaf positions. By 3 h after ^{32}P application, the ratio of ^{32}P activity per unit leaf area in the upper leaves gradually increased. These results suggest that P is preferentially transported to the upper leaves via the phloem flow after P is transported via the xylem flow.

1 Introduction

Phosphorus (P) is one of the essential macronutrients of plants. P is taken up from the roots and transported to the aerial parts of the plant via xylem flow and subsequently allocated to the leaves.[1)] Then, P is translocated from older leaves to young leaves and shoot apex via phloem.[2)] These two flows should work in concert to achieve the proper allocation of P, but individual contributions and mechanisms of coordination are not well understood. Using the deciduous woody plant poplar, we quantified and visualized the time course of P allocation, which has been unexplored.

2. Materials and methods

Poplar (*Populus alba* L.) shoots developed roots were planted in the vermiculite and supplied with 1/5 Murashige and Skoog Plant Salt Mixture. To sequentially visualize P movement in a living plant, continuous imaging was performed using a live imaging system, namely the real-time radioisotope imaging system (RRIS).[3, 4, 5)] Before performing the RRIS, 50 mL of hydroponic solution (1/5 MS) containing 5 MBq of ^{32}P was added to a plastic container with a poplar. The ratio of ^{32}P activity per leaf area of L1, L2, L5 and L10 was calculated using RRIS and Imaging plate (IP). The distribution of P in a leaf were quantified using IP.

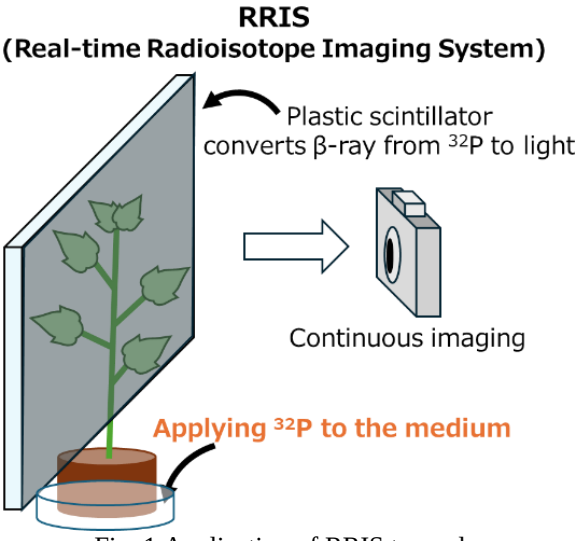


Fig. 1 Application of RRIS to poplar.

Copyright on 7th Asia-Pacific Symposium on Radiochemistry 2025

3. Results and Discussion

P was initially (0-1 h) allocated evenly across all leaves; subsequently, preferential transport to the upper leaves began. The uniform distribution of ^{32}P observed within 1 h after ^{32}P application in our study likely reflects rapid xylem-mediated transport. The subsequent changes in the ratios of ^{32}P activity observed 3 h after ^{32}P application can be attributed to phloem-mediated translocation from the middle and lower leaves to the upper leaves. In the upper leaves, the signal intensities were higher along the entire length from the leaf tip to the base, in both the leaf blade and the main vein. In contrast, the middle and lower leaves showed a marked increase was observed in the nectary gland region of the main vein. P may be accumulating in the nectary glands due to remobilization from the leaf blade, or its transport from the petiole to the leaf tip may be restricted.

4. CONCLUSIONS

In this study, time-course analysis of P transport from the roots was conducted using poplar as a model tree, and the allocation of P across leaves of different positions was quantified. These findings suggest that the preferential allocation of P to young leaves may be achieved by the cooperation of transport immediately after absorption by the xylem flow and translocation by the phloem flow. Furthermore, the pattern of P distribution within leaves appears to be determined by local sink capacity.

ACKNOWLEDGMENTS

This work was supported by JSPS KAKENHI Grant Number 19J00707 and 23K14208, 24H00499, and F-REI (JPFR25040101). We thank Prof. Kimitsune Ishizaki and Research Facility Center for Science and Technology of Kobe University for use of facilities.

References

[1] Wegner, L. H. Root pressure and beyond: Energetically uphill water transport into xylem vessels?, J Exp Bot, 65, 381–393 (2014)
[2] Kurita, Y. et al., Visualization of phosphorus re-trans location and phosphate transporter expression profiles in a shortened annual cycle system of poplar, Plant Cell Environ, 45, 1749–1764 (2022)
[3] Nakanishi, T. M. et al., Real-time imaging of ion uptake from root to above-ground part of the plant using conventional beta-ray emitters, J Radioanal Nucl Chem, 282 265–269 (2009)
[4] Kanno, S. et al., Real-time imaging of radioisotope labeled compounds in a living plant. J Radioanal Nucl Chem, 272, 565–570 (2007)
[5] Sugahara, K. et al., Plastic Scintillators Enable Live Imaging of 32P-labelled Phosphorus Movement in Large Plants, Radioisotopes, 68, 73–82 (2019)

Copyright on 7th Asia-Pacific Symposium on Radiochemistry 2025

Photosynthate Allocation in Soybean: Influence of Source-Sink spatial Relationships

Ai Kaiho-Soma[1], Yuko Kurita[1], Natsuko I. Kobayashi[1], Tomoko M. Nakanishi[1, 2], Keitaro Tanoi[1, 2]

[1]*Graduate School of Agricultural and Life Science, The University of Tokyo: 1-1-1 Yayoi, Bunkyo-ku, Tokyo 113-0032, Japan*
[2]*Fukushima Institute for Research, Education and Innovation: 6-1 Yazawa-machi, Gongendo, Namie town, Futaba County, Fukushima 979-1521, Japan*

Photosynthesis is known to convert water and carbon dioxide into sugars and oxygen using light energy. While young leaves consume most of the sugars they produce for their own growth, mature "source" leaves generate excess sugars that are transported to growing "sink" organs such as shoot apex, buds, young leaves, roots, pods, etc. Efficient allocation of these photosynthates is crucial for plant growth and influence on crop yield. In this study, we analyzed carbon allocation dynamics in soybean from specific source leaves using radioactive ^{14}C-labeled CO_2 or ^{14}C-labeled sucrose. The results showed that ^{14}C was preferentially translocated to sink pods or buds closer to the source leaves, and that the ratio of distribution to these sinks varied depending on the position of the source leaves within the plant. Considering that the uppermost meristem is the primary sink during the early developmental stage, our findings suggest that when new meristems emerge closer to specific source leaves, those leaves preferentially allocate photosynthates to the nearby sinks, and that source–sink translocation is influenced not only by distance but also by the relative position of source leaves within the plant.

1. MATERIAL AND METHODS

Seeds of soybean (*Glycine max*) were germinated in vermiculite and transferred to 1/2 Hoagland hydroponic solution. To investigate allocation to pods, plants were grown under an 8-hour light/16-hour dark condition, while for buds, a 16-hour light / 8-hour dark condition was used. To analyze of photosynthate allocation, $^{14}CO_2$ or ^{14}C-sucrose was supplied to specific mature leaves, and the plants were subsequently cultivated for 22-24 hours. Then, the amount of ^{14}C in sink organs was measured using liquid scintillation counting.

2. RESULTS AND DISCUSSION

When $^{14}CO_2$ was supplied to the 5th (L5) or 6th (L6) leaves during the reproductive growth, higher ^{14}C accumulation was observed in the nearest pods (fig. 1). Similarly, in vegetative growth plants with buds whose growth was promoted by pinching, ^{14}C-sucrose supplied to 1st (L1), 3rd (L3), or 4th (L4) leaves resulted in the highest ^{14}C levels in nearest buds. In the vegetative stage, a comparison was made by supplying ^{14}C-sucrose to either the 1st (L1) or 3rd (L3) leaves of soybean plants grown under the same conditions. When ^{14}C-sucrose was supplied to L1, 42–89% of the total radioactivity in buds was detected in the closest buds, whereas L3 application resulted in only 23–63% (fig. 2). These results indicate that photosynthate allocation is governed not only by proximity between source and sinks but also by overall balance and the position of source leaves within the plant.

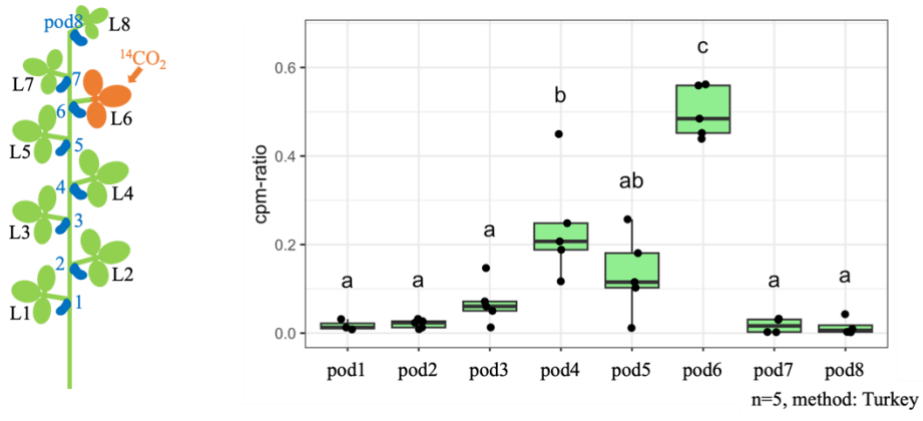


Fig.1 The ratio of ^{14}C translocated from 6th leaf (L6) to the pods

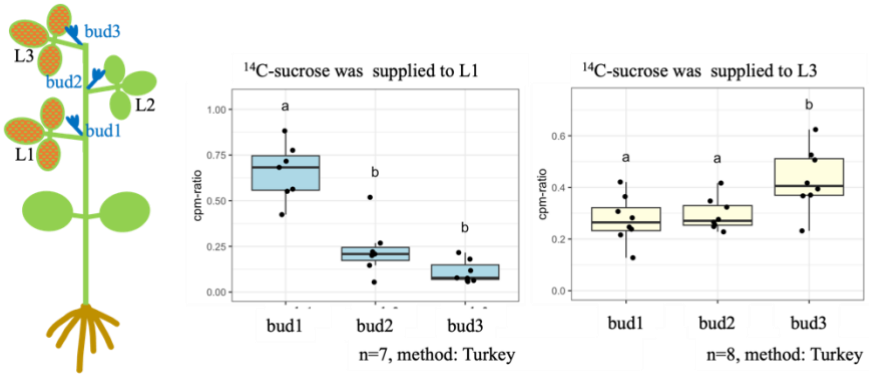


Fig.2 The ratio of ^{14}C translocated from 1st leaf (L1) or 3rd leaf (L3) to the buds

3. CONCLUSIONS

Photosynthate allocation in soybean is influenced by both the distance between source leaves and sink organs, and the overall spatial positioning of source leaves within the plant. Understanding these patterns provides insight into internal resource distribution and may provide some suggestions for improving crop productivity.

ACKNOWLEDGMENTS

This work was supported by JSPS KAKENHI Grant Number JP24H00499, and F-REI (JPFR25040101).

7th Asia-Pacific Symposium on Radiochemistry *September 14 ~ 19, 2025 • Kunibiki Messe • Shimane, Japan*

BIOIMAGING AND XPDT TREATMENT USING HIGHLY LUMINESCENT NANOCOMPOSITE SCINTILLATORS

Xenie Lytvynenko[1], Lenka Prouzová Procházková[1,2], Jan Bárta[1,2], Václav Čuba[1,*]

[1]*Department of Nuclear Chemistry, Faculty of Nuclear Sciences and Physical Engineering, Czech Technical University in Prague, Břehová 7, 115 19 Prague, Czech Republic*
[2]*Department of Optical Materials, Institute of Physics of the Czech Academy of Sciences, Cukrovarnická 10, Prague 162 53, Czech Republic*
** Corresponding Author Email: vaclav.cuba@fjfi.cvut.cz*

This work presents the synthesis and characterization of multimodal luminescent nanocomposites designed for applications in cathodoluminescence (CL) bioimaging and X-ray induced photodynamic therapy (XPDT). Using LuAG:Ce^{3+}, LuAG:Pr^{3+}, and CeF_3:Tb^{3+} nanoparticle cores, we developed functional systems with silica shells and surface-bound biomolecules or photosensitizers to enable specific cell targeting, biocompatibility, and radiation-induced activation. LuAG:Ce^{3+}-based nanocomposites showed stable and intense luminescence under electron beam irradiation and were successfully used for CL imaging of Saccharomyces cerevisiae and leukocytes. LuAG:Pr^{3+}@SiO_2-PpIX and CeF_3:Tb^{3+}@SiO_2-PpIX nanohybrids demonstrated efficient energy transfer to protoporphyrin IX and generation of singlet oxygen under X-ray exposure. Our findings support the feasibility of multifunctional nanocomposites in targeted bioimaging and XPDT, laying the groundwork for future development of advanced theranostic agents.

1. INTRODUCTION

Multimodal composite nanoparticles offer a powerful strategy for combining diagnostics and therapy within a single nanoscale system. By integrating luminescent cores, functional shells, and biologically active molecules, these materials can be engineered for precise targeting, imaging, and external activation by ionizing radiation to induce a photodynamic effect for cancer treatment. [1,2]. In this study, we focus on the design of radiation-responsive nanocomposites (Fig. 1) for two main biomedical applications: cathodoluminescence (CL) bioimaging and X-ray induced photodynamic therapy (XPDT).

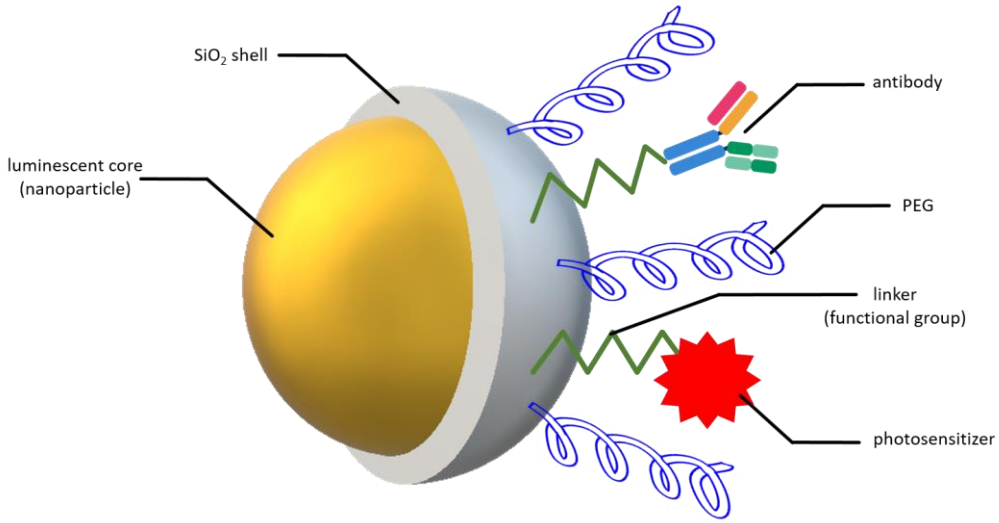


Fig. 1. Design of multimodal luminescent nanocomposite.

2.1 Materials for X-ray Induced Photodynamic Therapy (XPDT)

Two types of nanocomposites were prepared for XPDT: LuAG:Pr^{3+}@SiO_2-PpIX [3] and CeF_3:Tb^{3+}@SiO_2-PpIX [4]. The LuAG:Pr^{3+} core was prepared via a photo-induced precipitation method, while the CeF_3:Tb^{3+} core was synthesized by a sol–gel approach. Both were subsequently coated with silica and conjugated with protoporphyrin IX (PpIX). Upon X-ray excitation, energy transfer from the luminescent core to PpIX was confirmed via radioluminescence and time-resolved photoluminescence spectra. Singlet oxygen generation was demonstrated using APF chemical probes [5], and its

Copyright on 7th Asia-Pacific Symposium on Radiochemistry 2025

origin was verified through quenching experiments with NaN_3 [6]. These results confirm the efficient non-radiative energy transfer and the ability of these nanohybrids to generate reactive oxygen species, supporting their application in XPDT.

2.2 Materials for Cathodoluminescence Imaging

LuAG:Ce^{3+} nanoparticles were synthesized using a photo-induced method and encapsulated with amorphous or mesoporous SiO_2 shells. Surface functionalization with anti-Fas ligand (FasL) antibodies enabled receptor-specific targeting, and polyethylene glycol (PEG) increased biocompatibility. Under 10-keV electron beam excitation, these nanocomposites exhibited high CL intensity and stability. Imaging of *Saccharomyces cerevisiae* and leukocytes confirmed effective cell binding through both nonspecific sorption and targeted interactions [7].

3. CONCLUSIONS

The synthesized nanocomposites demonstrate high structural stability, tunable luminescent properties, and effective functionalization for biological applications. Their ability to withstand ionizing radiation while enabling either imaging or therapeutic singlet oxygen generation makes them promising candidates for further development as advanced multifunctional theranostic agents in biomedical applications.

ACKNOWLEDGMENTS

This work was carried out in the frame of the Crystal Clear Collaboration and supported by the Ministry of Education Youth and Sports, project SENDISO, grant number CZ.02.01.01/00/22_008/0004596.

References

[1] D.-E. LEE, *et al.*, "Multifunctional nanoparticles for multimodal imaging and theragnosis," *Chem. Soc. Rev.*, **41**, 7 (2012).
[2] X. LI, *et al.*, "Multimodality imaging in nanomedicine and nanotheranostics," *Cancer Biol. Med.*, **13**, 3 (2016).
[3] K. POPOVICH, *et al.*, "LuAG:Pr^{3+}-porphyrin based nanohybrid system for singlet oxygen production: Toward the next generation of PDTX drugs," *J. Photochem. Photobiol. B*, **179** (2018).
[4] K. POPOVICH, *et al.*, "Preliminary study on singlet oxygen production using CeF_3:Tb^{3+}@SiO_2-PpIX," *Radiat. Meas.*, **90** (2016).
[5] M. PIERCE, *et al.*, "Monitoring singlet oxygen and hydroxyl radical formation with fluorescent probes during photodynamic therapy," *Photochem. Photobiol.*, **85** (2009).
[6] M. BANCIROVA, "Sodium azide as a specific quencher of singlet oxygen during chemiluminescent detection by luminol and Cypridina luciferin analogues," *Luminescence.*, **26** (2011).
[7] K. POPOVICH, *et al.*, "Luminescent Nanocomposites for Biomedical Applications," *IEEE Trans. Nucl. Sci..*, **67**, 6 (2020).

7th Asia-Pacific Symposium on Radiochemistry *September 14 ~ 19, 2025 • Kunibiki Messe • Shimane, Japan*

EXPERIMENTAL SYSTEMS FOR INTERNAL AND EXTERNAL EXPOSURE OF SILKWORMS TO RADIOACTIVE CESIUM FOR THE EVALUATION OF BIOLOGICAL EFFECTS

Sota Tanaka[1], Sho Amano[2], Tadatoshi Kinouchi[3]

[1] *Faculty of Bioresource Sciences, Akita Prefectural University: 241-438 Kaidobata-Nishi, Nakano, Shimoshinjo, Akita City, Akita 010-0195, JAPAN, tanaka.sota@akita-pu.ac.jp*
[2] *Oita University Faculty of Medicine: 1-1 Idaigaoka, Hasama-machi, Yufu City, Oita 879-5593, JAPAN, m2341101@oita-u.ac.jp*
[3] *Institute for Integrated Radiation and Nuclear Science, Kyoto University: 2 Asashiro-Nishi, Kumatori-cho, Sennan-gun, Osaka 590-0494, JAPAN, kinouchi.tadatoshi.4v@kyoto-u.ac.jp*

INTRODUCTION

A large number of radioactive materials were released into the environment due to the accident at TEPCO's Fukushima Daiichi Nuclear Power Plant (FDNPP), raising concerns about the biological effects on the surrounding ecosystem. Radioactive cesium (Cs), which has a long half-life of approximately 30 years and accumulates near the ground surface, is expected to significantly impact ecosystems; thus, field surveys around the accident site are ongoing. In fact, morphological abnormalities and reductions in habitat density have been reported in insects that were previously considered to be relatively low in radiosensitivity. However, data on the effects of low-dose and low-dose-rate radiation on organisms, even insects, are incredibly scarce. Attempting to gather data from wild organisms presents several uncertainties that hinder quantitative evaluation, including the heterogeneity of environmental conditions and individual variations. As a result, our laboratory has researched the effects of low-dose and low-dose-rate radiation on organisms by constructing a simulated experimental system at the laboratory level using silkworms as model animals [1]. In other words, to simulate the internal exposure situation after the accident, silkworms were fed artificial diets containing drops of ^{137}Cs at 1,385 Bq/g- wet, three times the initial soil deposition after the accident, and were reared. Furthermore, there was no increase in the number of white eggs showing germ cell mutations, representing effects on the next generation. Based on these results, this study examined the *in vivo* dynamics of Cs in silkworms by feeding them artificial diets with drops of Cs.

METHODS

The silkworms were reared on artificial diets containing drops of ^{133}Cs (aqueous chloride solution) at concentrations of 4.19×10^{-4}, 5.32×10^{-2}, 5.32, and 5.32×10^{2} ppm (mg/kg-wet), fed this diet from the 1st to 5th instar (all larval stages). A Cs-concentration of 4.19×10^{-4} ppm (mg/kg-wet) was used as a non-radioactive control for ^{137}Cs (1,385 Bq/g-wet) utilized in a previous study.

To investigate the Cs biokinetics in silkworms, 5th instar larvae were dissected and divided into the principal organs of silkworm larvae: gut, reproductive organs, silk glands, muscle, skin, and other organs (primarily the head). Additionally, adult females were dissected, and eggs were collected to study Cs accumulation in the next generation. These samples were pretreated by microwave acid digestion, and Cs concentrations were measured by ICP-MS.

RESULTS and DISCUSSION

The Cs concentrations in different parts of the silkworm larvae were not significantly different among the reproductive organs, silk glands, and muscles. However, the skin had more than twice the Cs concentration compared to these organs, while the other organs (mainly the head) exhibited more than four times as much. This is thought to result from the silkworm skin and head being primarily composed of chitin, which chelates Cs, an alkali metal. The Cs concentrations of eggs collected from adult females were below the detection limit in silkworms reared on diets of 4.19×10^{-4} and 5.32×10^{-2} ppm (mg/kg-wet), respectively. On the other hand, the specific radioactivities of ^{137}Cs in eggs of adult females reared on diets containing 5.32 and 5.32×10^{2} ppm (mg/kg-wet) of Cs were estimated to be 9.78 and 53.4 (Bq/g-wet), respectively, indicating that approximately 1/250 to 1/1,400 of the Cs in the artificial diets was transferred into the eggs.

CONCLUSIONS

Copyright on 7th Asia-Pacific Symposium on Radiochemistry 2025 P-R6-08 -

In our previous study, no morphological abnormalities or radiation effects (germline mutations) were observed in the second generation of silkworms due to long-term low-dose exposure to ^{137}Cs [1]. However, adults of the pale grass blue butterfly collected in September 2011 in the area surrounding the FDNPP accident exhibited more severe morphological abnormalities than those collected in May of the same year [2]. This suggests that the effects of long-term low-dose exposure may be greater in the second and subsequent generations than in the first. Additionally, the Rad Silk project conducted on Kibō, which is the Japanese Experiment Module (JEM) for the International Space Station (ISS), has indicated that long-term low-dose space radiation exposure to embryo-expressing fertilized eggs of the silkworm can cause mutations in the next generation [3,4]. These studies are not directly comparable to our experimental results due to differences in species, radiation types, gravity, and experimental systems. However, since the specific activity of ^{137}Cs in silkworm eggs was estimated to be 9.78-53.4 Bq/g-wet by this study, it can be anticipated that silkworm eggs experience long-term low-dose exposure, and morphological abnormalities occurring after the second generation should also be examined in detail. Furthermore, we plan to conduct RNA-Seq analysis of Cs-localized tissues and eggs of the silkworm to investigate radiation responses at the gene level, even if no phenotypic/morphological abnormalities are observed in them.

ACKNOWLEDGMENTS

We thank Dr. Y. Banno and Dr. T. Fujii of Kyushu University for discussing the effects of radiation on silkworms and for their assistance with silkworm-rearing techniques. We appreciate Dr. M. Ikegami and Dr. D. Maki of the Institute for Integrated Radiation and Nuclear Science at Kyoto University for their technical support in handling radioisotopes and the grass rod dosimeter, as well as for the quantitative analysis of Cs using ICP-MS.

References

[1] S. TANAKA, T. KINOUCHI, et al., "Observation of Morphological Abnormalities in Silkworm Pupae After Feeding ^{137}CsCl-supplemented Diet to Evaluate the Effects of Low Dose-rate Exposure," *Scientific Reports*, **10**, 16055, (2020).

[2] A. Hiyama, et al., "The Biological Impacts of the Fukushima Nuclear Accident on the Pale Grass Blue Butterfly," *Scientific Reports*, **2,** 570, (2012).

[3] T. FURUSAWA, et al., "Introduction to the Proposed Space Experiments Aboard the ISS Using the Silkworm, *Bombyx mori,*" *Biological Sciences in Space*, **23**, 61-69, (2009).

[4] T. FURUSAWA, et al., "Targeted Heavy-ion Microbeam Irradiation of the Embryo but not Yolk in the Diapause-terminated Egg of the Silkworm, *Bombyx mori*, Induces the Somatic Mutation," *Journal of Radiation Research*, **50**, 371-375, (2009).

Copyright on 7th Asia-Pacific Symposium on Radiochemistry 2025 P-R6-08 -

Poster Presentation | [R9]Interdisciplinary and Multidisciplinary Topics

Wed. Sep 17, 2025 6:30 PM - 8:00 PM JST | Wed. Sep 17, 2025 9:30 AM - 11:00 AM UTC Poster

[Poster] R9

[P-R9-01]

ROBUST AND OPTIMIZED POLYGONAL MESH MODELING OF 3D-CAD/CG INTRICATE SHAPES USING THE INDUSTRIAL-STANDARD PRE/POST-PROCESSING TOOLS ON PHITS

*Minoru Sakama[1], Hiroto Nakano[1], Makoto Kobayashi[2], Takuya Saze[2], Ken'ichi Fujimoto[3] (1. Tokushima University (Japan), 2. National Institute for Fusion Science (Japan), 3. Kagawa University (Japan))

[P-R9-02]

In Vivo Tracking of ^{131}I-Cobravenom to Enhance Cobra Antivenom Production

*Nantanat Chailanggar[1], Wiranee Sriwiang[1], Piriya Kaeopookum[1], Surasak Akesowan[2], Orawan Khow[2], Narongsak Chaiyabutr[2] (1. Thailand Institute of Nuclear Technology (Thailand), 2. Queen Saovabha Memorial Institute (Thailand))

[P-R9-03]

THE IMPACT OF γ-IRRADIATION ON THE STABILITY OF VARIOUS CLAYS

*ALICIA Negron-Mendoza[1], Benjamín Leal-Acevedo [1], Isabel Gamboa De Buen[1], Javier Gutiérrez- Romero [1], Sergio Ramos-Bernal [1], Claudia Camargo-Raya[1], Elizabeth Chacón-Baca [2], Alejandro Heredia[1], Alfredo Rojas-Vivas[1], María José Rodríguez-Albarrán [1] (1. Instituto de Ciencias Nucleares, Universidad Nacional Autonoma de México (Mexico), 2. Facultad de Ciencias de la Tierra. Universidad Autónoma de Nuevo León (Mexico))

[P-R9-04*]

SMOOTHING OF ENERGY SPECTRUM DATA USING AN ε-FILTER FOR CONVOLUTIONAL NEURAL NETWORKS TO ESTIMATE DEPTH DISTRIBUTION OF RADIOISOTOPES IN SOIL

*Souya Horikawa[1], Kanata Nokubo[1], Ken'ichi Fujimoto[1], Minoru Sakama[2], Kazumasa Inoue[3], Masahiro Fukushi[4] (1. Kagawa University (Japan), 2. Tokushima University (Japan), 3. Tokyo Metropolitan University (Japan), 4. Tsukuba International University (Japan))

[P-R9-05]

Application of multi-point ^{14}C dating of fossil calcareous assemblages for reconstructing relative sea level fluctuation

*Yuzuko Tsukahara[1], Tetsuya Komatsu[1], Natsuko Fujita[1], Nariaki Nishiyama[1], Hideaki Maemoku[2] (1. Tono Geoscience Center (JAEA) (Japan), 2. Hosei University (Japan))

[P-R9-06]

Monitoring of TFWT concentrations in fish using Electrolytic Enrichment method for ALPS treated water discharged into the ocean

*Takaya Yabuta[1], Yurika Sasanami[1], Satoshi Tan[1], Takayuki Otsuki[1], Wataru Niita[1], Keiko Morimoto[2] (1. Japan Chemical Analysis Center (Japan), 2. Kyushu Environmental Evaluation Association (Japan))

[P-R9-07]

MODULATION TRANSFER SPECTROSCOPY OF CESIUM ATOMS TOWARD FULLY OPTICAL QUANTITATIVE ISOTOPE DETECTION

*Leo Matsuoka[1] (1. Hiroshima Institute of Technology (Japan))

©APSORC25

[P-R9-08]

ADSORPTION OF BA AND SR USING ZEOLITE SYNTHESIZED FROM INDUSTRIAL WASTES

*Takaaki Wajima[1] (1. Chiba Univeristy (Japan))

[P-R9-09]

PLATFORMS FOR SUPPLYING SHORT-LIVED RADIOISOTOPES FOR BASIC AND APPLIED SCIENCES IN JAPAN

*Hiroki Kanda[1], Takashi Nakano[1], Mitsuhiro Fukuda[1], Hiromitsu Haba[2], Noriko S. Ishioka[3], Hidetoshi Kikunaga[4], Kotaro Nagatsu[5], Atsushi Toyoshima[6,7], Hiroshi Watabe[8] (1. RCNP, Osaka University (Japan), 2. RIKEN Nishina Center (Japan), 3. QST Takasaki (Japan), 4. RARiS Mikamine, Tohoku University (Japan), 5. QST QMS (Japan), 6. IRS, Osaka University (Japan), 7. Osaka University (Japan), 8. RARiS Aobayama, Tohoku University (Japan))

©APSORC25

ROBUST AND OPTIMIZED POLYGONAL MESH MODELING OF 3D-CAD/CG INTRICATE SHAPES USING THE INDUSTRIAL-STANDARD PRE/POST-PROCESSING TOOLS ON PHITS

Minoru Sakama[1], Hiroto Nakano[1], Makoto Kobayashi[2], Takuya Saze[2] Ken'ichi Fujimoto[3]

[1]*Tokushima University: Kuramoto-cho 3-18-15, Tokushima City, Tokushima, 770-8509, JAPAN*
[2]*National Institute for Fusion Science (NIFS): Toki City, Gifu, 509-5292, JAPAN*
[3]*Kagawa University: Hayashicho 2217-20, Takamatsu City, Kagawa, 761-0396, JAPAN*

This work presents the current status of a pre/post-precessing workflow scheme consisting mainly for three steps for 3D mesh data imported from 3D-CAD designs with intricate entity shapes and 3D-Scan representative of industry-standard reverse engineering. SimLab and AcuSolve (Altair Engineering, Inc.) and MSC Apex modeler (HEXAGON AB) for tetrahedral meshing production of 3D-CAD/CG models, POLYGONALmeister (UEL Corporation) and VISI (HEXAGON AB) for editing processing for tetrahedral mesh intersections and face sharing errors that cannot be handled by this meshing production, and Paraview (Kitware, Inc.) for advanced visualization production for the Mote-Carlo based radiation transport calculation results obtained from PHITS ver.3.35 (the latest version).

1 INTRODUCTION

Currently, as represented by PHITS calculation codes, radiation and particle transport simulation calculations based on the Monte Carlo method, which are not only used in radiochemistry but also in the radiation industry, are effectively utilized in various situations and have become indispensable tools for researchers and engineers. We have utilized the PHITS code mainly for medical applications, radiation protection, radiation activation evaluation for medical accelerator, and next generation fusion reactor development. In particular, it is worth noting that in recent years, the number of start-up companies developing next-generation fusion reactors around the world has been steadily increasing, and each of these companies is competing fiercely to achieve their goals. As a startup company in Japan, Helical Fusion, Co. Ltd., established in 2021, has highlighed helical-type including stellarators as potential next generation fusion power reactors [1]. One of the most important issues of Monte-Carlo based calculations, including PHITS, is to set up a highly accurate and precise model of human bodies and structures equivalent to a real entity in a three-dimensional virtual space, i.e.,a intricate topology in which the real entities do not have to be actually constructed (manufactured or built). During these first stages, it is exactly essential to assess the feasibility of real entity concepts. It is important to emphasize that these concepts can vary significantly regarding their overall shape and allocation of space for each component, including the external vessel and skin structures with multi layers, internal parts and organ tissues, among others. To fulfill this challenges, it had been impossible to reproduce such complex topology groups in the 3D virtual calculation space due to very low software performance associated with older computer hardware performance (weak CPU and GPU performance and data transfer hardware) and insufficient 3D-CAD processing performance such as pre-post processing and solver processing using the finite element method, which is essential for 3D processing, and algorithms with slow code compilation processing. However the drastic improvement in computer performance combined with the growing needs of general-purpose industries in the automotive, aerospace, shipbuilding, and creator industries has led to remarkable technological progress in 3D-CG production, an integrated simulation environment that includes pre-post processing, solver processing, and 3D-CAD/CAE. In the PHITS code which should be involved as a solver processing for radiation and particle transport behavior, it has been now possible to export Nastran bulk data (.bdf format) corresponding to its code by integrating the latest methods for pre/post processing of intricate entities (human body, structures, etc.), namely, integrating Altair engineering SimLab and AcuSolve, and MSC Apex modeler with a design development platform with general-purpose 3D-CAD/CG functionality.

2 MATERIALS AND METHOD

This section provides each conceptual description of the industrial-standard and reliable pre/post-processing tools on the current state of generating tetrahedral mesh polygonal for 3D-CAD/CG models of various intricate shapes when imported to PHITS calculation space. Noteworthy is that the tools elaborated here have been developed in stages since FY2022 in our laboratory, and their maintenance is currently ongoing. In addition, the hardware performance of the workstation machines supporting these tools must also be robust and optimized, and the machine maintenance also has been carried out simultaneously.

2.1 SimLab and AcuSolve

SimLab and AcuSolve are provided by Altair Engineering, Inc. and both these tools can produce high-quality solid and surface mesh generation for intricate assemblies when simulating only particle and radiation transports but also multiple physics including structural, thermal, electromagnetic, and fluid dynamics (in particular, for AcuSolve coupled with HyperWorks CFD also supported by Altair Engineering, Inc.) in typical use such as manufacturing industries. And then, Both of

Copyright on 7th Asia-Pacific Symposium on Radiochemistry 2025

these tools are powerful enough to achieve high quality solid volume mesh models associated with the specific format (.bdf) of Nastran bulk data that addresses the requirements of PHITS.

2.2 MSC Apex Modeler

MSC Apex modeler is provided by HEXAGON AB, and also has specific features of mesh editing to implement any modification for the entities of interest, such as a face, edge or vertex, with pushing, pulling or dragging. In particular, this tool has enabled us to generate solid facet bodies that are editable in CAD from 3D polygonal data (.stl) obtained from a 3D scanner.

2.3 POLYGONALmeister and VISI as advanced mesh editing tools with highly capabilities

POLYGONALmeister is provided by UEL Corporation, and this tool offers powerful editing capabilities to locate complex polygon mesh errors, such as mesh intersections and face folding, and to edit them with any repair functions. While those tools already mentioned above have any similar capabilities, this POLYGONALmeister's correction algorithm has advantages over them. The same is valid for the other tool, VISI also provided by HEXAGON AB, which has been installed in our laboratory at an early stage and, therefore, has not yet fully utilized its many mesh repair features. However, one of the most notable features is the mesh morphing function. This morphing function can graphically repair the extremely thin, multi-layered mesh structure of the epidermis in the human phantom, which causes difficult intersection problems.

2.4 ParaView

ParaView provided by Kitware Inc. is an open source, cross-platform application for scientific visualization based on post-processing engine. Intended for interactive 3D visualization of large data sets, it has become an indispensable tool for researchers and engineers in the scientific and engineering fields. This tool can import many data formats. In this work, one of the data formats, OpenFOAM, can be exported via the PHITS calculations and we have obtain a variety of visualizations with advanced 3D post/processing by fusing radiation transport results with intricate shapes on ParaView.

3 RESULTS AND DISCUSSION

At the time of preparing this abstract, the latest version 3.35 of PHITS code had just been released on April 2025, nearly one year after the previous version. Because due to its timeliness, first impressions are that the tetrahedral mesh structure modeling relative to importing intricate shapes and computational stability associated with several previous program issues have been improved in comparison with the previous version 3.341. We will also address on the details of these improvements in this presentation. Figure 1 shows the current status of a pre/post-processing workflow scheme developed in this work, in which a mock-up simulated object with intricate shapes are handled by shape modification, remeshing, and solid volume meshing processings using SimLab and POLYGONALmeister.

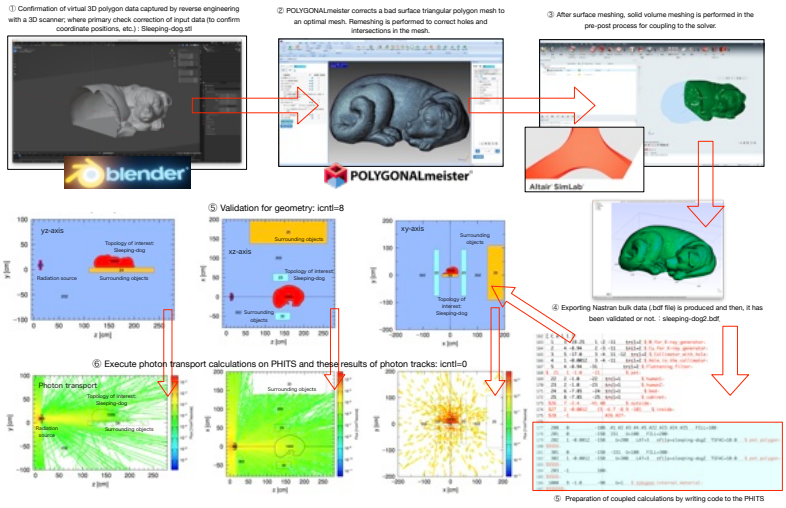


Fig. 1. Our development of the whole workflow with a coupled process in which a mock-up simulated object (e.g. a sleeping-dog) with complex topological shape are coped with shape modification, remeshing, and solid volume meshing to importing the data into PHITS calculation space.

4 CONCLUSIONS

In this study, we have utilized high-performance and reliable meshing tools based on industry specifications. Additionally, for the challenging errors that often generate during the meshing process, we addressed them using a tool with advanced mesh editing capabilities. This development enable us to import even the most intricate 3D-CAD/CG topologies into the PHITS computational space with flexibility.

ACKNOWLEDGMENTS

Some of this work have been carried out with the generous support of *Helical Fusion, Co. Ltd.*, through ongoing joint research activities. We would like to express our sincere gratitude for their support.

References

[1] J. Miyazawa and T. Goto, "Development of steady-state fusion reactor by Helical Fusion," Physics of Plasmas 30, 050601 (2023) http://doi.org/10.1063/5.0145222.

Copyright on 7th Asia-Pacific Symposium on Radiochemistry 2025

7th Asia-Pacific Symposium on Radiochemistry *September 14 ~ 19, 2025 • Kunibiki Messe • Shimane, Japan*

In Vivo Tracking of ^{131}I-Cobravenom to Enhance Cobra Antivenom Production

Nantanat Chailanggar[1], Wiranee Sriwiang[1], Piriya Kaeopookum[1], Surasak Akesowan[2], Orawan Khow[2], Narongsak Chaiyabutr[2]

[1]*Thailand Institute of Nuclear Technology, Ongkharak, Nakhon Nayok, 26120, Thailand. Email: nantanat@tint.or.th*
[2]*Queen Saovabha Memorial Institute, Bangkok, 10330, Thailand. Email: narongsak.c@chula.ac.th*

Snake envenomation continues to be a critical public health issue in Thailand and globally. The Thai cobra (Naja kaouthia) produces venom with a complex composition and highly potent neurotoxins, which are rapidly cleared from the body—limiting the time for effective antibody production. To overcome this challenge, adjuvants are used to prolong venom presence and enhance immune response. Among them, Freund's Incomplete Adjuvant (FIA) has shown superior performance in maintaining the activity of ^{131}I-labeled cobravenom compared to Alum or adjuvant-free formulations. Central to these advancements is the application of radiotracer techniques, which enable real-time, in vivo tracking of venom distribution and retention. This approach provides critical insights into the pharmacokinetics and biodistribution of cobra neurotoxins, contributing significantly to improving antivenom production efficiency and guiding more effective treatment strategies.

1 INTRODUCTION

Snake envenomation poses a significant public health challenge in Thailand, particularly among rural laborers [1]. The Queen Saovabha Memorial Institute (QSMI) produces seven monovalent and two polyvalent antivenoms targeting the most prevalent venomous snakes. While monovalent antivenoms are preferred due to their specificity and higher efficacy, polyvalent antivenoms are used when the snake species is unidentified, guided by clinical symptoms and patient history. However, their lower potency often necessitates higher doses, increasing the risk of adverse reactions and complicating treatment and production efforts [2,3]. Thus, the use of monovalent antivenoms still dominates snakebite treatment.

The venom of the Thai cobra (Naja kaouthia) contains a complex mixture of biologically active proteins, including enzymes, neurotoxins, and non-toxic molecules. Among these, neurotoxins—comprising approximately 10% of the total venom—are notably potent and represent a key target in antivenom production [4]. However, the immunogenicity of cobratoxin is relatively low; only 0–70% of horses immunized with cobratoxin produce antibody titers above the required threshold, compared to 80–100% when using toxins from other snake species. This results in limited antivenom yield, constraining supply to healthcare facilities and increasing treatment costs [2].

To enhance antivenom production, immunization protocols often incorporate adjuvants such as Freund's adjuvant and Alum. Freund's adjuvant, a water-in-oil emulsion, prolongs antigen retention at the injection site, thereby enhancing immune stimulation. Alum, composed of colloidal aluminum salts, increases antigen surface area to promote immune system activation [5,6]. Despite their widespread use, the underlying mechanisms of these adjuvants remain incompletely understood.

This study employed iodine-131 (I-131) to radiolabel cobratoxin via electrophilic substitution on the phenolic group of tyrosine residues (Fig. 1) [7]. The radiolabeled toxin, administered with either Freund's Incomplete Adjuvant, Alum, or without adjuvant, was tracked in vivo using gamma imaging. The resulting time-activity curves, biodistribution data, and dynamic scans in rat models provided insights into the pharmacokinetics of cobratoxin and the modulatory effects of adjuvants, contributing to the optimization of antivenom production protocols.

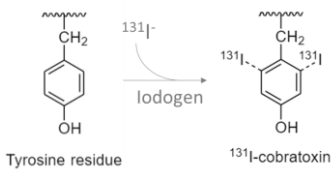


Fig. 1. The electrophilic substitution of ^{131}I on the phenolic group of tyrosine residue via Iodogen method.

Copyright on 7th Asia-Pacific Symposium on Radiochemistry 2025

2. CONCLUSIONS

Radiolabeling cobravenom with I-131 can be effectively accomplished using the Iodogen method. In the absence of FIA, it was observed that radiolabeled cobravenom could withstand metabolic processes for only a limited duration (data not shown). In contrast, the ^{131}I-cobravenom encapsulated in FIA remained intact, to some extent, throughout the 14-day observation period until elimination from the body. The highest uptake of ^{131}I-cobravenom in horses' blood was recorded at 24h post injection, followed by a decline in activity to nearly minimal levels at 96-120h post injection (4-5d post injection) (Fig. 2). A booster applied within these time frames could effectively enhance the antibody titer. Additionally, administering antivenom within 4-24 hours after a snakebite could ensure optimal neutralization capacity of the antivenom.

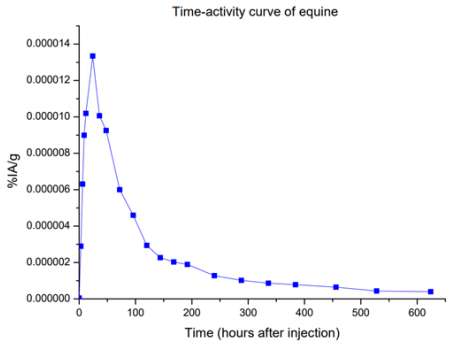


Fig 2. Time-activity curve of horses introduced radiolabeling cobravenom.

ACKNOWLEDGMENTS

This project has been funded by National Research Council of Thailand (NRCT) (Contract No. N12E660077).

References

[1] Chippaux, J.-P. Snakebite Envenomation Turns Again into a Neglected Tropical Disease! J Venom Anim Toxins Incl Trop Dis 2017, 23, 38.
[2] Leong, P. K.; Fung, S. Y.; Tan, C. H.; Sim, S. M.; Tan, N. H. Immunological Cross-Reactivity and Neutralization of the Principal Toxins of Naja Sumatrana and Related Cobra Venoms by a Thai Polyvalent Antivenom (Neuro Polyvalent Snake Antivenom). Acta Trop 2015, 149, 86–93.
[3] Ratanabanangkoon, K. Polyvalent Snake Antivenoms: Production Strategy and Their Therapeutic Benefits. Toxins. Multidisciplinary Digital Publishing Institute (MDPI) September 1, 2023.
[4] Sriprapat, S.; Aeksowan, S.; Sapsutthipas, S.; Chotwiwatthanakun, C.; Suttijitpaisal, P.; Pratanaphon, R.; Khow, O.; Sitprija, V.; Ratanabanangkoon, K. The Impact of a Low Dose, Low Volume, Multi-Site Immunization on the Production of Therapeutic Antivenoms in Thailand.
[5] Facciolà, A.; Visalli, G.; Laganà, A.; Di Pietro, A. An Overview of Vaccine Adjuvants: Current Evidence and Future Perspectives. *Vaccines*. MDPI May 1, 2022.
[6] Arguedas, M.; Umaña, D.; Moscoso, E.; García, A.; Pereira, C.; Sánchez, A.; Durán, G.; Cordero, D.; Sánchez, A.; Segura, Á.; Vargas, M.; Herrera, M.; Villalta, M.; Gómez, A.; Salas, C.; Díaz, C.; María Gutiérrez, J.; León, G. Comparison of Adjuvant Emulsions for Their Safety and Ability to Enhance the Antibody Response in Horses Immunized with African Snake Venoms. *Vaccine X* **2022**, *12*.
[7] Kumar, K.; Ghosh, A. Radiochemistry, Production Processes, Labeling Methods, and ImmunoPET Imaging Pharmaceuticals of Iodine-124. Molecules 2021, 26 (2).

THE IMPACT OF γ-IRRADIATION ON THE STABILITY OF VARIOUS CLAYS

Negrón-Mendoza Alicia[1], Leal-Acevedo Benjamín[1], Gamboa De Buen Isabel[1], Gutiérrez- Romero Javier[1], Ramos-Bernal Sergio[1], Camargo-Raya Claudia[1], Chacón-Baca Elizabeth[2], Heredia Alejandro[1], Rojas-Vivas Alfredo[1], María José Rodríguez-Albarrán María José[1]

[1]Instituto de Ciencias Nucleares, Universidad Nacional Autónoma de México (ICN-UNAM), Circuito Exterior s/n, Ciudad Universitaria, Coyoacán, 04510 CDMX, México
[2]Facultad de Ciencias de la Tierra. Universidad Autónoma de Nuevo León, Linares, México.

As a result of the distinctive physicochemical features that clays have, particularly their sorption abilities, these solids find widespread application in various sectors. Researching how radiation interacts with these materials is necessary to consider their potential applications in interdisciplinary and multidisciplinary research, such as chemical evolution, waste disposal, and sorption of emerging contaminants. This study involved exposing samples of Na-montmorillonite, Ca-montmorillonite, attapulgite, hectorite, and kaolinite clays to high doses of gamma radiation using the Gammabeam 651PT ^{60}Co source at ICN-UNAM. This research aimed to assess the structural changes in these clays following exposure to high gamma radiation fields.
The analysis of clays was by ATR-IR spectroscopy, X-ray diffraction (XRD), and electron paramagnetic resonance (EPR), which enabled us to examine an alteration in the structures of clays.
.

1 INTRODUCTION

One of the main research questions about the effects of radiation on minerals is to find broad patterns in the potential alteration of the physicochemical properties of clay minerals due to irradiation. For example, to use minerals for various purposes, it is crucial to understand how stable they are toward radiation. It is essential to predict the radiation stability of minerals that could be used as engineering barriers in storing radioactive waste, in prebiotic chemistry, to protect the sorbed organic compound, and to remove emerging contaminants through Advanced Oxidation Processes. In all these applications it is important to evaluate the stability of minerals.

1.1 Experimental Procedures

Clays

This study used five clays from the Source Clays Repository of the Clay Minerals Society, with no prior purification. The clays were kaolinite (KGa-1), Na-montmorillonite (SWy-2), Ca-montmorillonite (STX-1), hectorite (SHCa-1), and attapulgite (PF1-1).

Irradiation

The irradiation was conducted in a gamma source of ^{60}Co, Gammabeam 651 PT at Instituto de Ciencias Nucleares-UNAM with doses up to 11.21 MGy.

Analysis

FTIR spectroscopy. The clays were analyzed with infrared spectroscopy using a Perkin Elmer Spectrum 100 FT-IR spectrophotometer with an ATR technique.
X-ray spectroscopy (XRD) analyzed clay samples using a D5000 S diffractometer with filtered Cu Kα radiation, at 2θ angles from 2◦ to 15◦. The calibration of the spectrometer was using Si, quartz, and kaolinite reference materials.
For EPR analyses we used a spectrometer JES-TE300, Jeol, Japan, at the Instituto de Química, UNAM. 20 mg of the clay were analyzed working the X-band with a frequency of 9.437 GHz modulation and a cylindrical cavity in TE_{011} mode. The magnetic field was calibrated using a precision gaussmeter (ES-FC5, Jeol, Japan). The magnetic reading intervals were 800-600 mT, 260-410 mT, 330-344 mT.

1.1.1 Results

The results showed that high irradiation doses did not affect the mineral's crystalline structures in the examined clays, and the influence on their physicochemical characteristics was weak. RXD patterns showed that irradiation reduced clay crystallinity, specifically in kaolinite, since in this mineral two small peaks disappeared (Fig. 1). These findings support Plôtze et al. [1], who found low montmorillonite damage from intense irradiation doses. Other clay irradiation studies

Copyright on 7th Asia-Pacific Symposium on Radiochemistry 2025

suggest irradiated clays analyzed by EPR only causes paramagnetic defects [2]. More data is needed to evaluate clays' photo-physical and electronic energy storage capacities.

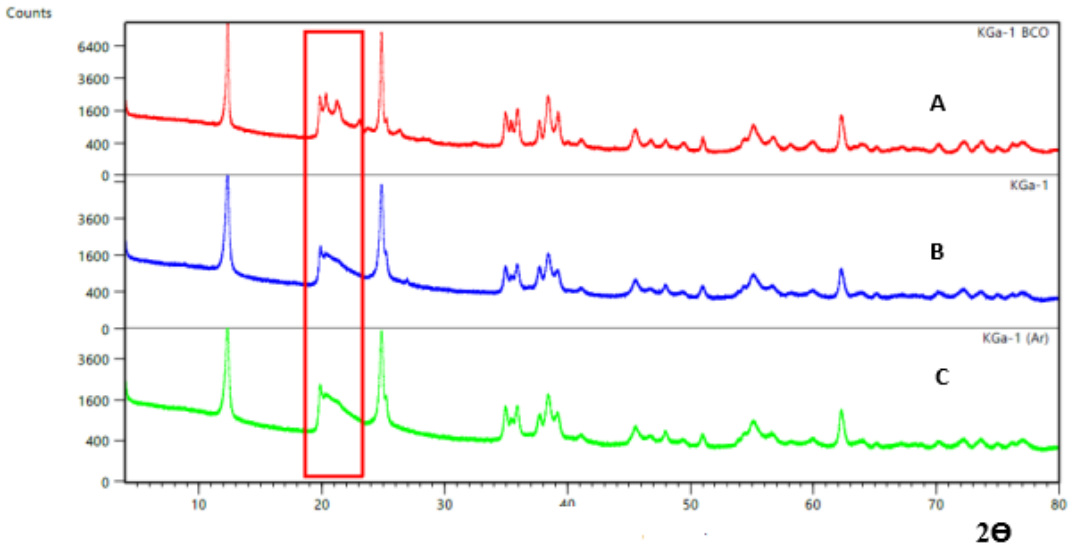


Fig. 1. X-ray spectra for kaolinite (A) Non-irradiated, (B) irradiated at 11.21 MGy (C) Irradiated at 11.21 MGy under an argon atmosphere.

2. CONCLUSIONS

These findings show that the examined clays may absorb significant radiation levels without substantial damage, making them proper materials for applications involving sorbed substances.

ACKNOWLEDGMENTS

Acknowledgement for financial support from DGAPA-PAPIIT IN113325 project, CONAHCYT I- 2604, and the CF-2439-CONAHCyT.
.

References

[1] M. M. PLOTZE, G. KAHR, G. HERMANNS, R. STENGELE, *Appl. Clay Sci*. **23** (1–4), 195 (2003).
[2] M. LAINE, E. BALAN, T. ALLARD, E. PAINEAU, P. JEUNESSE, M. MOSTAFAVI, J.L. ROBERT, S. LE CAER, *RSC Adv*. 7 (1), 526 (2017).

Copyright on 7th Asia-Pacific Symposium on Radiochemistry 2025 P-R9-03 -

SMOOTHING OF ENERGY SPECTRUM DATA USING AN ε-FILTER FOR CONVOLUTIONAL NEURAL NETWORKS TO ESTIMATE DEPTH DISTRIBUTION OF RADIOISOTOPES IN SOIL

Soya Horikawa[1], Kanata Nokubo[1], Ken'ichi Fujimoto[1], Minoru Sakama[2], Kazumasa Inoue[3], Masahiro Fukushi[4]

[1]*Kagawa University: 2217-20, Hayashi-cho, Takamatsu, Kagawa 761-0396, Japan*
[2]*Tokushima University: Kuramoto-cho 3-18-15, Tokushima, Tokushima 770-8509, Japan*
[3]*Tokyo Metropolitan University: 7-2-10, Higashi-Ogu, Arakawa-ku, Tokyo 116-8551, Japan*
[4]*Tsukuba International University: 6-20-1, Manabe, Tsuchiura, Ibaraki 300-0051, Japan*

To design efficient decontamination plan for soils contaminated with radioisotopes (RIs), we developed a portable measuring instrument that can accurately estimate the radioactivity of RIs distributed in the depth direction of soil. We also developed convolutional neural networks (CNNs) to estimate the depth distribution of soil radioactivity from radiation energy spectra measured with detectors. Although the CNNs have good estimation accuracy, it needs improvement for practical use. In this paper, to enhance CNNs' performance, we propose a method using an ε-filter for smoothing of the radiation energy spectra before inputting them into CNNs. We obtained results that the estimation accuracy of CNNs using the ε-filter was better than that with CNNs and a moving-average filter.

1 INTRODUCTION

The earthquake that occurred on March 11, 2011 caused serious damage to the Fukushima Daiichi Nuclear Power Plant. This accident resulted in the release of a large amount of radioactive materials in and around Fukushima. To design effective decontamination strategies for soils contaminated with these radioisotopes (RIs), it is essential to develop portable instruments capable of assessing the extent and depth of soil contamination.

We developed a prototype of a portable measuring instrument (AFT-DDS) with convolutional neural networks (CNNs) to estimate the depth distribution of soil radioactivity based on measured radiation energy spectra [1]. Although CNNs demonstrated promising estimation accuracy, further improvement is necessary for practical applications. In this paper, we propose a method for smoothing of the radiation energy spectra to enhance CNNs' performance by applying an ε-filter [2].

2 ESTIMATION SYSTEM AND SMOOTHING METHOD

The AFT-DDS has a rod-shaped design and equips 20 detectors at 2 cm intervals. It can count the number of photons in each depth layer of the soil. Based on measured photons, 20 energy spectra can be plotted. The scientific problem to design effective decontamination strategies is to estimate the distribution of RIs in each depth layer of soil from 20 energy spectra. We constructed two CNNs (CNN_1 and CNN_2) [1] that estimate the distribution of RI in 20 layers. We here assign the estimation in the 1–10th layers to CNN_1 and that in the rest of the 11–20th layers were assigned to CNN_2, i.e., CNN_1 receives 10 energy spectra in the 1–10th layers and outputs the radioactivity in the 1–10th layers. In the same way, CNN_2 receives 10 energy spectra in the 11–20th layers and outputs the radioactivity in the 11–20th layer. We defined CNNs' correct output as the error between CNN output and true values is within $\pm 5\%$ in layers where RI is present, and CNN output value is less than 0.1 in layers where RI is not present.

To enhance CNNs' performance, we propose a method using an ε-filter [2] for smoothing energy spectrum before inputting them into CNNs. Let be $x^\ell(k)$ $(k = 1, 2, \ldots, 165)$ the number of photons measured with the kth channel of detector in the ℓth layer. The output $y^\ell(k)$ of the ℓth ε-filter is defined as

$$y^\ell(k) = x^\ell(k) + \sum_{i=-N^\ell}^{N^\ell} a_i^\ell F^\ell(x^\ell(k+i) - x^\ell(k)), \quad F^\ell(z) = \begin{cases} z & \text{if } |z| \le \varepsilon^\ell \\ 0 & \text{if } |z| > \varepsilon^\ell \end{cases} \tag{1}$$

where N^ℓ, a_i^ℓ, and ε^ℓ are user-defined parameters. Based on the results in preliminary experiment, we set to $N^\ell = 5$, $a_i^\ell = 0.1$, and $\varepsilon^\ell = (x_{\max}^\ell - x_{\min}^\ell)/6.0$ for all i and ℓ, where $x_{\max}^\ell = \max\{x^\ell(1), \ldots, x^\ell(165)\}$ and $x_{\min}^\ell = \min\{x^\ell(1), \ldots, x^\ell(165)\}$.

3 RESULTS AND DISCUSSIONS

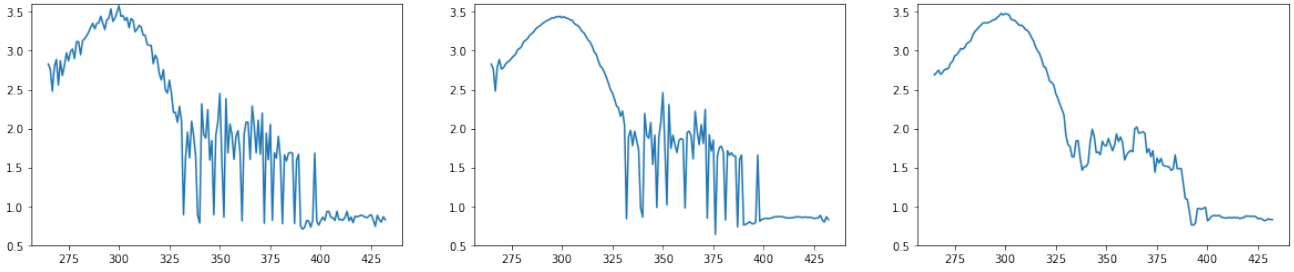
We used radiation energy spectra generated through numerical simulation using the particle and heavy-ion transport calculation code (PHITS) [3]. Moreover, we increased the number of energy spectra datasets using conditional generative adversarial networks (CGAN) [4]. An energy spectrum is composed of 1024ch data and we extracted only 168ch in the

Copyright on 7th Asia-Pacific Symposium on Radiochemistry 2025 P-R9-04* -

265–433ch, which are particularly affected by two types of RIs: ^{134}Cs and ^{137}Cs. Since the vertical range of energy spectrum is wide, the energy spectrum was logarithmically transformed before a filter was applied.

Figure 1(a) shows an energy spectrum generated by PHITS and CGAN in which the vertical values were logarithmically transformed. Figures 1(b) and 1(c) show the energy spectra processed by the proposed ε-filter and a five-point moving average filter for logarithmically transformed energy spectrum in Fig. 1(a), respectively. Comparing Figs 1(b) and 1(c), the shape of energy spectrum in the 265–330ch was similarly smoothed. However, we found a significant difference in the shape of the energy spectrum in the 330–433ch. In the use of the ε-filter, a part of fluctuations in 330–433ch was preserved. On the other hand, in the case of the five-point moving average filter, the shape of energy spectrum in the same range was quite smoothed.

We treated the cases that RIs with intensity of 1.0 were placed in two layers. Table 1 shows the estimation accuracy of CNNs for filterd energy spectra. For filterd energy spectra using the ε-filter, the estimation accuracy of CNN_1 and CNN_2 were 82.6% and 98.6%. In contrast, the use of the five-point moving-average filter reduced the estimation accuracy of CNN_1 and CNN_2 to 78.1% and 93.5%, respectively. The results demonstrated that the use of ε-filters with appropriate parameter values can improve the estimation accuracy of CNNs. Conversely, it was suggested that excessive smoothing can degrade the estimation accuracy of CNNs.



(a) Only logarithmically transformed (b) ε-filter (c) five-point moving-average filter

Fig. 1. Smoothing results of radiation energy spectrum using ε-filter or five-point moving-average filter.

TABLE 1. Estimation accuracy of CNNs for energy spectra smoothed by filters.

	ε-filter	five-point moving-average filter
CNN_1	82.6%	78.1%
CNN_2	98.6%	93.5%

4 CONCLUSIONS

To improve the estimation accuracy of CNNs, we proposed the smoothing of radiation energy spectra using an ε-filter. Comparing with two smoothing methods using the ε-filter or a five-point moving-average filter, we obtained the results that the estimation accuracy of CNNs using the ε-filter was better than that with the five-point moving-average filter.

ACKNOWLEDGMENTS

This work was supported by JSPS KAKENHI Grant Number JP23K11249.

References

[1] M. Azam B. M. Pauzi, et al., “Development of Convolutional Neural Networks to Estimate Depth Distribution of Radioisotope in Soil Layers,” Journal of Signal Processing, Vol. 27, No. 4, pp. 103–106, 2023.

[2] K. Arakawa, K. Matsuura, et al., “A Method of Noise Reduction for Speech Signals Using Component Separating ε-Filters,” IEICE TRANSACTIONS on Fundamentals of Electronics, Communications and Computer Sciences, Vol. J85-A, No. 10, pp. 1059–1069, 2002. (In Japanese)

[3] Y. Iwamoto, S. Hashimoto, et al., “Benchmark Study of Particle and Heavy-Ion Transport Code System Using Shielding Integral Benchmark Archive and Database for Accelerator-Shielding Experiments,” Journal of Nuclear Science and Technology, Vol. 59, No. 5, pp. 665–675, 2022.

[4] M. Mirza and S. Osindero, “Conditional Generative Adversarial Nets,” arXiv:1411.1784v1, 2014.

Copyright on 7th Asia-Pacific Symposium on Radiochemistry 2025 P-R9-04* -

Application of multi-point ^{14}C dating of fossil calcareous assemblages for reconstructing relative sea level fluctuation

Yuzuko Tsukahara[1], Tetsuya Komatsu[1], Natsuko Fujita[1], Nariaki Nishiyama[1], Hideaki Maemoku[2]

[1]*Tono Geoscience Center (JAEA): 959-31 Jorinji, Izumi-Cho, Toki-shi, Gifu, 509-5102, Japan*
tsukahara.yuzuko@jaea.go.jp
[2]*Hosei University: 2-17-1 Fujimi, Chiyoda-ku, Tokyo 102-8160, Japan*

1. INTRODUCTION

Many calcareous organisms live densely in intertidal zone of rocky coast, which remain as fossil after death. Fossils often form assemblage and are discovered above sea level. The elevation and ^{14}C age of fossil calcareous assemblages indicate the past sea level heights and periods and thus are useful to reconstruct the history of relative sea level fluctuations from the past to the present. However, not all fossils forming a single assemblage indicate the same age. Depending on the pattern of sea level fluctuations, calcareous organisms that lived in different periods may form a single assemblage [1] [2]. Maemoku [1] focused on the visually identifiable discontinuous boundary surfaces (hereinafter, referred as "boundary ") in fossil assemblages and dated the ^{14}C ages of each layer to estimate that this structure was formed by repeated relative sea level fluctuations. The formation process of fossil assemblages, however, is not understood in detail, and each layer may not necessarily correspond to a single sea level fluctuation. In this study, we randomly sampled a large number of fossils without regard to internal structure of assemblages and dated those ^{14}C ages. Subsequently we compared the ^{14}C ages with structural features such as boundaries and multilayered structures to examine the formation process of the fossil assemblages.

2. STUDY AREA AND METHOD

We collected fossil calcareous assemblages consisting mainly of polychaeta on the rocky coasts of Cape Gyoto and Cape Hane, Muroto Peninsula, Kochi prefecture. One fossil assemblage (Fig. 1: Gy) was collected in Cape Gyoto and three assemblages (Fig. 1: HN1, 2, and 3) were collected in Cape Hane.

The fossil assemblages were cut at the laboratory and identified the boundaries by visual observation of cross section (Fig. 1). The polychaeta fossils were sampled from the cross sections and dated ^{14}C. The samples of Cape Gyoto were dated using Compact-AMS at Paleo Lab Co., Ltd., while samples of Cape Hane were dated using JAEA-AMS-TONO-5MV at the Tono Geoscience Center. Conventional ages were calibrated using the Oxcal program version 4.4 [3] with the Marine20 curve [4]. The local calibration value (ΔR) is -150±51 yr based on age of shell in the Kii Peninsula [5]. This value was recalculated using CALIB [6], the Marine20 calibration curve [4] in this study.

3. RESULT AND DISCUSSION

The calibration ages of the polychaeta fossils are shown in Fig.2. Based on the ages, these of Cape Gyoto are divided into two age groups: 1925–1060 calBP and 985–630 calBP. The boundary between these age groups corresponds with boundary A. The boundary A with time gap of the polychaeta fossils is thought to have formed by the emergence of fossil assemblage due to sea level fall, as pointed out in the previous study [1]. On the other hand, there were no age differences between the outer and inner sides of the boundary B, and the polychaeta fossils of the outer and inner sides belong to the same age group. This indicates that the boundary is not necessarily caused by events with time gaps such as sea level fluctuations. The boundary can be formed by other factors such as changes in the species composition of calcareous organisms and instantaneous and powerful erosion caused by waves.

The calibration ages of the three fossil assemblages of Cape Hane cannot be divided into defined groups, unlike those of Cape Gyoto. However, there are some trends in the distribution of ages. Although the age ranges overlap within the 2σ, they can possibly be divided into three age groups: 2290–1510 calBP, 1700–1005 calBP, and 1215–605 calBP. HN2 and HN3 consisted of polychaeta fossils of different age groups even though no boundaries are identified. This suggests that boundaries do not always form even if events causing a time of gap occur, such as sea level fall. It is possible that significant erosion that creates distinct boundaries did not occur even when sea level fell.

This study reveals that forming boundaries do not necessarily correspond to sea level fluctuations, and that there are various patterns in the formation process of fossil calcareous assemblages. In the case of Cape Gyoto, boundaries without time gaps were identified by measuring approximately one polychaeta fossil per 10 cm² of section. When reconstructing

Copyright on 7th Asia-Pacific Symposium on Radiochemistry 2025

relative sea level fluctuation based on fossil assemblages, it is desirable to date ^{14}C ages of numerous calcareous organisms constituting a single assemblage to enhance the temporal resolution.

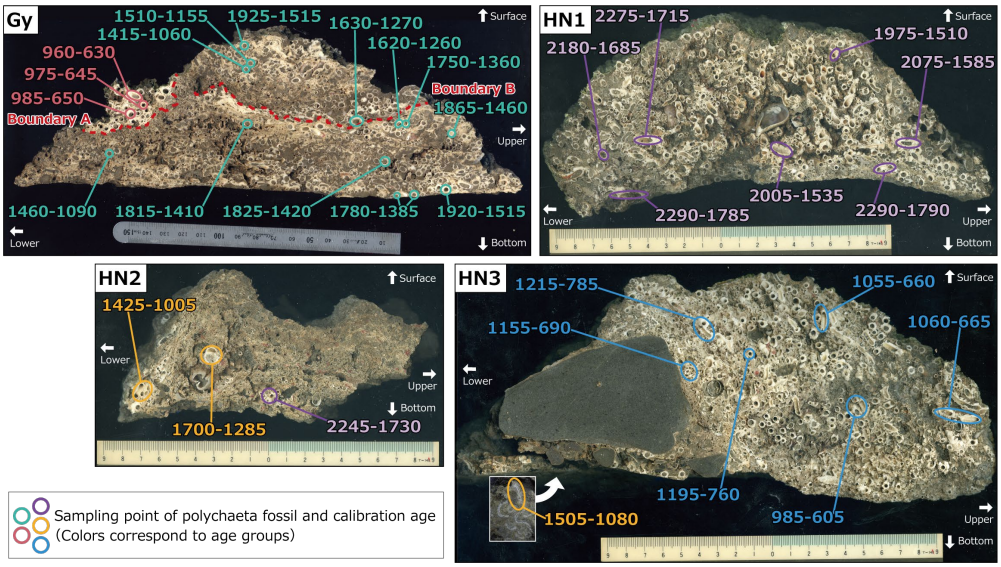


Fig. 1. Cross sections of the fossil assemblages with calibration ages and discontinuous boundary surfaces

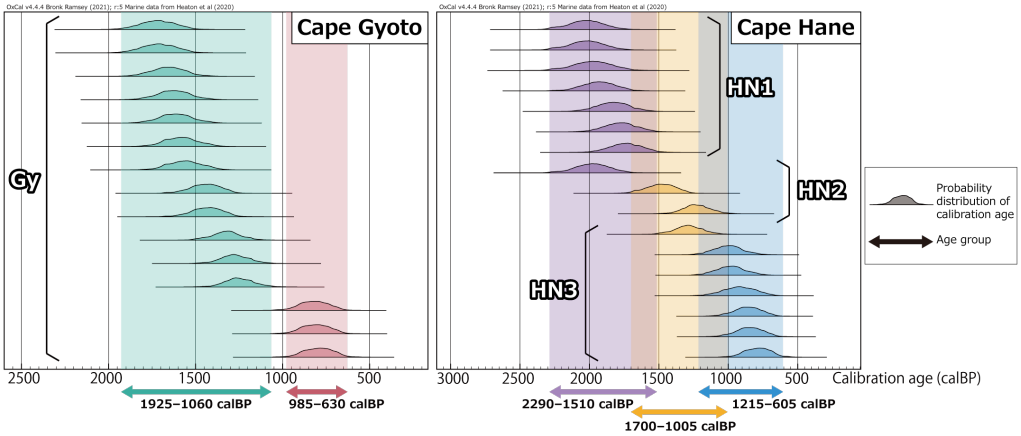


Fig. 2. Calibration ages of polychaeta fossils

ACKNOWLEDGMENTS

This study was funded by the Sector of Nuclear Fuel, Decommissioning and Waste Management Technology Development, Japan Atomic Energy Agency (JAEA) as part of developing young researchers and engineers and the Ministry of Economy, Trade and Industry (METI), Japan as part of its R&D supporting program for the geological disposal of high-level radioactive waste (JPJ007597).

References

[1] H. Maemoku, Reexamination of Coseismic Uplift of Cape Muroto, Southwestern Japan, Using AMS14C Ages of Raised Sessile Organisms, Journal of Geography, 110(4), pp. 479-490 (2001).
[2] M. Shishikura et al., Coseismic Uplift of Iwami-Tatamigaura during the 1872 Hamada Earthquake -Survey of Emerged Sessile Assemblage and Topography-, Zisin, 73, pp. 159-177 (2000).
[3] C. Bronk Ramsey, Bayesian analysis of radiocarbon dates, Radiocarbon, 51, pp. 337-360(2009).
[4] T. Heaton et al., Marine20 - the marine radiocarbon age calibration curve (0–55,000 cal BP), Radiocarbon, 62, pp. 779–820(2020).
[5] M. Yoneda et al., Pre-bomb marine reservoir ages in the western north Pacifc: Preliminary result on Kyoto University collection, Nuclear Instruments and Methods in Physics Research, 172, pp. 377-381(2000).
[6] M. Stuiver and P.J. Reimer., Extended 14C Data Base and Revised CALIB 3.0 14C Age Calibration Program, Radiocarbon, 35, pp. 215-230(1993).

Copyright on 7th Asia-Pacific Symposium on Radiochemistry 2025

Monitoring of TFWT concentrations in fish using Electrolytic Enrichment method for ALPS treated water discharged into the ocean

Takaya Yabuta[1], Yurika Sasanami[1], Satoshi Tan[1], Takayuki Otsuki[1], Wataru Niita[1], Keiko Morimoto [2]

[1]*Japan Chemical Analysis Center: 295-3 Sanno-cho, Inage-ku, Chiba City, Chiba Prefecture, 263-0002*
[2]*Kyushu Environmental Evaluation Association: 1-10-1 Matsukadai, Higashi-ku, Fukuoka City, Fukuoka Prefecture, 813-0004*

As part of marine environmental monitoring conducted by the Ministry of the Environment in response to the ocean discharge of Advanced Liquid Processing System (hereinafter" ALPS") treated water off the coast of Fukushima Prefecture, we report the results of Tissue Free Water Tritium (hereinafter "TFWT") in fish analyzed from 2022 to 2024. TFWT in fish collected four times a year, was concentrated by electrolysis and measured using a liquid scintillation counter.

Although TFWT concentrations increased slightly during the period in which ALPS-treated water was discharged into the ocean, once the discharge was stopped, the concentrations returned to those before the discharge began, and that tritium was not accumulating or concentrating in fish. In addition, the TFWT concentrations in fish were within the range of past fluctuations in tritium concentrations in seawater throughout Japan, and it was assessed that the impact of discharging ALPS-treated water into the ocean would be negligible on people and the environment in the conference consisting of environmental radioactivity experts, relevant ministries, and agencies in Japan.

1 INTRODUCTION

As part of the decommissioning process for the Fukushima Daiichi Nuclear Power Plant (hereinafter "FDNPS") operated by Tokyo Electric Power Company, water containing radioactive materials contained within the FDNPS building is being purified using ALPS or other equipment until radioactive materials other than tritium meet safety standards, and the water is then significantly diluted with seawater so that the tritium concentration fully meets safety standards, after which it is being discharged into the ocean. The treated water was discharged into the ocean a total of 10 times between August 2023 and November 2024. Because ALPS treatment cannot remove tritium, there is growing concern about the effects on the human body of ingesting fish in which tritium has absorbed. Therefore, the safety of ALPS-treated water must be confirmed before it is dischaged into the ocean, and marine monitoring is being continuously carried out by various Japanese ministries, local governments, and related organizations. We report on the results of monitoring of TFWT concentrations in fish conducted by the Ministry of the Environment from 2022 to 2024. The TFWT concentration in fish was expected to be extremely low, similar to the tritium concentration in the surrounding seawater, so an Electrolytic Enrichment method was adopted in this research to lower the detection limit.

2 MATERIALS AND METHODS

2.1 SAMPLING

From the ALPS-treated water discharge outlet 1km away from FDNPS, fish samples were collected at 3 sea areas; 1.5 km north, 0.4 km east and 2 km south away from discharge outlet (E-SF1, E-SF2, and E-SF3, respectively) (Fig. 1). Sampling was conducted four times a year from 2022 to 2024, and the most commonly collected fish was flounder.

2.2 ANALYSIS OF TFWT

The analysis flow chart is shown in Fig. 2. Fish sample was freeze dried and separated into water and dry matter. The obtained sample water was refluxed to decompose organic matter, and then was distilled to remove impurities. Distilled water applied electrolytic enrichment of tritium (See Fig. 3). After tritium enrichment, sample water was distilled again to remove alkali reagent. Distilled water was mixed with scintillator for measurement and the vial was shaken well to prepare the measurement sample.

The measurements were carried out using a low background liquid scintillation counter, with each sample measured over 500 minutes, and the tritium concentration was calculated.

Copyright on 7th Asia-Pacific Symposium on Radiochemistry 2025

3 RESULTS AND DISCUSSION

The TFWT analytical results are shown in Fig. 4. A slight increase in TFWT concentration was confirmed in the samples collected on October 18, 2023, July 9, 2024, and November 6, 2024. This is considered to be a temporary increase in concentration during or near the ALPS-treated water ocean discharge period, and it was shown that the concentration would return to the level before the discharge was started when the discharge was stopped. In addition, throughout the entire period, the TFWT concentrations were within the range of past tritium concentrations in seawater in Japan and surrounding sea areas. It was assessed that the impact of discharging ALPS-treated water into the ocean would be negligible on people and the environment.

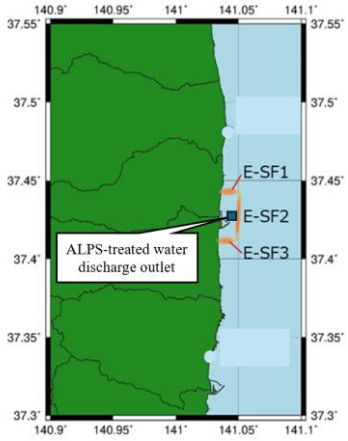


Fig. 1 Sampling points of fish

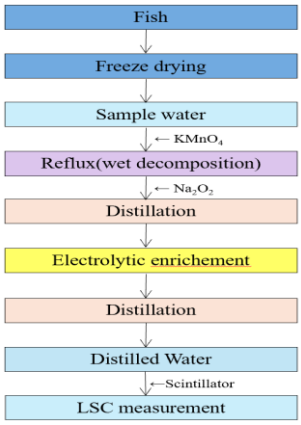


Fig. 2 TFWT analysis flow chart



Fig. 3. Electrolytic Enrichment equipment(e.g.)

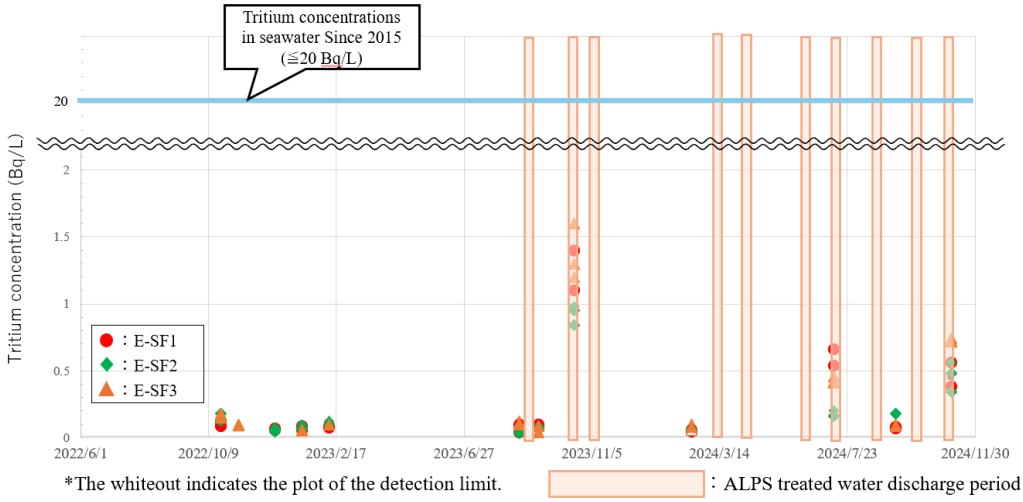


Fig. 4. TFWT analysis results for fish

4. CONCLUSIONS

As part of marine environmental monitoring efforts conducted by the Ministry of the Environment, TFWT analysis of fish was conducted using an Electrolytic Enrichment method. It was found that while TFWT concentrations increased slightly during the ocean discharge period, they returned to the concentration before discharge began when the discharge was stopped, confirming that tritium was not accumulating or concentrating in the fish. In addition, the TFWT concentration in fish is within the range of past tritium concentrations in seawater across Japan and it was assessed that the impact of discharging ALPS-treated water into the ocean would be negligible on people and the environment in the conference consisting of environmental radioactivity experts, relevant ministries, and agencies in Japan.

ACKNOWLEDGMENTS

* This work is one of the results of the " ALPS Treated Water Marine Monitoring " conducted by the Ministry of the Environment of Japan.

Copyright on 7th Asia-Pacific Symposium on Radiochemistry 2025

7th Asia-Pacific Symposium on Radiochemistry *September 14 ~ 19, 2025 • Kunibiki Messe • Shimane, Japan*

MODULATION TRANSFER SPECTROSCOPY OF CESIUM ATOMS TOWARD FULLY OPTICAL QUANTITATIVE ISOTOPE DETECTION

Leo Matsuoka[1]

[1]*Faculty of Engineering, Hiroshima Institute of Technology: 2-1-1, Miyake, Saeki-ku, Hiroshima, Hiroshima, 731-5193, r.matsuoka.65@cc.it-hiroshima.ac.jp*

We conducted a fundamental study to develop a fully optical method for quantitative cesium isotope detection by means of modulation transfer spectroscopy (MTS). MTS selectively amplifies signals from specific hyperfine transitions in the cesium D_2 line. By varying the current to a cesium-bismuth vapor source, we observed that the MTS signal intensity changes proportionally with vapor density. Comparison with absorption spectroscopy confirmed the quantitative behavior of the MTS signal within the non-saturated range. These findings demonstrate the potential of MTS for optical cesium isotope detection, providing a non-destructive and simplified alternative to conventional methods.

1 INTRODUCTION

Radioactive cesium plays a key role in radioactive waste management and environmental monitoring. A major challenge in isotope separation is accurately measuring the ratio between stable and radioactive cesium [1]. Conventional methods like ICP-MS (Inductively Coupled Plasma Mass Spectrometry) or Time-of-Flight (TOF) spectrometry are commonly employed; however, TOF methods can cause contamination of the measurement apparatus. In contrast, laser-based techniques enable isotope ratio measurements without breaking containment, offering an alternative solution to conventional methods. Nevertheless, measuring cesium isotopes using lasers is challenging due to the extremely small difference in their absorption wavelengths.

Modulation Transfer Spectroscopy (MTS) is a laser-based technique applicable to cesium atoms [2]. In MTS, a laser beam is split into two parts: the pump beam and the probe beam, which are introduced into the vapor from opposite directions. This configuration allows for Doppler-free detection of signals originating solely from atoms with zero velocity along the laser axis. By modulating the pump beam and performing lock-in amplification at the modulation frequency, MTS selectively enhances signals from specific hyperfine transitions (cycling transitions), resulting in highly sharp signals that enable clear separation of Cs isotope signals. This technique has traditionally been employed to generate reference signals for wavelength stabilization.

While MTS is widely used for wavelength stabilization, its potential for quantitative analysis has not been thoroughly explored. This study aims to investigate the feasibility of using MTS for fully optical quantitative detection of cesium isotopes, demonstrating the quantitative nature of the signals.

2 EXPERIMENTAL SETUP

The principle of MTS for cesium atoms has been discussed extensively in previous studies and will not be detailed here. Figure 1 shows our experimental setup. An external cavity diode laser (ECDL) [3], operating at a wavelength of 852 nm, which excites the cesium D_2 line, was divided into two beams: the pump beam and the probe beam. The pump beam passed through an Electro-Optic Modulator (EOM) and was introduced into the vacuum chamber in the opposite direction to the probe beam. The polarization of the counter-propagating lasers was adjusted to ensure a clear signal.

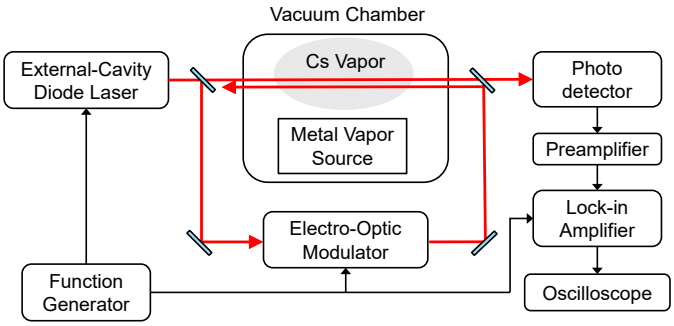


Fig. 1. A simplified diagram of the experimental setup. Thick arrows indicate the laser path, while thin arrows represent the flow of electrical signals.

Copyright on 7th Asia-Pacific Symposium on Radiochemistry 2025

Cesium vapor was generated by applying a direct current to a cesium-bismuth alloy vapor source, with the vapor density controlled by varying the current. The laser intensity was kept constant regardless of the current applied to the vapor source. The transmitted probe light was detected using a photodetector, amplified with a preamplifier, and subsequently processed through a lock-in amplifier. The EOM was modulated at 3 MHz, and the lock-in detection was performed at the same frequency. The output signal from the lock-in amplifier was recorded by an oscilloscope, and the vapor density of cesium was quantified based on the absorption signal.

3 RESULTS AND DISCUSSION

Figure 2 shows representative MTS signals for Cs-133. The obtained signals are notably sharp, demonstrating that signals from Cs-135 and Cs-137 can be effectively separated, even when they coexist. This indicates the high resolution of MTS in distinguishing cesium isotopes. The signal intensity was found to vary depending on the current applied to the vapor source. At low vapor densities, the MTS signal intensity exhibited a nearly proportional relationship with the vapor amount. As the vapor density increased, the signal intensity also increased; however, beyond critical density, the signal began to decrease. This reduction is likely caused by the attenuation of the pump light, resulting from increased absorption or scattering within the dense vapor. In addition, weak signals unrelated to the cycling transition were observed, particularly at high vapor densities. These signals are presumed to result from an increased relaxation rate of the excited states due to atomic collisions, which disturb the population balance among hyperfine levels during interaction and affect laser-based measurements.

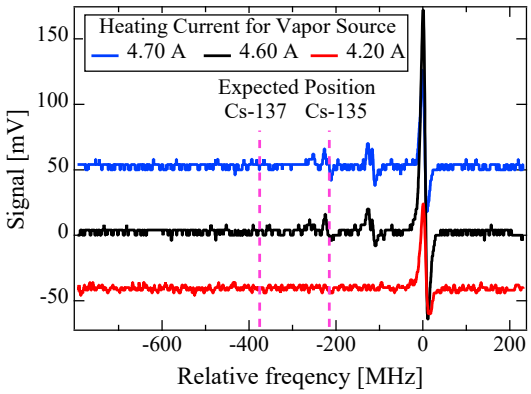


Fig. 2. An example of the variation in MTS signals of Cs-133 as a function of heating current. The three signals are plotted with appropriate offsets for clarity. The laser intensity is kept constant. Dashed lines indicate the expected positions of the peaks corresponding to Cs-135 and Cs-137.

4. CONCLUSIONS

This study demonstrated the quantitative nature of MTS signals, which had not been previously investigated. The potential of MTS as an efficient and non-destructive method for cesium isotope analysis was highlighted, establishing a foundation for fully optical isotope detection. Further studies will address the quantitative relationship between MTS signals and cesium vapor density, as well as the consistency with absorption spectroscopy. These aspects will be presented in subsequent reports.

ACKNOWLEDGMENTS

I would like to thank Noritaka Nishiya and Yuya Kusano for their contributions to the experimental setup.

References

[1] K. Yuki, T. Kobayashi, and L. Matsuoka, *Journal of Nuclear Science and Technology*, **54**, 1240–1250 (2017).
[2] J. H. Shirley, *Optics Letters.*, **7**, 537-539 (1982).
[3] X. Baillard, A. Gauguet, S. Bize, P. Lemonde, Ph. Laurent, A. Clairon, and P. Rosenbusch, *Optics Communications*, **266**, 609-613 (2016).

Copyright on 7th Asia-Pacific Symposium on Radiochemistry 2025

7th Asia-Pacific Symposium on Radiochemistry *September 14 ~ 19, 2025 • Kunibiki Messe • Shimane, Japan*

ADSORPTION OF BA AND SR USING ZEOLITE SYNTHESIZED FROM INDUSTRIAL WASTES

Takaaki Wajima[1]

[1]*Graduate School of Engineering, Chiba University: 1-33, Yayoi-cho, Inage-ku, Chiba, 263-8522, wajima@chiba-u.jp*

The adsorption of barium and strontium ions from aqueous solution using zeolitic materials synthesized from industrial wastes, waste stone powder and aluminum dross. Zeolitic materials including zeolite-X and zeolite-A can be synthesized from these wastes via alkali fusion, and that from the mixture of stone powder and dross (3:1) indicates higher adsorption abilities for Ba and Sr ions from aqueous solution than commercial zeolite-X and zeolite-A.

1 INTRODUCTION

Barium (Ba) and strontium (Sr) ions are the most toxic radionuclides present in relatively large amounts in radioactive liquid wastes arising from the reprocessing plants, and effective and simple methods are needed for the removal of these ions before disposing of their wastes in an aquatic system [1]. Adsorption has been established as an effective and economical technology, and zeolite is one of the representative adsorbent for removal of hazardous ions from aqueous solution.

During quarrying, waste stone powder is generated in the process of manufacturing a raw material of concrete as industrial wastes, and aluminum dross is a hazardous by-product generated primarily in aluminum smelters and aluminum recycling processes. For both of these industrial wastes, currently, effective utilization has not been established, and a large amount of these wastes is disposed in landfills.

In this study, we attempted to synthesize the zeolitic products from industrial wastes, waste stone cake and aluminum dross via alkali fusion, and its adsorption of Ba and Sr from aqueous solution was estimated for application of water purification.

2 EXPERIMENTAL

2.1 Sample

The waste stone powder was obtained from one of the quarry in Japan. Before the experiment, the powder was washed with distilled water and dried overnight in an oven at 60 °C. Aluminum dross used in this study was collected from an aluminum recycling company in Japan. Waste stone powder is mainly composed of SiO_2 (67.6 %) and Al_2O_3 (19.8 %), in the form of quartz (SiO_2) and albite ($NaAlSi_3O_8$), and aluminum dross mainly consisted of Al_2O_3 (65.3 %), SiO_2 (10.5 %), and MgO (13.3 %), in the form of metallic Al, alumina (Al_2O_3), spinel ($MgAl_2O_4$) and quartz (SiO_2), determined using X-ray fluorescence spectroscopy (XRF) (Epsilon 1, Malvern Panalytical) and powder X-ray diffraction (XRD) (Rigaku, MiniFlex600).

2.2 Synthesis

The stone powder and the dross were mixed with the mixed ratio of the dross to the mixture = 0, 0.25, 0.5, 0.75 and 1. The mixtures (10 g) and powdered NaOH (16 g) were mixed and added to a nickel crucible, which was heated at 600 °C in an electric furnace for 6 h. After heating, the crucible was cooled at room temperature under natural convection, and the resulting fused material was ground into fused powder (particle size < 500 μm) in a ceramic mortar. The fused powder (25 g) was added to 100 mL of distilled water and stirred for 24 h at room temperature to prepare the precursor and then heated at 80 °C for 8 h. After heating, the residual solids were filtered and dried overnight in a drying oven to obtain the products. It is noted that the products from the mixture with the mixed ratio of 0, 0.25, 0.5, 0.75 and 1 indicate Product-1, Product-2, Product-3, Product-4 and Product-5, respectively. The mineralogical composition of the product was analyzed using XRD. Cation exchange capacities (CECs) of the product was determined using the method reported by Wajima et al. [2], and compared with commercial zeolite-A (MS-4A) (Wako) and zeolite-X (MS-13X) (Wako).

2.3 Adsorption

The adsorption properties of Ba^{2+} and Sr^{2+} on the products were investigated using the products and commercial zeolites. The aqueous solutions of Ba^{2+} and Sr^{2+} with 0-2 mmol/L were prepared with $Ba(NO_3)_2$ and $Sr(NO_3)_2$, respectively, and pH of each solution was adjusted with nitric acid to become pH 6-8 after shaking. 0.02 g of sample was

Copyright on 7th Asia-Pacific Symposium on Radiochemistry 2025

added to 20 mL of each aqueous solution in 50 mL centrifuged tube, and the tube was shaken for 2 h. After shaking, the tube was centrifuged, and the concentrations of Ba^{2+} and Sr^{2+} in the supernatant was determined by atomic absorption spectrometry (AAS) (AAnalyst200, PerkinElmer). The corresponding adsorption amounts (q) were determined from the material balance as follows.

$$q = \frac{(C_0 - C) \cdot V}{w} \quad (1)$$

where C_0 and C are initial and measured concentrations of Ba^{2+} or Sr^{2+} in the filtrate (mmol/ L), V is volume of aqueous solution (L), and w is weight of the sample (g).

3. RESULTS AND DISCUSSION

Product-1, which was synthesized from only stone powder, contains zeolite-X ($Na_{22}Si_{26}Al_{22}O_{96}{\cdot}55H_2O$), and with increasing the aluminum dross content in the mixture, the mineralogical phases in the product was transformed from zeolite-X to zeolite-A ($Na_{12}Si_{12}Al_{12}O_{48}{\cdot}27H_2O$), and Product-2, Product-3, Product-4 and Product-5 contains zeolite-A with diminishing zeolite-X phases.

Table 1 shows the CEC of the products and commercial zeolite-A and zeolite-X. The CEC of Product-1 including zeolite-X is almost same as that of commercial zeolite-X, and with increasing the Al content, the CEC of the product increase, due to the transformation of zeolite-X into zeolite-A in the product (Product-2, Product-3), and then decrease due to the change of zeolite-A crystal morphology from cubic to spherical shape (Product-4, Product-5). Adsorption isotherms of Ba and Sr on zeolitic products and commercial zeolites are shown in Fig. 1.

TABLE 1. Cation exchange capacities of the products and commercial zeolites

	Product-1	Product-2	Product-3	Product-4	Product-5	Zeolite-X	Zeolite-A
CEC (mmol/g)	3.43	4.04	3.84	3.30	2.28	3.39	3.43

Adsorption isotherms of Ba and Sr on zeolitic products and commercial zeolites are shown in Fig. 1. Product-2 with highest CEC indicates the highest adsorption abilities of Ba^{2+} and Sr^{2+}, which is higher than commercial zeolites.

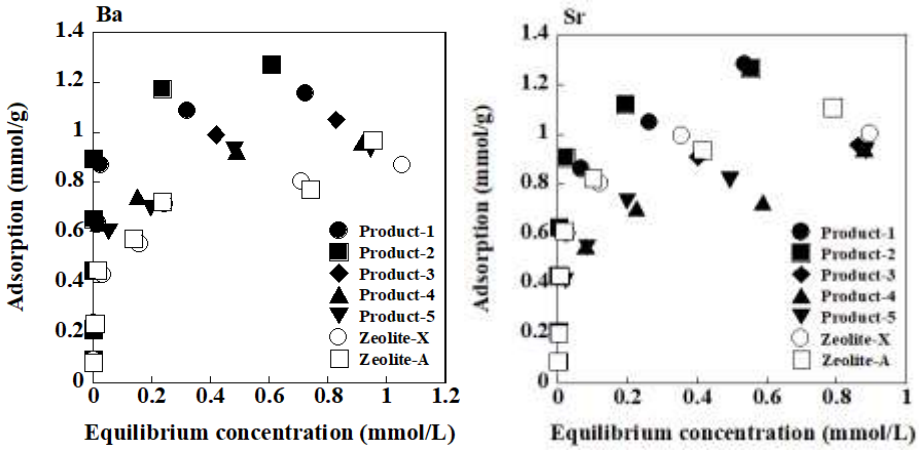


Fig. 1. Adsorption isotherms of Ba and Sr on zeolitic products and commercial zeolites.

4. CONCLUSIONS

Zeolitic materials including zeolite-X and zeolite-A with high cation exchange capacity can be synthesized from waste stone cake and aluminum dross, and indicate adsorption abilities for Ba and Sr from aqueous solution, which are higher than commercial zeolites.

References

[1] S. P. MISHRA and V. K. SINGH, "Radiotracer technique in adsorption study XIII, adsorption of barium and strontium ions on chromium (IV) oxide powder," *Appl.Radiat. Isot.*, 46, 847 (1995).
[2] T. WAJIMA and Y. IKEGAMI, "Synthesis of zeolitic materials from waste porcelain at low temperature via a two-step alkali conversion," *Ceram. Int.*, **33**, 1269 (2007)

7th Asia-Pacific Symposium on Radiochemistry *September 14 ~ 19, 2025 • Kunibiki Messe • Shimane, Japan*

PLATFORMS FOR SUPPLYING SHORT-LIVED RADIOISOTOPES FOR BASIC AND APPLIED SCIENCES IN JAPAN

Hiroki Kanda[1], Takashi Nakano[1], Mitsuhiro Fukuda[1], Hiromitsu Haba[2], Noriko S. Ishioka[3], Hidetoshi Kikunaga[4], Kotaro Nagatsu[5], Atsushi Toyoshima[6,7], Hiroshi Watabe[8]

[1]*Research Center for Nuclear Physics, Osaka University, 10-1 Mihogaoka, Ibaraki 567-0047, Japan, kandah@rcnp.osaka-u.ac.jp, nakano@rcnp.osaka-u.ac.jp, mhfukuda@rcnp.osaka-u.ac.jp*
[2]*Nishina Center for Accelerator-Based Science, RIKEN, 2-1 Hirosawa, Wako 351-0198, Japan, haba@riken.jp*
[3]*Department of Quantum-Applied Biosciences, Takasaki Institute for Advanced Quantum Science, National Institutes for Quantum Science and Technology, 1233 Watanuki, Takasaki 370-1292, Japan, ishioka.noriko@qst.go.jp*
[4]*Research Center for Accelerator and Radioisotope Science, Tohoku University,1-2-1 Mikamine, Sendai 982-0826, Japan, kikunaga@raris.tohoku.ac.jp*
[5]*Institute for Quantum Medical Science, National Institute for Quantum Science and Technology, 4-9-1 Anagawa, Chiba 263-8555, Japan, nagatsu.kotaro@qst.go.jp*
[6]*Institute for Radiation Sciences, Osaka University, Suita 565-0871, Japan, toyo@irs.osaka-u.ac.jp*
[7]*MS-CORE, FRC, Graduate School of Science, Osaka University, Toyonaka 560-0043, Japan, toyo@irs.osaka-u.ac.jp*
[8]*Research Center for Accelerator and Radioisotope Science, Tohoku University, 6-3 Aoba, Aramaki, Sendai 980-8578, Japan, hwatabe@tohoku.ac.jp*

We have been operating two platforms for supplying short-lived radioisotopes in Japan. One is Supply Platform of Short-Lived Radioisotopes (RIPF) and the other is Radioisotope Collaborative Interdisciplinary Development Platform (RIIP). RIPF aims to supply radioisotopes for the research projects supported by KAKENHI. RIIP aims to support research programs at any stage by supplying radioisotopes and by providing technical or legal information on the handling of radioisotopes. Both platforms consist of seven accelerator and radioisotope handling facilities in Japan which are capable of production and chemical purification of radioisotopes. The number of research programs which are supported by these platforms is more than 30 per year. Many important results from these research programs have come from a wide range of research fields. We are sure that these platforms are contributing to improve the quantity and quality of research using short-lived radioisotopes in Japan, and we hope to continue these activities for further support of research in the field of sciences with radioisotopes.

1 INTRODUCTION

The demand for radioisotopes in Japan has been increasing across various scientific fields, from basic research to applied sciences. However, short-lived radioisotopes are difficult to obtain commercially due to the small market size and transportation issues, and research using them has only been carried out by researchers affiliated with accelerator facilities or in collaboration with accelerator facilities, making it difficult to spread nationwide. To answer to the demand for the short-lived radioisotopes, we founded a system to supply the short-lived isotopes from accelerator facilities in Japan. The Supply platform of Short-lived Radioisotopes (RIPF) was founded in 2016 with four accelerator facilities in Japan [1] and continued by adding two more accelerator facilities [2]. Its aim is to support the research projects which are supported by KAKENHI by supplying the short-lived radioisotopes. The Radioisotope Collaborative Interdisciplinary Development Platform (RIIP) was started in 2023 with the same organization [3] to support research projects at all stages of research, from research at initial stages without any funding support to large-scaled research with the support of external funding.

2 PLATFORMS

The platform consists of seven accelerator and radioisotope facilities: Research Center for Nuclear Physics, Osaka University; Institute for Radiation Sciences (IRS), Osaka University; Radioactive Isotope Beam Factory (RIBF) at the RIKEN Nishina Center; Research Center for Accelerator and Radioisotope Sciences (RARiS-Aobayama and RARiS-Mikamine), Tohoku University; and National Institute for Quantum Science and Technology (QST-QMS and QST-Takasaki). These seven facilities produce and purify various radioisotopes according to their specific accelerator types and chemical processing capabilities, supplying over 50 different isotopes in diverse chemical forms tailored to user requirements. We also open our radioisotope facilities to the users according to their requests. Combinations of nearby facilities such as RCNP and IRS, and RARiS-Aobayama and RARiS-Mikamine share the production of radioisotopes, their chemical purification, and facility use for a single research project to support it.

Copyright on 7th Asia-Pacific Symposium on Radiochemistry 2025

Research projects that receive support such as RI supply are decided by an advisory committee's review of the research proposals using a peer review system. The facility for the support is selected based on the requests from the users but other facilities may be recommended by consideration of the facilities' operation and maintenance status. This kind of flexibility is one of the advantages of our platforms consisting of multiple facilities.

Over the past nine years, a total of 342 research projects have applied for support through our platforms, with 308 projects benefiting from RIPF and 22 from RIIP. Activities of users are quite high and distinctive and outstanding results with many papers and press releases have been published. Furthermore, projects requesting the supply of At-211 account for more than 40% of the projects submitted to our platform, and the results of these studies have led to investigator-initiated clinical trials currently being conducted at the Osaka University School of Medicine, as well as collaborative research with companies and large-scale research projects funded by large research grants. We have supported research projects to strongly promote investigations in wide fields of sciences which use short-lived radioisotopes. Our activities are mentioned as an important initiative in the Action Plan that aims to provide domestic radioisotopes developed by the Japan Atomic Energy Commission [4].

3 CONCLUSIONS

In order to address the increasing demand for short-lived radioisotopes in the broad field of science, we have been operating platforms for supplying commercially-not-available isotopes for researchers and since 2016. The system comprises seven accelerator and radioisotope facilities, each offering different isotopes and chemical forms tailored to users' needs. These facilities collaborate to optimize isotope production, purification, and research support. Research projects undergo advisory committee reviews, and facility selection depends on user requests and operational considerations. We have supported more than 300 research programs in 9 years of our activities. Many studies have led to high-profile publications, press releases, and significant findings, notably in At-211 supply, which has driven clinical trials and industrial collaborations. The initiative is recognized in Japan's Action Plan to enhance domestic radioisotope availability.

ACKNOWLEDGMENTS

This research was supported by JSPS Grant-in-Aid for Transformative Research Areas, Grant Number 22H04924 and by MEXT Promotion of Development of a Joint Usage / Research System Project: Coalition of Universities for Research Excellence Program (CURE) Grant Number: JPMXP1323015485.

References

[1] T. Nakano, M. H. Fukuda, H. Haba, Y. Sakemi, and H. Kikunaga, "Grant-in-Aid for Scientific Research on Innovative Area, 'Short-lived RI supplying platform' has started", Radiochemistry, Vol. 34, 2016, pp.44-45 (in Japanese).

[2] Mitsuhiro Fukuda, Takashi Nakano, Hiromitsu Haba, Yasuhiro Sakemi, Hiroshi Watebe, Hidetoshi Kikunaga and Tetsuhiko Yorita, "Supply platform of Short-lived Radioisotopes for Fundamental research", Kasokuki, Vol 14, 2017, pp. 81- 86 (in Japanese).

[3] Hiroki Kanda, Takashi Nakano, Mitsuhiro Fukuda, Tetsuhiko Yorita, Noriko S. Ishioka, Hidetoshi Kikunaga, Atsushi Toyoshima, Kotaro Nagatsu, Hiromitsu Haba and Hiroshi Watabe, "Radioisotope Collaborative Interdisciplinary Development Platform", Kasokuki, Vol. 21, 2024, pp. 208 – 211 (in Japanese).

[4] Mitsuru Uesaka, "The Action Plan for Promotion of Production and Utilization of Medical Radioisotopes and Follow-Up (2nd)", Kasokuki, Vol. 21, 2024, pp. 185-189 (in Japanese).

Copyright on 7th Asia-Pacific Symposium on Radiochemistry 2025 P-R9-09 -

Poster Presentation | [P2]ICP-MS Based Radioanalytical Chemistry and Related Applications

Wed. Sep 17, 2025 6:30 PM - 8:00 PM JST | Wed. Sep 17, 2025 9:30 AM - 11:00 AM UTC Poster

[Poster] P2

[P-P2-01]

Optimisation of conditions for the quantitative analysis of I-129 in smear samples collected inside the Fukushima Daiichi Nuclear Power Station by alkaline fusion and ICP-MS/MS

*Maki Honda[1], Asako Shimada[1], Yoshihisa Iida[1] (1. JAEA (Japan))

[P-P2-02]

Control of Zirconium-90 for Strontium-90 determination using thermal ionization mass spectrometry (TIMS)

*Norbert Kavasi[1], Tatsuo Aono[1] (1. Fukushima Institute for Research, Education and Innovation (F-REI) (Japan))

[P-P2-03]

Sensitivity improvement for radionuclide analysis using ICP-MS/MS with desolvating nebulizer

*YASUYUKI SHIKAMORI[1], CHIKAGE ABE[1], KAZUYA IDEMITSU[1], YASUYOSHI NAGAI[2] (1. Tohoku University (Japan), 2. Central Research Institute of Electric Power Industry (Japan))

©APSORC25

7th Asia-Pacific Symposium on Radiochemistry *September 14 ~ 19, 2025 • Kunibiki Messe • Shimane, Japan*

Optimisation of conditions for the quantitative analysis of I-129 in smear samples collected inside the Fukushima Daiichi Nuclear Power Station by alkaline fusion and ICP-MS/MS

Maki Honda[1], Asako Shimada[1], Yoshihisa Iida[1]

[1]*Japan Atomic Energy Agency: 2-4Shirakata, Tokai, Ibaraki, 319-1195, honda.maki@jaea.go.jp*

A method suitable for quantitative analysis of I-129 in smear samples taken from various locations inside the 1F reactor building was investigated. Since I-129 is quantified by ICP-MS/MS, this method is limited in that sufficient I-127 carriers cannot be added to ensure the recovery yield. Nevertheless, it has become possible to quantify the amount of I-129 presumed to be contained in 1F smear samples and low carrier amounts of 3 × 10^{-7} g by refining an analytical method through optimisation of the alkaline fusion procedure and suppression of iodine adsorption on the surface of the containers during the sample pretreatment process.

1 INTRODUCTION

Radioactive iodine with a short half-life and high volatility contributed to the initial radiation exposure doses in the accident at the Fukushima Daiichi Nuclear Power Station (1F). This study will contribute to advancing safety countermeasures for nuclear reactors by estimating the transport pathways of the radioactive iodine from the pressure vessels of 1F to the building interior and their transport mechanisms. For this purpose, a suitable method for quantitative analysis of I-129 in smear samples wiped off various surfaces inside the 1F reactor building was investigated. This study will enable the evaluation of the surface contamination level of I-129. I-129 has the same chemical properties as other radioactive iodine isotopes and is still detectable due to its longer half-life of 1.57 × 10^7 years. As smear samples may contain difficult-to-decompose substances, developing a method that decomposes refractory substances like silicate minerals while capturing free iodine in an alkaline solution is necessary. There are the conventional methods of alkaline fusion for analysing iodine in solid samples, involving the addition of approximately 10^{-3} g of I-127 carrier and measurement by radiochemical neutron activation analysis (RNAA) or accelerator mass spectrometry (AMS) [1, 2]. However, the smear samples are subject to regulations on nuclear fuel materials, and the I-129 quantification is performed by ICP-MS/MS (8900, Agilent Technologies) with permission to handle nuclear fuel materials. Therefore, an alkaline fusion method must be established to efficiently recover I-129 with minimal or no addition of the carrier to minimise contamination and memory effects of I-127 in the ICP-MS/MS. In this study, blank smear pieces (1/4 piece; approximately 0.05 g) cut to the approximate size of the actual sample were prepared, and solutions of I-127 and I-129 at known concentrations were added. The fluxing agent, method in fusion, and amount of iodine (I-127) carrier to be added were determined.

2 METHOD

A quarter of a smear sample and flux were placed in a 50 mL nickel crucible, the I-127 carrier was added, and the mixture was heated and dried at 120°C for 30 minutes using an electric furnace. The dried sample was then fused at 850°C for 60 minutes in the electric furnace. The fusion cake was dissolved in water after allowing the nickel crucible to cool, and the aqueous sample was collected in a polypropylene bottle. Carbon tetrachloride was added to the bottle to perform solvent extraction, followed by reverse extraction to separate iodine into approximately 15 mL of the aqueous layer. The aqueous layer samples were analysed by ICP-MS/MS to quantify I-127 and I-129. For the measurement of I-129, oxygen gas flowed at a rate of 0.9 mL/min to efficiently remove interfering Xe-129. The typical limits of detection were 1 × 10^{-11} g/g for I-127 and 2 × 10^{-13} g/g (10^{-6} Bq/g) for I-129. I-127 and I-129 were quantified using calibration lines prepared from the I-127 standard solution (1000 μg/g, Sigma-Aldrich) and I-129 radioactivity standard solution (0.686 kBq/g, containing 7.66 μg/g of I-127 carrier, Eckert&Ziegler), respectively. The matrix of the solutions for the calibration lines was matched to that of the aqueous layer sample. The variation in sensitivity during the measurement was calibrated using the Cs solution (990 ± 2 μg/g, Sigma-Aldrich) as an internal standard. The I-127 carrier and I-129 aqueous solutions added in the alkaline fusion process were the same as the I-127 standard solution and the I-129 radioactivity standard solution described above.

3 RESULTS AND DISCUSSION

Following conventional methods [1, 2], approximately equal amounts of I-127 carrier (1 × 10^{-3} g) were added to blank 1/4 pieces of smear samples and alkaline fusion were performed with NaOH. As a result, iodine was hardly recovered in this study (the recovery yield of I-127 was at most 6%). The cause of the low recovery yield is currently unexplained. Therefore, the flux was switched from NaOH to another typical flux of Na_2CO_3. Furthermore, an alternative fusion method was devised in which the smear sample was coated with Na_2CO_3 to prevent the volatilisation of iodine. As a result, approximately 93% of I-127 was recovered under the condition of 1 × 10^{-3} g of I-127 carrier. The recovery yield

Copyright on 7th Asia-Pacific Symposium on Radiochemistry 2025

of I-129 was not evaluated because ICP-MS/MS could not measure I-129 with a large amount of I-127 carrier (1×10^{-3} g). On the other hand, the recovery yield of I-129 was reduced to an average of 21 ± 5% (n = 3) under the condition of alkaline fusion with 2×10^{-9} g of I-127 (contained in the radioactive standard solution of spiked I-129; the amount of I-129 was 3×10^{-8} g). Even with this small amount of I-127 carrier and low recovery yield of I-129, it is still two orders of magnitude higher than the estimated iodine content of the actual smear sample ($\leq 5 \times 10^{-10}$ g for I-127, $\leq 1 \times 10^{-10}$ g for I-129, and no I-127 carrier). However, if the iodine recovery yields were less than 1%, the concentration of I-129 in the sample measured by ICP-MS/MS would be less than 10^{-12} g/g, which is near the limit of detection of I-129. Therefore, the amount of I-127 carrier added to the sample cannot be reduced to less than 10^{-9} g for evaluating the recovery yield of I-129, and this amount was set as the minimum amount. The results of the I-129 recovery yield in the alkaline fusion with varying amounts of I-127 showed that a certain amount of I-127 is essential to recover trace amounts of I-129 ($\leq 10^{-8}$ g) in the pretreatment process. Therefore, solvent extraction experiments were conducted by varying the amount of I-127 carrier from 3×10^{-8} to 1×10^{-3} g, and the relationship between the amount of I-127 carrier and the recovery rate of I-129 was evaluated in detail to determine the appropriate amount of I-127 carrier. As a result, there was a trend toward higher recovery rates of I-129 with increasing amounts of I-127 carrier, and it was found that the recovery rate of I-129 was 85 ± 3% (n = 3) on average when the amount of I-127 carrier was 3×10^{-5} g. The recovery rate of I-129 was obtained by solvent extraction using polypropylene bottles; when solvent extraction was performed using PFA bottles, the recovery rate reached an average of 102 ± 2% (n = 3). At this carrier amount, the background of I-127 can be readily reduced by flushing ultra-pure water or similar through the ICP-MS/MS for a specified time, even when measuring the aqueous layer sample without dilution. Furthermore, the bottles used for the solvent extraction and ICP-MS/MS measurement were changed from polypropylene to PFA to improve the recovery yield of I-129 (suppressing the adsorption of iodine to the surface of the container). As a result, the recovery yield was further improved. The amount of I-127 carrier to be added to the sample was determined to be 3×10^{-7} g based on the relationship between the I-127 carrier amount and the I-129 recovery rate. The recovery yield of I-129 achieved 52 ± 6% on average (n = 3, in the process from alkali fusion to solvent extraction) with the I-127 carrier amount of 3×10^{-7} g by optimising the alkaline fusion conditions and adopting PFA containers. This method was determined to be suitable for the I-129 quantification because, even though the carrier amount was four orders of magnitude less than the typical amount, a high iodine recovery yield was achieved in this study. In the future, smear samples wiped from the interior of the 1F reactor building will be analysed using the established alkaline fusion method.

4 CONCLUSIONS

Alkaline fusion was performed according to conventional methods; however, no significant amount of iodine was recovered in this study. Therefore, the analytical method was refined as follows: (1) select a good iodine recovery flux of Na_2CO_3, (2) devise the fusion method preventing iodine volatilisation, (3) optimise the amount of I-127 carrier, and (4) adopt PFA containers to prevent surface adsorption of iodine onto containers during the pretreatment process. By combining these techniques, the 52% recovery yield of I-129 was achieved even under the condition of the low carrier amount of 3×10^{-7} g. The outcome enabled the quantification of I-129, which is expected to be contained in 1F smear samples.

ACKNOWLEDGMENTS

We would like to express our sincere gratitude to Mr. Yonekawa and Mr. Terunuma of the Back-end Cycle Key Elements Research Facility (BECKY) at JAEA for their excellent technical support. This research was conducted with the support of the Nuclear Regulation Authority.

References

[1] M. Ebihara, Y. Oura, N. Shirai, Y. Nagakawa, N. Sakurai, H. Haba, H. Matsuzaki, H. Tsuruta, Y. Moriguchi, "A new approach for reconstructing the ^{131}I-spreading due to the 2011 Fukushima nuclear accident by means of measuring ^{129}I in airborne particulate matter", *J. Environ. Radioact*., **208-209**, 106000 (2019).

[2] S. Sekimoto and M. Ebihara, "Accurate Determination of Chlorine, Bromine, and Iodine in Sedimentary Rock Reference Samples by Radiochemical Neutron Activation Analysis and a Detailed Comparison with Inductively Coupled Plasma Mass Spectrometry Literature Data", *Anal. Chem*., **85**, 6336－6341 (2013).

Control of Zirconium-90 for Strontium-90 determination using thermal ionization mass spectrometry (TIMS)

Norbert Kavasi[1] and Tatsuo Aono[1]

[1]*Regional Environmental Co-Creation Unit, Fukushima Institute for Research, Education and Innovation (F-REI)*
F-REI Branch at Fukushima Medical University, 1 Hikarigaoka, Fukushima-city, Fukushima 960-1295, Japan
kavasi.norbert.h4v@research.f-rei.go.jp

The determination of Sr-90 by mass spectrometry is a reliable technique, particularly in the case of a nuclear accident; however, the control of Zr-90 is crucial to prevent isobaric interference. The aim of this study was to find the potential source of zirconium (Zr) for TIMS by examining various filament ribbons, specifically tantalum (Ta) and rhenium (Re), along with Ta activator solutions. Significant Zr contamination of the Re ribbon necessitates a specialized degassing method for Sr-90 analysis with TIMS.

1. BACKGROUND

Strontium-90 (Sr-90) ($T_{1/2}$=28.8 years) is a fission product of significant environmental and health concern due to its radiotoxicity and mobility in biological systems. Rapid, accurate and sensitive determination of Sr-90 in environmental and nuclear samples is essential for radiological assessment and nuclear forensics. Applying thermal ionization mass spectrometry (TIMS) for Sr-90 determination, removal of isobaric interference from zirconium-90 (Zr-90) is the main concern [1]. The analytical procedure involves chemical separation of strontium from complex matrices using extraction chromatography, followed by deposition onto Re ribbon for thermal ionization. The TIMS technique enables the detection of ultra-trace levels of Sr-90 with minimal isobaric interference from Zr-90, aided by chemical purification and difference in ionization potential [2, 3].

However, the Zr-90 contamination may originate from the sample matrix due to inadequate element-specific separation, impurities in the Ta activator solution, or the Re ribbon utilized for heating the analyte. Re does not exist as a separate mineral, mainly it is produced as the by-product of copper (Cu) mining along with molybdenum (Mo). Thus, even the zone refined Re, which has 99.999% purity, contains ultra-trace impurities of refractory metals such as Mo or Zr.

Tantalum exhibits chemical behaviors closely analogous to that of niobium (Nb), resulting in their frequent co-occurrence in minerals; hence, niobium is a common impurity in tantalum. Additionally, other transition metals, including vanadium (V), zirconium (Zr), hafnium (Hf), and tungsten (W), may also be present at ultra-trace concentrations (Fig. 1).

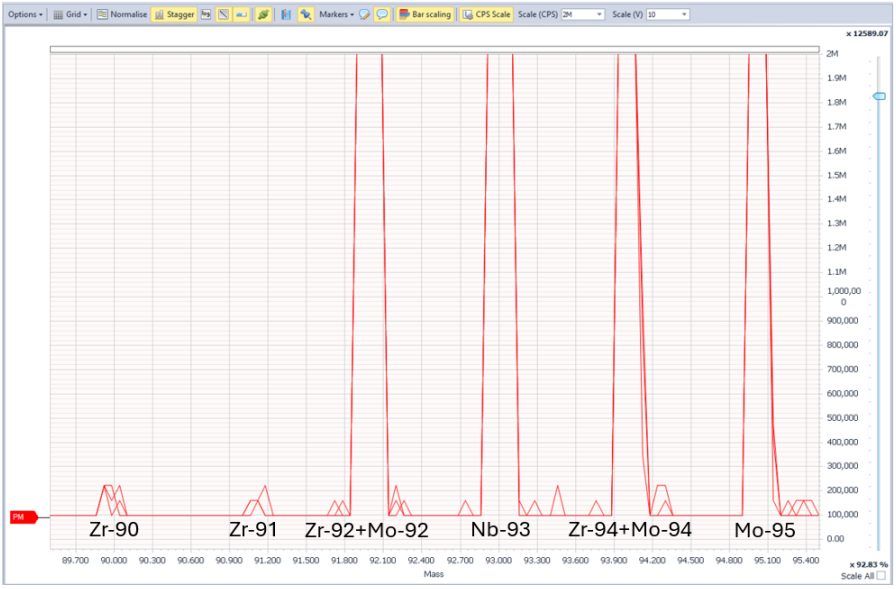


Fig. 1. Impurities on Ta filament

2. MATERIALS AND METHODS

All acid solutions were prepared using analytical grade Tamapure AA-100 reagents and Milli-Q2 purified water (>18 MΩ cm at 25 ◦C).The tantalum (V) fluoride (TaF5) activator solution was prepared as a mixture of tantalum (V) chloride ($TaCl_5$) (2 g) (Sigma-Aldrich 99.999 % trace metals basis), HF (38%, 1.6 mL), phosphoric acid H_3PO_4 (85%, 1.2 mL) (Sigma-Aldrich 99.999 % trace metals basis), HNO3 (68%, 20.6 mL) and Milli-Q2 purified water (>18 MΩ cm at 25 ◦C, 79 mL). Commercial-grade (99.99 %) and zone refined grade five (99.999 %) Re ribbons (H. Cross Co. USA) and commercial-grade (99.95 %) Ta ribbon (Nilaco Co. Japan) were used for the investigations.

Phoenix X62 TIMS (Isotopx Ltd., U.K.) mounted with a Daly detector system was used for the mass spectrometry analysis. The Zr-90 impurity was determined at 90 AMU with 60 sec integration time and 20 measurement cycles.

2. CONCLUSIONS

In this study, several degassing procedures of Re, Ta filament were studied along with Ta activator solutions in order to achieve the goal of completely removing the isobaric interference of Sr-90 that was caused by Zr-90. The amount of Zr that is present in Ta filament and Ta activator solution was found to be insignificant, whereas the Zr content of Re filament was much higher (Fig. 2.). Zr impurity in Re filament can be reduced with the use of an appropriate degassing procedure.

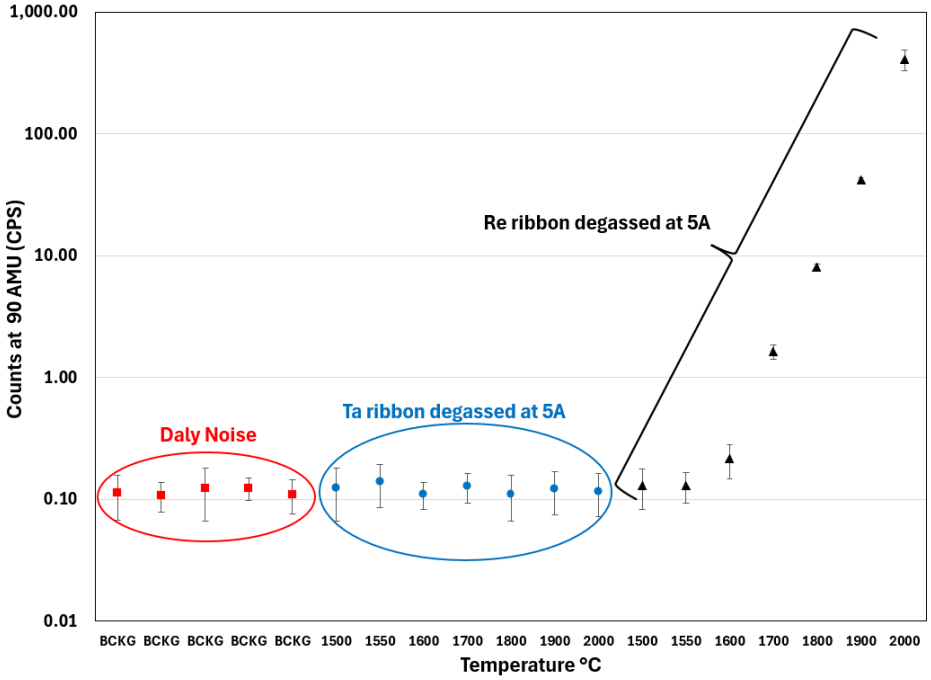


Fig. 2. Zr-90 impurity on different metal ribbons at different ionization temperatures

References

[1] N KAVASI and S.K. SAHOO, "Method for ^{90}Sr Analysis in Environmental Samples Using Thermal Ionization Mass Spectrometry with Daly Ion-Counting System," *Analytical Chemistry*, **91**, 4 (2019).

[2] N KAVASI, S.K. SAHOO, H. ARAE, T. AONO, Z. PALACZ, "Accurate and precise determination of ^{90}Sr at femtogram level in IAEA proficiency test using Thermal Ionization Mass Spectrometry," *Scientific Reports*, **9**, 1 (2019).

[3] J. AOKI, S. WAKAKI, H. ISHINIWA, T. KAWAKAMI, T. MIYAZAKI, K. SUZUKI, Y. TAKAGAI, "Direct Quantification of Attogram Levels of Strontium-90 in Microscale Biosamples Using Isotope Dilution-Thermal Ionization Mass Spectrometry Assisted by Quadrupole Energy Filtering," *Analytical Chemistry*, **95**, 11 (2023).

Copyright on 7th Asia-Pacific Symposium on Radiochemistry 2025

Sensitivity improvement for radionuclide analysis using ICP-MS/MS with desolvating nebulizer

Yasuyuki Shikamori, Chikage Abe, Kazuya Idemitsu, Yasuyoshi Nagai[a)]

Institute for Materials Research, Tohoku University, Oarai, Ibaraki,311-1313
[a]Present address; Energy Transformation Research Laboratory, Central Research Institute of Electric Power Industry, Yokosuka, Kanagawa 240-0196,
E-mail: yasuyuki.shikamori.b1@tohoku.ac.jp(Y.Shikamori), chikage.abe.a4@tohoku.ac.jp(C.Abe), kazuya.idemitsu.e4@tohoku.ac.jp(K.Idemitsu), nagai41262@criepi.denken.or.jp(Y.Nagai)

1 INTRODUCTION.

Reaction cell-inductively coupled plasma tandem mass spectrometry (ICP-MS/MS) is a highly sensitive elemental analysis technique that combines a collision/reaction cell, which reduces background-causing interference ions, and a pair of quadrupole mass spectrometers arranged in tandem before and after the reaction cell. This technique makes it possible to achieve selective ion species reactions in the MS/MS configuration, and to transfer analytes or interfering ions to ions of different measured masses (m/z) resulted from the reaction of various reaction gases (e.g., oxygen and nitrous oxide) in the cell. This allows more reliable reduction or elimination of background signals that cause strong spectral interference originated from argon plasma or coexisting matrix elements. Therefore, it has been widely used in radiochemistry and nuclear engineering for the analysis of radionuclides in complex matrix samples with high concentrations of uranium and other elements.

However, compared to conventional single ICP-MS, this technique inevitably suffers from lower ion transmission due to the tandem arrangement of the mass spectrometers and collisions with the cell gas in the cell. The decreased sensitivity obtained by ICP-MS/MS mode is a tradeoff of separating spectral interference and is inferior to that by the single ICP-MS mode, suggesting that some improvement is needed.

The membrane desolvation nebulizer is an option for sample introduction system in which the sample aerosol is passed through a heated spray chamber and a heated membrane desolvation module, and the water vapor leaking out of the membrane periphery is exhausted and removed by Ar sweep gas to introduce only elemental particles into the ICP. Since desolvation dramatically reduces the amount of water vapor introduced into the ICP while permitting almost all of the sample introduced, it is expected to improve sensitivity by increasing the sample aerosol introduction efficiency, but it has not been widely used in the past due in part to its unclear characteristics.

In this study, prior to the application of the reaction cell method in ICP-MS/MS in radiochemistry and nuclear engineering, we investigated the improvement of sensitivity by replacing a conventional nebulizer with a desolvating nebulizer in order to improve the sensitivity of the ICP-MS/MS instrument alone. Optimization of instrument conditions was carried out to systematically investigate the increase in sensitivity and the suppression of oxide ions associated with desolvation. In addition, the sensitivity and detection limits of radionuclides such as radioactive iodine and some actinides were also investigated.

2 EXPERIMENTAL

For the study, an Agilent Technologies 8900 ICP-MS/MS tandem inductively coupled plasma mass spectrometer and an Aridus3 desolvating nebulizer from Teledyne CETAC were used. The spray chamber of the 8900 ICP-MS/MS standard is a double-barrel Scott type.

For ICP-MS/MS, sensitivity changes were investigated under typical plasma conditions (RF 1500W or 1550W, sampling depth 8mm) for the standard sample introduction system of (1) x-lens and Micromist Nebulizer for matrix samples, (2) s-lens and MicroFlow Nebulizer for high sensitivity analysis, and (3) the combination of Aridus3+c-flow PFA 100 nebulizer for desolvating nebulization used in this study.

For the desolvating nebulizer, the Spray Chamber temperature and desolvating membrane temperature were set to 110°C and 140°C, respectively, and the Ar sweep gas was varied in steps from 4 to 8 L/min. Using tuning solution (containing 1 ng/mL each of Li, Co, Y, Ce, and Tl, 2% HNO_3), the conditions for maximum sensitivity were found by further varying the carrier gas flow rate at each sweep gas flow rate.

The plasma parameters were also optimized, and changes in sensitivity, oxide ion production ratio (CeO^+/Ce^+), and other characteristics were investigated.

3 RESULTS AND DISCUSSION

The comparison of results using the c-flow nebulizer are shown in Figure 1. When the c-flow nebulizer was

Copyright on 7th Asia-Pacific Symposium on Radiochemistry 2025

used alone, only 60,500 cps $^{89}Y^{+}$ was obtained for 1 ng/mL ^{89}Y under carrier gas control alone, but when optimized by adding make-up gas, sensitivity increased to 552,779 cps/1ng/mL ^{89}Y.

In using Aridus3 with the c-flow nebulizer, loose connection of the Ar sweep gas exhaust tube caused signal instability, so the signal instability could be improved by tightening the pipe connection.

When Aridus3 equipped with the c-flow nebulizer was connected to ICP-MS/MS and the carrier gas flow rate and Ar sweep gas flow rate were varied, the sensitivity response was found to be significantly different depending on the Ar sweep gas flow rate. Therefore, the carrier gas introduced into the c-flow nebulizer and the sweep gas flow rate introduced into the membrane of the desolvation nebulizer were optimized. As a result of optimization, a maximum sensitivity of 4,410,010 cps/1 ng/ml ^{89}Y was obtained at 0.7 L/min of carrier gas + 7 L/min of Ar sweep gas. The results of the study are summarized and compared in Figure 1.

Figure 1 shows that even when the c-flow nebulizer alone was used, adding make-up gas and controlling the balance with the carrier gas improved sensitivity by about 9 times compared to the carrier gas-only condition when the device was delivered. This was approximately the same or slightly higher sensitivity than that of a standard Micromist nebulizer normally used at a carrier gas flow rate of 1.05L/min.

When a desolvating nebulizer with a c-flow nebulizer was used, optimization of the carrier gas flow rate and sweep gas flow rate to the desolvating nebulizer resulted in an approximately 8-fold increase in sensitivity. This was an improvement in sensitivity that could not have been achieved by ICP-MS/MS alone.

In addition, findings were obtained regarding the cause of plasma lighting failure and signal instability, which had been a concern of existing users, and it was confirmed that a stable signal could be obtained.

On the other hand, when the desolvating nebulizer is used, the amount of water vapor introduced into the plasma is dramatically reduced, and the shape of the plasma changes, moving it closer to the ICP torch side, and the heat radiation to the torch is also thought to increase. When the desolvation nebulizer is used, it is expected that slightly increasing the auxiliary gas flow rate and slightly moving the plasma away from the torch relative to the torch will reduce the thermal radiation to the torch and not increase the background intensity.

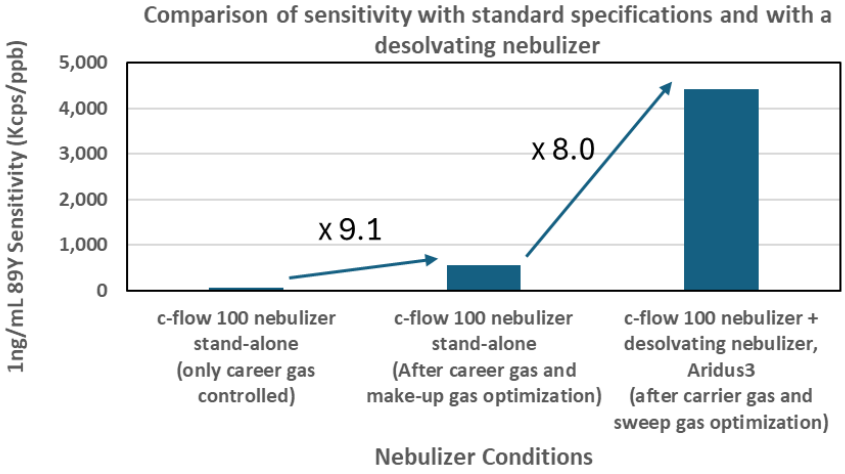


Figure 1 Comparison of sensitivity with standard specifications and with a desolvating nebulizer

4 CONCLUSION

The sensitivity improvement of the ICP-MS/MS system alone was investigated by replacing the conventional sample introduction system with a desolvating nebulizer. Optimization of the carrier gas flow rate and the Ar s weep gas flow rate introduced into the desolvating nebulizer system resulted in an approximately 8-fold increase in sensitivity for ICP-MS/MS.

This sensitivity increase factor by desolvating nebulizer is considered to be an effective method because it can fully compensate for the loss of sensitivity due to the tandem MS configuration in ICP-MS/MS.

Copyright on 7th Asia-Pacific Symposium on Radiochemistry 2025

Contributed Talk | [R3]Actinide Chemistry and Nuclear Energy Chemistry

Wed. Sep 17, 2025 11:00 AM - 12:00 PM JST | Wed. Sep 17, 2025 2:00 AM - 3:00 AM UTC Hall A(MP)

[R3] Actinide Chemistry and Nuclear Energy Chemistry

11:00 AM - 11:20 AM JST | 2:00 AM - 2:20 AM UTC

[R3-12]

Studies on Adsorption and Desorption Characteristics of Lanthanides using a Polydimethylsiloxane Sponge Incorporated with Soft-donor Ligands

*YIWEI ZHANG[1], Atsuro Furuichi[1], Ki Chul Park[1], Naokazu Idota[1], Takehiko Tsukahara[1] (1. Institute of Science Tokyo (Japan))

11:20 AM - 11:40 AM JST | 2:20 AM - 2:40 AM UTC

[R3-13*]

Mutual separation of lanthanides by extraction chromatography in hydrochloric acid solution

*WENZUN LUO[1], Putra Rahma Andri[1], Chikage Abe[2], Suzuki Tatsuya[1] (1. Nagaoka University of Technolygy (Japan), 2. Tohoku University (Japan))

11:40 AM - 12:00 PM JST | 2:40 AM - 3:00 AM UTC

[R3-14*]

Selective Recovery of Lanthanide Ions Using Spiropyran-Based Photoswitchable Adsorbents

*Kai Peng[1], Naokazu Idota[1], Takehiko Tsukahara[1] (1. Institute of Science Tokyo (Japan))

©APSORC25

7th Asia-Pacific Symposium on Radiochemistry *September 14 ~ 19, 2025 • Kunibiki Messe • Shimane, Japan*

Studies on Adsorption and Desorption Characteristics of Lanthanides using a Polydimethylsiloxane Sponge Incorporated with Soft-donor Ligands

Yiwei Zhang[1], Atsuro Furuichi[1], Ki Chul Park[1], Naokazu Idota[1], and Takehiko Tsukahara[1]

[1]*Laboratory for Zero-Carbon Energy, Institute of Integrated Research, Institute of Science Tokyo, 2-12-1-N1-6, Ookayama, Meguro, Tokyo, 152-8550, Japan.*

*Partitioning of minor actinide (MA) and lanthanide (Ln) plays an important role in reducing the potential risk of HLWs (*high-level radioactive waste*) and recovering valuable rare-earth metals. Advanced separation techniques based on solvent extraction and chromatography have been extensively investigated but have negative impacts on the environment and radiation workers. To overcome such limitations, in this study, we developed a novel porous functionalized PDMS (polydimethylsiloxane) sponge capable of adsorbing and desorbing target Ln ions from simulated HLWs by controlling chemical and mechanical stresses of the sponge and further explored their adsorption abilities. Moreover, selective desorption of adsorbed Ln ions was achieved within 30 min by squeezing the sponge in appropriate eluent solutions. These findings indicate that the new separation methodology using PDMS sponge holds great potential for various nuclear fields such as partitioning, decommissioning, and environmental remediation.*
Keywords: *PDMS sponge, High-level radioactive waste, Lanthanides, Adsorption, Desorption*

1. Introduction

Considering the growing demand for rare-earth elements, high-level radioactive waste (HLW) is promising to become a powerful secondary source. However, due to similar chemical properties and trivalent states of lanthanides and minor accidents, their mutual separation is still a challenging in nuclear waste management [1]. Although conventional separation techniques such as solvent extraction and chromatography are effective, they are complex and generate substantial secondary waste, posing potential environmental risks. Therefore, efficient and green separation strategies are urgently required.

Recently, polydimethylsiloxane (PDMS) sponges received great attention due to their unique features such as inherent hydrophobicity, flexibility, and chemically-mechanically robust [2]. In this study, we aim to create novel functionalized PDMS sponges incorporated with soft donor ligands and evaluate their adsorption-desorption abilities of lanthanides from simulated radioactive waste solutions. Di(2-ethylhexyl)phosphoric acid (D2EHPA), *N,N,N',N'*-tetraoctyldiglycolamide (TODGA) and 2-ethylhexyl diamide amine (ADAAM-EH) were selected as the hydrophobic soft donor ligands which can immobilized in the PDMS sponge surfaces owing to the hydrophobic interactions. Moreover, the adsorption-desorption performances and mechanisms are explored.



Figure 1. Optical Images of PDMS sponges

2. Experimental

A porous bare PDMS sponge (Figure 1) was fabricated by using sugar cubes as a sacrificial template to realize the porous structure. The selected ligands were first dissolved in dichloromethane and then added to a round-bottom flask containing the bare PDMS sponge. Ligands penetration and immobilization within the sponge were achieved via hydrophobic interactions by gradually reducing the pressure in the flask to evaporate the solvent. The resulting sponges were labelled D2EHPA/PDMS sponge, TODGA/PDMS sponge and ADAAM/PDMS sponge, respectively. Batch adsorption experiments were carried out in a simulated HLW solution containing 14 elements under various conditions, with lanthanide concentrations ranging from 1.40×10^{-3} M – 8.96×10^{-3} M, equivalent to their concentrations in practical HLW. Changes in lanthanide concentration before and after adsorption-desorption experiments were analyzed using inductively coupled plasma mass spectrometry (ICP-MS). Recovery efficiency, adsorption capacity and mass weighted partition coefficient were employed to evaluate the lanthanide adsorption performance and its selectivity against other elements existed in simulated HLW.

3. Results and Discussions

To quantitatively evaluate the amounts of each ligand immobilized in the sponge, thermogravimetric and differential thermal analysis was conducted. The thermal decomposition results suggest that the introduction of TODGA and ADAAM-EH suppressed the PDMS sponge framework degradation, with the amounts of each ligand immobilized in the sponge remaining are almost comparable to their initial concentrations used for functionalization. In addition, effects of the ligand concentrations, nitric acid concentrations, contact time, initial lanthanide concentrations and competitive interfering ions on adsorption were examined to further study the adsorption behaviour and mechanism of lanthanide ions (Ln(III)) on

Copyright on 7th Asia-Pacific Symposium on Radiochemistry 2025 - R3-12 -

functionalized sponges. Each sponge was found exhibiting distinctive lanthanide adsorption behaviours in solutions with different HNO_3 concentration, depending on their interactions with Ln(III) in each condition. Taking Sm(III) as a representative, the D2EHPA/PDMS sponge exhibited an adsorption efficiency of 41.6% between 1×10^{-4} - 1×10^{-3} M HNO_3. However, as the HNO_3 concentration increased, the adsorption efficiency rapidly decreased, falling to 17.7% at 0.01 M, 13.7% at 0.1 M HNO_3, and 0% at 1 M HNO_3, indicating that the D2EHPA/PDMS sponge is unsuitable for use in the strong acidic environment. In contrast, the TODGA/PDMS sponge demonstrated a much higher affinity for Sm(III) under strong acid conditions, with adsorption efficiency increasing from 24.64% at 0.1 M HNO_3 to 86.86% at 1M and 89.32% at 3 M.

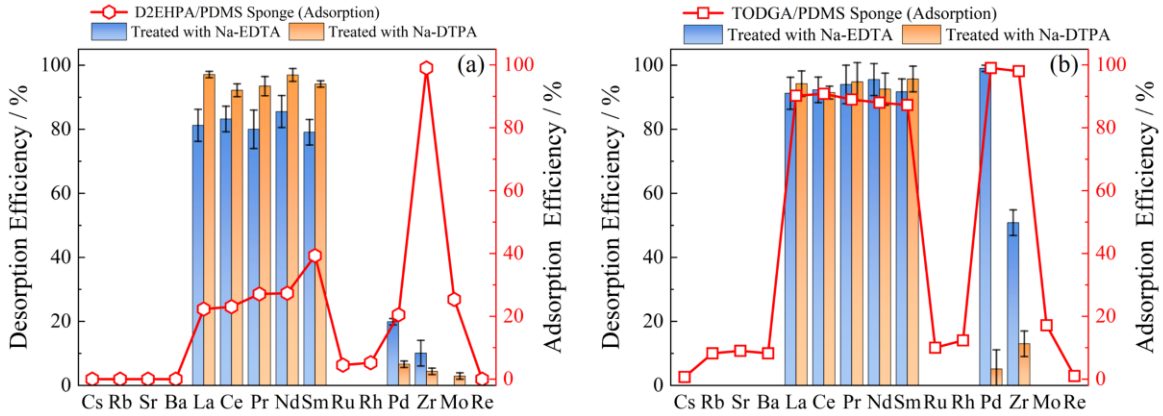


Figure 2. Adsorption-desorption performances of D2EHPA/PDMS sponge and TODGA/PDMS sponge in simulated HLW.

The ADAAM/PDMS sponge achieved its highest adsorption efficiency at 1M HNO_3. These differences are attributed to the protonation behavior of each ligand, which affects their interactions with Sm(III) by altering the availability and coordination ability of soft-donor sites. To verify the applicability of these sponges in HLW, additional batch adsorption experiments were conducted using simulated waste solutions under their respective optimal conditions. It was found that the adsorption percentages of Ln(III) (La – Sm) on the D2EHPA/PDMS sponge gradually increased from 22.3% to 39.2% (Figure 2 (a)), significantly higher than those of other elements except Zr. Moreover, nearly 100% of the Ln(III) present were adsorbed using the TODGA/PDMS sponge (Figure 2 (b)). These results suggest that both the D2EHPA/PDMS sponge and TODGA/PDMS sponge have the potential to selectively recover Ln(III) even from complex multi-component acidic solutions such as HLW. Interestingly, when these sponges loaded with adsorbed ions were manually squeezed in an eluent solution (EDTA·2Na or DTPA), lanthanide desorption was effectively promoted by chemical stresses coupled with mechanical stress. As shown in Figure 2 (a)-(b), nearly all adsorbed Ln(III) were successfully detached from the sponge. Such squeezing-based desorption was found more efficient than conventional desorption procedures by immersing the sponge in the eluent solution without applying mechanical pressure.

4.Conclusion

In this study, we successfully fabricated 3 PDMS sponges incorporating soft-donor ligands using a facile fabrication approach. These sponges demonstrated excellent abilities to selectively and efficiently recover lanthanide ions from complex waste solutions. The adsorption mechanism is derived from the coordination between the soft donor sites of each ligand and the lanthanide ions. These results prove that the fabricated PDMS sponge is a simple and easy-to-use separation material, enabling chemical and mechanically driven adsorption-desorption of lanthanides from waste solutions without generating any secondary radioactive wastes.

ACKNOWLEDGMENTS

This work was financially supported by the JAEA Nuclear Energy S&T and Human Resource Development Project Grant Number JPJA22F22717857 and Secretariat of the Nuclear Regulation Authority, Japan. The authors would like to thank Science Tokyo SPRING & BOOST and ISE for their help.

References

[1] T. Tsukahara and Y. Ikeda. Mutual separation of strontium, cerium, and uranium using pressure-driven flow in 100 nm-sized nanofluidic channels. Progress in Nuclear Energy, 53(7), 935-939 (2011).
[2] D. Zhu, H W. Stephan, X. Zhou. Recent progress in fabrication and application of polydimethylsiloxane sponges. Journal of Materials Chemistry A, 5(32), 16467-1642017 (2017).

7th Asia-Pacific Symposium on Radiochemistry *September 14 ~ 19, 2025 • Kunibiki Messe • Shimane, Japan*

Mutual separation of lanthanides by extraction chromatography in hydrochloric acid solution

Wenzun Luo[1], Andri Rahma Putra[1], Chikage Abe[2], Tatsuya Suzuki[1]

[1]*Nagaoka Univ. of Tech.: Kamitomiokamachi1603-1, Nagaoka, Niigata, 940-2137*
[2]*Tohoku Univ.: Katahira, Sendai, Miyagi, 980-8577*

The adsorption of lanthanides on Ln resin (HDEHP (di(2-rthylhexyl) orthophosphoric acid) impregnated resin, Eichrom Tech.) under different concentration of hydrochloric acid was investigated by chromatographic experiment. As results, the heavy lanthanides can be separated almost completely, and the light lanthanides achieved the different peak point of eluted curves. The variation trend of distribution coefficient with the hydrochloric acid changed was summarized. The trend be explained by the competition of hydrogen ion and the HDEHP adsorbent mutual complexation occurred.

1 INTRODUCTION

Environmental assessments necessitate the analysis of lanthanides present in irradiated nuclear fuel and debris. However, due to the presence of similar performance, effective mutual separation of these elements is required.

Currently, the most used methods for separating REEs include solvent extraction, extraction chromatography, and ion exchange chromatography [1-3]. In these methods, extraction chromatography has highly adsorption efficiency and stable physical performance due to its effectiveness in separating elements, including REEs [4].

In this study, we investigated the adsorption behavior of lanthanides by HDEHP-impregnated resin through chromatographic experiments conducted under various hydrochloric acid concentrations. The results showed the possibility of mutual separation of lanthanides. Additionally, the distribution coefficients obtained were systematically compiled and analyzed to evaluate the adsorption and selective ability of the resin under different hydrochloric concentrations.

2 EXPERIMENTAL

The REE ions were obtained from XSTC-1 standard solution in 2% nitric acid system by *SPEX CertiPrep*. The resin was supplied by *Eichrom Technologies Inc.*, the Ln resin (Particle size 100-150 μm). The column was bought from *Muromac*, L Size. An inductively coupled plasma-mass spectroscopy (ICP-MS Agilent 8900, Agilent Technologies) was used for all element measurements in this study.

Chromatographic experiments were carried out to study the selectivity of resins to REEs at different concentrations of hydrochloric acid. After packing the resin columns, the flow rate and column height were measured and conditioned as the same concentration in the experiments. Since the mass of the resin used each time was approximately the same, the flow rate and height of resin column were consistently maintained. And then 0.1 mL of the prepared feed solution was added. The feed solution contained REEs, except for Pm, and keep the same hydrochloric acid concentration as the experimental conditions. After added the feed solution, hydrochloric acid of a determined concentration was continuously added for elution. Eluate samples were collected and diluted for the analysis by ICP-MS. From these experiments, the value of the distribution coefficient (D_w, mL/g) can be obtained. The equation is as follows:

$$V_p = (D_w \times m_r) + V_0 \quad (1)$$

Where, the V_p is the peak point volume of metal ions (mL); V_0 is the dead volume (mL). m_r represents the mass of the resins (g).

Eluate samples were collected at regular intervals, diluted appropriately, and the concentrations of REEs in the eluate were determined by ICP-MS.

3. RESULT AND DISSCULTION

One of the experiment results (Fig. 1.) that shown as the sample. In 0.5M HCl condition, from 0 to 100 mL effluent volume, the element until Gd show the different peak points that show the possibility to achieve the mutual separation.

From the experiments, the distribution coefficient (mL/g) were calculated and summarized as the Fig. 2. With the equations that to evaluate the separation performance.

Copyright on 7th Asia-Pacific Symposium on Radiochemistry 2025- R3-13* -

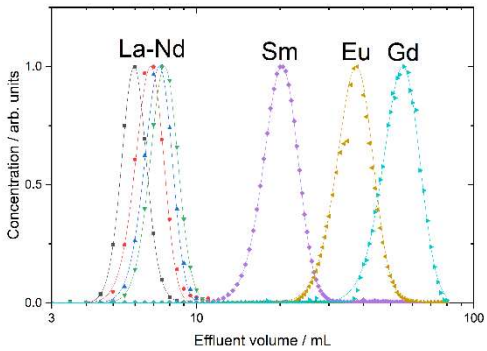


Fig. 1. Result of chromatography separation of REEs in 0.5M HCl condition.

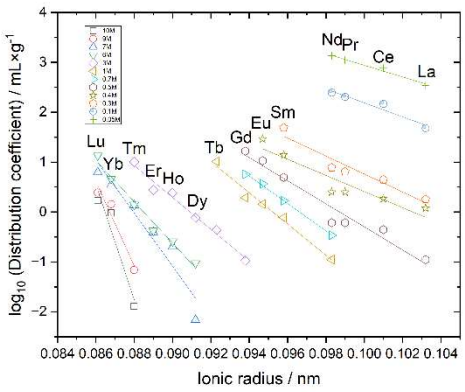


Fig. 2. Distribution coefficients (mL/g) for lanthanides (excluding Pm) with Ln resin in HCl.

3. CONCLUSION

The adsorption behavior of HDEHP-impregnated resin under hydrochloric acid system demonstrates its capability in separating REEs, especially its potential as an environmental-friendly alternative to traditional solvent extraction methods. The presence enables Ln resin to maintain satisfactory separation efficiency in hydrochloric acid environment, despite the relatively weak coordination of rare earth ions compared to other mineral strong acids.

Exclusive use of hydrochloric acid presents significant environmental advantages. Hydrochloric acid, as an inorganic acid, is non-toxic and less-flammable compared to organic solvents. The REEs separated using hydrochloric acid pose less risk to human health and the environment than those separated with other inorganic acids, expanding the potential applications of this method.

ACKNOWLEDGMENTS

This study was performed under the subsidy program “Project of Decommissioning, Contaminated Water and Treated Water Management” conducted by the Ministry of Economy, Trade and Industry of Japan.

References

[1] Fuks, L. and M. Majdan, “Review on hydrometallurgical recovery of rare earth metals," *hydrometallurgy*, **165**, 2 (2016)
[2] Hérès, X., et al., “Selective extraction of rare earth elements from phosphoric acid by ion exchange resins,” Metals, **8**, 682 (2018).
[3] Kifle, D., “Development and optimization of high-performance extraction chromatography method for separation of rare earth elements," *Journal of Chromatography A*, **1730**, 465120 (2024).
[4] Labb, S.A., et al., “Extraction and separation of rare earth elements using LN resins in hydrochloric acid,” Journal of Radioanalytical and Nuclear Chemistry, **333**, 6525 (2024).

Copyright on 7th Asia-Pacific Symposium on Radiochemistry 2025- R3-13* -

Selective Recovery of Lanthanide Ions Using Spiropyran-Based Photoswitchable Adsorbents

Kai Peng[1], Naokazu Idota[2], and Takehiko Tsukahara[1,2*]

[1]*School of Materials and Chemical Technology, Department of Chemical Science and Engineering, Institute of Science Tokyo*
[2]*Laboratory for Zero-Carbon Energy, Institute of Integrated Research, Institute of Science Tokyo, 2-12-1-N1-6,, Ookayama, Meguro-ku, Tokyo, 152-8550 Japan*

Photochromic hybrid silica-based spiropyran nanoparticles (SP@SiO_2) were synthesized via a two-step silane coupling strategy, employing 3-(Triethoxysilyl)propyl isocyanate (ICPTES) as the coupling agent, with spiropyran and porous silica as the primary raw materials. The structure and composition of the resulting nanoparticles were characterized using multiple analytical techniques. The prepared SP@SiO_2 nanoparticles were subsequently evaluated for their adsorption and desorption performance toward lanthanide ion solutions of varying concentrations. The experimental results confirmed the successful synthesis of the target material and demonstrated its effective, reversible adsorption and desorption capabilities for lanthanide ions.

1 Introduction

The efficient separation of lanthanides (Ln) and minor actinides (MA) from high-level liquid wastes (HLLWs) is essential for advancing partitioning and transmutation strategies in nuclear fuel recycling, owing to the strong neutron absorption characteristics of lanthanides that adversely affect MA transmutation [1]. Traditional separation methods, such as solvent extraction and chromatography, while effective, are constrained by issues including the generation of secondary waste and the complexity of operational procedures [2]. In this study, a sustainable and innovative approach is presented through the development of a spiropyran-based photoswitchable adsorbent immobilized on porous silica (SP@SiO_2), which enables ultraviolet/visible (UV/Vis) light-controlled adsorption and desorption of metal ions without the need for organic solvents or acidic eluents. This material offers significant potential to improve the efficiency and environmental sustainability of Ln/MA separation processes in nuclear waste management.

2 Experimental

Porous silica particles (SiO_2; pore diameter: 10 nm, particle size: 75–150 μm) were first activated by treatment with hydrogen peroxide. The activated SiO_2 was then reacted with 3-(Triethoxysilyl)propyl isocyanate (ICPTES) at a molar ratio of 1:2 and heated at 65 °C under an argon atmosphere for 20 hours to achieve silane coupling, resulting in ICPTES-immobilized silica (ICPTES-SiO_2). Subsequently, the ICPTES-SiO_2 was mixed with spiropyran in an acetonitrile solution and heated at 80 °C for 7 hours under an argon atmosphere. Through the reaction between the terminal isocyanate group of ICPTES and the hydroxyl group of spiropyran, spiropyran-immobilized silica (SP@SiO_2) was successfully synthesized. The resulting SP@SiO_2 nanoparticles were characterized using proton nuclear magnetic resonance (^{1}H-NMR) spectroscopy, thermogravimetric-differential thermal analysis (TG-DTA), Fourier-transform infrared (FT-IR) spectroscopy, ultraviolet-visible (UV/Vis) spectroscopy, and other analytical techniques.

Adsorption–desorption experiments for lanthanide (Ln) ions in aqueous solution were conducted using a UV/Vis irradiation setup. In a typical procedure, 10 mg of SP@SiO_2 was mixed with 5 mL of Ln ion solution (concentration range: 0.01–0.5 ppm). The mixture was irradiated with UV light for 5 minutes under dark conditions to promote adsorption of Ln ions. Subsequent desorption was induced by irradiating the solution with visible light (Vis) for either 30 minutes or 7 hours. The concentrations of Ln ions before and after UV/Vis irradiation were quantified by inductively coupled plasma mass spectrometry (ICP-MS), and the adsorption–desorption efficiencies were evaluated based on the observed changes in Ln ion concentrations.

3 Results and Discussion

Figure 1 presents the ^{1}H-NMR spectra of spiropyran-ICPTES, spiropyran, and ICPTES. The observed shifts in chemical shifts clearly indicate the successful covalent bonding between spiropyran and ICPTES. Thermogravimetric-differential thermal analysis (TG-DTA) was employed to evaluate the immobilization of ICPTES onto the silica particles. As shown in Figure 2, a distinct thermal decomposition peak corresponding to ICPTES was observed at approximately 228 °C. Based on the TG-DTA results, the amount of immobilized ICPTES was estimated to be 0.498 mg per 1 mg of ICPTES-SiO_2.

Copyright on 7th Asia-Pacific Symposium on Radiochemistry 2025- R3-14* -

The interaction between lanthanide (Ln) ions and spiropyran was further investigated by examining the color changes of the solutions. With increasing La(III)/spiropyran molar ratios, the solution color shifted progressively from purple to yellow, suggesting the formation of coordination complexes between La(III) ions and spiropyran molecules. Moreover, the absorbance at 349 nm exhibited a linear correlation with the La(III)/spiropyran molar ratio, further supporting the coordination interaction.

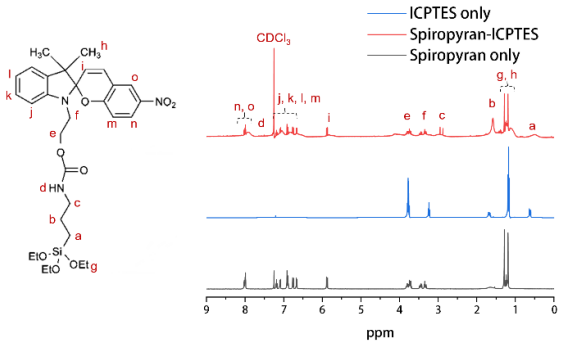


Fig. 1. ^{1}H-NMR spectra of spiropyran-ICPTES, pure spiropyran and pure ICPTES

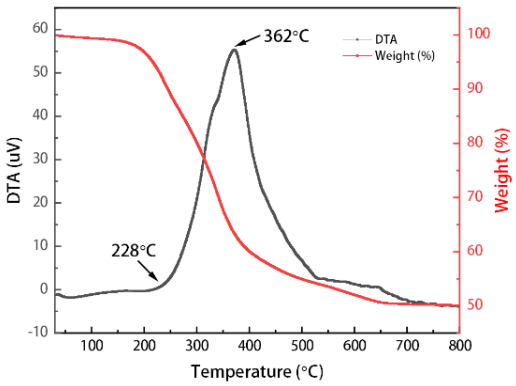


Fig. 2. TG-DTA curve of ICPTES-SiO_2

Adsorption–desorption experiments were subsequently carried out using the synthesized SP@SiO_2 nanoparticles, and the results are summarized in Figure 3. Under UV light irradiation, the adsorption rate of La(III) ions reached over 70% at an initial concentration of 0.01 ppm; however, the adsorption efficiency decreased with increasing La(III) concentration. Desorption of La(III) ions was achieved by visible light irradiation for 30 minutes, and the desorption rate was further enhanced by heating. Specifically, a desorption rate exceeding 17% was attained under visible light irradiation combined with heating at 60 °C for 7 hours. These findings suggest that the desorption behavior of Ln ions from the SP@SiO_2 surface is strongly dependent on both the duration of visible light exposure and the ambient temperature. Nevertheless, residual Ln ions remained on the SP@SiO_2 surface after treatment, indicating that precise control of visible light irradiation conditions is necessary to achieve complete desorption.

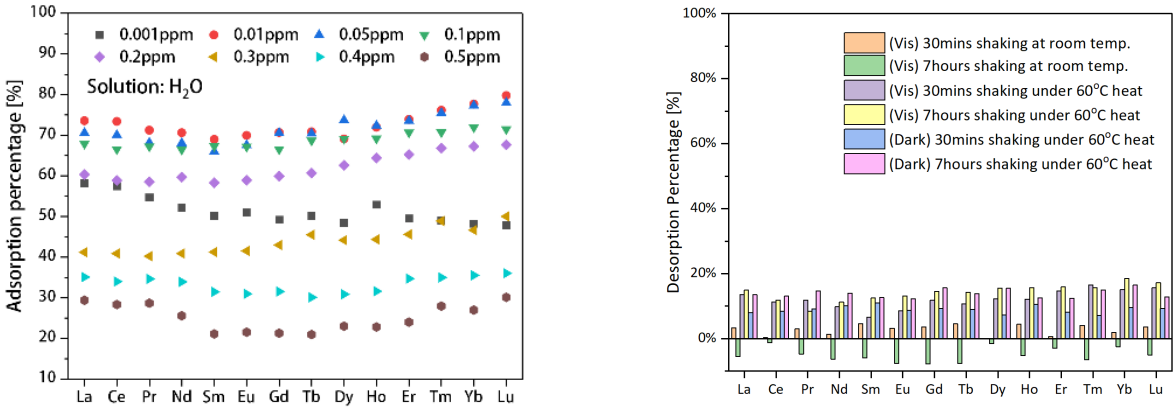


Fig. 3. Adsorption-desorption percentages of Ln ions by UV-Vis irradiation. (left; Adsorption, right; Desorption)

ACKNOWLEDGMENTS

This work was financially supported by the Secretariat of the Nuclear Regulation Authority, Japan.

References

[1] Xiaoyu Guan, Mengyan He, Photo-controllability of fluoride remediation by spiropyran-functionalized mesoporous silica powder, [Journal of Environmental Chemical Engineering, Volume 9, Issue 1,2021,104655]
[2] Berkovic, G.; Krongauz, V.; Weiss, V. Spiropyrans and spirooxazines for memories and switches. [Chem. Rev. 2000, 100, 1741−1754.]

Copyright on 7th Asia-Pacific Symposium on Radiochemistry 2025- R3-14* -

Plenary Talk | Plenary Talk

Thu. Sep 18, 2025 8:45 AM - 9:30 AM JST | Wed. Sep 17, 2025 11:45 PM - 12:30 AM UTC Hall S(Int'l)

[PL4] Plenary Talk 4 by Kazuhiko Ninomiya

8:45 AM - 9:30 AM JST | 11:45 PM - 12:30 AM UTC

[PL04]

ELEMENTAL ANALYSIS METHOD USING MUONS: APPLICATIONS FOR ASTEROID AND ARCHEOLOGICAL SAMPLES

*Kazuhiko Ninomiya[1,2] (1. Natural Science Center for Basic Research and Development, Hiroshima University (Japan), 2. Graduate School of Advanced Science and Engineering, Hiroshima University (Japan))

©APSORC25

ELEMENTAL ANALYSIS METHOD USING MUONS: APPLICATIONS FOR ASTEROID AND ARCHEOLOGICAL SAMPLES

Kazuhiko Ninomiya[1,2]

[1]*Natural Science Center for Basic Research and Development, Hiroshima University: 1-4-2, Kagamiyama, Higashi-Hiroshima City, Hiroshima, Japan, 739-8526, ninomiya-kazu@hiroshima-u.ac.jp*
[2]*Graduate School of Advanced Science and Engineering, Hiroshima University: 1-3-1, Kagamiyama, Higashi-Hiroshima City, Hiroshima, Japan, 739-8526*

In this plenary talk, we will present principle of elemental analysis method using muons. This method bases on characteristic muonic X-ray measurement emitted after muon stop in a material. Due to large mass of a muon, this method can quantify elements non-destructively, position selectively and multi-elementally. This method has already been applied for the analysis of asteroid and archeological samples, so some application studies will also be presented.

1 INTRODUCTION

Elemental analysis by measuring muonic X-rays emitted after muon stop in a material was firstly proposed about 60 years ago [1]. A muon is one of the elementary particles having a negative charge and a mass of 106 MeV/c^2. Due to its negative charge, the muon makes muon atomic orbit around a nucleus and forms an atomic system called a muonic atom. Since the muon has a large mass compare to an electron, high-energy characteristic X-rays called muonic X-rays are emitted after formation of muonic atoms. Furthermore, the muon stopping position, that is, muonic atom formation position in a material can be selected by adjusting incident muon energy. By measuring muonic X-rays, identification and quantification of elements at any position in a material are possible. This is the principle of muon elemental analysis method, MIXE: Muon Induced X-ray Emission.

Although some pioneering researches related to MIXE have been done in the past [2-5], it has not been established as an analytical method. On the other hand, recent advances in accelerator technology enable us to obtain high-intensity and mono-energetic muon beam, making it possible to perform various research projects using muons. Since MIXE research was restarted at J-PARC (Japan Proton Accelerator Research Complex, Japan) in 2008, MIXE was established as an analytical method [6-8]. In present, MIXE research has been carried out not only at J-PARC but also at muon facilities around the world, such as PSI (Paul Scherrer Institute, Switzerland), RAL (Rutherford Appleton Laboratory, United Kingdom) and RCNP (Research Center for Nuclear Physics, Japan), and various analysis researches are being performed.

Since MIXE allows non-destructive elemental analysis, it has been applied to valuable samples. In particular, the analysis of asteroid and cultural heritage samples has been very successful in J-PARC [9-12]. In this plenary talk, we will introduce these J-PARC achievements as well as recent progress and application researches of MIXE being conducted around the world.

2 ASTEROID SAMPLE ANALYSIS

Elemental composition of the solar system is important to understand the mystery of how the solar system was formed. In particular, the compositions of light elements such as carbon, nitrogen, and oxygen are strongly related to the birth of life on Earth. To understand the composition of the solar system, the meteorites containing volatile elements, called carbonaceous chondrites, have been analyzed. However, the meteorites may have been contaminated during their fall on Earth, so it was necessary to collect samples directly from the asteroid. Samples from asteroid Ryugu collected and brought back by asteroid explorer Hayabusa2 are valuable and important materials to solve the mystery of the solar system.

To investigate the bulk composition of asteroid Ryugu, MIXE was applied for 120 mg of Ryugu grains [9, 10]. The compositions of carbon, nitrogen, and oxygen are directly determined by muonic X-ray measurement without sample destruction, which had previously only been possible by destructive analysis method. In addition, the compositions of the other elements, such as Mg, Si and Fe, were determined by muonic X-ray spectrum

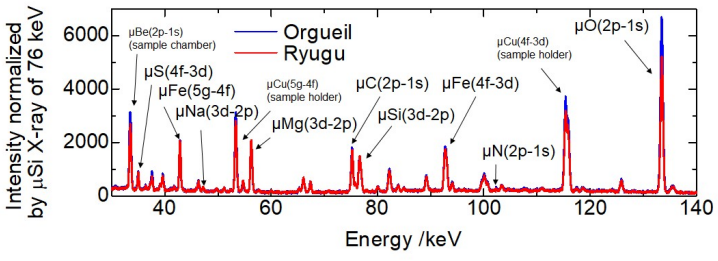


Fig. 1. Muonic X-ray spectra for Ryugu and Orgueil (CI chondrite)

Copyright on 7th Asia-Pacific Symposium on Radiochemistry 2025

as shown in Figure 1. The bulk composition of asteroid Ryugu was very similar to that of the Orgueil meteorite, which is considered one of the most primordial meteorite (CI chondrites), except for oxygen. The amount of oxygen in Ryugu is about 25% lower than that of Orgueil, indicating that Orgueil has been contaminated by terrestrial materials. In other words, the analysis showed that Ryugu grains are the most representative of solid materials in the solar system.

3 ARCHEOLOGICAL SAMPLE ANALYSIS

Analysis of archeological samples is important for investigation of the past human activities. In particular, elemental composition provides information about making process of the material, which in turn leads to understanding how the technology developed and spread. Because such cultural properties are valuable, only non-destructive analytical methods can be applied. However, in many cases, these objects have rusted on surface. MIXE is the only way to investigate the internal composition of such objects non-destructively.

As an example of application of MIXE for cultural property research, we will introduce the analysis of a bronze bell made in Japan about 2000 years ago [11]. The bronze bell was remained underground for a long time, so its surface was rusted. By changing the muon incident energy and selecting the muon stopping depth, muonic X-ray spectra were obtained as shown in Figure 2. In low incident energy conditions, oxygen derived from rust layer on the surface was observed, while in high incident energy conditions, oxygen was not observed, and only metal layer was analyzed. In addition, the composition (muonic X-ray intensities of Cu, Sn and Pb) of the bronze in the surface was different from that in deeply inside. By this analysis, the elemental composition of the bronze bell was determined to be 81.5±1.5% of copper, 8.6±1.1% of tin and 9.1±1.3% of lead. Also, this results indicated that elemental analysis for surface by X-ray fluorescence analysis does not give the correct elemental composition at manufactured.

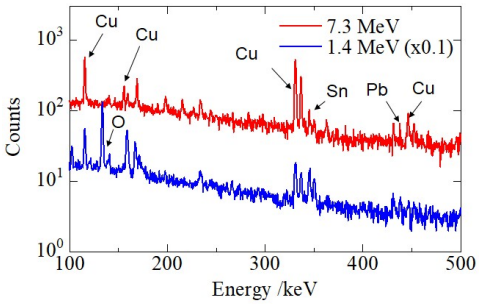


Fig. 2. Muonic X-ray spectra for the bronze bell with different incident muon energy

ACKNOWLEDGMENTS

The authors would like to thank all the staff at the facilities where muon experiments were conducted: J-PARC, RCNP, RAL and PSI.

References

[1] H. Daniel, “The muon as a tool for scanning the interior of the human body” *Nuclear-Medizin*, **8**, 311 (1969).
[2] E. Köhler et al, “Application of muonic X-ray techniques to the elemental analysis of archeological objects” *Nucl. Instrum. Meth. Phys. Res.* **187**, 563 (1981).
[3] H. Daniel et al., “Non-destructive Elemental Analysis Using Negative Muon” *Fresenius Z. Anal. Chem.* **321**, 65 (1985).
[4] Y. Hosoi et al., “Non-destructive elemental analysis of vertebral body trabecular bone using muonic X-rays” *British J. Radiology* **68**, 1325 (1995).
[5] M. K. Kubo et al., “Non-destructive elemental depth-profiling with muonic X-rays” *J. Radioanal. Nucl. Chem.* **278**, 777 (2008).
[6] K. Ninomiya et al., “Development of elemental analysis by muonic X-ray measurement in J-PARC” *Journal of Physics: Conference Series*, **225**, 012040 (2010).
[7] K. Ninomiya et al., “Development of Nondestructive and Quantitative Elemental Analysis Method using Calibration Curve between Muonic X-ray Intensity and Elemental Composition in Bronze” *Bulletin of the Chemical Society of Japan*, **85**, 228 (2012).
[8] K. Ninomiya et al., “Nondestructive Elemental Depth-Profiling Analysis by Muonic X-ray Measurement” *Analytical Chemistry*, **87**, 4597 (2015).
[9] T. Nakamura et al., “Formation and evolution of carbonaceous asteroid Ryugu: Direct evidence from returned samples” *Science*, **379**, eabn8671 (2022).
[10] K. Ninomiya et al., “Quantification of bulk elemental composition for C-type asteroid Ryugu samples with nondestructive elemental analysis using muon beam” *Meteoritics & Planetary Science*, **59**, 2044 (2024).
[11] T. Saito et al., “Non-destructive composition analysis of remaining metallic parts in the deeper layer of the rusty part of a Dotaku, bronze bell made in the Yayoi period, using muonic X-ray measurement” *Scientific studies on cultural properties*, **87**, 43 (2024)
[12] K. Shimada-Takaura et al., “A novel challenge of nondestructive analysis on OGATA Koan’s sealed medicine by muonic X-ray analysis” *Journal of Natural Medicines*, **75**, 532 (2021).

Copyright on 7th Asia-Pacific Symposium on Radiochemistry 2025

Invited & Contributed Talk | [R4]Nuclear Probe in Chemistry

Thu. Sep 18, 2025 9:35 AM - 10:45 AM JST | Thu. Sep 18, 2025 12:35 AM - 1:45 AM UTC Hall S(Int'l)

[R4] Nuclear Probe in Chemistry

9:35 AM - 10:05 AM JST | 12:35 AM - 1:05 AM UTC

[R4-01(Invited)]

Application of muon spin imaging spectroscopy to material science

*Mototsugu Mihara[1], S. Ishitani[1], K. M. Kojima[2], A. Sato[1], K. Yasuda[1], G. Takayama[1], T. Sugisaki[1], Y. Kimura[1], M. Fukuda[1], M. Fukutome[3], R. Taguchi[1], S. Shimizu[1], K. Horie[1], R. Imai[1], S. Ide[1], K. Shimizu[4], M. Kamon[4], M. Fukushima[4], Y. Mizoi[5], A. Koda[6], S. Kanda[6], W. Sato[7], D. Nishimura[8], M. Tanaka[9] (1. Department of Physics, The University of Osaka (Japan), 2. TRIUMF (Canada), 3. Niigata University (Japan), 4. KYOKUGEN, The University of Osaka (Japan), 5. Osaka Electro-Communication University (Japan), 6. KEK (Japan), 7. Kanazawa University (Japan), 8. Tokyo City University (Japan), 9. Kyushu University (Japan))

10:05 AM - 10:25 AM JST | 1:05 AM - 1:25 AM UTC

[R4-02]

^{61}Ni Mössbauer Spectroscopy on Hofmann-type coordination polymer

*Kosuke Kitase[1], Takafumi Kitazawa[1], Yasuhiro Kobayashi[2], Makoto Seto[2], Shinji Kitao[2], Takumi Kubota[3] (1. Toho University (Japan), 2. Institute for Integrated Radiation and Nuclear Science, Kyoto University (Japan), 3. Agency for Health, Safety and Environment, Kyoto University (Japan))

10:25 AM - 10:45 AM JST | 1:25 AM - 1:45 AM UTC

[R4-03]

LOCAL STRUCTURE OF CADMIUM IMPURITIES IN STRONTIUM TITANATE STUDIED BY THE TIME DEFFERENCIAL PERTURBED ANGULAR CORRELATION METHOD

*Sayaka Komatsuda[1], Wataru Sato[1], Akihiro Taniguchi[2], Yoshitaka Ohkubo[2] (1. Kanazawa University (Japan), 2. Kyoto University (Japan))

©APSORC25

APPLICATION OF MUON SPIN IMAGING SPECTROSCOPY TO MATERIAL SCIENCE

M. Mihara[1,†,*], S. Ishitani[1,†], K. M. Kojima[2,†], A. Sato[1], K. Yasuda[1], G. Takayama[1], T. Sugisaki[1,†], Y. Kimura[1,†], M. Fukuda[1], M. Fukutome[3], R. Taguchi[1], S. Shimizu[1], K. Horie[1], R. Imai[1], S. Ide[1], K. Shimizu[4], M. Kamon[4], M. Fukushima[4], Y. Mizoi[5,†], A. Koda[6,†], S. Kanda[6], W. Sato[7], D. Nishimura[8], M. Tanaka[9,†]

[1]*Department of Physics, The University of Osaka: 1-1 Machikaneyama, Toyonaka, Osaka 560-0043, Japan*
[2]*TRIUMF: 4004 Wesbrook Mall, Vancouver, British Columbia V6T 2A3, Canada*
[3]*Faculty of Science, Niigata University: 8050 Ikarashi 2-no-cho, Nishi-ku, Niigata 950-2181, Japan*
[4]*KYOKUGEN, Center for Science and Technology under Extreme Conditions, The University of Osaka, 1-3 Machikaneyama, Toyonaka, Osaka, 560-8531, Japan*
[5]*Osaka Electro-Communication University: 18-8 Hatsucho, Neyagawa, Osaka 572-8530, Japan*
[6]*Institute of Materials Structure Science, High Energy Accelerator Research Organization (KEK), 1-1 Oho, Tsukuba Ibaraki 305-0801, Japan*
[7]*College of Science and Engineering, Kanazawa University: Kakuma-machi, Kanazawa, 920-1192, Japan*
[8]*Tokyo City University: 1-28-1 Tamazutsumi,Setagaya-ku, Tokyo158-8557, Japan*
[9]*Faculty of Arts and Science, Kyushu University: 744 Motooka, Nishi-ku, Fukuoka 819-0395, Japan*
[†]*Open-It*
[*]*mihara@phys.sci.osaka-u.ac.jp*

The μSR spectroscopy has been used in various research fields as an extremely versatile measurement method. However, due to the difficulty of reducing the size of the muon beam, it has been difficult to apply the method to small sample volumes or samples confined in a limited space such as a high-pressure cell. In order to realize measurements in such limited sample environments and 3D imaging of various objects such as biological samples, meteorites, and archaeological materials, we have developed a new imaging technique, muon spin imaging, which adds spatial resolution to the conventional μSR spectroscopy. Currently, we have achieved an image resolution of 0.6 mm through instrument improvement and performance evaluation. At the conference, we will present the current status and future plans of this project.

1 INTRODUCTION

The muon spin rotation/relaxation/resonance (μSR) spectroscopy has been used in various research fields including material and life sciences as an extremely versatile measurement method. However, due to the difficulty of reducing the size of the muon beam, it has been difficult to apply the method to small sample volumes or samples confined in a limited space such as a high-pressure cell. In order to realize measurements under such limited sample environments or furthermore 3D imaging of various objects such as biological samples, meteorites, archaeological materials and so on, we have started to develop an imaging technique we call "muon spin imaging" that adds spatial resolution to the conventional μSR spectroscopy. The μSR method is a technique for measuring the time variation of muon spin polarization in a magnetic field using the asymmetric angular distribution of positrons emitted by the decay of spin-polarized muons. This enables us to

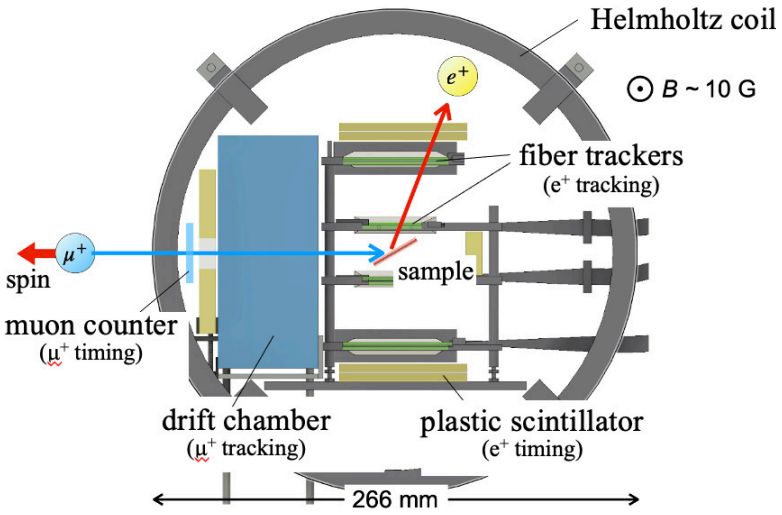


Fig. 1. Setup of the muon spin imaging spectroscopy experiment.

Copyright on 7th Asia-Pacific Symposium on Radiochemistry 2025 - R4-01 -

observe the internal magnetic field in materials with very high sensitivity and is used for various materials science research on magnetism, superconductivity, ion dynamics, chemical reactions, and so on. We have introduced a position sensitive detectors into the μSR spectrometer, as shown in Fig. 1, to track both incident muons (μ^+) and μ-e decay positrons (e^+) so that the μ^+ stop position can be determined. Imaging was performed by dividing the stop positions into pixels and acquiring μSR spectra for each pixel.

2 DEVELOPMENT AND PERFORMANCE TESTING OF MUON SPIN IMAGING DEVICE

In the present study, significant improvements were made to our muon spin imaging device based on the previous results [1,2]. One of the improvement was to minimize the misalignment of the scintillation fibers used for tracking e^+ particles, which was the main cause of image blurring. Another was to significantly reduce the dead time for data acquisition by incorporating the Kalliope system [3]. Third was to add a drift chamber for μ^+ beam tracking, which enables 3D imaging combined with the e^+ tracking. We have tested the performance of the improved device using a surface DC muon beam at TRIUMF, which showed that a clear 2D image is successfully created as shown in Fig. 2. The image resolution was deduced to be 0.6 mm from the material boundaries of the 2D image. At the conference, we will present the result of the 3D imaging which is in progress, together with the details of our imaging device and future plans of our project.

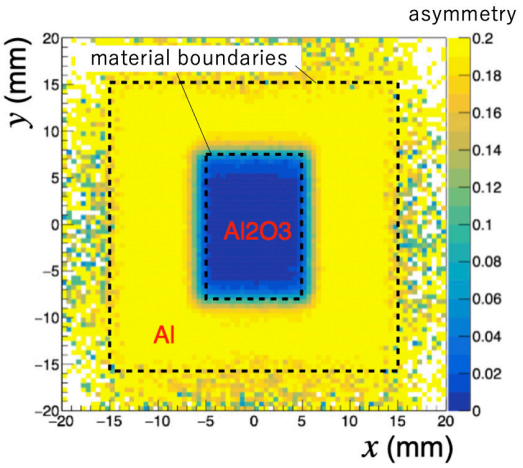


Fig. 2. 2D muon spin image of a test sample combining Al and single crystal Al_2O_3 plates.

ACKNOWLEDGMENTS

This work was supported by the Multidisciplinary PhD Program for Pioneering Quantum Beam Application (PQBA) at the University of Osaka, The University of Osaka Foundation for the Future, TRIUMF-KEK Exchange Program for Early Career Researchers (EPECR), Fundamental Electronics Research Institute (FERI) at Osaka Electro-Communication University, and JSPS Kakenhi Grant Number JP22H00110.

References

[1] T. Sugisaki et al., ”Development of muon spin imaging spectroscopy”, Interactions 245, 20 (2024).

[2] G. Takayama et al., ”Evaluation of image resolution of muon spin imaging”, Interactions 245, 32 (2024).

[3] K. M. Kojima et al., ”New μSR spectrometer at J-PARC MUSE based on Kalliope detectors”, J. Phys.: Conf. Ser. 551, 012063 (2014).

Copyright on 7th Asia-Pacific Symposium on Radiochemistry 2025 - R4-01 -

^{61}Ni Mössbauer Spectroscopy on Hofmann-type coordination polymer

Kosuke Kitase[1], Shinji Kitao[3], Yasuhiro Kobayashi[3], Takumi Kubota[4], Makoto Seto[3], Takafumi Kitazawa[1, 2]

1 - Department of Chemistry, Faculty of Science, Toho University, 2-2-1 Miyama, Funabashi, Chiba, 274-8510, Japan
2 - Research Centre for Materials with Integrated Properties, Toho University, 2-2-1 Miyama, Funabashi, Chiba, 274-8510, Japan
3 - Institute for Integrated Radiation and Nuclear Science, Kyoto University, 2 Asashiro-nishi, Kumatori, Sennan-gun, Osaka, 590-0494, Japan
4 - Agency for Health, Safety and Environment, Kyoto University, Gokasho, Uji, Kyoto 611-0011, Japan

Hofmann-type complex is one of the coordination polymer. Mössbauer spectroscopy is a valuable tool for elucidating fine structures around specific elements. However, Mössbauer spectroscopy on Hofmann-type complexes primarily focus on ^{57}Fe. Herein, we synthesized Ni Hofmann-type complexes and investigated it using ^{61}Ni Mössbauer spectroscopy.

1 INTRODUCTION

The spin-crossover (SCO) phenomenon is a reversible spin switching in metal ions between high-spin (HS) and low-spin (LS) states triggering by external stimuli.

The Hofmann-type complex is coordination polymer with metal ion and cyanometalate, and another ligand such as pyridine or pyrazine-type ligand.

^{57}Fe Mössbauer spectroscopy is a very powerful tool for iron(II) SCO materials because I.S. and Q.S. paramaters are very sensitive to iron(II) spin states. Hence, ^{57}Fe Mössbauer spectroscopy has been extensively used to study Hofmann complexes which has been used to study Fe-type SCO Hofmann complexes [1, 2]. In contrast, ^{61}Ni Mössbauer spectroscopy is only very few reported.

Now we have researched three Hofmann-type complexes Fe(Ethyl isonicotinate)$_2$[Ni(CN)$_4$], Fe(Allyl isonicotinate)$_2$[Ni(CN)$_4$] and Ni(Ethyl isonicotinate)$_2$[Ni(CN)$_4$] with ^{61}Ni Mössbauer spectroscopy it using ^{61}Ni Mössbauer spectroscopy with a 67.4 keV γ–ray probe because of the transition of nuclear spin from I = 5/2 (excited state) to 3/2 (ground state).

2 RESULTS AND DISCUSSION

Figure 1 shows the ^{61}Ni Mössbauer spectrum of reference material $Ni_{86}V_{14}$ alloy , {Fe(Ethyl isonicotinate)$_2$[Ni(CN)$_4$]}, {Fe(Allyl isonicotinate)$_2$[Ni(CN)$_4$]}, and {Ni(Ethyl isonicotinate)$_2$[Ni(CN)$_4$]} at 20 K. Additionally, Table 1 presents the Mössbauer parameters (IS, full width at half maximum (FWHM), and relative peak area) of reference material $Ni_{86}V_{14}$ alloy , {Fe(Ethyl isonicotinate)$_2$[Ni(CN)$_4$]}, {Fe(Allyl isonicotinate)$_2$[Ni(CN)$_4$]}, and {Ni(Ethyl isonicotinate)$_2$[Ni(CN)$_4$]}. Compared with the $Ni_{86}V_{14}$ alloy, these complexes exhibit slightly lower IS and wider FWHM in the ^{61}Ni Mössbauer spectrum. Also, {Ni(Ethyl isonicotinate)$_2$[Ni(CN)$_4$]} shows additional peak that exhibits slightly higher IS. These results show these complexes contain square planner divalent Ni site and {Ni(Ethyl isonicotinate)$_2$[Ni(CN)$_4$]} contains octahedral divalent Ni site. The thickness of the {Fe(Ethyl isonicotinate)$_2$[Ni(CN)$_4$]} (approximately 0.116 g cm^{-2} for Ni atoms), {Fe(Allyl isonicotinate)$_2$[Ni(CN)$_4$]} (approximately 0.270 g cm^{-2} for Ni atoms), and {Ni(Ethyl isonicotinate)$_2$[Ni(CN)$_4$]} (approximately 0.326 g cm^{-2} for Ni atoms) are all greater than that of the $Ni_{86}V_{14}$ alloy sample (0.0907 g cm^{-2}, approximately 0.0794 g cm^{-2} for Ni atoms). Nevertheless, the absorption intensity of the spectrum of these complexes are weaker than that of the $Ni_{86}V_{14}$ alloy. Considering the thickness of the sample, this absorption intensity is very low. This was attributed to the presence of long organic ligands in Hofmann-type coordination polymers and their flexible framework.

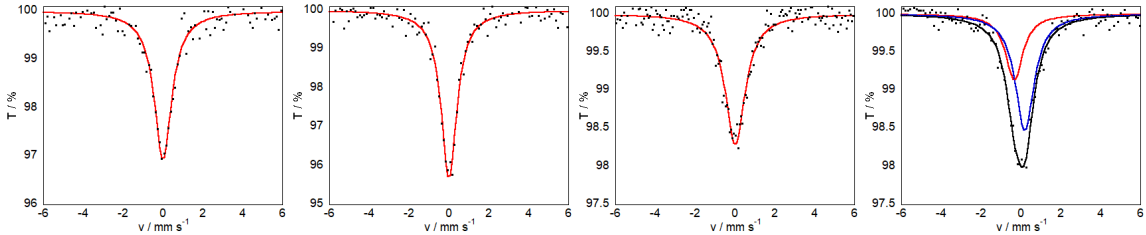


Fig. 1. ^{61}Ni Mössbauer spectroscopy of $Ni_{86}V_{14}$ alloy, Fe(Ethyl Isonicotinate)$_2$[Ni(CN)$_4$], Fe(Allyl isonicotinate)$_2$[Ni(CN)$_4$] and Ni(Ethyl Isonicotinate)$_2$[Ni(CN)$_4$]

Copyright on 7th Asia-Pacific Symposium on Radiochemistry 2025 - R4-02 -

Table 1. Parameter of ^{61}Ni Mössbauer spectroscopy

	weight [g]	Ni thickness [g cm^{-2}]	IS / [mm s^{-1}]	HW / [mm s^{-1}]	Peak area
$V_{86}Ni_{14}$ alloy		0.0794	0	0.95	0.0416
Fe(Ethyl Isonicotinate)$_2$[Ni(CN)$_4$]	0.809	0.116	-0.06	1.21	0.0208
Fe(Allyl Isonicotinate)$_2$[Ni(CN)$_4$]	1.969	0.270	-0.002	1.07	0.0329
Ni(Ethyl Isonicotinate)$_2$[Ni(CN)$_4$]	1.141	0.326	-0.34 0.19	1.06 1.15	0.00917, 0.0175

3. CONCLUSIONS

Now we have synthesized Hofmann-type complex {Fe(Ethyl isonicotinate)$_2$[Ni(CN)$_4$]}. That complex shows the SCO phenomenon. The result of X-ray absorption fine structure (XAFS) and ^{61}Ni Mössbauer spectroscopy suggest the SCO phenomenon of this complex only occurs in Fe sites. The ^{61}Ni Mössbauer spectroscopy of this complex suggests this complex doesn't have so much electric field gradient.

ACKNOWLEDGMENTS

This work was partially supported by the Joint Usage/Research of the Institute for Integrated Radiation and Nuclear Science, Kyoto University (KURNS) (No. R4P3-7, R5P1-2, R6P9-1).

References

[1] G. Molnár, T. Guillon, N. O. Moussa, L. Rechignat, T. Kitazawa, M. Nardone, A. Bousseksou, *Chem. Phys. Lett.*, 423, 152 (2006).
[2] T, Kitazawa, T. Kishida, T. Kawasaki, M, Takahashi, *Hyperfine Interact.*, 238(1), 1 (2017).

7th Asia-Pacific Symposium on Radiochemistry *September 14 ~ 19, 2025 • Kunibiki Messe • Shimane, Japan*

LOCAL STRUCTURE OF CADMIUM IMPURITIES IN STRONTIUM TITANATE STUDIED BY THE TIME DEFFERENCIAL PERTURBED ANGULAR CORRELATION METHOD

S. Komatsuda[1], W. Sato[2], A. Taniguchi[3], Y. Ohkubo[3]

[1]*Institute of Human and Social Sciences, Kanazawa University: / Kanazawa, Ishikawa, 920-1192*
[2]*Institute of Science and Engineering, Kanazawa University: / Kanazawa, Ishikawa, 920-1192*
[3]*Institute for Integrated Radiation and Nuclear Science, Kyoto University: / Kumatori, Osaka, 590-0458*

Strontium titanate ($SrTiO_3$) is a perovskite-type oxide widely studied for its photocatalytic applications. In this work, we investigated the local structural environment of Cd-doped $SrTiO_3$ by means of the time-differential perturbed angular correlation (TDPAC) method with $^{111}Cd(\leftarrow^{111m}Cd)$ probes. The TDPAC spectrum revealed three distinct electric field gradient (EFG) components. These results suggest that Cd^{2+} ions occupy multiple lattice sites, including defect-free A or B sites and B sites associated with structural defects. The observed EFG values closely resemble those obtained in our previous study on In-doped $SrTiO_3$ using a $^{111}Cd(\leftarrow^{111}In)$ probe, implying that Cd^{2+} is incorporated into the $SrTiO_3$ lattice in a similar substitutional manner to In^{3+}. Because In^{3+} acts as an effective dopant for enhancing the photocatalytic activity of $SrTiO_3$, Cd^{2+} might also enhance performance when occupying similar structural environments.

1 INTRODUCTION

Strontium titanate ($SrTiO_3$) is a cubic perovskite-type oxide (ABO_3) known for its wide range of electrical and catalytic properties. $SrTiO_3$ doped with metal ions as impurities exhibit a wide variety of electronic properties, and the effects of various dopants have been extensively investigated. Especially, $SrTiO_3$ doped with trivalent metal ions at Ti^{4+} site has attracted much attention because of their excellent photocatalytic activity [1]. For a practical use of $SrTiO_3$, it is necessary to obtain more microscopic information on the impurity site. In our previous study using time-differential perturbed angular correlation (TDPAC) measurements with $^{111}Cd(\leftarrow^{111}In)$ probes, we investigated the local structure around In^{3+} ions in $SrTiO_3$ [2]. The results revealed that In^{3+} ions are uniformly dispersed and occupy three types of sites; (i) the first site is a defect-free substitutional Sr^{2+} or Ti^{4+} site, and (ii) The second and third components, characterized by well-defined electric field gradients (EFGs) at the $^{111}Cd(\leftarrow^{111}In)$ probe site, are attributed to In^{3+} ions at Ti^{4+} sites associated with lattice defects such as oxygen vacancies. In order to investigate how different dopants influence the structure and photocatalytic properties of $SrTiO_3$, we examined the local structure of Cd-doped $SrTiO_3$ using the TDPAC method with $^{111}Cd(\leftarrow^{111m}Cd)$ probe and compared the results with those of In-doped $SrTiO_3$ obtained in our previous study.

2 EXPERIMENTAL

Stoichiometric amount of $SrCO_3$, $CdCO_3$, and TiO_2 powders were mixed in the mortar. The powders were pressed into disks. For TDPAC measurements, about 3 mg of CdO enriched with ^{110}Cd was irradiated with thermal neutrons in a pneumatic tube at Institute for Integrated Radiation and Nuclear Science, and radioactive ^{111m}Cd was generated by $^{110}Cd(n, \gamma)^{111m}Cd$ reaction. The neutron-irradiated CdO powder was dissolved in 6M HCl and added in droplets onto the pre-sintered $Cd_xSr_{1-x}TiO_3$ disk. The disk was sintered in air at 1373 K for 90 min. The TDPAC measurement was carried out for the 151-245 keV cascade γ rays of $^{111}Cd(\leftarrow^{111m}Cd)$ probe with the intermediate state of I = 5/2 having a half-life of 85.0 ns.

3 RESULTS

Figure 1 shows the TDPAC spectra of (a) $^{111}Cd(\leftarrow^{111}In)$ in $SrTiO_3$ from our previous work, and (b) $^{111}Cd(\leftarrow^{111m}Cd)$ in $Cd_{0.15}Sr_{0.85}TiO_3$ at room temperature from this work. The directional anisotropy on the ordinate, $A_{22}G_{22}(t)$, was deduced with the following simple operation for delayed coincidence events of the cascade:

$$A_{22}G_{22}(t) = \frac{2[N(\pi,t) - N(\pi/2,t)]}{N(\pi,t) + 2N(\pi/2,t)}. \quad (1)$$

Here, A_{22} denotes the angular correlation coefficient, $G_{22}(t)$ the time-differential perturbation factor as a function of the time interval, t, between the relevant cascade γ-ray emissions, and $N(\theta,t)$ the number of the coincidence events observed at angle, θ. The spectra in Fig. 1 can be reproduced by a fit with three unique quadrupole frequencies. The parameters of quadrupole frequencies between the two results of Fig.1(a) and (b) were the same within the fitting error range. These observations show that local fields at the $^{111}Cd(\leftarrow^{111m}Cd)$ probe in $Cd_{0.15}Sr_{0.85}TiO_3$ composite oxide is identical to that at the $^{111}Cd(\leftarrow^{111}In)$ probe in $SrTiO_3$. It is suggested from these results that the $^{111}Cd(\leftarrow^{111m}Cd)$ probe also reside at

Copyright on 7th Asia-Pacific Symposium on Radiochemistry 2025

three unique site; (i) for first component of zero EFGs, the ^{111}Cd(←^{111m}Cd) probe substitutes defect-free A or B sites in cubic perovskite structure, and (ii) for second and third components of well-defined EFGs, suggesting that the Cd^{2+} ions are located at Ti^{4+} sites where defect exists in the vicinity of the probes. These results also indicate that the cubic perovskite structure of $SrTiO_3$ is retained even at high Cd concentrations. Since In doping enhances the photocatalytic activity of $SrTiO_3$ as a dopant, Cd might also play a similar role when incorporated into $SrTiO_3$ structure.

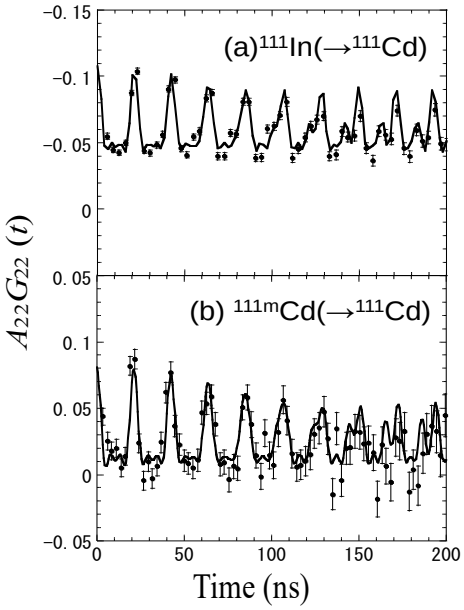


Fig. 1. TDPAC spectra of (a) ^{111}Cd(←^{111}In) in $SrTiO_3$, and (b) ^{111}Cd(←^{111m}Cd) in $Cd_{0.15}Sr_{0.85}TiO_3$.

4 CONCLUSIONS

In this study, TDPAC measurements were carried out to investigate the local structure of Cd-doped $SrTiO_3$ using ^{111}Cd(←^{111m}Cd) probe. The spectra revealed three distinct electric field gradient components, consistent with those observed previously in In-doped $SrTiO_3$, which suggests that Cd^{2+} ions occupy multiple sites, including defect-free A or B sites and defect-associated sites in the lattice. These results suggest that Cd^{2+} might be incorporated into the $SrTiO_3$ lattice site in a comparable manner to In^{3+}, influencing the local environment and photocatalytic performance.

ACKNOWLEDGMENTS

The present work was supported by the Grant-in-Aid for Early-Career Scientists (JSPS) Grant Number 21K17993. This work was accomplished as part of the Visiting Researcher's Program of Institute for Integrated Radiation and Nuclear Science, Kyoto University (KURNS).

References

[1] L.L. Rusevich et al., "Effects of Al Doping on Hydrogen Production Efficiency upon Photostimulated Water Splitting on $SrTiO_3$ Nanoparticles", *J. Phys. Chem. C* **126**:50, 21223-21233 (2022).

[2] S. Komatsuda et al., "Investigation of doping effect on the local structure and photocatalytic activity of $SrTiO_3$", *Interactions* **245**:37(2024).

Invited & Contributed Talk | [P3]Environmental Integrated Knowledge of Radionuclides Dynamics Studied from the Fukushima Accident

Thu. Sep 18, 2025 9:40 AM - 10:50 AM JST | Thu. Sep 18, 2025 12:40 AM - 1:50 AM UTC Hall B(Small)

[P3] Environmental Integrated knowledge of Radionuclides Dinamics Studied from the Fukushima Accident

9:40 AM - 10:10 AM JST | 12:40 AM - 1:10 AM UTC

[P3-01(Invited)]

How the forested areas have worked to radiocesium migration in a river system after the Fukushima nuclear accident

*Seiji Hayashi[1], Hideki Tsuji[1] (1. National Institute for Enviromental Studies (Japan))

10:10 AM - 10:30 AM JST | 1:10 AM - 1:30 AM UTC

[P3-02]

TREND OF CS-137 IN LEAVES, BRANCHES, AND TREE RINGS OF FIR (*Abies firma*) IN ISHINOMAKI AREA OF MIYAGI PREFECTURE, JAPAN

*MICHIKO FUKUSHIMA[1], takeshige MATSUTANI[1], Tomoyuki NEMOTO[1], Kiyotane YODA[1], Amares CHATT[2] (1. Ishinomaki Senshu University (Japan), 2. Dalhousie University (Canada))

10:30 AM - 10:50 AM JST | 1:30 AM - 1:50 AM UTC

[P3-03]

Increase in dissolved Cs-137 concentration in bottom water layer at summer stratification from a mountainous lake, Lake Akagi-Konuma in Gunma Prefecture, Japan

*Seiya Nagao[1], Shinji Otori[1], Kanako Shiozawa[2], Takashi Akutsu[2], Kyuma Suzuki[2], Shinya Ochiai[1] (1. Kanazawa University (Japan), 2. Gunma Prefectural Fisheries Experiment Station (Japan))

©APSORC25

How the forested areas have worked to radiocesium migration in a river system after the Fukushima nuclear accident

Seiji Hayashi[1], Hideki Tsuji[1]

[1] National Institute for Environmental Studies: 10-2, Fukasaku, Miharu, Tamura, Fukushima, 963-7700, Japan, and shayashi@nies.go.jp
[2] National Institute for Environmental Studies: 10-2, Fukasaku, Miharu, Tamura, Fukushima, 963-7700, Japan, and tsuji.hideki@nies.go.jp

Despite the limited transfer of radioactive cesium from forested areas contaminated by the Fukushima nuclear accident, there is continuous runoff in highly bioavailable forms, with forest litter as the source. The transfer has given rise to concerns regarding the contamination of freshwater ecosystems.

1. INTRODUCTION

Approximately 20% of the radioactive cesium released from the TEPCO Fukushima Daiichi Nuclear Power Plant accident (FDNPP) has been deposited on Japanese land, mainly in Fukushima Prefecture [1]. Despite forests covering most of the heavily contaminated areas in Fukushima Prefecture, the government has limited decontamination to the forest fringes. Radiocesium tends to bind to soil clay, with about 90% of Cs-137 originating from the accident still present in the soil at a depth of 10 cm [2]. Forests are a potential source of radiocesium to river systems and play a key role in cesium cycling. This presentation will report on the effects of forests on the transfer behaviour of radioactive cesium in river systems, as found in the studies of the National Institute for Environmental Studies (NIES) on forested river catchments after the FDNPP accident. It will also discuss issues for forested areas relating to environmental restoration and preparation for future nuclear disasters.

2. MATERIALS & METHODS

In the aftermath of the FDNPP accident, the NIES began riverine surveys including runoff during rainfall in the 0.68 km² forested watershed of Mt. Tsukuba in Ibaraki Prefecture. In 2012, similar surveys were initiated in the upstream forested areas of the Udagawa and Ohta Rivers (Udagawa: 0.34 km², Ohta: 21 km²) in the coastal region of Fukushima Prefecture. In each study watershed, river flow and suspended solid (SS) concentration were automatically and continuously observed. In the case of the runoff survey in Mt. Tsukuba, the focus was continuous water sampling during rainfall runoff for radiocesium related to SS. The collected SS was fractionated into four particle size fractions, and the concentration of radiocesium in each fraction was also measured. In forested rivers in the coastal region of Fukushima, river water samples were collected a monthly basis during base flow and continuously during rainfall runoff. The samples were then separated into dissolved radiocesium (Bq/L) and radiocesium in SS (Bq/kg-SS) using a special cartridge filter [3] at the site, and their respective radiocesium concentrations were measured. The radiocesium (^{134}Cs and ^{137}Cs) concentrations of the collected samples were measured using a germanium semiconductor detector.

3. RESULTS & DISCUSSION

3.1 Effect on Formation of Radioactive Cesium Concentration in River Water under Baseflow Conditions

Figure 1 shows the changes in ^{137}Cs concentrations in the dissolved and suspended forms, respectively, in the forested river water upstream of the Ohta River during baseflow conditions, along with SS concentrations. Both forms declined at a faster rate than the physical decay rate, similar to other forested river studies [4]. Extremely low SS concentrations indicate the dissolved form accounts for about 80-90% of the total radiocesium concentration in forested rivers during baseflow condition and is the main form. The dissolved form changes mainly during the summer, peaking in concentration, with forest litter being its main source, and temperature-dependent microbial decomposition

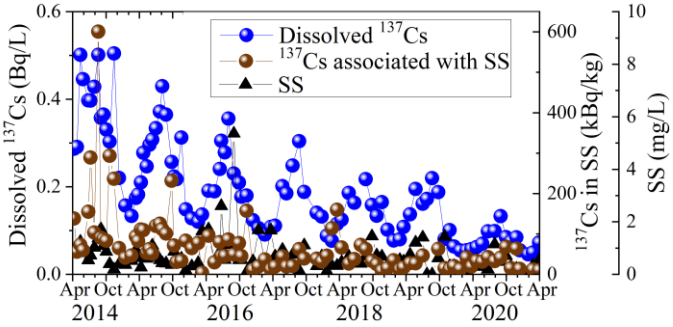


Fig.1 Changes in ^{137}Cs concentrations in the upstream of the Ohta River under baseflow conditions [4].

contributing to its elevated concentrations [5]. Since the dissolved form of radiocesium supplied from the forested river basin greatly influences the downstream dam lake's dissolved form concentrations, concern is affecting radiocesium concentrations in freshwater fish through the food chain.

3.2 Role as Source of Radiocesium Loadings

Despite the fact that the annual runoff ratio of ^{137}Cs to total deposition is strongly dependent on the rainfall characteristics, it is at most the order of 0.1% in each of the study watersheds, indicating limited transfer to downstream waters. As demonstrated in Figure 2, an instance of radiocesium runoff during rainfall is illustrated [6]. Despite the prevalence of particulate form of radiocesium adsorbed on SS in river water, attributable to sediment runoff, the dissolved form concentration in river water remains undiluted even at peak flow rate. This is a consequence of direct runoff of dissolved components from the litter. Consequently, dissolved radiocesium cannot be considered negligible, and further study is required on their involvement in contamination of the aquatic ecosystem. A survey conducted in the forested river catchment of Mt. Tsukuba demonstrated a strong positive correlation between the concentration of ^{137}Cs in SS fractionated by particle size and the organic matter content (Ignition loss) in the relatively coarse fraction (62 μm to 1 mm) (see Figure 3). This finding suggests that particulate organic matter (POM) derived from forest litter functioned as a transport medium for radiocesium. Furthermore, ^{137}Cs contained in POM accounted for at least 15-35% of the ^{137}Cs runoff load at the peak of rainfall-runoff. Given that POM is the initiating factor in the decay chain, POM may have a significant impact on the contamination of ecosystem in downstream water bodies. Consequently, a comprehensive investigation into the behaviour of radiocesium through POM is imperative.

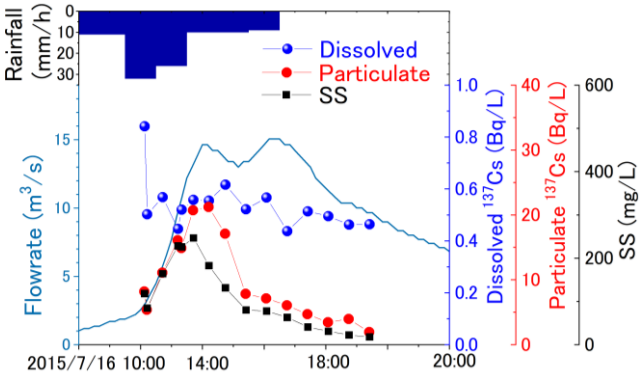


Fig.2 Changes in ^{137}Cs concentrations in the upstream of the Ohta River during a rainfall event [6].

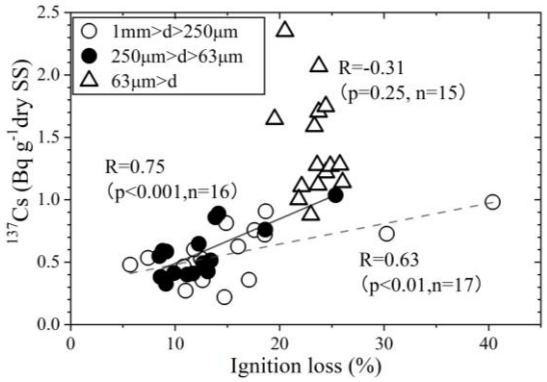


Fig.3 Relationship between ^{137}Cs and organic matter content in each of fractionized SS.

4 Future Issues

A survey by the Forestry Agency found that a lot of radioactive cesium in forested areas after the FDNPP accident was in the litter layer for about a year. This likely led to the transfer of radioactive cesium to downstream waters, mainly during rainfall runoff, in the form of dissolved and POM. However, there are few cases of runoff behaviour from forested areas being investigated after the accident, and we don't know how it behaved. It is imperative to elucidate how radioactive cesium behaved in the litter layer and reconstruct how the runoff field changed during the early post-accident period using detailed, accurate numerical simulations. This will help us review the transfer behaviour of radioactive materials from forested areas after the Fukushima nuclear plant accident and propose ways to control the transfer in river systems in the early stages of future nuclear disasters.

ACKNOWLEDGMENTS

This research was partially supported by a grant-in-aid for scientific research (JSPS KAKENHI Grant Number JP16H01791).

References

[1] Y. Morino et al. Geophysical Research Letters, 38, L00G11. (2011).
[2] T. Manaka et al. Journal of Environmental Radioactivity, 251–252, 106967 (2022).
[3] H. Tsuji et al. Journal of Radioanalytical and Nuclear Chemistry, 303, 1803–1810 (2014).
[4] S. Iwagami et al. Journal of Environmental Radioactivity, 166, 466–474 (2016).
[5] S. Hayashi et al. Journal of Hydrology: Regional Studies. 41, 101099 (2022).
[6] H. Tsuji et al. Journal of Geophysical Research: Biogeosciences, 121, 2588–2599 (2016).

Copyright on 7th Asia-Pacific Symposium on Radiochemistry 2025 - P3-01 -

TREND OF CS-137 IN LEAVES, BRANCHES, AND TREE RINGS OF FIR (*Abies firma*) IN ISHINOMAKI AREA OF MIYAGI PREFECTURE, JAPAN

M. Fukushima[1], T. Matsutani[1], T. Nemoto[1], K. Yoda[1], A. Chatt[2]

[1]*Ishinomaki Senshu University: 1 Minamisakai, Ishinomaki Miyagi, 986-8580 Japan, neko.fukusima@gmail.com*
[2]*Dalhousie University, Canada*

On 2011.03.11 an earthquake of magnitude 9.0 struck the North East coast, mainly Iwate, Miyagi and Fukushima prefectures, of the Main Island of Japan. This earthquake induced a huge Tsunami which in turn led to the serious accidents at Fukushima Daiichi nuclear power reactors. Our university is located in the Ishinomaki city of Miyagi Prefecture, which is about 99 km NNE of the Fukushima Daiichi nuclear power reactors. Although Iwate, Miyagi and Fukushima prefectures are located next to one other from north to south, the contamination was generally not so serious in the first two areas. We started a program of monitoring ^{137}Cs in tree leaves, plants, soils, sea water, and sediments of Oshika Peninsula in 2012 June. After the investigation of the collection efficiency for ^{137}Cs, we have chosen Fir for further extensive monitoring. We found radioactivity of ^{137}Cs in budded leaves and branches of Fir even after 6 yeas have passed from Fukushima Daiichi Accident. We found activities of ^{137}Cs were accumulated in the core part of trunk.

1 INTRODUCTION

Levels of radioactive Cs in Miyagi Prefecture are not high comparing the southern next Fukushima Prefecture. Radioactive plume was thought to pass through Oshika Peninsula (Fig. 1). We started a monitoring ^{137}Cs in environmental samples in Oshika Peninsula in 2012 June, and chose Japanese Fir (*Abies firma*) for further extensive monitoring. We have measured ^{137}Cs and ^{40}K in leaves and small branches of Fir trees cut in 2013, 2014 and 2017. Tree rings of Fir tree, which was supposed to fall down during the period of 2013 November – 2014 March, were striped from log and measured the radioactivity of ^{137}Cs and ^{40}K to find the accumulation position of ^{137}Cs .

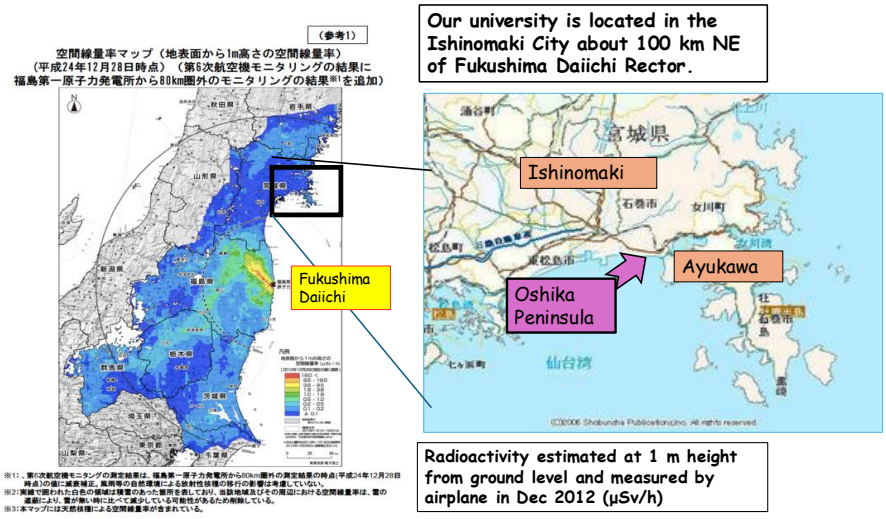


Fig. 1. Maps of Radioactivity within 200 km from Fukushima Daiichi and Oshika Peninsula, Miyagi Pref.

2. EXPERIMENTS

Fir (*Abies firma*) is evergreen tree and we can find them in natural forest in Miyagi Prefecture. Commonly it has corns at the top of branch and bud three new branches in April-May (Fig. 2). Our idea was that Fir needles keep the past ^{137}Cs contamination condition in old branches. For measuring ^{137}Cs, several branches were cut from these trees three times (2013, 2014, and 2017) during 2012 June - 2017 March, and leaves and small branches were separated from one another according to the budding year, freeze dried, and pulverized in a mill. Thus obtained dried powder was doubly sealed in polyethylene bags and placed in polyethylene counting bottles. From branches cut from two fir trees in 2017 March, leaves and small branches were separated each other according to the budding year; 2009 – 2016. Tree rings were striped from log of Japanese Fir which was fallen during the period of 2013 November – 2014 March and

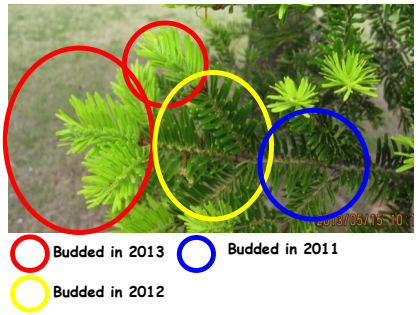


Fig. 2. Photo of Fir leaves (needles) in May 2013.

approximate age was 62 years by counting tree rings. Tree rings were separated each other according to year till 1975, small chips were freeze tried, then placed in polyethylene counting bottles.

3. RESULTS

Mean values of radioactivity of ^{137}Cs were 20.3 – 30.9, and 21.5 – 34.0 Bq/kg, DW, as for leaves and small branches budded 2012 – 2015, respectively. Also, even after 5 years have passed after Fukushima Daiichi Accident in 2011, mean values of ^{137}Cs were 36.8 and 69.8 Bq/kg, DW in all leaves and small branches budded in 2016, respectively. Levels of 137Cs in tree rings changed from 1.7 ± 3.1 (2011) to 41.5 ± 7.6 Bq/kg, DW (2006) depending on the year, and rather high levels of ^{137}Cs were found in core part of trunk. Results mean ^{137}Cs has migration system within fir tree, and accumulated in the core part of trunk.

ACKNOWLEDGMENT

We would like to thank Dr. K. MASUMOTO (KEK), Dr. T. OHTSUKI (Tohoku University, Kyoto University), Dr. H. KIKUNAGA (Tohoku Univeristy) for their support for measuring image by autoradiography and radioactivity.

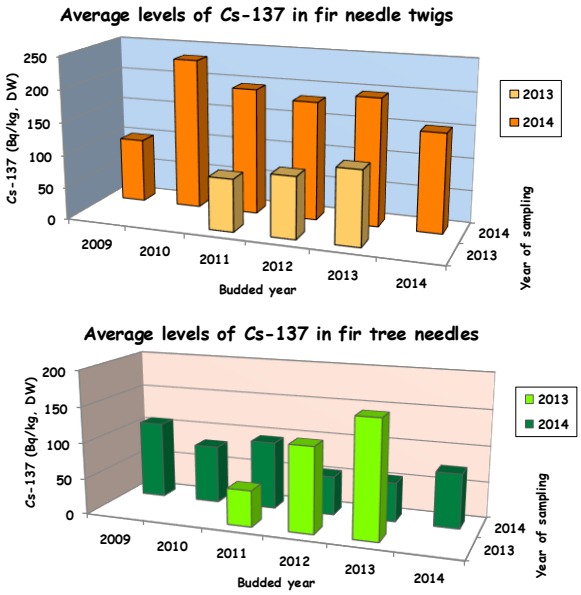


Fig. 3. Average levels of Cs-137 in Fir needle twigs and tree needles collected in 2013 and 2014.

7th Asia-Pacific Symposium on Radiochemistry *September 14 ~ 19, 2025 • Kunibiki Messe • Shimane, Japan*

Increase in dissolved Cs-137 concentration in bottom water layer at summer stratification from a mountainous lake, Lake Akagi-Konuma in Gunma Prefecture, Japan

Seiya Nagao[1], Shinji Otori[2], Kanako Shiozawa[3], Takashi Akutsu[4], Kyuma Suzuki[5], Shinya Ochiai[6]

[1] *Institute of Nature and Environmental Technology, Kanazawa University. Nomi, Ishikawa 923-1224, Japan. nagao37@staff.kanazawa-u.ac.jp*
[2] *Graduate School of Nature and Environmental Technology, Kanazawa University. Kakuma, Kanazawa, Ishikawa 921-1190, Japan. wangansoara@yahoo.co.jp*
[3] *Gunma Prefectural Fisheries Experiment Station, Maebashi, Gunma 371-0036, Japan. shiozawa-k@pref.gunma.lg.jp*
[4] *Gunma Prefectural Fisheries Experiment Station, Maebashi, Gunma 371-0036, Japan. akutsu-t@pref.gunma.lg.jp*
[5] *Gunma Prefectural Fisheries Experiment Station, Maebashi, Gunma 371-0036, Japan. suzuki-q@pref.gunma.lg.jp*
[6] *Institute of Nature and Environmental Technology, Kanazawa University. Nomi, Ishikawa 923-1224, Japan. sochiai@se.kanazawa-u.ac.jp*

This study conducted investigation at Akagi-Konuma, a semi-closed mountain lake with low electric conductivity (0.4-0.5 mS/m) in Gunma Prefecture, before and during summer stratification to understand the concentration level and behavior of Cs-137 in lake environments more than 10 years after the accident. As a result, the concentration of dissolved Cs-137 increased in the bottom water of the reducing environment during the summer stratification, suggesting elution from the bottom sediment.

1 Introduction

In the mountainous areas of Gunma Prefecture, Cs-137 from the Fukushima nuclear accident was deposited from the atmosphere in lakes and their drainage basin, and relatively high Cs-137 concentrations have been observed in soil, lake water, and lake bottom sediments [1-3]. In addition, it has been reported that when the bottom water transitions to a reducing environment during summer or winter stratification, the concentration of dissolved Cs-137 increases [4-5]. Therefore, understanding the concentration level and dynamics of Cs-137 in lake environments more than 10 years after the accident, that is, the elution process of Cs-137 in the bottom layer, will lead to an understanding of the environmental dynamics of radioactive cesium in freshwater lake environments, making it possible to predict reliable concentration fluctuations.

In this study, we measured the vertical distribution of dissolved and particulate phase of Cs-137 radioactivity concentrations during the summer stratification period in Akagi-Konuma, Gunma Prefecture, a semi-closed mountain lake at an altitude of 1,450 m, where the supply of radioactive cesium from the basin is limited to direct outflow from the lake basin due to rainfall and where the electrical conductivity of the lake water is about one order of magnitude lower (0.5 mS/m in surface water).

2 Materials and methods

Lake water samples were collected from the center of Lake Akagi-Konuma Lake in June 2023 and August 2024 at two points from the surface at 5 m depth intervals, and bottom water was collected 0.5 m above the bottom sediment (water depth 8.2 m) using a submersible pump. Water temperature and electrical conductivity were measured using a CTD instrument, and pH and dissolved oxygen concentration were measured for the collected water samples. The obtained lake water sample of approximately 20 L was filtered on-site using a cartridge filter with a pore size of 0.45 μm. The Cs-137 radioactivity concentration of the filtered and unfiltered samples was measured using a Ge semiconductor detector after precipitating and recovering Cs-137 using the AMP method. Samples for measuring nutrients, trace element, and major cation concentrations were also collected and analyzed after filtering using a pore size 0.45 μm membrane filter.

3 Results and discussion

Copyright on 7th Asia-Pacific Symposium on Radiochemistry 2025 - P3-03 -

In June 2023, before summer stratification, the electrical conductivity of the lake water was 0.62 mS/m in the bottom water, slightly higher than that of the surface water (0.41 mS/m), but the dissolved oxygen concentration was 7.1-8.7 mg/L. Dissolved Cs-137 was below the detection limit and mostly existed in suspended form, and was constant with depth at 10 mBq/L. On the other hand, in August 2024, during the stratification period, the electrical conductivity increased significantly to a maximum of 3.73 mS/m in the bottom water, and the NH_4^+ and Fe^{2+} ion concentrations were high at 0.44 mg/L and 5.69 mg/L, respectively. The dissolved Cs-137 concentration was also detected in the bottom water at 21.2 mBq/L. On the other hand, the particulate Cs-137 concentration was almost constant with depth at about 20 mBq/L. The concentration of Cs-133, which is thought to be due to ion exchange with Cs-137, increased 1.7-fold in the bottom water, and K^+ ions increased 2.8-fold in the surface water, but these concentrations were lower than those of NH_4^+ ions. These results suggest that the increase in dissolved Cs-137 concentration during the summer stratification period in Akagi-Konuma may have been caused by the addition of Cs-137 released by microbial decomposition of organic matter in the bottom sediment and Cs-137 eluted by ion exchange reactions with NH_4^+ ions in the bottom water that had shifted to a reducing environment.

References

[1] S. Nagao, M. Kanamori, S. Ochiai, K. Suzuki and M. Yamamoto “Dispersion of Cs-134 and Cs-137 in river waters from Fukushima and Gunma prefectures at nine months after the Fukushima Daiichi NPP accident,” *Progress in Nuclear Science and Technology*, **4**, 9 (2014).

[2] S. Aizawa, M. Mori, Y. Koike and K. Tsunoda “Radioactive cesium precipitated in Lake Onuma of Mt. Akagi emitted by the Fukushima Daiichi Nuclear Power Plant accident,” *BUNSEKI KAGAKU*, **66**, 271 (2017).

[3] M. Mori, K. Tsunoda, S. Aizawa, Y. Saito, Y. Koike, T. Gonda, S. Abe, K. Suzuki, Y. Yuasa, T. Kuge, H. Tanaka, H. Arai, S. Watanabe, S. Nohara, Y. Minai, Y. Okada and S. Nagao “Fractionation of radiocesium in soil, sediments, and aquatic organisms in Lake Onuma of Mt. Akagi, Gunma Prefecture using sequential extraction,” *Science of the Total Environment*, **575**, 1247 (2017).

[4] K. Suzuki, Y. Onozeki (Yuasa), H. Tanaka, E. Matsuoka, T. Kuge, K. Tsunoda, S. Aizawa, M. Mori, S. Nohara, Y. Minai, Y. Okada and S. Nagao “Estimation of the biological half-life of radioactive cesium in wakasagi *Hypomesus nipponenisis*,” *Nippon Suisan Gakkaishi*, **82**, 774 (2016).

[5] K. Suzuki, S. Watamabe, Y. Yuasa, Y. Yamashita, H. Arai, H. Tanaka, T. Kuge, M. Mori, K. Tsunoda, S. Nohara, Y. Iwasaki, Y. Minai, Y. Okada and S. Nagao “Radiocesium dynamics in the aquatic ecosystem of Lake Onuma on Mt. Akagi following the Fukushima Dai-ichi Nuclear Power Plant accident,” *Science of the Total Environment*, **622**, 1153 (2018).

Copyright on 7th Asia-Pacific Symposium on Radiochemistry 2025

Contributed Talk | [R2]Radioanalytical Chemistry and Nuclear Forensics

Thu. Sep 18, 2025 9:45 AM - 10:45 AM JST | Thu. Sep 18, 2025 12:45 AM - 1:45 AM UTC Hall A(MP)

[R2] Radioanalytical Chemistry and Nuclear forensics

9:45 AM - 10:05 AM JST | 12:45 AM - 1:05 AM UTC

[R2-05]

FROM SPECIATION TO SIGNATURE DISCOVERY: INTEGRATED APPROACHES IN THE CONSORTIUM FOR NUCLEAR FORENSICS

*Ken Ronald Czerwinski[1] (1. University of Nevada, Las Vegas (United States of America))

10:05 AM - 10:25 AM JST | 1:05 AM - 1:25 AM UTC

[R2-06]

VERIFICATION OF THE SEGMENTATION APPROACH IN PARTICLE SHAPE MEASUREMENT FOR ELECTRON MICROSCOPE IMAGE ANALYSIS - APPLICATION IN NUCLEAR FORENSICS

*Yoshiki Kimura[1], Tetsuya Matsumoto[2], Yuichi Kijima[1], Yutaka Tomita[1] (1. Japan Atomic Energy Agency (Japan), 2. Power Computer (Japan))

10:25 AM - 10:45 AM JST | 1:25 AM - 1:45 AM UTC

[R2-07]

Study of Rapid Analysis Methods for Pu Isotopes in Atmospheric Particulate Matter Samples

*Yang Shao[1], Lingling Ma[1], Ziao Li[1], Futao Xin[1] (1. Institute of High Energy Physics, Chinese Academy of Sciences (China))

©APSORC25

7th Asia-Pacific Symposium on Radiochemistry *September 14 ~ 19, 2025 • Kunibiki Messe • Shimane, Japan*

FROM SPECIATION TO SIGNATURE DISCOVERY: INTEGRATED APPROACHES IN THE CONSORTIUM FOR NUCLEAR FORENSICS

Ken Czerwinski

Radiochemistry Program, University of Nevada Las Vegas 4505Maryland Parkway, Las Vegas, NV USA 89154-4009

The identification and interpretation of nuclear forensic signatures are critical to attributing the origin and history of nuclear materials. A powerful approach to improving these capabilities lies in the use of radionuclide and radioelement speciation, which provides detailed chemical information on oxidation state, coordination, molecular structure, and trace composition. Speciation offers practical advantages in sample preparation and separation, reducing time-to-result for isotope identification and enabling more targeted analyses. This methodology forms the basis for molecular nuclear forensics, a growing field that leverages spectroscopic, microscopic, and compositional techniques to extract signatures related to synthesis conditions, material origin, and processing history. Examples of this approach include speciation studies of plutonium-containing particles and uranium oxides, where synchrotron-based spectroscopy and electron microscopy were used to reveal chemical form, morphological features, and trace element distributions, each providing insight into material provenance and production pathways.

Recognizing the scientific value and strategic importance of such work, the U.S. Department of Energy's National Nuclear Security Administration (NNSA) supports the Consortium for Nuclear Forensics (CNF). This multidisciplinary initiative brings together 16 universities and 7 U.S. National Laboratories to advance nuclear forensics through integrated research, education, and training. The CNF is structured into five Thrust Areas (TAs), Rapid Turnaround Forensics, Advanced Analytical Methods, Ultrasensitive Measurements, Signature Discovery, and Prompt Effects and Measurements, supported by cross-cutting themes in High-Performance Computing/Data Science and Workforce Development. These thematic pillars foster innovation in both science and technology while building the technical community essential for sustaining long-term nuclear forensic capabilities.

Within CNF, collaborative projects link academic and laboratory investigators in joint research that strengthens technical depth and enhances training. Undergraduate and graduate students engage directly with national laboratory scientists through internships, extended site visits, and mentorship, ensuring experiential learning aligned with current mission needs. CNF faculty and students also benefit from formal academic-laboratory integration, including participation on dissertation committees and coordinated research planning. International engagement is an additional cornerstone of CNF’s mission, with partnerships being pursued with global institutions such as the Atomic Weapons Establishment, fostering bilateral research, information exchange, and the development of harmonized methods in nuclear forensics.

Through this combination of speciation science, interdisciplinary collaboration, and strategic partnerships, the Consortium for Nuclear Forensics represents a transformative effort to enhance national and global capabilities in nuclear material attribution. It establishes a foundation for scientific innovation while ensuring the growth of a technically proficient, globally connected workforce prepared to address emerging threats and opportunities in the nuclear domain.

Copyright on 7th Asia-Pacific Symposium on Radiochemistry 2025 - R2-05 -

7th Asia-Pacific Symposium on Radiochemistry *September 14 ~ 19, 2025 • Kunibiki Messe • Shimane, Japan*

VERIFICATION OF THE SEGMENTATION APPROACH IN PARTICLE SHAPE MEASUREMENT FOR ELECTRON MICROSCOPE IMAGE ANALYSIS - APPLICATION IN NUCLEAR FORENSICS

Yoshiki Kimura[1], Tetsuya Matsumoto[2], Yuichi Kijima[1], Yutaka Tomita[1]

[1]*Japan Atomic Energy Aency: 2-4 Shirakata, Tokai-mura, Ibaraki, 3191195, kimura.yoshiki@zc.iir.isct.ac.jp*
[2]*Power Computer: 4-4-13 Ninomiya, Tsukuba, Ibaraki, 3050051, matsumoto.tetsuya@jaea.go.jp*

Morphological features such as particle shape distributions have been used as one of the nuclear forensics signatures for sample comparisons. This paper discussed the reproducibility of particle shape measurements by comparing different segmentation approaches for the particle shape measurement from electron microscope images by computer image analysis.

1 INTRODUCTION

Nuclear forensics analysis is a technical means to identify the origin and intended use of nuclear and other radioactive materials out of regulatory control by the measurement and interpretation of material characteristics called nuclear forensics signatures. A toolbox of various analytical tools is essential to obtain confident and timely results in nuclear forensics analysis. Morphological characteristics captured by optical and electron microscopes are used as one of the important nuclear forensics signatures [1, 2]. In order to obtain confident findings in the morphological analysis for nuclear forensics, it is necessary to address the issues that can lead to inaccurate or inconsistent results, such as reproducibility and human error. In recent years, several efforts have been made to quantitatively characterize the particle shape and surface patterns obtained from microscopic images using computer image analysis [3, 4]. In these methods, it has been pointed out that sample preparation, image acquisition conditions, and computer image analysis can cause variation in the analytical results [5]. One of the major challenges in the particle shape measurement from microscopic images is the segregation of overlapping particles. Since it is difficult to eliminate the overlapping in the sample preparation process, it is necessary to separate them by image processing, but this can cause additional variation. This paper discussed the reproducibility of particle shape measurements by comparing different segmentation approaches for the particle shape measurement from electron microscope images by computer image analysis.

2 MATERIALS AND METHODS

The scanning electron microscope images of UOC powder-certified reference materials (UCHI-1, UCLO-1, and UPER-1) [6-8] were used in this study. The investigated samples consist of two U_3O_8 (UCHI-1 and UCLO-1) and a UO_4 (UPER-1). They were respectively produced by their own defined synthesis process, which ensures their uniformity. A methodology for particle shape measurement of powder samples developed for nuclear forensics analysis was used [9]. Sample holders were prepared for each material in the UOC for image acquisition using SEM. Particle images were acquired at ×750 magnification using the secondary electron image mode of the *JCM-6000Plus NeoScope (JEOL Ltd.)*. A *Pelcotec G-1* silicon standard from *AISthesis Products* was used to calibrate the magnification. 15 images with 1280 × 960 pixel acquired from each sample holder were used for particle size measurement. The particle size of each sample was measured using the particle analysis program in *ImageJ* [10]. There are several particle shape descriptors that differ depending on the measurement method, but in this method, the equivalent circular diameter (ECD), circularity, and fitted ellipse aspect ratio were compared.

Three different methods were used to clean-up the overlapping particles observed in the SEM images. The first one was manual segmentation by human eyes, the second one was semi-automatic segmentation based on particle boundary detection using the Watershed function in the *OpenCV* [11] package, and the third one was semantic segmentation based on deep learning models. Segmentation by boundary detection using the Watershed is employed in the *MAMA* software [12] widely used in nuclear forensics analysis. Because the results of the clean-up would differ depending on the different users in the case of the manual and semi-automatic segmentation, the clean-up process was made independently by two different users. After the clean-up of overlapping particles using individual approach, the SEM images were pre-processed using the following procedures before particle size measurement: removal of noise or dust particles less than 4 pixels, and binarization. These pre-processing was made using the image processing program in the *ImageJ* software.

3 PRELIMINARY RESULTS AND DISCUSSIONS

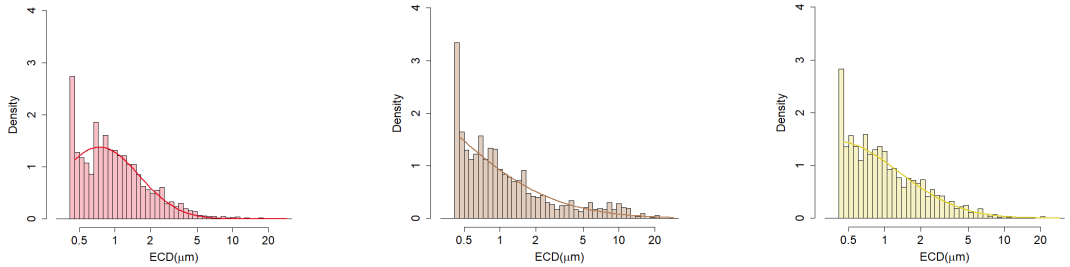
Copyright on 7th Asia-Pacific Symposium on Radiochemistry 2025 - R2-06 -

In preliminary results of particle shape measurements on SEM images prior to cleanup of overlapping particles (Table 1), it was observed that UCHI-1 has a relatively large mean and variance in ECD compared to the other two samples. The difference in the ECD is likely due to a greater abundance of particles larger than 5 µm in the samples from UCHI-1, as can be seen in Fig.1. The largest frequency at the minimum class interval (<0.5µm) observed in all of the three samples indicates that the size of particles smaller than that interval cannot be distinguished by image analysis at ×750 magnification. By fitting the measured size distribution with log-normal function and excluding the minimum class interval, it can be observed that all of the three powders have a similar size distribution centered around 1µm and only UCHI-1 has another small distribution centered around 10µm.

As mentioned earlier, the present method for particle shape measurement was originally developed to use the particle shape parameters as nuclear forensics signature. The results obtained using this measurement showed that particle size distribution can contribute to the discrimination of different UOC samples in nuclear forensics analysis and is likely to be one of effective approach for that purpose, but the reproducibility of the measurement by SEM image analysis needs to be verified. This paper will discuss this issue in the future by comparing the measurement results for SEM images cleaned up by the different segmentation approaches.

TABLE 1. Statistics of measured ECD and shape descriptors of UOC particles.

Sample	Particles	ECD (µm)		Circularity		Aspect ratio	
		mean	σ	**mean**	**σ**	**mean**	**σ**
UCLO-1	2402	1.2998	1.3113	0.853	0.173	1.424	0.384
UCHI-1	1309	1.8968	2.7491	0.789	0.232	1.504	0.458
NPER-1	2246	1.4402	1.7507	0.854	0.193	1.424	0.384



(a) UCLO-1 (b) UCHI-1 (c) UPER-1

Fig. 1. UOC powder particle size distribution in ECD histograms. Note that in density, lines show log-normal functions fitted by excluding the minimum class intervals.

ACKNOWLEDGMENTS

This work was supported by the Ministry of Education, Culture, Sports, Science and Technology (MEXT) of Japan.

References

[1] V. FEDCHENKO, *New Nuclear Forensics*, Oxford University Press, Harvard, Vancouver (2015).
[2] E. KEEGAN, M.J. KRISTO, M. COLELLA et al, *Forensic Sci. Int.*, **240**,111-121 (2014).
[3] A.L. TAMASI, L.J. CASH, C. ELEY, et al., *J Radioanal Nucl Chem*, **307**, 1611–1619 (2016).
[4] L. FONGARO, D.M. HO, K. KVAAL, et al., *New perspective in nuclear forensics*, Talanta. **152,** 463-474 (2016).
[5] NATIONAL RESEARCH COUNCIL CANADA, DOI 10.4224/crm.2020.uchi-1 (2020).
[6] A. ROSS, R. KIPS, Y. KIMURA et al., LLNL-CONF-826125 (2021).
[7] NATIONAL RESEARCH COUNCIL CANADA, DOI 10.4224/crm.2020.uclo-1 (2020).
[8] NATIONAL RESEARCH COUNCIL CANADA, DOI 10.4224/crm.2020.uper-1 (2020).
[9] Y. KIMURA, N. SHINOHARA, T. MATSUMOTO, *Progress Nucl. Sci. Tech.*, 5, 188-191 (2018).
[10] C.A. SCHNEIDER, W.S. RASBAND, K.W. ELICEIRI, *Nature Methods*, **9(7)**, 671-675 (2012).
[11] G. BRADSKI, *Dr. Dobb's Journal of Software Tools* (2000).
[12] B.K. GASCHEN, J.J. BLOCH, R. PORTER, et al., LA-UR-16-25116 (2016).

Copyright on 7th Asia-Pacific Symposium on Radiochemistry 2025 - R2-06 -

Study of Rapid Analysis Methods for Pu Isotopes in Atmospheric Particulate Matter Samples

Yang Shao, Lingling Ma, Ziao Li, Futao Xin

Institute of High Energy Physics, Chinese Academy of Sciences, 19B Yuquan Road, Shijingshan District, Beijing, China, 100049, shaoyang@ihep.ac.cn, malingling@ihep.ac.cn, liziao@ihep.ac.cn, xinft@ihep.ac.cn

1 Introduction

During the application of nuclear energy, a large number of radionuclides such as uranium and plutonium are released into the environment due to human activities such as nuclear weapon tests, nuclear power plant accidents, nuclear waste reprocessing and satellite disintegration. The released radionuclides have long half-lives and high chemical toxicity and receive great concern in environmental safety evaluation, geological disposal of nuclear waste and biological effects. The isotopic ratios of uranium and plutonium have significant application value in nuclear emergencies and accidents, including identifying the sources of nuclear materials, assessing the severity of incidents, monitoring the spread of contamination, supporting emergency decision-making, and researching accident mechanisms. These analytical results provide crucial scientific evidence for the response to and management of nuclear accidents.

For most environmental samples, traditional strong acid digestion is currently the most commonly used method. In nuclear emergencies, nuclear accidents, and even nuclear forensics situations, traditional methods are not applicable, as they are too complex and time-consuming to meet the demand for quickly obtaining fingerprint characteristics and conducting source tracing analysis. Therefore, a rapid and accurate method is needed to enhance sample processing efficiency, thereby assisting the governor in addressing these dangerous situations.

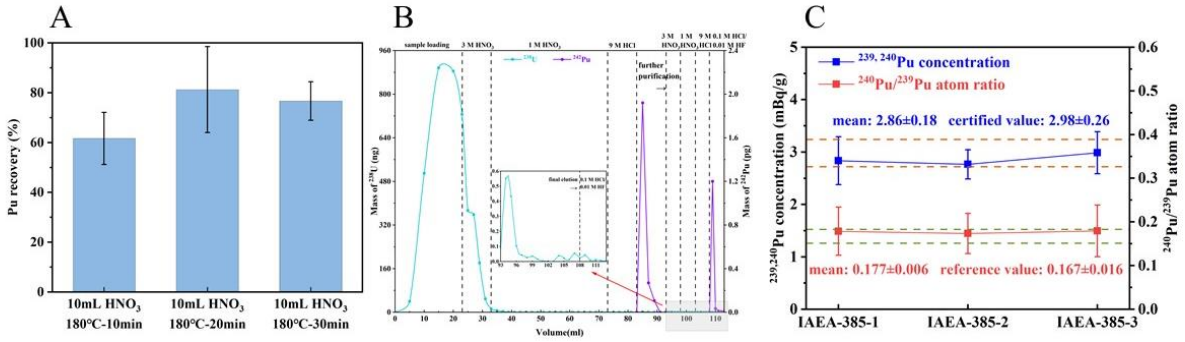
2 The rapid method for determination of ultra-trace level Pu isotopes in atmospheric particulate matter samples

2.1 Experiment

The atmospheric particulate matter samples were ashed in a muffle furnace at 450 ℃ for 8 hours and microwave digested with 10 mL concentrated HNO_3 for 20 minutes. After dilution, $TiCl_3$, Ca, La and HF were added to the sample solution. After centrifugation, the precipitate was reserved and dissolved in 20 mL 3 M HNO_3, and $NaNO_2$ was added to adjust the valence state to Pu (IV). A 2 mL TEVA resin was first used to primary purification and plutonium was eluted with 10 mL 0.1 M HCl/0.01 M HF. For further purification of Pu fraction, a second TEVA resin (0.5 mL) was used to remove U from Pu. Finally, Pu was collected in a PFA vessel by eluting the resin with 5 mL 0.1 M HCl/0.01 M HF. The sample was evaporated to dryness and dissolved in 1 mL 2 % HNO_3 and prepared for SF-ICP-MS measurements.

2.2 Results

Fig 1(A) shows results of microwave digestion optimization, with Pu recovery of higher than 80 % in 10 mL HNO_3-180 ℃-20 min, which is more efficient than strong acid digestion. Fig 1(B) shows the purification effect of TEVA resin. About 81.3 % of Pu was recovered after the separation of a 2 mL TEVA resin and a 0.5 mL TEVA resin. The concentration of ^{238}U in the final elution was 19.6 ppt, corresponding to the DF(U) to be 4.1×10^4. Fig 1(C) shows the results of simulated atmospheric particulate matter sample using IAEA 385. The $^{239, 240}Pu$ activity concentrations and $^{240}Pu/^{239}Pu$ atom ratios were all fall into the certified values, indicating the practicability of the developed method. The developed method enables the analysis of Pu in atmospheric particulate matter within 16 hours with high Pu recovery (80~90%)



Copyright on 7th Asia-Pacific Symposium on Radiochemistry 2025 - R2-07 -

Fig. 1. Rapid analysis method optimization for Pu isotopes in atmospheric particulate matter. (A), microwave digestion optimization; (B), TEVA resin elution; (C) method validation with simulated sample using IAEA 385.

3. CONCLUSIONS

The developed methods can be directly utilized in nuclear emergency response, rapid monitoring, and tracing in nuclear forensics, where rapid analysis and high-precision measurement of Pu isotopes are required for environmental samples, including soil, sediment, and atmospheric particulate matter.

ACKNOWLEDGMENTS

The authors are grateful to the financial support from the National Natural Science Foundation of China (Grant Numbers: 12105311)

References

[1] F. XIN, M. Luo, C. Li, L. Ma, D. Xu, G. Xu, X. Li, Y. Shao, "A rapid method for determination of ultra-trace level Pu isotopes in atmospheric particulate matter samples using SF-ICP-MS and TEVA resin", *J RADIOANAL NUCL CH*, 10.1007/s10967-025-10126-x

[2] Y. Shao, J. ZHANG, M. Luo, D. Xu, L. Ma, "A Review of Anthropogenic Radionuclide ^{236}U: Environmental Application and Analytical Advances", *J ENVIRON RADIOACTIV*, **251-252**, 106499 (2022).

[3] X. Liu, Y. Shao, M. Luo, L. Ma, G. Xu, M. Wu, "Progress of the Analytical Methods and Application of Plutonium Isotopes in the Environment", *Processes*, **11**, 1430 (2023).

Contributed Talk | [R2]Radioanalytical Chemistry and Nuclear Forensics

Thu. Sep 18, 2025 11:00 AM - 11:40 AM JST | Thu. Sep 18, 2025 2:00 AM - 2:40 AM UTC Hall A(MP)

[R2] Radioanalytical Chemistry and Nuclear forensics

11:00 AM - 11:20 AM JST | 2:00 AM - 2:20 AM UTC

[R2-08*]

Development of Graphene–Macrocycle Hybrid Nanomaterials and Its Application to Cesium Separation

*Jiawei Xu[1], Naokazu Idota[2], Takehiko Tsukahara[1,2] (1. Department of Materials Science and Engineering, Institute of Science Tokyo (Japan), 2. Laboratory for Zero-Carbon Energy, Institute of Integrated Research, Institute of Science Tokyo (Japan))

11:20 AM - 11:40 AM JST | 2:20 AM - 2:40 AM UTC

[R2-09]

Decontamination of contaminated Raspberry Pi module as a surrogate for sensitive electronics by Cyber Clean® Putty

*Zakir Kazi[1], Jaleh Semmler[2], Tim Munsie[1] (1. Defence Research & Development Canada (DRDC) (Canada), 2. Canadian Nuclear Laboratories (CNL) (Canada))

©APSORC25

7th Asia-Pacific Symposium on Radiochemistry *September 14 ~ 19, 2025 • Kunibiki Messe • Shimane, Japan*

Development of Graphene–Macrocycle Hybrid Nanomaterials and Its Application to Cesium Separation

Jiawei Xu[1], Naokazu Idota[2], Takehiko Tsukahara[1,2]

[1]*Department of Materials Science and Engineering, Institute of Science Tokyo*
[2]*Laboratory for Zero-Carbon Energy, Institute of Integrated Research, Institute of Science Tokyo, 2-12-1-N1-6, Ookayama, Meguro-ku, Tokyo, 152-8550*

Isotopic analysis of $^{135}Cs/^{137}Cs$ ratios provides valuable insights into the environmental behavior of cesium, which is critical for the decommissioning of nuclear-related facilities. However, conventional methods are limited by labor-intensive chemical procedures and the generation of secondary waste. In this study, we developed a novel graphene–macrocycle hybrid nanomaterial to enable rapid and efficient adsorption of cesium ions (Cs^+) and direct detection of cesium isotopic ratios. The hybrid material (BOB-GNPs) was synthesized by intercalating a macrocyclic calix compound (BOB) into graphene nanoplatelets (GNPs) and was characterized using various spectroscopic techniques. Cs^+ adsorption experiments under different solution conditions were conducted, and adsorption performance was evaluated by fluorescence X-ray analysis (XRF) mapping. The results demonstrated that BOB-GNPs exhibited excellent Cs^+ adsorption capabilities, which varied depending on the BOB-to-GNPs ratio. Furthermore, an inverse relationship was observed between the GNP content and crystallinity in the BOB-GNPs adsorbents.

1. Introduction

A substantial amount of highly radioactive cesium, including ^{134}Cs ($T_{1/2}$ = 2.1 y), ^{135}Cs ($T_{1/2}$ = 2.3 × 10^6 y), and ^{137}Cs ($T_{1/2}$= 30.2 y), has been released into the environment not only by nuclear accidents, such as those at Chernobyl and Fukushima, but also by global fallout from nuclear weapon tests and chronic releases from nuclear facilities during normal operation. To facilitate the decommissioning of nuclear facilities, it is essential to verify that the surrounding environment is safe without requiring further radiation control measures. The measurement of cesium isotopic ratios is a key tool for this purpose, as the isotopic signatures vary depending on the contamination source. Specifically, the $^{135}Cs/^{137}Cs$ ratios are approximately 2.62 for global fallout, 0.52 for the Chernobyl accident, and 0.35 for the Fukushima accident [1]. Conventional determination of cesium isotopic ratios in environmental samples, such as soil, typically involves chemical separation techniques (e.g., solvent extraction and chromatography) combined with mass spectrometric analyses (e.g., ICP-MS and TIMS). However, these methods are often hindered by labor-intensive operations, long processing times, and the generation of large amounts of secondary waste. Therefore, the development of novel separation methods that enable rapid and selective recovery of Cs^+ ions from complex radioactive matrices is highly desirable. Calix[4]arene derivatives, particularly Calix[4]arene-bis(t-octylbenzo-18-crown-6) (BOBCalix6), are known for their high Cs^+ selectivity due to the size-matching between Cs^+ and the crown ether cavity [2]. Moreover, macrocyclic compounds with benzene rings can interact with graphene layers via π–π interactions [3]. Based on these insights, we designed a novel hybrid nanomaterial by intercalating BOBCalix6 (BOB) between graphene nanoplatelets (GNPs), aiming to create a solid-state adsorbent (BOB-GNPs) that allows rapid and effective Cs^+ adsorption and enables direct detection of cesium isotopic ratios. The conceptual diagram of BOB-GNPs is shown in Fig. 1. In this study, we synthesized and evaluated the separation performance of the BOB-GNPs.

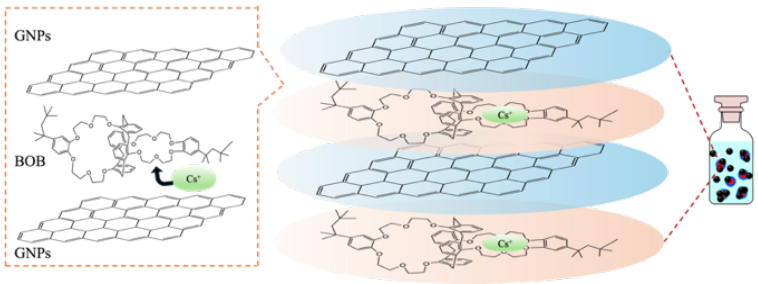


Fig. 1. Conceptual illustration of BOB-GNPs

2. Experimental

A 0.01 M solution of BOB in 1-octanol was prepared, and GNPs were added at mass ratios of 1, 10, 20, and 50. After agitation at room temperature for 1 hour, the mixtures were left to stand overnight for sedimentation. The

Copyright on 7th Asia-Pacific Symposium on Radiochemistry 2025- R2-08* -

precipitates were collected, dried, and designated as BOB-GNPs-1, BOB-GNPs-2, BOB-GNPs-3, and BOB-GNPs-4 according to the BOB-to-GNP mass ratio. The structures and compositions of the synthesized BOB-GNPs were characterized by attenuated total reflection infrared spectroscopy (ATR-IR), Raman spectroscopy (Raman), scanning electron microscopy (SEM), Thermogravimetry-Differential Thermal Analysis (TG-DTA) and X-ray diffraction (XRD). Cs^+ adsorption experiments were carried out by immersing the samples in 1 M HNO_3 under agitation for three days at room temperature. The Cs^+-adsorbed solids were then analyzed by X-ray fluorescence (XRF) to evaluate their adsorption performance.

3. Results and Discussion

ATR-IR and Raman measurements showed that the synthesis of BOB-GNPs compounds was succeeded. From SEM images, it was observed that the microscopic layer thickness of BOB-GNPs increased with increasing BOB contents. The contents of each component in BOB-GNPs could be confirmed by TG-DTA. In addition, from XRD spectra of the samples, we found that the crystallinities of BOB-GNPs increased with decreasing amounts of GNPs.

XRF measurements were conducted on the recovered solutions after the Cs^+ adsorption experiments to evaluate the adsorption performance of BOB-GNPs samples. The Cs^+ concentrations were quantified by analyzing the pixel intensities of Cs signals in the XRF mapping images which is shown in Fig. 2. The results clearly indicated that BOB-GNPs exhibited significant Cs^+ adsorption abilities, with the adsorption efficiencies varying depending on the BOB-to-GNP ratio. Among the samples, BOB-GNPs-1 showed the highest Cs^+ adsorption, while BOB-GNPs-4 exhibited the lowest. In addition, a linear relationship was observed between the amount of GNPs and the crystallinity of the BOB-GNPs adsorbents. In contrast, no significant Cs^+ adsorption was observed for BOB or GNPs alone.

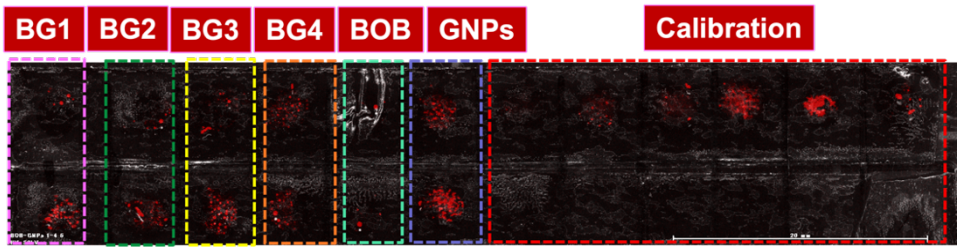


Fig. 2. XRF mapping images

4. Conclusions

A novel Cs^+ adsorbent was prepared by intercalating a macrocyclic calix compound (BOB) into graphene nanoplatelets (GNPs) and characterized using spectroscopic techniques. An XRF mapping method was also established to directly quantify Cs^+ adsorption on the solid BOB-GNPs. The BOB-GNPs exhibited high Cs^+ uptake, with adsorption capacities varying according to the BOB-to-GNP ratio.

ACKNOWLEDGMENTS

This work was financially supported by the Secretariat of the Nuclear Regulation Authority, Japan.

References

[1] M. S. Snow, A. L. Tretbar, and R. W. Williams, “Cesium isotope ratio analysis by TIMS,” *International Journal of Mass Spectrometry*, 381–382, 17–24 (2015).
[2] B. C. Russell, J. T. Trevors, and M. A. Frisch, “Analysis of cesium isotopes in environmental samples,” *Analytical Chemistry*, 86, 11890–11896 (2014). [3]M. P. BROWN and K. AUSTIN, “With or Without Title of Paper,” *Title of Journal*, **36**, 102 (2024).
[3] A. A. Kadam, J. Lee, and D. S. Lee, “Graphene-based composite materials for cesium ion removal,” *Bioresource Technology*, 216, 391–398 (2016).

Copyright on 7th Asia-Pacific Symposium on Radiochemistry 2025- R2-08* -

7th Asia-Pacific Symposium on Radiochemistry *September 14 ~ 19, 2025 • Kunibiki Messe • Shimane, Japan*

Decontamination of contaminated Raspberry Pi module as a surrogate for sensitive electronics by Cyber Clean® Putty

Zakir Kazi[1], Jaleh Semmler[2], Tim Munsie[1]

[1]*Defence Research & Development Canada: Box Number 4000, Stn Main, Medicine Hat, AB, T1A 8K6, Zakir.Kazi@drdc-rddc.gc.ca*
[2]*Canadian Nuclear Laboratory: 86 Plant Road, Chalk River, ON, Canada, K0J 1J0, jaleh.semmler@cnl.ca*

1 Introduction

Electronics are widely used in household, scientific research, and military equipment. These components can be contaminated with radioactive materials from incidents including experimental use, radiological dispersal devices, and accidental releases. The ability to decontaminate while functionally restoring operational capability is crucial for the recovery of information and reuse of the equipment. The Raspberry Pi (rPi) module, a single-board computer, was considered as a surrogate for general, sensitive electronics for decontamination studies because of its structure and affordability. It has a relatively smooth side and a rough side. Figure 1(a, b) shows photographs of a rPi circuit board. The dimensions of an rPi 3 (Model B) are approximately 8.5 cm × 5.6 cm × 2.0 cm.

Sensitive equipment, including a rPi, cannot be decontaminated by commonly used methods such as corrosive aqueous and organic based liquid decontamination products without degradation of their performance. Special treatments, such as the use of neutral/mild reagents, and a gentler approach are required for their decontamination. Cyber Clean® putty (Figure 1c), available commercially, was found to be effective for removal of radionuclide contamination. Very little secondary radioactive waste is produced from this decontamination method, which is optimal in field operational settings. The putty method was evaluated in terms of degree of contaminant removal and continued functionality post-decontamination treatment metrics.



Fig. 1. Raspberry Pi module, (a) rough-side view (left), (b) smooth-side view (middle), and (c) Cyber Clean putty in bulk (right).

1.1 Experimental Results

In a decontamination trial, rPi coupons were contaminated separately with a radionuclide solution mixture containing ^{60}Co, ^{137}Cs and ^{241}Am by nitrogen dispersion at ambient conditions (normal temperature, humidity). The radionuclide solution contained 75% methanol and 25% water. The dwell times, the time between application of the contaminant and the start of decontamination, were two and 24 hours. The contaminated modules were initially γ-counted using a CANBERRA ISOCS spectrometer. This was followed by an initial decontamination of individual modules using Cyber Clean putty (Round 1). A second γ-counting of the surfaces was carried out after the decontamination followed by a second decontamination step (Round 2). A third γ-counting of the surfaces was carried out after this second decontamination step.

There were two objectives in the trial: (1) rate of decontamination, and (2) to assess the survival for post-decontamination functionality. The rate of decontamination of the rPi modules was estimated by measuring the radioactivity before and after the decontamination. The functionality assessment methodology included assessing the system function of the rPi modules such as mouse, keyboard, HDMI connection to a monitor, SD card, USB function, and copying files/videos to USB from the rPi unit via rsync. All these functions were run and tested by a script. Functionality tests after decontamination for the modules were conducted by simulating the contamination with aqueous-methanol solutions, without the use of longer-lived radionuclides (^{60}Co, ^{137}Cs and ^{241}Am) for personal safety.

Copyright on 7th Asia-Pacific Symposium on Radiochemistry 2025 - R2-09 -

1.1.1 Results and Discussion

Decontamination efficiencies were estimated using the percentage activity removed (% AR) from the pre- and post-decontamination radioactivity measurements on rPi modules, expressed by the equation 1.

$$\%AR = \left[1 - \left(\frac{\text{Final Activity}}{\text{Initial Activity}}\right)\right] \times 100\% \qquad \text{Eq. 1}$$

Tables 1 and 2 show decontamination effectiveness (%AR) values for two tests based on sample dwell time. Table 1 shows the data for tests in which the dwell time was two hours, and Table 2 shows the data for the tests in which 24 hours dwell time was used. The rPi functionality tests for modules treated with Cyber putty resulted in 100% retainment of functionality for all the modules used.

TABLE 1. %AR values after decontamination of ^{60}Co, ^{137}Cs and ^{241}Am from the surfaces of rPi modules two hours after deposition of radionuclides (n=3)

Radionuclides	Round 1 decontamination, %	Round 2 decontamination, Cumulative %
^{60}Co	60±1	63± 2
^{137}Cs	67±3	70± 4
^{241}Am	48±2	50±3

TABLE 2. %AR values after decontamination of ^{60}Co, ^{137}Cs and ^{241}Am from the surfaces of rPi modules 24 hours after deposition of radionuclides (n=3)

Radionuclides	Round 1 decontamination, %	Round 2 decontamination, Cumulative %
^{60}Co	60±11	62±10
^{137}Cs	72±11	76±10
^{241}Am	35±7	37± 6

2. CONCLUSIONS

The objective of this work was to evaluate a decontamination method using Cyber Clean putty on rPi modules contaminated by radionuclides. This testing measured decontamination efficiency and coupon survivability. Decontamination after 24 hours of contaminant exposure resulted in an average efficiency of 60 ±11 %, 72±11 % and 35 ±7 % for ^{60}Co, ^{137}Cs and ^{241}Am, respectively. Decontamination immediately after contamination, considered to be within 2 hours of contaminant exposure, resulted in a similar efficiency for ^{60}Co, and ^{137}Cs, but ^{241}Am registered a higher decontamination, 48±2 %. Operational functionality tests for the post-decontamination rPi found 100 percent survivability. The results of these tests suggest that rPi module represents as a surrogate of electronic equipment with respect to radioactive decontamination.

Copyright on 7th Asia-Pacific Symposium on Radiochemistry 2025 - R2-09 -

Contributed Talk | [R4]Nuclear Probe in Chemistry

Thu. Sep 18, 2025 11:00 AM - 12:00 PM JST | Thu. Sep 18, 2025 2:00 AM - 3:00 AM UTC Hall S(Int'l)

[R4] Nuclear Probe in Chemistry

11:00 AM - 11:20 AM JST | 2:00 AM - 2:20 AM UTC

[R4-04]

Chemical state of Fe and electrical conduction properties of dense sintered $Sr_{1-x}Ln_xFeO_{3-\delta}$ and $SrFe_{1-x}Ln_xO_{3-\delta}$ (*Ln*: Y, lanthanoid) with cubic perovskite structure

Keina Nagai[1], Chihiro Kato[1], Taizo Yoshino[1], Ryutaro Maehara[1], Kosuke Shido[1], Takayuki Sugimoto[1], *Takuya Hashimoto[1], Fumito Fujishiro[2], Motoyuki Matsuo[3] (1. Nihon University (Japan), 2. Kochi University (Japan), 3. The University of Tokyo (Japan))

11:20 AM - 11:40 AM JST | 2:20 AM - 2:40 AM UTC

[R4-05]

Mechanism of Half-Iron Morin Transition in the Nb-Doped Hematite

*Satoru Nakashima[1], Habibur Rahman[1], Shiro Kubuki[2] (1. Hiroshima University (Japan), 2. Tokyo Metropolitan University (Japan))

11:40 AM - 12:00 PM JST | 2:40 AM - 3:00 AM UTC

[R4-06]

Preparation and ^{61}Ni Mössbauer Spectroscopy for Supramolecular Bridging Cyanide Complexes containing $[Ni(II)(CN)_4]^{2-}$ unit

*Takafumi Kitazawa[1,2], Kosuke Kitase[1], Shinji Kitao[3], Yasuhiro Kobayashi[3], Takumi Kubota[4], Makoto Seto[3] (1. Department of Chemistry, Faculty of Science, Toho Universityoho University (Japan), 2. Research Centre for Materials with Integrated Properties, Toho University (Japan), 3. Institute for Integrated Radiation and Nuclear Science, Kyoto University (Japan), 4. Agency for Health, Safety and Environment, Kyoto University (Japan))

©APSORC25

7th Asia-Pacific Symposium on Radiochemistry *September 14 ~ 19, 2025 • Kunibiki Messe • Shimane, Japan*

Chemical state of Fe and electrical conduction properties of dense sintered $Sr_{1-x}Ln_xFeO_{3-\delta}$ and $SrFe_{1-x}Ln_xO_{3-\delta}$ (*Ln*: Y, lanthanoid) with cubic perovskite structure

Keina Nagai[1], Chihiro Kato[1], Taizo Yoshino[1], Ryutaro Maehara[1], Kosuke Shido[1], Takayuki Sugimoto[1], Takuya Hashimoto[1, *], Fumito Fujishiro[2], Motoyuki Matsuo[3]

[1]*Department of Physics, College of Humanities and Sciences, Nihon University: 3-25-40 Sakurajousui, Setagaya-ku, Tokyo 156-8550, Japan*
**Corresponding author, e-mail: hashimoto.takuya@nihon-u.ac.jp*
[2] *Faculty of Science and Technology, Kochi University: 2-5-1 Akebono-cho, Kochi-shi, Kochi 780-8520, Japan*
[3] *Isotope Science Center, The University of Tokyo: 2-11-16 Yayoi, Bunkyo-ku, Tokyo 113-0032, Japan*

The crystal structures and chemical state of Fe of $Sr_{1-x}Ln_xFeO_{3-\delta}$ and $SrFe_{1-x}LnO_{3-\delta}$ (Ln: Y, lanthanoid) were investigated using X-ray diffraction measurements, X-ray absorption spectroscopy and Mössbauer spectroscopy. Ln with small ionic radii, such as Tm, Yb, and Lu, could be partially substituted for both Sr and Fe sites, resulting in cubic perovskite structure, whereas larger Ln, such as Y and La, were substituted only Sr site. The chemical state of Fe in cubic $Sr_{1-x}Ln_xFeO_{3-\delta}$ and $SrFe_{1-x}LnO_{3-\delta}$ was determined not by the kind of cation but by the substituted site. $Sr_{0.9}Yb_{0.1}FeO_{3-\delta}$ exhibited higher conductivity than $SrFe_{0.9}Yb_{0.1}O_{3-\delta}$, which was ascribed to higher $Fe^{3.5+}$ content observed by Mössbauer spectroscopy.

1. INTRODUCTION

Perovskite oxides with random distribution of oxide ion vacancies attract interest as material for solid oxide fuel cells, gas separation and so on because high oxide ion and hole mixed conducting property is expected. Tetragonal $SrFeO_{2.875}$ and orthorhombic $SrFeO_{2.75}$, including ordered arrangement of oxide ion vacancies at room temperature [1], undergo structural phase transition to cubic perovskite with random distribution of oxide ion vacancies at ~300 ºC and ~420 ºC, respectively. Because abrupt increases of electrical conductivity were observed at the both phase transitions [2], cubic $SrFeO_{3-\delta}$ at high temperature is promising as new oxide ion and hole mixed conducting material. However, mechanical instability owing to sudden increase in volume at the phase transition was a problem for practical application. To improve stability of the cubic phase at temperature, partial substitution of Ln^{3+} (Ln; Y, lanthanoid) for Sr site was examined. At present, preparation of cubic $Sr_{1-x}Ln_xFeO_{3-\delta}$ where *Ln*=La, Y, Gd, Sm [3] was reported; however, preparation of the cubic phase by partial substitution of Ln^{3+} for Fe site has not been reported although preparation of $BaFe_{1-x}Ln_xO_{3-\delta}$ with cubic perovskite was reported [4]. In this study, partial substitution of Ln^{3+} for Sr or Fe sites has been examined. It has been revealed that the substitution site is determined by the difference in ionic radii between Ln^{3+} and Sr^{2+} or $Fe^{3.5+}$. Mössbauer spectroscopy clarified that not kind of Ln^{3+} but the substitution site determines the chemical state of Fe. The difference in chemical state of Fe by substitution site corresponds to higher electrical conductivity of Sr site substituted specimens.

2. EXPERIMENTAL PROCEDURE

The specimens were prepared by the Pechini method from $SrCO_3$, Ln_2O_3 and $Fe(NO_3)_3 \cdot 9H_2O$. A nominal amount of each raw material was weighed. $SrCO_3$ was dissolved in dilute HNO_3. Solution of Ln_2O_3 was prepared using hot HNO_3. H_2O_2 was added for acceleration of solution for some Ln_2O_3. $Fe(NO_3)_3 \cdot 9H_2O$ was dissolved by distilled H_2O. After mixing three kinds of solutions, citric acid and ethylene glycol, the mixture was heated at ~400 ºC, resulting in a solid precursor. The precursor was ground into powder, followed by calcination at 750 ºC for 17 h in air. The calcined powder was pressed into pellets and sintered at 1200 ºC for 17 h in air. The sintered pellets were reground into powder and subjected to X-ray diffraction measurement (XRD: CuK_α, 50 kV, 250 mA, RINT-2500, Rigaku Corp.) and Mössbauer spectroscopy (TOPOLOGIC SYSTEMS MFD-110D, ^{57}Co/Rh source) for analysis of crystal structure and chemical state of Fe, respectively. X-ray absorption spectroscopy of the pellets obtained by pressing the mixture of specimen and powder boron nitride was also performed to confirm the substitution site of Ln^{3+} at BL-9C in Photon Factory, KEK.

For Mössbauer spectra, the isomer shifts were expressed with respect to the centroid of the spectrum of metallic Fe foil. The curve fittings of the obtained Mössbauer spectra were performed using a least-square method, assuming that the spectra were composed of peaks with Lorentzian line shape as shown in our preceding paper [1]. The identification of constituent Fe species and evaluation of relative content of individual Fe species were performed as described in [1]. For $Sr_{0.9}Y_{0.1}FeO_{3-\delta}$, mean Fe valence, *i. e.*, oxygen content was also evaluated by iodometric titration.

For measurement of electrical conductivity and morphology of sintered specimens, the obtained powder was pressed into a cuboid shape with approximately $3 \times 4 \times 14$ mm^3 by cold isostatic pressing and sintered at 1200 ºC for 17 h in air, again. The total electrical conductivity at various temperatures in air was measured at a heating rate of 1 ºC/min

Copyright on 7th Asia-Pacific Symposium on Radiochemistry 2025 - R4-04 -

with four probe method, with which mesh and line made of platinum were employed as electrodes for current and voltage, respectively.

3. RESULTS AND DISCUSSION

XRD measurements revealed that Tm, Yb and Lu, which have smaller ionic radius than those of Y and other lanthanoid, could be partially substituted for both Sr and Fe sites, resulting in a cubic perovskite structure. Also revealed that the larger trivalent ion, such as Y, La, Sm and so on, substituted for Sr site only. This tendency shows agreement with assumption that *Ln* predominantly substitute site with a smaller radius difference, which could be applicable for substitution site of *Ln* for $BaFeO_{3-\delta}$ [4]. YbL_{III} absorption edge of X-ray absorption near edge structure (XANES) of $Sr_{1-x}Yb_xFeO_{3-\delta}$ and $SrFe_{1-x}Yb_xO_{3-\delta}$ (x=0.1, 0.2) showed a single white line and splitting ones, respectively. The peak splitting indicated that Yb successfully substitute for Fe site because it can be attributed to splitting of 5d orbital owing to octahedral coordination [5].

Figure 1 shows Mössbauer spectra of $Sr_{0.9}Ln_{0.1}FeO_{3-\delta}$. For $Sr_{0.9}Y_{0.1}FeO_{3-\delta}$, the valence of Fe and 3-δ were determined to be 3.5+ and 2.80 by iodometric titration. The mean valence of Fe obtained by iodometry agreed with that evaluated from the area of decomposed each Fe peak. Although the evaluation of Fe valence in $Sr_{0.9}Ln_{0.1}FeO_{3-\delta}$ (*Ln*=Tm, Yb, Lu) with iodometry was not succeeded because the specimen was not completely dissolved by HCl, the chemical state of Fe in $Sr_{0.9}Ln_{0.1}FeO_{3-\delta}$ was deduced to be almost same regardless of kind of *Ln* because almost the same spectra were obtained. Figure 2 shows Mössbauer spectra of a single phase of cubic $SrFe_{0.9}Ln_{0.1}O_{3-\delta}$. The observed spectra were almost the same with a mean Fe valence of 3.5+ irrespective of kind of *Ln*. Although the mean valence of Fe was almost same, chemical state of Fe deduced from Mössbauer spectroscopy showed a difference by substitution site. The intensity of the peak assigned as 3.5+ was smaller and those as 3.0+ and 4.0+ was larger for the Fe site substituted specimens. This suggested lower mobility of holes in Fe site substituted specimens, presumably because of longer Fe-Fe distance and hole scattering by Yb substituted for Fe site. The lower electrical conductivity of $SrFe_{0.9}Yb_{0.1}O_{3-\delta}$ than $Sr_{0.9}Yb_{0.1}FeO_{3-\delta}$ showed agreement with the chemical state of Fe deduced from Mössbauer spectroscopy.

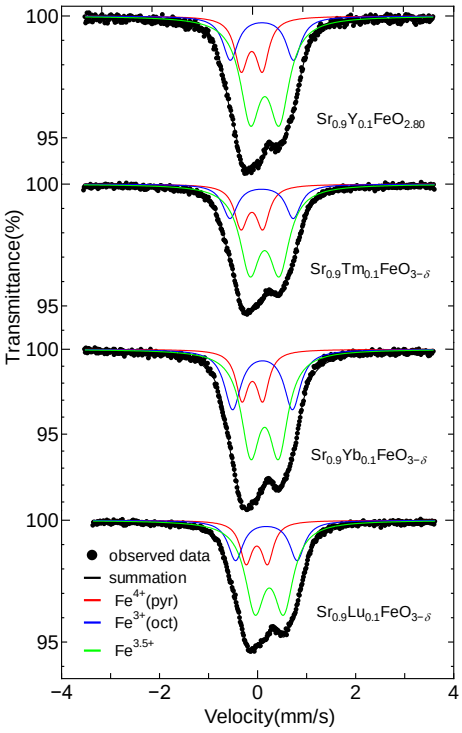


Fig. 1 Mössbauer spectra of cubic single phase of $Sr_{0.9}Ln_{0.1}FeO_{3-\delta}$. Oxygen content of $Sr_{0.9}Y_{0.1}FeO_{3-\delta}$ was determined to be 2.80 by iodometric titration.

4. CONCLUSIONS

Cubic perovskite with random distribution of oxide ion vacancies were prepared by partial substitution of Ln^{3+} (*Ln*=Y, lanthanoid) for $SrFeO_{3-\delta}$. The substitution site was determined by the difference in ionic radii between Ln^{3+} and Sr^{2+} or $Fe^{3.5+}$. Tm, Yb and Lu with small ionic radius could be substituted for both Sr and Fe sites, whereas Y, La, Sm and so on with larger ionic radius substituted for the Sr site only. Mössbauer spectroscopy revealed that not kind of *Ln* but the substitution site determined the chemical state of Fe, showing agreement with higher electrical conductivity of $Sr_{0.9}Yb_{0.1}FeO_{3-\delta}$ than that of $SrFe_{0.9}Yb_{0.1}O_{3-\delta}$.

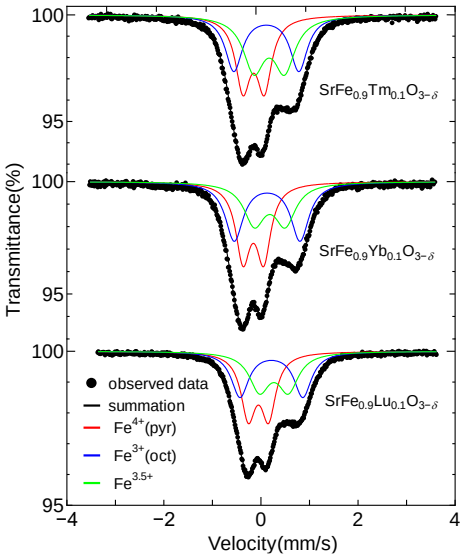


Fig. 2 Mössbauer spectra of cubic single phase of $SrFe_{0.9}Ln_{0.1}O_{3-\delta}$.

ACKNOWLEDGMENTS

X-ray absorption spectroscopy was performed under the approval of the Photon Factory Program Advisory Committee (Proposal No. 2022G547 and 2025G103).

References

[1] K. SHIDO et al., *Interactions*, **245**, 299 (2024).
[2] T. YOSHINO et al., *Solid State Ionics*, **422**, 116768 (2025).
[3] A. S. URUSOVA et al., *Ceram. Inter.*, **46**, 24718 (2020).
[4] Y. MATSUMOTO et al., *J. Ceram. Soc. Jpn.*, **128**, 898 (2020).
[5] K. UEDA et al., *J. Phys. Chem. C*, **127**, 15641 (2023).

Copyright on 7th Asia-Pacific Symposium on Radiochemistry 2025 - R4-04 -

7th Asia-Pacific Symposium on Radiochemistry *September 14 ~ 19, 2025 • Kunibiki Messe • Shimane, Japan*

MECHANISM OF HALF-IRON MORIN TRANSITION IN THE Nb-DOPED HEMATITE

Satoru Nakashima[1], Habibur Rahman[2], Shiro Kubuki[3]

[1]*Natural Science Center for Basic Research and Development (N-BARD), Hiroshima University, 1-4-2 Kagamiyama, Higashi-Hiroshima, Hiroshima 739-8526, Japan. E-mail: snaka@hiroshima-u.ac.jp*
[2]*Chemistry Program, Graduate School of Advanced Science and Engineering, Hiroshima University, 1-3-1 Kagamiyama, Higashi-Hiroshima, Hiroshima 739-8526, Japan. E-mail: hbb_rahman7@yahoo.com*
[3]*Department of Chemistry, Graduate School of Science, Tokyo Metropolitan University, 1-1 Minami-Osawa, Hachioji, Tokyo 192-0397, Japan. E-mail: kubuki@tmu.ac.jp*

Nb-doped hematite shows a half-iron Morin transition. The mechanism was discussed from the position of Nb site. Nb was thought to enter first the interstitial site. But when more than 2% Nb is introduced, it also enters the lattice site. When calcined at 700°C, Nb in the lattice site pairs with Fe and is released out of the hematite, producing $FeNbO_4$. The hematite particles gather to form larger particle. There are two ways in which Nb escapes, i.e., one leaves the crystallographically equivalent irons and the other leaves crystallographically inequivalent irons. At low temperatures, the former becomes antiferromagnetic, but the latter remains weakly ferromagnetic. The escape ratio is 1:1, and it is thought that the effect spreads throughout the crystal, showing Morin transition of half iron.

1 INTRODUCTION

Hematite is antiferromagnetic at low temperatures, but when heated to about 260 K, it undergoes a Morin transition and becomes weakly ferromagnetic. This Morin transition is accompanied by a reversal of the sign of the quadrupole splitting in the Mössbauer spectrum of hematite. From the Mössbauer spectra of Nb-doped hematite, it was shown that half of the iron undergoes the Morin transition, but the other half does not [1]. However, the details of the half-iron Morin transition are unknown. In the present study, we discussed the positions of Nb in hematite and the cause of half-iron Morin transition. The present results suggest that the Nb is introduced in interstitial site first and then in lattice site and the removal of Nb with Fe occurs from lattice site to form $FeNbO_4$, which explains the half-iron Morin transition.

2 MORIN TRANSITION

2.1 Antiferromagnetism and Weak Ferromagnetism

The isotropic exchange interaction energy between two spins $\mathbf{S}_1$ and $\mathbf{S}_2$ is expressed as $-2J_{12}S_1S_2\cos\theta$, where $J_{12} = J_{21}$. When $J_{12}<0$, $\mathbf{S}_1$ and $\mathbf{S}_2$ are antiferromagnetic. Conversely, when $J_{12}>0$, the material becomes ferromagnetic. In addition to the isotropic exchange interaction $J(\mathbf{S}_1\cdot\mathbf{S}_2)$, the antisymmetric exchange (Dzyaloshinsky-Moriya) interaction acts as $\mathbf{D}\cdot[\mathbf{S}_1\times\mathbf{S}_2]$, where $J_{12} = -J_{21}$. In classical vector terms, the energy can be expressed as $E_{DM}=DS_1S_2\sin\theta$. If both interactions are in play, $\theta=0$ or $\theta=\pi$ cannot become a minimum of the total energy. If $J_{12}<0$, i.e., $\mathbf{S}_1$ and $\mathbf{S}_2$ are antiparallel, then θ will be slightly smaller than π. This is weak ferromagnetism. Also, if $J_{12}>0$ and they are parallel, then θ will form a slight angle.

2.2 Crystal Structure and Dzyaloshinsky-Moriya Interaction

The Morin transition is affected by the symmetry of the crystal. When $\mathbf{S}_1$ and $\mathbf{S}_2$ are crystallographically equivalent, the Hamiltonian must remain unchanged when $\mathbf{S}_1$ and $\mathbf{S}_2$ are interchanged. In this case, the Dzyaloshinsky-Moriya interaction is eliminated. There are four Fe^{3+} atoms in the unit cell of hematite (Fig. 1). The iron atoms in A and B positions are crystallographically equivalent, and the iron atoms in C and D positions are crystallographically equivalent. However, the iron atoms in A and C, or the iron atoms in A and D, are not crystallographically equivalent. The spin direction is perpendicular to the c-axis above 260 K and is aligned along the c-axis below 260 K. The symmetry of Fe^{3+} is important for the Dzyaloshinsky-Moriya interaction.

2.3 Morin Transition and Mössbauer Spectroscopy

The Morin transition is reflected by a change in sign of the quadrupole splitting of the Mössbauer spectrum. Especially the absolute QS values become 1:2 by the change in sign of the quadrupole splitting.

3 RESULTS AND DISCUSSION

3.1 Half-Iron Morin Transition and the Formation of $FeNbO_4$

At 0 and 2 % Nb doping, the Morin transition is completely observed by the measurement of Mössbauer spectra at 298 and 78 K. When 7.4% Nb is doped, 50% of the iron does not undergo the Morin transition. When half-iron Morin transition is observed, the formation of $FeNbO_4$ was confirmed by Mössbauer spectroscopy, PXRD, and TEM-eds. Even if more Nb is added, the proportion of iron undergoing the Morin transition remains essentially at 50%. That is, at room

Copyright on 7th Asia-Pacific Symposium on Radiochemistry 2025

temperature, all irons are weakly ferromagnetic, but as the temperature is lowered, the proportion of iron undergoing the Morin transformation remains essentially at 50%. This suggests the possibility of a stable phase in which the iron that becomes antiferromagnetic and the iron that remains weakly ferromagnetic exist in a 1:1 ratio, i.e., the phase of half-iron Morin transition is stabilized

3.2 Mössbauer Spectra at Lower Temperature

Mössbauer spectrum at 20 K of the sample doped with 7.4% Nb showed that the proportion of the iron undergoing Morin transition was not significantly different from that at 78 K. This also suggests that the structure showing half-iron Morin transition is stable.

3.3 Position Where Nb Is Introduced

Up to 2% Nb doping in hematite 100 % irons show the Morin transition. Nb^{5+} has no spin. It is speculated that this Nb first occupies the interstitial site of hematite. The Nb in the interstitial sites does not magnetically interact with the Fe in the lattice site, and does not disturb the magnetic interaction between the iron ions in the lattice sites. Furthermore, by increasing the Nb concentration, Nb also enters the lattice site (Fig. 1), and this Nb affects the interaction between Fe spins. It is thought that the Nb is systematically introduced at lattice sites, and it is thought that this is why the sample calcined at 600°C becomes ferrimagnetic-like and is attracted to the magnet despite the hematite structure [1].

3.4 How Nb Is Removed

When Nb leaves the hematite structure, it comes out as $FeNbO_4$, therefore it is thought that Fe in the lattice site next to Nb leaves the system in pairs.

The way how it escapes is shown in Figure 1. There are two ways in which Nb substituted at the lattice site escapes in pairs with Fe. That is, the way surrounded by red oval and the way surrounded by green oval. When it escapes as surrounded by red, the rest two spins are crystallographically equivalent (dashed red oval) and become antiferromagnetic at low temperatures. On the other hand, when it escapes as surrounded by green, it is thought that the rest two spins are crystallographically inequivalent (dashed green oval) and may remain weakly ferromagnetic even at low temperatures. Since the ways of escape are random, the two patterns coexist in a 1:1 ratio. Also, 25% of Fe is not substituted with Nb. That is, it is thought that the effect of a portion of Nb and Fe being paired and released spreads to the entire crystal. The dashed red oval pairs align, when Nb and Fe in red circle are released. And the dashed green oval pairs align, when Nb and Fe in green circle are released. By considering the Nb site when it is introduced and it is removed, it can be explained that the iron that undergoes the Morin transition and the iron that does not are 1:1.

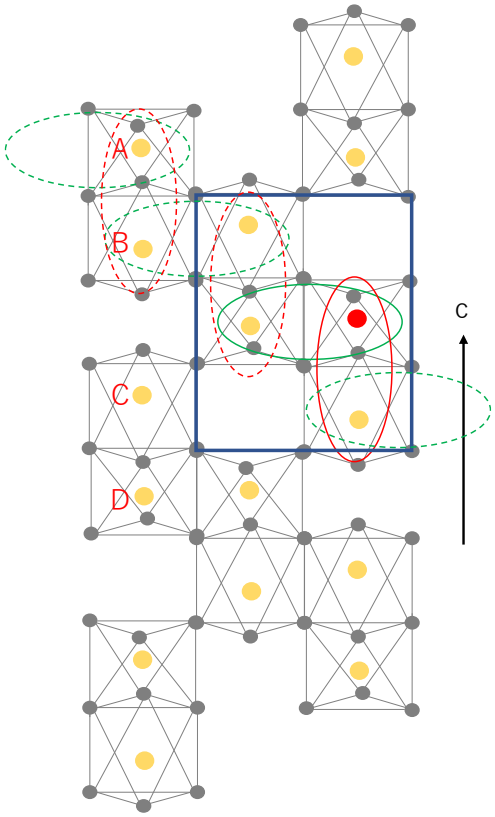


Fig. 1. Schematic diagram of the hematite structure. The Fe atoms (yellow ball) in A and B, and the Fe atoms in C and D are crystallographically equivalent. This shows the case where Nb (red ball) is introduced into a lattice site. The two types of combination in which Nb and Fe are released in pairs to form $FeNbO_4$ are shown by red and green ovals. The effect expands in the crystal as shown in dashed red and green ovals.

4. CONCLUSIONS

We considered the cause and mechanism of the half-iron Morin transition in Nb-doped hematite. The doped Nb first enters the interstitial site, but when more than 2% is introduced, it is thought that Nb also enters the lattice site. When calcined at 700°C, Nb in the lattice site makes a pair with Fe and is released out of the hematite, producing $FeNbO_4$. There are two ways how it escapes: one that leaves the crystallographically equivalent irons and the other that leaves crystallographically inequivalent irons. At low temperatures, the former becomes antiferromagnetic, but the latter remains weakly ferromagnetic. The escape ratio is 1:1, and it is thought that the effect spreads throughout the crystal, and it is considered that there is a 1:1 ratio of iron that undergoes the Morin transition and iron that does not. It is thought that such a stable state exists and this is the reason of half-iron Morin transition.

References

[1] H. Rahman and S. Nakashima, Applied Phys. A, **128**, 564 (2022).

Copyright on 7th Asia-Pacific Symposium on Radiochemistry 2025 - R4-05 -

Preparation and ^{61}Ni Mössbauer Spectroscopy for Supramolecular Bridging Cyanide Complexes containing $[Ni(II)(CN)_4]^{2-}$ unit

Takafumi Kitazawa[1, 2], Kosuke Kitase[1], Shinji Kitao[3], Yasuhiro Kobayashi[3], Takumi Kubota[4], and Makoto Seto[3]
,

[1]1 - Department of Chemistry, Faculty of Science, Toho University, 2-2-1 Miyama, Funabashi, Chiba, 274-8510, Japan
2 - Research Centre for Materials with Integrated Properties, Toho University, 2-2-1 Miyama, Funabashi, Chiba, 274-8510, Japan
3 - Institute for Integrated Radiation and Nuclear Science, Kyoto University, 2 Asashiro-nishi, Kumatori, Sennan-gun, Osaka, 590-0494, Japan
4 - Agency for Health, Safety and Environment, Kyoto University, Gokasho, Uji, Kyoto 611-0011, Japan

INTRODUCTION: The Mössbauer Effect has been found for about 100 nuclear transitions in some 80 nuclides in nearly fifty elements. The Mössbauer technique is a very valuable and helpful tool to the material sciences linking to molecular magnetisms such as spin crossover (SCO) behaviors.

As associated with temperatures, pressure and lights, 3-d block transition metal ion coordination compounds with d^4-d^7 configuration in an octahedral crystal field allow a possibility of SCO between the low spin (LS) and the high spin (HS) state. Octahedral iron(II) SCO systems with $3d^6$ can be transited between the diamagnetic $(t_{2g})^6$ and the paramagnetic $(t_{2g})^4(e_g)^2$ configuration. Coordination polymers with bistable systems between the LS and the HS states, usually triggered by external stimuli, such as temperature, light, pressure and guest molecules, are a class of potential candidates for smart materials. As the very important history of SCO researches of the Hofmann-like coordination polymers, the SCO in $Fe^{II}(pyridine)_2Ni(CN)_4$ was found using ^{57}Fe Mössbauer spectroscopy and SQUID measurements in 1996 [1], SCO supramolecular Hofmann-like metal-organic frameworks containing 2D layers and 3D structures, with octahedral iron(II) ions linked by cyanidemetallates along the in-plane directions, have been investigated thoroughly for the development of interesting SCO materials in order to obtain potential applications in smart materials [3-6]. Ni(II) ions states are associated with Fe(II) ions state. Now we have carried out Ni-61 Mössbauer spectroscopy for three Hofmann type SCO compounds which act as different spin transition temperatures and behaviors including LS spin and HS spin ratios; $Fe(pyridine)_2Ni(CN)_4$, $Fe(3\text{-Methyl-py})_2Ni(CN)_4$, and $Fe(3\text{-Cl-py})_2Ni(CN)_4$, and mononuclear $K_2[Ni(CN)_4]$.

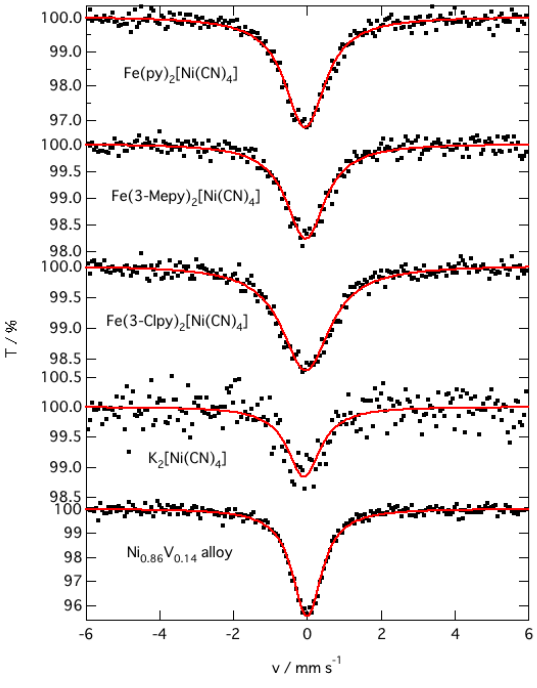


Fig.1 ^{61}Ni Mössbauer Spectroscopy for Supramolecular Bridging Cyanide Complexes

Copyright on 7th Asia-Pacific Symposium on Radiochemistry 2025 - R4-06 -

EXPERIMENTS: We freshly synthesized $Fe(pyridine)_2Ni(CN)_4$, $Fe(3\text{-}Methyl\text{-}py)_2Ni(CN)_4$, and $Fe(3\text{-}Cl\text{-}py)_2Ni(CN)_4$, according to the applied methods [1,5-7] and mononuclear $K_2[Ni(CN)_4]$.

Ni-61 source production associated with $^{62}Ni(\gamma, p)^{61}Co$ was done using activation with Bremsstrahlung from the Electron beam of the KURNS-LINAC. Ni-61Mössbauer measurements were carried out conventional methods, Since the half-life of Co-61 is about100 minutes, about three hours measurements were done for one cycle. For one SCO compound sample, three times cycles are carried out in order to get suitable Mössbauer spectra. All spectra were obtained at 16 K. Ni-14at%V alloy was used for characterizations of velocities.

RESULTS: As shown in Fig. 1, Ni-61 Mössbauer spectra three kinds of SCO compounds with MOF(Metal Organic Framework) were found for the first time at 16K. Obtained IS values are corresponding to Ni(II) ions. There are very small differences in IS shifts for these compounds coordinated by different pyridine-type ligands. Obtained Isomer Shift δ (mm/sec) parameters are associated with Ni(II) oxidation states, electronegativity of ligands coordinating to Ni(II) atoms, character of bonds to Ni(II) ions and spin states of Ni(II) containing d^8 electrons.

The obtained Mössbauer parameters have relationship with the square planar crystal field of $[Ni(CN)_4]_{2-}$ units composed for coordination polymer $Fe(pyridine)_2Ni(CN)_4$, $Fe(3\text{-}Methyl\text{-}py)_2Ni(CN)_4$, and $Fe(3\text{-}Cl\text{-}py)_2Ni(CN)_4$.

ACKNOWLEDGMENTS This work was partially supported by the Joint Usage/Research of the Institute for Integrated Radiation and Nuclear Science, Kyoto University (KURNS) (No. R4P3-7, R5P1-2, R6P1-2).

REFERENCES:

[1] Kitazawa, T.; Gomi, Y.; Takahashi, M.; Takeda, M.;Enomoto, M.; Miyazaki, A.; Enoki, *J. Mater. Chem.* 1996, 6(1) 119-121, DOI:10.1039/JM9960600119.

[2] Kitazawa, T. Synthesis and Applications of New Spin Crossover Compounds. *Crystals* **2019**, *9*(8), 382;, DOI:10.3390/cryst9080382.

[3] K. Kitase, D. Akahoshi and T. Kitazawa, Inorg. Chem., 60, 7, 4717–4722 (2021).

[4] K. Kitase T. Kitazawa,, Dalton. Trans., 49, 12210-12214 (2020). (Back Cover)

[5] Gábor, M.; Guillon T.; Moussa, N. O.; Rechignat, L.; Kitazawa,T.; Nardone,M.; Azzedine ,B.;, *Chem. Phys. Lett.* 2006, **423**(1-3), 152-156.

[6] Kitazawa, T.; Eguchi,M.; Takeda, M; "Crystal structures of two-dimensional coordination polymer $Fe(methylpyridine)_2Ni(CN)_4$" T, *Mol. Cryst. Liq. Cryst. Sci Tech. A*, 2000, 341, 527-532 DOI:10.1080/10587250008026193

[7]T. Kitazawa, Mi. Takahashi, Ma. Takahashi, M. Enomoto, A. Miyazaki, T. Enoki, M. Takeda "^{57}Fe Mossbauer spectroscopic and magnetic study of a spin-crossover polymer complex, $Fe(3\text{-}chloropyridine)_2Ni(CN)_4$" , *J. Radioanal. Nucl. Chem.* 1999, 239(2), 285-290. DOI:10.1007/BF02349498

Contributed Talk | [P3]Environmental Integrated Knowledge of Radionuclides Dynamics Studied from the Fukushima Accident

Thu. Sep 18, 2025 11:00 AM - 12:00 PM JST | Thu. Sep 18, 2025 2:00 AM - 3:00 AM UTC Hall B(Small)

[P3] Environmental Integrated knowledge of Radionuclides Dinamics Studied from the Fukushima Accident

11:00 AM - 11:20 AM JST | 2:00 AM - 2:20 AM UTC

[P3-04]

Activity ratio of Sr-90 and Cs-137 in different environmental samples collected from the Fukushima exclusion zone

*Norbert Kavasi[1], Tatsuo Aono[1] (1. Fukushima Institute for Research, Education and Innovation (F-REI) (Japan))

11:20 AM - 11:40 AM JST | 2:20 AM - 2:40 AM UTC

[P3-05*]

Fundamental study on the rapid analytical method for radioactive Cs-containing particles by PHITS

*Tsubasa Matsumura[1], Shinya Yamasaki[2], Keisuke Sueki[2], Yudai Shigekawa[2], Aya Sakaguchi[2] (1. Graduate School of Science and Technology, Degree Programs in Pure and Applied Sciences, Master's Program in Chemistry,University of Tsukuba (Japan), 2. Institute of Pure and Applied Sciences,University of Tsukuba (Japan))

11:40 AM - 12:00 PM JST | 2:40 AM - 3:00 AM UTC

[P3-06]

Development of an analytical method for ^{90}Sr in using ICP-DRC-MS/MS with O_2+NH_3 reaction gas

*Kazuma Koarai[1], Makoto Matsueda[1], Kayo Yanagisawa[1], Yusuke Watanabe[1] (1. Japan Atomic Energy Agency (Japan))

©APSORC25

Activity ratio of Sr-90 and Cs-137 in different environmental samples collected from the Fukushima exclusion zone

Norbert Kavasi[1] and Tatsuo Aono[1]

[1]*Regional Environmental Co-Creation Unit, Fukushima Institute for Research, Education and Innovation (F-REI)*
F-REI Branch at Fukushima Medical University, 1 Hikarigaoka, Fukushima-city, Fukushima 960-1295, Japan
kavasi.norbert.h4v@research.f-rei.go.jp

Moderate positive correlation was revealed between Sr-90 and Cs-137 and higher mobility of the Sr-90 was confirmed in Japanese soil. The activity ratio of 85% for Sr-90/Cs-137 was in the range of 5.0×10^{-5} to 5.0×10^{-4} with a median of 1.2×10^{-4}.

1. BACKGROUND

Sr-90 is an artificial pure beta emitting radionuclide that has been released into the environment through nuclear accidents and detonation of nuclear weapons. Due to its biochemical similarities to Ca, there is a risk of internal radiation dose increment for living beings. Fourteen years after the severe accident at the Fukushima Dai-ichi Nuclear Power Station (FDNPS), available data on Sr-90 contamination in the Fukushima exclusion zone are still relatively limited compared to those of radiocesium (Cs-134 and Cs-137). There are two explanations for this phenomenon. First, the accident emission rate of the semi-volatile Sr-90 was much lower than that of the volatile radiocesium. Second, radiocesium determination is a straightforward, simple process because highly penetrating gamma photons with a discrete energy spectrum emitted during the radioactive decay of radiocesium are detected. Contrarily, Sr-90 analysis is a much more complex procedure since only low penetrating beta particles with a continuous energy spectrum are emitted and that necessitates a time-consuming sample preparation and a chemically based element separation.

In regard to the emission pattern of radionuclides, volatility has the highest importance if the protective containment system is able to maintain its functionality (inhibiting radionuclide releases) during an accident. In the FDNPS accident, despite the hydrogen explosions and fuel meltdowns, the protective containment system held back most of the radioactive nuclides, resulting in radiocesium and Sr-90 releases that were one and two orders of magnitude lower than at Chernobyl. Consequently, the discharged activity ratio of Sr-90 and Cs-137 changed considerably: 7.7×10^{-2} for the Chernobyl accident and 5.0×10^{-4} for the FDNPS accident. However, according to the latest atmospheric discharge estimations, the FDNPS accident-released Cs-137 could be in the range of 6–40 PBq, while Sr-90 could be around 2.7–3.6 TBq [1], resulting in the Sr-90/Cs-137 activity ratio in the range of 9.9×10^{-5} to 1.2×10^{-4} which clearly indicates dominance of the volatile Cs-137 over the semi-volatile Sr-90 and the effectiveness of the containment system. The atmospheric Sr-90 released by the FDNPS accident (0.14 PBq) [2] is negligible (~0.1 and 0.002%) when compared to the Chernobyl accident (10 PBq) and to global atmospheric fallout (622 PBq) from nuclear weapon tests [3]. Therefore, the Sr-90 deposited on land has not caused a significant increase compared to the background level in Fukushima Prefecture; notable differences occur only in samples from the Fukushima exclusion zone [1]. Consequently, this work focuses on analysis of samples collected from the exclusion zone to uncover the details of Sr-90 deposition and migration in the context of Cs-137 occurrence.

2. MATERIALS AND METHODS

Samples: soil, litter, rain gutter deposit, roadside sediment, fish and mushroom samples were collected from different locations within the Fukushima exclusion zone (less than 30 km from the FDNPS) in 2013, 2015, 2016, 2017, 2018, 2023 and 2024.

Analysis: Extraction chromatography Sr resin was used for element separation and Sr-90 was determined with radiometric and mass spectrometric methods. Cs-137 was measured with gamma-spectrometry.

3. CONCLUSIONS

Correlation

In this study, a moderate positive correlation (R^2=0.64, n=76) was confirmed between Sr-90 and Cs-137 in soil samples as can be seen in Figure 1, [4].

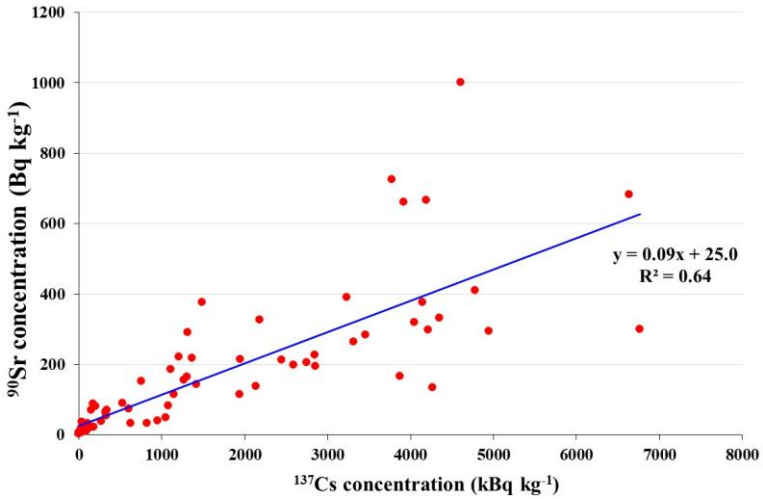


Figure 1. Correlation of Sr-90 and Cs-137 in soil samples collected from the Fukushima exclusion zone (Reference date: March 15, 2011)

Sr-90/Cs-137 activity ratio

Because of the similarity in half-life, the Sr-90/Cs-137 activity ratio is informative regarding the environmental migration process for both radionuclides. The frequency distribution of the Sr-90/Cs-137 activity ratio, presented in Figure 2, [4]. The most frequent ratios (~45%) were between 1.1×10^{-4} and 2.5×10^{-4}, while 85 % percent of the ratios were between 5.0×10^{-5} and 5.0×10^{-4}. This study found Sr-90/Cs-137 activity ratios that suggested Sr-90 emission should be around 1-10 TBq. Mark I containment system protection caused low-level pollution, compared to Chernobyl and other nuclear incidents. Thus, agricultural, forestry, and urban areas in the Fukushima exclusion zone, as well as all other portions of Fukushima Prefecture and other Japanese prefectures, cannot expect significant Sr-90 contamination above the background level

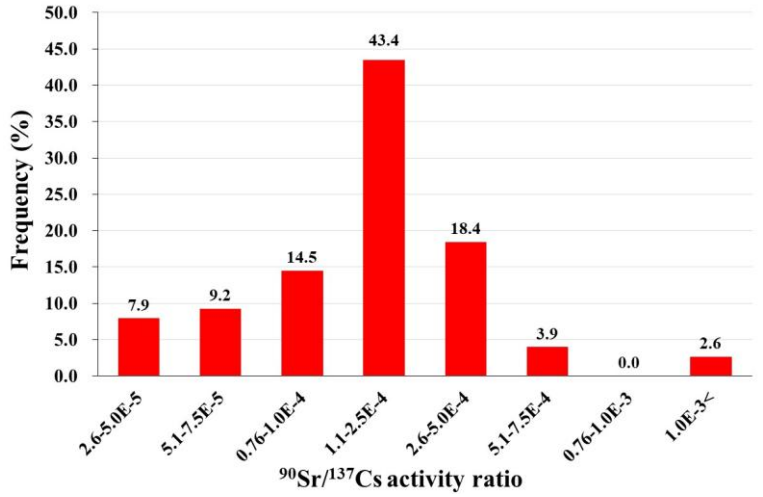


Figure 6. Frequency distribution of Sr-90/Cs-137 activity ratio in samples from the Fukushima exclusion zone (Reference date: March 15, 2011)

References

[1] K. HIROSE, "Sr-90 Deposition Observed in Central and Northeast Honshu Island, Japan, after the Fukushima Dai-ichi Nuclear Power Plant Accident," *International Journal of Earth & Environmental Sciences*, **2**, 134 (2017).
[2] P. POVINEC, K. HIROSE, M. AOYAMA, *Fukushima Accident Radioactivity Impact on the Environment*, pp. 75–95, Elsevier, Amsterdam (2013).
[3] UNITED NATIONS SCIENTIFIC COMMITTEE ON THE EFFECTS OF ATOMIC RADIATION, *Sources, Effects and Risks of Ionizing Radiation. Scientific Annex C: Exposures to the public from man-made sources of radiation*, United Nation, New York (2002).
[4] N. KAVASI, H. ARAE, T. AONO, S. K. SAHOO, "Distribution of strontium-90 in soils affected by Fukushima Dai-Ichi nuclear power station accident in the context of cesium-137 contamination," *Environmental Pollution*, **326**, (2023).

Copyright on 7th Asia-Pacific Symposium on Radiochemistry 2025 - P3-04 -

Fundamental study on the rapid analytical method for radioactive Cs-containing particles by PHITS

Tsubasa Matsumura[1], Shinya Yamasaki[2], Keisuke Sueki[2], Yudai Shigekawa[2], Aya Sakaguchi[2]

[1] *Graduate School of Science and Technology, Degree Programs in Pure and Applied Sciences, Master's Program in Chemistry,University of Tsukuba: 1-1-1 Tennodai, Tsukuba, Ibaraki, 305-8577*
[2] *Institute of Pure and Applied Sciences,University of Tsukuba: 1-1-1 Tennodai, Tsukuba, Ibaraki, 305-8577*

The aim of the present study was to reduce the analysis time of highly radioactive Cs-containing particles, CsMPs, by locating them using a scanning electron microscope (SEM) equipped with β- particle detectors. We investigated the optimal structure of the detection system, by simulations using the calculation code PHITS.

1 INTRODUCTION

The accident at the Fukushima Daiichi nuclear power plant led to the release of large amounts of radioactive cesium (Cs), resulting in widespread soil contamination. Insoluble, highly radioactive Cs-bearing particles (cesium-rich micro-particles, CsMPs) along with natural minerals have been reported as a retention medium for radioactive Cs in soil [1]. CsMPs are significant due to their small size and high radioactivity, which pose both biological [2] and environmental risks. However, the analysis of CsMPs is a time-consuming and laborious research problem, as it requires radioactivity-based particle screening and particle identification by electron microscopy. To reduce screening time and promote the study of CsMPs, the present study aimed to establish a CsMP identification system by combining an electron microscope and a radiation detector, and to investigate the structure of a suitable device using the calculation code PHITS (Particle and Heavy Ion Transport code System) [3], which simulates the behavior of radiation.

2 MATERIALS AND METHODS

2.1 Comparison of measured and calculated spectra using a β-ray detector

To check the reliability of PHITS simulations, the spectra obtained from actual measurements of radioactive particles with a β-ray detector using a plastic scintillator were compared with those simulated by PHITS.

2.2 Invention and study of a system for locating CsMPs

In this study, four plastic scintillators were employed as detectors in the simulation, and they were placed equidistantly from the center. Two types of scintillator geometry were set up: cylindrical (Fig. 1) and rectangular (Fig. 2), and the counting rate of each detector was simulated for these systems by varying the position of the radioactive particles. The four detectors were then divided into two groups based on the direction of particle movement (Fig. 3), and the difference in counting rates (ΔC) between the groups was calculated.

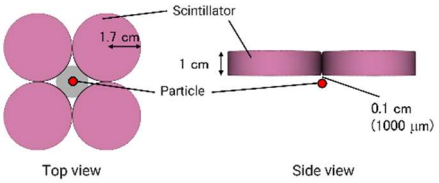


Figure 1 Schematic diagram of the CsMP locating system (cylinder) (left: top view, right: side view)

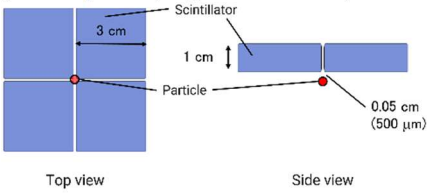


Figure 2 Schematic diagram of the CsMP locating system (rectangular) (left: top view, right: side view)

3 RESULTS AND DISCUSSIONS

The spectra from actual measurements and PHITS simulations showed good agreement (correlation coefficient of 0.98), validating the reliability of the simulations. This allowed the plastic scintillator and detector to be used in subsequent simulations. The simulation was then performed for the system shown in Figure 1, and the obtained ΔC values were plotted against the relative position of the particles (the center of the detector is 0 μm) (Figure 4). As a result, a linear relationship between the particle position and ΔC was observed although we expected that the particle position could be identified by searching the position where C was zero. However, in the cylindrical scintillator, the particle positions where the ΔC was closest to 0 were off-center. This was likely due to the absence of a scintillator above

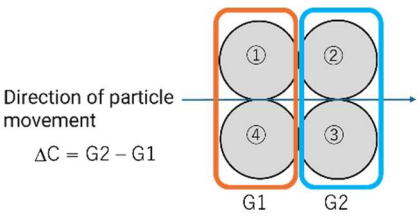


Figure 3 Grouping in determining ΔC

Copyright on 7th Asia-Pacific Symposium on Radiochemistry 2025- P3-05* -

the particle, a consequence of the scintillator's shape. This issue could be improved by changing the shape of scintillators and reducing the gap above the particle. The relative error E(%) in relation to the number of counts N is defined by

$$E = \frac{100}{\sqrt{N}} . \quad (1)$$

From equation (1), the formula for the relationship between the number of counts and accuracy at the graph slope a cps/μm is expressed as

$$N = \frac{4\,n^2}{x^2\,a^2}. \quad (2)$$

(x: accuracy of measurement (±x μm), n: counting rate (cps), a: graph slope (cps μm^{-1}))
From equation(2), the relationship between the measurement time t(s) and accuracy can be expressed as

$$t = \frac{4\,n}{x^2\,a^2} . \quad (3)$$

From equation (3), it was estimated that approximately 700,000 counts are required to locate the position with an accuracy of ±10 μm, requiring approximately 20 hours of measurement for a radioactive particle of 100 Bq. To reduce this measurement time, the scintillator was modified to a rectangular shape to cover the area above the particle and to shorten the distance to it (Fig. 2), resulting in increased counting efficiency and reduced deviation from the center (Fig. 5). The time required for an accuracy of ±10 μm was reduced to approximately 20 minutes, indicating the potential for faster and more precise determination of the position of CsMPs. By integrating this detection system into SEM, the method could be applied to the rapid identification of CsMPs in environmental samples.

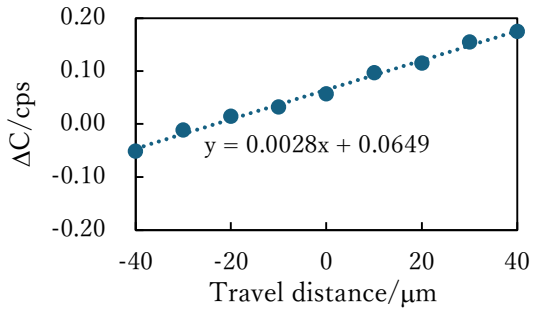


Figure 4 ΔC plot of cylindrical scintillator

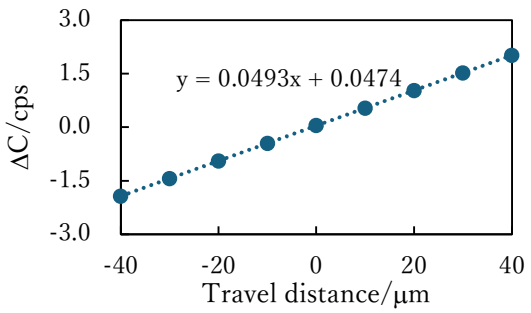


Figure 5 ΔC plot of a rectangular scintillator

4 CONCLUSIONS

This study demonstrated that PHITS simulations agreed closely with actual measurements (r = 0.98), confirming the reliability of the proposed detector system. By redesigning the scintillator from a cylindrical to a rectangular geometry—thereby improving coverage and reducing the distance to the particle—the counting efficiency increased dramatically, cutting the time required for ±10 μm positioning accuracy from roughly 20 hours to about 20 minutes. Incorporating this optimized detection setup into a scanning electron microscope offers a rapid and precise method for identifying cesium-rich micro-particles in environmental samples.

ACKNOWLEDGMENTS

This work was supported by JSPS KAKENHI Grant Number JP24K22345.

References

[1] Y. Igarashi, T. Kogure, Y. Kurihara, H. Miura, T. Okumura, Y. Satou, Y. Takahashi, N. Yamaguchi, A review of Cs-bearing microparticles in the environment emitted by the T Fukushima Daiichi Nuclear Power Plant accident, Journal of Environmental Radioactivity 205-206,101-118(2019).
[2] Mizuki Suetake, Yuriko Nakano, Shinya Yamasaki, Gareth T.W. Law, Toshihiko Ohnuki, Bernd Grambow, Rodney C. Ewing, Satoshi Utsunomiya, Radioactive cesium-rich microparticle (CsMP): A window into the damaged reactors and its environmental impacts (8) Dissolution kinetics of Cs-rich microparticle in a simulated body fluid,Atomic Energy Society of Japan2017 Fall Meeting collection of abstracts.
[3] T. Sato, Y. Iwamoto, S. Hashimoto, T. Ogawa, T. Furuta, S. Abe, T. Kai, Y. Matsuya, N. Matsuda, Y. Hirata, T. Sekikawa, L. Yao, P.E. Tsai, H.N. Ratliff, H. Iwase, Y. Sakaki, K. Sugihara, N. Shigyo, L. Sihver and K. Niita, Recent improvements of the Particle and Heavy Ion Transport code System - PHITS version 3.33, J. Nucl. Sci. Technol. 61,127-135(2024).

7th Asia-Pacific Symposium on Radiochemistry *September 14 ~ 19, 2025 • Kunibiki Messe • Shimane, Japan*

Development of an analytical method for ^{90}Sr in using ICP-DRC-MS/MS with O_2+NH_3 reaction gas

Kazuma Koarai[1], Makoto Matsueda[1], Kayo Yanagisawa[2], Yusuke Watanabe[1]

[1]*Collaborative Laboratories for Advanced Decommissioning Science (CLADS), Japan Atomic Energy Agency: 790-1 Otsuka-Motooka, Tomioka-machi, Futaba-gun, Fukushima, 979-1151, and Email Address*
[2]*Nuclear Science and Engineering Center (NSEC), Japan Atomic Energy Agency: 2-4 Shirakata-shirane, Tokai-mura, Naka-gun, Ibaraki, 319-1195*

An analytical method for the determination of ^{90}Sr was developed using inductively coupled plasma dynamic reaction cell tandem mass spectrometry (ICP-DRC-MS/MS) with a mixed reaction gas of O_2 and NH_3. This study aimed to improve detection sensitivity and effectively remove spectral interferences, which are critical issues in ^{90}Sr quantification. Zr, the main source of such interference, is present in environmental samples and at elevated levels in decommissioning materials from the Fukushima Daiichi Nuclear Power Station (1F) due to the use of Zircaloy cladding.

Under the conventional O_2-only reaction condition [1], isobaric interference from ^{90}Zr appears at concentrations above 0.1 ng mL^{-1}, while polyatomic interferences such as $^{74}Ge^{16}O$ and $^{74}Se^{16}O$ remain problematic. In contrast, the mixed O_2 + NH_3 reaction gas effectively suppresses Zr interference up to 1 ng mL^{-1} and also removes interferences from Ge and Se, which cannot be eliminated by O_2 alone. These improvements are attributed to the formation of cluster ions such as $ZrNH_{1-2}(NH_3)_{4-5}^+$, $GeNH_2(NH_3)_{1-2}^+$, and $SeNH_2^+$, which shift these species away from the detection pathway.

This enhanced interference removal expands the method's applicability to both radiological screening and ultra-trace analysis. For radiological screening, it enables rapid ^{90}Sr measurement in contaminated water from 1F without chemical separation, provided that Zr levels are below 1 ng mL^{-1}. For ultra-trace environmental analysis, the detection limit (LOD) was improved from 3.7 Bq L^{-1} (O_2 only) to 2.2 Bq L^{-1} (O_2 + NH_3). The method was validated using certified reference material NIST SRM-4354, which contains ^{90}Sr at a $^{90}Sr/^{88}Sr$ isotopic ratio on the order of 10^{-10}. The measured values showed good agreement with the certified activity, confirming the method's accuracy and robustness for low-level ^{90}Sr determination in environmental samples.

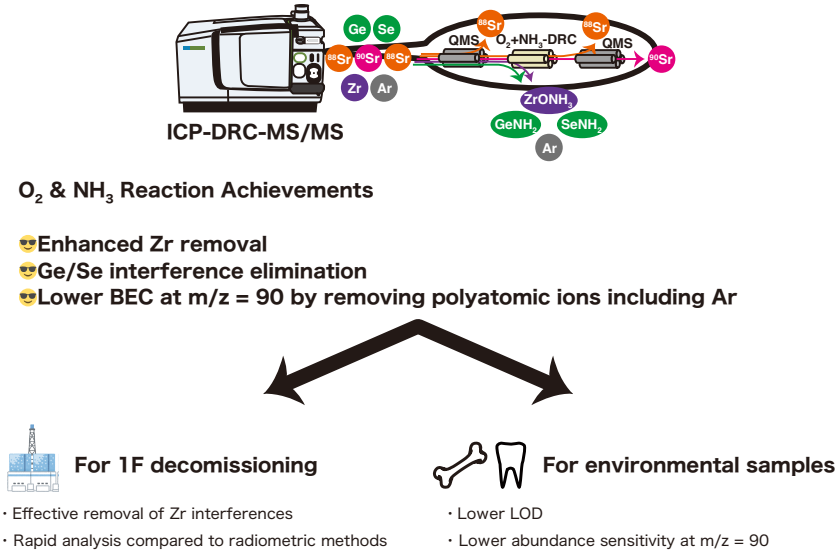


Figure 1. Application of O_2 + NH_3 Reaction for ^{90}Sr Analysis in ICP-MS

References

[1] K. Koarai et al., *JAAS*, 1678-1682 (2021).

Acknowledgment
This study was partly performed under the subsidy program "Decommissioning, Contaminated Water and Treated Water Management (Research and Development of Processing and Disposal of Solid Waste)" conducted by the Ministry of Economy, Trade and Industry of Japan.

Contributed Talk | [R1]Nuclear Chemistry

Fri. Sep 19, 2025 9:00 AM - 10:00 AM JST | Fri. Sep 19, 2025 12:00 AM - 1:00 AM UTC Hall S(Int'l)

[R1] Nuclear Chemistry

9:00 AM - 9:20 AM JST | 12:00 AM - 12:20 AM UTC

[R1-13]

Development of Radiochemical Techniques for the Measurement of (n,2n) Cross Sections at the National Ignition Facility

*John Despotopulos[1], Kelly Kmak[1], Daniel Pitman-Weymouth[2], James Benstead[2], Tom Braun[1], Tony Huynh[1], Justin Jeet[1], William Kerlin[1], Samantha Labb[1], Elvin Monzon[1], Rhyan Reynolds[1], Nicholas Ruof[1], Brian Sammis[1], Dawn Shaughnessy[1], Keenan Thomas[1], Todd Wooddy[1], Charles Yeamans[1] (1. Lawrence Livermore National Laboratory (United States of America), 2. Atomic Weapons Establishment (UK))

9:20 AM - 9:40 AM JST | 12:20 AM - 12:40 AM UTC

[R1-14]

Measurement of the ^{73}As(n,g) cross section at thermal neutron energies

*Kelly Nora Kmak[1], John Despotopulos[1], Connor Holiski[1], William Kerlin[1], Nicholas Scielzo (1. Lawrence Livermore National Laboratory (United States of America))

9:40 AM - 10:00 AM JST | 12:40 AM - 1:00 AM UTC

[R1-15]

Experimental study on noble gas transport in liquid lead using the Gas-jet facility at PSI

*Haohan Zhang[1], Robert Eichler[1,2] (1. Paul Scherrer Institut (Switzerland), 2. University of Bern (Switzerland))

©APSORC25

7th Asia-Pacific Symposium on Radiochemistry *September 14 ~ 19, 2025 • Kunibiki Messe • Shimane, Japan*

Development of Radiochemical Techniques for the Measurement of (n,2n) Cross Sections at the National Ignition Facility

John Despotopulos[1], Kelly Kmak[1], Daniel Pitman-Weymouth[2], James Benstead[2], Tom Braun[1], Tony Huynh[1], Justin Jeet[1], William Kerlin[1], Samantha Labb[1], Elvin Monzon[1], Rhyan Reynolds[1], Nicholas Ruof[1], Brian Sammis[1], Dawn Shaughnessy[1], Keenan Thomas[1], Todd Wooddy[1], Charles Yeamans[1]

[1]*Lawrence Livermore National Laboratory: 7000 East Ave, Livermore, CA, 94550, United States*
[2]*Atomic Weapons Establishment: Aldermaston, Reading, Berkshire, RG7 4RS, United Kingdom*

Measurements of (n,2n) cross sections on radioactive species at 14.1 MeV are challenging due to the difficulty in obtaining and handling target material in quantities required for accelerator-based experiments. A platform has been developed at the National Ignition Facility (NIF) to add radioactive target material to the inner surface of ignition capsules. Using this method only 10^{13} atoms are required to make a cross section measurement, far less than an equivalent accelerator experiment (>10^{16} atoms). The first measurement of the ^{88}Y(n,2n)^{87}Y cross section at NIF using this platform will be discussed.

1 SUMMARY

The NIF is an Inertial Confinement Fusion (ICF) research facility at Lawrence Livermore National Laboratory (LLNL). During an ICF shot, a high-density carbon (HDC) capsule filled with deuterium and tritium (DT) is compressed to extreme densities and temperatures with 192 high energy laser beams. The resulting DT fusion produces alpha particles and a significant yield (≤10^{18}) of 14.1 MeV neutrons in a short pulse (~100 ps). Material on the inside of the target capsule sees extremely large neutron fluxes ($10^{27\text{-}33}$ n/s/cm^2), allowing cross section measurements to be made with low amounts of target material (~10^{13} atoms). These measurements are unique due to the NIF high energy density (HED) plasma environment and neutron spectrum (14.1 MeV) with minimal contributions from lower energy neutrons, such as down scattered or 2.45 MeV (DD) neutrons. Furthermore, the exceedingly small amount of target material required for measurements allows for the study of reactions that cannot be measured at conventional nuclear reactor or particle accelerator facilities.

To take advantage of these unique capabilities for cross section measurements at NIF, target material must be added to the inner surface of HDC NIF capsules. These capsules are 2-mm (outer diameter) with a 10 μm fill hole, which is used to add the DT fuel. Any dopant added to the capsule must be extremely pure and contained in a very small volume of solution. The total volume of the capsules is only ~3 μL and contaminants, such as salt (Na, K, Ca, etc.), can easily plug the microscopic fill hole after solution is added and dried. Three systems have been successfully developed with capabilities for doping NIF capsules. The first, Apparatus for NIF-Doping Automated Robotic Injection System for Targets (ANDARIST), is based on microinjection of material through the fill hole with a micro-capillary. The second system, Vacuum Optimized Radionuclide-to-Capsule Administer for NIF (VORCAN), uses a vacuum to pull liquid into the capsule. The final system, Pressure Assisted Radiochemical Apparatus for Liquid Doping (PARALD) also uses vacuum to pull liquid into the capsule but can accommodate larger solution volumes

To measure a cross section at NIF, the capsule must not only be doped with the nuclide of interest, but also a flux monitor with a well-characterized cross section to enable accurate calculation of the unknown cross section. However, this requires the isotopes with known and unknown cross sections to be intimately mixed and chemically similar to minimize fractionation in the NIF shot. Both isotopes must have an additional tracer isotope to quantify for both the insertion into the capsule and the post-shot collection efficiency. Based on these stringent parameters, a specific radionuclide cocktail must be determined for each experiment. New radiochemical techniques that have been developed to meet these needs will be discussed. Reaction products are collected via Solid Radiochemistry Collectors (SRC) in the NIF target chamber. These can be removed post-shot for gamma-ray spectroscopy and radiochemical separations, as needed, to analyze the reaction products.

Measurements at NIF are currently focused on the ^{89}Y(n,2n)^{88}Y and ^{88}Y(n,2n)^{87}Y reactions, which can be used as a benchmark for future cross section measurements such as ^{173}Lu(n,2n)^{172}Lu. Results on the first measurement of ^{89}Y(n,2n)^{88}Y and ^{88}Y(n,2n)^{87}Y in an HED plasma at NIF will be presented.

2. CONCLUSIONS

Nuclear data measurements on radioactive species at 14.1 MeV are lacking in literature. For many radioactive isotopes cross section measurements are impossible to perform at traditional accelerator facilities due to the required amounts of target material. The NIF platform provides a means to measure these cross sections on extremely small quantities of target

Copyright on 7th Asia-Pacific Symposium on Radiochemistry 2025 - R1-13 -

material. Development of this nuclear data measurement technique has huge benefits for nuclear physics and radiochemical applications.

ACKNOWLEDGMENTS

This work was performed under the auspices of the U.S. Department of Energy by Lawrence Livermore National Laboratory under Contract DE-AC52-07NA27344. This material is based upon work supported by the U.S. Department of Energy, Office of Science, Office of Nuclear Physics, under Work Proposal No. SCW1781.

7th Asia-Pacific Symposium on Radiochemistry *September 14 ~ 19, 2025 • Kunibiki Messe • Shimane, Japan*

Measurement of the ^{73}As(n,g) cross section at thermal neutron energies

Kelly Kmak[1], John Despotopulos[1], Connor Holiski[1], William Kerlin[1], Nicholas Scielzo[1]

[1]*Lawrence Livermore National Laboratory: 7000 East Ave, Livermore, CA, 94550*

Arsenic-73 is a radioactive isotope with a half-life of 80.3 days. There is currently no available data in the literature for neutron capture of this isotope, likely because nuclear reaction measurements can be challenging on unstable isotopes. Irradiations of ^{73}As were conducted at the Missouri University Research Reactor (MURR) to determine the cross section for the ^{73}As(n,g) reaction. Extensive nuclear decay counting was performed at LLNL to quantify the production of ^{74}As in these irradiations. Preliminary data for this novel cross section measurement is presented here.

1 SUMMARY

As part of a collaboration with the Facility for Rare Ion Beams (FRIB), Lawrence Livermore National Laboratory (LLNL) has been studying radiochemical and nuclear reaction properties arsenic isotopes. As FRIB comes online, radioarsenic species will be some of the first isotopes available, and there are plans to harvest these isotopes for applications in biochemistry, nuclear medicine and national security. As part of this work, there have been five publications on novel arsenic and selenium radiochemistry with three more pending. Alongside the radiochemistry efforts, a series of nuclear data measurements are in progress at LLNL to fill in gaps in the available data for arsenic isotopes.

The first of these experiments is to measure the thermal neutron capture of ^{73}As, which is a useful isotope for environmental tracer studies and is also of interest to the LLNL Stockpile Stewardship Program (SSP). This cross section has not been reported in the literature, likely due to difficulties in obtaining ^{73}As in an isotopically pure form as well as challenges related to handling radioactive target materials. For these experiments, ^{73}As was obtained from Los Alamos National Laboratory, where it is produced via the proton irradiation of germanium, and allowed to decay for several months to eliminate other shorter-lived radioarsenic isotopes, particularly ^{74}As, that are co-produced with the ^{73}As. Two ^{73}As samples, ~300 µCi each, were then sealed in quartz tubes for reactor irradiation at MURR. Monitor foils (Zr, Y, Mo, Fe) were irradiated alongside the ^{73}As samples to assess the neutron flux during the irradiation. Samples were characterized extensively with gamma spectroscopy at the Nuclear Counting Facility (NCF) at LLNL before and after irradiation. Initial results from these neutron capture experiments will be discussed.

Further work on arsenic measurements is planned in coordination with the National Ignition Facility (NIF), which is a unique source of high flux, 14 MeV neutrons. This work began with measurements of the ^{75}As(n,2n) cross section as a proof of concept for a ride-along method of cross section measurements. While the ^{75}As(n,2n) cross section has been measured before, there is a large variance in the measurements in the literature, therefore a new measurement will improve the available nuclear data as well as demonstrate a method for measuring (n,2n) cross sections at NIF on samples of ~$1x10^{16}$ to $1x10^{20}$ atoms. For smaller samples ($1x10^{13}$ atoms), a platform for performing (n,2n) measurements on radioactive species at NIF has been demonstrated. These measurements are accomplished by doping the material of interest into the NIF capsule, which is then filled with deuterium-tritium fuel that undergoes fusion, producing 14.1 MeV neutrons, during the NIF shot. Both methods will be evaluated as an avenue for measuring the ^{73}As(n,2n) reaction to provide nuclear data in a regime more relevant for SSP. The capsule-based measurement route requires extremely laborious sample preparation as any mass present in the solution with the radionuclide can occlude the extremely small (10 µm) fill holes of NIF capsules, which themselves are only 2 mm in diameter. Collection of debris from a NIF shot for analysis is also a challenge. However, the ride-along method requires more activity, which poses a logistical challenge for target fabrication when working with radioactive species.

These experiments contribute to ongoing efforts at obtaining high fidelity nuclear data on radioactive species, which is an active area of research at LLNL and is vital for constraining models that use calculated, rather than measured, nuclear reaction data.

2. CONCLUSIONS

Nuclear data measurements on radioactive species are critical to reaction cross section networks used by LLNL. These measurements present a range of challenges as compared to similar measurements on stable isotopes and innovation is needed in this area to make new contributions to nuclear data sets. Obtaining this nuclear data, and establishing new techniques for these measurements, has benefits for a wide range of radiochemical and nuclear physics applications.

Copyright on 7th Asia-Pacific Symposium on Radiochemistry 2025 - R1-14 -

ACKNOWLEDGMENTS

The authors thank the NCF staff at LLNL, particularly Keenan Thomas, for their nuclear counting expertise. This work was performed under the auspices of the U.S. Department of Energy by Lawrence Livermore National Laboratory under Contract DE-AC52-07NA27344. This work was funded by the Laboratory Directed Research and Development Program at LLNL under project tracking code 23-SI-004. LLNL-ABS-2006208

7th Asia-Pacific Symposium on Radiochemistry *September 14 ~ 19, 2025 • Kunibiki Messe • Shimane, Japan*

EXPERIMENTAL STUDY ON NOBLE GAS TRANSPORT IN LIQUID LEAD USING THE GAS-JET FACILITY AT PSI

Haohan Zhang[1], Robert Eicher[1, 2]

[1]*Laboratory of Radiochemistry, Paul Scherrer Institut (PSI), Forschungsstrasse 111, 5232 Villigen, Switzerland*
[2]*Department of Chemistry, Biochemistry and Pharmaceutical Sciences, University of Bern, Freiestrasse 3, 3012 Bern, Switzerland*

Monitoring and timely detection of nuclear fuel failures are critical challenges in the development and optimization of next-generation lead-cooled fast reactors (LFRs). Noble gas fission products are among the first radioactive species released in fuel failure scenarios, making their detection essential for early failure identification. However, studies on noble gas release and transport in liquid lead remain limited. This study provides experimental data on noble gas transport in liquid lead using a newly developed experimental setup. Designed to replicate LFR operating conditions, the setup enables controlled experimental conditions and real-time, online detection of noble gas fission products. Noble gas fission products are generated via fission of ^{235}U and extracted for transport experiments by using the Gas-jet facility at PSI. The results offer valuable insights for designing and validating fuel pin failure detection systems in LFRs, contributing to improved reactor safety and reliability.

1 INTRODUCTION

The lead-cooled fast reactor (LFR) concept is one of the six reactor technologies that have been selected in the technical roadmap of the Generation IV International Forum (GIF) for further research and development. LFRs have gained significant interest because of its advanced concepts in terms of sustainability and in proliferation resistance and physical protection [1]. However, the success deployment of this technology requires a comprehensive evaluation of its safety performance.

A key aspect of nuclear safety is preventing the release of radioactive materials, which is generally ensured through a multi-barrier design. The nuclear fuel matrix and fuel cladding serve as the first barrier against radioactive release. While the probability of fuel cladding failure is very low, it is not impossible. This issue has been well recognized and extensively studied in water-cooled nuclear reactors [2-4]. For LFRs, experimental data on noble gas fission product release remains scarce [5, 6]. The complexity of LFR designs—such as the use of non-transparent liquid lead as a coolant and higher operating temperatures (~500 °C) compared to water-cooled reactors—poses significant experimental challenges. Additionally, noble gases are intentionally introduced into fuel cladding tubes in LFRs as fingerprinting tracers to facilitate early detection of fuel pin failures. To assess the effectiveness of this approach, experimental studies on noble gas transport in liquid lead are essential.

This study aims to provide experimental data on noble gas fission product transport in liquid lead under conditions similar to LFR operational conditions. Relevant noble gas fission products are made available through the Gas-jet facility at the Swiss Neutron Spallation Source (SINQ), where products of ^{235}U nuclear fission can be directly extracted and used for experiments [7]. Additionally, a specialized experimental setup has been developed to enable precise control and monitoring of temperature and oxygen concentration during liquid lead experiments. Macroscopic amounts of noble gases can be easily admixed to the fission product gas-jet to observe the behavior of larger quantities in contact with lead using the fission gases as tracers for quantification.

2 EXPERIMENTAL SETUP AND PRELIMINARY RESULTS

To conduct noble gas fission product transport experiments under LFR-like conditions, having a leak-tight experimental setup is essential. The system should be able to maintain liquid lead at approximately 500 °C, enable the controlled introduction and extraction of noble gases for measurement, and regulate oxygen concentration to prevent lead oxide formation. To meet these requirements, a sealed compartment equipped with a heating element has been designed to melt the lead (as shown in Fig.1). Noble gas fission products are introduced via a quartz tube with a quartz propeller at the end, ensuring effective mixing in the liquid lead. A vertically movable oxygen sensor monitors oxygen concentration, while released fission gases are collected and directed to a gas trap above a gamma detector for real-time monitoring.

A cryogenic trap has been implemented to enhance noble gas retention and ensure precise measurement by gamma spectrometry. The trap consists of a copper tube filled with a mixture of charcoal and zeolite, providing a high surface

Copyright on 7th Asia-Pacific Symposium on Radiochemistry 2025 - R1-15 -

area for gas adsorption. It is cooled using liquid nitrogen (boiling point: -196 °C), allowing krypton and xenon (boiling points: -153 °C and -108 °C, respectively) to liquefy and be effectively retained within the trap.

Preliminary transport experiments were conducted by introducing radioactive xenon into the setup both with and without liquid lead. A comparison of the xenon breakthrough curves indicates little or no retention of xenon by liquid lead. Further experiments will be carried out to confirm and better understand this observation.

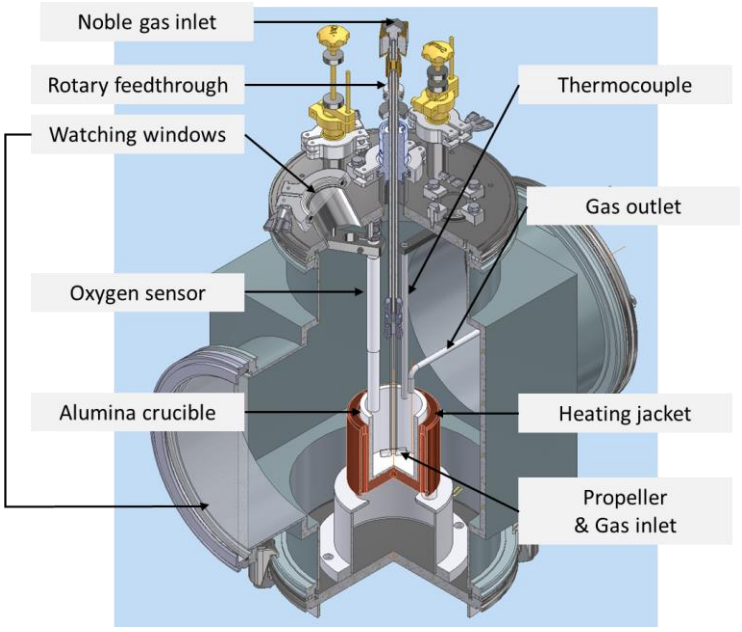


Fig. 1. Schematic illustration of experimental setup

ACKNOWLEDGMENTS

This project has received funding from the European Union's Horizon EURATOM 2021 research and training program under Grant Agreement No 101061185: ANSELMUS (Advanced Nuclear Safety Evaluation of Liquid Metal Using Systems) https://cordis.europa.eu/project/id/101061185.

References

[1] H. Kamide *et al*., "Generation IV International Forum - GIF, Annual Report 2020," NEA (2021).
[2] D. H. Locke, *Nuclear Engineering and Design*, **21**, 318-330 (1972).
[3] B. J. Lewis *et al*., *Journal of Nuclear Materials*, **489**, 64-83 (2017).
[4] M. S. Veshchunov, *Nuclear Engineering and Design*, **343**, 57-62 (2019).
[5] J.S. Bell *et al*., *Annals of Nuclear Energy*, **148**, 107683 (2020).
[6] M. Epstein *et al*., *Annals of Nuclear Energy*, **181**, 109499 (2023).
[7] G. Tiebel *et al*., *Nuclear Instruments and Methods in Physics Research Section A: Accelerators, Spectrometers, Detectors and Associated Equipment*,**1041**, 167360 (2022).

Copyright on 7th Asia-Pacific Symposium on Radiochemistry 2025 - R1-15 -

Contributed Talk | [R3]Actinide Chemistry and Nuclear Energy Chemistry

Fri. Sep 19, 2025 9:00 AM - 10:00 AM JST | Fri. Sep 19, 2025 12:00 AM - 1:00 AM UTC Hall A(MP)

[R3] Actinide Chemistry and Nuclear Energy Chemistry

9:00 AM - 9:20 AM JST | 12:00 AM - 12:20 AM UTC

[R3-23]

Burnup determination of irradiated U-Mo dispersion fuel by chemical methods

*Hyejin Cho[1], Nam uk Kim[1], Yang-Soon Park[1], Minjae Ha[1], Junhyuck Kim[1], Hye-Ryun Cho[1], Jai Il Park[1] (1. Korea Atomic Energy Research Institute (Korea))

9:20 AM - 9:40 AM JST | 12:20 AM - 12:40 AM UTC

[R3-24]

Small-Scale Experiments, Big-Scale Impact: Insights into Anion Exchange Chemistry in Pu Recovery

*Maryline G Kerlin (Ferrier)[1], Bradley C Childs[1], Scott A Simpson[1], Silvina A Di Pietro[1], Tsuyoshi A Kohlgruber[1], Emma R Tardiff[1], Hiroshi H Saito[1], Saurabh Narain[1], Kiel S Holliday[1], Lawrence Eddy Banks[1] (1. Lawrence Livermore National Laboratory (United States of America))

9:40 AM - 10:00 AM JST | 12:40 AM - 1:00 AM UTC

[R3-25]

Experimental Study on Pyrolytic Incineration Mechanism of trialkylphosphine oxide(TRPO)

*Duo Ma[1], Wei Xu[2], Meng Wei[1], Longhao Cao[1] (1. CNNC Longan Co., Ltd. (China), 2. China Institute for Radiation Protection (China))

©APSORC25

7th Asia-Pacific Symposium on Radiochemistry *September 14 ~ 19, 2025 • Kunibiki Messe • Shimane, Japan*

BURNUP DETERMINATION OF IRRADIATED U-MO DISPERSION FUEL BY CHEMICAL METHODS

Hyejin Cho, Namuk Kim, Yang-Soon Park, Minjae Ha, Junhyuck Kim, Hye-Ryun Cho, Jai Il Park

Affiliation Information: Korea Atomic Energy Research Institute, 111 Daedeok-daero-989, Yuseong-gu, Daejeon 34057, and hcho921@kaeri.re.kr

The determination of burnup is a crucial step for assessing nuclear fuel performance. Employing both non-destructive and destructive techniques, researchers aim to quantify the number of fissions per heavy atom (mass ≥ 232) initially present in the fuel. Destructive methods were employed to determine the burnup of U-Mo dispersion fuel irradiated in the HANARO at KAERI. Through precise analysis and measurement, the burnup of the U-Mo dispersion fuel was accurately determined.

1. INTRODUCTION

The irradiated fuel samples discussed here were submitted for chemical analysis after completing the HAMP-2 (HANARO Mini-Plate irradiation test - 2) irradiation experiment at the High-flux Advanced Neutron Application Reactor (HANARO), located within Korea Atomic Energy Research Institute (KAERI). Hereafter, these samples will be referred to as HAMP-2. This paper details the procedure for determining the burnup (atom % fission) of heavy isotopes (M ≧ 232) in the HAMP-2 samples.

1.1 Burnup Overview

Burnup is generally represented as a percentage of the initial fissile material atoms (% FIMA) that have undergone fission or as the energy released per unit mass of fuel (GWd/tU). Approximately, 1 atom % burnup corresponds to about 9.6 GWd/tU. Chemical burnup analysis techniques are considered destructive methods, directly quantifying heavy elements and specific fission products. These can be broadly categorized into two main approaches: i) Direct measurement of changes in heavy isotopes before and after irradiation, which is based on the decrease or increase of U-235, Pu-239, and other isotopes due to burnup, and ii) Quantifying specific indicators (burn-up monitor elements) among the heavy elements and fission products to calculate burnup [1-2].

This paper presents a study where Nd-148 was used as an indicator element for analyzing the burnup of HAMP-2 samples, and the results are compared with those calculated using the Nd-(145+146), Cs-137 measurements and code calculations.

1.2 Fuel Overview

The Ki-Jang Research Reactor (KJRR) is a research reactor under construction for the production of medical isotopes and neutron doping. It is designed to employ a plate-type U-7Mo fuel with low-enriched uranium (LEU). The fuel consists of metal alloy (U-7Mo) particles dispersed in an aluminum-silicon alloy matrix (Al-5Si). The cladding material for the fuel plates is aluminum 6061 alloy. This structure plays a crucial role in maintaining the safety and combustion efficiency of the fuel. The HAMP-2 irradiation test involved loading an irradiation capsule with a miniaturized U-Mo dispersed fuel assembly into the OR-3 irradiation port at the HANARO reactor. The irradiation test spanned from June 10, 2018 to April 25, 2022 [3].

The irradiated HAMP-2 was prepared as samples for chemical analysis at a hot cell in the KAERI irradiation materials examination facility (IMEF). Each sample consisted of 1~3 pellets, punched at three locations: Top (4-C-3), Mid (4-C-2), and Bottom (4-C-1-1). One sample contained 1~3 round cylindrical punches with diameters of 1.5 mm. The prepared HAMP-2 samples were then transported to the chemical hot cell in the chemical analysis facility (CAF) for analysis.

2. RESULTS AND DISCUSSIONS

The solid samples received from the IMEF underwent dissolution in a mixture of mineral acids to obtain a solution of the fuel. This solution was then transported using a transfer device to the glovebox. The transferred solution was diluted for gamma-ray measurement and for separating U, Pu, and Nd to determine the quantities of each isotope.

2.1 Fuel Dissolution, Separation and Measurement of U, Pu, and Nd

The dissolution procedure involves two sequential steps for the dissolution of cladding material and dispersion fuel. The fuel sample was completely dissolved in a mixture of 6 M HCl and 14 M HNO_3 - 1 M HF, maintained at 60 ~ 90 °C

Copyright on 7th Asia-Pacific Symposium on Radiochemistry 2025 - R3-23 -

for 6 hours under reflux conditions.

A small aliquot of the fuel solution was diluted with 8 M HNO_3 by weight to achieve a concentration of approximately 100 ng of Nd-148 per gram of solution. The solution was then divided into three portions, with one portion transferred to a vial for γ-spectrometric measurement of Cs-137. The remaining two portions were subjected to the determination of U, Pu, and Nd isotopes with and without triple spikes of U-233, Pu-242, and Nd-150 addition, followed by two sequential anion exchange resin separation procedures.

Nd and other fission products were passed through the first column with 6 mL of 12M HCl. This portion was collected and stored for the second separation. Pu was eluted from the first column using a 12 M HCl-0.1 M HI mixture, followed by the elution of U with 0.1 M HCl. The Nd fraction was isolated from other fission products on the second column using a methanol (MeOH)-HNO_3 medium, specifically a 0.04 M HNO_3-99.6% MeOH (1:9) eluent, under established chromatographic conditions.

The isotopic compositions of U, Pu, and Nd in each isolated and concentrated fraction were measured using a thermal ionization mass spectrometer (TIMS). Sample solutions of U, Pu, and Nd in the range of μg to ng were loaded onto a rhenium filament and then measured. The contribution of natural Nd was corrected for all the Nd isotopes measured.

2.2 Burnup Calculation

The total burnup (F_T) value in atom% fission was calculated by using different Nd and Cs isotope monitors according to Eq. (1) [1].

$$F_T = \left[\frac{N/Y}{(N/Y + N(U) + N(Pu))}\right] \times 100 \quad (1)$$

Where, N: number of atoms of the monitor Nd or Cs isotope in the irradiated fuel solution,
Y: effective fission yield of the monitor Nd or Cs isotope from the fissile elements,
$N(U)$, $N(Pu)$: number of U and Pu atoms in the irradiated fuel solution, respectively.

Table 1 gives the total burnup determined by the Nd isotope, Nd-148, together with the corresponding results calculated by the McCARD (Monte Carlo Code for Advanced Reactor Design and Analysis) program for HAMP-2 fuel samples. The number of fissions by the Nd-148 monitor was calculated by correcting the excess Nd-148 produced from the neutron capture of Nd-147, where the correction factor(K) was obtained from the HANARO operation conditions.

TABLE 1. Total burnup of HAMP-2 fuel

	HAMP-2 burnup (GWD/tU)		
	4-C-1-1(bottom)	4-C-2(mid)	4-C-3(top)
Nd-148	115.7 ± 7.2	115.8 ± 7.2	108.4 ± 6.8
McCARD calculation	117.880 ~ 121.82	109.055 ~ 109.62	108.116 ~ 108.87

3. CONCLUSIONS

This study concludes with the successful application of the highly accurate Nd-148 method to determine the burnup of HAMP fuel. The experimental conditions and methods were established using unirradiated samples, and through TIMS and IDMS techniques, U, Pu, and Nd from irradiated HAMP samples were successfully dissolved, separated, measured, and quantified. Burnup values calculated via the Nd-148 method matched those obtained with the Nd-(145+146) method and McCARD calculations within uncertainty, showing consistency. This consistency highlights the reliability and precision of the employed methodologies, thereby validating their applicability in fuel burnup assessments.

ACKNOWLEDGMENTS

This work was supported by the KAERI Institutional Program (Project No. 524620-25).

References

[1] American Society for Testing and Materials Standard Method E 321-20, “Atom Percent Fission in Uranium and Plutonium Fuel (Neodymium-148 Method)”, 1 (2020).

[2] J. S. Kim, S. H. Han, M. Y. Suh, K. S. Joe and T. Y. Eom, ″Burnup Measurement of Irradiated Uranium Dioxide Fuel by Chemical Methods”, *J. Korean Nucl. Soc*. **21**(4), 277 (1989).

[3] G. Jung, et al., “PIE Report on the HANARO Mini Plate Irradiation II (HAMP-2)”, KJ-374-KN-468-007, Rev. 0. (2024).

Copyright on 7th Asia-Pacific Symposium on Radiochemistry 2025 - R3-23 -

7th Asia-Pacific Symposium on Radiochemistry *September 14 ~ 19, 2025 • Kunibiki Messe • Shimane, Japan*

SMALL-SCALE EXPERIMENTS, BIG-SCALE IMPACT: INSIGHTS INTO ANION EXCHANGE CHEMISTRY IN PU RECOVERY

Maryline G. Ferrier (Kerlin)[1*], Bradley C. Childs[1], Scott A. Simpson[1], Silvi A. Di Pietro[1], Tsuyoshi A. Kohlgruber[1], Emma R. Tardiff[1], Hiroshi H. Saito[1], Saurabh Narain[1], Kiel S. Holliday[1], and Lawrence E. Banks[1]

[1]*Lawrence Livermore National Laboratory, Livermore, California, United States*
** email: kerlin4@llnl.gov*

After nearly a decade of demolition, construction, and readiness assessments, the Pu Recovery Glovebox Lines at LLNL were approved for startup in April of 2022. This renovated facility provides a critical capability for medium-scale plutonium (Pu) purification, capable of reprocessing a wide variety of feed materials. The overall chemistry is well-established: the dissolved Pu solution is adjusted to a +IV oxidation state and a nitric acid concentration of 7-9 M before being loaded onto an anion exchange column. Here, Pu remains on the column while impurities are washed out, and elution is achieved using a low nitric acid solution (0.5 M). This solution is collected, and Pu is reduced to a +III oxidation state, precipitated with oxalic acid, and calcined to produce Pu oxide.
At this operational scale, the process is run by technicians rather than scientists with expertise in Pu chemistry. As a result, small-scale experiments are conducted to better understand the chemical processes and determine approaches that are most suitable for large-scale operations. This talk will focus on understanding the anion exchange column chemistry, focusing on key operational parameters such as valence adjustments, flow rates, volumes, concentrations, and temperatures. Experiments can easily be conducted in small scale and being translated to a larger scale as long as the Pu flux is standardized. To investigate the influence of process parameters on Pu concentration and valence, experiments are monitored using UV-visible spectroscopy, while the purity of the final product is assessed via mass spectrometry. These studies aim to ensure the production of high-purity Pu solutions with minimal impurities while maintaining operational simplicity for non-experts.

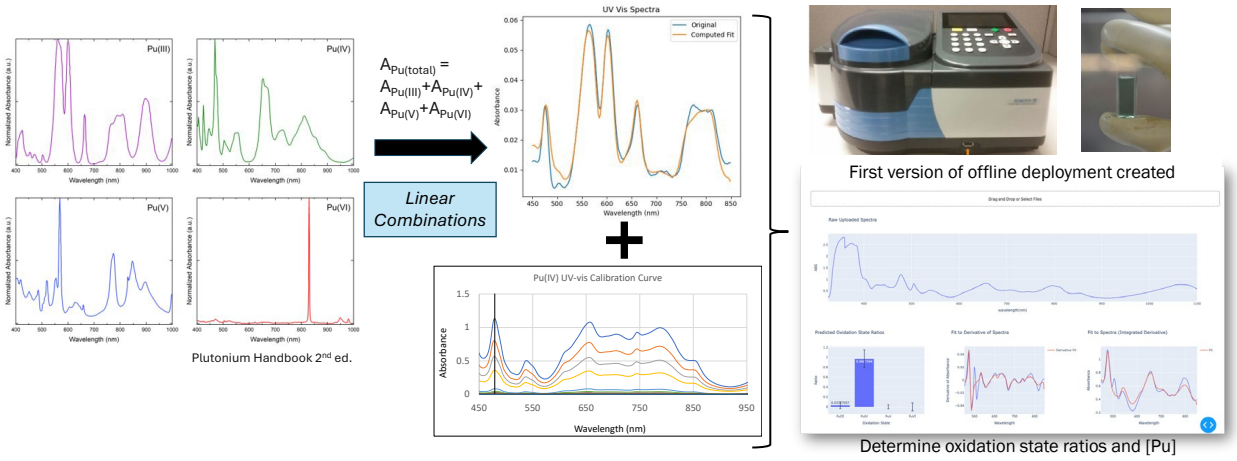


Figure introducing the technique used to analyze raw UV-Visible spectra in order to obtain automatically an output showing the percentage of each oxidation state of plutonium present in solution.

ACKNOWLEDGMENTS

This work was performed under the auspices of the U.S. Department of Energy by Lawrence Livermore National Laboratory under Contract DE-AC52-07NA27344. LLNL-ABS-2005307.

Copyright on 7th Asia-Pacific Symposium on Radiochemistry 2025 - R3-24 -

7th Asia-Pacific Symposium on Radiochemistry *September 14 ~ 19, 2025 • Kunibiki Messe • Shimane, Japan*

Experimental Study on Pyrolytic Incineration Mechanism of trialkylphosphine oxide(TRPO)

Duo Ma[1], Wei Xu[2], Meng Wei[1], Longhao Cao[1]

[1]*CNNC Longan Co., Ltd.: Beijing, China*
[2]*China Institute for Radiation Protection: Taiyuan,China*

Trialkylphosphine oxide(TRPO) is an extractant used in the separation process of advanced spent fuel reprocessing. It can separate high exothermic fission products (Sr, Cs) and long-lived minor actinides (Am, Cm) from high level radioactive waste liquid. However, the engineering application of this separation process must solve the problem of disposal waste TPRO as a radioactive organic waste. TRPO and TBP used in Purex process of spent fuel reprocessing are both organophosphorus extractants, so the pyrolysis incineration mechanism of TRPO was studied by referring to the pyrolysis incineration of waste TBP. According to the properties of organophosphorus compounds, the functional groups of Cyanex923 TRPO are linear alkyl groups, which can be decomposed and disproportionated to produce higher and lower organophosphorus compounds. Phosphorus mainly exists in lower and higher organophosphorus compounds. The pyrolysis products of pure TPRO and TRPO+ Ca $(OH)_2$ were pyrolytic anhydride, phosphine (R3P), middle phosphine (H3P), alkene, phosphonic acid $(RP(O)(OH)_2)$ and phosphorus oxide (PxOy). However, phosphorus fixation experiments show that phosphorus fixation rate is lower than 5%, and adjusting the type of emulsifier has no obvious effect on improving phosphorus fixation rate. It is preliminarily indicated that it is not feasible to treat TRPO organic waste liquid by pyrolysis incineration process for treating TBP, and it is necessary to seek other destructive treatment methods, such as direct incineration, supercritical water oxidation, etc.

Keyword:High level liquid waste separation, trialkylphosphine oxide(TRPO), Waste solvent treatment, Pyrolysis incineration

Copyright on 7th Asia-Pacific Symposium on Radiochemistry 2025 - R3-25 -

Contributed Talk | [P3]Environmental Integrated Knowledge of Radionuclides Dynamics Studied from the Fukushima Accident

Fri. Sep 19, 2025 9:00 AM - 10:00 AM JST | Fri. Sep 19, 2025 12:00 AM - 1:00 AM UTC Hall B(Small)

[P3] Environmental Integrated knowledge of Radionuclides Dinamics Studied from the Fukushima Accident

9:00 AM - 9:20 AM JST | 12:00 AM - 12:20 AM UTC

[P3-07]

Aging Effect on the Decontamination Efficiency of ^{137}Cs from Clay Minerals Using Cationic Surfactant

Akihito Matsushima[1], Herry Wijayanto[2], *Satoru Nakashima[1] (1. Hiroshima University (Japan), 2. National Research and Innovation Agency of Indonesia (Indonesia))

9:20 AM - 9:40 AM JST | 12:20 AM - 12:40 AM UTC

[P3-08]

Impact of plutonium originating from Fukushima Daiichi Nuclear Power Plant accident in the environment: an overview of a decade studies

*Jian Zheng[1], Junwen Wu[2], Keiko Tagami[1], Guosheng Yang[1], Tatsuo Aono[3] (1. National Institutes for Quantum Science and Technology (QST) (Japan), 2. Shantou University (China), 3. Fukushima Institute for Research, Education and Innovation (Japan))

9:40 AM - 10:00 AM JST | 12:40 AM - 1:00 AM UTC

[P3-09]

Effect of Gamma Dose and pH on Methyl Iodide Formation in 2 mM NaI and 5 mM MEK Aqueous Solutions

*Jei-Won Yeon[1], Minsik Kim[2] (1. Korea Atomic Energy Research Institute (Korea), 2. Korea Institute of Toxicology (Korea))

©APSORC25

AGING EFFECT ON THE DECONTAMINATION EFFICIENCY OF ^{137}Cs FROM CLAY MINERALS USING CATIONIC SURFACTANT

Akihito Matsushima[1], Herry Wijayanto[2], Satoru Nakashima[1,3]

[1]*Natural Science Center for Basic Research and Development (N-BARD), Hiroshima University, 1-4-2 Kagamiyama, Higashi-Hiroshima, Hiroshima 739-8526, Japan. E-mail: masha@hiroshima-u.ac.jp*
[2]*Research Center for Nuclear Materials and Radioactive Waste Technology (PRTBNLR), Research Organization of Nuclear Technology (ORTN), National Research and Innovation Agency (BRIN) of Indonesia, South Tangerang 15314, Indonesia. E-mail: herry.wijayanto@brin.go.id*
[3]*Graduate School of Advanced Science and Engineering, Hiroshima University, 1-4-1 Kagamiyama, Higashi-Hiroshima, Hiroshima 739-8526, Japan. E-mail: snaka@hiroshima-u.ac.jp*

In order to investigate the aging effect on the decontamination efficiency from clay minerals contaminated with ^{137}Cs, four types of clay minerals (illite, kaolinite, Na-bentonite, Ca-bentonite) that had adsorbed ^{137}Cs were decontaminated with two types of cationic surfactants (benzyldodecyldimethylammonium bromide (BDAB) and dodecyltrimethylammonium bromide (DTAB)). No change in decontamination efficiency over aging time was observed for kaolinite and Ca-bentonite, while the change was observed for illite and Na-bentonite. The difference was discussed from the point of the equilibrium of $Cs^+_{aq/sol} \rightleftharpoons Cs^+_{aq/clay} \rightleftharpoons Cs^+_{adsorption}$ + aq in the clay mineral.

1 INTRODUCTION

Of the radionuclides found in Fukushima soil after Fukushima Daiichi Nuclear Power Plant accident, radioactive cesium is still of major concern because of its long half-life and consecutive effect on human health and surrounding environment for an extended period. It is known that ^{137}Cs adsorbed to soil is extremely difficult to decontaminate. This is thought to be because Cs^+ ions are strongly adsorbed to the clay minerals contained in the soil. Four types of clay minerals (illite, kaolinite, Na-bentonite, Ca-bentonite) adsorbed ^{137}Cs were decontaminated using two types of cationic surfactants (benzyldodecyldimethylammonium bromide (BDAB) and dodecyltrimethylammonium bromide (DTAB)) [1]. In the present study, we investigated how the decontamination efficiency of BDAB and DTAB changes over aging time after ^{137}Cs adsorption treatment of the above four types of clay minerals.

2 EXPERIMENTAL

2.1 Preparation of Cs-adsorbed samples

10 g of each clay mineral (illite, kaolinite, Na-bentonite, and Ca-bentonite) was added into 225 ml centrifuge tube. To this tube 100 ml of 100 mM CsCl (100 Bq/ml) was added. Radioisotope ^{137}Cs was added to the CsCl solution in advance with concentration ratio 0.001 mmol/1 Bq (CsCl/^{137}Cs). The mixture was equilibrated for 24 h at 25 ℃ on horizontal shaker, then followed by centrifugation at 2400 rpm for 10 min to separate solid samples from supernatant. To assure Cs was tightly adsorbed, the solid samples were washed several times using distilled water until released ^{137}Cs was not detected in the rinse solution using gamma counter. Cs-adsorbed samples were collected by drying at 80 ℃ for 24 h.

2.2 Desorption experiments

The ^{137}Cs-adsorbed clay minerals were aged for 1 day, 10 days, 20 days, 30 days, 60 days at room temperature. Cs desorption experiment was performed by mixing each Cs-adsorbed sample (0.125 g) with 1.25 ml of 0 mM, 5 mM, 10 mM, 30 mM, 50 mM, 100 mM BDAB or DTAB. The mixture was agitated at 25 ℃ for 24 h on vortex mixer equipped with head-disc type. The samples were then centrifuged and washed three times with distilled water before being dried in oven at 80 ℃ for 24 h.

The dried samples were measured using HP-Ge detector to determine the remaining Cs in the solid phase after desorption treatment (solid-based measurement). Cs desorption efficiency was calculated.

2.3 Radioactivity measurement

Radioactivity concentration of ^{137}Cs in the dried Cs-adsorbed samples was measured (solid-based measurement) using HP-Ge detector and was calculated using the following equation:

$$RC=CPS/(E*I_\gamma*m) \quad \text{eq 1}$$

where RC is radioactivity concentration (Bq/g), CPS is net counts per second ($CPS=CPS_{sample} - CPS_{background}$), E is counting efficiency of HP-Ge detector obtained from calibration, I_γ is emission rate (85.00%) of selected gamma-ray (661.49 keV), and m is sample mass (g). Finally, the amount of Cs bound to clays was calculated using eq 2 by considering CsCl/^{137}Cs concentration ratio,

$$C = RC*r \quad \text{eq 2}$$

where C is amount of Cs in the Cs-adsorbed samples (mmol/g), and RC and r are radioactivity concentration of ^{137}Cs obtained from eq 1 and CsCl/^{137}Cs concentration ratio, respectively.

3 RESULTS AND DISCUSSION

3.1 Cs Adsorption

$C_{initial}$ was 0.0275, 0.0148, 0.3479, 0.4425 mmol/g for illite, kaolinite, Na-bentonite, Ca-bentonite, respectively. The concentrations are lower than the corresponding literature concentrations [1]. But the order of the concentration is the same with the literature. This may suggest that the present washing is thorough. Number of washing not to detect Cs in the rinse solution was 7 times for kaolinite and Ca-bentonite, while 12 times for illite and Na-bentonite. We consider the equilibrium in the clay or on the clay as below

$$Cs^{+}_{aq/sol} \overset{K_1}{\rightleftharpoons} Cs^{+}_{aq/clay} \overset{K_2}{\rightleftharpoons} Cs^{+}_{adsorption} + aq, \quad \text{eq 3}$$

where $Cs^{+}_{aq/sol}$ and $Cs^{+}_{aq/clay}$ are hydrated Cs^{+} in solution and in the clay, respectively, and $Cs^{+}_{adsorption}$ is a naked Cs^{+} adsorbed to clay. Not only K_1 but also K_2 should be considered for washing.

3.2 Cs desorption from Cs-adsorbed samples and aging effect on decontamination efficiency

BDAB had a higher decontamination efficiency than DTAB for all clay minerals. The decontamination efficiency increased with an increase of surfactant concentration. The decontamination efficiency decreased by 30 days aging for Na-bentonite and illite, while the efficiency remained almost constant over aging time for Ca-bentonite and kaolinite.

The change in decontamination efficiency over aging time for 30 mM of cationic surfactant concentration was compared. Figure 1 shows the result for Na-bentonite. The change in decontamination efficiency can be seen. Similar change was also observed for illite. On the other hand, no change in decontamination efficiency over aging time was observed for kaolinite and Ca-bentonite. The aging effect was particularly noticeable for DTAB. Decontamination efficiency of DTAB is slightly worse than BDAB. The lower decontamination efficiency of DTAB is easily affected by 30 days aging.

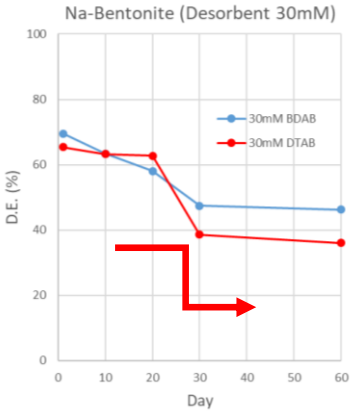


Fig. 1 Decontamination efficiency (D.E.) from Na-bentonite over aging time using 30 mM of cationic surfactant.

The layer charge can be calculated using the chemical formula of each clay mineral to be -0.8, -0.6, -0.4, 0 for illite, Na-bentonite, Ca-bentonite, and kaolinite, respectively, although the charge changes depending on pH. The aging effect tends to appear when the layer charge is more negative. This means $Cs^{+}_{aq/clay}$ is more easily dehydrated to be naked Cs^{+} and adsorbed to the clay having more negative charge. To discuss the aging effect, we consider K_2 shown in eq 3. The $Cs^{+}_{aq/clay}$ interacts with the layer to become $Cs^{+}_{adsorption}$. From the layer charge, the K_2 of equilibrium constant is thought to be relatively larger for illite and Na-bentonite. We assume that the $Cs^{+}_{aq/clay}$ can be decontaminated, while the $Cs^{+}_{adsorption}$ is not easily decontaminated. It is known that the hydration energy of Cs^{+} is relatively small. When Cs^{+} is adsorbed to frayed-edge site, dehydration occurs and it becomes hard to decontaminate.

It is interesting that illite and Na-bentonite showed the aging effect. We thought that K_2 in eq 3 moved to the right by aging. From the structure, it is thought that the mechanism is different between illite and Na-bentonite. We have to consider the relatively smaller region of frayed-edge site for illite and larger interlayer area for Na-bentonite. For illite, it is thought that over aging time, hydrated Cs^{+} ions diffused, gradually dehydrated, and penetrated deeper place via frayed-edge site to the area where the decontamination of the cationic surfactant could not reach. In addition, the dehydrated K^{+} ions located in the interlayer near the frayed-edge site became hydrated because the hydration energy of K^{+} is higher than Cs^{+}. As a result, the positions of Cs^{+} and K^{+} were exchanged, causing Cs^{+} to migrate deeper into interlayer [2]. This suggests that, at least for a decontamination time of 24 hours, the cationic surfactant does not penetrate deep into the interlayer and cannot decontaminate the Cs^{+} ions. In the case of Na-bentonite, other possibility can be considered. This is intercalation compound and it includes water. When the time goes, the interlayer water will be evaporated, and the $Cs^{+}_{aq/clay}$ changes to $Cs^{+}_{adsorption}$ + aq to compensate the evaporated water. On the other hand, Ca^{2+} has higher hydration energy and tends to keep water molecules in the interlayer of Ca-bentonite.

Other explanation can be considered for the difference in aging effect between Na-bentonite and Ca-bentonite. Not all Na^{+} and Ca^{2+} were exchanged by Cs^{+} [3]. The retention trend is Ca^{2+}>Cs^{+}>Na^{+}. This means Cs^{+} is relatively easily desorbed for Ca-bentonite, while Cs^{+} tends to be retained for Na-bentonite.

4. CONCLUSIONS

Aging effect of cesium desorption from clay minerals was investigated. Illite and Na-bentonite showed the aging effect, while kaolinite and Ca-bentonite did not show the aging effect, which was explained by the equilibrium.

References

[1] H. Wijayanto and S. Nakashima, Applied Clay Science, **228**, 106649 (2022).
[2] S. M. Park, et. al., Journal of Hazardous Materials, **369**, 569-576 (2019).
[3] J.-Y. Goo, et al., Applied Clay Science, **245**, 107141 (2023).

Copyright on 7th Asia-Pacific Symposium on Radiochemistry 2025 - P3-07 -

Impact of plutonium originating from Fukushima Daiichi Nuclear Power Plant accident in the environment: an overview of a decade studies

Jian Zheng[1], Junwen Wu[2], Keiko Tagami[1], Guosheng Yang[1], Tatsuo Aono[3]

[1]*Institute for Radiological Sciences,National Institutes for Quantum Science and Technology (QST), Japan.*
Email: zheng.jian@qst.go.jp
[2]*Institute of Marine Sciences, Shantou University, China*
[3]*Fukushima Institute for Research, Education and Innovation, Japan*

On March 11, 2011, a magnitude 9.0 earthquake occurred in the western North Pacific about 130 km off the northeast coast of Japan followed by a tremendous tsunami which arrived at Fukushima Daiichi Nuclear Power Plant (FDNPP) about 45 min later. The tsunami severely damaged the nuclear reactor cooling system, leading to hydrogen explosions in the reactor buildings. As a result, massive radionuclides were released into the environment. As one of the most important actinides, Pu isotopes attracted great public attention after the FDNPP accident because they present a high risk for internal radiation exposure via ingestion of contaminated agricultural crops and seafood. It has been estimated that the total amount of ^{137}Cs released from the FDNPP accident ranged from 15-35 PBq, while for the refractory actinides, in particular, Pu isotopes, tiny amount ($2x10^{-5}$% of the core inventory) was released into the environment [1,2].

This study reviewed the current knowledge of plutonium (Pu) isotopic composition (the atom or activity ratios) and activities of ^{238}Pu, ^{239}Pu, ^{240}Pu, and ^{241}Pu derived from the Fukushima Daiichi Nuclear Power Plant (FDNPP) accident in 2011. In this critical review, we documented the characteristic values of Pu atom or activity ratios (fingerprints) and presented its spatial distributions around the FDNPP site. Based on multiple Pu fingerprints (^{238}Pu/$^{239+240}$Pu activity ratio, ^{240}Pu/^{239}Pu atom ratio, and ^{241}Pu/^{239}Pu atom ratio), we clarified there received the Pu contamination from the FDNPP accident in a restricted terrestrial area, while Pu in the northwest Pacific Ocean is still predominately sourced from the Pacific Proving Grounds (PPG) fallout and the global fallout. Using a simple two end–member mixing model, the contributions of Pu from the FDNPP accident were calculated to be on average 27±34% (n=149) in soils, 55±32% (n=38) in litter samples, and 67±26% (n=129) in the air dust/black substances, respectively. In the marine environment, the PPG source contributed 45±15% (n=76) in the seawaters and 42±12% (n=48) in the sediments [3]. The spatial distribution of Pu atom or activity ratios based on existing studies suggested that: 1) the Pu contamination in the northwestern FDNPP site was mainly observed in an area within 50 km radius; 2) in the southwestern FDNPP site, the Pu contamination was mainly observed in a zone within 30 km radius. The studies of Cs-bearing radioactive particles indicated that Pu occurred as Pu oxide and the fuel fragments containing Pu were released from the reactors to the surrounding environment associated with micron-scale Cs-bearing radioactive particles [4]. It should be noted that the fractionation between Pu and other radionuclides occurred after release. Finally, these new findings about the Pu fingerprints around the FDNPP site help us to establish a reference background database for the coming environmental risk assessment and geochemical study in this region.

References

[1] J. Zheng, K. Tagami, Y. Watanabe, S. Uchida, T. Aono, N. Ishii, S. Yoshida, Y. Kubota, S. Fuma, S. Ihara, Isotopic evidence of plutonium release into the environment from the Fukushima DNPP accident. Sci. Rep. 2, 304 (2012).

[2] J. Zheng, K. Tagami, S. Uchida, Release of Plutonium Isotopes into the Environment from the Fukushima Daiichi Nuclear Power Plant Accident: What Is Known and What Needs to Be Known. Environ. Sci. Technol. 47 (17), 9584–9595 (2013).

[3] J. Wu, X. Zheng, J. Chen, G. Yang, J. Zheng, T. Aono, Distributions and impacts of plutonium in the environment originating from Fukushima Daiichi Nuclear Power Plant accident: an overview of a decade studies. J. Environ. Radioact. 248, 106884 (2022). Doi:10.1016/j.jenvrad.2022.106884.

[4] J. Igarashi, K. Ninomiya, J. Zheng, Z. Zhang, M. Fukuda, T. Aono, H. Minowa, H. Yoshikawa, K. Sueki, Y. Satou, A. Shinohara, Fukushima Daiichi Nuclear Power Plant Accident: Understanding Formation Mechanism of Radioactive Particles Through Sr and Pu Quantities. Environ. Sci. Technol. 58, 14823-14830 (2024). https://pubs.acs.org/doi/full/10.1021/acs.est.4c03428.

7th Asia-Pacific Symposium on Radiochemistry *September 14 ~ 19, 2025 • Kunibiki Messe • Shimane, Japan*

Effect of Gamma Dose and pH on Methyl Iodide Formation in 2 mM NaI and 5 mM MEK Aqueous Solutions

Jei-Won Yeon [1,*], Minsik Kim [2]

[1]Nuclear Chemistry Technology Division, Korea Atomic Energy Research Institute, 111, Daedeok-daero 989beon-gil, Yuseong-gu, Daejeon, 34057, Republic of Korea, *yeonysy@kaeri.re.kr*
[2]BioHealth Research Center, Korea Institute of Toxicology, 17, Jegok-gil, Munsan-eup, Jinju-si, Gyeongsangnam-do, 52834, Republic of Korea, *minsik.kim@kitox.re.kr*

The effects of gamma dose and pH on the formation of CH_3I in a mixed solution of 2 mM sodium iodide (NaI) and 5 mM methyl ethyl ketone (MEK) were investigated. Under acidic conditions, the pH increased from 3.5 to 5.5 due to the oxidation of I^- to I_2. Under neutral conditions, no significant change in pH was observed. Under alkaline conditions, the pH decreased slightly from the initial 11.9 due to the decomposition of MEK. Although I_2 is required for CH_3I formation, the formation of CH_3 radicals, which compete with I_2 formation, was also involved. Under acidic and neutral conditions, CH_3I was formed at levels of 5-6 μM, but under alkaline conditions, CH_3I was not formed because I_2 was not stable.

1 INTRODUCTION

The decomposition of alkyl ketone compounds by ionization energy has been of interest in various fields of research. In the field of nuclear power, volatile organoiodines such as CH_3I are the main chemical forms of volatile radioactive materials released into the atmosphere during a severe accident at a nuclear power plant, and thus are important from the perspectives of accident prevention and prediction [1-3]. In the event of an accident, radioactive iodine in CH_3I is supplied from irradiated nuclear fuels, and the organic components are supplied from the decomposition of various organic substances present in the reactor building, such as epoxy paint. Organoiodines are formed when radioactive iodine combines with organic substances under radiation conditions, and many studies have been conducted on their formation and behavior. In this study, the effects of gamma dose and pH on the formation of CH_3I in an aqueous solution of sodium iodide (NaI) and methyl ethyl ketone (MEK) were investigated.

2. METHODS AND RESULTS

2.1 Experimental Method

All chemicals used in our experiments were analytical reagent grade. The experimental and calibration solutions were made from NaI (> 99.5 wt%, Sigma-Aldrich), MEK (2-butanone, > 99.7%, Sigma-Aldrich), toluene (> 99.9%, Sigma-Aldrich), CH_3I(> 99%, Sigma-Aldrich) and deionized water (>18.2 MΩ·cm, EMD-Millipore). The experimental solutions were prepared as a mixture of NaI and MEK. The pH values of all mixed solutions were measured before and gamma irradiations. Calibration of the pH meter (Metrohm model 827) was carried out before the pH measurements.

The gamma irradiation experiment was carried out at a high gamma irradiation facility. The gamma dose rates were 10 kGy h^{-1}, and the irradiation times were 0, 2, and 4 h. The NaI and MEK solutions (5 mL) were prepared in 20 ml vials as experimental solutions. All vials were sealed with a Teflon cap to avoid the evaporation of the volatile reaction product, CH_3I. After gamma irradiation, toluene (5 mL) was injected into the vials using a gas-tight glass syringe, and the liquid/liquid extraction was performed for 1.5 h to extract organic iodides into the toluene phase. After the liquid/liquid extraction, we sampled the 1 mL of the solution from the toluene phase by the syringe. Subsequently, we measured the concentrations of CH_3I dissolved in toluene using a GC–MS (Perkin Elmer Clarus 680/SQ 8T, USA) [4].

2.2 Results and Discussion

The pH change of the NaI and MEK mixed solution according to the gamma irradiation dose is shown in Figure 1. In the acidic pH region, the pH increased with the increase in gamma dose. In the neutral pH region, the pH decreased slightly, but there was no significant change. In the alkaline region, the pH decreased slightly with the increase in gamma dose.

The increase in pH in the acidic region was analyzed as the oxidation reaction of I^- to I_2, and it was also confirmed by the increase in the concentration of I_2 in the solution. A small amount of I_2 formation was observed along with the decrease in pH in the neutral pH region. This can be interpreted as a competition between the I_2 formation reaction that causes the increase in pH and the decomposition reaction of MEK that causes the decrease in pH. The decrease in pH in the alkaline region is not large, but it is a significant concentration change considering the concentration scale of

Copyright on 7th Asia-Pacific Symposium on Radiochemistry 2025

hydroxyl ions. This is analyzed as the decomposition reaction of MEK, which is the largest, although several influencing factors were involved.

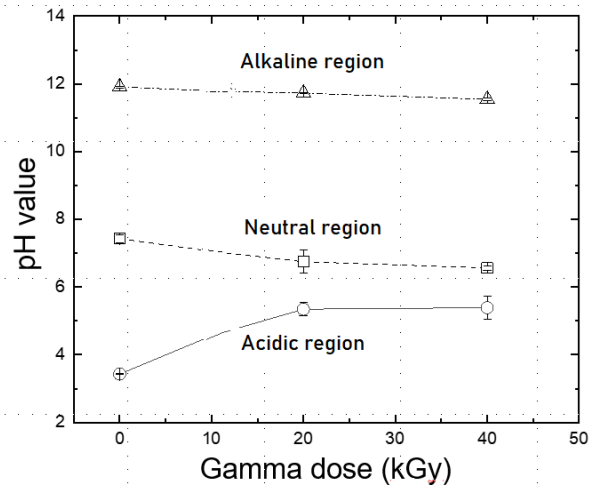


Fig. 1. pH changes of 2 mM NaI and 5 mM MEK solutions according to gamma dose.

The concentrations of I_2 and CH_3I formed in the experimental solutions corresponding to Figure 1 were also measured. The I_2 concentrations were measured to be up to 500 μM, 200 μM, and 0 M in the acidic, neutral, and alkaline regions, respectively, and the CH_3I concentrations were measured to be 4.4 μM, 5.8 μM, and 0 M in each condition. Under acidic conditions, it was analyzed that the OH radical, which is a radiolysis product of water, was mainly used for the oxidation of I^-, and under neutral conditions, it was interpreted that the OH radical was appropriately used for the oxidation reaction of I^- and the decomposition of MEK. In addition, under alkaline conditions, it was understood that the formation of CH_3I did not proceed because I_2 did not exist stably due to disproportionation. These results suggest that the I_2 from the oxidation of I^- and the CH_3 radical from the decomposition of MEK are essential for the formation of CH_3I. In addition, it shows that CH_3I formation is relatively easy under conditions where the concentrations of I_2 and CH_3 radicals are appropriately balanced and not biased to one side.

3. CONCLUSIONS

When a mixed solution of 2 mM NaI and 5 mM MEK was exposed to high-dose (up to 40 kGy) gamma irradiation, I_2 and CH_3I were formed together. I_2 was formed from the oxidation of I^-, and CH_3I was formed from the reaction of I_2 with the CH_3 radical formed from the decomposition of MEK. CH_3I was formed in the acidic and neutral pH regions, but neither I_2 nor CH_3I was observed in the alkaline region. The pH affects the I_2 formation of the decomposition of MEK, and the CH_3I formation proceeded well at a pH where the concentrations of I_2 and CH_3 radicals were appropriately maintained.

ACKNOWLEDGMENTS

This work was supported by the National Research Foundation of Korea (NRF) Grant funded by the Korean government (MSIT: the Ministry of Science and ICT) (NRF Nos. 2017M2A8A4015281, 2021M2E3A3040092, RS-2022-00144202, RS-2023-00261146)

References

[1] J. PAQUETTE, D. F. TORGERSON, J. C. WREN, Volatility of Fission Products during Reactor Accidents. J Nucl Mater., **130**, 129 (1985).
[2] K. ISHIGURE, H. SHIRAISHI, H. OKUDA, N. FUJITA, Effect of Radiation on Chemical Forms of Iodine Species in Relation to Nuclear Reactor Accidents. Radiat Phys Chem., **28**, 601 (1986).
[3] M. KIM, T. KIM, J.-W. YEON, Formation of CH_3I in a NaI and Methyl Alkyl Ketone Solution under Gamma Irradiation Conditions. J. Radioanal. Nucl. Chem., **316**, 1329 (2018).
[4] M. Kim, J.-W. YEON, Accuracy Analysis on Concentration Determination of Molecular Iodine in Gamma Irradiated Solutions. J. Radioanal. Nucl. Chem., **330**, 469 (2021).

Copyright on 7th Asia-Pacific Symposium on Radiochemistry 2025 - P3-09 -

Contributed Talk | [R3]Actinide Chemistry and Nuclear Energy Chemistry

Fri. Sep 19, 2025 10:10 AM - 10:50 AM JST | Fri. Sep 19, 2025 1:10 AM - 1:50 AM UTC Hall A(MP)

[R3] Actinide Chemistry and Nuclear Energy Chemistry

10:10 AM - 10:30 AM JST | 1:10 AM - 1:30 AM UTC

[R3-26]

Complexation and Redox Behavior in Np(V)-HA-Fe(II) System

*Yuxiao Guo[1], Chao Xu[1] (1. Tsinghua University (China))

10:30 AM - 10:50 AM JST | 1:30 AM - 1:50 AM UTC

[R3-27]

HARNESSING BIOPOLYMERS FOR SUSTAINABLE REMOVAL OF RADIOACTIVE ELEMENTS

*Mohammed Fouda Hamza[1], Yuezhou Wei, Xiangbiao Yin, Amr Fouda, Eric Guibal (1. Prof. School of Nuclear Science and Technology, Univ. of South China, Hengyang 421001, China (China))

©APSORC25

7th Asia-Pacific Symposium on Radiochemistry *September 14 ~ 19, 2025 • Kunibiki Messe • Shimane, Japan*

Complexation and Redox Behavior in Np(V)-HA-Fe(II) System

Yuxiao Guo, Chao Xu*

Institute of Nuclear and New Energy Technology, Tsinghua University, Beijing 100084,China
**Email: xuchao@tsinghua.edu.cn*

The long-term radiotoxicity of transuranic elements, such as neptunium (Np), presents significant challenges for nuclear waste management. Due to their extended radiotoxic lifetimes, these elements can persist in the environment for millennia, underscoring the need for a comprehensive understanding of their physicochemical behavior to mitigate potential risks. This study investigates the pH-dependent interactions of Np(V) with humic acid (HA) and Fe(II) under anoxic conditions. Experimental results show that at pH 5–6, Fe(II) promotes the formation of HA-Fe(II) colloids and enhances the reduction of Np(V) to Np(IV). Under neutral to alkaline conditions (pH 7–8), Np(V) undergoes near-complete reduction (~98%), and the resulting Np(IV) forms stable colloidal complexes with HA. These findings underscore the critical roles of pH, Fe(II), and HA in controlling the speciation and mobility of actinides in subsurface environments, providing valuable insights for the safety assessment of nuclear waste repositories.
Keywords: Neptunium; Humic acid; Fe^{2+}; Complexation; Redox

1 INTRODUCTION

The management of actinides, particularly long-lived transuranic elements such as neptunium (Np), is a key challenge in mitigating the long-term environmental risks associated with nuclear waste. Owing to their extended radiotoxic lifetimes, these elements can persist in the environment for thousands of years, highlighting the importance of a comprehensive understanding of their physicochemical behavior [1]. Humic acid (HA), a ubiquitous natural organic macromolecule enriched with redox-active functional groups [2], plays an essential role in the environmental fate of transuranic elements through complexation and redox interactions. Under anoxic conditions, HA can additionally interact with naturally occurring ferrous iron (Fe^{2+}) to form HA-Fe(II) colloids, which may further modify the speciation and mobility of actinides in environmental systems [3-4]. This study focuses on the pH-dependent mechanisms governing the interactions between Np(V), HA, and Fe(II) under anoxic conditions, providing insights into the processes that influence actinide mobility in subsurface environments.

2. CONCLUSIONS

This study demonstrates that Fe(II) significantly enhances the reduction of Np(V) to Np(IV) under mildly acidic conditions (pH 5–6), promoting the formation of less mobile Np(IV) species. At neutral to alkaline pH (7–8), the reduction of Np(V) reaches near-completion (~98%), and the resulting Np(IV) is stabilized through complexation with humic acid (HA), forming stable colloidal complexes. These findings highlight the critical roles of Fe(II) and HA in controlling the speciation and mobility of Np in subsurface environments. By providing mechanistic insights into the redox and complexation processes, this study contributes valuable information for improving the long-term safety assessments of nuclear waste repositories, particularly in terms of predicting actinide behavior and mobility in anoxic environments.

ACKNOWLEDGMENTS

We thank for the financial support from National Natural Science Foundation of China (22325603).

References

[1] Zhou Y. *Energy Policy*, 2011, 39(7): 4360-4369.
[2] Sachs S et al. J. *Radioanal. Nucl. Chem.*, 2011, 290(1):17-29.
[3] Marquardt C et al. *Radiochim. Acta*, 1998, 80(3): 129-138.
[4] Liao P et al. *Environ. Sci. Technol.*, 2020, 54(7): 4256-4266.

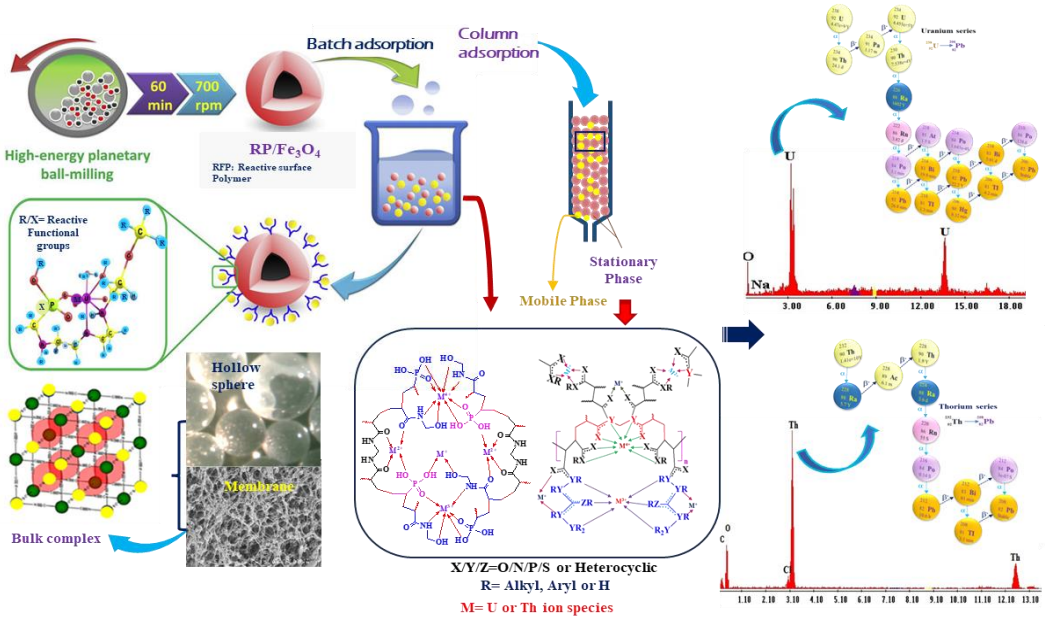
Copyright on 7th Asia-Pacific Symposium on Radiochemistry 2025 - R3-26 -

7th Asia-Pacific Symposium on Radiochemistry *September 14 ~ 19, 2025 • Kunibiki Messe • Shimane, Japan*

HARNESSING BIOPOLYMERS FOR SUSTAINABLE REMOVAL OF RADIOACTIVE ELEMENTS

Mohammed F. Hamza,[1,*], Yuezhou Wei,[1,2] Xiangbiao Yin,[1] Amr Fouda[3], Eric Guibal,[4]

[1] *School of Nuclear Science and Technology, University of South China, Heng Yang 421001, China. (m_fouda21@usc.edu.cn (MFH), yzwei@usc.edu.cn (Y.W), yinxb@usc.edu.cn (X.Y))*
[2] *School of Nuclear Science and Engineering, Shanghai Jiao Tong University, Shanghai, China (yzwei@usc.edu.cn (Y.W)).*
[3]*Botany and Microbiology Department, Faculty of Science, Al-Azhar University, Nasr City, Cairo 11884, Egypt (amr_fh83@azhar.edu.eg)*
[4] *Polymers Composites and Hybrids (PCH), IMT Mines Ales, Alès, France (eric.guibal@mines-ales.fr)*



Abstract

The growing demand for energy has recently given a new impulse to the development of nuclear power plant and facilities. Fueling nuclear power units became a strategic issue. Uranium and thorium were mostly considered as the fuel source for the nuclear technology. With several reasons that in fact-oriented researchers and governments to paid attention for promoting the development of such alternative technology: i.e., extend abundance of uranium and thorium in Earth's crust. Indeed, using Th in nuclear plant is expected to minimize hazardous nuclear wastes and to diminish the risks for nuclear dissemination. The ores remain the principal source for commercial production of these ions. The conventional (and commercial) ore processes may produce residues containing low-level concentrations (which may be poorly competitive for recovery by conventional resins or solvent extraction), considered as the source of pollution, poses a serious hazard to the ecosystem and human being. These effluents can represent a meaningful U and Th resources for alternative processes (using sorbents). The valorization of these residues requires developing new sorbents (design to be highly selective) bearing highly reactive functions, with fast uptake and strong stability (at reuses). To reach these objectives, the current studies adopted a dual strategy based on the appropriate selection of reactive groups combined with the application of an ion-imprinting step in the synthesis of the sorbent. The effect of light irradiation on sorption properties and mechanisms, enhance the selectivity of uranium through in-situ precipitation. The overall process involve 1) Synthesizing of novel acid-resistant adsorbent (bearing numerous N-, -P, -O and S groups with large specific surface area); 2) Evaluating the sorption performances (high adsorption capacity, and fast kinetics) and selectivity characteristics, 3) Demonstrating the stability of the sorbent for successive reuses and 4) Optimizing the efficiency of the new sorbent for the recovery of U and Th from pre-treated leachate with high selective separation, further treatment for the crude cake on the medical isotope separation (especially radium), which considered as the main source of it.

Keywords: *Novel Biopolymers adsorbent, Light irradiation, Nuclear power, Pre-treated leachate.*

Contributed Talk | [S2]Radiopharmaceutical Sciences

Fri. Sep 19, 2025 10:10 AM - 11:10 AM JST | Fri. Sep 19, 2025 1:10 AM - 2:10 AM UTC Hall S(Int'l)

[S2] Radiopharmaceutical Sciences

10:10 AM - 10:30 AM JST | 1:10 AM - 1:30 AM UTC

[S2-15]

^{225}Ac/^{213}Bi MEDICAL GENERATOR FOR RAPID PRODUCTION OF RADIOLABELED PEPTIDES

*Aleksandr N. Vasiliev[1], Stanislav V. Ermolaev[2], Elena V. Lapshina[2], Darya R. Khaliullina[2], Boris L. Zhuikov[2] (1. Shenzhen MSU-BIT University (China), 2. Institute for Nuclear Research of the Russian Academy of Sciences (Russia))

10:30 AM - 10:50 AM JST | 1:30 AM - 1:50 AM UTC

[S2-16]

Investigating radiopharmaceuticals for targeted alpha therapy with Direct Alpha Spectroscopy on living cell cultures

*Peter Kunz[1,2], Mahsa Farasat[1], Behrad Saeedi[1], Luke Wharton[1], Sidney Shapiro[3], Chris Vinnick[2], Corina Andreoiu[2], Hua Yang[1,2], Madison Daignault[2], Meghan Kostashuk[4], Nicholas Pranjatno[2], Myla Weiman[1] (1. TRIUMF (Canada), 2. Simon Fraser University (Canada), 3. University of British Columbia (Canada), 4. McMaster University (Canada))

10:50 AM - 11:10 AM JST | 1:50 AM - 2:10 AM UTC

[S2-17]

Production of ^{225}Ac via the ^{226}Ra(p,2n)^{225}Ac reaction at RIKEN

*Akihiro Nambu[1], Yousuke Kanayama[1], Hiromichi Shimizu[1], Masataka Imamura[1,2], Shota Kimura[1,2], Daiki Mori[1,2], Yuichiro Wakitani[2], Takahiro Mikamoto[2], Yudai Shigekawa[1], Sayantani Mitra[1], Hiromitsu Haba[2] (1. Nishina Center for Accelerator-Based Science, RIKEN (Japan), 2. Japan Radioisotope Association (Japan))

©APSORC25

^{225}Ac/^{213}Bi MEDICAL GENERATOR FOR RAPID PRODUCTION OF RADIOLABELED PEPTIDES

Aleksandr N. Vasiliev[1,2,3], Stanislav V. Ermolaev[1], Elena V. Lapshina[1], Darya R. Khaliullina[1,3], Boris L. Zhuikov[1]

[1]*Institute for Nuclear Research of the Russian Academy of Sciences, 60-letiya Oktyabrya prospekt 7a, Moscow, Russia, 117312, vasiliev@inr.ru*
[2]*Faculty of Materials Science, Shenzhen MSU-BIT University, International University Park Road 1, Shenzhen, China, 518172*
[3]*Lomonosov Moscow State University, Leninskie Gory 1, Moscow, Russia,119991*

A method for high-scale ^{225}Ac-production for medical application from a massive metallic ^{232}Th-target irradiated with 160 MeV-protons has been developed. This process can yield up to 100 GBq of ^{225}Ac per one irradiation run, which takes 7–10 days. The produced ^{225}Ac can be used as a source of short-lived ^{213}Bi in a ^{225}Ac/^{213}Bi generator. The circulating ^{225}Ac/^{213}Bi generator developed at INR RAS provides a ^{213}Bi-labeled bioconjugate as a final product. While a conventional synthesis route including generator milking, bioconjugate labeling and size-exclusion purification takes >20 min, the duration of radiopharmaceutical's production by the proposed method is reduced to 6–8 min.

1 PRODUCTION OF ^{225}Ac FOR MEDICAL APPLICATION

Alpha emitting radionuclides ^{225}Ac ($T_{1/2}$= 10 d) and its daughter ^{213}Bi (45.6 min) are currently being trialed for use in alpha therapy for various types of cancer. A highly efficient method for producing ^{225}Ac involves the irradiation of natural metallic thorium with medium-energy protons [1]. This approach was first proposed at the Institute of Nuclear Research of the Russian Academy of Sciences (INR RAS) more than 15 years ago and has since been actively promoted in Russia, the United States, Canada, and China. The process developed at INR RAS can yield up to 100 GBq of ^{225}Ac per one irradiation run, which takes 7–10 days. The target was made of a metallic Th disk of few mm thickness encapsulated in Nb shell using diffusion welding that provided effective target cooling under an intensive proton beam. An original processing procedure comprises selective dissolution of niobium target windows diffusion-welded to thorium, liquid–liquid extraction of thorium macro-amount, and chromatographic purification of actinium fraction with extraction chromatographic sorbents DGA-, LN- and TRU-resins (Fig. 1). Three successive chromatographic stages are realized according to the ''end-to-start'' technique, which assumes that the eluate of the previous column is directly transferred to the column with the next sorbent. The achieved total chemical yield of ^{225}Ac was 87% and radionuclidic purity was better than 99.8%. However, the ^{225}Ac produced from irradiated thorium also contains a chemically inseparable impurity of the long-lived radionuclide ^{227}Ac (approximately 0.2% by the end of bombardment). While the direct medical use of ^{225}Ac with this small amount of ^{227}Ac is still debated, it can be used as the parent radionuclide in a ^{225}Ac/^{213}Bi generator.

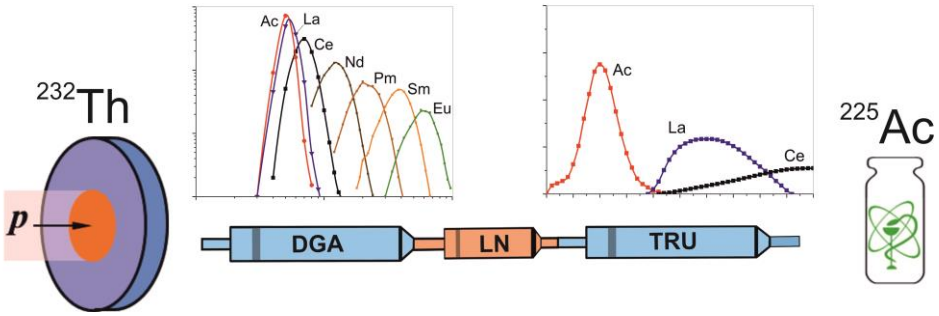


Fig. 1. Illustration of the proposed method for producing ^{225}Ac [1].

2 CIRCULATING ^{225}Ac/^{213}Bi GENERATOR

^{225}Ac/^{213}Bi generators based on ion exchange (AG MP-50, AG 1, BioRad) and extraction chromatography resins (Actinide Resin, UTEVA Resin, Triskem Int.) are well described. However, all the generators have been developed for isotopically pure ^{225}Ac, while the presence of ^{227}Ac and its decay products in ^{213}Bi eluate may be important. One of the main challenges to the early proposed ^{225}Ac/^{213}Bi generator systems is the decay loss of ^{213}Bi during the conventional

process of producing radiopharmaceuticals that includes generator milking, bioconjugate labeling and size-exclusion purification.

A two-column generator that allow accumulating ^{213}Bi separately from the parent ^{225}Ac and producing directly ^{213}Bi-labeled bioconjugates has been developed at the INR RAS [2]. The formation and concentration of ^{213}Bi in the second column was realized by continuous separation of intermediate ^{221}Fr (4.9 min) from ^{225}Ac fixed in the first column filled with Actinide Resin sorbent arranged in circulation mode (Fig. 2). The two-column construction allows us to vary the size of the first column and distribute ^{225}Ac uniformly without compromising the characteristics of the generator. ^{213}Bi can be extracted from the second column filled with cross-linked dextran gel Sephadex G-25 using a suitable complexing agent, including bioconjugates of chelators and proteins. In order to demonstrate the feasibility of the proposed approach, ^{213}Bi-DTPA-Nimotuzumab for radioimmunotherapy of EGFR-overexpressing carcinomas and ^{213}Bi-DOTA-Substance P for glioma treatment were synthesized. The total production time was reduced to 6-8 minutes, three to four times faster than conventional synthesis protocols.

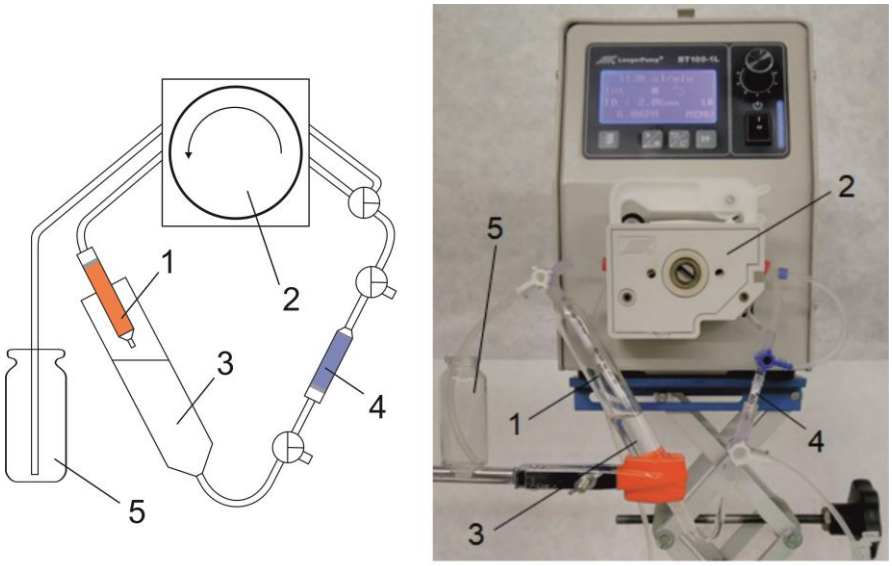


Fig. 2. Scheme and photo of a laboratory circulating ^{225}Ac/^{213}Bi generator. 1 – column with parent ^{225}Ac, 2 – peristaltic pump, 3 – tube for ^{221}Fr decay, 4 – column for ^{213}Bi accumulation and extraction, 5 – additional line for fast transfer of ^{213}Bi from the decay tube to the second column [2].

2. CONCLUSIONS

Unique technologies have been developed at the INR RAS that make it possible to produce high-purity medical ^{225}Ac, which can be applied for the rapid synthesis of ^{213}Bi-containing radiopharmaceuticals using a circulating ^{225}Ac/^{213}Bi generator system. The proposed approaches make it possible to produce radiopharmaceuticals based on ^{213}Bi with high efficacy and activity sufficient for their routine use.

References

[1] S. V. ERMOLAEV, A. N. VASILIEV, E. V. LAPSHINA, et al., "Production of ^{225}Ac for medical application from ^{232}Th-metallic targets in Nb-shells irradiated with middle-energy protons," *New Journal of Chemistry*, **48**, 18 (2024).

[2] S. V. ERMOLAEV, A. N. VASILIEV, A. K. SKASYRSKAYA, et al., "^{225}Ac/^{213}Bi generator for direct synthesis of 213Bi-labeled bioconjugates," *Nuclear Medicine and Biology*, **140**, 108975 (2025).

Investigating radiopharmaceuticals for targeted alpha therapy with Direct Alpha Spectroscopy on living cell cultures

Peter Kunz[a,c], Mahsa Farasat[a], Behrad Saeedi[b], Luke Wharton[b], Sidney Shapiro[d], Chris Vinnick[c], Madison Daignault[c], Meghan Kostashuk[g,b], Nicholas Pranjatno[e], Myla Weiman[a,h], Corina Andreoiu[c], Hua Yang[b,c,f]

[a] *Accelerator Division, TRIUMF, 4004 Wesbrook Mall, Vancouver, BC V6T 2A3, Canada*
[b] *Life Sciences Division, TRIUMF, 4004 Wesbrook Mall, Vancouver, BC V6T 2A3, Canada*
[c] *Department of Chemistry, Simon Fraser University, Burnaby, BC V5A 1S6, Canada*
[d] *Physics and Astronomy, University of British Columbia, Vancouver, BC V6T 1Z4, Canada*
[e] *Department of Physics, Simon Fraser University, Burnaby, BC V5A 1S6, Canada*
[f] *Department of Chemistry, University of British Columbia, Vancouver, BC V6T 1Z1, Canada*
[g] *McMaster School of Biomedical Engineering, McMaster University, Hamilton, Ontario L8S 4L7 , Canada*
[h] *Department of Physics and Astronomy, University of Waterloo, Waterloo, Ontario, Canada N2L 3G1 , Canada*

Targeted alpha-particle therapy (TAT) works with radionuclides conjugated to tumor-targeting molecules to deliver localized α radiation to cancer cells. Among these radionuclides, Actinium-225 has emerged as a clinically promising candidate. Efficient retention of ^{225}Ac and its decay products at the target cells is critical to limit toxicity. To investigate uptake and retention efficiencies on living cell cultures, we developed a method to detect α emissions directly from cells incubated with TAT vectors. In first proof-of-principle experiments, AR42J rat pancreatic tumor cells were incubated with [^{225}Ac]Ac-crown-TATE, [^{225}Ac]Ac-PSMA-617, and [^{225}Ac]Ac^{3+}. The results revealed distinctly different decay spectra between radiolabeled cells and reference samples. Identification of ^{213}Po enables to investigate retention and release of decay products from cells. The results of experimental studies are supported by Geant4 simulations.

1 Introduction

TRIUMF's large cyclotron was built to support research in nuclear structure, astrophysics and material science. Now it is increasingly used to produce a wide range of medical isotopes by irradiating targets with its 500 MeV proton beam. ^{225}Ac ($T_{1/2}$=9.9 days) is of particular interest. It is separated chemically from irradiated thorium metal targets on a regular basis [1][2]. Very pure samples of ^{225}Ac are also obtained at the Isotope Separation and Acceleration facility (ISAC) [3] wich is also a source for more exotic isotopes such as ^{226}Ac, ^{149,155}Tb and ^{209,211}At. The isotopes or their precursors are collected from a radioactive ion beam (RIB). Essential for the collection process is knowledge of the RIB composition and intensity which is obtained mainly through α, β and γ spectroscopy [4]. The establishment of a cell culture laboratory at TRIUMF and expertise in RIB characterization motivated a spin-off, using essentially the same technology for detecting α-emitters in RIB to probe α-emissions from cell samples.

In a collaboration between the TRIUMF Accelerator and Life Science divisions we have developed a customized α-spectroscopy setup that allows to obtain the complex ^{225}Ac decay spectrum from living cell samples. The resolution is sufficient to distinguish the ^{213}Po decay which is a good indicator of retention due to its relatively long-lived decay chain precursor ^{213}Bi ($T_{1/2}$=45.61 min). The project is still at an early stage though we can report on first proof-of-principles measurements with some well-known TAT targeting vectors that demonstrate the method's feasibility.

2 Results

The development of a *Bio-Sample Alpha Detector* (BAD) and associated sample preparation and measurement procedures enabled in-vitro investigations of ^{225}Ac-labeled pharmaceuticals. This work was motivated by the lack of diagnostic capability to monitor α emissions directly when the targeting vector interacts with cells. The goal is to be sensitive to uptake efficiencies as well as metabolic processes in living cultures.

First results of direct alpha spectroscopy on AR42J rat pancreatic tumor cells under ambient conditions demonstrate the potential of this new method. Cell samples were incubated with [^{225}Ac]Ac-crown-TATE, [^{225}Ac]Ac-PSMA-617 and [^{225}Ac]Ac^{3+}. The measurement results revealed distinctly different uptake behaviour. α decay spectra shown in Fig. 1 indicate significant uptake of [^{225}Ac]Ac-crown-TATE by the cells. Less efficient uptake was observed for ^{225}Ac-PSMA-617 consistent with the lack of PSMA-617 receptors on AR42J cells. These results were achieved by placing typically several hundred thousand cells after incubation under ambient conditions in a custom sample cup filled with 200-400 μL of cell media. The cells settle very close to the detector surface on the cup floor, made of a 2.5 μm Mylar foil, thus, limiting the energy loss of α particles. Most of the attenuation is caused by the cells themselves. With an average cell diameter of 13 μm the attenuation is significant but not prohibitive.

Copyright on 7th Asia-Pacific Symposium on Radiochemistry 2025 - S2-16 -

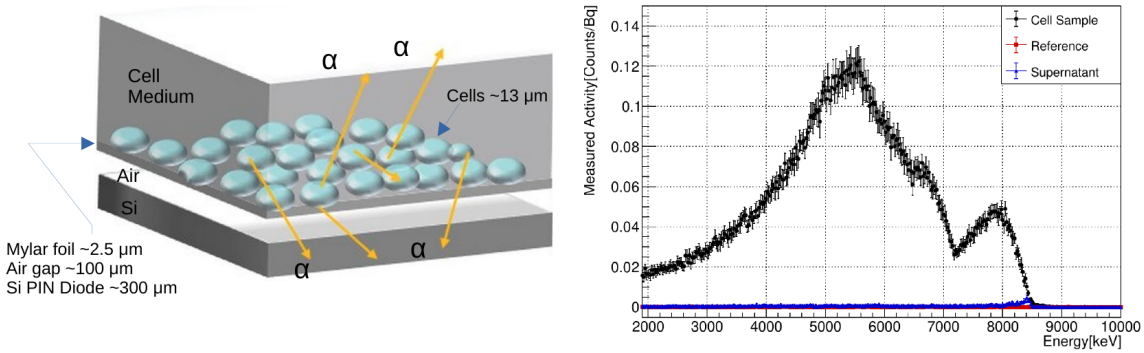


Fig. 1. **Left**: Schematic representation of the detection setup. The configuration of detector and sample is designed to keep the attenuation of α particles at a minimum. **Right**: α-decay spectra of [^{225}Ac]Ac-crown-TATE obtained from the cell sample (black), supernatant (blue), and reference sample (red, no cells)

The spectrum in Fig. 1 also shows the clear separation of ^{213}Po at $\sim$8 MeV from its α-emitting precursors in the decay chain. This enables the measurement of ^{213}Bi redistribution from the cells into the surrounding media and potential consequences on dosimetry and toxicity. These measurements were validated with Geant4 simulations by tracking trajectories and energy loss of α particles in a similar geometry as depicted in Fig. 1 (Left).

3 Conclusions

The results so far demonstrate the feasibility to determine the uptake efficiency of radiopharmaceuticals for TAT by directly probing α emissions from live cell samples. Continuing studies are underway to explore other cell types, different radiolabeled compounds, and improved detector designs. Continuous efforts are made to improve detection systems, data acquisition and data analysis. Further developments on sample preparation and measurement procedures a underway with the goal to enhance the reproducibility and statistical robustness of results.

ACKNOWLEDGMENTS

TRIUMF receives federal funding via a contribution agreement through the National Research Council of Canada. We also acknowledge added support through the New Frontiers in Research Fund - Exploration NFRFE-2019-00128 and Discovery Grants from the Natural Sciences and Engineering Research Council of Canada, (NSERC): SAPIN-2021-00030 (P. Kunz) and RGPIN-2022-03887 (H. Yang). Many thanks to the Life Science Laboratory team.

References

[1] V. Radchenko, A. Morgenstern, A. R. Jalilian, C. F. Ramogida, C. Cutler, C. Duchemin, C. Hoehr, F. Haddad, F. Bruchertseifer, H. Gausemel, et al., Production and supply of α-particle–emitting radionuclides for targeted α-therapy, Journal of nuclear medicine 62 (11) (2021) 1495–1503.

[2] A. K. Robertson, B. L. McNeil, H. Yang, D. Gendron, R. Perron, V. Radchenko, S. Zeisler, P. Causey, P. Schaffer, 232th-spallation-produced 225ac with reduced 227ac content, Inorganic Chemistry 59 (17) (2020) 12156–12165.

[3] P. Kunz, C. Andreoiu, V. Brown, M. Cervantes, J. Even, F. H. Garcia, A. Gottberg, J. Lassen, V. Radchenko, C. F. Ramogida, et al., Medical isotope collection from isac targets, in: EPJ Web of Conferences, Vol. 229, EDP Sciences, 2020, p. 06003.

[4] P. Kunz, C. Andreoiu, P. Bricault, M. Dombsky, J. Lassen, A. Teigelhöfer, H. Heggen, F. Wong, Nuclear and in-source laser spectroscopy with the isac yield station, Review of Scientific Instruments 85 (5) (2014).

Copyright on 7th Asia-Pacific Symposium on Radiochemistry 2025 - S2-16 -

Production of ^{225}Ac via the ^{226}Ra(*p*,2*n*)^{225}Ac reaction at RIKEN

Akihiro Nambu[1], Yousuke Kanayama[1], Hiromichi Shimizu[1], Masataka Imamura[1,2], Shota Kimura[1,2], Daiki Mori[1,2], Yuichiro Wakitani[2], Takahiro Mikamoto[2], Yudai Shigekawa[1], Sayantani Mitra[1], and Hiromitsu Haba[1]

[1]*Nishina Center for Accelerator-Based Science, RIKEN, 2-1 Hirosawa, Wako-shi, Saitama 351-0198, Japan*
[2]*Japan Radioisotope Association, 2-28-45 Honkomagome, Bunkyo-ku, Tokyo 113-8941, Japan*

Toward establishing a domestic production of ^{225}Ac via the ^{226}Ra(p,2n)^{225}Ac reaction at the RIKEN AVF cyclotron, a ^{226}Ra target was prepared by recoverying legacy ^{226}Ra needles for brachytherapy. ^{225}Ac was purified through multi-step column chlomatography. The production yield, radionuclidic purity, and chemical purity of the purified ^{225}Ac were discussed.

1 INTRODUCTION

^{225}Ac ($T_{1/2} = 9.92$ d) is one of the most world-wide trended radioisotopes applied for targeted alpha-particle therapy [1]. Most of ^{225}Ac has been produced by ^{229}Th generator system, but its supply has been limited due to the shortage of ^{229}Th in recent years. Therefore, the import of ^{225}Ac into Japan has been unstable and scarcely available over the past few years. To ensure a stable supply, a domestic production route for ^{225}Ac has been desired.

Recently, several nuclear reactions have been suggested for ^{225}Ac production. One of the most promising reaction is ^{226}Ra$(p, 2n)^{225}$Ac [1]. The use of ^{226}Ra is very restricted because of its decay product, ^{222}Rn ($T_{1/2} = 3.8$ d), the alpha-emitting noble gas which readily disperses into the atmosphere and poses a significant contamination risk. Despite such difficulties, a high production yield is expected for the ^{226}Ra$(p, 2n)^{225}$Ac reaction due to its high production cross section [2]. To produce a sufficient radioactivity of ^{225}Ac, a ^{226}Ra target with a high areal density is required because only a limited amount of the element can be used due to its rarity.

In this research, ^{225}Ac was produced via the ^{226}Ra$(p, 2n)^{225}$Ac reaction using ^{226}Ra recovered from legacy radiotherapeutic needles. Then, ^{225}Ac was purified through multi-step column chromatography.

2 MATERIAL AND METHODS

2.1 Radium-target preparation

A glove-box system with radon-trap system was employed in this study to ensure the safe handling of ^{226}Ra. The internal air of the glove box was circulated through pre-dehydrators maintained at $-20°$C and $-80°$C, followed by a charcoal radon trap cooled to $-80°$C. All procedures for target preparation and chemical separation (sec. 2.3) were performed in this system.

Three legacy radiotherapeutic needle sources contained $\sim$4 mg of ^{226}Ra in total (74, 33, and 33 MBq). Each platinum-alloy needle was cut into small pieces and stored in water. All pieces including insoluble compound of Ra were subjected to ultrasonication for approximately three days uncontinuously until Ra was released from the pieces of needles. Here radium sulfate in water is in an equilibrium state of $RaSO_4 \rightleftarrows Ra^{2+} + SO_4^{2-}$. In this study, cation exchange resin (Muromac 50WX8 200-400 mesh, CIX) and anion exchange resin (Dowex Monosphere, 550A(OH), AIX) were used to adsorb Ra^{2+} and SO_4^{2-}, respectively, in order to decompose $RaSO_4$ [3]. For this process, 300 mg of AIX was packed in a 110-mesh nylon fiber sheet. After ultrasonication, this packet was sank in the suspension of $RaSO_4$ with the same weight of unpacked CIX. After they were shaked for 1–3 day together, ^{226}Ra was adsorbed on the CIX resin. The ^{226}Ra-adsorbed CIX was transfered to an empty column, and ^{226}Ra was eluted with 4 M nitric acid. In order to remove ^{nat}Ba carrier possibly mixed with ^{226}Ra in the legacy needles, additional purification by using extraction chromatography (Sr resin 100-150 μm, 0.1 M HPF_6 and 3 M HNO_3) [4, 5] and cation exchange chromatography (Muromac 50WX8 100-200 mesh, 0.5 M and 4 M HNO_3) were carried out. The above procedure was performed for each of three legacy needles. The purified ^{226}Ra solution was transfered into a ϕ4-mm hole of the tantalum target holder and heated to dryness, then sealed with a 6.73 μm Havar foil. Finally, 104 MBq of $^{226}Ra(NO_3)_2$ target was prepared, providing the apparent target areal density of 22.5 mg/cm^2 as ^{226}Ra.

2.2 Irradiation

The target holder was installed in an irradiation chamber and taken out from the glove box to the E7 vertical beamline at the RIKEN AVF cycrotron. In the irradiation chamber, the target was double-sealed with two Havar foils, which were cooled with He gas in two isolated lines during irradiation. The bottom of the tantalum target holder was cooled with $\sim$5°C water.

Copyright on 7th Asia-Pacific Symposium on Radiochemistry 2025 - S2-17 -

The target was irradiated by a ϕ3-mm vertical proton beam. The incident energy of the beam was measured to be 13.97 MeV by a time-of-flight method before irradiation. Energy loss in the window materials and He gas layers was calculated using the SRIM code [6], resulting in an energy of 13.60 MeV. The beam current was initially 0.1 μA and gradually increased to a maximum of 10 μA over 2 h to avoid sudden damage to the target material. The irradiation at maximum beam current was then maintained for approximately 20 h.

2.3 Chemical separation

The target chamber was carried into the glove box and the ^{226}Ra target was retrieved for ^{225}Ac purification. The chemical separation of ^{225}Ac was performed mainly based on the previous procedures [2, 7]. The target material was dissolved with nitric acid and ^{225}Ac was separated from ^{226}Ra with the Eichrom LN resin column. In order to remove ^{210}Pb ($T_{1/2}$ = 22.2 y) produced as a descendant of ^{226}Ra, an additional purification was performed by using the Sr resin column which possess high capacity factor (k') for Pb [8]. Actinium was then purified with the Eichrom branched DGA resin, according to Ref. [7]. Finally, anion exchange chromatography using the Muromac 1x8 resin column was performed twice with different concentrations of hydrochloric acid to reduce potential contamination by inorganic metals such as iron and zinc. After separation, the ^{226}Ra was collected, purified, and recovered to reuse for the next irradiation.

2.4 Measurements

The purified Ac was measured by a Ge detector to qualify ^{225}Ac, the undesired ^{226}Ac ($T_{1/2} = 29.4$ h), and the remaining ^{226}Ra target. The radioactivity of ^{225}Ac was evaluated with the γ ray of ^{221}Fr ($T_{1/2} = 4.8$ min, 218 keV, $I_\gamma = 11.4\%$) in a radioactive equilibrium with ^{225}Ac. Radioactivity of ^{226}Ac was evaluated by its γ ray (230 keV, $I_\gamma = 26.9\%$).

The radioactivities of remaining ^{226}Ra target and biproduct ^{227}Ac ($T_{1/2} = 21.8$ y) were measured by α-ray spectrometry using a Si detector after more than two months cooling. The amounts of other impure elements were measured using ICP-MS 7800 (Agilent Technologies).

3 RESULTS AND DISCUSSION

The radioactivities of $^{225,\,226}$Ac produced in the target were 110 and 14 MBq at the EOB, respectively. The radionuclidic purity of ^{225}Ac was 88.8% at the EOB, which is expected to reach 99.9% after 10 d, considering a typical case of purification and delivery. A production yield of 0.59 MBq/(μA h) for ^{225}Ac was achieved. Other results will be discussed in the presentation.

4 CONCLUSION

We successfully produced 110 MBq of ^{225}Ac at the end of bombardment through the ^{226}Ra(p,2n)^{225}Ac reaction with 104 MBq of ^{226}Ra target recovered from the legacy radiotherapeutic ^{226}Ra needles. An enhancement of the production yield is under development.

References

[1] W. Jalloul *et al.*, Pharmaceuticals, **16**, 1679 (2023).

[2] C. Apostolidis *et al.*, Applied Radiation and Isotopes, **62**, 383 (2005).

[3] W. Dedek, Fresenius' Zeitschrift für analytische Chemie, **173**, 399 (1960).

[4] D. V. Filosov *et al.*, Solvent Extraction and Ion Exchange, **33**, 496 (2015).

[5] A. N. Vasiliev *et al.*, Radiochimica Acta, **104**, 539 (2016).

[6] J. F. Ziegler *et al.*, Nuclear Instruments and Methods in Physics Research Section B: Beam Interactions with Materials and Atoms, **268**, 1818 (2010).

[7] K. Nagatsu *et al.*, European Journal of Nuclear Medicine and Molecular Imaging, **49**, 279 (2021).

[8] E. P. Horwitz *et al.*, Solvent Extraction and Ion Exchange, **10**, 313 (1992).

Copyright on 7th Asia-Pacific Symposium on Radiochemistry 2025 - S2-17 -

Contributed Talk | [P2]ICP-MS Based Radioanalytical Chemistry and Related Applications

Fri. Sep 19, 2025 10:10 AM - 11:10 AM JST | Fri. Sep 19, 2025 1:10 AM - 2:10 AM UTC Hall B(Small)

[P2] ICP-MS Based Radioanalytical Chemistry and Related Applications

10:10 AM - 10:30 AM JST | 1:10 AM - 1:30 AM UTC

[P2-10]

Rapid Determination of Uranium isotopes and Ra-226 in Water Samples Using ICP-QQQ-MS

*Ivana Coha[1,2], Norbert Kavasi[3], Marko Štrok[2], Leja Rovan[2], Dorice Seif[4], Marta Jagodic Hudobivnik[2], Željko Grahek[1] (1. Ruđer Bošković Institute (Croatia), 2. Jožef Stefan Institute (Slovenia), 3. Fukushima Institute for Research, Education and Innovation (Japan), 4. University of Dar es Salaam (Tanzania))

10:30 AM - 10:50 AM JST | 1:30 AM - 1:50 AM UTC

[P2-11]

The application of ICP-MS/MS for the analysis of actinides and Sr-90 in bioassay samples for rapid dose assessment in radiation emergency medicine

*Guosheng Yang[1], Eunjoo Kim[1], Jian Zheng[1], Hirofumi Tazoe[2], Munehiko Kowatari[1], Osamu Kurihara[1] (1. National Institutes for Quantum Science and Technology, Japan (Japan), 2. Institute of Radiation Emergency Medicine, Hirosaki University (Japan))

10:50 AM - 11:10 AM JST | 1:50 AM - 2:10 AM UTC

[P2-12]

Determination of trace level I-129 by ozone reaction ICP-QMS/QMS

*Yanbei Zhu[1], Daiki Asakawa[1] (1. National Institute of Advanced Industrial Science and Technology (Japan))

©APSORC25

Rapid Determination of Uranium isotopes and Ra-226 in Water Samples Using ICP-QQQ-MS

Ivana Coha[1,2], Norbert Kavasi[3], Marko Štrok[2], Leja Rovan[2], Dorice Seif[2,4], Marta Jagodic Hudobivnik[2], Željko Grahek[1]

[1]*Laboratory for radioecology, Division for Marine and Environmental Research, Ruđer Bošković Institute, Bijenička cesta 54, Zagreb, Croatia, 10000, ivana.coha@irb.hr, zgrahek@irb.hr*
[2]*Department of Environmental Sciences, Jožef Stefan Institute, Jamova cesta 39, Ljubljana, Slovenia, 1000, marko.strok@ijs.si, leja.rovan@ijs.si, marta.jagodic@ijs.si*
[3]*Regional Environmental Co-Creation Unit, Fukushima Institute for Research, Education and Innovation, Fukushima, Japan, 960-1295 Norbert Kavasi, kavasi.norbert.h4v@research.f-rei.go.jp*
[4]*Physics department, University of Dar es Salaam, Dar es Salaam, Tanzania, P.O Box 35063, doricers85@gmail.com*

Monitoring and managing radionuclide levels in water is essential to ensure compliance with safety standards and guidelines, thereby protecting both human health and the environment. The assessment of human exposure to radionuclides in drinking water has received considerable global attention over the past decades. The EU Drinking Water Directive sets derived concentrations for the most common natural and artificial radionuclides in water intended for human consumption [1]. Natural waters contain both alpha- and beta-emitting radionuclides, with concentrations varying widely depending on geological and environmental conditions. Alpha activity in water samples is typically attributed to dissolved uranium isotopes (U-234, U-235, U-238) and Ra-226. According to the Directive, the recommended limit for Ra-226 in drinking water is 0.5 Bq/L, and 3 Bq/L for each of U-234 and U-238. Uranium poses a greater health risk due to its chemotoxicity rather than its radiotoxicity, and according to EU Directive 2020/2184 [2], its concentration in drinking water should not exceed 30 µg/L (375 mBq/L). In most EU countries, the determination of gross alpha radioactivity is mandatory for drinking water as an indirect measure of their presence. However, this approach does not allow their identification and individual quantification. Traditionally, for their identification and quantitative determination, long-term, labor-intensive radiometric methods are used, including the use of various chemicals and the generation of considerable waste. On the other hand, mass spectrometry offers a promising solution to overcome the limitations of radiometric techniques. Although initially expensive and less accessible for routine laboratory analysis, advances in instrumentation have significantly increased both the availability and sensitivity of these methods. This is particularly important, as radionuclide determination typically requires measurements at concentrations in the pg/mL or even fg/mL range, which poses considerable analytical challenges.

The triple quadrupole mass spectrometry (ICP-QQQ-MS), due to its potential for efficient spectral interference removal without sacrificing sensitivity along with its ability to quasi-simultaneously screening for multiple radionuclides, appears to be a very promising choice for the measurement of uranium isotopes and Ra-226. Therefore, in this study, a novel method for the direct determination of Ra-226 and uranium isotopes (U-234, U-235, U-238) in water samples was developed using ICP-QQQ-MS. The ICP-QQQ-MS was operated in a single quadrupole mode, with or without helium as a collision/reaction gas. For uranium isotopes, optimal performance was achieved using a helium flow rate of 2 mL/min, with no significant interferences observed. Ra-226 was measured using the same mode and quantified using the standard addition method to account for matrix effects. The newly developed method involves direct measurement using only 10 mL of water sample, thereby significantly reducing the required sample volume compared to conventional approaches (50 mL up to 30 L), and drastically shortening analysis time while eliminating complex pre-treatment steps.

The method was validated and successfully applied to real water samples. Results were compared with those obtained from alpha spectrometry, demonstrating good agreement between the two techniques. The lowest detection limit achieved for the direct determination of Ra-226 was 3.6 mBq/L, while for uranium isotopes it was 14 µBq/L for U-234, 0.4 µBq/L for U-235, and 1.4 µBq/L for U-238, respectively.

This approach offers a rapid, efficient, and accurate alternative for the determination of radionuclides in water, making it highly suitable for routine environmental monitoring and radiological risk assessment.

ACKNOWLEDGMENTS

This work was supported in part by the Croatian Science Foundation under the project number HRZZ-MOBODL-23-08-3540, the European Union's Horizon 2020 research and innovation programme under the Marie Sklodowska-Curie grant agreement No 101003359, the Slovenian Research and Innovation Agency programme P2 0075 and the project 21GRD09 MetroPOEM.

References

[1] Council of the European Union, "Council Directive 2013/51/Euratom of 22 October 2013 laying down requirements for the protection of the health of the general public with regard to radioactive substances in water intended for human consumption," *Official Journal of the European Union*, L296, 12–21 (2013).

[2] European Parliament and Council, "Directive (EU) 2020/2184 of 16 December 2020 on the quality of water intended for human consumption," *Official Journal of the European Union*, L435, 1–62 (2020)

The application of ICP-MS/MS for the analysis of actinides and Sr-90 in bioassay samples for rapid dose assessment in radiation emergency medicine

Guosheng Yang[1], Eunjoo Kim[1], Jian Zheng[1], Hirofumi Tazoe[2], Munehiko Kowatari[1], Osamu Kurihara[1]

[1]*National Institutes for Quantum Science and Technology (QST), 4-9-1 Anagawa, Inage, Chiba 263-8555, Japan*
yang.guosheng@qst.go.jp
[2]*Institute of Radiation Emergency Medicine, Hirosaki University, 036-8564, Aomori, Japan*

For the rapid response after an internal exposure accident of radionuclides, such as actinides and Sr-90, different collision/reaction gases have been introduced in the collision/reaction cell to mitigate the polyatomic and isobaric interferences and increase the sensitivity of the target radionuclide during the tandem mass spectrometric analyses. For method validation, the reference materials provided by PROCORAD (Association for the PROmotion of Quality COntrol in RADiotoxicological Analysis), France, were analyzed, and satisfactory results were shown using the performance index of Z-score. The certifications of TOP LABOs in the PROCORAD indicate our developed bioassay techniques could perform rapid and accurate dose assessment to provide timely information for medical treatment after an internal exposure accident.

1 ACTINIDE BIOASSAY

Internal exposure to alpha-particle emitters, such as ^{238}U, ^{237}Np, ^{238}Pu, ^{239}Pu, ^{240}Pu, ^{241}Am, and ^{244}Cm, is likely to bring about a large radiation exposure dose even if the intake amount is small. For dose assessment of radionuclides, such as isotopes of actinides, urine and fecal analyses have been used extensively. Urinary bioassay has the merit for verification of solubility classification (S, slow; M, moderate; F, fast) of actinides in order to select the proper biokinetic models for dose calculation in an early phase. In the very early phase, the contents of actinides in the fecal excretion are approximately serval orders of magnitude higher than that in the urinary excretion, which makes the fecal bioassay is more sensitive for concentration assessment [1].

Compared with the conventional radiometric spectrometric techniques, the required urinary samples were reduced to 20 mL from 0.5–1 L allow us to analyze spot urine to study the efficiency of decorporation agents (such as DTPA) during radiation emergency medicine [2]. Since the distribution of radionuclides in fecal samples is uneven, total digestion of the whole fecal samples is required. After shortening the time for drying and ashing to 8 h, we conducted a complete decomposition based on borate fusion for the ash of a 150 g fecal sample. Subsequently, sequential column chromatographic separation using AG MP-1M resin and DGA resin were performed. Using triple-quadrupole inductively coupled plasma−mass spectrometry (ICP-MS/MS) with helium collision gas provided the method detection limits for ^{237}Np, ^{239}Pu, ^{240}Pu, ^{241}Pu, ^{241}Am, and ^{244}Cm of 9.99, 30.4, 18.2, 16.5, 16.5, and 4.95 ag/mL, respectively, for the 20 mL urinary sample, and 1.33, 4.05, 2.43, 2.21, 2.21, and 0.660 ag/g, respectively, for the 150 g fecal sample [1,2].

2 SR-90 BIOASSAY

As pure β^- emitters, the potential beta energies of ^{90}Sr (0.546 MeV, 100%; $t_{1/2}$ = 28.74 y) and its daughter nuclide ^{90}Y (2.28 MeV, 100%; $t_{1/2}$ = 64 h) are very high [3]. Like calcium, Sr belongs to the alkaline earth element and is known as a bone seeker when incorporated into the human body, resulting in its long biological half-life (~ 18 y) in the human body [4,5]. For those under 20 y of age, the age-specific ingestion dose coefficients applied in case of internal intake are higher for ^{90}Sr, at (4.7−23) × 10^{-8} Sv/Bq, than they are for ^{137}Cs, at (0.96−2.1) × 10^{-8} Sv/Bq [6]. Therefore, ^{90}Sr should be also regarded as one of the radioisotopes that the public needs to be protected from internal radiation exposure following large-scale radiological or nuclear disasters and/or nuclear terrorist attack.

The primary drawback of conventional radiometric methods is long analytical time (2–3 weeks) mainly due to the waiting time for the secular equilibrium state between ^{90}Sr and ^{90}Y. For rapid public screening after a large-scale radiological and/or nuclear accident, we developed a novel ^{90}Sr bioassay for small-volume urine samples using ICP-MS/MS [7]. After organic matter decomposition of 10 mL urine by HNO_3, stacked DGA and Sr resin cartridges were used directly for chromatographic separation and purification of Sr. Yields of Sr were measured as 94±5% (n=12) for the whole procedure, using stable ^{88}Sr originally in the urine sample as a yield tracer. CO_2 proved to be a better reaction gas than O_2, to overcome isobaric/polyatomic interferences, especially those caused by Zr and Ge. With a conventional introduction system + s lens + 75% CO_2 flow rate in the 4$^{\#}$ cell gas line, the method detection limit was estimated to be

Copyright on 7th Asia-Pacific Symposium on Radiochemistry 2025 - P2-11 -

0.978 pg/L (5 Bq/L) in 10 mL urine, meeting the public screening requirement for judging ingestion/inhalation exposure beyond 1 mSv Committed Effective Dose Equivalent, with a reasonable throughput (~ 6 h for 12 samples).

3. METHOD VILIDATION AND APPLICATION

For method validation, the reference materials provided by PROCORAD (Association for the PROmotion of Quality COntrol in RADiotoxicological Analysis), France, were analyzed (U in urine, actinides in urine, DTPA-actinides in urine, actinides in fecal ashes, and Sr-90 in urine). Each year around 75 laboratories participate in the interlaboratory comparison exercises offered by PROCORAD. Satisfactory results were shown using the performance index of Z-score (|Z-score| ≤2 indicates satisfactory performance). The developed methods were also applied to the urinary samples collected in a Pu/Am internal exposure accident, and the results of ICP-MS/MS were consistent to that of conventional alpha spectrometric analysis. Both the results from the developed ICP-MS/MS analysis and the conventional beta counting were consistent for the analysis of ^{90}Sr in urine. During the PROCORAD, our laboratory has been certified as TOP LABOs in the items of U in fecal ashes, actinides in urine, DTPA-actinides in urine, and Sr-90 in urine. The high throughput and high sensitivities of our proposed methods will allow greater numbers of related laboratories to be involved in screening activities for unexpected actinide exposure, such as in the case of a large scale radiological and/or nuclear disaster.

ACKNOWLEDGMENTS

This work was supported by the Japan Society for the Promotion of Science KAKENHI (17k00537, 22K12384 and 23H03142) and the Managing Director's Fund of the Quantum Medical Science Directorate, QST. The authors also thank Hatsuho Seno, Norikazu Kogure, Taira Fujita, Akira Sakuma, Kohei Iwaya, and other staff for their assistance in the experiment.

References

[1] G. Yang, et al., Bioassay for multiple actinides in large-size feces using ICP-MS/MS after borate fusion and chromatographic separation by AG MP-1 M and DGA resins. *Microchem. J.*, **209** (2025). https://doi.org/10.1016/j.microc.2025.112659.
[2] G. Yang, et al., Rapid analysis of ^{237}Np and Pu isotopes in small volume urine by SF-ICP-MS and ICP-MS/MS. *Anal. Chim. Acta*, **1158** (2021), https://doi.org/10.1016/j.aca.2021.338431.
[3] JAEA Nuclear Data Center, https://wwwndc.jaea.go.jp.
[4] K. Koarai, et al., ^{90}Sr in teeth of cattle abandoned in evacuation zone: record of pollution from the Fukushima Daiichi Nuclear Power Plant accident, *Sci. Rep.*, **24077**, (2016), https://doi.org/10.1038/srep24077.
[5] N. B. Shagina, et al., An application of in vivo whole body counting technique for studying strontium metabolism and internal dose reconstruction for the Techa River population, *J. Phys.: Conf. Ser.*, **41**, 433–440, (2006).
[6] ICRP, Age-dependent Doses to the Members of the Public from Intake of Radionuclides – Part 5 Compilation of Ingestion and Inhalation Coefficients, ICRP Publication 72, Ann. ICRP, **26**(1), 15–83, (1995).
[7] Yang et al. ^{90}Sr bioassay in small-volume urine by ICP-MS/MS with CO_2 as the reaction gas. *J. Anal. At. Spectrom.*, **38**, 2562−2570 (2023).

Determination of trace level I-129 by ozone reaction ICP-QMS/QMS

Yanbei Zhu & Daiki Asakawa

National Metrology Institute of Japan, National Institute of Advanced Industrial Sciences and Technology, Japan. E-mail: yb-zhu@aist.go.jp, d.asakawa@aist.go.jp

Online generated ozone was introduced as the reaction gas for tandem quadrupole inductively coupled plasma mass spectrometry (ICP-QMS/QMS),[1] permitting the measurement of $^{129}I^+$ as $^{129}I^{16}O^+$ and $^{129}I^{16}O_2^+$ after ion-molecule reactions.[2] By using ozone as the reaction gas, the reactions of ($^{129}I^+ \rightarrow ^{129}I^{16}O^+$) and ($^{129}I^+ \rightarrow ^{129}I^{16}O_2^+$) were both improved significantly in comparison to those observed with oxygen as the reaction gas. Typical spectral interferences related to $^{129}Xe^+$ were completely removed by introduction of hydrogen as an additional cell gas to ozone, resulting in free-of-spectral-interference measurement of ^{129}I without mathematic correction. In isotopic ratio ($^{129}I/^{127}I$) analysis, the formation of ($^{127}I^1H_2^+ \rightarrow$) $^{127}I^{18}O^+$ resulted in a blank ratio of 4.4×10^{-8} for natural iodine in the measurement of ($^{129}I^+ \rightarrow ^{129}I^{16}O^+$)/($^{127}I^+ \rightarrow ^{127}I^{16}O^+$), while a much lower blank ratio of 6.7×10^{-10} can be achieved by the measurement of ($^{129}I^+ \rightarrow ^{129}I^{16}O_2^+$)/($^{127}I^+ \rightarrow ^{127}I^{16}O_2^+$). The mechanism for separating spectral interference is shown in Figure 1.

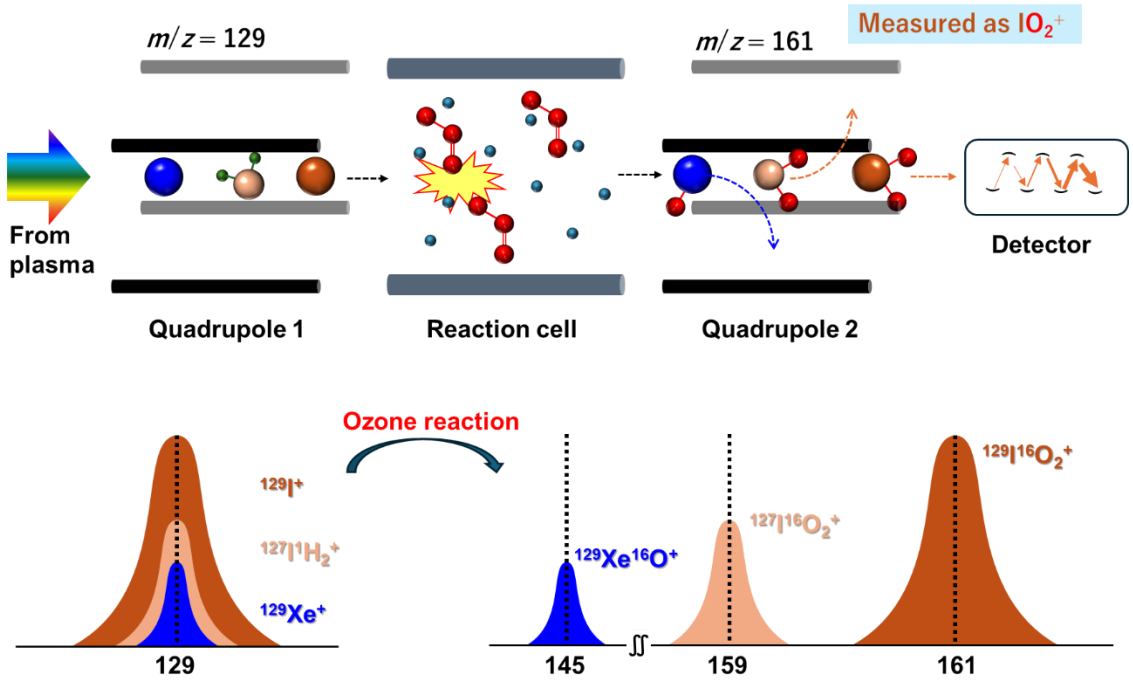


Figure 1. The mechanism for separating spectral interferences in the measurement of I-129 by ozone reaction ICP-QMS/QMS

References

1. Y. Zhu, *Chem. Comm.*, 2024, **60**, 3974-3977.
2. Y. Zhu, D. Asakawa, *iScience*, 2024, **27**, 111138.

Closing Ceremony

Fri. Sep 19, 2025 11:20 AM - 11:45 AM JST | Fri. Sep 19, 2025 2:20 AM - 2:45 AM UTC Hall S(Int'l)

[CL] Closing Ceremony

11:20 AM - 11:45 AM JST | 2:20 AM - 2:45 AM UTC

Closing Ceremony

©APSORC25